



University  
of Glasgow

Aly, Samir El-Sayed (1979) *Investigations into the effect of heat and mass transfer on flow across tube bundles*. PhD thesis.

<http://theses.gla.ac.uk/2194/>

Copyright and moral rights for this thesis are retained by the author

A copy can be downloaded for personal non-commercial research or study, without prior permission or charge

This thesis cannot be reproduced or quoted extensively from without first obtaining permission in writing from the Author

The content must not be changed in any way or sold commercially in any format or medium without the formal permission of the Author

When referring to this work, full bibliographic details including the author, title, awarding institution and date of the thesis must be given

INVESTIGATIONS INTO THE EFFECT OF HEAT AND MASS TRANSFER  
ON FLOW ACROSS TUBE BUNDLES

by

Samir EL-Sayed Aly,  
Dipl. Ing., Dr. Ing.

On leave from Reactors Dept., A.E.E., Cairo, Egypt.

Thesis submitted for the degree of Doctor of Philosophy  
in the Faculty of Engineering, University of Glasgow.

Department of Mechanical Engineering,  
James Watt Building,  
University of Glasgow.

May, 1979.

**BEST COPY**

**AVAILABLE**

Poor text in the original  
thesis.

ABSTRACT

The thesis describes an investigation into the effect of different parameters on the detailed flow structure in a heat exchanger model. The problems related to the flow and heat transfer in tube bank configurations are discussed. A literature review is incorporated and the approximate consistency between different investigations is shown.

The aim of the study was to determine the effect of parameters such as surface roughness, turbulent intensity, mass transfer and heat transfer on the simultaneously measured local parameters such as wall shear stress, normal pressure and heat transfer coefficient distributions around circular cylinders in cross flow.

A newly developed instrument was built to measure the local shear stress around the test cylinder surface. A literature review for different experimental techniques used in this field is presented and the difficulties connected with their usage are discussed. The developed device was of the null seeking servo-force balance type which showed a high accuracy and reliability with instantaneous response. This device was also used to measure the vortex shedding frequency.

These studies were of air flow, using an open circuit wind tunnel working in the suction mode. Measurements were obtained for single cylinder and individual cylinders along the/...



the depth of a seven rows tube bank. The bank was of the staggered type with equal pitch to diameter ratios of 1.5. Using the same set up through the whole programme of study made it possible to separate the effect of individual parameters on the local flow characteristics.

Using a hydrodynamic analogy, the condensation process in a surface steam condenser was simulated by homogeneous extraction of air through the surface of a porous test cylinder. Experiments involving simultaneous heat and mass transfer were also carried out and their effect on the local parameters around the cylinder was investigated.

Tests covered a range of main stream Reynolds number up to 70,000, surface roughness up to  $53 \times 10^{-5}$ , suction parameter up to 1.2 and input heat loads up to 18 Watt /Cm<sup>2</sup>.

Results of the studies are presented for the local parameters around the cylinder surface. These are also presented in terms of the relative contribution of shear stress and pressure drag to the total drag. Results are also presented for the overall pressure drop and heat transfer rate over different rows in the tube bank.

Measurements of the Strouhal number for a single cylinder agreed with other investigators and showed an independence of the Reynolds number.

Results showed that even with small surface roughness, the shear stress was increased considerably. The effect of/...

of increasing the turbulence intensity was to increase the shear stress and to cause a reduction in the pressure drag.

Flow and heat measurements showed that the entrance effect in the tube bank extended up to the third row and stable conditions were reached from the fourth row onwards.

The pressure drop per row decreased as the number of rows increased and the percentage contribution of the shear stress to the total drag was about 2 to 4 per cent.

Results with mass extraction showed that for a typical condenser loading, the suction had a considerable effect on the values of the wall shear stress which was increased by increasing suction rate. Although suction caused slight changes in the normal pressure distribution, the changes in the pressure drag due to suction effect were not significant. Furthermore, beyond a certain suction rate flow transition took place due to the surface roughness relative to the reduced thickness of the boundary layer.

Heat transferred across the sucked boundary layer caused an increase in the wall shear stress with no significant effect on the normal pressure distribution.

The distribution of the heat transfer coefficient showed a relative minimum value at the FSP while its peak was reached in the region of the shear stress peak and its minimum value was reached beyond the flow separation point. Moreover/...

Moreover, all the rows in the bank showed heat transfer coefficients which were higher than those for a single cylinder.

Flow visualisation showed the general effect of suction on the flow around the cylinder and efforts made to develop a theoretical model for such cases are also discussed.



## ACKNOWLEDGMENTS

I would like to acknowledge, with sincere gratitude, the help and constant encouragement I received from Professor R.S. Silver during the course of this work.

Thanks are due to Mr. J. Cunningham for acting as the project supervisor, for many useful discussions and for his advice and comments.

I am also grateful to Dr. D. Macvean. The control system of the shear stress sensor could not have been developed to its present standard without his valuable assistance and co-operation.

I would also like to thank the technical staff of the Departments of Mechanical Engineering and Aeronautics and Fluid Mechanics, without whose efforts the study would not have been possible.

Thanks are also due to Miss M.B. Simpson for typing the manuscript. I am also thankful to my wife Fahima and my children for their patience and support whilst I was studying the subject.

The work was financed by the Science Research Council whose grant was highly appreciated.

CONTENTS

	Page
Title page	i
Abstract	ii
Acknowledgments	vi
Contents	vii
List of tables	xiv
List of figures	xv
Chapter 1.      Introductory	1
1.1      General introduction	1
1.2      Aim and scope of the present work	7
1.3      Nomenclature	14
Chapter 2.      Measurement of shear stress on solid boundaries	18
2.1      Introduction	18
2.2.      Indirect skin friction measurements	20
2.2.1   Total head tube	21
2.2.2   Hot wire anemometer	23
2.2.3   Surface tubes	25
2.2.3.1. Stanton tube	25
2.2.3.2. Preston tube	30
2.2.3.3. Effective centre of the velocity head probe	32
2.2.4   Surface heated probe	35
2.2.5   Measurements of skin friction on circular cylinder using indirect methods.	36
2.3      Direct measurements of skin friction	39
2.3.1   Direct measurement of average shearing forces.	39

Chapter 2.	(cont'd.)	Page
2.3.2	Direct measurement of local shearing force	41
2.3.3	Direct measurements of skin friction on a circular cylinder	43
2.4	Discussion and concluding remarks	44
Chapter 3.	Development of a device for the measurement of skin friction and flow dynamics around a circular cylinder.	47
3.1	Introduction	47
3.2	Possible sources of error	47
3.2.1	Clearance gap effect	47
3.2.2	Flushness with the rest of the model surface	49
3.2.3	Buoyancy effect	50
3.2.4	Drag piece dimensions	51
3.3	Direct force measuring techniques	51
3.3.1	Deflected devices	51
3.3.2	Null-positioning devices	52
3.4	Description of the developed device	52
3.4.1	Mechanical description of the device	54
3.4.2	The controller and electronic equipments	58
3.4.2.1.	Choice of system	59
3.4.2.2.	Analysis of the system	61
3.5	Calibration of the device	64
3.6	Concluding remarks	65
Chapter 4.	Pressure drop and heat transfer in tubular heat exchangers	67
4.1	Pressure drop in cross flow	67
4.1.1	Introduction	67
4.1.2	Single cylinder in a cross flow	69

Chapter 4.	(cont'd.)	Page
4.1.3	Turbulence and cylinder in a cross flow	72
4.1.4	Tube in a bank in cross flow	73
4.1.5	Pressure drop for banks of tubes in a cross flow	76
4.1.6	Rectangular tube banks in an isothermal cross flow	77
4.1.7	Pressure drop in non isothermal cross flow	86
4.1.8	Effect of condensation on pressure drop in tube banks	88
4.1.9	Reynolds model and pressure drop across tube banks	92
4.1.10.	Pressure drop in cylindrical banks of tubes	95
4.2	Heat transfer in cross flow	96
4.2.1	Introduction	96
4.2.2	Heat transfer of a single cylinder in cross flow	99
4.2.3	Turbulence and heat transfer of a single cylinder	104
4.2.4	Distribution of heat transfer around single cylinder	113
4.2.5	Heat transfer in relation to skin friction around cylinder	117
4.2.6	Heat transfer for a tube in a staggered bank	129
4.2.7	Heat rate distribution in a staggered bank	133
4.2.8	Heat transfer in cylindrical bank in cross flow	136
4.3	Concluding remarks	137
Chapter 5.	Apparatus and experimental procedure	139
5.1	Introduction	139
5.2	Experimental apparatus	140



Chapter 5.	(cont'd.)	Page
5.2.1	Wind tunnel	140
5.2.2	Test cylinder	146
5.2.3	Static pressure measurements on the test cylinder	150
5.2.4	Skin friction measurements	153
5.2.5	Hot wire anemometer	155
5.2.6	Two-dimensionality of the tunnel	158
5.2.7	Tunnel blockage	160
5.2.8	Simulated condensation tests	164
5.2.8.1.	Mass transfer during condensation	165
5.2.8.2.	Heat transfer during condensation	168
5.2.8.3.	Temperature measurements	172
5.3	Experimental procedure	178
5.3.1	Single cylinder	178
5.3.2	Tube bank	180
5.4	Concluding remarks	184
Chapter 6.	Results I: Vortex shedding	187
6.1	Introduction	187
6.2	Vortex shedding for a bluff body	187
6.3	Measurements of the vortex shedding frequency	190
6.4	Present device and shedding frequency measurements	193
6.5	Concluding remarks	195
Chapter 7.	Results II: Cross flow through a tube bank	197
7.1	Introduction	197
7.2	Single cylinder in cross flow	198
7.2.1	Shear sensor's gap effect on the recorded skin friction	199
7.2.2	Procedure and reduction of observations	203

Chapter 7.	(cont'd).	Page
7.2.3	Effect of surface roughness	205
7.2.3.1.	Surface roughness in cross flow	205
7.2.3.2.	Results and discussion	207
7.2.4	Turbulence level effect	215
7.2.4.1.	Turbulence level in cross flow	215
7.2.4.2.	Experimental procedure	216
7.2.4.3.	Results and discussion	217
7.3	Staggered tube bank experimental results	220
7.3.1	Cross flow around a cylinder in a tube bank	220
7.3.2	Procedure and reduction of observations	222
7.3.3	Results and discussion	224
7.4	Total pressure drop in the tube bank	233
7.5	Concluding remarks	236
Chapter 8.	Results III: Effect of mass transfer on a tube bank in a cross flow	240
8.1	Introduction	240
8.2	Mass extraction from circular cylinders in cross flows	242
8.3	Single cylinder with suction	246
8.3.1	Experimental procedure and reduction of observations	246
8.3.2	Results and discussion	248
8.4	Tube bank experiments	257
8.4.1	Experimental procedure and reduction of observations	258
8.4.2	Results and discussion	258
8.5	Concluding remarks	272

		Page
Chapter 9.	Results IV: Heat and mass transfer on a tube bank in cross flow	276
9.1	Introduction	276
9.2	The simulation of a condensation process	278
9.3	Measurement of local heat transfer rate	280
9.4	Experimental results	285
9.4.1	Single cylinder measurements	285
9.4.2	Tube bank measurements	299
9.4.2.1.	Flow characteristics in the tube bank	301
9.4.2.2.	Heat distribution in the tube bank	305
9.5	Summary and discussion	315
Chapter 10.	Flow visualisation	321
10.1	Introduction	321
10.2	Experimental arrangement	322
10.2.1	The buoyant bubble system	322
10.2.2	Smoke filament system	324
10.3	Results and discussion	326
10.4	Concluding remarks	331
Chapter 11.	Theoretical approach	333
11.1	Introduction	333
11.2	The potential flow model	333
11.3	Application for the law of the wall	336
11.4	Concluding remarks	343
Chapter 12.	Summary and conclusions	344
12.1	Summary	344
12.2	Conclusions	347

Chapter 12.	(cont'd)	Page
12.2.1	The development of the shear stress sensor	347
12.2.2	Effect of different parameters on flow characteristics	348
12.2.3	Effect of mass extraction on flow characteristics	350
12.2.4	Effect of the simultaneous heat and mass transfer	350
12.3	Suggestions for further work	353
References		355

## Figures

Appendix 1	:	Electronic circuit and computer programme
2	:	Difficulties and failures
3	:	Published article
4	:	Published article
5	:	Mechanical description of the shear stress sensor

LIST OF TABLES

	Page
7.1. Blockage ratio and turbulence intensity	209
7.2. Pressure drag for smooth and rough surfaces	209
7.3. Shear stress for smooth and rough surfaces	212
7.4. Pressure drag and skin friction with turbulence intensity	219



## LIST OF FIGURES

- 3.1 Light beam arrangement
- 3.2 Block diagram of the system
- 3.3 Transducer with the vane
- 3.4 Vane OA
- 3.5 Transducer vane OA
- 3.6 Block diagram of instrument
- 3.7 Dynamic response of the transducer
- 3.8 Natural frequency of the vane
- 3.9 Root locii of denominator of  $H_1(s)$
- 3.10 Moduli of transfer functions versus frequency
- 3.11 Static calibration of the device
- 5.1 Test section arrangement
- 5.2 Velocity distribution across the test section
- 5.3 Turbulence distribution across the test section
- 5.4 Schematic diagrams of the assembled device
- 5.5 Two-dimensionality check
- 5.6 Heaters arrangements and wiring diagram
- 5.7 Test section arrangement
- 5.8 Thermocouples arrangement
- 5.9 Thermocouples calibration curves
- 5.10 Hot wire anemometer calibration curve
- 6.1 Spectrum analysis,  $Re = 0.27 \times 10^5$  at  $\theta = 50^\circ$
- 6.2 Spectrum analysis,  $Re = 0.27 \times 10^5$  at  $\theta = 160^\circ$
- 6.3 Spectrum analysis,  $Re = 0.47 \times 10^5$  at  $\theta = 50^\circ$
- 6.4 Spectrum analysis,  $Re = 0.47 \times 10^5$  at  $\theta = 160^\circ$
- 6.5 Spectrum analysis,  $Re = 0.7 \times 10^5$  at  $\theta = 160^\circ$
- 7.1 Skin friction distribution around a circular cylinder
- 7.2/...

- 7.2 Skin friction on a smooth cylinder
- 7.3 Effect of roughness on static pressure distribution
- 7.4 Normal pressure around a rough circular cylinder in a cross flow
- 7.5 Effect of roughness on skin friction
- 7.6 Effect of roughness on skin friction
- 7.7 Effect of roughness on skin friction
- 7.8 Percentage effect of roughness on friction drag
- 7.9 Effect of turbulence and surface roughness on pressure distribution
- 7.10 Effect of turbulence and surface roughness on skin friction
- 7.11 Effect of turbulence on pressure distribution for rough surface
- 7.12 Effect of turbulence on skin friction for rough surface
- 7.13 Effect of turbulence level on skin friction
- 7.14 Effect of turbulence level on skin friction
- 7.15 Pressure coefficient distribution around first row of tube bank
- 7.16 Skin friction distribution for the second row in the bank
- 7.17 Skin friction distribution for the third row in the bank
- 7.18 Skin friction distribution for the fourth row in the bank
- 7.19 Skin friction distribution for the fifth row in the bank
- 7.20 Reynolds number variations for a staggered tube bank
- 7.21 Pressure drag on different rows in the bank
- 7.22 Skin friction distribution on the staggered bank,  
 $R_{\infty} = 0.27 \times 10^5$
- 7.23 Skin friction distribution on the staggered bank,  
 $R_{\infty} = 0.47 \times 10^5$
- 7.24./...



- 7.24 Skin friction distribution on the staggered bank,  
 $R_{\infty} = 0.7 \times 10^5$
- 7.25 Predicted and measured skin friction, first row  
in the bank
- 7.26 Predicted and measured skin friction, second row  
in the bank
- 7.27 Measured and predicted skin friction for third  
row in the bank
- 7.28 Measured and predicted skin friction for fourth  
row in the bank
- 7.29 Measured and predicted skin friction, fifth row  
in the bank
- 7.30 Hydraulic resistance of a staggered bank,  
referred to one row
- 7.31 Pressure drop in the bank
- 8.1 Effect of suction on skin friction
- 8.2 Effect of suction on skin friction
- 8.3 Effect of suction on friction drag
- 8.4 Skin friction on a circular cylinder fitted  
with wire at rear
- 8.5 Effect of wire fitted at rear on skin friction  
with suction
- 8.6 Average skin friction with mass transfer on  
single cylinder
- 8.7a Pressure drag on rough cylinder
- 8.7b Skin friction ratio against suction parameter  
for single cylinder
- 8.8 Skin friction with suction on the first row of  
the bank,  $Re = 0.6 \times 10^5$
- 8.9 Skin friction with suction on the first row  
of the bank.
- 8.10 Effect of suction on pressure distribution,  
second row,  $Re = 0.76 \times 10^5$
- 8.11 Effect of suction on pressure distribution,  
second row,  $Re = 1.3 \times 10^5$
- 8.12 Suction effect on skin friction distribution,  
second row,  $Re = 1.75 \times 10^5$
- 8.13 Effect of suction on skin friction for the third  
row in the bank,  $Re = 0.6 \times 10^5$
- 8.14/...

- 8.14 Effect of suction on skin friction for the third row in the bank,  $Re = 0.94 \times 10^5$
- 8.15 Effect of suction on skin friction for the third row in the bank,  $Re = 1.3 \times 10^5$
- 8.16 Effect of suction on skin friction for the fourth row in the bank,  $Re = 0.56 \times 10^5$
- 8.17 Effect of suction on skin friction for the fourth row in the bank,  $Re = 1 \times 10^5$
- 8.18 Effect of suction on skin friction for the fifth row in the bank,  $Re = 0.6 \times 10^5$
- 8.19 Suction effect on skin friction, fifth row in the bank,  $Re = 1 \times 10^5$
- 8.20 Average skin friction with mass transfer on the bank at  $Re_\infty = 0.27 \times 10^5$
- 8.21 Average skin friction with mass transfer on the bank at  $Re_\infty = 0.47 \times 10^5$
- 8.22 Average skin friction with mass transfer on the bank at  $Re_\infty = 0.7 \times 10^5$
- 9.1 Effect of main stream temperature on single cylinder
- 9.2 Effect of main stream temperature with mass transfer on single cylinder
- 9.3 Effect of heat and mass transfer on shear stress around single cylinder
- 9.4 Effect of heat and mass transfer on shear stress around single cylinder
- 9.5 Shear stress with heat and mass transfer around single cylinder
- 9.6 Coefficient of heat transfer with mass transfer around single cylinder
- 9.7 Heat transfer with suction around single cylinder
- 9.8 Heat transfer with mass transfer around single cylinder
- 9.9 Heat transfer with mass transfer around single cylinder
- 9.10 Average heat transfer coefficient round single cylinder
- 9.11 Effect of main stream temperature on first row in the bank
- 9.12/...

- 9.12 Effect of main stream temperature with mass transfer on first row in the bank
- 9.13 Effect of heat and mass transfer on shear stress, first row in the bank
- 9.14 Heat and mass transfer effect on first row in the bank
- 9.15 Shear stress with heat and mass transfer round first row in the bank
- 9.16 Heat transfer with mass transfer around first row in the bank
- 9.17 Heat transfer with mass transfer around first row in the bank
- 9.18 Heat transfer with mass transfer around first row in the bank
- 9.19 Heat transfer with mass transfer around first row in the bank
- 9.20 Average heat transfer coefficient for first row in the bank
- 9.21 Effect of main stream temperature on second row in the bank
- 9.22 Effect of main stream temperature with mass transfer on second row in the bank
- 9.23 Shear stress with heat and mass transfer for second row in the bank
- 9.24 Shear stress with heat and mass transfer for second row in the bank
- 9.25 Shear stress with heat and mass transfer for second row in the bank
- 9.26 Heat transfer with mass transfer for second row in the bank
- 9.27 Heat transfer with mass transfer for second row in the bank
- 9.28 Heat transfer with mass transfer for second row in the bank
- 9.29 Heat transfer with mass transfer for second row in the bank
- 9.30 Average heat transfer coefficient for second row in the bank
- 9.31 Effect of main stream temperature on third row in the bank
- 9.32/...



- 9.32 Effect of main stream temperature with mass transfer, third row in the bank
- 9.33 Effect of heat and mass transfer on shear stress, third row in the bank
- 9.34 Effect of heat and mass transfer on shear stress, third row in the bank
- 9.35 Shear stress with heat and mass transfer, third row in the bank
- 9.36 Heat transfer with mass transfer, third row in the bank
- 9.37 Heat transfer with mass transfer, third row in the bank
- 9.38 Heat transfer with mass transfer, third row in the bank
- 9.39 Heat transfer with mass transfer, third row in the bank
- 9.40 Average heat transfer coefficient, third row in the bank
- 9.41 Effect of main stream temperature on fourth row in the bank
- 9.42 Shear stress at different main stream temperature with suction, fourth row in the bank
- 9.43 Shear stress with heat and mass transfer, fourth row in the bank
- 9.44 Shear stress with heat and mass transfer, fourth row in the bank
- 9.45 Shear stress with heat and mass transfer, fourth row in the bank
- 9.46 Heat transfer with suction, fourth row in the bank
- 9.47 Heat transfer with mass transfer, fourth row in the bank
- 9.48 Heat transfer with mass transfer, fourth row in the bank
- 9.49 Heat transfer with mass transfer, fourth row in the bank
- 9.50 Average heat transfer coefficient, fourth row in the bank
- 9.51 Effect of main stream temperature on fifth row in the bank
- 9.52/...

- 9.52 Shear stress with mass transfer at different main stream temperature, fifth row in the bank
- 9.53 Shear stress with heat and mass transfer, fifth row in the bank
- 9.54 Shear stress with heat and mass transfer, fifth row in the bank
- 9.55 Shear stress with heat and mass transfer, fifth row in the bank
- 9.56 Heat transfer with mass transfer, fifth row in the bank
- 9.57 Heat transfer with suction, fifth row in the bank
- 9.58 Heat transfer with suction, fifth row in the bank
- 9.59 Heat transfer with suction, fifth row in the bank
- 9.60 Average heat transfer coefficient, fifth row in the bank
- 9.61 Heat transfer with tube position,  $V_w = 0.012$  m/s.
- 9.62 Heat transfer with tube position,  $V_w = 0.018$  m/s.
- 9.63 Heat transfer with tube position,  $V_w = 0.025$  m/s.
- 10.1 Flow visualisation with buoyant bubble system
- 10.2 Flow visualisation with smoke,  $Re = 13,600, 24,000$ .
- 10.3 Flow visualisation with smoke,  $Re = 35,000, 45,000$ .
- 10.4 Flow visualisation with smoke,  $Re = 55,000, 66,000$ .
- 10.5 Flow visualisation with smoke,  $Re = 77,000, 87,000$ .
- 10.6 Flow visualisation with smoke,  $Re = 98,000, 108,000$ .
- 11.1 Predicted pressure distribution along streamline body.

## CHAPTER 1

### INTRODUCTION

#### 1.1. General introduction

The study of flow normal to banks of tubes continues to attract interest because of the importance of this flow configuration in the design of heat exchangers, items of equipment, which are widely used in thermal and chemical engineering. In fact, a detailed knowledge of heat transfer and flow phenomena in heat exchanging equipment may be considered a prerequisite to obtaining a reliable design.

Flow characteristics within a heat exchanger tube bank represent some of the major factors in the overall performance of the exchanger. As the geometry of the exchanger becomes more complicated, it is necessary to develop experimental procedures in order to obtain a fundamental knowledge of flow characteristics for such configurations.

A study of the literature shows that, from the thermal stand point, there are still uncertainties regarding the way in which heat is transferred between a single phase flow and circular tube test models. In addition, the rate of transfer varies around the tube's circumference and the influence of different parameters on those variations is not yet fully understood. Of course, the situation will be more complicated for heat exchangers where a change of phase is taking place.

Processes/...



Processes involving change of phase with simultaneous heat and mass transfer represent basic engineering problems in heat transfer. While there are many industrial processes in which such phenomena are involved, e.g., transpiration or mass transfer cooling, drying processes, refrigeration and chemical engineering, the main interest in the present work is related to situations where condensation is taking place in a heat exchanger, i.e., steam condensers.

Steam condensation represents an essential part of many industrial processes but its most important application is for surface condensers in conjunction with steam turbine for the generation of electricity in power stations and in desalination plants to produce fresh water for public utilities. Due to the important role the condenser plays in the steam process cycle together with its proportionally large capital cost, one of its major requirements is efficiency of performance at an economical cost. The performance of the unit is closely connected to the heat transfer that takes place during the condensation process on the immediate cost of some pressure drop across the condenser.

In particular, pressure drop between the vapour entry to the exchanger and the air ejector section in the condenser, has an important effect on the efficiency of the power generation plant. Besides its thermal effect, e.g., excessive undercooling of the condensate which has to be compensated in the feed heaters or boiler and decreasing the heat transmission performance of the unit, it has a considerable effect on the duties of the air ejector. Since the ejector is/...



is a volume displacement equipment, it is reckoned that for a pressure drop of 12.5 mm Hg in the range of 711 to 737 mm vacuum, the ejector has to handle as much as three times its capacity without this extra pressure drop (122).

From the economy point of view, a marginal improvement in the pressure drop in a condenser could lead to a significant saving in the running costs of a conventional power station. It has been estimated (242) that an improvement in condenser vacuum of 2.5 mm Hg for a 500 MW plant would result in a saving of about £60,000 annually with the fuel price in 1976. With the present rate of increase in the fuel price, it is relevant to consider these problems more seriously.

With the increasing size of plant there has been a corresponding increase in the condenser requirement. Accordingly, it has become necessary to have a more detailed knowledge of the flow characteristics in tube bank configurations to enable condenser designers to overcome the new problems with which they are faced due to increasing size of the unit. Indeed, the increased interest in these problems is reflected in the growing volume of research in this field undertaken in recent years.

In a real condenser, however, it is rather difficult to obtain measurements in the tube bank arrangement in order to discover the flow and heat transfer processes response to changes of the parameters in the exchanger. It is also difficult to separate the influence of different parameters due to the complexity of the processes involved.

In/...

In order to investigate the physical processes of flow and heat transfer in tube banks and their response to the change of different factors, it is a common practice to make experiments on properly chosen, simple geometrical models in which it is possible to obtain data for the local parameters and to investigate the influence of only one separate parameter at a time.

Although there are some articles dealing with the measurements of the mean as well as the local values of the cross flow parameters in tube banks, the picture of the detailed characteristics for the flow in a condenser tube bank is far from being completely known due to the complicated geometries and the great number of factors involved in the process.

As far as the flow characteristics in steam condensers are concerned, a study of the literature shows a limited amount of available data on its detailed variations and in most cases these were obtained on tube arrangements under adiabatic or isothermal flow conditions.

To provide for studies into the effect of condensation on the flow structure on a test model, a hydrodynamic analogy is usually used. This analogy is based on the assumption that the effect of the liquid phase of the condensate is not significant and condensation process is simulation by mass extraction from the main stream into the surface of the test model, e.g., references 57, 70, 72 and 227.

However/...



However, from the literature survey it is found that:

a) The discrepancies and inconsistencies between different investigations, using different test conditions and instrumentation, make it difficult to determine the effect of the interaction of different parameters on the characteristics of the cross flow through the tube bank arrangements. Consequently, qualitative rather than quantitative comparisons are usually made.

b) The studies are usually carried out for investigating the effect of one or two parameters on flow characteristics within the bank and there is no work which is performed, using the same instrumentation and test conditions, to study simultaneously factors such as surface roughness, turbulent intensities, mass transfer and heat transfer on the variations of these characteristics in the bank.

c) There is a considerable need for more detailed investigations to be carried out in order to improve the understanding of the structural variations in the flow characteristics in tube bank condenser.

d) As far as the thermal side of the characteristics is concerned, it is of great importance scientifically as well as from the stand point of design to determine the variations of the heat transfer around cylinders in cross flow in general and that on the steam side in a condenser unit in particular.

Considering the above mentioned points, the present investigation/...

investigation programme is designed to study the influence of different parameters usually encountered in condensers on the flow and heat transfer characteristics around circular models, whether for an isolated single cylinder or tube bank arrangement in cross flows.

While in an actual condensation process heat and mass transfer are coupled together, in that the heat transfer rate is determined by the condensation rate, in the present work these are decoupled by simulating mass transfer by mass extraction through the surface. This simulation provides an opportunity for measurements to be realised on the effect of only one parameter separately and independently from the flow conditions around the test model.

Flow characteristics such as wall shear stress, normal pressure and heat transfer coefficient distributions around the cylindrical models circumference are measured simultaneously using special techniques developed for this purpose. Measurements are carried out over a limited range of mass extraction, surface roughness, turbulence intensity, heat loads and Reynolds number.

Except for the effect of gravity on the condensate drainage, the present work is connected to the condensation on vertical tube exchangers in a cross flow of vapour. These are found primarily in the previous forms of vertical tube evaporators. Some of the steam condensers are occasionally built to operate in this manner. The cleaning problem is one of the main reasons which make the vertical/...



vertical tube condensers not as common in industrial practice as horizontal tube condensers. Whereas this problem does not limit the design, it seems that vertical tube condensers deserve more serious consideration and an accurate method for predicting its flow and heat transfer characteristics becomes of considerable importance.

For such types of condensers there are only a few publications reported in the literature. Even then, there are quite a number of limitations on the variables studied and in most cases only overall characteristics have been obtained. In general, the subject of flow characteristics within vertical tube condensers has not received enough attention as that for the non-condensing medium because of the experimental difficulties involved in the subject.

From the thermal stand point, it was shown (207) that with steam flowing at fairly high velocity across such condensers, it blows away the condensate liquid which is carried downstream with the main flow. Under such circumstances, the heat transfer rate must approach, as mass flow increases, the limiting value of the interface coefficient (254). In the present work, however, an effort was made to determine variations of the heat transfer coefficient around the test model and along the depth of the tube bank over a limited range of variables.

## 1.2. Aim and scope of the present work

The aim of this investigation was, therefore, to determine/...

determine the effect of individual parameters such as surface roughness, turbulent intensity, mass transfer, heat load and Reynolds number on the simultaneously measured flow and heat characteristics such as wall shear stress, pressure drag and heat transfer rate on single cylinders and tube bank models for a vertical tube condenser in cross flow of vapour.

The separation of the influence of different parameters on the flow characteristics was straight-forward except for the case of the heat and mass transfer in the condenser model. In order to separate between these two effects, with provision for measuring flow local parameters, it was found necessary to decouple the heat and mass transfer phenomena.

Recognising the difficulties faced by other research workers and to provide for the aforementioned requirement, mass extraction through the porous wall of a test cylinder offered a convenient method for decoupling the effect of heat and mass transfer. In this way the rate of mass transfer extracted could be separately controlled to any desired value independent of the flow conditions. Of course, in this case, the condensate is regarded as a solid (250) and the effect of the liquid phase on the cross flow is neglected (72). Due to the very small thickness of normal condensate layer (219) the local measurements of the flow parameters were then carried out on the surface of the test cylinder.

It/...

It was decided that the investigation programme should be divided into four main parts:

1) Development of an instrument which would be capable of providing, accurately, the necessary information about the distribution of the shearing forces on the surface of a circular cylinder in an external cross flow.

2) An investigation into the effect of different parameters such as surface roughness, turbulent intensity and Reynolds number on the flow local characteristics around the test models.

3) A study of the influence of mass transfer with Reynolds number on the cross flow around the circumference of the test models under adiabatic flow conditions.

4) An investigation into the effect of simultaneous heat and mass transfer at different Reynolds numbers, in non isothermal conditions, on the simultaneously measured distributions of wall shear stress, normal pressure and heat transfer coefficient around the perimeter of the test models.

Part (1) above was completed after about eighteen months work. Chapter 2 gives a review for the available techniques for measuring wall shear stress together with an analysis and an overall assessment of different instruments used in this field.

Chapter/...



Chapter 3 gives the theory behind the developed instrument together with its functional description. The mechanical and electronic construction are also given. A theoretical analysis of the automatic control system showing the limitations imposed on the design is demonstrated.

It was intended to design the developed instrument with the minimum possible dimensions, so it could be fitted on to the middle length of a test cylinder with a practical size for condenser tubing. However, in addition to the practical limitations imposed on the dimensions of the instrument itself, there were other factors which played a part in deciding the final size of the test cylinder.

For example, it was necessary to provide for the uniformity of suction velocity around the cylinder together with provisions for the cooling of its inner surface area. All these restrictions combined together resulted in a minimum dimension, for the test cylinder, of 76.2/63.5 mm OD/ID.

Although the flow conditions on a condenser tube is a three-dimensional one, the experiments are performed in a nominally two-dimensional manner. An experimental apparatus with a wind tunnel, suction made, is designed for the study. Chapter 5 gives a description for the detailed construction of different parts in the experimental rig.

Chapter 6 shows some preliminary results using the developed instrument for measuring the shedding frequency for a single cylinder in cross flow. The main purpose/...

purpose of these measurements was to show the reliability of the new instrument for determining not only the 'static' characteristics of the flow as the time average values of the shearing force distribution but also the 'dynamic' characteristics of the flow around a circular cylinder in cross flow.

Chapter 7 shows the investigations for part (2) in the above programme. The simultaneously measured results show the variations in the flow characteristics around a single cylinder in cross flow as a direct influence of variations in the surface roughness and turbulent intensity in the incident stream. Two surface roughnesses were used, one was aerodynamically smooth while the other had a roughness parameter of  $K_s/D$  about  $53 \times 10^{-5}$ . Besides, two levels of the turbulent intensity are used with intensity in the main stream direction of 1.2 and 6 per cent. The range of the Reynolds number used was that from 27000 up to 70000 based on the cylinder diameter and the main stream velocity.

It is understood that this range for  $Re$ , in general, is higher than the values usually encountered in conventional condensers, nevertheless, it is still useful since the Reynolds number can occasionally reach quite a high value (141). Of course, it could have been worthwhile to extend the Reynolds number range to a lower limit than that used, but the minimum value which is set by the minimum flow rate of the exhaustor on the rig was about 15000. However, the present values of  $Re$  are within the subcritical range.

Experiments/...



Experiments were to be performed using different types of tube bank arrangements but for practical reasons the study is limited to only one type of tube arrangement, i.e., staggered type. It is of the equal pitches type with a pitch diameter ratio of 1.5.

Except for measurements of the overall characteristics on the tube bank, e.g., pressure drop, the range of the main stream Reynolds number is limited in some cases to three particular values, namely, 27,000, 47,000 and 70,000. Chapter 7 shows also the total pressure across the bank with different depth and the bank entrance effect is demonstrated and results are compared with the available data and correlations from the literature. Measurements of the wall shear stress distribution around the test models are compared with the approximate theories for the boundary layer flows and comparisons are presented.

Chapter 8 demonstrates the investigation for part (3) in the programme of studies for single cylinder and tube bank arrangement. The effect of mass extraction on the simultaneously measured distributions for wall shear stress and pressure drag is shown. Also, the influence of suction on the boundary layer separation and transition due to the combined effect of mass transfer and Reynolds number is shown for suction parameter  $CQ \sqrt{Re}$  from 0. to 1.13.

Chapter/...



Chapter 9 shows the study for part (4) in the investigation programme and the simultaneously measured distributions of wall shear stress, normal pressure and heat transfer coefficient, around the test models are presented. The effect of the viscosity gradient, due to the non-isothermal conditions at the cylinder's wall, on the measurements of the shearing forces around the model is demonstrated. The influence of the simultaneous heat and mass transfer on the local parameters for different Reynolds numbers is presented. The heat transfer coefficient distributions around the perimeter of the test model and along the depth of the tube bank are presented for the range of suction and Reynolds number previously mentioned over a heating load range from 6 to 18 watt /Cm<sup>2</sup> based on the total heat input and the area of the working section.

Chapter 10 shows flow visualisation around a single cylinder and an inner tube in a bank in a cross flow with emphasis on the effect of suction on the flow pattern around the test models used.

Chapter 11 demonstrates the effort made to build a theoretical model for the case of a cylinder with suction in a cross flow.

Chapter 12 lists the main conclusions of the present work together with the author's thoughts on how future work in this field should be continued to reach as close as possible to the full picture of the flow and heat characteristics in vertical tube bank condensers.

### 1.3. Nomenclature

A	cross sectional area
a	cylinder's radius
b	distance between photocells and pivots
C	constant (equation 4.4)
$C_d$	pressure drag (equation 5.6)
$C_F$	coefficient of friction (equation 2.3)
$C_F$	friction contribution to total drag (equation 7.4)
$C_p$	pressure coefficient (equation 7.1)
$C_Q$	suction to main flow velocity ratio
d	height of surface tube opening (equation 2.2)
$d_1$	diameter of Preston's tube (equation 2.3)
d	distance from the wall where velocity equals $U_1$ (equation 2.6)
d	cylinder diameter (equation 6.1)
D	cylinder diameter
$D_V$	hydraulic diameter (equation 4.7)
$\frac{D}{X}$	blockage ratio
Eu	Euler's number
f	friction factor (equation 4.4)
FSP	front stagnation point on the cylinder surface
h	height of surface tube (equation 2.4)
h	heat transfer coefficient (equation 9.2)
H	length of the test cylinder (equation 7.10)
$H_1(s)$	transfer function (equation 3.1)
J	moment of inertia
$K_f$	friction factor (equation 7.3)
$K_D$	pressure drag contribution to total drag (equation 7.2)

$K_s$	thermal conductivity (equation 9.1)
$K_s$	roughness equivalent diameter (table 7.2)
$\frac{K_s}{D}$	roughness parameter (table 7.2)
$K$	constant (equation 2.7)
$K_o$	velocity feed back factor
$K_1$	proportional factor )
	) (equation 3.1)
$K_2$	integral factor )
$L$	length of the heated surface probe (equation 2.10)
$L$	longitudinal pitch to diameter ratio (equation 4.1)
$M_p$	shearing moment
$M_q$	balancing moment
$n, m$	constants (equation 4.13)
$Nu$	Nusselt's number
$N$	number of major flow restrictions (equation 4.1)
$n$	shedding frequency (equation 6.1)
$P$	shearing force (equation 3.1)
$\Delta P$	pressure head from Preston's tube (equation 2.3)
$\Delta P$	total pressure drop (equation 4.1)
$P_w$	wake pressure (equation 7.8)
$P$	normal pressure on the solid surface
$Pr$	Prandtl's number
$Q$	balancing force from the magnetic field
$q$	Heat flux
$Re$	Reynolds number
$S$	Strouhal's number (equation 6.1)
$SL$	centre-to-centre distance (equation 4.7)
$t$	temperature
$T$	transverse pitch to diameter ratio (equation 4.1)
$T.L.$	turbulence level
$Tu$	turbulence level



u	flow velocity component parallel to the surface
U	flow velocity
$u^*$	shear velocity $= \sqrt{\frac{\tau_w}{\rho}}$
U <sub>l</sub>	velocity measured by surface tube (equation 2.2)
$u^1$	rms axial fluctuations
X	curvilinear ordinate parallel to cylinder surface
y	curvilinear ordinate normal to cylinder surface
$\tau$	shear stress
$\mu$	coefficient of viscosity
$\nu$	kinematic viscosity
$\delta$	displacement of the surface tube's effective centre (equation 2.4)
$\alpha$	thermal diffusivity (equation 2.10)
$\theta$	angle measured from the FSP on the cylinder surface
$\epsilon$	Reynolds flux
$\tilde{\omega}_n$	natural frequency
$\tilde{\zeta}$	damping coefficient
$\rho$	density

### Subscripts

a	approach to the model
av	average value
c	corrected for blockage
d	diameter of the tube
h	for heat transfer calculations
i	inner diameter
m	mean value
max	maximum value
O	outside diameter
P	for pressure drop calculations

x      value at positive x from the FSP  
z      value for the Zth row  
w      value at the wall, i.e.,  $y = 0$   
 $\infty$     in the undisturbed main stream  
 $\omega_i$     value at the inner surface of the cylinder  
 $\omega_o$     value at the outer surface of the cylinder  
 $\theta$      value at angle  $\theta$  from the FSP

## CHAPTER 2.

### Measurements of Shear Stress on Solid Boundaries

#### 2.1 Introduction

An object moving through a real fluid with a relative velocity to the body of the fluid experiences a fluid resistance to its motion. The existence of the wall of the object has a strong influence on the velocity profile in its vicinity and energy is dissipated as viscous shearing forces which is proportional to the velocity gradient at the surface.

Most of investigations into the nature of the flow in boundary layers involve a knowledge of this sort of resistance which is called skin friction or wall shear stress. The contribution of such resistance to the total resistance of the object varies from representing a significant part of it, for flat plates for instance, to just a few per cent of the resistance for the case of a circular cylinder in a cross flow.

It is highly desirable, both from practical and theoretical stand points, that the accuracy of the skin friction determination should be improved. A better understanding of the flow dynamics of moving objects demands accurate measurements of the skin friction.

Such measurements have so far proved to be difficult to accomplish. According to Thwaites, "to measure accurately the skin friction is an exceedingly difficult task which stands as a perpetual challenge to the experimenter". The only/...



only flow configuration for which skin friction is known with some confidence is the case of fully developed flow in circular cross section, small diameter long pipes where the skin friction, through a momentum balance, may be deduced from measurements of pressure drop. For an immersed body, the relationship between the pressure drop and skin friction is not clear and a different approach must be adopted in order to estimate the wall shear stresses. The situation becomes more complicated whenever turbulent boundary layers exist since a relationship for the shearing stresses due to turbulent exchange is not known (1). In such cases, the necessary data for wall friction must be determined by experimental methods.

Under the assumption of continuum flow and no slip of the real fluids at the solid boundaries, the shear stress  $\tau$  at any point on the solid boundaries is defined and given by the Newton's formula

$$\tau = \mu \left( \frac{\partial u}{\partial y} \right)_{y=0} \quad 2.1$$

where  $\mu$  and  $\frac{\partial u}{\partial y}$  are the dynamic viscosity and the velocity gradient at the solid boundary. This is a general formula which is valid for both laminar and turbulent boundary layers. Any attempt to estimate the skin friction must satisfy the above expression by measuring the quantities on either side of the equality sign. Methods which endeavour to measure quantities on the RHS of the equality sign are usually called indirect methods for measuring the skin friction. Methods which endeavour to measure the LHS of the/...

the above expression are called direct methods for measuring the skin friction. In the next part both types of methods will be dealt with in more detail.

It must be understood that the present chapter is not intended to give a comprehensive review for all the existing methods for skin friction measurements, which is outside the scope of the present work, instead it was decided to give a general outlook at the main devices used in this field with an overall assessment for each one of them.

## 2.2. Indirect skin friction measurements

This category includes attempts made to measure the skin friction by any means other than the direct measurements of the skin friction force itself. Normally, these include devices for measuring the velocity gradient at the surface (from measurements of the velocity distribution across the boundary layer thickness) to satisfy the RHS of expression 2.1. The most commonly used devices for this purpose are :

- 2.2.1. Total head tubes
- 2.2.2. Hot wire anemometer

Amongst this category are devices which measure physical quantities related to skin friction at the solid boundary such as :

- 2.2.3. Surface tubes
- 2.2.4. Surface heated probe



### 2.2.1 Total head tube

An estimation of skin friction by a total head tube involves the measurements of the velocity distribution throughout the thickness of the boundary layer. This is normally carried out in the narrow region in the immediate vicinity of the surface where the whole of the influence due to the solid boundary may be considered to operate. This is achieved by measuring the impact pressure (time average) at the mouth of the probe in relation to its height normal to the surface of the object, together with static pressure measurements at the same section. In the case of a boundary layer flow, experiments (2,3) showed that the variation of static pressure across the boundary layer was negligible. Consequently, the static pressure could be measured by a single tapping on the surface. The total head probes usually used for scanning the boundary layer thickness can be circular of a very small diameter, e.g., 1.4 mm (4) or a small bore tube with its tip flattened out to form a narrow rectangular mouth. The flattened end height can be as small as 0.2 mm and 2 mm wide (5). O'Donnell (6) used a probe with a width to height ratio of 4.8 and claimed that the results from such a probe are satisfactory as long as the ratio of the probe height to boundary layer thickness was no greater than 0.22. The rectangular opening of the probe should be aligned perpendicular to the direction of the flow with its narrow side normal to the surface and should be free of burrs and imperfections. The probe is mounted on a micrometer traversing mechanism from either underneath or above the surface (7) and the static pressure orifice used with this sort of device could be 0.9 mm diameter drilled perpendicular to the surface. The zero position/...



position of the probe can be obtained visually using a traversing microscope or electrically using an electric circuit which is energized when the probe makes contact with the surface or optically with a cathetometer and dial gauge (8). These methods were reported (5) to give an accuracy in indicating the zero position within 0.02 mm if both wall and probe were kept clean and free of all foreign matter. Normally the probe had a "Shepherd's Crook" form so that readings could be obtained with it practically touching the wall. The difference between the impact pressure recorded by such probes and that of a static probe is proportional to  $\rho u^2$ , assuming that the static pressure along each normal line is constant and equal to that measured at the wall (9). Some investigators, however, mounted both total head probe and static pressure probe onto the velocity measurement traversing mechanism (10). Signals from the probe could be read using a precision alcohol manometer of the Zahn type (2). or a manometer type filled with a tetrabromoethane fluid (5). Dutton (11) used a very small rectangular probe which was 0.12 mm in height and the minimum possible distance (12) close to the surface was 0.012 mm.

It is believed that the largest source of error is that of the distortion of the boundary layer due to the presence of the probe (13). The slower stream lines near the wall sensing being displaced sideways and the faster stream lines, located away from the wall, being displaced towards the wall. This could account for a probe near the wall higher velocities than would normally be expected. Where the/...

the probe interference is significant (6), the effect was either to cause early transition of the laminar boundary layer or to distort the velocity profile so that higher average skin friction was measured. Factors which could affect the accuracy of velocity measurements by total head probe are as follows :

Local Reynolds number of the probe

Possible static pressure variations within the boundary layer

Allowance for turbulent components

Displacement of effective centre near the wall

Error in zero adjustment in both touching and leaving the model's surface.

While Monaghan and Johnson (14) reported no effect of the probe size until it was touching the wall, O'Donnell (2) reached the conclusion that the smaller the height of the rectangular opening the more accurate the measurement of skin friction.

## 2.2. Hot wire anemometer

Hot wire anemometry is used for the measurement of the mean velocity in boundary layers at low speeds where the effect of compressibility can be neglected. Usually the hot wire anemometer is used as a calibrated instrument. In principle it depends for its application on the heat loss from a small diameter wire which is electrically heated. Normally, the wire is made from a tungsten alloy 0.01 mm diameter. Therefore for a given temperature difference between the heated wire and the surrounding medium, the amount/...



amount of heat transferred is proportional to the square root of the mass flow rate (15). Bradshaw (17) used a hot wire fixed just above the surface to measure the velocity, then calculated the skin friction. Wires of 0.005 mm diameter platinum-rhodium alloy were used. The height of the wire above the surface was nominally 0.05 mm. The wire length was about 2 mm fed with a constant current of 40 m.A. The conduction of heat to the wall is always a source of trouble when a hot wire is used very close to a surface (16). It was shown (17) that a wire ten diameters from a perfectly conducting wall loses 30 per cent of heat supplied to it by conduction to the wall. With a hot wire anemometer in use, the distance of closest approach to the solid wall was about 0.03 mm (145). Preston (18) described the factors affecting the accuracy of velocity measurements by hot wires as follows :

Dust affecting consistence of calibration

Effect of radiation, conduction and convection  
when close to a surface.

The main conclusion is that, the behaviour of hot wires, like that of total head probes and the boundary layer should be thick to accommodate the probe. Due to the physical dimensions of the probe, velocity cannot be measured right up to the wall and the velocity profile has to be extrapolated to the wall. Such an extrapolation could cause a significant error especially when the boundary layer thickness is small.



### 2.2.3. Surface Tubes

#### 2.2.3.1. Stanton tube

With the validity of the inner velocity law  $\frac{u}{u^*} = f\left(\frac{yu^*}{\nu}\right)$  a shearing stress measurement, in theory, will be a simple matter. It simply calls for a measurement of velocity at any distance  $y$  and then the solution of the equation of the inner law of the velocity to get  $u^*$ . The result will be the shearing stress. But, practically, the velocity must be measured at very small distance, within the laminar sublayer where the inner law is applicable with some confidence. It has been suggested that the solid surface in a turbulent flow, for flow mean speeds above the critical, there may exist a thin layer in which the flow is laminar in character. Assuming no slip at the solid wall, the shear stress could be determined from the slope of the velocity profile in that layer, which is called the laminar sublayer, and the coefficient of viscosity of the fluid expressing this in symbols, the boundary condition is  $\mu \left( \lim_{y \rightarrow 0} \left( \frac{du}{dy} \right) \right) = \tau$ . But the smallest rectangular total head probe (12) was 0.1 x 0.8 mm. In order to come even closer to the wall, the wall of the total head probe adjacent to the wall was removed and replaced by the solid surface itself. By carrying the outer wall of the probe on a traverse micrometer it was possible to obtain readings up to the solid wall. As Stanton was the first to use this type of device it was named after him. Therefore, the Stanton tube is a special type of total head probe in which the inner wall of the tube is formed by the surface itself. Stanton showed that in a turbulent flow there exists a thin layer of fluid in laminar motion, which/...

which has zero velocity at the solid boundary. Since the velocity changes rapidly near the surface, the velocity gradient can only be predicted reliably when the velocity observations are taken very close to the surface. Fage and Falkner (9) used a similar type of surface tube to that of Stanton with a slight modification. Then the probe was constructed on the top of a circular rod of diameter 5 mm designed to pass through holes, with a very small clearance, in the surface of the model. The outer wall of the tube was formed by a thin steel cap, ground at the front edge to a thickness of 0.015 mm. A hole of fine bore drilled along the axis of the rod served to transmit the pressure at the mouth of the tube to a manometer. The tube then had to be calibrated to determine the position of the "effective centre" corresponding to the speed deduced from the measured pressure. Taylor (19) called the Stanton tube a half pitot tube. Such half tubes were used by Fage and Falkner (23) to measure the skin friction on aerofoil. These tubes were calibrated in a rectangular pipe under laminar flow conditions for which skin friction could be calculated. A special design for the Stanton tube was used to measure the skin friction in the separated and recirculation region (7). The probe unit had one upstream facing line and another similar rearward facing line, with height 0.05 - 0.15 mm. But there was a risk of air leakage between the forward and the rearward facing holes. It was recommended that the probe should be calibrated in similar conditions to those in which it is going to be used. Several types of the Stanton tubes were investigated (29) where steel wedges 7.6 mm in height were screwed to the surface to leave a gap about 0.12 mm high./...



high. Hool (20), Smith (21), Winter and Smith (22) modified the technique and used razor blades soldered to the surface giving a gap of about 0.076 mm. Fage and Falkner (23) used a modified Stanton tube by placing a sharp knife edge approximately 0.005 mm above an ordinary pressure orifice at the measurement point. The pressure rise below the knife edge with respect to the undisturbed static pressure gives a measure of the wall shear stress. Bellhouse (24) and Bellhouse and Schultz (25) used Stanton tubes together with a static pressure orifice to detect the separation location (when the reading from the tube equalled the local static pressure). Hool (20) developed a simple empirical correlation to provide means of determining approximate values of skin friction from values of the surface velocity  $u_1$ . The correlation reads as follows :

$$\tau = 0.481 u_1^{1.25} \rho^{0.25} (\mu/d)^{0.75} \quad 2.2$$

Wyatt and East (26) devised a very simple type of surface tube by attaching a razor blade segment magnetically to the model by small magnet flush with the surface. This way of mounting improves on the soldered technique in coping with a flow whose direction changes with incidence. In such cases the direction could be determined using the oil flow visualisation technique (27) and then aligning the segment with the surface flow direction. Moreover, the gap height could be measured accurately as half the blade thickness which can be predetermined accurately using a sensitive micrometer. This improves on the optical/...



optical measurements of the gap height in the case of soldered razors to an accuracy of about 0.01 mm, which gives an error in the gap height about 20 per cent for 0.05 mm gap. In spite of all these attractive points there are two sources of possible error, the first is the possible leakage between the razor blade and the magnet surface such as was reported in reference 9, the second is the error due to possible movement at the rear of the razor blade. A rear displacement of 0.01 mm would lead to a 15 per cent reduction in the registered skin friction with 0.05 mm blade. Bradshaw and Gregory (17) used a square hole and a piece of metal shim with a chamfered leading edge while Smith et al (21) ground away most of the razor blade above the sharp leading edge in their surface tube. This technique was used by Turner and Walker (28) in a slender wing free flight model in order to establish the ratio between the rms pressure fluctuations and local skin friction.

The sort of surface tubes mentioned above, showed sensitivity to dust contaminated flow. Special care had to be taken to ensure that the tubes did not become partially blocked during each run. Moreover, the time required for the tests represent one of the disadvantages of such devices (29). Another difficulty is the alignment of the narrow opening (which must project into the boundary layers) with the flow direction. This necessitates small sizes and accurate machining and positioning to give readings close to the surface and, at the same time, cause minimum disturbances. This type of device has a drawback in its slow response which makes it unsuitable for measurements in unsteady flow. There is also a tendency for/...

for the mouth of the tube to become partially blocked with fine dust particles and it is necessary to clean out the mouth of the probe on occasions and whenever this is done the tube has to be recalibrated in order to account for the small alterations in the shape of the mouth which occurred during the cleaning process. One of the major troubles is the possibility of leakage occurring at the edge of the outer wall (9). The surface tube depends on the fluid density and viscosity which calls for recalibration of the unit for use in different fluids and temperatures. Bradshaw (17) mentioned that an application of laminar calibration to the turbulent flow gives incorrect answers for skin friction. Moreover, the turbulent velocity fluctuates in the linear sublayer and the static pressure fluctuations at the wall below the turbulent boundary layer may influence the shear stress results as the rms of the latter is about the same order as the wall shear stress. Smith (21) showed that it is difficult to give precise estimates of the accuracy of the calibration procedure due to uncertainties about the expected value of shearing stress. The accuracy was found to range up to  $\pm 25$  per cent. The major source of inaccuracy of the calibration curve arises from errors in measuring the gap height  $h$ . Here the accuracy might improve with modern techniques. Errors can result if the size of the static hole " $d$ " was too small and Smith (21) suggested that providing  $d/h > 3$  the standard calibration can be used. Bradshaw (17) has shown that the effect of finite static hole size on the recorded pressure is considerable. The largest source of error in the measured " $\Delta p$ " was likely to be from insufficient accuracy in positioning of the upper leading edge relative to the leading/...



leading edge of the static hole. East (20) concluded the following :

- a) The calibration is significantly affected by changes in the dimensions of the probe configuration and reliable data can be obtained provided that mouth width  $b/h = 36$ ,  $d/h = 6$  and  $b/d > 5$ .
- b) A major source of error arises from inaccuracy of positioning the blade relative to the static hole.
- c) The removing of the thickness above the leading edge so as to reduce its effect upon the external flow, will change the calibration.

#### 2.2.3.2. Preston tube

In 1953 Preston (31) showed that at subsonic speeds the pressure on the mouth of a circular pitot tube placed on a test surface can be related to local skin friction. He based his suggestions on Prandtl-Karman's "law of the wall" for turbulent flow, which states that the fluid properties near the wall are related to the surface shear stress. Preston assumed that this was valid for both turbulent pipe flow and boundary layer flow (11). Based on the experiments of Ludwig and Tillman (1), he assumed that for any solid surface there is a region near the wall in which  $\frac{u}{u^*} = f\left(\frac{yu^*}{\nu}\right)$  where  $u$  is the velocity at a distance  $y$  normal to the surface and  $u^*$  is a friction velocity defined as  $u^* = \sqrt{\frac{\tau}{\rho}}$ . Guided by the method used by Stephen (32), Preston suggested that similarity parameters for a surface pitot tube might be obtained from the law of the wall/...



wall and that these factors correlate the effects of Reynolds number and tube size. Preston's resulting functional equation is :

$$\frac{\Delta p \cdot d^2}{4\rho v^2} = f \frac{\tau \cdot d^2}{4\rho v^2} \quad \text{or} \quad R_d^2 C_p = f R_d^2 C_F$$

$$\text{where } R_d C_p = 8 \frac{\Delta p \cdot d^2}{4\rho v^2} \quad \text{and} \quad R_d C_F = 8 \frac{\tau \cdot d^2}{4\rho v^2} \quad 2.3.$$

and  $\Delta p$  is pressure measured by pitot.  $d$  is the diameter of the tube. In this way the Preston tube, which is simply a circular pitot tube touching the surface, is a preferable instrument to the surface tube suggested by Stanton, because a larger tube could be used which is more robust, easier to mount and gives larger pressure difference with a better time response (24). Nevertheless, two precautions are necessary, (a) the tube must lie entirely in a region within 1/10 of the boundary layer thickness and (b) the tube dimensions must be small compared with dimensions of the model. Dutton (11) found that the region of local dynamical similarity extends up to 1/5 of the boundary layer thickness. It was also shown that the Preston tube Reynolds number limits are  $300 < \frac{u^* d}{\nu} < 350$ . (20). A probable limitation to the use of the Preston tube in two dimensional boundary layer is that its calibration is significantly affected by strong pressure gradients. Smith and Walker (5) indicated that, in general, the Preston tube device indicates smaller skin friction than the floating element device which is used for the direct measurements of shear stress and it could be useful in the range of

$5 < \frac{\Delta p d^2}{4 \rho v^2} < 7.5$  with zero pressure gradient. Furthermore, in a given favourable pressure gradient condition, errors actually increased with decreasing Preston tube diameter (4). Fage (4) showed that the inner law for the velocity distribution in turbulent pipe flow is different from that for turbulent boundary layer flow over flat plate. Therefore, calibration of the Preston tube in a turbulent pipe flow will not provide the accurate calibration method needed for the tube to be used on a flat plate.

#### 2.2.3.3. Effective centre of the velocity head probe

In 1928 Thom (34) showed that when a pitot is placed with its end in a field where the total head varies rapidly, it may not be correct to assume that the pressure reading given by the tube corresponds to the total head at the centroid of the end. Also, there is the effect of the proximity of the surface when the tube is very close to it. Such effects increase as the tube comes closer to the wall. Taylor (19) analysed the data of Stanton and of Fage and Falkner and suggested a correlation which involves the idea of the "effective centre" of the pitot tube. Obviously introducing the probe into the boundary layer causes flow disturbance. This disturbance may be propagated upstream a sufficient distance to modify the boundary layer ahead of the pitot tube, so that the pressure at the mouth of the tube would not correspond to that in the same position of an undisturbed flow (35). This necessitates that the probe diameter should be very small in comparison with the local thickness of the boundary layer. However, this requirement can lead to practical/...



practical difficulties since a reduction in the probe size will decrease its response to pressure variations. The effective centre of the probe gives a measure of the interference of the flow near the walls due to the presence of the probe body. Young (36) demonstrated that when the diameter of the bore of the probe to its outer diameter is of the order of  $0.6d$ , displacement ratio  $\delta/d = 0.18$  was found to be independent of " $d$ " provided that the pressure gradient was constant across the face of the probe. In general there exists a considerable velocity gradient across the face of the probe. For rectangular face probe, the suggested formula is as follows :-

$$\frac{\bar{\delta}}{h} = 0.24 \quad \text{where } h = \text{height of the probe} \quad 2.4.$$

For circular probe it takes the following form :-

$$\frac{\bar{\delta}}{d} = 0.131 + 0.082 \left( \frac{d_i}{d} \right) \quad 2.5.$$

where  $d_i$  and  $d$  are ID and OD of the probe.

Bradshaw (17) indicated that only when  $\frac{u^*d}{\nu} = 3$  will the tube read the dynamic head at its geometrical centre. On the other hand Hool (20) showed that the effective centre of a surface tube varies with the fluid velocity. The distance of the effective centre from the wall  $d^1$  can be expressed as :-

$$d^1 \propto u_1^{-0.25}$$

or

$$d^1 = 2.08 d^{0.75} \frac{\nu}{u_1^{0.25}} \quad 2.6$$



Taylor (19) from a momentum balance in the plane of the probe mouth assumed that the limiting pressure on a very small probe must be proportional to the tangential stress :-

$$\Delta p = K \mu \frac{u}{d^1} = \frac{1}{2} \rho u^2 \quad 2.7.$$

Therefore  $d^1 = \sqrt{2K\nu/u}$  with K experimentally found to be 1.2. Fage and Falkner (9) indicated that the distance from the wall corresponding to a velocity u is given by the ratio  $d^1 = \left\{ 1 - \sqrt{1 - \frac{2u}{3u_m}} \right\} \frac{d}{2}$  where  $u_m$  is the mean velocity during calibration.

Young and Maas (36) from measurements in a wake concluded that the streamline displacement ( $\frac{\delta}{h}$ ) is approximately 0.25 which seems to be small for turbulent boundary layer and lacks the Reynolds number dependence. Preston (31) account for the displacement effect close to the wall by introducing the following expression :-

$$\left( \frac{\Delta p}{\rho v^2} \right) y^2 = \phi \left( \frac{\tau y^2}{\rho v^2}, \frac{y}{h} \right) \quad 2.8.$$

and the effective displacement can be written as :-

$$\frac{\bar{\delta}}{h} = \psi \frac{\tau y^2}{\rho v^2}, \frac{y}{h} \quad \text{where } h \text{ is the height of the probe.}$$

$$\frac{\bar{\delta}}{h} = 0.2 \text{ (D1)} \text{ or } \frac{\bar{\delta}}{h} = 0.25 \text{ (G1)} \quad 2.9$$

#### 2.2.4. Surface heated probe

This method depends on the Reynolds analogy between the transport of momentum and that of heat. The former being responsible for the skin friction while the latter for the heat transfer. Ludwig (37) assumed that at a smooth wall the velocity profile next to the wall is dependent, aside from the material constants of the flowing medium, only on the shearing stress transmitted to the wall even with pressure rise or pressure drop (1). Consequently the heat transfer from a small electrically heated element flush with the model surface and thermally insulated from it, is a measure of the wall shearing stress. By keeping the length of the element small, the thickness of the warm boundary layer can be kept small. It is assumed that the velocity field is not affected by the temperature field. The relationship between the heat transfer and the skin friction could be as follows :-

$$Nu = 0.807 \frac{L^2}{\mu a} \tau^{1/3} \quad 2.10.$$

The heat flow is measured by the amount of electrical energy supplied to the heated probe. This method was first used by Fage and Falkner (38) in 1931 for a laminar boundary layer. They used a heated generator strip of a circular cylinder to estimate the average skin friction on the frontal part of a cylinder with an OD of 50 mm. Liepman and Skinner (16) showed that a very simple instrument could be used instead of that of Ludwig. They used an ordinary hot wire 0.01 mm diameter platinum wire cemented into a groove in the surface of an ebonite plate and flush mounted with it.

One of the main drawbacks of the surface heated probes is the/...

the assumption that the thermal boundary layer remains within the laminar sublayer which calls for small dimensions of the device which create construction difficulties. In addition small temperature differences create problems in the insulation and measurement of the probe surface temperature. Preston (18) showed that the heat probe method is inherently inaccurate since the measured quantity is proportional to  $1/3$  power of the shearing stress. One disadvantage of this sort of instrument is the time taken for the surface to reach thermal equilibrium with its surroundings which may be considerable (19).

Bellhouse (24) and Bellhouse and Schultz (25, 39) used a small thin film heated probe. They indicated that such a probe has the advantage of having quick response. Due to the fact that the thermal layer and the friction layer do not originate at the same point, calibration is needed. Again, this device needs to be calibrated in a situation where skin friction is known or measured by one of the other methods.

#### 2.2.5. Measurements of skin friction on circular cylinder using Indirect Methods

Measurements of skin friction on the surface of a circular cylinder in cross flow started with Thom (34) who measured it using a small pitot tube on a 114 mm OD cylinder. The pitot was mounted on a micrometer arrangement so that the end of the tube could be traversed along the normal to the outer surface of the cylinder. He noticed that when the bore of the probe was less than 0.1 mm, the damping effect was so great that the tube was practically useless and/...



and 0.2 mm was recommended as a lower limit for the outer diameter of the probe. Fage (40) obtained total head observations close to the surface with an exceedingly small pitot tube. The minimum distance from the surface at which observations were taken was about 0.09 mm which is the thickness of the probe wall. It was shown that the measurements were not accurate when the height of the probe represented a large fraction of the region of total head gradient near the surface. Fage (41) mentioned that the pressure gradient existing around a circular cylinder profoundly affected the flow in the boundary layer. Green (42) used a 1 mm probe to measure the velocity distribution normal to the cylinder surface. He showed that with a flow where the velocity gradient was large, the problem of interference (when the probe was very close to the surface) could produce readings which were slightly too large. On the other hand, Fage and Walker (23) used a surface tube of the Stanton type on two cylinders 74 mm and 150 mm outer diameters. They found that the assumption of linear relationship between normal distance and velocity measured by the probe was difficult to fulfill especially on the frontal part of the cylinder. In order to account for the displacement of the "effective centre" of the probe, the intensity of skin friction was given by the relation :

$$\tau = K \mu \left( \frac{u}{y} \right) \quad 2.11.$$

where K was found to be 1.16

According to their analysis, they concluded that reliable measurements with the surface tube on a circular cylinder could/...

could only be obtained provided that the boundary layer was not too thin, a condition which was not satisfied on the 74 mm cylinder. Giedt (43) used a Stanton type of tube projecting about 0.09 mm above the cylinder surface while its opening was  $2 \times 0.07$  mm, to study the effect of the turbulence level in the main stream on the shear stress around the cylinders. The static pressure tap was located 38 mm on either side of the probe. Through calibration he arrived at the following expression for the intensity of skin friction :

$$\tau = 4.625 \times 10^{-2} \mu (\Delta p)^{0.7} \quad 2.12.$$

It has also been demonstrated that a very small error in positioning of the surface tube may account for a difference of the order of 30 per cent in the results of skin friction coefficient at Reynolds number of  $10.6 \times 10^4$  for 76.2 mm diameter cylinder (23).

Giedt (44) showed from his experiments that since both the point heat transfer coefficients and skin friction intensities rise from coincident minimums on the front half of the cylinder and drop to coincident minimums on the back half, he concluded that, it is quite reasonable to assume that the maximum values in between occur near the same point. Achenbach (45) used a modified technique by placing a "fence" which transversely projected only some hundredths of a millimeter to the boundary layer. The idea of using such a boundary layer fence was started by Konstantinov and Dragnysh (46) in 1955 and was used later by Ziugzda and Ruseckas (47) to/...



to study the effect of main stream temperature on skin friction distribution around a cylinder in cross flow. Achenbach showed that such a fence could cause a premature boundary layer transition.

### 2.3. Direct measurements of skin friction

The devices used in this sort of measurements are designed to give their output signals as a direct measure of the shearing forces. Direct measurements could be carried out to give either an average estimation of the shear forces acting on the whole model or as a local value on the surface over which measurements were to be conducted.

#### 2.3.1. Direct measurements of average shearing forces

The first attempt of this type was conducted by Kempf in 1929 (48) by towing tests on pontoons in a ship tank. He was able to obtain skin friction factors at large Reynolds numbers. In 1932 a similar principle was used by Fronde and Kempf in determining the fluid resistance of bodies in water. Later in 1940 Schultz-Grunow (49) used a similar technique for the measurement of skin friction in a low speed wind tunnel. For measurements of the total frictional resistance for ship models, Schoenherr (50) used a similar procedure to that of Froude. The models are towed in a small towing tank by means of a falling weight, accelerating, until the resistance is equal to the towing weight and travelling thereafter at constant speed. His experiments covered a range of Reynolds number between  $10^3$  to  $6 \times 10^4$ . Geiger and/...



and Collucio (51) measured the average skin friction on the surface of a circular cylinder (fitted with splitter plate) by means of a pyramidal strain gauge balance. Drag readings were determined directly from the digital read out of the balance. In 1956 Sommer and Short (52) obtained values for the average skin friction of a turbulent boundary layer in presence of severe aerodynamic heating at Mach number of up to 7. Skin friction forces were calculated from measurements of the total drag of spin-stabilised hollow-cylinder models. Identical cylindrical models, except for length, were gun launched under the same conditions and total drag coefficients were computed from deceleration data. The difference between the deceleration factors of two different models then was a measure of the average skin friction drag over the difference in areas between them. In 1965, White (53) designed a balance to measure the skin friction on the inner convex surface of an annulus. The main body of the balance is constructed in two pieces, one sliding inside the other and fixed by a body adjusting plate and springs at the forward end of it. A null method was used in which the spring mounted element, having been deflected by the drag force, was pushed back to its initial position. The displacement indicator consisted of three coils, two of which were attached to the main body of the model, the third to the floating piece. An A.C. voltage supplied to the outer coils induced a voltage in the inner coil which depended on its position relative to the other two coils. By moving one of the outer coils and varying the supply frequency, the sensitivity of the transformer could be adjusted/...

adjusted to determine the inner coil position. The measurement of the drag force was done by applying a constant D.C. current to the outer coils while a variable current was fed to the inner coil. This D.C. current was charged until the electromagnetic force developed was sufficient to push the floating element back to its original position.

### 2.3.2. Direct measurements of local shearing force

Usually this can be carried out by making part of the surface, over which fluid flows, moveable under the effect of the drag force exerted from the flow against it. The next step is to measure the drag forces which cause such movement of this drag piece. Normally, the drag forces work against some sort of restoring force. These are calibrated so that the frictional forces and hence the skin friction can be ascertained. The drag piece has to be quite small compared with the dimensions of the body on which the measurements are to be taken. Moreover, the shearing forces are bound to be small so that the drag force measuring mechanism has to be extremely sensitive.

In 1950 Attinder (54) supported his drag piece by small columns from underneath the plate where the measurements were to be made, then measured the drag forces by using column strain gauges. Dhawan (2) in 1952 used a small drag piece supported from the ceiling of the transonic wind tunnel at California Institute of Technology. The piece was supported by a four-bar linkage which allows it to translate in the plane of a flat plate model without rotation./...



rotation. Smith and Walker (5) followed the same line as Dhawan and used a similar technique to measure the local skin friction on a small element of the surface of a flat plate. Matting and Coworkers (13) measured the local skin friction in a turbulent boundary layer on a 57 mm diameter disc, by means of a differential transformer. The drag piece was simply deflected under the effect of the shearing forces and the deflection was measured to indicate the amount of shear stress on the drag piece. Garringer (55) used a drag piece which was mounted on small wire flexures and held centered by electromagnets. Any shearing force attempting to displace this floating element along the sensitive axis of the device caused a change in voltage to the electromagnets. Thus a restoring force was produced that balanced the drag force on the element. In 1977 Depooter and Coworkers (56) used what they called a thrust balance which, in principle, is similar to that of Garringer. Their balance incorporated a feedback system which provided self centering of the floating element. They used their balance on a porous plate where mass transfer took place. But they could not succeed in eliminating or controlling the flow induced vibrations of the element electronically and instead they adopted the known method of using some 20,000 centistoke silicon fluid to overcome the mechanical vibrations transmitted from the wind tunnel. In 1959 Smith and Walker (5) used a nulling device to measure the local skin friction on a flat plate. When the element position indicator showed that the element had started to move from its no-load neutral position, the strength of a powerful electro/...



electro magnet was varied until the element returned to its no-load neutral position.

### 2.3.3. Direct measurements of skin friction on a circular cylinder

In 1973, Morsy (57) devised an instrument to measure the skin friction distribution around a circular cylinder (89 mm diameter). In general his device had the main features of Dhawan's device (2). The drag piece was 51 x 3.2 mm separated from the rest of the cylinder surface by a clearance gap and the rectangular window through which the element was projected was 0.3 mm wider than the element. The element was supported vertically on two, manually adjusted, jewel bearings located at the centre of the cylinder. The element was allowed to move under the effect of the shear force against bias springs. A linear variable differential transformer (LVDT) was used to indicate the position of this drag piece. Torsional springs (the restoring force mechanism) with varying stiffness were used to accommodate the different shearing force ranges associated with the range of Reynolds number used. By connecting two side slots on the leading and trailing edges of the element, he maintained that it was possible to eliminate the buoyancy forces due to pressure gradient over the cylinder surface.

Due to the fact that the flow around cylinder in cross flow is normally associated with vibrations and oscillating forces acting essentially at the vortex shedding frequency, the forces on the jewel bearings were not purely static ones. Such vibrations can increase the pressure between jewel and pivot/...

pivot considerably and jewel mounting with spring loading should have been used (58) instead of those used by Morsy. Moreover, due to the effect of the drag force, the moving element must move a measurable distance, to either side of the clearance gap, and this causes an increase or decrease in the gap size. In the case of a considerable movement of the drag piece, this could lead to a significant effect of the pressure forces on the measured drag force. Another difficulty in Morsy's device is the inconvenience encountered by using torsional springs for different ranges of Reynolds number. This calls for previous knowledge of the shearing force applied together with the recalibration necessary whenever the torsional springs were changed. Again, in order to damp the mechanical vibrations, an oil dash pot was used, which restricted the operation of the device in the vertical position.

It will be shown in the next chapter that by making use of the recent developments in bearings design and control systems, it is possible to devise such an instrument which would not have the drawbacks outlined above.

#### 2.4. Discussion and concluding remarks

As far as the indirect methods are concerned, most of the devices call for calibration in a similar condition to that in which it is going to be used. Although it is easy to calibrate a particular device by placing it in a long circular pipe, doubts arise as to whether the results obtained apply in other flow configurations.

With/...



With surface tubes and Preston tubes compressibility effects, perhaps, render inapplicable calibration data obtained in incompressible flow (7). As was pointed out by Taylor in 1932 and subsequently verified by Laufer (59) the name laminar sublayer is appropriate except that it implies that the viscous shear stress predominates over the turbulent one in the region of the wall. An ultra-microscope with a rotating objective was used (60) to examine the flow nature in the vicinity of the wall of a water channel. This showed that the flow near the wall is approximately in laminae parallel to the wall but the motion of the particles is no longer rectilinear and is in general sinuous. This shows how the flow nature close to a solid boundary is not that easily defined. One of the major troubles in using velocity probes is due to its finite size and therefore measurements cannot be made right up to the wall. The problem of the effective centre for the probe and the uncertainty regarding the definition of the velocity measured by the probe is clearly demonstrated in the previous sections in this chapter. Furthermore, since these instruments have to be calibrated under conditions which are difficult to be reproduced exactly during the actual measurements, such effects may cause large changes in the calibration constants. Beside these technical problems, the skin friction has to be determined by differentiation of the measured velocity profiles. The results of differentiation, even for accurate velocity measurements, can be quite inaccurate. More than that, in flows involving pressure gradient and mass transfer through the surface upon which measurements are/...



are to be carried out, the velocity direction in the vicinity of the surface becomes indeterminate and the situation becomes worse.

Since the direct methods for measuring the skin friction do not rely on any physical assumptions regarding the nature of the flow, so any defect in the experimental set-up does not alter the calibration of the device. The confidence in this sort of technique led to its application in the laboratories as a standard reference to calibrate other devices against, e.g., (references 61, 62, 37). Shearing stress measurements by direct methods have two main advantages; first, the only calibration needed is the determination of the force restoring constant in the device. Second, the output signal yields the shearing force directly.

The preceeding discussion showed that experimental estimation of skin friction using methods other than direct methods is subject to many errors. On account of this it was decided to apply the principle of direct shear stress measurements to estimate the skin friction distribution on the present set up.

## CHAPTER 3

### DEVELOPMENT OF A DEVICE FOR THE MEASUREMENT OF SKIN FRICTION AND FLOW DYNAMICS AROUND A CIRCULAR CYLINDER.

#### 3.1. Introduction

From the preceeding chapter, it was felt that the principle of direct measurements is the technique which involves the minimum source of errors if it is properly used. Nevertheless, there is some possible sources of errors in such devices which must be dealt with carefully if the aim is to reach a device capable of providing the necessary information about the flow characteristics around circular cylinders.

#### 3.2. Possible sources of errors

These could be summarised mainly as follows :-

- 1) Clearance gap around the drag piece
- 2) Flushness of the drag piece with the surrounding surface
- 3) Buoyancy effect due to pressure gradient
- 4) Drag piece dimensions

##### 3.2.1 Clearance gap effect

The fact that the drag piece must be free to move means that it must be separated from the rest of the surface, over which measurements are to be carried out, by a surrounding clearance gap. The effect of this gap is not well understood and may be important particularly in flows with a large pressure gradient over the surface.

Such/...

Such a case exists on the surface of a circular cylinder (53). Moreover, doubts may perhaps arise concerning the effect of these gaps. It was Schultz-Grunow (49) who mentioned the possible effects of these clearance gaps. In spite of the fact that the pressure on both sides of his drag piece was equal, he indicated that these gaps manifest flows which produce uneven suction and pressure on the drag piece and may falsify the measurements. On the other hand, Dhawan (2) showed that the clearance gaps may cause changes in the velocity and pressure distribution in their immediate vicinity. Since the no slip condition at the surface is not satisfied, within the gap width, a sudden disturbance in the slope of the velocity profile at the wall may occur as a result of the sudden break in the continuity of the boundary layer. The magnitude of such disturbance is a function of the gap dimensions and flow characteristics in its vicinity. Presumably the balance, drag piece, would give a correct estimation for the shear force if the width of the clearance gap is zero, for then there would be no interference with the flow and no leakage of air through the gaps under the drag piece. If the gaps were made very small compared to the drag piece dimensions, the pressure underneath the drag piece will be almost uniform and the error due to pressure forces could be minimised. This point was examined by White et al (53) with a variable clearance gap width ranging from 0.03 mm to 0.7 mm in order to reach the gap dimensions which would not disturb the velocity profile. From the graphical representation of their results, the effect was not serious provided the gap width is kept small, about 0.08 mm, and the measured/...



measured shearing force could be accepted with some confidence. Dhawan (2) studied the effect of gap size on flow over a flat plate by means of Schlieren photography. The continuity in a laminar boundary layer seemed to be unaffected by the presence of the gap until its width exceeded 0.25 mm. For a turbulent boundary layer, very faint wave seen originating at the clearance gap location. Searching for pressure variations at the gap location and measurements for the velocity profiles in the vicinity of a 0.2 mm gap by a hot wire anemometer confirmed that the flow structure and the shearing force were not affected by such a slot. Dhawan's choice for the clearance gap dimensions was adopted later by Morsy (57) in having clearance of 0.1 mm and 0.2 mm inch at the leading and trailing edges of the drag piece respectively.

### 3.2.2 Flushness with the rest of the model surface

The drag piece and the test model surface must at all times be at the same level. One way to do it is to lap the piece flush with the test surface after assembly. It has been shown Schultz-Grunow (49) that 0.1 mm vertical displacement between the drag piece and the surrounding horizontal surface yields about 6 per cent change in the estimated force. Dhawan (2) indicated that even small inclinations (of the order of  $1/50^\circ$ ) of the piece would introduce large errors into the measured forces. While Smith and Walker (5) mentioned that a depression of the piece as much as 0.01 mm will have effect on the readings, Matting et al (13) indicated that such a depression may produce force values about 2 per cent low. Allan (63) in his/...

his analysis of the direct methods and its applicability showed that a depression is equally serious as protrusion in destroying the accuracy of the measured shearing force.

### 3.2.3 Buoyancy effect

In flows with a pressure gradient like those which exist on the surface of a circular cylinder, the pressure gradient over the length of the drag piece is likely to create an extra force in addition to that of the shearing force. This extra force, a buoyancy force, is equal to the product of the drag piece side area and the difference in pressure at its leading and trailing edges. Therefore the force measurements require a correction for the apparent forces due to the pressure gradient. This is one of the reasons why Liepman (16) showed that direct techniques are restricted to cases of zero or at least small pressure gradients while Coles (16) recommended this technique for moderate pressure gradient provided it is precalibrated for this purpose. Morsy (57) tried to eliminate the effect of normal pressure difference by connecting together two slots cut into the supporting frame opposite to the leading and trailing edges of the drag piece. But it is possible that this can produce an air flow through the surrounding gaps from the higher to the lower pressure side which results in a break in the boundary layer and in the velocity profile in the vicinity of the clearance gap. As a consequence the measured values will be coloured by this kind of disturbance.



#### 3.2.4. Drag piece dimensions

For local measurements of the shearing forces, the drag piece has to be very small compared with the dimensions of the body over which the friction measurements are to be made. Since the drag force on the surface of a circular cylinder is bound to be small, these small dimensions (width) of the drag piece will result in very small forces acting on the element. This requires that the force measuring technique must be extremely sensitive.

#### 3.3. Direct Force measuring techniques

The magnitudes of the friction forces exerted on the drag piece from the main flow are usually measured using one of the following methods.

- 1) Measurements of the "free" drag piece deflection under the influence of shear force.
- 2) Measurements of a counter force which is necessary to restore the "controlled" drag piece to its no load neutral position.

##### 3.3.1. Deflected Devices

In this class of device, the deflection (angular or linear) is proportional to the amount of force applied on to the drag piece. In this case the piece is left to deflect freely under the influence of the shearing force. Deflection is measured through a calibration curve and directly indicates the magnitude of the drag force applied. Measurements of such small deflections could be carried out using optical methods, strain gauges or reactance gauge pickups (2, 57). The reactance type is similar, in principle/...



principle, to the strain gauges but the percentage change is several times larger than that of the mechanical change for the former while it is of the same order of magnitude as the mechanical change for the latter. Normally, this sort of device is equipped with some sort of restoring force mechanism. This can either be in the form of flexural linkage (2) or torsional springs (57). Restoring forces with different capacity were used and thus provided different levels for the parameter to be measured.

### 3.3.2. Null-positioning Devices

Such instruments are usually called null-seeking servo force balances. Here the parameter to be measured (drag force) produced by the flow against the drag piece is counteracted by an externally applied force to restore the drag piece to its no-load neutral position. The amount of counterforce is thus proportional to and a measure of the drag force. In this sort of instrument, the applied force deflects the moveable drag piece assembly, the signal is detected and is sent through a force balancing mechanism generating the restoring force required to bring the drag piece back to its no-load position. In these devices the motion detectors could be capacitive (10, 13, 64) or using a linear differential transformer (5, 13).

### 3.4. Description of the developed device

Although the idea of using a direct force balance to estimate the shear force is obvious and simple, its application/...

application to the present investigation was not an easy one. The instrument was planned to be used to measure skin friction on the outer surface of a cylinder placed in a crossflow. This raised the first restriction to the design, i.e., the effect of flow with pressure gradient on the measurements. In one part of the programme it was decided to investigate the effect of surface roughness on the distribution of skin friction around the cylinder. This raised the second restraint to the design, i.e., the homogeneity of the surface nature and flushness between the drag piece and the rest of the test cylinder surface. In another part of the investigation, it was planned to study the effect of distributed section on the shearing force around the test model. Here the problem was how to keep the dimensions as small as possible to reduce the disturbance caused to the sucked boundary layer due to the presence of the drag piece. It was also planned to make a simulation between the test cylinder and a condenser tube where both heat and mass transfer processes go simultaneously side by side. It was, therefore, decided to cool the inside wall of the test cylinder with a film of cooling water run over the interior surface while hot air was sucked through the porous wall of the test cylinder. This implies that it was important to use as little as possible of the interior space of the test cylinder. The problem of reducing the dimensions of the device to fulfill these requirements was a troublesome one and resulted in a minimum dimension for the test cylinder as 76.2/63.5 mm OD/ID. Keeping an eye on the likely sources of errors mentioned in Chapter 2 and in the previous part of/...



of the present chapter, the task was to develop a device which could meet the following requirements :-

- A) The drag piece width along the cylinder's circumference should be made as small as possible to reduce the effect of buoyancy correction.
- B) The drag piece must be made from the same material as that of the test cylinder. This was a difficult task to do, since the test cylinder was made from a sintered bronze, a material which is very brittle and not easy to handle or machine.
- C) The clearance gap, surrounded and isolated the drag piece from the test of the cylinder surface, and should be kept as small as possible.
- D) The total frontal width of the device, including the drag piece, clearance gaps on both sides plus the supporting frame, should be kept as small as possible to reduce to a minimum the disturbances to the sucked boundary layer.
- E) The overall dimensions of the device should be quite small relative to the internal available space inside the test cylinder.
- F) The drag piece should be flush with the surrounding supporting frame and the rest of the test cylinder surface.

The developing procedure was divided into two stages, first, to design and construct a device which could meet the above requirements. Secondly, to develop a controller capable of matching the accuracy required for such a device.

#### 3.4.1. Mechanical description of the device

A schematic diagram of the device within the cylinder test section is shown in Fig. 5.4. The test cylinder was 76.2/63.5 mm OD/ID porous cylinder. The drag piece was rectangular/...



rectangular 50 mm along the length of the cylinder, 2 mm wide along the cylinder circumference and it was made out of a circular ring sector cut from the body of the test cylinder to keep the surface nature of the drag piece the same as the surrounding cylinder surface. The sides of the drag piece were 1 mm wide. This piece was exposed to the main flow replacing a part of the outer surface of the cylinder through a 2.16 mm wide rectangular supporting frame using accurately cut spacers. There was about 80 microns clearance gap on each side of the drag piece when it was in the no load position. Clearance gaps at the top and bottom of the piece were about 100 microns. The leading surface of the piece was aligned flush with the supporting frame and the surrounding cylinder surface using a dial indicator with  $\pm 5$  microns. On each side of the element 0.25 mm wide, 50 mm long slot was cut in the supporting frame facing the leading and trailing edges of the drag piece and running parallel to it. These slots were connected separately to an inclined manometer. The supporting frame body replaced a part of the cylinder surface 6 mm wide along the circumference of the test cylinder. This was the minimum possible width of the frame in order to bring the porous surface, where mass transfer was going to take place, as close as 3 mm away on each side of the middle axis of the drag piece. This rectangular drag piece represents the leading end of a mass balanced-beam, or vane, pivoted along the longitudinal axis of the test cylinder and made from a non-magnetic material. It was pivoted on a pair of crossed spring frictionless flexural cantilever type pivots. The pivots were supplied by Messrs./...

Messrs. Field Tech. Ltd. These pivots offer a small spring restoring force and a negligible friction (65). These pivots were fitted in such a way that one end was fitted to the beam while the other end was mounted on an adjustable frame. The fitting of the pivot using set screws or other mechanical methods, after careful consideration, was rejected due to its effect on the annular space (which was about 40 microns) between the moving parts of the pivot. Finally, it was decided to glue the pivot using a resin epoxy. Two types of these pivots, 5000 series cantilever type, were tested 5004 - 800 and 5006 - 600 which gave the beam natural frequencies of 4.5 and 24 Hz respectively. The spring factor of these pivots were measured using known weights together with a travelling microscope and they were found to be 30 per cent and 10 per cent too high for the tabulated values for the two types of pivots used respectively. The other end of the swinging beam was equipped with a photo-electric displacement-to-voltage converter (66) plus the counter force mechanism. The light beam for the photo electric system was produced at right angles to the beam plane using a 'vitality lens end lamp TL - 1½'. This lamp was placed in a small enclosure so that the light beam from the lens would pass through a rectangular slit 4 x 0.2 mm at one end of the enclosure. The light beam passes through a rectangular slot 3 x 1.5 mm cut in the swinging beam and placed 20 mm away from the flexural pivots. On this slot two sharp ends of razor blades were mounted in an adjustable fashion to let the light beam pass through a rectangular slit 3 x 0.2 mm cross section area. To reduce/...



reduce the scattering of the light downstream the razor blades, a "light cone" 6 mm long was mounted on the beam opposite to the light source. Inlet cone area was  $3 \times 1.5$  mm to give a light beam through a  $3 \times 0.2$  mm rectangular outlet section. The inside of the cone was coloured matt black. Thereafter, the light beam was received on a BP x 48 differential diode producing a signal proportional in amplitude to the illuminated area difference, for a precision pair of photocells, for a constant intensity of illumination. The advantage of using such a diode is its insensitivity to variations in thermal conditions and light intensity. Such sensitivity is an inherited character of normal photo-cell diodes. The BP x 48 was mounted on an adjustable frame surrounded by a matt black painted light shield except from the front which faced the light beam coming from the outlet of the light cone placed 0.5 mm away from the photo diodes. The arrangement for the light beam is shown in Figure (3.1). The counter force mechanism was placed 27 mm away from the flexural pivots. A permanent magnet 400 gauss strength was placed in the field of a pair of electromagnetic coils with soft iron core driven by a DC servo amplifier. The coils electrical resistance was 43 MOH. The total weight of the complete pivoted assembly unit including the flexural pivots and their seats was 10.6 grams (shown in Figure 3.4). The drag piece leading surface area subjected to the flow was 100 square millimeters. The device was tightly sealed to prevent flow through the leading end surrounding gap clearance.



### 3.4.2. The controller and electronic equipments

Since the effect of any change in the clearance gap dimensions is not well known, it was decided to operate the present device with a fixed position of the drag piece within the gap. Therefore, the system was designed to work as a null-seeking device. The use of the servo force balance principle represents a valuable improvement on previous instruments because, firstly, the sensing element is held in a fixed position by integral control (I) guaranteeing a constant local flow field and, secondly, the proportional feedback (P) can be used to increase the natural frequency of the system thus enabling the accurate and sensitive detection of not only the required skin friction forces but also such dynamic features of the flow such as vortex shedding frequencies. The use of velocity or derivative feedback (D) instead of oil damping (2, 56, 57) allows operation of the device in an arbitrary orientation. Using PID control system the clearance gap, surrounding the drag piece, was kept to a minimum (80 microns) while the flow dynamics was measured accurately and the accurate correction for the buoyancy forces was possible. The main target in developing the control system was to achieve the following :-

- 1) Suitable servo-amplifier
- 2) Force transducer with linear current versus shearing force characteristics
- 3) Circuit to produce a stable proportional plus integral controller.

### 3.4.2.1 Choice of system

A schematic diagram of the system is shown in Figure (3.5). The basic element in the system is the beam OA mounted on the crossed springs at O. The shearing force  $P$  produces a moment  $M_p = aP$  which is balanced by moment  $M_q = bQ$  of the internally generated force  $Q$  so as to maintain the two gap distances  $g_1$  and  $g_2$  constant and equal. For this reason a displacement transducer is fitted to the beam as far from O as possible (Figure 3.3). The major considerations in choosing a displacement transducer are long-term stability, freedom from mechanical flexibility, extreme high sensitivity and linearity in the interest of simplified stability analysis. Inductive, capacitive or optical methods are available. Inductive methods are quite common. However, there is no real alternative to a magnetic method of producing the small balancing force  $Q$ , and since the displacement to be resolved is extremely small, problems of stray interaction can be reduced by choosing a non-magnetic displacement system. Capacitive systems have certain attractions but, as a general rule, an increase in sensitivity of such a system necessitates increasing the areas of the capacitor plates which is ultimately restricted by: firstly, the physical dimensional restrictions imposed by the nature of the test set-up and, secondly, by the need to avoid high frequency modes of mechanical vibrations in the whole system. The optical displacement-to-voltage system recommended by Havenstein (66) has proved to meet the above considerations. In this system parallel light beam passes the arrangement shown in Figure (3.1). to a BP x 48 procession pair of photocells, connected/...



connected in a differential mode thus giving immunity from variations in thermal conditions and light intensity. The sensitivity of this system using the recommended TAA 861 amplifier is about 80 volt/mm or with the photocells unit 20 mm from point O, 1600 V/rad. The balancing force  $Q$  was produced on a permanent magnet, 400 Gauss strength, fixed to the beam assembly and placed into the field of a pair of electro-magnetic coils with soft iron cores driven by a D.C. servo amplifier. It was realised that it is more advantageous to eliminate the soft iron core from the electro magnetic coils and a good current versus shearing force linearity was achieved by using air cored coils.

The simplest possible servo-system would consist in feeding the output signal of the displacement transducer, error signal, directly and with suitable polarity to the force actuator. Using the above displacement transducer and the small space available for the magnetic force actuator, an equivalent stiffness of  $K = 0.4 \text{ N.m./rad}$  could be achieved. With a beam inertia of  $4.2 \times 10^{-6} \text{ Kg m}^2$  this simple proportional control could have a natural frequency of 50 HZ. Figure (37) shows a recording of the skin friction on the cylinder that would have a shedding rate of 25 HZ if the Strouhal number was 0.2. Hence the natural frequency of 50 HZ would guarantee a constant transducer gain over the band width of interest. However, the loads to be measured are in the range  $10^{-5}$  to  $5 \times 10^{-3} \text{ N}$ , with the above stiffness,  $K$ , the upper limit of the load would cause a change in the gap clearance of 23 micron. This was too large compared with our target of 80 micron gaps. In principle, there is no/...



no limit to the amplification of the error signal before it is applied to the force activator. However, in practice, the amplification is limited by such things as noise in the photocells and instabilities at high frequencies. Hence integral action must be added to reduce gap clearance variations. The stability of the required control system was reached by adding some sort of velocity feedback, or derivative action, to achieve artificially viscous damping. Differentiation can only be accurate over a limited bandwidth; this means that the action must be "rolled off" in a suitable manner above a carefully chosen frequency. In the present case the first mode of flexural vibration of the beam at 350 HZ gave trouble until additional reinforcements were made to raise this frequency to 600 HZ. Then the derivative action was rolled off about 500 HZ with a four-pole Bessel filter supplied by Messrs. Barr & Stroud. The choice of the roll-off frequency and type of filter was a critical experimental choice. It appeared that the relatively small phase shift in the Bessel L.P. filter was favourable for stability. A block diagram for the electronic circuit is shown in Figure (3.2).

#### 3.4.2.2. Analysis of the system

The transducer beam, or vane, has a moment of inertia  $J$  which by virtue of the crossed spring flexural pivot, has a 'low' natural frequency  $\tilde{\omega}_n$  and damping coefficient  $\tilde{G}$ . These were determined from a free vibration test as shown in Figure (3.8). For the theoretical analysis and optimization of parameters, the velocity action was represented by an ideal differentiation with transfer function  $K_0 S$ . The block diagram/...

diagram of the instrument is thus as given in Figure (3.6), and the closed loop transfer function between applied moment  $M_p$  and balance moment  $M_Q$  is,

$$H_1(S) = M_p(s)/M_Q(s) = b(K_0 S^2 + K_1 S + K_2) / (S^3 + 2\zeta\omega_n S^2 + \omega_n^2 S + \eta\omega_n^3) \quad 3.1.$$

where:

$K_0$ ,  $K_1$  and  $K_2$  are determined by the parameters in the PID controller.

$$b = 1/J$$

$$2\zeta\omega_n = bK_0 + 2\tilde{\zeta}\tilde{\omega}_n$$

$$\omega_n^2 = bK_1 + \tilde{\omega}_n^2$$

$$\eta\omega_n^3 = bK_2$$

The optimum setting of the instrument now requires a choice of the control parameters  $K_0$ ,  $K_1$  and  $K_2$ . However, the optimum values depend on the dynamic performance indices adopted. The criteria considered are: (1) transient response, (2) steady state frequency response, and (3) variations of the drag piece clearance gaps, i.e. variations from the null position. Before these theoretical criteria are examined there is the practical consideration of random noise in the system. This sets an effective maximum value on the proportional factor  $K_1$  and hence  $\omega_n$ , provided the permissible velocity feedback factor  $K_0$ , which emphasizes noise, lies in a restricted range. Hence the restricted optimisation of  $\eta$  and subject to  $0.6 < \zeta < 1.5$  and  $\omega_n = 725$  rad/sec. was considered. The transient response of the system/...



system under various velocity feedback actions is shown in Appendix 1. The transient behaviour of the balance moment  $M_Q$  is depicted by the root loci of the denominator of  $H_1(s)$  as shown in Figure (3.9) for various values of  $\eta$  and  $\xi$ . Small values of  $\eta$  correspond to a highly damped oscillatory term plus a non-oscillatory term of long time constant (cf points marked +), whereas large values of  $\eta$  reverse the situation, i.e., oscillations of long time constant and a non-oscillatory term of short time constant (cf typical points marked X). Optimum transient response with equal true constants is achieved with the parameter pairs  $(\xi, \eta\omega_n) = (0.6, 200), (0.7, 190), (0.8, 170), (0.9, 130), (1.0, 120)$  and  $(1.5, 100)$ . Such optimum settings are non-oscillatory for  $\xi > 0.9$ , but at the same time the rapid change in the shape of the root loci indicates sensitivity which may be undesirable (237). Figure (3.10a) depicts the steady state frequency response of the balance moment  $M_Q$  for a range of values with the corresponding optimum values of  $\eta$ . The larger  $\xi$  is the flatter the frequency response.

However, Figure (3.10b) depicting :

$$J. \text{ MOD } (\theta(i\omega)/M_p(i\omega)) = \omega / \{ (\eta\omega_n^3 - 2\xi\omega_n\omega^2)^2 + \omega^2(\omega_n^2 - \omega^2) \}^{1/2} \quad 3.2.$$

shows that very little reduction in the largest amplitude of  $\theta$  can be gained by increasing  $\xi$ . This has an important implication concerning the gap clearance criteria. There is always a frequency where the angular amplitude reaches  $2 \times 10^{-6}$  MP/J (rad.). Thus a fluctuating load of 150 milligram on the leading end of the drag piece, corresponding to an amplitude of/...



of  $M_p = 56 \times 10^{-6}$  Nm. acts at the worst possible frequency, the amplitude of  $\theta$  will be  $(2 \times 10^{-6} \times 56 \times 10^{-6}) / 4.2 \times 10^{-6}$  rad. with the chosen beam inertia  $J = 4.2 \times 10^{-6}$  Kg m<sup>2</sup>. The gap clearance variations will thus be  $28 \times 10^{-6} \times 38$  mm < 2 micron which is quite satisfactory. Hence in choosing the beam inertia  $J$  a compromise must be made between the need to increase  $\omega_n$  by decreasing  $J$  to obtain a wide dynamic band width and the need to increase  $J$  to restrict the side gap variations.

### 3.5. Calibration of the device

Among the great number of tests and checks made to the device, tests were made to check the static and dynamic response of the instrument under different loading conditions. In fact, any variations of the side clearance gap were imperceptible within the range of working loads. The servo amplifier gain and pick off sensitivity can be made very high so that a displacement of the drag piece as small as a micron can generate full output. Adjustment of the drag piece position, to create equal clearance gaps on both sides of it was done using an offset current fed to the buffer of the servo amplifier.

Under static conditions, the instrument was able to discriminate load increments of 1/10 of a milligram ( $10^{-6}$  N). The maximum permissible load was limited by the maximum current allowed through the electro magnetic coils which correspond to 500 milligram force to give a shear stress equal to 50 N/m<sup>2</sup>. Calibration of the device was made by hanging small pieces of wire of known weight on the drag piece and recording/...

recording the voltage output developed across the electromagnetic coils using a SE Laboratories digital voltmeter. The error due to the inductance of the coils involved in the measurements in its dynamic mode was negligible. The output signal recorded is directly proportional and a measure for the applied force onto the loading end of the moving assembly. Sample calibrations indicating the linearity and repeatability of the device may be seen in Figure (3.11). It is worth mentioning here that these calibration values were independent of the type of controller and flexural pivot used. The skin friction force, in an experimental run, was measured as the difference between the no load and loading conditions according to the predetermined calibrations. Therefore, any error which could occur in the alignment of the centre of mass, for the moving assembly, with that for the flexural pivots would appear as an output of the system with the no load forming the zero shear stress signal. Another point is that, since the counter force is produced parallel to the force applied to the drag piece, it is immaterial whether the device was calibrated horizontally or vertically.

Characteristics of the developed device and performance are given in Appendix 5.

### 3.6. Concluding remarks

The addition of servo force balancing to the instrument of the direct measurements of wall skin friction leads to available improvement in performance without losing the convenience of direct calibration. The integral control allows/...

allows the clearance gaps to be reduced to limits set only by mechanical tolerances; in the present device gaps of 80 microns were chosen. The proportional control allows the natural frequency of the system to be increased to a limit set only by the signal-to-noise ratio in the displacement-to-voltage transducer. The optical displacement system has proved to be robust, reliable and sensitive. The suggested criteria for optimising the control system have proven to give a satisfactory instrument that has already revealed valuable information about the dynamics of the flow around circular cylinders in cross flow as it will be demonstrated in the next chapters.



## CHAPTER 4

### PRESSURE DROP AND HEAT TRANSFER IN TUBULAR HEAT EXCHANGERS

#### 4.1. Pressure Drop in Cross Flow

##### 4.1.1. Introduction

The most common type of heat exchangers found in practice is the conventional shell-and-tube exchanger. The tube geometry for such exchangers is one of four arrangements, of course the tube arrangement can take any arbitrary pattern but these are the most commonly used ones. One is in-line square, an in-line arrangement with the tubes in pattern of square, where the transverse spacing  $T$  is equal to the longitudinal spacing  $L$ . The others are staggered arrangements, rotated square, equilateral triangular and equal spacing arrangement.

In a rotated square matrix the tubes are arranged in a square pattern rotated through 45 degrees. Here the transverse spacing is equal to twice the longitudinal spacing of the rows. An equilateral triangular arrangement consists of tubes in a pattern of equilateral triangles, with the flow in the main stream normal to the bases of the triangles. For this arrangement  $L$  is equal to  $T \sin 60^\circ$ . For the equal spacing bank arrangement, isosceles triangular spacing, the tubes are displayed in a pattern of triangles in which the base is equal to the height, with the main flow normal to the base. In this arrangement  $L$  is equal to  $T$ .

For most of the heat exchangers where these tube arrangements are/

are used, the ratio between the tubes pitch and tube diameters is between 1.25 and 1.75. The lower limit for the pitch ratio is set by the maintenance aspect of the exchanger, e.g., the need to clean the outside surface of tubes mechanically, while the upper limit is determined by both heat transfer and hydraulic resistance of the unit. In fact, the pitch ratio in special cases could be lower or higher than these values. It is known that with higher pitch ratios, the cost and the space of the exchanger will also be higher.

In these exchangers, the flow velocity is neither perpendicular to the tubes nor is it uniform through the tube bundles. Of course the situation becomes more complicated in steam surface condensers due to the presence of both steam and condensate within the shell.

The fluid mechanics of the shell side flow within a tubular exchanger is important since the thermal performance of the unit depends upon these fluid characteristics. Moreover, large heat exchangers such as steam condensers for power stations and desalination plants account for a high proportion of the capital cost of the plant, so there is a considerable incentive to improve the design and performance of such exchangers.

For most of the shell-and-tube exchangers, it is the shell side fluid which dominates and controls the overall thermal performance of the unit. Moreover, it is the shell side pressure loss which is particularly costly in the case of steam surface condensers, for instance. Therefore, it is not/...



not surprising that the shell side fluid mechanics has drawn the attention of many research workers. Furthermore, a better understanding of the shell side flow is necessary when modelling work is carried out to predict prototype heat transfer and pressure loss performance or when existing experimental data is being used for heat exchanger design.

In the present chapter we shall be concerned with problems of pressure drop and heat transfer for single cylinder and banks of tubes, mainly staggered arrangements in cross flow. Although there is a fairly extensive literature on these problems, it is not the intention of this chapter to discuss each available investigation in the subject. That sort of survey cannot be accommodated here and it is more appropriate to discuss only the relevant investigations to the present study.

In the following, problems associated with cross flow over single cylinder will be considered first and then it will be followed with those associated with a tube in bank.

#### 4.1.2. Single cylinder in a cross flow

When fluid flows past a cylinder, the fluid is accelerated as it passes over the forward portion of the body as a result of going around the cylinder starting from the forward stagnation point (FSP). Due to the viscosity of real fluids, a laminar boundary layer is formed on the front part of the cylinder surface which faces the flow. The thickness of this layer increases downstream as its Azimuthal span increases from the FSP. According to/...



to the ratio of inertial and viscous forces in the flow, characterised by the Reynolds number, several types of flow regimes can be distinguished.

Under sufficiently high Reynolds numbers, the kinetic energy of the fluid in the boundary layer is increased due to the acceleration over the forward portion of the cylinder. A certain amount of this energy is consumed in overcoming friction in the boundary layer and is thus dissipated. As the fluid in the main stream goes past the cylinder, the expanding cross-section of flow on the rear of the cylinder produces a deceleration of the fluid and a corresponding increase in pressure. The boundary is thus moving against an adverse pressure gradient as it moves around the cylinder. The remainder of the kinetic energy of fluid in the boundary layer, which is gained over the forward portion after allowing for dissipated energy due to friction, does not suffice to overcome that adverse pressure gradient on the rear of the cylinder. Fluid particles of the boundary layer that have a low velocity because of friction become even slower. This will continue until these particles stop and eventually a local reversal of the flow in the boundary layer will occur. In order to maintain flow in the direction of the adverse pressure gradient, the boundary layer separates from the solid surface and continues in space. Fluid sheets of opposite movements begin to curl and give rise to vortices that shed from the cylinder. Consequently, the area behind the cylinder becomes an area of disturbed flow and vortices formed on the rear portion consume a part of the energy of disturbances of the separated boundary layer. The remainder of the energy/...

energy dissipates in the wake in the form of small turbulent vortices. With this sort of regular vortex shedding, there is a constant and intensive exchange of momentum and mass between the circulation region and the main flow.

As the fluid flows across a cylinder, the fluid encounters a resistance which is known as hydraulic resistance or simply called drag. This resistance or total drag of the cylinder in a cross flow is equal to the sum of the forces of friction and pressure drag. The frictional drag is mainly due to the viscous forces in the boundary layer developed on the frontal part of the cylinder. On this portion, it is assumed that the fluid in contact with the surface has zero velocity and the frictional resistance retards the moving particles near the solid surface of the cylinder. Although, these frictional forces constitute a few per cent of the total drag, it influences, however, the flow by affecting the separation of the boundary layer. Moreover, the flow pattern around the cylinder may be judged from the friction force distribution around the cylinder.

As a result of flow separation and vortex formation close to the rear, a broad wake is developed behind the cylinder. Consequently, the pressure behind the cylinder will be less than the corresponding pressure at the forward portion. As a result, a force will act on the cylinder called pressure drag. This force is caused by flow separation and depends on the width of the circulation region. The large width of the wake in the subcritical region corresponds to the large/...



large value of the pressure drag coefficient in that region.

#### 4.1.3. Turbulence and a cylinder in a cross flow

The turbulence level in the incident flow exerts a certain influence on the flow pattern around a circular cylinder. In fact, Taylor (97) was the first to show that the drag of bodies of revolution is affected by the intensity of turbulence in the main stream. He demonstrated that the turbulence in the incident stream can cause transition through the action of small eddies which are also responsible for energy dissipation. Petrie and Simpson (98) obtained measurements of the pressure distribution around cylinder of 19.1 mm diameter at  $5000 < Re < 35000$ . They found that the free stream turbulence is only effective in the region of  $40^\circ < \theta < 140^\circ$  measured from the FSP. Even in this region, however, turbulence levels below 2.63 per cent had no measureable effect on the pressure distribution around the cylinder. On the other hand the results of Zijnen (99) agreed with Petrie and Simpson that for  $Re > 20000$ , the effect of turbulence on the pressure distribution starts at about 50 degrees from FSP. Moreover, the results showed that, instead of limiting the turbulence effect at  $\theta = 140^\circ$  (98), the negative pressure on the entire down stream side of the cylinder and, in particular, at the rear stagnation point is affected by the turbulence intensity.

The roughness of the cylinder surface has also an effect on the drag coefficient and flow pattern around the cylinder. Indeed the results from a number of investigations (80, 100, 101)/...



101) showed that as the relative roughness of the surface ( $\frac{KS}{D}$ ) increases, the Reynolds number at which the critical flow region is established decreases. Moreover, the pressure drag coefficient increases in the critical flow region with increasing surface roughness (102).

#### 4.1.4. Tube in a bank in cross flow

For the case of a cylinder within a tube bank, the flow pattern is influenced by the surrounding cylinders in addition to the factors previously discussed. In the longitudinal gap between adjacent cylinders of a transverse row, the pressure changes even more rapidly than without this sort of contraction. As a consequence of this, a corresponding change of velocity distribution in the boundary layer and of the flow pattern in the rear of the cylinder is to be expected. Another factor which contributes to the flow complexity in the bank is the tube pattern within the bank. In tube bank arrangements, the cylinders in the intermediate and inner rows are located in the wake of those in the preceeding rows. That means that the flow approaching the inner rows is a vortical non-uniform one.

Apart from the first row, which is in a way similar to single cylinders in cross flow, the flow pattern in subsequent rows changes according to the tube arrangement. Flow patterns in an in-line bank could be comparable with those in straight channel and the velocity distribution in the minimum cross section of an inner row is mainly determined by the pitch ratio. In staggered banks, however, /...

however, the flow pattern is comparable with that in a curved channel of periodically converging and diverging cross section. In these banks, away from the entrance region which extends through the first few rows, the velocity distribution around cylinders in different rows is expected to have a similar character.

In a staggered tube bank, at Reynolds number more than  $10^3$  vortices appear as the flow in the bank becomes turbulent and flow between tubes becomes vortical with a higher degree of turbulence. Nevertheless, a laminar boundary layer persists on the front portion of an inner cylinder as if it was in a uniform flow (103). The pattern of flow, with a laminar boundary layer on the cylinder under the influence of a turbulent flow stream together with an intensive vortical flow in the wake region, could be described as mixed flow. Consequently, on any of the inner tubes of a staggered bank, the pressure in front of the separation point is higher than that on a single tube due to the movement of the separation point towards the rear of the cylinder.

Studies of flow pattern in banks of tubes, should also include the influence of the pitch to tube ratio. For staggered banks, an increase in the longitudinal pitch leads to a longer pass for the flow with less interference for the wakes and an increase of the hydraulic resistance of the bank is to be expected. The resistance of the bank is influenced by the amount of free space available for the flow between tube array. Therefore, a decrease in/...



in the longitudinal pitch could result in a reduction in the flow free section which may lead to higher thermal performance together with a higher hydraulic resistance of the bank. As far as the effect of transverse pitch is concerned, a decrease of its value will result in a higher velocity through the longitudinal gap between tubes in the same transverse row. Pearce (104) measured the flow velocity in the centre of straight gaps in a staggered bank and found that it varied with position within the bank and with cylinder spacing. Increasing the transverse pitch caused changes in the velocity distribution across the longitudinal gaps. With wider pitches, Pearce's results showed that the flow was pushed towards the sides of the gap. As a result, the flow was concentrated close to the cylinder sides with smaller velocities in the centre of the gaps. This movement of the peak of the flow velocity distribution towards the gap edges was attributed to the reduction in the ratio between the boundary layer thickness and the gap width. With a decrease in the transverse pitch this ratio becomes relatively large in the contraction region and the velocity near the cylinder surfaces decreases. According to Zukauskas et al (190) the flow velocity profile in the gap region was straightened when the transverse gap was decreased due to the influence of viscous forces at its sides.

Pearce indicated that the characteristics of the accelerated flow through the longitudinal gap, with much of the fluid passing near the edges of the gap, is the general trend of flow pattern within staggered tube banks. He/...



He found that for a pitch ratio  $1.3 > T > 1.5$ , the velocity over the central part of the longitudinal gap was equal to the nominal gap velocity in this region, but rose to a peak about 10 per cent higher towards the edges, before dropping rapidly within the boundary layer thickness. On the other hand for a pitch ratio equal to 1.5 the velocity at the gap centre was lower than the nominal gap velocity and the peak towards the side reached about 35 per cent higher than nominal velocity before it dropped in the boundary layer region. These peaks in the velocity profile, towards the edges of the gaps, showed that the fluid tended to take the shortest way through the gap from the upstream diagonal gap right into the wake.

#### 4.1.5. Pressure Drop for banks of tubes in a cross flow

Hydraulic resistance represents an important characteristic of heat exchangers and it is characterised by the total pressure drop in flow across the tube banks. This total pressure drop is a function of flow velocity, bank arrangement and physical properties of the flowing medium. The resistance encountered by viscous fluids of constant density flowing across a tube bank is expressed by the following functional relationship:

$$\Delta P = f(U, D, N, L, T, \mu, \rho) \quad 4.1.$$

Usually, the pressure drop for flow past a bank of tubes is expressed in non-dimensional terms such as the pressure drop per row as a fraction of the dynamic head of the incident/...

incident flow based on the nominal velocity in the narrowest gap between tubes. The nominal velocity could be calculated based on either the transverse pitch width or the diagonal pitch width as appropriate. The number of rows  $N$  refers to the number of major flow restrictions in the bank, so that if the nominal velocity is that based on the transverse pitch,  $N$  will be equal to the number of rows, whereas, when the nominal velocity is that based on the diagonal pitch between tubes of adjacent rows,  $N$  will be equal to the number of diagonal gaps, one less than the number of rows.

The simplest expression for the dimensionless pressure drop is the Euler number which is defined by the following equation :

$$Eu = \frac{\Delta P}{\frac{1}{2} \rho U^2 N} \quad 4.2.$$

where  $\Delta P$  is the total pressure drop across the tube bank. A friction factor ' $f$ ' equal to one quarter of the Euler number is normally used and it is this factor or coefficient which is usually calculated for the bank of cylinders.

#### 4.1.6. Rectangular tube banks in an isothermal cross flow

There is a large volume of published data on the pressure drop characteristics for isothermal, non-condensing, flow across experimental tube banks. These investigations were usually carried out using rectangular working sections where the banks were mounted across it. Measurements of total pressure drop across these banks were carried out by recording/...



/recording the difference in pressure between two tappings inserted upstream and far enough down stream of the bank. Thereafter, the obtained results were correlated with the tube arrangement and the Reynolds number based on the velocity through the narrowest free section.

When a fluid emerges from between the cylinders of the final row in a bank, it tends to emerge in jets. In the wake, these jets diffuse and beyond a certain distance down stream there will be a more or less uniform flow distribution across the wake. Through the diffusion of the jets, a certain amount of static pressure recovery takes place in the wake behind the bank, and this is about complete by the time the uniform flow distribution region is reached.

A wall tapping, however, situated close behind the bank could read any of a range of pressures, depending upon whether the fluid passing over it was in a jet or the more stagnant fluid between jets. Therefore, the pressure tapping down stream of the bank should be situated far enough from the bank and placed where the uniform velocity is reached indicating that the pressure recovery is about complete.

In generalising the experimental results, the choice of the nominal velocity to calculate the friction factor and number of rows to which pressure drop is related is of considerable importance. The maximum flow velocity passing through the smallest gap or the average main flow velocity could be used. In most of the investigations, the/...



the maximum velocity is adopted as a reference velocity.

It has long been recognised that the size and spacing of tubes in a staggered bank will affect the hydraulic resistance encountered by fluid flowing across the tubes in the bank. The available literature shows that Chilton and Generaux (106), in 1933, suggested a relationship for calculating the pressure drop in a tube bank. They noticed that the ratio of friction factor of a tube bank to a single cylinder is increased in proportion with the transverse pitch ratio in the bank. Consequently, they concluded that the transverse pitch is the controlling dimension in the pressure drop data. This conclusion was used as a basis for their correlation. Assuming that the flow across the bank resembles that through a series of orifices, the pressure drop is therefore caused by successive  $N$  contraction and expansion in addition to the surface friction loss. They expressed their correlation in the classic form of the general Fanning equation for flow inside tubes and it reads as follows :-

$$\Delta P = 4 f N \left( \frac{1}{2} \rho U_{\max}^2 \right) \quad 4.3.$$

$$\text{where the friction factor } f = C (Re_{\max})^n = 0.75 (Re_{\max})^{-0.2} \quad 4.4.$$

Here  $Re_{\max}$  is the Reynolds number based on the maximum velocity through the bank and the transverse gap between adjacent tubes in a row (i.e. T-D). In applying such a correlation it was appreciated that it did not show the effect of the longitudinal spacing on the calculated pressure drop. Later in 1937 Pierson (107) carried out an extensive/...

extensive study on a large number of tube arrangements, using small scale model banks for both convective heat transfer and hydraulic resistance with gaseous fluids. For Reynolds number between 2000 and 40000, thirty-eight tube arrangements with different pitch ratios were tested. He found that friction factors varied with the Reynolds number to a power index ranging from 0.2 to about -0.3. Moreover, for specific Reynolds number, the friction factor varied markedly with changes in tube arrangement. Pierson indicated that while the friction factor remained constant or decreased slightly as Reynolds number was increased, the tube arrangements influenced the absolute value of the friction factor. To complete the picture obtained by Pierson, Huge (108) investigated the effect of tube size on heat transfer and flow resistance for different tube bank arrangements. Over a Reynolds number range from 2000 to 70000, three tube sizes were tested using six tube arrangements, two staggered and four in-line banks. Similar to Pierson's results, Huge found that the friction factor was not only related to the Reynolds number but varied with the tube arrangement. Furthermore, Huge showed that results obtained from small scale and full scale apparatus were in good agreement which implied that the effect of tube size was negligible.

The data obtained by Pierson and by Huge was analysed by Grimson (109) who gave a summary of their experimental results on heat transfer and pressure drop across exchangers in relation to transverse and longitudinal spacing in terms of tube diameter and tube arrangement for  $2000 < Re < 40000$ ./...



$Re < 40000$ . Grimison presented his correlation in a graphical form of charts in which parameters such as Reynolds number (based on tube diameter) pitch ratio and friction factor, were drawn.

Because it is sometimes difficult to use the graphical correlations, Jakob (110) developed expressions to correlate Pierson's and Hoge's data for different tube arrangements. As far as staggered banks are concerned, the correlation reads :

$$f = (Re)^{-0.16} \{0.25 + 0.1175 (T-1)^{-1.08}\}^{4.5}.$$

This formula is not applicable to a bank in which the minimum free area is that through the diagonal slit between succeeding rows of tubes. It is obvious that this correlation is valid only over the same flow range used by Pierson and Hoge, in other words, up to Reynolds numbers of 40000. It should be noted that this formula is a function of the transverse pitch,  $T$ , rather than the longitudinal pitch,  $L$ , whose effect was reported to be restricted to the in-line tube arrangements. As Pierson and Hoge used ten row banks to realise their data, a correlation like that of Jakob which is based on their work is only strictly applicable for banks having that number of rows.

Jakob found that his correlation was in a good agreement with the experimental results of Pierson over a range of spacing between the tubes up to  $T = L = 3$  except for transverse/...



transverse spacing ratio of 1.5 with the staggered arrangement. For this pitch ratio, Dwyer and Coworkers (112) used the following expression which was reported to be in a good agreement with their results of  $T = 1.5$ , the expression reads :

$$f = (Re)^{-0.15} \{0.23 + 0.11 (T-1)^{-1.08}\} \quad 4.6.$$

This formula was used for a Reynolds number which exceeds the range originally investigated by Pierson and Huge.

Jakob's correlation for calculating the pressure drop in in-line and staggered arrangements were criticised by Gunter and Shaw (111) who proposed a simple single correlation for an arbitrary tube arrangement in cross flow. The correlation covers both isothermal and non isothermal cases and reads:

$$\frac{f}{2} = \left( \frac{\Delta P}{\frac{1}{2} \rho U^2} \right) \frac{DV}{L} \left( \frac{M}{\mu \omega} \right)^{0.14} \left( \frac{DV}{T} \right)^{-0.4} \left( \frac{SL}{T} \right)^{-0.6} = \phi (Red) \quad 4.7.$$

where the friction coefficient for the turbulent flow,  $Red > 200$ , is calculated as follows

$$f = 1.92 (Red)^{-0.145} \quad 4.8.$$

To apply the above formula for non-isothermal flow conditions, the fluid properties were calculated at the average flow temperature. The arbitrary bank term  $SL$  is defined as the centre-to-centre distance from a tube in one row to the nearest tube in the next row transverse to flow. The two characteristic/...

characteristic dimensions which appear in the correlation were  $L$  the fluid flow length and the volumetric hydraulic diameter  $DV$  which was defined as:

$$DV = \frac{4 \times \text{net free volume}}{\text{friction surface}}$$

Gunter and Shaw claimed that their correlation has a deviation from the data of Pierson in the order of magnitude, in general, of not more than 10 or 15 per cent. Indeed this was very similar to the deviation in Jakob's correlation as pointed out by Boucher and Lapple (113) who found that Grimison's graphical correlation and Jakob's formula represented Pierson's data fairly well with an average deviation of 13 per cent for staggered arrangements.

In 1950, Bergelin et al (114) carried out investigations using three different tube arrangements in cross flow with different tube sizes and pitch ratios in seven banks. They obtained data upon the effect of tube size and spacing in the region of viscous flow. These data for Reynolds number up to a thousand were correlated well by using the Gunter and Shaw formula. From this data Bergelin et al concluded the following :-

- a) at constant flow velocity for a given arrangement and tube size, the pressure drop is lower when pitch is increased.
- b) at constant flow velocity for a given arrangement and pitch ratio, the pressure drop is lower when the tube diameter increased.

Later/...



Later, the range of these investigations was extended up to  $Re = 6000$  by Bergelin et al (115) in 1952. Data was obtained for five tube arrangements using oil as the shell side fluid and isothermal tests. Their graphical correlation is reproduced by McAdams (116).

One of the most extensive investigations, as far as the pressure drop is concerned, was carried out by Zukauskas (105). He measured the rate of reduction of the friction factor with Reynolds number and gave a prediction of its value over a wide flow range which exceed the Grimison's 40000 up to  $2 \times 10^6$ . His pressure drop measurements covered fifty-three different banks in cross flow of air and other fluids such as transformer oil and water. These measurements suggested that the resistance encountered by the flow was mainly influenced by the amount of free space between the tubes in the bank which was determined mainly by the transverse pitch and the bank resistance increases with a decrease of this pitch.

On increasing the longitudinal pitch ratio  $L$ , the larger space between two neighbouring rows permits the formation of vortices, which in many cases affects the resistance of the bank. Moreover, the pressure drag of tube in the bank is highly affected by the longitudinal pitch due to its effect on the pitch along the diagonal of the bank which applied for transverse pitch ratios less than 2. Here a decrease of the longitudinal pitch involves a decrease of the free section along the diagonal and this reflects on the hydraulic resistance of the bank.



Zukauskas (105) presented his measurements for the pressure drop across banks of tubes in a group of charts which gave the overall Euler number, four times the friction factor, as a function of Reynolds number, tube arrangement and tube spacing. His results are presented by the Euler number referred to one row or to a bank of ten rows.

The effect of the ratio between transverse pitch and longitudinal pitch was investigated by Stasjuljawschjus et al (117). Their results indicated that the friction coefficient for deep banks decreases with an increase in the Reynolds number and at  $Re > 2 \times 10^5$  it became independent of the Reynolds number if the ratio  $\frac{T}{L}$  was less than 1.7. For this arrangement this independence on  $Re$  being abrupt.

It should be pointed out that the pressure drop across the bank is affected by the entrance and exit conditions of the bank. Moreover, with a decreasing number of rows in the bank, these conditions contribute more to the total loss of kinetic energy of the incident stream. Inside the bank, the entrance conditions can continue to affect the flow characteristics around tubes in the first few rows in the bank. This is supported by the measurements obtained by Pearce (104) for flow velocities within the bank. He found that the velocity in the longitudinal gap decreased from the first row to the second row. From the third row onward he measured no further changes in the velocity and its value was slightly higher than the nominal gap velocity./...

velocity.

A good survey of the characteristics of different tube arrangements is given by Kays and London (118) and by Boucher and Lapple (113).

#### 4.1.7. Pressure drop in non isothermal cross flow

In determining the friction factor for non-isothermal flows from isothermal data, allowance should be made for the variations of fluid's physical properties, e.g., viscosity, in the boundary layer at the model surface. It was in 1936 when Sieder & Tate (119) found that, for non-isothermal flow in pipes, the pressure drop could be calculated by applying a viscosity correction factor to the data obtained from isothermal flow at the same mixed mean temperature. The correction factor was the ratio of viscosity in the flow to that calculated at the wall temperature raised to power index of 0.14. The deviation of the non-isothermal data from that of isothermal flows was also noticed by Omohundro et al (120). In 1949, they carried their investigation to study fluid friction and heat transfer in idealised models and in commercial tubular heat exchangers at low range of Reynolds number using oil as a flowing medium. They attributed this deviation between isothermal and non-isothermal data to the increase in the frictional resistance caused by the colder surface of the tubes in the exchanger raising the viscosity of the fluid in contact with them. They tried two different viscosity correction factors in an effort to correlate their non-isothermal data with that of an isothermal flow condition. The first correction factor tried, was that/...



that recommended by Sieder and Tate as  $(\frac{\mu}{\mu_w})$  raised to the power 0.25. The second factor was that recommended by Gunter and Shaw (111) as  $(\frac{\mu}{\mu_w})$  raised to power 0.14. The results from these corrections were not satisfactory. Consequently, Omohundro and Coworkers concluded that a single viscosity ratio correction factor was not adequate for their correlation. Moreover, they recommended that the  $\frac{\mu}{\mu_w}$  ratio should be some function of the flow rate. Their line of investigation was continued by Bergelin et al (121) using a similar medium, oil flowing across three vertical tube arrangements. They tested three once-flow through units with equilateral triangular in-line tube arrangements and a staggered square bank. It was indicated that variations of fluid properties occurring with heat transfer caused the physical properties at the tube wall to differ from those within the main body of the flowing medium. Furthermore, they showed that the degree of increase in pressure drop in the non isothermal cases appears to be a function of the ratio of the bulk medium viscosity to the viscosity at the tube wall. It is also an inverse function of the Reynolds number. Accordingly, they suggested a correction term for the viscosity ratio raised to the power 'n', where 'n' was required to bring the friction factors for non-isothermal cases into an agreement with the isothermal friction factors. The functional relationship related the index 'n' to the flow Reynolds number and took the following form:

$$n = 0.56 - 0.16 \log Re$$

4.9.

This/...



This index was found to be in agreement with that reported by Bergelin et al (114) who introduced another form for the index 'n' for the lower range of Reynolds number as a first estimation of the viscosity ratio correction in both cooling and heating flow conditions. The relation reads as follows :

$$n = 0.57 \text{ Re}^{-0.25} \quad 4.10.$$

Later in 1952, Bergelin et al (115) from measurements taken across five tube arrangements for Re up to 10000, indicated that such index relationship were not fully adequate for both heating and cooling flow conditions. Indeed, the index 'n' for the viscosity ratio should be different for heating and cooling and should be a function of the flow Reynolds number.

#### 4.1.8. The effect of condensation on pressure drop in tube banks

Apart from the entrance region of the bank, the pressure drop in a non-condensing flow across a tube bank varies almost linearly with the number of tube rows. Whereas, in the case of a condensable medium, the pressure drop is expected to vary non-linearly with the tube rows due to the variations of the mass velocity through the depth of the exchanger.

In recognising the above situation, Guy and Winstanley (122) correlated their pressure drop data, obtained from a number of commercial condensers, with some equivalent or average velocity/...

velocity which reflected the effect of varying the steam mass velocity through the tube bundles due to condensation. However, the applicability of their data was limited due to the fact that the condenser loads have increased many fold since the time of their investigation. Nowadays, steam loads for moderate commercial condensers can go up to about  $0.012 \text{ Kg/m}^2\text{.sec.}$  (242).

Extensive studies were carried out by Diehl (123) and Diehl and Unruh (124) on four tube arrangements using different flow mediums, e.g., air, methane vapour and pentane vapour for Reynolds number up to  $1.5 \times 10^6$ . They showed that pressure drop for condensable gases could be predicted by using a two phase correlation. In this way the predicted values were within a maximum deviation of  $\pm 30$  per cent of the test data. Although these investigations were fairly comprehensive ones, it was not indicated clearly whether condensation reduces the resistance encountered by the flow across the tube banks tested. The effect of condensation on pressure drop in a down flow across the tube bank was also demonstrated by Chisholm and McFarlane (125). They adopted Faks's view (126) in that the pressure drop across the bank can be calculated by subtracting the kinetic energy pressure change which was calculated neglecting the kinetic energy of the condensate from the isothermal data. Of course, that does not represent the actual case, however, it could be used to provide a first estimate for the pressure drop in condensable gases.



Fujii et al (127) measured heat transfer and hydraulic resistance of low pressure, saturated steam which passed horizontally across different tube banks. Both in-line and staggered tube arrangements with equal spacing ratio of 1.5 were tested. They showed that the flow resistance encountered in a staggered bank was twice as much as that experienced through an in-line arrangement. More importantly, Fujii et al suggested that condensation may reduce the pressure drop in the same way as suction of the boundary layer would do for an external flow across a cylinder and this effect is greater for in-line than for staggered banks.

In an effort to study the hypothetical similarity between condensation and suction effect, Drummond (72) investigated the flow characteristics in a condenser model tube bank arrangement. Condensation on the tube surface was simulated, ignoring the effect of condensate, by mass extraction through porous test tubes. His result showed that a reduction in the pressure drop was only recorded at high extraction rates. Consequently, he concluded that condensation or mass extraction reduces the pressure drag and the higher the extraction rate the greater the reduction in the pressure drag.

Bearing in mind that the extraction rates used by Drummond reached 13.5 per cent of the inlet flow to the working section of the tunnel, for single cylinders, it is not clear whether the reported reduction in the pressure drag was due to a reduction in the friction losses, such as flow inside pipes, or due to a reduction in the pressure drag/...



drag around the cylinder.

In 1973, Morsy (57) investigated the effect of condensation on pressure drop following Drummond's experiments as a guide line. He used a staggered tube arrangement of equal spacing type and condensation was aerodynamically simulated by air extraction through a perforated copper plate fitted to the experimental cylinder. The inner side of the plate was covered with canvas cloth to increase the pressure drop across the plate relative to the circumferential pressure variations. Air was sucked through staggered holes 0.75 mm dia. and 6.35 mm apart which gave the surface an average porosity of about 1 per cent. Morsy reached a suction velocity to main stream velocity ratio of 16 per cent and concluded that by mass extraction, for typical condenser range, a reduction of up to 30 per cent of the pressure drag could be achieved. As was stated by Morsy (128), the suction rates in his experiments were measured by a rotameter which was calibrated at normal pressure and temperature with no allowance for the pressure drop across the cylinder wall. Due to the nature of the perforated wall beside its low porosity, the pressure drop across the wall might have been considerable and the rotameter readings should have been corrected for the pressure drop across the wall. Without such correction the suction ratio reported by Morsy might be overestimated.

On the other hand, the pressure drag in Drummond's investigations was obtained using a normal pressure tapping/...

tapping drilled through the porous wall of his test cylinder. Due to reasons given in section 5.2.3. the reported results might be over estimated because of the stagnation effect.

#### 4.1.9. Reynolds flux model and pressure drop across tube banks

Available methods for predicting the pressure drop of condensable gases, are quite limited. One approach which attracted many investigators, is the possibility of such prediction using the Reynolds flux model.

As early as 1874, Reynolds (129) pointed out the nature of connection between heat transfer and surface friction in a pipe through which a turbulent fluid stream is passing. He assumed that the momentum and heat are transferred within the fluid in the same way. Moreover, the lateral mass flux responsible for the momentum transfer to the surface of the pipe is proportional to the lateral flux responsible for the heat transfer process assuming that the turbulence extended to the pipe walls.

Later in 1916, Nusselt (130) extended the application of Reynolds concept to combustion process of solid fuels. He assumed that the burning of a carbon surface in a gas stream was controlled by the rate of mass transfer of oxygen to the surface during the combustion process. On a similar line of thinking, Silver (131) put forward the assumption that all the oxygen molecules transported to the surface entered into a reaction with the carbon surface. Applying the Reynolds concept for this case, with/...



with complete combustion, Silver reached a simple relationship for the reaction rate at the solid fuel surface.

Silver (132) extended his applications for the Reynolds concept and showed theoretically that it was possible by condensation to recover the inlet kinetic pressure head. But this theory was based on flow over flat plate, conditions under which Reynolds concept is easily applicable, i.e., where the pressure drop is mainly caused by the frictional drag.

Indeed, the application of the Reynolds concept to processes involving mass and heat transfer at a surface or a phase interface has been the subject of quite a number of publications. Some of them are those of Silver (133), Spalding (134), Silver and Wallis (135), Wallis (136, 137) and Sherwood (138).

When Silver (132) extended his theory to a bank of tubes, an inconsistency arose from the fact that the resistance encountered by the cross flow over the bank consisted not only of frictional drag but to a much greater extent of pressure drag. At this point, Simpson (141) indicated that the analysis given by Silver, according to Spalding's theory, was valid only for flows over flat plates where the Reynolds concept is applicable. In other words, for flows with no pressure gradient in the stream direction tangential to the surface.

Nevertheless, Silver (139) mentioned that his theory for banks/...



banks of tubes could still be fruitful, by assuming that the modifications of the flow over a bluff body will modify the pressure drag to a reduced value in the same way as the skin frictional resistance is changed.

On the other hand, Drummond (140) continued Silver's line of thinking but adopted a different point of view. He suggested that the total pressure drop for condensing gases could be calculated by adding the pressure drag completely unmodified by condensation to the frictional resistance as modified by condensation. Furthermore, he came to the conclusion that a pressure recovery in the condenser would not be possible until the steam velocity was reduced to a very low value where the situation will be far from practice and the magnitudes of pressure drop are unimportant.

Drummond reported pressure recoveries of the order of half the inlet kinetic head when all the flow passes through the working section was extracted through the porous cylinder which was fitted with 0.8 mm dia. wire at its rear stagnation point.

In spite of that, Morsy (57) tried to apply the Reynolds concept to the case of a cross flow over tube bank. He made use of the Blasius solution (142) for shear stress on flat plate and the boundary layer thickness,  $\delta$ , for flow on flat plate to define the Reynolds flux,  $\epsilon$ , as follows :

$$\epsilon = 1.66 \mu / \delta$$

Whenever/...

Whenever a pressure gradient does exist, the momentum equation was used neglecting the inertia effects.

Assuming that the velocity profile in the boundary layer is geometrically similar (there exists a function of one variable). He expressed the velocity distribution using a power series of that function.

Morsy made the assumption that the boundary layer thickness at point X on the cylinder surface is given by:

$$\delta = \beta \sqrt{\frac{v x}{U_{\infty}}}$$

with  $\beta$  chosen to be 1.56. However, in the text there was no justification for this value of  $\beta$ , and it seems that it may have been chosen to fit some of his experimental results. However, that does not seem to be the case. In reviewing this theory, Milne (143) found that the constants in Morsy's shear stress expression were indeed varying around the cylinder surface.

#### 4.1.10. Pressure drop in cylindrical banks of tubes

In the preceeding sections, most of the investigations mentioned were carried out using rectangular cross sections containing the tube banks. This situation is not commonly used in practice and instead the tube bank is in the form of a bundle which is enclosed within a cylindrical shell. Under these conditions, the flow configurations are expected to be different from those in a rectangular working section.

In such banks, cylindrical type, the flow free area across the/...

the bundle varies from one row to the other and some sort of a mean effective area must be used in order to utilise the available pressure drop data obtained from rectangular banks of tubes. To facilitate this utilisation process, Emerson (144) developed an expression for calculating the mean effective area rather than using the arithmetic mean area of the bundle. Emerson's formula for the effective area across the cylindrical shell reads as follows :-

$$A_p = \frac{N}{\sum_{1}^N (AZ)^{-2}}^{0.5} \quad 4.11.$$

where AZ is the effective area at the Zth row of tubes.

That expression was based on a similarity between different rows in the bundle which is not strictly true; however, it can be used as best available for first estimation of the flow effective area across tube bundle in a cylindrical shell.

## 4.2. Heat transfer in cross flow

### 4.2.1. Introduction

The process of heat transfer from a circular cylinder in cross flow is determined mainly by stream velocity, physical properties of the flowing medium, heat flux intensity, direction of heat flux and the geometrical surroundings in the neighbourhood of the cylinder. The dimensionless functional relationship for this process reads :

$$Nu \equiv f (Re, Pr, \frac{\mu'}{\mu_w}, \frac{K}{K_w}, \frac{CP}{CP_w}, L, T) \quad 4.12.$$

where/...



where L and T define the longitudinal and transverse configurations in the cylinder surroundings relative to the main flow.

Normally this form of relationship is not used and a power equation is used instead as follows :-

$$Nu = C Re^n Pr^m \quad 4.13.$$

where constants C, n and m are functions of the main flow characteristics, i.e., whether it is subcritical or critical flow. For gases of constant Prandtl number the equation becomes ;

$$Nu = C Re^n \quad 4.14.$$

Variations in the flow pattern around the cylinder might lead to changes in the power indices in the previous expression. Since the surface temperature gradient affects the thermal boundary layer thickness. Variations in the surface temperature result in differences in the heat transfer coefficient compared to those calculated for a constant wall temperature. The boundary layer thickness varies under the influence of a surface temperature gradient, causing corresponding variations in the heat transfer coefficient which is inversely proportional to the thickness of the thermal boundary layer.

The effect of heat flux direction will manifest itself in a viscosity gradient at the surface. According to Drew and Ryan/...

Ryan (145) it is impossible to expect that the velocity distribution in the boundary layer at the cylinder surface be the same under non-isothermal as under isothermal conditions. For the case of heating air, for instance, the effect of the varying fluid viscosity in the boundary layer may result in a decrease in the velocity gradient as the wall is approached. Consequently the velocity distribution in the laminar layer, or sublayer, should be a curve and not a straight line. Indeed, the effect of the heat flux direction on the flow characteristics was also noticed by Bergelin et al (115) when they could not correlate their pressure drop data for heating and cooling conditions using a single viscosity correction factor. As a result, they recommended different correction factors for heating and cooling conditions.

One of the main difficulties encountered in the calculations of the heat transfer coefficient (equation 4.14) is the choice of a reference temperature at which the physical properties are to be evaluated. Normally, this is done according to one of two methods as appropriate. The first method is to evaluate the properties at the main flow temperature and introduce a compensating parameter in the heat transfer formula to account for the properties variation. This method was used by Perkins and Leppert (82) who accounted for these variations by using a viscosity ratio with an appropriate exponent similar to that proposed by Sieder and Tate (119). The second method, is to evaluate the physical properties at a chosen temperature between that of the main flow and the cylinder wall.



It is a common practice, for a bundle, to correlate heat transfer in the bundle using one of the previous expressions, against the flow velocity in the narrowest free cross section, that is to the maximum Reynolds number in the bundle.

#### 4.2.2. Heat transfer of a single cylinder in cross flow:

It is apparent that a knowledge of the peripheral variation of the rate of heat transfer from the surface of cylinders to a fluid flowing transversely, is necessary for the successful design of heat exchangers.

The complexity of the flow pattern around a circular cylinder has been recognised for a very long time. The same could be said about the mechanism heat transfer around a cylinder. Experimental investigations have led to the development of expressions describing the variations of the average heat transfer coefficient (191) and the variations of the local heat transfer coefficient around the forward part of the cylinder (103).

While it is possible to analyse, on a theoretical basis, the flow characteristics on the front portion of the circular cylinder using the boundary layer theory (146), the flow beyond the point of flow separation in the rear portion of the cylinder is a vortical one which is difficult to analyse on theoretical grounds. This difficulty is connected with the difficulties of determining the local velocity at the rear of the cylinder and the unavailability of a detailed description of the flow details in the circulation/...



circulation region. Moreover, heat transfer at the front stagnation point and separation region has some peculiar features.

However, the flow mechanism in the rear part of the cylinder in cross flow has drawn the attention of a number of investigators, e.g., Petrie (147). The first known measurement of the flow velocity in the circulation region was that carried out in 1913 by Morris (148). He used a hot wire anemometer to explore the region in the vicinity of a circular cylinder in a cross flow. Because the hot wire could not show the direction of the flow he could not tell too much about the flow mechanism in the circulation region. However, by plotting his measurements on a polar plot, the velocity distribution around the cylinder looked like a butterfly with low velocities at the front, sides and back of the cylinder and high velocities at intermediate points. The circulation region was noticed also by Drew and Ryan (145) in 1931 through photographic pictures. They observed that the fluid motion in the rear of the cylinder was opposite to that in the main flowing stream. Giedt (43) tried to measure the magnitude of velocity in that reversed flow using a surface tube. Due to the high flow fluctuations in this region, he was not able to obtain velocity measurements in the circulation region. Andreas Acrivos et al (150) and Grove et al (149) used a stroboscopic air bubble tracer technique to investigate the back flow at the rear of the cylinder. They indicated that after the vertical path was established behind the cylinder, for Reynolds number more than 25, the pressure coefficient at the rear remains unchanged as the Reynolds number increased.

Under/...

Under these circumstances, the maximum back flow velocity within the circulation region reached a finite limit which lay approximately between 30 to 50 per cent of the velocity in the undisturbed flow. Moreover, it was indicated by Petrie and Simpson (98) that, in the circulation region, there was an opposite flow which has a boundary layer with constant thickness over the area from  $\theta = 140^\circ$  to  $180^\circ$  measured from FSP at  $Re = 35000$ . As indicated by Sogin (151), the effect of such strong eddies at the rear was to cause a large proportion of the temperature drop between the wall and the fluid to occur in a very thin layer near the wall.

In order to facilitate calculations of heat transfer at the rear of the cylinder, Matsui (152) proposed the following correlation:

$$Nud = 0.229 Re^{0.63} Pr^{0.4} \left\{ 1 - \left( \frac{180-\theta}{90} \right)^2 \right\} \quad 4.15.$$

He attributed the high heat transfer at the rear of the cylinder to the existence of a strong reverse flow in this region. This expression is similar to that developed by Sogin (151) for the wake of all the configurations he tested except that the constant value was 0.2 and the Reynolds number index was 0.66.

The effect of the wake region on the heat transfer from the cylinder in cross flow was also recognised by Boulos and Pei (85). They indicated that the wake, was, in fact, subdivided into two distinct regions, the secondary vortex region which covers the area after the separation point until/...



until about  $\theta = 130 - 150$  degrees. The rest of the rear of the cylinder was the main vortex region. They stated that these two regions had different heat transfer characteristics and separate heat transfer contributions from these regions should be considered. To account for these separate contributions, they recommended the following expression for heat transfer in the wake region:

$$Nu_w = a Re^K + b Re^E \quad 4.16.$$

where the first term on the r.h.s. represents the contribution of the secondary region, while the second term the main vortex region in the wake. The value for the constant  $E$  was chosen to be 0.67 while constant 'b' was a function of the free stream turbulence conditions.

Fand and Keswani (153) utilised the available data and developed a correlation equation for heat transfer from circular cylinders to air in cross flow for Reynolds number range from  $10^{-2}$  to  $2 \times 10^5$ . The correlation reads as follows :

$$Nu \psi = C_0 + C_1 Re^{0.5} + C_2 Re^X \quad 4.17.$$

Here the properties were calculated at the mean film temperature while  $\psi$  was the ratio between mean film and ambient absolute temperature raised to power -0.17. The constant  $C_0$  accounts for the total heat transfer from cylinder by free convection and is equal to 0.184. The second term on r.h.s. represents the convective heat transfer to the boundary layer prior to the separation point while the/...



the third term represents the heat transfer by convection from the rear of the cylinder. Values for the index 'X' were a function of the Reynolds number as follows :

$$X = 0.247 + 0.0407 \text{ Re}^{0.168}$$

In general, at low Reynolds number, as long as the vertical path is formed at the rear of the cylinder, the coefficient of heat transfer drops from its value at the front of the cylinder to reach a minimum at the rear portion of the cylinder.

For higher values of Reynolds number, the vortex shedding favours the access of a fresh cold mass of fluid, for cooling conditions, to the cylinder surface. Consequently the coefficient of heat transfer reaches its minimum around the separation point and then increases downstream in the vertical region at the rear of the cylinder. The improvement of heat transfer in the circulation region is due to the increased transverse exchange of fluid in the separated region. The strength of eddies in this region is clear from the measurements taken by Matsui (152) who showed that, for Reynolds number of 27000, the root of the time mean square of the oscillating flow in the wake was found to be about 50 per cent of that in the mainstream velocity. In fact, these measurements were confirmed by the earlier observation of Acrivos et al (150).

At relatively low Reynolds numbers,  $\text{Re} < 8000$ , the heat transfer at the front is higher than that in the rear (154).  
With/...

With increasing Reynolds number,  $Re > 20000$ , the heat transfer in the vortical region increases and eventually at  $Re > 40000$ , the maximum heat transfer occurs at the rear instead of the front of the cylinder.

#### 4.2.3. Turbulence and heat transfer at single cylinder

It was recognised by many research workers that heat transfer from a circular cylinder in a cross flow is influenced by the turbulence in the mainstream. In fact, the effect of turbulence in the incident flow is to cause transition in boundary layer and wake at a lower Reynolds number than normal. The higher the Reynolds number the closer is the boundary layer to becoming turbulent and the lower the incident flow turbulence required to induce this transition. Once transition has been induced by the incident turbulence, the effect of increasing the turbulence level further is relatively small.

As heat transfer is affected by a modification of flow in the boundary layer and wake, its value is expected to increase considerably by increasing the turbulence level in the incident stream. This was observed as early as 1925 by Reiher [155] who reported an increase in the rate of heat transfer of 50 per cent in a highly turbulent stream compared to a low turbulent one.

The location of the cylinder relative to the turbulence generator has a significant effect on the heat transfer characteristics from the cylinder. Almost all grid generated turbulence is anisotropic in nature, being at best/...



best homogenous in planes parallel with the grid before the influence of the cylinder model takes place. A source of inaccuracy arises when the cylinder is placed too close to the turbulence generator. Here the velocity field is not uniform and it is not possible to separate the combined effects on the heat transfer of non-uniform flow and turbulence. The minimum distance that can be safely used is a complicated function of the mesh length and dimensions of the coils in the grid.

In the region where the distance from the turbulator is less than 10 mesh lengths, the turbulence intensity would not be homogeneous and its magnitude would vary greatly over the diameter of the cylinder (156).

While it was reported by Kestin and Wood (157) that the turbulence intensity and not the turbulence scale was the dominant variable, it was mentioned by Petrie and Simpson (98) that the turbulence scale, linked with the cylinder diameter, might have some effect when different sizes of cylinder were used. Indeed it was shown by Zignen (99) that the Nusselt number was a function of the Reynolds number, turbulence intensity and the ratio between the scale of turbulence and cylinder diameter. At a constant Reynolds number and turbulence intensity, Zignen showed that heat transfer varied with increasing turbulent scale to diameter ratio increasing to a maximum value when the ratio was about 1.5 to 1.6 and then decreasing. This was explained by assuming that at the maximum value of the heat transfer some effective frequency of turbulence coincided with/...



with the frequencies of the transition eddies which result in an interaction between the wake motion and the induced oscillation.

A similar explanation was provided by Petrie and Simpson (98) when they reported that the improvement in heat transfer in the wake was the result of a resonant interaction between the wake motion and the free stream fluctuations.

The effect of turbulence level on the heat transfer characteristics of a cylinder in cross flow was one of the topics which attracted the attention of a large number of investigators. In 1948 Cummings and Coworkers (158) carried out their investigations to study the variations of the overall heat and mass transfer ratio from circular cylinders in a crossflow of air stream. Two cylinders were used for the heat transfer experiments, one cylinder was steam heated and the other was electrically heated over a range of Reynolds number from 400 to 20000. They found that at constant  $Re$ , increasing the turbulence level in the incident stream caused a maximum of 25 per cent increase in the rate of heat transfer. They also noticed that the influence of turbulence was more pronounced at higher  $Re$  while its influence was either small or negligible at smaller Reynolds number. They concluded that the effect of turbulence level on the Nusselt number, for Reynolds number more than 1750, could be expressed as follows :-

$$Nu = 25.6 \left( \frac{Re}{1750} \right)^n$$

where the index  $n$  is a function of the turbulence level.

$n = 0.63 - \frac{0.07}{T.L.\%}$ . Beside its effect on increasing the Nusselt number, it was shown that turbulence had an effect on the movement of the separation point and a change of flow mechanism in the separated region. Indeed the increase in the local flow parameters with turbulence level was consistent with an effective increase in the  $Re$  as shown by Surry [193]. On the other hand, he was not able to detect variations in the separation point due to its continuous oscillation.

Giedt (43) investigated the effect of turbulence intensity from 1 to 4 per cent, on the local heat transfer and skin friction around cylinders in a cross flow of air. In agreement with the previous investigators, his measurements showed that turbulence produced results characteristic of velocities higher than those indicated by the free stream velocity. But as he reported, at the stagnation point and up to approximately  $\theta = 8^\circ$ , with a high turbulence level, the readings of his skin friction probe, surface tube, were negative with reference to the local static pressure. As this might mean a flow opposing the main stream at the front of the cylinder, Giedt omitted the skin friction results in that region. This was attributed to the possibility that the original rise in dynamic pressure in a turbulent air stream due to the turbulent velocity fluctuations was registered on the static pressure tapings but not on the surface tube at the front of the cylinder. If this was the case, this would make it difficult to compare Giedt's results with other investigators. Moreover, it will leave the/...



the higher dynamic head registered by Surry (193) with reference to the local static pressure, under high turbulence intensity, unexplainable. On the quantitative side of the experiments, Giedt indicated that an increase of the heat rate of 10 to 20 per cent was recorded by increasing the turbulence level in the incident stream. Furthermore, the relative amounts of heat transferred from the front and back halves of the cylinder varied with increasing the turbulence level.

For low turbulence levels the ratio of the front to back half of the cylinder heat transfer was measured by Giedt to be about 85 per cent while this ratio increased to about 110 per cent with a higher level of turbulence. Giedt attributed this to both increase of heat transfer on the front half and to a decrease on the back half of the cylinder. In fact, if one assumes that increasing the turbulence is in a way equivalent to an increase in the flow Reynolds number, which has been agreed upon by most of the previous investigators, then the changes in the front to back half heat transfer ratio measured by Giedt cannot be explained. Because, in comparing these ratios and the reasoning for them given by Giedt with other results, for example, Schmidt and Wenner (162) and Fand and Keswani (153), it is possible to notice that for higher Reynolds number, the contribution for the rear portion was increased. On the other hand, the increase in the local heat transfer rate at the FSP by 25 per cent by increasing the T.L. up to 4 per cent reported by Giedt was also recorded near the FSP by Smith and Kuethe (160). They reported an increase of the local heat transfer of 70 per cent by increasing the T.L. from 0.1 to 6 per cent for  $Re = 240,000$ .



Some other investigators relied on experiments in which the heat transfer coefficient was determined by an analogy between heat transfer and mass diffusion. This analogy is based on the similarity of the differential equation governing diffusion to that applying to thermal conduction. That is done usually using the equations of Chilton and Colburn (161) relating heat and mass transfer coefficients to the 'j' function in moving media. A method which according to Schmidt and Wenner, (162), is afflicted with sources of error.

However, this method was used by Kestin and Wood (157) to study the effect of freestream turbulence on the local heat transfer inferred from mass transfer measurements of a 2.4 m thick layer of Paradichlorobenzene coated on a 101 mm diameter plexiglass cylinder in a cross flow of air. They measured the rate of mass transfer by the local reduction of the coating layer thickness. The turbulence intensity was measured upstream of the cylinder at a location which corresponds to 1.5 times the cylinder diameter. At that location, they indicated that the effect of the cylinder presence started to influence the mainstream. Through their measurements, they suggested that even the slightest amount of turbulence could trigger flow instability and results in an increase in the mass and momentum transferred across the boundary layer. This could be attributed to the flow conditions in their experiments, since they carried out the investigation near the critical range of Reynolds number where the required turbulence to cause transition is at a minimum. It was also reported that the effect of turbulence/...

turbulence was to multiply the theoretically predicted values,  $T.L. = 0$ , by a nearly constant factor over the front portion of the cylinder up to  $\theta = 60^\circ$ .

Mizushima et al (159) carried out an investigation which was similar in nature to that of Kestin and Wood (157) but the technique they used was different. They used an electro-chemical method to measure the mass transfer around circular cylinders in a cross flow in a water tunnel over a Reynolds number range from 3870 to 10380. This technique was based on a diffusion controlled electrode reaction and the mass transfer rate was detected by measuring the electric current on a small electrode isolated from the surrounding mass transfer electrode surface. In contrast to Kestin and Wood's observations, they indicated that the effect of turbulence on the local mass transfer became larger with the increase in the azimuthal angle  $\theta$  from the FSP. Since the effect of turbulence increases with increasing  $\theta$ , then it is to be expected that turbulence effect becomes quite large near the separation point and eventually could promote some sort of movement of the flow separation location on the surface.

Mizushima's results showed that the increased turbulent intensity in the free stream caused the separation point to move in the upstream direction. These results are in disagreement with the observations of Zijnen (99) who indicated that by increasing the turbulence level the boundary layer flow penetrates further downstream and the wake of the cylinder more intensely turbulent which results in/...



in an increased heat transfer coefficient.

Richardson (194), stated that the free stream turbulence intensity did not appear to have a major effect upon heat transfer at the rear stagnation point of a bluff body, in distinct contrast with its effect at the forward stagnation point. On the other hand, a recent investigation carried out by Simonich and Bradshaw (195) showed that for a turbulent boundary layer, in zero pressure gradient, the effect of the generated free stream turbulence was to increase the heat transfer by almost five per cent for each one per cent r.m.s. increase of the longitudinal intensity.

These findings contrast with those of Kestin et al (199) who demonstrated that the free stream turbulence does not exert a local effect on the coefficient of heat transfer through a laminar or a fully developed turbulent boundary layer in zero pressure gradient. They showed that the imposition of a favourable pressure gradient over the test plate restored the effect of turbulence intensity on the local rate of heat transfer.

That point was investigated by Petrie and Simpson (98) who investigated the effect of turbulence on heat transfer in the rear region of a cylinder for  $5000 < Re < 35000$ . They demonstrated the sensitivity of that region to free stream turbulence intensity and showed that an increase in T.L. to 10 per cent resulted in improvement of heat transfer of 100 per cent at the rear of the cylinder. Obviously/...



Obviously, such results do not coincide with the observations of Giedt (43) for  $Re = 95000$ . In agreement with Zijnen's results, they showed that the point of minimum pressure and consequently the flow separation point was moved downstream by increasing the main stream turbulence intensity.

Recent investigations (169) suggested that the local heat transfer of a circular cylinder increases considerably with turbulence level in the incident flow. Furthermore, it was shown that the critical flow regime could be established in as low Reynolds number as 39000 by increasing the turbulence level to 11.5 per cent.

Kestin and Wood (198) provide an evidence to show that the flow field in the laminar boundary layer formed in the neighbourhood of the FSP in a two dimensional blunt body is three dimensional in character. Moreover, the effect of free stream turbulence on heat and mass transfer rates from the forward portion of the cylinder, in cross flow, is indirect.

A relationship between the ratio of heat transfer with an arbitrary turbulence intensity to that with zero intensity and the product of the Reynolds number and turbulence level was suggested by Dyban and Epick (169). The relation reads as follows :-

$$\frac{Nu_{\theta \text{ T.L.}} / 0}{Nu_{\theta \text{ T.L.}} = 0} = 1 + 0.01 (Re. (T.L.))^{0.5} \quad 4.19.$$

This/...

This relationship was recommended for the evaluation of the influence of turbulence on heat transfer rate from the FSP up to  $\theta = 60^\circ$ , that is at the base of the laminar boundary layer at the front portion of the cylinder.

Lowery and Vachon (201) presented an equation that enables the stagnation point heat transfer as a function of turbulence intensity to be determined. For the range of  $0 < Tu Re^{\frac{1}{2}} < 64$ , the correlation reads :-

$$Nu/Re^{\frac{1}{2}} = 1.01 + 2.624 \left\{ \frac{Tu Re^{\frac{1}{2}}}{100} - 3.07 \frac{Tu Re^{\frac{1}{2}}}{100} \right\}^2$$

#### 4.2.4. Distribution of heat transfer around single cylinder

Theoretical predictions of the local heat transfer rate at the forward part of the cylinder surface in a cross flow is usually carried out in a form of equation similar to 4.14, calculated using local flow parameters. Using a power distribution to the velocity outside the boundary layer. Frossling (170) developed the following equation:

$$Nu_x = \{0.945 - 0.7696 \left(\frac{X}{D}\right)^2 - 0.3478 \left(\frac{X}{D}\right)^4\} Re^{0.5} \quad 4.20.$$

where  $X$  is the distance along the cylinder's circumference measured from the FSP. It is obvious that such formula yields a maximum heat transfer rate at the FSP which gradually diminishes with increasing distance  $X$ .

On the experimental side of the investigations, there is disagreement among the research workers not only on the local/...

local values but also on the shape of the distribution of heat transfer around the cylinder. The peculiar features of the heat transfer at the front stagnation point will be dealt with in section 4.2.5.

In recognising the difficulties encountered by individual investigators in measuring the heat transfer parameters, e.g., accurate temperature measurements, which might partially explain the large variations in the absolute values of the reported  $Nu$ . The following review is based mainly on a qualitative rather than a quantitative study. As it will be shown in this section, the measurements from different sources are not in agreement even between those realised by the same techniques and this kind of disagreement appears almost for every technique found in the literature.

The first available reported distribution of heat transfer around cylinders is that of Reiher (155) who measured the rate of heat transfer for a non-isothermal cylinder for Reynolds numbers up to 4400. As far as the distribution is concerned, his measurements indicated that there was a maximum in the heat transfer at the FSP which decreased gradually until it reached a minimum at the rear stagnation point of the cylinder. He realised these measurements by measuring the outer surface temperature of a 28 mm O.D. tube carrying cold water with hot air flowing externally across the tube, then the outer surface temperature variations should indicate the variation of heat transfer around the cylinder.



Measurements reported by Drew and Ryan (145) for  $Re = 39600$  around a steam heated cylinder in cross flow of cold air, while their distribution shape agreed with that obtained by Lohrisch (165), it did not agree with that obtained by Reiher. The measured local heat transfer rate, detected by the amount of condensate from various longitudinal internal divisions, showed that it was decreasing from the FSP until it reached  $\theta = 180^\circ$ . They attributed the distribution for the cooling water within his tube or to some peculiarity of air flow existing in the vicinity of the cooled pipe. On the other hand, they attributed the discrepancies between their results and those of Lohrisch which were inferred from the mass analogy technique, to the effects of the hot walls of the cylinder in their investigations upon the velocity field near the sides and rear of the cylinder. By comparing Drew and Ryan's results with those of Lohrisch, it is possible to notice that, under similar flow conditions, the minimum values which are related to the region of separation do not correspond to the same location at the cylinder surface. Consequently, the discrepancies between these two groups of results could be due to the difference in the turbulence levels in both studies. However, this was not mentioned in their papers.

Thomson et al (154) carried out an investigation in which they recorded, for  $Re < 8000$ , a heat transfer rate distribution which agrees with that of Reiher. The rate continuously fell from its peak at the FSP to reach a minimum at the rear stagnation point. Their work had substantiated/...

substantiated Reiher's work and extended it to a higher Re.

Fujii et al (164) predicted a heat transfer distribution around a circular cylinder in cross flow, which was similar to that obtained by Reiher. For Re equal to 60000 they showed that the distribution had a maximum value at the FSP and decreased gradually to reach a minimum at the rear stagnation point.

Petrie and Simpson (98) noticed that the variations in heat transfer around the cylinder in their investigation were not only in magnitude but also in trend at a great discrepancy with other investigators. From the measurements obtained for pressure and velocity together with the heat transfer results, they concluded that their measurements with small gradients around the cylinder appeared the most satisfactory ones. This seems to be the case according to Thomson and Coworkers (154) who found that there was an almost flattening of the distribution when they considered the variation of the heat transfer on the cold side of a water cooled cylinder in a hot air cross flow. They attributed this flattening effect to the lateral conduction of heat due to the circumferential temperature gradient. This effect of lateral conduction was also reported by Cess and Grosh (185) who indicated that such an effect can give results 10 per cent lower than those based on the surface temperature.

In 1935, Small (166) used a surface thermopile to measure the local variations of heat transfer rate around a uniformly/...



uniformly heated cylinder using steam as a heating medium. Small showed that he obtained considerably higher rates by correlating the measurements with his overall parameters and the distribution around the cylinder was quite steep with equal peaks on FSP and at rear stagnation point. On the other hand, Schmidt and Wenner (162) flattened Small's distribution by correlating his measurements against the correlation given by Fishenden and Saunders (167) rather than the parameters measured by Small. It was shown by Schmidt and Wenner that these recorrelated measurements of Small were in good agreement with theirs obtained using an electrically heated strip isolated from the rest of the isothermal surface of the cylinder.

#### 4.2.5. Heat transfer in relation to skin friction around cylinders

The sort of heat transfer rate distribution mentioned in the previous section, apart from the possibility of having some minimum value around the separation point, does not give clear impressions about the relationship between the flow characterised by the skin friction and the heat transfer around a cylinder in cross flow.

In 1931, Fage and Falkner (38) indicated that, provided the flow velocity was sufficiently great for the free convection at the surface to be ignored, there was a linear relationship between the heat rate and the square root of the mainstream velocity for constant  $\theta$  ( $\theta < 60^\circ$ ). With and without a turbulator in the tunnel, they recorded a/...



a heat transfer rate distribution which showed a trend that might be coupled with that of the skin friction distribution in the area between the FSP and the flow separation point.

For Reynolds numbers in the subcritical range, the heat transfer distribution was a relative minimum at the FSP, following the skin friction trend. This minimum gradually increased until it showed maximum value about  $\theta = 50$  degrees, in the region where maximum skin friction was recorded. Thereafter, the rate of heat transfer, decreased to reach a minimum around the region where the skin friction reached zero indicating the position of flow separation on the cylinder circumference. Whenever there was a transition from laminar to turbulent boundary layer which manifests itself by a drop in the skin friction followed by a sharp rise, that was also shown on their measurements of heat transfer being characterised by a minimum followed by a second maximum in the heat transfer rate.

These observations of Fage and Falkner drew the attention of Small (166). Nevertheless, his measurements showed a maximum heat rate at the FSP which gradually decreased to its minimum in the separation region and no explanation was offered for the discrepancies between the two investigations in the neighbourhood of the FSP.

In 1937, Baker and Mueller (197) carried out an investigation to study the heat transfer variations around the circumference/...

circumference of a horizontal tube in a downward flow of condensing pure and mixed vapour. Their measurements with pure steam showed a maximum rate at the FSP which then gradually decreased with increasing  $\theta$  from the front of the cylinder. Adding Benzine to the steam caused the H.T. rate to increase from the FSP to reach a maximum value at about  $\theta = 35$  degrees and then gradually decrease to reach a minimum at  $\theta = 180^\circ$ , bottom of the cylinder, with high rates of condensation. On the other hand, adding Heptane to the steam, caused the maximum rate of heat transfer to be at about  $\theta = 90^\circ$  with low rates of condensation. No explanation was offered for such peculiar behaviour for heat transfer distribution around the cylinder perimeter.

The trend observed by Small near the FSP was also noticed by Winding and Cheney (171) using the mass transfer analogy to obtain results for the heat transfer around a single cylinder. The effect of changes in dimensions on the aerodynamic conditions around their naphthalene coated cylinder was neglected as the maximum radial variations were about 6 per cent. Using a streamlined tube the distribution was quite different.

Schmidt and Wenner (162) noticed that the heat distribution at the front of a circular cylinder was modified when the cylinder was streamlined at the back. They reported a slight drop in the heat transfer at the FSP, a phenomenon which was attributed to the effect of the facilitated flow off at the back. On the other hand, using the mass transfer analogy over a streamlined tube, Winding and Cheney showed/...



showed a relative minimum heat rate at the FSP which increased to reach a maximum at either side of the FSP.

Giedt's measurements (44), apart from the FSP region, showed a correlation between heat transfer and skin friction around a non-isothermal cylinder surface. As noticed earlier by Fage and Falkner (38), Giedt noticed that the heat transfer reached a minimum at the separation point and whenever there was a second peak in the skin friction, due to transition, there was a corresponding maximum in the heat transferred.

According to the available literature, it appears that research workers continued to report a similar trend to that obtained by Giedt and the trend shown in the thirty's by Fage and Falkner was not reported again until the early sixty's.

In 1961 Grassmann and Trub (163) used an electrochemical technique to measure the local mass transfer coefficients in analogy to those of the heat transfer around a circular cylinder. Over a subcritical flow range up to a Reynolds number of 12000, all their experimental runs down to  $Re = 460$  showed a minimum coefficient at the FSP which increased to reach a maximum at  $\theta = 12$  degrees and then decreased gradually to reach a minimum value at the flow separation region.

As this phenomenon at the FSP might be attributed to the influence of boundary layer flow fluctuations in the front region/...

region of the cylinder, Grassman and Trub measured the local turbulence in that region. Their observations indicated that there was no or negligible fluctuations at the FSP with  $Re = 10500$ . At  $\theta = 2.5$  degrees the turbulence increased and corresponded to that in the flowing medium but from  $\theta = 5$  degrees the turbulence disappeared as the laminar boundary layer developed over the frontal portion of the cylinder circumference.

Similar characteristics at the FSP were recorded in 1972 by Mizushina et al (159) using the electrochemical mass transfer technique in a water tunnel. They checked their data, by recording the mass transfer coefficients at two symmetrical positions around the cylinder's FSP, and the discrepancy of both values was about 2 per cent, at most. These data for flow and turbulence conditions similar to that of Grassmann and Trubeg for  $Re = 10380$ , were in agreement about the distribution trend at the forward portion of the cylinder and that there were, in both sets of data, at a minimum at the FSP. But this agreement was lost as far as the position of the peak after the FSP was concerned. While data of Grassmann and Trub showed the peak around 12 degrees from the FSP, Mizushina et al recorded their peak at about 40 degrees from FSP which was very close to the region of maximum shear stress. The effect of different turbulence levels on their distribution was that, the smaller the turbulence intensity, the flatter the distribution but with all the intensities used the peak was recorded around the location of the shear stress peak at the front of the cylinder./...



cylinder. Their results in this region were contrasted with those theoretically predicted, e.g., Frossling (170) but no explanation was offered for such discrepancies.

The idea to attribute these measurements and its trend at the front of the cylinder to the type of technique used by Grassmann and Trub and Mizushima et al was rejected by the evidence provided in its favour by Zeev Rooten (173). He indicated that the advantage of using diffusion controlled electrochemical technique was the ease and accuracy of measurements. Its main advantage was the high level of results reproducibility provided that extreme cleanliness was exercised during tests. But its major disadvantages were the limitations as to the choice of test fluid, probe material, solute and supporting electrolyte.

Referring to direct measurements of heat transfer rate, the relationship between heat transfer and skin friction on the frontal part of the cylinder was recorded by Bellhouse and Schultz (24, 174). They used an electrically heated thin metallic film to measure the mean skin friction in laminar and turbulent flow across a circular cylinder. The film probe acted as both a heat source and a heat transfer gauge, and the heat supplied to the air flow could be deduced from electrical power supplied to the probe. Under the conditions of a constant-temperature feed back controlled probe fed by a constant voltage, the probe current was directly related to the heat transfer rate to the flowing air stream. Plotting the film current against the azimuthal angle  $\theta$ , they/...

they recorded a minimum heat rate at the FSP which increased to reach a peak at the region of maximum shear stress.. These results confirmed the existence of a relationship between the heat transfer and flow at the frontal part of the cylinder as found earlier by Fage and Falkner (38).

While Bellhouse and Schultz found it necessary to calibrate their probe for different levels of temperature elevation, Rotem (173) used a probe made of a thin strip of metal alloy whose electrical resistance did not change much with change of temperature. Moreover, while Bellhouse and Schultz's probe aimed at creating an isothermal surface, the Rotem's constant, a Nichrome probe aimed at the creation of a surface of approximately constant heat flux. Measurements with this probe for heat transfer and mass transfer in oil tunnel showed that both distributions had a relative minimum at the FSP which gradually increased to reach a peak at the region of maximum shear stress. Thereafter both distributions decreased to reach their minimum towards the flow separation point. Again, these results confirmed those of Fage and Falkner.

One of the extensive investigations into the local flow parameters around single cylinders in cross flow over a wide range of  $Re$ , was that carried out by Achenbach (175, 45, 80, 176). Although, experiments for heat transfer and skin friction were made separately, a quantitative study into the relation between the two parameters is possible. It must be noticed that he measured the rate of heat transfer/...



transfer using a probe which, in principle, is similar to that of Bellhouse and Schultz, in other words, an electrically heated probe isolated from, and working on, an isothermal cylinder surface. And again, the value of the electrical input was used for the determination of the local heat flux.

Using that probe on a smooth cylinder, Achenbach (175), obtained results similar in character to those reported by Krujilin (180) which showed that the heat transfer rate was a maximum at the FSP which diminishes with distance towards the flow separation point. Apart from that, Achenbach's distribution of heat rate followed the trend of the flow, skin friction, in the boundary layer until flow finally separated from the cylinder surface.

However, when Achenbach used a roughened cylinder (80, 175), the picture was different from that for smooth cylinders. For the subcritical  $Re$ , it was possible to notice that the heat transfer rate on the frontal part of the cylinder had just followed that for the shear stress distribution up to the separation point. Besides, the minimum values obtained at the FSP, normalised by the square root of  $Re$ , were higher than those for smooth cylinders.

Achenbach attributed the changes in the heat rate characteristics at the front of the cylinder to the effect of surface roughness on the flow at  $Re > 10^5$ , and eventually the transcritical flow range was assumed to be established by increasing the roughness up to  $\frac{KS}{D} = 300 \times 10^{-5}$ . Consequently/...

Consequently, the transition from laminar to turbulent flow in the boundary layer took place close to the FSP and any further increase in the surface roughness had no effect on the flow and heat distribution around the cylinder. These conclusions of Achenbach at the transcritical flow conditions around a bluff body are in disagreement with the observations of Rhodes and Bloxom (177) in 1962. They need a special point which had been developed to change through three visible spectral orders for various wall temperatures on spheres with diameters up to 14.2 mm. At Mach numbers over 10, results showed that the heat transfer rate fell off on the sphere from its maximum value at the FSP and diminished towards the rear of the cylinder. Indeed, such a distribution does not follow the skin friction distribution around spheres at these flow conditions (103) and it is obvious that it contradicts with the conclusions drawn by Achenbach at the transcritical flow around bluff bodies.

Of course, one might question the possibility of the influence of blockage ratio used by different investigators as an explanation for these discrepancies reported about the heat transfer characteristics at the frontal part of the cylinder in relation to the flow in that region. Since it is known that when the cylinder occupies a large part of the channel cross sectional area (high blockage ratio  $\frac{D}{X}$ ) changes occur in the pressure distribution, transition, separation point and heat transfer around the cylinder.

These/...



These changes due to the blockage effect were shown by the investigations carried out by Akelbaev et al (178) around 57.8 mm diameter, uniformly heated cylinder. Their theoretically predicted values, following the method of Merk (179), demonstrated that for  $\frac{D}{X} > 0.39$ , the heat transfer rate increased at the FSP with increasing blockage ratio. Their results showed that for high blockage ratio,  $\frac{D}{X} > 0.6$ , the heat transfer distribution deviated from that characterised by its maximum at the FSP. Over the range of  $12000 < Re < 125000$ , experiments showed that with higher blockage ratio,  $\frac{D}{X} > 0.7$ , the minimum at the FSP gradually increased to reach a peak at about  $\theta = 70^\circ$  from the FSP.

The effect of blockage ratio on heat transfer distribution was also reported by Perkins and Leppert (82) who showed that this distribution became less steep at the front of the cylinder by increasing  $\frac{D}{X}$  from 0.2 to 0.4 while such effects for  $\frac{D}{X} = 0.42$  were not reported by Schmidt and Wenner (162).

Such changes associated with different blockage ratio cannot be attributed simply to the increase in the effective Reynolds number approaching the cylinder as a result of the blockage effect, e.g., reference 248. This was clear when a comparison was made between Akelbaev's data at main stream Reynolds number of 50,000 with  $\frac{D}{X} = 0.83$  and Achenbach's data for  $Re = 3 \times 10^5$ .

The idea of attributing the discrepancies between different investigators, around the front of the cylinder, to the effect/...

effect of blockage ratio does not seem to be reasonable. That was obvious, since data of Small (166), Krujilin (180), Giedt (44) and Achenbach (45) on one hand, and Fage and Falkner (38), Grassmann and Trub (163) and Mizushina et al (159) on the other, were carried out under blockage ratio ranging from 0.125 to 0.2 and the effect of blockage ratio seemed to be a secondary one.

Moreover, these investigations were made using cylinders with span to diameter ratio ranging for 3.3 to 16. However, it was indicated by Achenbach (176) that the effect of this ratio on the flow at mid-height of the cylinder is only considerable when this ratio was less than 3. Consequently, attributing discrepancies at the front of the cylinder in the above mentioned investigations to the span to diameter ratio effect was also unreasonable.

As to the reasoning given by Achenbach (45), that the finite width of his probe as well as the conduction of heat in a circumferential direction falsifies the true experimental results, that was not the case. It is true that the circumferential conduction could flatten out the distribution as shown by Thomson et al (154), but nevertheless, the maximum and minimum could not be falsified completely by the probe width since it subtended a small angle of  $2.3^\circ$  to the axis of the cylinder.

One of the important features of the relationship between flow and heat transfer around the cylinder in a cross flow is the dependence of the variations in the heat transfer on/...



on the relationship between flow and heat transfer around the cylinder in a cross flow is the dependence of the variations in the heat transfer on variations in the flow. As was noticed by Schmidt and Wenner (162) the point of minimum pressure around the cylinder was located prior to the location of minimum heat rate. A similar observation was made by Giedt (44) and he showed that the minimum heat transfer occurred at about 10 degrees further back along the cylinder circumference than the point of minimum static pressure. One of the important results of Achenbach (45) is that the minimum point of heat transfer lagged downstream of the flow separation point as a consequence of vanishing skin friction downstream the point of minimum pressure around the cylinder.

This was also clear from the measurements of Winding and Cheney (171) when they reported a minimum heat transfer coefficient which was further downstream of the point of minimum pressure for streamlined tube (172).

From the previous discussion, it is clear that most of the research workers agreed that, apart from the region in the front of the cylinder, there is a relation between the local heat rate and shear stress around the cylinder prior to the final flow separation point. Moreover, the relationship is accepted for the overall heat transfer, (e.g., Davies and Fisher (181)).

While the discrepancies and disagreements could be understandable in the circulation region, which is far too complicated/...

complicated to analyse, the disagreement around the front of the cylinder, where the boundary layer exists, is not exactly understandable. This is really confusing in particular when investigations were carried out under similar flow conditions and using similar techniques of measuring the local parameters.

The departure of the heat transfer from a circular cylinder from that predicted by boundary layer analysis was investigated by Lee and Richardson (200). They showed that this departure may be attributed to the effect of the boundary layer curvature.

Finally, since the measurements showed that both point unit heat transfer coefficients and shear stress rise from coincident minimums on the front half of the cylinder and drop to coincident minimums on the back half, it is quite reasonable to assume the maximum values in between occur near the same point.

#### 4.2.6. Heat transfer for a tube in a staggered bank

In the beginning of this century condenser tests showed variations in the characteristics of individual tubes according to their location in the tube bundle. These variations were determined mainly by the flow pattern which depends to a great extent on the tube arrangement in the bundle. Moreover, an inner tube in the bundle is expected to be influenced by the highly turbulent flow emerging from the preceeding rows.

Although/...



Although there are some theoretical approaches to help in the design calculations of heat exchangers (e.g. Roetzel (182)), the prediction of heat exchangers performance was still relied upon in the experimental investigations carried out in the field. These investigations indicated that the heat transfer from a cylinder in the first row is similar to that of a single cylinder in cross flow except at its rear part which may show the effect of interference from the succeeding row. This interference with the first row's wake depends on the tube spacing in the bundle. This could have an effect on the turbulence in the wake which could cause changes in its mean heat transfer. As the fluid passes through the first row, it is disturbed. The turbulence produced causes an increase in heat transfer in subsequent rows.

Eventually, once the turbulence in the bank reaches its stable conditions, the heat transfer becomes more or less stable and similar heat transfer is obtained from rows deep in the bundle. The intensity of the turbulence produced from the preceeding rows depends upon the longitudinal pitch ratio between two successive rows and consequently the heat transfer will change with changes in that pitch ratio.

The effect of the longitudinal pitch ratio on heat transfer of a tube in the bank, could resemble the effect on a tube placed at various distances from a turbulence generator. Austin and Coworkers (183) investigated the manner in which the heat transfer coefficient, of an equilateral triangles staggered bundle, might be affected by varying the pitch to/...

to diameter ratio. Their results with a pitch ratio of 1.25 indicated similar effect as that of 1.58 obtained by Dwyer et al (112).

An extensive investigation was carried out by Stasjuljawitschjus et al (117) to study the heat transfer on staggered bundles with different pitch ratio. They came to the conclusion that, the larger the inter-tube space, ratio of  $\frac{T}{L}$ , the greater the heat transfer and apparently the greater the turbulence. The effect of this ratio was to multiply the heat transfer functional relationship (equation 4.14) by the factor  $(\frac{T}{L})^{-5.35}$  for  $\frac{T}{L}$  from 1.27 to 1.94.

The heat transfer on a tube could increase with a decrease in the distance from the turbulator, preceeding row. However, the efficiency of the bank in an exchanger depends not only on its heat transfer rates but also on its hydraulic resistance and a decrease in the longitudinal pitch involves a reduction of the available area for the flow which leads to a higher hydraulic resistance of the bank.

In dealing with flow normal to bank of tubes, a relationship of the form given in equation 4.14 is usually used to express the functional relationship between heat transfer and flow parameters.

While for single cylinder constants C and n are correlated against the main free stream Reynolds number, e.g., Hilpert (168), for the case of tube bank, the Reynolds number is based/...



based on the maximum velocity calculated through the minimum free area available for flow in the bank.

Obviously, different values for the constants  $c$  and  $n$  will be needed to correlate data obtained under different flow conditions through the staggered bank. The heat transfer in this case will be that averaged over the entire tube bank and is based on the rate of total heat transfer.

For the subcritical range, the exponent of  $Re$ ,  $n = 0.6$  is accepted for most staggered banks whereas in the critical range the exponent rises to  $0.79 - 0.93$  for smooth tube banks (117). But for a tube bundle which has the natural unpolished surface of a rolled tube with  $\frac{KS}{D} = 50 \times 10^{-5}$ , Hammeke et al (184) showed that the index ' $n$ ' for the Reynolds number was raised from  $0.67$  to  $0.96$  when the flow changes from subcritical to critical flow.

These changes in the heat transfer functional dependence on the Reynolds number was attributed to the change in the flow conditions and associated with turbulence in the boundary layer (183). However, the difference in the index value ' $n$ ' between the two investigations in references (117) and (184) in similar flow regimes is due to the effect of the difference in the surface roughness in both investigations.

This point was supported by the investigations carried out by Groehn and Scholz (101) who found that by increasing the surface roughness parameter, the critical Reynolds number was reduced from  $2 \times 10^5$ , for technically smooth tubes, to 25000 by reaching  $\frac{KS}{D} = 0.017$ .

As/...

As a result, the value of the index 'n' for the Reynolds number in the heat transfer relationship is not only influenced by flow parameters but also by surface roughness.

#### 4.2.7. Heat rate distribution in a staggered bank

In 1948, Winding and Cheney (171) showed that for a tube in a staggered bank up to  $Re = 80000$ , the heat rate was maximum at FSP dropped to a minimum at about  $\theta = 90^\circ$ , rose rapidly to another peak at  $\theta = 120^\circ$ , dropped again and then increased until the rear stagnation point was reached. They also showed that all these values were greater than those obtained for a single cylinder at the same approach velocity. Of course, that might be due to the turbulence produced in the bank around that cylinder.

Thomson et al (154) showed that this sort of large variation around a tube in the bank could be flattened out if the lateral conduction of heat due to the circumferential temperature gradient was taken into consideration. As far as the variation within the bank was concerned, they recorded the maximum convective heating and circumferential temperature gradient around the second row of the bank. Moreover, the minimum temperature in the first and second rows was moved towards the front by increasing the Reynolds number. For the third row, the minimum temperature moved nearer to the rear by increasing  $Re$  while the succeeding rows, in the equal pitch bank, had a minimum value at the rear stagnation point for all values of  $Re$ .

In/...



In dealing with banks of tubes, staggered type, the entrance effect on the heat transfer rate variations within the bank must be mentioned. This was shown by Thomson et al (154) who showed that the variation in the heat transfer distribution became smaller, the farther the tube was from the front of the bank and the entrance effect extended through the first three rows in the bank.

Thomson's heat rate distributions were integrated by Snyder (186) and compared with his own results. He found that both sets of data agreed about the effect of the entrance of the bank on the flow pattern. Both sets of data were increased sharply and linearly from the first to third row. But while Thomson's values showed a reduction in the heat rate after the third row, Snyder's data showed a constant heat rate between third and fourth row which dropped at the fifth row. Such differences might be attributed to the difference in entrance conditions in both investigations.

The important conclusion from these two sets of data is that, the heat transfer from the first row was lower than the rest of the tubes in the bank. While Snyder's results (obtained in air tunnel) showed that it was 35 per cent below the average heat transfer from 10 rows deep bank, it was found by Dwyer et al (112) to vary with the Reynolds number. For  $Re = 10^5$ , it was 30 per cent below the whole bank, while at  $Re = 10^6$ , it was about 40 per cent below. Moreover, the average heat transfer from the first row was related to  $Re$  raised to power 0.65 compared by 0.8 for the rest of the rows.

The entrance effect was also reported by Welch and Fairchild (187) who used a long calming section with straightening vanes upstream of the bank. Under these conditions for  $Re = 20000$ , the entrance effect continued through the first four rows in the bank. For the succeeding rows, the bank induced turbulence created some common average coefficient of heat transfer except for the last row which was influenced by the free wake following and it attained a higher coefficient of heat transfer.

It seems that the variations in heat transfer in the front portion of the bank and the extent to which the entrance effect can go deep into the bank depends on the flow nature upstream of the bank. In other words, when the bank is exposed to an essentially uniform flow with low turbulence intensity, the entrance effect will extend deeper into the bank. And whenever the upstream flow conditions were turbulent, the flow approaching the first part of the bank could resemble the turbulent flow within the bank and consequently there will be no or negligible variations of heat transfer through the bank.

This situation was shown by Austin and Coworkers (183) when they recorded, in turbulent flow, coefficients at the front row tubes which were only a little lower than those deeper in the bank. By increasing the Reynolds number the coefficients were approximately equal for all the rows in the bank. This might explain the results obtained by Osment et al (188, 189) who measured the overall heat transfer coefficient with the film condensation of steam in a/...



a water cooled surface condenser model. For an equilateral triangular pitch bank, they indicated that the measured overall coefficients for the three top row tubes, middle and far ends of the row, were practically identical under the same flow conditions. And only slight variations were recorded across the bundle on tubes in the fourth and ninth rows of the bank.

A similar observation was noticed by Katz (196) with a tube bank in a turbulent flowing stream, when there was a fan upstream of the tubes. Under these conditions, he indicated that no effect of the position of a tube in the bank was found. Moreover, there was a very little difference in heat transfer with tubes as to whether it was the first, second or third row.

It was shown by Zdravkovich (192) that the variations on the front part of the staggered bank is purely due to the entrance effect. From experiments carried out on two and six rows deep triangular banks, he indicated that neither the first nor the second rows are typical representatives of the tube bank. Furthermore, the flow pattern around the first two rows in the bank was essentially unchanged by the addition or removal of succeeding rows.

#### 4.2.8. Heat transfer in cylindrical bank in cross flow

Most of the laboratory investigations are usually carried out using tube banks mounted vertically or horizontally in a cross flow through rectangular working sections.

Results obtained from such arrangements cannot be applied directly to the case of bundles in cylindrical shells without some configuration modifications. An effective value for the flow area is required in order to calculate the effective Reynolds number through the shell. While the arithmetic mean area for the bundle could be used as first approximation, Emerson (144) developed an expression to calculate the effective area for a cylindrical bank.

As the effective Reynolds number is proportional to the inverse of the effective area, the effective heat transfer coefficient should be proportional to the inverse of the effective area raised to power  $n$  (equation 4.14). Choosing the value of  $n = 0.6$ , for subcritical flow, Emerson obtained the following equation for calculating the effective area in a cylindrical bank:

$$Ah = \left\{ \frac{N^{1.67}}{\sum_{1} (AZ)^{-0.6}} \right\} \quad 4.21.$$

where  $N$  is the number of rows in cross flow

$AZ$  is the effective area at the  $Z$ th row of tubes.

#### 4.3. Concluding remarks

In this chapter a literature survey was given and which is considered by no means to be complete. This review, collected from investigations carried out by other research workers, is used to build up a reasonable picture for the flow mechanism around test models, whether it is a single cylinder or a tube bank arrangement, in a cross flow. It is also useful in providing the basic nature of the problems/...



problems encountered by fluids flowing across circular cylinders in particular.

The survey is divided into two main parts, one dealt with the problems of the hydraulic resistance of the test models in cross flow while the other part is dealing with problems connected with the heat transfer or the thermal side of it. Each part was subdivided into different sections to handle separately, as far as possible, the influence of different parameters, relating to the present study, such as surface roughness, turbulent intensity, Reynolds number and heat transfer on the flow pattern around circular test models.

Apart from the discrepancies between different investigations, the review showed that the picture of the detailed flow structure within tube bank arrangements is not fully understood. Moreover, deviations and inconsistencies, probably due to differences in test conditions or instrumentations, made it difficult sometimes to separate the effect of individual parameters on the flow across the tube bank. As a result, qualitative rather than quantitative comparisons are usually carried out.

One important outcome from the survey is that, there is a big need for improving the understanding of the changes in the flow characteristics across the bank arrangements. Furthermore, information about the influence of different parameters on these characteristics represent some fundamental knowledge for a heat exchanger designer as well as for a research worker.

## CHAPTER 5

### APPARATUS AND EXPERIMENTAL PROCEDURE

#### 5.1. Introduction

The experimental work described below was designed to improve the understanding of the flow structure with tube banks in heat exchangers in general and in condensers in particular. The investigation programme was also planned to provide data, which would supplement that available from the literature, on the effect of different parameters, such as, surface roughness, turbulence level, Reynolds number, suction parameter, location within the tube bank and heat transfer rate on a model of a tube bank condenser. It was the intention to collect data on the effect of those parameters on the tube bank characteristics such as skin friction, form drag, pressure drop and contribution percentage of the skin friction to the total drag in a tube bank exchanger under different flow conditions.

This information together with a greater understanding of the flow behaviour may then be useful to improve the design and performance of heat exchangers in general and steam condensers in particular.

In the present chapter a description will be given for the basic equipment employed in studies of the fluid flow (air) over a single cylinder and tube matrix simulating the flow over banks of tubes normally existing in heat exchangers.

In/...



In the first few sections, the wind tunnel and flow measurement equipment is described with details of calibration and use of those equipments. In later sections, the simulation for part of a tube bank is described. The measurements made in the flow on the simulated model are indicated.

## 5.2. Experimental apparatus

### 5.2.1. Wind Tunnel

Most of the experimental work, except the flow visualisation, was carried out using an open type low speed tunnel working in the suction mode, designed and built to satisfy the planned experimental programme in the Thermodynamic Laboratory of the James Watt Building, University of Glasgow. The tunnel is shown schematically in figure (5.1.).

Air was drawn from the laboratory atmosphere into the intake section and passed through a fine 6.3 meshes per cm. 0.3 mm wire diameter damping screen. This screen was erected on the upstream side of the working section to reduce the turbulence level at the intake section. The air was accelerated through a bell shaped intake section, 1.8 m long, designed to produce a flat velocity profile and to reduce the turbulence level in the flow passes through the rectangular working section. The downstream side of the working section was connected to a contraction leading to a circular section. Finally, the air passed to the suction side of a variable speed centrifugal fan and was discharged into the laboratory.

The/...

The inlet section was 1.30 m wide and 1.22 m high, giving an inlet area of 1.586 square meters. The working section was 1.22 m in length, 0.34 m wide by 0.381 m high, so that the cross sectional area of the working section was 0.13 square meters and the contraction area ratio is 1.586 : 0.13 or 12.2:1.

The walls of the wind tunnel were made from sheet metal with a welded construction. The working section consists of a steel angled frame to which sheet metal at the top and bottom were bolted in. The sides of the working section were made of perspex sheet so that the interior of the working section could be viewed from outside the tunnel.

The working section frame, the downstream contraction and the circular section leading to the fan were bolted securely to the floor of the laboratory. The downstream circular section was attached to the suction side of the fan by a short section of flexible ducting so that any vibrations induced by the fan were confined to the fan away from the working section. In this way vibrations of the walls of the test section were kept to a minimum. Moreover, rubber sheet was used between the base of the working section frame support and the laboratory's floor.

The fan had a suction capacity of 1.9 cubic meters per second, 100 mm water head at ambient conditions and it was driven by a 15 horse power direct current motor. The fan rotor speed was controlled electrically using a D. Budworth set and this allowed the rate of air flow through the tunnel to be/...



varied. When the motor was running, the fan speed could not be reduced to zero so that there was a minimum velocity available at about 500 R.P.M. giving the maximum allowed velocity at 3000 R.P.M. that gives maximum velocity to minimum velocity ratio of about 6. Thus the air velocity can be varied in the tunnel by a factor of about six times.

The inlet nozzle and the bell shaped intake were constructed on a supporting frame carried on wheels. The outlet of the intake section was connected to the inlet of the working section by means of bolted rectangular frame. In this way access to the upstream of the test section was facilitated. As will be seen later, this was quite useful. For example, to insert or withdraw the turbulence generator and the heater banks upstream of the working section.

Wall pressure tapping tubes were inserted into the walls of the working section at two stations (figure 5.1), one near the inlet downstream of the end of the contraction (station 1) and one at the downstream end of the working section at the upstream of the contraction leading to the fan suction side (station 2). At each station a set of four wall pressure tappings were made, one on each wall of the rectangular test section in an axial plane to the mainflow direction. These pressure tappings, at each section, were connected to each other and the average output gave the pressure at the corresponding station.

These pressure tappings were connected (using flexible clear plastic tubing) to a variable angle twenty-four limb manometer/...

manometer which has a reservoir of manometer fluid.

Hexan fraction, specific gravity 0.66. The manometer was supported on four legs with adjusting screws whose length may be adjusted to make the base of the instrument horizontal as indicated by small spirit level. A protractor fitted with a vernier was used to measure the angle of inclination of the limbs.

Flow rates were controlled by adjusting the motor speed. The magnitudes were determined by measuring the velocity profile in the 254 mm diameter circular section erected between the contraction downstream of the working section and the suction side of the centrifugal fan. This was carried out using a pitot tube probe with an outside diameter of 2 mm. The probe was carried on an automatic traversing mechanism and traverses were made across the circular section at a distance of about 1.5 meters downstream of the test section. For a certain motor speed the undisturbed free stream velocity  $U_{\infty}$  at the entry to the test section, was calculated by dividing the corresponding rate of flow by the cross-sectional area of the working section. Whenever the tunnel was working with a substantial blockage, with cylinders across the entire width of the working section, this velocity was used as the nominal approach velocity to cylinders in the working section.

The velocity distribution across the upstream of the working section was investigated using a D.I.S.A. hot wire anemometer. The probe was mounted on a traversing mechanism and traverses were made across the central horizontal plane 0.6 meters upstream/...



upstream of the first row in the bank. The velocity profiles obtained are shown in figure(5.2.) It is clear that the profiles are flat over the central area of the working section outside the boundary layer. Towards the wall the local velocity dropped rapidly as the boundary layer was reached. In each case the velocity outside the boundary layer did not vary by more than about three per cent of the average values integrated over working cross section.

Under normal conditions the density of the air  $\rho$  is approximately  $1.18 \text{ Kg/m}^3$  and its viscosity is about  $1.8 \times 10^{-5} \text{ Kg/m.sec.}$  and so the Reynolds number, based on the cylinder diameter is as follows:  $Re = 5080 U_0$  where  $U_0$  is the velocity approaching the test model corrected for the blockage effect.

Most of the tests were carried out with undisturbed free stream velocities between 3 and 13.7 meters per second, so that the Reynolds number varied from about  $0.15 \times 10^5$  to  $0.7 \times 10^5$ , based on the undisturbed free stream velocity. At such high Reynolds number turbulent flow would be expected in the working section and the level of turbulence depends on the quality of the wind tunnel.

Turbulence level was investigated using a hot wire probe (section 5.2.2) in the centre of the working section assuming isotropic turbulence. At different flow velocities the anemometer was operated in its normal mode. All measurements were taken with the probe located in the central/...

central horizontal plane of the working section.

The percentage or level of turbulence, the ratio of the root mean square velocity to the mean velocity varied little with the mean velocity  $U_0$ . Compared with the high quality wind tunnels, the intensity of turbulence measured in the present wind tunnel was high. The average level of turbulence considered for the present set up was about 1.2 per cent. These turbulence levels were measured in the centre of the working section, where turbulence would be expected to be lowest. It was found that the level of turbulence was higher in positions remote from the centre, especially in the boundary layers close to the tunnel walls, e.g., figure 5.3.

During the course of the experiments a number of holes were drilled in the tunnel walls of the working section, especially in the floor and roof. Three holes were used for locating the test cylinder and dummy ones inside the tunnel. These holes were clearance ones through which screws passed. Moreover, bigger holes were needed, to have an access to the inside of the working section, and were big enough to pass the cylinders used in the test. Holes were also necessary for the hot wire probe and its mount (section 5.2.5). In addition, a hole was required for passing pressure tubing which used in the working section two dimensional checks (section 5.2.6). Where any hole was not in use, it was blocked, either using plasticine or by sticking a small piece of adhesive tape over it. If a hole had been left unblocked, the pressure difference between/...



between inside and outside of the working section, when the tunnel is running, would have caused air to be sucked in through the hole, which would have altered local conditions in the working section leading to increased flow turbulence as well as an increase in the flow rate downstream of the hole.

#### 5.2.2. Test cylinder

The instrumented test cylinder was made of a porous material and it had an outer diameter of 76.2 mm while the inside one was 63.5 mm. It was necessary to use this size of tube diameter in order to accommodate the developed shear stress sensor (Chapter 3). The cylinder was mounted vertically and centered between the two perspex side walls of the working section in the wind tunnel. The cylinder was centered in position using 63.5 mm diameter guiding extension, bottom extension, which passes through a similar hole cut into the bottom steel plate of the working section. The length of the cylinder was extended, top extension, with its full outer diameter until it passed through a hole cut into the upper top steel plate of the tunnel. This hole was a clearance one and the cylinder was located vertically in the working section using a girding circular frame. The top of the test cylinder was connected to a rotating mechanism and could be rotated around its vertical longitudinal axis to any desired angular position around its circumference.

The porous cylinder was supplied by Messrs. Sintered Products Ltd. ('porosent', grade A). The cylinder was made/...

made by the powder metallurgy technique. It was manufactured by the moulding and sintering of spherical particles made from bronze (89% Cu, 11% Sn). The particles of this grade of porosity have a range of size from 37 to 43 micron with an average particle diameter of about 40 microns.

It was intended that the suction velocity along the cylinder circumference be reasonably uniform. A cylinder was selected that would have a pressure drop across its porous wall much greater than the changes in pressure around its circumference. Therefore the thickest available cylinder was chosen. The porous cylinder has a wall thickness of about 6.4 mm with a nominal filtration rating of 2.5 microns and having an overall porosity of 22 per cent..

As the porous cylinder was not available in the full length of the test cylinder, 381 mm, which is the height of the working section in the tunnel, the test cylinder was constructed from three parts. The length of the porous cylinder was 227 mm which was equally extended from both ends to give the test cylinder total length of 381 mm. These end extensions were made from aluminium tubing whose dimensions from the outer and inner diameters were the same as the porous cylinder. Each extension was connected to either end of the porous tube by equally overlapping both ends longitudinally by 6.5 mm length. Then the overlapped parts were secured together using eight 6BA screws equally distributed along the circumference of the cylinder. The screws/...



screws passing through holes drilled through the thickness of the two overlapped ends. That part of the holes passing through the porous thickness was made wider to pass the 6BA screw while that part passing through the aluminium thickness was threaded to fit that screw. Although the overlapped ends were cut together accurately to have a smooth fit, force fit was avoided due to the fragile nature of the sintered bronze tube. Any possibility of leakage through the overlapped section was avoided using 'Hermetite' on both ends before assembly securing with the 6BA screws.

The top extension for the test cylinder was closed and sealed using a circular metallic disc. This disc was secured to the top of the cylinder using eight 6BA screws fitted axially into the wall thickness. 'Hermetite' was used to prevent leakage between the two surfaces. The extension was ended by a rod 12 mm diameter welded to the top disc. This rod was used as a top guide for the test cylinder to the rotating mechanism. Air leakage was prevented using rubber gaskets.

The upper end of the bottom extension was connected to the bottom end of the porous cylinder in a similar way for the top extension. The lower end of the extension was closed using a 18 mm thick and 76.2 mm diameter metallic plate.

At one side of this plate and for 6 mm of its thickness the diameter was reduced to 65.5 mm and it rests on a supporting ring which was pushed, forcefit, into the bottom of the aluminium extension tubing. The supporting ring/...

ring was resting on 1 mm wide circular ring cut into the inner side of the aluminium bottom extension. Using O-ring and Hermetite, the 18 mm thick plate was fitted on the supporting ring and then it was secured with eight 6BA screws. These passed through clearance holes, drilled through to the middle 6 mm of the plate thickness and screwed in threaded holes drilled axially into the thickness of the aluminium tubing. The diameter of the last 6 mm in the thickness of the plate was reduced to 63.5 mm and passed through an identical hole cut into the bottom steel plate of the working section in the tunnel. This part of the plate was working as a bottom guide for the test cylinder while it rotated. Leakage through the bottom hole was prevented by using O-ring between the lower end of the test cylinder and the bottom plate. Grease was used to ease the friction between the O-ring and steel plate.

It was necessary to choose that thick plate (18 mm thick) in order to accommodate the small stuffing boxes necessary for passing the suction tubing to the inside of the cylinder, pressure taps leads and electrical connections to the shear stress sensor.

The test cylinder was instrumented with the servo-force balance shear stress sensor (section 5.2.4). It was mounted vertically along its length and at its mid-height. Two pressure tappings were located at equal distances above and below mid-section of the cylinder at the same generator as the shear stress sensor. The  $45^{\circ}$  inclined sides/...



sides of the sensor were pressed against the sides of a groove cut from the interior side of the test cylinder, the sides of the groove were cut at the same angle, i.e.,  $45^{\circ}$ . Four screws pass through clearance holes, one at each corner of the sensor's frame, were secured into a mounting set up built into the interior of the cylinder. The access to the inner side of the porous cylinder was made through the back side, relative to the sensor, which was sealed after assembly. Air leakage was prevented using Hermetite and plastic filler on contact surfaces. The assembled test cylinder is shown in figure 5.4.

#### 5.2.3. Static pressure measurements on the test cylinder

On an impermeable surface, static pressure is normally measured by means of pressure taps inserted into the surface so that their axis is perpendicular to the flow direction. Under such circumstances the flow direction in the vicinity of the pressure tappings is parallel to the surface over which measurements are to be made. Usually pressure tappings are made by inserting a short length of hypodermic tubing into an undersized hole drilled normal to the surface of the model.

Whenever a normal velocity is applied to a surface in main flow, the flow direction is no longer parallel to the surface and so becomes indeterminate. Therefore, if pressure tappings on a permeable surface are made in the same fashion as for an impermeable surface (67, 68, 69, 70) the pressure readings obtained will probably over estimate/...

estimate the actual static pressure due to stagnation effects.

Aggarwal (71) forced the flow to remain parallel to the wall, in the vicinity of a pressure tap, inserted into a porous surface, by applying a small quantity of paraffin wax to the porous surface around the pressure orifice. But when suction into the surface is applied, the area covered with wax could be affected and the flow direction could become indeterminate in the vicinity of the pressure tapping. Drummond (72) tried to avoid the difficulty of measuring the static pressure in a canvas hose, where normal velocity exists at the wall. He conducted his measurements about 13 mm downstream of the hose and in a brass tube fitted at the end of it.

From above, it is clear that the flow should be made to go parallel to the surface in the vicinity of the location where static pressure is to be measured using pressure tappings. In the present work, static pressure taps, to measure static pressure distribution around the porous cylinders were formed from two brass rectangular stubs each with a central hole of diameter 0.5 mm drilled normally to it along its length.

The width chosen for the brass stubs was 6 mm running along the cylinder circumference, cut from a circular ring sector so that the streamlines would run locally parallel to the wall in the vicinity of the pressure orifice. This means that the pressure tapping was preceded/...



preceeded and succeeded by 3 mm impermeable surface.

These pressure tappings stubs were made to form the upper and lower ends of the shearing stress sensor's supporting frame (section 3.4.1). The pressure orifices were located 30 mm above and below the mid-height of the test cylinder on the same generator as the shearing stress sensor. They were fitted in such a way that they were nearly flush with the surrounding porous surface but did not protrude it. The stub is shown in appendix 5. The length of the stub was made more than the thickness of the test cylinder so that on the outer end of it the pressure orifice facing the flow was 0.5 mm diameter while the outlet on the other end was a threaded tap to fit 10BA screwed end of a pressure lead from the interior of the test cylinder and parallel to its vertical axis. These pressure leads passed through stuffing box fitted to the bottom end of the test cylinder. By means of plastic tubing these pressure leads were connected to an inclined manometer.

Static pressure distribution around the cylinder circumference was obtained by averaging the reading from the two pressure tappings, above and below the mid-height of the test cylinder. As the cylinder could be rotated to any angular position around its vertical axis, the average of these pressure tappings gave the local static pressure at that peripheral position ' $P_\theta$ '. The local pressure ' $P_\theta$ ' together with the static pressure  $P_o$  in the undisturbed free stream, averaged over the four sides of the tunnel, were monitored and the pressure difference  $P_\theta - P_o$  was/...

was divided by the dynamic head of the incident flow to give the pressure coefficient distribution along the cylinder circumference as a function of its angular position measured from the front stagnation point (FSP).

#### 5.2.4. Skin friction measurements

Local measurements of shear stress around the circumference were taken in five degrees intervals. As the distribution around the cylinder was believed to be symmetrical about the meridian, measurements were taken from  $0^{\circ}$  (FSP) to  $180^{\circ}$  from the front stagnation point by rotating the test cylinder around its vertical longitudinal axis.

The values of skin friction around the cylinder were picked up by means of a servo-force balance type of instrument (section 3.4). The output signal from the balance was displayed on an oscilloscope screen during the whole experimental work to watch the positioning of the drag piece within the gap clearance. During the investigation any displacement from the null position was insignificant and the sensing element was at the neutral position practically all the time.

Before any experimental run was started, the instrumented test cylinder was turned around its vertical axis so that the sensing element of the servo balance was facing the incident air flow. From normal pressure readings round the  $0^{\circ}$  position, the point of maximum pressure accurately determined the location of the front stagnation point/...



point and errors in positioning the protractor, on the top of the cylinder, relative to the angle scale were highly reduced. Then the protractor vernier was adjusted to read  $0^{\circ}$ .

The air flow rate passing through the tunnel was adjusted by changing the speed of the fan driving motor. Using a Bryans X-Y recorder type 29000 series the output signal from the servo force balance was recorded. The signal was fed to the Y coordinate while the X coordinate was moved in equal steps to represent the circumference of the test cylinder. With the drag piece facing the incident main stream (at the front stagnation point) the signal was recorded to give the "zero" shear signal. Then the cylinder was rotated starting from the FSP until the highest signal was recorded, the peak of the shear stress, consequently the Y scale on the recorder was set to suit the range between the two signals.

Starting from the FSP the servo balance signal was recorded along the circumference of the cylinder in equal  $5^{\circ}$  steps until the protractor read  $180^{\circ}$ . Due to the nature of the flow around the cylinder and due to the fact that the flow field around it in a cross flow is affected by the shedding vortices in the wake, the output signal oscillated around its mean value, fundamentally, with the shedding frequency. In such a case the shear stress taken was that of a time mean average value.

According to the precalibration data, the skin friction was calculated as  $\tau$  in  $\text{N/m}^2$ . This shear stress was divided by the/...

the dynamic head of the incident air flow to give the friction factor,  $K_f$ , distribution around the cylinder circumference as a function of its angular position measured from the front stagnation point.

#### 5.2.5. Hot wire anemometer

Measurements of velocity and turbulence intensity in the wind tunnel were made using a D.I.S.A. hot wire, mainly boundary layer or probe type 55P15. The wire of the probe was tungsten, plated with platinum for protection against corrosion, with a length of 3 mm and 0.005 mm diameter and the wire resistance at 20°C was 3.5 MOH.

When in use the probe was mounted on standard D.I.S.A. probe support and had a long reach necessary for the survey across the working section in the tunnel. The probe support was mounted on a steel angle frame mounted outside the wind tunnel. The probe support was held in position by two screws on one end of the mount. The other end of the mount was screwed to the supporting rectangular frame that connected the upstream of the working section to the intake contraction of the tunnel. The length of the mount, from the centre of the probe support location hole to the other end was about 170 mm. The support passes through a hole in the perspex side wall of the working section. The probe and the probe support were positioned in the horizontal plane passing through the mid height of the tunnel. A fine meter coaxial cable, specially designed for use with hot wires, connected the hot wire, via its probe support, to a D.I.S.A. constant temperature anemometer type.

Hot/...



Hot wire is most sensitive to those components of velocity which are in the plane at right angles to the wire axis.

In the present investigation the bulk of air flow was passing horizontally in the tunnel and it was assumed that the vertical component of induced velocity fluctuations was small in comparison with the horizontal component.

Therefore, the axis of the hot wire was kept vertical.

The anemometer is fitted with two volt meters which read the voltage across the hot wire. One reads the steady DC component which was a measure of the mean flow velocity across the hot wire, while the other read the fluctuating r.m.s. component which was a measure of the velocity fluctuations in the vicinity of the hot wire.

For operation the probe cold resistance was increased by 80 per cent, giving an over heat ratio of 1.8, the value recommended for use in air. The DC voltage was then read off giving the value for zero air flow velocity,  $V_{0_1}$ . The tunnel was started up and the air velocity increased to the required value; then the DC voltage ( $V$ ) and the AC voltage ( $V_{r.m.s.}$ ) were read off. The air velocity increased in a number of steps up to the maximum available velocity in the tunnel. At each velocity the DC voltage across the wire was noted as well as the manometer readings at stations 1 and 2 (section 5.2.1) together with a pitot tube survey in the circular cross section downstream of the working section.

In order to relate the DC voltage to the air flow velocity across the hot wire, the wire must be calibrated.

Calibration/...

Calibration was carried out in a round duct connected to two compressors with different capacities in order to get a wide range of air flow rate. The flow was increased to the desired value, the flow velocity at the centre line of the round duct was measured using a standard precalibrated pitot-static probe 1.5 mm diameter whose signal was read on a manometer filled with Hexan fraction with specific gravity of 0.66. The manometer was equipped with a vernier scale so that readings down to 0.01 mm head were measured. The hot wire probe was inserted into the flow replacing the pitot tube.

King (73) showed that the heat transfer rate in forced convection from a hot wire is proportional to the square root of the flow velocity. But the heat produced by resistance heating in the hot wire is equal to  $V^2/R$ , where  $R$  is the hot wire resistance, so that a relation between the voltage  $V$  and the flow velocity  $U_\infty$  may be expressed as follows:

$$\frac{V^2}{R} = a + b U_\infty^{\frac{1}{2}} \quad \text{where } a, b \text{ are constants, } a = \frac{V_0^2}{R}$$

$$\text{that gives } \frac{V^2 - V_0^2}{R} = b U_\infty^{\frac{1}{2}}$$

$$\text{or } V^2 - V_0^2 = (bR) U_\infty^{\frac{1}{2}} \quad 5.1.$$

Thus a graph of  $V^2 - V_0^2$  plotted against  $U_\infty^{\frac{1}{2}}$  should be a straight line. Calibration curve in these coordinates were not convenient for the present use. However, the calibration was expressed as a direct plot of the output parameters/...



parameters of the calibration process, i.e., DC voltage  $V$  against velocity  $U_\infty$ . A typical calibration is shown in figure (5.10).

The anemometer r.m.s. voltmeter reading was used to calculate the magnitude of the velocity fluctuations in the vicinity of the hot wire. Velocity fluctuations are often expressed in terms of the percentage turbulence, defined as  $\frac{U_{\infty \text{ rms}}}{U_\infty} \times 100\%$ . In conjunction with the probe calibration equation  $V^2 - V_0^2 = (bR_1) U_\infty^{\frac{1}{2}}$  it can be shown that the percentage of turbulence is given by

$$U_{\infty \text{ rms}} = \frac{4V}{V^2 - V_0^2} \times 100\% \quad 5.2.$$

This expression is only true for moderate velocities so that straight line calibration for the probe is applicable. It is also valid for low level of turbulence, i.e., less than about 10 per cent. Since our concern was with the mid-area in the working section where the level of turbulence was within that range so, the previous relation was used in the present work. The level of turbulence, therefore, is defined as:

$$Tu = \text{r.m.s. axial fluctuations/time averaged axial velocity.}$$

#### 5.2.6. Two-dimensionality of the tunnel

The experimental investigations were confined to the horizontal plane passing through the median section of the/...

the instrumented porous test cylinder. This is vertically mounted in the centre of the working section where the flow had been regarded as two-dimensional. In order to check the two dimensionality of the flow, the instrumented cylinder was removed and replaced with another identical dummy cylinder. This cylinder was made from aluminium having the same dimensions as the test cylinder. On this cylinder three pressure tappings 0.5 mm diameter each were drilled radially at right angles (through the wall thickness) to its longitudinal axis along the same generator on the cylinder surface. Short hypodermic tubings were inserted through these, undersized, holes force fit from outside of the dummy cylinder.

The location of the three pressure tappings was aligned together, one at the mid height of the cylinder while the other two taps were located 100 mm on either side above and below the middle one. The extra length of the hypodermic tubing above the outer surface of the cylinder was fitted out and it was machined to remove the burrs from the pressure tappings. From the inner side of the dummy cylinder, the hypodermic tubing was connected (using flexible plastic tubing) to a variable angle multi-limb manometer filled with Hexan fraction whose specific gravity is 0.66.

The cylinder was rotated around its vertical axis and at each peripheral angle the readings from the three pressure tappings were noted. At any angular position, relative to the incident air flow, the readings from the two side taps were/...



were averaged and compared with those from the tap located at the mid-height of the cylinder. The velocity of the air flow was varied and the procedure was repeated for each velocity. Typical results are shown in figure (5.5). From these graphs it is clear that the air flow in the mid-horizontal section of the tunnel approximates to two dimensional flow. This is shown in the similarity of the pressure distributions along the mid height of the cylinder.

#### 5.2.7 Tunnel blockage

When a model is located within the working section in a closed tunnel it reduces the cross sectional area through which the air will flow. The presence of the model in conjunction with the confining effect of the tunnel walls can give rise to a substantial blockage within the tunnel. Boundary layers are formed on the walls of the tunnel and in order to maintain a constant flow rate, the air in the centre of the tunnel accelerates, so that the actual approach velocity to the model in the working section is higher than the average velocity upstream of the tunnel. This increase in velocity due to the presence of the model in the tunnel may be considered constant over the length of the model in the main stream direction and is called 'solid blocking'. This effect arises as a result of the inability of the stream to expand laterally as freely as it would in an unconfined space. It is a function of the physical dimensions of the model, e.g., model length, thickness and size.

The flow of real fluids with practical Reynolds numbers over a bluff body, such as a cylinder, is associated with the formation of/...

of a wake downstream of the model. In these circumstances, it is obvious that the flow velocity, streamwise component, is equal to zero at the rear stagnation point of the bluff body and thereafter it must increase steadily until it reaches the value of the average velocity of the main flow some distance downstream of the model. As a result of this process, the mean velocity in the wake behind the bluff body is lower than that of the free stream. The velocity deficit in the wake of the model and the requirements of overall mass continuity imply that the velocity outside the wake of the bluff body should be higher than those in the free stream in order to maintain a constant flow rate of air passing through the tunnel.

The velocity distribution in the wake and the corresponding variations in the main stream velocities, outside the wake, put the bluff body in a zone of pressure gradient which extends upstream of the wake and results in a velocity increment at the model.

From above it is obvious that the model of the bluff body together with its wake have effect on the actual approaching of the model in a closed tunnel. Consequently any attempt to account for the tunnel blockage effect on the flow around a bluff body should include the effect of both the solid and wake blockage.

Of course one way to avoid or at least to minimise this interference between the wind tunnel walls and the flow past bluff bodies, is to use small models. On the other hand, larger/...



larger models are not only easier to work with but may be needed to achieve large Reynolds numbers or possibly chosen to accommodate specific instrumentations such as the present work.

For the case of a circular cylinder, a small change in the flow conditions might lead to significant movements of separation point and consequently to significant changes in the pressure distribution and in the characteristics of the wake. It is not surprising, therefore, to find that the available analytical treatments of blockage had specifically excluded such cases, e.g., Maskell (238). One of the earliest calculations for the tunnel blockage corrections was carried out by Fage (74) for different Rankine oval shapes and cylinders in cross flow.

Lock (75), Glauert (76) and Goldstein (77) analysed the effect of solid blockage upon the flow of an ideal fluid about asymmetric airfoil section at zero incidence.

For the case of a circular cylinder the velocity increment  $U_1$  at the location of the model was calculated, using the following formula:

$$\frac{U_1}{U_\infty} = 0.821 \left(\frac{D}{X}\right)^2 \quad 5.3.$$

where  $U$  is the approach velocity in the tunnel and  $X$  is the width of it.

Allen and Vincenti (78) made the first attempt to include wake blockage in an analytical treatment. The velocity increment/...

increment  $U_2$  due to the existence of the wake of the cylinder was expressed as follows :

$$\frac{U_2}{U_\infty} = \frac{C_d}{4} \left(\frac{D}{X}\right) \quad 5.4.$$

where  $C_d$  is the drag coefficient measured in the tunnel.

By adding Lock's solid blockage correction  $U_1$  and the wake correction  $U_2$  to the velocity  $U$  of the oncoming flow one obtains a corrected velocity  $U_c = U_\infty + U_1 + U_2$  given as follows:

$$\frac{U_c}{U_\infty} = 1 + 0.821 \left(\frac{D}{X}\right)^2 + \frac{C_d}{4} \left(\frac{D}{X}\right) \quad 5.5.$$

In order to correct for the drag coefficient, Allen and Vincenti proposed the relationship:

$$1 - C_{p_c} = \left(\frac{U}{U_c}\right)^2 (1 - C_p)$$

which gives the following relationship:

$$\frac{C_{d_c}}{C_d} = 1 - 0.5 C_d \left(\frac{D}{X}\right) - 2.5 \left(\frac{D}{X}\right)^2 \quad 5.5.$$

But this correction does not include a correction for the pressure gradient induced by the wake blockage and it implies that the pressure distribution is invariant under constraint. Dalton (239) showed that the correction formula of Allen and Vincenti is valid only up to a blockage ratio  $\frac{D}{X} = 0.1$ . Farrell et al (240), for blockage ratio up to 0.25, suggested the following expression which takes the form:



$$1 - C_{p_c} = \frac{C_{d_c}}{C_d} (1 - C_p) \quad 5.6.$$

where the difference between  $\frac{C_{d_c}}{C_d}$  and  $\frac{(U_\infty)^2}{U_c^2}$ , in the two expressions, involves the extra correction for the pressure gradient induced by the wake blockage  $(2.5 \left(\frac{D}{X}\right)^2 - 2 \times 0.821 \left(\frac{D}{X}\right)^2)$ .

However, Roshko (79) and Achenbach (80) used the suggested expressions of Allen and Vincenti for circular cylinders with blockage ratio of 0.136 and 0.166 respectively. Following the same line of approach these corrections are used in the present work as best available recommended by Pope (81) and Perkins et al (82).

#### 5.2.8. Simulated condensation tests

Condensation process was simulated in the present programme of investigations in order to evaluate its effect on the flow characteristics in a tube bank condenser.

Whenever the conditions allow condensation to take place on a surface, the condensable vapour flows from the main stream towards the cooling surface. By condensation the vapour releases heat in the form of latent, and possibly, sensible heat which is carried away by conduction through the thickness of the cooling surface and eventually will be removed by means of the cooling medium. Therefore, it is possible to say that condensation is a process where both heat and mass transfer exist side by side. Consequently an experimental investigation to simulate condensation process should include both heat and mass transfer.

##### 5.2.8.1./...

#### 5.2.8.1. Mass Transfer during condensation

The investigation was carried out to study the interaction between the vapour and the surface of the condensate film.

For this purpose, it was assumed that the condensate film is in solid form and the frictional coefficient at the surface of condensate film was regarded as that at the surface of a cylinder whose diameter is  $D_1$  where an inward velocity exists at its surface. As  $D_1$  is nearly equal to  $D + 2\Delta$ , where  $\Delta$  is the film thickness, then it was assumed that  $D_1 \approx D$ .

On the cylinder condensation was simulated by homogeneous suction of the flowing medium, air, along the periphery through the wall of the test cylinder (section 5.2.2.). To ensure satisfactory homogeneous suction along the circumference it was chosen to be the thickest available 6.4 mm in the fine grade A of the porous tubing. The air was sucked through the whole surface area of the porous material except that part occupied with the front part of the shear stress sensor. This amounts to a length of about 6 mm along the cylinder's circumference and 70 mm along the middle length of the cylinder (0.7 per cent of the suction area). The skin friction sensor was isolated from the interior of the cylinder and it was built in a sealed compartment.

The extracted air through the thickness of the cylinder wall was sucked through a 19 mm diameter circular tube inserted through the bottom plate of the test cylinder. This tube was pushed into the cylinder until its top touched the skin friction sensors sealed compartment. The top of the tube through which air passed was made in an inverse U-shape.

One /...



One end of the U-tube was connected to the suction tube while the other end was enlarged conically and opened to the interior of the cylinder. This was done in order to avoid sucking the cooling water film (explained later). The exit of the suction tube was connected to a rotameter to measure the suction flow rate. This was connected to the suction side of a Reavell NRD rotary exhaustor type R 3½ x 5 MK9 with capacity range from 0 to 0.6 cubic meter per minute. In order to facilitate the cylinder rotation around its vertical axis while connected to the suction line, the connection was made from clear thick plastic tubing secured with Jubilee Clips. The tubing was twisted twice to avoid being blocked when the cylinder rotated.

During the period of adjustment of the suction rate, with the cooling film covering the cylinder's interior surface, there was a possibility for water to be drawn into the air suction line. Hence, a water separator was fitted between the suction pump and the outlet of the rotameter while another separator was placed upstream of the rotameter.

Since the suction pump is an oil film positive type, the flow rate was controlled by means of a bypass valve fitted to the pump. The pump was coupled to an electric motor and the set was carried on spring loaded shock absorbers. The outlet of the pump was fitted with a car exhaust silencer to reduce the noise and vibration levels in the pump.

The pressure in the interior of the porous cylinder was measured/...

measured using a hypodermic tubing about 1.5 mm diameter inserted through a stuffing box fitted to the bottom plate which closes the lower end of the test cylinder. The top of this pressure tap was enlarged and connected to a cone facing downward for the same reason explained for the suction tube. The pressure tap reaches the middle height of the test cylinder while its other end was connected to a manometer filled with mercury using plastic tubing to minimise restrictions from the rotation of the test cylinder.

The pressure inside the cylinder, equal to the average pressure over the inner surface of the cylinder  $P_i$ , and the normal pressure  $P_o$  on the outer surface of the cylinder was monitored, the pressure difference  $P_o - P_i$  being measured using an inclined mercury tube manometer. For analysis this pressure difference was used, in the case with no cooling film, together with values of the porosity of the material given by the manufacturer to estimate the suction flow rate. The values calculated were compared with those obtained using a calibrated rotameter. Agreement between the two methods was reasonable with  $\pm 5\%$ .

It is worth mentioning that there is no suction applied through the front of the shear stress sensor together with the supporting frame. Since the suction area was located at about 3 mm on both sides of the loading and centre line, it was felt that the skin friction measured could, although not strictly true, reasonably represent those on a porous surface. Moreover, adding suction to the drag piece may cause the flow direction tube indeterminate on its surface. That/...



That could have added complications to the design of the sensor to separate the tangential component of force which is needed for calculating the shearing forces. Therefore, as in any instrument a compromise was necessary and it was decided to leave the drag piece as a surface where the flow direction is parallel to it.

#### 5.2.8.2. Heat transfer during condensation

In order to go one step further towards a complete simulation for the condensation process the simultaneous heat transfer together with the mass transfer should be carried out. Keeping in mind that our test cylinder is made from a porous material and is instrumented with the developed shear stress sensor, quite a number of precautions must be applied to fulfill that objective.

Since the effect of heat transfer direction on the behaviour of the flow around cylinders is not completely known, it was intended to apply the heat transfer in the same direction as in a condenser tube. While it could have been easier to apply it in the other direction, heat was transferred from the hot medium to the cold surface of the test cylinder.

The air medium was heated using an open bank of electrical air heaters fitted upstream of the working section. The bank of heaters is mounted between the outlet of the bell shaped intake section and the inlet to the working section of the wind tunnel. It was supported on a frame so that it was easy to be removed or to be fitted to the rig. The bank/...

bank was constructed from steel frame with the heater coils mounted horizontally across its section. It is constructed from eighteen separate equal units with a total power consumption of 24 KWH. The coils were made spirals with 12 mm diameter and they are wound from 2 mm diameter 80/20 nickel-chrome resistance wire supported on porcelain refractory formers.

The test cylinder leading edge was 1040 mm downstream of the heater bank. Heaters were supplied with 240 AC voltage and the temperature in the tunnel was controlled by an XD6 Eltron control system. This consisted of a Statchwell Climatronic wall mounting integral action controller type C x T 1602 to give a controlled temperature range of 20 to  $65^{\circ}\text{C} \pm 1^{\circ}\text{C}$ . This was used with a Statchwell temperature detector type DD 1402 fitted downstream of the working section in the tunnel. The integral action adjustment was set to position 7 as recommended by the manufacturer. This was connected to a modulating and two positions light duty motor Statchwell type XRM 1201. The motor shaft drove a step controller through a tongue and groove connection. The step controller was a light duty type MC 1202 with nine active single pole switches. A recyclic switch was attached to return the controller to the start position before the load is reconnected after any interruption of the power supply. Electrical power points were supplied to the heaters bank through nine 20 ampere C20 T contactors.

Power fed to the coils was distributed in such a way so that the first contactor was connected to the lateral horizontal coil/...



coil and this is distributed alternatively above and below this central one. The arrangement and wiring diagram is shown in figure (5.6). The bank was protected against overheating by a high temperature safety cut-out which is wired in series with the operating coil of a controlling contactor. To protect the air heaters against any failure in the main air flow, the wind tunnel was equipped with a 'Londex sail switch' type AS mounted through the wall of the tunnel upstream of the heater bank with 'off' normal position. By means of an adjustable balancing weight, this switch will stay off until a predetermined air velocity in the tunnel is reached. In the present cast the minimum speed of 4 meters per second moves the switch to 'ON' position. Arrangement is shown in Figure (5.7).

To cool the walls of the porous test cylinder, two ways were tested. First method was to fill the top aluminium extension for the test cylinder with cold water and then let the water fall on to the porous wall as a thin film of water by means of the device shown in Appendix 5. But this method was found to be very critical and sensitive to any tilting and caused problems in its application. In the second method the cylinder walls are cooled by a thin film of water sprayed on it from a special type of nozzle. For this purpose a hollow cone type of nozzle was chosen. Two nozzles Delavan's Mini-SDX type AE40 and AE50 were used to cover a range of water flow rate of 4 to 30 litres per minute. The sprayed cone angle was varied from  $65^{\circ}$  to  $75^{\circ}$  for water pressure varying from 0.3 to 5 bar.

The/...

The nozzle was mounted in a short cylindrical tube which was mounted in a central hole in the plate covering the top extension of the test cylinder. The water film sprayed with the lowest water supply pressure covers almost half of the top aluminium extension before it flows down on the porous surface.

Cooling water was supplied using a centrifugal pump with regulated capacity. Through a Delavan H1 strainer and a dual chamber Delavan 23017 pressure relief valve, the water was fed tangentially at right angles to the top of the hollow core spray nozzle. A calibrated rotameter and a thermometer were used to measure the cooling water flow rate and the inlet water temperature respectively. Pressure of the cooling water supply was measured using a pressure gauge upstream of the nozzle. The water jet reached the nozzle eccentrically from a swirl chamber with a single inlet spiral configuration. The water at the outlet attained a rotational speed besides its speed and it takes the form of a thin film sprayed on to the wall of the test cylinder.

The water collected in the lower aluminium extension of the test cylinder was carried away, to avoid flooding of the cylinder, using a tube inserted through a stuffing box in the bottom plate of the cylinder. The tube is adjusted to be lower than the height of the lower aluminium extension. This was connected to a level indicator. Nevertheless, this was found to be unsatisfactory and sometimes flooding of the test cylinder could not be completely avoided. The method/...



method adopted was to fit a tube 19 mm diameter through the bottom of the cylinder and flush with the bottom plate. The other end of this tube was extended to pass through one end of a sealed perspex tube 58 mm diameter and 285 mm in length, through the lower side of the perspex tube a connection was made to a centrifugal pump to drain the collected cooling water. In fact this perspex tube worked as a part of the test cylinder with one advantage, that the water level could be controlled and flooding of the porous cylinder was avoided. The pressure in the interior of the cylinder is transferred to the top of the water level in the perspex tube by connecting them via a small stop-cock. The water filled lines were made using thick plastic tubing. The outlet temperature of the cooling water is measured before the water through the pump to the drain.

#### 5.2.8.3. Temperature measurements

Knowledge is needed about the temperature of hot air surrounding the test section, temperature difference of the cooling water before and after it cools the cylinder and the surface temperature of the porous surface.

Temperature in the wind tunnel is controlled by adjusting the control system to the desired temperature and its variations are, as recommended by the manufacturer,  $\pm 1^{\circ}$  C. Temperature measurements are made at three axial stations located centrally in the working section. The DD 1402 temperature detector was fitted downstream of the working section beside the two chromel allumel calibrated thermocouples, one inserted upstream of the working section while the other was/...

was downstream of the instrumented test cylinder. To detect temperature variations around the test cylinder a thermocouple was mounted to rotate with the cylinder and its hot junction was fixed on a bracket fitted to it about 12 mm from its surface. The thermocouple was fabricated from 36 gauge Teflon-coated copper constantan wire with the junction made by spot welding which gave about 0.2 mm spherical head.

Temperature of the cooling water was measured at both inlet and outlet of the test cylinder using accurate mercury thermometers reading down to  $\pm 0.1^{\circ}$  C. Thermometers were inserted into the cooling water line. The temperature difference between these two thermocouples is used to calculate sensible heat carried by cooling water.

Accuracy of the measurements of local convective heat transfer coefficients is dependent upon the accuracy of a surface temperature measurement. The most common methods of using a thermocouple to measure the surface temperature is to attach the thermocouple to the surface by brazing, peening or capsule couples, e.g., copper-constantan pressed in contact with the surface.

In using one of these methods two basic difficulties are encountered. The first is that the thermocoupling only indicates the temperature of its sensitive element, i.e., the junction between the two metals. Thus the sensitive element must make a perfect thermal contact with the surface. However, this must be done without perturbing the heat flux through/...



through the surface of affecting phenomena occurring on the surface, e.g., suction through the surface. The second problem is that if the positive element is in perfect thermal contact with the surface, heat can be conducted along the thermocouple wires causing the surface temperature in the vicinity of the junction to be changed. Further, the insertion of the thermocouples must have some effect on the conduction pattern in the tube wall.

After some consideration, the technique finally selected required that the metallic surface formed part of one arm of the thermocouple, the second arm was made from a pointed probe of a thermoelectrically dissimilar metal which was pressed against the surface. The probe must be in a good electrical contact with the surface such that extraneous Seeback voltages are not introduced. To achieve this, a constantan wire was pressed on to the surface and the junction between the wire and the metal of the surface represented the thermoelectric element or the hot junction of the thermocouple. Temperature measured by the junction so formed must be the surface temperature at the point of contact. Heat conduction through the wires was minimised by making the tip of the probe as sharp as possible. This also minimised the effect of the measuring instrument on the heat flux occurring at the surface. The constantan wire was supported in a porcelain two bored tube so that the wire passes through one bore at one end of the tube to the other end which faces the porous surface and is then bent  $180^{\circ}$  to pass through the other hole in that end back to the inlet end and then twisted around itself. In this way the contact end/...

end of the constantan wire was strengthened, the twisted end was collapsed and shaped to give a good contact when pressed against the porous surface. When the wire was in touch with the surface, the porcelain end was about 1.5 mm away from the cylinder wall. The porcelain tube was supported up to about 7 mm, from its end, by hypodermic tubing. This was spring loaded in an axial direction to press the constantan wire radially against the porous wall.

The probe was fitted to the outer surface of the cylinder at an angle of  $40^{\circ}$  to the longitudinal axis of the cylinder. In order to complete the thermocouple circuit without introducing a foreign metal, the connection between the cylinder surface and the cold junction of a thermocouple should be made from the same composition as that of the porous surface. A strip 1.5 mm thick and 4 mm wide of the same grade as that of the cylinder porous material is used to connect the second arm of the thermocouple to the cold junction. This strip was attached to the cylinder surface by pressing the two surfaces together. The point of attachment was sufficiently remote from the probe location so its presence did not affect the measurement of the surface temperature. Since the porous strip has a fragile nature it was reinforced and supported in a stainless steel tubing which passed through a small stuffing box mounted centrally in the bottom of the test cylinder and extended vertically until it reached the cold junction. The cold junction was dipped into a glass tube filled with mercury which was placed into/...



into the ice pot. The temperature of the outer surface of the cylinder was measured only at one point on the rotating generator assuming that it was uniform along that generator.

The temperature of the inner surface of the cylinder was measured at two stations along the same generator which coincided with that for the outer surface. These were made in a similar way to those of the outer thermocouple with two main differences:

- a) Probes were mounted at right angles to the cylinder longitudinal vertical axis.
- b) Length of the probe was extended radially across the cylinder diameter, spring loaded from outside the cylinder,  $180^{\circ}$  to the rotating generator, passed through the thickness of the wall to touch the opposite side of the cylinder internal surface.

The arrangement for mounting the thermocouples is shown in figure (5.8.).

The outer probe was mounted 42 mm above the mid-height of the test cylinder and on the same longitudinal generator as the shear stress sensor (section 5.2.4). On the inner surface the probes were mounted at equal distances above and below the shear stress sensor's compartment. The upper one was adjusted to face the outer probe across the wall thickness.

The connection to the cold junction, porous strip, was used as/...

as a common second arm to all of the three thermocouples measuring the surface temperatures. By means of a selector switch the thermocouple was chosen and the temperature measured will always be that at the dissimilar metal probe junction.

In the analysis, the output readings from the two inner probes were averaged to give an estimate of the temperature at the mid section of the test cylinder.

As with any thermocouple, to obtain good accuracy, the thermocouples required calibration. However, if the materials are carefully chosen and high accuracy is not required, calibration could be omitted. In the present case with one arm of the thermocouple is constantan and the other arm is the porous material, calibration of the instrument becomes necessary.

Calibration was carried out by immersing the test cylinder with the probes in place into one of the standard temperature controlled water bath type. Typical calibration curves are shown in figure (5.9).

All thermocouples involved in the measurements were connected to a multi-channel MB Mini-logger unit where the microvolt output scanned over the thermocouples could be displayed using a data teletype.



### 5.3. Experimental Procedure

#### 5.3.1. Single cylinder

A logical step before investigating the flow in a complete tube bank exchanger is to study the case of a single circular cylinder in a cross flow. A single cylinder facing the undisturbed free stream flow could be considered to resemble a part of a tube bank especially those tubes existing in the first row in the bank.

Provisions were made in the tunnel to facilitate mounting and removal of the test cylinder from the working section. Clearance holes are necessary to protect the porous cylinder against being damaged by the edge of the hole. To locate and hold the test cylinder centrally in its vertical position, a supporting guide circular frame of 100 mm diameter is used on the top plate of the working section guided by eight equally spaced short 4BA screws. This frame guides the 12 mm diameter rod at the top of the test cylinder. Air leakage was prevented using rubber sheet between the metallic surfaces.

The mean corrected approach velocity  $U_c$  of the flow past the cylinder was estimated by applying the correction for the blockage effect (section 5.2.7). to the velocity of the undisturbed stream  $U_\infty$  to give the velocity which would have been observed in the working section had the cylinder been removed. The air flow rate passing through the tunnel was varied and the following measurements were made with each free stream velocity under adiabatic conditions.

1. Pressure at upstream and downstream of the working section.
2. Peripheral angle measured from FSP.
3. Output signal developed across the shear stress servo-balance.
4. Normal pressure to the cylinder surface at each angle from FSP.
5. Pressure difference across the floating element (drag piece) of the servo-balance.

Whenever a normal velocity is applied to the porous surface, the following parameters are to be measured together with the previous ones:

6. Suction rotameter reading.
7. Pressure in the interior of the test cylinder.

Under diabatic conditions, with heat transfers between the main stream and the test cylinder, the following are extra parameters to be measured in conjunction with the previous parameters:

8. Cooling water flow rate.
9. Temperature difference, increase, for the cooling water.
10. Mainstream and surface temperatures.

The air velocity was varied between about 5.29 and 13.4 meters per second, giving a range of Reynolds number, based on the approach velocity and the cylinder diameter of  $0.27 \times 10^5$  to/...



to  $0.7 \times 10^5$ . At each chosen velocity the hot air together with the pitot-static probe were used to estimate the flow velocity and turbulence level in the tunnel.

### 5.3.2. Tube bank

Reliable data on flow within the commonly used tube bank arrangements is limited. However, due to time restrictions it was decided to study only one tube arrangement, namely, equal spacing staggered pattern in the present investigation with the intention to cover the rest of the arrangements later in a separate project.

For the tests, the transverse and longitudinal spacing distance were chosen to be 1.5 tube diameter, since this is an intermediate step between the two limits used in the most of exchangers, i.e., 1.25 and 1.75 tube diameter. Thus for the cylinders of 76.2 diameter, the transverse and longitudinal spacing were 114.3 mm each.

Since heat transfer was to be simulated in the tunnel using the hot air to simulate the shell fluid of exchanger, therefore, the dummy tubes chosen have a metallic surface. The ratio of tube length to diameter was chosen to be 5 to decrease the end wall effect on the central horizontal section of the cylinders where the flow measurements were to be made.

For these tests the tube bank consisted of twenty-one tubes arranged in staggered arrangement, three rows wide and seven rows deep. Since the tubes were to be used in a fixed geometry/...

geometry, the method of constructing the bank was to hold the tubes between a pair of end plates with holes in equal spacing pattern where the tubes were screwed to the plates. These end plates fixed the geometrical arrangement and the transverse as well as the longitudinal spacings.

The tubes are mounted vertically in the working section and each tube has the same dimensions as the instrumented test cylinder, i.e., 76.2 mm OD and 381 mm in length. The cylinders spanned the height of the working section while the test cylinder could be rotated from outside the tunnel.

The dummy tubes were made of aluminium tubing with 6.4 mm wall thickness. The cylinder surfaces are turned and machined so as to give a smooth surface finish. Cylinders were fitted with end pieces inserted into both ends of each cylinder and secured to the cylinder walls by three screws  $120^{\circ}$  apart. These end pieces were threaded, to fit a 1/4 inch BSF screw, along the longitudinal axis of the test cylinder. By this means, the cylinders could be secured, using short screws, between the top and bottom 0.8 mm thick steel plates in the tunnel. The screws passed through holes arranged in equal spacing staggered pattern. A total of twenty-three holes of diameter 6.5 mm were drilled through each end plate arranged to suit the bank pattern. Each plate is 393 mm wide, equal to the width of the working section plus the supporting frame width.

The distance from the outer cylinders, in a row, to the tunnel walls are equal to half the normal spacing of the cylinders./...



cylinders. This reduced effects of the wall on the flow in the central area of the tunnel. The holes being 114.5 mm apart and positioned so that the spaces between the outer holes and the plate edge was equal to half the normal hole spacing plus the supporting frame width.

There were seven rows of cylinders, with alternate rows containing three complete cylinders or two complete cylinders with two half cylinders at row ends, so that the effect of the side walls on the flow is reduced.

Possible air leakage between the tunnel walls and the half cylinders at the ends of each alternate row was prevented by machining the flat sides of the half cylinders.

Moreover, long eye and screws are hooked to the half cylinders from outside the tunnel, through the side walls of the working section. These screws are used to tighten the half cylinders flat ends against the tunnel perspex 5 mm thickness side walls.

Although the spacing between the cylinders in the bank are correct on average, manufacturing tolerances meant that the actual spacing of individual cylinders varied from the average value. The tolerance in the positions of holes in the end plates was  $\pm 0.25$  mm, and this, combined with the tolerance of  $\pm 0.1$  mm allowed for the positioning of the screw passing through the holes and a tolerance of  $\pm 0.15$  mm between the centre of the thread in the cylinder fixing end plates and the geometric axis of the cylinder, gives a maximum malpositioning of a cylinder axis of  $\pm 0.5$  mm, or between/...

between 0.6 per cent and 0.7 per cent of the cylinder diameter. Thus the maximum possible variations in the cylinder spacing is approximately 1 per cent of the cylinder diameter in any direction, although, in practice, few cylinders will be more than 0.7 per cent out of perfect alignment.

Most measurements were carried out at a range of Reynolds numbers, based on the cylinder diameter and the undisturbed free stream velocity between  $0.27 \times 10^5$  and  $0.7 \times 10^5$ . The lower limit was set to facilitate comparison with available data in the literature while the upper limit was controlled by the capacity of the centrifugal fan fitted to the rig.

The determination of the local parameters around a cylinder in the tube bank has been realised by the instrumented test cylinder (section 5.2.2) which could be inserted in different positions within the tube bank. The test cylinder was located in the middle section of the bank. It was the middle cylinder in a row containing three complete cylinders. This row is followed by two rows of the dummy tubes to eliminate the effect of any variations in downstream for different rows. This arrangement was fixed during the experiments, while changes in the relative tube position, for different rows, within the bank are made by moving the other dummy rows in upstream direction.

In addition to the local values the total pressure drop of the flow through the whole bank was measured.

The experimental procedure started by fixing the rear three rows/...



rows in the bank with the instrumented cylinder in the middle of the first row. For a certain flow rate the approach velocity was measured and corrected (section 5.2.7). The local parameters recorded were similar to those of the single cylinder (section 5.3.1) measured around the cylinder in equal steps of 5 degrees.

The flow rate was varied and the procedure is repeated for the planned range of Reynolds numbers. After completion of first row experiments, the instrumented cylinder was moved to each of the successive rows by adding rows of the aluminium dummy tubes upstream of that containing the test cylinder while its downstream is unchanged. Therefore, data collected shows the effect of any changes in the upstream direction. For each row a complete set of experiments similar to that of a single cylinder was carried out.

It must be understood that, as far as the tube dimensions are concerned, trials and effort were made to choose ones of exchanger engineering interest. Nevertheless, the physical dimensions of the developed shear stress sensor and the nature of the investigation add more restrictions to the tube diameter choice. However, it was felt that this disadvantage is not very serious as the effect of the tube diameter is allowed for in the Reynolds number.

#### 5.4. Concluding remarks

In this chapter a description of the experimental apparatus is given. Besides the constructional details for different/...

different parts of the rig, a functional description in relation to the proposed experimental programme is also given.

It is clear that in designing the present apparatus, provision is made for separating the individual effect of each parameter involved in the planned project, on the flow across the test models whether it is an isolated single cylinder or an individual cylinder inside an equally pitched staggered tube bank.

The developed shear stress sensor, servo-force balance, as a first step in the project, was used to determine the dynamic characteristics of the cross flow of air on an isolated single cylinder and the vortex shedding frequency. Results compared with available data are analysed and discussed in Chapter 6.

Various flow conditions were studied over a certain range of parameters such as Reynolds number, surface roughness, turbulent intensity and cylinder position relative to the tube bank. For each test, simultaneous measurements of local parameters such as wall shear stress and normal pressure were carried out around the test cylinder's circumference. Results of pressure drop across the tube bank with different depth are compared with data and correlations from the literature. The measurements are analysed and discussed in Chapter 7.

For both the isolated single cylinder and tube bank, detailed studies were made for the effect of mass extraction on/...



on the local parameter around the test model over a certain range of suction and Reynolds number. Different flow regimes under these conditions were obtained and determined in terms of these parameters. Effect of mass extraction on different flow conditions are analysed and discussed in Chapter 8.

Over a certain range of Reynolds number, mass extraction and heat load, local parameters such as wall shear stress, normal pressure and heat transfer coefficient around the test model were determined simultaneously. The effect of simultaneous heat and mass transfer on the flow across single cylinder and tube bank arrangement is analysed and discussed in Chapter 9.

## CHAPTER 6

### VORTEX SHEDDING

#### 6.1. Introduction

In a previous chapter, 3, details of the design and construction of an instrument to measure directly the shearing forces on circular cylinders in an external cross flow are given. In this chapter, it will be demonstrated how this instrument is successfully used to give a picture for the flow dynamics around a cylinder such as the vortex shedding frequency. Only data concerning flow around single cylinders will be shown while the data concerning the bank of tubes are outside the scope of the present work.

#### 6.2. Vortex shedding from a bluff body

Steady external flow over a bluff body, e.g., a circular cylinder, experiences different flow characteristics than that over a streamlined body. Over a bluff body, the pressure rise on the rear side of the cylinder is sufficient not only to let the particles existing in the boundary layer and slowed down by the friction come to rest before reaching the stagnation point, but also to repulse them (83) and, further downstream the tendency is for a back flow. The effect of this is that the forward flow in the boundary layer is forced to leave the surface, and a sheet of discontinuity is formed which ultimately breaks up. The separated shear layer, roll-up due to instability and mean velocity gradient. This breaks/...



breaks up into vortices which are shed into the wake. The exact form of this process depends on the Reynolds number and turbulence in the fluid flow.

For Reynolds number less than about three, the flow is called Stoke's flow and is characterised by the absence of vortices behind the cylinder. With increasing Reynolds number, streamlines widen and at about  $5 < Re < 40$  a pair of fixed vortices are formed immediately behind the cylinder. A further increase in Reynolds number causes the vortices to elongate in the flow direction and become less stable in asymmetric disturbances. Such a disturbance may cause the fixed vortices to break away from the rear of the cylinder. This leads to the formation of a new pair of vortices which break away too, the process repeats itself and a state of alternate periodic vortex-shedding is reached. The boundary value for the Reynolds number of 40 (for the shedding of the vortices) is valid only for flows in a free field. If measurements are made in a wind tunnel, the tunnel walls extend a stabilizing action on the separated boundary layer, so that the final collapse into individual vortices could take place at higher approach Reynolds number which is a function of the blockage ratio (84).

The process of breaking away of the vortices can occur at Reynolds numbers as low as ninety and then a Karman street is formed in the wake of the cylinder. For Reynolds number up to 150, the flow in the vortices is laminar and the vortex street is preserved for many diameters downstream.

As the Reynolds number increases from 150 to 300, the free vortex layers "spring" away from each separation point on each side of the cylinder to become turbulent before shedding away into the vortex street. The vortices are diffused as they move downstream and at about fifty diameters downstream there is pure turbulence with no evidence of periodicity. As the Reynolds number reaches 300, a transition from laminar to turbulent flow at the separation points occurs and periodic turbulent vortices are shed into the wake of the cylinder and decay rapidly with distance downstream.

This situation is believed to remain up to the critical Reynolds number, about  $2 \times 10^5$ . This range is known as the subcritical range of Reynolds number. At the critical Reynolds number, the flow transition from laminar to turbulent occurs in the boundary layers and this causes the separation to be delayed and the separation points move backwards towards the rear of the cylinder. This causes the wake to be much narrower, periodic vortex shedding is suppressed and the pressure drag falls to a minimum.

Boundaries between the subcritical and the critical ranges tend to be at lower Reynolds numbers by increasing the turbulence level in the incident stream, since transition to turbulent flow in the wake or boundary layer then occurs at a lower Reynolds number.



### 6.3 Measurements of the vortex shedding frequency:

The rate at which the vortices are shed from the sides of the cylinder is usually measured using one or a combination of the following methods :

- 1) Strain gauges on the cylinder surface
- 2) Hot wire anemometer in the Karman vortex sheet
- 3) Microphones inside or outside the tunnel
- 4) Capacitive or inductive transducer supported on the channel wall and kept a small distance from the wall.
- 5) Platinum film sensors deposited on the surface with frequency response calibration (85).

The field of the vortices is by no means a purely sinusoidal one; its second harmonics may be strong. If one of the mechanical natural frequencies of the cylinder or the channel walls happens to coincide with this second harmonic, a strong vibration or noise with this frequency may be detected if one of the methods 1, 3 or 4 are in use.

The source for such noise is not necessarily the field column perpendicular to the flow and parallel to the cylinder longitudinal axis inside the channel, but could also come from the radiation of the vibrations of the channel wall. Measurements of this type could lead to a shedding frequency twice as high as the real one in the channel.

Hot wire anemometry is used extensively in measuring the shedding frequency. The hot wires are tungsten wires of

5 microns in diameter and the electronic circuit is a linearized constant temperature type. In these cases, the hot wire should be placed in the mainstream some distance away from the axis of the Karman vortex street.

Hot wire measurements have indicated that the flow structure and particularly the frequencies of flow oscillations can change rapidly in the vicinity of the solid surface.

Roshko (86) reported a frequency twice the shedding frequency at close proximity to the cylinder by a hot wire anemometer. Moreover, the presence of the probe could affect the flow structure around the cylinder.

The drawback in using strain gauges is that, to ensure an adequate or reliably measurable strain, the cylinder needs to be sufficiently flexible (87). Under these circumstances there is a real danger of contamination of the result from the cylinder dynamics.

Hussain and Ramjee (89) showed that periodical signal, from a hot wire, in the cylinder wake at  $Re = 145$  increases in amplitude from the rear of the cylinder to about four diameters distance and then decreases progressively with distance from the cylinder. Moreover, increasing the free stream turbulence will disturb the wake vortices. The otherwise stable and periodic wake is disturbed by the three dimensional free stream turbulence and the distortion will be complete at 60 diameters downstream of the cylinder.

In the case of the tube banks, Strouhal number measurements are/...



are more difficult than those of an isolated cylinder. Chen (90) during experiments to determine the Strouhal number for tube banks of various geometries interpreted his hot wire measurements in terms of vortex shedding. He suggested that different types of vortex patterns exist for different types of tube bank geometries. On the other hand, Owen (91) from similar experiments to those of Chen interpreted his hot wire signal in terms of turbulence which does not involve vortex shedding. Further, he suggested that deep inside a tube bank system the flow is essentially turbulent and exhibits no regular features apart from the general motion through the tube bank. By using microphones to pick up the pressure fluctuations, Baully (92) tried to measure the vortex shedding in a tube bank. The predominant frequency was determined from the microphone signal frequency spectrum. He concluded that the Strouhal number in the bank can depend upon the number of cylinder rows. Vortex shedding frequencies were also measured by Borges (93) for two row banks of tubes. The technique adopted was to vary the position of the hot wire between the two rows until a near sinusoidal output was obtained. This signal is stored on a screen of a storage oscilloscope and frequency is measured directly from the oscilloscope record and an average obtained from a number of samples. From measurements in a single row bank, Ishigai (94), suggested that the shedding frequency recorded by the hot wire for transverse pitch of  $< 1.5$  was somewhat irregular and the periodic velocity fluctuations caught were not due to the Karman vortex but to unknown reasons. Stevenson (95) used two hot wires placed in the rear of the cylinder/...

cylinder row and he reached the same conclusion. For more details about this topic reference should be made to the critical survey made by Zdravkovich (255).

#### 6.4 Present device and shedding frequency measurements

It has been realised that it would be more accurate to estimate the shedding frequency on the cylinder surface if such measurements are made on a part of the surface producing such vortices. For this purpose, the present device developed for measuring the shearing force (Chapter 3) which is constructed at the middle height of the test cylinder was used to measure such frequencies.

Measurements of the dynamic response of the device were made at two angular positions around the circumference of the cylinder. In the analysis this dynamic response is used to determine the dominant shedding frequency in the flow around the cylinder. First position was chosen where there was known to be a definite boundary layer at the frontal part of the cylinder, namely at  $\theta = 50^\circ$  measured from the front stagnation point. Second angular position was located in the main vortex region (85) and it was chosen to be at  $\theta = 160^\circ$  from the front stagnation point in the wake region of the test cylinder.

The dominant frequency, vortex shedding, was measured from the dynamic response of the shearing force device when it was exposed to the external flow across the cylinder.

The technique adopted was to rotate the cylinder around its vertical axis to the first chosen position, at  $50^\circ$ , and the signal/...



signal developed across the servo-force balance was displayed on the screen of an Advance Instruments OS/000A oscilloscope. Then the signal was recorded using a data lab DL 901 transient recorder. The recorded signal was transferred on to a tape which was fed to a computer programme for analysing the spectrum obtained using the fast fourier transformation (FFT) technique to determine the frequency - amplitude characteristics of the spectrum. The dominant frequency, indicated the shedding frequency in the tunnel. The procedure was repeated at the second angular position, i.e.,  $160^\circ$  from the F.S.P. the frequency was estimated and an average was obtained from a number of samples.

At each position at least ten samples were taken, from each flow rate, of the output signal of the servo-force balance. From these samples the dominant shedding frequency was estimated. The highest amplitude recorded, averaged over the sampling period, was recognised to correspond to the vortex frequency of the fluid column perpendicular to the flow direction. A typical frequency amplitude characteristics are shown in Figures 6.1 to 6.5 as 'first trial' which correspond to main stream velocities  $U_\infty$  of 5.3, 9.3 and 13.4 meters per second.

From the measured frequency the Strouhal number defined as :-

$$S = \frac{nd}{U_\infty} \quad 6.1.$$

was estimated, where  $n$  is the dominant shedding frequency of/...

of the unsteady flow,  $d$  is the cylinder diameter and  $U_\infty$  is the free stream velocity. The Strouhal number was estimated to be about 0.2 and was independent of the Reynolds number of the main flow around the cylinder.

The experimental runs were repeated and results are shown on the corresponding figures as the 'second trial'. It is apparent that the servo force balance shows a quite satisfactory level of repeatability. The point which is worth mentioning here is the detection of the same dominant vortex shedding frequency at the frontal part of the cylinder at  $50^\circ$ , measured from the FSP which was similar to that detected in the vortex region in the wake of the cylinder. Bruun (96) from measurements of the unsteady pressures around a cylinder, using pressure transducers connected to equally spaced pressure tappings, noticed that in the sub-critical range, the vortex shedding dominated the surface pressure field. This result together with the present results, suggest that the shedding of the vortices is affecting the whole flow structure over the cylinder surface. It is obvious that the amplitude of the signal is not as dominant at the frontal part of the cylinder compared to the rear. Nevertheless, it is possible to ask whether the assumption for laminar boundary layer and laminar separation is still holding for this 'shaken' boundary layer on the frontal part of the cylinder.

#### 6.5. Concluding Remarks

From previous sections it is possible to conclude that by analysis of the dynamic response of the developed  
 : servo/...



servo force balance, vortex shedding frequency can be estimated. The results are in agreement with the reported values in the literature. The main conclusion reached is that the present device works satisfactorily and could be used with some confidence for investigating static and dynamic characteristics of the flow across circular cylinders.

## CHAPTER 7

### RESULTS II: CROSS FLOW THROUGH A TUBE BANK

#### 7.1. Introduction

The study of flow across tube bank configurations continues to attract interest because of the importance of this flow type in the design of heat exchangers. From the literature survey presented in Chapter 5, it is clear that while much work has been done on the overall characteristics in the tube banks, a limited number of investigations dealt with the details of the flow within the bank configurations. This shows the need for more work to be carried out to provide more information about the detailed characteristics inside the tube bank. Due to this need the present work was undertaken.

The present study is mainly concerned with studies into the flow characteristics within tube banks in general and equal pitches staggered type in particular for the case of a cross flow normal to the tube axis in a model of a vertical tube condenser. A complementary approach to this will be considered in separate successive stages, in Chapters 7, 8 and 9.

This chapter deals with the first stage in the present investigation, i.e., the influence of different flow parameters which might affect the flow around a circular cylinder whether single or within a tube bank. The parameters involved are those of the surface roughness, Reynolds/...



Reynolds number and turbulence intensity for single cylinder in a cross flow. Thereafter, the effect of the cylinder's relative position within the tube bank is investigated.

The flow parameters distribution around the test cylinder was carried out using the experimental rig explained in Chapter 5. Data was recorded for the variations in the normal pressure and wall shear stress around the test cylinder under different flow conditions. Whenever possible, this is compared with the relevant work reported by other research workers.

Local values of the wall shear stress were measured using the specially developed sensor described in Chapter 3 and using the experimental procedure as explained in Chapter 5.

First, data is presented for the flow across a single cylinder and, thereafter, it is followed by results obtained using the tube bank model.

## 7.2. Single cylinder in a cross flow

This part of the study is subdivided into sections to accommodate the individual influence of parameters such as surface roughness and turbulence intensity on the flow characteristics around the cylinder circumference.

The experiments were performed using the porous cylinder, section 5.2.2., spanning the height of the working section and located in its middle plan between the side walls.

Local/...

Local measurement of the wall shear stress and normal pressure were made using the servo-force balance with its built in pressure tappings, Chapters 3 and 5. The length and diameter of the tubes connecting the pressure tappings to the manometer were chosen to minimise the response of the flow fluctuations and time average values were thus obtained.

As the distributions around the cylinder circumference were believed to be symmetrical about the meridian, measurements were recorded from  $\theta = 0^\circ$  up to  $180^\circ$  from the front stagnation point (FSP) by rotating the cylinder around its vertical longitudinal axis. The angle  $\theta$  was read by the protractor fitted to the test cylinder.

From static pressure readings around the position  $\theta = 0^\circ$ , the point of maximum pressure accurately determined the location of the front stagnation point and errors in positioning the protractor relative to the angle scale were thus highly reduced.

#### 7.2.1. Shear sensor's gap effect on the recorded skin friction

From the external cross flow around the cylinder view point, the drag piece of the sensor whilst flush with the cylinder surface, was separated from it by a surrounding 80  $\mu\text{m}$  clearance gap.

Presumably, the balance would give a better reading if that clearance gap was zero, for then there would be no floating drag/...



drag piece. Since the surface area of the drag piece is quite large compared to the very small clearance gaps (over 25 times), the pressure underneath this area will be quite uniform and errors due to pressure forces could be minimised.

However, it seems reasonable to assume that modifications of the flow over the outer surface of the test cylinder is slight if the clearance gap's width is kept small. The magnitude of the disturbance caused to the flow eventually depends on the dimensions of the gap width as well as the flow characteristics in the gap vicinity.

Dhawan (2) carried out measurements of the velocity profile together with Schlieren photographs in the vicinity of 2 mm gap in a thick turbulent boundary layer and 0.25 mm gap in supersonic flow. He concluded that, provided that the drag piece is flush with the surrounding model surface, the flow characteristics were essentially unaltered by the presence of these gaps. Moreover, it was indicated by White (53) that, provided that the gap width is kept small, about 80  $\mu\text{m}$ , the effect of the gaps is not serious and readings of the balance may be accepted with some confidence.

It is apparent that more accurate information about gap effect on the measured skin friction could be obtained from an experimental investigation solely devoted to such studies. It was felt, however, that in view of the limitations imposed by the present set up's physical dimensions, it would not be wholly satisfactory for this purpose./...

purpose. Indeed, such an investigation would best be performed using larger devices in a working section with extremely uniform and accurately controlled, repeatable flow conditions.

However, the published data in the available literature provides an approximate picture of the clearance gap effect and its influence on the measured shear stress values.

The first estimate is that given by Hoerner (245, 246) who considered the deep clearance gaps as a sort of imperfection in the surface and indicated that the drag caused by these gaps is a function of their width and depth. For gaps with depth to width ratio of more than 0.7, the gap drag coefficient reached a constant value and the pressure forces were those corresponding to a dynamic pressure calculated on a height equal to the width of the gap. This means that, for the case of the present floating drag piece, the effect is approximated to twice the magnitude of the skin friction based on the gap area.

In 1955, Hakkinen (247) showed that these clearance gaps introduce a force equal to at least the skin friction based on some effective gap area acting on the solid surfaces as pressure forces. These forces act on the side of the gap as increased skin friction on the surface of the drag piece exposed to the main flow. With gap clearance equal to 11% of the deflected drag piece area, Hakkinen estimated the effective area to be 50% of the total clearance area.

Moreover/...



Moreover, he reported that in a null-type transducer system, the gap effect could be even smaller.

Recently, a smaller gap effect was reported by Depooter et al (56) who demonstrated that the effective gap area was reduced to 36.5% of the total clearance area. They pointed out that the difference between their results and those of Hakkinen were due to the fact that they used a null-type device while he used a deflected type of instrument where the gaps upstream and downstream of the drag piece were not equal under loading conditions.

Indeed, an investigation which is designed only to provide data on the effect of the gap clearance is the answer for the major question: How much can the gaps affect the measured skin friction?

Such an investigation was carried out by Allen (63) using a drag piece with different sizes over a wide range of gap width to drag piece area ratio. Within the scatter of the obtained results for the variation in the measured skin forces, with zero protrusion, as a function of the gap size, very little effect is indicated for the gap size on the total friction forces.

Moreover, Allen (63) indicated that there was no advantage in using small gap size and a larger gap size was recommended for it was less sensitive to protrusion error. While this might be the case on a flat plate where the incident main stream is parallel to the drag piece surface, the/...

the situation is different on the surface of a circular cylinder. In this case the drag piece together with the clearance gaps face the incident stream with different angles as they rotate around the cylinder circumference. It was felt, however, that it was much more advisable to use the smallest possible clearance gap width on the present test cylinder rather than the big one.

It is obvious that, considering the above, an approximate percentage of the error involved in the present skin friction measurements due to the presence of the clearance gap could be estimated. On the one hand, applying the approach used by Hoerner (245, 246) to the problem in hand gives the maximum possible error of about 8% overestimated. On the other hand, applying the other extreme found by Depooter et al (56) provides the minimum possible error in the measured shear stress of about 3% overestimated.

#### 7.2.2. Procedure and reduction of observations:

For a certain main air flow rate, the undisturbed force stream velocity was calculated from measurements of flow velocities by the pitot traversing mechanism located in the circular section downstream of the working section.

Moreover, the velocity head was recorded by a Prandtl tube just upstream of the test cylinder and was compared with that obtained from the static pressure taps on the cylinder at the FSP. The agreement was reasonable about  $\pm 2$  per cent and the velocity head recorded at the FSP was used, accordingly, to calculate the main stream velocity  $U_{\infty}$ .

This/...



This velocity was then corrected for the blockage effect through equations 5.5, and thus  $U_a$  was obtained.

The normal pressure distribution was measured from the signal recorded by the tappings located at the test porous cylinder referred to the static pressure averaged over the side walls of the working section upstream of the test cylinder in the undisturbed region ( $P_\infty$ ).

The static pressure around the cylinder circumference was made non-dimensional in the form of pressure coefficient  $CP$  against angle  $\theta$  measured from FSP.

$$CP_\theta = \frac{P_\theta - P_\infty}{P_{\theta=0} - P_\infty} \quad 7.1.$$

where  $P_\theta$  is the normal pressure measured at the peripheral angle  $\theta$  and  $P_\infty$  is the static pressure of the undisturbed incoming stream.

The pressure drag contribution to the total drag coefficient is calculated using the following formula :-

$$KD = \int_0^\pi CP_\theta \cos\theta \, d\theta \quad 7.2.$$

On the other hand, wall shear stress,  $\tau_\theta$ , was measured from the output signal of the servo force balance and presented in a dimensionless form by the dynamic pressure as the friction factor  $K'_{f\theta}$  :

$$K_{f\theta} = \tau_{\theta}/\frac{1}{2} \rho U_a^2 \quad 7.3.$$

The values of this coefficient are estimated to be within 3 to 8 per cent overestimated (section 7.2.1).

Drummond (72) suggested that the frictional drag could be obtained by integrating the wall shear stress from the FSP up to the flow separation on the cylinder surface while Morsy (57) integrated the skin friction distribution graphically to obtain the average coefficient of shear stress.

In this work the shear drag contribution to the total drag coefficient is estimated as following (23) :

$$CF = \int_0^{\pi} K_{f\theta} \sin\theta \, d\theta \quad 7.4.$$

The ratio contribution of the wall shear stress and pressure drag is :

$$\frac{\Delta P \text{ skin friction}}{\Delta P \text{ press drag}} = \frac{CF}{KD} \quad 7.5.$$

and the turbulence intensity of the incoming air stream is :

$$T.L.\% = \frac{\sqrt{u'^2}}{U_{\infty}} \times 100 \quad 7.6.$$

### 7.2.3. Effect of surface roughness

#### 7.2.3.1. Surface roughness in cross flow:

Smoothness/...



Smoothness or roughness of a surface is a relative quantity. It is a common practice, however, to regard a surface as smooth when it is so even that no roughness or points are perceptible to the touch. In aerodynamics the surface roughness influence on the flow structure is a function of the type of flow together with the boundary layer structure over the surface in hand.

Sometimes permanent surface treatment is used to enhance the heat transfer in heat exchangers to raise the efficiency of the unit. This could be achieved by applying hydrophobic coatings for condensing surfaces, porous coatings for boiling and textured or formed surfaces for both condensing and boiling (24).

Therefore, an investigation into the effect of surface roughness on the flow around circular cylinders was considered to be relevant to the present study. Surface roughness with a cross flow on cylindrical surfaces was also studied by Achenbach (80) for roughness parameter up to  $45 \times 10^{-5}$ . Since his probe was not able to detect shear stress values for Reynolds number less than  $10^5$ , he concluded that, based only on static pressure measurements, the surface roughness does not affect that flow regime.

In the present work, the outer surface of the test cylinder with its porous nature was considered to have a rough surface with  $\frac{K_s}{D} = 53 \times 10^{-5}$ , where  $K_s$  is the average diameter of the spherical bronze particles from which the cylinder was made. Thereafter the cylinder's outer surface was made 'aerodynamically' smooth by applying a sheet of transpaseal self/...

self adhesive plastic, 50  $\mu\text{m}$  thick to it. The sheet was applied to the whole surface including the drag piece of the shear force sensor together with its supporting frame. Care was taken to keep the same squared clearance gaps around the drag piece.

#### 7.2.3.2. Results and discussion

First of all, it was decided to compare the present results with those obtained by other investigators around a smooth surface single cylinder in a cross flow using different types of probe for realising the wall shearing forces.

Fig. 7.1 shows the measurements of Achenbach (176), Giedt (43), Fage (41) and Zingzda and Ruseckas (47) together with some of the present results. The results of these investigators cover a range of Reynolds number from 29000 to 100,000 and were obtained using a variety of indirect shear stress measuring techniques. For example, data of Achenbach and Zingzda and Ruseckas were realised using a boundary layer fence similar to that developed by Konstantinov and Dragnysh (46). On the other hand, results of both Fage and Giedt were obtained using surface tubes.

It is interesting to note that while Achenbach was not able to obtain shear stress data, using the boundary layer fence, for Reynolds number less than 100,000, Zingzda and Ruseckas, using the same technique, managed to record skin friction forces around the cylinder for Reynolds numbers as low as 29,000.



From figure 7.1, it is clear that the disagreement between the present measurements and those for the mentioned research workers, cannot be attributed to variations in the turbulence intensity since they are performed with T.L.% within 1.2 per cent. Neither, could it be caused by different blockage effect since the maximum correction could be within 11 per cent of the recorded values. Consequently, a question could be raised about the effect of the probes used on the final outcome of the shearing forces, i.e., the applicability of indirect devices on cylinder surface.

Depooter et al (244) showed that the boundary layer fence could be useful in those cases where there is no longitudinal pressure gradient. However, round a cylinder in a cross flow a large pressure gradient exists and the flow picture is expected to be quite different than on a flat plate. Patel (4) indicated that the readings of the boundary layer fence were affected by a pressure gradient but to a lesser degree than the corresponding surface tube readings. These observations show that, in a large pressure gradient, the readings of the boundary layer fence and the surface tube might be appreciably in error. Indeed, it was reported by Achenbach (176) that the results obtained using surface tubes and boundary layer fence were too low.

TABLE 7.1. /...

TABLE 7.1

<u>Author</u>	<u>L/D</u>	<u>D/X</u>	<u>T.L.%</u>
Fage (41)	16	0.06	-
Giedt (43)	10	0.11	1.
Achenbach (176)	3.3	0.16	0.7
Zingzda et al (47)	2	0.25	-
Present	5	0.22	1.2

From the above discussion, the main conclusion reached was the doubt as to the usefulness of the indirect measuring techniques in estimating the wall shear stress on the cylinder circumference where large pressure gradient does exist.

Figure 7.3 shows the effect of changing the cylinder's surface nature on the normal pressure distribution around its circumference. In figure 7.4, the present pressure coefficients are compared with those of Morsy (57) and Achenbach (80). From these figures, the pressure drag is calculated and given in Table 7.2.

TABLE 7.2

<u>Author</u>	<u>Re x 10<sup>-5</sup></u>	<u>KD (Smooth)</u>	<u>KD (Rough)</u>
Present	( 0.27	0.92	1.03)
	( 0.47	0.95	1.08)
	( 0.7	0.91	1.03 )
Ref. (57)	( 0.3	1.29	-
	( 0.46	1.18	-
Ref. (80)	( 1.	1.12	0.75)

The/...



The present results (corrected for the blockage effect) show a slight increase in the pressure drag ( $K_D$ ) with the natural roughness of the porous surface. In general, these results agreed with the values obtained from the analysis of the data reported by Fage and Warsap as shown in Figure 9, in Reference number 80. The reduction in the pressure drag with the rough surface reported by Achenbach (80) might be due to the fact that his measurements were in the neighbourhood of the critical range where large changes in the pressure drag are expected.

Figures 7.5, 7.6 and 7.7 demonstrate the present results for "rough" and "smooth" test cylinders together with those of references 57 and 80. These figures show the wall shear stress factor  $K_f$  versus angle  $\theta$  measured from the forward stagnation point.

The general trend of the present results of  $K_f$  values is similar to that noticed by other investigators. Magnitudewise, however, the similarity was not that clear. The similarity between the presented data lies mainly at the FSP where  $K_f$  starts from zero value and at the separation point where  $K_f$  was reduced to zero value. However, Morsy's data in figures 7.5 and 7.6, did not show a drop in  $K_f$  to zero value in the separation region. Instead, positive shear stress was recorded all the way up to the rear stagnation point which Morsy attributed to the small values of  $Re$  used and that negative values of  $K_f$  at the back half of the cylinder could be obtained if Reynolds number is raised to 107,000.

By/...

By placing a perforated copper plate on the mid section of his cylinder, Morsy reported that the roughness caused by the drilled holes, 0.76 mm diameter and 6.35 mm apart, resulted in a zero value of  $K_f$  at separation point. On the rear of the cylinder, after separation, negative  $K_f$  values were reported which changed to positive from  $\theta = 125^\circ$  up to  $\theta = 180$  from FSP.

In fact, the trend of measurements obtained on the rear of the smooth cylinder by Morsy (57) is in complete disagreement with the observations of other investigators and the positive  $K_f$  on the rear part of the cylinder seems unrealistic. For example, the negative or the reversed flow motion on the rear of a cylinder in cross flow was noticed as early as in 1931 (145) and for Reynolds numbers as low as 25 (149), this point is explained in detail in section 4.2.2. Furthermore, the available literature shows that negative wall shear stress in the circulation region was recorded for Reynolds number equal to 29,000 by Zingzda et al (47).

It is possible to notice that the present measurements agreed, trendwise, with those observed by Achenbach (80, 176). However, there is a considerable difference in the recorded values of  $K_f$ . That might be due to the difference between the devices used in each case. As mentioned earlier, Achenbach reported that the results realised by the boundary layer fence were too low (176). Since Achenbach's lowest Reynolds number, for the shear stress measurements, was 100,000, the corresponding reported results are/...



are presented in Figure 7.7 for comparison.

The present results generally speaking, feature the following points. First, the peak in the  $K_f$  distribution was higher for the rough cylinder surface than for the smooth one. Second, the peak was slightly moved towards the rear of the cylinder for the rough surface. The separation point is not significantly influenced by the present changes in the surface nature, neither were the recorded values beyond the separation point significantly varied for the present conditions.

The shear stress contribution to the total drag according to expression 7.4 and results are shown in Table 7.3.

TABLE 7.3

<u>Author</u>	<u>Re x 10<sup>-5</sup></u>	<u>CF (Smooth) x 10<sup>3</sup></u>	<u>CF (Rough) x 10<sup>3</sup></u>
Present	( 0.27	8.2	15.8
	( 0.47	13.4	20.8
	( 0.7	21.7	29.4
Ref. (57)	( 0.3	30	29
	( 0.46	23	20
Ref. (80, 176)	( 1.	8.2	16.1

From this table together with Table 7.2, it is noticeable that the percentage contribution of surface friction to the total drag of a cylinder in cross flow is quite small. With a smooth surface, this amounts to about 0.7 per cent of the total drag at  $Re = 27,000$  and it becomes 1.8 per cent at/...

at  $Re = 70,000$ . For rough surfaces, the percentage contribution ranges from 1 to 2 per cent for the Reynolds number range tested. These are shown in figure 7.8.

Morsy (57), from graphical integration of his  $K_f - \theta$  distributions, suggested that the average skin friction coefficient was about 30 per cent higher for the 'rough' surface than the smooth one. Reprocessing Morsy's data, according to expression 7.4 and tabulated in Table 7.3, the results showed that CF was, in fact, decreasing for the "rough" surface and less than that for the smooth surface ones. On the other hand the increase in the CF value due to roughness effect noticed in the present work is similar to the observations noticed by Achenbach as shown in Table 7.3.

It is worth mentioning here, that the output signal from the servo force-balance was subjected to high oscillations on the rear of the cylinder and, in particular, near the flow separation point. The observations near this area suggested that there might be a separation region rather than a flow separation point.

In the beginning, it was thought that this might be due to the "finite" width of the drag piece which subtended an angle of about  $\Delta\theta = 3$  degrees at the axis of the cylinder. But such oscillations were also noticed by other investigators. Hurley and Thwaites (67) indicated that such phenomena is possible in a laminar boundary layer.

Indeed/...



Indeed these oscillations could be attributed to the influence of the shedding of vortices that took place at the rear of the cylinder. Boulos and Pei (85) noticed a pronounced periodicity in the heat transfer rate, at the separation point which has a frequency equal to the vortex shedding frequency at the back of the cylinder. Their observations showed clearly that the flow separation point was continuously oscillating over an arc of 10 degrees over the cylinder surface. This point is explained further in section 9.4.2.1.

One of the noticeable features of the shear stress distributions is the non zero magnitudes at  $\theta = 180^\circ$  measured from the FSP. Similar observations are reported by Zingzda et al (47) using a boundary layer fence as a shear stress probe. Indeed this should not be the case if this position,  $\theta = 180^\circ$ , on the cylinder surface was the rear stagnation point of the flow.

However, this phenomena could be explained, following Pankhurst and Thwaites (68), by assuming that the rear stagnation point was away from the cylinder. According to Schwabe (83), there might be a pressure minimum between the rear stagnation point at the cylinder surface and this free stagnation point. Moreover, this free stagnation point could be unstable due to the shedding of the vortices from the rear of the cylinder together with the tendency for disturbances to be amplified in a region of rising pressure.

7.2.4./...

#### 7.2.4. Turbulence level effect:

##### 7.2.4.1. Turbulence level in cross flow

In a tubular heat exchanger, when shell side fluid flows with realistic values of Reynolds number, some degree of turbulence will be present. These may be generated in one or more of a number of ways and the magnitude of flow fluctuations involved are dependent to some extent on the flow velocities encountered.

One source of turbulence is that of normal turbulent flow when the flow Reynolds number exceeds a value which depends on the shape of the channel through which the fluid is flowing. For example, upstream of a tube bank, much of the turbulence may be of this type. Within the tube bank, separation of the boundary layer that built up on an obstacle, presents the major source of turbulence inside the bank. Also, turbulence is generated at abrupt changes in the flow cross section, e.g., at entry to the shell.

Therefore, it is obvious that a study of the effect of turbulence intensity on cross flow characteristics around circular cylinders seems relevant to the present work since it was designed to study the influence of different parameters normally encountered in heat exchangers in general and in vertical tube condensers in particular.

A study of the effect of turbulence on the flow around a circular cylinder, from observations taken in wind tunnels, should be based on a comparison between the flow characteristics measured in tunnel streams which have been purposely/...



purposely disturbed with those measured in the ordinary undisturbed stream.

Artificial turbulence was produced by introducing a turbulence generator such as a rope netting or wire screen upstream of the test cylinder at such a distance that the flow through the generator is not influenced by the presence of the model.

A small fraction of the generated turbulent energy is dissipated at a given distance behind the generator. Since disturbances in the vicinity of a body diminish in intensity down its length, these can only be regarded as reasonably uniform when the model length is small compared with the distance behind the generator.

#### 7.2.4.2. Experimental procedure

Data was taken first with a 16 mesh damping screen placed upstream of the wind tunnel, attached to the bell shaped intake to decrease the turbulent fluctuations occurring in the normal tunnel stream.

A constant temperature hot wire anemometer was used to measure the turbulence intensity in the incoming air stream to the working section. Turbulence intensity of the incident undisturbed stream was estimated at a location more than 1.5 cylinder diameters upstream of the test cylinder FSP, since at this distance the turbulence level might have just begun to be affected by the presence of the cylinder model (157). The estimated turbulence level of the air stream (rms stream wise component relative to free stream velocity) was/...

was about 1.2%.

Thereafter, the turbulence intensity was artificially increased in the flowing airstream by inserting a turbulence generator, i.e., the heater banks, explained in section 5.2.8.2., upstream of the test cylinder with the plane of the generator normal to the flow direction. This generator consisted of spiral coils 12 mm diameter which were wound from 2 mm diameter wire. The cylinder's leading edge was 1040 mm downstream the generator and the estimated turbulence intensity in this case was in the order of 6%.

Turbulence intensity variations across the working section were shown in figure 5. It is clear that in the central part of the test section, the change in the recorded level of turbulence is not significant and it increases slowly towards the side walls of the tunnel with a rapid increase in the boundary region.

#### 7.2.4.3. Results and discussion

Under conditions of high stream turbulence level, the structure of the flow field would be expected to be quite different with and without imposed turbulence.

Data showing the distribution of normal pressure for two surface conditions, explained in section 7.2.3.1, under two turbulence levels of the incident flow is presented in figure 7.9 for  $Re = 27,000$ . Figure 7.10 shows the wall shear stress measurements corresponding to the flow conditions in figure 7.9.

The/...



The data shows that the effect of T.L. on the pressure coefficient distribution is not significant. Figure 7.10 shows that increasing the T.L. caused an increase in the skin friction on both surface conditions, smooth and rough. Variations in the  $K_f$  values were quite small in the region from the FSP to about  $\theta = 30$  degrees. The peak of the  $K_f$  distribution was displaced at a higher value towards the flow separation point by increasing the turbulence intensity. Due to the lack of a fixed separation point, at any particular condition, the influence of increasing the T.L. on the flow separation was difficult to determine.

Figure 7.11 shows the normal pressure distribution on the present "rough" surface for two Reynolds numbers at the two turbulence levels investigated. From the FSP up to  $\theta = 60^\circ$ , variations in CP values are quite small, and within the accuracy of the measurements, data in that region collapses on one curve. At the rear of the cylinder, however, it seems that the increased turbulence level caused the back pressure to increase and consequently the pressure drag (uncorrected for blockage effect) was reduced as shown in Table 7.4.

Figure 7.12 shows the wall shear stress simultaneously measured with data of figure 7.11. Up to  $\theta = 40^\circ$  from the FSP, changes in  $K_f$  values are not significant, thereafter the local values of  $K_f$  were increased by increasing the turbulence intensity.

Figures 7.13 and 7.14 show a comparison between the present results and those of Fage (23) and Giedt (43). The present turbulence/...

turbulence intensities were 1.2 and 6 per cent, those of Giedt were 1 and 4 per cent and Fage did not specify the turbulence level in his tunnel.

TABLE 7.4

<u>Author</u>	<u><math>\text{Re} \times 10^{-5}</math></u>	<u>KD</u>		<u>CF</u>			
		1.2	6	1.2	6	1	4
						n.s.	b.r.
Present	(0.47	1.3	1.05	13.4	17.3		
	(0.7	1.16	0.85	21.6	23		
Fage (23)	0.6						10.6 17.2
Giedt (43)	0.9					11	13.6

Both Fage and Giedt used surface tubes as shear stress probes, thus they were able to measure  $K_f$  values only up to the flow separation point. Due to the nature of these probes, they recorded no measurements in the circulation region or at the very front of the cylinder (23). In fact, Giedt (43) recorded negative values for  $K_f$  in the neighbourhood of the FSP up to  $\theta = 8^\circ$ , with 4 per cent turbulence intensity. As these were unrealistic measurements, Giedt omitted data recorded in this region.

The general trend shown in the presented results is that, for a certain flow rate, increasing the turbulence intensity causes an increase in the local wall shear stress as demonstrated in Table 7.4. However, there is a disagreement, as far as the absolute values are concerned, between the results presented in that table. This disparity could be mainly attributed to the difference in the measuring techniques used in each investigation and length to diameter ratio.



### 7.3. Staggered tube bank experimental results:

#### 7.3.1. Cross flow around a cylinder in a tube bank

Flow around a circular cylinder in a tube bank is influenced by the presence of other cylinders in its neighbourhood (besides other factors) and this is normally dependent upon the pitch to diameter ratio used. This ratio, in practice, is usually not less than 1.25 to avoid excessive pressure drop and to give access to mechanically clean the outside surface of the tubes inside the bank. The pitch ratio is normally not more than 1.75 in order to avoid reduction of the flow velocity which plays a role in the thermal characteristics of the shell side fluid through the tube bank. Larger pitch ratios usually lead to a higher cost of the heat exchanger and a larger area for its installation.

A literature survey showed that, although some work has been done on the flow within tube banks, e.g., references numbers 57, 234, 235, 236, the picture inside the tube bank configuration is by no means complete and called for more investigations in this direction. Therefore, it was decided to carry out a detailed study for the flow parameters in a tube bank that would normally be used in practice. The choice settled down to a staggered tube bank with equal pitch ratios of 1.5, since this was an intermediate value between the pitch limits mentioned earlier.

It was a seven rows deep equally spaced, transverse and longitudinal pitch ratio, with the instrumented test cylinder, used in section 7.2, located in the middle of a transverse row/...

row of three tubes in the working section. This row was followed by a permanent two dummy rows to avoid the effect of free wakes, encountered in the case of single row and last row in the bank. With these downstream conditions unaltered, the row containing the test cylinder was placed at different depths inside the bank by changing the number of the dummy rows in its upstream direction.

The flow conditions upstream the tube bank were the same as for single cylinder experiments (section 7.2.4) with the heater banks used as a turbulence generator and the estimated turbulence intensity for the undisturbed stream about 6 per cent at the mid height of the entrance to the working section.

Flow parameters such as local values of normal pressure and wall shear stress around the test cylinder were carried out simultaneously, similar to that for single cylinder section 7.2, in 5 degree steps around the cylinder circumference starting from  $\theta = 0^\circ$  to  $180^\circ$  measured from the FSP. Some checks were made and measurements were done over the whole cylinder circumference with no significant difference observed between the two halves of the cylinder. This was repeated for each row over the Reynolds numbers investigated. Then the row containing the instrumented cylinder was located at each one of the successive rows, from first to fifth row in the bank, and measurements were carried out for each row accordingly.



### 7.3.2. Procedure and reduction of observations

For studies of cross flow within a tube bank, the dimensionless presentation of the local values of pressure coefficient (CP) and wall shear stress ( $K_f$ ) for different rows in the depth of the bank, cannot be carried out in the same way as that used for single cylinders. This is simply due to the fact that there is no undisturbed flow upstream of the internal rows in the bank to which the flow parameters could be correlated.

Two ways, however, are used in the literature for presenting the dimensionless normal pressure distribution for different rows in the tube bank. The first of these, is that described by Achenbach (234) who defined a hypothetical dynamic pressure based on a maximum flow velocity,  $U_{max}$ , calculated from the mass flow through the smallest free area. As a result, the local pressure coefficient at angle  $\theta$  from the FSP will be :

$$CP = 1 - \frac{P_{\theta} - P_0}{\frac{1}{2} \rho U_{max}^2} \quad 7.7.$$

This choice of the reference velocity, however, allows no comparison between various rows in the tube bank since velocity variations through the depth of the bank are not taken into account. Indeed, flow velocity variations along the tube bank were confirmed from the investigations carried out by Pearce (104).

The second way of presenting the pressure coefficient for different rows in the tube bank is that used by Morsy (57).  
For/...

For an arbitrary row in the bank, the flow velocity head was measured from the pressure rise at the front stagnation point, for a cylinder in this row, referred to the wall static pressure measured in the longitudinal gap between this row and the preceding one. The wall pressure tappings were located at about  $0.2 D$  upstream of the row in hand and the final approach velocity to this row was obtained by multiplying that pressure rise by a factor of 1.15.

Since there is no apparent justification for the figures and factors used by Morsy, it was decided to adopt an alternative approach for the non-dimensional presentation of the normal pressure in different rows in the bank. The method used here is similar, in principle, to that of a single cylinder, i.e.,

$$CP_{\theta} = \frac{P_{\theta} - P_W}{\frac{1}{2} \rho U_a^2} \quad 7.8.$$

This method allowed the changes of the flow velocity inside the tube bank to be accounted for; in addition, no correction factors were needed for the presentation of the pressure coefficient.

Where  $P_W$  is the wake pressure in the preceding row measured at the rear of cylinder in that row.  $U_a$  is the approach velocity to the row in hand which brings the value of  $CP_{\theta}$  to be equal unity at  $\theta = 0$ .

For the first row in the bank, the approach velocity was that of/...



of the main stream corrected for the blockage effect using the formula of Allen and Vincenti (78) as shown in section 5.2.7.

Based on the estimated approach velocity, the local wall shear stress is presented in the following dimensionless form:

$$K_{f\theta} = \tau\theta / \frac{1}{2} \rho U_a^2 \quad 7.9.$$

The contribution of the pressure drag and shear stress to the total drag are estimated by integrating the local values according to expressions 7.2 and 7.4 respectively.

### 7.3.3. Results and discussion

The distribution of wall shear stress ( $K_f$ ) and normal pressure coefficient (CP) around a cylinder in the 1st, 2nd, 3rd, 4th and 5th row in the bank is shown in figures 7.15, 7.16, 7.17, 7.18 and 7.19 respectively. The change in the flow characteristics from one row to another is quite noticeable.

In the first row, pressure coefficient around the test cylinder drops quite rapidly from its unity value at the FSP to reach a minimum value, at  $\theta = 85^\circ$ , which depends slightly on the Reynolds number used. Whereas the peak of the  $K_f$  distribution is located at about  $\theta = 70^\circ$  and its value, too, depends on the value of the flow Reynolds number. Increasing Re value for this row results in an increase in the shear stress and the negative pressure coefficient as well.

Figure/...

Figure 7.15a shows that the  $K_f$  distribution indicates that the flow separation occurs at about 100 degrees from FSP. The CP distribution, on the other hand, Figure 7.15b, shows a slight inflection at  $\theta = 100^\circ$  and instead of having a zero gradient on the rear of the cylinder, as normally expected after separation occurs, the back pressure increased slightly and then decreased until it reached  $\theta = 160^\circ$  where it continued with constant value up to  $\theta = 180^\circ$ . This change in the flow characteristics between  $\theta = 100^\circ$  and  $160^\circ$  is also shown in the corresponding  $K_f$  distribution in Figure 7.15a. This figure shows that, after the flow was almost separated at  $100^\circ$ , it reaches again to the surface, indicated through the positive  $K_f$  values recorded, and it finally separates at  $\theta = 160^\circ$  where  $K_f$  recorded signal is zero. These figures indicate that the flow on the first row may resemble that around a single cylinder and the measurements were similar to those of a single cylinder in the critical range of Reynolds number.

In the second row, flow characteristics are markedly different from those on the first row. Figure 7.16 shows that the CP values drop from unity at FSP, with less steep gradient compared with first row, to reach a minimum at a position which depends on the Reynolds number used. At  $Re = 76,000$ , the  $K_{f_\theta}$  reaches its maximum value at  $\theta = 30^\circ$  while the point of minimum pressure lies at about  $\theta = 70$  degrees. After  $K_{f_\theta}$  drops from its peak at  $\theta = 30^\circ$  to  $\theta = 60^\circ$  the distribution flattened out in a region of a corresponding flattening out in the CP distribution. The rapid change in CP around  $\theta = 95^\circ$  is followed by a similar change/...



change in the  $K_f$  distribution and flow separation,  $K_f = 0$ , seems to occur at  $\theta = 130^\circ$  with small variations on the rear of the cylinder.

Increasing the Reynolds number results in an increase in the minimum CP obtained together with a shift towards the rear of the cylinder and an inflection point at about  $\theta = 50$  degrees from FSP. This is shown in Figure 7.16a, the  $K_f$  drops slightly from its peak at  $\theta = 30^\circ$  until it reaches  $\theta = 50^\circ$  where a change in the gradient occurs and a second peak is recorded at about  $\theta = 70^\circ$ , from which a rapid drop followed with a gentle drop occurs until  $\theta = 120^\circ$  is reached. Afterwards, the  $K_f$  distribution continues with a small positive value and the flow, eventually, separates nearby the rear stagnation point. These changes are also clear in the CP -  $\theta$  distribution, figure 7.16b, where the distribution continues, however, with small gradient, up to the rear of the test cylinder.

Figure 7.17 shows the flow characteristics around a cylinder in the third row of the tube bank. This figure demonstrates the change in the pressure coefficient and its drop from the unity value at FSP to reach the point of minimum pressure at about  $\theta = 85^\circ$  with a tendency of some recovery on the rear of the cylinder until the flow eventually separates and the region of uniform pressure is reached at about  $\theta = 120^\circ$ . The same features are also clear in the corresponding measurements of the wall shear stress. At  $Re = 60,000$ , the  $K_f$  value increases from its zero magnitude at FSP, with high rate, until  $\theta = 30^\circ$  and then with a smaller rate it reaches  $\theta/\dots$

$\theta = 70^\circ$  where it starts to drop until flow is separated around  $\theta = 100^\circ$ . Downstream of the separation region, the rear of the cylinder is occupied by a circulation region which covers the rest of the cylinder surface up to  $\theta = 180^\circ$ .

Increasing the flow Reynolds number across the third row caused the point of minimum pressure to acquire a higher negative value. However, the contrast pressure region on the back of the cylinder was not significantly changed. On the other hand, increasing the Reynolds number caused the  $K_f = \theta$  distribution to be more uniform with a single peak at about  $\theta = 70^\circ$  while the downstream part of the distribution remained unchanged and the flow separation was at  $\theta = 100^\circ$ . A comparison between figures 7.18 and 7.19 illustrates that, cylinders in the fourth and fifth rows have very similar flow characteristics to each other. On these rows, pressure drops steadily from its maximum at the FSP to reach its minimum value at about  $\theta = 85^\circ$ , after some recovery, the flow separates from the cylinder surface and the constant pressure region on the cylinder rear starts at about  $\theta = 130^\circ$ . Of the shear stress measurements, the  $K_f$  value increased from its zero magnitude at FSP rapidly until  $\theta = 30^\circ$ , with an inflection point at  $\theta = 50^\circ$ , it continued with a high rate of increase up to  $\theta = 70^\circ$ . Downstream of this region, the  $K_f$  value drops to reach zero and thus flow separates at about  $\theta = 100^\circ$  where the circulation region begins to grow until it covers the rear of the cylinder, with its characteristic feature of negative wall shear stress indicating the reverse of the flow direction in this region.

The/...



The variations of the flow velocity approaching different rows in the tube bank is shown in figure 7.20. This figure indicates that velocity variations occurred mainly in the first part of the bank while from the fourth row onwards the approach velocity reached the values measured at the first row in the bank. Indeed, this was noticeable also from the similar flow distribution, i.e.,  $CP$  and  $K_f$ , experienced on the fourth and fifth row in the tube bank. These variations along the depth of the bank, in general, are in agreement with the observations of Pearce (104) who showed that steady flow conditions could be reached from row four onwards.

The change in the pressure drag encountered by the flowing air stream over different rows in the tube bank is shown in figure 7.21. In general, the pressure drag decreases with increasing the Reynolds number and data for single cylinders is presented in this figure for comparison.

Due to the high acceleration of the incoming uniform flow while passing over the first row with the associated large pressure gradient, the pressure drag encountered on the first row is quite high. Its value is about five times that encountered on a single cylinder under similar undisturbed flow conditions.

On the other hand, the second row offers the smallest pressure drag in the bank. This is because of the small negative pressure on the back of cylinders in that row which is probably due to the insufficient width of the jet emerging from/...

from the transverse gap between cylinders in the first row, compared to the cylinder diameter.

Because of the flow retardation after passing over the second row, it is possible that some pressure gain could happen over the rear of cylinders in this row. In fact, negative pressure drag over the second row is reported by Morsy (57). Since that means that there is not only a pressure recovery but also an increase in the pressure of the main flow, a result which is very interesting, these pressure drag results were recalculated. From Morsy's original pressure distributions, the pressure drag was calculated, according to expression 7.2, and results showed that the pressure drag acquires a small positive rather than negative values. This shows that the flow experienced, however small, some pressure drop in passing over the second row in the tube bank as well.

It is possible to assume that, although the flow was highly retarded over the second row, the retardation is almost complete over the third row in the tube bank used.

Moreover, the apparent steadiness of the flow after passing over the third row might be due to the turbulence caused by preceding rows which could have reached some maximum value at this section in the bank. As a result, similar flow characteristics were obtained on the fourth and fifth tube rows. Accordingly, no justification was found for going any further in the present bank deeper than the fifth row.

For the task of comparing different rows behaviour under similar/...



similar flow conditions, data are grouped for each undisturbed flow condition and results are shown in figures 7.22, 7.23 and 7.24. Although effort was made to control the flow rate, when running tests from row to row, inevitably slight differences are to be expected; however, these were considered within the accuracy of the measurements and the nominal values of the Reynolds number were used.

From these figures it is clear that the largest pressure gradient in the tube bank occurs in cylinders placed in the first row. This is mainly due to the blockage effect of the side cylinders, to the test cylinder, on the main incoming air stream. As the blockage increases, the velocity around the cylinder, outside the boundary layer, increases and the pressure distribution changes accordingly. Such blockage will cause flow acceleration in the transverse gap between cylinders in that row which is accompanied by large pressure gradient in this gap.

In fact the flow around cylinders in the first row is similar to that around a single cylinder in cross flow under similar blockage restrictions. These observations are confirmed through the investigations carried out by Akelbaev et al (178) who measured the pressure distribution around a single cylinder under different blockage constraints.

Figure 7.22b shows the possible effect imposed from cylinders placed in the second row on flow distribution around those in the first row. Accordingly, instead of having a constant pressure on the rear of a cylinder in the first row as expected/...

expected from the measurements of Akelbaev et al, pressure started to drop slightly after  $\theta = 130^\circ$  gradually until it reached the rear of the cylinder. Increasing the Reynolds number, e.g., figures 7.23b, 7.24b, the back pressure at the cylinder rear gets flattened out. Therefore, increasing the Re values, possibly, results in wakes with smaller width and the interference of cylinders in the second row into the flow in the first row is reduced.

From figure 7.22b, it is noticeable that the point of minimum pressure for the five rows, except the second row, lies between  $\theta = 85^\circ$  and  $90^\circ$ . In fact it was shown by Akelbaev et al that increasing the blockage constraint, for a single cylinder, from 0 to 0.8 causes the point of minimum pressure to be displaced from  $\theta = 70^\circ$  to  $\theta = 90^\circ$  from the FSP. .

The unique characteristics of the second row is due to the fact that, a cylinder placed in this row is exposed partly to the accelerated main flow emerging from the gap between adjacent cylinders in the first row at its front portion. As a result, the flow approaches the second row at a much higher velocity compared with that approaching the first row in the bank.

As far as the flow parameters on the second row are concerned, figure 7.22b shows that the point of minimum pressure lies somewhere about  $\theta = 70^\circ$  while the maximum shear stress lies at  $\theta = 30^\circ$  from FSP. Increasing the Reynolds number causes the point of minimum pressure to be displaced to  $\theta = 85^\circ - 90^\circ$  as/...



as shown in figures 7.23b, 7.24b and the shear stress spreads over a larger portion of the cylinder surface with a second peak at about  $\theta = 70^\circ$ , figure 7.23a. Further increase in the Reynolds number causes the second peak to acquire higher value than that at  $\theta = 30^\circ$  and eventually the second row joins the other four rows in the tube bank with their points of minimum pressure at  $\theta = 85^\circ - 90^\circ$ .

The available approximate solutions for the laminar boundary layers developed by Thom (34) and by Thwaites (243) were used to predict the shear stress around the frontal part of the cylinder at different rows in the tube banks. This was achieved by feeding the recorded normal pressure distributions to a computer programme to calculate the local parameters needed for the above mentioned theories.

Experimental wall shear stress compared with the predicted values from Thom's and Thwaites theories are shown in figures 7.25, 7.26, 7.27, 7.28 and 7.29 for 1st, 2nd, 3rd, 4th and 5th rows respectively. It is noticeable that the predicted values are considerably different from the experimental results, from row to row along the depth of the tube bank.

Since the flow across the first row is mainly uniform in nature, this row provides the best possible agreement, compared to other rows, between the predicted and measured values, figure 7.25. For the successive rows, in general, and the second row, in particular, the difference between the two results is very high indeed.

It/...

It is obvious that this sort of disagreement is to be expected due to the nature of these two theories and that they are mainly based on laminar layers which may exist on the surface of a single cylinder with a smooth surface and placed in a nearly turbulence free tunnel. Deep inside the tube bank, e.g., fourth and fifth rows, the predicted values are about 40 to 50 per cent of the measured wall shear stress. Of course, the prediction is only possible on the front of the cylinder.

#### 7.4. Total Pressure Drop in the tube bank

In addition to the detailed study of the flow characteristics around cylinders in different rows inside the tube bank, the total pressure drop across the bank with different depth was also measured.

Total pressure drop was realised by measuring the pressure difference between two stations, the first station was located upstream of the bank, in the undisturbed area, by more than  $1.5 D$  before the influence of the blockage begins (157). The second station was located far enough downstream of the bank and located at more than  $2L$ ,  $L$  is the longitudinal pitch ratio, from the last row where the pressure recovery is almost complete (104). At each station a set of four wall tappings were used, one on each side of the rectangular working section, to provide the average pressure at that station.

Figure 7.30 shows the drag coefficient, presented in the form of Euler number, referred to one row as a function of the Reynolds/...



Reynolds number based on the flow velocity in the minimum free area in the bank. In this figure, data presented for different number of rows from single to seven row bank. Data for single cylinder by Stasjuljawitshius et al (117) with a transverse pitch of 1.5 and by Achenbach (235) with a transverse pitch of 2, are presented in that figure for comparison.

The results indicate that, as would be expected, the shallower the tube bank the higher the drag coefficient per row and the deeper the bank, the lower the drag factor per row. Each row acts as an artificial turbulator for the succeeding one. After flow passes across a certain number of rows, this effect causes stable flow conditions to be reached. From figure 7.30, it is clear that flow stability is reached from the fourth row onwards. There is no apparent reason for the higher value measured by Achenbach which is expected to be lower, due to its larger transverse pitch ratio, than other data in that figure.

Displacement of the curves towards smaller Reynolds number, for bigger number of rows, is attributed to the increase in the amount of turbulence that occurs with increasing the number of rows in the bank. From the present work, however, stable conditions set in at about the fourth row onwards.

In order to facilitate the comparison between results of suction 7.3 and 7.4, it is assumed that the middle cylinder in each transverse row in the bank is representative of all tubes in that row. While this is not strictly true, due to the/...

the tunnel's wall effect, it is considered to be a reasonable approximation to reality. If this is the case, the flow will encounter similar resistance around all cylinders in any particular row.

By neglecting the effect of the working section side walls, the percentage of momentum loss for each row could be computed by integrating the local static pressure and wall shear stress distributions to yield the contributions of pressure drag and shear stress respectively to the total drag, according to expressions number 7.2 and 7.4. The summation of these two contributions should yield the pressure drop.

Accordingly, the pressure drop for the cross flow in passing over a particular row in the bank could be calculated as follows:

$$\Delta P.A. = (KD + CF) \cdot \frac{1}{2} \rho U_a^2 D.H.N \quad 7.10.$$

This expression was applied to each of the five rows, starting from the first row, in the tube bank and results are correlated with the Reynolds number based on the velocity through the minimum free area. The calculated outcome of the pressure drop in  $N/m^2$  is presented in figure 7.31 compared with data of Achenbach (234), Jakob (110), Grimson (109) and Zuskawskas (105).

This figure shows that pressure drop per row decreases as the flow moves deeper through the bank. It is also noticeable/...



noticeable that the integrated values over the fifth row, as a limiting curve for deep exchangers, are higher than those calculated from the total pressure drop measurements by about twenty to thirty per cent. This might be due to the difference in surface conditions for both cases, since the total pressure drop was measured across banks of smooth surface cylinder and the integrated values were estimated over the porous cylinder whose roughness parameter  $K_{s/D}$  equal to  $53 \times 10^{-5}$ . (The effect of this roughness is explained in section 7.2.3).

One of the surprising results is the high values calculated for the first row in the present tube bank compared with those reported by Achenbach (234). The reason for this sort of difference might be due to the difference in the transverse pitch used in each investigation.

#### 7.5. Concluding Remarks

Comparison between the present data on a single smooth surface, cylinder with the available literature showed that the present developed device for measuring the wall shear stress is adequate for the planned project. Moreover, as far as the time factor is concerned, the device is superior to other devices and quick in providing accurate estimation for the shearing forces on the cylindrical surface.

A. Single cylinder experiments showed the following:

1. Even for small surface roughness,  $K_s = 53 \times 10^{-5}$ , the shear stress contribution to the total  $\frac{D}{D}$  drag is increased/...

increased considerably. Moreover, the peak of the  $K_f - \theta$  distribution, region of highest flow velocity, moved towards the rear of the cylinder, however small, and the distribution becomes more steep towards the flow separation point.

2. The coefficient of skin friction was increased by increasing the turbulence intensity of the main air stream; however, this effect was less than the effect of surface roughness.

3. The pressure drag showed similar characteristics to those of other investigators and it decreased by increasing the turbulence intensity.

4. The percentage contribution of the shear stress to the total drag of a single cylinder amounts to about 2 per cent at the highest Reynolds number used (i.e., 70,000).

5. The measurements of shear stress on a single cylinder showed lack of a fixed point for the flow separation and observations suggested the existence of a separation region rather than a separation point which led to a difficulty in detecting the influence of surface roughness and turbulence intensity on the flow separation.

6. There was no real stagnation point at  $\theta = 180^\circ$  from the FSP relative to the main flow.

B. Tube bank experiments showed that the flow characteristics varied considerably with the cylinder position/...



position along the depth of the bank. However, the main conclusions were as follows :-

1. The entrance effect is extended probably up to the third row in the bank.
2. The flow reached its stable conditions of the self-modelling nature from the fourth row onwards.
3. Apart from the downstream possible effect on its rear, a cylinder in the first row acts in a similar manner to a single cylinder under similar flow restraints.
4. The first row in the bank offers the highest drag coefficient in the bank which could be as much as five times that of a single cylinder at similar undisturbed conditions.
5. The second row in the bank, with its highest flow approach velocity, provides the lowest drag coefficient in the tube bank.
6. The pressure drop, per row, decreased with increasing the number of tube rows.
7. The percentage contribution of the wall shear stress to the total drag ranges from 2 to 4 per cent for the flow range investigated. While these values could mean that the shear stress contribution does not significantly influence the results of the total drag, they do, however, influence/...

influence the flow by affecting the position of separation on the cylinder surface, the width of the circulation region and consequently the pressure drag.

8. The high experimental wall shear stress compared with the predicted one, could be explained through the investigations of Pearce (104) who showed that the flow in the bank is pushed towards the sides of the straight gaps between adjacent cylinders. Consequently, the velocity outside the boundary layer on the cylinder could reach a peak of about 35 per cent higher than that for the nominal gap velocity in the free section.



## CHAPTER 8

### RESULTS III: EFFECT OF MASS TRANSFER ON A TUBE BANK IN A CROSS FLOW

#### 8.1. Introduction

Since the present project is devoted mainly to studying the influence of different factors affecting the flow through heat exchangers in general and vertical tube surface condensers in particular, a natural extension of the investigation presented in Chapter 7 is to study the effect of condensation on the cross flow through the present tube bank configuration.

In a real condensation process it is difficult to investigate the detailed response of the main cross flow to the condenser surface, to the changes in the condensation rate or heat transfer rate. In such cases it is difficult to apportion the influence of different parameters involved.

To facilitate such an investigation with the possibility of determining the flow local parameters, it was found necessary to split the physical processes involved in a condensation process, i.e., heat and mass transfer. Such a coupling effect is usually associated with common condensation phenomena, in which heat transfer rate is controlled by the heat released by the condensate, from the main stream, being condensed on the colder condenser surface.

To/...

To accomplish the aforementioned requirement, suction of the flowing medium through the test cylinder's porous surface offered a convenient means of decoupling the heat and mass transfer effects. The absolute rate of mass transfer could thus be separately and independently controlled at any desired value for the same main stream flow conditions.

As far as the interaction between the vapour and the surface of the condensate film is concerned, it was assumed in the present analogy that the condensate was in a solid form (250) and the friction coefficient at the surface of condensate film was regarded as that at the surface of a cylinder in cross flow whose diameter is  $D_1$ . As  $D_1$  is nearly equal to  $D + 2\Delta$ , where  $\Delta$  is the film thickness which is very small (219) and could be neglected relative to the cylinder's dimensions, it is assumed that  $D_1 \approx D$ . The liquid phase effects are ignored according to the observations of Drummond (140) for condensation in pipes.

The hydrodynamic analogy of the condensation process by an inward velocity towards the surface was also used in the investigations carried out by Wallis (70), Morsy (57), Drummond (72) and Kotake (227).

The present chapter will deal only with the influence of the mass transfer or extraction, on the characteristics of the cross flow while the simultaneous effect of heat and mass transfer will be the subject of the next chapter.

8.2./...



## 8.2. Mass extraction from circular cylinders in cross flow

As far as the effect of mass extraction on the flow local parameters on either a single cylinder or tube bank configuration is concerned, only a few investigations could be found in the available literature. One of these was the early work of Pankhurst and Thwaites (68) who measured the pressure distribution around the circumference of a single porous cylinder under conditions of continuous high suction rates. They assumed that the scale effect could be wholly taken into account by using the suction parameter  $CQ\sqrt{Re}$  where  $CQ$  was the ratio between the suction velocity to the undisturbed main flow velocity. Their experiments were performed for  $CQ\sqrt{Re} > 25$ .

Another work was that carried out by Drummond (72) for a single cylinder and porous tube bank for suction rates equal to 13.5 per cent of the inlet flow rate to the working section. He concluded that such a high rate of mass extraction might reduce the pressure drag on the cylinder.

It is obvious that these two investigations, previously mentioned, dealt with high suction rates which are beyond the range encountered in steam condensers. For practical condensers, typical condensation loading is about  $0.0113 \text{ Kg/m}^2\cdot\text{sec}$ . with mass velocity of steam of  $0.5$  to  $3 \text{ Kg/m}^2\cdot\text{sec}$ . at absolute pressures of  $4.5 \text{ KN/m}^2$  (242). Under these conditions the analogous hydrodynamic 'suction parameter'  $CQ\sqrt{Re}$  was estimated to vary from about  $0.3$  to  $0.8$ .

An/...

An investigation which dealt with low suction rates was that of Hurly and Thwaites (67), who studied the boundary layer development on a porous cylinder using low suction rates,  $CQ\sqrt{Re} = 0$  to 3. But they were mainly concerned with the development of a laminar layer under conditions of continuous suction rather than the distribution of local parameters around the cylinder perimeter. Nevertheless, they indicated that, for such a situation, the suction parameter was not the only determining parameter in deciding the values of the flow velocities outside the boundary layer.

The effect of mass extraction on local flow parameters around a circular cylinder in cross flow was reported by Morsy (57). Since that work has a similar nature to the present study, it deserves a good deal of our interest. Around a circular cylinder circumference he measured the local normal pressure and shear stress using a deflected type floating element, 3.2 mm wide, skin friction sensor. The sensor's supporting body was 38 mm, along the circumference, by 63.5 mm along the length of the 89 mm OD plain test cylinder and mounted at its mid height.

To conduct the mass extraction experiments, Morsy covered the test cylinder with a perforated copper plate lined with a tightly woven canvas cloth and air was sucked through a recess in the test cylinder under the perforated plate. The plate was drilled with staggered holes 0.76 mm diameter with equal pitch of 6.35 mm which gave the surface of the plate an average porosity of about 1 per cent. The thickness/...



thickness of the perforated plate together with the canvas cloth was about 1.7 mm.

In order to bring the suction area as close as possible to the floating element, drag piece, the perforated lined copper plate was made to cover the test cylinder circumference except for a rectangular, 17.5 mm wide, window through which the drag piece was seen by the external flow. Consequently, the floating element was in a recess from the external surface of the cylinder by the thickness of the perforated plate and its canvas liner, i.e., in a recess of about 1.7 mm from the surface on which measurements were to be carried out.

The minimum suction rate used by Morsy was equivalent to  $CQ\sqrt{Re} = 4.5$  up to a maximum of about 29 measured by a rotameter with its standard calibration chart at normal pressure and temperature. Since the average porosity of the perforated plate was quite small, 1%, a high pressure drop across it should be expected and the rotameter readings should have been corrected for this new operating pressure.

Comparison between the shear stress results obtained by Morsy from the plain cylinder surface and those for the cylinder when it was covered with the perforated plate, with no suction, showed great discrepancies in both trend and magnitude. He reported that the increase of the shear stress, with the perforated plate in place, of 30 per cent was due to the roughness caused by the drilled holes in the rolled copper plate. On the other hand, no explanation was offered for the existence of clear separation/...

separation points with the perforated plate while none were recorded for the plain surface at similar Reynolds numbers. In this case, the negative shear stress recorded on the rear of the cylinder contradicts with his findings and conclusions on the plain cylinder in that such negative values are characteristics of flow with Reynolds where  $> 107000$ .

The recess of Morsy's drag piece might have caused a considerable error to the measured values of skin friction. It was shown by Allen (63) that even a small recess could cause a great error with the results from the force balance systems. Furthermore, Garringer (55) indicated that a recess of the floating element of about 0.013 mm below the surrounding surface could produce errors of -2 per cent in the measured shear stress values. Moreover, it is possible to assume that the recess of the floating element could cause an effect similar to the shallow gaps as reported by Hoerner (245).

In these cases it is also surprising to find that Morsy's results for shear stress with suction showed a reduction of 10 to 26 per cent of the recorded values without suction at the frontal part of the cylinder up to  $\theta = 30$  degrees from the FSP. Suction was applied up to  $\frac{V_w}{U_\infty} = 0.08$  and  $12000 < Re < 32000$ . This was a rather disappointing result, since it is well known that at that part of the cylinder surface there is a laminar boundary layer which will be highly affected by suction and a higher wall shear stress is to be expected.

The/...



The inconsistency of Morsy's measurements makes it difficult to rely upon the recorded measurements of his deflected floating element especially those concerned with the suction experiments. Accordingly, a comparison between the present results and those reported by Morsy (57), as far as suction effect is concerned, is omitted in the present report.

### 8.3. Single cylinder with suction

#### 8.3.1. Experimental procedure and reduction of observations

It was intended to have a reasonably uniform suction velocity along the model circumference, rather than use series of perforated holes distributed over the surface. Also a material was required which could be reasonably smooth to the boundary layer flow.

The experiment for the single cylinder in cross flow was carried out using the porous test cylinder, section 5.2.2., and the arrangement was the same as was described in section 7.2.

It should be mentioned here, that mass transfer or extraction was applied to the whole of the cylinder circumference except on the drag piece, 2 mm wide, and its supporting frame which extended 2 mm upstream and downstream of the drag piece. In other words the suction took place on areas which proceeded and succeeded the axis of the drag piece by about 3 mm along the cylinder circumference. However, the measurements of Gregory and Walker (220), using perforated strips on a flat plate, showed that the sucked boundary layer could keep its identity for a distance equal/...

equal to 3.2 mm downstream of the suction area.

Accordingly, the measurement recorded on the axis of the drag piece could be considered to be that of the sucked boundary layer proceeding the sensor.

Since the output signal from the shear stress sensor was the average over the total width of the drag piece, and the downstream half was not effectively within the suction area, therefore the measured shearing forces were expected to be a bit smaller than those if the whole drag piece had been subjected to suction. However, the output of the sensor, which was between 3 and 8 per cent too high, as explained in section 7.2.1, is presented without correction with the view that such a small overestimation might counteract the small reduction expected on the rear half width of the drag piece.

The test procedure was the same as that explained in section 7.2.2. except that, for each value of the main stream, Reynolds numbers, measurements were taken for the local parameters around the cylinder circumference over a range of suction rates, i.e.,  $CQ\sqrt{Re} = 0$  to 1.13.

It should be emphasised here that, although the flow Reynolds number was controlled to achieve values similar to those used in Chapter 7, inevitably slight differences occurred. These were tolerated at times and the errors involved in the estimation of the Reynolds number for the whole study amounted to about  $\pm 5$  to 8 per cent of the nominal values presented in the data figures.

As/...



As shown in Chapter 7, the free stream  $Re$  is adjusted and corrected for the blockage effect and the turbulence intensity is estimated to be about 6 per cent with the turbulator explained in section 7.2.4. placed upstream of the working section.

Measurements of  $K_f$  and  $CP$  were mainly carried out from  $\theta = 0^\circ$  to  $180^\circ$  with few checks around the whole circumference which showed reasonable agreement between both halves of the cylinder. These parameters are correlated against the dimensionless suction parameter  $CQ\sqrt{Re}$  according to Pankhurst and Thwaites (68).

### 8.3.2. Results and Discussion

Characteristic examples of the progressive development of the wall shear stress ( $K_f$ ) distribution around the porous test cylinder with mass extraction are shown in figures 8.1 and 8.2. These data are presented for undisturbed main stream's Reynolds number of 47000, with the working section free from the turbulence generator, and the turbulence intensity for such conditions was about 1.2 per cent.

These figures cover a range of suction parameter  $CQ\sqrt{Re} = 0$  to 0.3 for figure 8.1 while figures 8.2 covers the range from 0.35 to 1.13. The pressure drag did not change significantly for this suction range and its value was about  $1.2 \pm 5\%$ . The pressure distribution in these cases was very similar to those shown in figure 7.11 at similar Reynolds number. The presentation of these distributions was omitted in the present chapter for the sake of decreasing/...

decreasing the number of graphs shown in this report. The reason for such an unchanged character of the normal pressure distribution will be discussed later on.

From figures 8.1 and 8.2, it is possible to notice that the position where the flow separates from the cylinder surface is delayed, as a direct influence of the air suction, from about  $\theta = 80^\circ$ , for the no suction case, gradually until it reaches  $\theta = 122^\circ$  by increasing the suction rate from 0 to 1.102. It is to be noticed also, that the rate of delay is higher at the small rates of suction and the rate reduces at the top of the suction range.

At the rear of the cylinder, after about  $\theta = 165^\circ$ , increasing suction rate caused the shear stress to acquire positive values close to the rear stagnation point. The tentative feeling at this part of the cylinder surface is that, increasing the suction rate might have disturbed the wake structure nearby the rear stagnation point and further increase in the suction rate may have created small vortices in this region whose direction would be opposite to the main wake.

It is also noticeable, from figure 8.1, that the peak in the shear stress distribution moves steadily from  $\theta = 50^\circ$  to about  $\theta = 75^\circ$  from the front stagnation point. With increasing suction rate, e.g., figure 8.2, the peak is still delayed but with a decreasing rate of change of position.

For/...



For the last top suction rates, the shape of the shear stress distribution deviates from the laminar like shape noticed for the low suction rates. These top rates correspond to a suction velocity to main stream velocity ratio of 0.0029, 0.0033, 0.0037, 0.0043 and 0.0047. Using these rates the ( $K_f = 0$ ) distribution shows two peaks, a characteristic which is normally associated with flow transition from laminar to turbulent.

Similar characteristics were noticed by Head (249) who noticed that the boundary layer, developed on a porous surface consisting of calendered nylon stretched over a phosphor-bronze gauze, was laminar with low suction rates but became turbulent as the suction rate was increased. This change in the boundary layer characteristics was attributed to the existence of a surface imperfection ahead of the measuring station. To investigate this phenomena, Head used a single isolated roughness with different heights, upstream of the measuring station. From the results, he concluded that, if the roughness height was about 125 microns, the boundary layer remained laminar over a small range of low suction and became turbulent for high suction rates. The maximum rate used by Head was equivalent to  $\frac{V_w}{U_\infty} = 0.0025$ .

The effect of distributed roughness on the transition when suction is applied to a porous surface was reported in reference number 251 and it was shown that since no porous surface can be entirely free from irregularities, if only at the holes through which the air is sucked, there is, for every porous surface a lower limit for the flow speed below/...

below which it can be regarded as aerodynamically smooth and an upper limit beyond which no suction will prevent transition.

The reason for this sort of behaviour is that, although distributed suction increases the flow stability, it decreases the boundary layer thickness and the transition to turbulence is caused then by, amongst other reasons, the significance of the surface irregularities relative to the thickness of the boundary layer.

In the present study, therefore, it is reasonable to assume that, for the high suction rates used, the roughness of the porous surface became significant relative to the thickness of the boundary layer and flow transition occurred which manifested itself by the appearance of a second peak in the shear stress distribution.

The shear stress contribution to the total drag, defined by expression 7.4, is presented in figure 8.3 and correlated against the suction parameter  $CQ\sqrt{Re}$ . Some of the scattering of the data points can be accounted for by errors due to the unsteady nature of the flow. However, an average curve drawn through the points provides a good description of the results. For the suction range tested, the percentage contribution of the wall shear stress to the total drag is increased from 2 to 29 per cent when  $CQ\sqrt{Re}$  was varied from 0 to 1.02 respectively.

From figure 8.3., it is noticeable that 'CF' increases rapidly/...



rapidly with increasing suction rate in the low range and the increasing rate became less around  $CQ\sqrt{Re} \approx 1$ , i.e.,  $\frac{V_w}{U_\infty} = 0.005$ . There is no convincing explanation for this behaviour which could be offered at the present stage, except that, it is possible at these very high suction rates, relatively speaking, some major changes in the external flow could have occurred.

Since it was planned to use the test porous cylinder, later on in the programme, in experiments involving heat and mass transfer, it was decided to prepare the cylinder in its final form for the rest of the investigation. In other words, to mount the heating banks, turbulence generator, at the intake of the working section and to equip the test cylinder with the thermocouples required for the heat transfer measurements, as explained in section 5.2.8.3. The constantan leads of the thermocouples were collected together at the rear of the cylinder,  $180^\circ$  from the drag piece generator on the cylinder surface, running along the length of the model. This collection of the thermocouples lead is referred to, in the figures, as a 'wire' at the rear of the cylinder.

Under these conditions, local flow parameters were measured over the suction and Reynolds number range planned for the investigations. Three values of the undisturbed flow Reynolds number were used, 27000, 47000 and 70000, while the suction velocities were chosen as 0.012, 0.018 and 0.025 m/s which yielded velocities ratios of  $\frac{V_w}{U_\infty}$  from 0.0009 to 0.0047. The turbulence intensity of the incident stream was measured and/...

and it is estimated as  $T.L. = 6$  per cent. The results of wall shear stress and normal pressure distributions around the cylinder with the 'wire' mounted on it are shown in figures 8.4 and 8.5.

In order to investigate the influence of the 'wire' only on the local parameters, measurements from figures 8.4 and 8.5, with no extraction, should be compared with the corresponding ones at figures 7.10 to 7.12 under similar surface, flow and turbulence conditions.

Comparison between figure 8.4.a, no suction, and figure 7.10 at  $Re_{\infty} = 27000$ , shows that the effect of the 'wire' is to reduce the peak value of the shear stress by about 18 per cent together with a similar reduction in the negative values, in the circulation region, to about 40 per cent of its value on the plain cylinder. This is also clear in figures 8.4b and 8.5a when the peak in the shear stress distribution, with no suction, are reduced by about 15 to 18 per cent of its value on the plain cylinder. The reduction in the shearing force values is quite clear in the circulation region due to the presence of the 'wire'.

The influence of the 'wire' on the recorded normal pressure distribution is shown in figure 8.5b for the three main Reynolds numbers used in the investigation. The effect on the base pressure is quite noticeable at the lower Reynolds number of 27,000 while increasing the negative value of the point of minimum pressure is clear at the highest Reynolds number of 70,000 due to the presence of the 'wire' /...



'wire' on the cylinder surface. The distributions in figure 8.5b were integrated according to expression 7.2 to yield the contribution of the pressure drag to the total drag, i.e.,  $KD$ , and results are shown in figure 8.7a where the presented data are not corrected for the blockage effect.

From figure 8.7a, it is obvious that the presence of the 'wire' caused a reduction in the form drag,  $KD$ , by about 18 to 20 per cent from its value on the plain cylinder. Although, this 'wire' is not strictly similar to the fixed splitter used by Apelt et al (252), or by Pankhurst and Thwaites (68), at different angles of  $\theta$ , the reduction in the measured pressure drag due to the presence of the present 'wire' agreed, in general, with the findings of these investigators.

This reduction in the  $KD$  values together with the corresponding reduction in the recorded wall shear stress are probably due to some sort of stabilizing effect caused by the presence of the 'wire' on the cylinder surface. In fact, a reduction in the shear stress was noticed also when air suction was applied to the surface with the mounted 'wire' on it. Comparing figures 8.4b, with suction, and figure 8.1, a reduction of approximately 40 per cent of the values recorded on the cylinder with plain surface is noticeable. However, these were carried out at different turbulence intensities.

The/...

The effect of suction, in the investigated range, on the normal pressure distributions was not significant and within the accuracy of the measurements the distributions were very much the same as the values with no suction as shown in figure 8.5b.

It is noticeable that while the shear stress distribution for Reynolds numbers of 27,000 and 47,000, with air extraction continued to behave in a laminar like boundary layer, at Reynolds number of 70,000 the distribution showed two peaks normally indicating the boundary layer transition to turbulence. Since at  $Re = 70,000$ , with no suction, the distribution shows a laminar behaviour for the boundary layer, the transition to turbulence with mass extraction could be explained according to the argument given in reference (251). In other words, suction caused a decrease in the boundary layer thickness, together with the high level of turbulence of 6 per cent, the relative size of the porous surface roughness to the thickness of the boundary layer became significant before the flow has been sufficiently stabilised. Under these conditions, the flow speed might have exceeded the upper limit above which no reasonable suction will maintain laminar flow over the cylinder surface. Consequently, the surface irregularities combined with the influence of the external disturbances, which were insufficient to cause transition with no suction, became able to cause transition when suction was applied and the boundary layer thickness was reduced (249).

With no suction, it is possible to notice the movement of the/...



separation point as a direct influence of increasing the Reynolds number, as shown in figures 8.4 and 8.5. For  $Re = 27000$  separation occurs at about  $\theta = 75^\circ, 80^\circ$  for  $Re = 47000$  and  $85^\circ$  with  $Re = 70000$ . According to the observations of Achenbach (176), the present observations could mean that the flow conditions at  $Re = 70000$  with T.L. of 6% is, in fact, in the neighbourhood of the critical flow regime where the separation point is delayed further downstream on the back of the cylinder and the shear stress distribution is characterised by the appearance of two peaks. This is confirmed from figure 8.7a where a drop in the pressure drag is noticed at  $Re = 70000$ . This does not seem surprising since it was reported (169) that the critical range could be reached at Reynolds numbers as low as 39000 when the turbulence intensity was 11.5%.

On the back of the cylinder, downstream separation region, it is obvious that air suction has caused an increase in the negative values of the shear stress in the circulation region. This is probably due to the same reasons argued on the frontal part of the cylinder when suction has removed the slow moving boundary layer fluid.

The shear stress contribution to the total drag (CF) is calculated from figures 8.4 and 8.5 according to expression 7.4 and correlated against suction to mainstream velocity ratio as shown in figure 8.6. From this figure, the value of CF is increased by increasing the suction quantities. However, with a differing rate with different Reynolds numbers in the main flow, the figure shows that data does not/...

not collapse on to a single curve. Replotting the data points as a ratio of CF with and without suction,  $\phi$ , as recommended by Wallis (253), the data are shown in figure 8.7b. Within the scatter of the points, an average curve is drawn to demonstrate the influence of suction on the wall shear stress contribution to the total drag. This figure shows that the contribution ratio,  $\phi$ , increases with increasing the suction rate and it could reach as much as seven in the suction range investigated in the present study.

#### 8.4. Tube bank experiments

Drummond (72) and Morsy (57) separately showed that condensation, simulated by mass extraction, could modify the total pressure loss encountered by a cross flow through a tube bank, by reducing the pressure drag contribution in the tube bank arrangements. On the other hand, Silver (139) suggested that, it is possible to assume that by condensation the pressure drag, or form drag, is modified in such a way as to preserve the ratio for the total pressure drop to frictional pressure drop similar to non-condensing conditions.

The present investigation was carried out with the intention of studying the effect of mass extraction, within a practical range, under adiabatic flow conditions, on the flow characteristics through the depth of the tube bank explained in section 7.3.

##### 8.4.1/...



#### 8.4.1. Experimental procedure and reduction of observations

Tests were carried out on the model used previously in section 7.3 and the flow conditions at its upstream were similar to those used with single cylinder, section 8.3.2. Also, the turbulence intensity in the incident stream was about 6 per cent over the range of Reynolds numbers used.

Wall shear stress and normal pressure values are recorded simultaneously around the perimeter of the test cylinder following the procedure explained in section 7.2.

At each value of the nominal Reynolds numbers, air is extracted through the porous walls of the test cylinder over the suction range used for single cylinder experiments as explained in section 8.3.2. and local flow parameters are repeatedly measured, for each suction rate, around the cylinder perimeter.

#### 8.4.2. Results and discussion

The simultaneous measurements of the pressure coefficient ( $C_p$ ) and wall shear stress ( $K_f$ ), on individual cylinders along the depth of the tube bank, are presented over a range of nominal main stream Reynolds numbers of 27000 to 30000 covering a range of suction to main velocity ratio from 0.0009 to 0.0047.

Figures 8.8 and 8.9 present data measured on the first row in the tube bank. The progressive increase in the wall shear stress due to the effect of mass extraction is quite noticeable. With no suction applied, the ( $K_f - 0$ ) distribution/...

distribution, figure 8.8, shows a peak value at about  $\theta = 65^\circ$ . From this peak, with increasing angle  $\theta$ , the shear stress is reduced to a value very close to zero and instead of showing flow separation, it continued with slight increase in the positive direction, indicating that the flow was penetrating to the back of the cylinder. Thereafter the shear stress is reduced and finally the flow separation occurred around  $\theta = 160^\circ$  from the FSP.

In fact, these measurements showed that, without suction, there is no real circulation region as such at the rear of the cylinder. Applying suction to that row caused a displacement of the shear stress peak to  $\theta = 80^\circ$  and flow separation occurred at  $\theta = 110^\circ$  with the highest suction rate used. Of course the well defined circulation region behind the cylinder when suction is applied was a surprising result. Possibly this might be explained by assuming that the weak boundary layer flow, confirmed by the small positive shear stress values, which were able to exist on the rear of the cylinder, as a result of penetration from the highly accelerated flow on that row, was removed by suction. By doing so, it gave a means for the circulation region, which probably was there all the time, to come in contact with the surface of the cylinder. The small rise at  $\theta = 180$  degrees to a positive value in a similar fashion to that noticed with a single cylinder, is probably due to, although there is no proof, the formation of small vortices at that part of the surface and whose direction would be opposite to the main vortices in the circulation region.

Figure/...



Figure 8.9, a and b, show the wall shear stress over the first row in the tube bank at  $Re = 10^5$  and  $1.4 \times 10^5$  respectively. The most noticeable feature of these figures is that the distribution which showed a laminar flow, with single peak at  $Re = 60000$ , acquired a turbulent flow characteristic, two peaks, when suction was applied at the higher Reynolds numbers. This change in the boundary layer characteristics could be explained in the manner used for a single cylinder. This change might be due to the fact that, under such high values of the Reynolds number, e.g.,  $10^5$ , suction has reduced the boundary layer thickness enough for the surface irregularities (251) to be significant relative to the boundary layer thickness and transition to turbulent flow within the boundary layer occurred.

In fact, it has been reported by Hurly and Thwaites (67) that in conditions of continuous suction, the flow around the cylinder appears to be especially sensitive to the surface irregularities, or disturbances, even when these are very small. Using a porous cylinder of a similar grade to the present one, they showed that transition might have had gradually started when  $Re$  was about 98000 and the suction parameter was  $CQ\sqrt{Re} = 0.55$ .

In the present work, however, in the laminar part before the transition took place, the shear stress acquired higher values than the corresponding values without suction, possibly due to the thinning of the boundary layer with suction, figure 8.9a. After transition at about  $\theta = 40^\circ$ , the shear stress value became less than the corresponding value/...

value without suction probably due to the increased thickness of the turbulent boundary layer. Similar results are reported by Achenbach (80) where local shear stress was lower for the turbulent layer than that for the boundary layer before transition.

Increasing suction rate, however, will tend to reduce the thickness of the laminar sublayer, after the transition with the smallest suction rate had occurred, which would result in an increase in the local wall shear stress.

From figure 8.9b, with the smallest suction rate used, transition occurred at  $\theta = 25^\circ - 30^\circ$ . The laminar layer, before transition, acquired higher local shear stress than the corresponding value with no suction. After transition and due to the increased thickness of the turbulent region, the shear stress became lower than the corresponding values with no mass extraction. Increasing suction rate, will cause an increase in the local values of the shearing forces due to the reduction of the boundary layer thickness with increasing suction. However, with the highest suction rate used, the peak value was still lower than the corresponding value without suction.

The upstream movement of the transition from  $\theta = 40^\circ$  to  $25^\circ$  by increasing the Reynolds number from  $10^5$  to  $1.4 \times 10^5$  respectively is in agreement with the observations of other investigators, e.g., Achenbach (80).

Figures/...



Figures 8.9 a and b show that the accelerated main flow on the cylinder surface at the first row at high Reynolds numbers was able to penetrate further downstream on the cylinder rear without allowing a real circulation region to be formed close to the cylinder surface. Moreover, applying suction to that cylinder delayed the flow separation up to  $\theta = 140^\circ$  with  $Re = 1.4 \times 10^5$ .

It should be mentioned here, that the normal pressure distribution on the first row in the tube bank was not significantly affected by suction in the range used in the present study and it was very similar, within  $\pm 2$  per cent, to that obtained without mass extraction, as shown in figure 7.15. This is quite an important result since it means that the pressure drag was more or less the same as without suction, thus the total drag must vary according to the variations of the wall shear stress contribution in this range of suction rates.

The unchanged values of the pressure drag due to suction could be explained by the following argument:- With no suction, the normal pressure is a function of the flow velocity outside the boundary layer, thus variations in the normal pressure should be expected whenever variations in the wall shear stress occurred or vice versa. For a particular Reynolds number, as long as the effect of the mass extraction is within the boundary layer, i.e., the effect is limited to the reduction of the boundary layer thickness, very small variations of the flow velocity outside the boundary layer are to be expected (67). Consequently/...

Consequently, the variations in the normal pressure would be very small too. On the other hand, variations in the normal pressure, should be expected when excessive suction is applied, e.g., Pankhurst and Thwaites (68), possibly because suction in this case affected the flow pattern beyond the boundary layer into the external flow.

Figures 8.10 to 8.12 present flow characteristics around a cylinder in the second row of the tube bank for Reynolds number from 76000 to 175000 respectively. From figure 8.10, the increase in the wall shear stress due to suction at  $Re = 76000$  is quite obvious. Even with no suction, it seems that transition had already developed at about  $\theta = 60^\circ$  from the FSP. Applying suction at that Reynolds number, the distribution keeps its identity with the two peaks, characterising transition phenomena, and the local values acquired higher magnitudes all over the surface until the flow separates.

On the second row, it seems that there is not much room for the suction to affect the flow separation and all the curves in figure 8.10a show flow separation at about  $\theta = 140^\circ$ . Again, suction, at its highest rate, helps to establish, however, small, a circulation region at the rear of the cylinder.

Figure 8.10b shows the small variations in the normal pressure distribution as a result of mass extraction through the cylinder porous surface. The transition which has shown itself at  $\theta = 60^\circ$  on the shear stress distribution, figure 8.10a, is also/...



also shown, especially at the highest suction rate, in the normal pressure distribution at  $\theta = 70^\circ$  with two points of inflection at  $\theta = 55^\circ$  and  $95^\circ$  which correspond to the two peaks noticed in the shear stress distribution at  $\theta = 30^\circ$  and  $80^\circ$  respectively.

Increasing the Reynolds number for the second row, e.g., figure 8.11, shows that transition moved upstream slightly to  $\theta = 50^\circ$  which corresponds to an inflection in the normal pressure distribution at about  $\theta = 60^\circ$ . The point of minimum pressure is moved downstream to  $\theta = 100^\circ$  from the FSP which corresponds to the peak of the shear stress at  $\theta = 95^\circ$ . It is noticeable that the effect of suction on the normal pressure distribution at that high Reynolds number is mainly concentrated around the back half of the cylinder. For a lower Re, but with the same suction rate, this effect was also noticeable on a portion of the front of the cylinder, figure 8.10. The shear stress distribution shows that, with no suction, the flow is nearly separated at  $\theta = 160^\circ$  when  $Re = 130000$ , applying suction, however, enables the flow to penetrate further on the rear of the cylinder until the rear stagnation point.

Comparison between figure 8.10a and 8.11a shows that increasing the Reynolds number has caused the second peak in the shear stress distribution, after the assumed transition, to acquire values higher than those for the first peak at the frontal part of the cylinder.

A/...

A further increase in the Reynolds number on the second row, figure 8.12, produced a rather interesting result. The shear stress, with the smallest suction rate, started at about  $\theta = 10^\circ$  to acquire values which are lower than the corresponding values without suction. These runs were repeated and the results were very much the same, with the repeatability of the measurements and flow conditions. On the other hand, when the tests were finished for the second row, the picture became clear. From the general trend noticed in figures 8.10 and 8.11, it was obvious that there was a gradual decrease in the values of the shear stress at the frontal part of the cylinder with the smallest suction relative to the no suction case. This is possibly because of the gradual movement of the transition point towards the front stagnation point, with suction, by increasing the Reynolds number. Then it was realised that the recorded results with  $Re = 175000$ , figure 8.12, were to be expected. For this case the transition, with the lowest suction, might have moved further upstream under the influence of the external disturbances imposed on the flow, and could have occurred at around  $\theta = 10^\circ$ . If this is the case, the shear stress could acquire values lower than the corresponding ones, without suction, after the position of boundary layer transition. Increasing suction in this case, would increase the shear stress values while keeping the boundary layer all the way over most of the cylinder surface and causing an increase in the downstream part of the distribution, i.e.,  $\theta = 110^\circ$ , to a comparable value with that at  $\theta = 40^\circ$ .

Figure/...



Figure 8.12b shows the changes in the normal pressure distribution at  $Re = 175000$  with suction. The assumed transition close to the front stagnation point which was noticed at  $\theta = 10^\circ$ , in the shear stress distribution, was not noticed in that region on the  $(CP - \theta)$  curves. This is understandable, since it is well known that the pressure distribution at the front of the cylinder is independent from the flow regime used (235). By applying suction, the point of minimum pressure acquires an even higher negative value with a tendency for spreading the minimum value over a wider area. This seems to be corresponding to the spreading out of the shear stress distribution over a wider area of the cylinder, figure 8.12a.

The influence of suction on flow separation at  $Re = 175000$  was very similar to that noticed with lower Reynolds numbers. In fact, for the second row, no separation point,  $K_f$  equal zero, was clearly shown in the  $(K_f - \theta)$  curves. This indicates that the boundary layer flow developed at the front of the cylinder was able to penetrate all the way through the back of the cylinder until the rear stagnation point. However, due to loss in energy, as viscous dissipation, there was no complete pressure recovery at the rear of the cylinder. In fact, the variations in the pressure drag on a cylinder in the second row, due to the suction effect, were slightly more than those for the first row and within +8 to -13 per cent of the values with no suction.

Figures 8.13 to 8.15 show the simultaneous measurements of shear stress and normal pressure distribution on the middle cylinder/...

cylinder of the third row in the tube bank arrangement for Reynolds numbers from 60000 to 130000 respectively.

At  $Re = 60000$ , figure 8.13a, shows that applying suction to the cylinder surface caused an increase in the recorded wall shear stress on both front and back of the cylinder. A further increase in the suction rate results in a corresponding increase in the values of the shearing forces. The delay of the flow separation due to suction is also quite noticeable. The interesting result is that, all the three suction rates used caused a displacement of the separation point to, almost, a single position at  $\theta = 125^\circ - 130^\circ$  instead of  $\theta = 95^\circ$  for the no suction case. The increase of the recorded shear stress in the circulation region, with reversed flow, at the back of the cylinder is explainable in the same manner as that at the front of the cylinder. In other words, suction removes the slow moving particles allowing the faster particles to come in contact with the cylinder surface causing an increase in the measured wall shear stress.

Although there is some variation in the normal pressure distribution due to suction effect, in figure 3.13b, the variations in the pressure drag were not significant.

The reason for this was explained earlier in the discussion.

Figure 8.14 shows that increasing the Reynolds number to 94000 caused flow transition to the boundary layer when suction was applied to the surface of the cylinder.

Consequently, after transition, the shear stress acquired values which are smaller than the corresponding ones without/...



without suction due to the bigger thickness of the boundary layer due to transition effect. The effect of suction rate variations on the recorded skin friction followed the same trend noticed earlier in figure 8.13.

An increase suction rate at that Reynolds number, 94000, results in an increase in the shear stress values and all suction rates caused the separation point to move downstream from  $\theta = 95^\circ$ , with no suction, to a similar position at  $\theta = 125^\circ$ .

Again, although suction caused some variations in the normal pressure distribution, the values of the pressure drag were very much the same as those without suction, within the accuracy of the measurements, it was considered unaffected by the present range of suction rates.

Further increase in the magnitude of the Reynolds number to 130000, figure 8.15, showed that the shear stress at the frontal part of the cylinder, with suction, was higher than those without suction. This is probably due to a transition in the boundary layer flow which might happen because of the combined effect of surface irregularities on the sucked thin boundary layer together with the effect of the external disturbances from the experimental arrangement. These changes were not noticed on the normal pressure distribution. Although suction caused some changes in the middle part of the distribution, towards a slightly higher negative value, the integrated pressure drag over the whole surface showed no significant variation from its value without/...

without suction.

Flow characteristics around middle cylinders in the fourth and fifth row were shown in figures 8.16 to 8.19. These figures demonstrated the general trend noticed on the previous rows. At lower Reynolds numbers, figures 8.16 and 8.18, increasing the suction rate caused an increase in the wall shear stress around the cylinder surface. Suction caused a downstream movement of the flow separation point from  $\theta = 95^\circ$  to a common position for all the three suction rates used at  $\theta = 125 - 130^\circ$  from FSP. On the rear of the cylinder, increasing suction resulted in an increase in the shear stress in the circulation region in the same fashion as on the frontal part of the cylinder surface. The variations in the pressure drag due to suction were insignificant and were about  $\pm 2$  per cent of its value with no mass extraction despite small variations recorded in the normal pressure distributions.

Increasing the Reynolds number, figures 8.17 and 8.19, the suction tended to decrease the boundary layer thickness and the relative size of surface irregularities became important which eventually caused transition to occur at  $\theta = 30^\circ - 40^\circ$  from FSP. The ratio of the shear stress with suction to that without suction differ on both sides of the transition region. While this ratio was more than one in the upstream of transition, the ratio became less than one on the downstream of transition which was probably due to the thickening of the boundary layer.

Further/...



Further increase in the suction rate resulted in an increase of the wall shear stress and all the suction rates displaced flow separation downstream to  $\theta = 120^\circ - 125^\circ$  instead of 95 degrees with no mass extraction. On the rear of the cylinder there was an increase in the shear stress of the circulation region and the pressure distribution was changed slightly from its value with no suction but the pressure drag remained insignificantly changed by suction from its value with no mass extraction.

The effect of mass extraction on the shear stress contribution to the total drag through the depth of the tube bank is calculated following expression 7.4. Results are shown in figures 8.20 to 8.22 for three undisturbed flow conditions, namely for Reynolds numbers of the main flow equal to 27000 to 70000 respectively. Results for the single cylinder are included for comparison.

Since the highest suction rate in the experiments amounts to only 0.2 per cent of the incoming flow rate to the working section, the effect of mass extraction on the flow velocity distribution through the tube bank is neglected.

As is expected, mass extraction, increases the shearing forces over the whole bank, however, with different degrees for different rows in the tube arrangement.

Figure 8.20 shows that cylinders located in the first and second rows in the tube bank have joined the single cylinder in having lower values of 'CF' compared to those in the third/...

third row onward at similar suction rates. Increasing the Reynolds number, e.g., figure 8.21, caused different rows to come closer to each other but with a lower rate of increase of the 'CF', with increasing suction rate, than that for lower Reynolds number. This trend is continued and for  $Re_{\infty} = 70000$ , in figure 8.22, 'CF' was decreased at the lowest suction rate used. Thereafter, CF is increased by increasing the rate of mass extraction.

This could be explained by the fact that mass extraction had reduced the boundary layer thickness and produced the flow characteristics of higher Reynolds numbers; together with the fact that, the turbulence intensity in the main stream was quite high, 6 per cent, it is possible to assume that the critical flow conditions are approached when the mainstream's Reynolds number was 70000 when the lowest suction rate is applied.

It is worth mentioning here that, it was noticed that the recorded signal from the shear stress sensor, servo-force balance, was subject to strong oscillations on the rear side of the test cylinder, which became even stronger in the separation region, in particular, in those experiments dealing with mass extraction. These oscillations are attributed to the effect of the vortices shedding at the back of the cylinder (35).

In all the experiments, it was noticed that the separation point had a very unstable nature and, in fact, it was moving backward and forward of a mean value which is presented in the experimental data. This point, together with the non zero values/...



values at  $\theta = 180^\circ$  from FSP, were discussed earlier in section 7.2.3.2.

#### 8.5. Concluding remarks

In this chapter investigations were carried out to determine the effect of mass extraction on circular cylinders in cross flow in a rectangular working section. By using a porous cylinder of a fine grade, uniformity of the suction velocity around the cylinder perimeter was reasonably insured.

On single cylinder and individual cylinders through the depth of a staggered tube bank, simultaneous measurements of the wall shear stress and normal pressure distributions were carried out for different flow and suction conditions.

It should be emphasised that, there are no other measurements in the literature to compare with these simultaneous measurements performed on a porous cylinder and at small suction rates of less than  $CQ\sqrt{Re} = 1$ .

As far as the effect of mass extraction on the local flow parameters is concerned, the main concluding points will be separated according to whether it is for single cylinder or for tube bank arrangement.

#### A - Single Cylinder experiments:

1. Mass extraction delays the position of the flow separation towards the cylinder rear.
2. With suction, there are some small changes in the normal/...

normal pressure distribution especially around the point of minimum pressure, however, the contribution of the pressure drag to the total drag was within  $\pm 5$  per cent of its value without suction. Within the accuracy of the measurements, it is concluded that the present suction range has no significant effect on the pressure drag of the single cylinder in cross flow.

3. Mass extraction can cause a considerable increase in the shear stress both as local values and as a contribution to the total drag.

4. Increasing the suction rate beyond a certain limit, can cause the surface irregularities to be significant relative to the reduced thickness of the boundary layer and flow transition would occur.

5. Increasing suction rate will reduce the area occupied by the circulation region at the rear of the cylinder, accompanied by an increase in the local values of the shear stress.

6. Placing a 'wire' at 180 degrees relative to the measuring generator on the cylinder surface caused a reduction in the shear stress values compared with the cylinder without the 'wire' at similar flow conditions with and without suction.

7. The 'wire' also caused a reduction in the pressure drag by up to 20 per cent of its value on the plain cylinder which was not significantly affected by suction.



B - Tube Bank experiments:

Within the repeatability of the measurements, the nominal values for the Reynolds number used in this chapter were similar to those reported in Chapter 7. The velocity changes and the corresponding variations in the flow Reynolds number through the depth of the tube bank were similar to those reported in section 7.3. Tests with mass extraction demonstrated the following:

1. The influence of suction on the flow characteristics differs according to the relative position of the cylinder within the tube bank arrangement.
2. Generally speaking, the contribution of the pressure drag to the total drag did not change considerably from its value without suction while the shear stress contribution was very sensitive to the range of suction used in the experiments.
3. Mass extraction delays the flow separation and helps the boundary layer flow which developed on the forward part of the cylinder to penetrate further on the back of the test cylinder.
4. Whenever a circulation region exists, suction tends to reduce it and higher values of the negative shear stress, characterising reversed flow, are recorded.
5. With high main stream Reynolds number, transition is noticed in the boundary layer at the lowest suction rate used./...

used. Increasing Reynolds number further, caused transition to move towards the front stagnation point.

6. For an isothermal non-dimensional mass extraction rate equivalent to a typical loading in a steam condenser, suction might have some influence on the normal pressure distribution on different rows in the tube bank. However, the effect of suction on the pressure drag contribution to the total drag is not significant.

7. Shear stress distribution is very sensitive to the suction rate and local values are considerably increased with mass extraction.

8. The present suction rates are considered to be working within the boundary layer region with very little effect on the external flow which controls the normal pressure distribution. This might explain the 'almost unchanged' pressure drag in the present experiments when suction was applied to the cylinder surface. This conclusion is in agreement with the observations of Hurly and Thwaites (67), however, for relatively higher rates of suction. They showed that under such conditions of continuous suction, mass extraction is not the only determining parameter in deciding the values of the flow velocities outside the boundary layer.



## CHAPTER 9

### RESULTS IV: HEAT AND MASS TRANSFER IN A TUBE BANK IN CROSS FLOW

#### 9.1. Introduction

In a vertical tube condenser, the real significance of the effect of vapour cross flow on the unit thermal performance could be obtained from analysis of the steam side heat transfer coefficient. This makes the measurement of the coefficient of heat transfer on the steamside, in the surface condenser, quite important for a designer knowledge.

While such measurements are available for the case of steam cross flow on a horizontal tube, e.g., Rauscher et al (202), the literature survey showed that the corresponding values for steam flow across vertical tube condensers, on the other hand, are not available. However, there are a number of investigations in which studies were carried out with steam flowing axially through the condenser. A good survey could be found in reference numbers 203 and 204.

For single vertical tube condensers, the majority of studies were performed with the steam flowing, outside the tube, longitudinally along the length of the tube condenser. With pure vapour (205) or vapour with noncondensable gases (206), these studies were focused on the overall performance of the unit. This was changed by varying conditions on either side of the tube metal boundary.

Vertical/...

Vertical tube banks, on the other hand, were dealt with as one unit and no detailed studies were performed within the banks. In most cases the overall coefficients of heat transfer only were obtained, e.g., Kirschbaum et al (209).

The mode in which the heat transfer rate is distributed in a vertical tube condenser in a steam cross flow has been visualised by some investigators, e.g., Furman and Hampson (207) and Ede (208). They reached the point of recognising that an uneven distribution of heat transfer round the perimeter of the vertical tube condenser would be expected. It was indicated that, due to the decreasing effect of gravity relative to vapour drag on the condensate film, at increasing cross flow velocity, such a distribution is somewhat similar to that of single phase heat transfer around circular cylinders in diabatic cross flow. Moreover, the condensate film development and its breakaway from the tube were developed in the same way as with single phase flow.

Indeed, the measurement of the heat transfer coefficient depends upon the measurement of the surface temperature, which is a peculiarly difficult problem, in general, and particularly where condensation takes place. In fact, measuring the temperature of the metallic surface under these conditions represents a major problem in the studies of condensation mechanism (218). This is confirmed by the observations of Furman and Hampson (207) who indicated that, the different conditions, around the vertical tube condenser, precluded any surface measurements even at discrete points around/...



around the perimeter, from which a steam side coefficient could be directly determined.

Appreciating the difficulties encountered by many investigators, in determining the influence of the flow parameters on the condensation process, a thermal hydrodynamic analogy was, therefore, justified to simulate the basic processes which take place in steam condensation on the outer surface of a vertical tube condenser.

It is the intention of the present chapter to take the adiabatic simulation used in Chapter 8, one step further towards the mechanism that takes place in a surface condenser.

## 9.2. The simulation of a condensation process

It is clear from the previous section that more information about the heat transfer around vertical tube condensers in steam cross flow is needed. Also, the realisation of this information under actual condensation conditions is known to be rather difficult. Therefore, a thermal hydrodynamic simulation was thought of as an alternative technique under which, flow parameters for a filmwise condensation on a surface condenser could be investigated.

It should be admitted, that such a simulation is not exactly what might be going on in a real condensation process. However, the present analogy was the nearest one obtainable in the present investigation.

On/...

On the surface of a vertical tube condenser, heat transfer takes place due to mass transfer from the flowing stream of vapour towards the condensate surface. Consequently, condensation process was considered, in the present simulation, as two processes, namely heat and mass transfer which are simultaneously taking place from the main stream towards the tube condenser surface.

Since the condensate film thickness for a typical condenser loading is normally very small, in the order of 30 microns (219), its effect on the curvature of the boundary layer could be neglected relative to the test tube diameter. Accordingly, the simultaneous heat and mass transfer, in the present simulation, were carried from the main stream to the surface of the test cylinder.

Care was taken, therefore, to perform the two simultaneous transfer processes, in the present work, in the same direction which they take in a surface condenser, i.e., from the flowing stream towards the surface of the test cylinder.

What was needed then, is the addition of a heat flux, to the mass extraction, as explained in Chapter 8, from the flowing air stream to the walls of the test cylinder.

In incompressible flows, however, heat is exchanged between the flowing medium and the cylinder only if the temperature of the wall is lower than that of the fluid. Accordingly, first the air flow through the tunnel should be/...



be raised to a higher temperature level, second, cooling the walls of the porous test cylinder and, third, provide a possibility for measuring the distribution of the heat transfer coefficient around the cylinder circumference.

The first task was the easiest and heating the flowing air stream was done using the heater's banks with its control, as described in section (5.2.8.2.). The second task, i.e., cooling the porous cylinder, with mass extraction, was carried out using the spraying method, as shown in section (5.2.8.2). It was the third task, local heat transfer coefficient distribution that took some time to achieve.

### 9.3. Measurement of local heat transfer rate

Brundrett and Baines (212) proposed a technique for the local measurement of heat flux based upon the inner law correlations for velocity and temperature. They placed a thermocouple at a specified location, in the inner law region, and the temperature difference from the wall value was a function of the variables which control the inner law temperature correlation, e.g., wall shear stress, kinematic viscosity, distance from the wall and Prandtl number.

Since this technique required the use of a Preston tube, a condition which is difficult to meet on the porous test cylinder without affecting the porosity of the surface, it was considered to be unsuitable for the present investigation.

Butterworth et al (213), presented a method for measuring the local heat flux and wall temperature for condensation experiments/...

experiments inside a horizontal tube. The local heat flux was obtained from the temperature difference between pairs of thermocouples inserted at different depths in a thick walled tube. This temperature difference is proportional to the local heat flux and hence this flux may be determined provided that the thermal resistance between the two thermocouples is known.

This technique was adopted in the present investigation and the original idea of inserting thermocouples within the thickness of the tube wall was replaced by measuring the temperature difference between the outer and inner surface of the tube wall whose thickness and hence its thermal resistance could be determined with confidence. However, the choice of a suitable method for measuring the surface temperature of the test porous cylinder was a difficult one.

Because of the nature of the porous surface and the fact that there is a normal suction velocity towards the surface, it was necessary to select a method for measuring that surface temperature, which would cause the minimum disturbance to the characteristics of the surface.

The major portion of the work done on the surface temperature measurement has been carried out using thermocouples, because of their inherent economy and flexibility of installation. Nevertheless, thermocouples have their own problems, e.g., the hot junction must be in perfect thermal contact with the surface without perturbing the local heat flux through the surface or affecting phenomena/...



phenomena occurring on the surface.

Consequently, methods using heat flux disc (214) or chord hole-groove and plug and recess (210) were considered to be unsuitable for the present studies. Neither the technique used by Green (215) with a total radiation pyrometer nor that used by Hampson (211) with inserted thermocouples in the surface was selected as a suitable method for surface temperature measurement in the present investigation.

Wiekhardt and Ritchie (216) demonstrated that a surface temperature could be measured accurately if the surface was made to form one arm of the thermocouples with the second arm made from a pointed probe of a thermoelectrically dissimilar metal which is pressed against the surface. They indicated that the probe must be in good electrical contact with the surface such that extraneous Seebeck voltages are not introduced.

That technique was by no means new and it was applied twenty years earlier in 1951 by Grootenhuis and Coworkers (217). By pressing a constantan wire on to the surface of a porous plate, they used the junction between this wire and the test plate as the thermoelectric element. Under these circumstances, the measured temperature is the true surface temperature where the contact point is located.

The method used for the surface temperature measurement in this investigation is similar to that developed by Grootenhuis et al and it is described in section (5.2.8.3.).

Particular/...

Particular care was taken in the measurement of all temperatures and calibration of the devices used was performed against a standard thermocouple calibrated by Dr. Nisbet of the Mechanical Engineering Department of Glasgow University.

It was necessary to use a multi-channel recording instrument for measuring the temperatures since the surface temperature underwent rapid and large oscillations with increasing angle  $\theta$  measured from the front stagnation point of the test cylinder. These could not be read on a manually balanced potentiometer, nor could an adequate mean temperature be determined from these fluctuations by using a static temperature measuring device.

Local heat transfer rate was calculated from the temperature difference across the test tube porous wall together with the thermal conductance of the porous material, as a heat conductor, per unit area based on the geometrical cross sectional area (217).

For a given position at angle  $\theta$  from the FSP, with surface temperatures  $t_{wo}$  and  $t_{wi}$  for outside and inside surface respectively, the local heat transfer rate is calculated as follows:

$$q_{\theta} = \frac{K_s}{x} (t_{wo} - t_{wi}) \quad 9.1.$$

where  $K_s$  is the thermal conductivity of the porous material and  $x$  is the wall thickness between inner and outer thermocouples/...



thermocouples junction. With main stream temperature  $t_{\infty}$ , measured at sufficient distance from the cylinder walls, the local heat transfer coefficient is:

$$h_{\theta} = q_{\theta} / (t_{\infty} - t_{wo}) \quad 9.2.$$

Having the local coefficient of heat transfer been determined around the cylinder perimeter, the mean heat transfer of the cylinder, as a whole, can be determined. This is obtained by integrating the local coefficients of heat transfer as follows :-

$$h_{av} = \frac{1}{\pi} \int_0^{\pi} h_{\theta} d\theta \quad 9.3.$$

It is estimated that the values of the heat transfer coefficient presented in this report are accurate within about 10 - 15 per cent. The sources of inaccuracy were:

- a) the unsteady nature of the flow
- b) the time averaging of the local measurements
- c) the accuracy of the heating control system
- d) the possible variations in the cooling water temperature
- e) accuracy of the thermocouples
- f) averaging effect of the curve smoothening
- g) possible stagnation effect for outer probe

In the following section, results obtained using single cylinders will be analysed first, followed by results recorded along the depth of a staggered tube bank.

#### 9.4. Experimental results:

##### 9.4.1. Single cylinder measurements

Tests for single cylinder in cross flow with heat and mass transfer were carried out covering a heat load range from 6 to 18 Watt/Cm<sup>2</sup> based on the cross section area of the tunnel working section. The mass extraction, suction, rates were similar to those used in the adiabatic cold experiments, Chapter 8.

The investigations were performed using a constant flow rate for the cooling water, sprayed on the inside surface of the porous cylinder. About 3.8 LPM flow rate was sprayed using a Dallavan hollow cone type of nozzle. Temperatures of the cooling water were measured at both inlet and outlet of the test cylinder using a precision glass mercury thermometer with smallest division of 0.1° C.

With cooling water sprayed on the inside surface of the porous cylinder, it was found that resistance from the suction pump, pressure drop across the test cylinder walls, for a specific rate of air extraction, was increased by about 30 per cent over that without cooling water. These resistance variations were measured at adiabatic flow conditions. This increase in resistance was probably due to the reduction in wall porosity because of cooling water capillary action. It was assumed further that this resistance variation would be the same for diabatic as well as adiabatic flow conditions.

After/...



After an initial run of the wind tunnel and the main air stream velocity had reached a steady state, with the heater banks switched on, small but constant temperature variations of up to  $\pm 1.5^{\circ}\text{C}$  had to be tolerated during the experiments.

It is noticeable that the test data points were recorded as the local time average values over the mid height of the test cylinder where the flow parameters were to be measured. In general, the local measurements were limited to one half of the cylinder circumference, but as a check on the symmetry, a few runs were carried out over the entire surface. No substantial differences between both halves were observed.

The investigations were carried out using the porous test cylinder and the test procedure was as explained in section (5.3). Wall shear stress was realised using the sensor described in Chapter 3.

On the sensor's drag piece, 2 mm width, there was no heat transfer as such and the transfer processes, mass and heat, were taking place on area preceeding and succeeding the axis of the drag piece by about 3 mm distance along the cylinder circumference.

Gregory and Walker (220), used perforated strips to maintain laminar boundary layers on a flat plate, their measurements showed that an adiabatic sucked boundary layer could keep its identity for a distance equal to 3.2 mm downstream/...

downstream of the suction area. Accordingly, it is assumed that the present diabatic sucked boundary layer would keep its identity over the shear stress drag piece whose axis was less than 3.2 mm apart from the suction area. Consequently, the measured values of shear stress were assumed to be those for a diabatic sucked boundary layer.

Tests were started by investigating the effect of temperature level in the mainstream on the recorded skin friction and normal pressure distribution around the cylinder perimeter.

Heater banks were switched on and the air was circulated through the tunnel for a certain flow rate that would achieve a mainstream Reynolds number similar to that used for the adiabatic cold tests (Chapter 8). It should be mentioned here that, although the Reynolds number was controlled as closely as possible when running tests from cold to hot adiabatic conditions, the recorded parameters correspond to a slightly different main stream Reynolds number. These slight variations, however, were considered to be satisfactory within the accuracy limits imposed on the present investigations and different tests were carried out under similar nominal Reynolds numbers.

For a certain air flow, temperature level steady state was observed on a double pen chart recorder together with the test cylinder's surface temperature reaching the main flow temperature. Extracting hot air through the porous walls was carried out to speed up the heating of the test cylinder.

After/...



After the steady state was reached, the free stream velocity was adjusted for the desired Reynolds number. Shear stress and normal pressure distributions around the cylinder were correlated to the Reynolds number based on the cylinder diameter and the flow approach velocity.

Typical distributions for two temperatures are shown in figure 9.1 (a,b). Increasing the temperature of the main stream decreases slightly the shear stress on the frontal part of the cylinder associated with a reduction in the corresponding values of the pressure coefficient,  $C_p$ . Variations in the air temperature result in corresponding changes in its kinematic viscosity. This will influence the thickness of the velocity boundary layer and will lead to variations in the shear stress recorded compared with that for colder air stream.

It is also clear that the hot adiabatic conditions have produced a less steep pressure coefficient gradient around the cylinder. This is particularly clear in the region of  $\theta = 50^\circ$  to  $120^\circ$  from the FSP.

The second stage of the investigation was to study the effect of the main stream temperature level on the shear stress and normal pressure distributions on the sucked boundary layer on the porous surface.

Typical results are presented in figure 9.2 (a,b) for two Reynolds numbers, namely  $0.47 \times 10^5$  and  $0.7 \times 10^5$ . As in the cases without suction, local values of the shear stress reduced/...

reduced on the frontal portion of the cylinder with increasing air stream temperatures. This is particularly clear with the lower Reynolds number, where local shear stress values are higher and differences in the recorded magnitudes can be observed.

Adding suction shows the influence of the air stream temperature on the wall shear stress in the region of circulation at the cylinder rear. Heating the main stream and increasing its kinematic viscosity will tend to decelerate the boundary layer which may lead to a shift in the flow separation point. However, such a shift was difficult to identify due to the unstable nature of the separation point.

The next step in the investigation was to add a heat flux across the sucked boundary layer to simulate a condensation process where both heat and mass transfer processes go side by side. Since the governing fluid properties are the fluid viscosity, thermal conductivity and density are temperature dependent, variations exist across the boundary layer if there is a temperature difference between the solid boundary and the flowing main stream. These variations would be expected to affect the flow in the boundary layer.

Flow conditions with heat and mass transfer processes simultaneously taking place at the solid surface is a bit complicated. In general, applying a heat flux from the main stream towards the cylinder surface to the tests with mass extraction, adds among possibly other effects, a new parameter/...



parameter to the boundary layer, i.e., a viscosity gradient across the boundary layer.

Figures 9.3 to 9.5 are typical examples of the results obtained with heat and mass transfer compared with those for adiabatic cold flow conditions. Cooling the cylinder surface lower than the main stream caused an increase in the wall shear stress around the cylinder circumference relative to the adiabatic sucked boundary layer at a similar main flow Reynolds number. These results, as far as the influence of cooling is concerned, are in agreement with other investigators.

Wazzan (221) showed numerically that the stability of a two-dimensional incompressible laminar boundary layer flow, in water, is enhanced with heating the solid boundary more than the main stream. Moreover, heating the wall could cause a delay for the flow separation. This conclusion was reached numerically by Poots and Ragget (222) and experimentally by Smith et al (223). They showed that by heating the solid surface of a circular cylinder, in water flow, the laminar flow separation would shift slightly towards the rear stagnation point. In fact, Smith et al, indicated that heating the wall can substantially increase the  $u'$  component of the velocity in the laminar boundary layer of a water flow past a hot sphere. With  $\Delta T$  of  $72.2^{\circ}\text{C}$ , a maximum increase in  $u$  of 50 per cent in the boundary layer occurs. Furthermore, the velocity boundary layer thickness was changed only slightly by heating or cooling.

Since/...

Since the air viscosity is increased by heating, opposite to the effect in liquids, it would be expected that cooling the cylinder surface in air flows would tend to delay flow separation, stabilise the flow and increase the  $u$  component in the boundary layer velocity. Therefore, cooling the present test cylinder lower than the air flowing stream temperature would enhance the acceleration effect of the main flow, in the acceleration region, which, depending on the flow viscosity, may increase the wall shear stress.

Back et al (224), used a Preston tube type of device to measure the shear stress on a flat plate, whose surface was cooled, in an airstream. They demonstrated that cooling the solid boundary at a lower temperature than the air stream temperature has the effect of increasing the friction coefficient above the constant property air flow values. The increase in the friction values, above the adiabatic case, with cooling amounts to about 20 per cent at a ratio of wall-to-free stream temperature of 0.5.

Examination of figures 9.3 to 9.5 shows that heat transfer rate and the wall to main stream temperature ratio are not the only factors influencing the flow characteristics around the cylinder. The possible effect of the surface temperature will be discussed in connection with the distribution of heat transfer coefficient around the cylinder. Unfortunately, this point was not fully investigated due to the limitations imposed on the present studies and only one test was made with three temperature levels for the cooling water. This will be discussed later in this section. Therefore, it should be understood/...



understood that the heat transfer part of the investigation is far from being complete.

It is worth mentioning that the pressure coefficient distributions were simultaneously measured with the heat transfer and shear stress all through the investigation. It was expected that pressure distribution taken with heat transfer towards the cylinder surface would be different than that for adiabatic conditions. By comparing the pressure results under those two circumstances, within the accuracy of the measurements, no significant differences were found. Accordingly it was decided to omit the presentation of the pressure distribution with the heat transfer for the sake of decreasing the number of graphs presented in this thesis.

The distributions of heat transfer rate around the cylinder circumference for two typical flow conditions are shown in figures 9.6 to 9.9. Each figure contains data collected from tests carried out under the same main flow conditions for three rates of air extraction and show the influence of mass transfer on the heat transfer distribution around the cylinder perimeter.

Figures number 9.6 and 9.7 demonstrate the heat transfer distribution for four heating loads at  $Re = 0.47 \times 10^5$ . In general, the local values of the heat transfer coefficients were decreased by decreasing the heat load in the tunnel. On the other hand, increasing the rate of mass extraction caused, over the investigated range, either no or slight increase in the local heat transfer rate recorded./...

recorded. Indeed this is in agreement with the observations of Boulos and Pei (225). Their measurements indicated that, over a mass transfer parameter  $CQ\sqrt{Re}$  range similar to the present one, the average heat transfer rate from a sphere was changed very slightly.

The way in which the heat transfer coefficient was distributed around the single cylinder under the present flow conditions needs more careful consideration. It should be emphasised, however, that this is the first time heat transfer coefficient has been measured around a circular cylinder while there is a simultaneous mass extraction taking place through the cylinder surface.

Kotake (227) analytically demonstrated that the increase of the normal velocity at the interface of a liquid-gas flow, associated with phase changing, modifies the velocity and temperature profiles. For the case of evaporation, these modifications will result in a reduction in the shear stress at the interface and the opposite would be expected in the case of condensation.

Luikov (226) in describing the process of heat and mass transfer, between a capillary porous body and the main flow stated that, the process mechanism under these conditions are very complicated and cannot be described by the common methods of heat and mass transfer of matter. Furthermore, he showed that there is a necessity for special and detailed experimental investigations on heat and mass transfer mechanism under these circumstances.



Heat transferred to the cylinder, from integrated local values, was checked against the heat transferred by the cooling water sprayed on the inside surface of the test cylinder. The calculated sensible heat carried away with the cooling water was found to amount only to about 20 per cent of the measured heat transferred to the cylinder. Obviously, the rest of the heat transferred must have been carried away by some sort of evaporative cooling of the capillary moisture. In fact, that is the most probable explanation for the high heat transfer coefficients obtained in the present tests in comparison with those for the net heat transfer with all other conditions equal.

This explanation agrees with the investigations of Lebedev (228, 229) who showed that the transfer of moisture in capillary-porous body, towards the surface due to the moisture content gradient, would accelerate the molecular heat transfer, thus causing an increase in the heat transfer coefficient over that with only heat transfer. This was also confirmed by investigations of Finlay and Coworkers (230, 231) who indicated that, depending on the moisture content in the main mist stream, the heat transfer from a heated circular cylinder in cross flow could be improved by up to twenty times the corresponding dry gas values.

In the present case, water vapour produced in the evaporative cooling process should be either carried into the inside of the test cylinder or carried away through the porous surface into the air main stream. If the vapour was carried to the inside of the test cylinder, it would either/...

either condense when it came in contact with the colder cooling water or be carried away, through the suction line, outside the cylinder. In this case, the heat carried by the vapour will show itself, by condensation, as an increase in the sensible heat of the cooling water. This was not the case and cooling water temperature increase accounted for only 20 per cent of the heat transferred to the porous surface. In the second case, the vapour would be partially condensed in passing through the suction tube which was surrounded by a pool of cold water in the bottom of the test cylinder and eventually this moisture would be separated in the water separator fitted to the suction line. Again, that was not the case.

In fact, if the water vapour was sucked instead of air from the main stream, then the suction capacity or the pressure drop across the porous wall would have had to have been increased considerably to carry away the produced volume of water vapour. On the other hand, the recorded magnitudes for the wall shear stress indicated that air was being sucked, not water vapour, from the external main flow. The values of the wall shear stress obtained were higher than those measured with the corresponding adiabatic flow conditions with other conditions equal. These measurements prove nothing, but the presence of a sucked boundary layer similar in nature to that which exists under adiabatic conditions.

Obviously this situation is far from being a simple one, and the above discussion shows that the conditions on the cylinder surface could be visualised as follows: While the water vapour/...



vapour was released into the main stream, the sucked boundary layer on the porous surface was active and did not seem to be affected by the vapour transfer from the surface towards the main air stream.

This puzzling situation was clarified in the light of the investigations carried out by Luikov (226). He measured the distribution in the boundary layer, on a moistened porous plate in a stream of hot air, of the flow velocity, temperature and vapour partial pressure. His measurements showed that the vapour was, in fact, moving from a lower partial pressure at the solid surface to the higher one in the main stream. Consequently, he concluded that the water vapour pressure cannot be considered as a potential of mass injection into the boundary layer. This conclusion was confirmed by Luikov's measurements of the velocity distribution in the boundary layer over the porous surface with and without evaporation. Over a Reynolds number range from 8000 to 100,000, he found that the mass transfer associated with the evaporation of the moisture in the surface had no influence on the velocity distribution across the boundary layer.

On the other hand, Luikov demonstrated that the direction of mass transfer depended on the marked difference in molecular weights of air and water vapour and the gradient of the kinetic energy (in the external boundary layer). Moreover, it was shown to be theoretically possible for moisture to be transferred against the water vapour partial pressure gradient if these two effects are sufficiently large (232).

Guided by Luikov's observations, it seemed reasonable to assume that his conclusions are also valid for the porous surface with a normal velocity towards the surface. In other words, the velocity distribution across the sucked boundary layer was assumed not to be influenced by the water vapour released into the boundary layer and the present simulation to condensation processes was valid.

Figures numbers 9.6 and 9.7 show that distribution of heat transfer, starting at the FSP with either zero or positive gradient. On the rear of the cylinder, the heat transfer coefficient reaches a minimum value at a location beyond the point of flow separation. The lag between the point of minimum heat transfer and flow separation was also noticed, for single phase flow, by Giedt (44), Achenbach (45) and Schmidt and Wenner (162).

By decreasing the heat load, in the working section, the point of minimum heat transfer coefficient was moved slightly towards the rear of the cylinder and the distribution of the heat transfer coefficient was flattened out. Downstream of the point of minimum coefficient of heat transfer there was an increase in the local heat transfer coefficient due to the effect of vortices being shed in the circulation region which encouraged mixing in the fluid and improved the heat transfer in this region.

Figures 9.8 and 9.9 demonstrate the distribution of heat transfer coefficient around the cylinder surface circumference for  $Re = 0.7 \times 10^5$ . The general trend shown previously with/...



with  $Re = 0.47 \times 10^5$ , has shown itself again in this case.

Figure 9.9.a shows the effect of increasing the cooling water temperature on the heat transfer distribution with other conditions equal. Three temperature levels for cooling water equal to  $15^\circ\text{C}$ ,  $19^\circ\text{C}$  and  $22^\circ\text{C}$  were used with  $CQ\sqrt{Re}$  equal to 0.15, 0.23 and 0.37 respectively.

These tests were carried out by recirculating the cooling water through the test cylinder, since the main mechanism of heat transfer in the present set-up was the evaporation of some of the cooling water, it is clear that increasing the temperature of the cooling water resulted in an increase in the recorded heat transfer rate. Since it was demonstrated that the suction rates used have no or slight effect on the local heat transfer coefficient, therefore, differences shown in figure 9.9.a. should be attributed to the influence of cooling water temperature, sprayed on the inside of test cylinder, on the recorded values.

It is to be noticed that the heat transfer coefficient at the rear stagnation point was very similar to the corresponding values obtained at the front stagnation point.

Average heat transfer coefficients were evaluated by integrating the local coefficients distribution of the type shown in figures 9.6 to 9.9., according to formula number 9.3. When the average values so obtained are plotted against the main stream temperature, as shown in figure 9.10, the data form curves of constant Reynolds numbers.

It/...

It is clear that there is some scatter in the results at the heat loads tested. Although some of the scatter was probably due to circumferential variations in the recorded results, some of the scatter is also due to the accuracy of the measurements and an average curve drawn through the data points should provide a good description of the results.

Figure 9.10 shows the effect of the air stream cross velocity on the heat transfer coefficient of a single cylinder as a function of the main stream temperature, heat load with Reynolds number as a parameter. In agreement with the observations of Furman and Hampson (207) for vertical tube condenser, the overall heat transfer rate was increased by increasing the cross flow velocity.

#### 9.4.2. Tube bank measurements

Investigations of the flow characteristics within the staggered bank were started by locating the instrumented porous test cylinder in the middle of a transverse row across the tunnel working section. Two permanent dummy rows were located downstream of the row containing the test cylinder to simulate the natural sequence found in heat exchangers. This was done to avoid the free wakes effect encountered in single rows of cylinders and the effect of deflected gap flow encountered in the last row of banks with tube spacings used in practice (94).

For a certain main stream flow rate, the approach velocity to the row concerned was carefully adjusted to be as close as possible to that used in the adiabatic tests. Although an/...



an effort was made to control the flow rates, for similar values, when running tests from row to row, inevitably slight differences were noticed for different rows in the tube bank tested. However, the data are collected and correlated against the values of the nominal Reynolds number.

Moreover, the temperature level of the air main flow could not be maintained constant from test to test and small variations have had to be tolerated during the investigation.

For a specific Reynolds number, normal pressure and heat transfer coefficient distributions together with those of the wall shear stress were measured around the cylinder circumference in 5 degree steps following the procedure used with the single cylinder in section 9.4.1. The recorded values of skin friction are presented as a fraction of the incoming kinetic energy of the approach velocity, as the coefficient of wall shear stress  $K_f$ . The local values of the normal pressure, relative to the kinetic energy upstream the row, was calculated as the pressure coefficient  $C_p$ . The values of the local coefficient are then plotted as functions of the angle  $\theta$  measured from the front stagnation point.

This procedure was repeated over the suction and heat load ranges used in the investigation. The suction rates used were the same all the way through the whole programme of study.

The flow rate of the main flow was then changed and the whole procedure/...

procedure repeated for that particular row in the tube arrangement over the Reynolds number range covered in present work.

By changing the number of the dummy aluminium tube rows upstream of the row containing the test cylinder, with the downstream unaltered, the investigations were continued and the whole previous procedure was repeated through the depth of the tube bank from the first to the fifth tube row.

#### 9.4.2.1. Flow characteristics in the tube bank

The effect of increasing the temperature level of the main air flow on the wall shear stress and normal pressure distributions, compared with adiabatic cold flow, around individual cylinders in the 1st, 2nd, 3rd, 4th and 5th row of the staggered tube bank is shown in figures 9.11, 9.21, 9.31, 9.41 and 9.51 respectively.

If the slight differences in flow rates are tolerated, then increasing the air temperature would cause either no or slight change in the shear stress on the frontal part of the cylinders in different rows in the tube bank. Because of the interconnection between the normal pressure and the wall shear stress under these conditions, e.g., boundary layer equations, similar changes were also observed in the recorded values of the pressure distributions.

On the cylinder in the first row, the trend was more or less similar to that noticed for a single cylinder, and shear stress distributions together with normal pressure distributions/...



distributions showed a slight decrease in the local values with adiabatic hot air compared to the adiabatic cold air.

In the second row there was a slight increase in the local wall shear stress with heating of the air stream. This might be due to the effect of the hot jet, high viscosity, discharged from the straight gap between adjacent cylinders in the first row, on the recorded values.

For the third row, the changes in the local values of the wall shear stress, with changing the temperature level of the main stream, were not significant and it was considered to be fairly constant. Similar observations were also noticed in the normal pressure distribution in that row.

The fourth and fifth rows showed similar characteristics, and air increase in the wall shear stress due to increasing the temperature of the air stream was recorded.

Examples of the progressive effect of the main stream temperature level on the wall shear stress distribution around the cylinder are shown in figures 9.12, 9.22, 9.32, 9.42 and 9.52 for cylinders in the 1st, 2nd, 3rd, 4th and 5th tube row respectively. These figures show that the effect of increasing the air temperature, with air extraction, varies along the depth of the tube bank.

First and second tube rows showed characteristics similar to those observed with a single cylinder and local shear stress on the frontal portion of the cylinder in these rows was reduced/...

reduced by raising the temperature of the main stream. In the rear of the cylinder's circulation region, local negative values of the wall skin friction were increased with increasing air temperature. On the third row, the wall shear stress could either slightly decrease or increase with increasing air temperature. Again fourth and fifth rows showed similar behaviour and local shear stress was slightly increased with increasing the main flow temperature.

The influence of adding heat flux to the sucked boundary layer, on the skin friction within the tube bank for different heat loads is presented in figures 9.13 to 9.15, 9.23 to 9.25, 9.33 to 9.35, 9.43 to 9.45 and 9.53 to 9.55 for the successive rows from the first to fifth tube row respectively.

The general trend in these figures is an increase in the recorded wall shear stress with the diabatic sucked boundary layer over that with the adiabatic cold tests. These are similar for the five rows in the bank and consistent with the single cylinder observations.

On the rear side of the cylinders, after the flow is separated from the surface, the negative values of the local shear stress were enhanced with the diabatic flow over those with the corresponding adiabatic cold stream. Corresponding variations in the normal pressure distributions, however, were not observed and pressure coefficients around the cylinder were very similar to those measured using adiabatic hot flow.

A/...



A question could be raised here about the circulation region with reversed flow, in the present study at the rear of the cylinders and how far it simulates the actual case in a surface vertical tube condenser. The answer lies in the observations of Furman and Hampson (207) with actual condensation on a vertical tube. On the rear of the cylinder, after the break away lines, they noticed that there was a movement of condensate drops towards the break away lines. In other words, similar to single phase flow, there was a reverse flow in the "circulation region".

Similar observations were noticed by Finlay and McMillan (230) who found that liquid droplets on the rear of the cylinder, in a cross mist flow, were moving towards the separation point of the water film that was formed at the forward portion of the cylinder with Reynolds number 29000 to 95000.

It can be noted that the flow conditions within the tube bank, in general, were of the unsteady type and the recorded local values were temporal values. Consequently, the small movements for the point of flow separation were expected and for each flow condition there was a flow separation region rather than a fixed separation point.

The existence of a separation region was also confirmed with the observations of Bloor (233) when a periodic laminar flow was observed inside the separated boundary layer at  $Re = 45000$ . Furthermore, the investigations of Finlay and McMillan (230) showed that the ridge, at which the water film formed on the forward part of a heated cylinder in a transverse mist flow, was/...

was unstable and continually receded and advanced with a frequency of motion which increased with increasing the mist flow velocity.

Unfortunately, the non-existence of a fixed separation point makes it difficult to identify the individual effect of heat transfer on this region. It seems, however, that the suction rate together with the powerful influence of the strong adverse pressure on the back of the cylinder plays the major part in determining the characteristics of flow separation. And this combined effect cannot be significantly influenced by the properties variations of the boundary layer flows. Accordingly, the small movements recorded for the flow separation point were considered to be within the separation region observed at any particular test.

#### 9.4.2.2. Heat distribution in the tube bank

Distribution of heat transfer coefficient around first tube in the bank is shown in figures 9.16 to 9.19. As a common feature, in these figures, the suction rate has either no or very little influence on the heat transfer coefficient distribution around a cylinder in the first row in the tube bank. The progressive reduction in the local values of heat transfer rate as a result of reducing the heat load on the working section is quite noticeable.

The distribution starts at the forward stagnation point,  $Re = 60,000$ , with either zero or positive gradient, increases to about  $\theta = 60^\circ$  (maximum shear stress area in figure 9.11a) and then drops gradually to a minimum at or near the rear stagnation/...



stagnation point. This point of minimum heat transfer coefficient was located beyond the flow separation point, about 30 degrees downstream the corresponding point on a single cylinder.

Figures 9.18 and 9.19 show the heat transfer coefficient distributions for the first row at  $Re = 10^5$ , the Reynolds numbers were determined as shown in Chapter 7. At this Reynolds number there is a relative minimum value of the heat transfer coefficients at the forward stagnation point, increased gradually to reach a maximum around the area of maximum wall shear stress, e.g., figures 9.13 to 9.15. Thereafter, there is a continuous reduction in the heat transfer coefficient until it reaches a minimum at or near the rear stagnation point of the cylinder at a location beyond the point of flow separation.

In this row, variations in the present suction rates have little to contribute to the heat transfer coefficient around the cylinder circumference. The coefficient of heat transfer at the rear stagnation point varies from about 50 to 100 per cent of the values at the front stagnation point with increasing the flow Reynolds number. For a particular Reynolds number, the dominating factor influencing the local values was the heat load on the working section (air stream temperature).

Figure 9.20 shows the average coefficient of heat transfer obtained by integrating the local values around the cylinder perimeter using expression 9.3. The scatter of the data (as shown in that figure) was due to experimental sources of error/...

error, accuracy of measurements and integration procedure. Nevertheless, the curves drawn through these points provide a description of the results. These show that the average coefficient of heat transfer was controlled mainly by the cross flow velocity and the main stream air temperature. For a specific heat load, and air temperature, increasing the Reynolds number resulted in an increase in the coefficient of heat transfer.

The distribution of heat transfer rate around a cylinder in the second row in the tube bank, is shown in figures 9.26 and 9.27 for  $Re = 76,000$ . The continuous reduction in the measured coefficient of heat transfer,  $h$ , with decreasing the main stream temperature is quite noticeable.

In this row, the distribution started at the front stagnation point then increased to reach a maximum, around the peak region of the shear stress distribution figure 9.21. Thereafter, the heat transfer rate decreased slowly to its minimum at or near the rear stagnation point close to the area of minimum wall shear stress.

Figures 9.28 and 9.29 demonstrate the variations in the values of  $h_0$  around the cylinder for  $Re = 1.3 \times 10^5$ . The effect of suction rate on the heat transfer distribution, which was not clear at the three main extraction rates used previously, was investigated further by reducing the suction rate to the lowest possible magnitude. In this context, the lowest possible rate means that, lower than this rate cooling water from inside the porous tube (under capillary action/...



action without air flowing through the tunnel) was observed on the outer surface of the test cylinder as water moisture. For these conditions, the lowest possible rate of suction parameter reached was  $CQ\sqrt{Re} = 0.01$ .

From figure 9.28a, it is clear that this minimum suction rate produced lower values from the local heat transfer rates. Comparison between these values with those obtained with the next highest suction rate, i.e.,  $CQ\sqrt{Re} = 0.1$ , shows that although the variations in the suction rates were ten times, variations in the heat transfer was about 20 per cent. In fact, a general correlation for the effect of suction rates on the heat transfer rate was not reached.

A closer look at figures 9.28 and 9.29 in relation to figures 9.24b, 9.25b demonstrates a possible relationship between the heat transfer and flow distribution around the cylinder perimeter.

It is clear that the value of  $h_0$  increased to reach a peak value in the peak region of the shear stress distribution. The gradual reduction from this peak towards the rear of the cylinder was very similar to the reduction in the values of  $K_f$ . Whenever a steep gradient in the value of  $K_f$  was observed a steep gradient in the heat transfer distribution was also observed. The value of  $h_0$  reached minimum 10 degrees downstream of the region of diminishing value of  $K_f$ .

The second peak value appeared in figure 9.28a and was, in fact, there all the time. It is identifiable even with the lowest/...

lowest suction rate used. These second peaks became more obvious with the increasing rate of air extraction. Furthermore, changes in the applied heat load did not cause changes in the general features observed with higher loads.

For a cylinder in the second row in the bank, heat transfer coefficient at the rear stagnation point was always less than the corresponding values recorded at the front stagnation point for all the tests. Increasing the Reynolds number results in a further relative reduction of this at the rear compared with that at the FSP.

The average heat transfer coefficient,  $h_{av}$ , for a cylinder in the second row is shown in figure 9.30. This was obtained from the integration of the local values of the heat transfer coefficient distribution,  $h_{\theta}$ , as shown in figures 9.26 to 9.29 and plotted against the main stream air temperature, with the Reynolds number as a parameter. Within the scatter of the points, average curves drawn through them, show that  $h_{av}$  is increasing with Reynolds number and air temperature (heat load).

The distribution of heat transfer coefficient around cylinder located at the third row in the tube bank is shown in figures 9.36 to 9.39. A general feature is the small effect of the suction rate on the recorded values of  $h_{\theta}$ . Although, sometimes, a slight effect does exist, a general relationship between these two parameters could not be deduced. Indeed, suction rate variations might have an effect on the values of  $h_{\theta}$  using higher rates than those presently/...



presently used. However, the small variations in the recorded coefficient of heat transfer for the present range of mass transfer agreed with the results of Boulos and Pei (225).

Figures 9.36 and 9.37 show the measured values of  $h_\theta$  around the cylinder circumference for  $Re = 60,000$ . The distribution begins at the forward stagnation point with a relative minimum value which increases with increasing angle  $\theta$  to reach some higher values in the neighbourhood of the FSP. It is then slightly reduced and then increased again, with increasing  $\theta$ , to reach a second peak around  $\theta = 100^\circ$  from FSP. In connection with the distribution of the wall shear stress,  $K_f$  in figure 9.33a, it is possible to notice that there is a second peak in  $K_f$  values around 90 degrees from FSP. Although the peak for  $K_f$  is a weak one, figure 9.34a, it still exists and it is the shear stress distribution which is flattened out at its top. In fact, the second peak is also shown in figure 9.35a with a small inflection at  $\theta = 90^\circ$ .

Unlike the second row, a cylinder located at the third row in the bank showed a minimum value of  $h_\theta$  which is delayed downstream of the flow separation point by 30 to 40 degrees and then it increases again until it reaches the rear stagnation point. The recorded magnitudes for the heat transfer coefficient at  $\theta = 180^\circ$  were always less than the corresponding magnitudes measured at  $\theta = 0^\circ$ .

Figures 9.38 and 9.39 demonstrate the distribution of  $h_\theta$  in the third row at  $Re = 94,000$ . These figures show that  $h_\theta$  started at the FSP with a relative minimum which increased with/...

with increasing angle  $\theta$ . The appearance of two peaks in the  $h_\theta$  distribution is noticeable especially at the highest heat load, investigated as shown in figure 9.38a. In relation to the wall shear stress distribution, this seems to be due to the influence of the flow distribution around cylinders in that row. After the second peak is reached, values of  $h_\theta$  rapidly decrease to reach minimum value downstream of the corresponding separation point, thereafter increasing again slowly until reaching the rear stagnation point.

The heat transfer coefficient at the rear stagnation point was comparable with that at the FSP when  $Re = 60,000$ , but it became less than that at the FSP for  $Re = 94,000$ .

The average heat transfer coefficient over a cylinder in the third row is shown in figure 9.4.0, plotted against the main stream air temperature for the Reynolds numbers tested.

This row shows the common features for the previous rows and the values of  $h_{av}$  increase with increasing Reynolds number and air temperature.

The distribution of heat transfer coefficient on the cylinder circumference at the fourth row in the tube bank is shown in figures 9.46 to 9.49. These will be analysed in relation to the wall shear stress distribution obtained in the same tests.

It is clear that, even with no air extraction as in figure 9.41a, there are two peaks in the shear stress distribution and it is their relative magnitudes which change whenever suction/...



suction is applied. Although with suction there is a tendency for the distribution to flatten these two peaks together with the area between them, the peaks are still identifiable. Accordingly, it would be expected that the  $h_\theta$  distributions would have peaks corresponding to those observed in the  $K_f$  distribution. However, they might be delayed or lag behind the peaks in the wall shear stress.

The recorded local heat transfer coefficients show that, indeed, that was the case. This showing itself clearly with the highest heat load used (e.g., figures 9.46 to 9.49). By decreasing the mainstream air temperature, the heat transfer distribution gets flattened out and the peaks gradually became difficult to identify, possibly due to the accuracy of measurements. Since figures 9.48a, b and 9.49a, b are plotted from data collected under the same flow conditions, the incoming air temperature was the only variable encountered, there was no obvious reason why all of them should not show some common main features. Therefore, the vanishing peaks could be only attributed to the accuracy of heat transfer measurements whose value was estimated to be about 15 per cent.

Local values of  $h_\theta$ , recorded at the FSP for a cylinder in the fourth row, showed a value whose magnitude increased with increasing angle  $\theta$  to reach its first maximum peak on the front of the cylinder and reached its second peak at about  $\theta = 100$  degrees from the FSP which nearly corresponds to the second peak location in the  $K_f$  distribution. After the second peak for  $h_\theta$  is reached, it drops gradually to reach a/...

a minimum value downstream of the flow separation point by about 30 degrees towards the rear stagnation point and then increased again until it reached  $\theta = 180^\circ$ .

Magnitudes of heat transfer coefficient at the rear of the cylinder in that row were very similar to those recorded at the FSP with  $Re = 56,000$ . Increasing the Reynolds number to  $10^5$ , caused the rear stagnation point heat transfer coefficient to be lower than the corresponding values at the front stagnation point.

Integration of the  $h_\theta$  distribution such as in figures 9.46 to 9.49, yield the average heat transfer coefficients for a cylinder in that row. Similar to the trend found with previous rows, the heat transfer coefficient increased with increasing Reynolds number and heat load in the working section.

Data obtained for the fifth rows in the bank, presented in figures 9.56 to 9.59, show the  $h_\theta$  distributions at Reynolds number equal to 60,000 and  $10^5$ . These figures together with the wall shear stress distributions, simultaneously measured under the same flow conditions, show a general behaviour which is similar to that noticed on the fourth row.

At the front stagnation point, the value of  $h_\theta$  is a relative minimum whose value increases with angle  $\theta$  to reach its first peak in the neighbourhood of the FSP, then decreases slightly on the middle part of the forward half of the cylinder. Thereafter/...



Thereafter, heat rate increases again to reach another peak which corresponds to the area of the second peak in the wall shear stress distribution at about  $\theta = 100^\circ$  from FSP. Heat rate drops thereafter to reach its minimum value at a position downstream the corresponding point of flow separation by about 30 degrees towards the rear stagnation point where its value starts to increase until it reaches  $\theta = 180^\circ$ .

The magnitude of second peak in  $h_\theta$  distributions was slightly higher than that close to the FSP at  $Re = 60,000$ . Increasing the Reynolds number caused the second peak to reach even higher values than those recorded at the FSP.

Values of  $h_\theta$  at the rear stagnation point are very similar to those measured at the FSP for  $Re = 60,000$ . With a higher Reynolds number,  $h_\theta$  at the rear of the cylinder becomes lower than the corresponding values at  $\theta = 0^\circ$ .

It is noticed that the variations in the suction rates tested had little influence on the heat transfer characteristics and a general correlation for this influence could not be deduced.

The average heat transfer coefficient for a cylinder located in the middle of the fifth row was obtained by integrating the distribution of local values using expression 9.3 and results are shown in figure 9.60. In accordance with the general characteristics of the previous rows, heat transfer coefficient for that row increases with increasing/...

increasing flow Reynolds number and air temperature.

#### 9.5. Summary and discussions

Heat and mass transfer were used simultaneously to simulate a condensation process in a vertical heat exchanger model. On a single cylinder and a seven rows deep staggered tube bank, detailed investigations were carried out to measure simultaneously the distributions of normal pressure, wall shear stress and heat transfer coefficient around the circumference of the test cylinder. For the tube bank tested, this was carried out for the middle cylinder in a transverse row from first to fifth rows. Stable flow characteristics for fourth and fifth rows indicated that they could resemble deep rows in the tube bank and no justification was found to proceed further beyond the fifth row in the present study.

Data for single cylinder showed that, increasing the air temperature in an adiabatic flow caused slight reduction in the local wall shear stress compared with the adiabatic cold flow. This was also the case when suction was applied to the cylinder surface and  $K_f$  values were decreased with increasing the air temperature in a diabatic flow at a similar Reynolds number. Moreover, the negative shear stress values at the rear of the cylinder were increased with raising air temperature levels.

Adding heat transfer across the sucked boundary layer caused an increase for both wall shear stress values on the front and rear of the cylinder compared with the constant property/...



property flow conditions.

The influence of properties variations on the flow separation point from the cylinder surface was not noticeable and the small movements recorded for the separation point were considered to be within the separation region observed at any particular flow conditions. It was concluded that, within the present range of variables, suction rate and adverse pressure on the rear of the cylinder are the dominating factors in determining the flow separation compared with the possible effect of properties variations across the boundary layer.

Distribution of  $h_\theta$ , around single cylinder, had either zero or positive gradient at FSP with a tendency of reaching higher values in the region of higher values in the  $K_f$  distribution.

Values of  $h_\theta$  reached minimum at locations downstream of the flow separation point, and heat transfer coefficients recorded at the rear stagnation point were very similar to the corresponding values at FSP.

Results for the tube bank indicated that the influence of raising air temperature level, adiabatic flow, is different with the row position inside the bank and in particular when suction was applied to the test cylinder. Compared with cold flow conditions, this caused a reduction in the  $K_f$  magnitudes on first and second rows in the tube bank. On a cylinder in the third row, the variations in  $K_f$  were either/...

either towards no or slight reduction compared with cold adiabatic flow conditions. For the fourth and fifth rows there was an increase in the  $K_f$  magnitudes relative to the cold flow conditions at similar Reynolds number.

Applying a heat flux across the sucked boundary layer results, in general, in an increase in the recorded wall shear stress around the test cylinder all the way through the investigated depth of the tube bank.

The influence of adding heat transfer to the boundary layer on the flow separation on cylinders in different rows was not confirmed and the little movements of the separation point were, in fact, within the separated region at any particular air flow rate. This agreed with the observations of other investigators who showed that this region can cover as much as 10 degrees arc on the cylinder surface (85). Similar to the single cylinder case, suction rate and adverse pressure on the back of a cylinder within the bank are determining the flow separation characteristics and the effect of property variation could be negligible compared to their combined influence.

For the five rows investigated, heat transfer coefficient was a relative minimum on the FSP which increased with angle  $\theta$  to reach maximum wherever the wall shear stress distribution showed a maximum. Moreover, the point of minimum heat transfer coefficient was located downstream of the flow separation point by up to 30 degrees towards the rear stagnation point of the test cylinder.

Values/...



Values of  $h_\theta$  at  $\theta = 180^\circ$  relative to that at FSP in the front portion of the tube bank were different than those recorded deep inside the bank. First, second and third rows showed  $h_\theta$  at  $\theta = 180^\circ$  which was less, in general, than the corresponding value recorded at  $\theta = 0^\circ$ . Cylinders in the fourth and fifth rows showed similar characteristics to those noticed with a single cylinder, and  $h_\theta$  at the rear stagnation point were very similar to those measured at FSP.

As far as the heat transfer distribution along the depth of the tube bank is concerned, data for different rows from different tests are replotted, within the measurements accuracy which is estimated to be about 15 per cent, to show different row heat transfer characteristics. Results for the average heat transfer coefficient over the tube bank are shown in figures 9.61, 9.62 and 9.63 for the three main extraction velocities,  $V_w$ , used in the study 0.012, 0.018 and 0.025 m/s respectively. Within the scatter of the data, the general heat transfer characteristics along the depth of the tube bank are shown as hatched area.

From these figures, it is quite clear that the average heat transfer coefficient,  $h_{av}$ , increases rapidly from first to third row, then drops towards the fourth row and with a decreasing gradient it reaches the fifth row. As would be expected, all these values were greater than those obtained for a single cylinder with all other flow conditions equal and  $h_{av}$  obtained for the first row were about 10 to 20 per cent lower than that measured for a deep row in the bank, e.g., fifth row. This is probably due to the high turbulence/...

turbulence level in the incoming air stream,  $T.L. = 6\%$ .

The peaks in  $h_{av}$  at the third row are similar to those found by Snyder (186) in his analysis for the work of Thomson et al (154). While Snyder's own results showed a constant value for  $h_{av}$  between the third and fourth rows, the present results, in general, are in agreement with those found by Thomson et al. Their results showed a gradual continuous reduction in the rate of heat transfer from the third to the sixth row in the tube bank. This is possibly due to the fact that, the sixth row in their experiments was the last row in the bank. That is clear from the present results where the reduction in  $h_{av}$  between fourth and fifth rows is less than the reduction in the average heat transfer coefficient between third and fourth rows.

The change in the heat transfer characteristics of the bank at the third row was also observed with the wall shear stress measurements for the sucked boundary layer under the influence of hot adiabatic flow when first and second rows on one side behaved differently from the fourth and fifth rows on the other. This change in character across the third row was noticed from the measurements of wall shear stress and pressure drag for different rows in the bank (described in Chapter 7). The high drag measured for the first row, which could be attributed to the effect of laminar flow due to free air streaming results in a low heat transfer coefficient. At the second and third rows the flow turbulence increases and results in an increase in the value of  $h_{av}$ .

As/...



As a general feature of this chapter, there was a small effect from the suction rates used on the variations of the heat transfer coefficient. Due to the limited range of suction data obtained, it was not felt a realistic correlation of this data could be made.

Finally, it is important to mention here that the investigation under diabatic flow conditions is by no means complete and it is hoped that the data presented in this chapter would contribute towards a better understanding of the flow through staggered tube banks surface condensers. More investigations on this side of the present work are needed to cover more heat loads and suction rates under smaller Reynolds numbers, preferably comparable to those found normally in an actual surface condenser.

As the experiments with heat and mass transfer were carried out at three values, sometimes only two, of the Reynolds number, a correlation which would satisfactorily relate the heat transfer coefficient to the flow  $Re$  was not reached.

## CHAPTER 10

### FLOW VISUALISATION

#### 10.1 Introduction

Many investigations have been made to study, by means of flow visualisation, the flow that passes across circular models, whether a single cylinder or a group of cylinders, e.g., Zdravkovich (256, 257). These studies have been carried out at low Reynolds numbers  $< 300$ , to investigate the flow pattern in the wake of the test models.

The present observations, however, were conducted to show the flow field around circular cylinders in a cross flow of air with high Reynolds numbers with an emphasis on the effect of distributed suction on the flow around a porous circular cylinder in a cross flow of air with high Reynolds numbers with an emphasis on the effect of distributed suction on the flow around a porous circular cylinder.

From the previous chapters, it was demonstrated that mass extraction or suction through the walls of a porous cylinder caused a delay of the point where the flow separates from the cylinder surface and that the boundary layer flow was in contact with the surface for a longer distance compared to the case with no suction.

The aim of the present work was to outline the path of flow streamlines, outside the boundary layer, under the effect of suction, which would envelope the test cylinder with its immediate wake region.



## 10.2. Experimental arrangement

The present observations were conducted in the horizontal low speed wind tunnel of the Aeronautical Department, University of Glasgow.

The study was made using a model with the same dimensions as that used in the previous chapters. The porous test cylinder was 76.2/63.5 mm OD/ID and its construction was similar to that explained in section 5.2.2. except that, in this case, there was no shear stress sensor fitted to its body. The cylinder was connected to a suction pump on one end of it and the suction rate was measured using a calibrated rota meter at the operating pressure.

The wind speed was varied over a range of flow velocities similar to that used in the main programme, i.e., Chapters 7, 8 and 9. The Reynolds number varied from 19500 to 108000.

Two techniques were used to provide means of visualising the flow around the test model. These were the buoyant bubble and smoke filament techniques.

Since good flow conditions were only obtainable by taking short exposures, the photographs suffer somewhat in intensity. The photographs were taken directly, by employing a camera mounted outside the wind tunnel.

### 10.2.1. The buoyant bubble system

This technique was based on implanting small buoyant bubbles generated using a special head in an air flow and then/...

then photographing the bubble's motion which would indicate also the motion of the air flow (258).

For the present work, the bubbles were generated using a low speed head (a pencil shaped device) approximately 6.5 mm OD with a total length of 27.5 mm. This head was able to produce a high rate of about 500 bubbles per second with bubble diameter of about 1.5 mm in air flow with velocities up to 25 m/sec. The bubbles were first formed inside the head and then injected into the surrounding air stream. They accelerated quickly and reached the mainstream velocity after travelling a short distance. The head was installed upstream of the model far enough to avoid any disturbing effect from the model on to the generated stream of bubbles.

The head basically consisted of a concentric array of three tubes, the outermost one being the body of the head itself. Air was fed through the innermost tube and soap solution fed through the intermediate tube which extended slightly beyond the inner tube.

For the present study, the soap solution chosen was a commercial 'green fairy' soap liquid based on household detergents. This soap has a good bubble forming characteristic and it was fed to the head using a small positive head displacement pump.

The air and soap liquid interact in such a way, downstream of the tip of the inner tube, to generate air filled bubbles continuously at the tip of the intermediate tube. Compressed air was fed to the third outmost tube, or the body of the head/...



head to blow the bubbles off the tip after the bubble has reached a particular diameter.

The velocity of the compressed air was the determining factor for the bubble size and generation rate. With too little air flow, the bubbles did not separate properly from the tip of the head. With too much air flow, the bubbles did not have a chance to inflate properly and the process degenerated into blowing small droplets of soap solution.

The constituents were fed to the head through flexible small diameter plastic tubing which fitted over the connecting pieces of hypodermic tubing which protruded from the head body.

Compact, high intensity lamps were installed upstream and downstream of the model to illuminate the bubbles at right angles with respect to the viewing direction. The lamps had narrow beams which were directed along the bubbles trajectories to minimise reflection and stray light.

The motion of the bubbles and therefore the air flow was viewed and photographed on ASA 125 films from the side of the tunnel using a Nikon camera. The exposure time was set in such a way that a number of bubbles pass through the field of view during the exposure.

#### 10.2.2. Smoke filament system

The smoke was to be dense and white as possible for visibility and had to be released into the air stream with a quite/...

quite low velocity, so that the disturbances to the flow were minimised.

The smoke was generated by the vapourisation of Shell 'ondina 17' oil using a T.E.M. smoke generator type B.FVSP/B with pressurised control unit FVSP 104.

The oil was forced through a small diameter tube and vapourised immediately adjacent to the axial exit orifice by an integral electric heating coil. The volume of smoke was controlled to produce a plume in the air flow with clear boundaries, provided that the pressure in the oil reservoir was maintained constant.

The smoke was introduced through a small pipe placed upstream of the test model, so that the flow around the model could be made visible. As the action of the test cylinder was to disturb the smoke concentration in a cross section of the main air stream, the situation was made visible by illumination through a plane sheet of light parallel to the tunnel axis. This light sheet was produced by focussing a slit-shaped light source on to the centre of the flow field. In this illuminated 'smoke screen' the flow field around the model was observed.

Since the mixing between the smoke and air was quite intense, therefore the stability of the smoke filament marked by the smoke depends upon the flow conditions inside the wind tunnel. With the present tunnel; however, it was possible to obtain stabilised filament for Reynolds numbers up to 110,000. The numerical/...



numerical values of the Reynolds numbers are only correct within the accuracy of the measuring equipment.

### 10.3. Results and discussion

Examples of the results obtained for the flow visualisation are shown in figures 10.1 to 10.6. Figure 10.1 was obtained using the buoyant bubble technique while the rest of the figures were obtained using the smoke filament system.

Figure 10.1 shows the flow field around an inner tube in a staggered tube bank arrangement with equal pitch to diameter ratios, i.e.,  $L = T = 1.5$ . The photographs were taken at Reynolds numbers from 19,000 to 32,000. Since the bubbles followed the air flow path lines, the bubbles rarely collided with the test model and were quite durable.

For the case of no suction ( $\frac{V_w}{U} = 0.0$ ) the flow path lines produced by the path of the bubbles during the exposure time were clear and the photographs showed how the incoming stream was divided at the forward half of the cylinder body.

When suction was applied, however, the porous surface was stained especially at the frontal part of the cylinder and eventually it was partially blocked when the soap bubbles came in contact with the cylinder porous surface. Although few shots were taken with suction, it was difficult to maintain the operation for any reasonable length of time without getting into the trouble of blocking the pores in the porous surface.

These/...

These photographs are presented in figure 10.1 and they show that suction caused the flow stream lines to be brought closer to the cylinder surface. For  $\frac{V_w}{U}$  ranging from 0.01 to 0.017 the suction reduced the dividing of the mainstream on the front of the cylinder and the stream lines followed the cylinder contour for a longer distance compared to the no suction case. Also the circulation behind the cylinder was shown clearly with more flow coming along the cylinder surface when suction was applied.

Because of the difficulties encountered by the porous surface with the buoyant bubbles when suction was applied to the cylinder surface, this technique was stopped and experiments were continued using the smoke filament technique instead.

Introducing a radial plume of smoke along the horizontal axis of the test cylinder did not show the expected deflection of the filament when suction was applied. This was due to the rapid diffusion of the smoke into the boundary layer and the circulation region. Shifting the smoke filament to another vertical plane close to that of the cylinder axis proved useful in demonstrating the general influence of suction on the flow field around the porous cylinder.

The wake region was visualised separately by introducing the smoke probe downstream of the cylinder rear stagnation point along the horizontal plane passing through the cylinder axis. This was done in order to outline the shape of the immediate wake under different conditions of continuous suction.

Results/...



Results are shown in figures 10.2 to 10.6 for Reynolds numbers from 13,600 to 108,000 respectively. The suction to the main stream velocity ratio ranged from 0.0014 to 0.044 with normal velocity towards the surface ranging from 0.032 to 0.125 m/sec.

For a certain Reynolds number, the photographs are arranged in a vertical array with the top one representing the case of no suction. Suction was then applied and the bottom photograph in the array represents the flow around the cylinder with the highest suction rate used.

The suction rates used in these tests were higher than those used in the previous chapters. When small suction rates were used, i.e., up to  $V_w = 0.025$  m/sec., it was difficult to trace any changes in the filament movement due to suction. In fact, these observations for such small suction rates confirmed our previous conclusion that, these small suction rates mainly affected the boundary layer without too much influence on the flow outside the boundary layer which determines the normal pressure distribution along the surface.

In the circulation region, the suggested back flow was very marked. The strength of the circulation demonstrated itself by the almost uniform diffusion of the smoke into that region giving clear boundaries for the downstream of the test cylinder.

The upstream smoke filament shows clearly how the path lines were/...

were following the cylinder contour for a longer distance when suction was applied. The progressive deflection of the filament especially at the downstream side of the cylinder due to suction effect is obvious.

On the other hand, photographs taken for the wake region did not show a significant effect of the suction rate on the flow separation point. Presumably, this was due to the combined effect of the strong circulation at the back of the cylinder and the instability of the flow separation point which would result in intensifying the smoke diffusion further upstream of the separation region.

In order to demonstrate the influence of the distributed suction on the flow field around the test cylinder, the deflection of the smoke filament relative to the cylinder surface was measured from the photographs obtained for the study. It should be mentioned here, that these photographs were taken using the same setting of the test cylinder and the smoke generator and the variables were the Reynolds numbers and the suction rates.

The photographs were enlarged about twenty times its size on a screen and the distance between the cylinder surface and the smoke filament was measured from  $\theta = 30^\circ$  (where the incident filament started to follow the cylinder contour) up to  $\theta = 135^\circ$ . It was difficult to continue the measurements up to the rear stagnation point due to the rapid diffusion of the smoke in the circulation region.

Although/...



Although this procedure is not accurate on a quantitative basis, it is to be appreciated that the main purpose of this study was to demonstrate the changes the smoke filament undergoes around the cylinder due to suction effect on a qualitative basis.

As is shown in the photographs, the narrowest gap or the smallest distance between the smoke filament and the cylinder surface, for the no suction case, was at about  $\theta = 68^\circ$  from the FSP. Applying suction to the surface caused this point to move downstream towards the rear of the cylinder. With  $V_w = 0.03$  m/sec. the point of minimum gap moved slightly to about  $\theta = 70^\circ$  and increasing the suction velocity to  $V_w = 0.062$  m/sec. pushed the point of minimum gap downstream to about  $\theta = 75^\circ$ . Increasing the suction velocity further to  $V_w = 0.093$  m/sec caused the point of minimum gap to occur at about  $\theta = 80^\circ$  and at  $V_w = 0.125$  m/sec. this point was delayed further to occur at about  $\theta = 90^\circ$ .

The displacement of the smoke filament downstream of the point of minimum gap towards the cylinder surface due to suction effect was also noticeable. Increasing the suction velocity brought the downstream side of the suction filament closer to the surface compared to that without suction. This trend continued and at the highest suction velocity used ( $V_w = 0.125$  m/sec.) the smoke filament trace showed a similarity in the distribution upstream and downstream of the point of minimum gap (at about  $\theta = 90^\circ$ ).

It/...

It is interesting to notice that similar characteristics for the above mentioned were observed over the whole range of Reynolds number from 13,600 to 108,000. This was expected due to the characteristics of the wind tunnel of being commercially designed with low turbulence intensities. Accordingly all the Reynolds numbers used were in the subcritical range.

#### 10.4 Concluding remarks

Obviously any conclusions based on a qualitative study must be also qualitative in nature. Although it is premature to draw conclusions, the following points could be made:

a. The buoyant bubble technique could be useful in flow visualisation even in a complex geometry such as tube bank arrangement without suction. Applying suction into the model's surface would influence the porosity of the surface.

b. With high Reynolds numbers, the smoke filament is useful only for short distances along the model and accordingly the test model was limited to a single cylinder in a cross flow of air.

c. It is difficult to demonstrate the effect of suction on the flow separation point due to its unstable nature which affects the smoke diffusion in that region.

d./...



d. A displaced smoke filament introduced upstream of the model was useful in demonstrating the effect of distributed suction on the flow field around the cylinder.

e. The influence of suction was traced by observing the movement of the point of minimum gap between the smoke filament and the cylinder surface. Increasing suction rate caused this point to be delayed towards the rear of the cylinder.

f. The application of suction caused the filament to follow the cylinder contour for a longer distance compared to that without suction.

g. Small suction rates have no significant effect on the flow outside the boundary layer region.

## CHAPTER 11

### THEORETICAL APPROACH

#### 11.1. Introduction

It is the intention of this chapter to present the attempts made to develop a theoretical model for the problem in hand, i.e., circular cylinder in a cross flow with mass transfer at its surface.

Since the theoretical models of Thom (34) and Thwaites (243), as explained in Chapter 7, were applicable for the case of no mass transfer, two different approaches were followed in this chapter in an effort to solve this problem. These approaches were the potential flow and an application for the law of the wall on the cylinder surface.

It must be admitted, however, that neither of these models succeeded in providing reasonable results for the present study. Nevertheless, it is worthwhile to present the stages reached in these directions in order to assist any developments of the present work which might be carried out in future. It is also hoped that the following presentation will stimulate further work in these directions.

#### 11.2. The potential flow model

The application of the potential flow theory around circular cylinders in cross flow was reported by Schwabe (83) who replaced the vortex pair behind the cylinder by a source-sink flow superimposed on the potential flow around the cylinder/...



cylinder surface. He used this method for cross flows with Reynolds numbers up to 735.

A similar approach was also used by Roshko (259) in which a potential flow was considered to exist outside the free stream lines defining the wake behind the cylinder. In this case, a single parameter was chosen (base-pressure parameter) which would bring the calculated and the measured pressure distributions together.

The application of the potential flow on a cylinder surface was also reported by Rotteveel (260) to predict the pressure distribution along the cylinder axis when suction was applied to its surface.

From the flow visualisation, explained in Chapter 10, the intuitive feeling was that, under the influence of suction, the external flow outside the boundary layer and the circulation region might have been following the contour of an imaginary stream line body. This body enveloped the test cylinder together with its immediate wake. Following this line of thinking, once the approximate shape of the streamline body could be outlined from the flow visualisation, a potential flow could be applied to its surface and the outcome would be the pressure distribution around the test model.

This idea was based on the shape of the displaced boundary around the cylinder surface due to the effect of the Reynolds/...

Reynolds number, in the main stream, and suction velocity towards the cylinder surface. In the asymptotic case when the Reynolds number approaches zero, the displacement thickness, for a certain suction rate effect, should have no preference to a particular direction and the displaced boundary is a concentric circle around the porous cylinder. As the Reynolds number increases the circulation region begins to appear and the circular displaced boundary starts to deform. Such a deformed circle could be approximated by a streamline shaped body where potential flow existed outside its boundary. The shape of such a body would be outlined using the flow visualisation as shown in Chapter 10.

The shape of the stream line body was fed to the computer programme developed by Katsanis (261) after being modified to suit the present case.

An example of the pressure coefficient distribution around the body is shown in figure 11.1 with the transverse pitch in a transverse row in a tube bank as a parameter. It is clear that this sort of distribution was not similar to the measured one and the pressure recovery at the rear of the body was in contrast to that obtained by experiments.

Despite these rather disappointing results, there are two features in that figure which are worth mentioning. First, when the transverse pitch was 1.5, which is equal to that used in the staggered bank, section 7.3, the pressure coefficient reached a minimum value of - 10. This value is close/...



close to that obtained on the first row in the bank (figure 7.15) and it confirmed the conclusion reached previously that, the cylinders in the first row were acting in a similar way to single cylinders under similar flow restrictions or blockage ratios. The second feature is that, the conditions around single cylinders in the working section, as explained in Chapter 7, was not exactly acting as an isolated cylinder and, therefore, a blockage correction was justified.

### 11.3 Application for the law of the wall

Since flow transition was noticed in the boundary layer when suction was applied to the cylinder surface (Chapter 8) it was thought that it might be appropriate to deal with the boundary layer on the cylinder surface (downstream the neighbourhood of the FSP) using the law of the wall as follows:-

When the Navier-Stokes equations are written in terms of mean velocities and fluctuations from the mean and then averaged with respect to time, the resulting total shear stress will be :-

$$\tau = \mu \left( \frac{\partial u}{\partial y} \right) - \rho \overline{u'v'} \quad 11.1.$$

The first term on the RHS represents the effect of viscosity on the mean flow whereas the second term is the Reynolds stress. Further away from the wall of a smooth surface the second term predominates while the first term predominates closer to the surface.

According/...

According to Prandtl (262), the Reynolds stress can be calculated from:-

$$-\overline{\rho u'v'} = \rho \ell^2 \left( \frac{\partial u}{\partial y} \right)^2 \quad 11.2.$$

where  $\ell$  is the mixing length. Further it was assumed that  $\ell = Ky$  where  $K$  is called the universal mixing constant and equation 11.1 became :-

$$\tau = \mu \left( \frac{\partial u}{\partial y} \right) + \rho K^2 y^2 \left( \frac{\partial u}{\partial y} \right)^2 \quad 11.3.$$

In order to account for the effect of the nearness of the solid surface on the mixing length, Van Driest (263) proposed a damping factor which forces the mixing length to zero at the wall. Therefore, in the region near the surface, the mixing length will be :-

$$\ell = Ky \{1 - \exp(-y/A)\} \quad 11.4.$$

where  $A$  is a factor which is limited to an incompressible turbulent boundary layer with negligible pressure gradient and zero mass transfer.

In terms of dimensionless quantities equation 11.4 became :-

$$\ell^+ = Ky^+ \{1 - \exp(-y^+/A^+)\} \quad 11.5.$$

where  $y^+ = yV^*/\nu$  ,  $V^* = \sqrt{\tau/\rho}$

$A^+$  was calculated by Van Driest to fit the experimental measurements of the velocity distribution on flat plates and/...



and in this case  $A^+$  became an effective viscous sublayer thickness. Under these conditions  $A^+$  had the value of 26 when  $K = 0.4$ .

In order to include the roughness effect of the porous cylinder on the velocity profile, the method of Van Driest was adopted by adding another factor to the damping factor as follows :-

$$l^+ = Ky^+ \{1 - \exp(-y^+/A^+) + \exp(-60 y^+/A^+ KS^+)\} \quad 11.6.$$

where  $KS^+ = KS.V^*/\nu$

and the velocity profile, including the roughness effect became :-

$$u^+ = \int_0^{Y^+} 2 dy^+ / \{1 + (1 + 4K y^+ \{1 - \exp(-y^+/A^+) + \exp(-60 y^+/A^+ . KS^+)\}^2)^{0.5}\} \quad 11.7.$$

As mentioned by Spalding (264) this equation as developed by Van Driest was applicable over the whole boundary layer.

In the case of a boundary layer under the influence of pressure gradient, in the flow direction along the model surface, the non dimensional velocity profile may be expressed by the following expression (256) :-

$$u^+ = f(y^+, ) \quad 11.8.$$

$$\text{where } = \frac{V}{\rho V^*} \cdot \frac{dp}{dx} \quad 11.9.$$

Moreover/...

Moreover, for the case of mass transfer and pressure gradient, it is necessary to express the factor  $A^+$  as a function of a mass transfer parameter and a pressure gradient parameter. Cebeci (266) introduced these parameters into the damping constant  $A^+$  which became :-

$$A^+ = 26 \left\{ \frac{\alpha}{V_w^+} \{ \exp (11.8 V_w^+) - 1 \} + \exp (11.8 V_w^+) \right\}^{-\frac{1}{2}} \quad 11.10.$$

$$\text{where } V_w^+ = V_w / V^*$$

Substituting equation 11.10 into equation 11.7, the result will be a velocity profile on a rough surface with mass transfer and pressure gradient along the surface. This profile was introduced into the boundary layer governing equations as follows :-

The differential equations and boundary conditions describing a plane, incompressible boundary layer are as follows :-

$$\text{momentum :} \quad u \frac{\partial u}{\partial x} + v \frac{\partial u}{\partial y} = - \frac{1}{\rho} \frac{dp}{dx} + \frac{1}{\rho} \frac{\partial T}{\partial y} \quad 11.11.$$

$$\text{continuity:} \quad \frac{\partial u}{\partial x} + \frac{\partial v}{\partial y} = 0 \quad 11.12.$$

and the boundary conditions are :

$$u(x, 0) = 0 \quad 11.13.$$

$$u(x, \delta) = U_1(x) \quad 11.14.$$

$$v(x, 0) = V_w \quad 11.15.$$

where/...



where  $U_1$  is the velocity at the edge of the boundary layer whose thickness is  $\delta$  at position  $x$  and  $x, y$  are the orthogonal curvilinear coordinates measuring distance along and normal to the model surface respectively.

Integrating equation 11.12 and applying the boundary conditions yields :-

$$v = v_w - \int_0^y \frac{\partial}{\partial x} u \, dy \quad 11.16.$$

which in the dimensionless notations of the law of the wall will be :-

$$v = v^* v_w^+ - \frac{v}{v^*} \int_0^{y^+} \frac{\partial}{\partial x} u \, dy^+ \quad 11.17.$$

and  $\frac{\partial u}{\partial x} = \frac{\partial}{\partial x} (u^+ v^*) = v^* \frac{\partial u^+}{\partial x} + u^+ \frac{dv^*}{dx}$

$$= v^* \frac{\partial u^+}{\partial y^+} \frac{\partial y^+}{\partial x} + u^+ \frac{dv^*}{dx}$$

$$= \frac{\partial u^+}{\partial y^+} y^+ \frac{dv^*}{dx} + u^+ \frac{dv^*}{dx} = \frac{dv^*}{dx} \left\{ y^+ \frac{\partial u^+}{\partial y^+} + u^+ \right\} \quad 11.18.$$

$$\frac{\partial u}{\partial y} = \frac{\partial}{\partial y} (u^+ v^*) = v^* \frac{\partial u^+}{\partial y^+} \frac{\partial y^+}{\partial y}$$

$$= \frac{v^{*2}}{v} \frac{\partial u^+}{\partial y^+} \quad 11.19.$$

Substituting equation 11.18 into equation 11.17 yields :-

$$\begin{aligned}
 V &= V^* V_w^+ - \frac{v}{V^*} \int_0^{y^+} \left\{ V^* \frac{\partial u^+}{\partial x} + u^+ \frac{dV^*}{dx} \right\} dy^+ \\
 &= V^* V_w^+ - \frac{v}{V^*} \frac{dV^*}{dx} y^+ u^+ \quad 11.20.
 \end{aligned}$$

Substituting equations 11.18, 11.19, 11.20 into equation 11.11 yields :-

$$\begin{aligned}
 u^+ V^* \left\{ y^+ \frac{\partial u^+}{\partial y^+} + u^+ \right\} \frac{dV^*}{dx} + \left\{ V^* V_w^+ - \frac{v}{V^*} \frac{dV^*}{dx} y^+ u^+ \right\} \frac{V^{*2}}{v} \frac{\partial u^+}{\partial y^+} = \\
 - \frac{1}{\rho} \frac{dp}{dx} + \frac{V^*}{\rho v} \frac{d\tau}{dy^+}
 \end{aligned}$$

Therefore :-

$$\rho V^{*2} V_w^+ \frac{\partial u^+}{\partial y^+} + \rho v u^{+2} \frac{dV^*}{dx} = - \frac{v}{V^*} \frac{dp}{dx} + \frac{d\tau}{dy^+} \quad 11.21.$$

Integrating equation 11.21 with respect to  $y^+$  yields :-

$$\begin{aligned}
 \rho V^{*2} V_w^+ u^+ + \rho v \frac{dV^*}{dx} \int_0^{y^+} (u^+)^2 dy^+ &= \frac{v}{V^*} \frac{dp}{dx} y^+ + \{\tau\}_0^{y^+} \\
 &= - \frac{v}{V^*} \frac{dp}{dx} y^+ + \rho V^{*2} \frac{\partial u^+}{\partial y^+} - \rho V^{*2} \quad 11.22.
 \end{aligned}$$

Replacing the upper limit in the integration by  $\delta^+$ , i.e., at the edge of the boundary layer, yields :-

$$\rho V^{*2} V_w^+ U_1^+ + \rho v \frac{dV^*}{dx} \int_0^{\delta^+} (u^+)^2 dy^+ = - \frac{v}{V^*} \frac{dp}{dx} \delta^+ - \rho V^{*2} \quad 11.23.$$

A/...



A refinement of equation 11.22 could be obtained by following the procedure developed by Volkov (267) by affecting a second integration into it from the wall ( $y^+ = 0$ ) to  $\delta^+$  we obtained:-

$$\begin{aligned} & \rho V^{*2} V_w^+ \int_0^{\delta^+} u^+ dy^+ + \rho v \frac{dV^*}{dx} \left\{ \int_0^{\delta^+} dy^+ \int_0^{y^+} (u^+)^2 dy^+ \right\} \\ &= - \frac{v}{V^*} \frac{dp}{dx} \frac{\delta^{+2}}{2} + \rho V^{*2} U_1^+ - \rho V^{*2} \delta^+ \end{aligned}$$

dividing by  $\rho V^{*2}$  yields :-

$$\begin{aligned} & V_w^+ \int_0^{\delta^+} u^+ dy^+ + \frac{v}{V^{*2}} \frac{dV^*}{dx} \left\{ \int_0^{\delta^+} dy^+ \int_0^{y^+} (u^+)^2 dy^+ \right\} \\ &= - \alpha \frac{\delta^{+2}}{2} + U_1^+ - \delta^+ \end{aligned} \quad 11.24.$$

it is to be realised that the boundary conditions at the wall :-

$$y^+ = 0, \quad \tau = \mu \frac{\partial u}{\partial y}$$

are satisfied by equation 11.22.

Using the velocity profile defined by equations 11.7 and 11.10, equations 11.23 and 11.24 will be two equations in two unknowns, namely,  $\delta^+$ ,  $V^*$ . A computer programme was developed to solve these equations, a version of it is included in Appendix 1.

Unfortunately, as far as the shear stress distribution was concerned, the results were disappointing and the predicted values/...

values were much less than the measured ones. In fact, the predicted values were less than 20 per cent of the measured ones.

Therefore, it was decided, for the time being, that this procedure was to be postponed until further analysis could be done into this problem in some future work.

#### 11.4 Concluding remarks

This chapter presented two approaches used in an effort to develop a theoretical model for the case of a circular cylinder in a cross flow where suction is applied to its surface.

Potential flow and an application of the law of the wall were used but none was successful in providing a reasonable picture for the flow around the cylinder.

It was felt, that it is quite important to show and to demonstrate the steps taken towards the solution of this problem. Although they were not successful in the present case, they might be proved useful in assisting any further work towards the solution of such cases.



## CHAPTER 12

### SUMMARY AND CONCLUSIONS

#### 12.1 Summary

This section sets out to summarise the programme of investigation for the dissertation. The thesis begins with a general introduction for the problem of flow characteristics in tubular heat exchangers and in particular for steam condensers to show the areas where previous investigations had indicated that a knowledge is lacking. Indeed, they showed that what was needed most is more information about the detailed behaviour of a cross flow through tube bank configurations and its response to changes in different parameters.

The aim of the investigation was then outlined showing the necessary steps needed in order to obtain the required information. It must be pointed out that the present work was concerned mainly with problems associated with vapour flowing externally across vertical tube bundles. For that purpose, a test model with a simulation for a condensation process is proposed.

A further area for study arose from that situation. It was an instrumentation problem concerned with the measurement of small forces, such as shearing forces on the external surface of a circular cylinder in cross flow. A review of that topic was incorporated. The review shows different types of the available devices and their limitations were/...

were also discussed. Accordingly, it was decided to develop a device which could adequately provide the necessary information for the proposed project.

Care was taken in designing the developed instrument together with its control system and time was required in order to reach to the final form of the developed device. The repeatability and response of the system were demonstrated through measurements in comparison with the available data in that field. The accuracy and reliability of the system was also checked on the dynamics side of the flow such as measurement of the vortex shedding frequencies.

In accordance with a study of the literature, the scope of the investigation is decided and an experimental apparatus was built to fulfill the requirements of the investigation.

Tests were carried out in steps so that the individual parameters could be separated on test models. Flow conditions (over a range of variables) were studied on plain cylinders first, motion was then applied and thereafter heat transfer was included in the investigation. For all the tests, flow characteristics such as wall shear stress, normal pressure and heat transfer coefficient were measured simultaneously at the mid height of a rotated generator on the test cylinder surface around its longitudinal axis.

Results are presented, discussed and analysed and whenever appropriate, comparison is made with available data or approximate/...



approximate theories from the literature.

Before proceeding, however, it will be recalled that in Chapter 1 it was stated that "The aim of this investigation was, therefore, to determine the effect of individual parameters such as surface roughness, turbulent intensity, mass transfer, heat loads and Reynolds number on the simultaneously measured flow and heat characteristics such as wall shear stress, pressure drag and heat transfer rate on single cylinders and tube bank models for a vertical tube condenser in cross flow of vapour".

The effects referred to may be summarised as follows :-

- i) Do small changes in the surface roughness have an effect on the flow characteristics across a circular cylinder?
- ii) Do changes in turbulence level (with changes in surface roughness) influence the subcritical flow regime?
- iii) Does condensation or mass extraction, for a typical condenser loading, affect the pressure drag across the condenser or exchanger?
- iv) Does the additional complexity with the simultaneous heat and mass transfer affect the flow characteristics in the tube bank model?

Just how far these questions have been satisfactorily answered may be judged to some extent from the major conclusions listed in the following section. For a fuller picture, reference should be made to discussions made in previous chapters.

## 12.2 Conclusions

This section sets out to list the main conclusions of the work described earlier in this dissertation.

### 12.2.1. The development of the shear stress sensor

The use of the servo-force balance principle represents a valuable improvement on previous instruments because of the following.

- i) The drag piece is held in a fixed position by an integral control, guaranteeing a constant local flow field.
- ii) The use of a velocity, or derivative, feed back instead of oil damping, allows operation of the developed transducer in an arbitrary orientation.

The main improvement of the present instrument over previous ones are as follows :-

- i) The successful application of the servo-force balance, null-seeking device, allows the clearance gaps (downstream and upstream of the drag piece) to be reduced to limits set only by mechanical tolerances. For the present purpose gap widths of 80  $\mu\text{m}$  are chosen thus their effect on the boundary layer flow is reduced. The estimated effect of these gaps, however, was to produce results which are 3 to 8 per cent too high. Buoyancy correction (due to pressure difference between upstream and downstream of the drag piece) was estimated to be about 3 per cent of the measured values.

ii)/...



- ii) The optical voltage-to-displacement system has proved to be robust, reliable and a sensitivity of about 70 times greater than that of previous devices is reached. With this sensitivity, the width of the drag piece is reduced to 2 mm and the system was able to discriminate load increments of 1/10 milligram ( $10^{-6}$  N).
- iii) Newly developed frictionless pivots are used to avoid errors that might occur if jewel bearings are used.
- iv) By using the servo-force balance a previous knowledge of the shearing force is not required.
- v) Ability to measure the temporal mean values of the shearing force as well as flow dynamics such as vortices shedding frequency at the rear of the cylinder. When the same frequency was detected at the front of the cylinder, it indicates that the whole field around the cylinder is oscillating at the shedding frequency.
- vi) As far as the time factor is concerned, the device is superior to other ones in providing an accurate and quick estimation of the flow characteristics around the cylinder.
- vii) The transducer is mounted on a scintered bronze test cylinder with homogenous surface roughness (including the drag piece) to ensure minimum disturbances to the boundary layer flow.
- viii) Using the same test cylinder throughout the whole study, the effect of different parameters is detectable without replacement and recalibration of the device.

#### 12.2.2. Effect of different parameters on flow characteristics

Investigations on single cylinders showed the following:

- i) Even for small surface roughness ( $\frac{K_s}{D} = 53 \times 10^{-5}$ ) the shear stress distribution was raised to a higher value/...

value together with a shift for its peak position towards the rear of the cylinder.

- ii) Increasing the turbulence intensity from 1.2% to 6% leads to an increase in the shear stress. However, this is small compared to that due to surface roughness. It also causes a reduction in the pressure drag.
- iii) The percentage contribution of the shear stress to the total drag amounts only to about 2 per cent.
- iv) There is a lack of a fixed point for the flow separation on the cylinder surface, instead there might be a separation region.
- v) There is no rear stagnation point as such at  $\theta = 180^\circ$  from the forward stagnation point.

Measurements on tube bank showed that:

- i) The entrance effect could extend up to the third row and stable conditions are reached from the fourth row onwards.
- ii) Cylinders in the first row offered the highest pressure drag in the bank and it acted similar to cylinders under similar flow restrictions.
- iii) The second row in the bank provides the lowest drag in the bank.
- iv) The percentage contribution of the shear stress is about 2 to 4 per cent of the total drag in the bank.
- v) The pressure drop per row decreased as the number of rows increased.
- vi) Mounting an axial 'wire' at 180 degrees from the measurement generator caused a reduction of about 20 per cent of the pressure drag on a plain cylinder.



### 12.2.3. Effect of mass extraction on flow characteristics

The use of a fine grade porous material for the test cylinder ensured a reasonable level of suction uniformity around its circumference. Measurements of suction rates equivalent to a typical condenser loading showed the following:

- i) Suction causes considerable delay of the flow separation.
- ii) The shear stress increases rapidly with increasing suction rate. That increase will be reduced by placing an axial 'wire' 180 degrees from the measurement generator on the cylinder.
- iii) Although some changes in the normal pressure distribution were recorded (due to suction) the final pressure drag contribution to the total drag was practically unaltered.
- iv) Beyond certain flow conditions, suction might cause transition through the influence of surface irregularities on the reduced thickness of the boundary layer.

### 12.2.4. Effect of the simultaneous heat and mass transfer

Compared with the cold (atmospheric) adiabatic flow conditions, single cylinder showed that:

- i) Increasing the temperature level in adiabatic conditions causes a slight reduction in the shear stress recorded at the front of the cylinder while an increase was recorded at its rear side.
- ii) Heat transfer across the 'sucked' boundary layer (towards the surface) causes an increase in the wall shear stress over the cylinder surface.
- iii)/...

- iii) Within the present range of variables, the influence of heat transfer on the flow separation was very difficult to estimate probably due to the unstable nature of the flow and the lack of a fixed point for the separation position.
- iv) The heat transfer coefficient is not a maximum at the FSP and it has a tendency to reach a higher value nearby the location of the peak in the shear stress distribution.
- v) The heat transfer rate is minimum downstream of the separation point and then increases to reach the rear stagnation point with a very similar value to the corresponding one at FSP.
- vi) Within the tested range of variables, mass extraction variations showed little influence on the recorded values of heat transfer rate.

Investigation on tube banks showed the following points in addition to some of the general points noticed earlier for single cylinder (e.g., items iii and vi previously mentioned):

- i) The effect of raising the temperature level in an adiabatic flow on the shear stress is to reduce its value on first and second row to produce no significant change on the third and to cause an increase of its value on fourth and fifth rows.
- ii) Shear stress is higher for the non-isothermal conditions than that for the cold adiabatic conditions.
- iii) For all the rows in the bank the heat transfer coefficient is at a relative minimum at FSP which increases with angle  $\theta$  to reach a maximum near the region of maximum shear stress.
- iv) The point of minimum heat transfer is downstream of the separation point by up to 30 degrees.

v)/...



- v) The heat transfer at the rear stagnation point is less than the corresponding value at FSP for rows from the first to third while it is very similar to that at the FSP for the fourth and fifth rows.
- vi) The average heat transfer coefficient increases rapidly from first to third row, thereafter it drops suddenly to the fourth row and then reduces slightly as it reaches the fifth row in the bank.
- vii) The measurements of the heat transfer along the depth of the tube bank showed that the entrance effect could extend up to the third row in the bank and 'stable' conditions are reached from fourth row onwards.
- viii) All the rows in the bank showed a heat transfer coefficient which is higher than that for a single cylinder by about 20 per cent.

It should be emphasised that the longitudinal axis of the "drag piece" was preceded and succeeded by about 3 mm (along the cylinder circumference) where there is no heat or mass transfer. Consequently, the recorded values of the shear stress differs towards smaller values than that on a porous surface. Nevertheless, for reasons mentioned in the thesis, it is believed that such differences will be quite small and the measurements could be accepted with some confidence.

Although the studies reported here represent an improvement in the understanding of the flow and heat characteristics in tube bank configuration, considerable further work needs to be done before the whole picture in a steam condenser is completely understood. It could be argued that the present method of simulation does not properly represent/...

represent the actual condensation process in the condenser, nevertheless, the data obtained in this investigation has shed some light on the flow characteristics in a tube bank condenser.

### 12.3. Suggestions for further work

Understanding of the shell-side fluid flow characteristics under practical conditions is still, however, far from complete and there are other aspects of the problem in which improved understanding and information would be valuable. For several reasons, the range of the variables investigated in the present work was limited. However, with the confidence in the study that has now been gained its extension to deal with different test models should present no basic difficulty.

The areas in which further studies could be useful include the following:

- i) Flow and heat transfer characteristics in tube banks of geometry other than those studied here, including triangular and other staggered and in-line arrangements.
- ii) Since the flow direction relative to the tubes varies with position within a real exchanger, the effect of such a factor could be studied by using other types of flows other than the cross flow type. This could be done, for example, by rotating the banks as a whole about their axis to create different components for the flow through the tube bank.
- iii) /...



- iii) More detailed studies of the flow dynamics inside the bank with different pitch to diameter ratios are also needed.
- iv) Effort should be made to investigate tube banks with different length to diameter ratio.
- v) More emphasis on the thermal side of the exchanger to cover a wider range of variables could be valuable.
- vi) Non-adiabatic tests with a predetermined surface temperature (for example by using cooling water at different temperature levels) could be useful.
- vii) Increasing the range of variables (used in the present work) on both ends to reach a wider scope for the processes involved in the exchanger.
- viii) A parallel research programme using the present techniques for the case of horizontal heat exchangers would be very valuable.

Finally, in examining the present work, a feeling that there are certain gaps in the study and that there are possibly few data in certain areas where a particular variable is under study is present. However, it must be appreciated that the time available for the investigation is considered to be a limitation in relation to the number of variables included in the study.

It is believed, however, that the present results obtained under careful experimental conditions for the parameters involved on the same rig with the developed instrumentation would help in clarifying some of the discrepancies found in the literature.

## REFERENCES

1. LUDWIEG, H. and Tillmann, W.  
Investigations of the wall shearing stress in turbulent boundary layers.  
Nat. Adv. Comm. Aero., TM 1285, 1950.
2. DHAWAN, S.  
Direct measurements of skin friction.  
Nat. Adv. Comm. Aero. Tech. No. 2567, 1952.
3. STANTON, T.E.  
The mechanical viscosity of fluids.  
Proc. Royal Society, Series A, V.85, pp.366-376 (1911)
4. PATEL, V.C.  
Calibration of the Preston tube and limitations on its use in pressure gradients.  
J. Fluid Mech., V.23, part 4, pp. 185-208, 1965.
5. SMITH, D. and Walker, J.H.  
Skin friction measurements in incompressible flow.  
Nat. Aero. Space Adm., Tech. R. R-26, 1959.
6. O'DONNELL, R.M.  
Experimental investigation at a Mach number of 2.41 of average skin friction coefficients and velocity profiles for laminar and turbulent boundary layers and an assessment of probe effects.  
Nat. Adv. Comm. Aero., Tech. Note 3122, 1954.
7. GADD, G.E. et al.  
Heat transfer and skin friction measurements at a Mach number of 2.44 for a turbulent boundary layer on a flat surface and in regions of separated flow.  
Aero. Res. Coun. R. & M. 3148, 1960.
8. PAPPAS, C.C.  
Measurements of heat transfer in the turbulent boundary layer on a flat plate in supersonic flow and comparison with skin friction results.  
Nat. Adv. Comm. Aero. Tech. N. 3222, 1954.
9. FAGE, A. and Falkner, V.M.  
An experimental determination of the intensity of friction on the surface of an aerofoil.  
Aero. Res. Comm. R & M. 1315, 1930.
10. HOPKINS, E.J. et al.  
Direct measurements of turbulent skin friction on a non-adiabatic flat plate at Mach number 6.5 and comparisons with eight theories.  
Nat. Aero. Space Adm. Tech. N. D-5675, 1970.
11. DUTTON, R.A.  
The accuracy of measurement of turbulent skin friction by means of surface Pitot-tubes and the distribution of skin friction on a flat plate.  
Aero. Res. Coun. R. & M. 3058, 1957.

12./...



12. STANTON, T.E. et al.  
On the conditions at the boundary of a fluid in turbulent motion.  
Proc. Roy. Soc., Series A, V.97, pp.413-434 (1920)
13. MATTING, F.W. et al.  
Turbulent skin friction at high Mach numbers and Reynolds numbers in air and Helium.  
Nat. Aero. Space Adm. Tech. R. R-82, 1961.
14. MONAGHAN, R.J.  
The measurements of heat transfer and skin friction at supersonic speeds.  
Aero. Res. Coun., C.P. No. 64, 1952.
15. SCHUBAUER, G. and Klebanoff, P.  
Investigation of separation of the turbulent boundary layer.  
Nat. Adv. Comm. Aero. Tech. No. 2133, 1950.
16. LIEPMANN, H. and Skinner, G.  
Shearing-stress measurements by use of a heated element.  
Nat. Adv. Comm. Aero. Tech. No. 3268, 1954.
17. BRADSHAW, P. and Gregory, N.  
The determination of local turbulent skin friction from observations in the viscous sub-layer.  
Aero. Res. Coun. R. & M. 3202, 1961.
18. PRESTON, J.H.  
Note on the turbulent velocity distribution near a wall and on the turbulent skin friction for a flat plate.  
Aero. Res. Coun. 17443. F.M. 2198, 1955.
19. TAYLOR, G.I.  
Measurements with a half Pitot tube.  
Proc. Roy. Soc., Series A, v. 166, pp. 476-481 (1938)
20. HOOL, J.N.  
Measurement of skin friction using surface tubes.  
Aircraft Engineering, V.28, pp. 52-54, 1956.
21. SMITH, K.G. et al.  
The use of surface Pitot tubes as skin friction meters at supersonic speeds.  
Aero. Res. Coun., R. & M. 3351, 1964.
22. WINTER, K.G. and Smith, K.G.  
Measurements of skin friction on a cambered Delta wing at supersonic speeds.  
Aero. Res. Coun. R. & M. 3501, 1967.
23. FAGE, A. and Falkner, V.  
The flow around a circular cylinder.  
Aero. Res. Comm., R. & M. 1369, 1931.
- 24./...

24. BELLHOUSE, B. and Schultz, D.  
Determination of skin friction, separation and transition with a thin film-heated element.  
Aero. Res. Coun., R. & M. 3445, 1966.
25. BELLHOUSE, B. and Schultz, D.  
The measurement of skin friction in supersonic flow by means of heated thin film gauges.  
Aero. Res. Coun., R. & M. 3490, 1968.
26. WYATT, L. and East, L.  
Low speed measurements of skin friction on a slender wing.  
Aero. Res. Coun., R. & M. 3499, 1968.
27. WYATT, L. and East, L.  
Low speed measurements of skin friction on a large half-model slender wing.  
Aero. Res. Coun., C.P. No. 1007, 1968.
28. TURNER, K. and Walker, D.  
Measurements of pressure fluctuations and skin friction on the upper surface of a slender wing at Lift ( $M = 0.8$  to  $2$ )  
Aero. Res. Coun., C.P. No. 985, 1968.
29. STAFF OF AERO. DIV.  
On the measurements of local surface friction on a flat plate by means of Preston tubes.  
Aero. Res. Coun., R. & M. 3185, 1961.
30. EAST, L.F.  
Measurement of skin friction at low subsonic speeds by the razor-blade technique.  
Aero. Res. Coun., R. & M. 3525, 1968.
31. PRESTON, J.H.  
The determination of turbulent skin friction by means of Pitot-tubes.  
J. Roy. Aero. Soc., Vol. 58, pp. 109-121, 1954.
32. STEPHENS, A. and Haslam, J.  
Flight experiments on boundary layer transition in relation to profile drag.  
Aero. Res. Coun., R. & M. 1800, 1938.
33. FAGE, A.  
Note on Report A.R.C. 17,025.  
Aero. Res. Coun., 17,320 - F.M. 2175, 1955.
34. THOM, A.  
The boundary layer of the front portion of a cylinder.  
Aero. Res. Comm., R. & M. 1176, 1928.
35. MONAGHAN, R.J.  
The use of Pitot tubes in the measurement of laminar boundary layers in supersonic flow.  
Aero. Res. Coun., R. & M. 3056, 1957.
- 36./...



36. YOUNG, A. and Maas, J.  
The behaviour of a Pitot tube in a transverse total pressure gradient.  
Aero. Res. Comm., R. & M. 1770, 1936.
37. LUDWIEG, H.  
Instrument for measuring the wall shearing stress of turbulent boundary layers.  
Nat. Adv. Comm. Aero., Tech. M. 1284, 1950.
38. FAGE, A. and Falkner, V.  
Relation between heat transfer and surface friction for laminar flow.  
Aero. Res. Comm., R. & M. 1408, 1931.
39. BELLHOUSE, B. and Schultz, O.  
The measurement of fluctuating skin friction in air with heated thin film gauges.  
J. Fluid Mech., Vol. 32, Part 4, pp. 675-680, 1968.
40. FAGE, A.  
The air flow around a circular cylinder in the region where the boundary layer separates from the surface.  
Aero. Res. Comm., R. & M. 1179, 1929.
41. FAGE, A.  
The skin friction on a circular cylinder.  
Aero. Res. Comm., R. & M. 1231, 1929.
42. GREEN, J.J.  
Viscous layer associated with a circular cylinder.  
Aero. Res. Comm., R. & M. 1313, 1930.
43. GIEDT, W.H.  
Effect of turbulence level of incident air stream on local heat transfer and skin friction on a cylinder.  
J. Aero. Sci., V. 18, pp. 725-730, 1951.
44. GIEDT, W.H.  
Investigation of variation of point unit heat transfer coefficient around a cylinder normal to an air stream.  
Trans. A.S.M.E., pp. 375-381, May, 1949.
45. ACHENBACH, E.  
Total and local heat transfer from a smooth circular cylinder in cross flow at high Reynolds number.  
Int. J. Heat Mass Transfer, V.18, pp. 1387-1396, 1975.
46. KONSTANTINOV, N. and Dragnysh, G.  
The measurement of friction stress on a surface.  
Department of Scientific and Industrial Research U.K., R.T.S. 1499 (1955).
47. ZIUGZDA, J. and Ruseckas, B.  
Temperature effect on circular cylinder (in Latvian).  
Mokslas ir Teknika, 61 (3), 1971.
- 48./...

48. KEMPF, G.  
Neue Ergebnisse der Widerstands for schung.  
Werft. Reederei, Hafen, Bd. X, Heft 11, pp. 234-239,  
1929.
49. SCHULTZ-Grunow, F.  
New frictional resistance law for smooth plates.  
Nat. Adv. Comm. Aero., Tech. M. 986, 1941.
50. SCHOENHERR, K.  
Resistance of flat surfaces moving through a fluid.  
The society of Naval Architects and Marine Engineering,  
Transactions, V. 40, pp. 279-313, 1932.
51. GEIGER, G. and Collucio, S.  
The heat transfer and drag behaviour of a heated  
circular cylinder with integral heat conducting  
downstream splitter plate in cross flow.  
J. Heat Transfer, pp. 95-99, Feb. 1974.
52. SOMMER, S. and Short, B.  
Free flight measurements of skin friction of  
turbulent boundary layers with high rates of heat  
transfer at high supersonic speeds.  
J. Aero. Sci., pp. 536 - 542, June, 1956.
53. WHITE, J. and Franklin, R.  
Measurements of skin friction in an annulus by  
the floating element technique.  
Aero. Res. Coun., C.P. No. 814, 1965.
54. ATTINELLO, J.  
A proposed experimental method for measuring skin  
friction drag at supersonic speeds.  
Research Division, R. 1159, Navy Dept. Bureau of Aero.,  
Washington, D.C., Jan. 1950.
55. GARRINGER, D. and Saltzman, E.  
Flight demonstration of a skin friction gauge to a  
local Mach number of 4.9.  
Nat. Aero Space Adm., Tech. No. D-3830, 1967.
56. DEPOOTER, K. et al.  
Direct measurement of wall shear stress with mass  
transfer in a low speed boundary layer.  
J. Fluids Engineering, pp. 580-584, Sept., 1977.
57. MORSY, M.  
Skin friction and form pressure loss in tube bank  
condensers.  
Ph.D. Thesis, Univ. of Glasgow, Scotland, U.K., 1973.
58. NEALE, M.  
Tribology Handbook.  
Butterworth, London, 1973.
59. LAUFER, J.  
Investigation of turbulent flow in a two-dimensional  
channel.  
Nat. Adv. Comm. Aero., Report 1053, 1951.
- 60./...



60. FAGE, A. and Townend, H.  
An examination of turbulent flow with an Ultramicroscope.  
Proc. Roy. Soc., Series A, V. 135, pp.656-677, 1932.
61. ALLEN, J.  
Use of Baronti-Libby transformation and Preston tube calibrations to determine skin friction from turbulent velocity profiles.  
Nat. Aero. Space Adm., Tech. N. D-4853, 1968.
62. KEENER, E. and Hopkins, E.  
Use of Preston tubes for measuring hypersonic turbulent skin friction.  
Nat. Aero. Space Adm. Tech. N., D-5544, 1969.
63. ALLEN, J.  
Experimental study of error sources in skin friction balance measurements.  
J. Fluids Engineering, pp. 197-204, March, 1977.
64. PAROS, J.  
Application of the force-balance principle to pressure and skin friction sensors.  
16th Annual Tech. Meeting - Proc. Inst. Environmental Science. The Environmental Challenge of the 70's.  
April, 1970.
65. BENDIX  
Spring-supported flexural pivot forms a frictionless bearing.  
Design Engineering, pp. 11-14.  
October, 1975.
66. HAUENSTEIN, A.  
Displacement-to-voltage converter and follower control circuit using the differential photodiode BP X 48.  
Siemens Electronic Components Bulletin, V. 6, No. 3, pp. 76-77, 1971.
67. HURLEY, D. and Thwaites, B.  
An experimental investigation of the boundary layer on a porous circular cylinder.  
Aero. Res. Coun., R. & M. 2829, 1955.
68. PANKHURST, R. and Thwaites, B.  
Experiments on the flow past a porous circular cylinder fitted with a Thwaites flap.  
Aero. Res. Coun., R. & M. 2787, 1953.
69. QUAILE, J. and Levy, E.  
Laminar flow in a porous tube with suction.  
J. Heat Transfer, pp. 66-71, Feb., 1975.
70. WALLIS, G.  
Pressure gradients for air flowing along porous tubes with uniform extraction at the walls.  
Proc. Inst. Mech. Eng., V. 180, Part 1, No. 1, 1965-66.

71./...

71. AGGARWAL, J. et al.  
Experimental friction factors for turbulent flow with suction in a porous tube.  
Int. J. Heat Mass Transfer, V.15, pp. 1585-1602, 1972.
72. DRUMMOND, G.  
Pressure recovery in condensation processes.  
Ph.D. Thesis, Heriot-Watt Univ., Scotland, U.K., 1966.
73. KING, L.V.  
On the convection of heat from small cylinders in a stream of fluid; determination of the convective constants of small Platinum wire with application to hot wire anemometry.  
Phil. Trans. Roy. Soc. (London), V.214A, pp. 373-432, 1914.
74. FAGE, A.  
On the two dimensional flow past a body of symmetrical cross section, mounted in a channel of finite breadth.  
Aero. Res. Comm., R. & M. 1223, 1929.
75. LOCK, C.  
The interference of a wind tunnel on a symmetrical body.  
Aero. Res. Comm., R. & M. 1275, 1929.
76. GLAUERT, H.  
Wind tunnel interference on wings, bodies and air screws.  
Aero. Res. Comm., R. & M. 1275, 1929.
77. GOLDSTEIN, S.  
Two-dimensional wind tunnel interference.  
Part II, Aero. Res. Comm., R. & M. 1902, 1942.
78. ALLEN, H. and Vincenti, W.  
Wall interference in a two-dimensional flow wind tunnel, with consideration for the effect of compressibility.  
Nat. Adv. Comm. Aero. Tech. R. 782, 1944.
79. ROSHKO, A.  
Experiments on the flow past a circular cylinder at very high Reynolds number.  
J. Fluid Mech., V. 10, pp. 345-356, 1961.
80. ACHENBACH, E.  
Influence of surface roughness on the cross flow around a circular cylinder.  
J. Fluid Mech., V. 46, part 2, pp. 321-335, 1971.
81. POPE, A..  
"Wind tunnel testing".  
Wiley, Second Edition, N.Y. 1954.
- 82./...



82. PERKINS, H. and Leppert, G.  
Local heat transfer coefficients on a uniformly heated cylinder.  
Int. J. Heat Mass Transfer, V. 7., pp. 143-158, 1964.
83. SCHWABE, M.  
Pressure distribution in non uniform two dimensional flow.  
Nat. Adv. Comm. Aero. Tech. M. 1039, 1943.
84. SHAIR, F. et al.  
The effect of confining walls on the stability of the steady wake behind a circular cylinder.  
J. Fluid Mech., V. 17, 4, pp. 546- 550, 1963.
85. BOULOS, M. and Pei, D.  
Dynamics of heat transfer from cylinders in a turbulent air stream.  
Int. J. Heat Mass Transfer, V.17, pp. 767-783, 1974.
86. ROSHKO, A.  
On the development of turbulent wakes from vortex streets.  
Nat. Adv. Comm. Aero. Tech. N. 2913, 1954.
87. SAVKAR, S.D.  
Buffeting of single cylinders.  
Session 2. Flow induced vibration in heat exchangers.  
Keswick, U.K., May, 1978.
88. SCHILLER, L. and Linke, W.  
Druck und Reibungs wider stand des Zylinders bei Reynoldsschen zahlen 5000 bis 40000.  
Zeitschrift fur Flugtechnik und Motorluftschiffahrt, Nr. 7, pp. 193-198, 1933.
89. HUSSAIN, A. and Ramjee, V.  
Periodic wake behind a circular cylinder at low Reynolds numbers.  
Aero. Quart., pp. 123-142, May, 1976.
90. CHEN, Y.N.  
Flow induced vibration and noise in tube bank heat exchanger due to von Karman streets.  
A.S.M.E. Paper No. 67, VIBR-48, 1967,  
J. Engng. Industry, Series B, V. 90, No. 1, pp. 134-146, Feb., 1968.
91. OWEN, P.  
Buffeting excitation of boiler tube vibration.  
J. Mech. Engng., Sci., V.7, No. 4, pp.431-439, Dec., 1965.
92. BAULY, J.  
Vortex shedding in tube banks.  
Symposium on internal flows.  
Univ. Salford, paper 25, April, 1971.
- 93./...

93. BORGES, A.  
Vortex shedding frequencies of the flow through two-row banks of tubes.  
J. Mech. Engng., Sci., V.11, No. 5, pp.498-502, 1969.
94. ISHIGAI, S. and Nishikawa, E.  
Experimental study of structure of gas flow in tube banks with tube axis normal to flow.  
Part II: On the structure of gas flow in single-column, single row and double row tube banks.  
Bulletin of the JSME, V. 18, No. 119, pp. 528-535, May, 1975.
95. STEVENSON, D. and Tang, T.  
Flow induced noise and vortex shedding in tube bank systems.  
5th Australasian Conf. Hydr. Fluid Mech., New Zealand, 1974.
96. BRUUN, H. and Davies, P.  
An experimental investigation of the unsteady pressure forces on a circular cylinder in a turbulent cross flow.  
J. Sound and Vibration, V.40 (4), pp. 535-559, 1975.
97. TAYLOR, G.  
Statistical theory of turbulence, V - Effect of turbulence on boundary layer.  
Proc. Roy. Soc. London, Series A, V. 156, pp. 307-317, 1936.
98. PETRIE, A. and Simpson, H.  
An experimental study of the sensitivity to freestream turbulence of heat transfer in wakes of cylinders in cross flow.  
Int. J. Heat Mass Transfer, V. 15, pp. 1497-1513, 1972.
99. ZIJNEN, B.  
Heat transfer from horizontal cylinders to a turbulent air flow.  
Appl. Sci. Res. Section A, V.7, pp.205-223, 1958.
100. ACHENBACH, E.  
Evaluation of measurements of the local and total heat transfer from smooth and rough surface cylinders in cross flow. Heat and Mass Transfer. 5th All-Union Conference, pp. 1-4, Minsk, 1976.
101. GROEHN, H. and Scholz, F.  
Heat transfer and pressure drop of in-line banks of tubes with artificial roughness.  
Heat and Mass Transfer. Source Book. 5th All-Union Conference, pp. 21-24, Minsk, 1976.
102. FAGE, A. and Warsop, J.  
The effects of turbulence and surface roughness on the drag of a circular cylinder.  
Aero. Res. Comm., R. & M. 1283, 1929.
- 103./...



103. GOLDSTEIN, S.  
Modern developments in fluid dynamics.  
Oxford. Clarendon Press, 1938.
104. PEARCE, H.  
Noise and vibration in heat exchangers.  
Ph.D. Thesis, Oxford, England, 1973.
105. ZUKAUSKAS, A.  
Heat transfer of banks of tubes in cross flow  
at high Reynolds numbers.  
Int. Centre for Heat and Mass Transfer, 1972.  
Int. Seminar, Trogir, Yugoslavia, Aug. 30 - Sept. 6,  
Session C, 1972.
106. CHILTON, T. and Genereaux, R.  
Pressure drop across tube banks.  
Amer. Inst. Chem. Engrs., Transactions, V.29,  
pp. 161-173, 1933.
107. PIERSON, O.  
Experimental investigation of the influence of  
tube arrangement on convection heat transfer  
and flow resistance in cross flow of gases over  
tube banks.  
Trans. A.S.M.E., V. 59, pp.563-572, 1937.
108. HUGE, E.  
Experimental investigation of effects of equipment  
size on convection heat transfer and flow  
resistance in cross flow of gases over tube banks.  
Trans. A.S.M.E., V. 59, pp. 573-581, 1937.
109. GRIMISON, E.  
Correlation and utilisation of new data on flow  
resistance and heat transfer for cross flow of  
gases over tube banks.  
Trans. A.S.M.E., V. 59, pp. 583-594, 1937.
110. JAKOB, M.  
Discussion on heat transfer and flow resistance in  
cross flow of gases over tube banks.  
Trans. A.S.M.E., V. 60, pp.384-386, May, 1938.
111. GUNTER, A. and Shaw, W.  
A general correlation of friction factors for  
various types of surfaces in cross flow.  
Trans. A.S.M.E., pp. 643-660, Nov., 1945.
112. DWYER, O. et al.  
Cross flow of water through a tube bank at Reynolds  
numbers up to a million.  
Industrial and Engineering Chem., V.48 (10), pp.  
1836-1846, Oct., 1956.
113. BOUCHER, D. and Lapple, C.  
Pressure drop across tube banks.  
Chem. Engng. Progress., V. 4 (2), pp. 117-134, 1948.
- 114./...

114. BERGELIN, O. et al.  
Heat transfer and fluid friction during viscous flow across banks of tubes - III, A study of tube spacing and tube size.  
Trans. A.S.M.E., pp. 881-888, Aug., 1950.
115. BERGELIN, O. et al.  
Heat transfer and fluid friction during flow across banks of tubes - IV, A study of the transition zone between viscous and turbulent flow.  
Trans. A.S.M.E., pp. 953-960, Aug., 1952.
116. McADAMS, W.  
Heat transmission. 3rd edition. N.Y.  
McGraw, Hill, 1954.
117. STASJULJAWITSCHJUS, I. et al.  
Heat transfer and fluid dynamics of staggered tube banks in cross flow at  $Re > 10^5$ .  
J. Engineering Physics, Vol. 7 (11), pp. 10-15, 1964.
118. KAYS, W. and London, A.  
Compact heat exchangers.  
McGraw-Hill, 2nd edition, 1964.
119. SIEDER, E. and Tate, G.  
Heat transfer and pressure drop of liquids in tubes.  
Industrial and Engineering Chem., V. 28 (12), pp. 1429-1435, Dec., 1936.
120. OMOHUNDRO, G. et al.  
Heat transfer and fluid friction during viscous flow across banks of tubes.  
Trans. A.S.M.E., pp. 27-34, Jan., 1949.
121. BERGELIN, O. et al.  
A study of three tube arrangements in unbaffled tubular heat exchangers.  
Trans. A.S.M.E., pp. 369-374, May, 1949.
122. GUY, H. and Winstanley, E.  
Some factors in the design of surface condensing plant.  
Proc. Inst. Mech. Eng., V. 126, pp. 227-273, Feb., 1934.
123. DIEHL, J.  
Calculate condenser pressure drop.  
Petroleum Refiner, V. 36, pp. 147-153, 1957.
124. DIEHL, J. and UNRUH, C.  
Two-phase pressure drop for horizontal cross flow through tube banks.  
A.S.M.E., Paper No. 58-HT-20, Sept., 1958.
125. CHISHOLM, D. and McFarlane, M.  
The prediction of condenser performance using a digital computer.  
NEL Report No. 161, 1964.
- 126./...



126. FUKS, S.  
The resistance to flow in tube banks during steam condensation (in Russian).  
Teploenergetika, V.1 (4), pp. 26-28, 1954.
127. FUJII, T. et al.  
Heat transfer and flow resistance in condensation of low pressure steam flowing through tube banks.  
Int. J. Heat Mass Transfer, V.15, pp. 247-260, 1972.
128. MORSEY, M.  
Private Communications, 1978.
129. REYNOLDS, O.  
On the extent and action of heating surfaces of steam boilers.  
Proc. Lit. Phil. Soc., Manchester, V. 14, pp. 7-12, 1874-5.
130. NUSSELT, W.  
Die Verbrennung die Vergasung der Kohle auf dem Rost.  
Z. Ver. Dtsch. Ing., 60, 102-107, 1916.
131. SILVER, R.  
Application of the Reynolds analogy to combustion of solid fuels.  
Nature, V. 165, pp. 725-728, May, 1950.
132. SILVER, R.  
An approach to a general theory of surface condensers.  
Inst. Mech. Engrs. Proc., V. 178, pp. 339-376, 1963-4.
133. SILVER, R.  
Some personal views and experiences in heat transfer design.  
Proc. 3rd Int. Heat Transfer Conference.  
A. Inst. Chem. Engrs., N.Y., 1966.
134. SPALDING, D.  
Convective mass transfer.  
Edward Arnold Ltd. (Pub.).., 1963.
135. SILVER, R. and Wallis, G.  
A simple theory for longitudinal pressure drop in the presence of lateral condensation.  
Proc. Instn. Mech. Engrs., V. 180, pp.36-40, 1965-6.
136. WALLIS, G.  
Use of the Reynolds flux concept for analysing one-dimensional two-phase flow, I. Derivation and verification of basic analytical techniques.  
Int. J. Heat Mass Transfer, V.11, pp.445-458, 1968.
- 137./...

137. WALLIS, G.  
Use of the Reynolds flux concept for analysing one-dimensional two-phase flow. II. Applications to two-phase flow.  
Int. J. Heat Mass Transfer, V.11, pp. 459-472, 1968.
138. SHERWOOD, T. et al.  
Mass Transfer.  
Chemical Engineering Series.  
McGraw-Hill, 1975.
139. SILVER, R.  
Author reply to the discussion of reference 132.  
Proc. Instn. Mech. Engrs., V.178, 1963-64.
140. DRUMMOND, G.  
Steamside pressure gradients in surface condensers.  
Proc. Instn. Mech. Engrs., V. 186, 10-72, 1972.
141. SIMPSON, H.  
Discussion of reference 132.  
Proc. Instn. Mech. Engrs., V.178, 1963-64.
142. BLASIUS, H.  
The boundary layers in fluids with little friction.  
Nat. Adv. Comm. Aero. Tech. M. 1256, 1950.
143. MILNE, H.  
Private communications, 1976.
144. EMERSON, W.  
Shell-side heat transfer and pressure drop with turbulent flow in segmentally baffled shell-and-tube heat exchangers. A. survey.  
NEL Report No. 45, 1962.
145. DREW, T. and Ryan, W.  
The mechanism of heat transmission: distribution of heat flow about the circumference of a pipe in a stream of fluid - I.  
Am. Inst. Chem. Engrs., Trans. V. 16, pp. 118-147, 1931.
146. JOSHI, N. and Sukhatme, S.  
An analysis of combined free and forced convection heat transfer from a horizontal circular cylinder to a transverse flow.  
J. Heat Transfer, pp. 441-448, Nov., 1971.
147. PETRIE, A.  
The prediction of heat transfer in the wake of cylinders in cross flow.  
Int. J. Heat Mass Transfer, V.18, pp.131-137, 1975.
148. MORRIS, J.  
The distribution of wind velocity in the space surrounding a circular rod in a uniform current of air.  
Engineering, pp. 178-181, Aug., 1913.
- 149./...



149. GROVE, A. et al.  
An experimental investigation of the steady separated flow past a circular cylinder.  
J. Fluid Mech. V. 19 (1), pp. 60-80, 1964.
150. ANDREAS ACRIVOS et al.  
The steady separated flow past a circular cylinder at large Reynolds numbers.  
J. Fluid Mech., V. 21 (4), pp. 737-760, 1965.
151. SOGIN, H.  
A summary of experiments on local heat transfer from the rear of bluff obstacles to a low speed air stream.  
J. Heat Transfer, pp. 200-202, May, 1964.
152. MATSUI, H.  
Heat transfer phenomena in wake flow of cylinder.  
4th Int. Heat Transfer Conference, Paris, paper FC5.9, 1970.
153. FAND, R. and Keswani, K.  
A continuous correlation equation for heat transfer from cylinders to air in cross flow for Reynolds numbers from  $10^{-2}$  to  $2 \times 10^5$ .  
Int. J. Heat Mass Transfer, V. 15, pp.559-562, 1972.
154. THOMSON, A. et al.  
Variation in heat transfer rates around tubes in cross flow.  
Proc. of the general discussion on heat transfer.  
Inst. Mech. Engrs., London and American Society of Mech. Engrs., N.Y., pp.177-180, 1951.
155. REIHER, H.  
Warmeubergang von Stromender Luft an Rohre und Rohrenbündel im Kreuzstrom. Mitt Forschungsarbeiten, 269, 1925.
156. KUETHE, A.  
Contribution to discussion of reference 157.  
J. Heat Transfer, pp. 326, Nov., 1971.
157. KESTIN, J. and Wood, R.  
The influence of turbulence on mass transfer from cylinders.  
J. Heat Transfer, pp.321-326, Nov., 1971.
158. COMINGS, E. et al.  
Air turbulence and transfer processes, flow normal to cylinders.  
Ind. and Engineering Chem., pp. 1076-1082, Jan., 1948.
159. MIZUSHINA, T. et al.  
Effect of free stream turbulence on mass transfer from a circular cylinder in cross flow.  
Int. J. Heat Mass Transfer, V.15, pp.769-780, 1972.
- 160./...

160. SMITH, M. and Kuethe, M.  
Effects of turbulence on laminar skin friction  
and heat transfer.  
The Physics of Fluids, V. 9(12), pp. 2337-2344,  
Dec., 1966.
161. CHILTON, T. and Colburn, A.  
Mass transfer (absorption) coefficients.  
Prediction from data on heat transfer and fluid  
friction.  
Industrial Engineering Chem., V.26, pp. 1183-1187,  
1934.
162. SCHMIDT, E. and Wenner, K.  
Heat transfer over the circumference of a heated  
cylinder in transverse flow.  
Nat. Adv. Comm. Aero. Tech. M. 1050, 1944.
163. GRASSMANN, P. and Trub, J.  
Elektrochemische Messung von Stoffubergangszahlen.  
Chemie-Ingenieur-Tech., V.33(8), pp.529-584,  
Aug., 1961.
164. FUJII, T. et al.  
Laminar filmwise condensation of flowing vapour  
on a horizontal cylinder.  
Int. J. Heat Mass Transfer, V.15, pp.235-246, 1972.
165. LOHRISCH, W.  
Bestimmung von Barmeubergangszahlen durch Diffusion-  
sversuche.  
Mitt. Forschungsarbeiten Ing-Wes. No. 322, 46, 1929.
166. SMALL, J.  
The average and local rates of heat transfer  
from the surface of a hot cylinder in a transverse  
stream of fluid.  
Phil. Magazine, Series 7, V. 49, pp. 251-260, 1935.
167. FISHENDEN, M. and Saunders, O.  
The calculation of heat transmission.  
H. M. Stationary Office, London, July, 1931.
168. HILPERT, R.  
Warmeabgabe von geheizten Drahten und Rohren  
im Luftstrom.  
Forschung, Bd. 4, Heft 5, pp.215-224, 1933.
169. DYBAN, E. and Epick, E.  
Some heat transfer features in the air flows of  
intensified turbulence.  
Heat Transfer 1970, V.2., FC 5.7., Paris-Versailles,  
1970.
170. FROSSLING, N.  
Verdunstung, Wärmeübergang und Geschwindigkeit-  
sverteilung bei zweidimensionaler und rotationsymmet-  
rischer laminarer Grenzschichtströmung.  
Lunds Universitets Arsskrift, N.F. Avd. 2, V.36(4)  
1940.
- 171./...



171. WINDING, C. and Cheney, A.  
Mass and heat transfer in tube banks.  
Industrial and Engineering Chem., V. 40 (6),  
pp. 1087-1093, June, 1948.
172. SMITH, R.  
Aerodynamic theory and test of strut forms -  
part II.  
Report Nat. Adv. Comm. Aero. pp. 725-759, 1929.
173. ROOTEM, Z.  
The heated surface probe for measuring shear  
stress at the wall in laminar boundary layers.  
The Can. J. Chem. Engng., V.45, pp. 175-178,  
June, 1967.
- 174.. BELLHOUSE, B. and Schultz, D.  
Determination of mean and dynamic skin friction,  
separation and transition in low speed flow  
with a thin-film heated element.  
J. Fluid Mech., V. 24, Part 2, pp. 379-400, 1966.
175. ACHENBACH, E.  
Heat transfer from smooth and rough surfaced  
circular cylinders in a cross flow.  
Int. Heat Transfer Conf., Tokyo, V.11, pp.229-233,  
1974.
176. ACHENBACH, E.  
Distribution of local pressure and skin friction  
around a circular cylinder in cross flow up to  
 $Re = 5 \times 10^6$ .  
J. Fluid Mech., V.34, part 4, pp. 625 - 639, 1968.
177. RHODES, B. and Bloxsom, D.  
Experimental effect of bluntness and gas rarefaction  
on drag coefficients and stagnation heat transfer  
on axisymmetric shapes in hypersonic flow.  
J. Aerospace Sci., V. 29, pp. 1429-1432, Dec., 1962.
178. AKILBAEV, Zh. et al.  
The influence of blockage on the local coefficient  
of heat transfer from uniformly heated single  
cylinder (in Russian).  
Preb. teplo. Prikltepflofiz, V.3, pp. 179-198, 1966.
179. MERK, H.  
Rapid calculations for boundary layer transfer using  
wedge solutions and asymptotic expansions.  
J. Fluid Mech., V. 5, pp. 460-480, 1959.
180. KRUSHILIN, G.  
The heat transfer of a circular cylinder in a  
transverse air flow in the range of  $Re = 6000 -$   
425,000.  
Tech. Physics of the USSR, V.5(4), pp.289-297,  
1938.
- 181./...

181. DAVIES, O. and Fisher, M.  
Heat transfer from electrically heated cylinders.  
Proc. Roy. Soc., Series A, V.280, pp.486-527,  
1964.
182. ROETZEL, W.  
Heat exchanger design with variable transfer  
coefficients for cross flow and mixed flow  
arrangements.  
Int. J. Heat Mass Transfer, V.17, pp.1037-1049,  
1974.
183. AUSTIN, A. et al.  
Convective heat transfer in flow normal to banks  
of tubes.  
I. & EC Process Design and Development, V.4(4),  
pp. 379-387, Oct., 1965.
184. HAMMEKE, K. et al.  
Warmeübergangs und Druckverlustmessungen an  
querangestromten Glattrohrbündeln, insbesondere  
bei hohen Reynolds-Zahlen.  
Int. J. Heat Mass Transfer, V. 10, pp. 427-446,  
1967.
185. CESS, R. and Grosh, R.  
Heat transmission to fluids with low Prandtl  
numbers for flow through tube banks.  
Trans. A.S.M.E., pp. 677-682, April, 1958.
186. SNYDER, N.  
Heat transfer in air from a single tube in a  
staggered tube bank.  
Symposium Series No. 5, Chem. Eng. Progress.,  
V. 49, Heat Transfer, pp. 11-20, 1953.
187. WELCH, C. and Fairchild, H.  
Individual row heat transfer in a cross flow  
in-line tube bank.  
J. Heat Transfer, pp. 143-148, May, 1964.
188. OSMENT, B. et al.  
Experimental condenser for heat transfer  
measurements.  
NEL Report No. 160, 1964.
189. OSMENT, B. et al.  
Heat transfer with filmwise condensation of  
steam in an experimental condenser.  
NEL Report No. 193, 1965.
190. ZUKAUSKAS, A. et al.  
Heat transfer in banks of tubes in cross flow  
of fluid.  
Mintis, Vilnius (in Russian), 1968.
191. ECKERT, E.  
Die Berechnung des Wärmeübergangs in der Laminaren  
Grenzschicht Umstromter Körper.  
Forschungsheft 416, VDI Verlag, Berlin, Germany,  
pp. 26, Oct., 1942.



192. ZDRAVKOVICH, M. et al.  
Flow structure within both stationary and vibrating tube banks with triangular pitch.  
B.N.E.S. - Vibration in Nuclear Plant,  
Session 2. Flow induced vibration in heat exchangers.  
Keswick, U.K., May, 1978.
193. SURRY, D.  
Some effect of intense turbulence on the aerodynamics of a circular cylinder at subcritical Reynolds number.  
J. Fluid Mech., V. 52, Part 3, pp. 543-563, 1972.
194. RICHARDSON, P.  
Heat and mass transfer in turbulent separated flows.  
Chem. Engng. Sci., V. 18, pp. 149-155, 1963.
195. SIMONICH, J. and Bradshaw, P.  
Effect of free stream turbulence on heat transfer through a turbulent boundary layer.  
J. Heat Transfer, V. 100, pp. 671-677, 1978.
196. KATZ, D.  
Contribution to discussion of Reference 186.  
Symposium Series No. 5, Chem. Eng. Progress., V. 49, Heat Transfer, pp. 18-20, 1953.
197. BAKER, E. and Mueller, A.  
Condensation of vapours on a horizontal tube, temperature variation around the perimeter of a tube on condensing pure and mixed vapours.  
Ind. Eng. Chem., V. 29 (9), pp. 1065-1067, 1937.
198. KESTIN, J. and Wood, R.  
The mechanism which causes free-stream turbulence to enhance stagnation line heat and mass transfer, 4th Int. Heat Transfer Conf., paper F.C. 2.7, Paris-Versailles, 1970.
199. KESTIN, J. et al.  
The influence of turbulence on the transfer of heat from plates with and without a pressure gradient.  
Int. J. Heat Mass Transfer, V.3, pp. 133-154, 1961.
200. LEE, C. and Richardson, P.  
Forced convection from a cylinder at moderate Reynolds numbers.  
Int. J. Heat Mass Transfer, V. 17, pp. 609-613, 1973.
201. LOWERY, G. and Vachon, R.  
The effect of turbulence on heat transfer from heated cylinders.  
Int. J. Heat Mass Transfer, V.18, pp. 1229-1242, 1975.

202./...

202. RAUSCHER, J. et al.  
Experimental study of film condensation from steam-air mixtures flowing downward over a horizontal tube.  
J. Heat Transfer, pp.83-88, Feb., 1974.
203. CHISHOLM, D. et al.  
A review of heat and mass transfer during condensation in surface heat exchangers.  
NEL Report No. 96, 1963.
204. MONRAD, C. and Badger, W.  
The condensation of vapours.  
Ind. Eng. Chem., V. 22(10), pp. 1103-1112, 1930.
205. KIRKBRIDE, C.  
Heat transfer by condensing vapour on vertical tubes.  
Trans. Amer. Inst. Chem. Eng., V.30, pp. 170-193, 1933-34.
206. CUNNINGHAM, J.  
Condensation on a vertical tube in the presence of air, paper number 12. Report of a meeting at NEL 17-18 Sept., 1974. Steam turbine condensers.  
NEL Report No. 619.
207. FURMAN, T. and Hampson, H.  
Experimental investigations into the effects of cross flow with condensation of steam and steam-gas mixtures on a vertical tube.  
Proc. Instn. Mech. Engrs., V. 173 (5), pp. 147-159, 1959.
208. EDE, A.J.  
Contribution to the discussion of Reference number 207.  
Proc. Instn. Mech. Engrs., V. 173 (5), pp. 159-160, 1959.
209. KIRSCHBAUM, E. et al.  
The thermal behaviour of flowing saturated and super heated steam during film and dropwise condensation also the heat transfer between the wall and cooling water flowing inside a vertical tube (in German).  
Chem. Ing. Tech., V. 23 (15/16), pp. 361-367, Aug., 1951.
210. HEBBARD, G. and Badger, W.  
Measurement of the wall temperatures in heat transfer experiments.  
Ind. Eng. Chem., Anal. Ed. 5(6), pp. 359-362, 1933.
211. HAMPSON, H. and Ozisik, N.  
An investigation into the condensation of steam.  
Proc. Instn. Mech. Eng., London (B), V.1B, pp. 282-294, 1953.

212/...



212. BRUNDRETT, E. and Baines, W.  
A temperature probe for the determination of heat transfer at a wall in turbulent flow.  
Int. J. Heat Mass Transfer, V. 10, pp. 973-981, 1967.
213. BUTTERWORTH, D. et al.  
A technique for measuring local heat transfer coefficients for condensation in a horizontal tube.  
The Instn. Chem. Engrs., Symposium Series, V. 1, No. 38, April, 1974.
214. CONNELL, M. et al.  
Condensation inside a horizontal tube.  
Instn. Chem., Engrs., Symp. Series, V.1, No. 38, 1974.
215. GREEN, L.  
Heat transfer in a power-producing porous solid.  
Proc. 3rd U.S. National Congress of Applied Mechanics, pp. 747-751, 1958.
216. WEICKHARDT, P. et al.  
Surface temperature measurement.  
Short communications.  
The Chem. Engng. Journal, pp. 212-214 (2), 1971.
217. GROOTENHUIS, P. et al.  
Heat transfer to air passing through heated porous metals. General discussion on heat transfer.  
Instn. Mech. Engrs., London, pp. 363-366, 1951.
218. LeFEVRE, E.  
Contribution to discussion of Reference number 207, Proc. Instn. Mech. Engrs., V. 173(5), pp. 162-163, 1959.
219. SILVER, R.S.  
Proceedings of the Int. Heat Transfer Conference, Part 2, pp. D.121, 1961-62.
220. GREGORY, N. and Walker, W.  
Experiments on the use of suction through perforated strips for maintaining laminar flow: Transition and drag measurements.  
Aero. Res. Coun., R. & M. No. 3083, 1958.
221. WAZZAN, A.  
The stability and transition of heated and cooled incompressible laminar boundary layers.  
Paper FC1.4, 4th Int. Heat Transfer Conference, Paris, 1970.
222. POOTS, G. and Raggett, G.  
Theoretical results for variable property, laminar boundary layers in water with adverse pressure gradients.  
Int. J. Heat Mass Transfer, V.11, pp. 1513-1534, 1968.
- 223./...

223. SMITH, M. et al.  
The effect of wall temperature on the growth and separation of the laminar boundary layer of a sphere.  
Int. J. Heat Mass Transfer, V.19, pp.33-40, 1976.
224. BACK, L. et al.  
Effect of wall cooling on the mean structure of a turbulent boundary layer in low-speed gas flow.  
Int. J. Heat Mass Transfer, V.13, pp. 1029-1047, 1970.
225. BOULOS, M. and Pei, D.  
Simultaneous heat and mass transfer from a single sphere to a turbulent air stream.  
The Can. J. Chem. Engrg., V.47, pp. 30-36, Feb., 1969.
226. LUIKOV, A.  
Application of methods of thermodynamics of irreversible processes to investigation of heat transfer in a boundary layer.  
Int. J. Heat Mass Transfer, V.3, pp.167-174, 1961.
227. KOTAKE, S.  
Heat transfer and skin friction of a phase-changing interface of gas-liquid laminar flows.  
Int. J. Heat Mass Transfer, V.16, pp. 2165-2176, 1973.
228. LEBEDEV, P.  
Heat and mass transfer during the drying of moist materials.  
Int. J. Heat Mass Transfer, V.1, pp.294-301, 1961.
229. LEBEDEV, P.  
Heat and mass transfer between moist solids and air.  
Int. J. Heat Mass Transfer, V.1, pp. 302-305, 1961.
230. FINLAY, I. and McMillan, T.  
Heat transfer during two-component mist flow across a heated cylinder.  
Proc. Instn. Mech. Engrs., V. 182, Pt.3H, paper number 29, pp. 277-288, 1967-68.
231. FINLAY, I.  
An analysis of heat transfer during flow of an air/water mist across a heated cylinder.  
The Can. J. Chem. Engrg., V.49, pp. 333-339, June, 1971.
232. FULFORD, G.  
A survey of recent Soviet research on the drying of solids.  
The Can. J. Chem. Engrg., V.47, pp.338-391, Aug., 1969.
233. BLOOR, M.S.  
The transition to turbulent in the wake of a circular cylinder.  
J. Fluid Mechanics, V. 19, Part 2, pp.290-304, 1964.
- 234./...

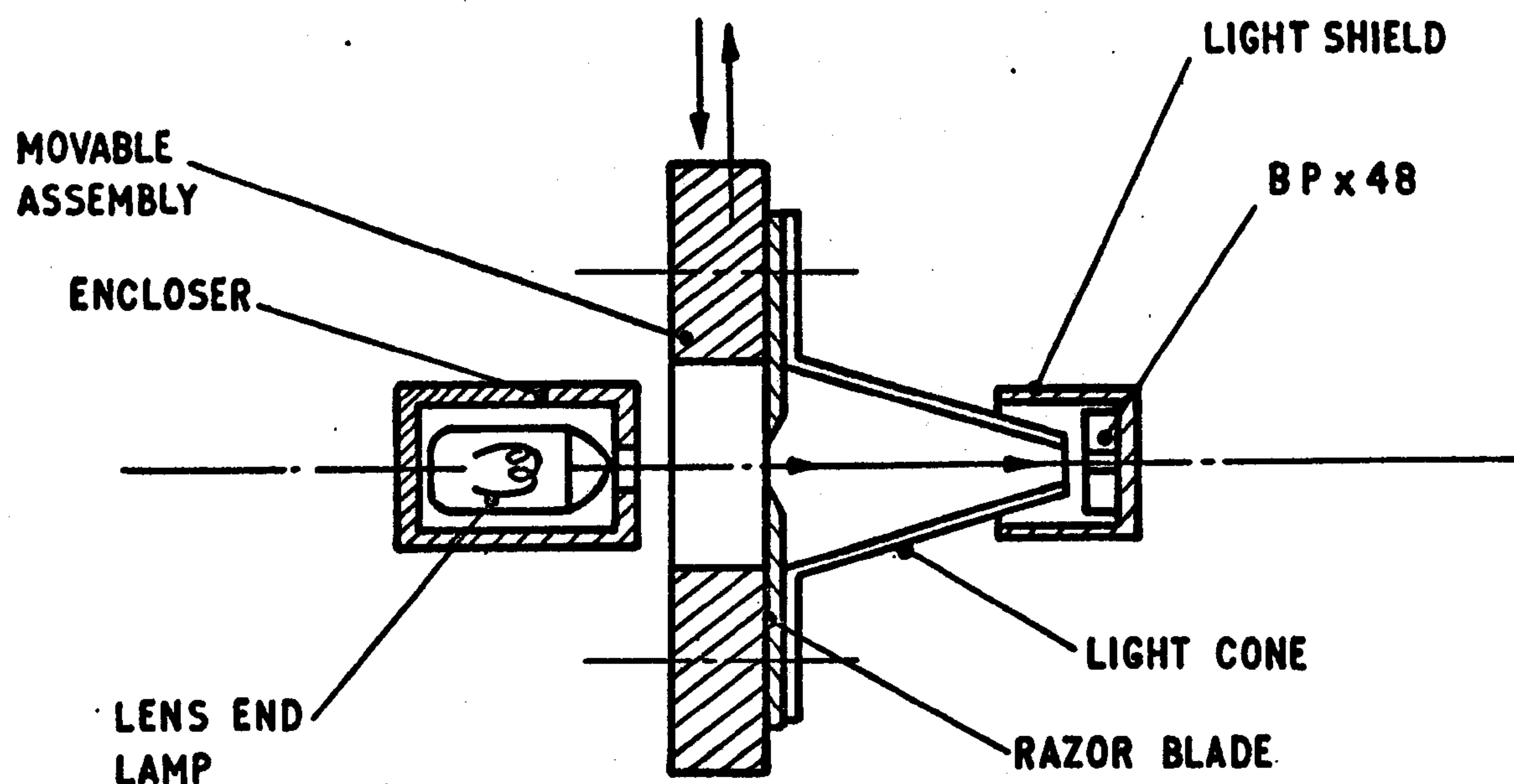


234. ACHENBACH, E.  
Investigations on the flow through a staggered tube bundle at Reynolds numbers up to  $Re = 10^7$ .  
Warme-und Stoffubertragung, Bd.2, S.47-52, 1969.
235. ACHENBACH, E.  
Influence of surface roughness on the flow through a staggered tube bank.  
Warme-und Stoffubertragung, Bd. 4, S.120-126, 1971.
236. ACHENBACH, E.  
On the cross flow through in-line tube banks with regard to the effect of surface roughness.  
Warme-und-Stoffubertragung, Bd. 4, S.152-155, 1971.
237. TOMOVIC, R. et al.  
General sensitivity theory.  
New York, Elsevier, 1972.
238. MASKELL, E.  
A theory of the blockage effects on bluff-bodies and stalled wings in a closed wind tunnel.  
A.R.C. 25 730, R. & M. 3400, 1963.
239. DALTON, C.  
Allen and Vincenti blockage corrections in a wind tunnel.  
AIAA Journal, V.9(9), 1864-1865, Sept., 1971.
240. FARELL, C. et al.  
Effect of wind-tunnel walls on the flow past circular cylinders and cooling tower models.  
J. Fluid Engineering, pp. 470-479, Sept., 1977.
241. CARNAVOS, T.  
Some recent developments in augmented heat exchange elements.  
Int. Centre for heat and mass transfer.  
Int. Seminar, Trogir, Yugoslavia, Serie C, Aug-Sept., 1972.
242. PRESTON, S. et al.  
Laboratory measurements of heat transfer coefficient during condensation of steam on horizontal tubes. Steam turbine condensers, Report of a meeting at N.E.L., 17-18 Sept., 1974, NEL Report No. 619.
243. THWAITES, B.  
Approximate calculation of the laminar boundary layer.  
The Aero. Quarterly, V.1, pp.245-280, 1949.
244. DEPOOTER, K. et al.  
The calibration of Preston tubes in transpired turbulent boundary layers.  
J. Fluid Engineering, V.100, pp. 10-16, 1978.
245. HOERNER, S.  
Aerodynamic drag.  
Ottenbein Press (Dayton, Ohio), 1951.
- 246./...

246. HOERNER, S.  
Fluid-dynamic drag.  
Library of Congress Cat. Card No. 64-19666 (1965).
247. HAKKINEN, R.J.  
Measurements of turbulent skin friction on a flat plate at transonic speeds.  
NACA TN 3486 (1955)
248. OKA, S. et al.  
Investigation of the heat transfer processes in tube banks in cross flow.  
Chapter 23, pp. 617-636, Heat exchangers: Design and theory source book.  
McGraw-Hill, 1974.
249. HEAD, M.  
The boundary layer with distributed suction.  
Aero. Res. Coun., R. & M. No. 2783, 1955.
250. SUGAWARA, S. et al.  
The condensation of vapour flowing normal to a horizontal pipe.  
Proc. 6th Japan Nat. Cong. App. Mech.,  
pp. 385-388, 1956.
251. The Cambridge Univ. Aero. Lab. Experiments on distributed suction through a rough porous surface.  
Aero. Res. Coun., R. & M. No. 3118, 1959.
252. APELT, C. et al.  
The effects of wake splitter plates on the flow past a circular cylinder in the range  $10^4 < Re < 5 \times 10^4$ .  
J. Fluid Mech., V.61 (1), pp.187-198, 1973.
253. WALLIS, G.  
Contribution to discussion on paper number 49, Volume 189.  
Proc. Instn. Mech. Engrs., 1977.
254. THOMAS, T.F.  
Contribution to discussion of reference number 132.  
Proc. Instn. Mech. Engrs., V.178, pp.363-364, 1963-64.
255. ZDRAVKOVICH, M.  
Review - review of flow interference between two cylinders in various arrangements.  
J. Fluids Engng., Trans A.S.M.E., pp. 618-633, Dec., 1977.
256. ZDRAVKOVICH, M.  
Smoke observations of the wake of a group of three cylinders at low Reynolds number.  
J. Fluid Mech., V. 32(2), pp.339-351, 1968.
257. ZDRAVKOVICH, M.  
Smoke observations of wakes of tandem cylinders at low Reynolds numbers.  
Aero. J., pp.108-114, Feb., 1972.
- 258./...

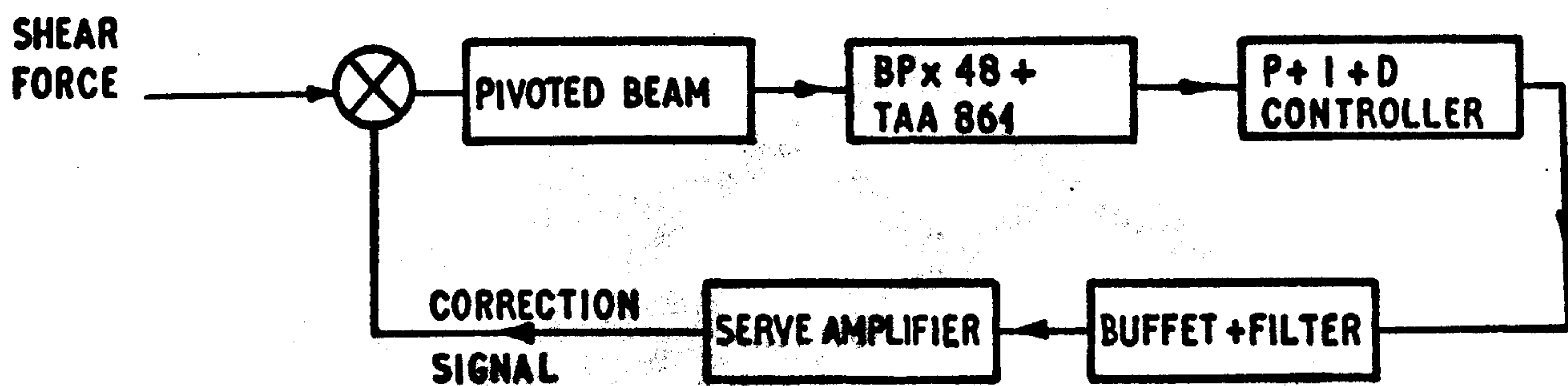


258. HALE, R. et al.  
Experimental investigation of several neutrally-buoyant bubble generators for aerodynamic flow visualisation.  
Naval. Research Reviews, pp. 19-24, June, 1971.
259. ROSHKO, A.  
A new hodograph for free-streamline theory.  
Nat. Adv. Comm. Aero., Tech. Note 3168, 1954.
260. ROTTEVEEL, B.  
Mass transfer through a porous tube. Part 1, Theory and Computer Programme.  
Univ. Witwatersrand, Johannesburg, Report No. 62, Sept., 1975.
261. KATSANIS, T.  
A computer programme for calculating velocities and streamlines for two-dimensional, incompressible flow in axial blade rows.  
Nat. Aero. Space Adm., T.N. D-3762, 1967.
262. CEBECI, T. and Smith, A.  
Analysis of turbulent boundary layers.  
Academic Press, 1974.
263. Van DRIEST, E.  
On turbulent flow near a wall.  
J. Aero. Sci., V.23, pp.1007-1011, 1956.
264. SPALDING, D.  
A single formula for the "law of the wall".  
J. Applied Mech. Trans. A.S.M.E., pp.455-458, Sept., 1961.
265. GRANVILLE, P.  
Integral methods for turbulent boundary layers in pressure gradients.  
J. Ship Research, V.16, pp.191-204, Sept., 1972.
266. CEBECI, T.  
Behaviour of turbulent flow near a porous wall with pressure gradient.  
AIAA Journal, V.8(12), pp. 2152-2156, Dec., 1970.
267. VOLKOV, V.  
A refinement of the Karman-Pohlhausen integral method in boundary layer theory.  
J. Engng Physics, V.9(5), pp.371-374, Nov., 1965.



LIGHT BEAM ARRANGEMENT

FIG. 3.1



BLOCK DIAGRAM FOR THE SYSTEM

FIG.3.2



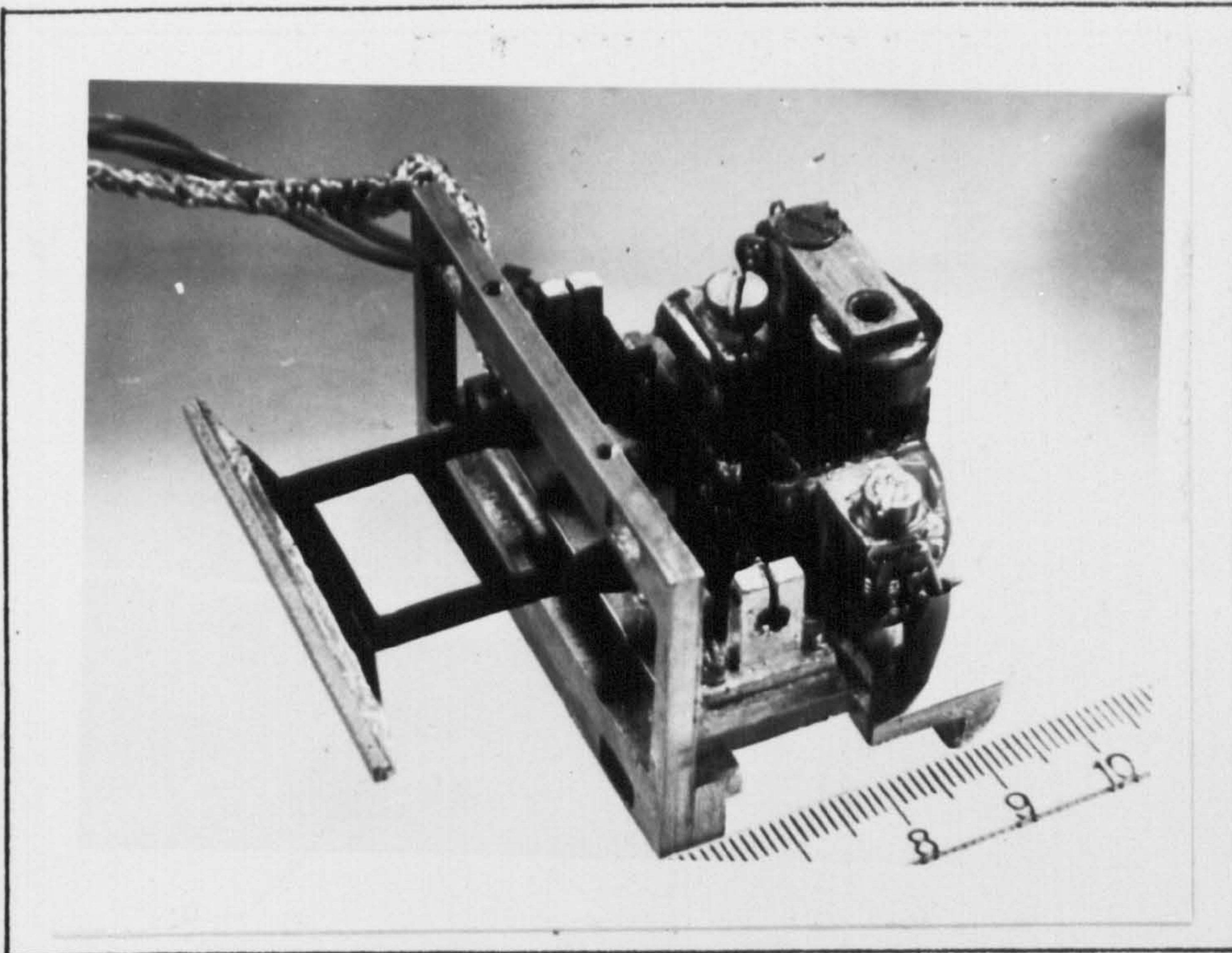


Fig.3.3 TRANSDUSER WITH THE VANE

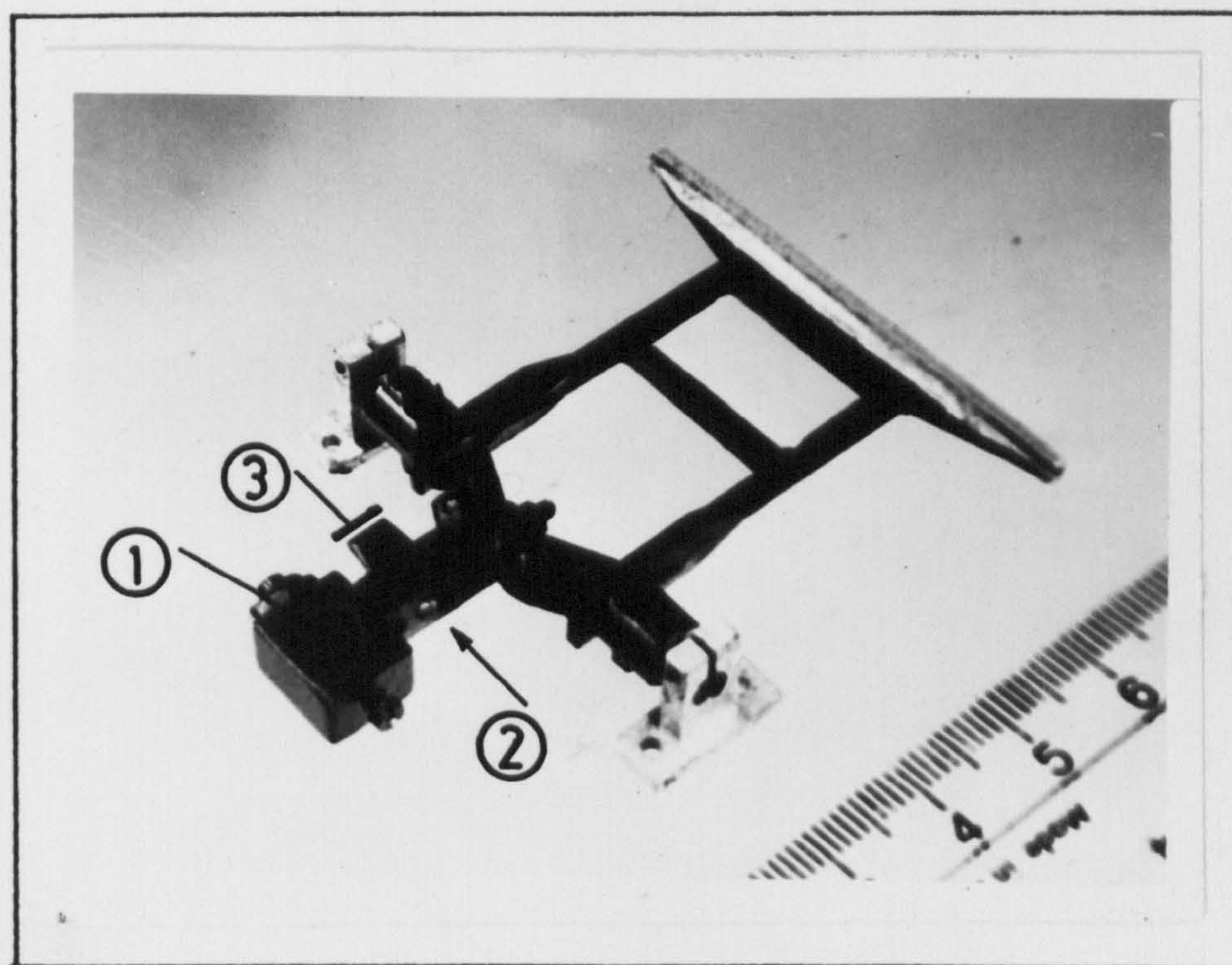


Fig.3.4 VANE OA

- ① Magnet
- ② Light source
- ③ Photo cells



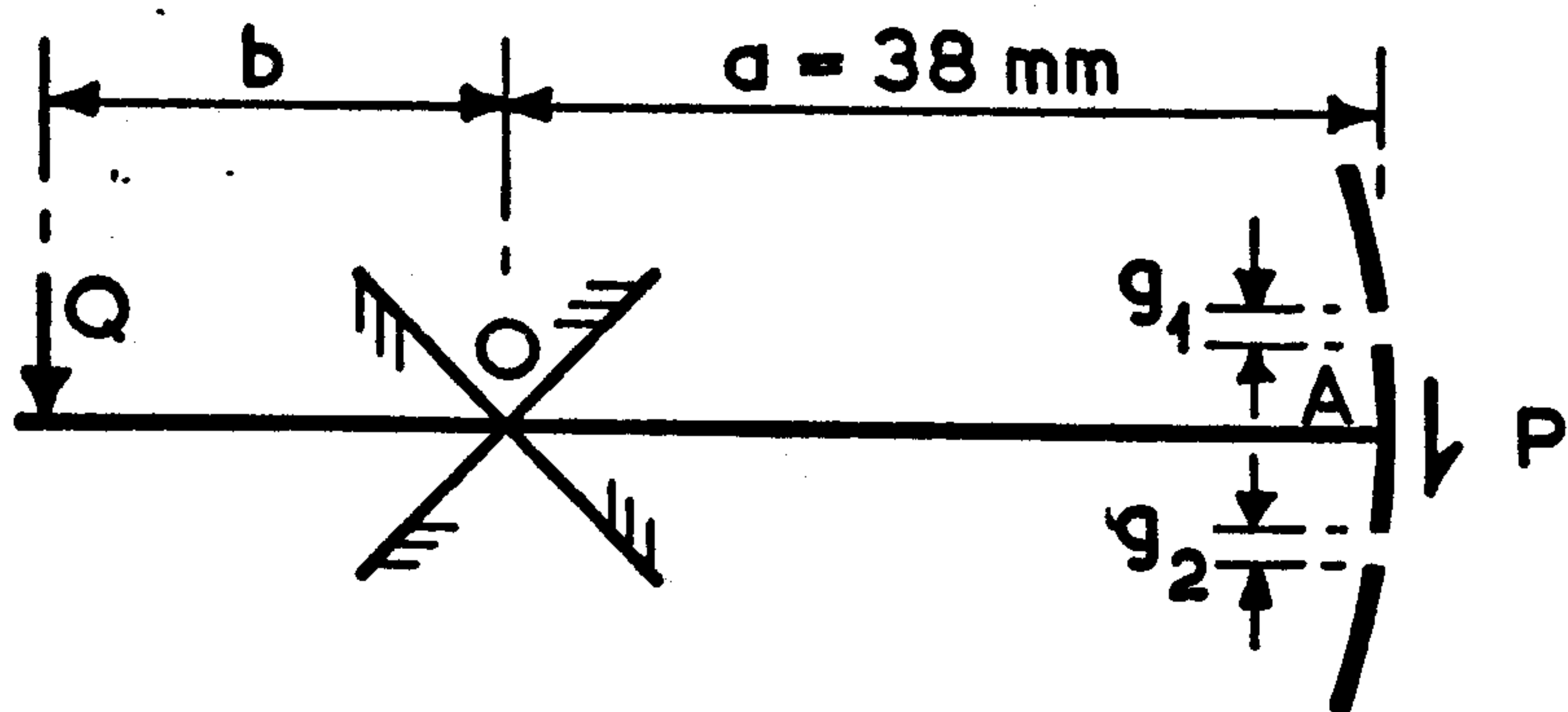


Fig.3.5 Transducer vane OA



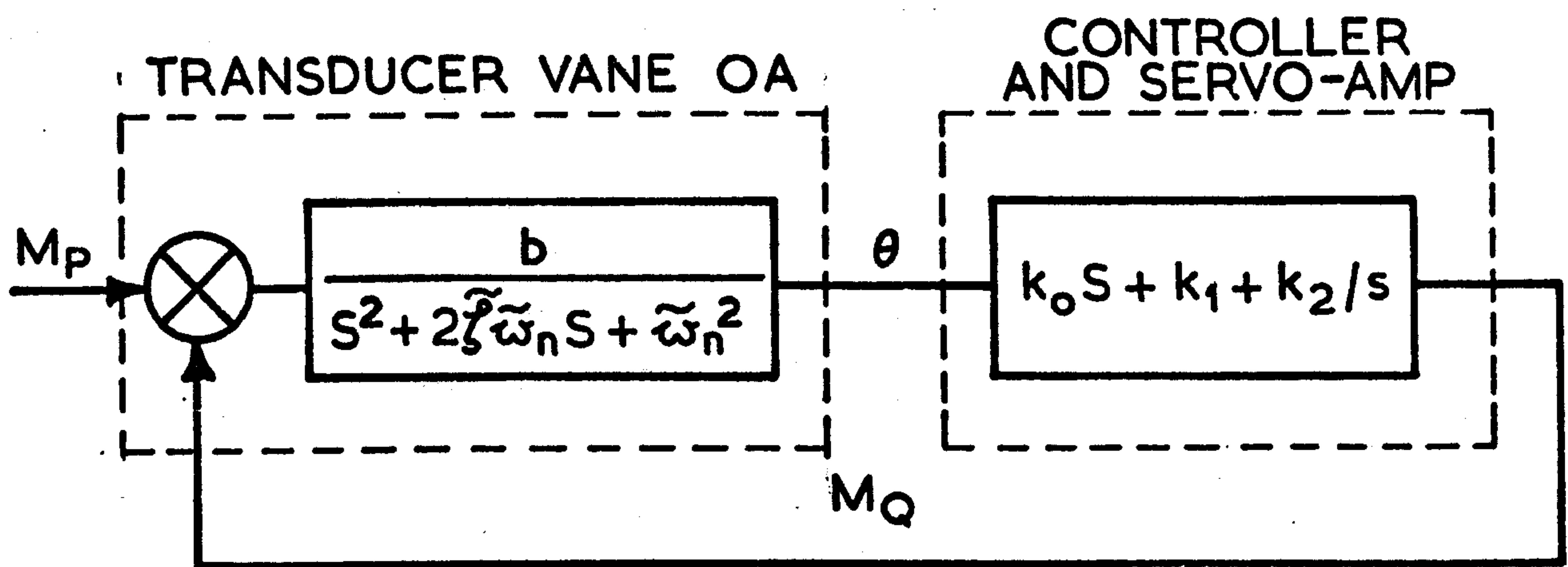
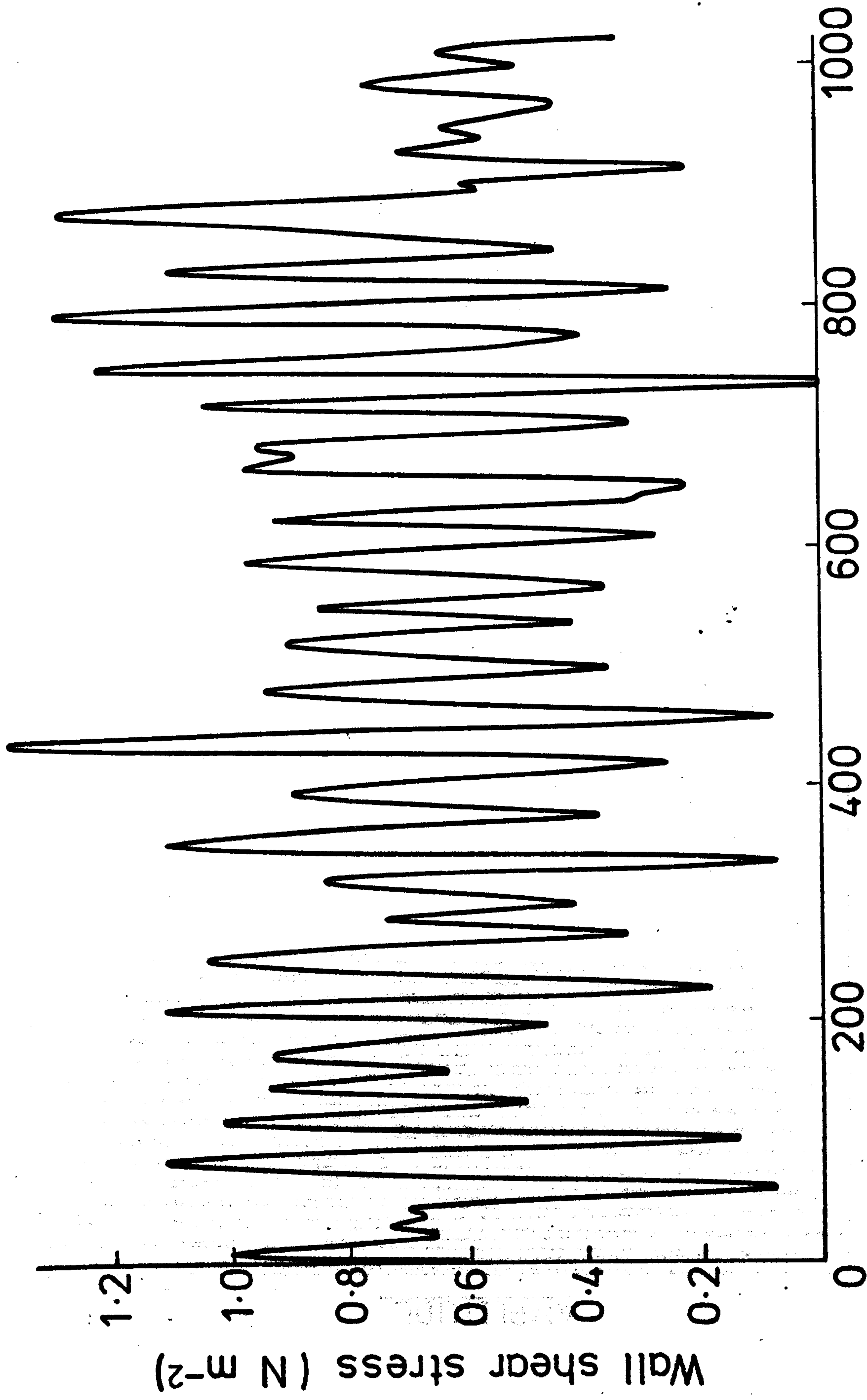


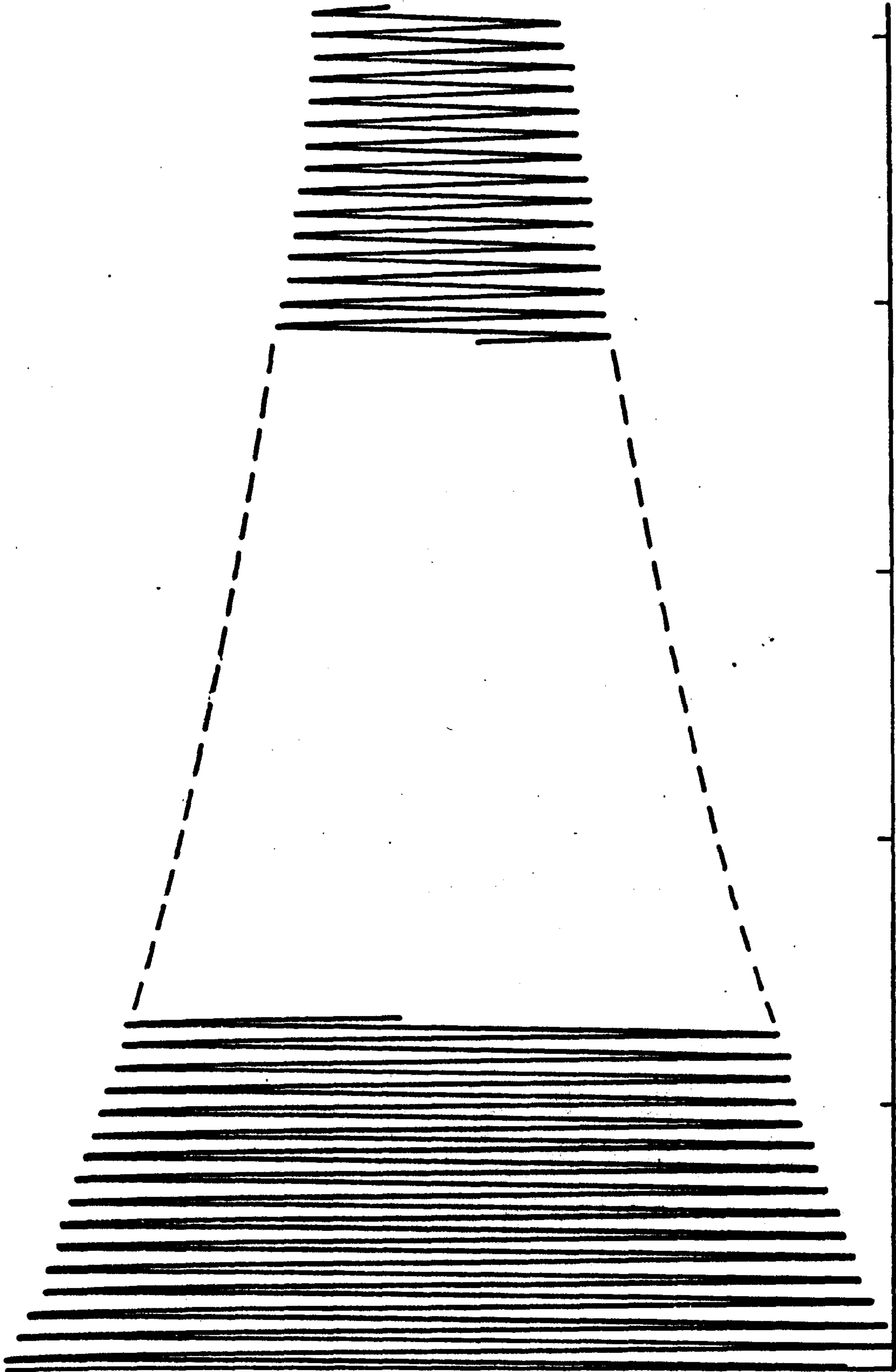
Fig.5.6 Block diagram of instrument



Dynamic response of the transducer

Fig. 3.7





AMPLITUDE

TIME

Natural frequency of the vane

Fig. 3.8

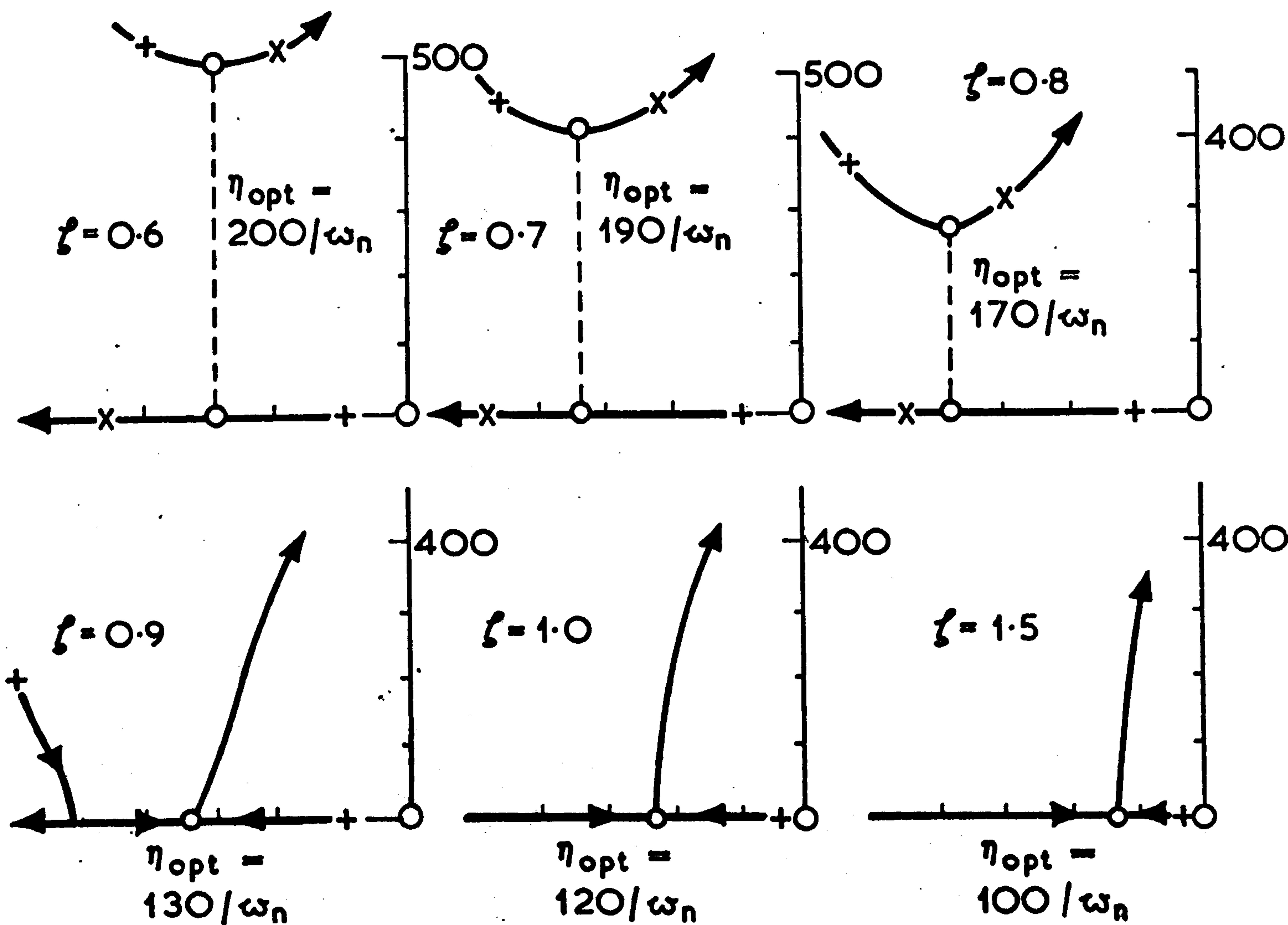


Fig.3.9 Root locii of denominator of  $H_1(s)$ ,  
i.e.  $S^3 + 2\zeta\omega_n S^2 + \omega_n^2 S + \eta\omega_n^3$  for  $\omega_n = 728 \text{ rad/s}$   
(Arrows are in direction of increasing  $\eta$ .)



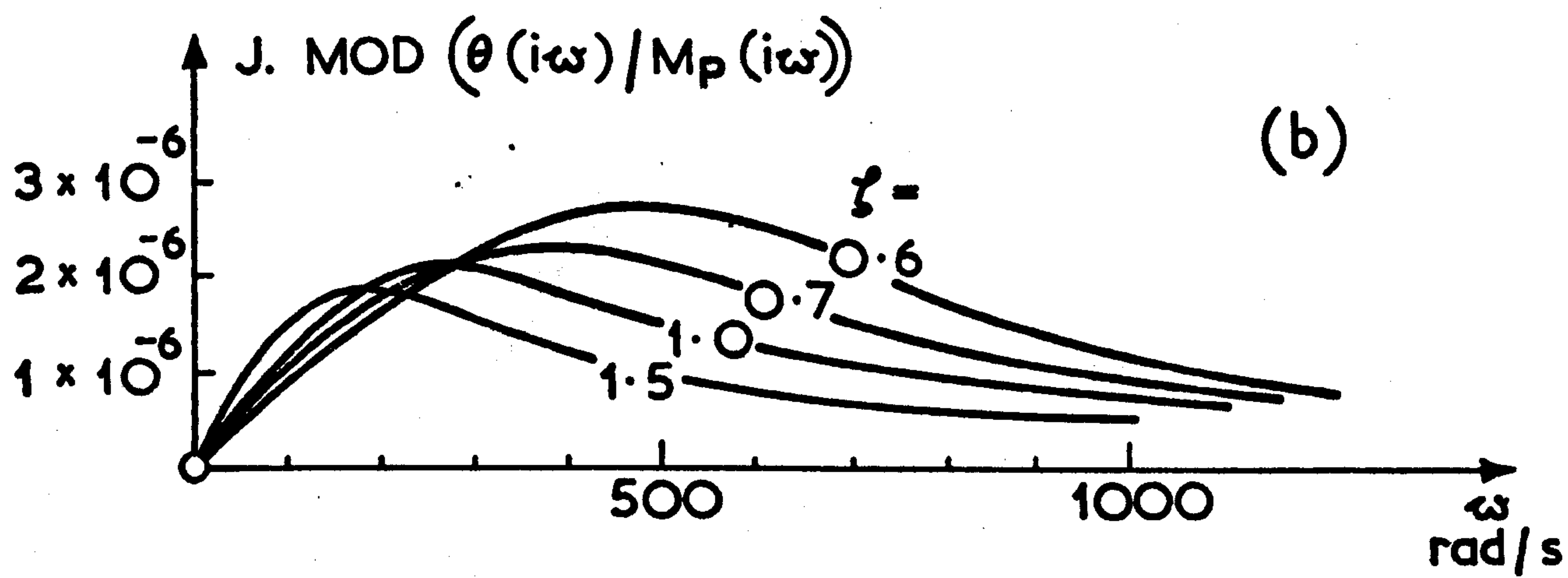
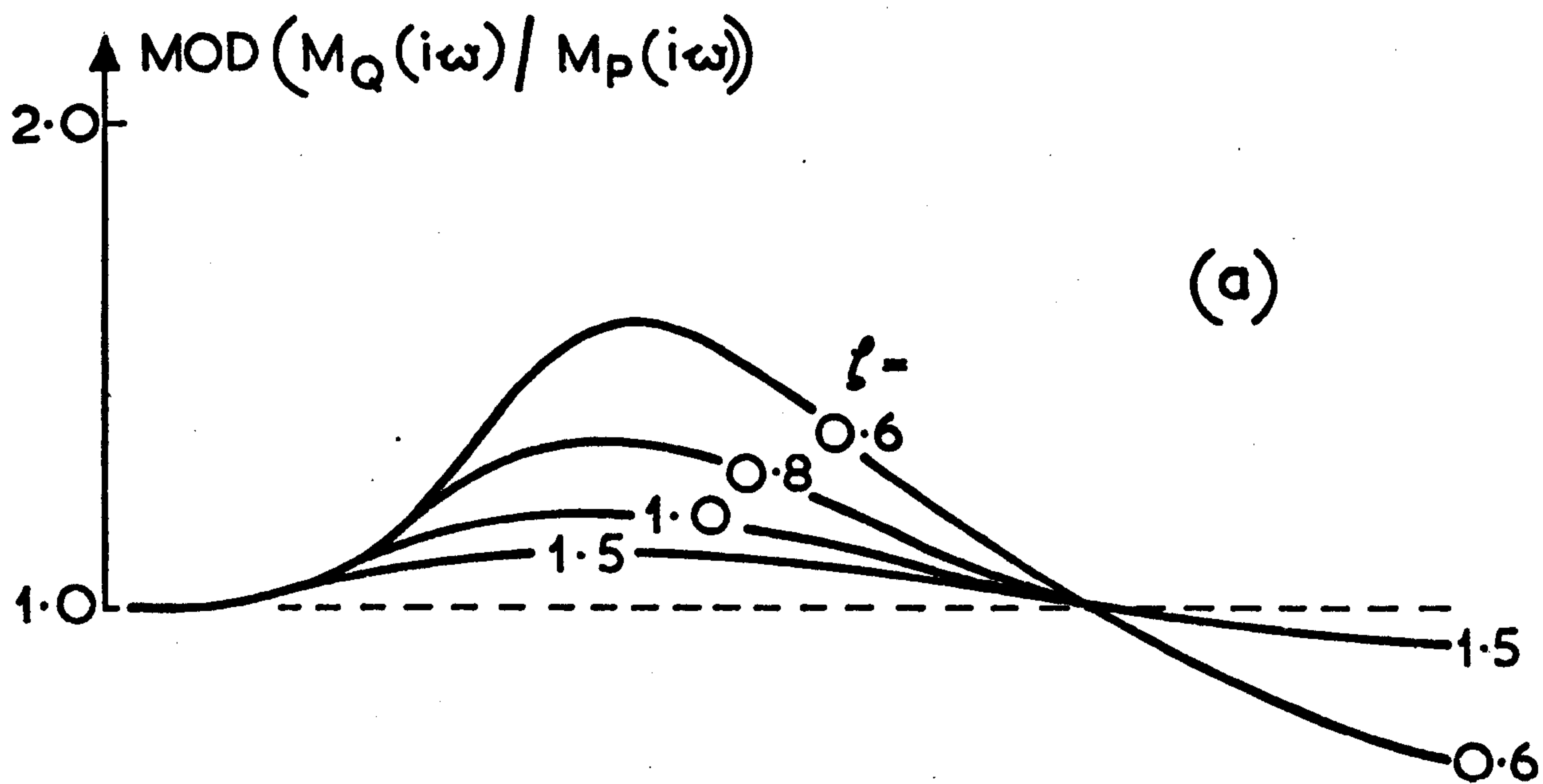
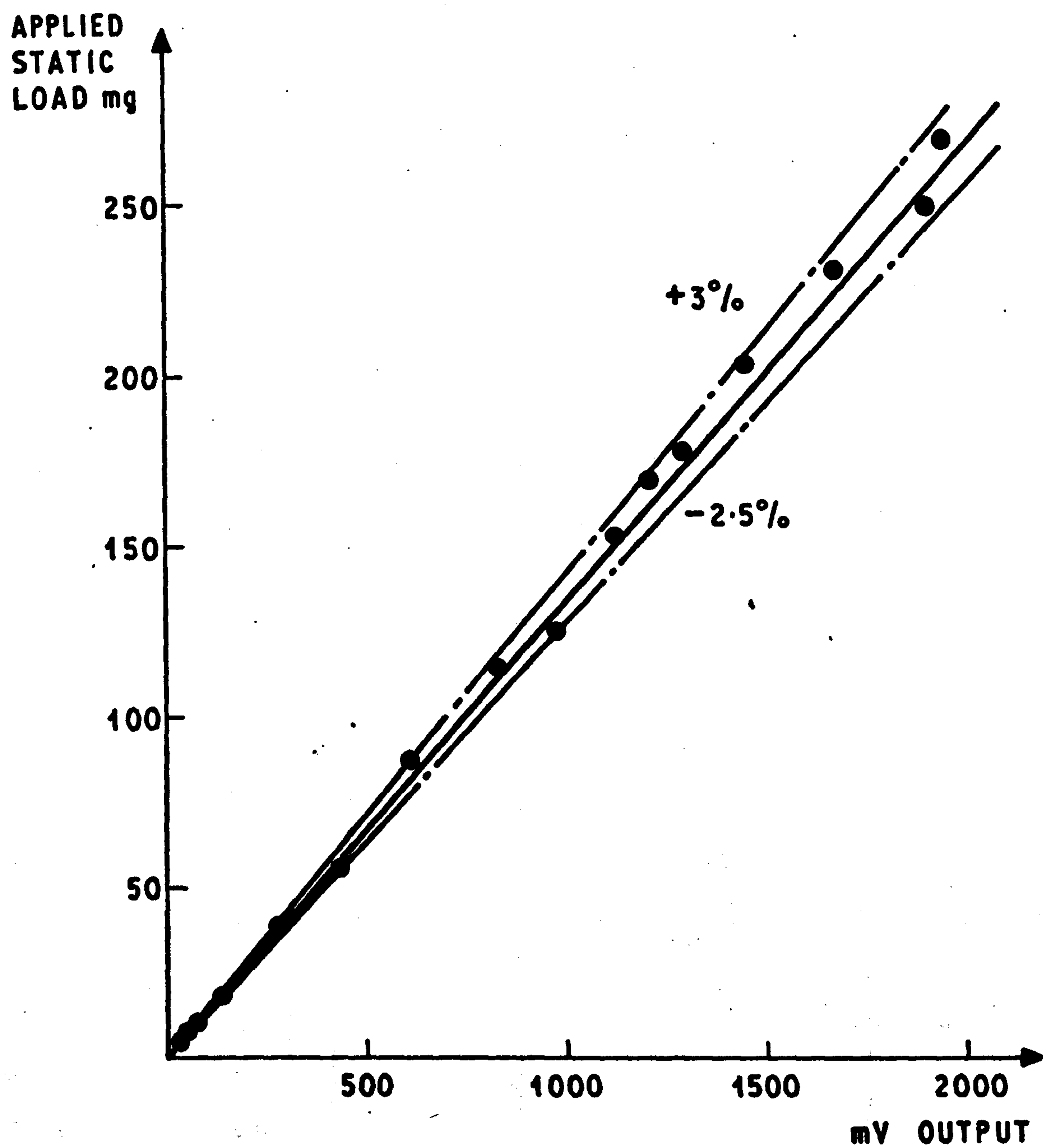


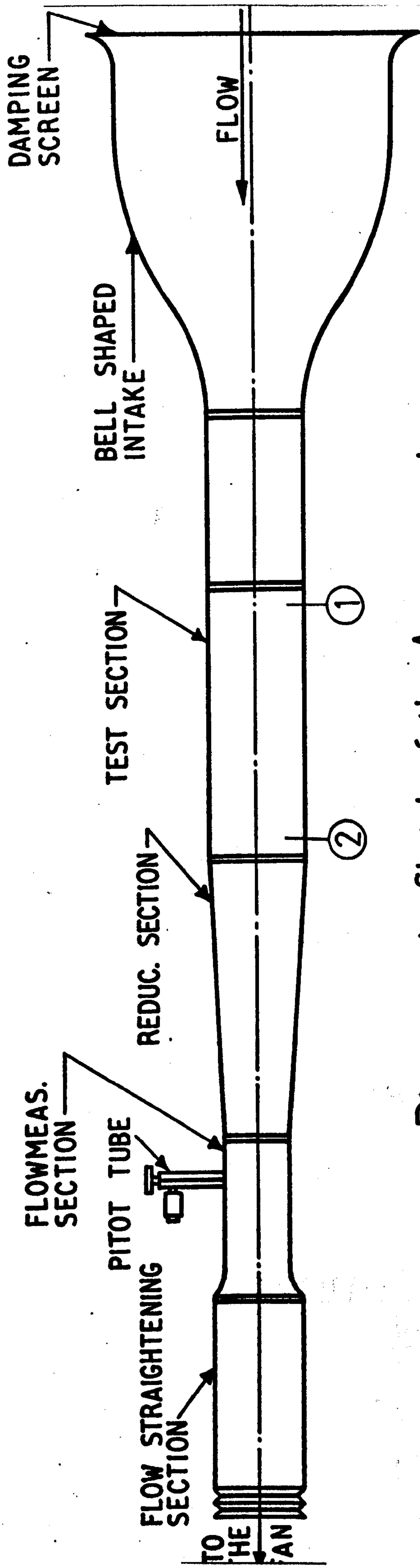
Fig.3.10 Moduli of transfer functions versus frequency.



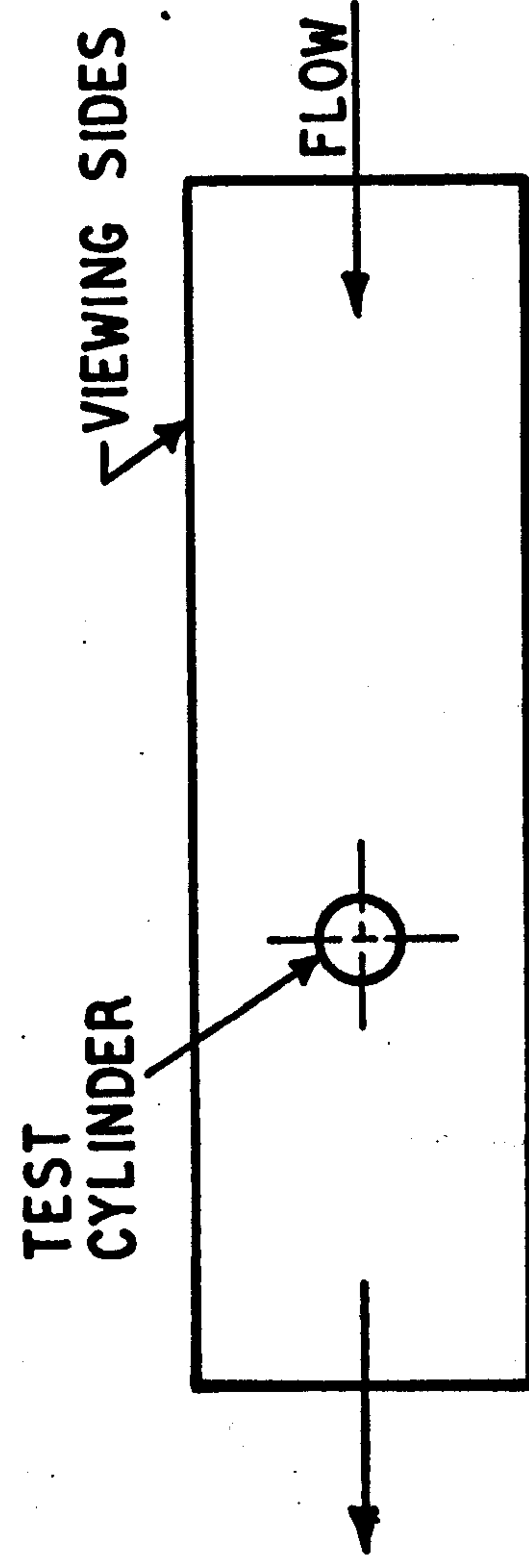
STATIC CALIBRATION OF THE DEVICE

FIG. 3.11





Diagrammatic Sketch of the Arrangement



Test Section Arrangement

Fig. 5.1

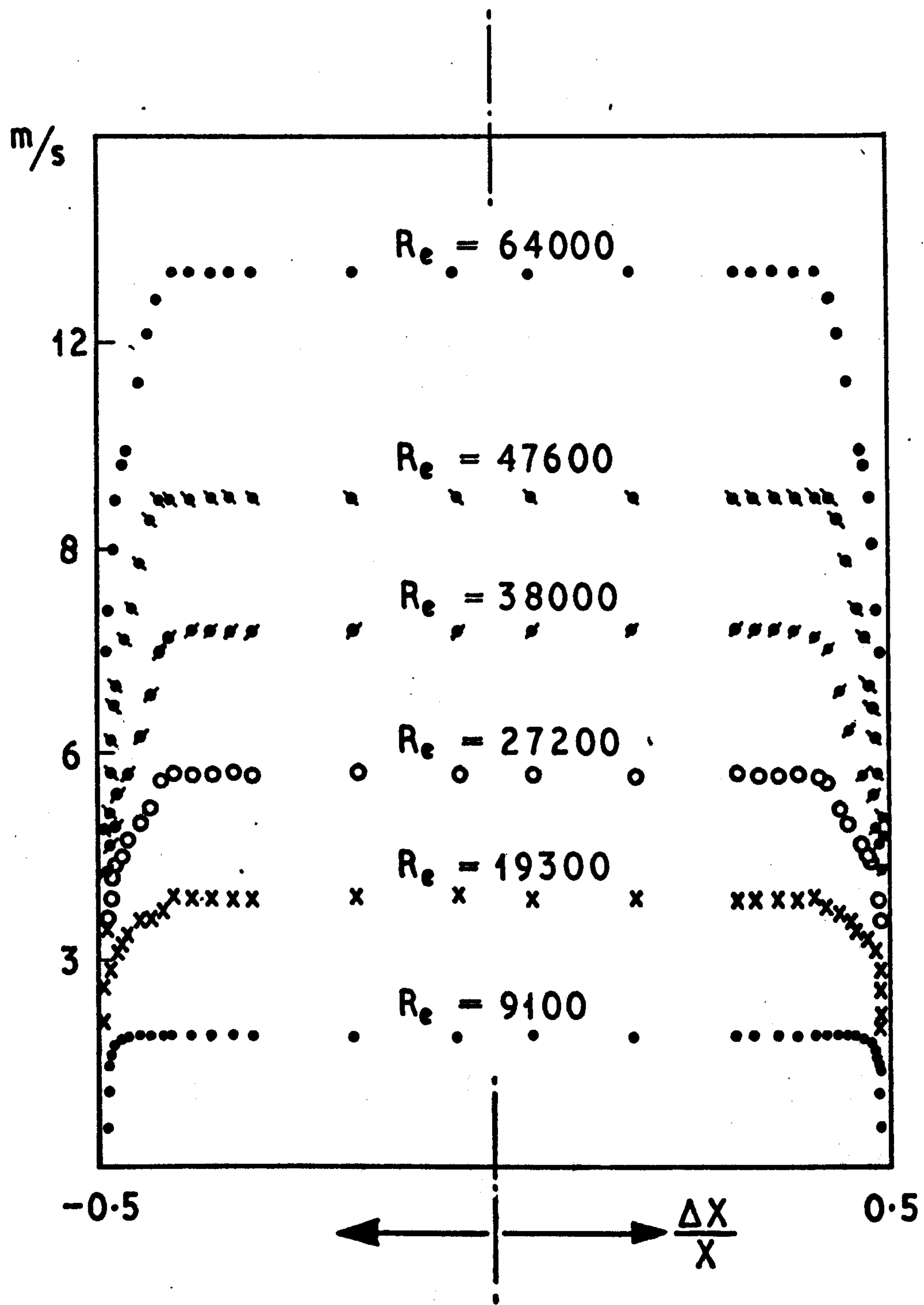


Fig. 5.2

Velocity Distribution Across the  
Test Section



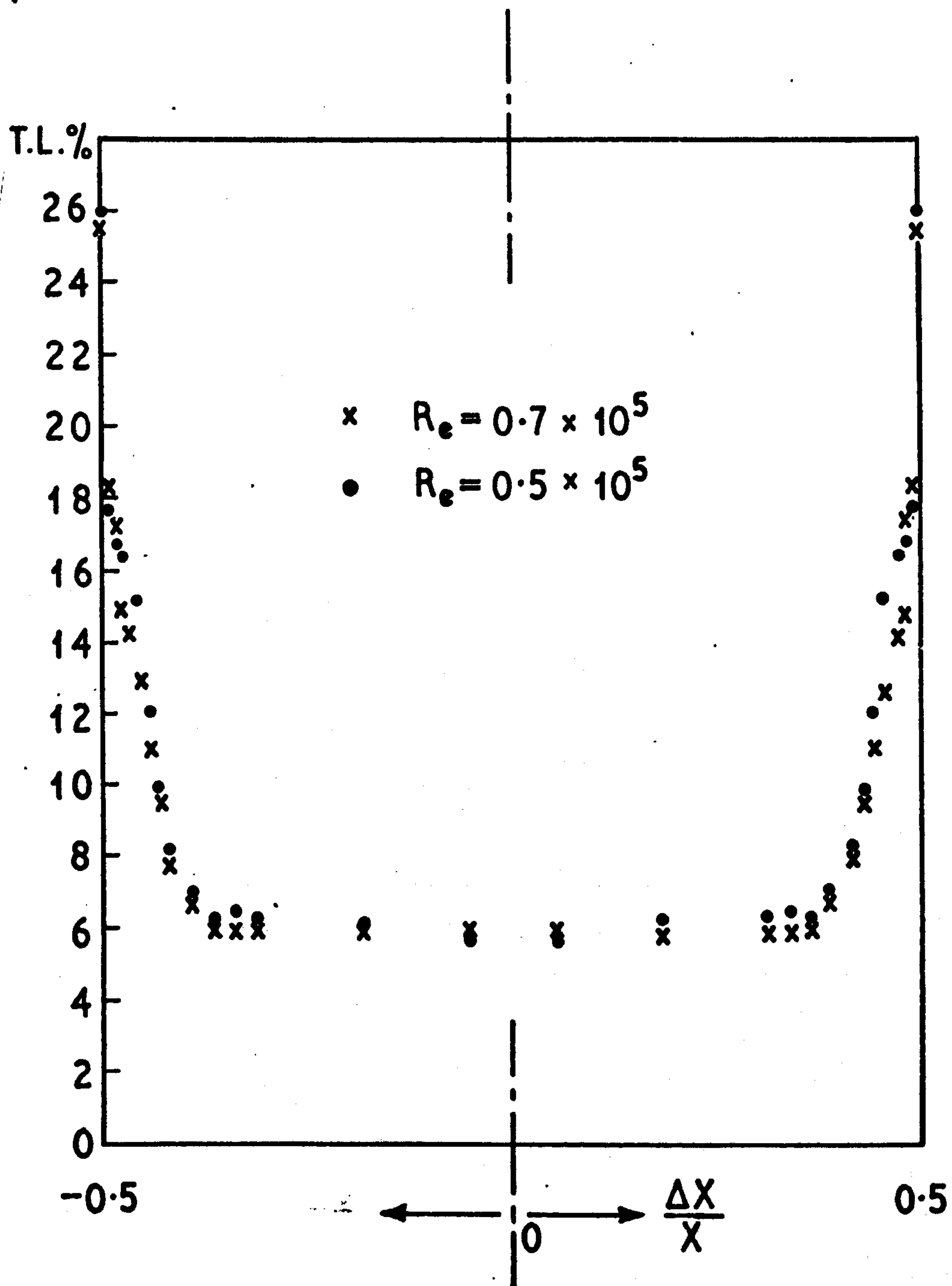
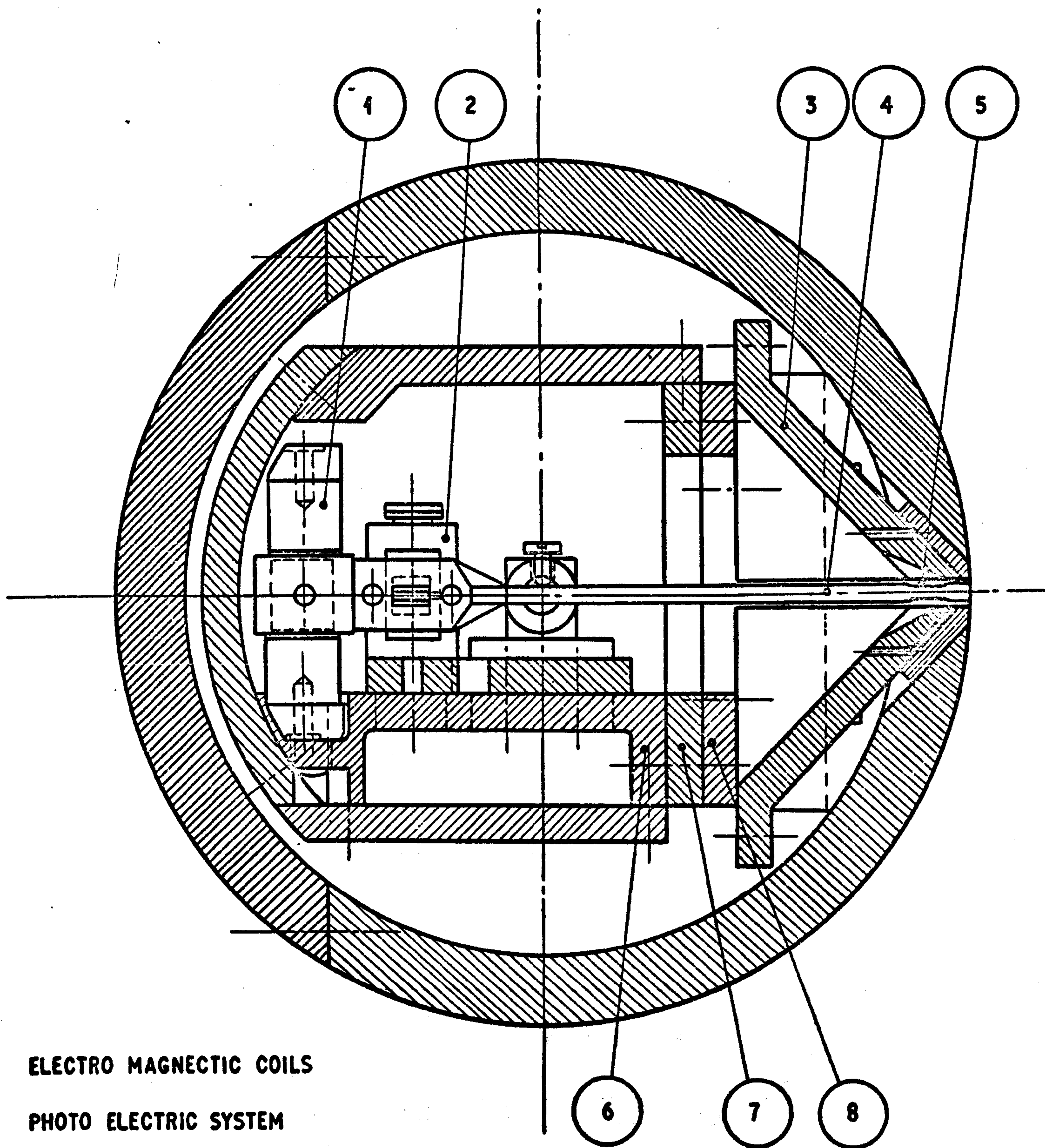


Fig.5.3

Turbulence Distribution Across the Test Section



- 1. ELECTRO MAGNETIC COILS
- 2. PHOTO ELECTRIC SYSTEM
- 3. SUPPORTING FRAME
- 4. MOVABLE ASSEMBLY
- 5. SIDE SPACERS
- 6. ADJUSTABLE CARRIER
- 7&8. SLIDING ADJUSTABLE FRAMES.

SCHEMATIC DIAGRAMS OF THE ASSEMBLED DEVICE

FIG. 5.4



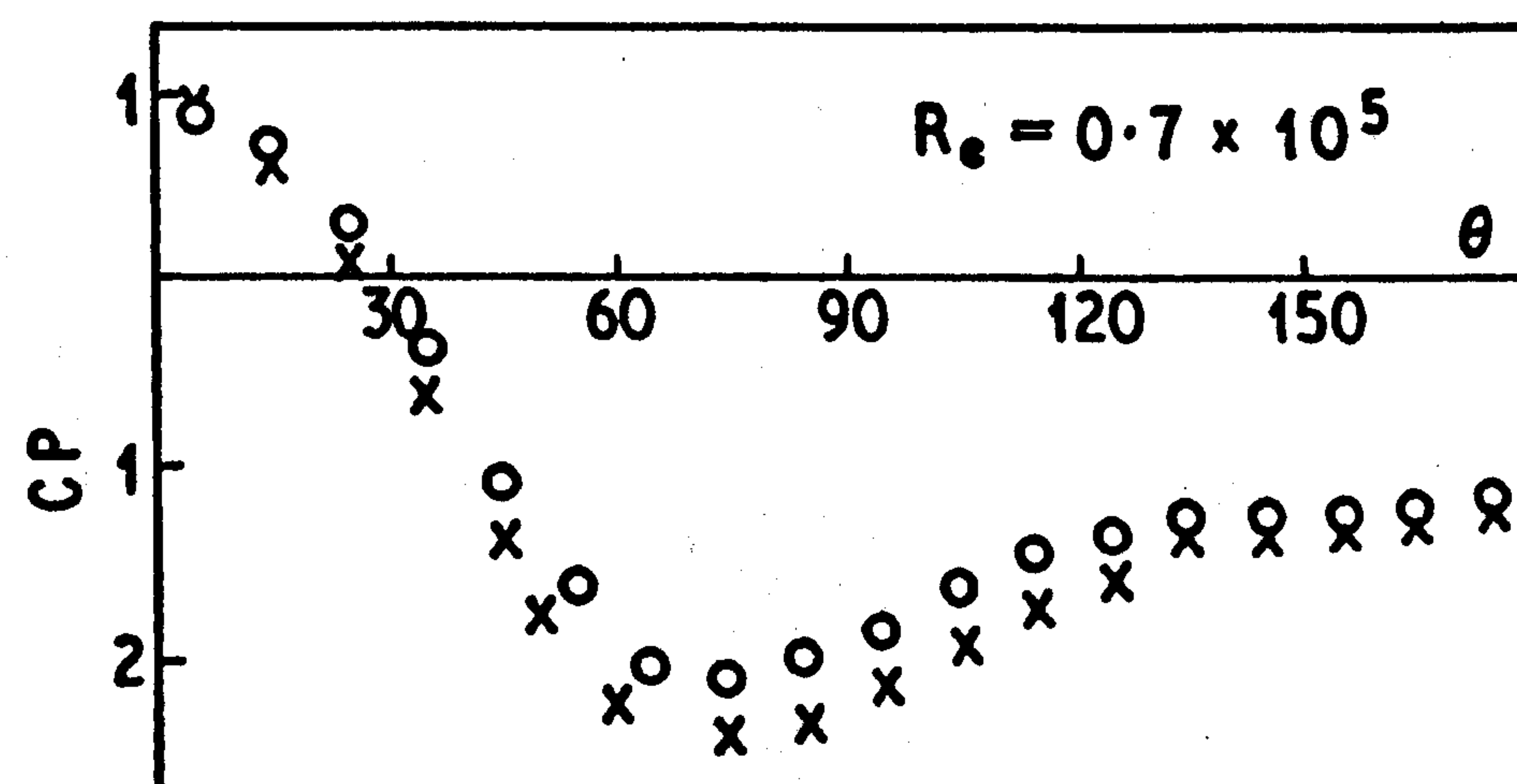
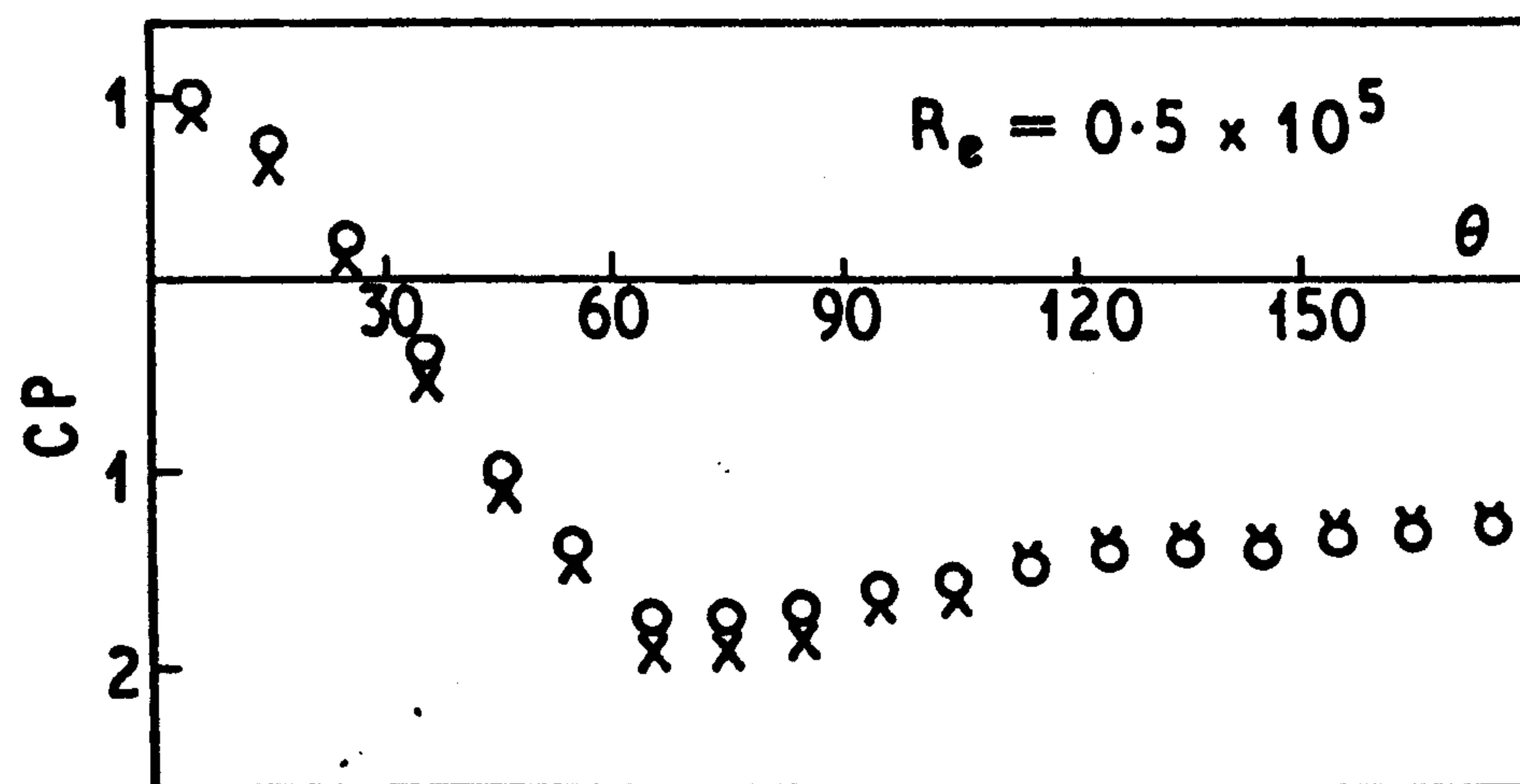
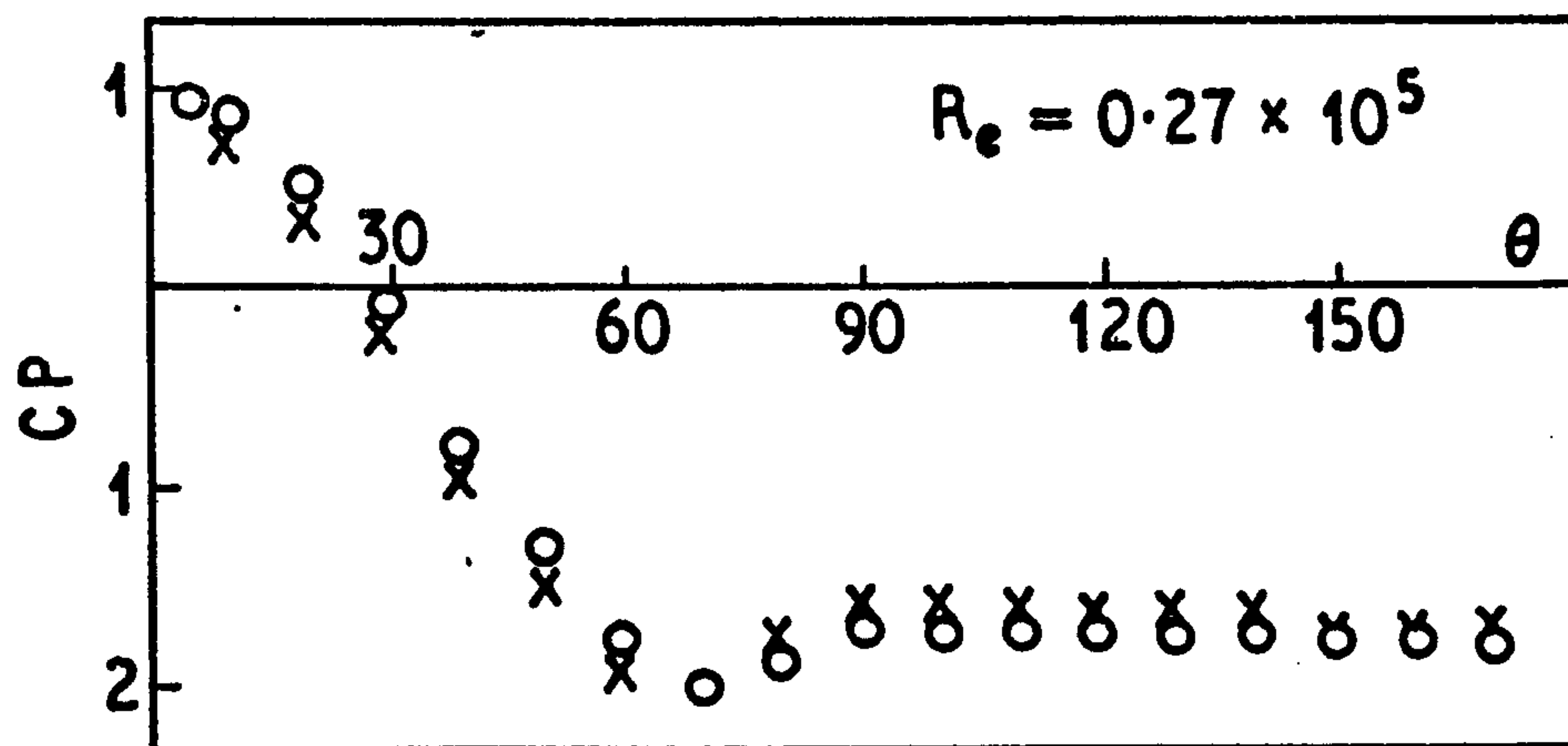
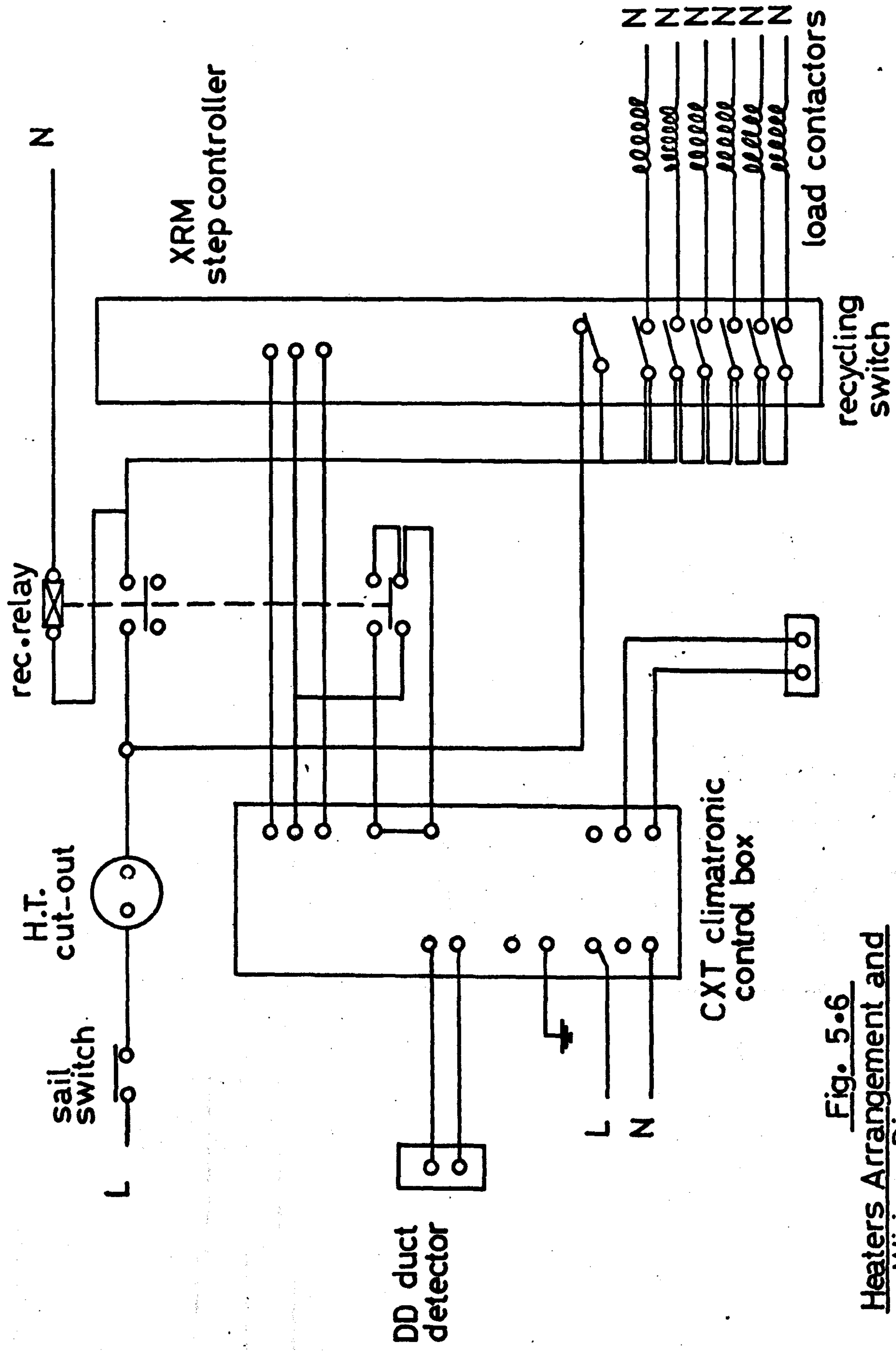


Fig. 5.5

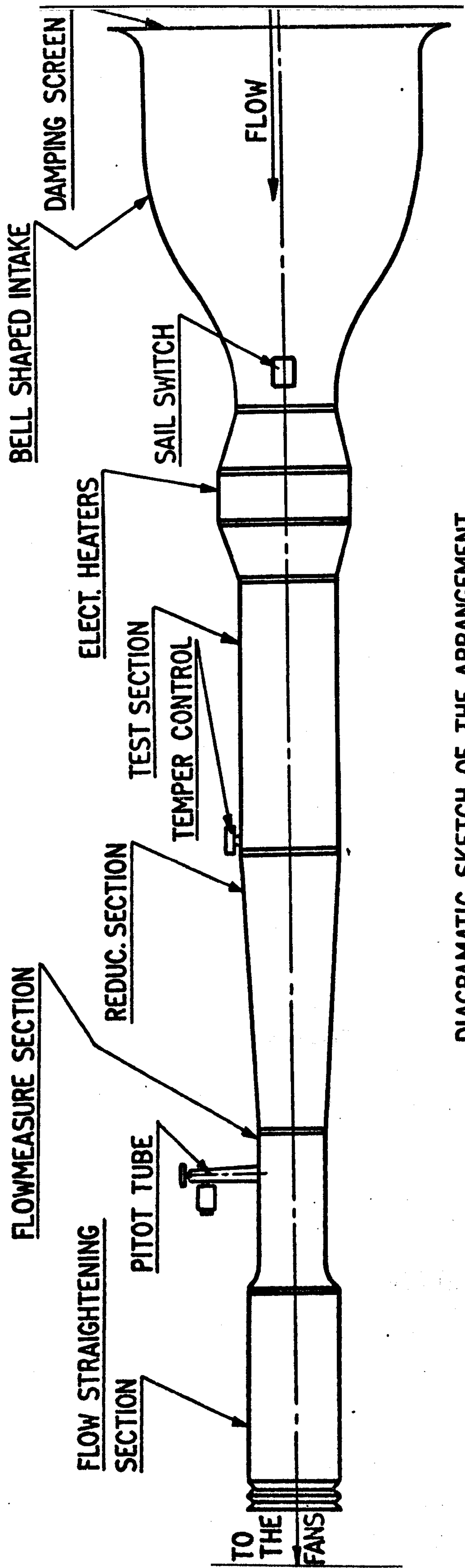
Two - Dimensionality Check

o CENTRE  
x MEAN PRESSURE

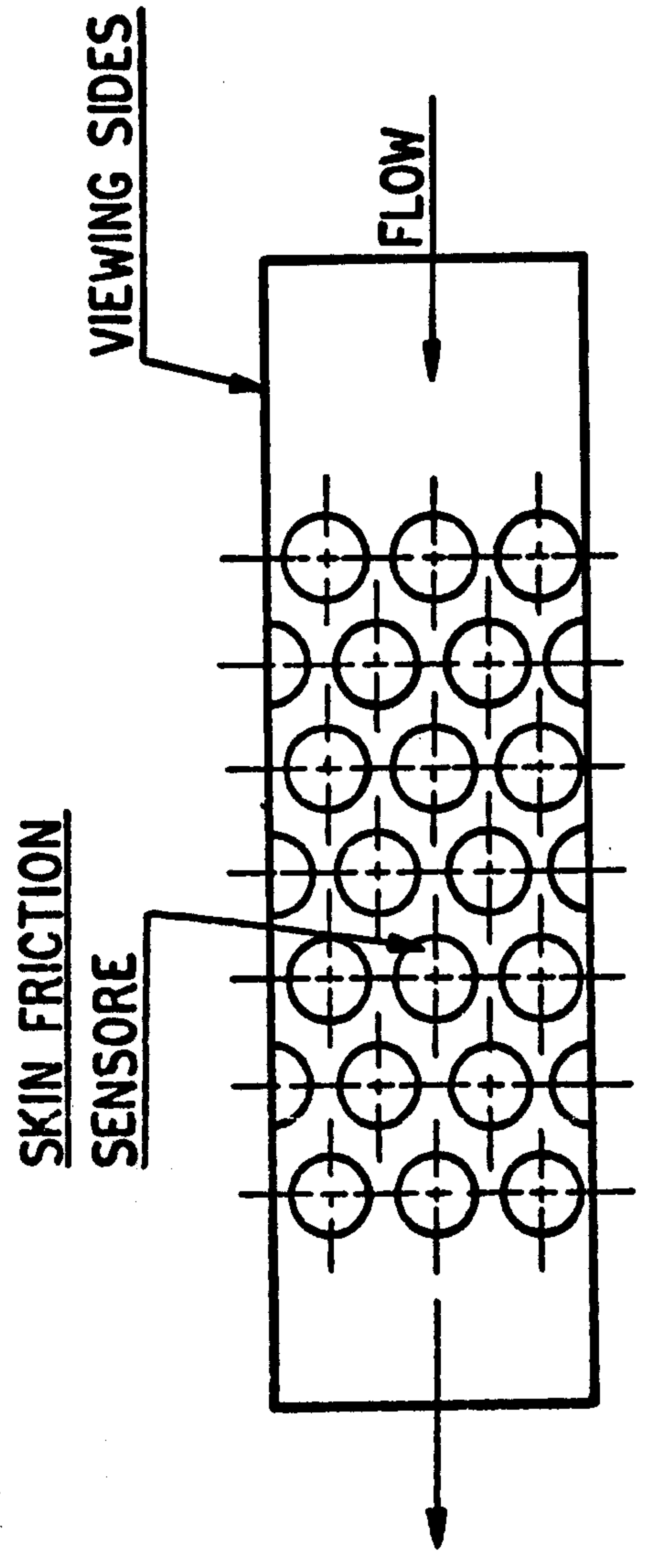


**Fig. 5.6**  
**Heaters Arrangement and**  
**Wiring Diagram**





DIAGRAMATIC SKETCH OF THE ARRANGEMENT



TEST SECTION ARRANGEMENT.

Fig.5.7

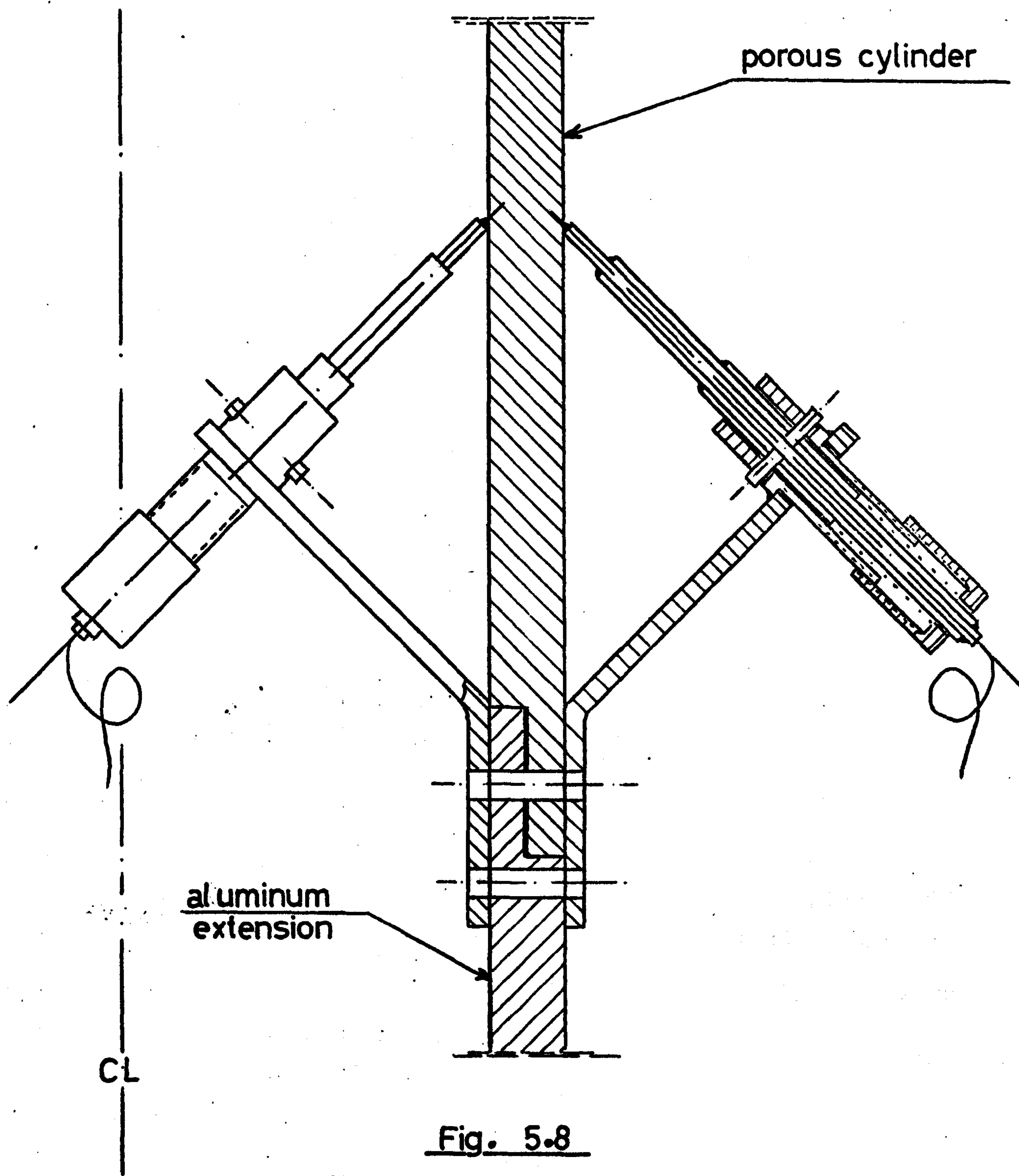


Fig. 5.8  
Thermocouples Arrangement



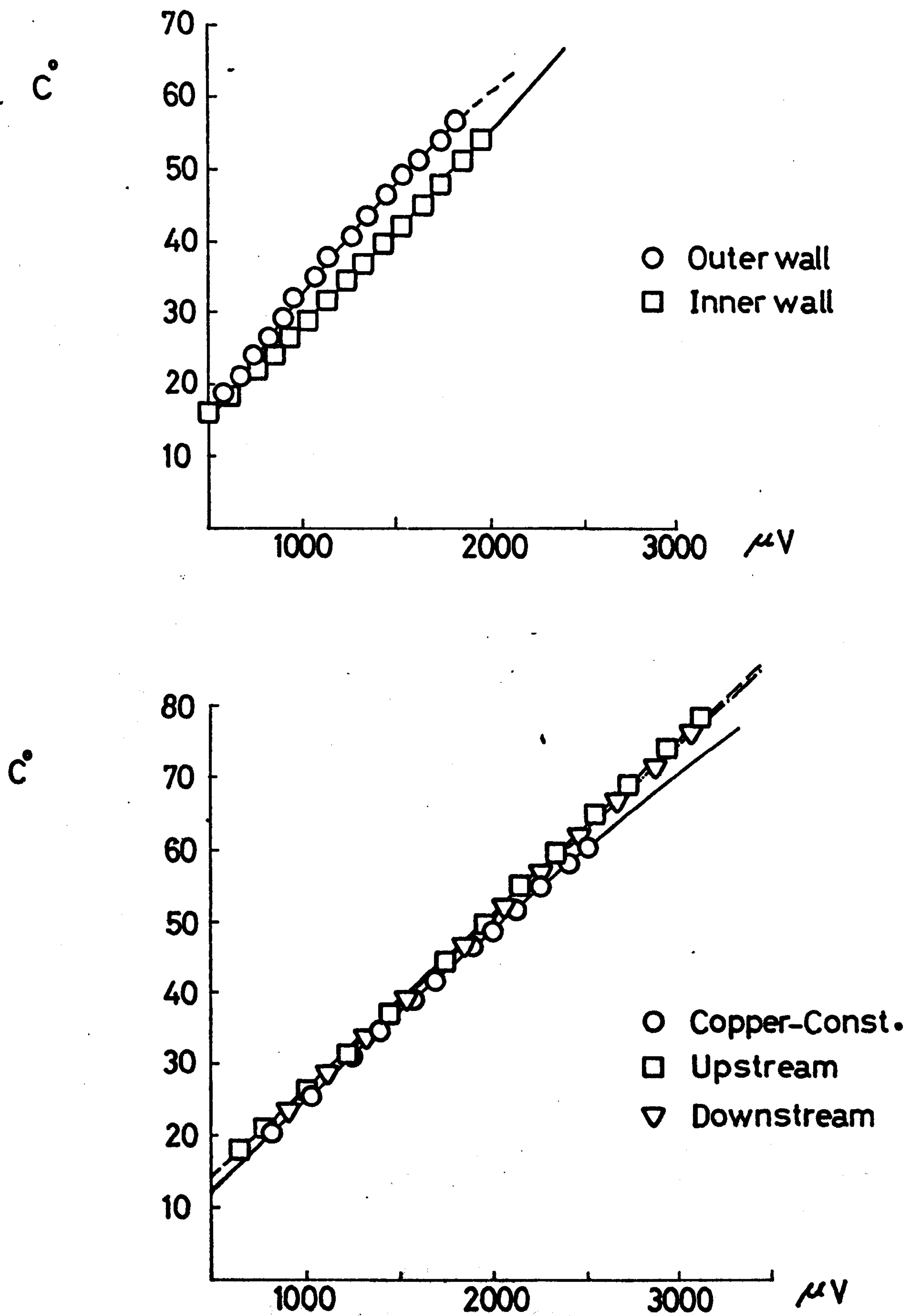


Fig. 5.9  
Thermocouples Calibration Curves

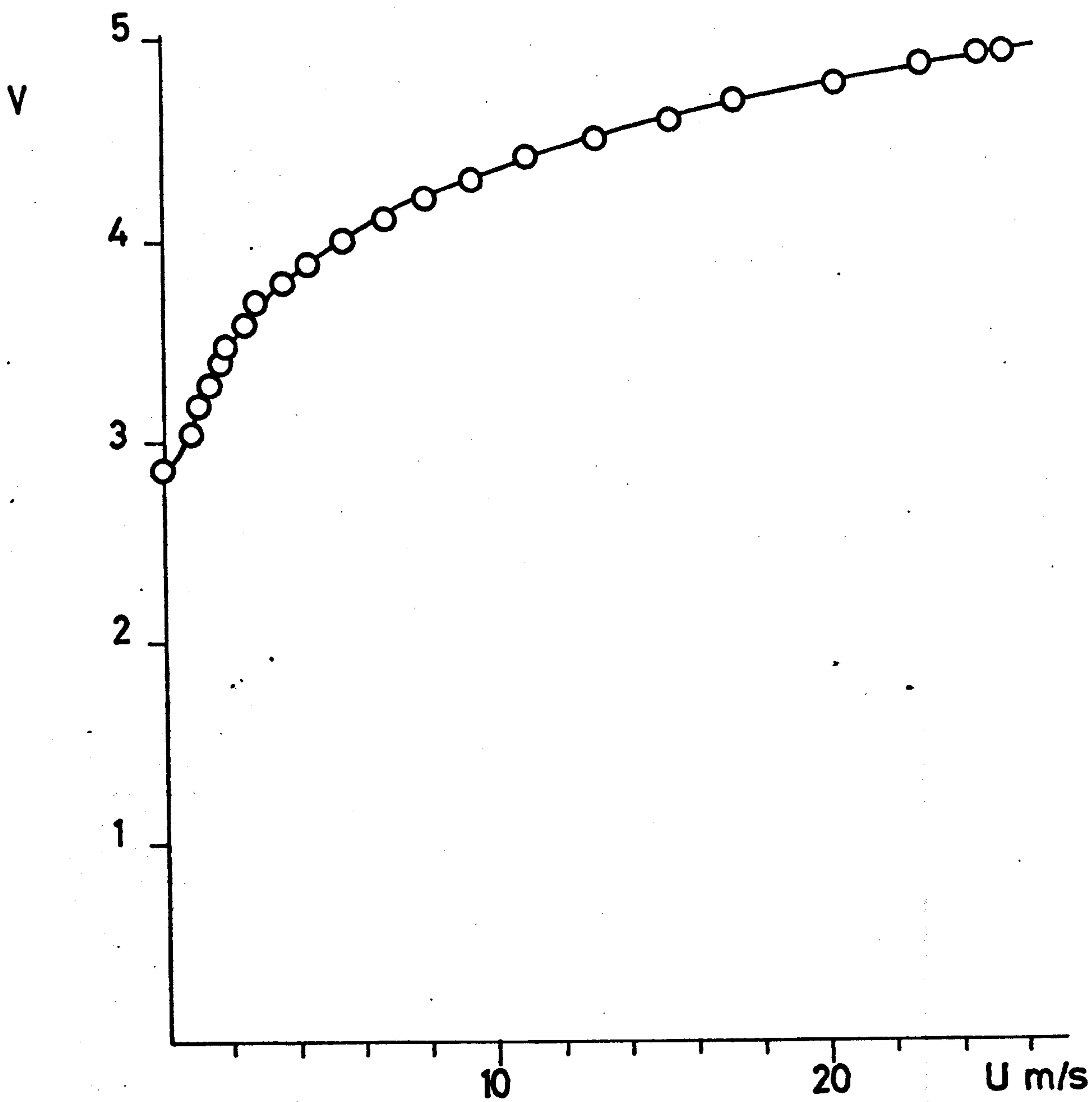
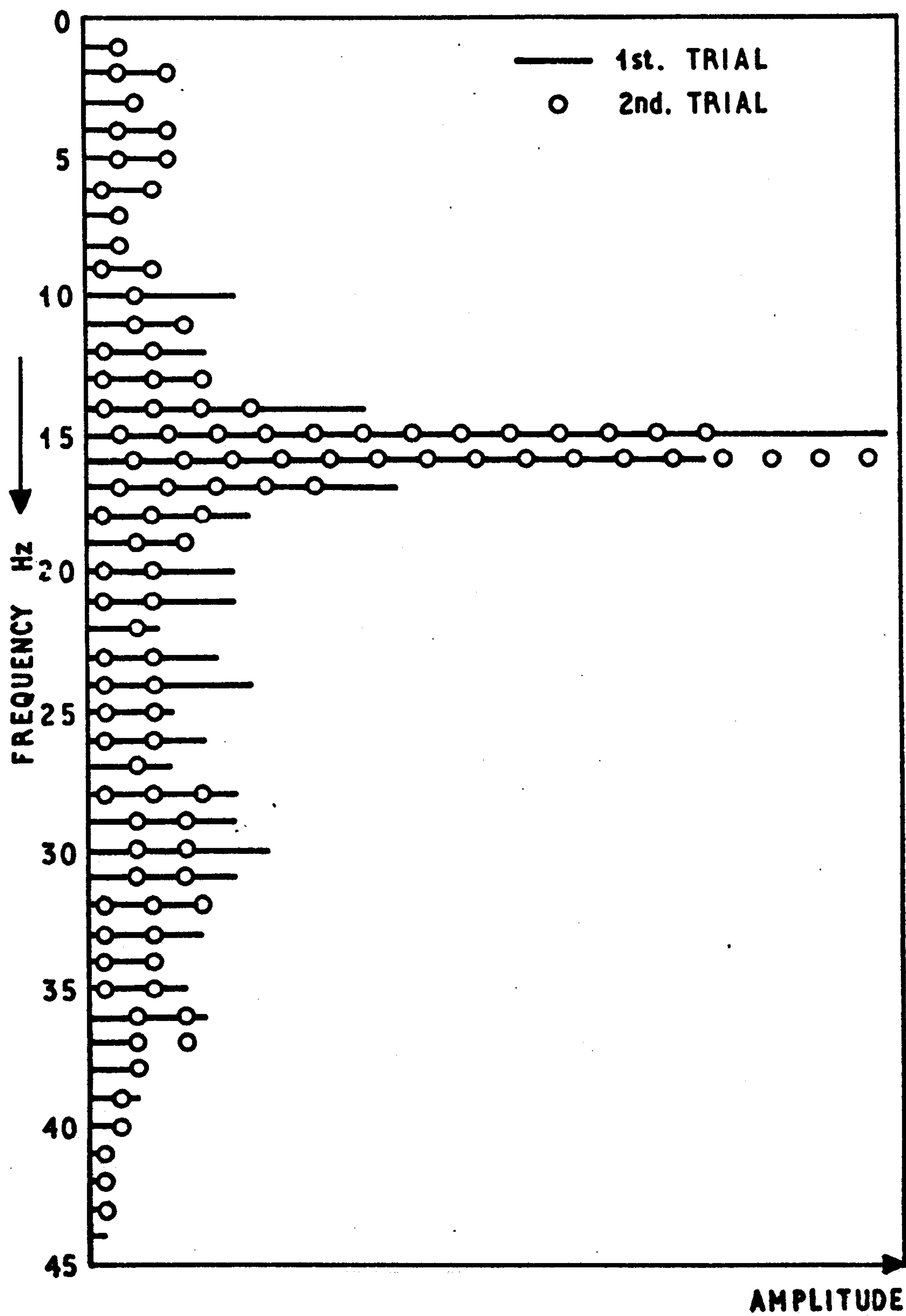


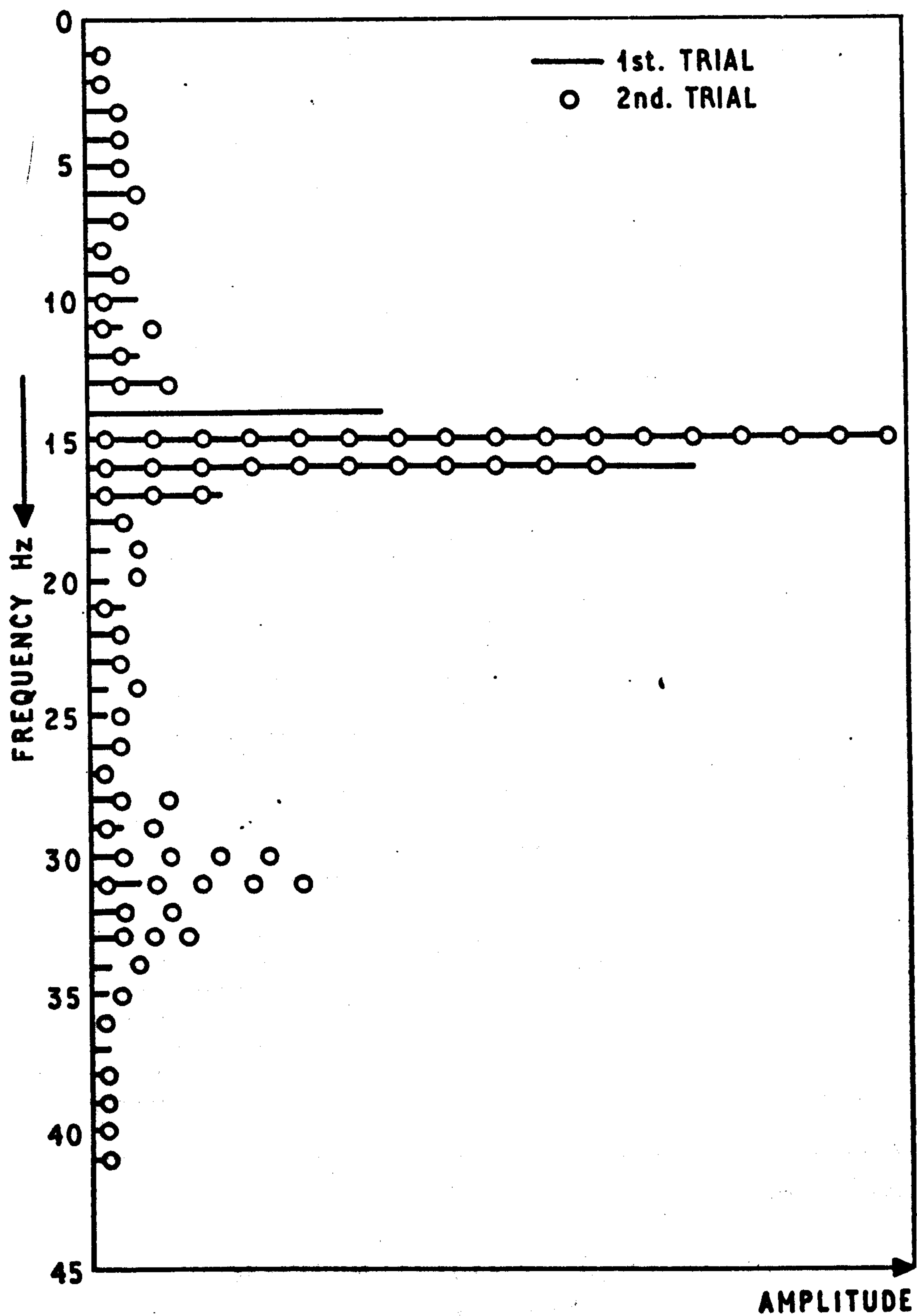
Fig. 5.10  
Hot wire anemometer  
calibration curve





SPECTRUM ANALYSIS,  $R_e = 0.27 \times 10^5$   
 $\theta = 50^\circ$

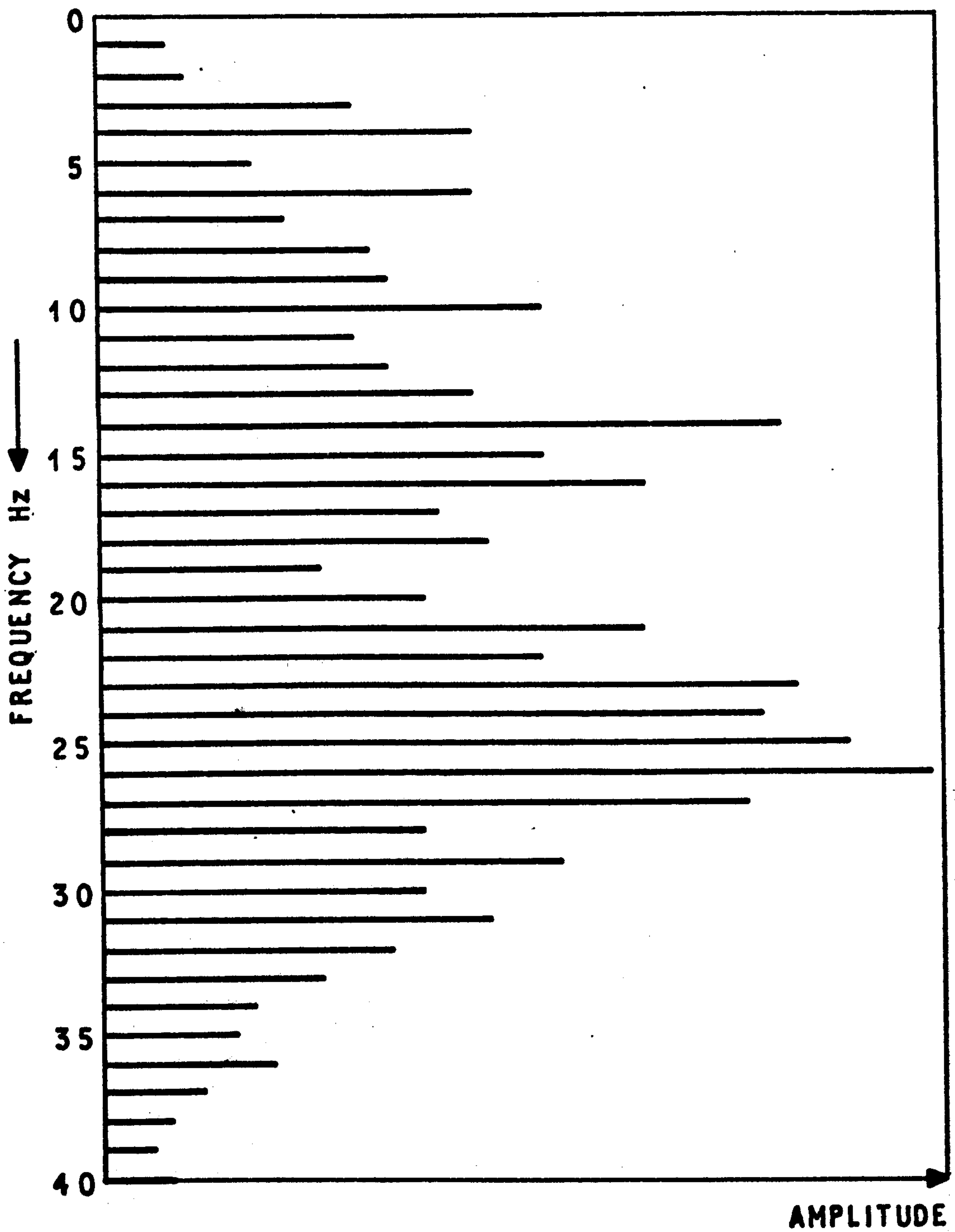
FIG. 6.1



SPECTRUM ANALYSIS ,  $R_e = 0.27 \times 10^5$   
 $\theta = 160^\circ$

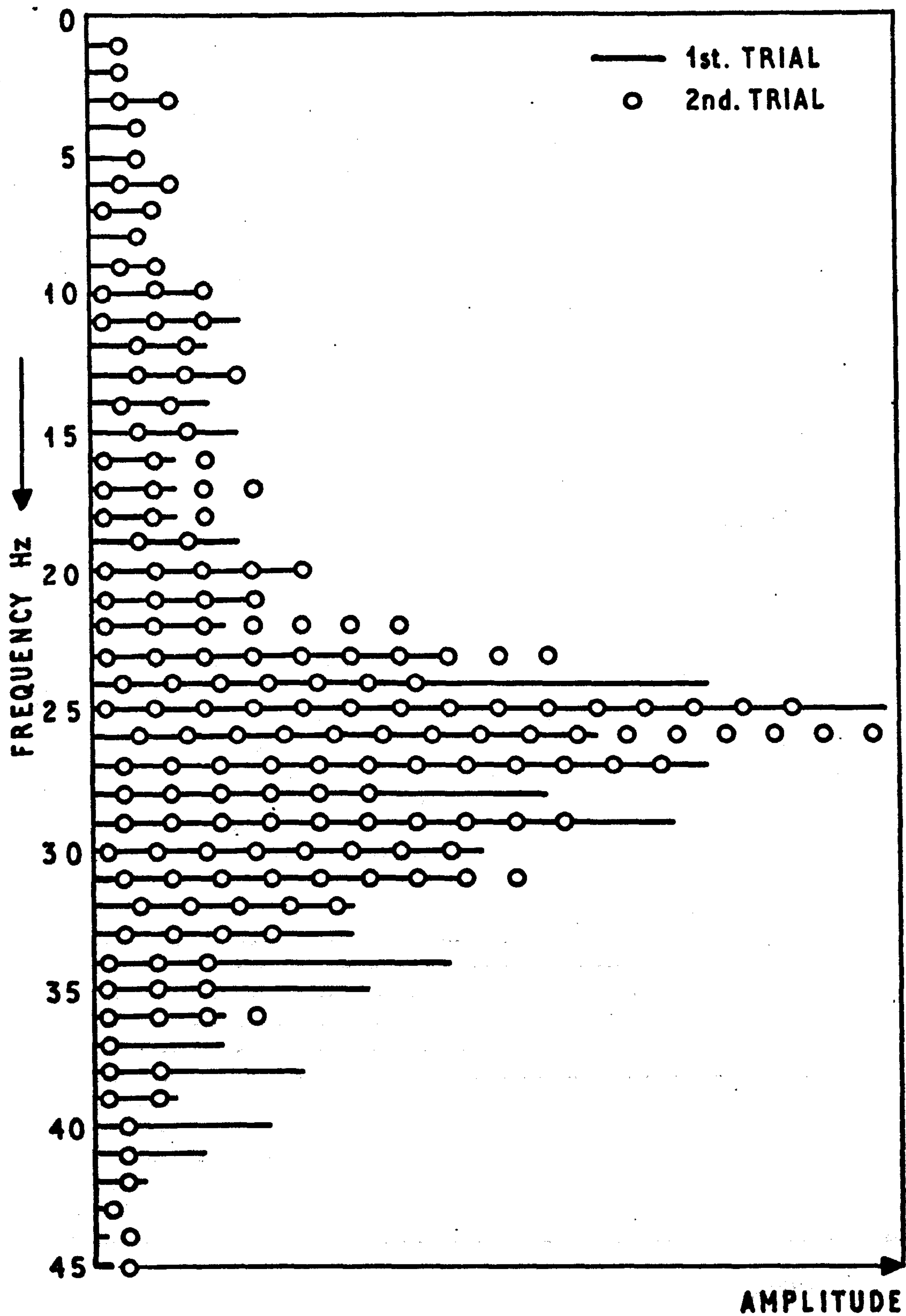
FIG. 6.2





SPECTRUM ANALYSIS ,  $R_e = 0.47 \times 10^5$   
 $\theta = 50^\circ$

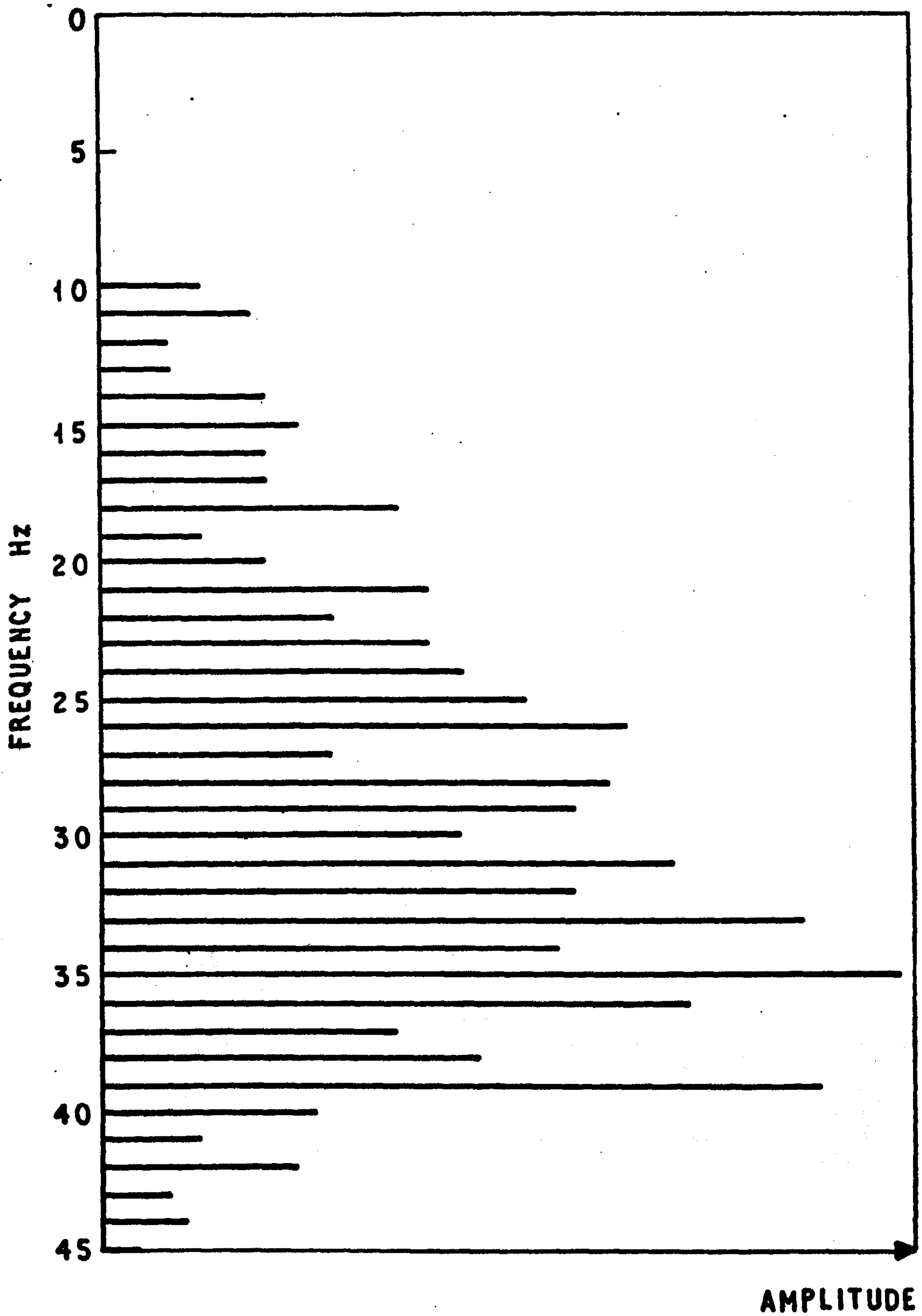
FIG.6.3



SPECTRUM ANALYSIS,  $R_e = 0.47 \times 10^5$   
 $\theta = 160^\circ$

FIG. 6.4





SPECTRUM ANALYSIS,  $R_s = 0.7 \times 10^5$   
 $\theta = 160^\circ$

FIG. 6.5

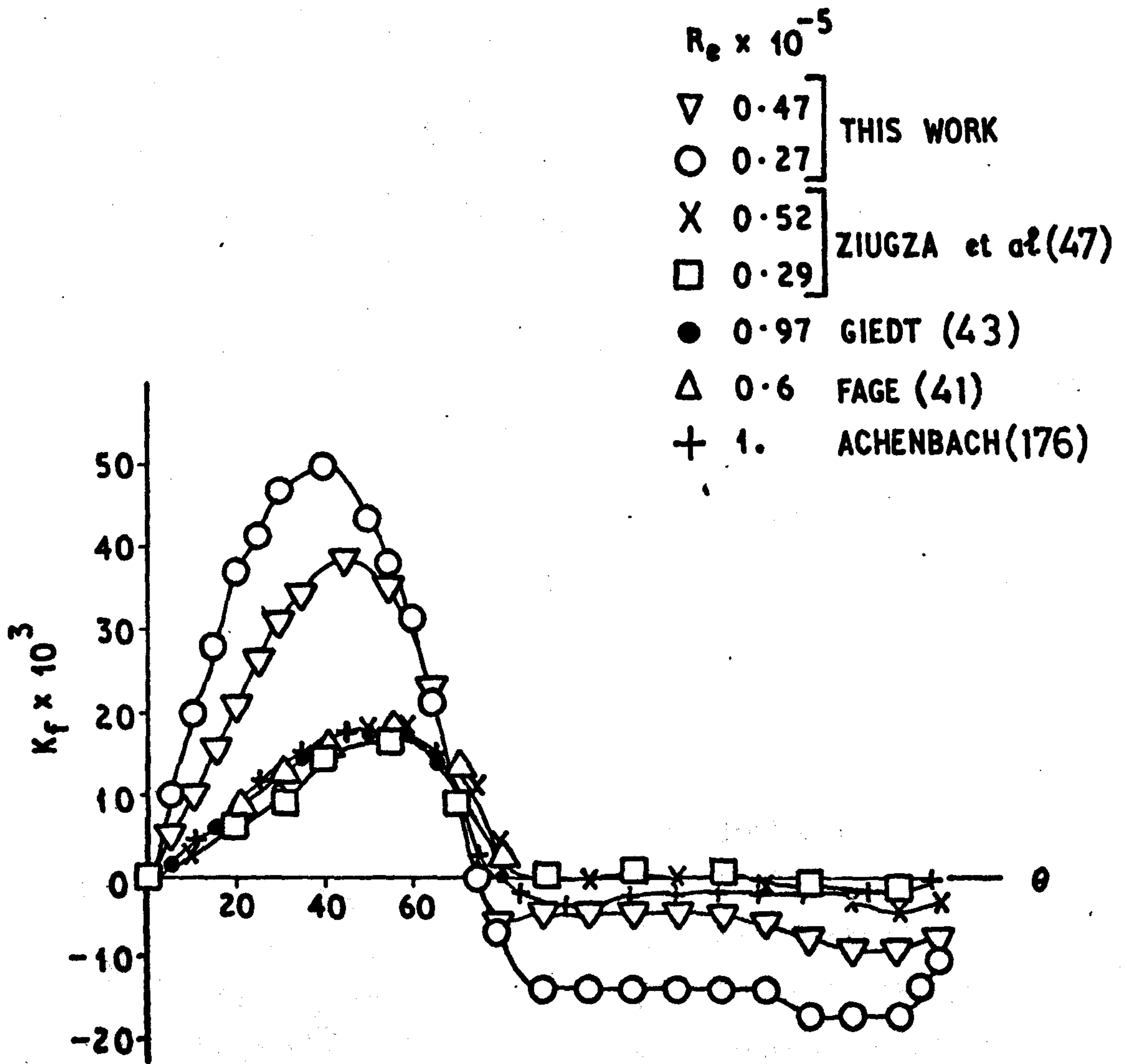


**Fig. 7.1.**  
SKIN FRICTION DISTRIBUTION AROUND  
A CIRCULAR CYLINDER



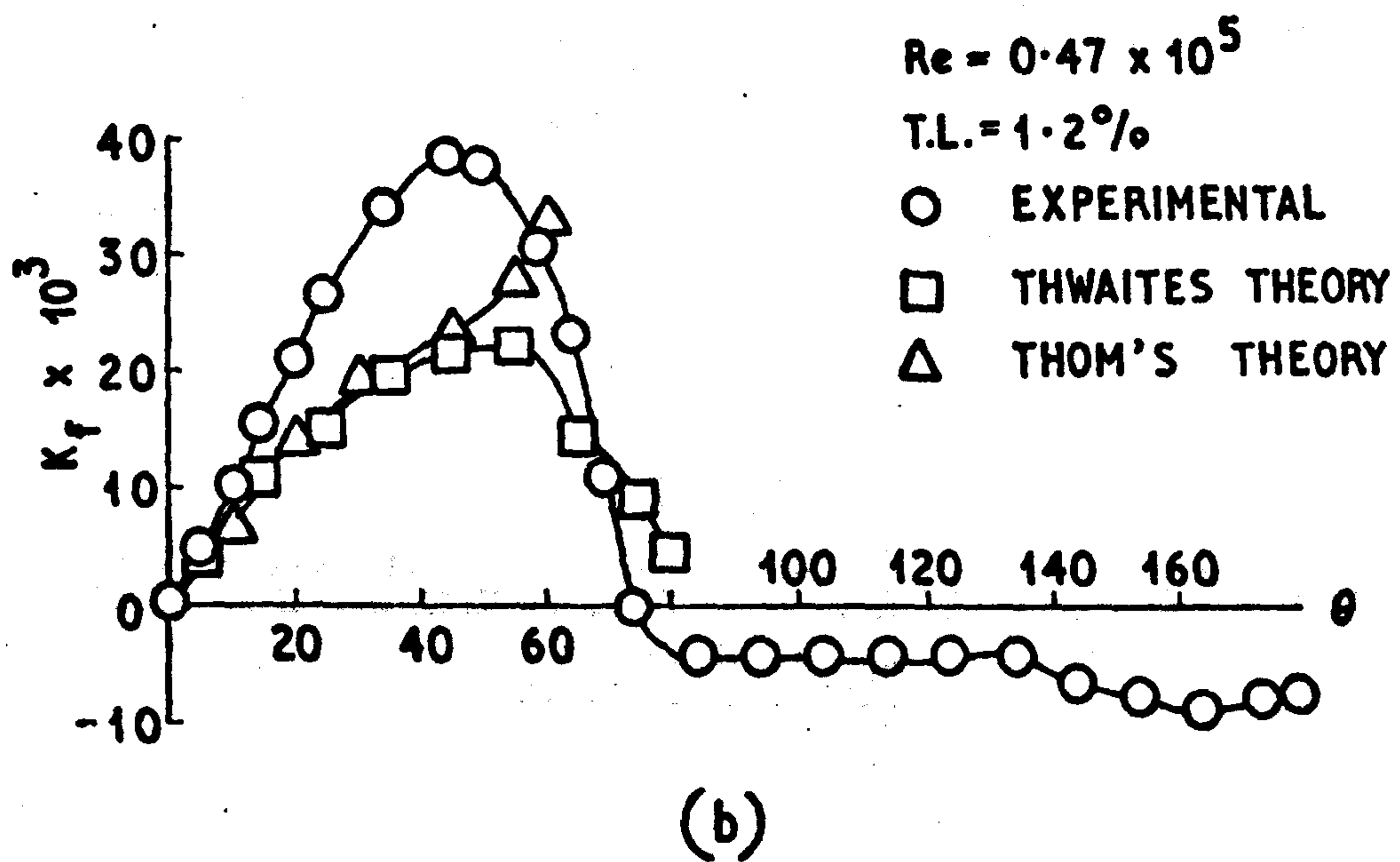
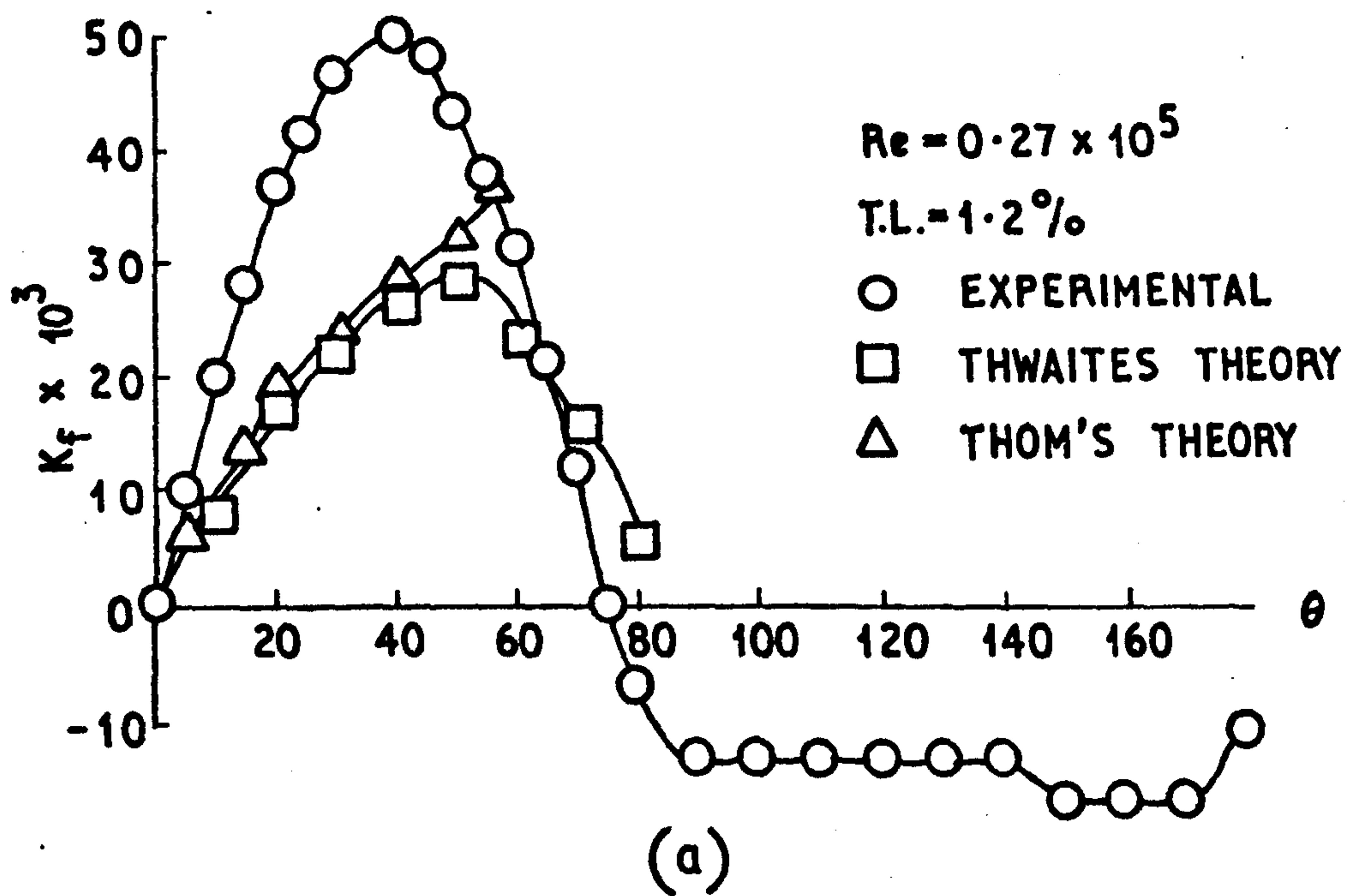
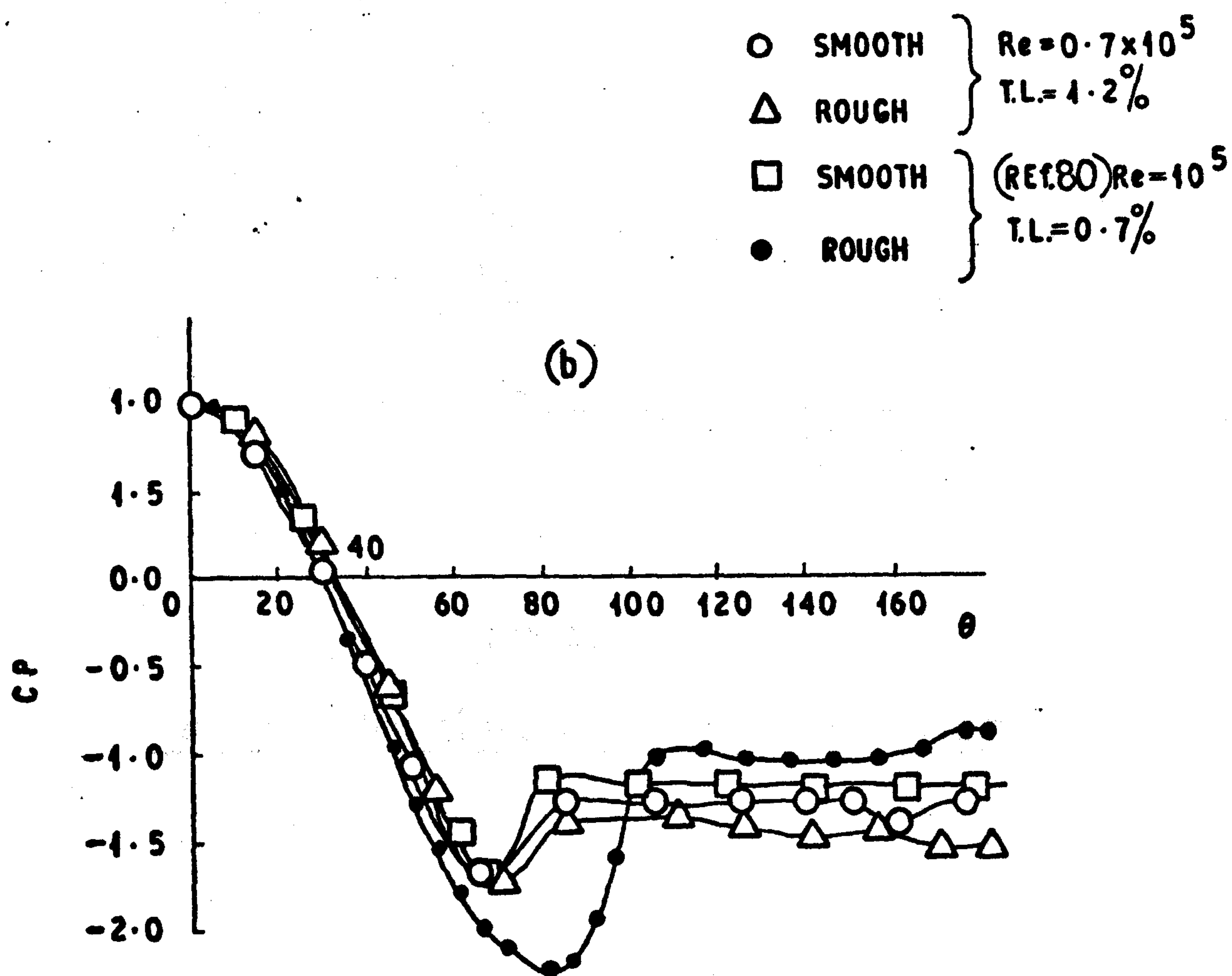
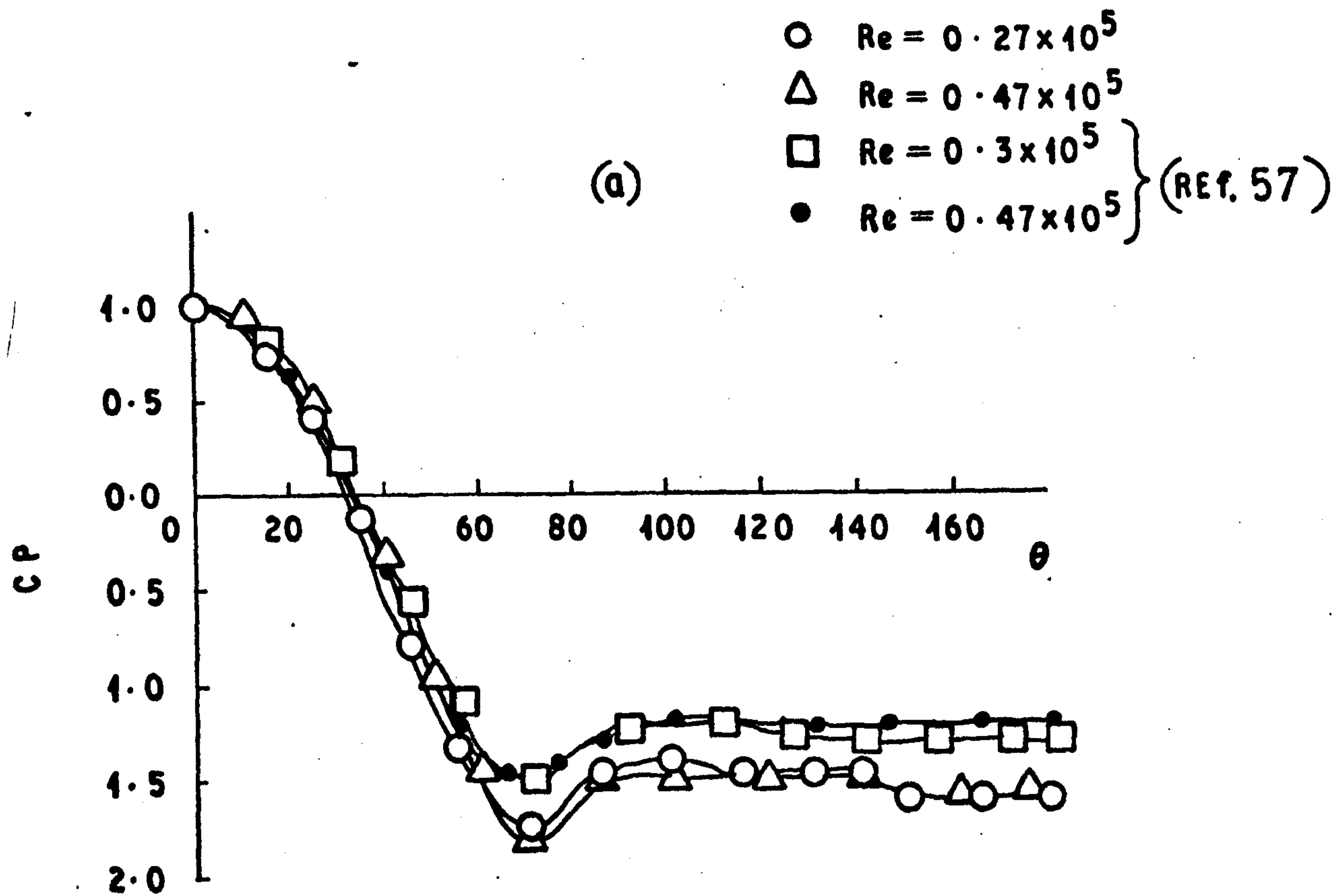


Fig. 7.2  
SKIN FRICTION ON A SMOOTH CYLINDER







**Fig. 7.4**  
**NORMAL PRESSURE AROUND A ROUGH CIRCULAR**  
**CYLINDER IN A CROSS FLOW**

x	SMOOTH	} $R_e = 0.27 \times 10^5$
$\Delta$	ROUGH	
o	SMOOTH	} REF. (57)
$\nabla$	ROUGH	
		} $R_e = 0.3 \times 10^5$

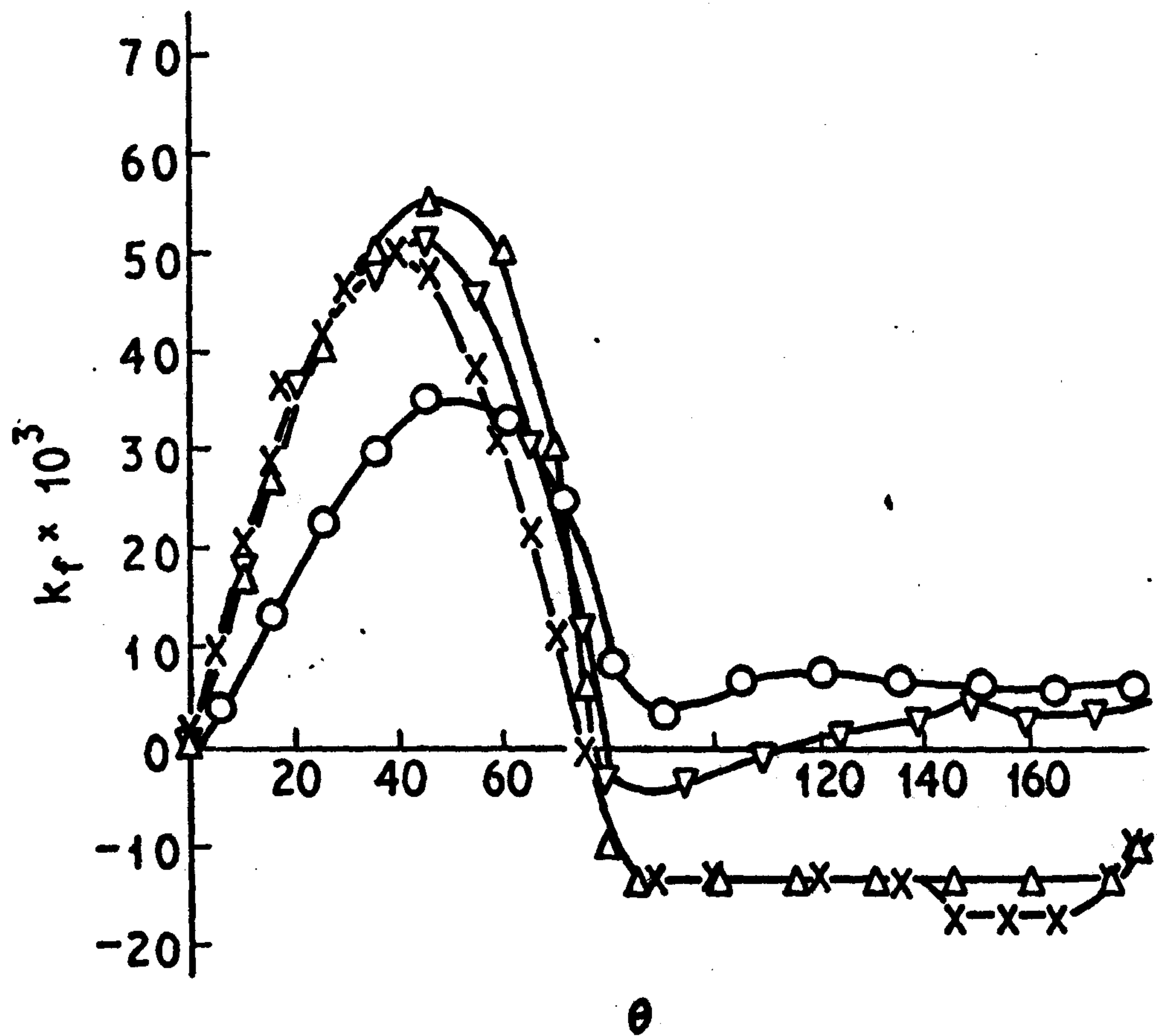


Fig.7.5

Effect of Roughness on Skin Friction



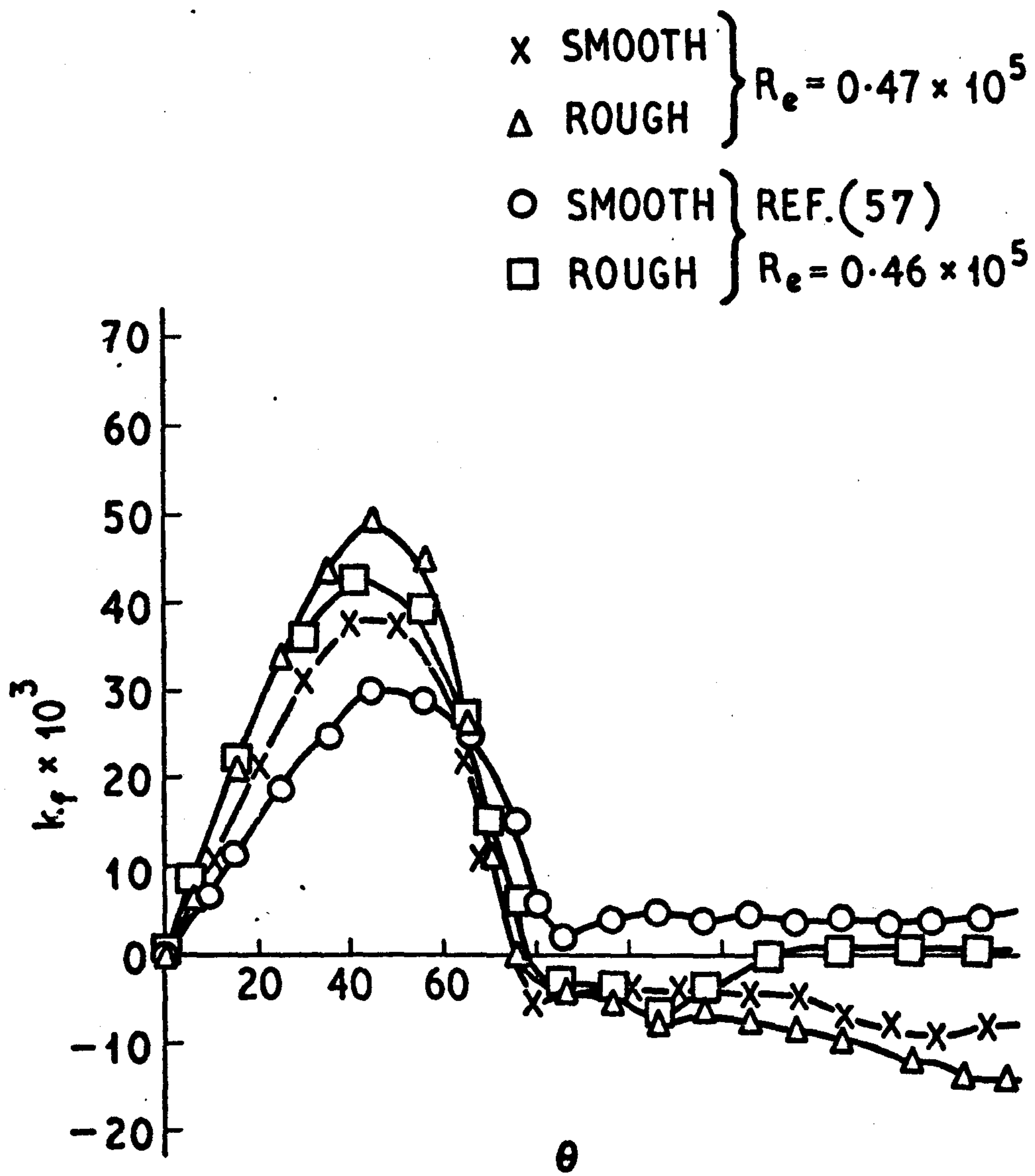


Fig. 7.6

Effect of Roughness on Skin Friction

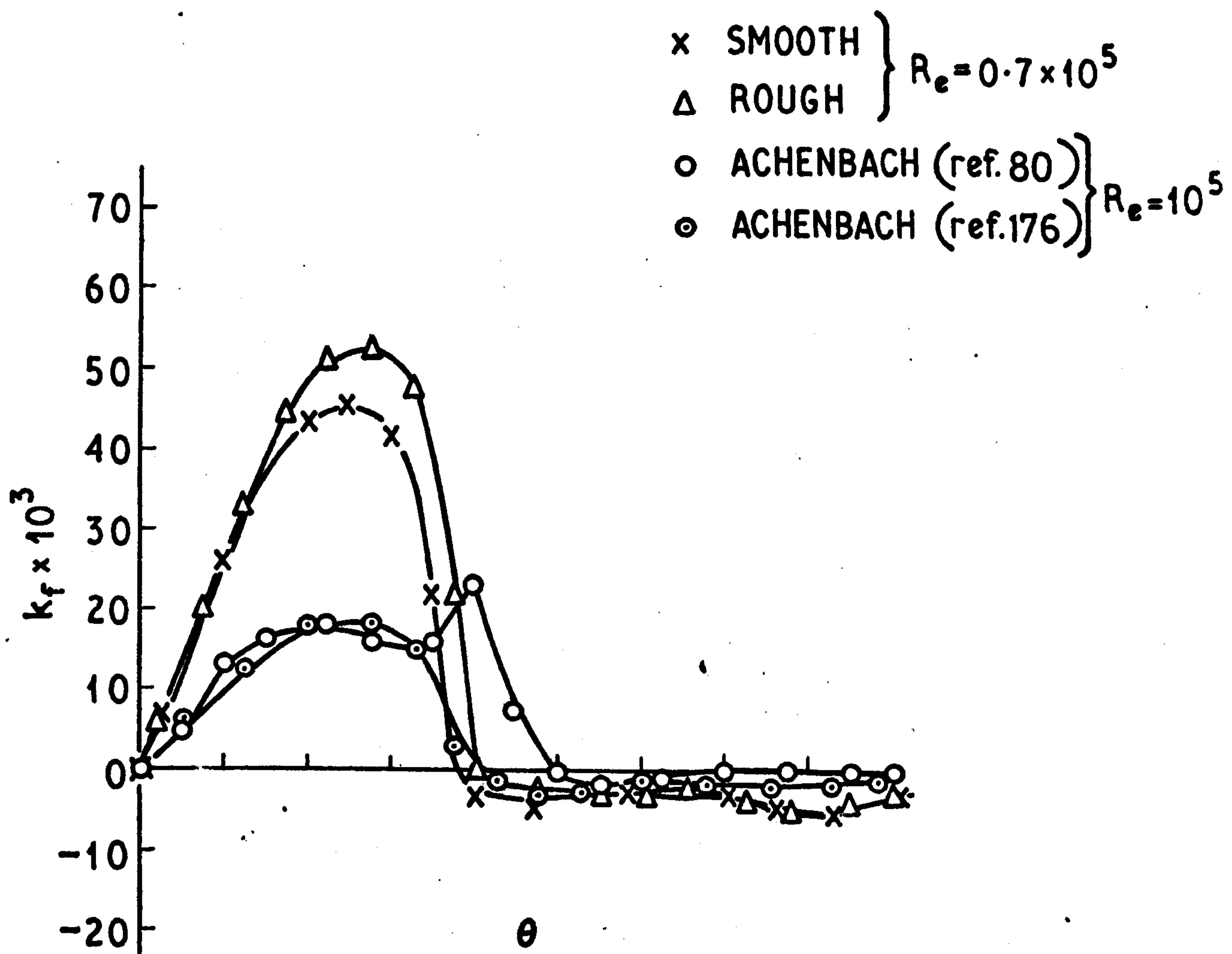


Fig. 7.7

Effect of Roughness on Skin Friction



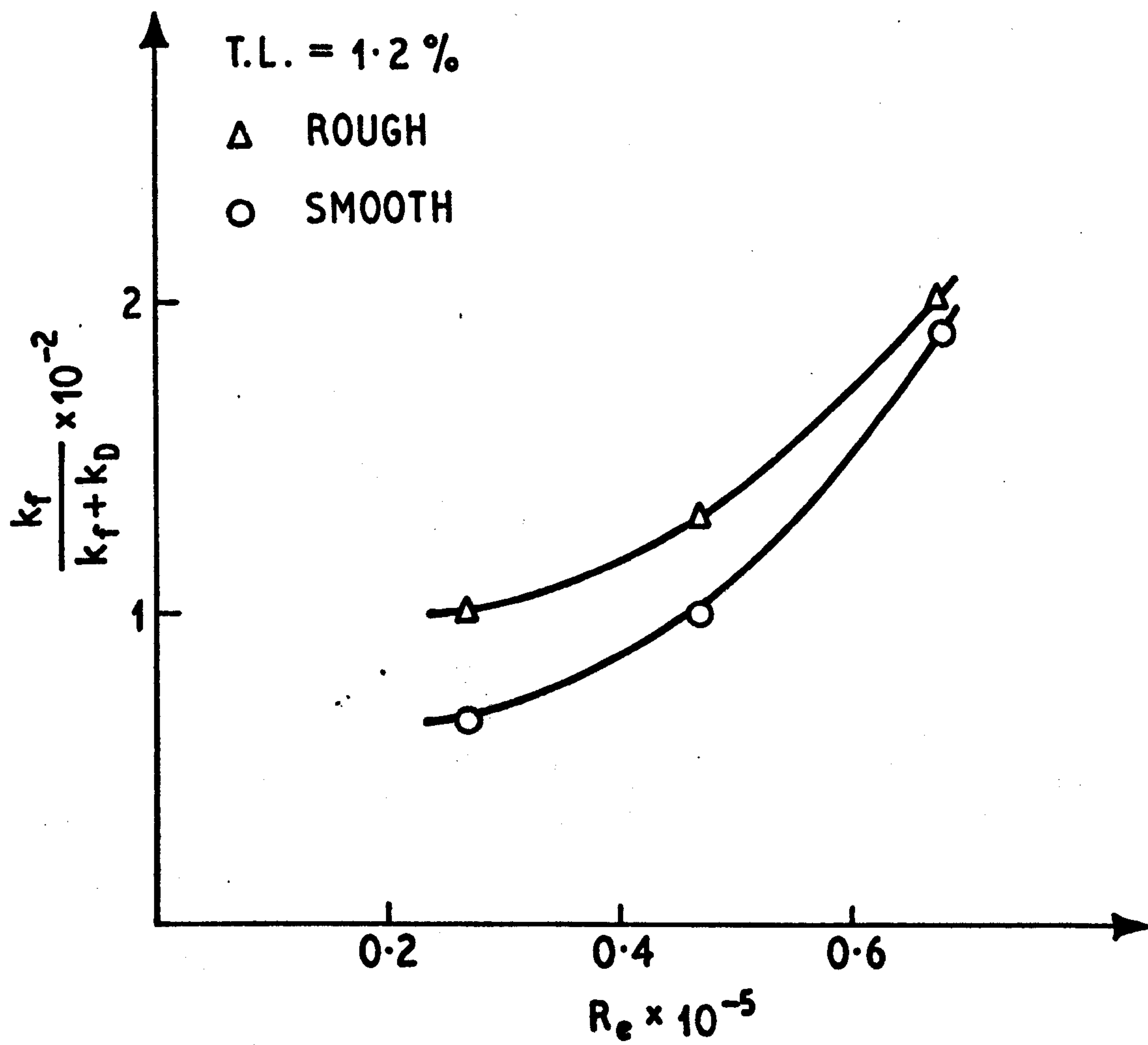


Fig. 7.8

Percentage Effect of Roughness on  
Friction Drag.

x	T.L. % = 1.2	} SMOOTH	} $R_e = 0.27 \times 10^5$
○	T.L. % = 6		
Δ	T.L. % = 1.2	} ROUGH	
●	T.L. % = 6		

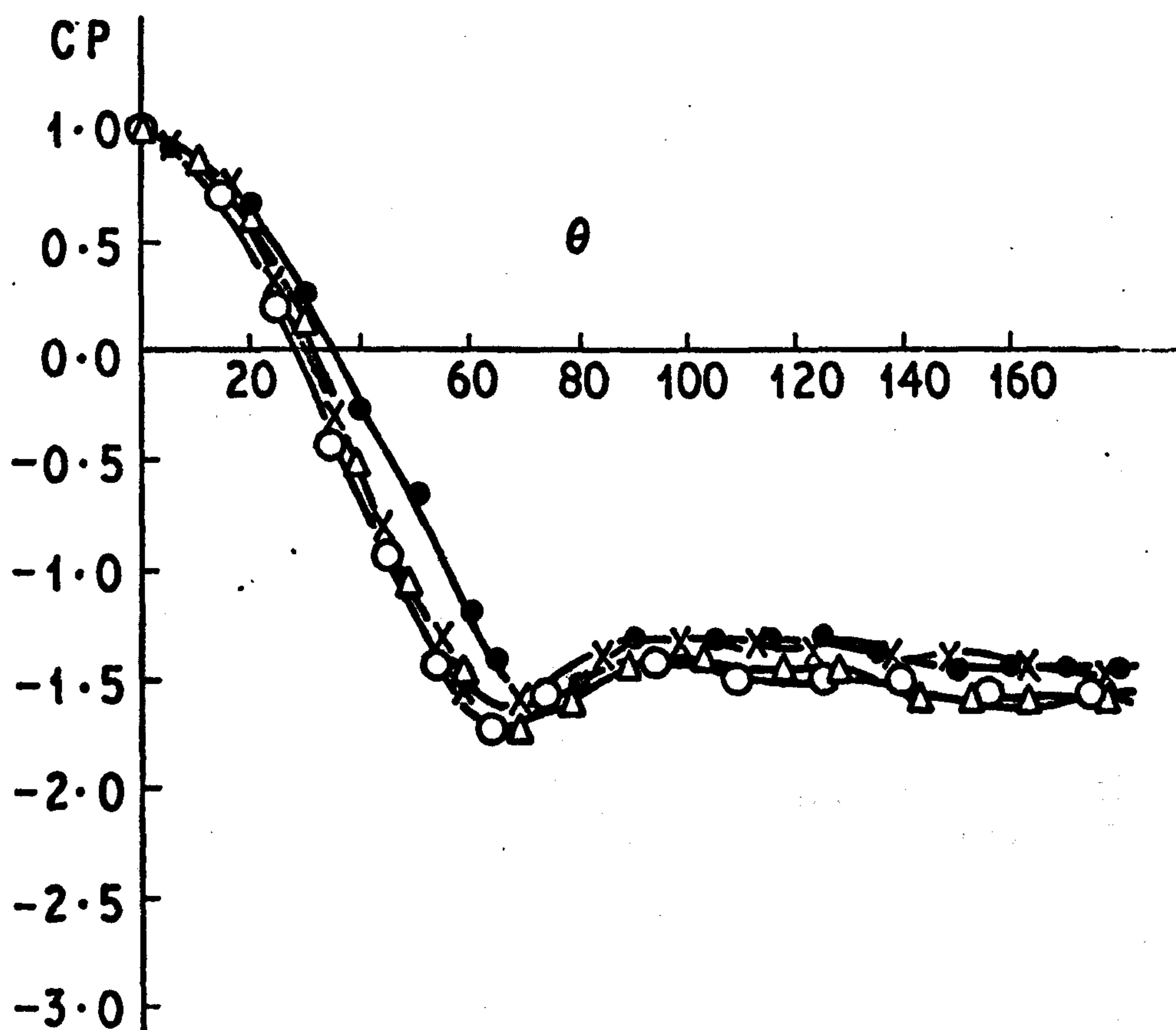


Fig. 7.9

Effect of Turbulence and Surface Roughness  
on Pressure Distribution



$\times$  T.L.% = 1.2  
 $\circ$  T.L.% = 6  
 $\Delta$  T.L.% = 1.2  
 $\bullet$  T.L.% = 6

} SMOOTH  
 } ROUGH

$R_e = 0.27 \times 10^5$

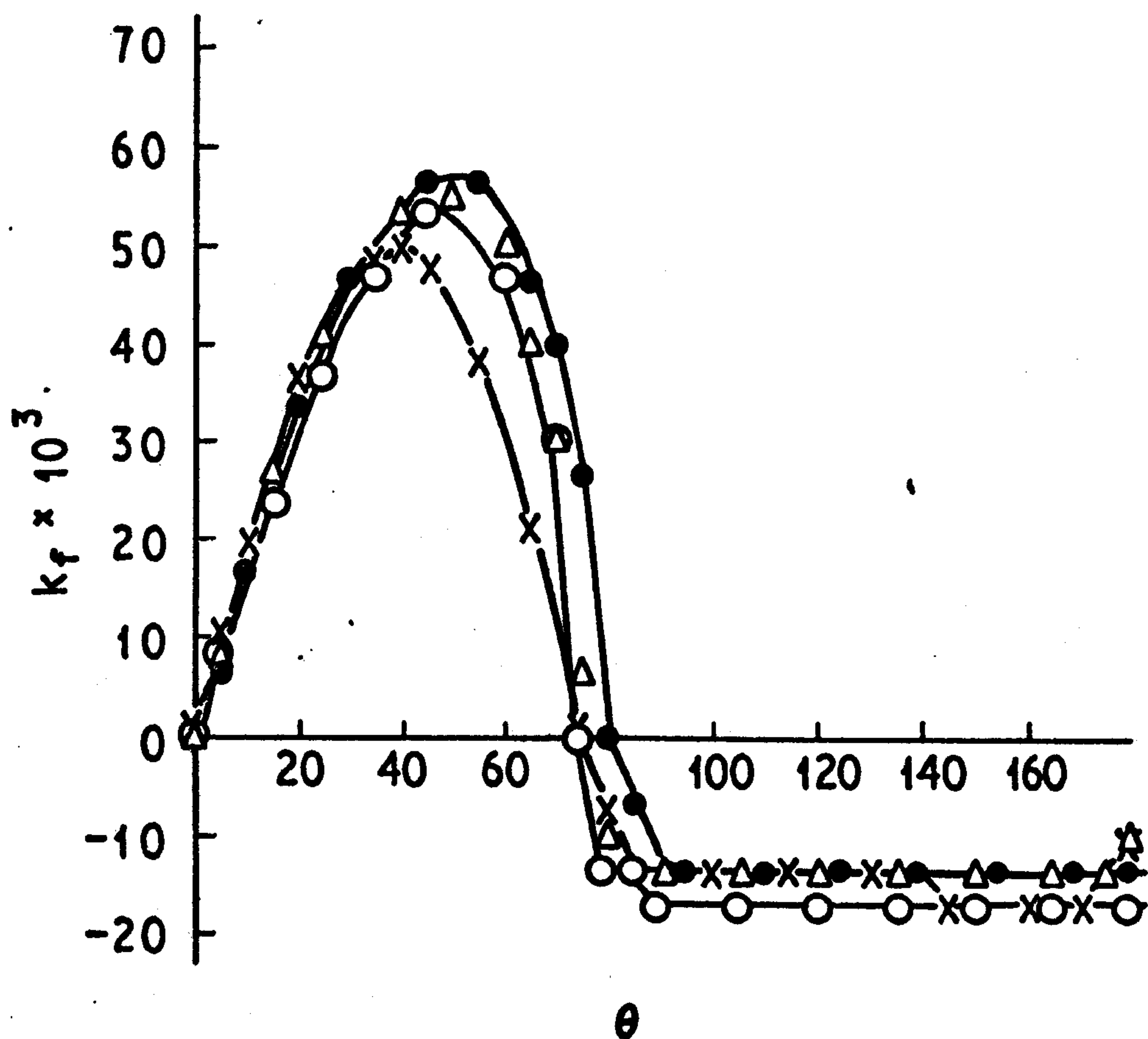


Fig. 7.10

Effect of Turbulence and Surface Roughness  
on Skin Friction

$$\begin{array}{l} \times \quad \text{T.L.\%} = 1.2 \\ \circ \quad \text{T.L.\%} = 6 \end{array} \left. \vphantom{\begin{array}{l} \times \\ \circ \end{array}} \right\} R_e = 0.47 \times 10^5$$

$$\begin{array}{l} \Delta \quad \text{T.L.\%} = 1.2 \\ \bullet \quad \text{T.L.\%} = 6 \end{array} \left. \vphantom{\begin{array}{l} \Delta \\ \bullet \end{array}} \right\} R_e = 0.7 \times 10^5$$

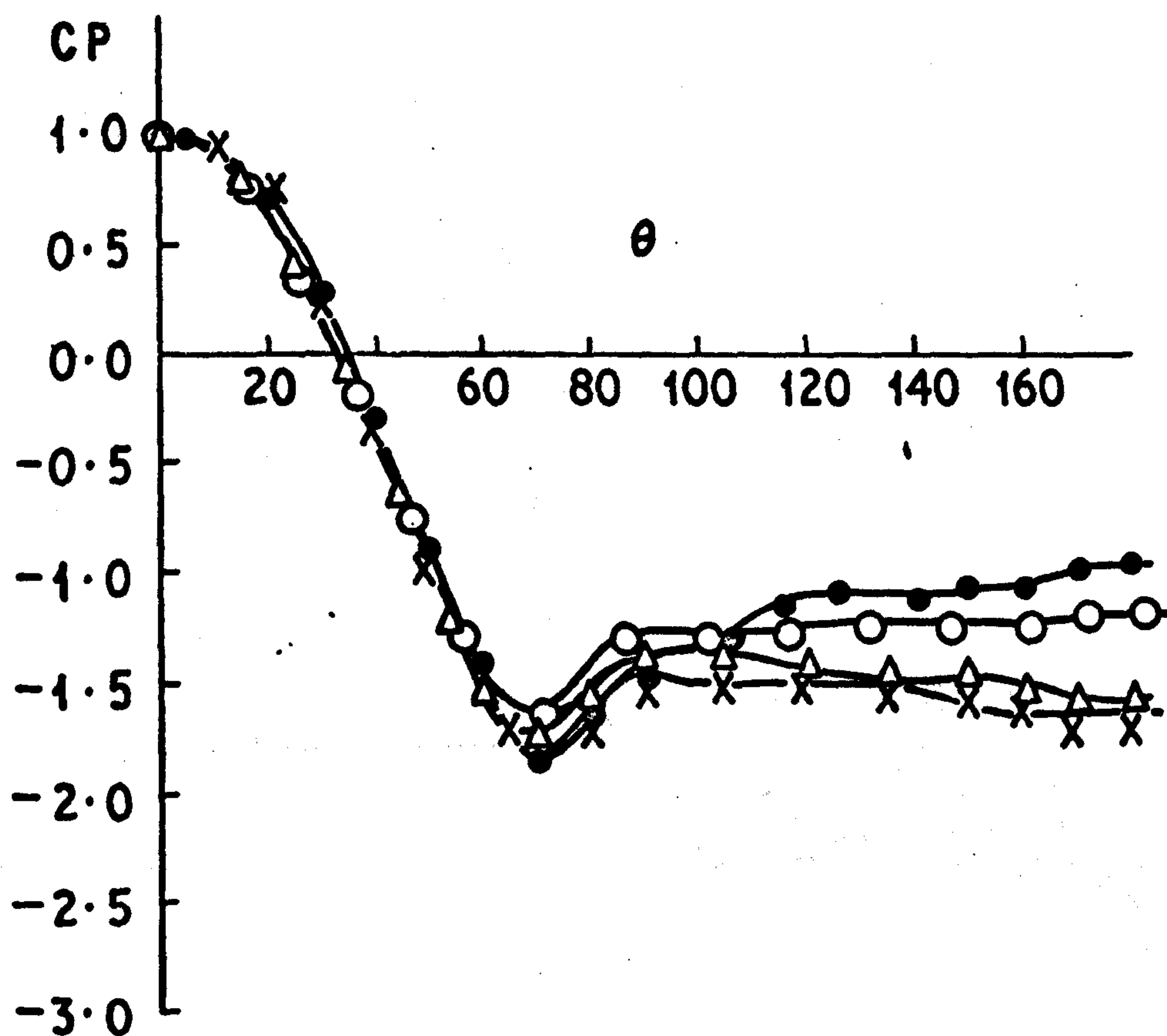


Fig. 7.11

Effect of Turbulence on Pressure Distribution  
for Rough Surface



$\times$  T.L.% = 1.2  $\left. \vphantom{\begin{matrix} \times \\ \circ \\ \Delta \\ \bullet \end{matrix}} \right\} R_e = 0.47 \times 10^5$   
 $\circ$  T.L.% = 6  
 $\Delta$  T.L.% = 1.2  $\left. \vphantom{\begin{matrix} \times \\ \circ \\ \Delta \\ \bullet \end{matrix}} \right\} R_e = 0.7 \times 10^5$   
 $\bullet$  T.L.% = 6

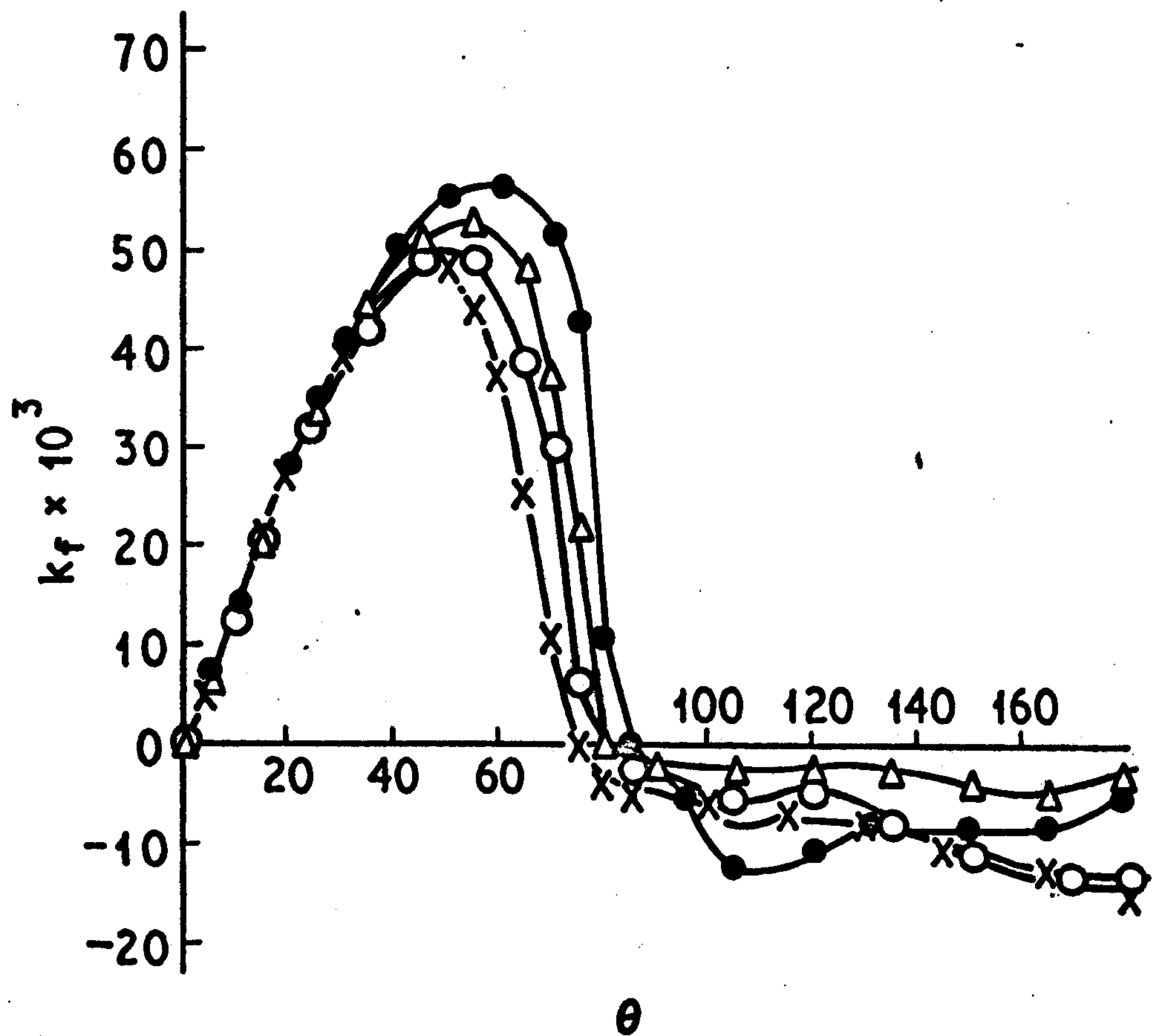


Fig. 7.12

Effect of Turbulence on Skin Friction  
for Rough Surface

$$\left. \begin{array}{l} \times \text{ T.L.\%} = 1.2 \\ \Delta \text{ T.L.\%} = 6 \end{array} \right\} R_e = 0.47 \times 10^5$$

$$\left. \begin{array}{l} \circ \text{ NORMAL STREAM} \\ \bullet \text{ BEHIND ROPE NETTING} \end{array} \right\} \begin{array}{l} \text{REF. (23)} \\ R_e = 0.6 \times 10^5 \end{array}$$

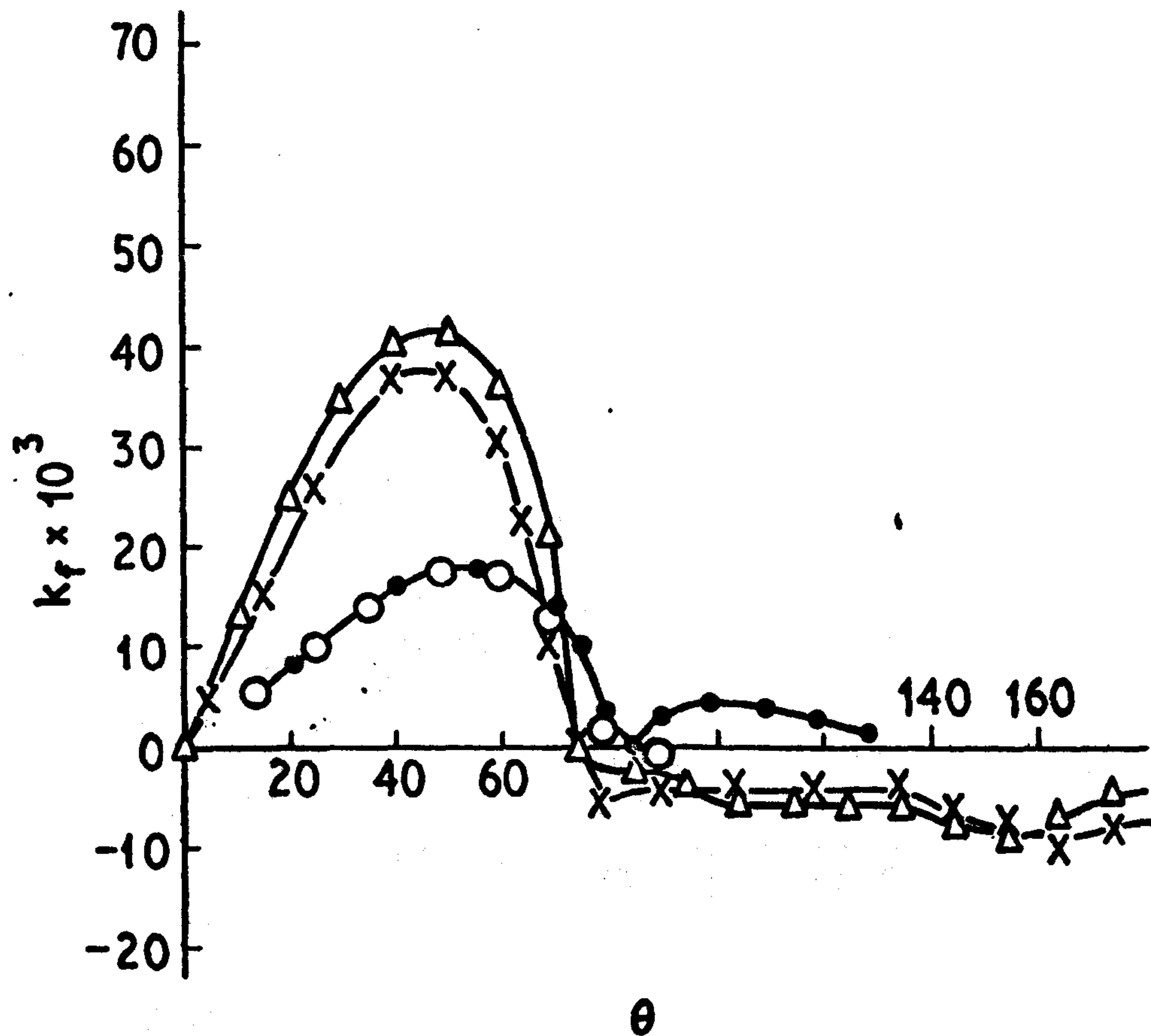


Fig. 7.13

Effect of Turbulence Level on Skin Friction



$$\left. \begin{array}{l} \times \text{ T.L. \%} = 1.2 \\ \Delta \text{ T.L. \%} = 6 \end{array} \right\} R_e = 0.68 \times 10^5$$

$$\left. \begin{array}{l} \circ \text{ BEHIND SCREEN } R_e = 0.97 \times 10^5 \\ \nabla \text{ BEHIND NET } R_e = 0.9 \times 10^5 \end{array} \right\} \text{REF. (43)}$$

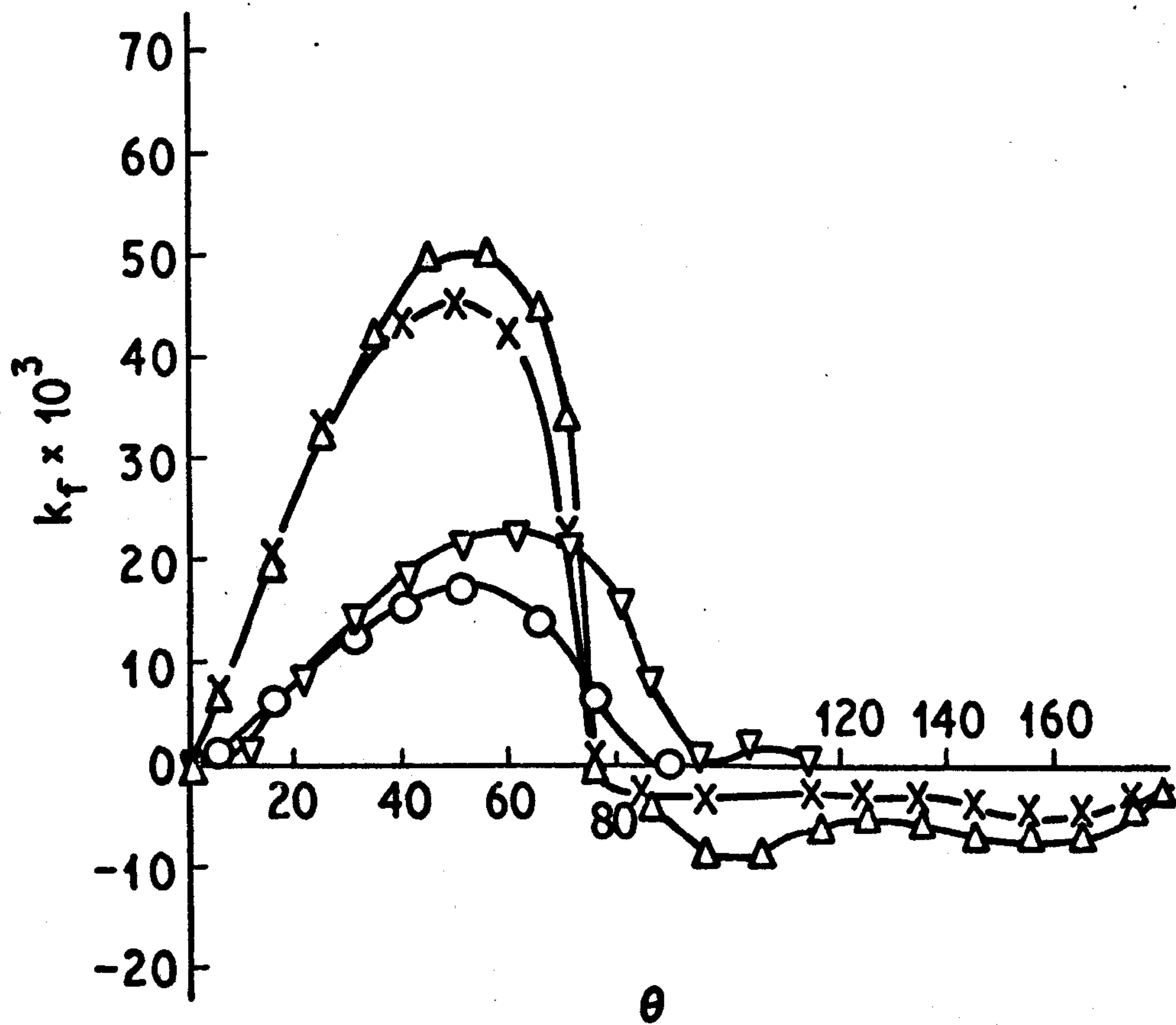
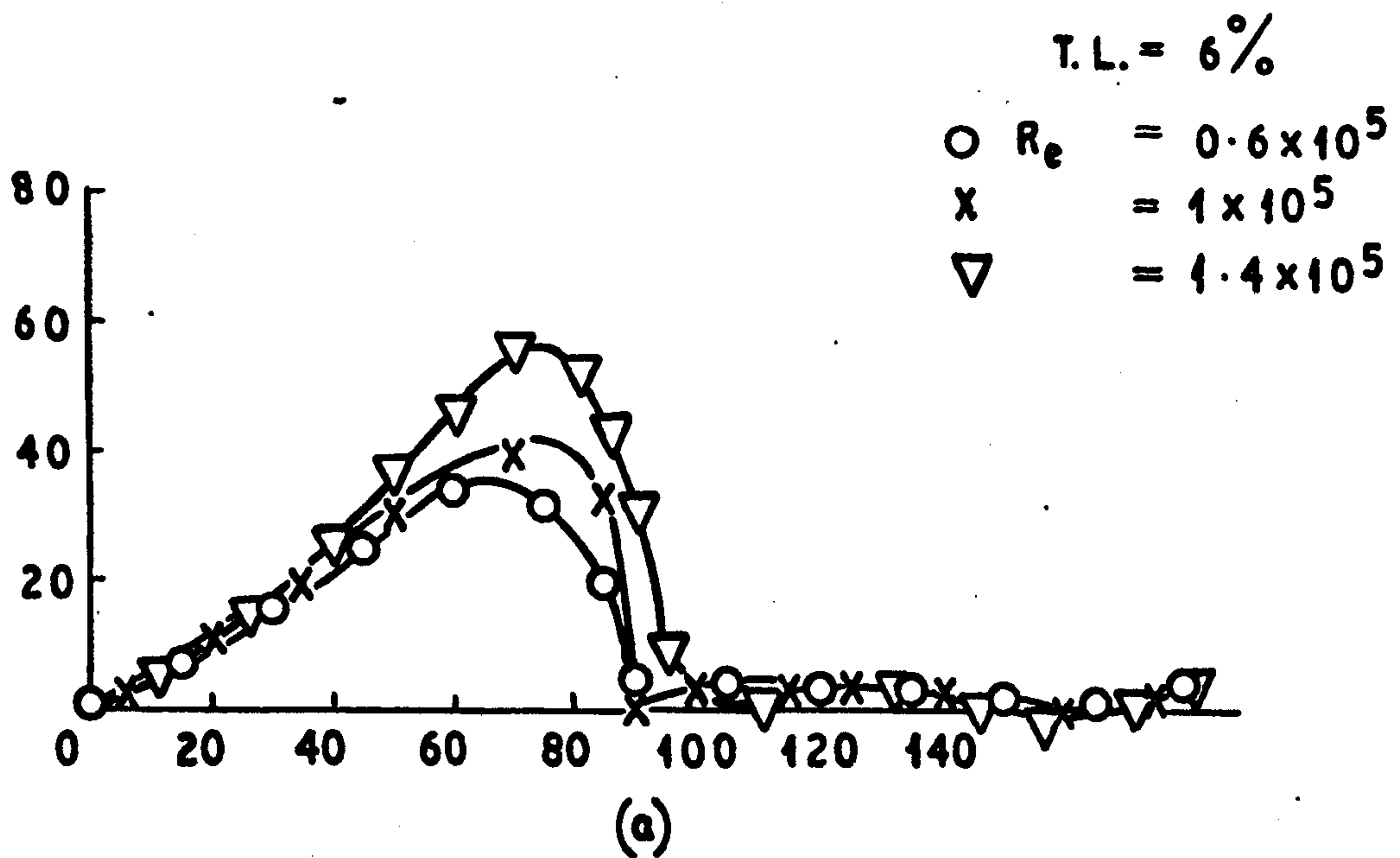
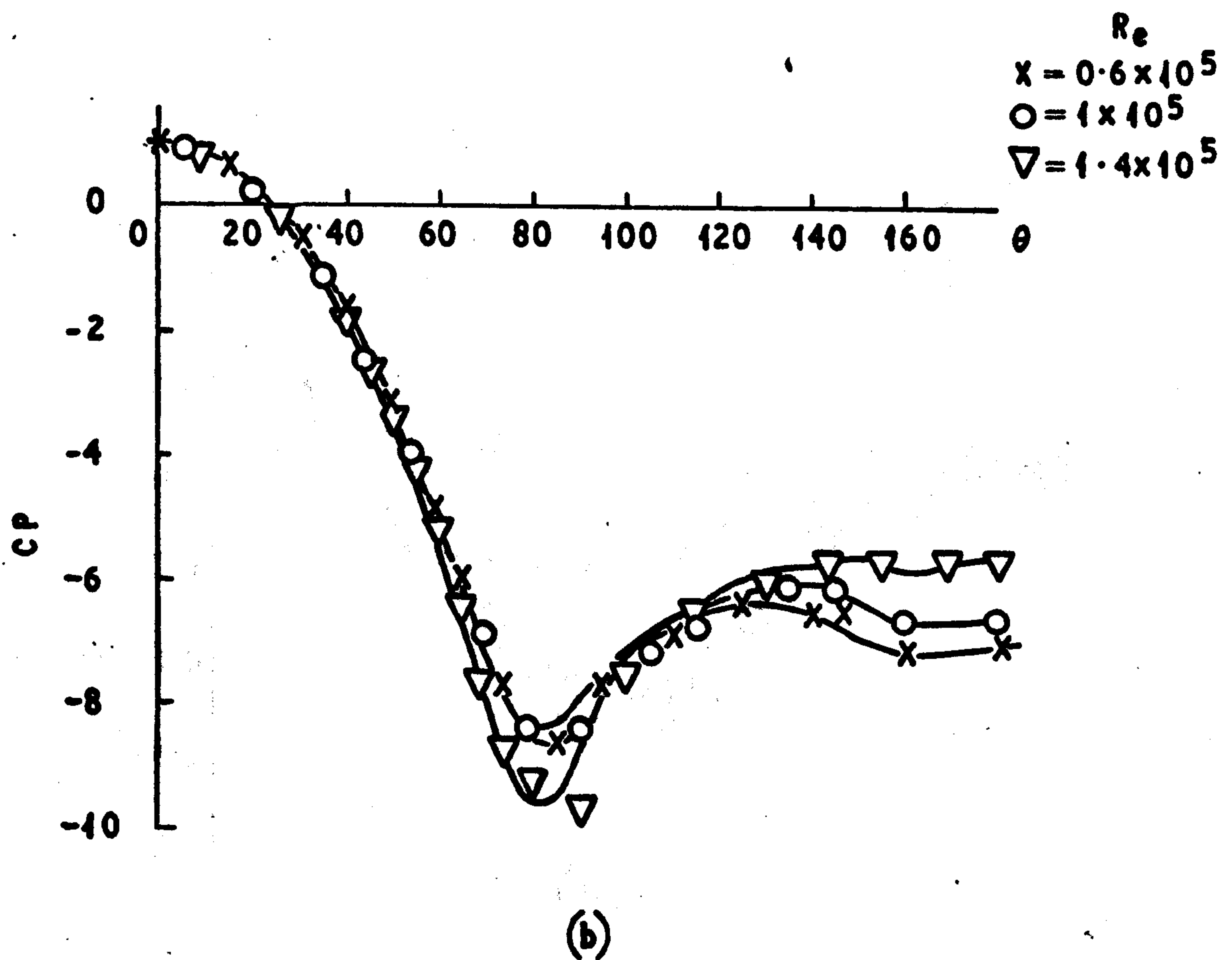


Fig. 7.14

Effect of Turbulence Level on Skin Friction



MEASURED SKIN FRICTION AROUND  
FIRST TUBE IN THE BANK



PRESSURE COEFFICIENT DISTRIBUTION AROUND  
FIRST ROW OF TUBE BANK  
FIG. 7.15



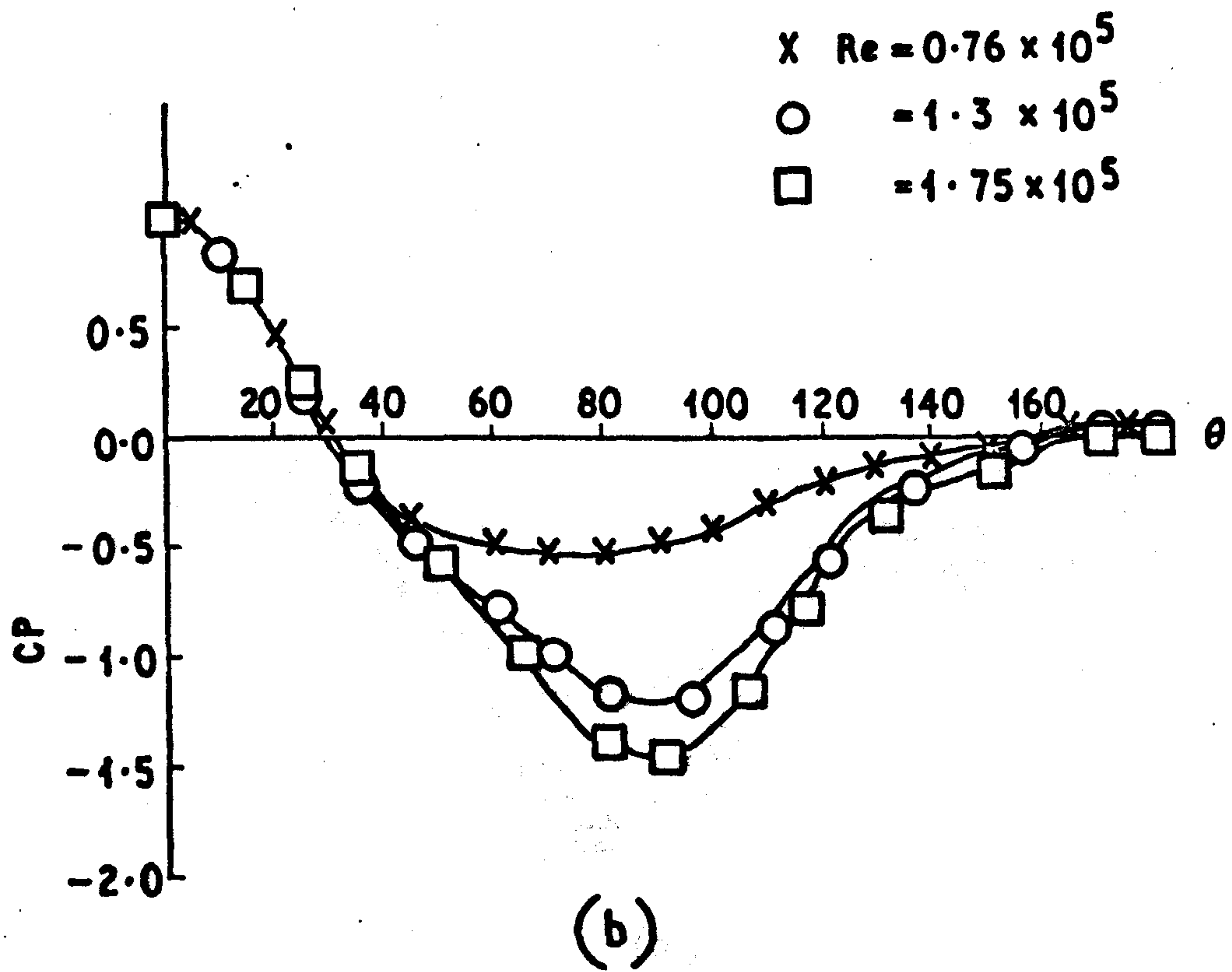
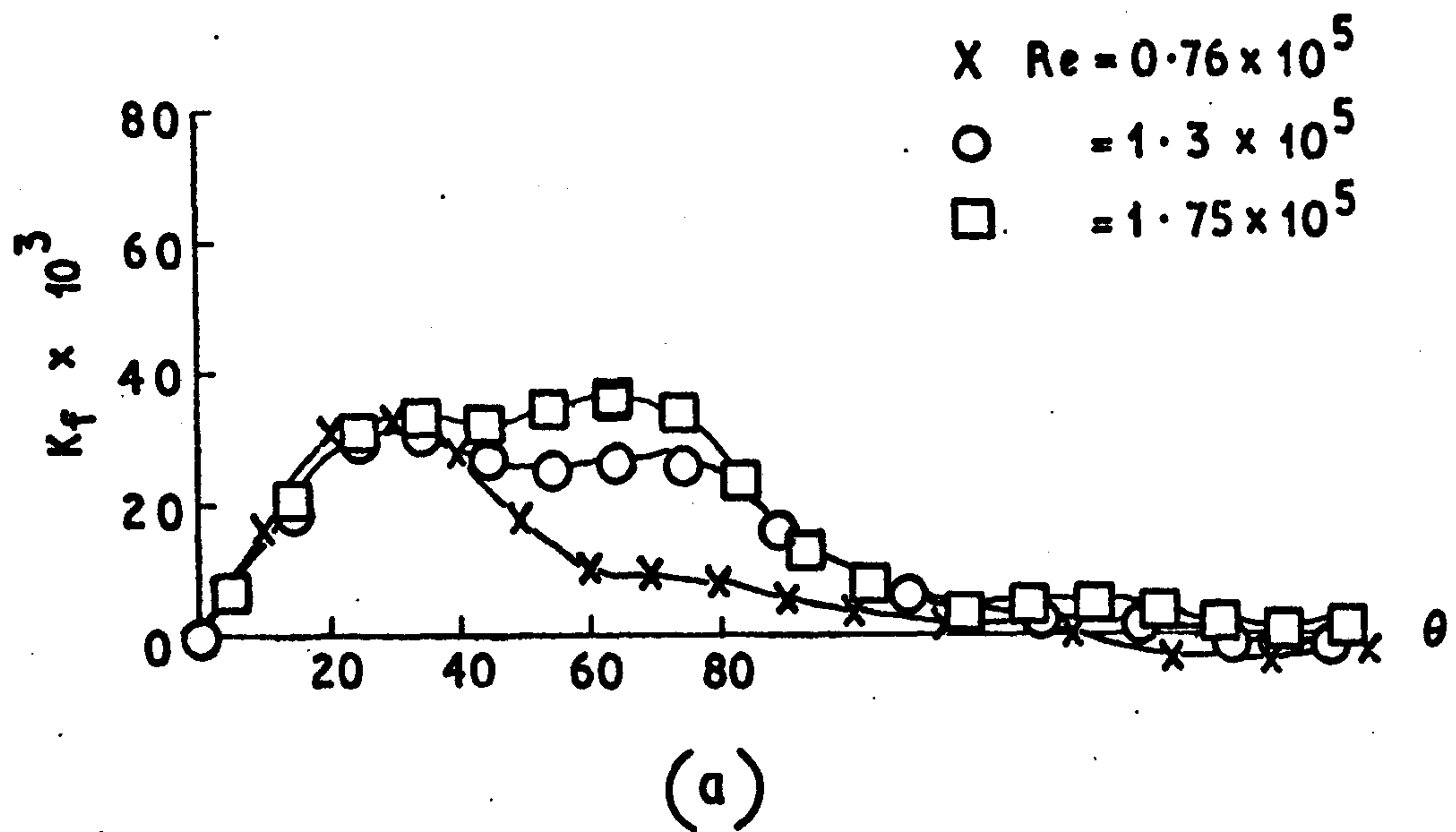
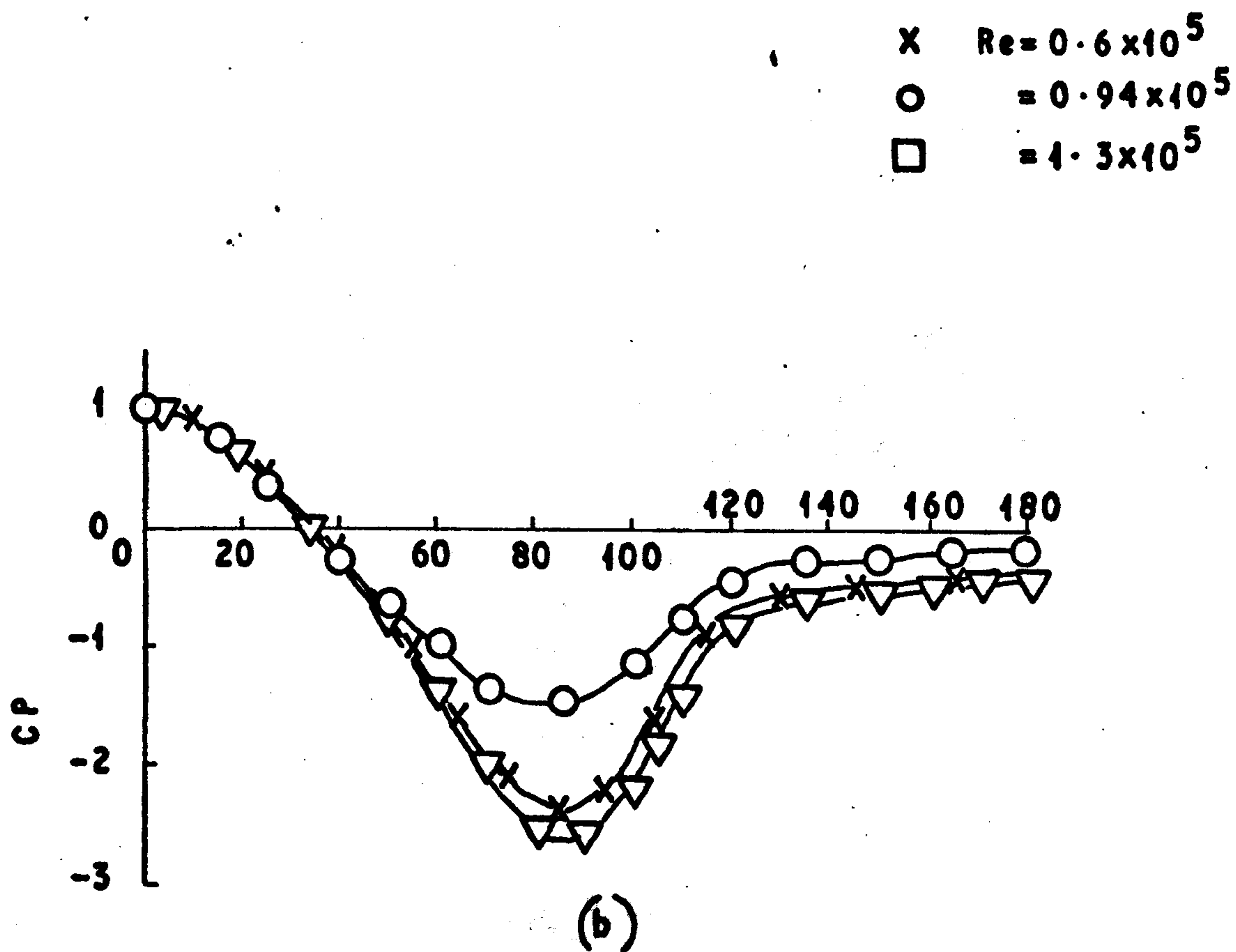
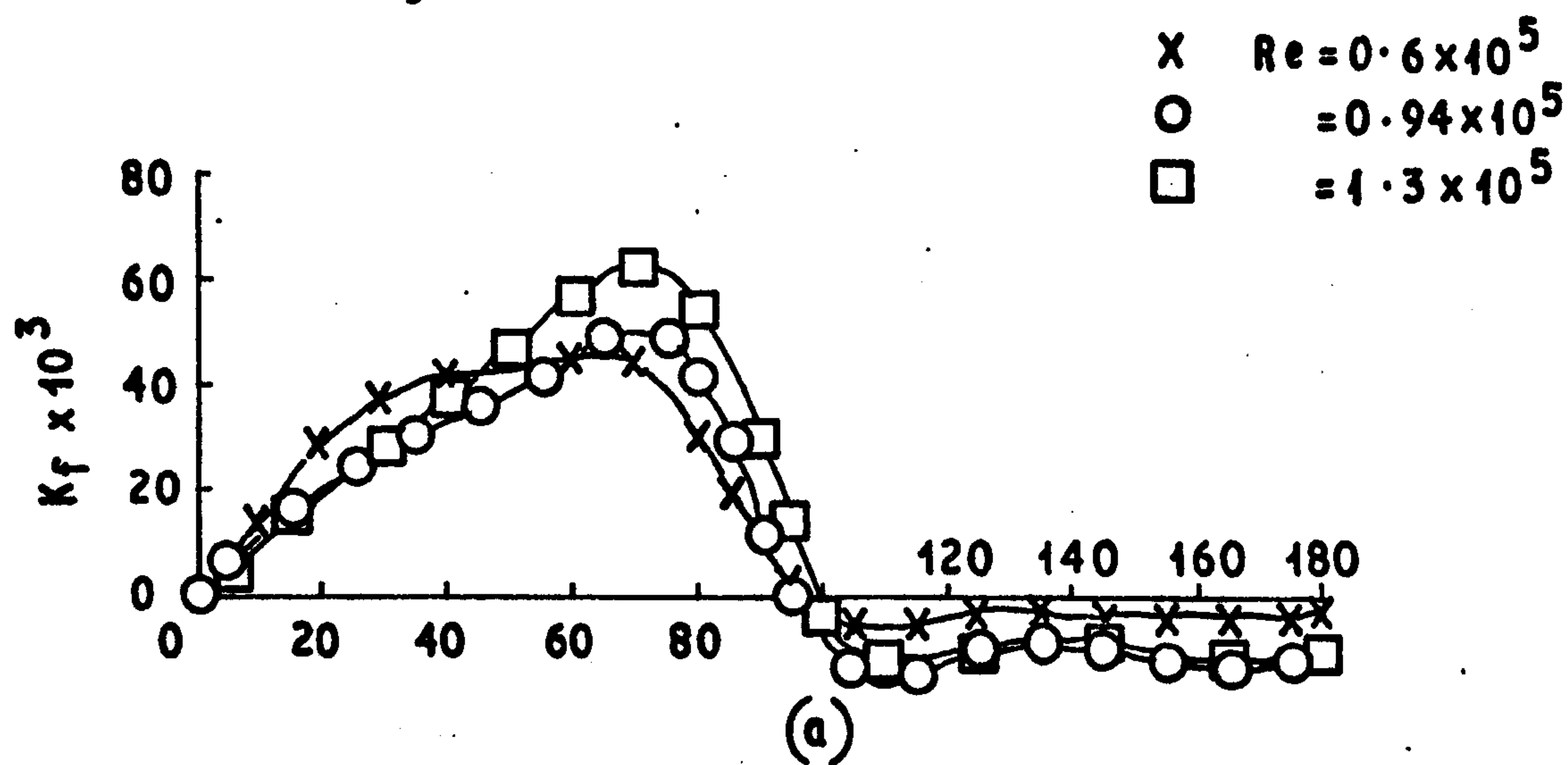


Fig. 7.16  
SKIN FRICTION DISTRIBUTION FOR THE  
SECOND ROW IN THE BANK



**Fig. 7.17**

**SKIN FRICTION DISTRIBUTION FOR THE THIRD ROW**  
**IN THE BANK**



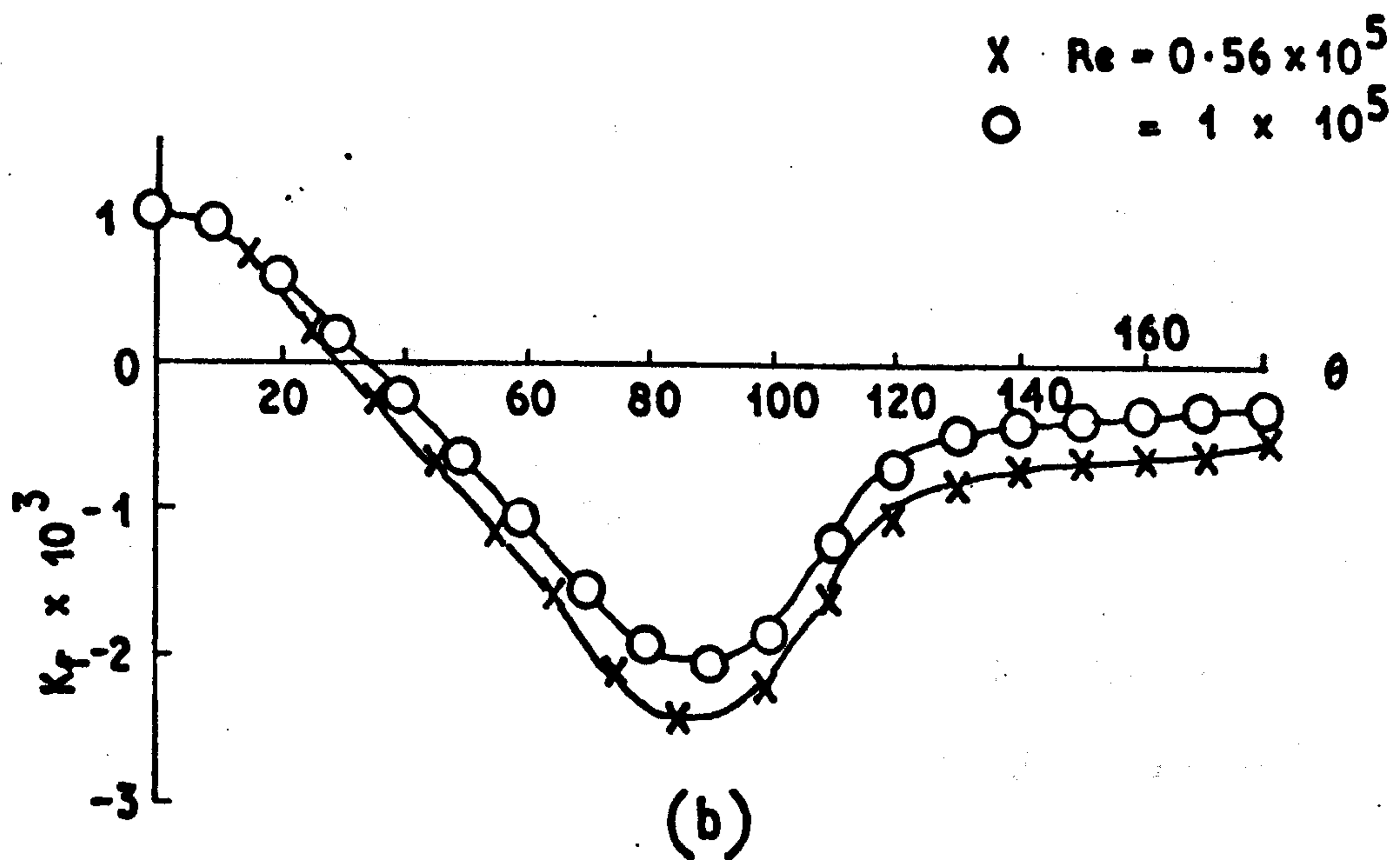
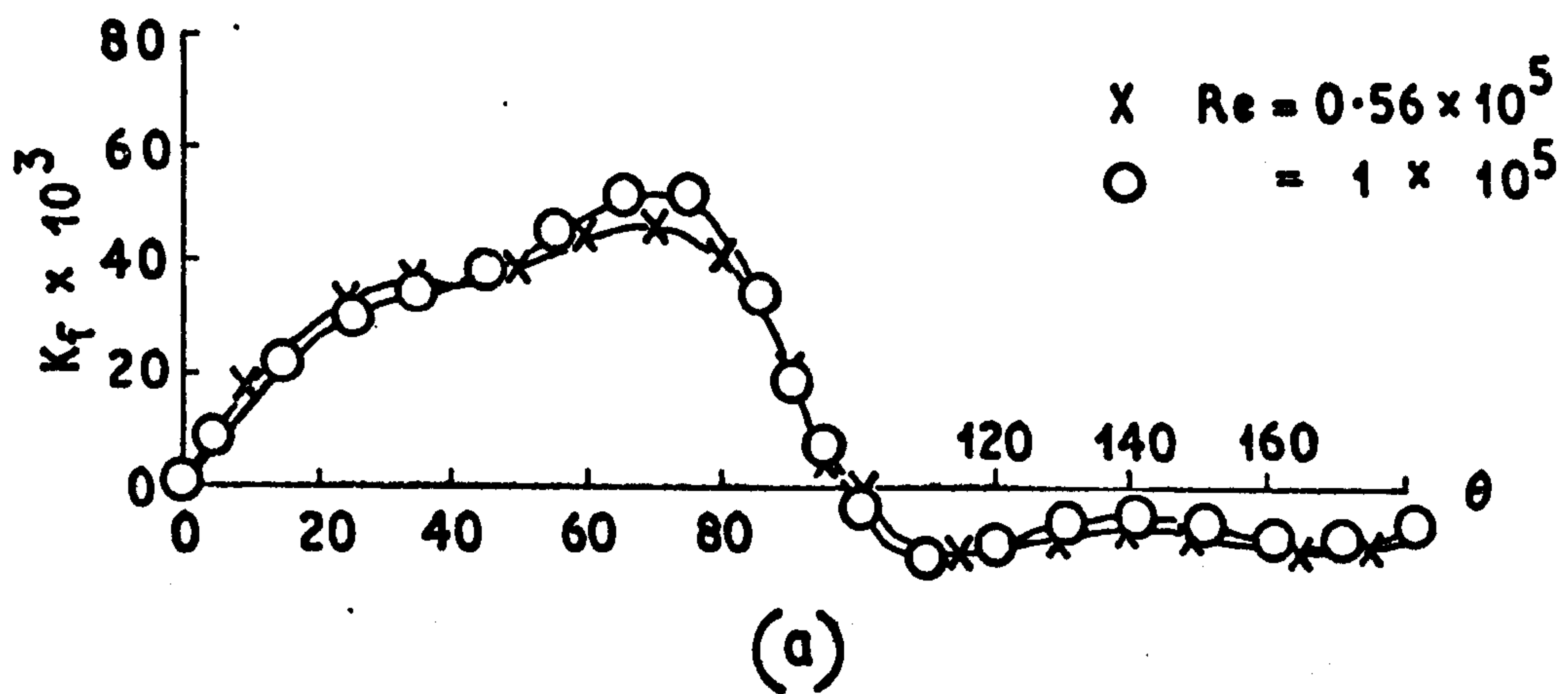


**Fig. 7.18**  
SKIN FRICTION DISTRIBUTION  
FOR THE FOURTH ROW IN THE BANK

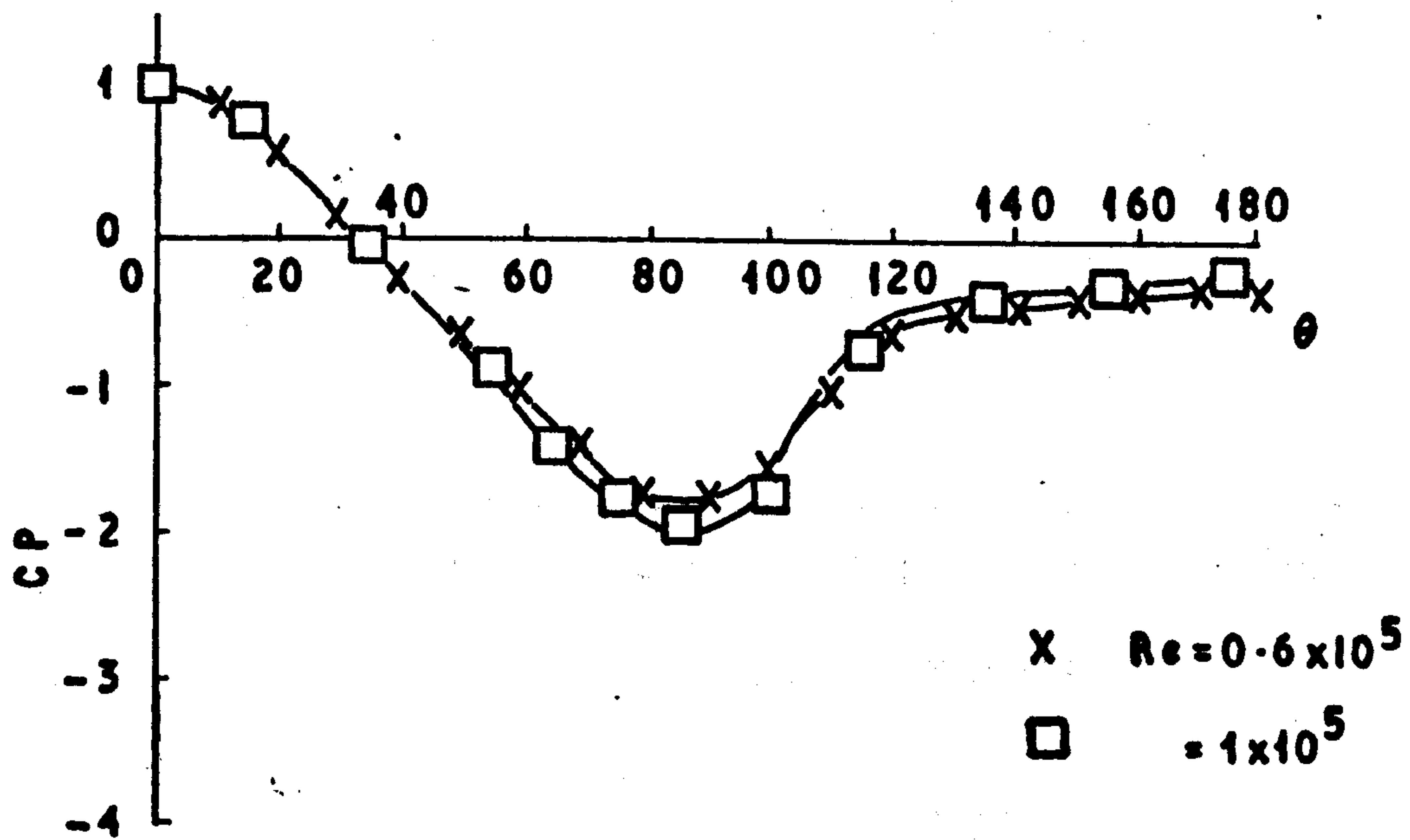
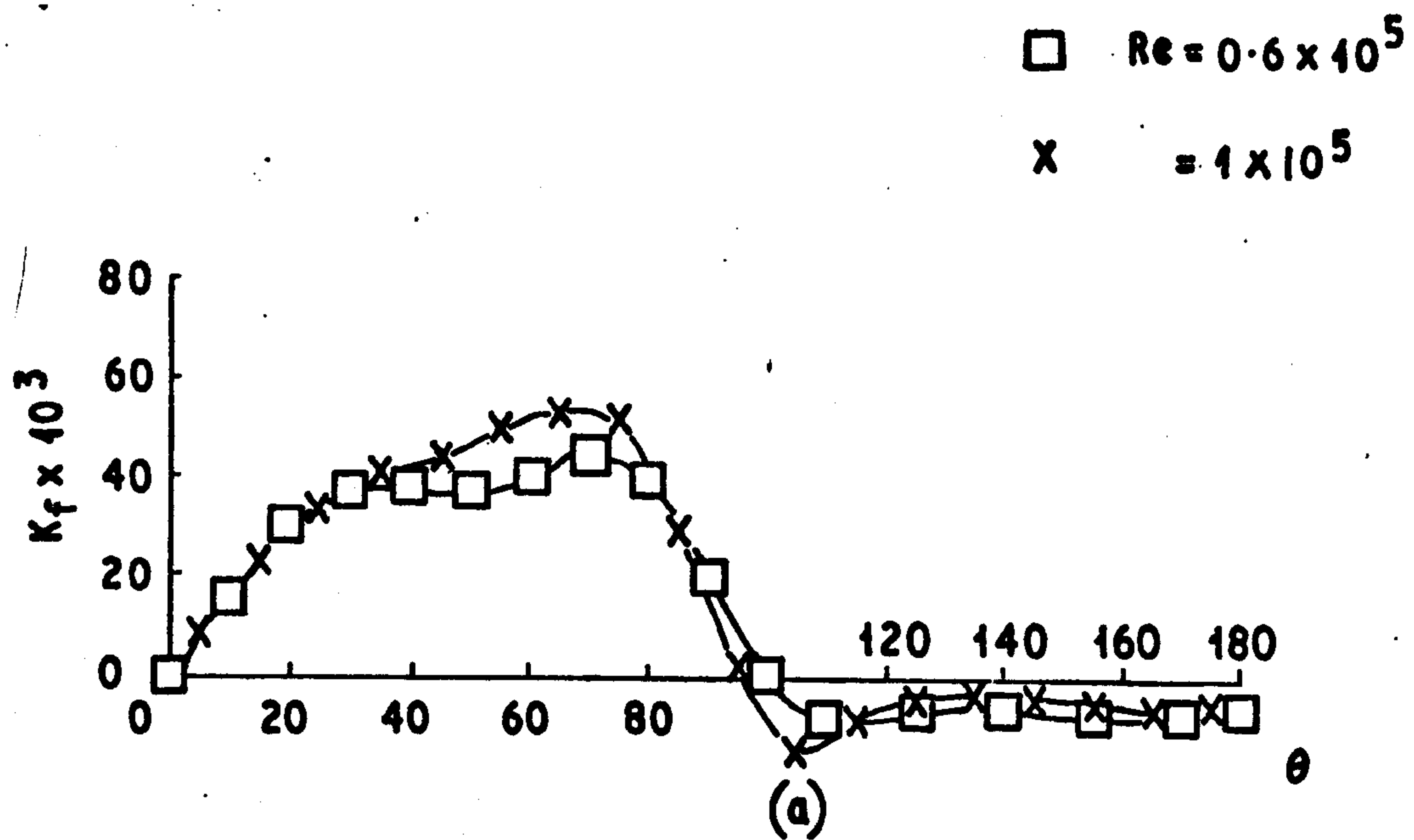


Fig 7.19

SKIN FRICTION DISTRIBUTION FOR THE FIFTH ROW  
IN THE BANK



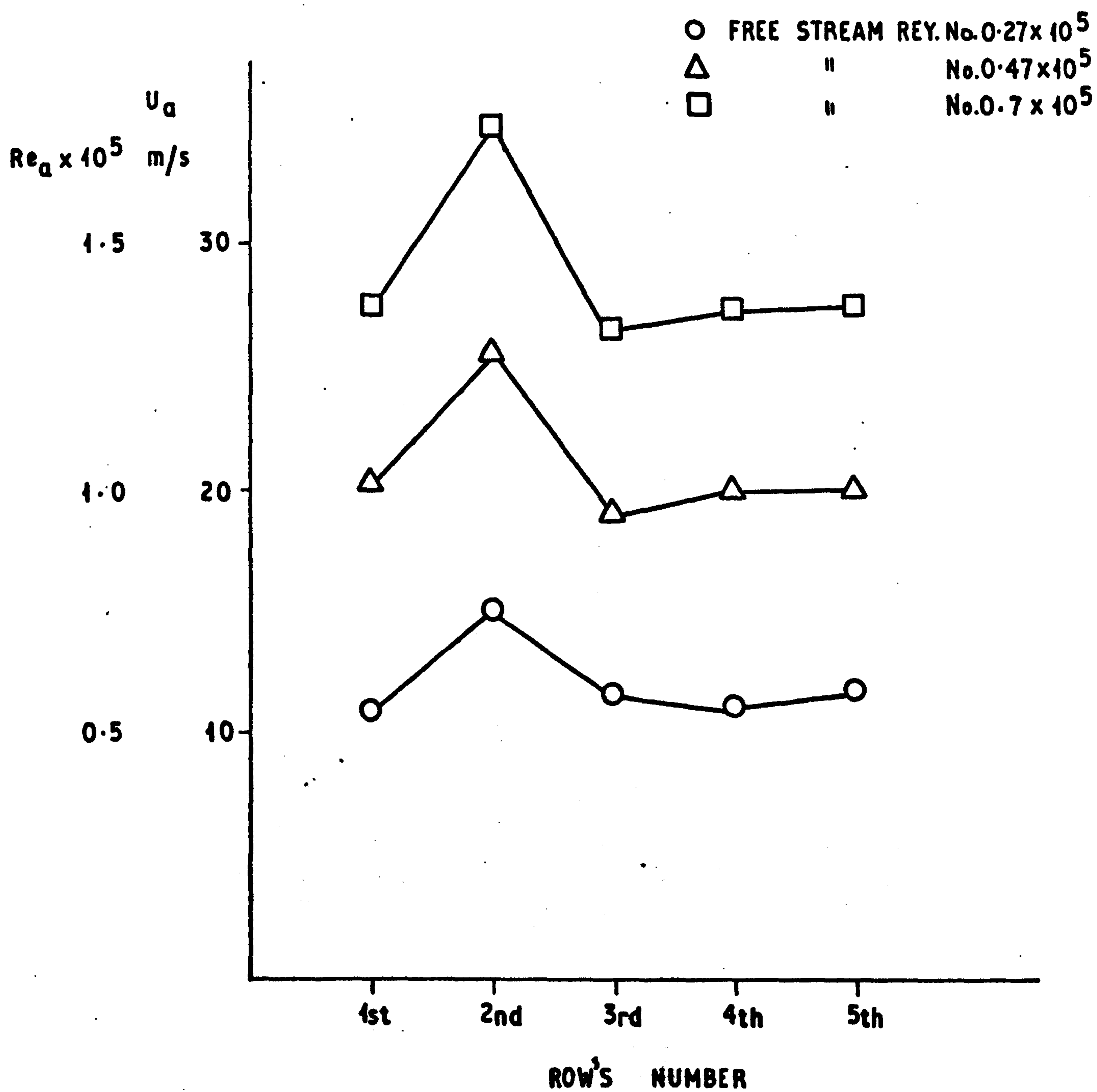


Fig.7.20

REYNOLDS NUMBER VARIATIONS FOR  
A STAGGERED TUB BANK

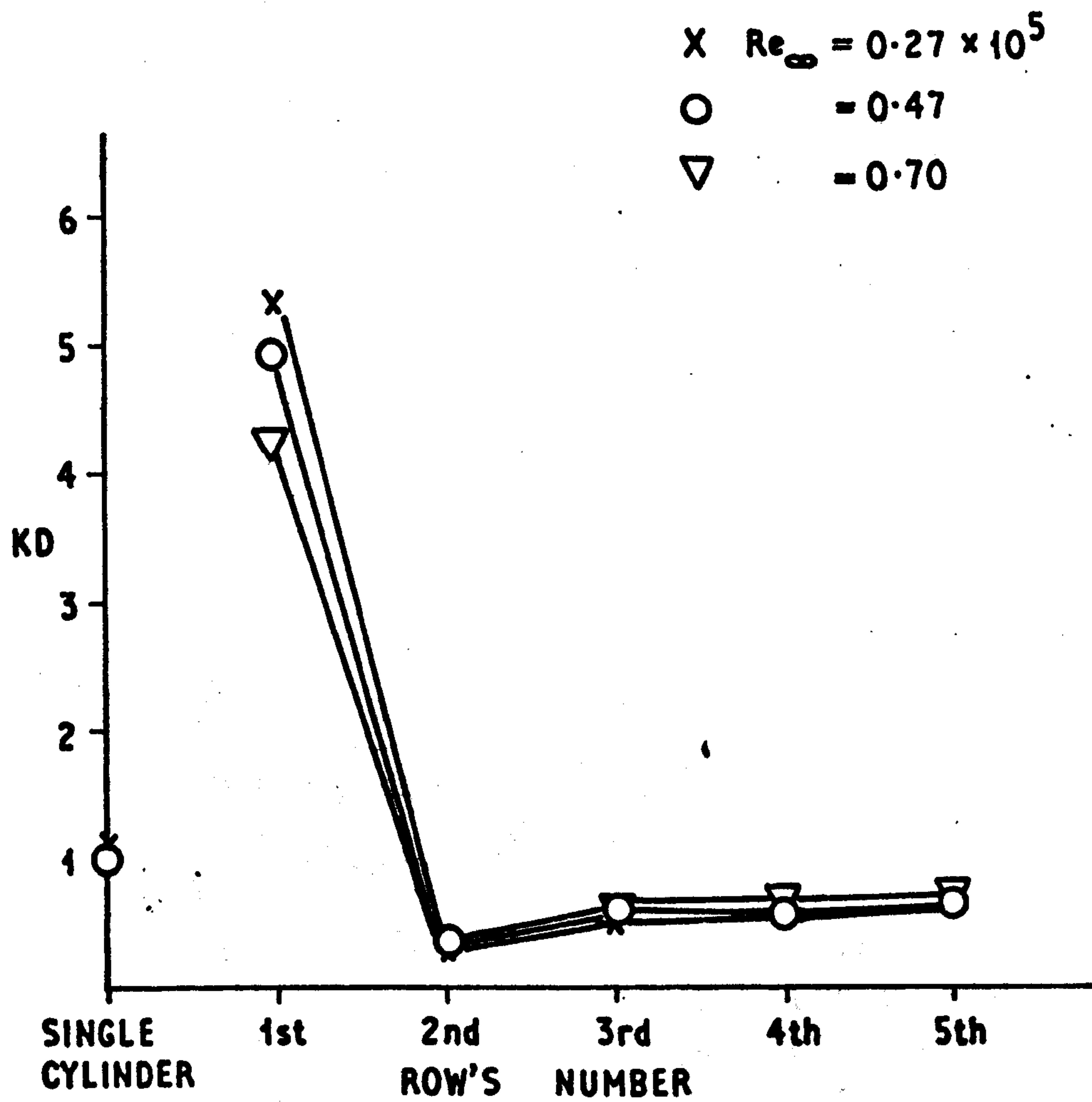
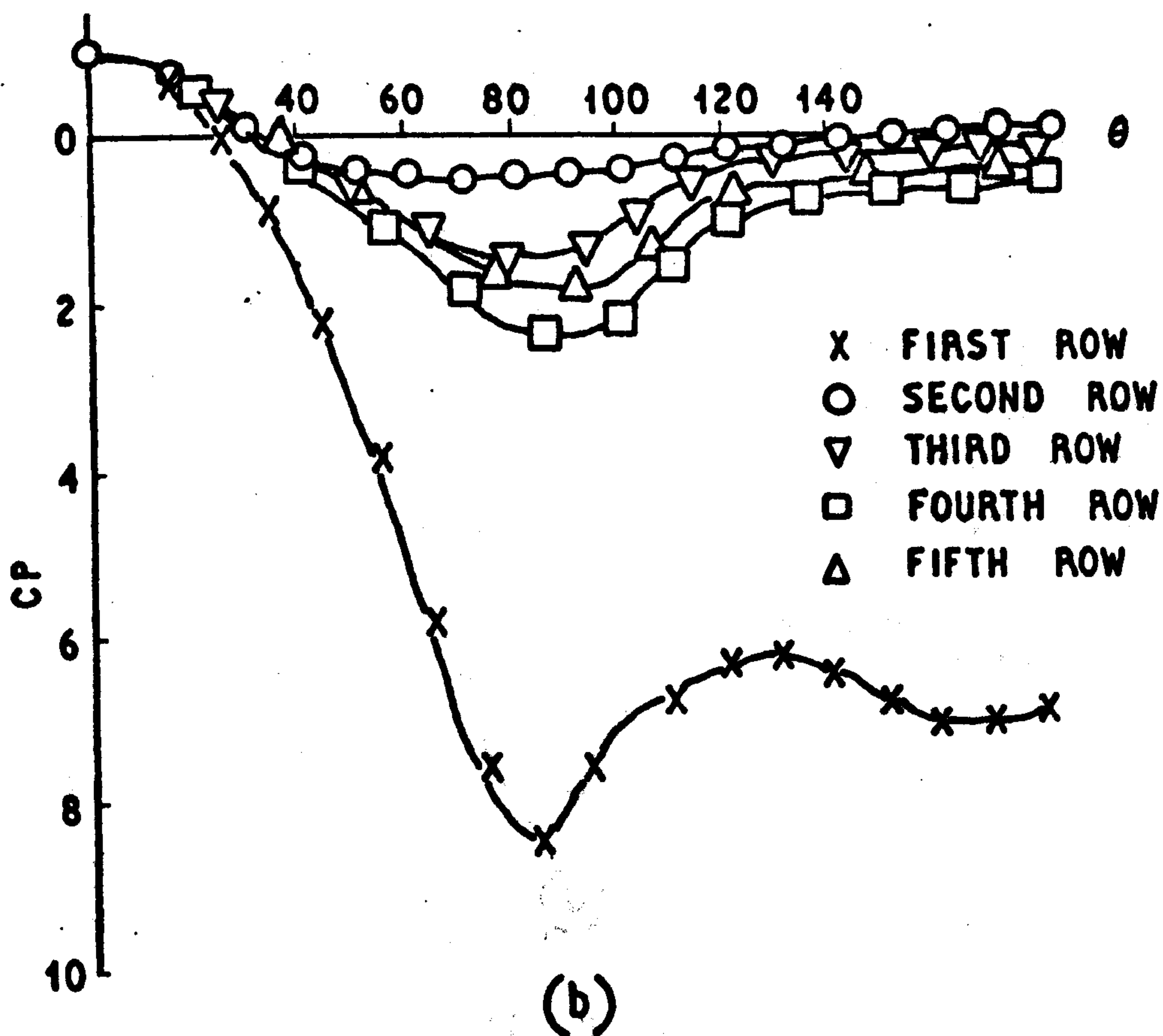
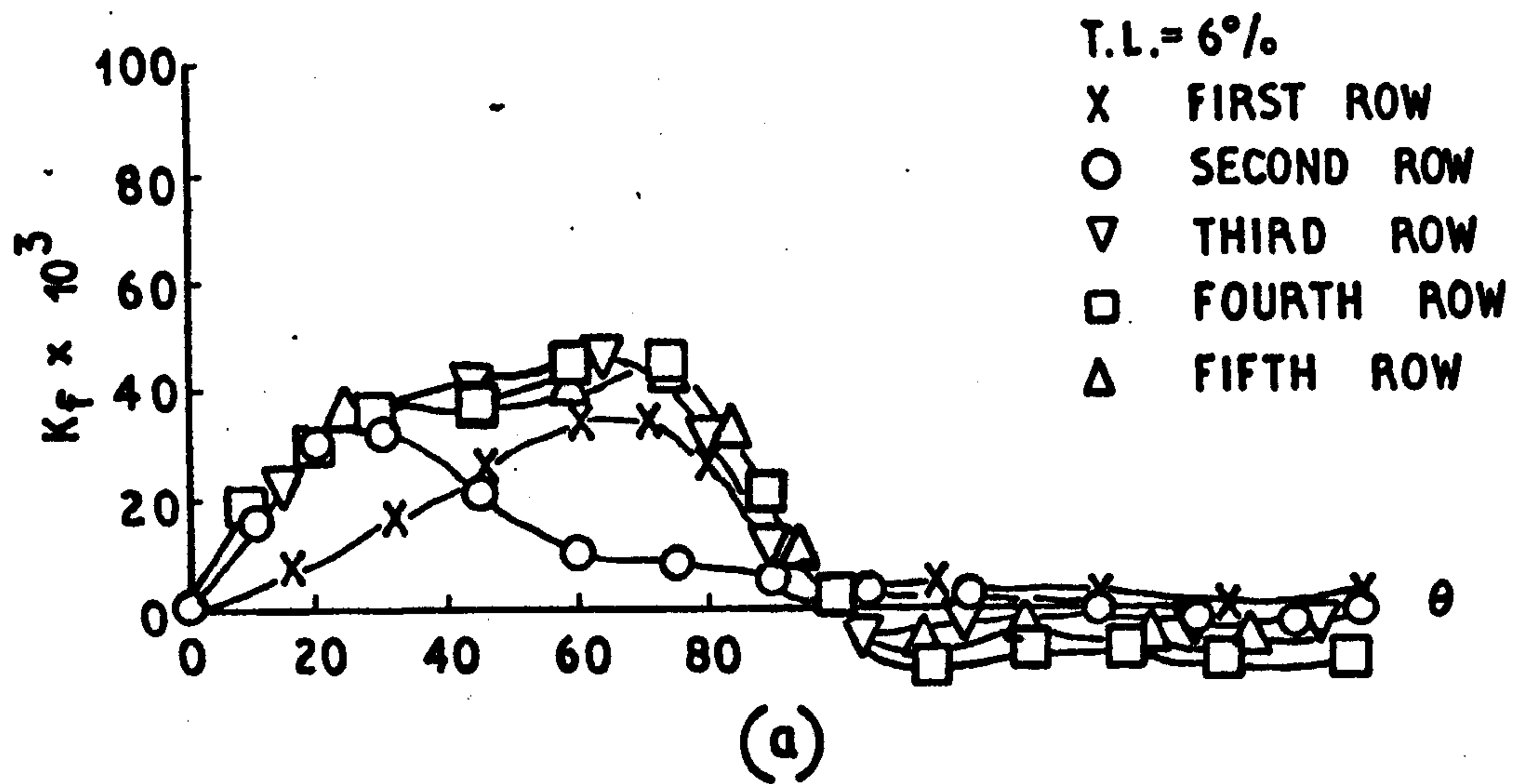


Fig. 7.21  
PRESSURE DRAG ON DIFFERENT ROWS  
IN THE BANK

IN THE BANK  
 ON THE SURFACE OF THE BANK  
 RE = 0.27 x 10^5



**Fig. 7.22**  
**SKIN FRICTION DISTRIBUTION**  
**ON THE STAGGERED BANK**  
 $R_{\infty} = 0.27 \times 10^5$



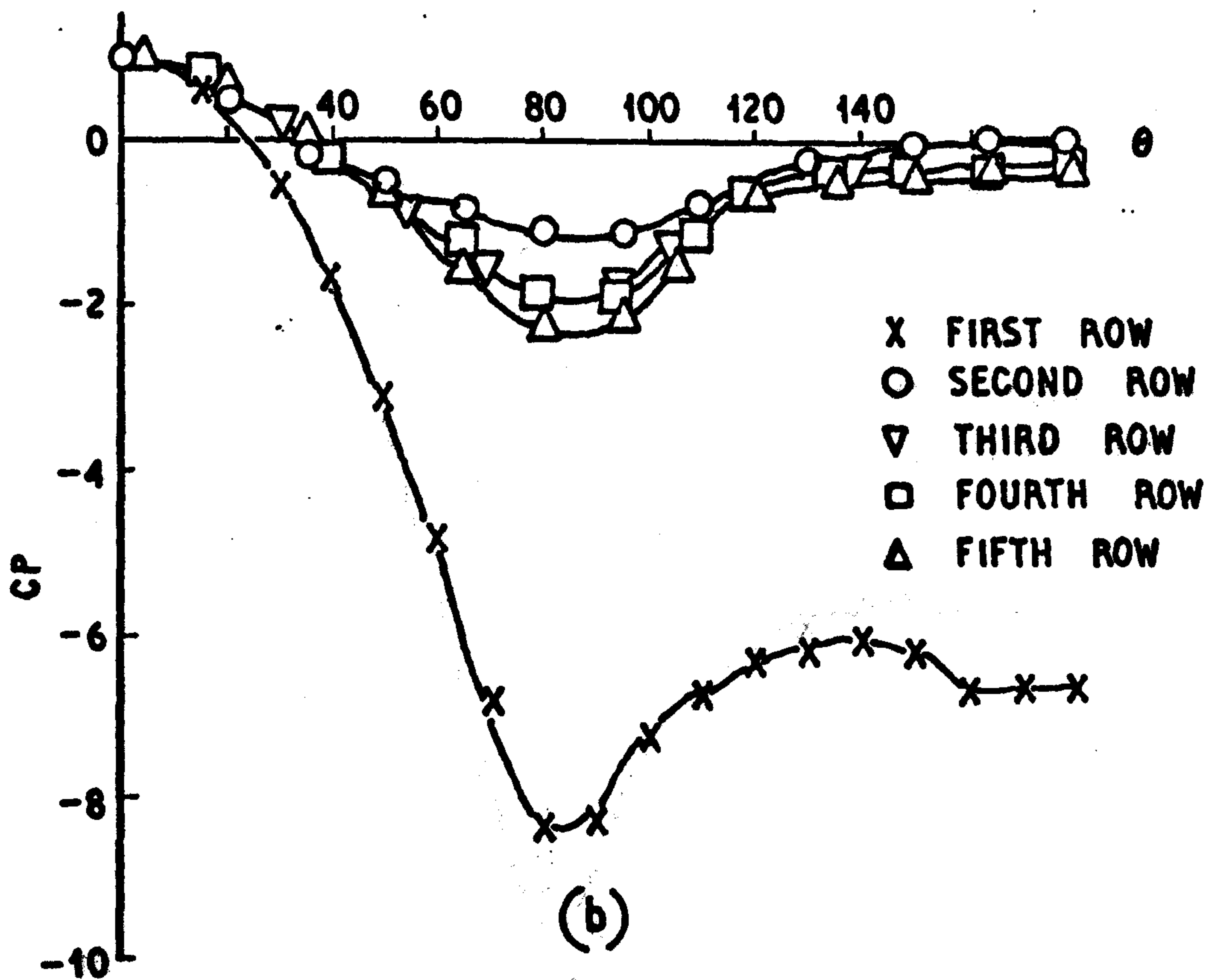
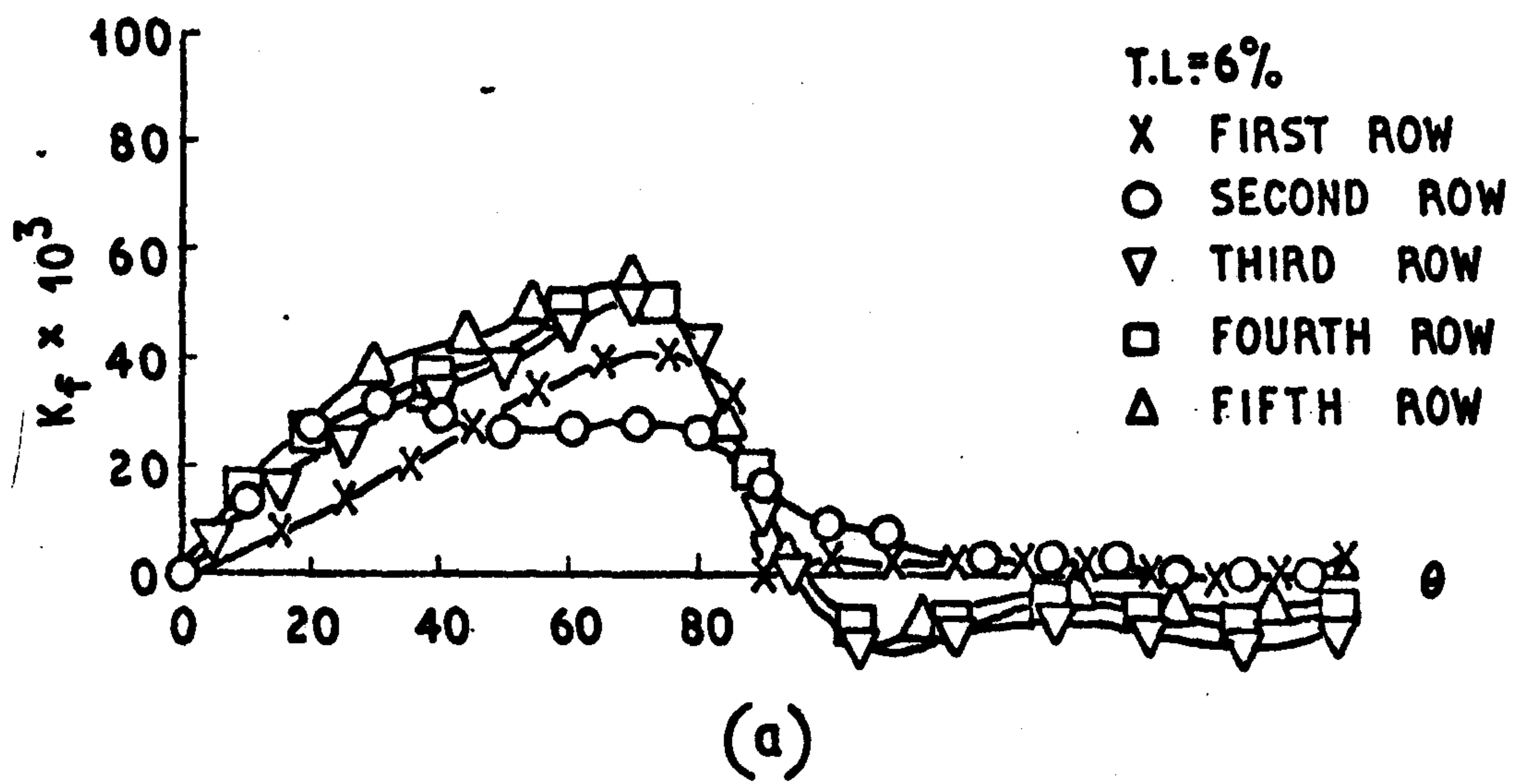
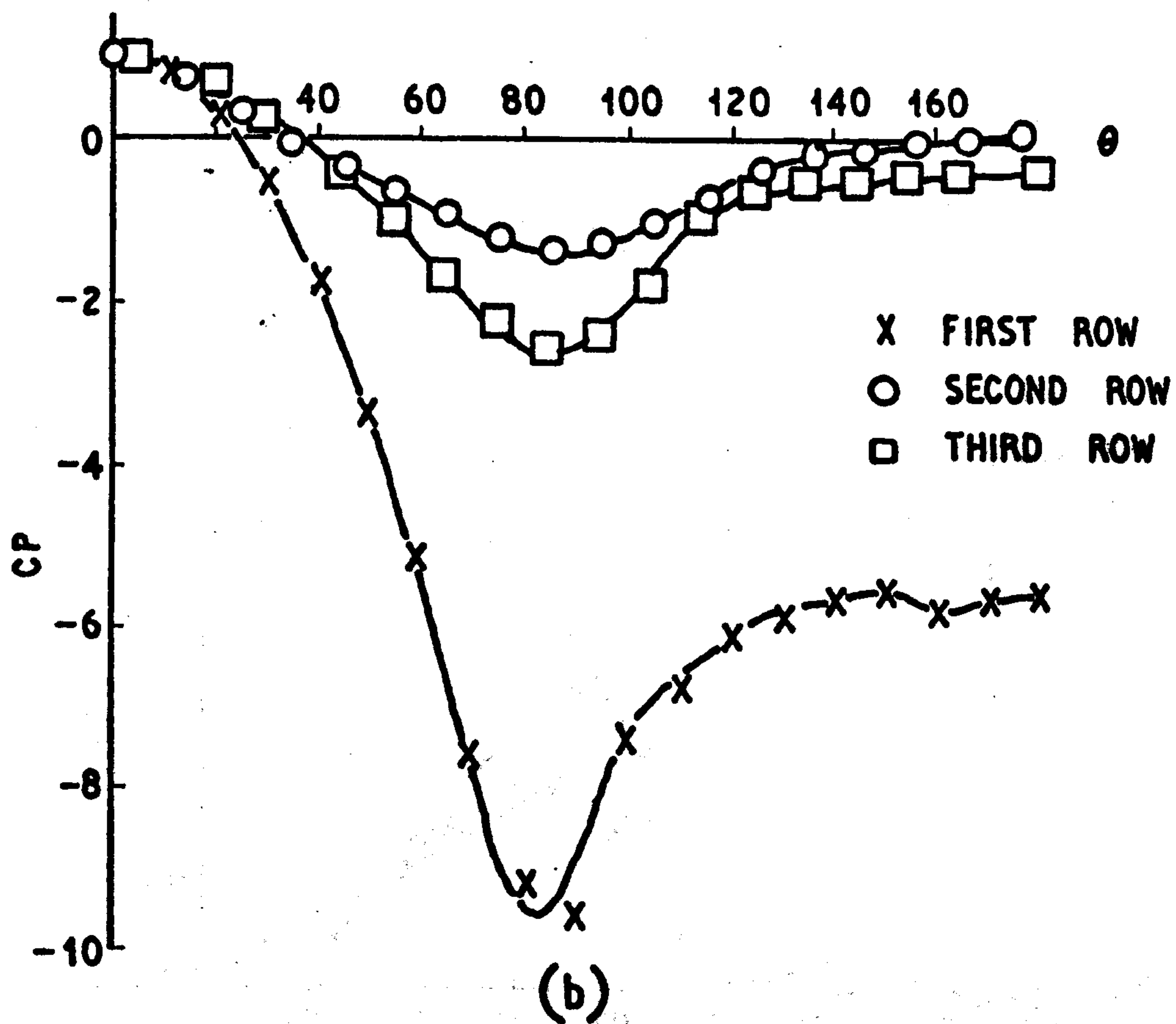
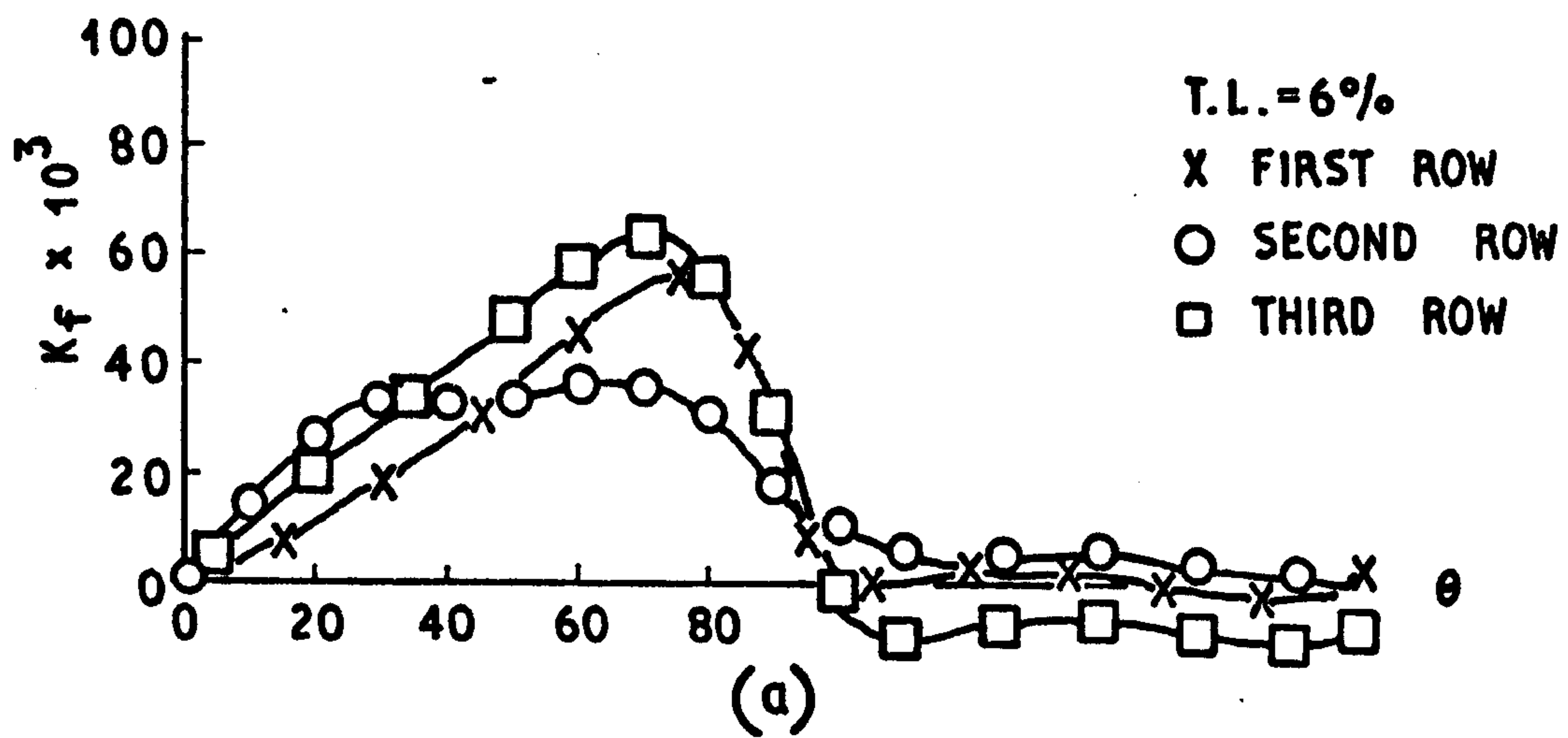
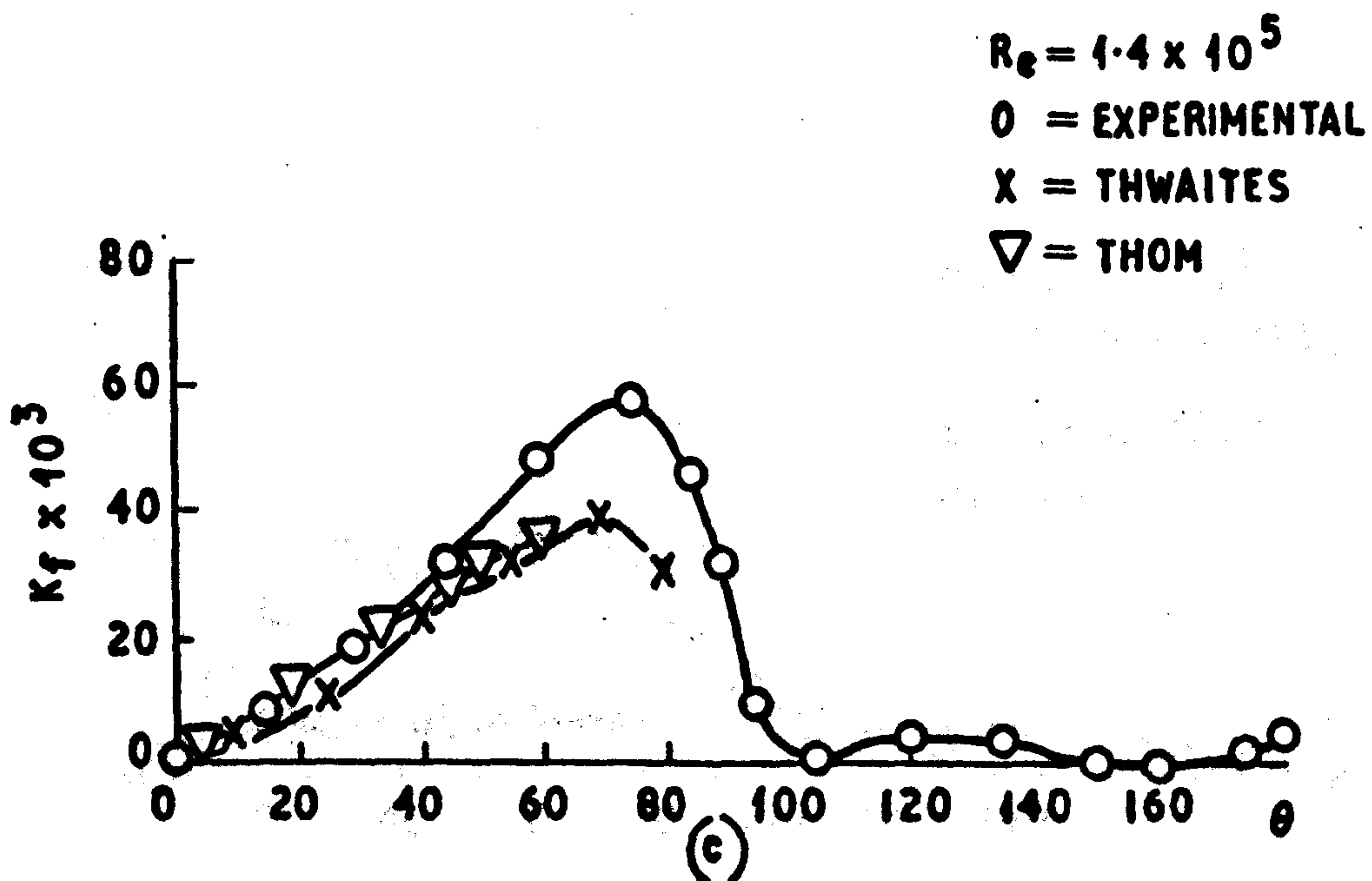
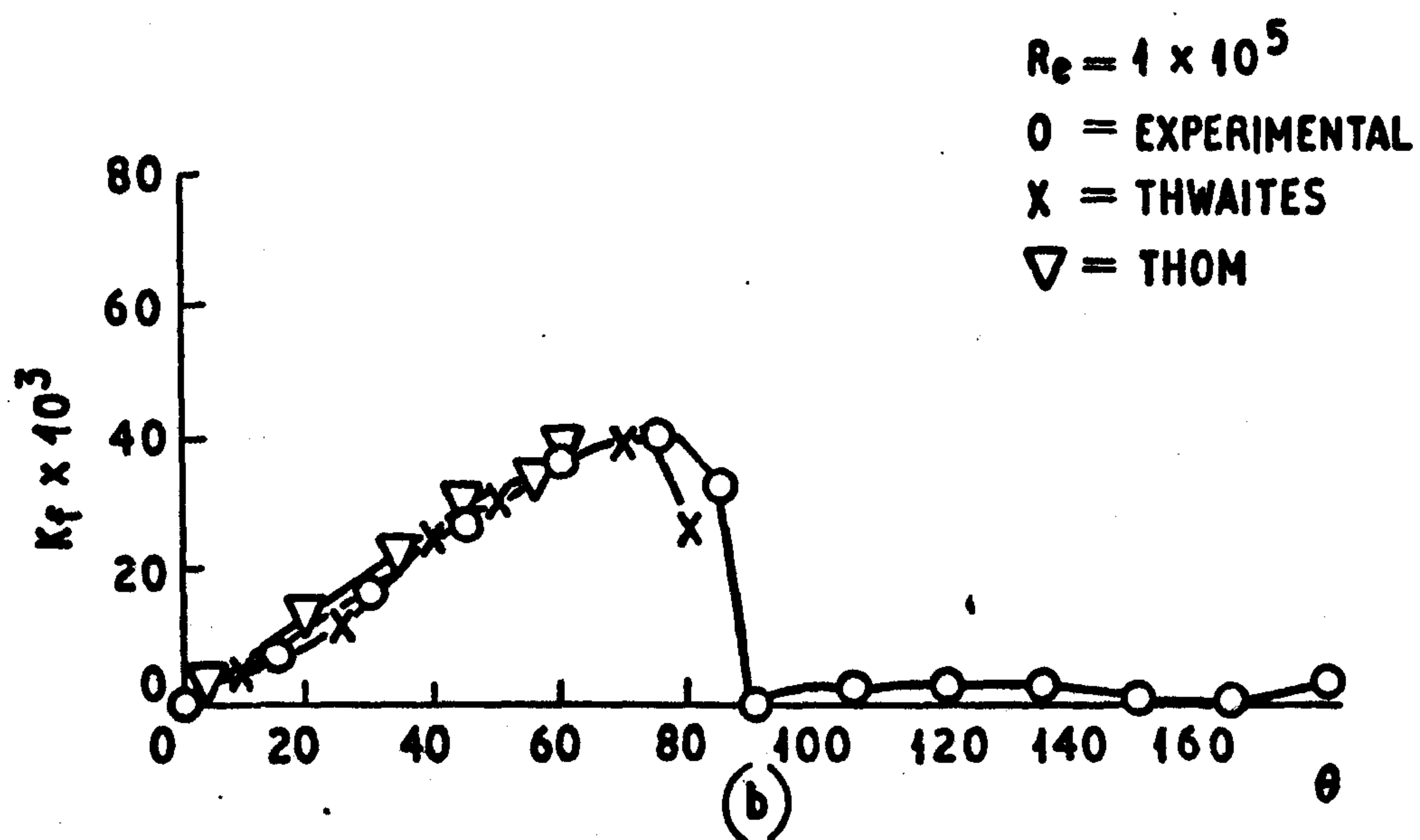
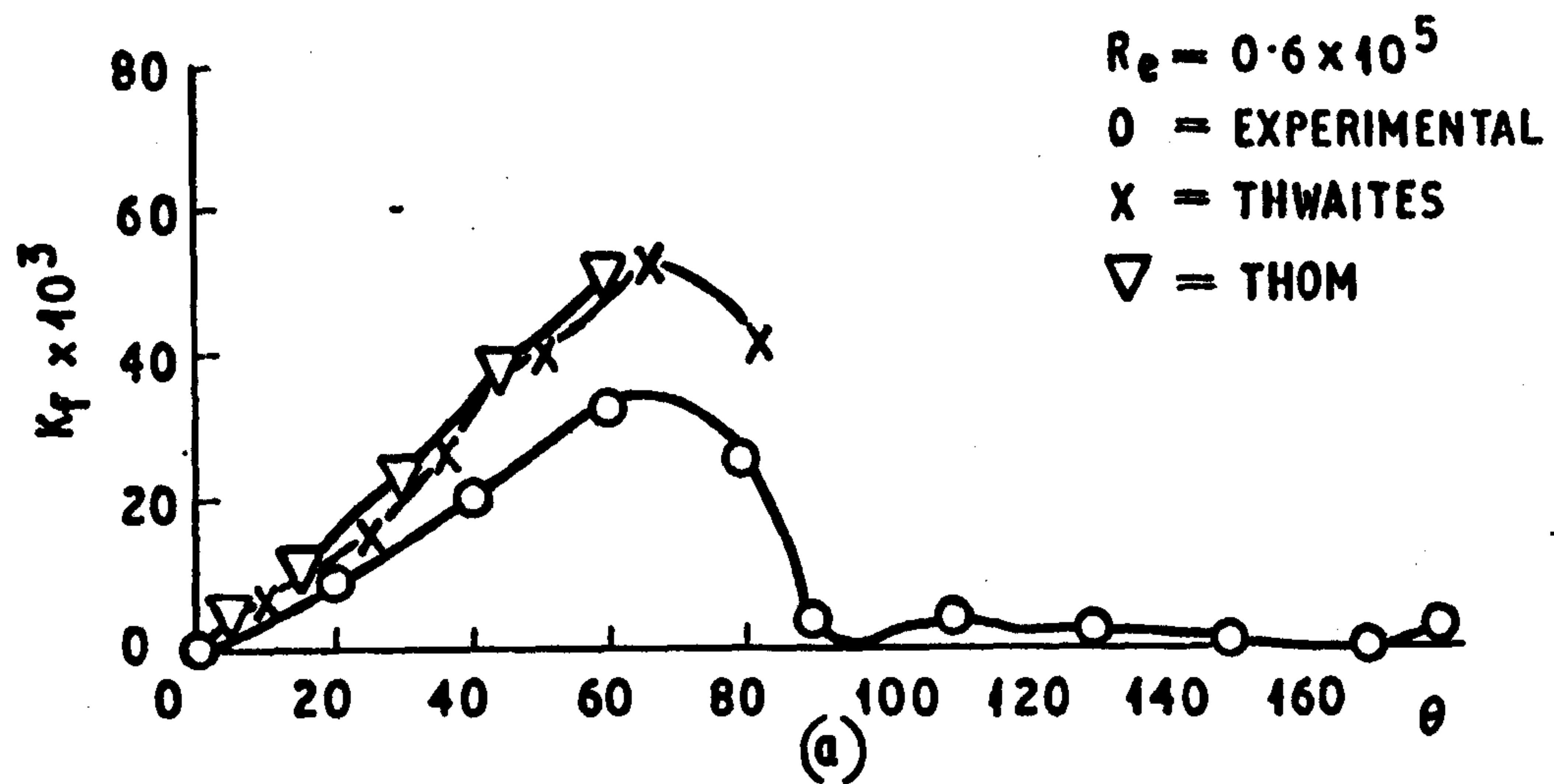


Fig. 7.23  
SKIN FRICTION DISTRIBUTION  
ON THE STAGGERED BANK  
 $R_{\infty} = 0.47 \times 10^5$



**Fig. 7.24**  
**SKIN FRICTION DISTRIBUTION**  
**ON THE STAGGERED BANK**  
 $R = 0.7 \times 10^5$



PREDICTED AND MEASURED  
SKIN FRICTION  
FIRST ROW IN THE BANK  
FIG. 7.25



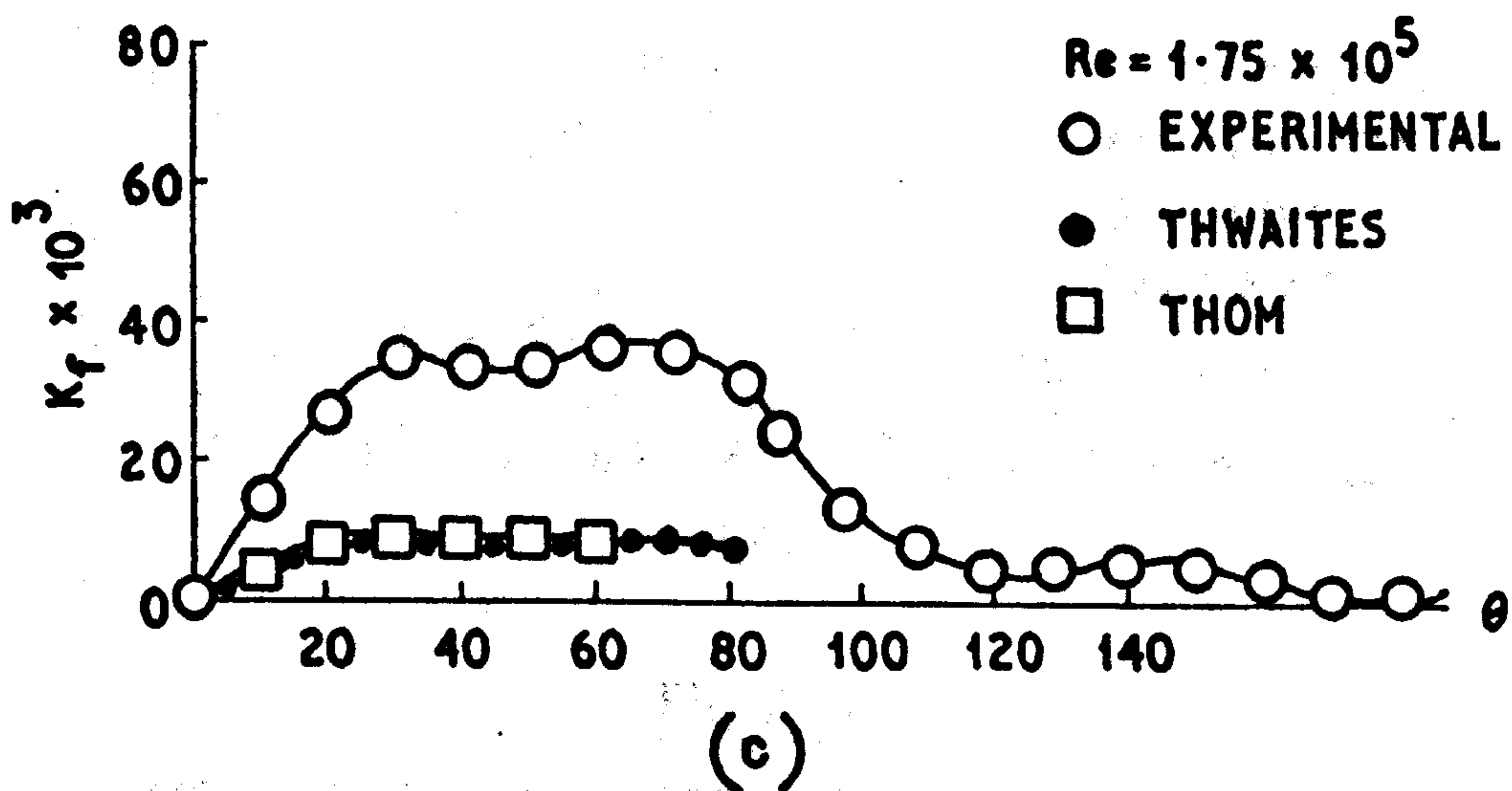
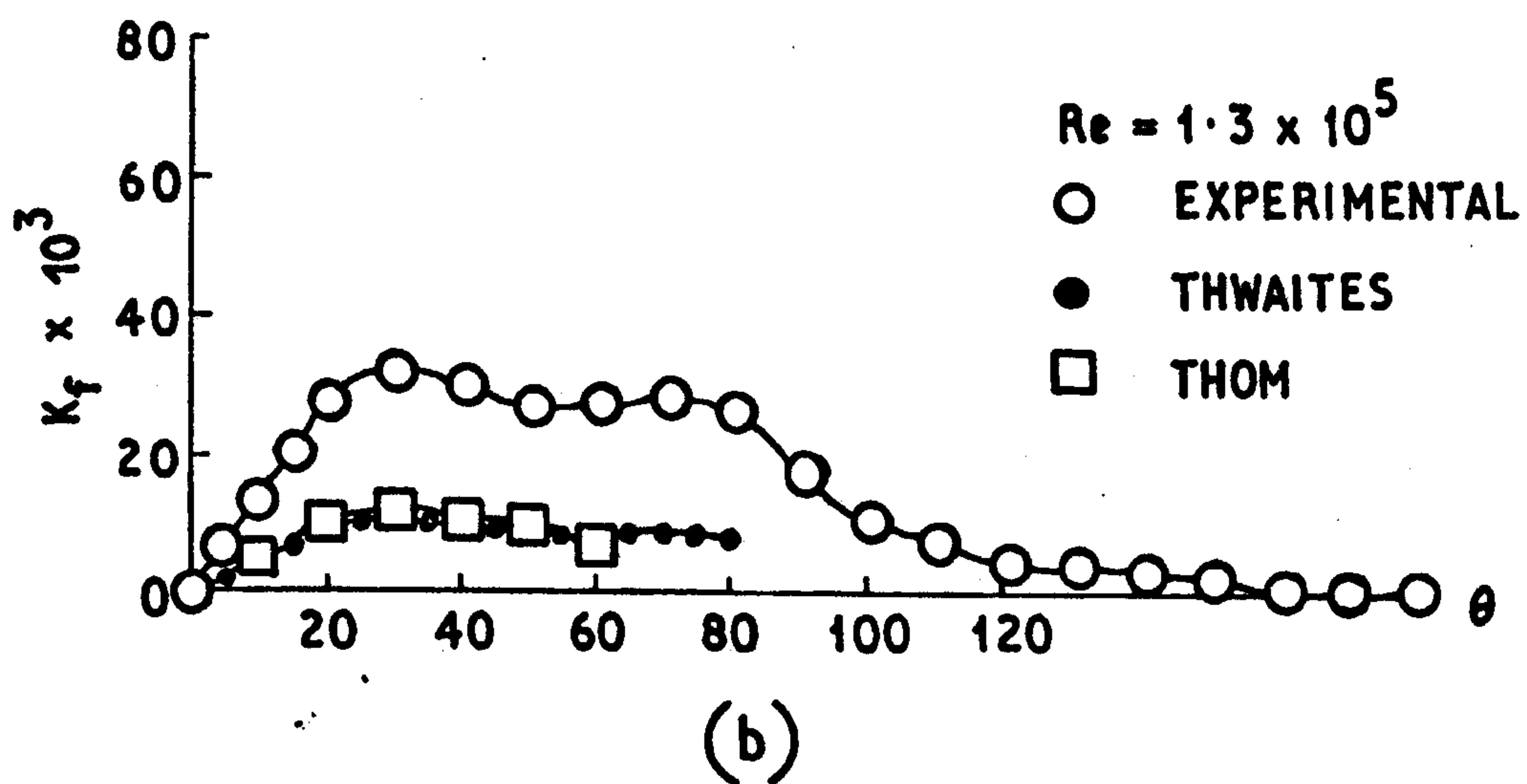
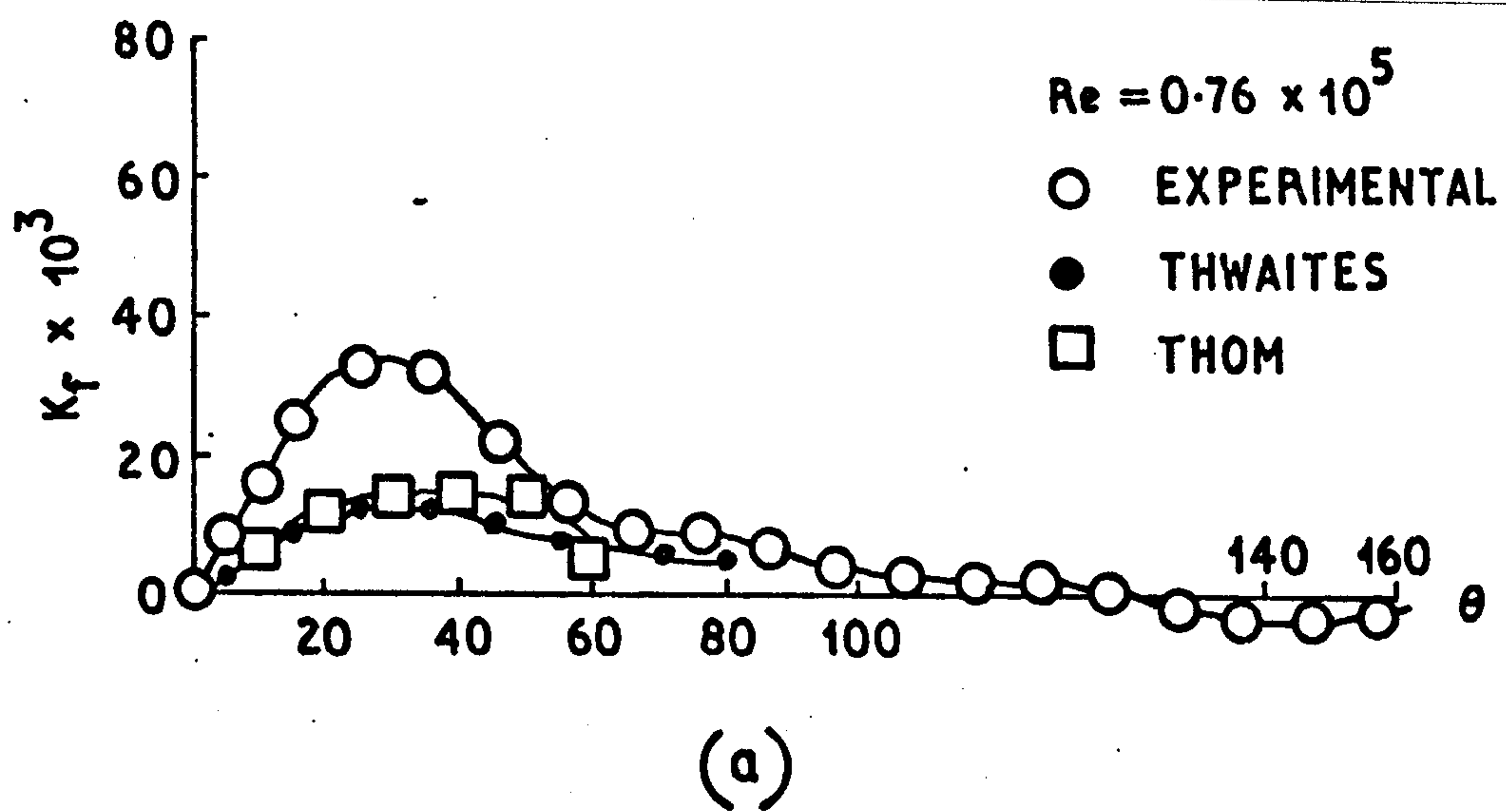


**Fig.7.26**  
**PREDICTED AND MEASURED SKIN FRICTION**  
**SECOND ROW IN THE BANK**

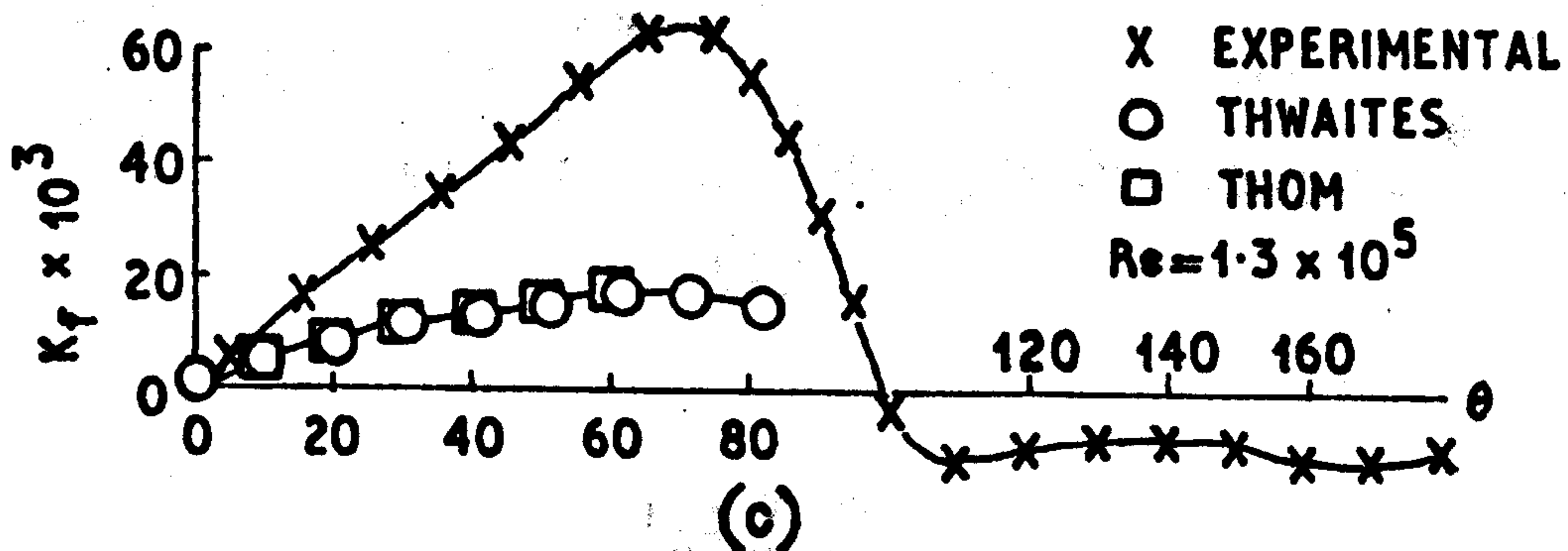
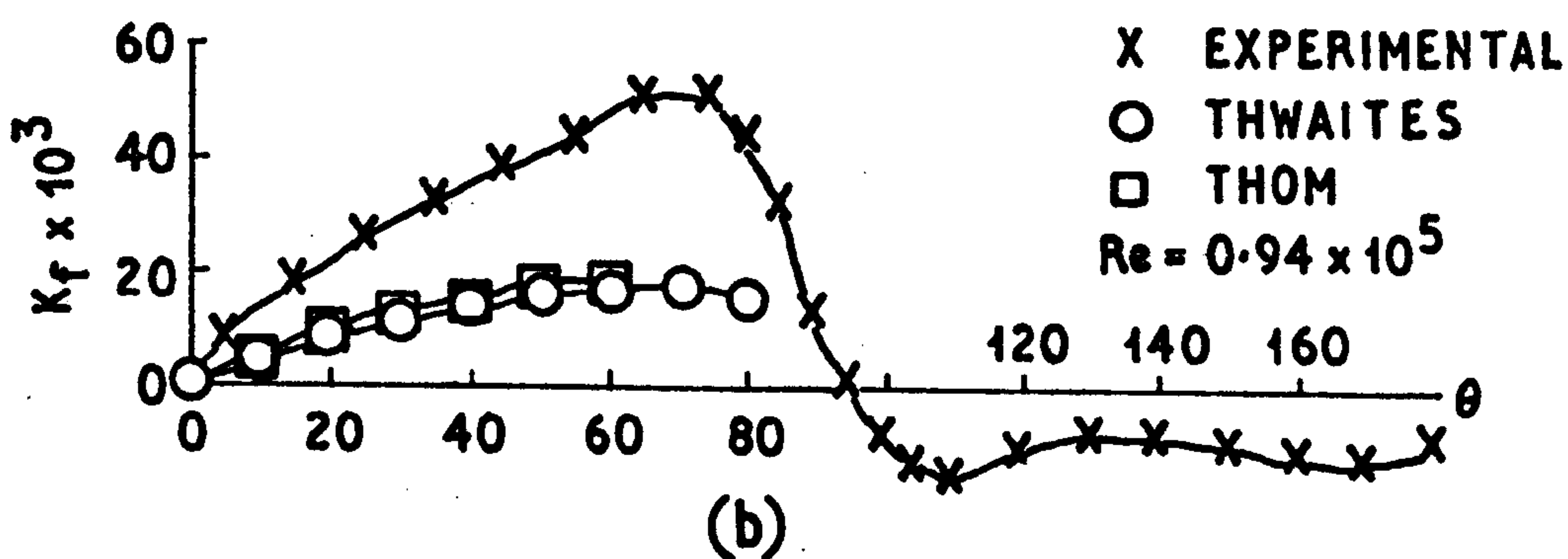
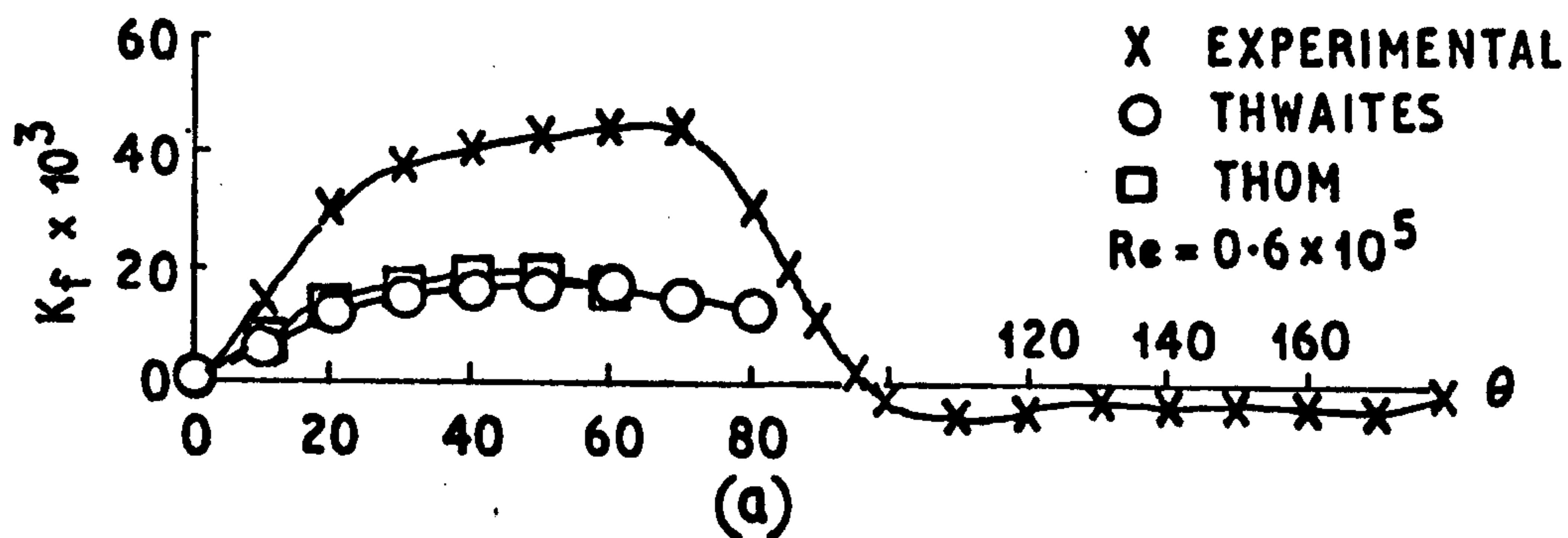


**Fig. 7.27**  
**MEASURED AND PREDICTED SKIN FRICTION**  
**FOR THIRD ROW IN THE BANK**

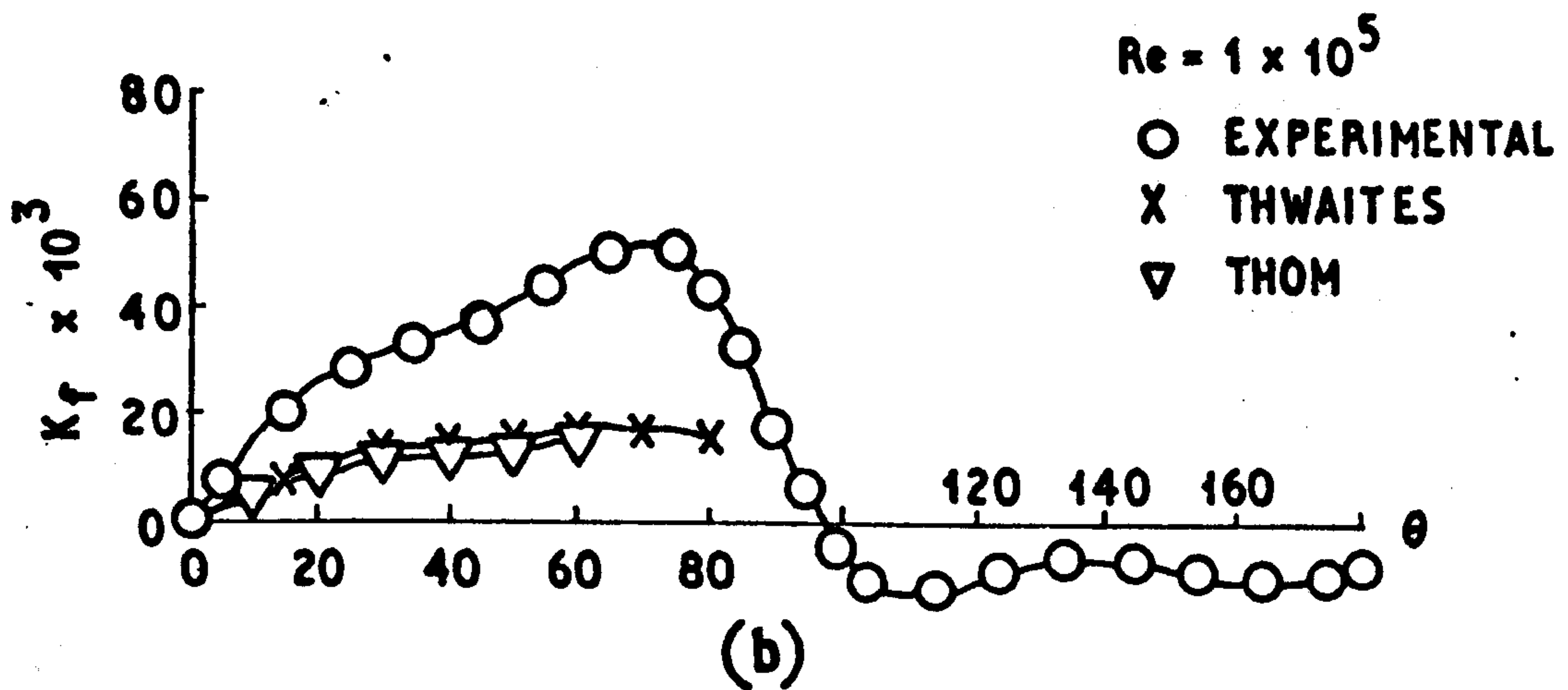
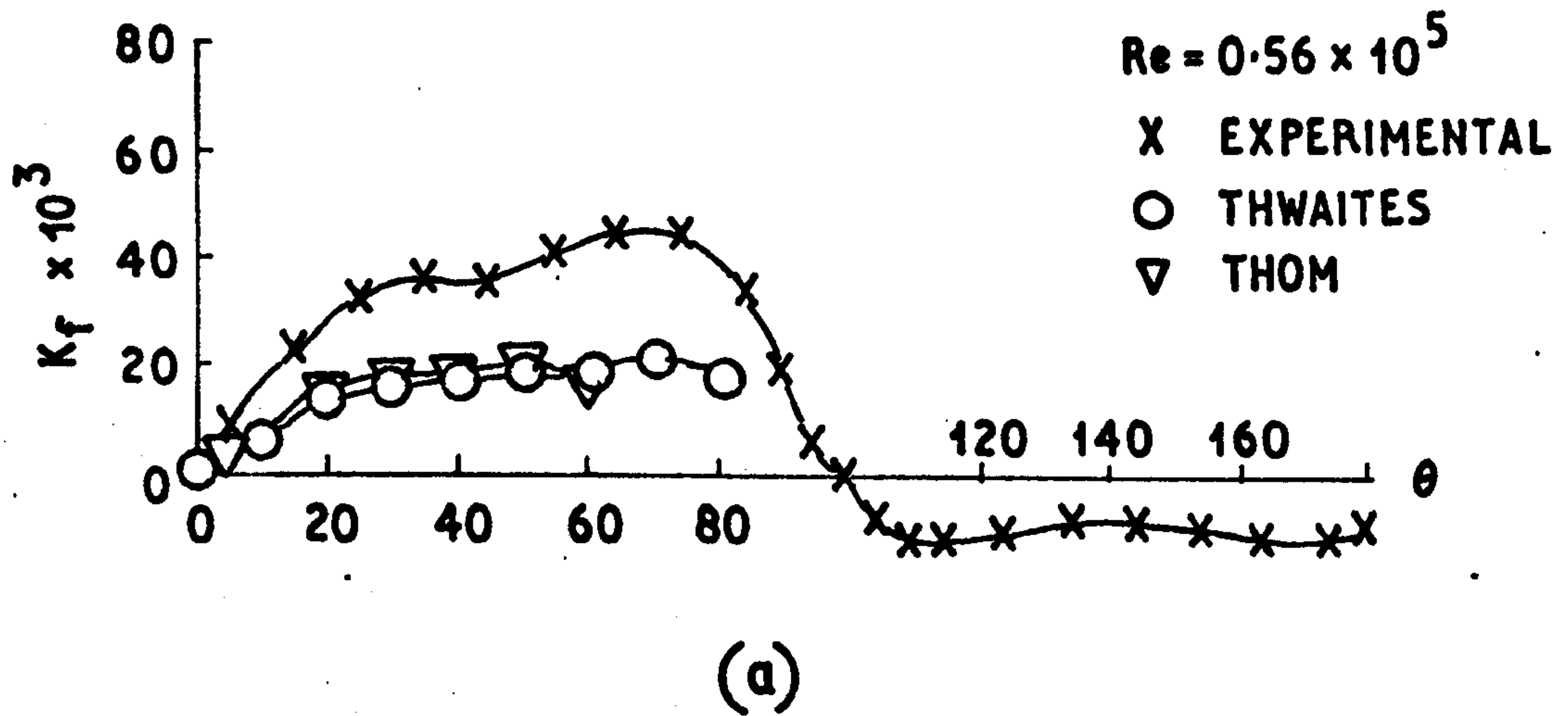


**Fig. 7.28**  
**MEASURED AND PREDICTED SKIN FRICTION**  
**FOR FOURTH ROW IN THE BANK**

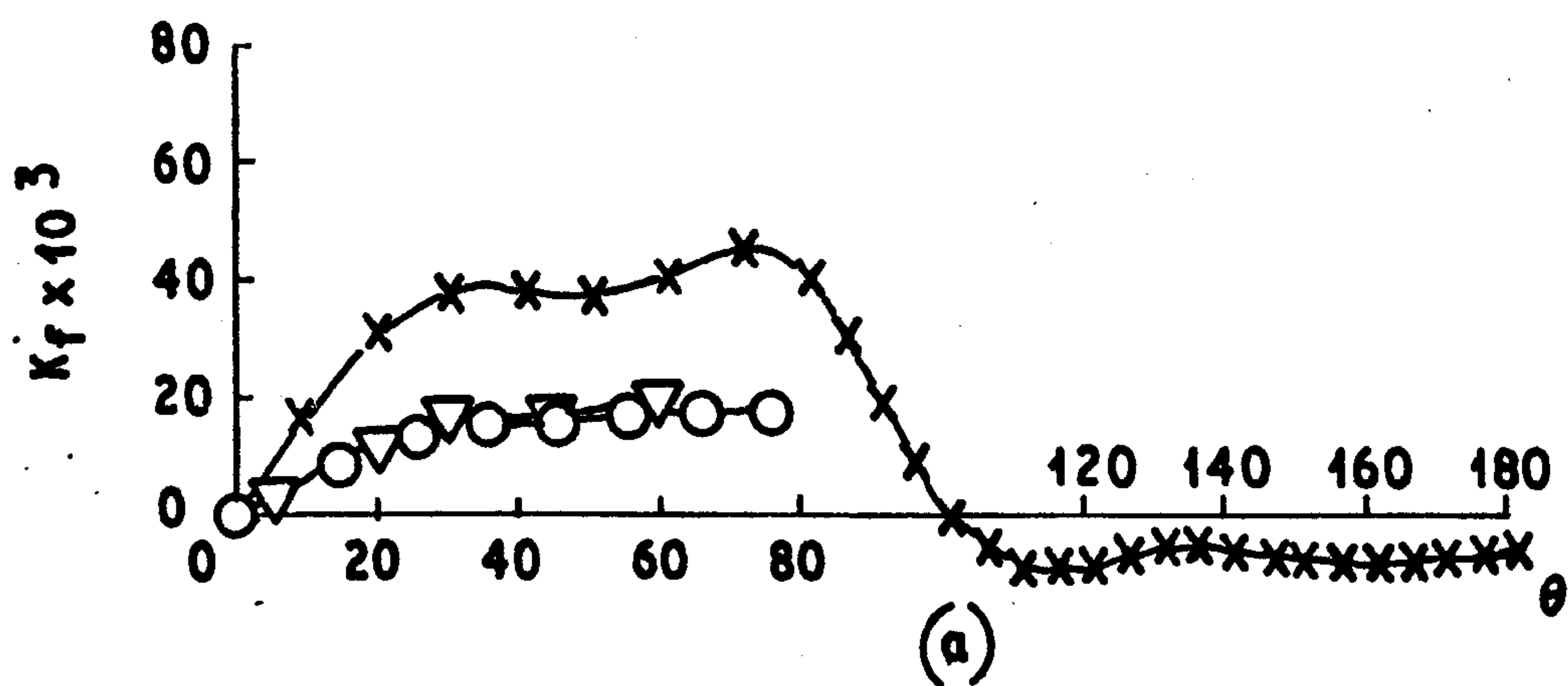


X EXPERIMENTAL

O THWAITES

▽ THOM

$Re = 0.6 \times 10^5$



X EXPERIMENTAL

O THWAITES

▽ THOM

$Re = 1 \times 10^5$

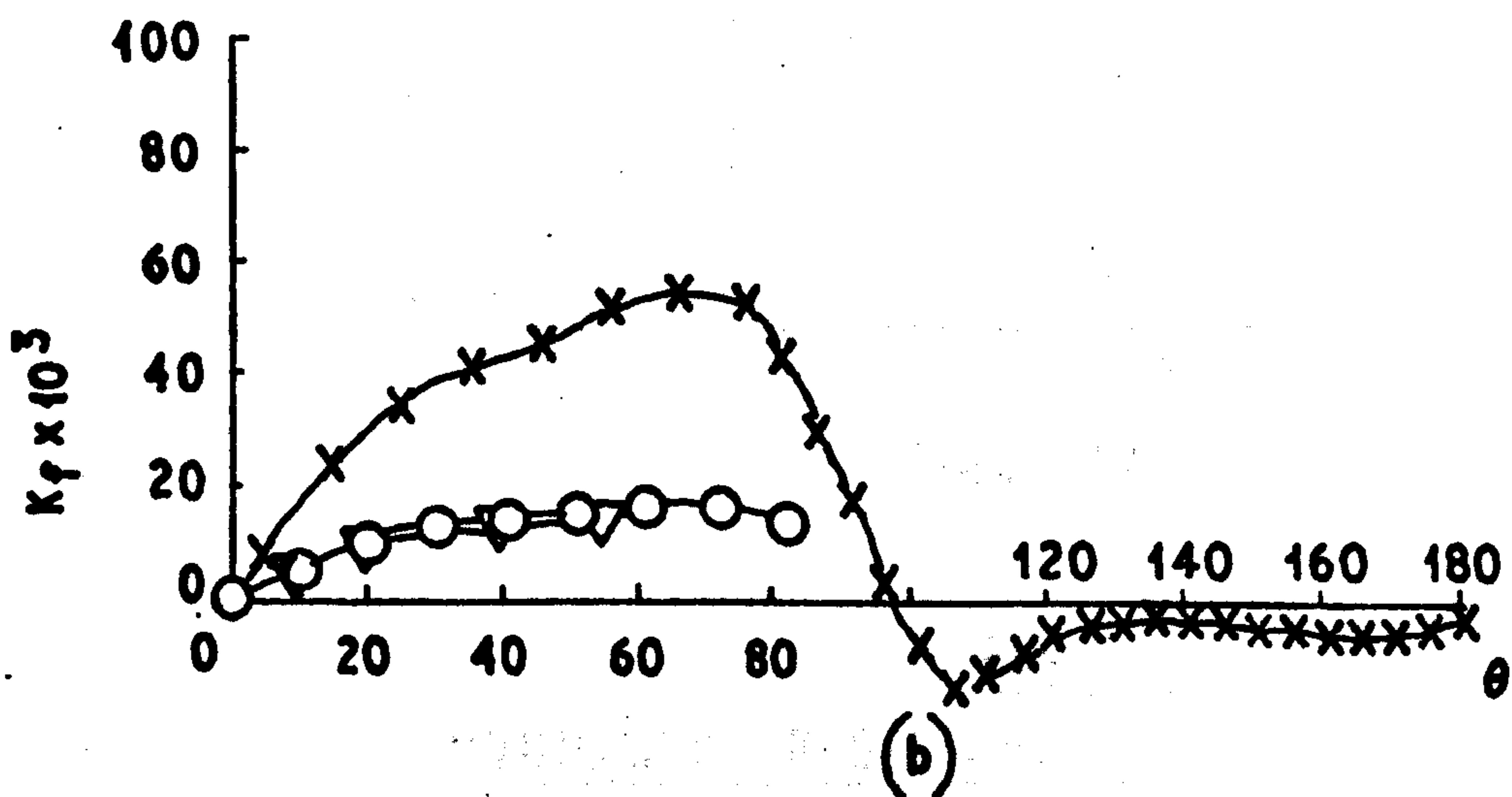
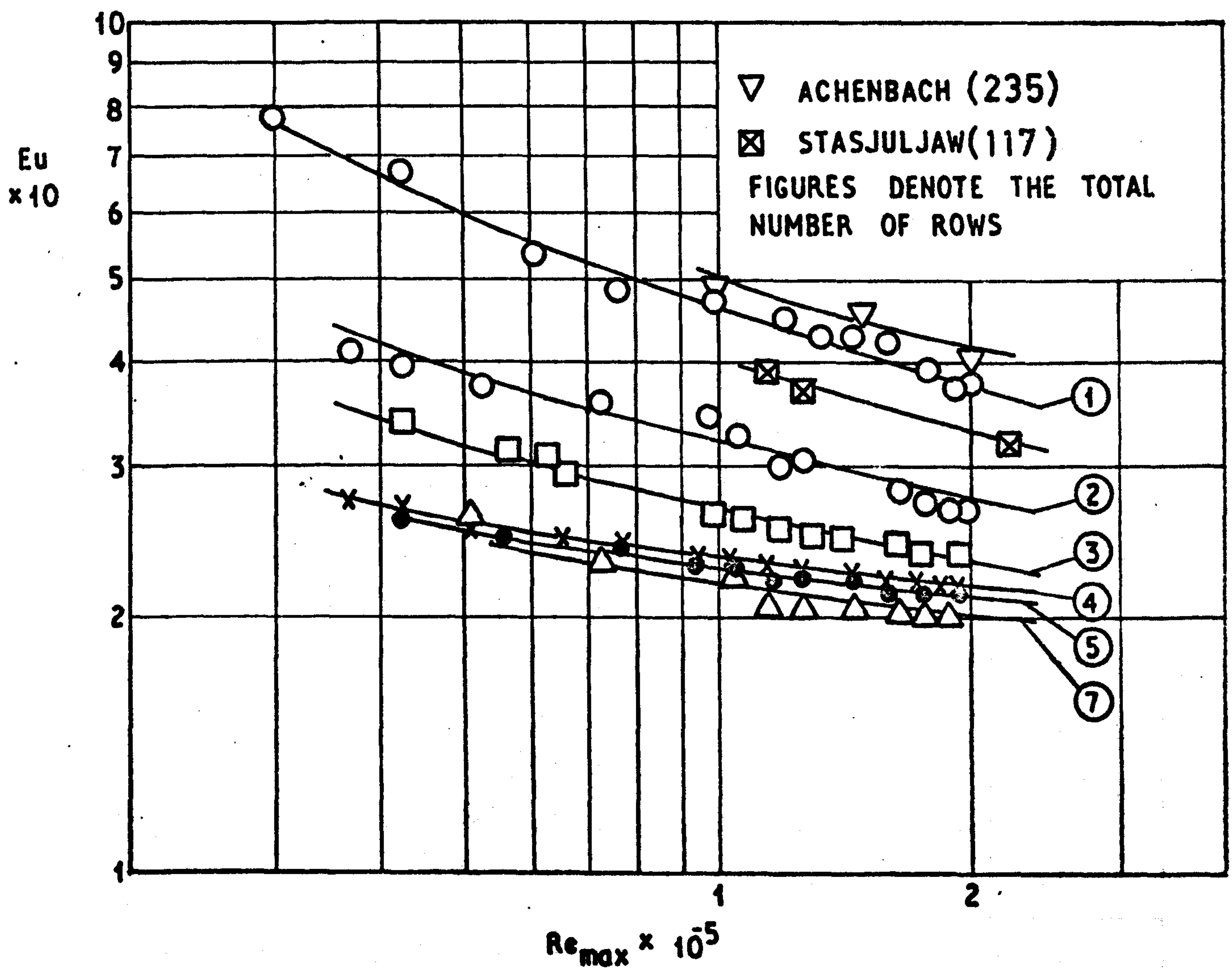


Fig. 7.29

MEASURED AND PREDICTED SKIN FRICTION FIFTH ROW  
IN THE BANK



**Fig. 7.30**  
**HYDRAULIC RESISTANCE OF A STAGGERED BANK,**  
**REFERRED TO ONE ROW**

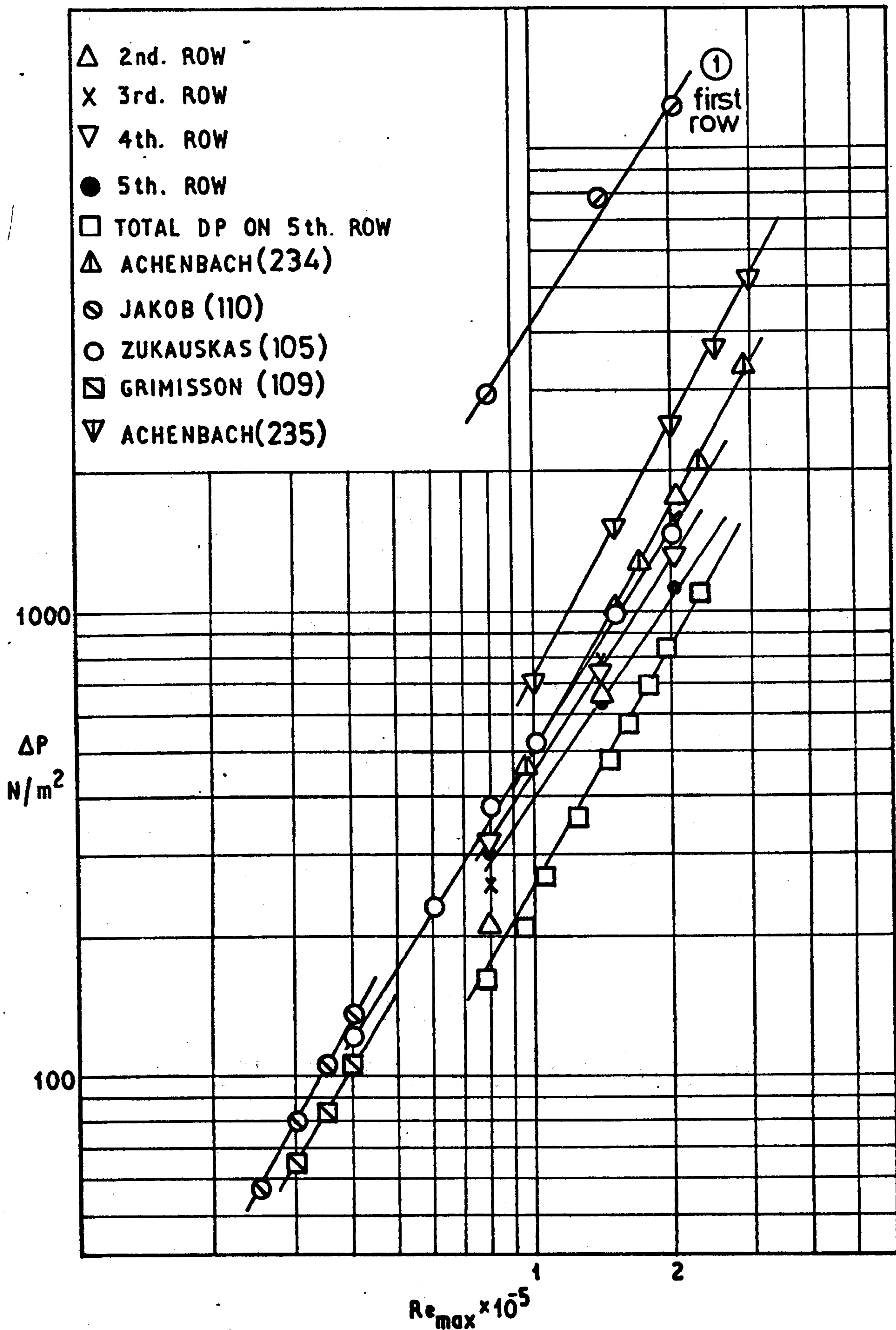


Fig. 7.31  
 PRESSURE DROP IN THE BANK



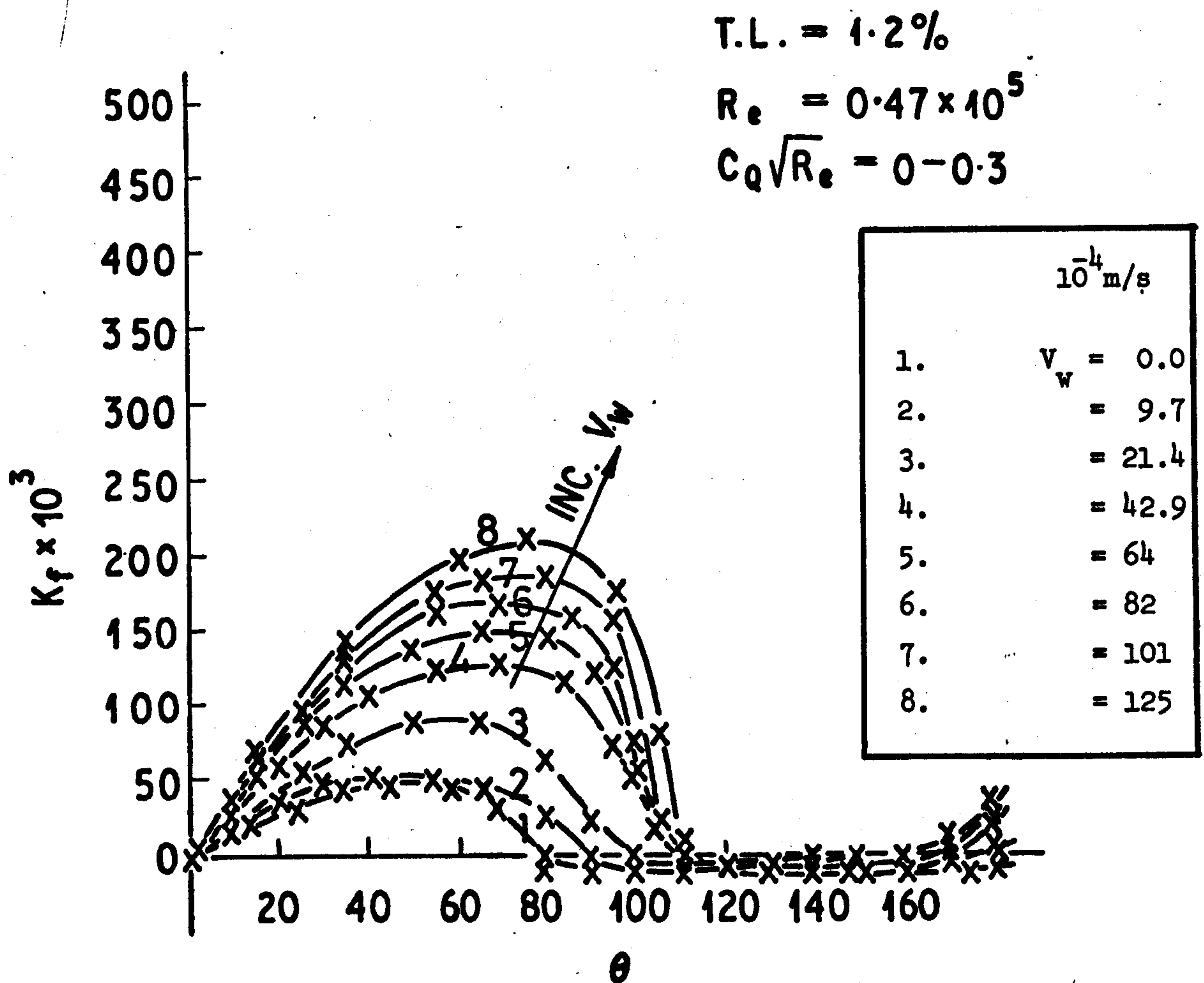


Fig. 8.1

Effect of Suction on Skin Friction

$$T.L. = 1.2\%$$

$$R_e = 0.47 \times 10^5$$

$$C_D \sqrt{R_e} = 0.35 - 1.02$$

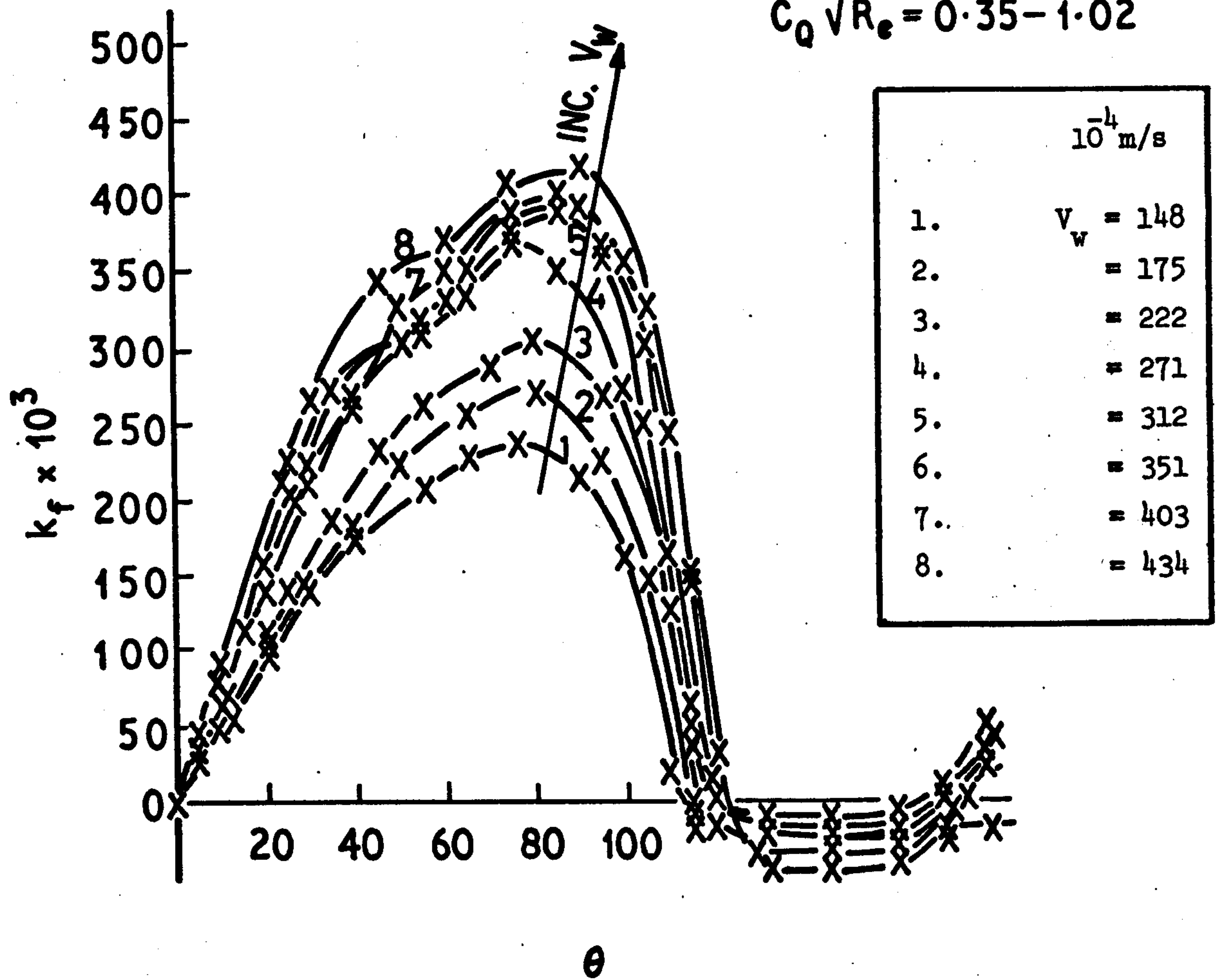


Fig. 8.2

Effect of Suction on Skin Friction

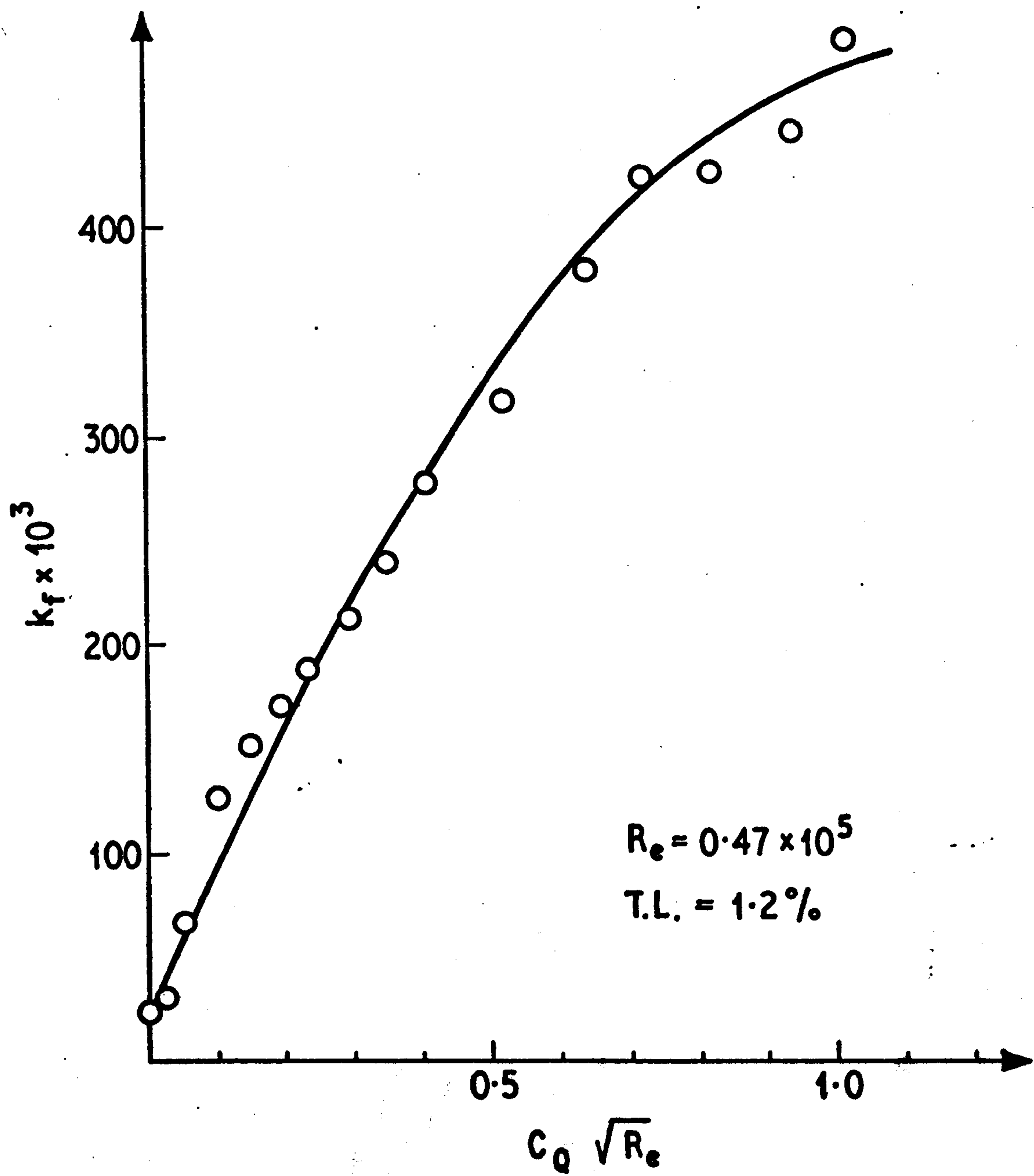


Fig. 8.3  
Effect of Suction on Friction Drag.



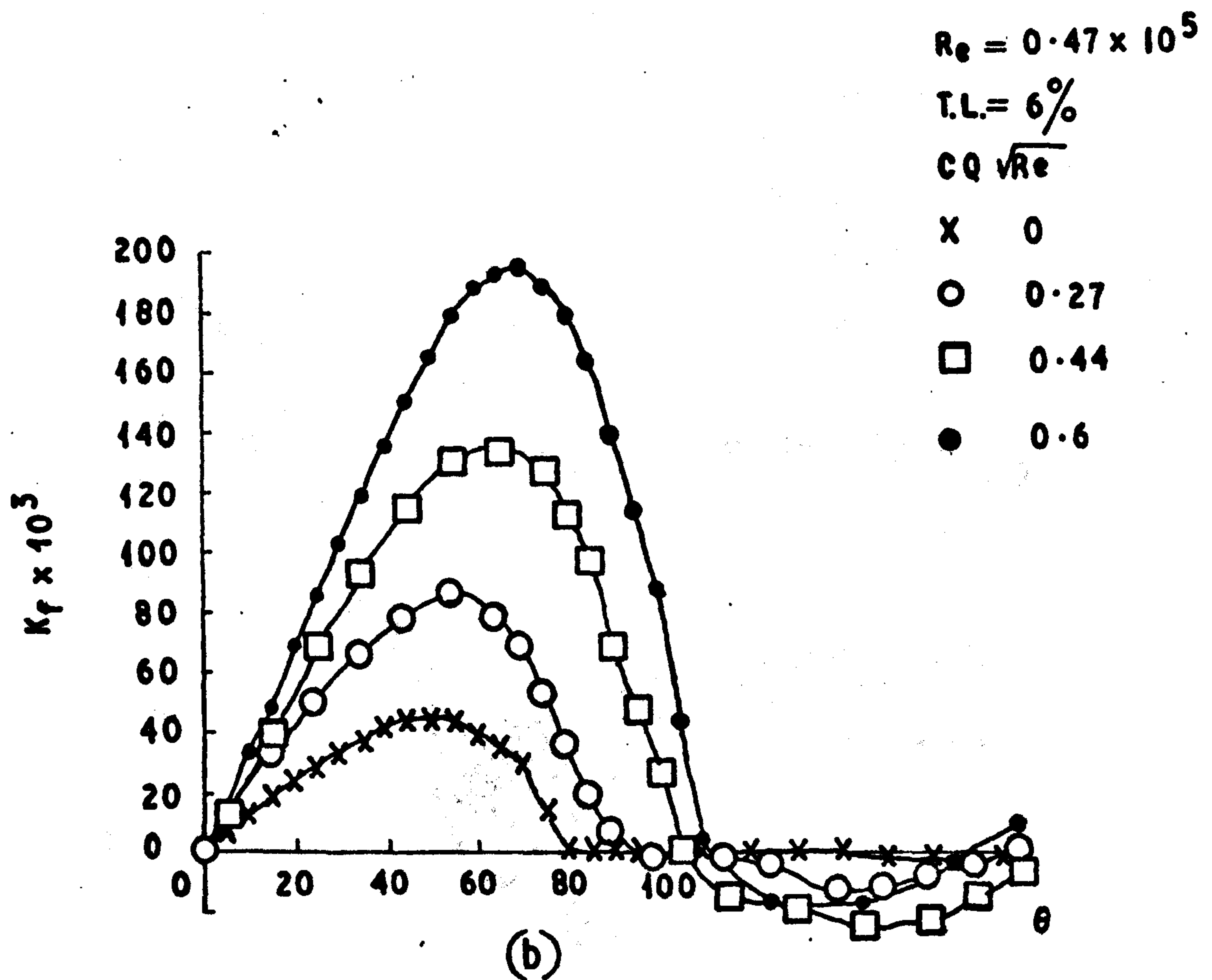
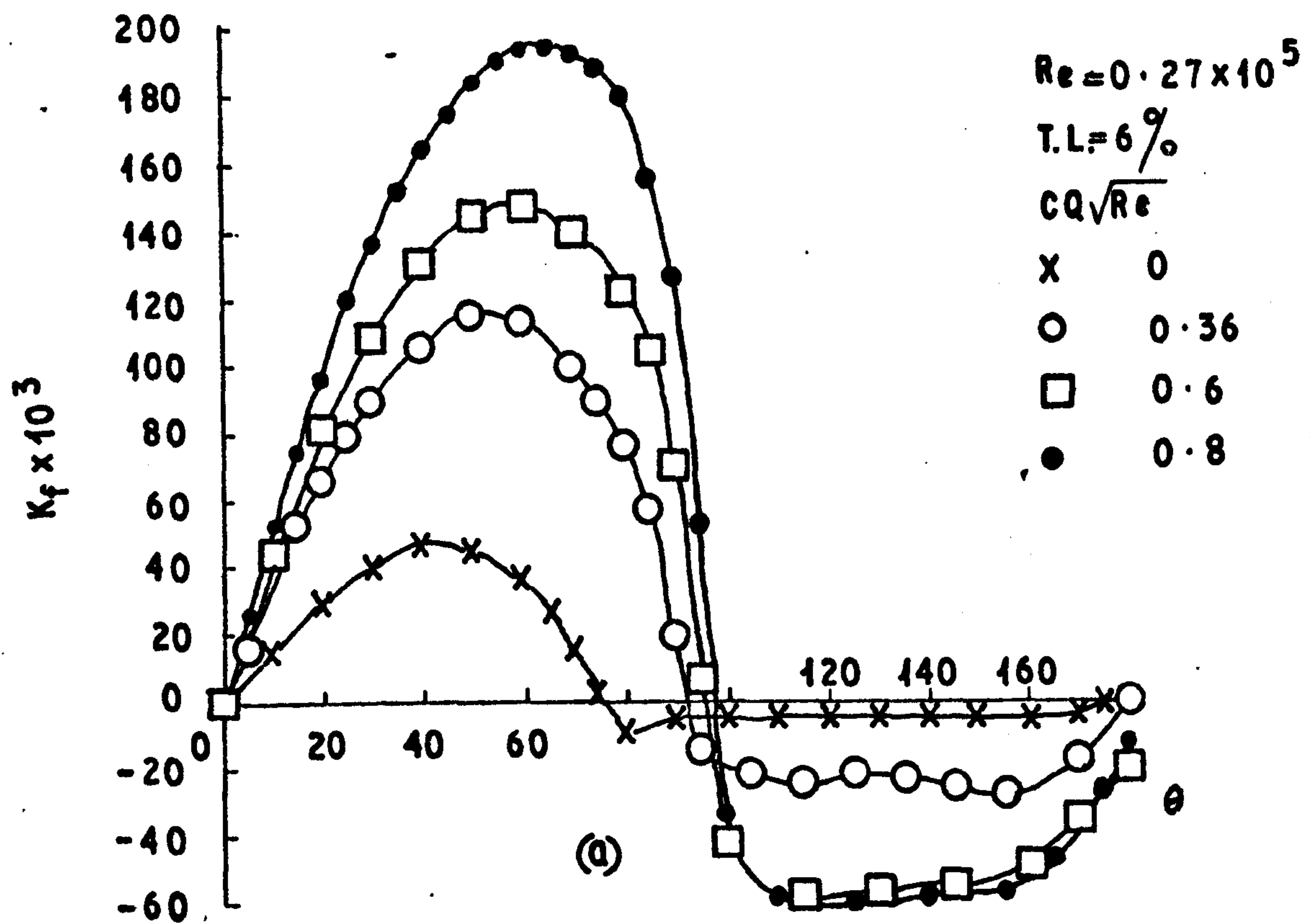
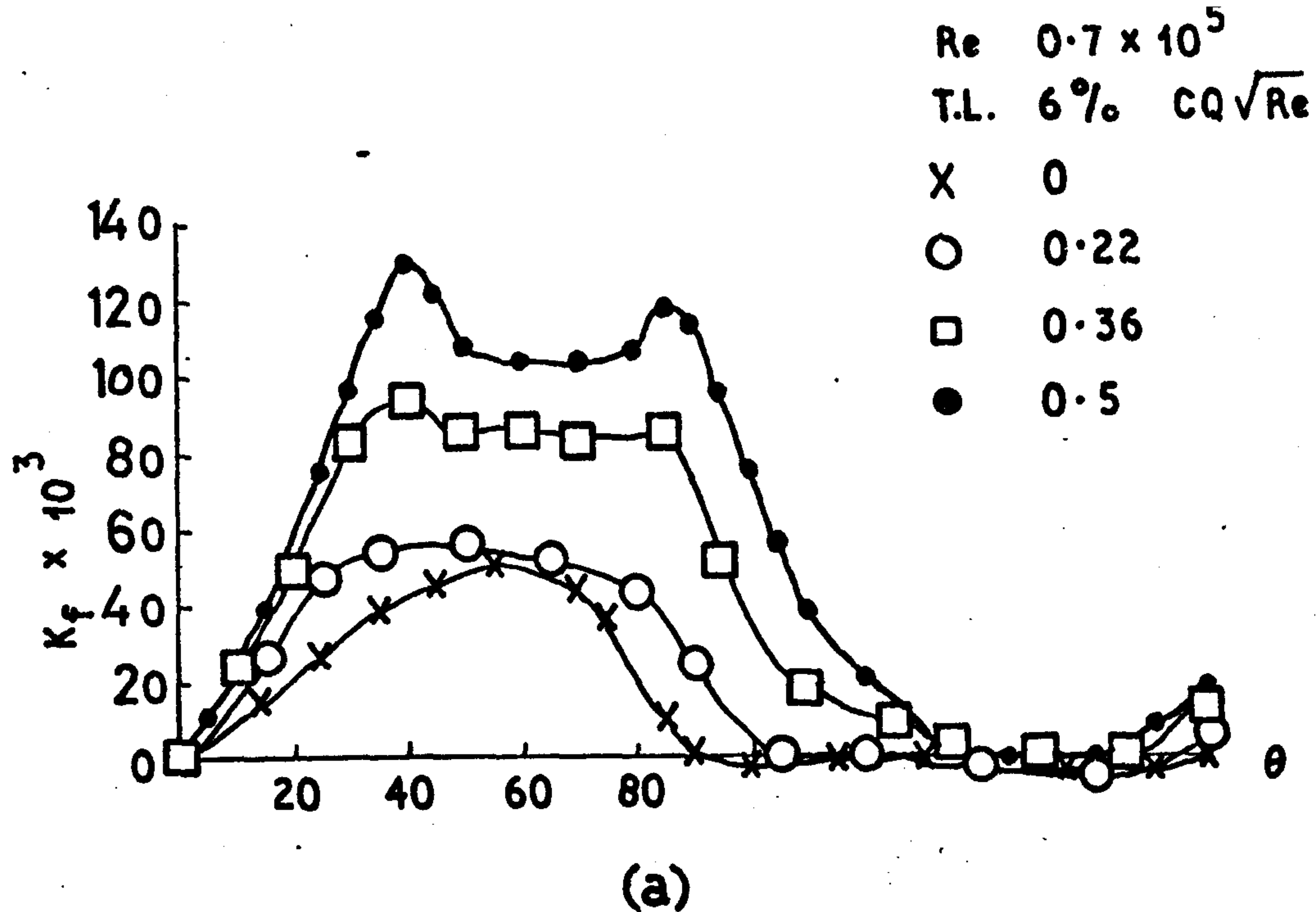


Fig. 8.4

SKIN FRICTION ON A CIRCULAR CYLINDER  
FITTED WITH WIRE AT REAR



SKIN FRICTION ON A CIRCULAR CYLINDER  
FITTED WITH WIRE AT REAR

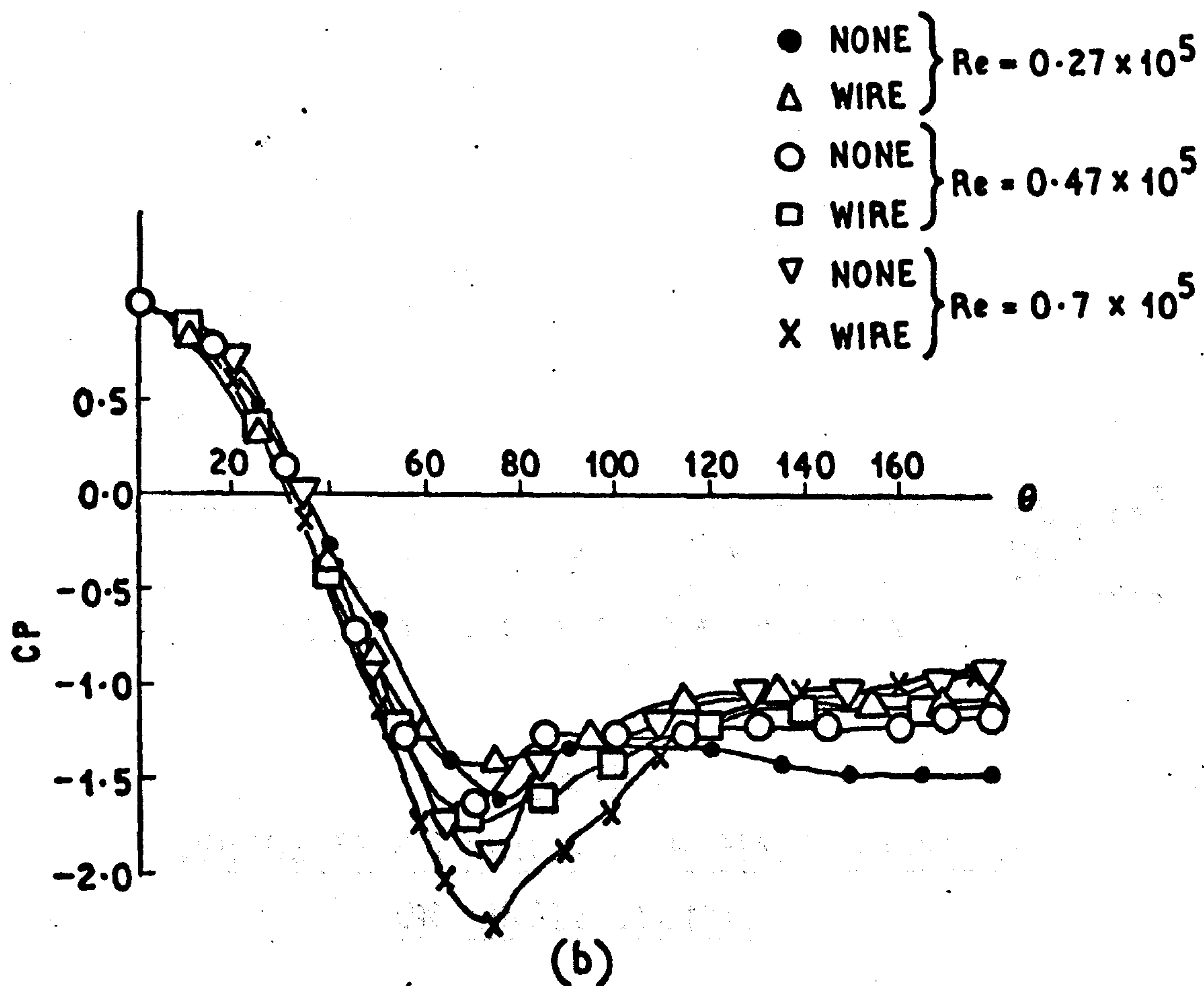
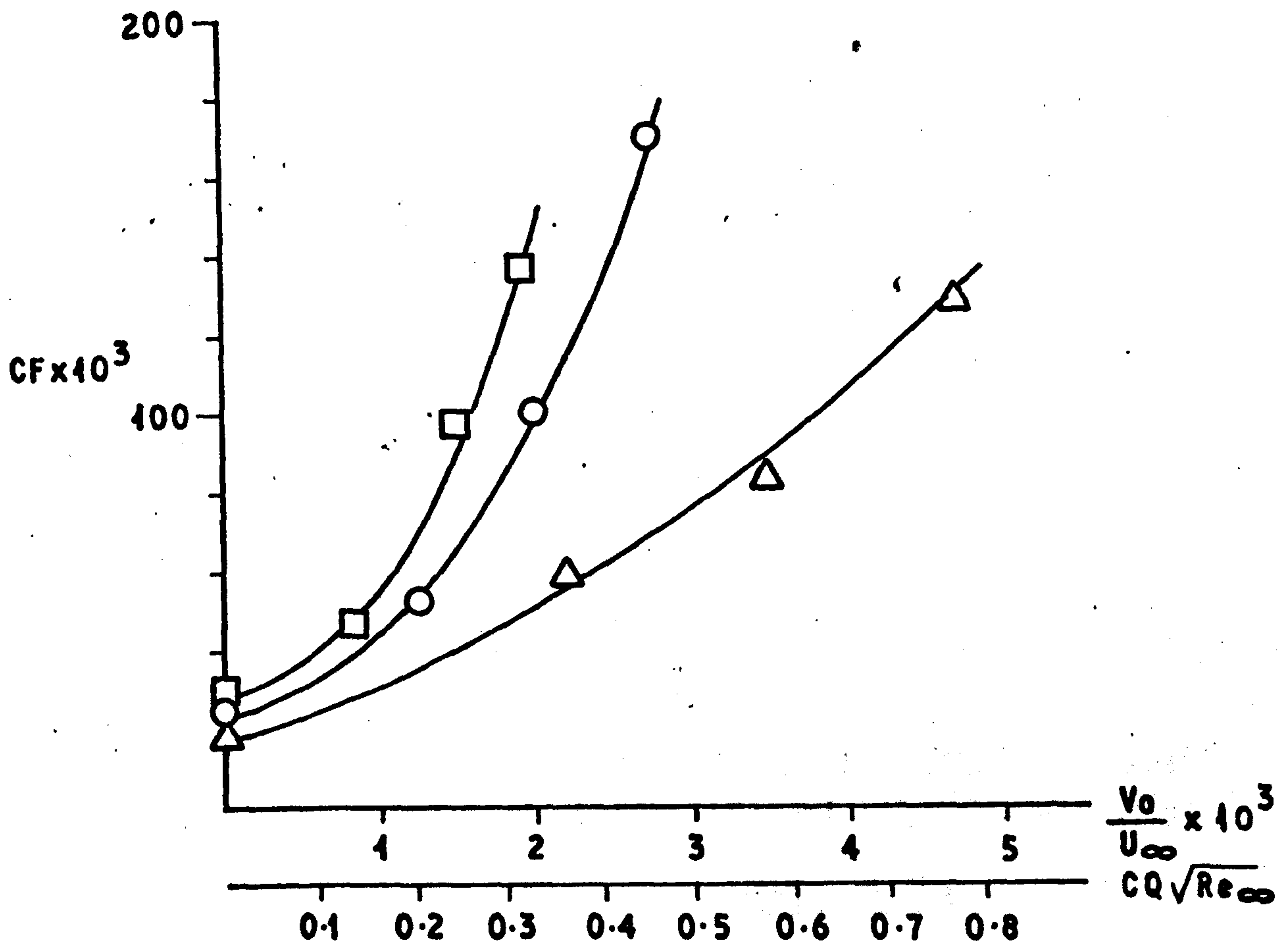


Fig. 8.5  
EFFECT OF WIRE FITTED AT REAR ON  
SKIN FRICTION WITH SUCTION

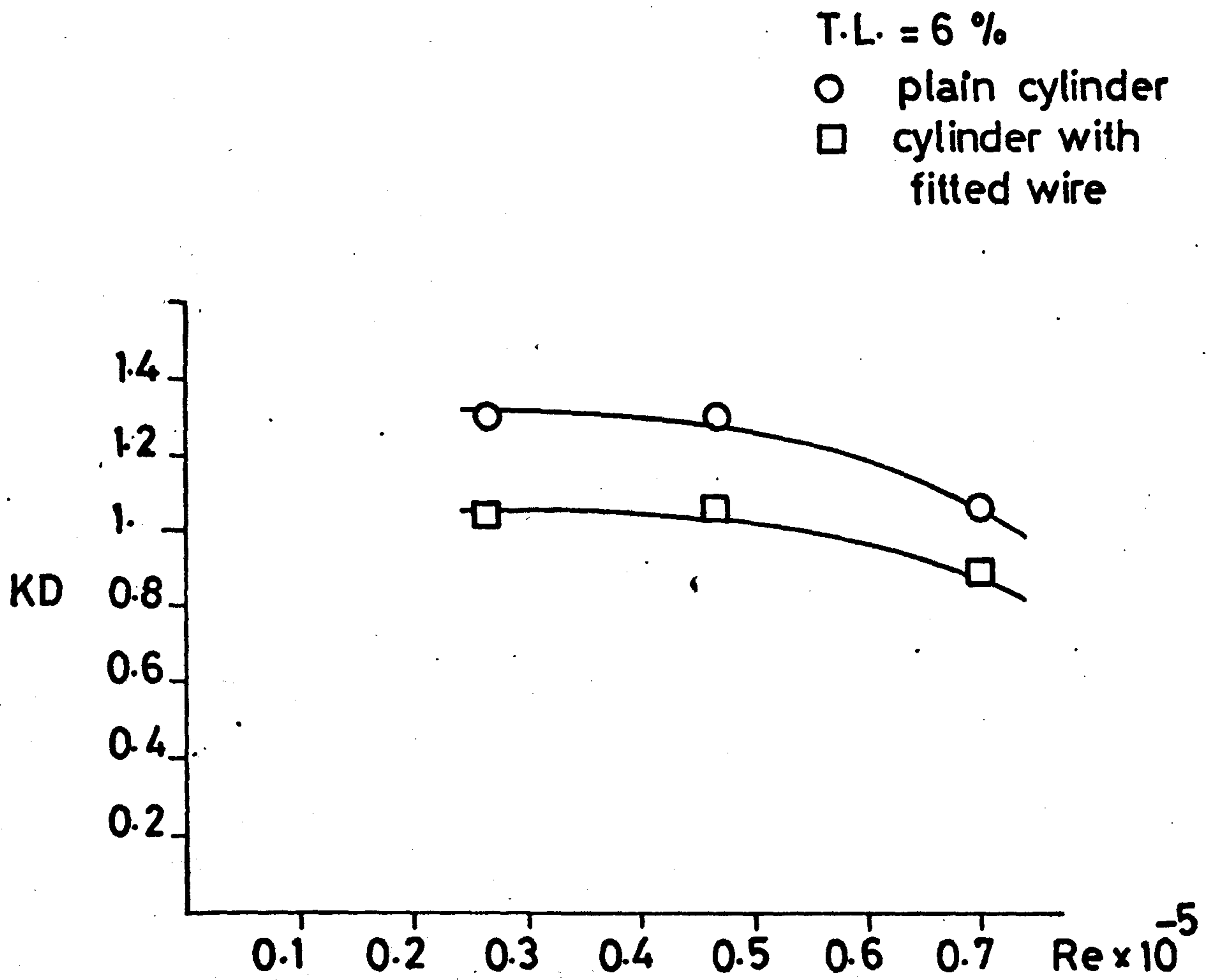
$\nabla$   $Re_{\infty} = 0.27 \times 10^5$   
 $\circ$   $= 0.47$   
 $\square$   $= 0.7$



**Fig. 8.6**

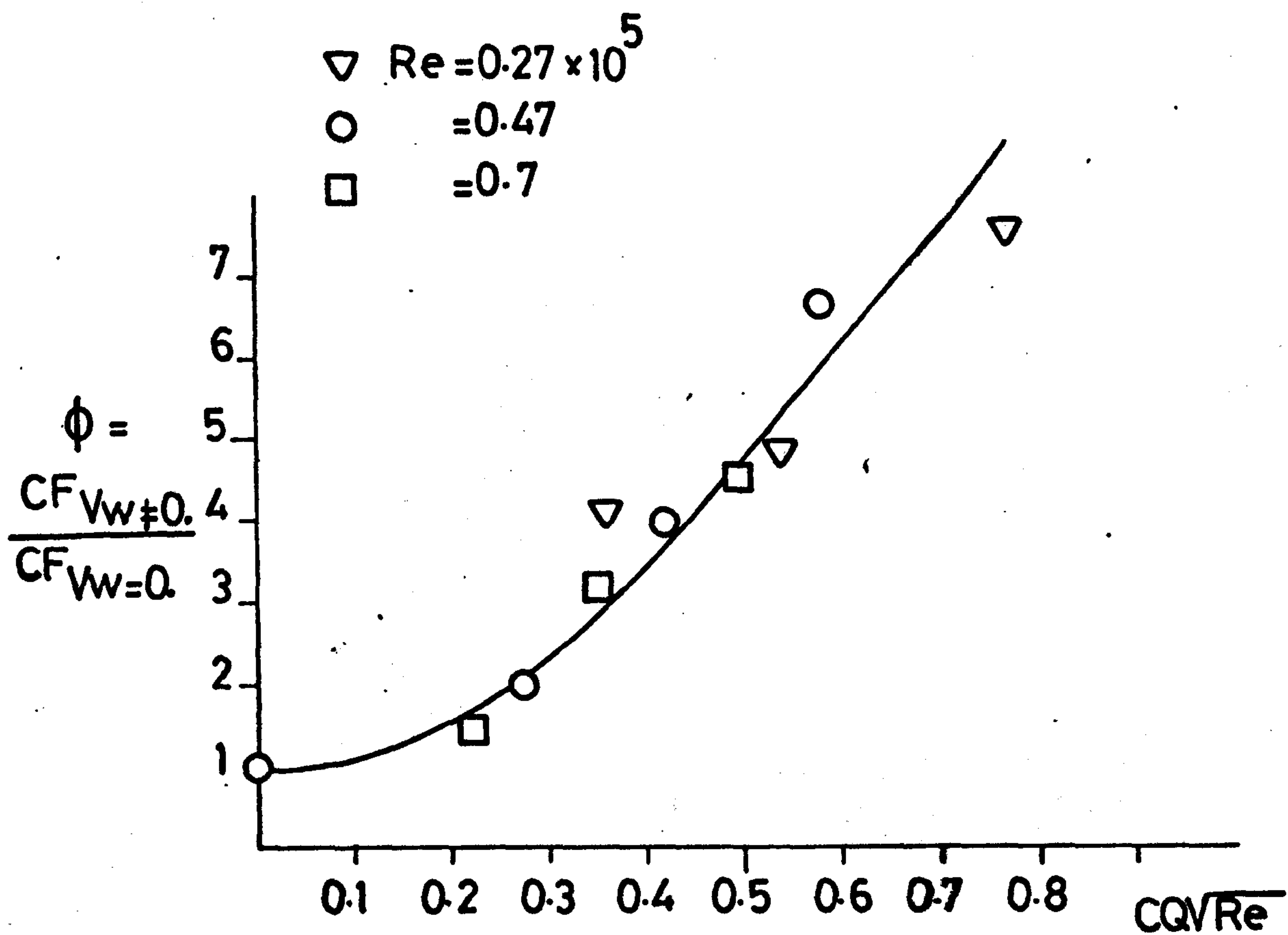
**AVERAGE SKIN FRICTION WITH MASS TRANSFER**  
**ON SINGLE CYLINDER**





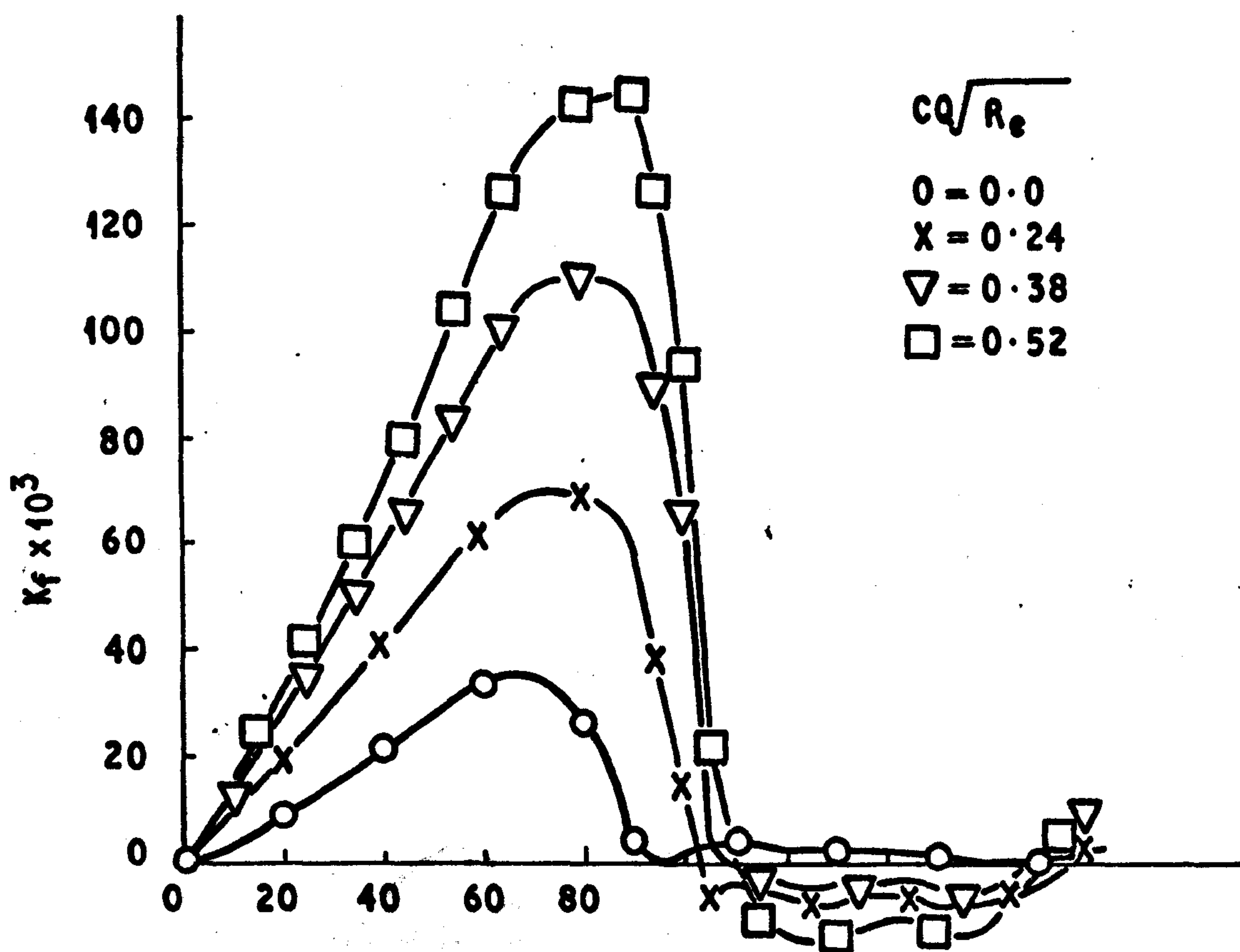
Pressure drag on rough cylinder  
(uncorrected for blockage effect)

Fig. 8.7a



Skin friction ratio against suction parameter, single cylinder

Fig. 8.7 b

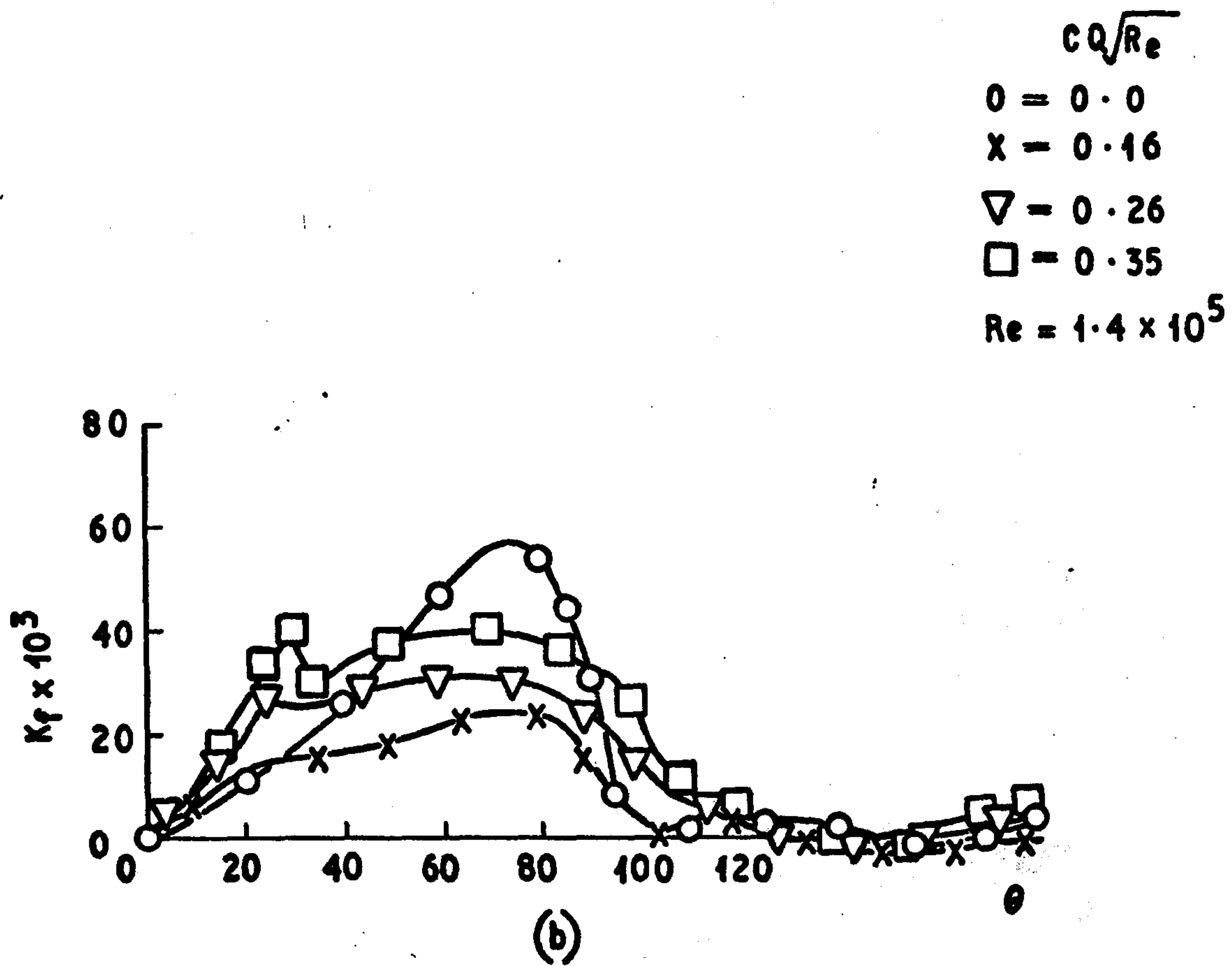
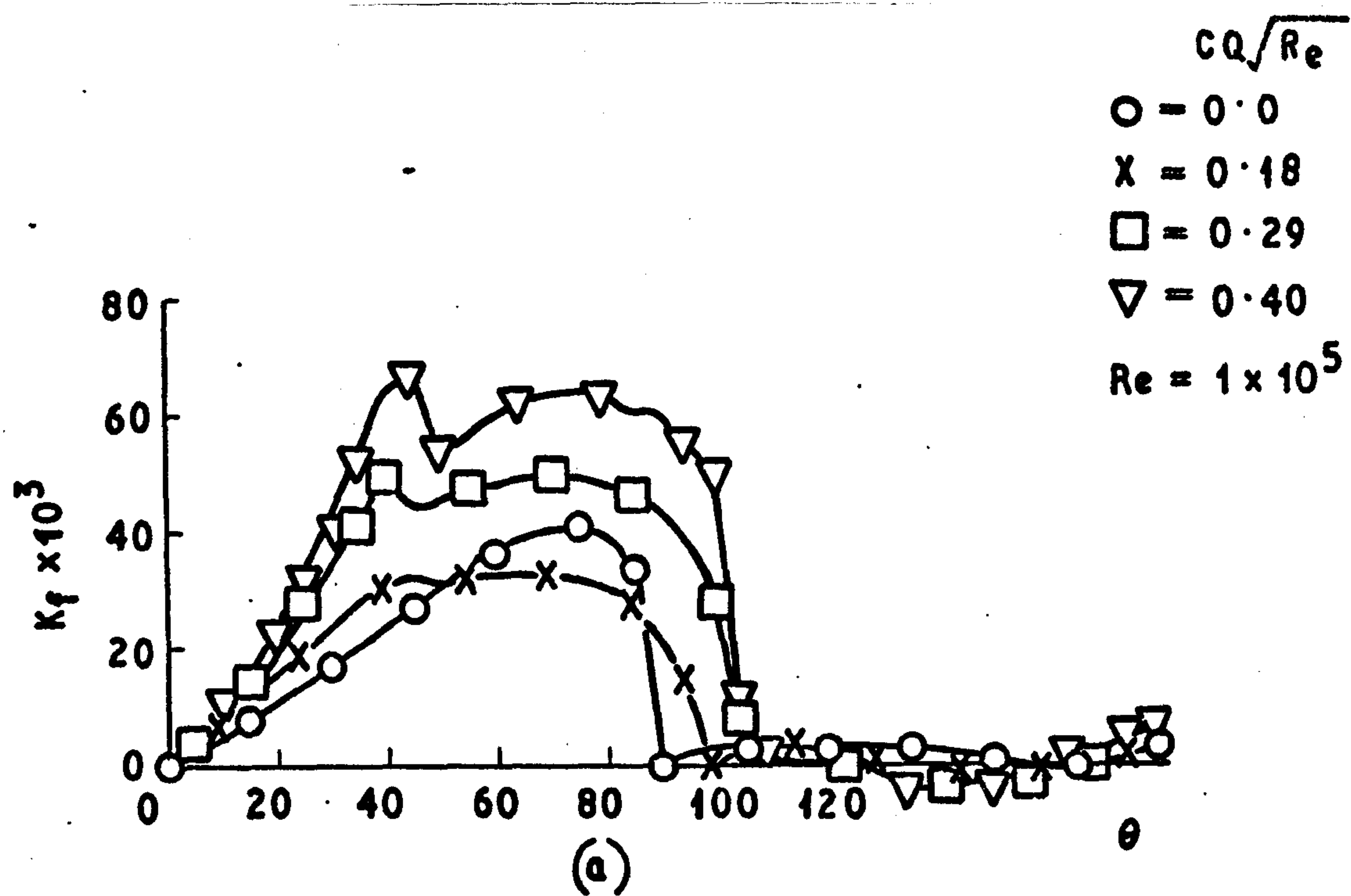


**SKIN FRICTION WITH SUCTION**  
**ON THE FIRST ROW OF THE BANK**

$R_e = 0.6 \times 10^5$

**FIG. 8.8**





SKIN FRICTION WITH SUCTION  
ON THE FIRST ROW OF THE BANK

FIG. 8.9

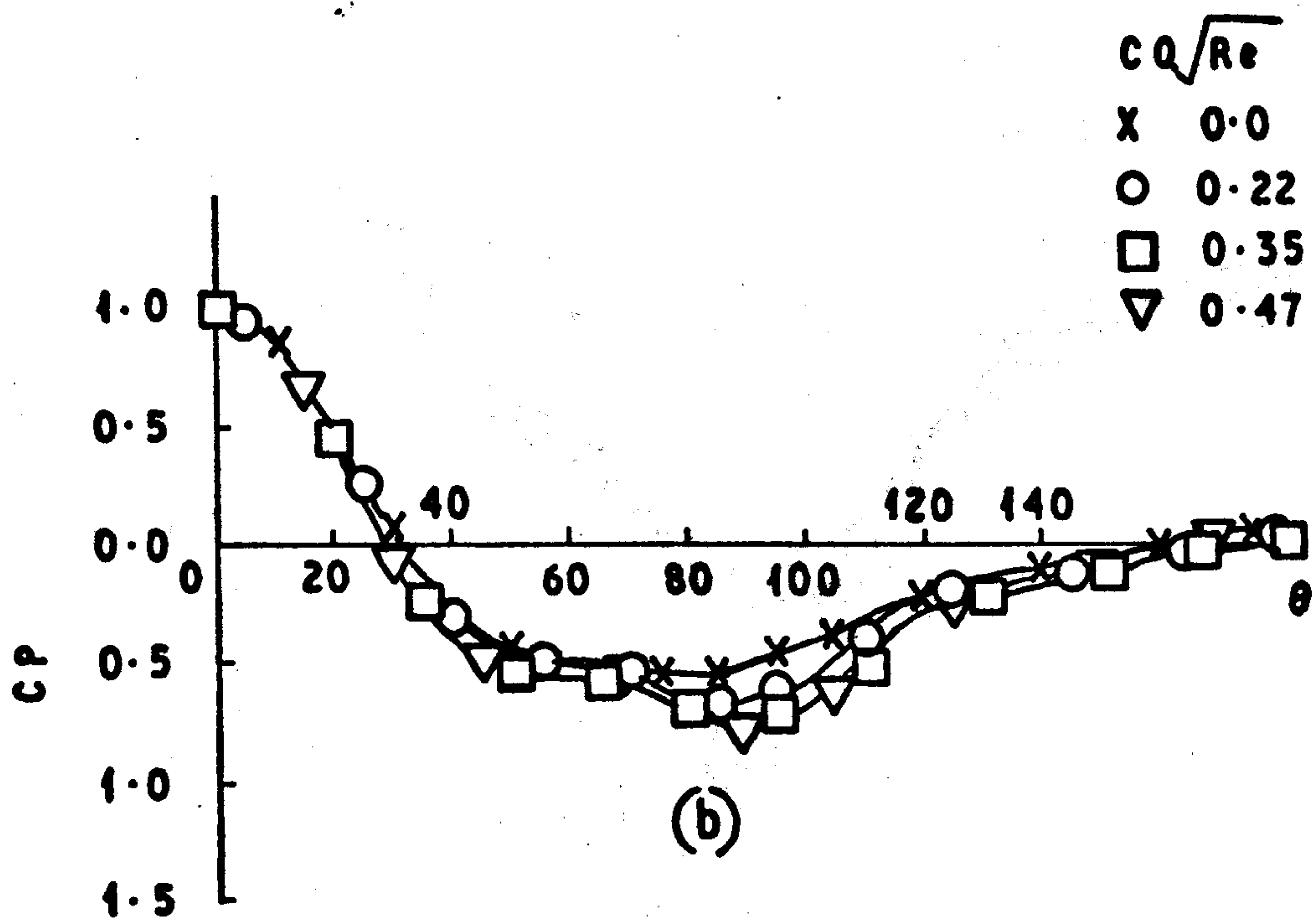
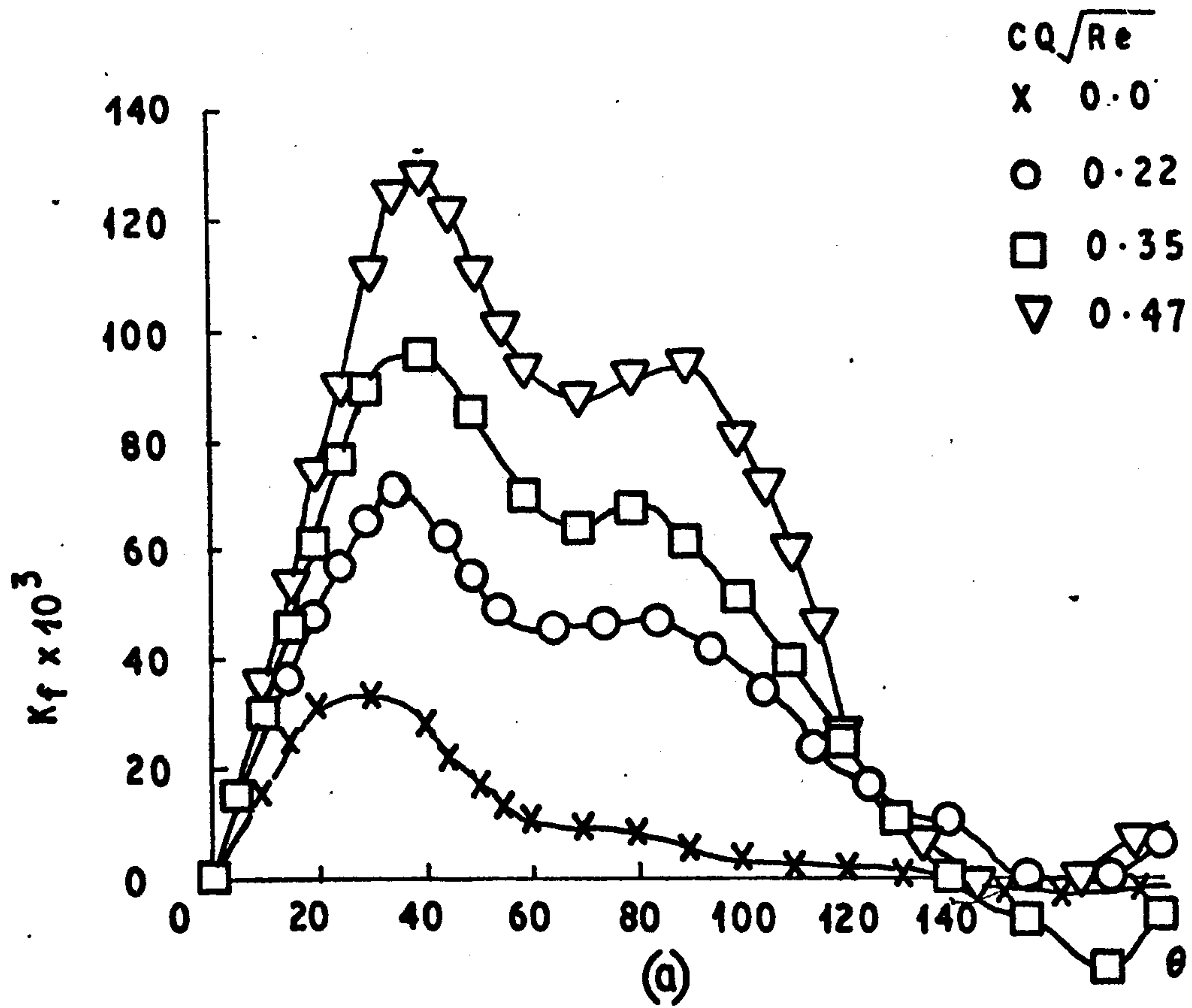


**Fig. 8.10**  
**EFFECT OF SUCTION ON PRESSURE DISTRIBUTION**  
**SECOND ROW,  $Re = 0.76 \times 10^5$**

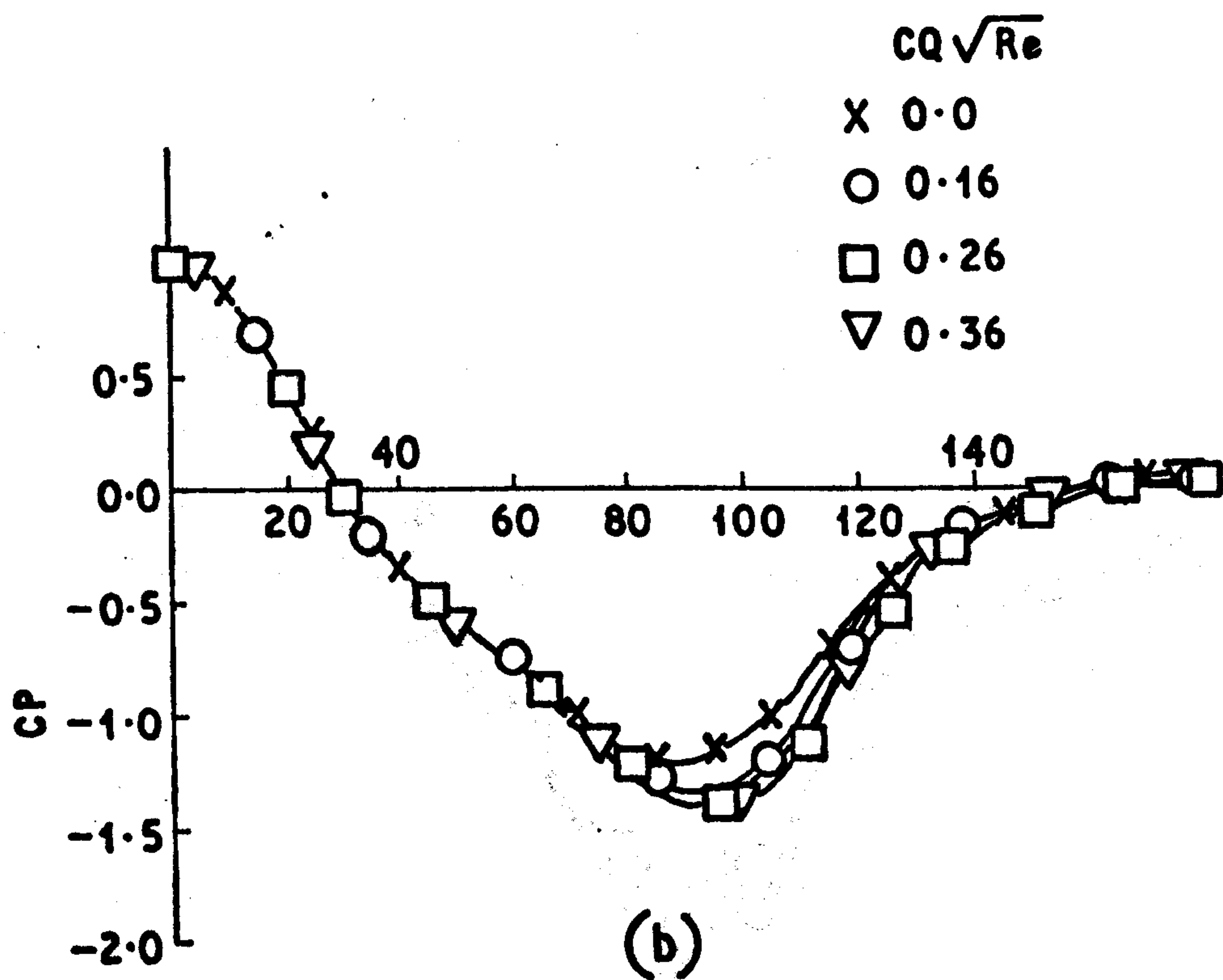
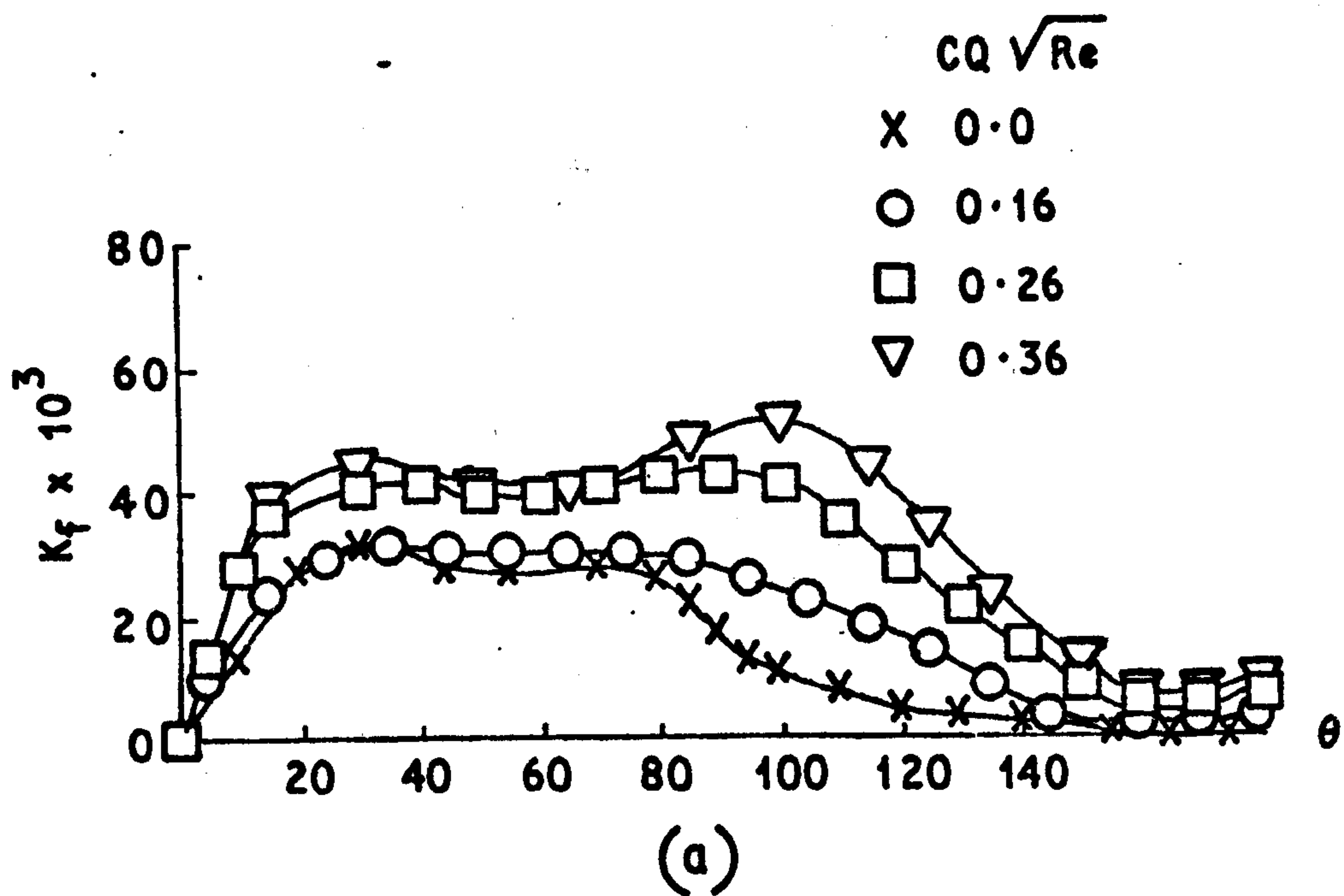


**Fig. 8.11**  
**EFFECT OF SUCTION ON PRESSURE DISTRIBUTION**  
**SECOND ROW,  $Re = 1.3 \times 10^5$**



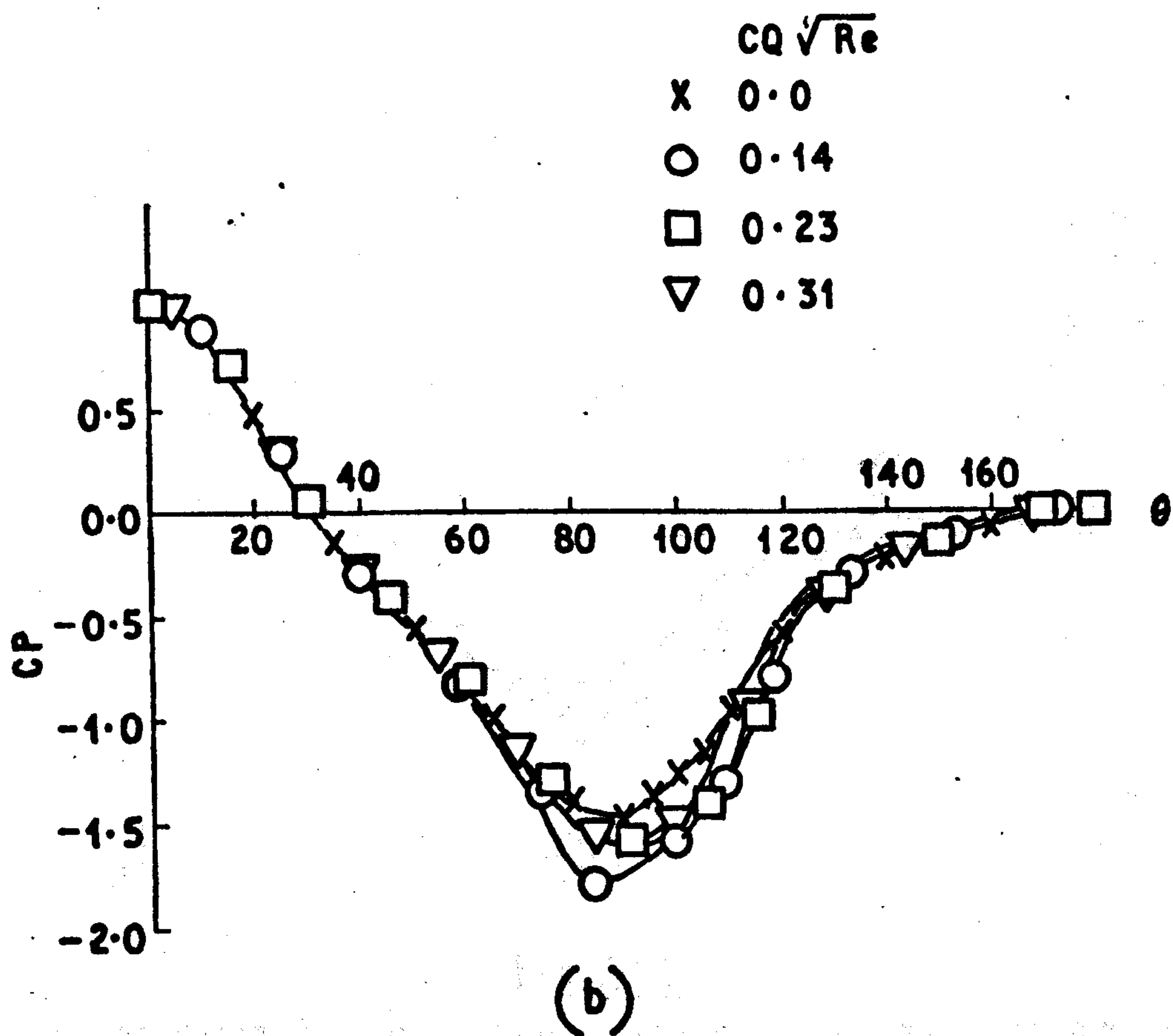
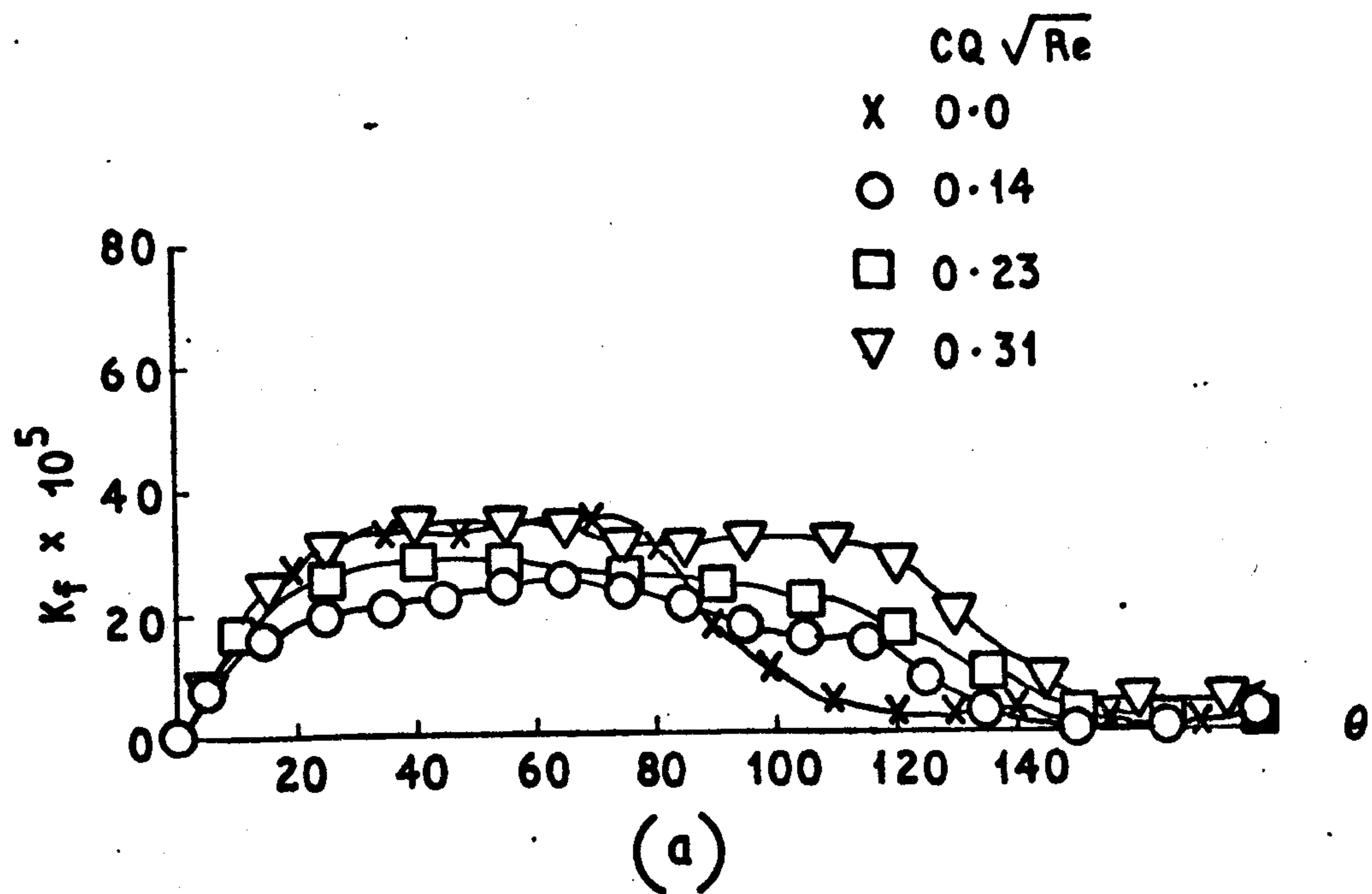


**Fig. 8.12**  
SUCTION EFFECT ON SKIN FRICTION DISTRIBUTION,  
SECOND ROW,  $Re = 1.75 \times 10^5$

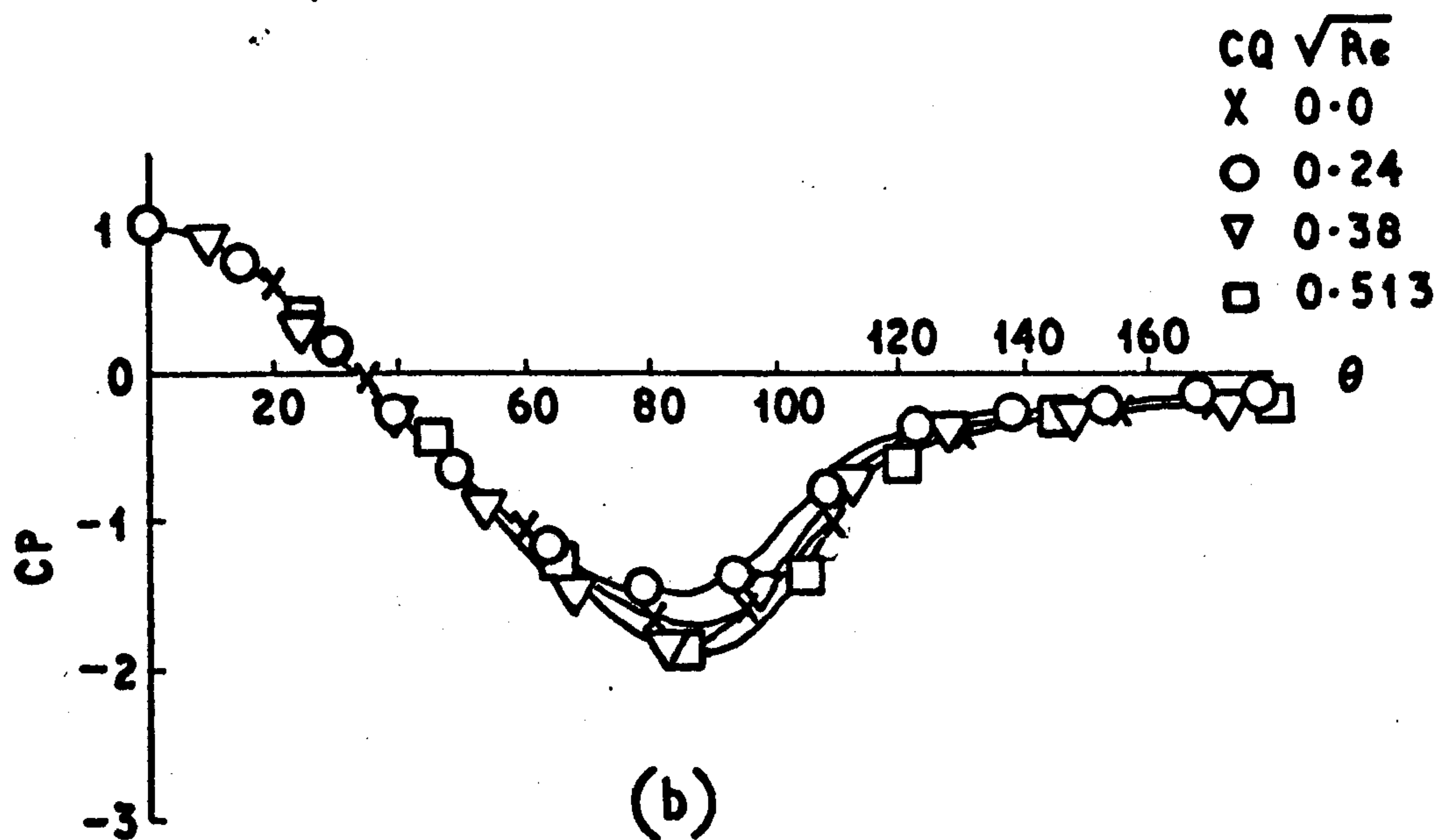
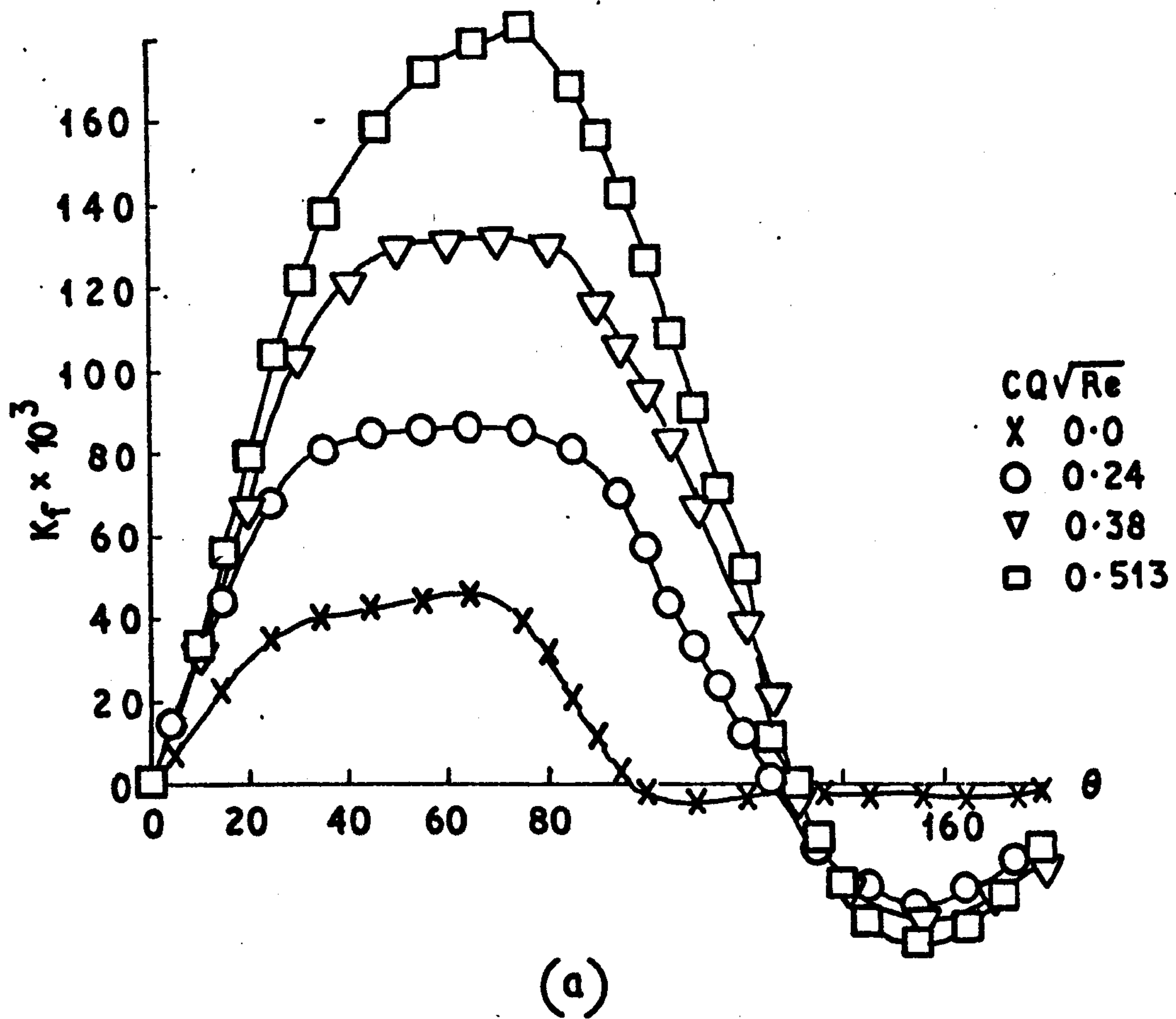


**Fig. 8.13**  
**EFFECT OF SUCTION ON SKIN FRICTION FOR THE THIRD ROW**  
**IN THE BANK**  
 **$Re = 0.6 \times 10^5$**

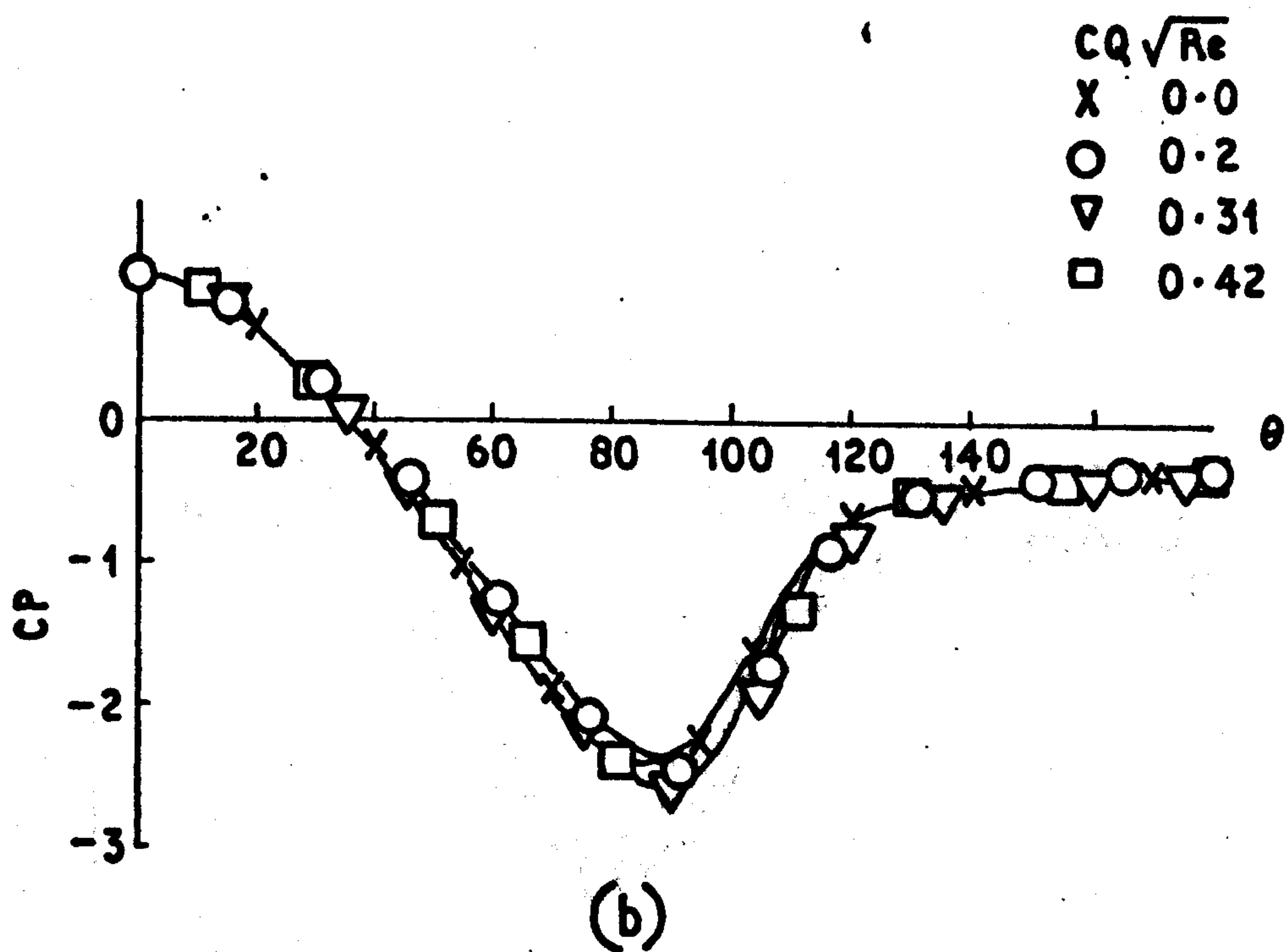
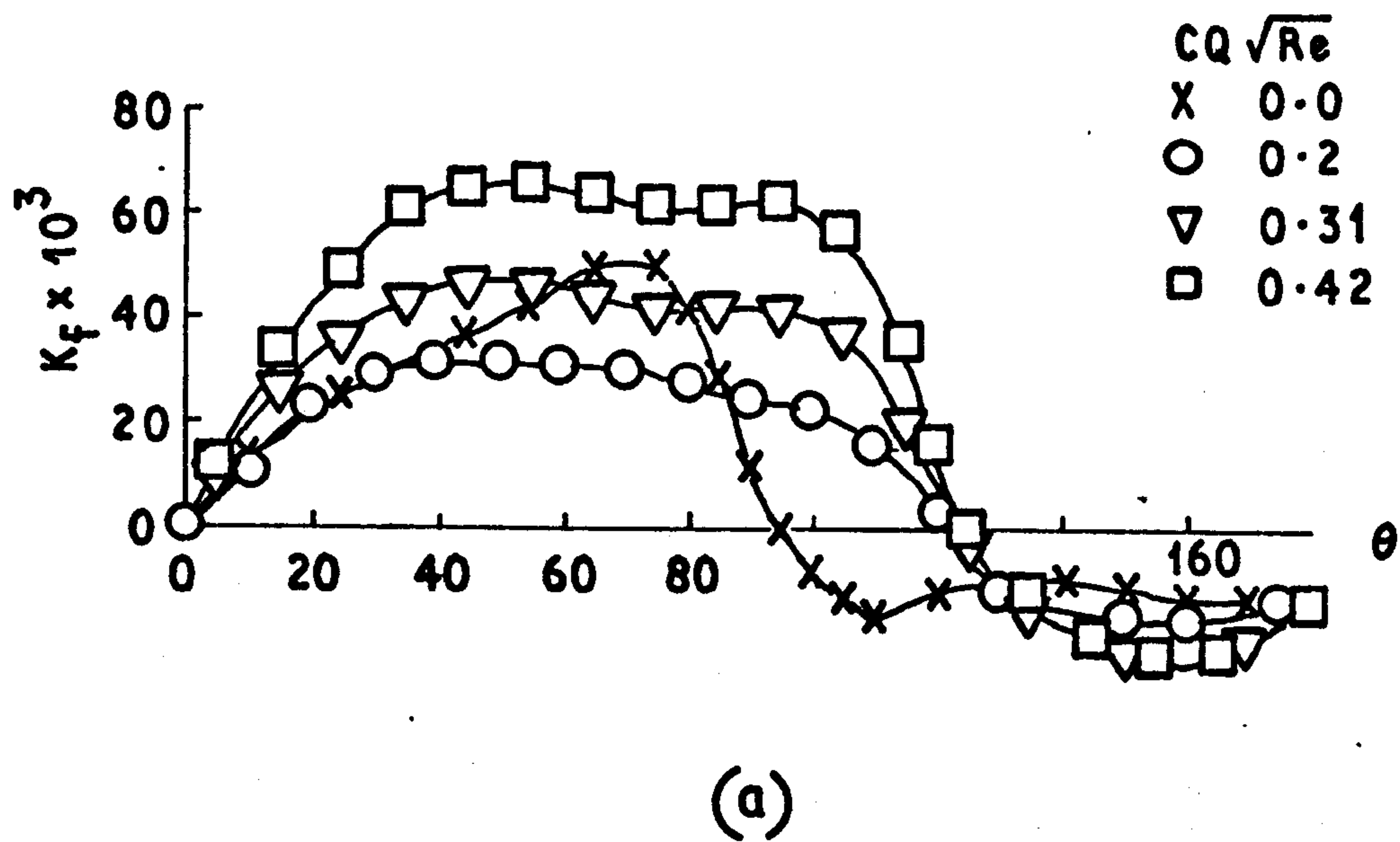


**Fig.8.14**  
**EFFECT OF SUCTION ON SKIN FRICTION FOR THE THIRD ROW**  
**IN THE BANK**  
 **$Re = 0.94 \times 10^5$**



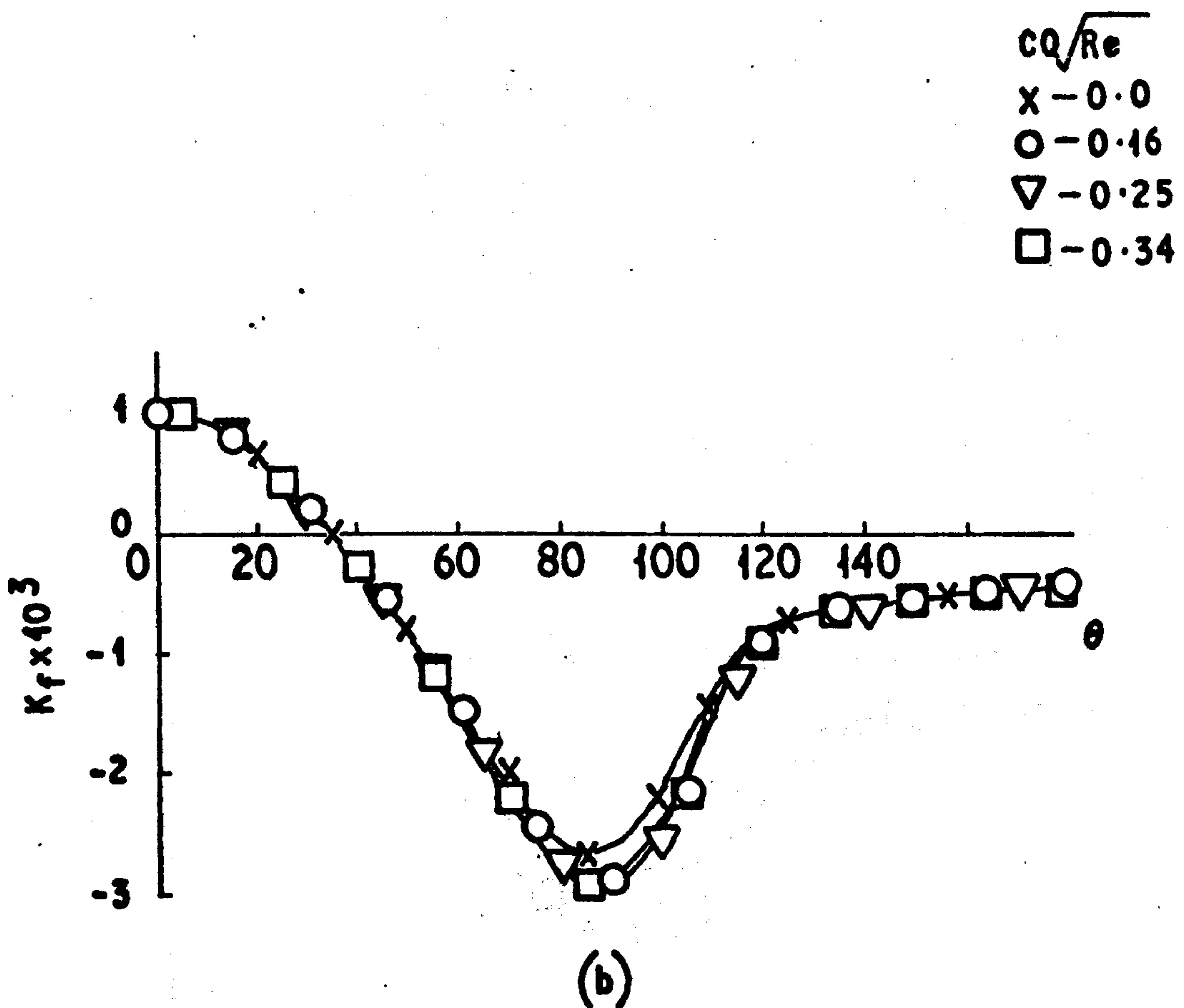
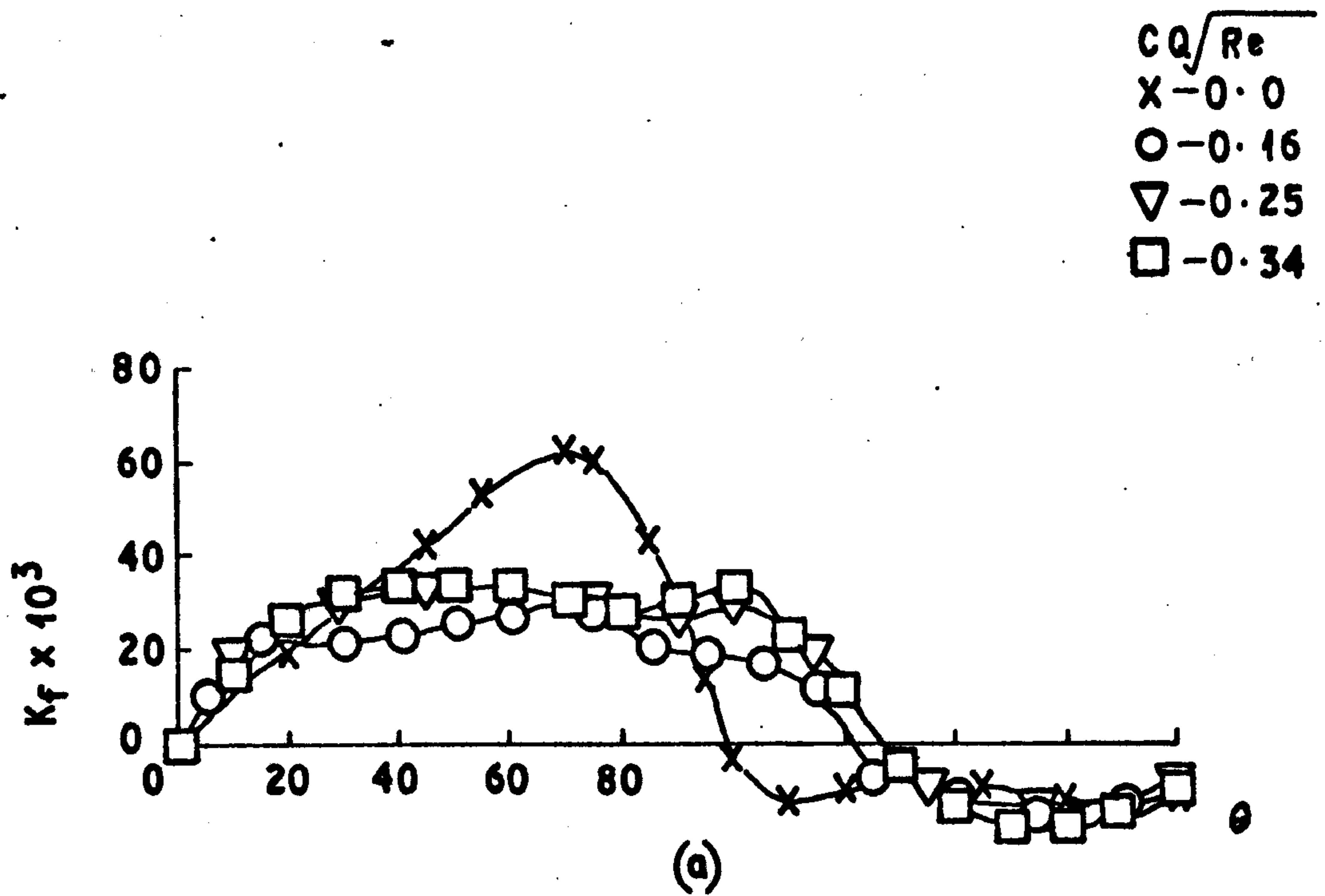


**Fig. 8.15**

**EFFECT OF SUCTION ON SKIN FRICTION FOR THIRD ROW**

**IN THE BANK**

**$Re = 1.3 \times 10^5$**

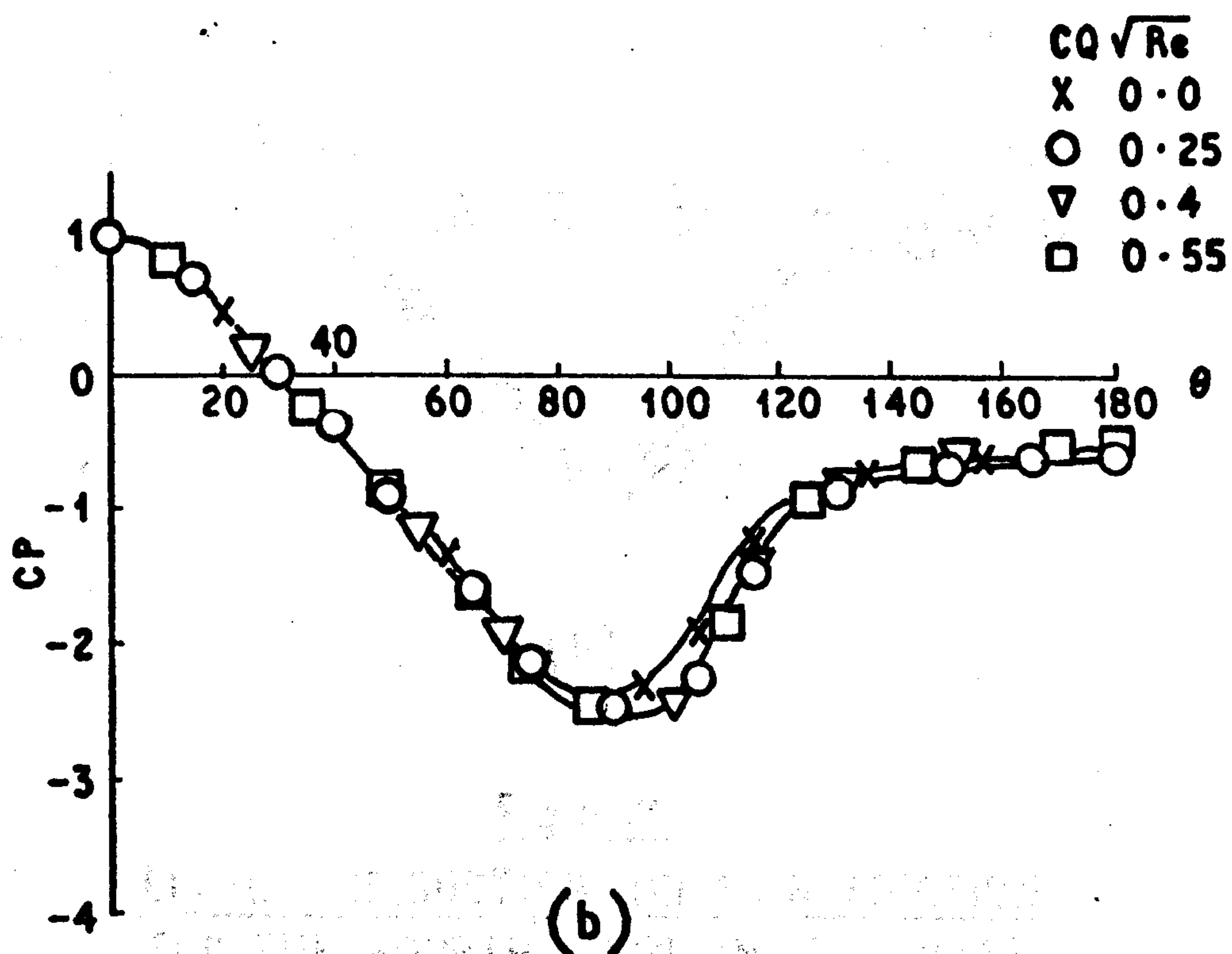
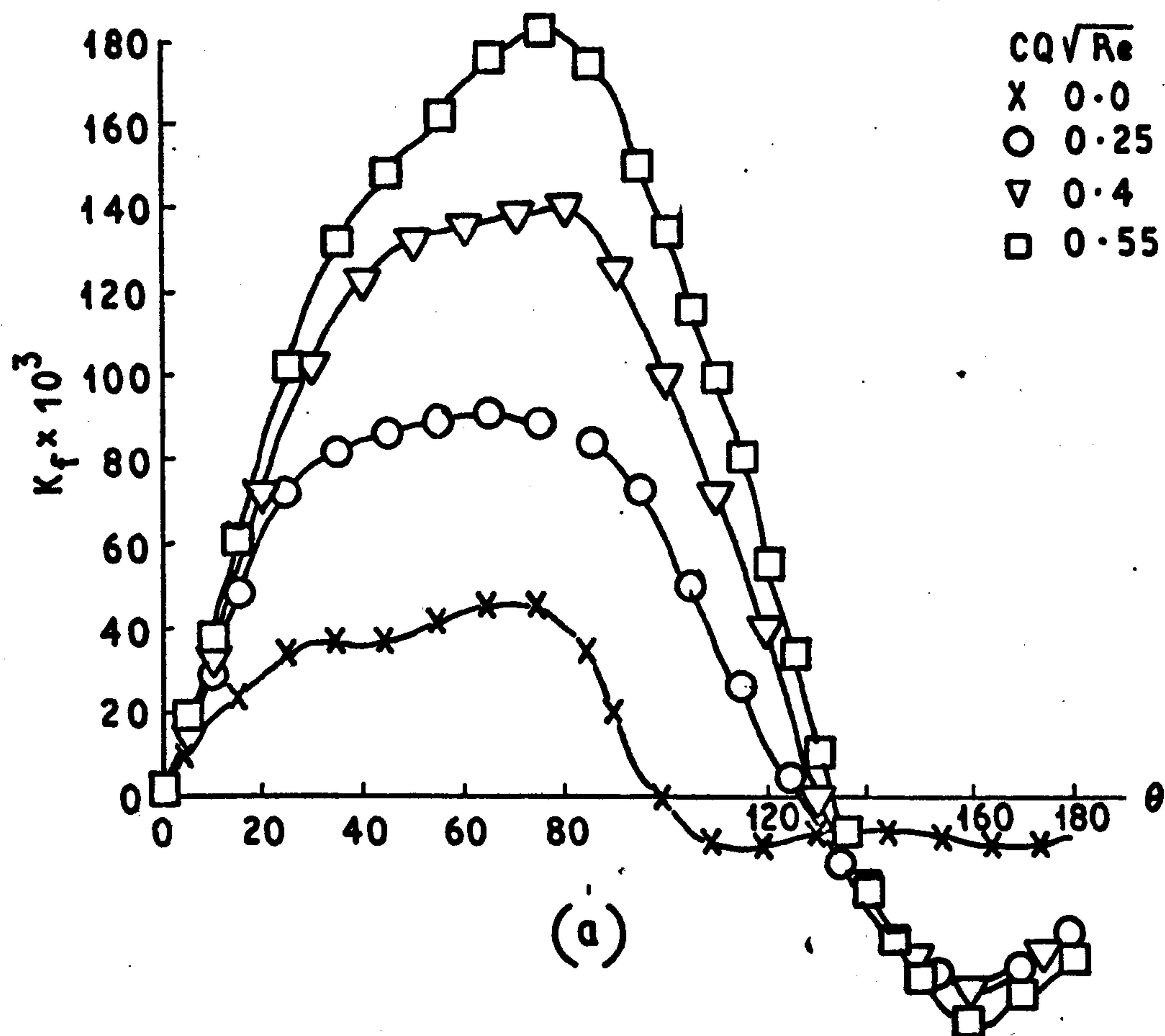


**Fig. 8.16**  
**EFFECT OF SUCTION ON SKIN FRICTION**  
**FOR THE FOURTH ROW IN THE BANK**  
 **$Re = 0.56 \times 10^5$**

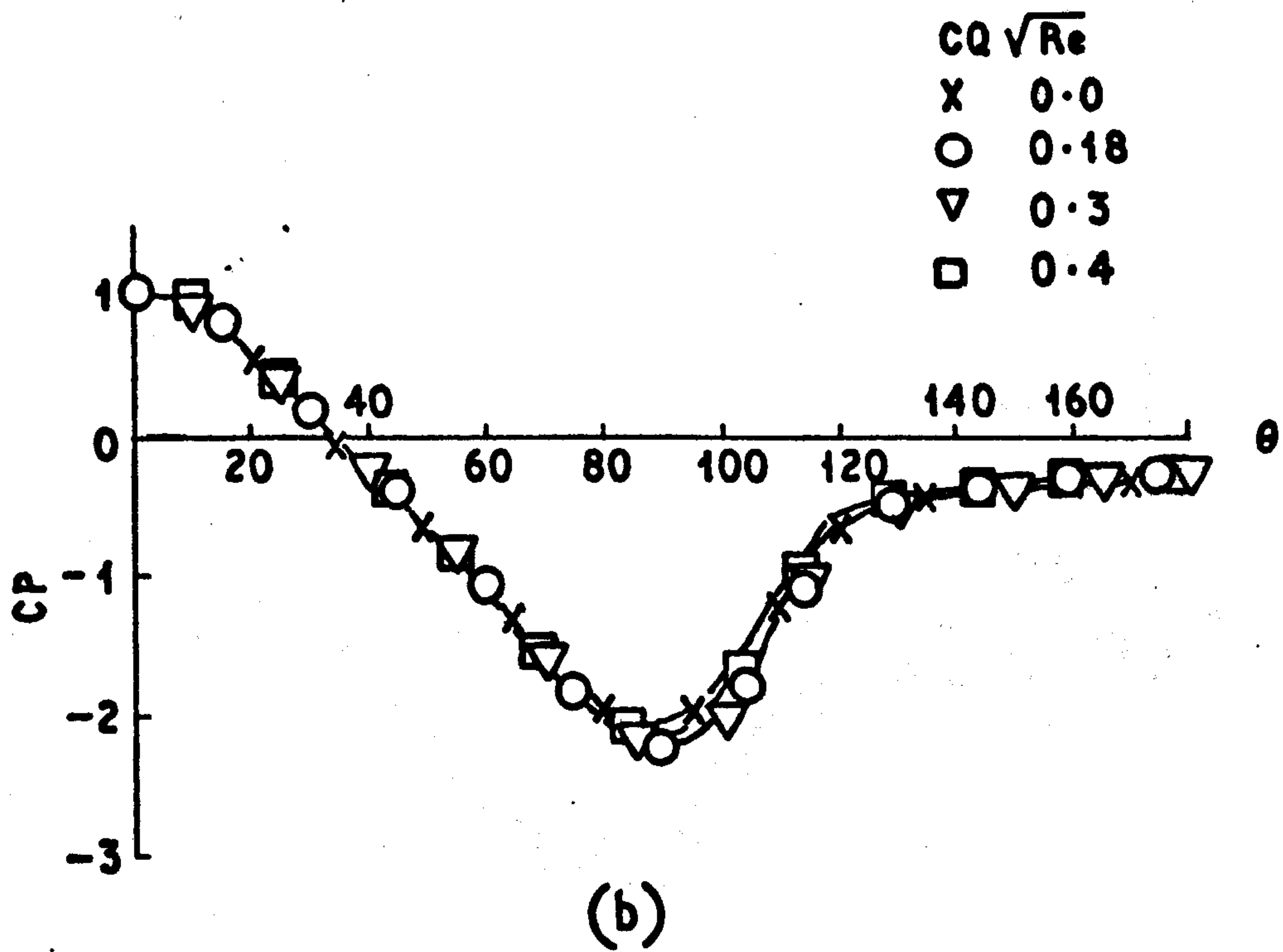
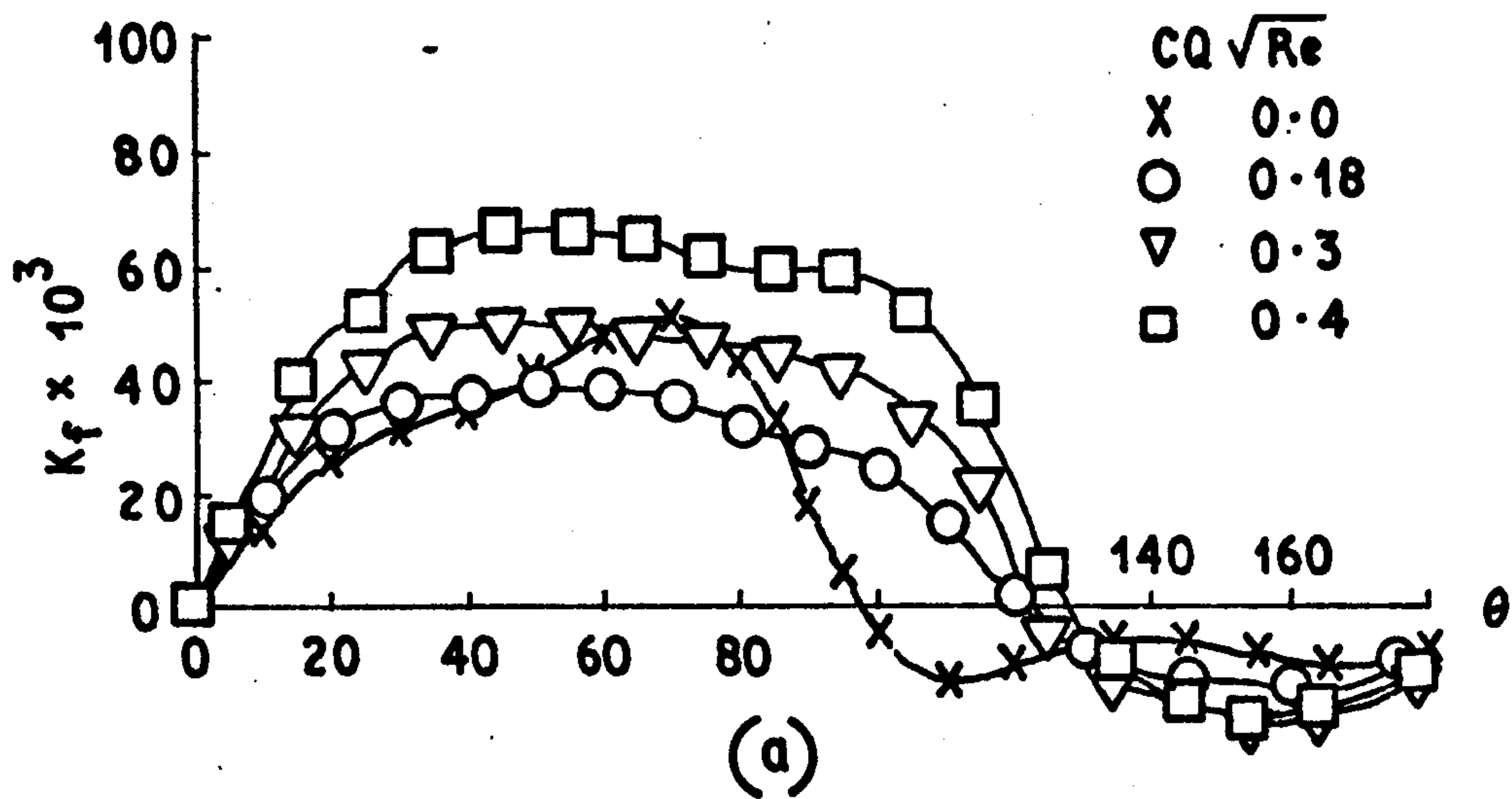


**Fig. 8.17**  
**EFFECT OF SUCTION ON SKIN FRICTION**  
**FOR THE FOURTH ROW IN THE BANK**  
 **$Re = 1 \times 10^5$**



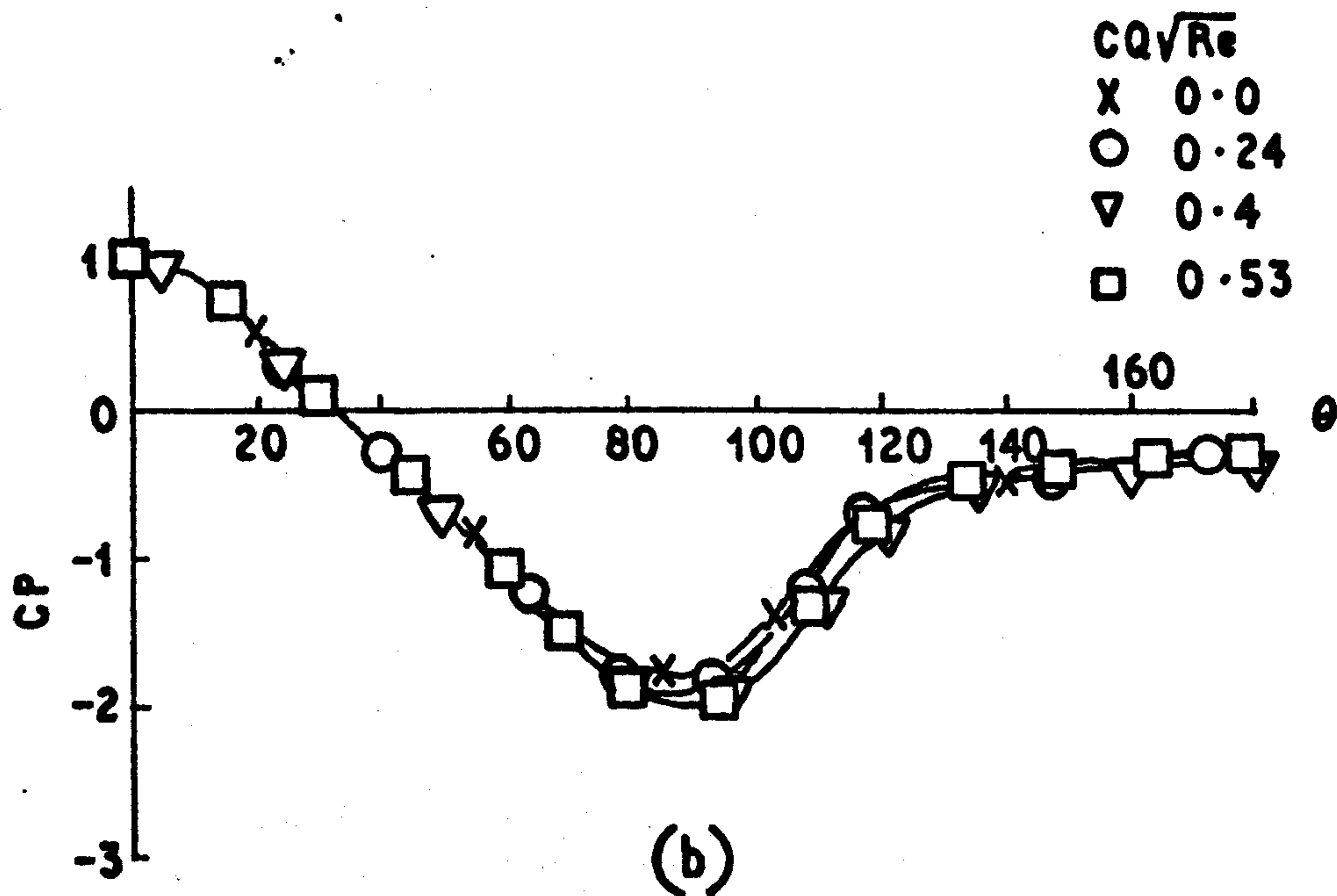
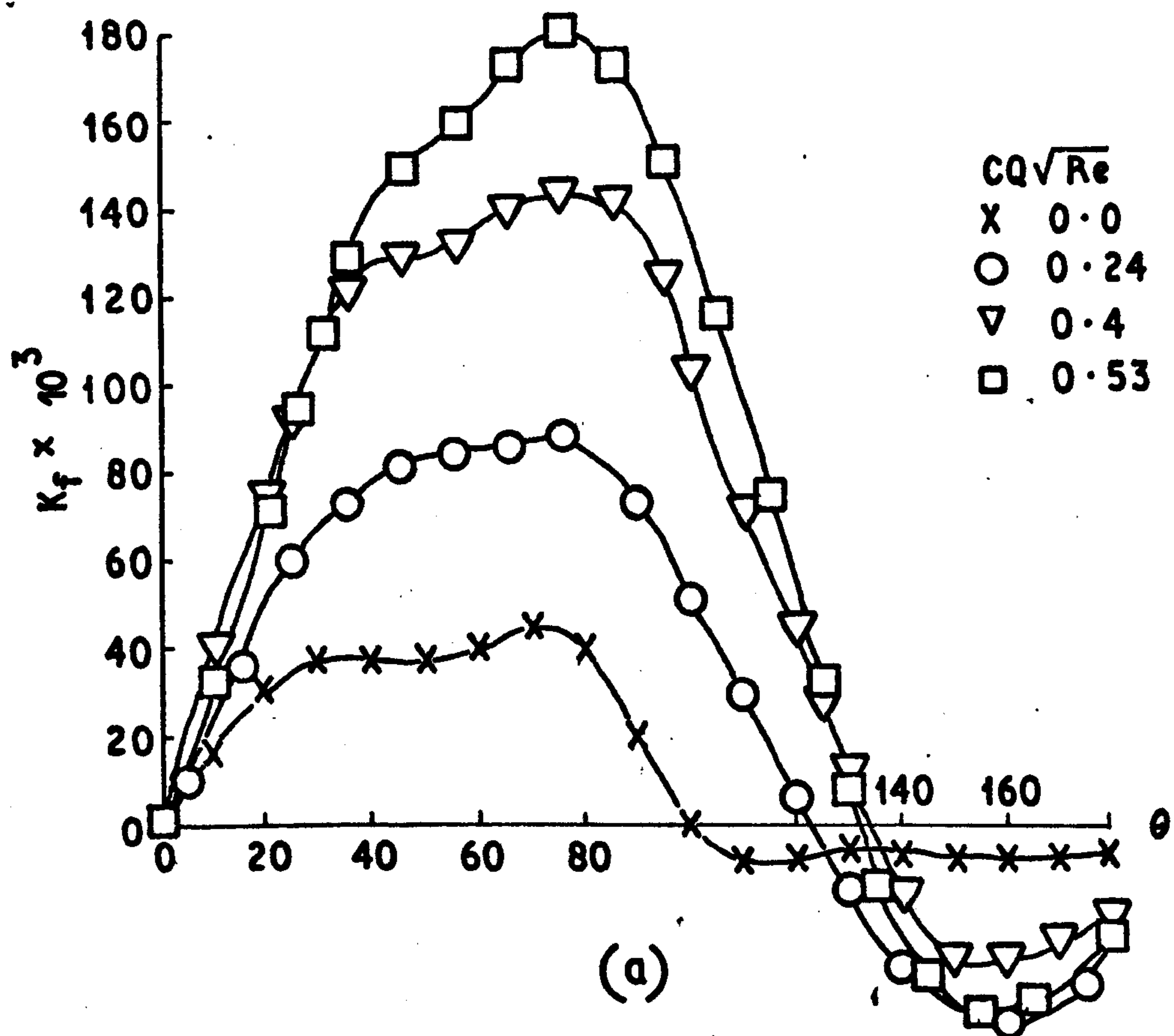


**Fig. 8.18**  
**EFFECT OF SUCTION ON SKIN FRICTION**  
**FOR THE FIFTH ROW IN THE BANK**  
 $Re = 0.6 \times 10^5$

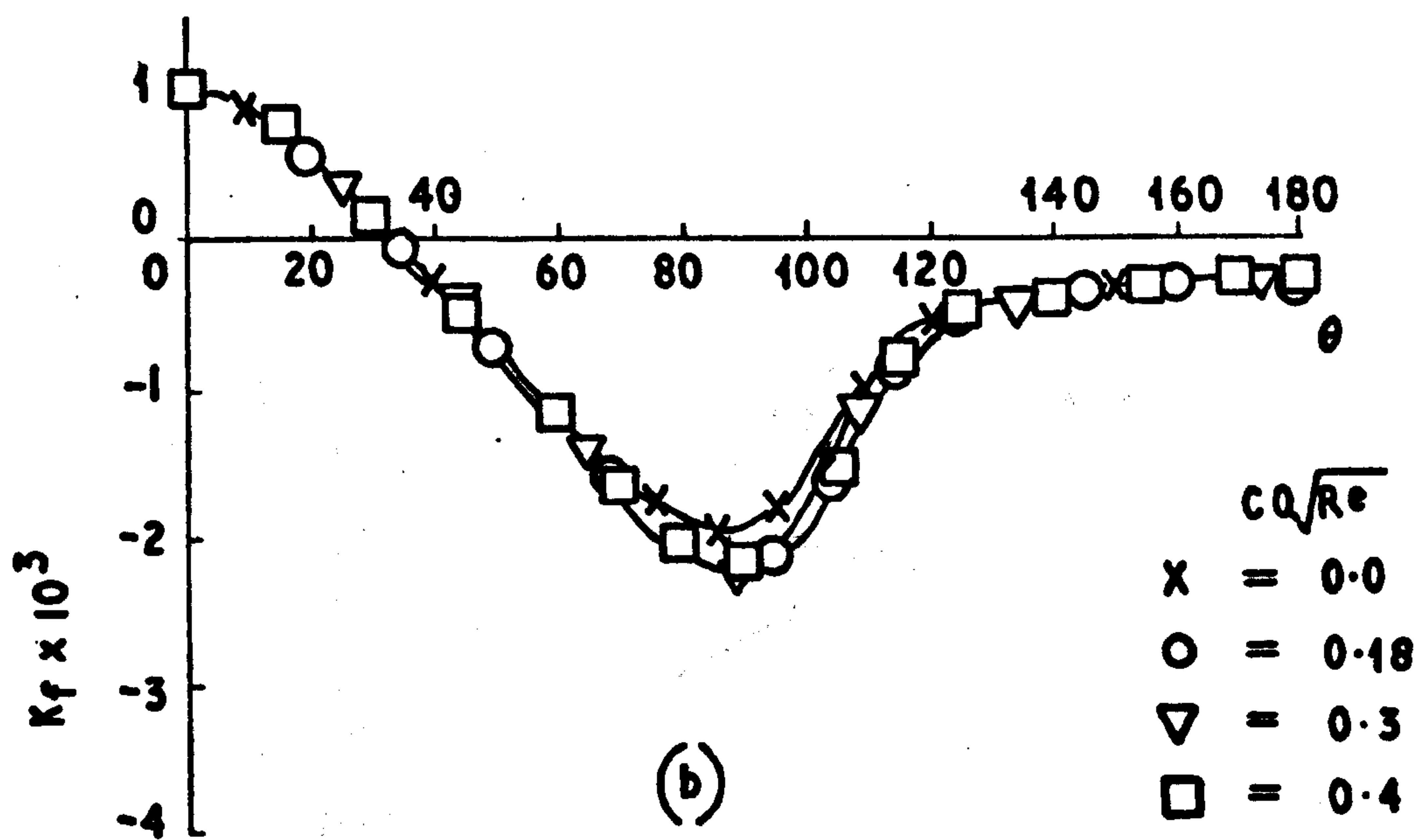
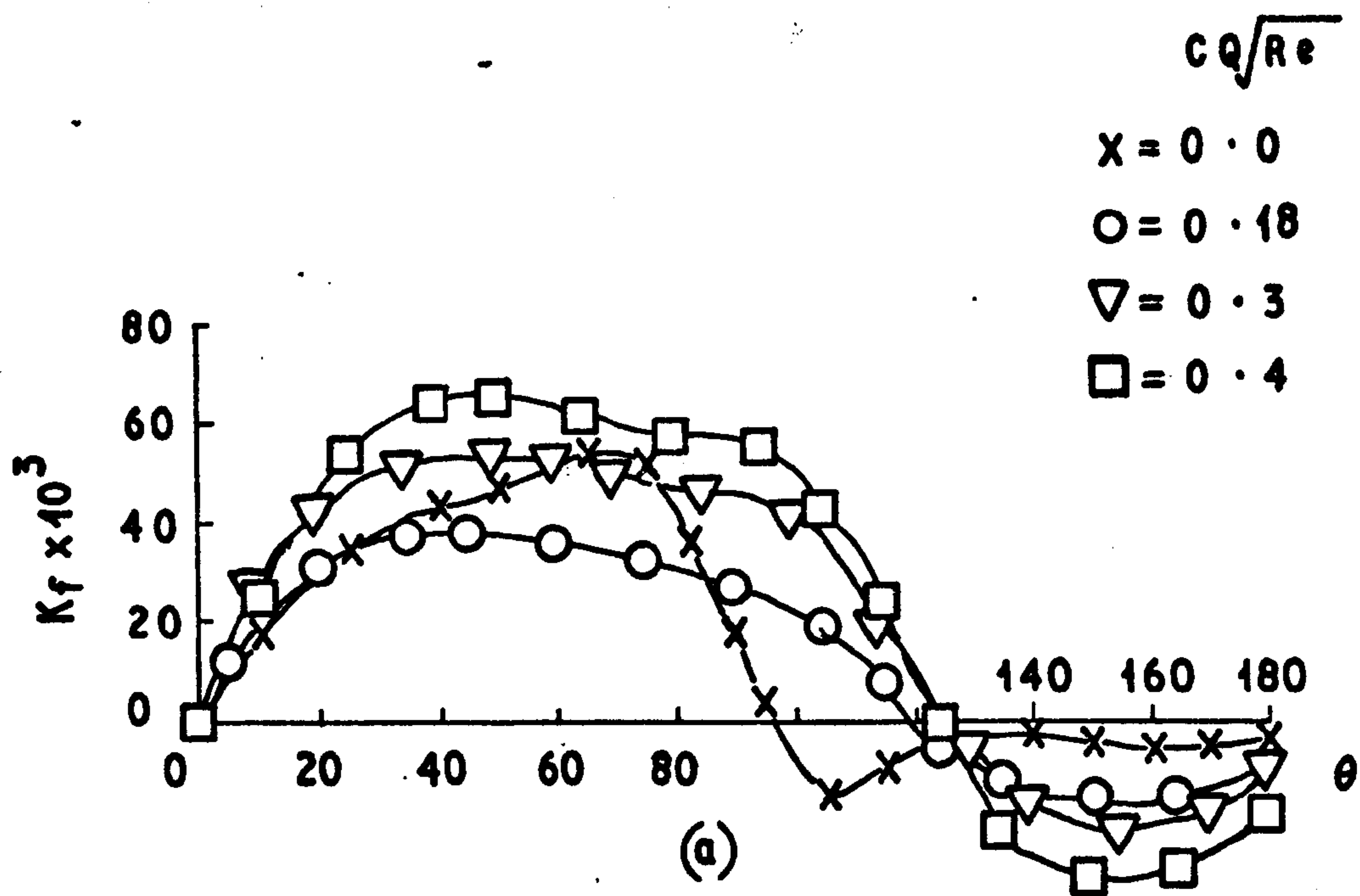


**Fig. 8.19**  
**SUCTION EFFECT ON SKIN FRICTION FIFTH ROW**  
**IN THE BANK,**  
 **$Re = 1 \times 10^5$**

$$Re_{\infty} = 0.27 \times 10^5$$

- X 1st. ROW
- 2nd. ROW
- ▽ 3rd. ROW
- △ 4th. ROW
- 5th. ROW
- single

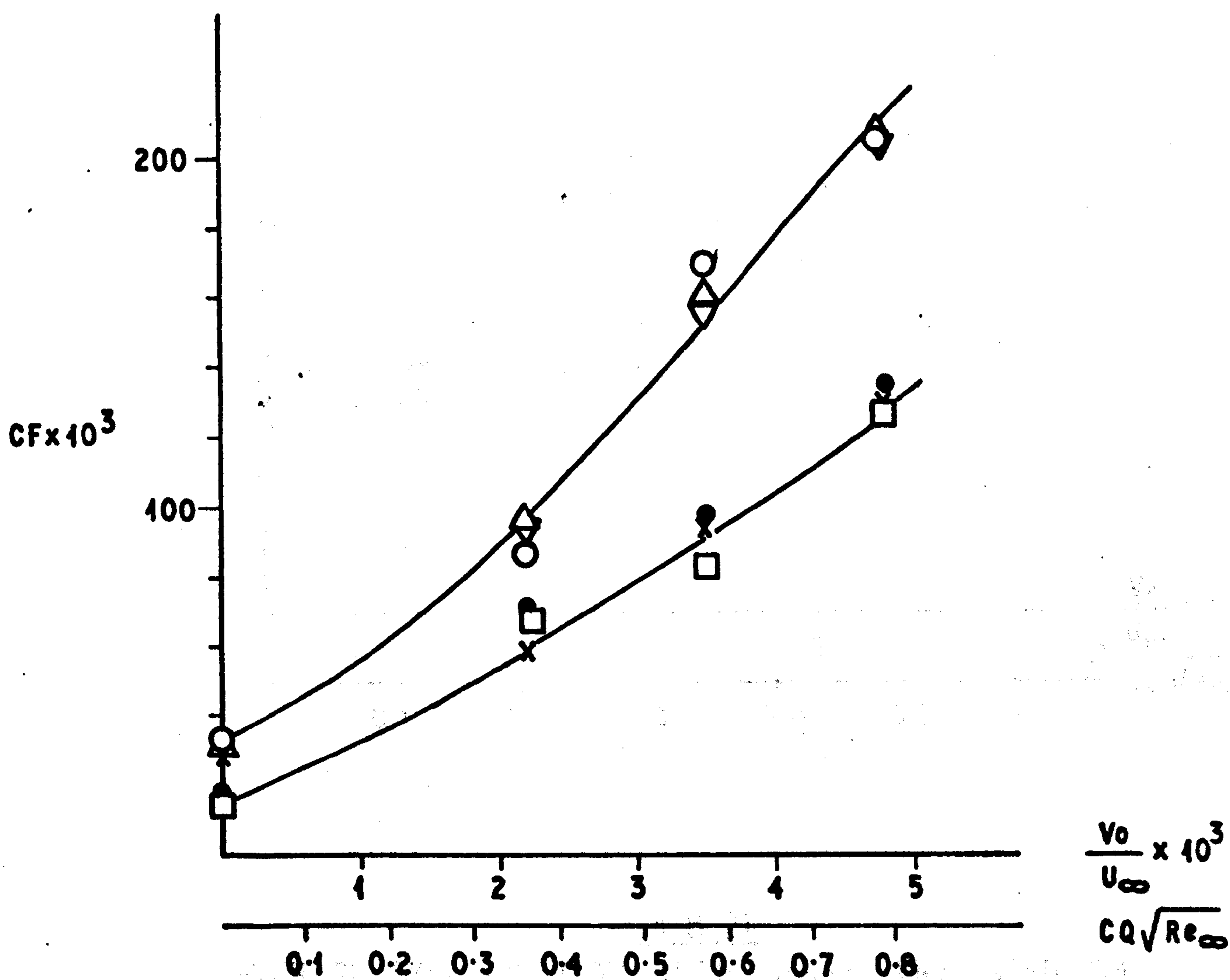


**Fig. 8.20**

**AVERAGE SKIN FRICTION WITH MASS TRANSFER ON  
THE BANK AT  $Re_{\infty} = 0.27 \times 10^5$**



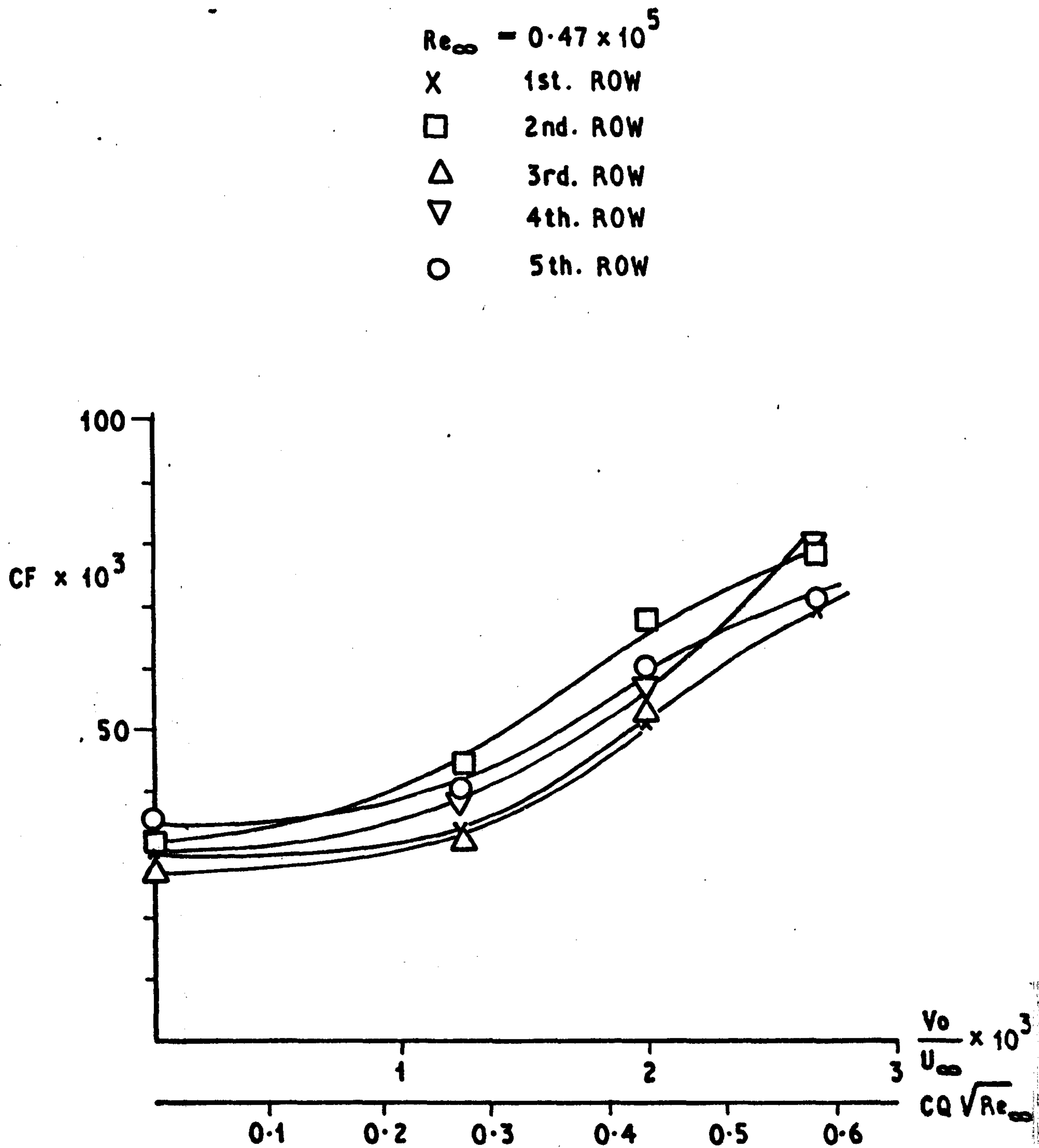


**Fig. 8.21**  
AVERAGE SKIN FRICTION WITH MASS TRANSFER ON  
THE BANK AT  $Re_{\infty} = 0.47 \times 10^5$

$$Re_{\infty} = 0.7 \times 10^5$$

▣ 1st. ROW

○ 2nd. ROW

▽ 3rd. ROW

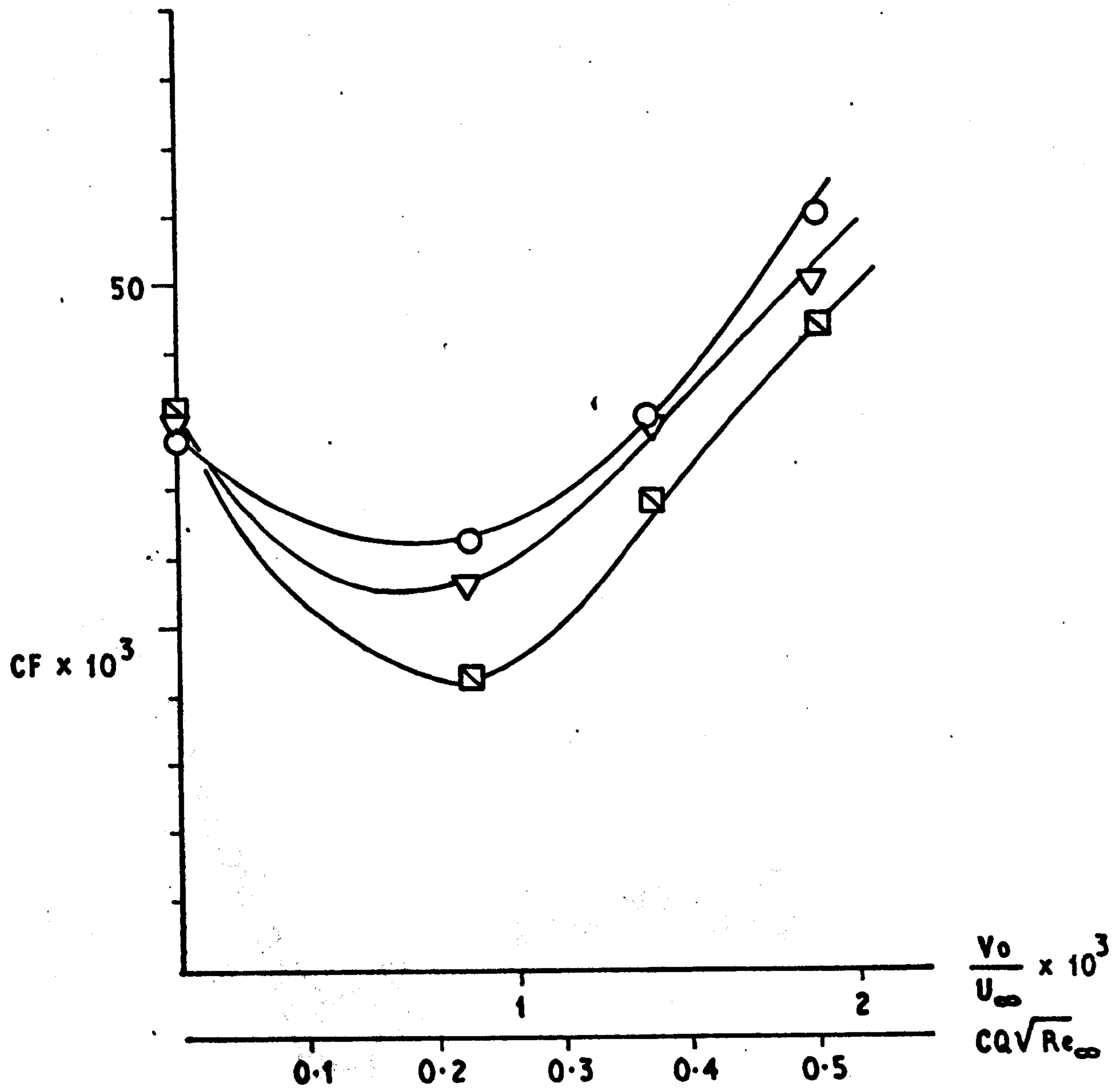


Fig.8.22

AVERAGE SKIN FRICTION WITH MASS TRANSFER IN  
THE BANK AT  $Re_{\infty} = 0.7 \times 10^5$

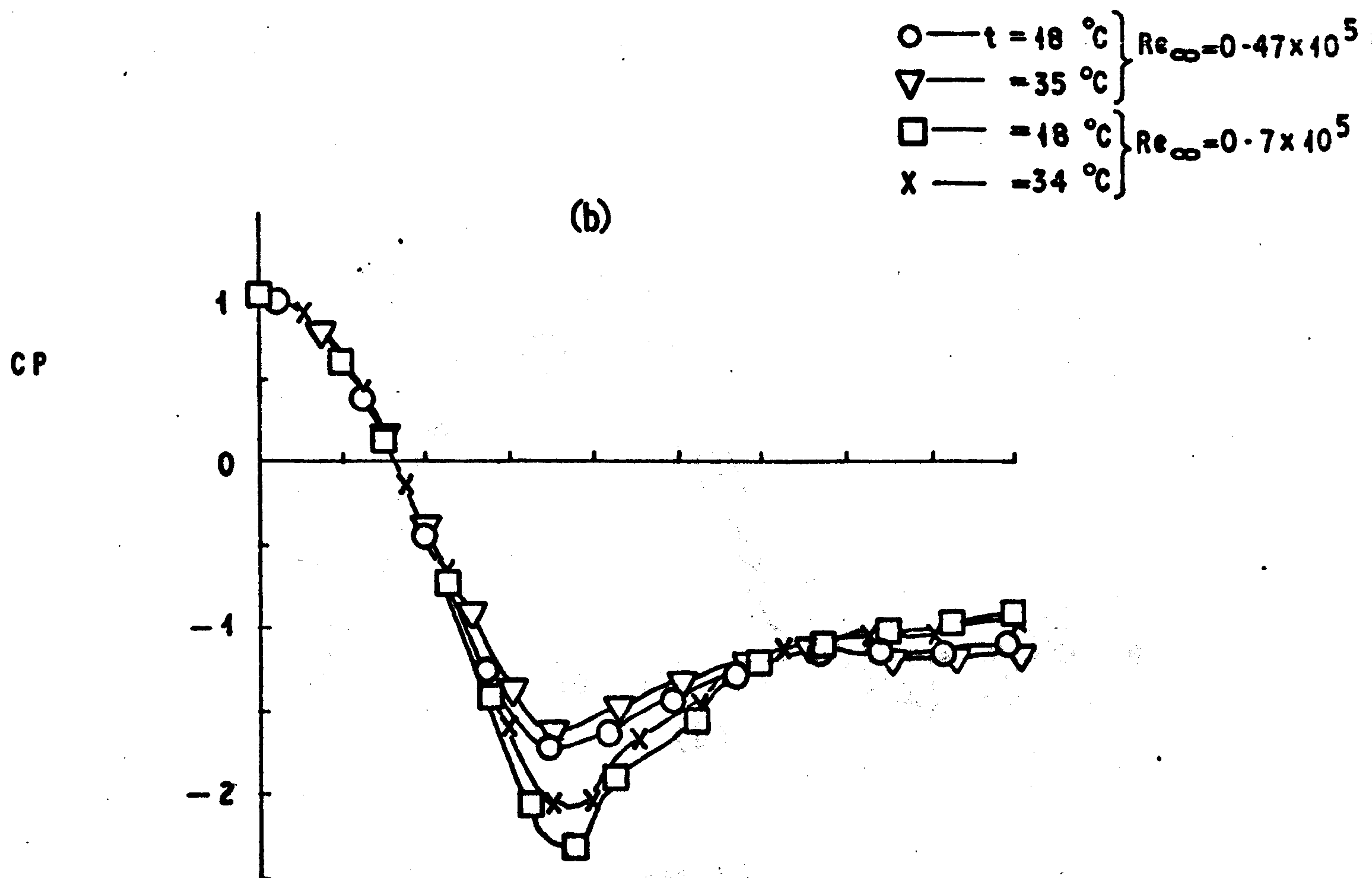
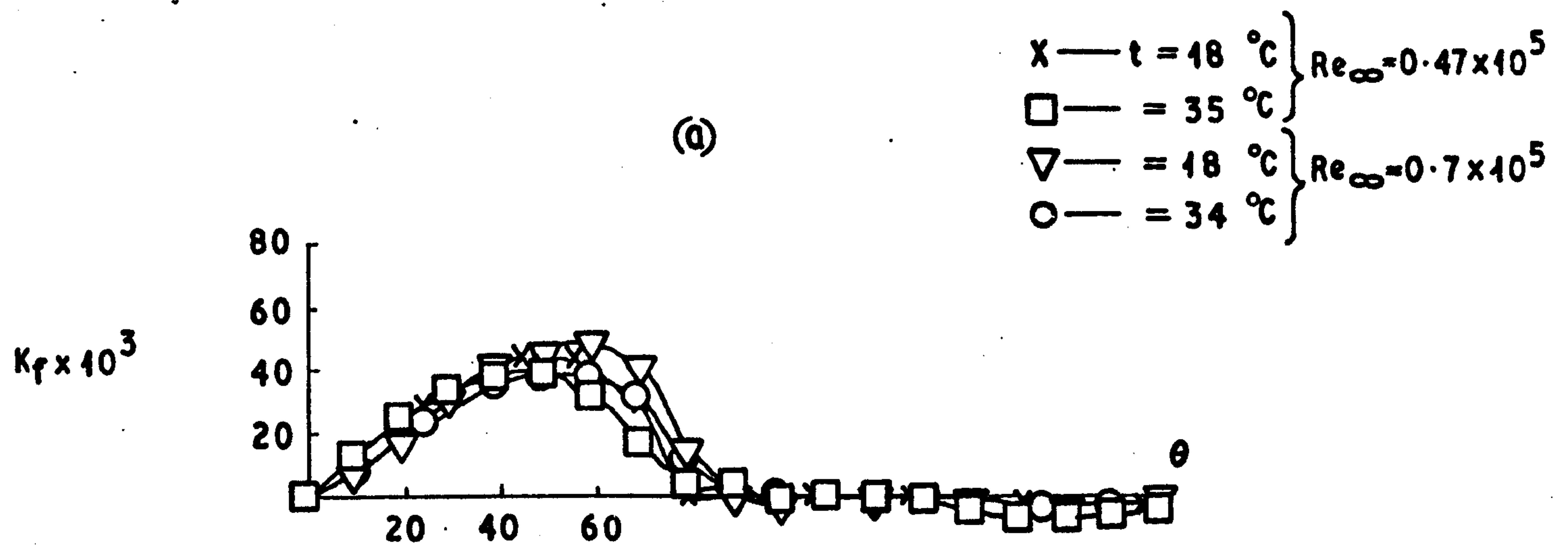
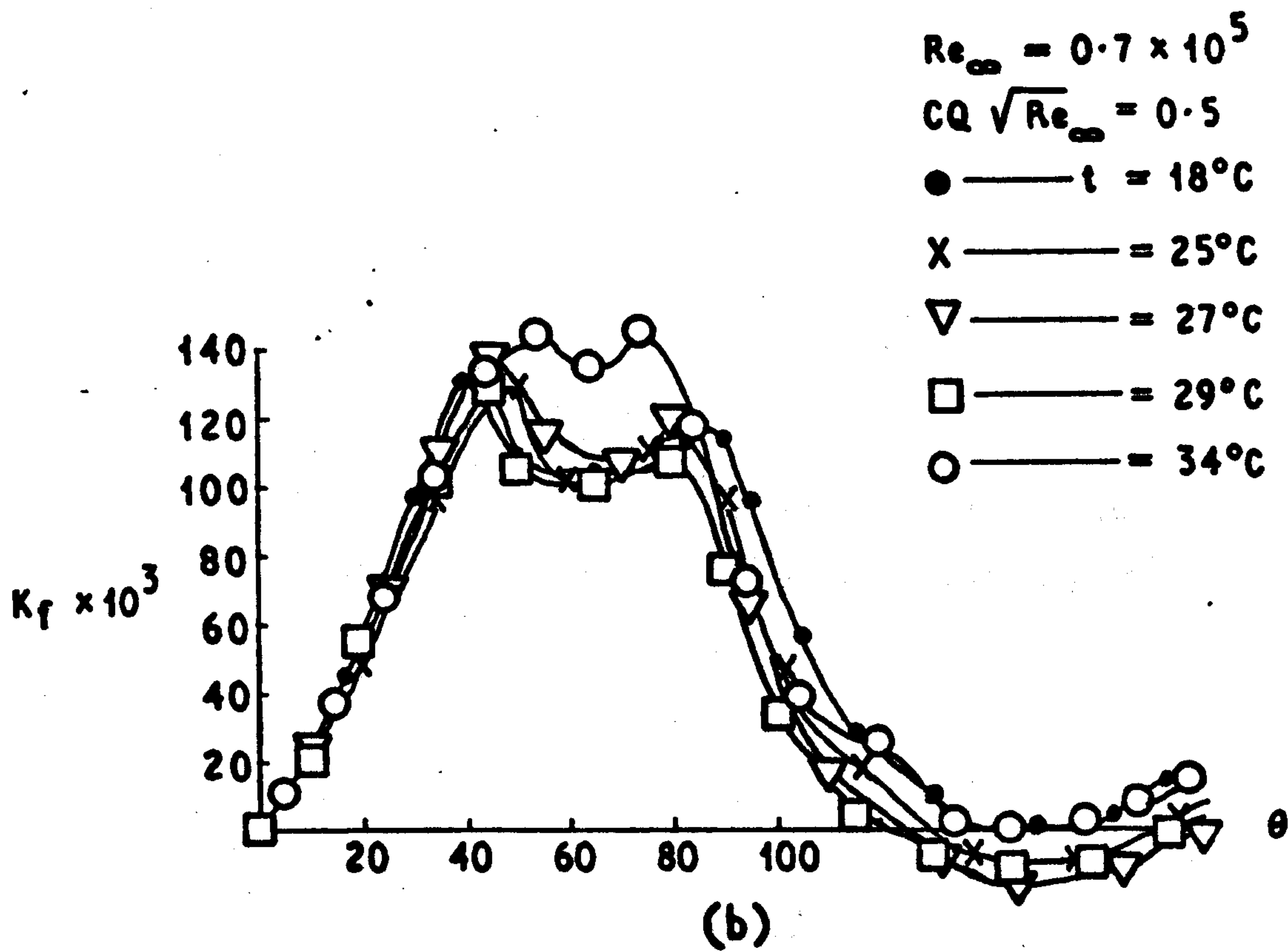
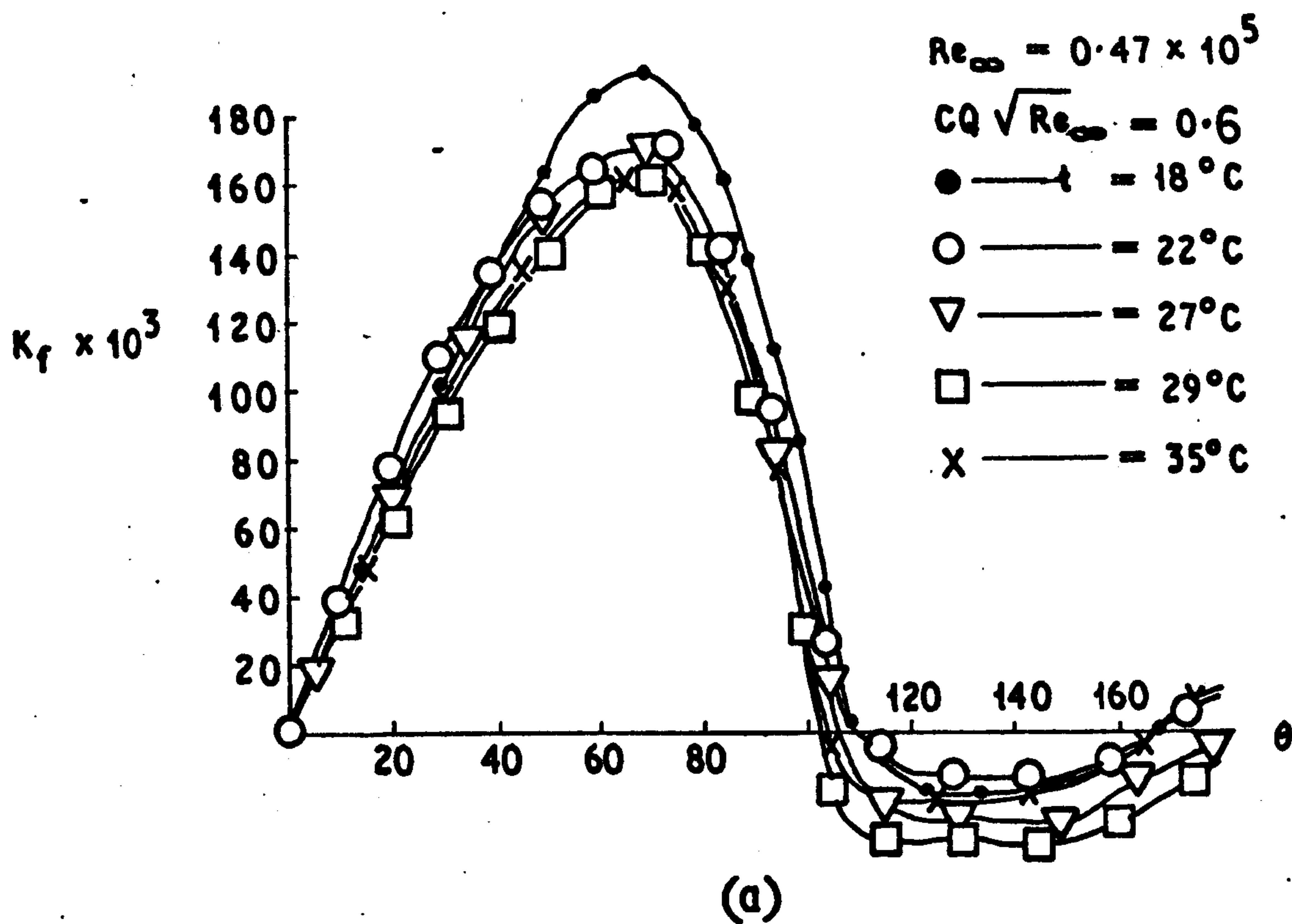


Fig. 9.1

EFFECT OF MAIN STREAM TEMPERATURE  
ON SINGLE CYLINDER





**Fig.9.2**  
**EFFECT OF MAIN STREAM TEMPERATURE WITH MASS**  
**TRANSFER ON SINGLE CYLINDER**

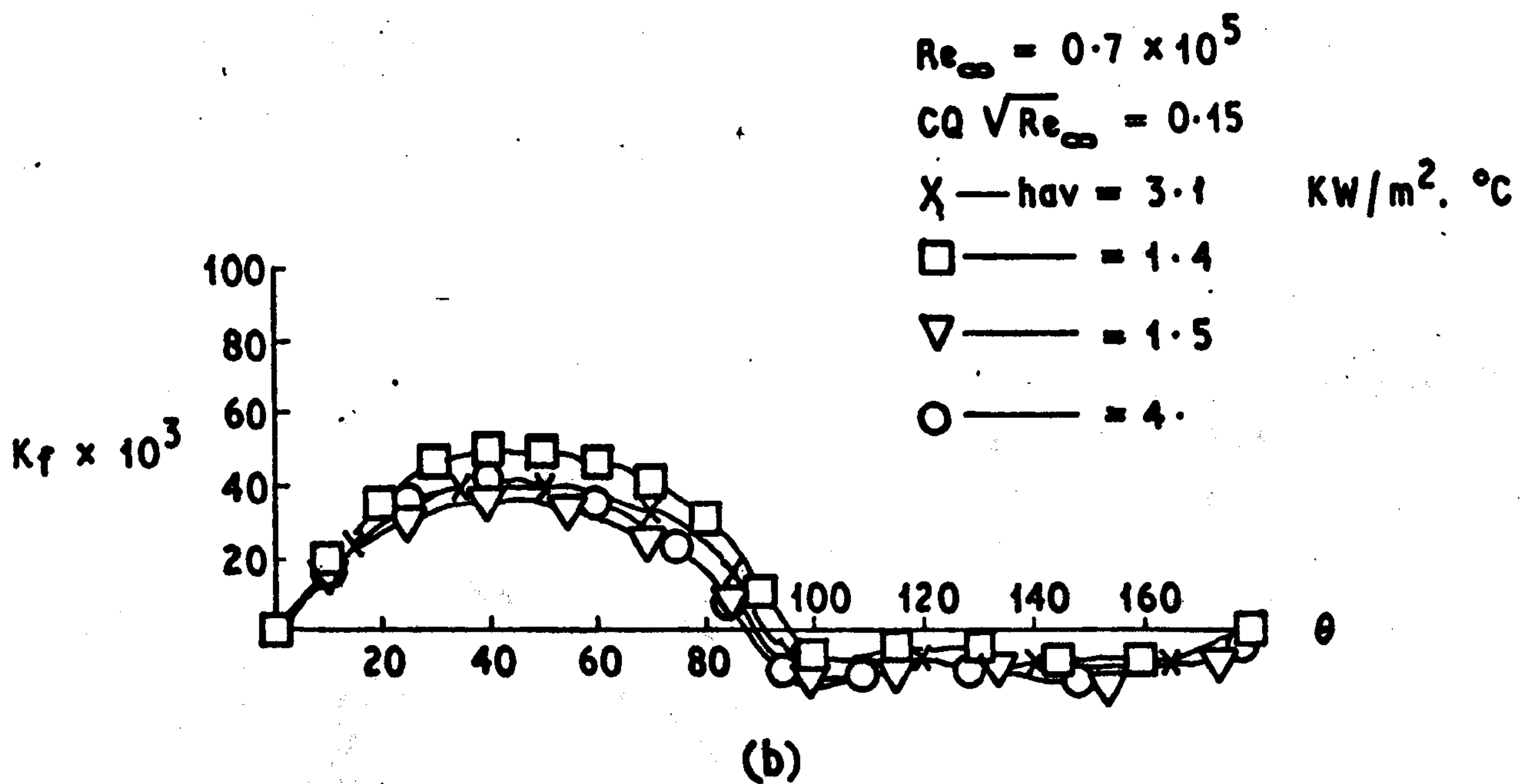
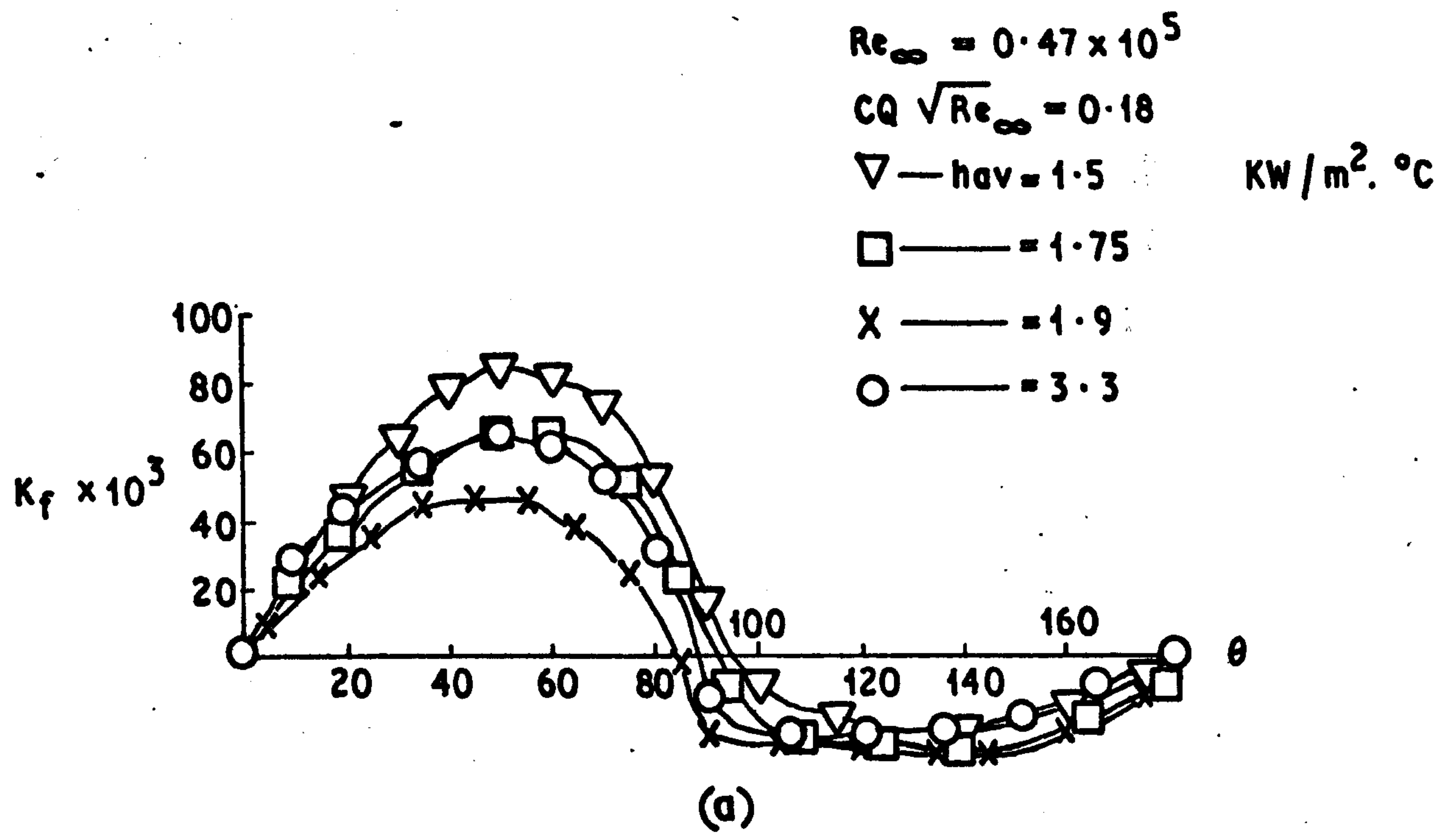


**Fig.9.3**  
**EFFECT OF HEAT AND MASS TRANSFER ON SHEAR**  
**STRESS ROUND SINGLE CYLINDER**

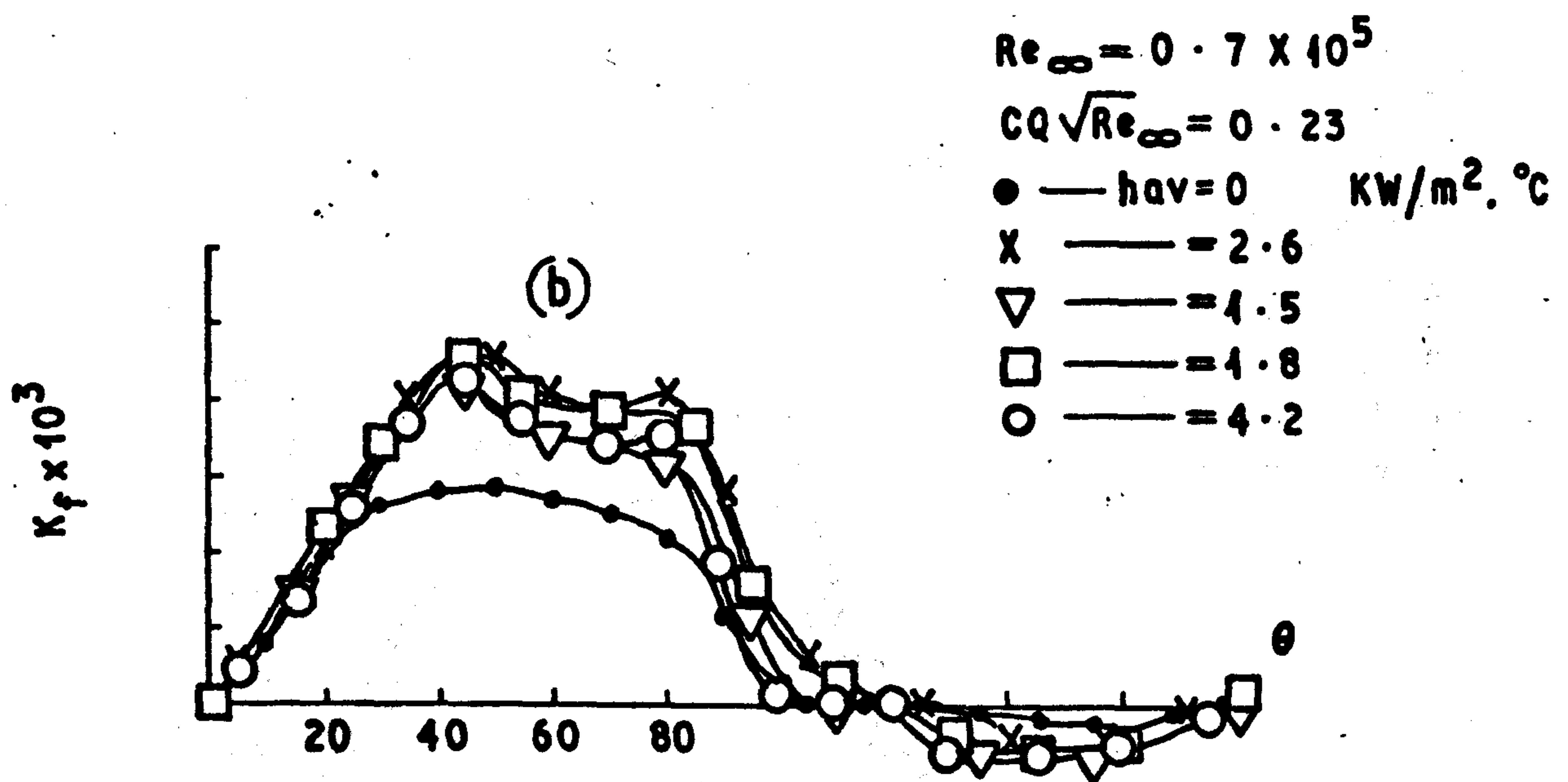
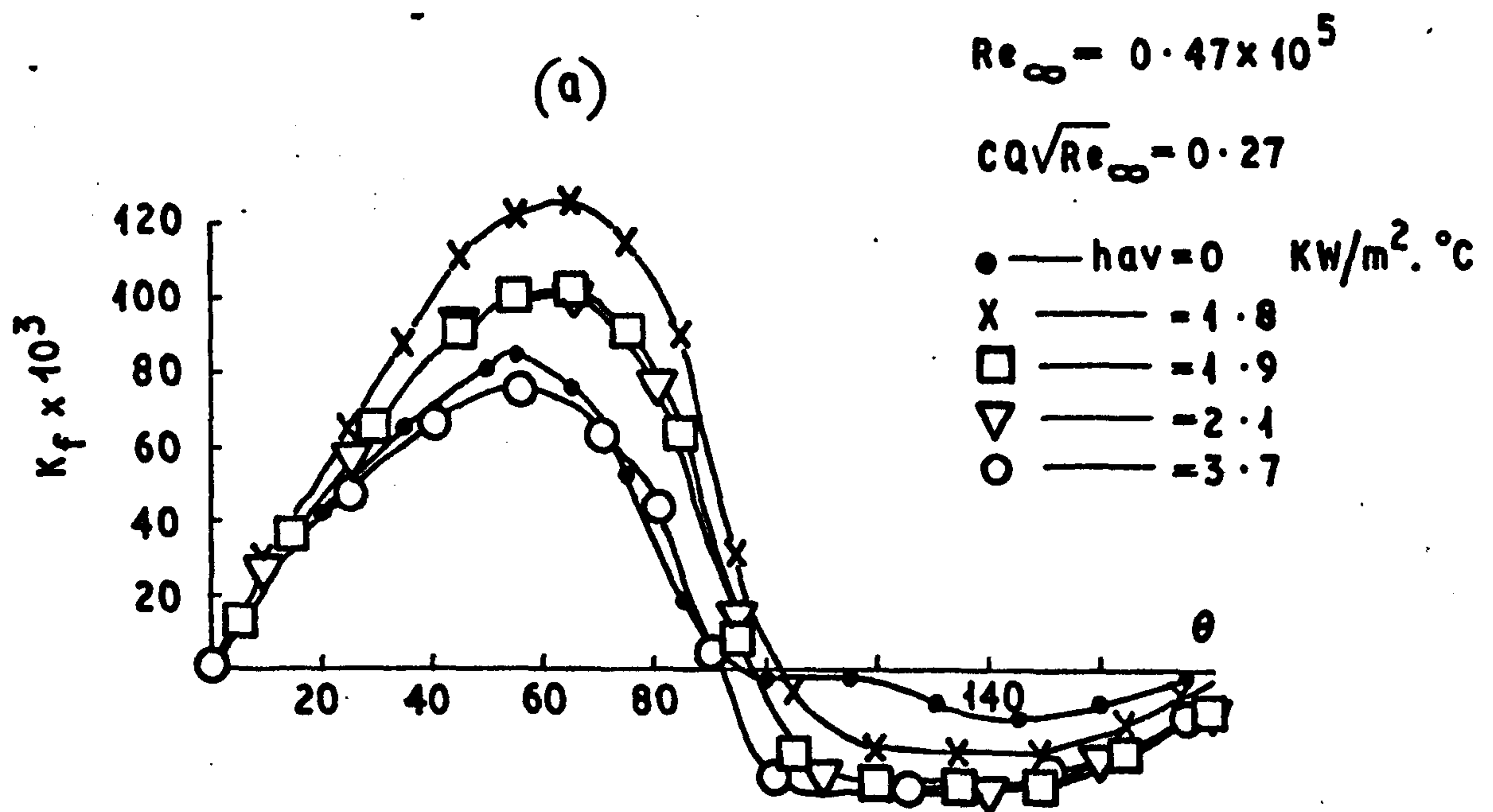
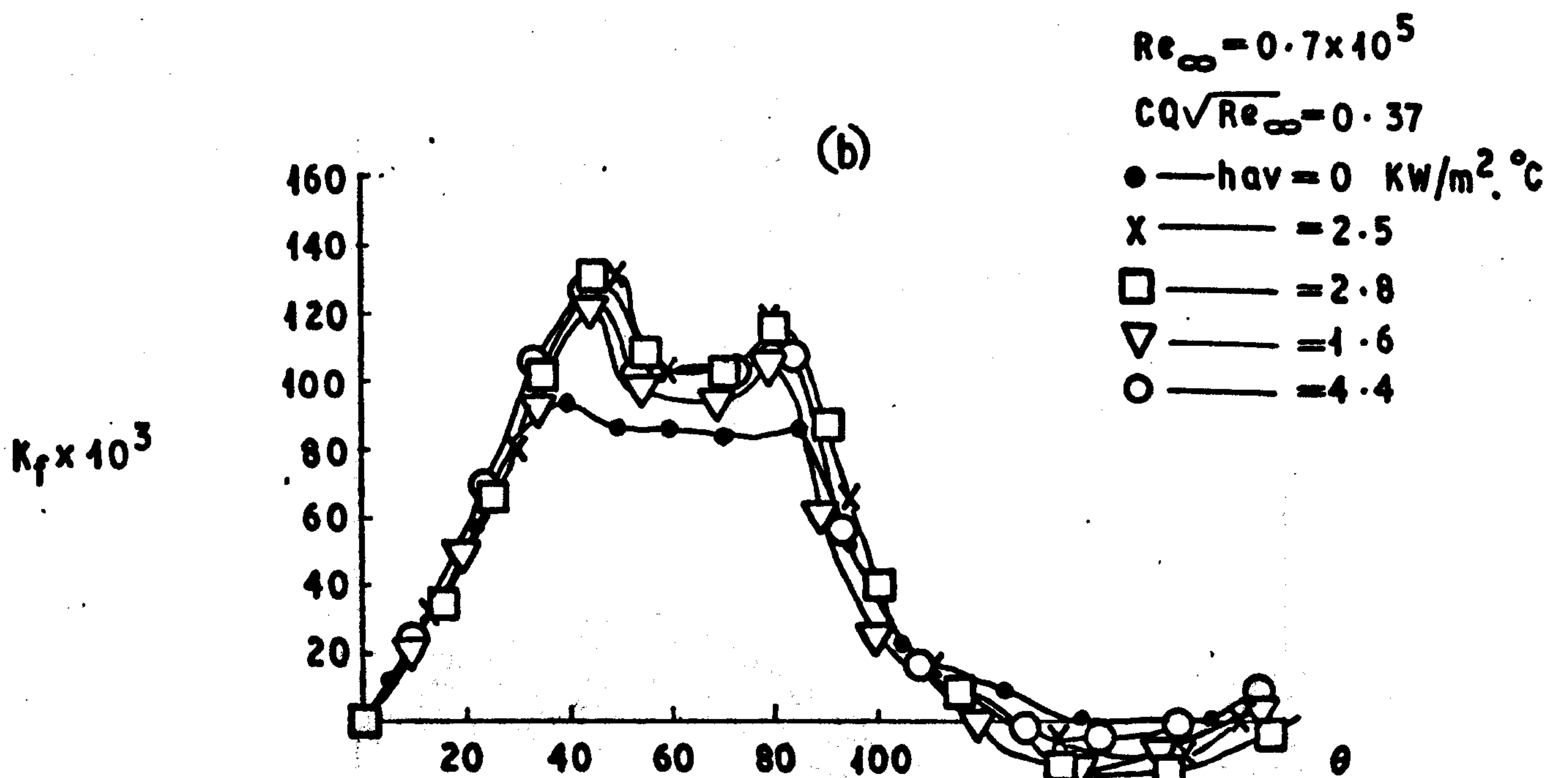
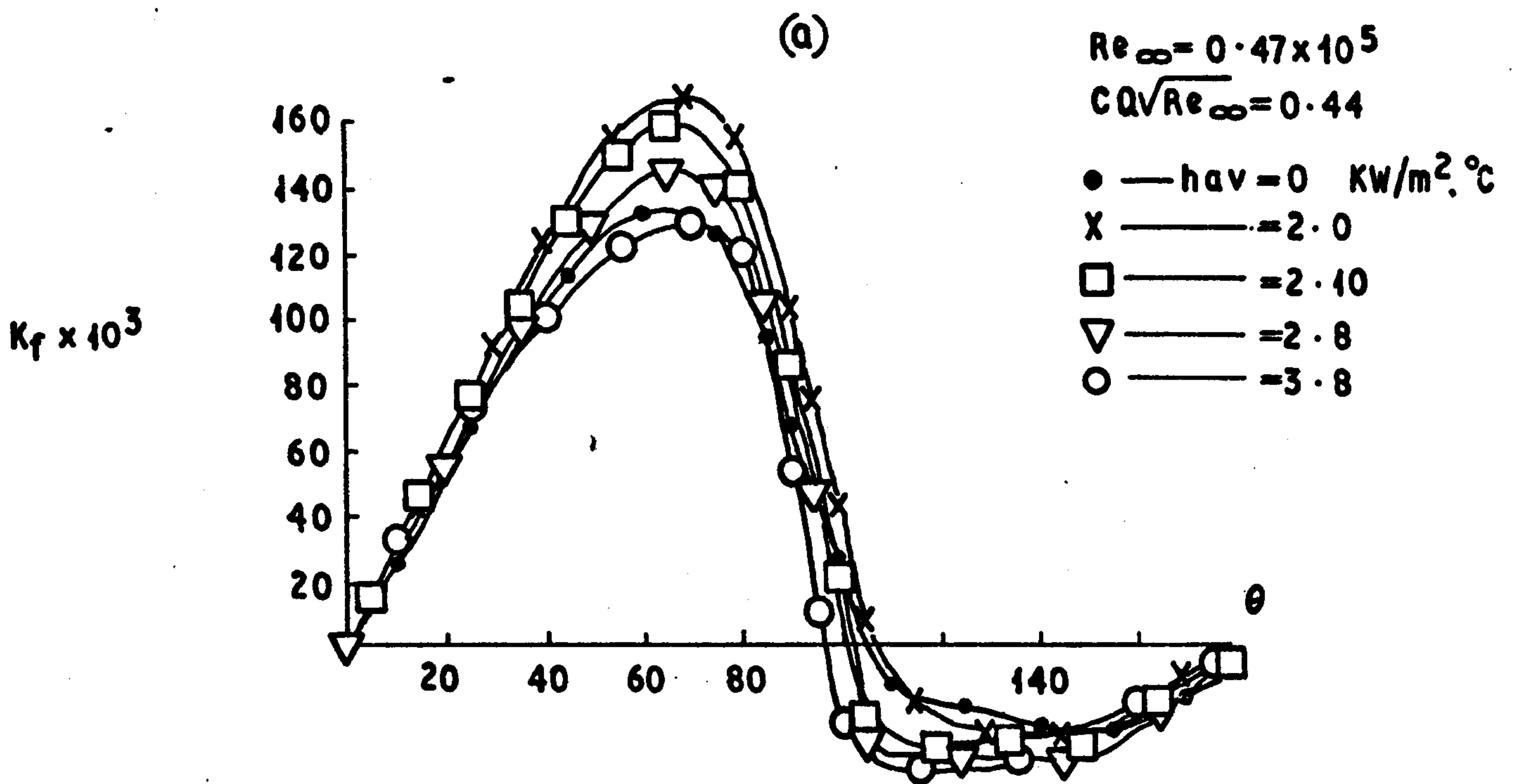


Fig. 9.4

EFFECT OF HEAT AND MASS TRANSFER ON  
SHEAR STRESS ROUND SINGLE CYLINDER





**Fig 9.5**  
**SHEAR STRESS WITH HEAT AND MASS TRANSFER**  
**ROUND SINGLE CYLINDER**

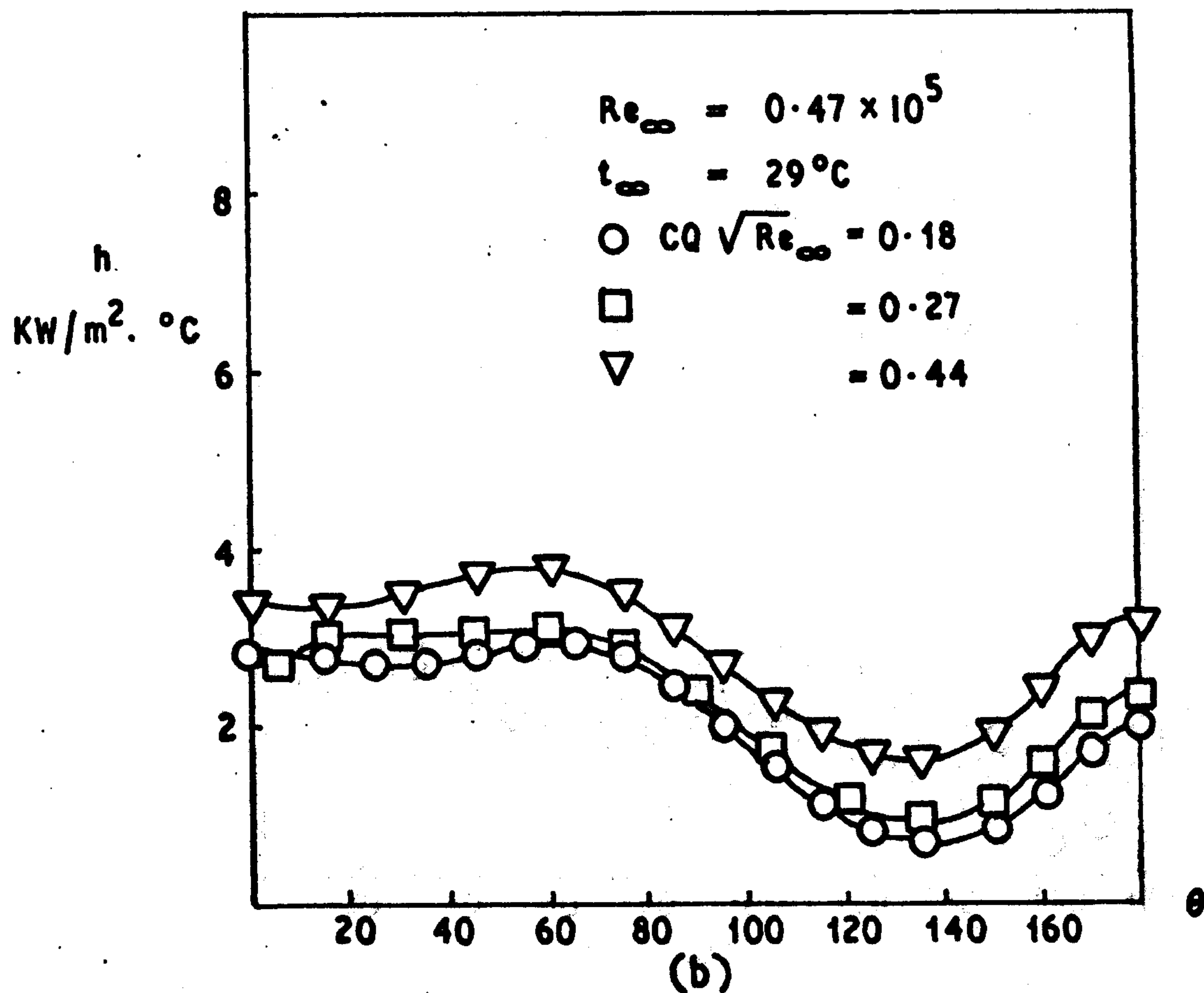
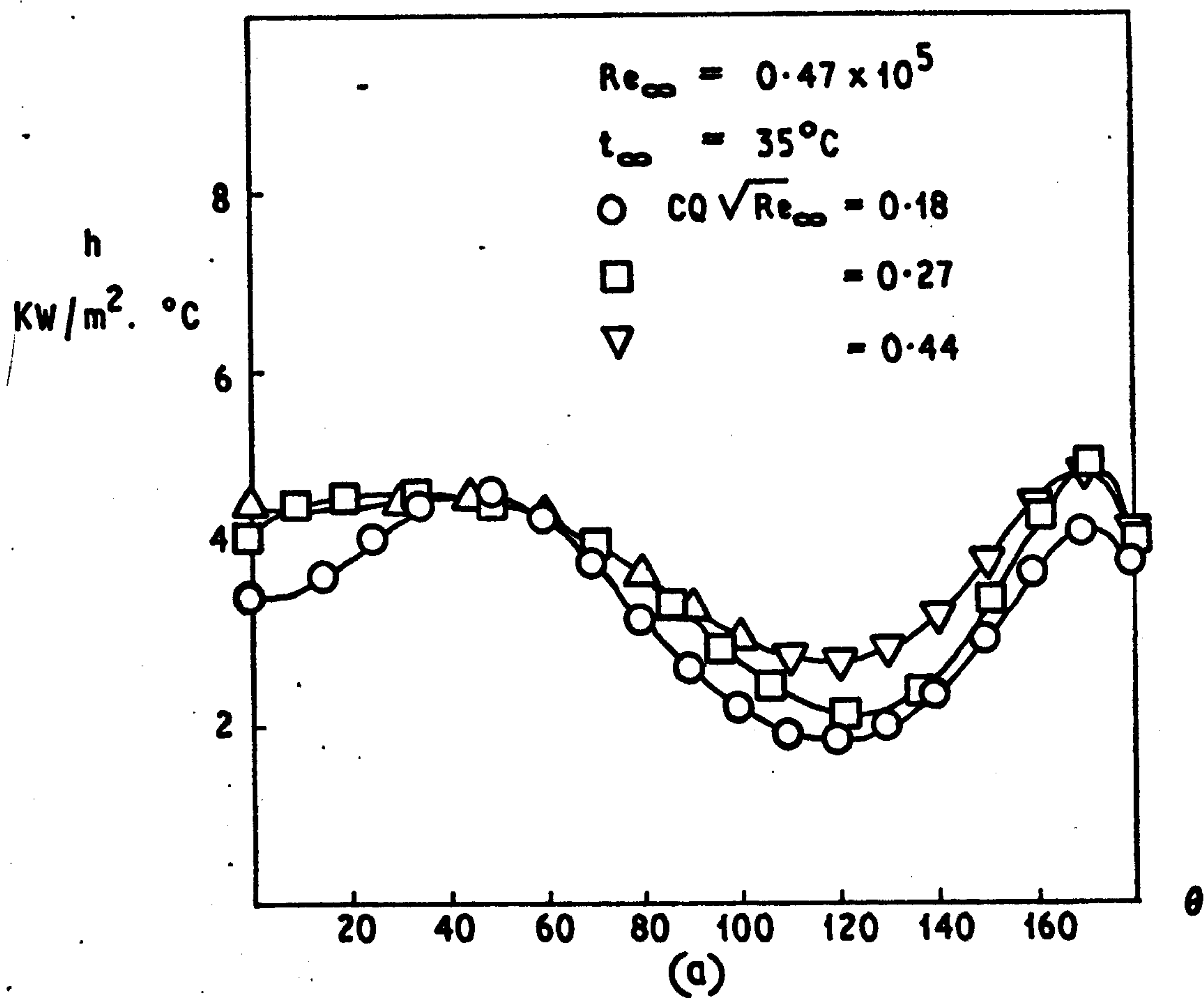
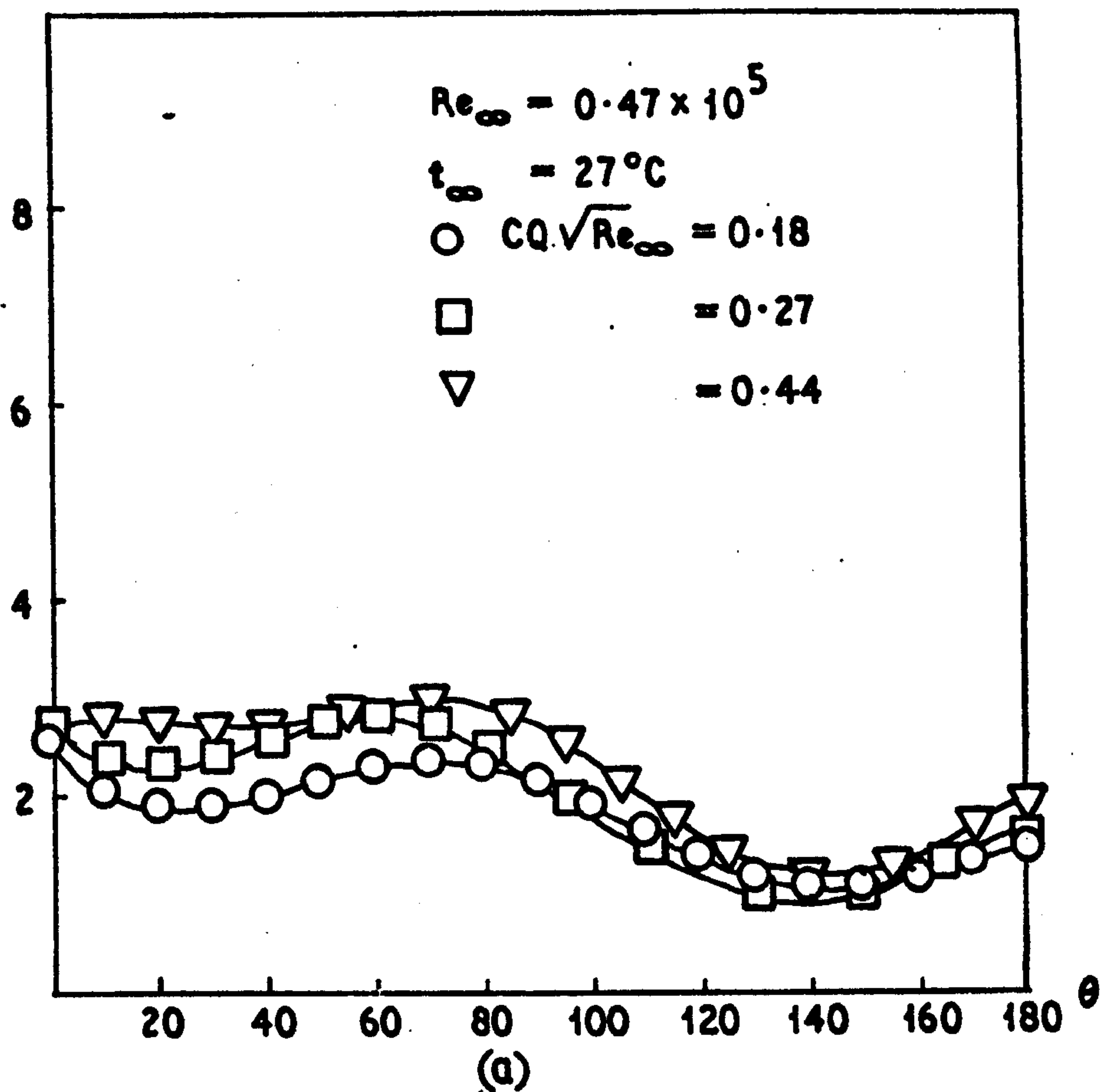


**Fig. 9.6**  
**COEFFICIENT OF HEAT TRANSFER WITH MASS TRANSFER**  
**ROUND SINGLE CYLINDER**

$h$   
KW/m<sup>2</sup>. °C



$h$   
KW/m<sup>2</sup>. °C

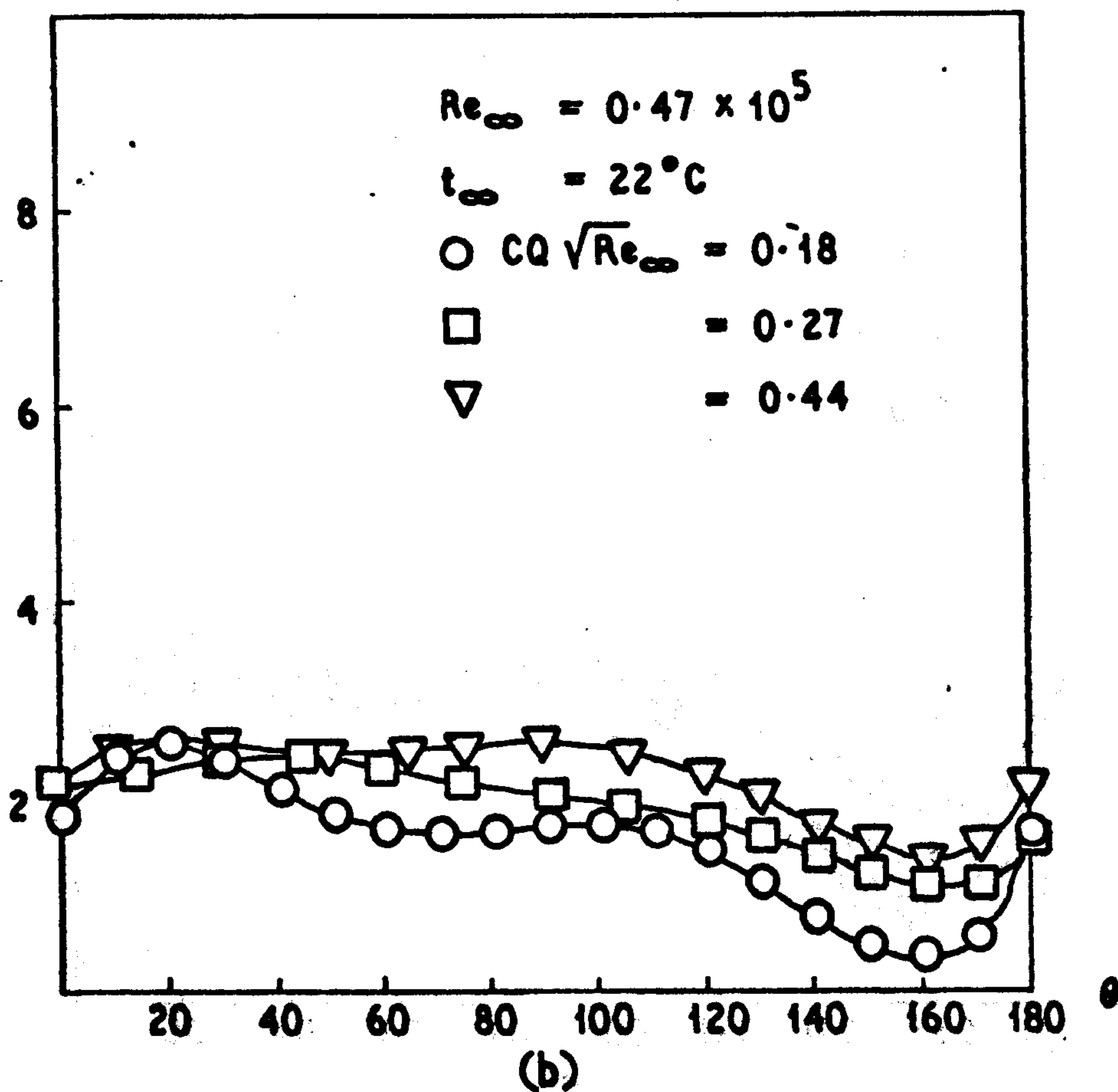
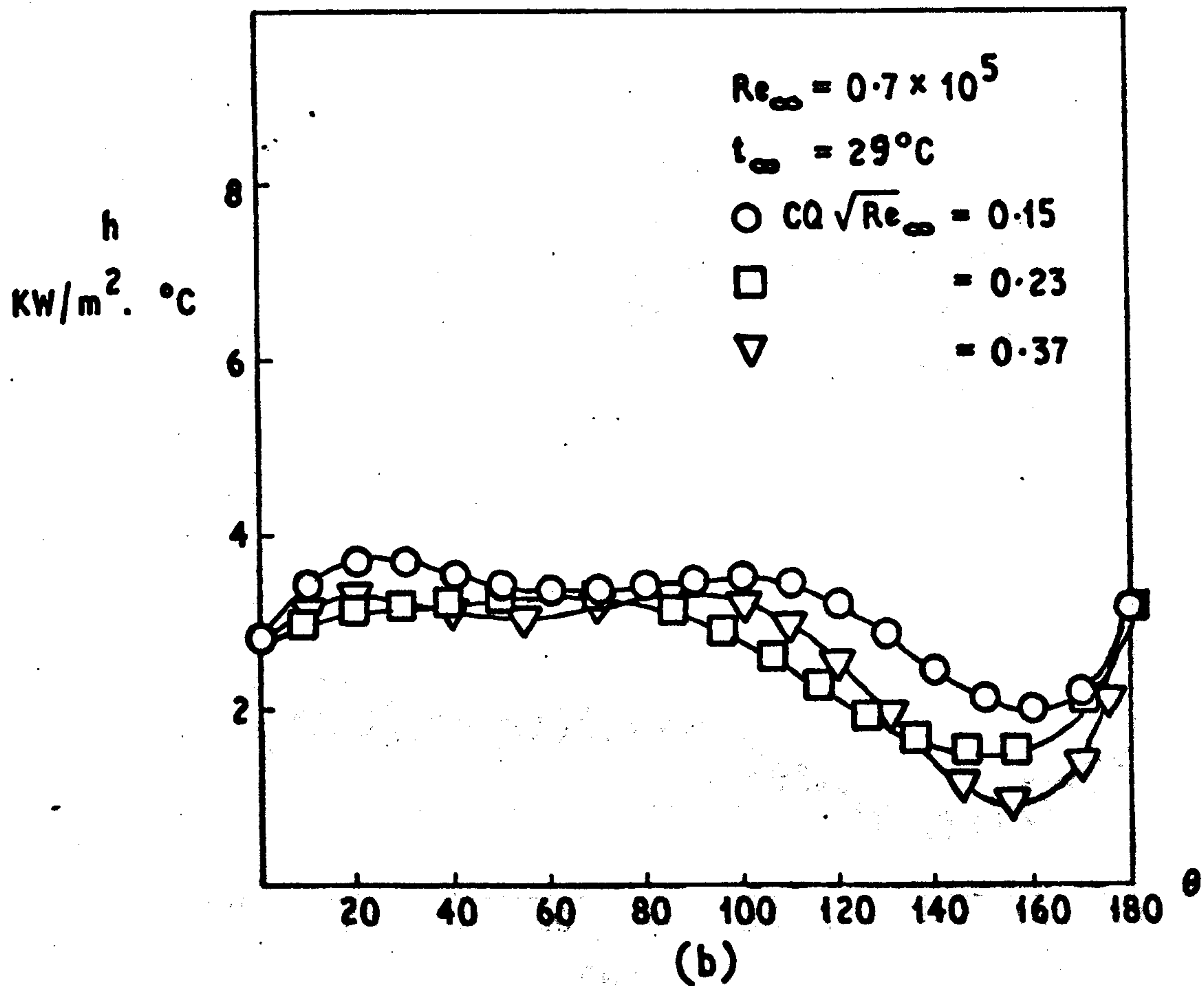
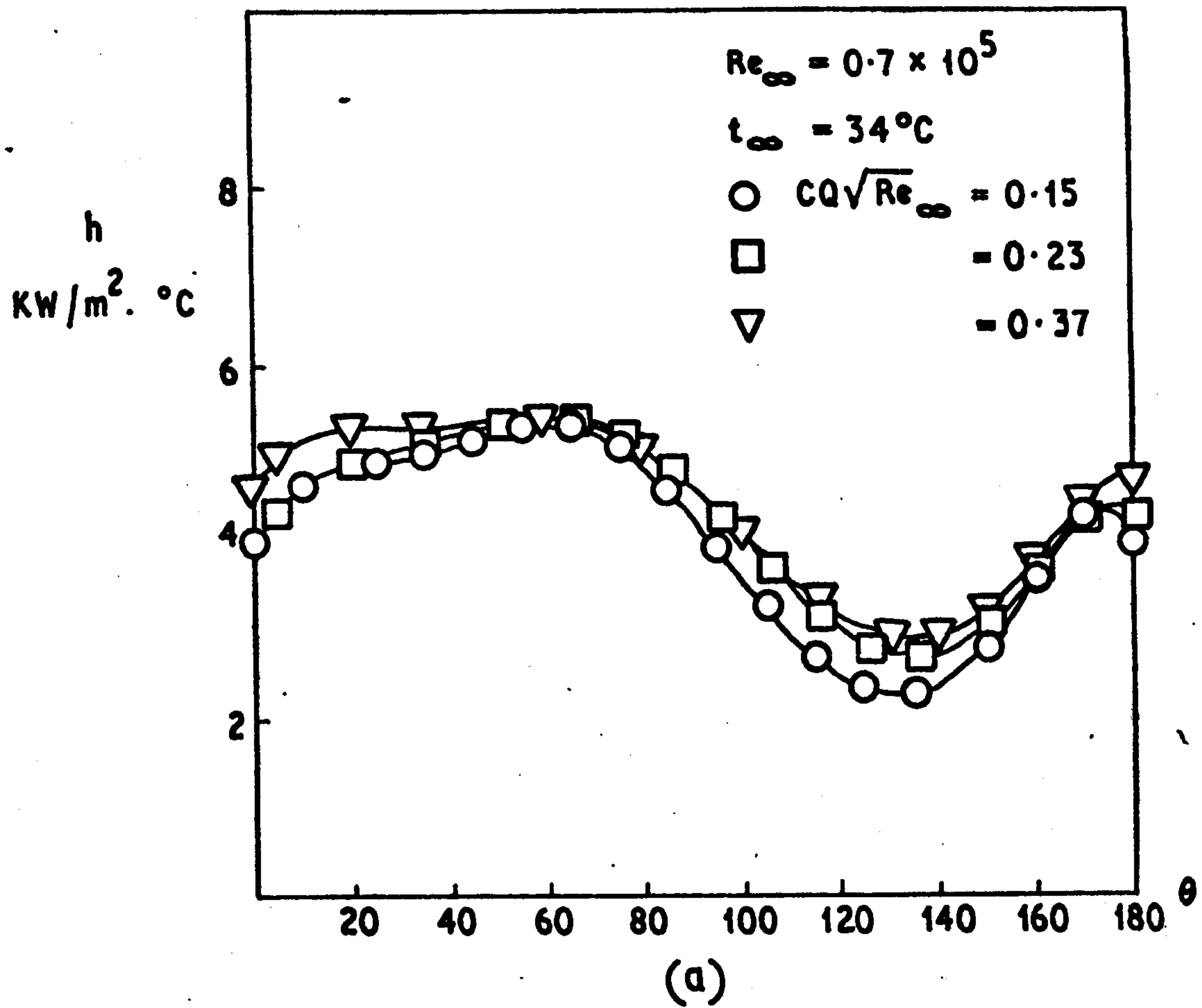


Fig. 9.7  
HEAT TRANSFER WITH SUCTION ROUND  
SINGLE CYLINDER





**Fig. 9.8**  
**HEAT TRANSFER WITH MASS TRANSFER**  
**ROUND SINGLE CYLINDER**

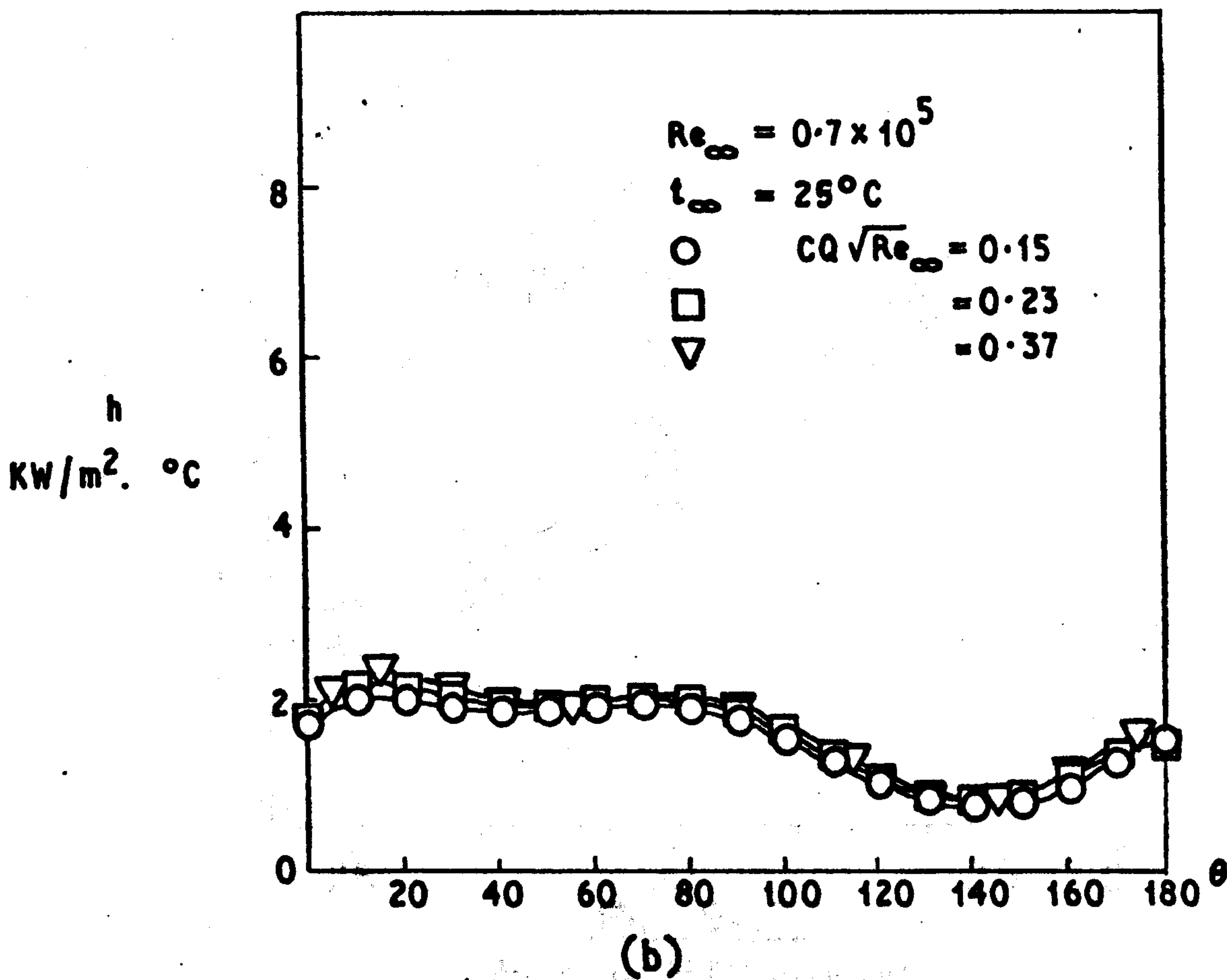
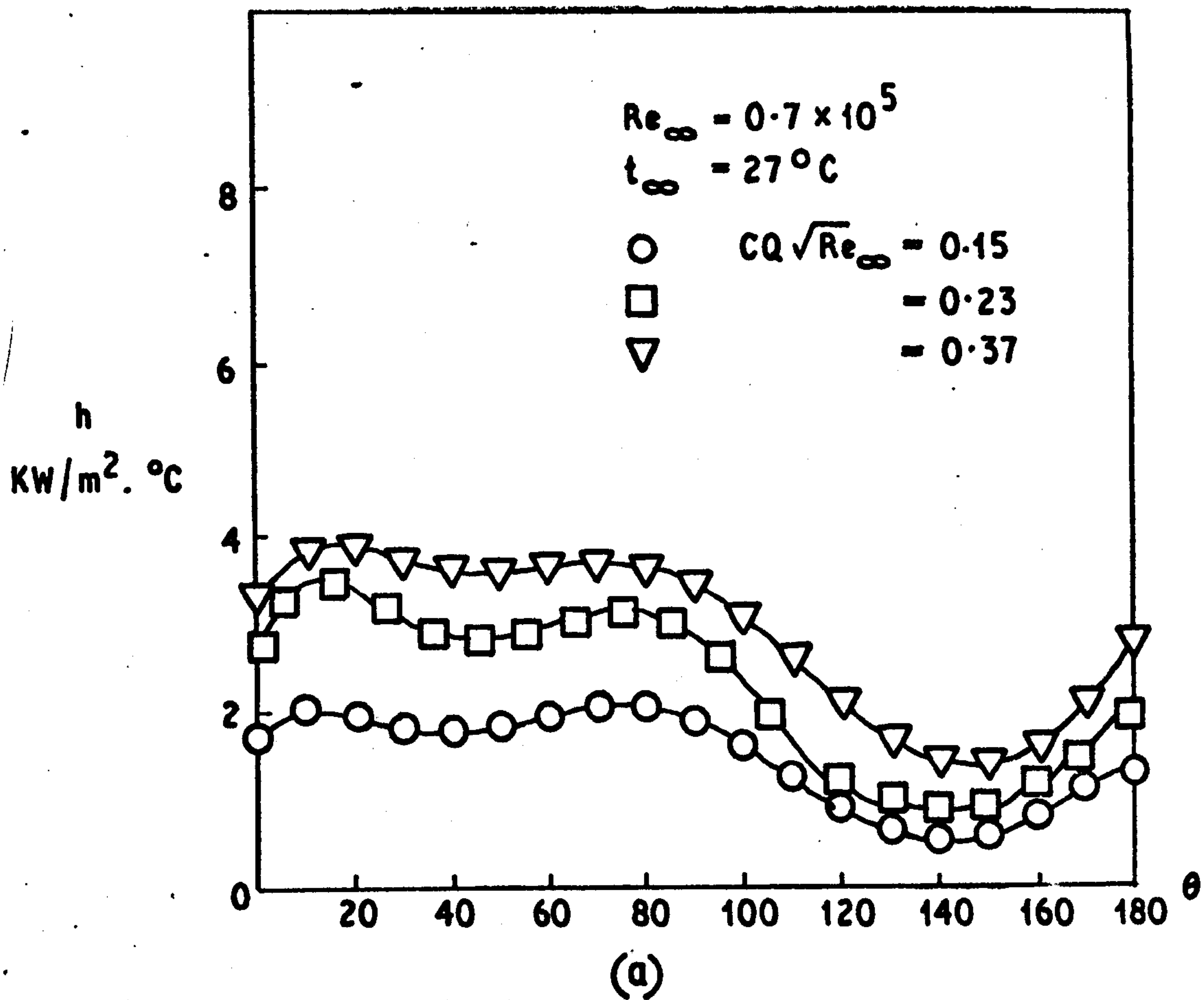


Fig. 9.9

HEAT TRANSFER WITH MASS TRANSFER  
ROUND SINGLE CYLINDER

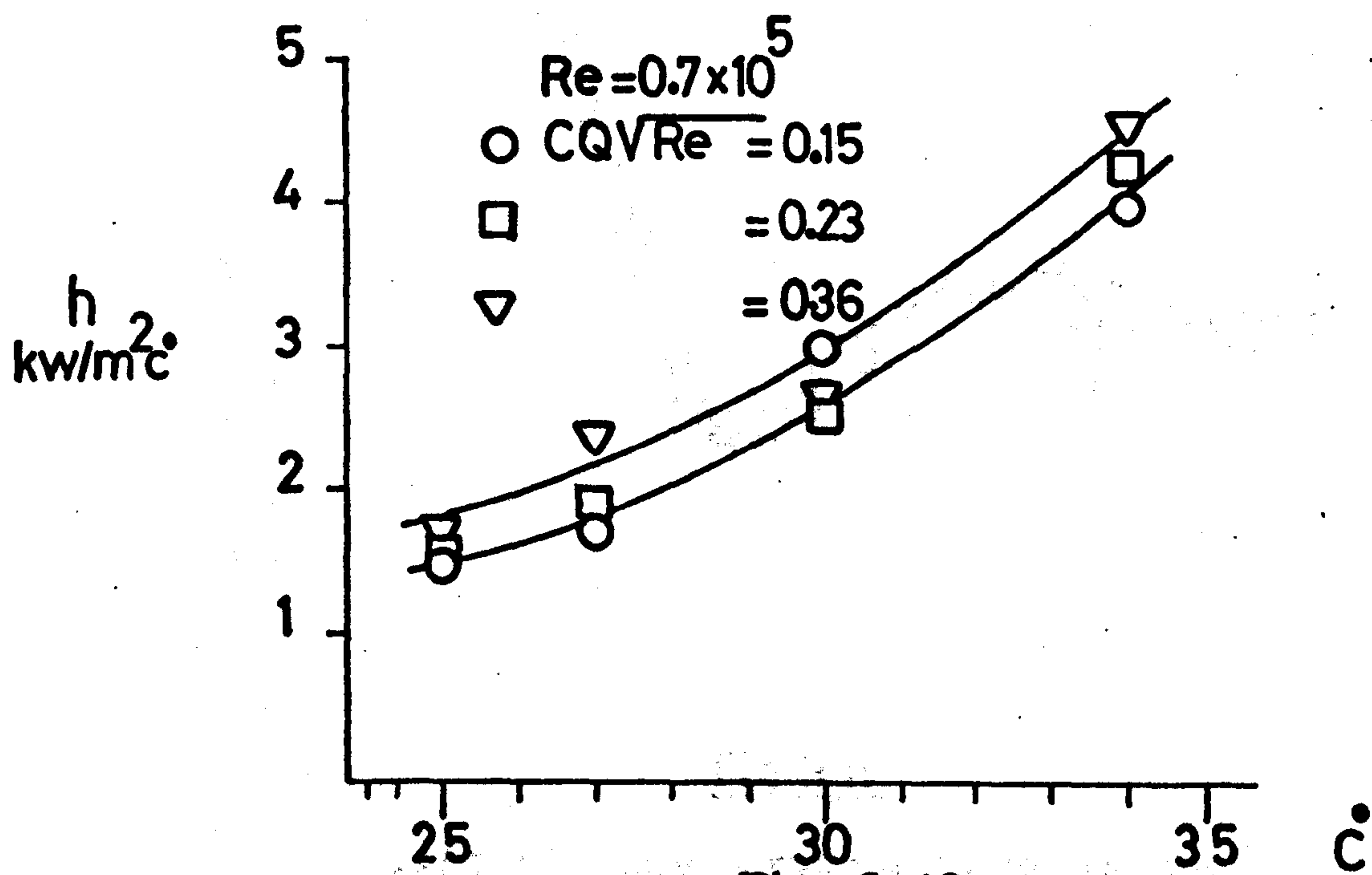
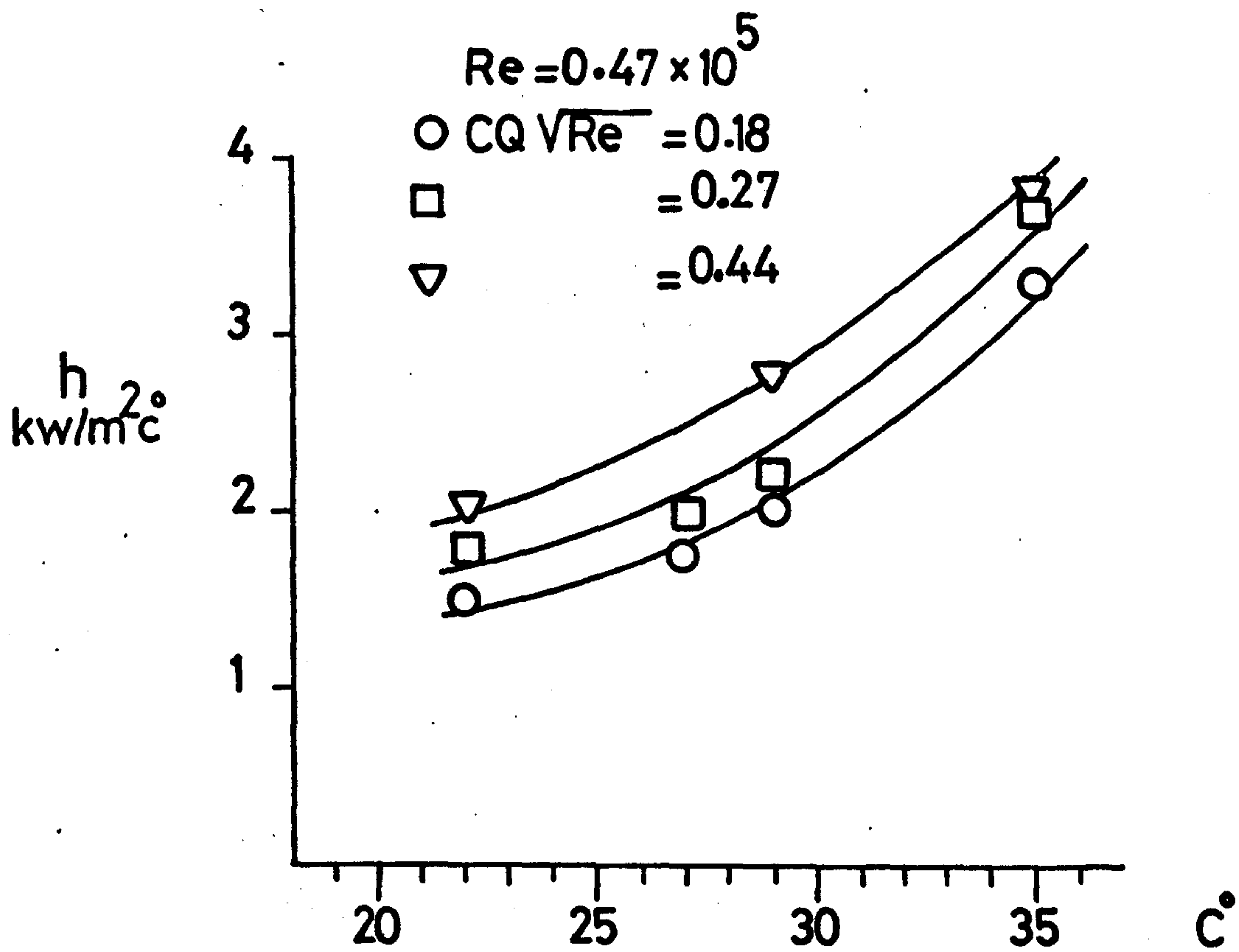
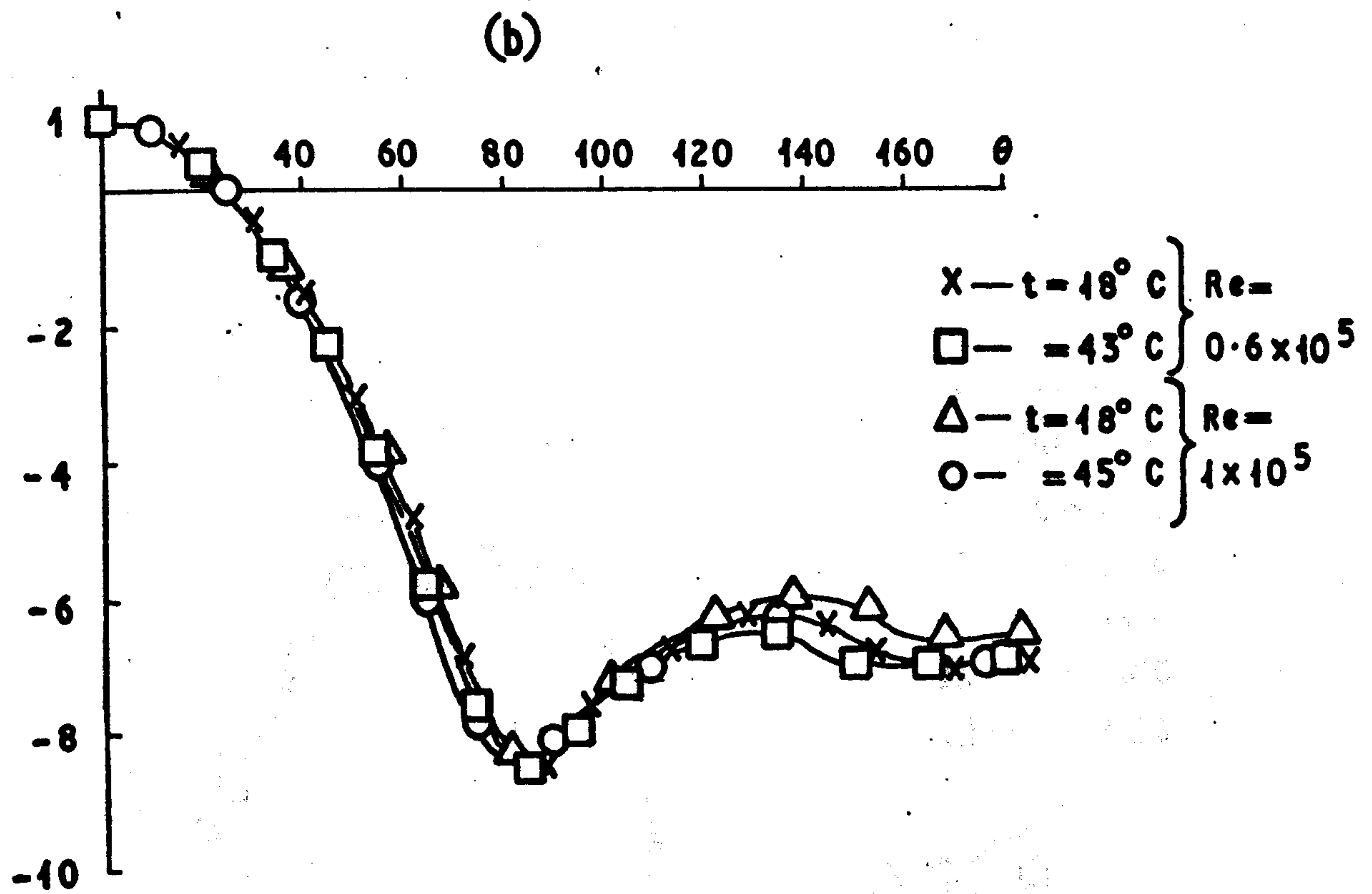
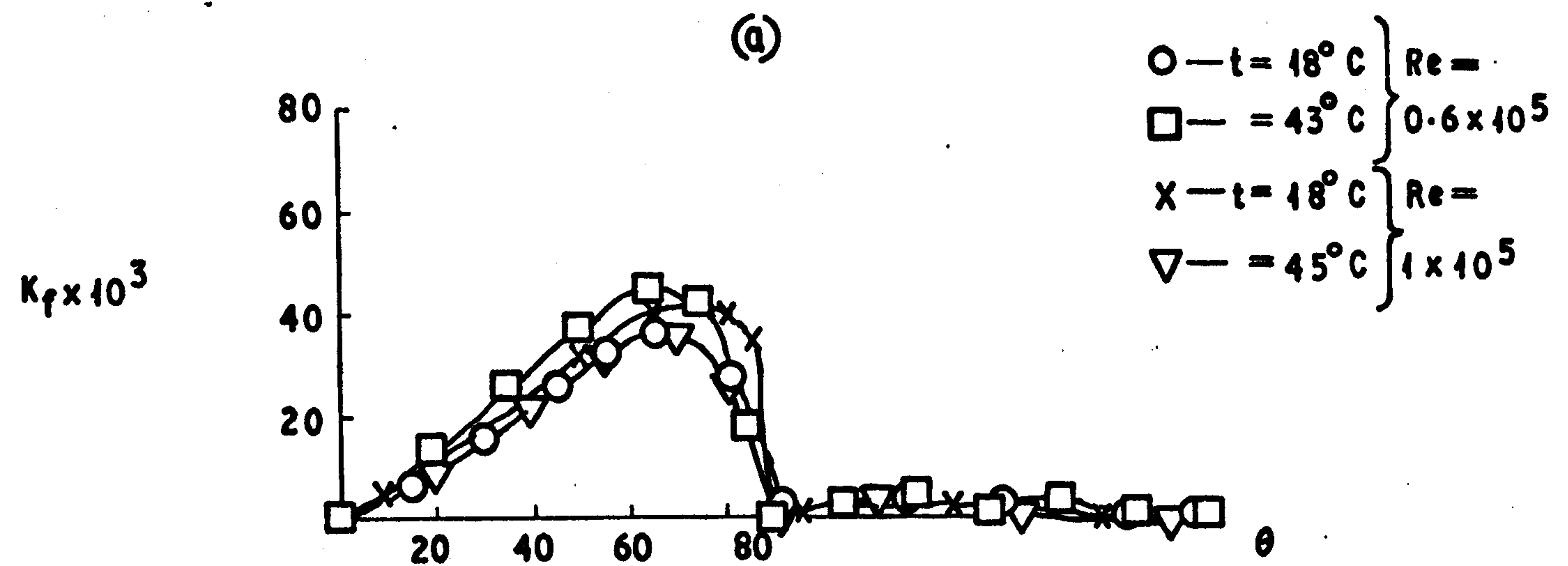


Fig. 9.10

Average HTC around  
single cylinder

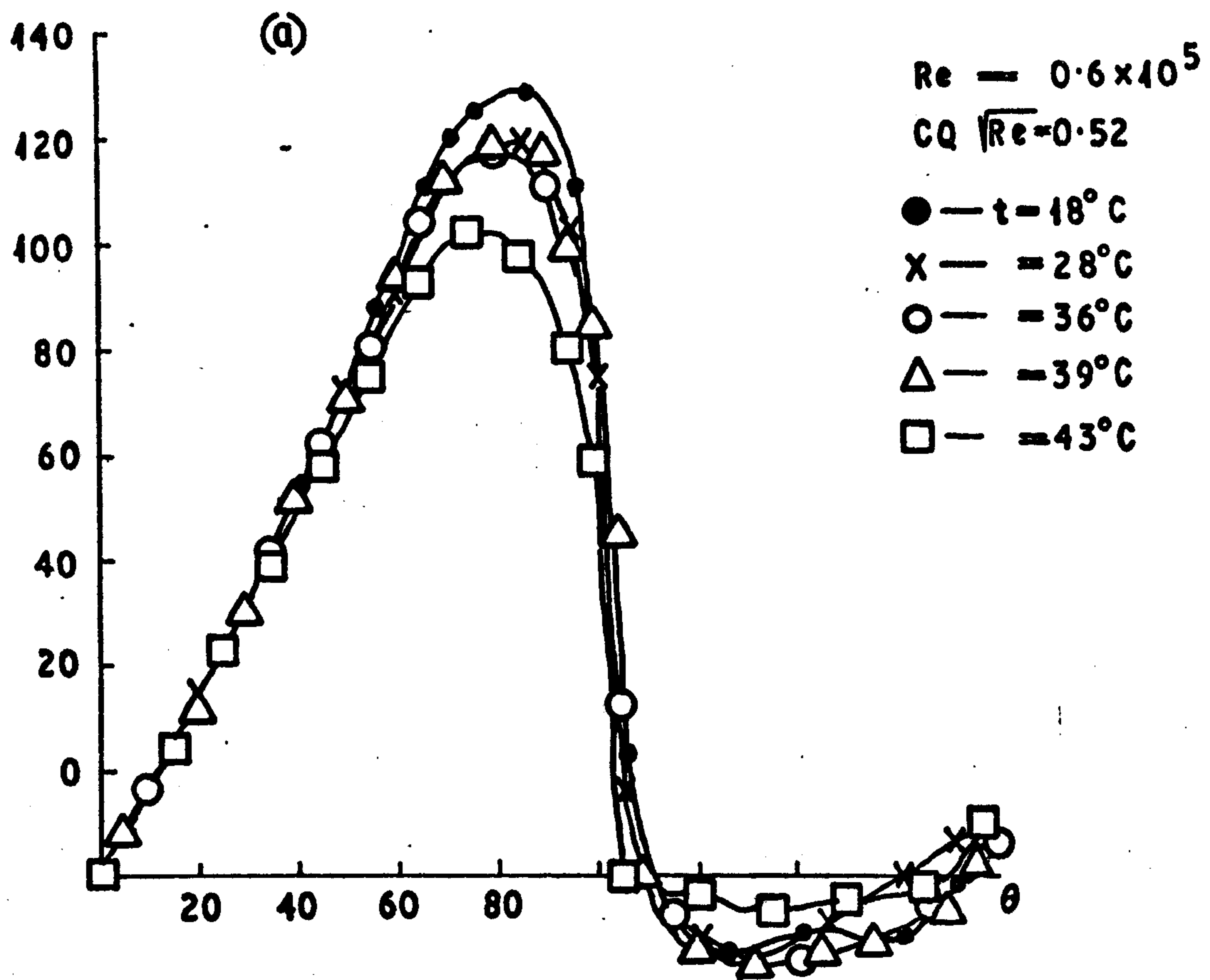




**Fig 9.11**

**EFFECT OF MAIN STREAM TEMPERATURE**  
**ON FIRST ROW IN THE BANK**

$K_f \times 10^3$



$K_f \times 10^3$

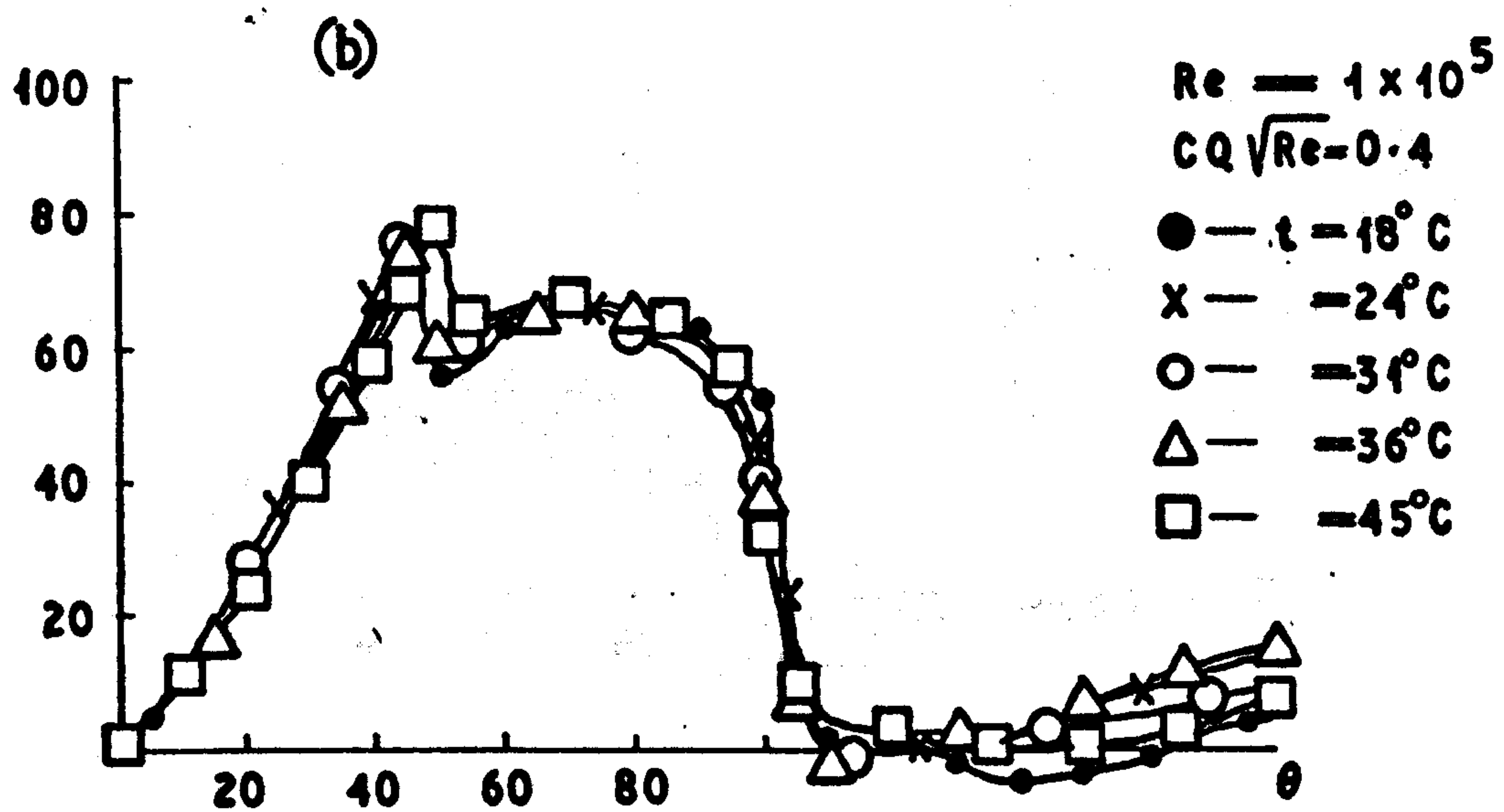


Fig 9.12

EFFECT OF MAIN STREAM TEMPERATURE  
WITH MASS TRANSFER ON FIRST ROW IN THE BANK

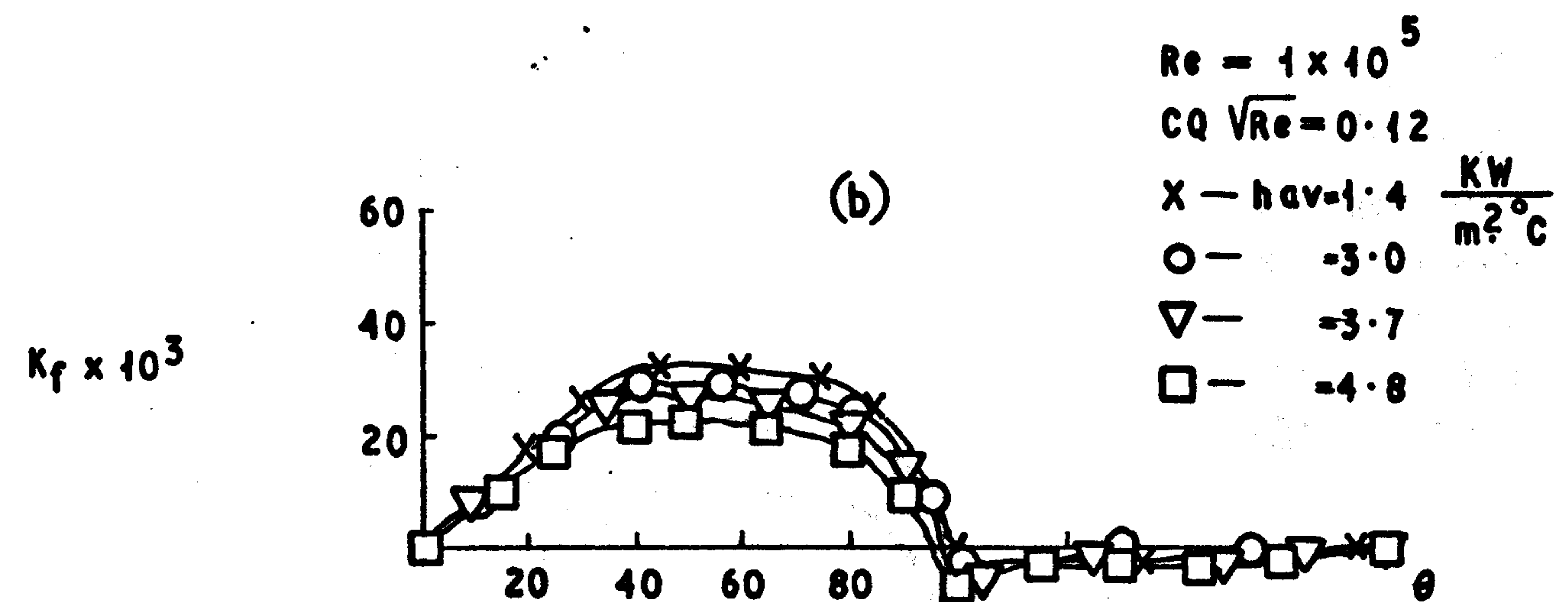
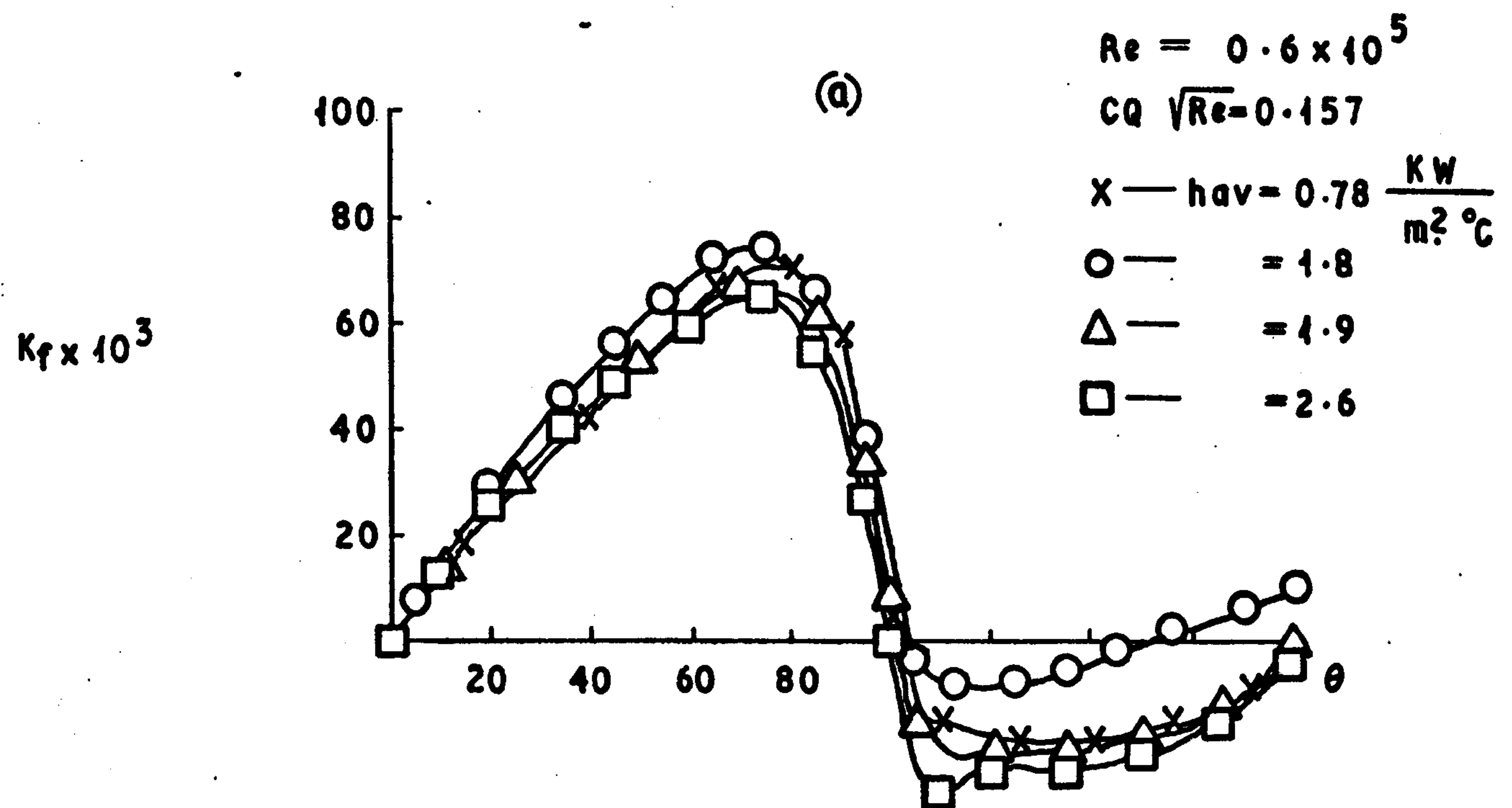
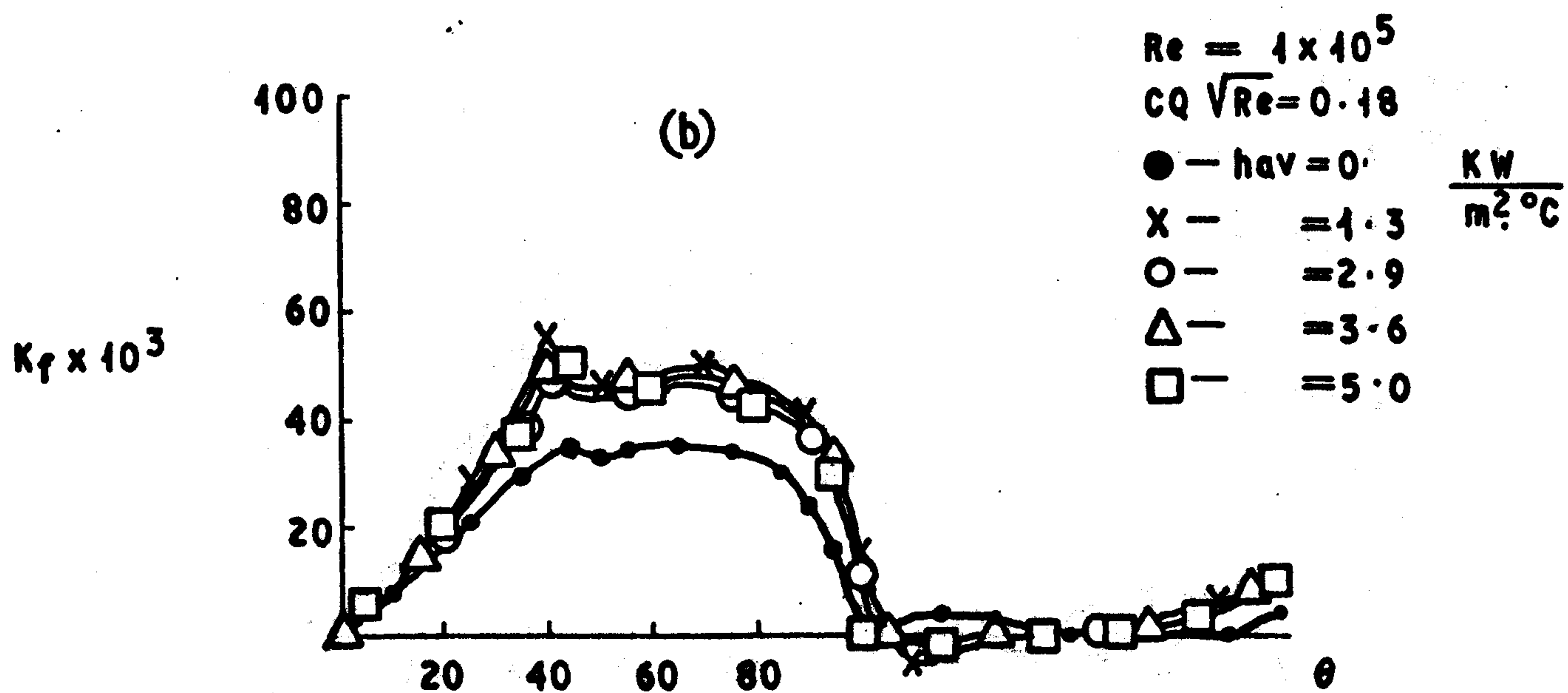
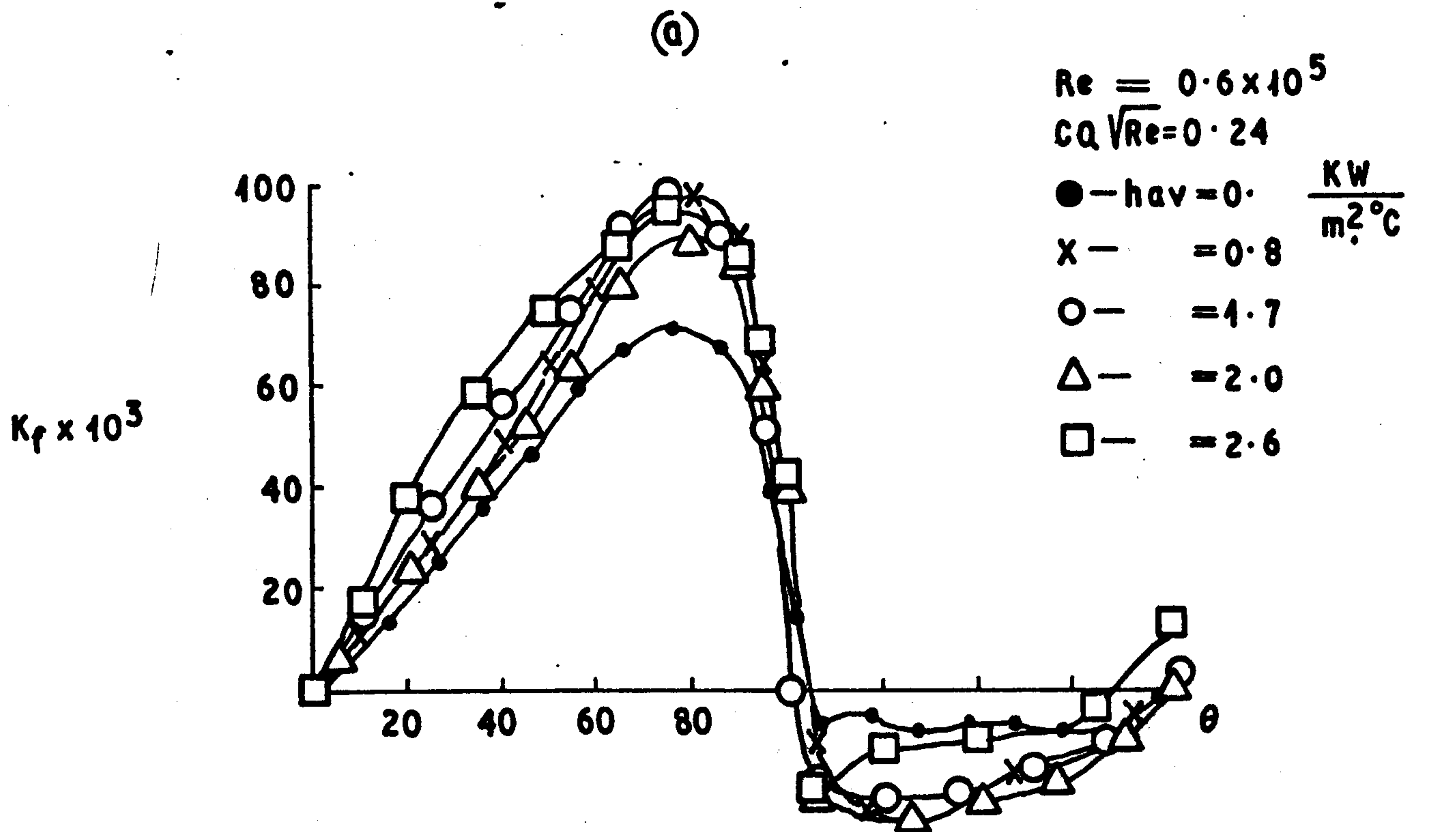


Fig.9.13

EFFECT OF HEAT AND MASS TRANSFER ON

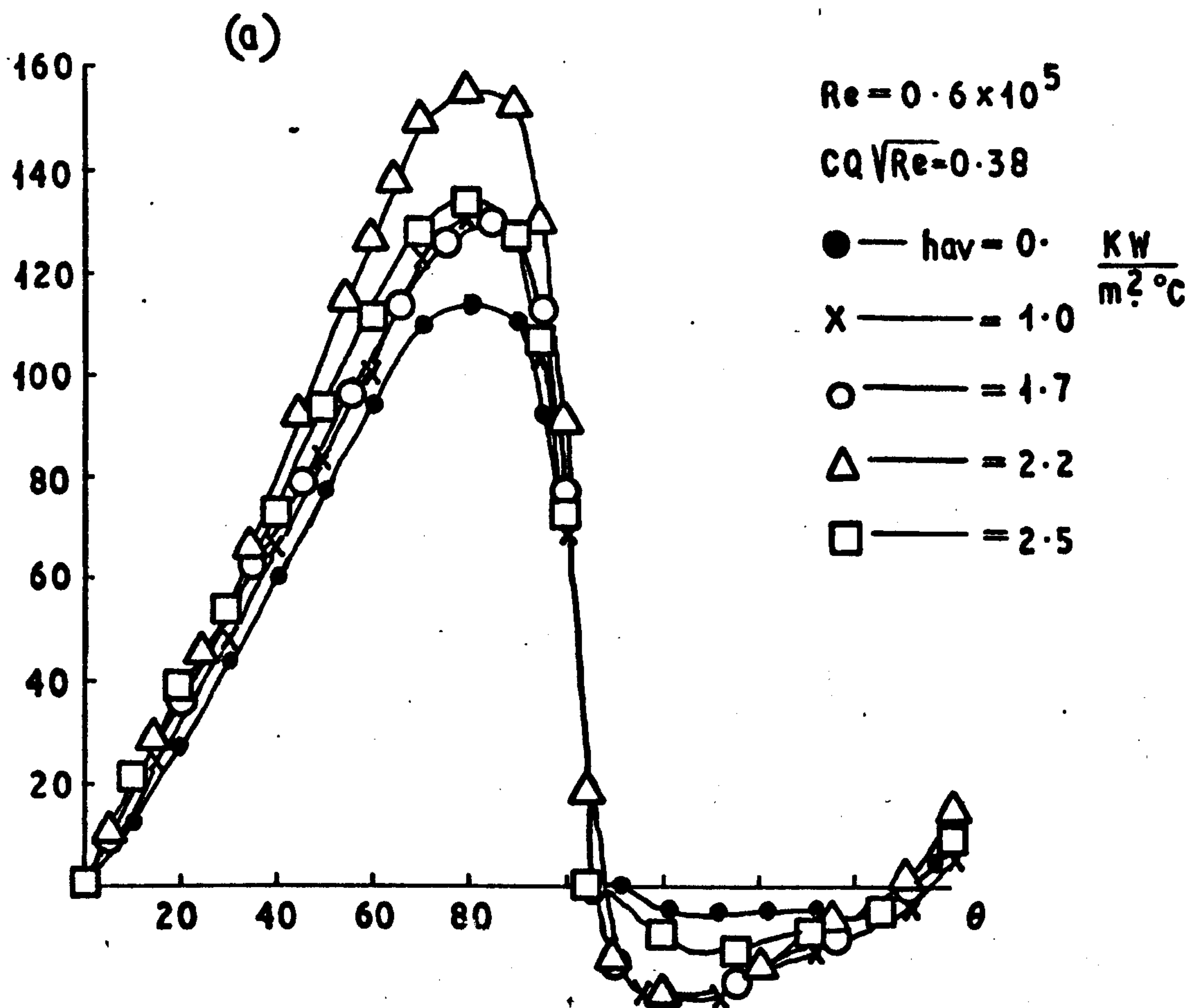
SHEAR STRESS, FIRST ROW IN THE BANK.





**Fig 9.14**  
**HEAT AND MASS TRANSFER EFFECT ON**  
**FIRST ROW IN THE BANK**

$K_f \times 10^3$



$K_f \times 10^3$

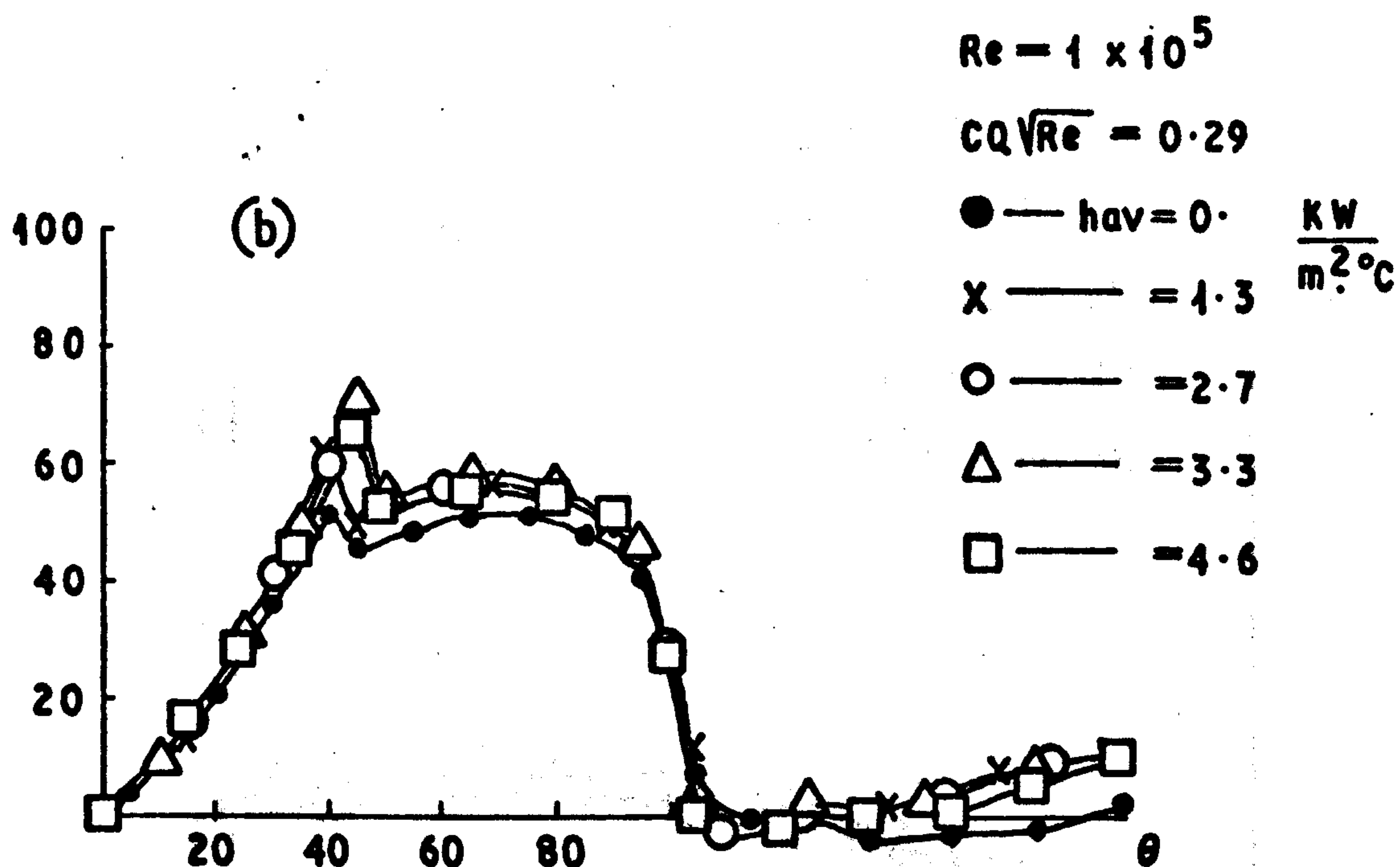


Fig 9.15

SHEAR STRESS WITH HEAT AND MASS TRANSFER

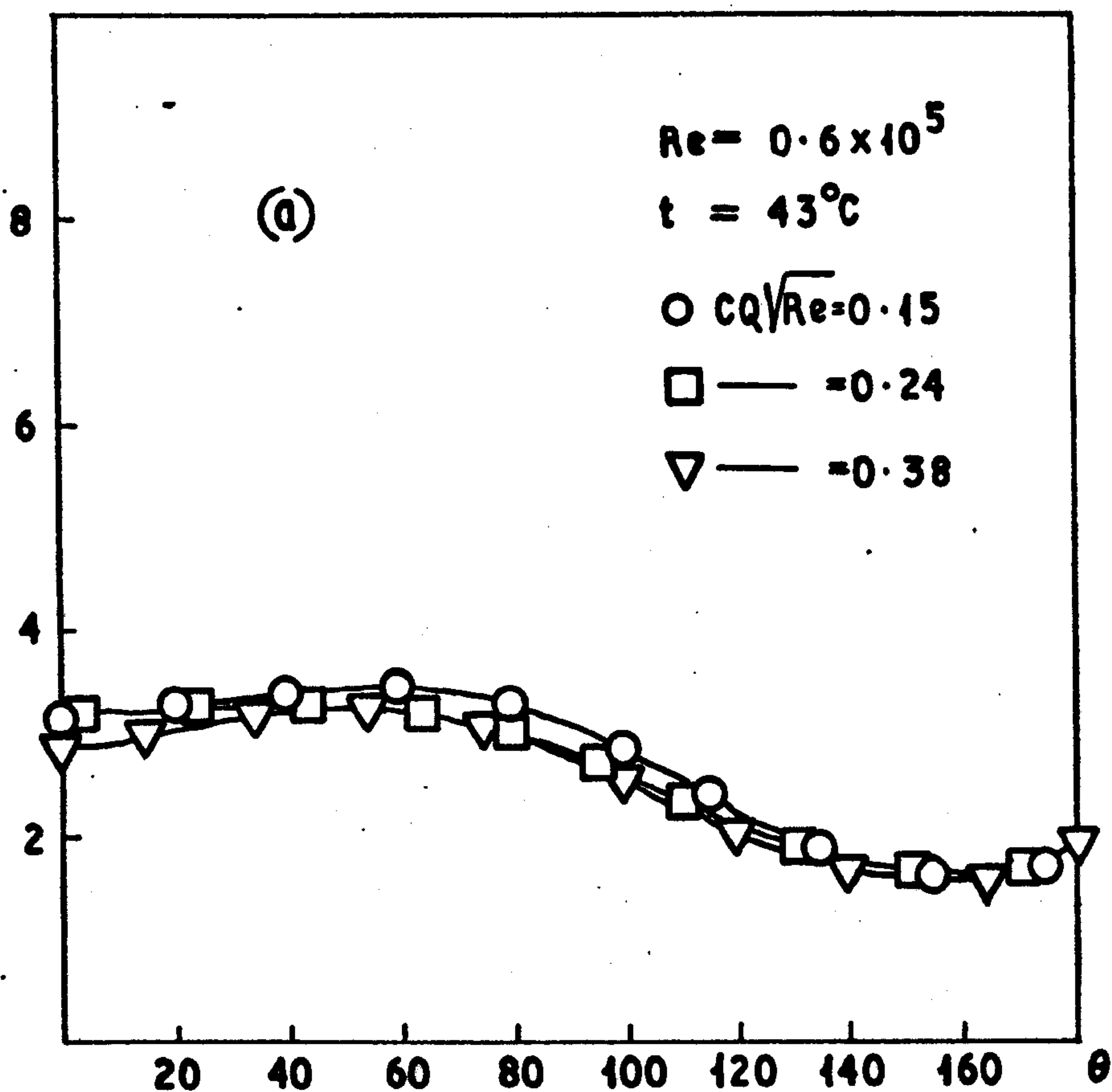
ROUND FIRST ROW IN THE BANK

Fig 9.15

HEAT TRANSFER WITH MASS TRANSFER

ROUND FIRST ROW IN THE BANK

$h$   
 $\frac{KW}{m^2 \cdot ^\circ C}$



$h$   
 $\frac{KW}{m^2 \cdot ^\circ C}$

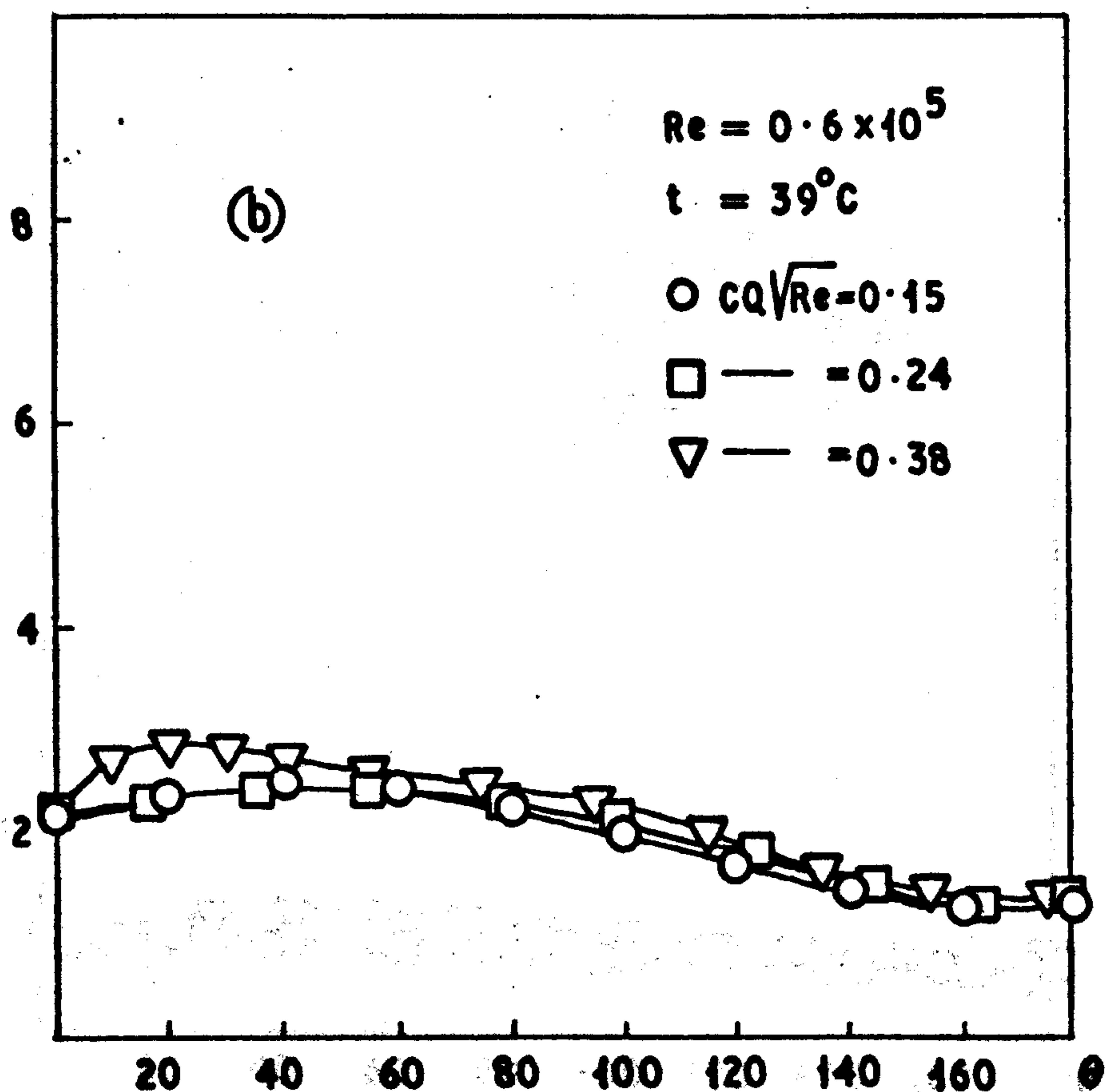
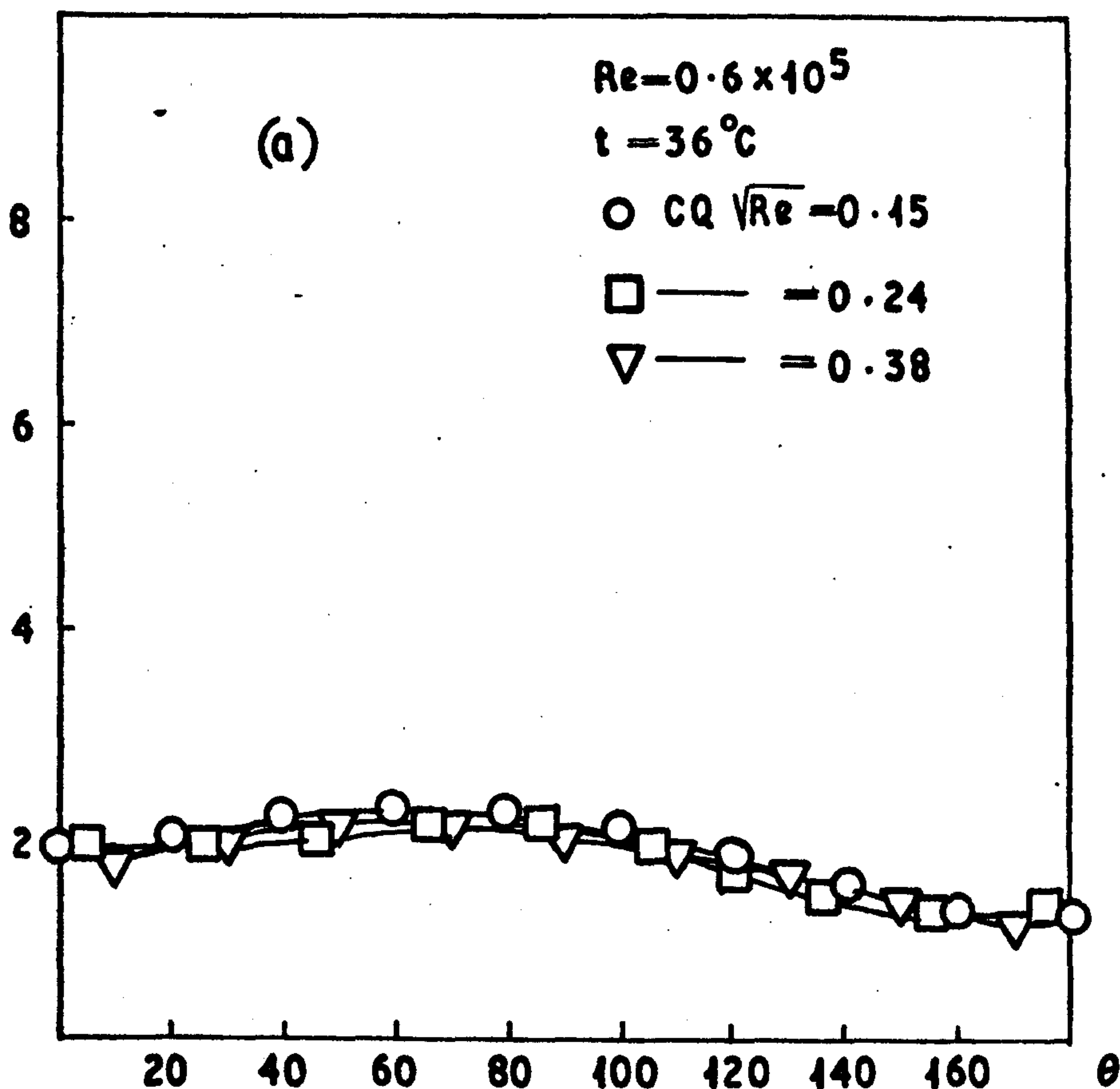


**Fig 9.16**

**HEAT TRANSFER WITH MASS TRANSFER  
AROUND FIRST ROW IN THE BANK**



$$\frac{h}{\text{KW}} \frac{\text{m}^2}{^\circ\text{C}}$$



$$\frac{h}{\text{KW}} \frac{\text{m}^2}{^\circ\text{C}}$$

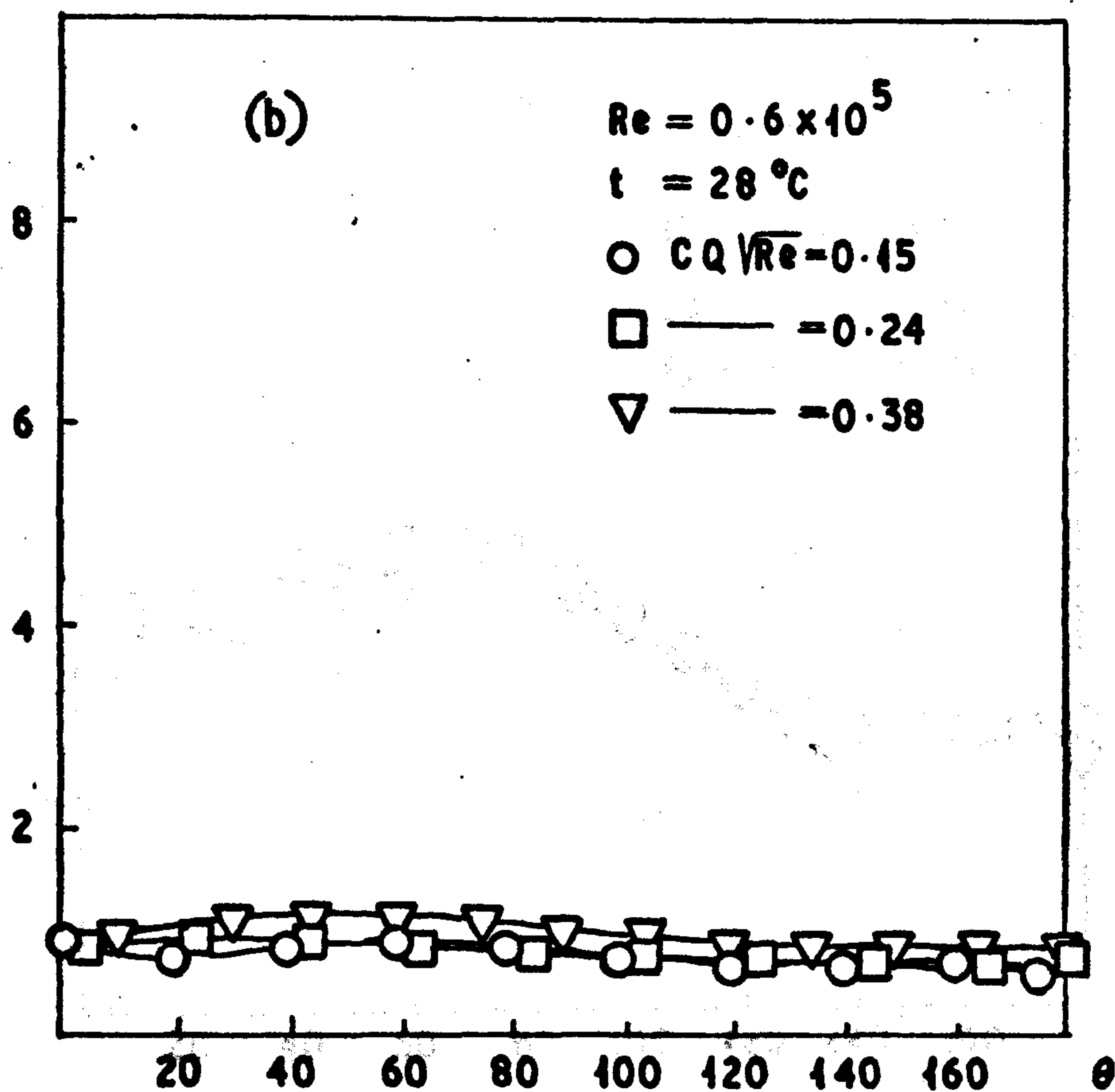


Fig 9.17

HEAT TRANSFER WITH MASS TRANSFER

AROUND FIRST ROW IN THE BANK

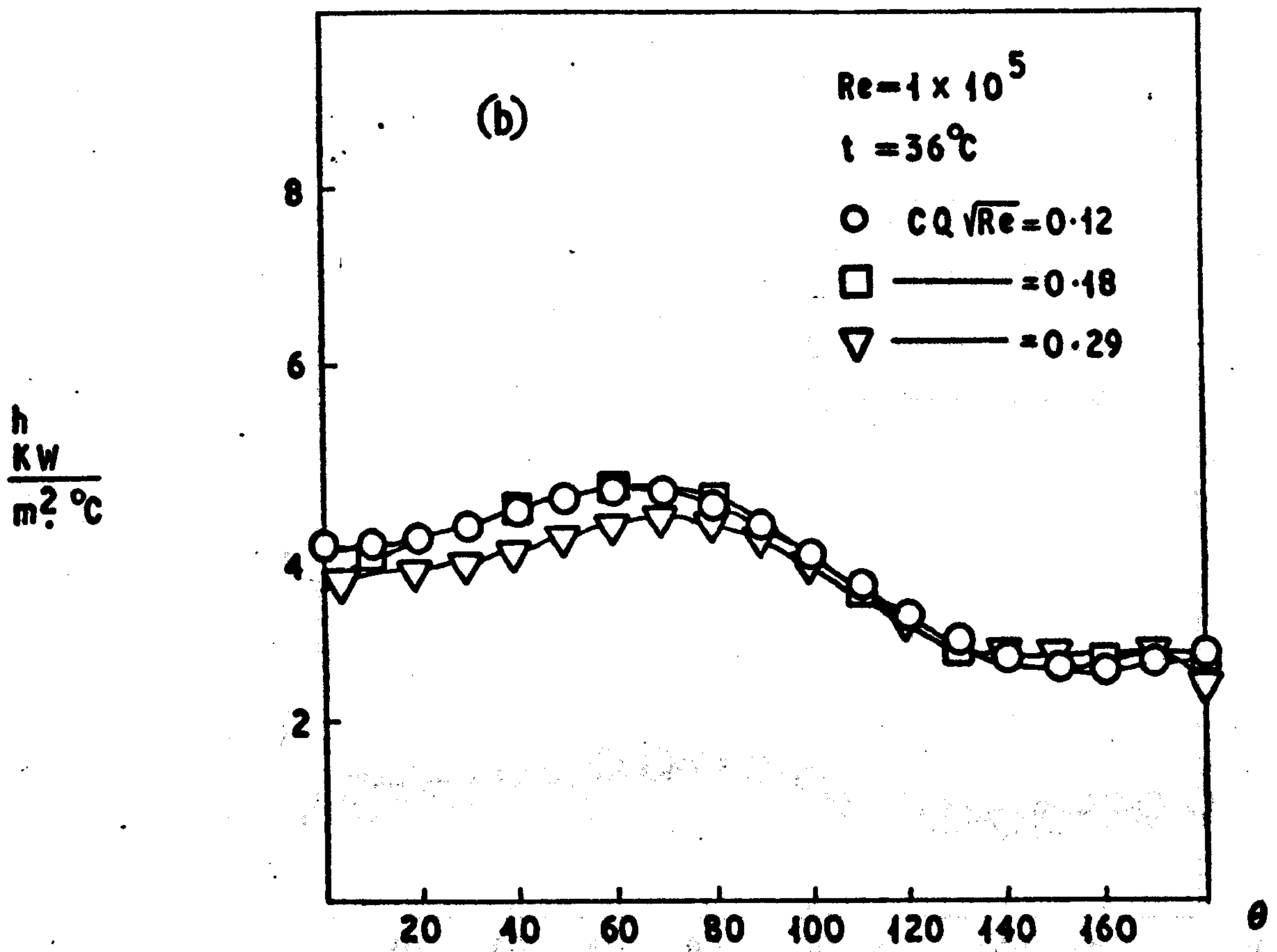
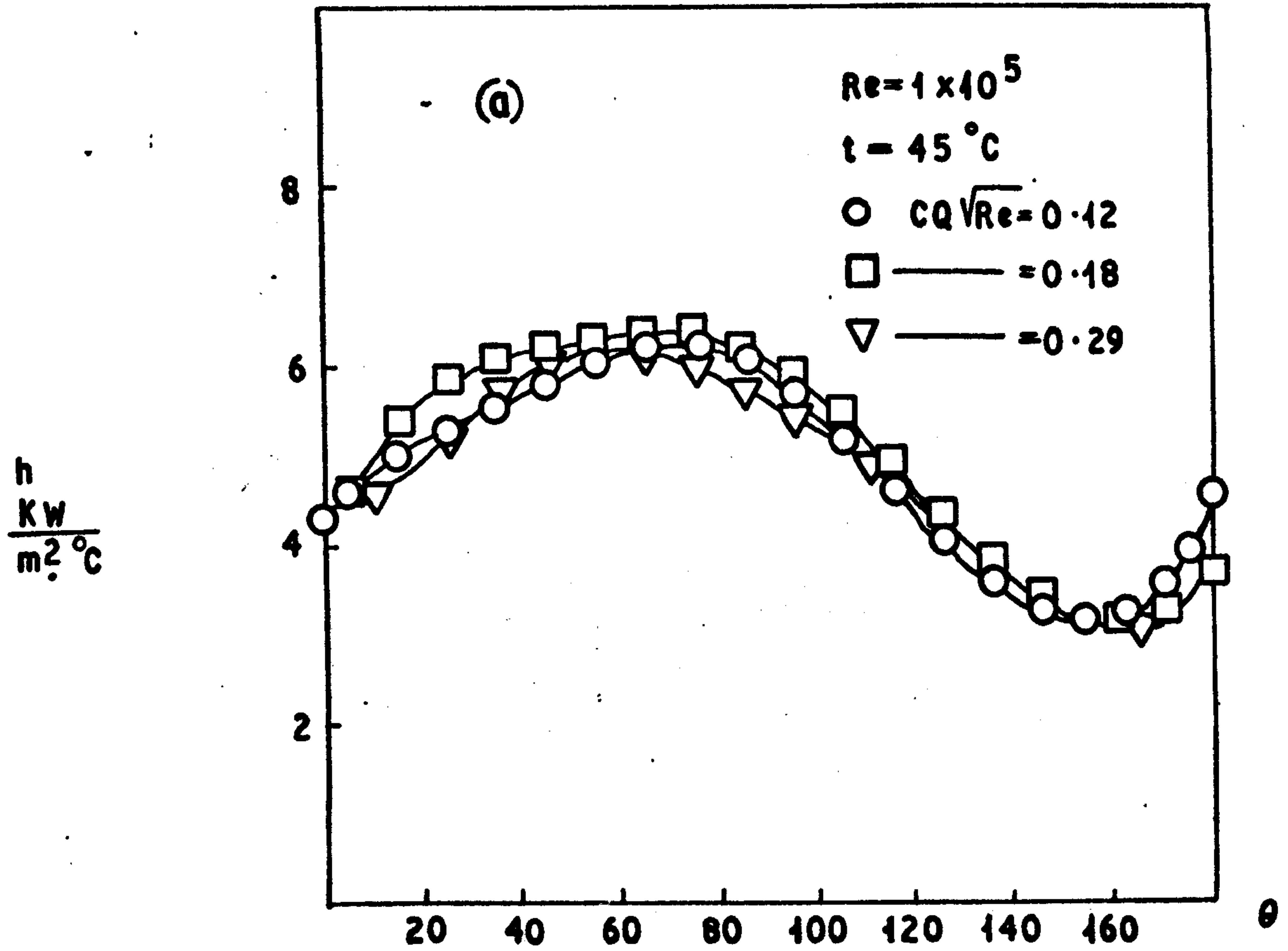
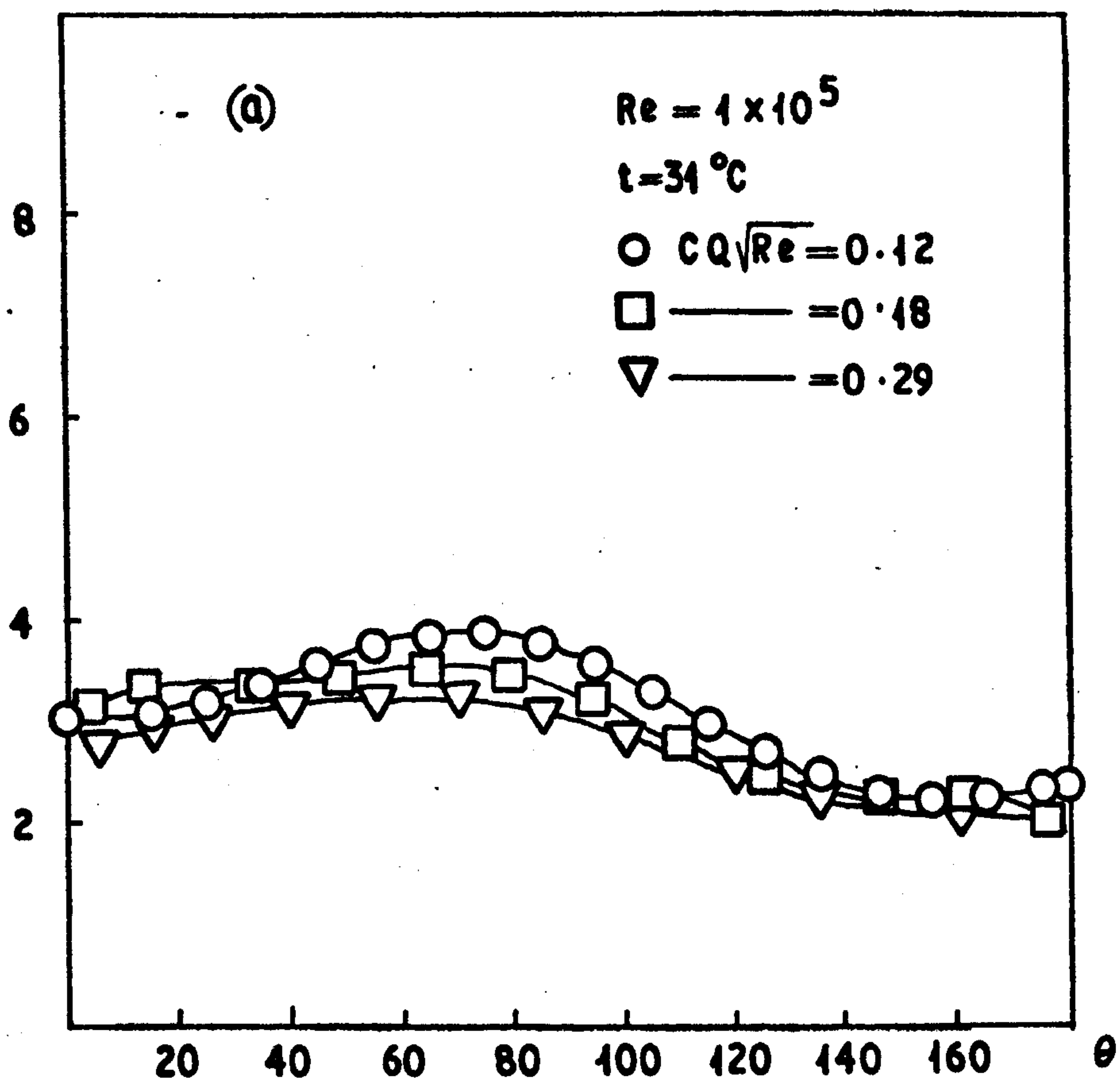


Fig. 9.18

HEAT TRANSFER WITH MASS TRANSFER  
AROUND FIRST ROW IN THE BANK

$\frac{h}{KW}$   
 $\frac{m^2}{m^2 \cdot ^\circ C}$



$\frac{h}{KW}$   
 $\frac{m^2}{m^2 \cdot ^\circ C}$

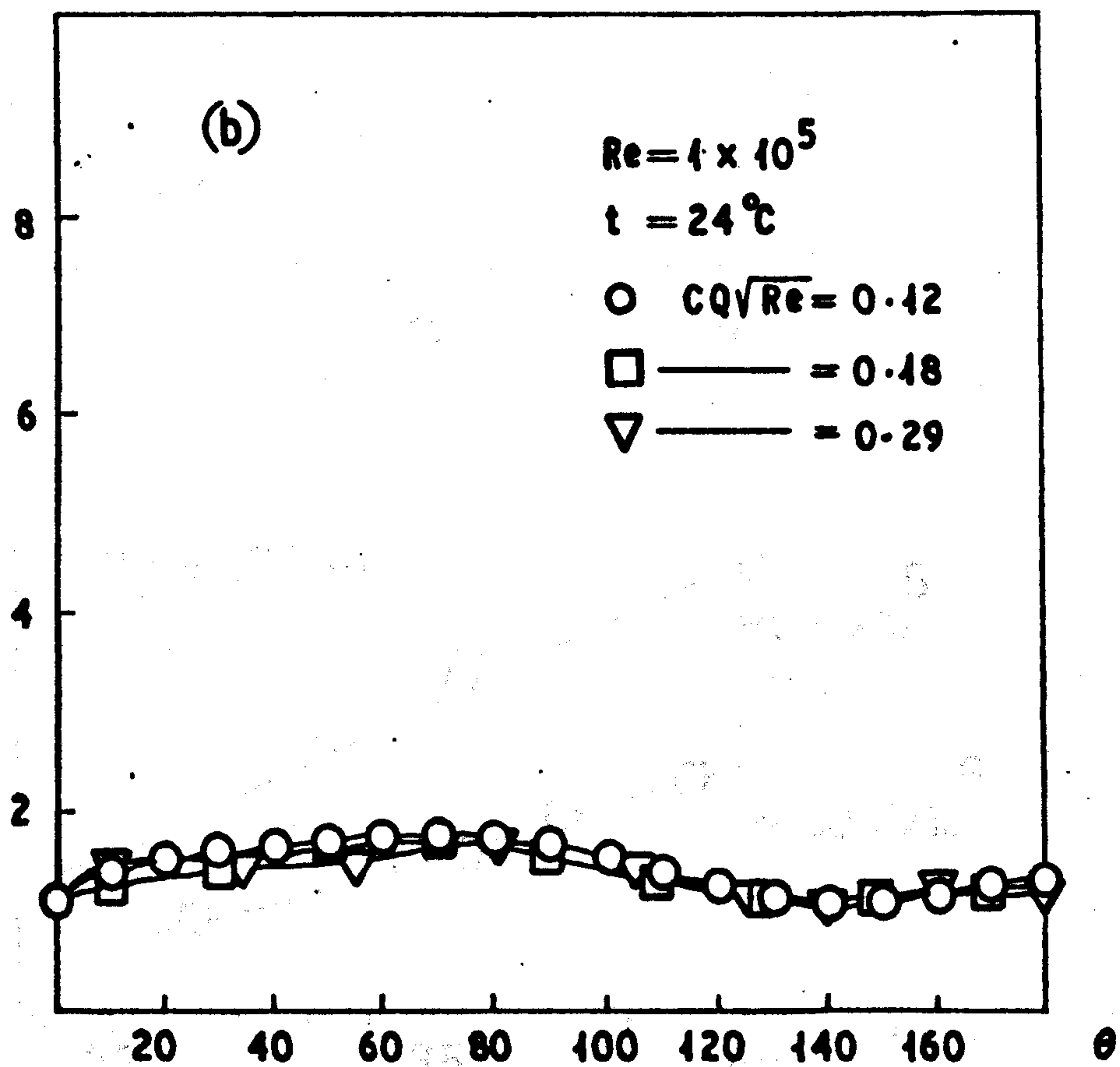


**Fig 9.19**  
**HEAT TRANSFER WITH MASS TRANSFER**  
**AROUND FIRST ROW IN THE BANK**



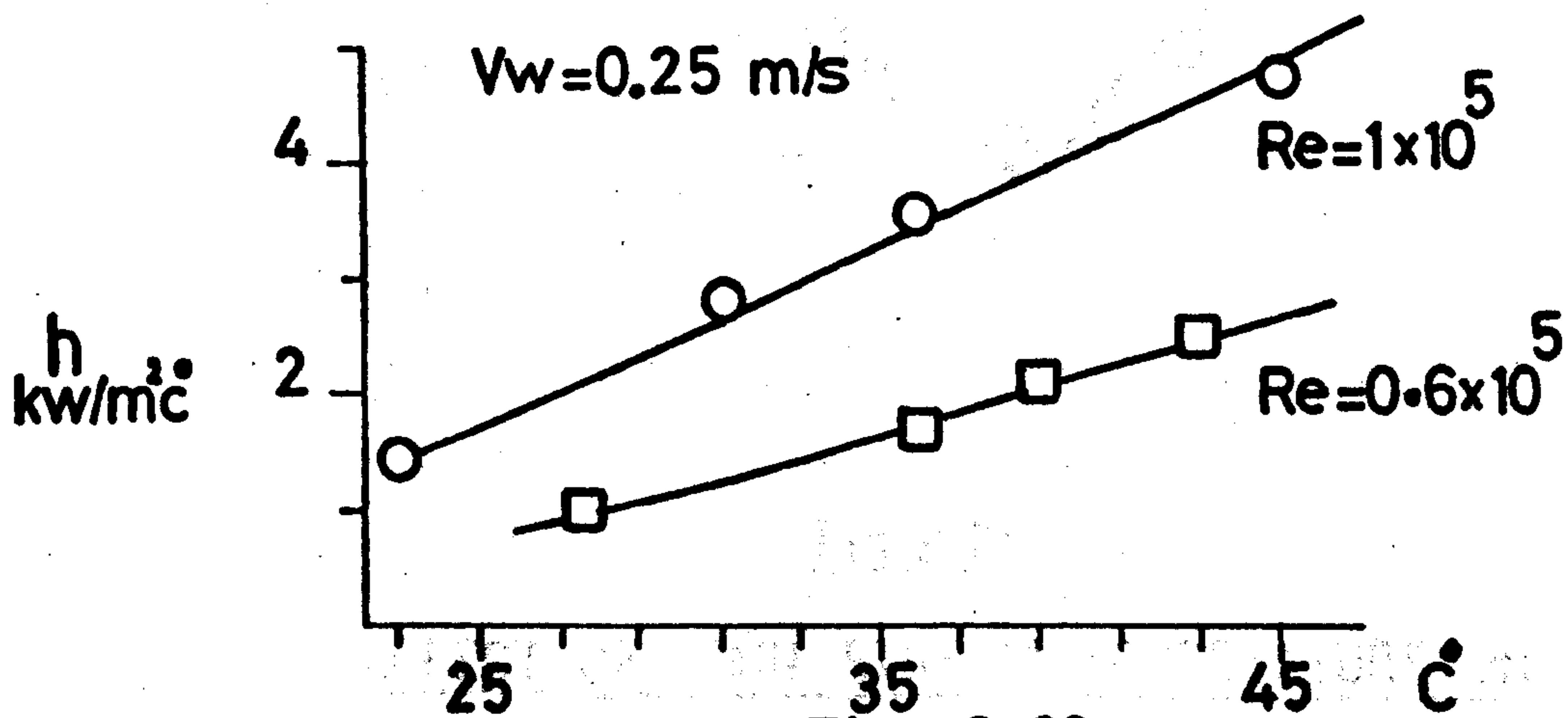
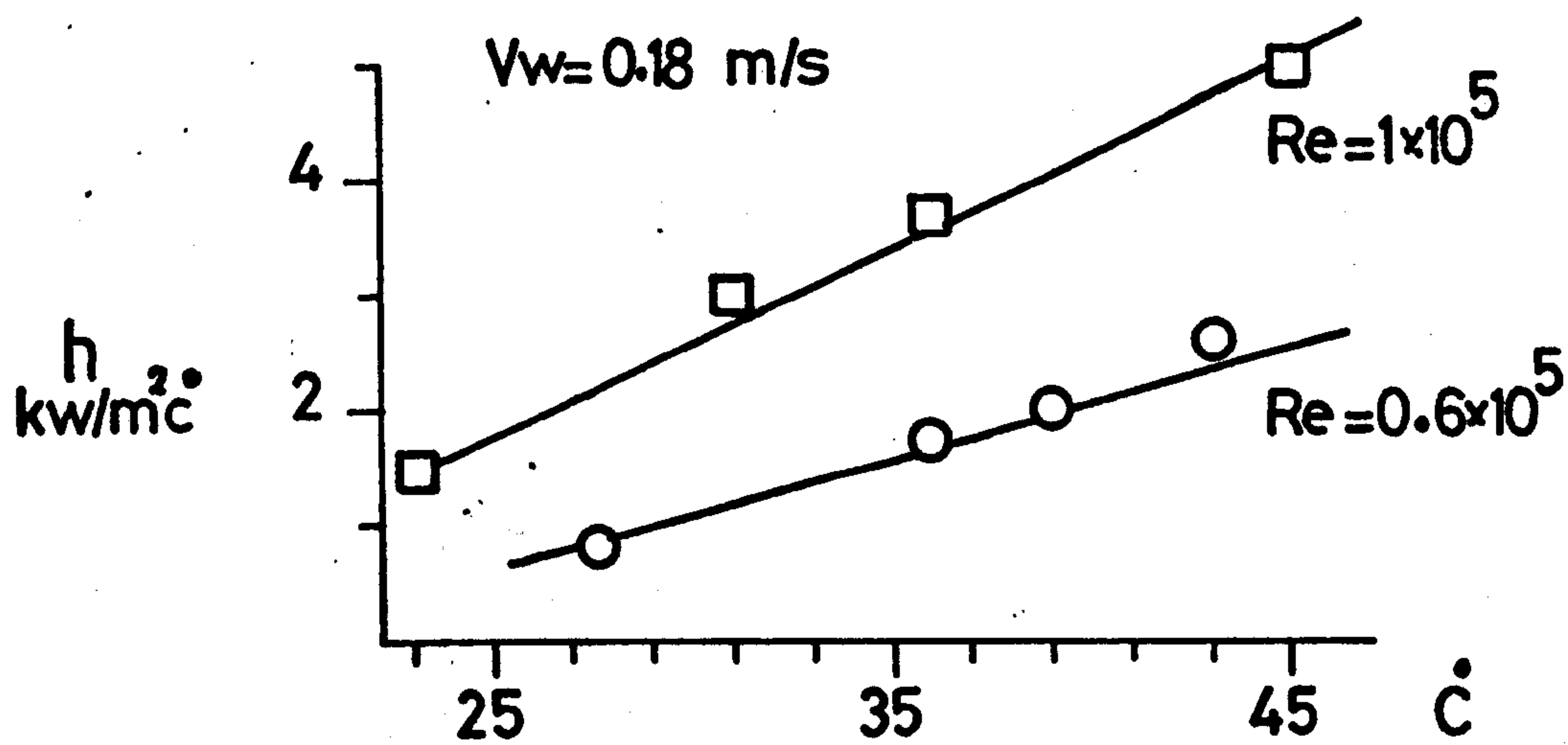
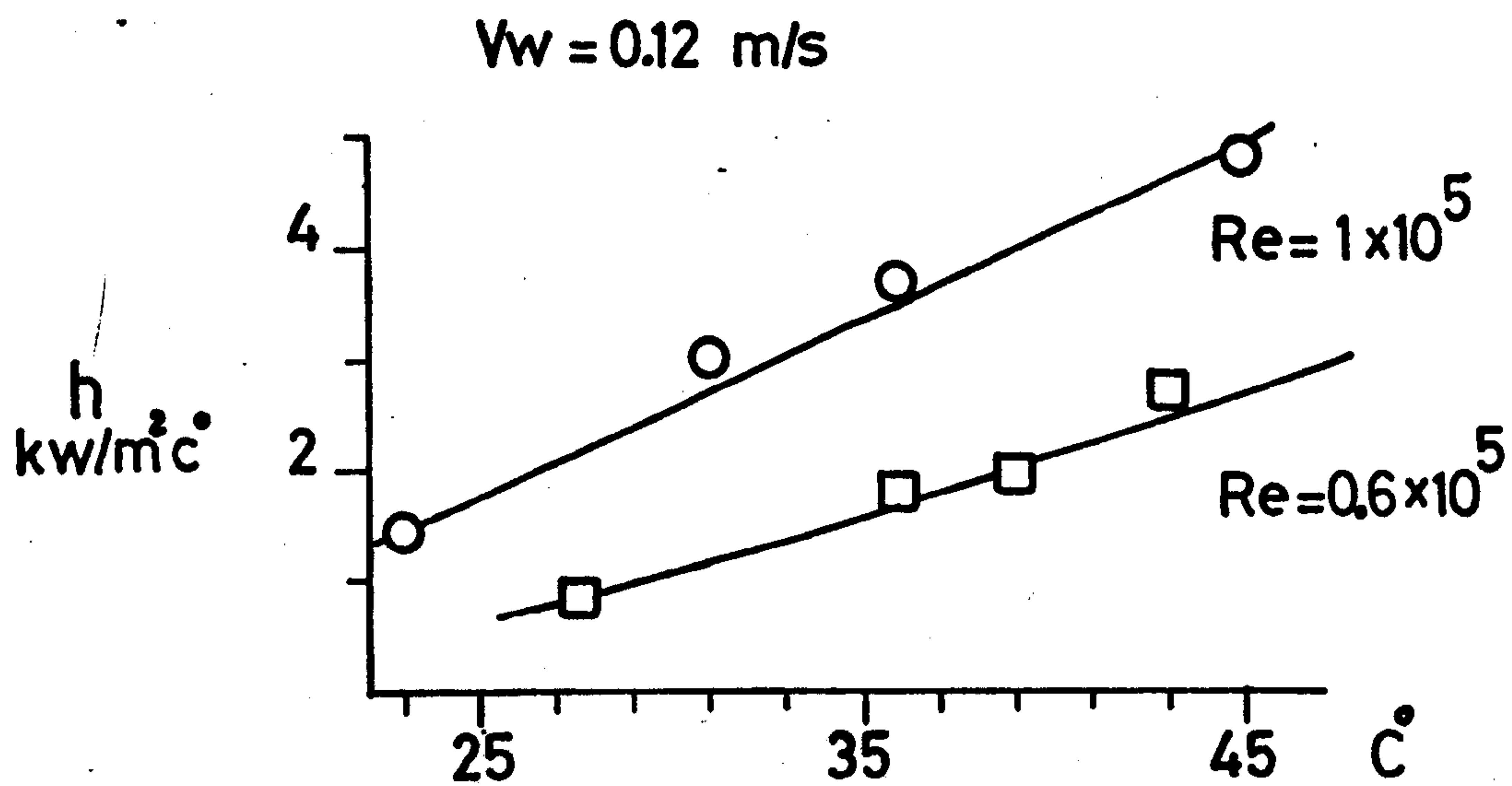


**Fig. 9.20**  
Average HTC for first row  
in the bank

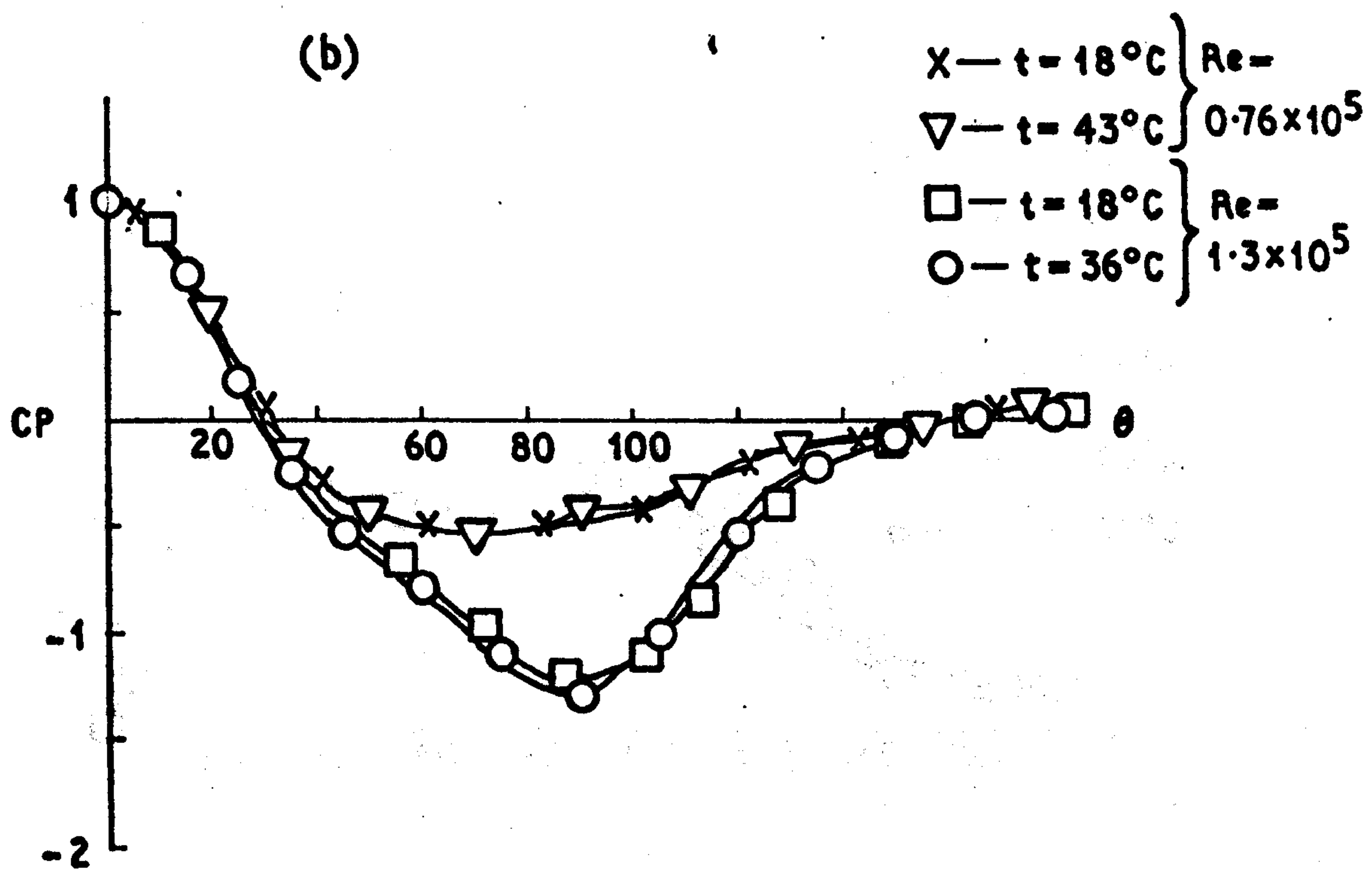
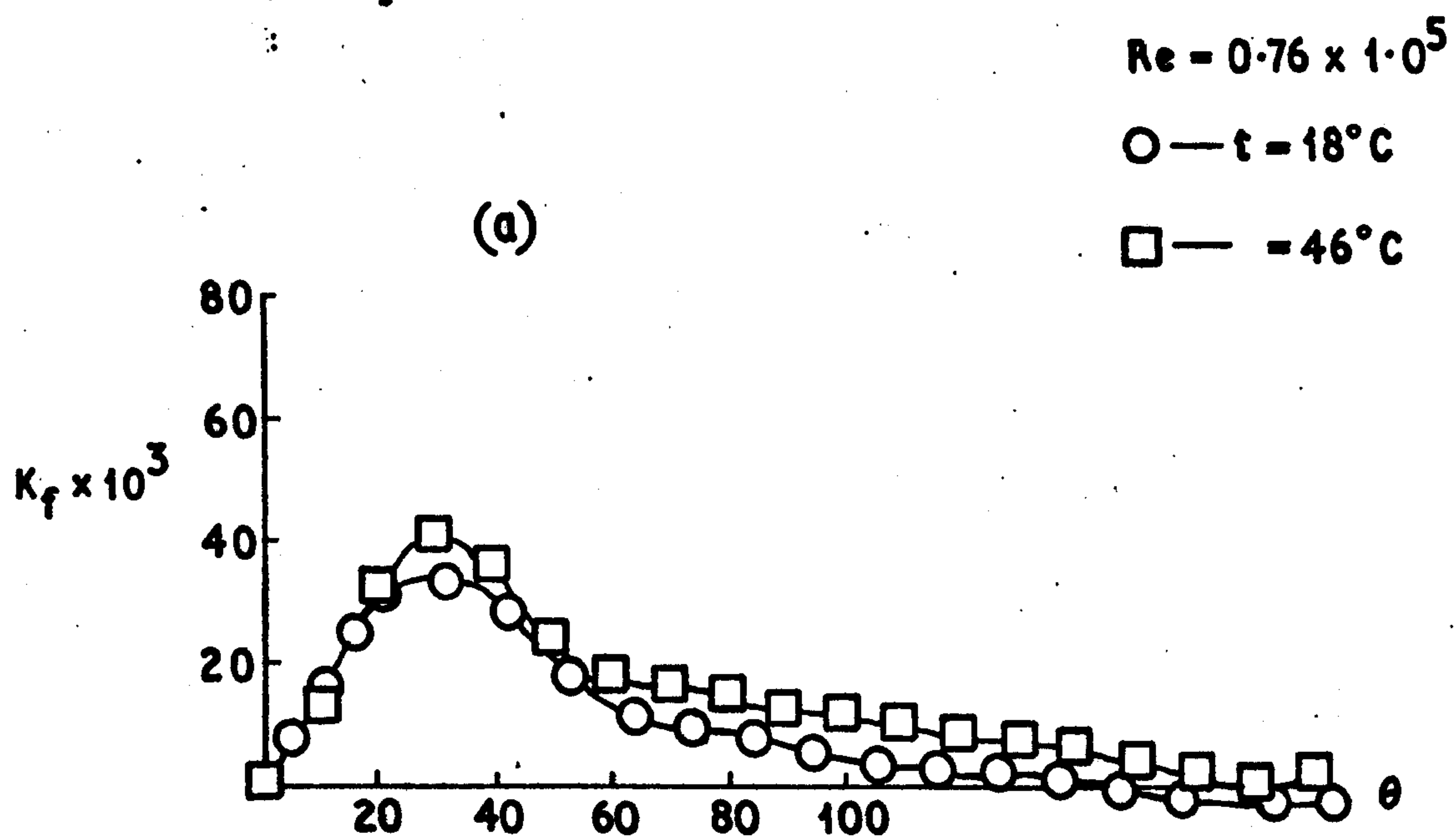


**Fig. 9.21**

**EFFECT OF MAIN STREAM TEMPERATURE ON**  
**SECOND ROW IN THE BANK**

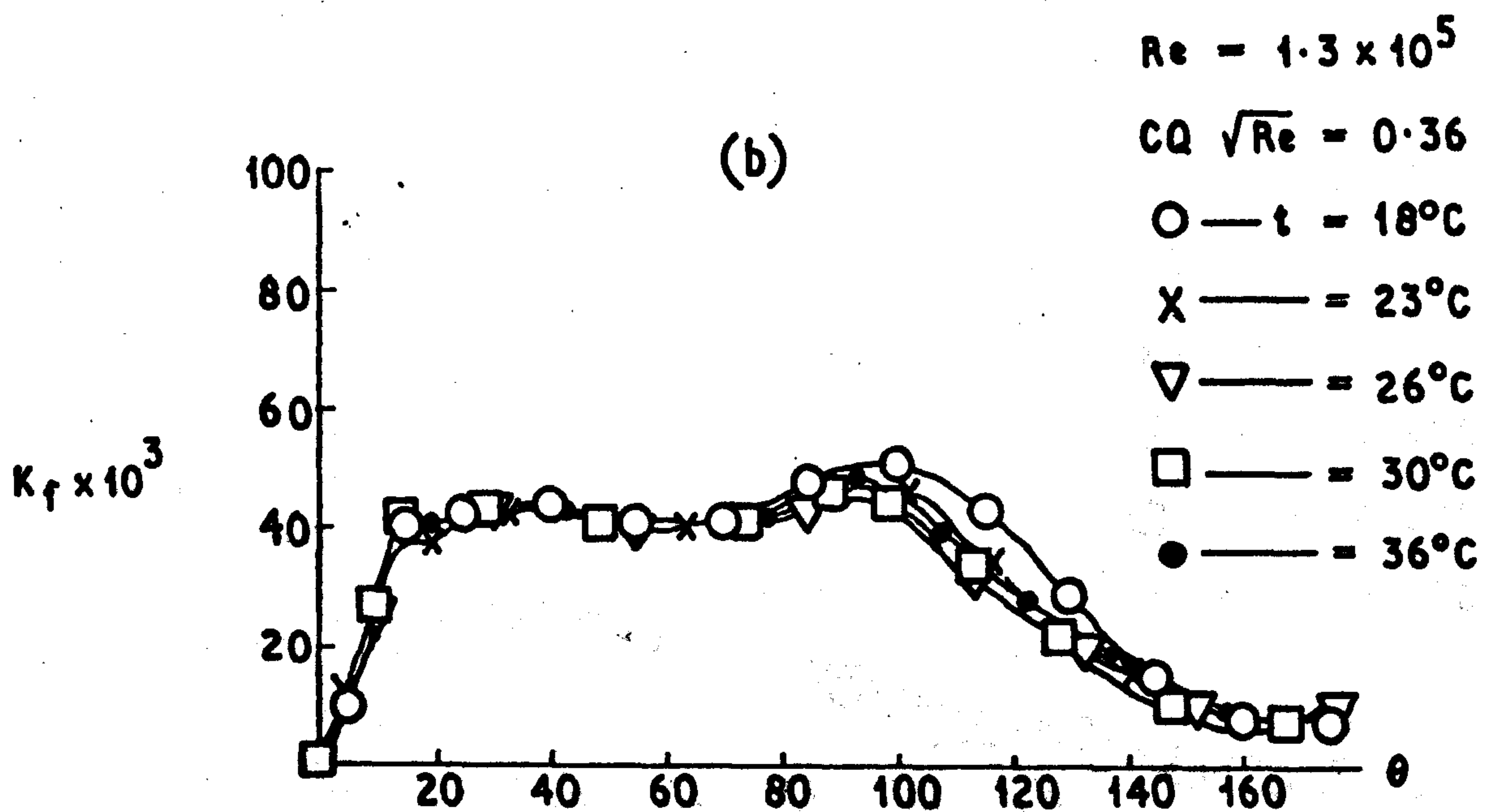
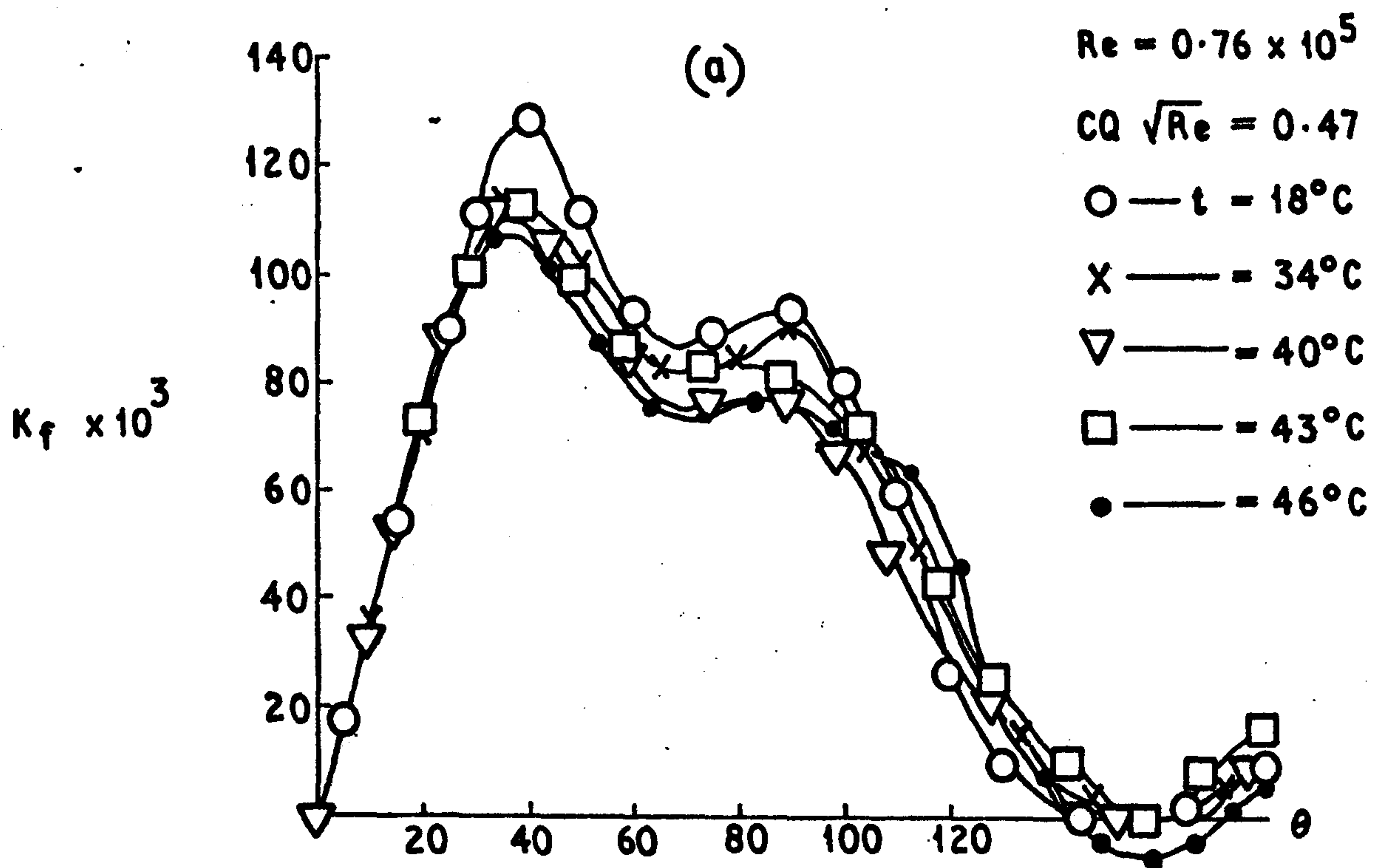


**Fig.9.22**

**EFFECT OF MAIN STREAM TEMPERATURE  
 WITH MASS TRANSFER ON SECOND ROW IN THE BANK**



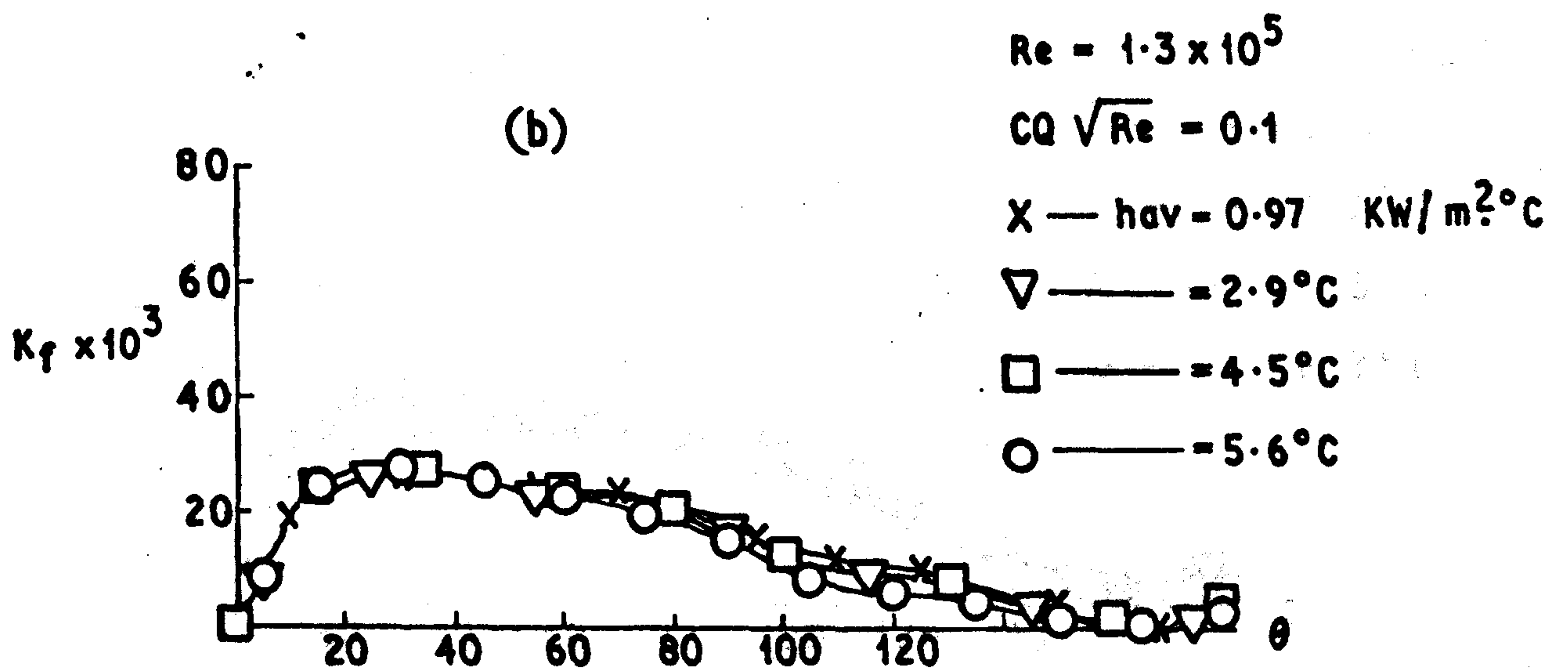
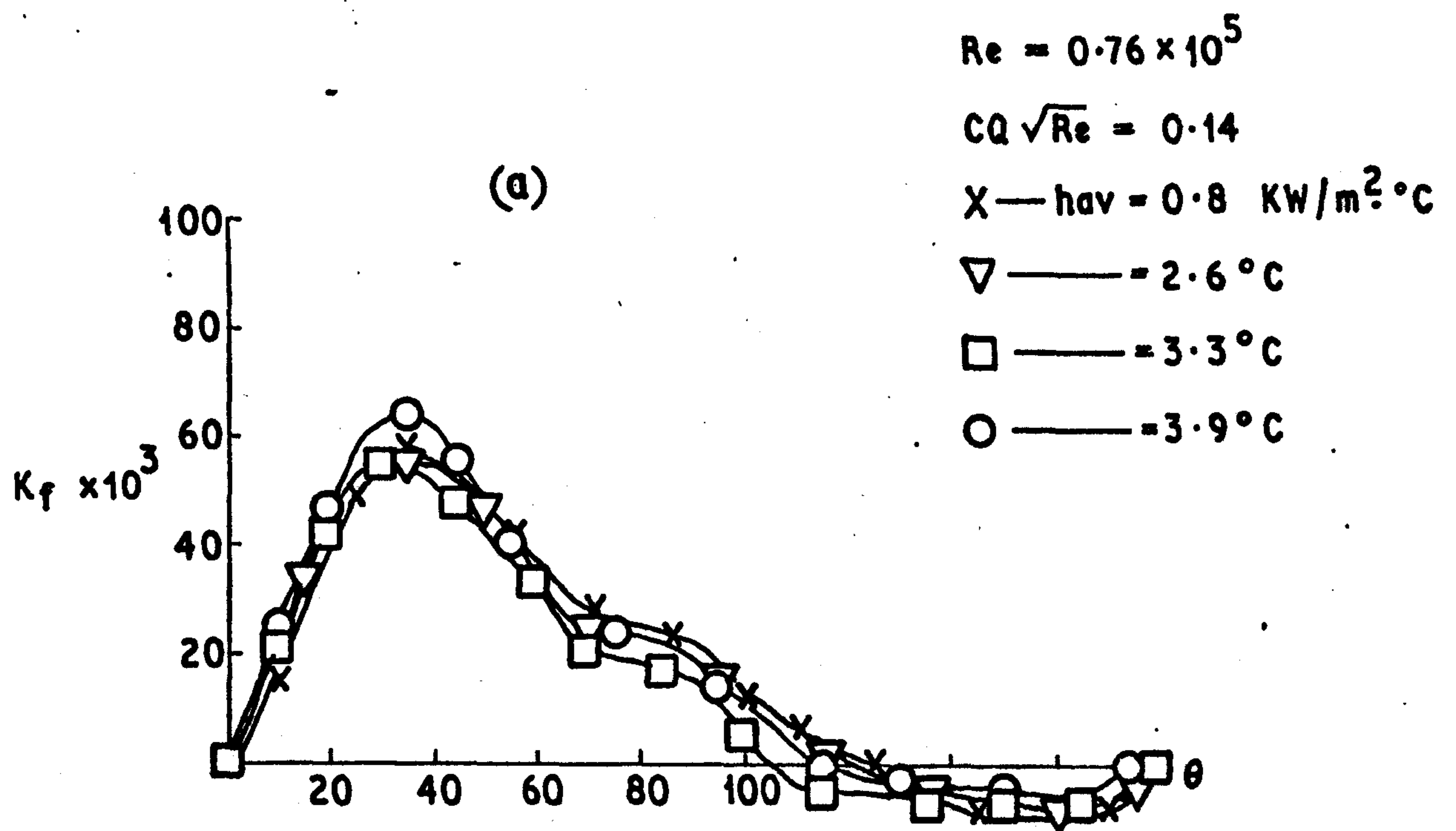


**Fig.9.23**

**SHEAR STRESS WITH HEAT AND MASS TRANSFER**  
**FOR SECOND ROW IN THE BANK**

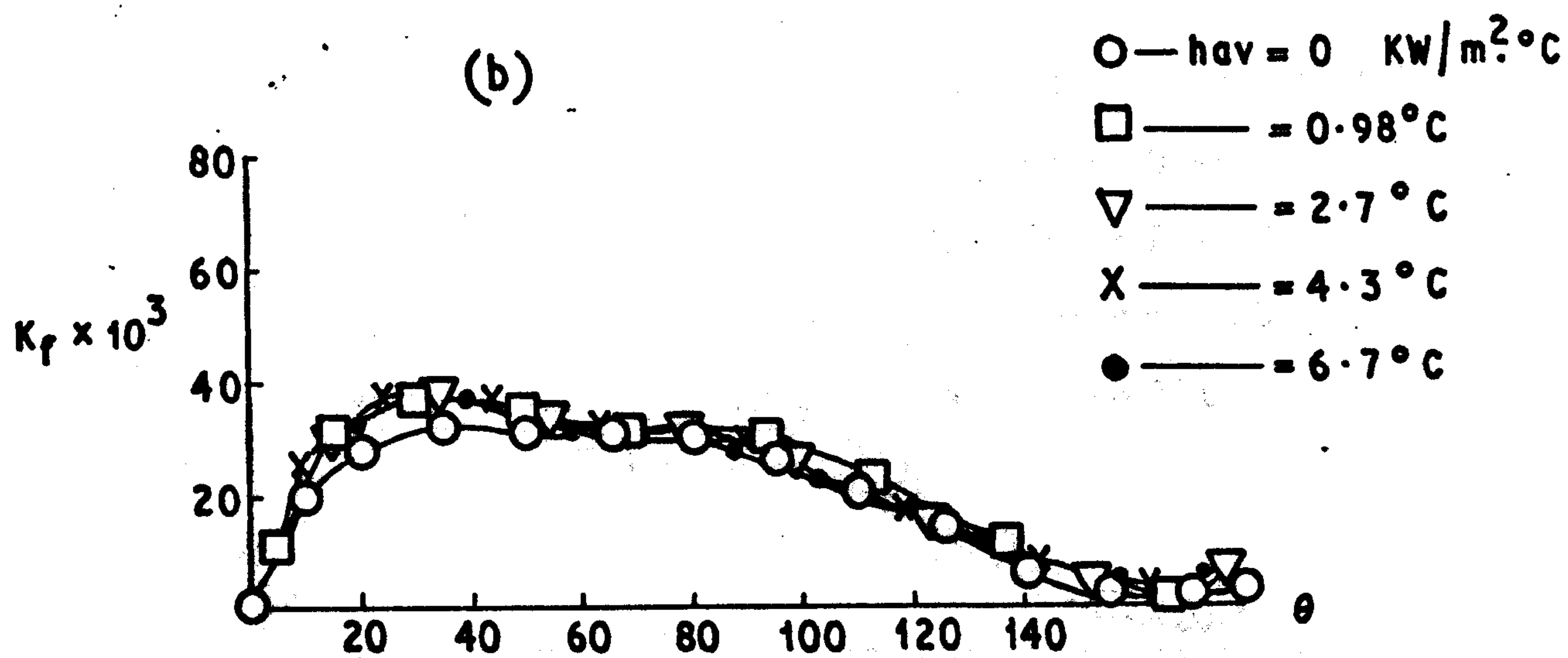
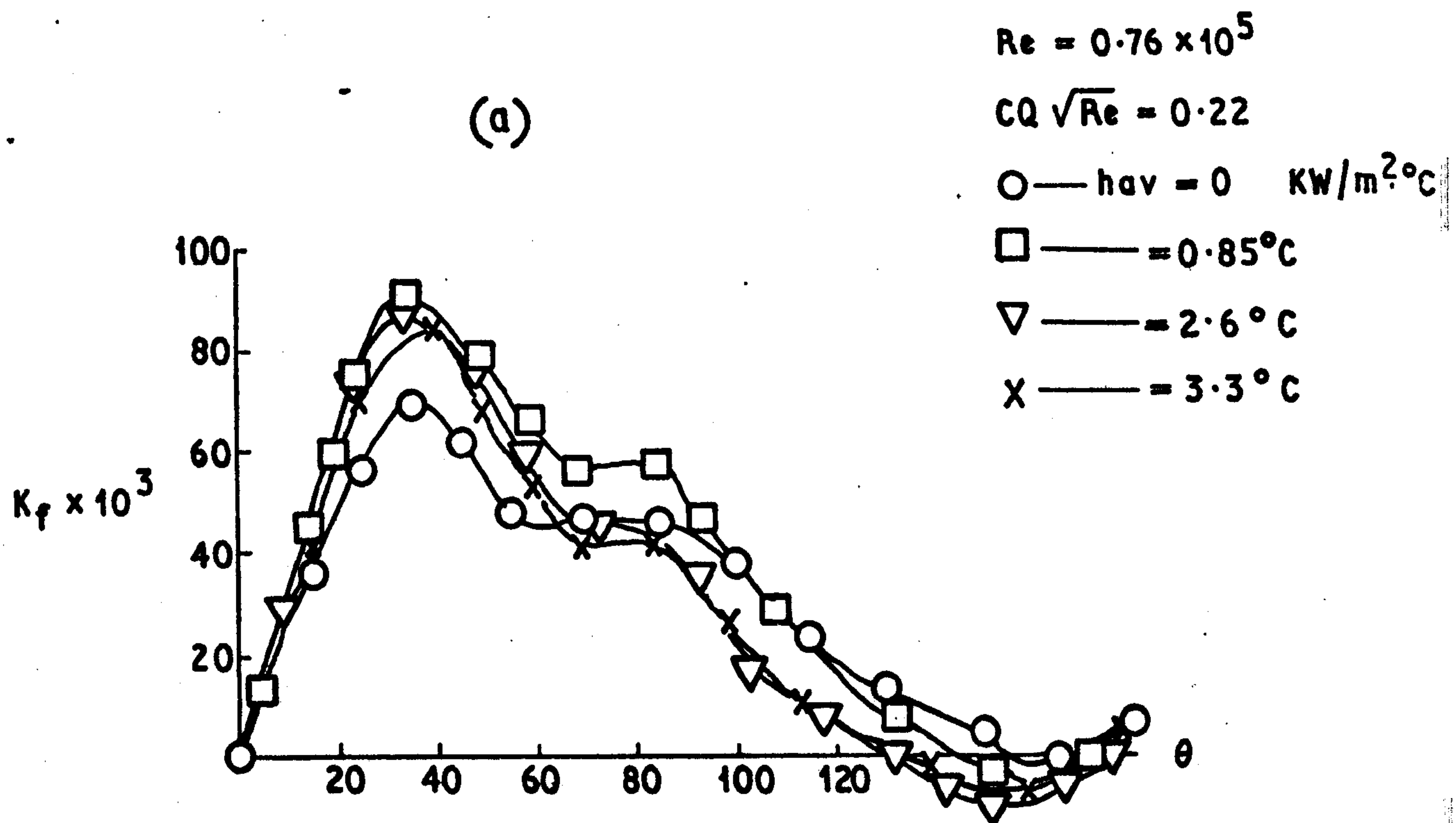
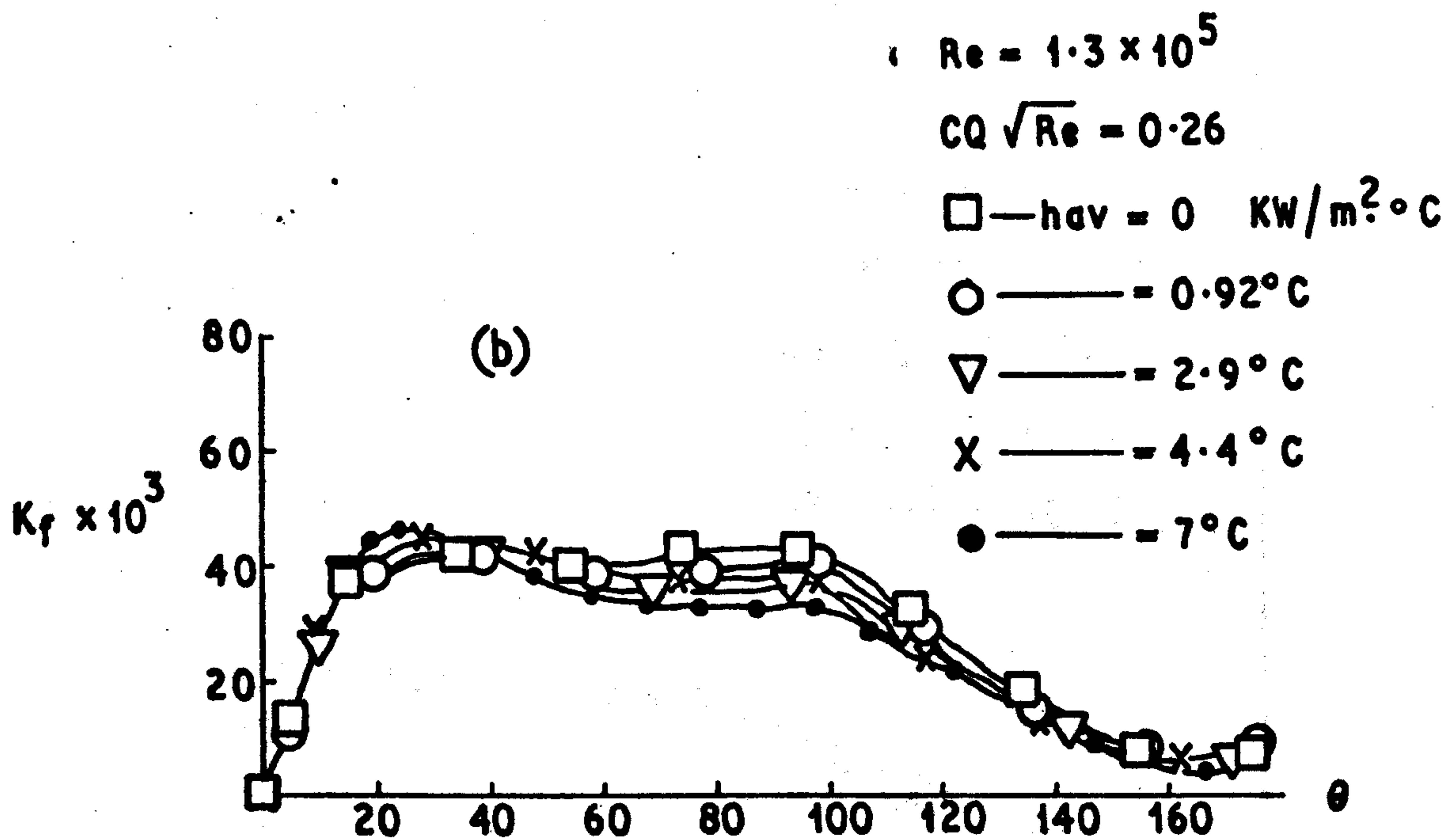
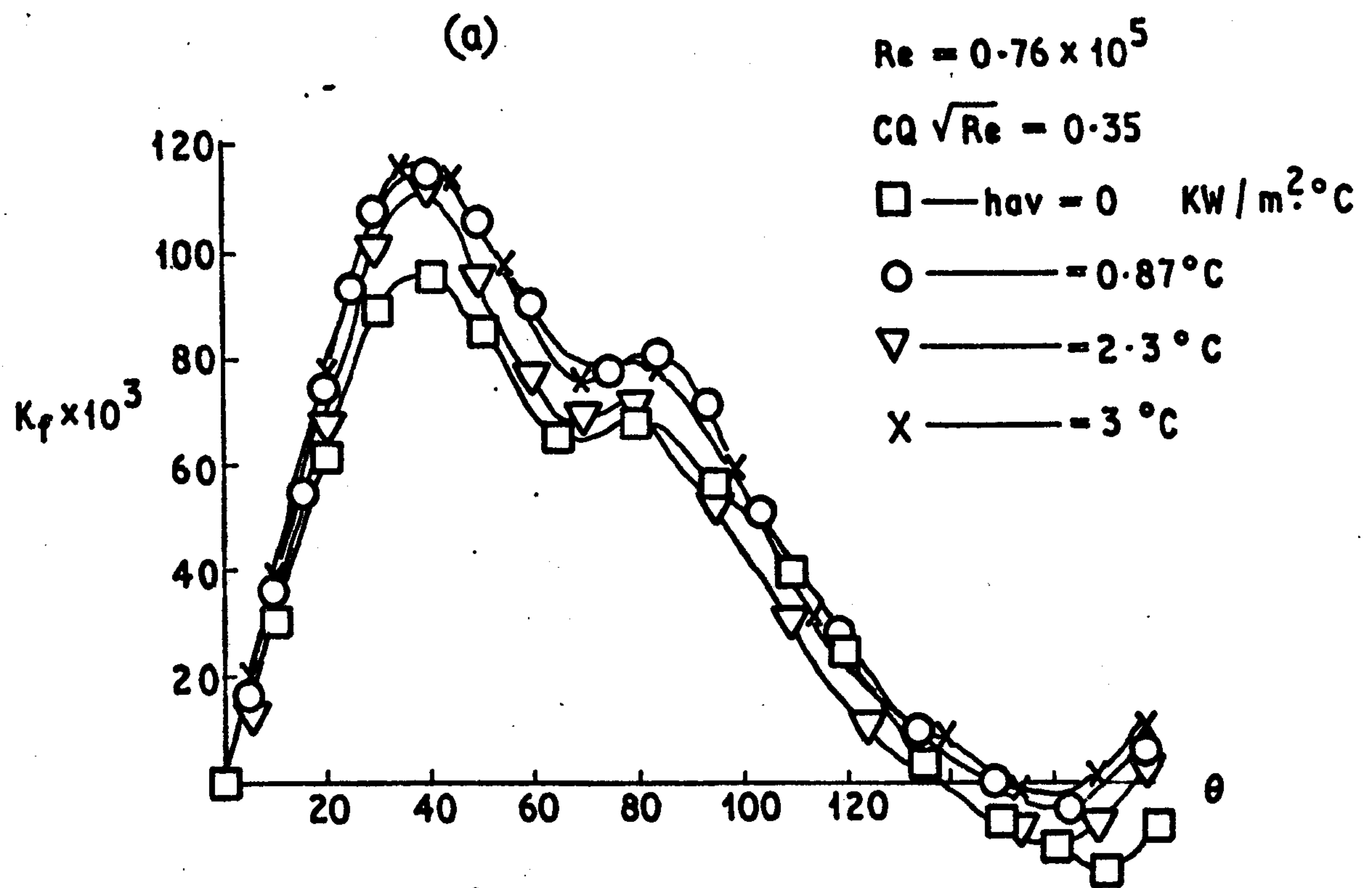


Fig. 9.24

SHEAR STRESS WITH HEAT AND MASS TRANSFER  
FOR SECOND ROW IN THE BANK



**Fig. 9.25**  
**SHEAR STRESS WITH HEAT AND MASS TRANSFER**  
**FOR SECOND ROW IN THE BANK**



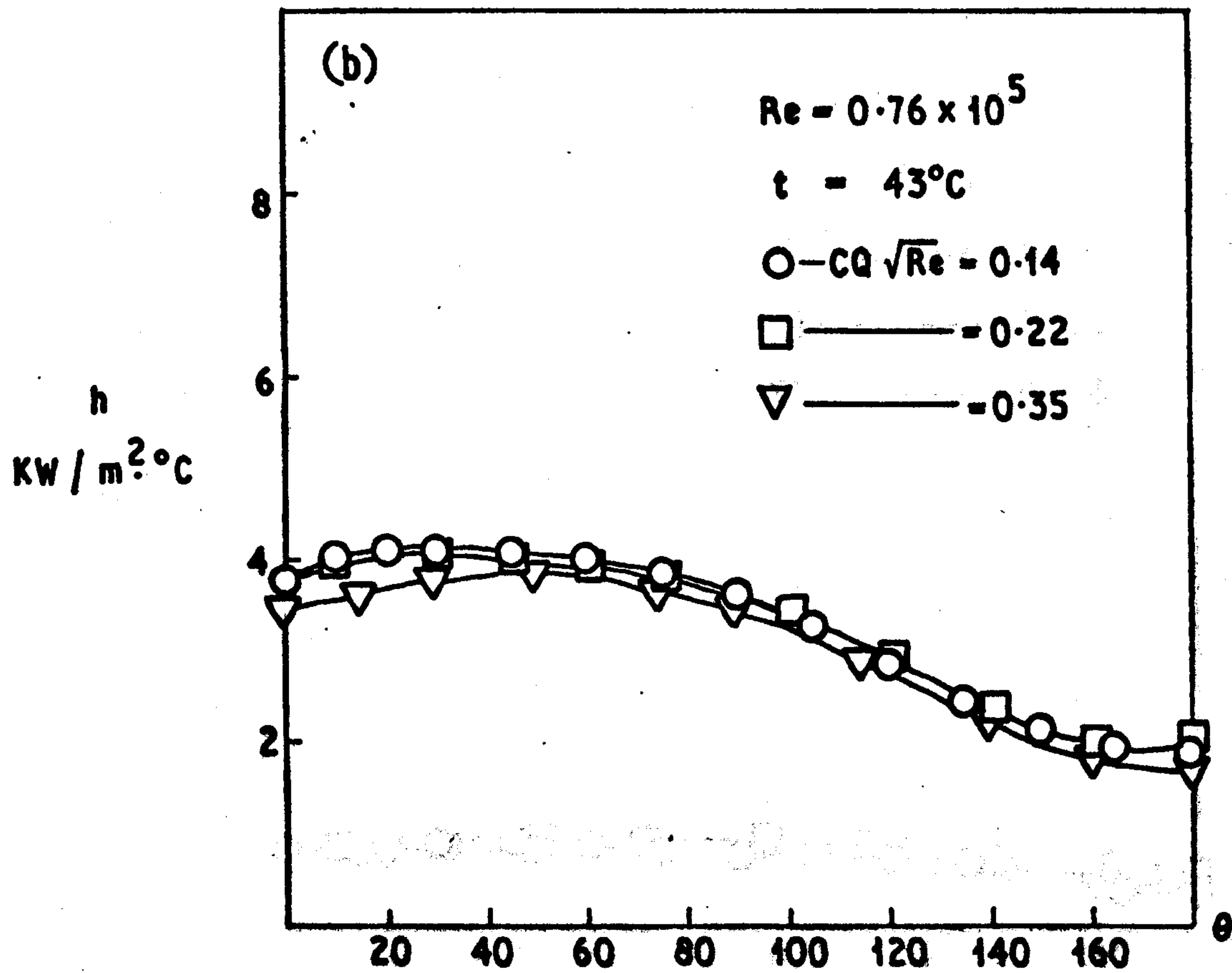
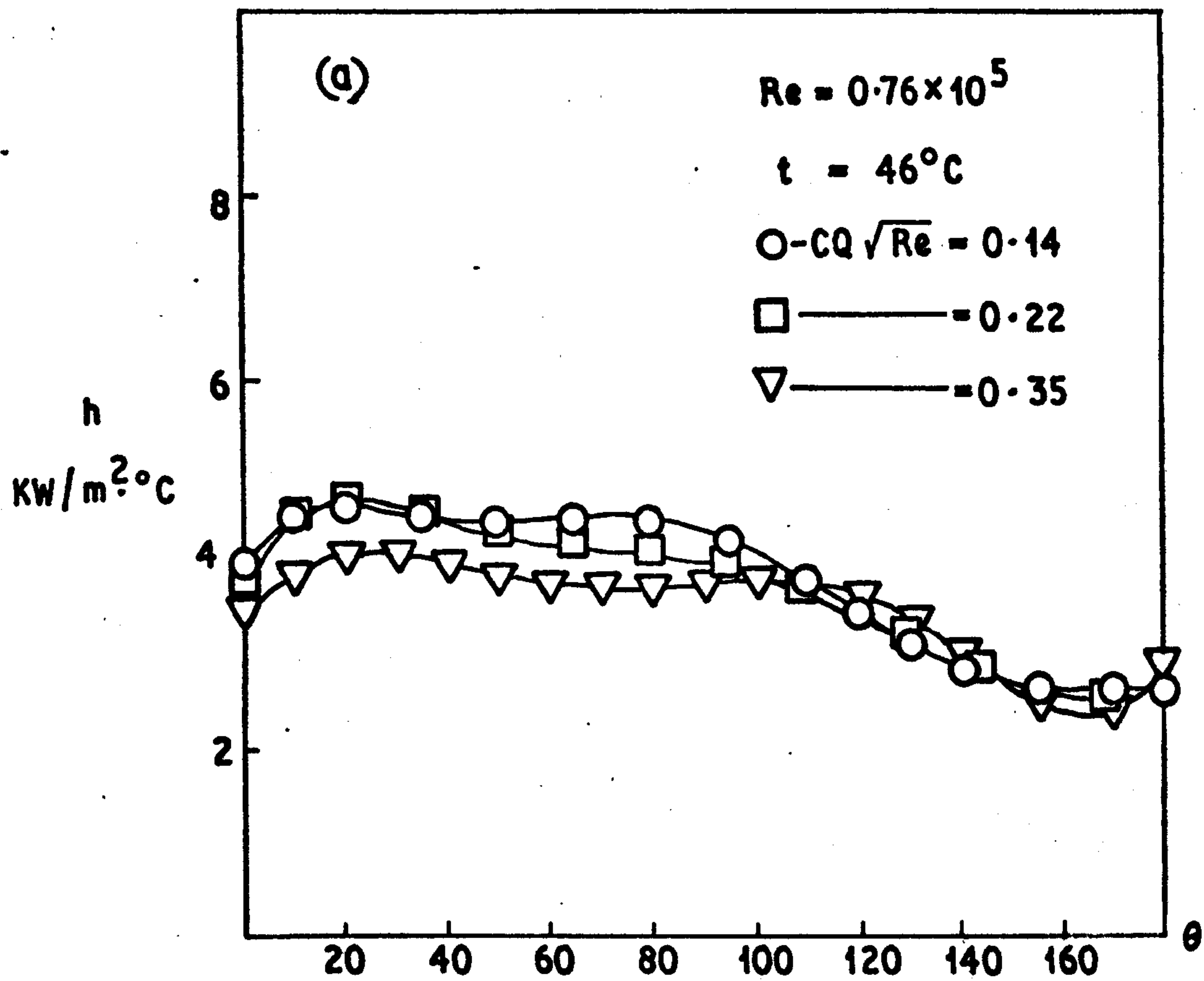


Fig. 9.26

HEAT TRANSFER WITH MASS TRANSFER  
FOR SECOND ROW IN THE BANK

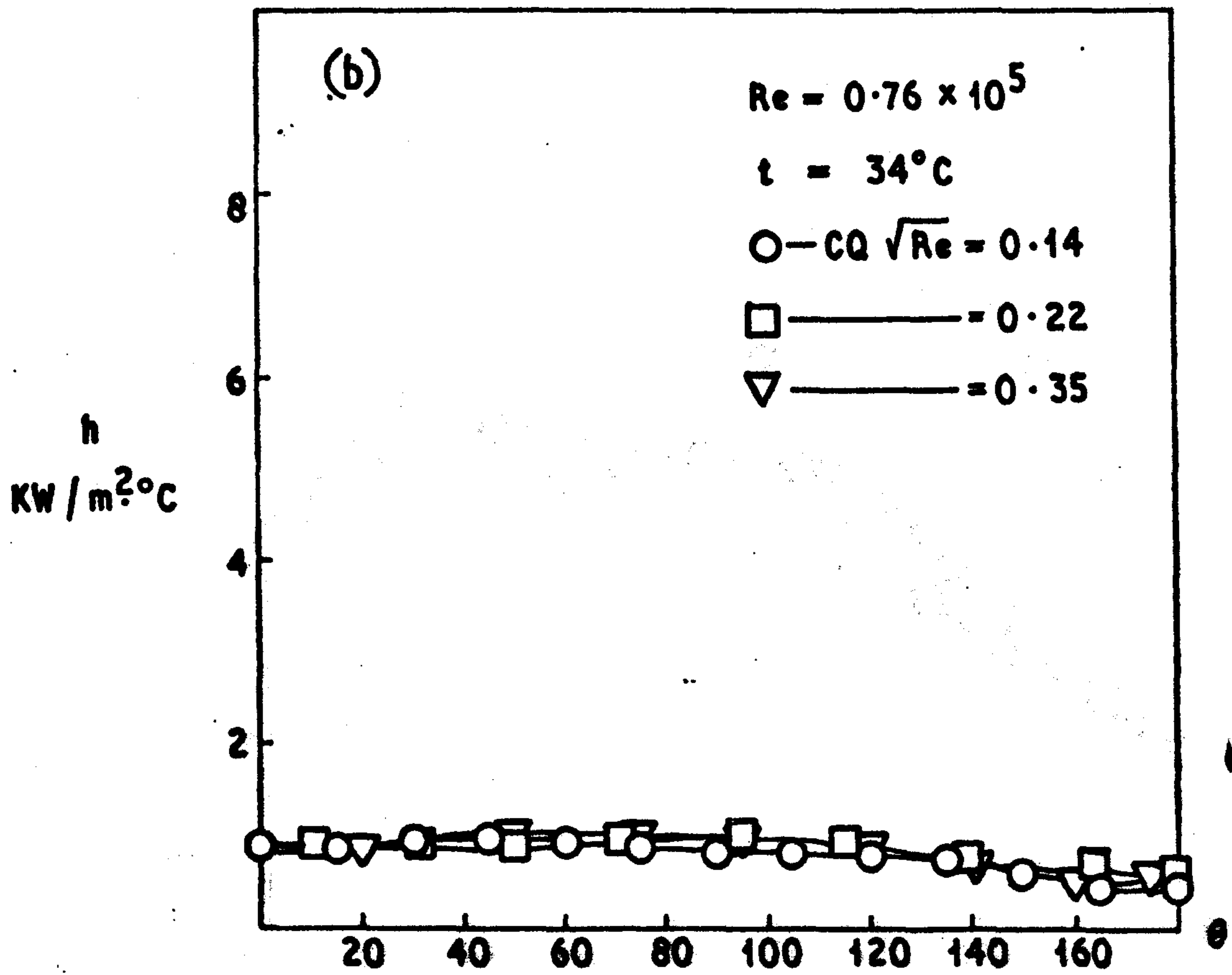
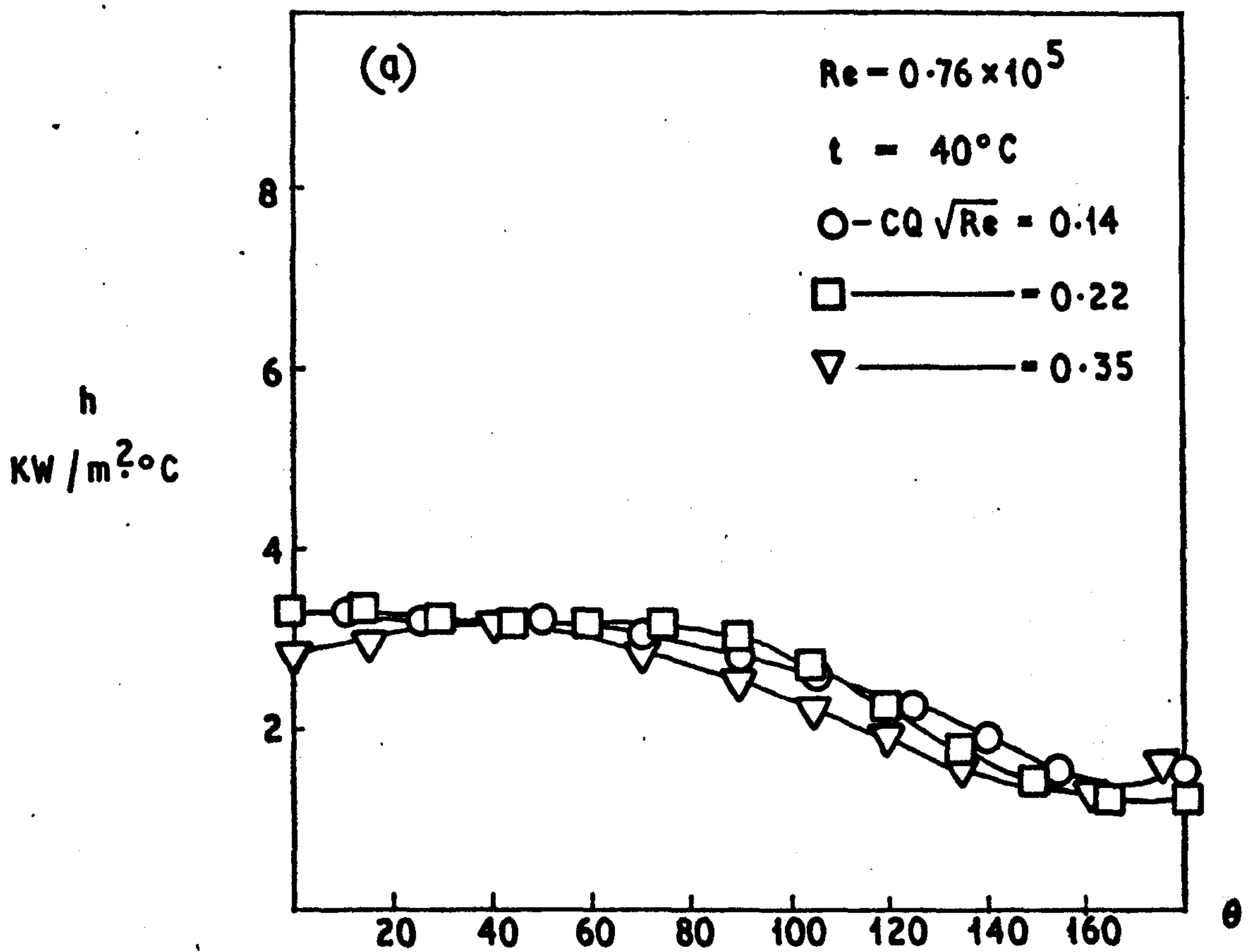
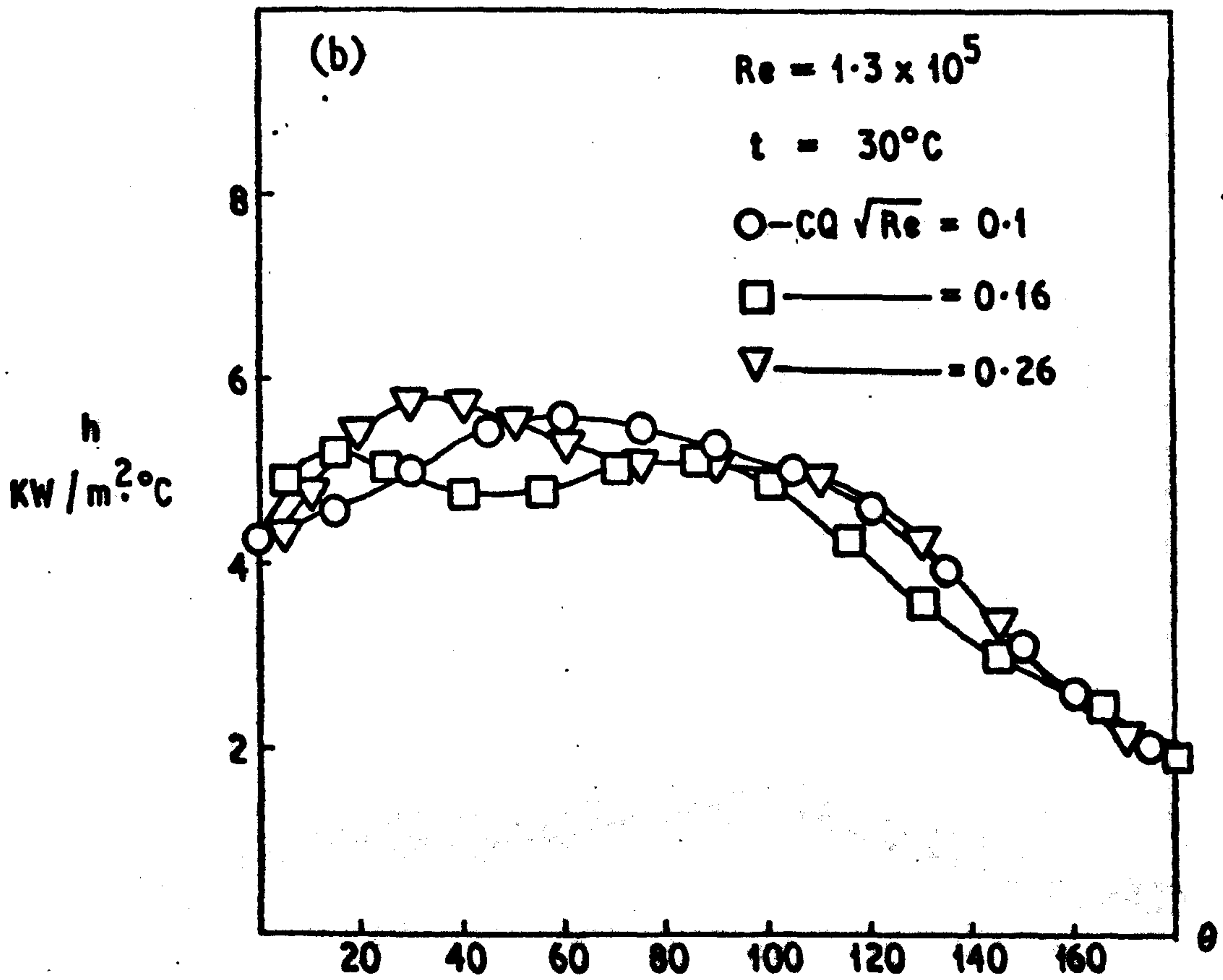
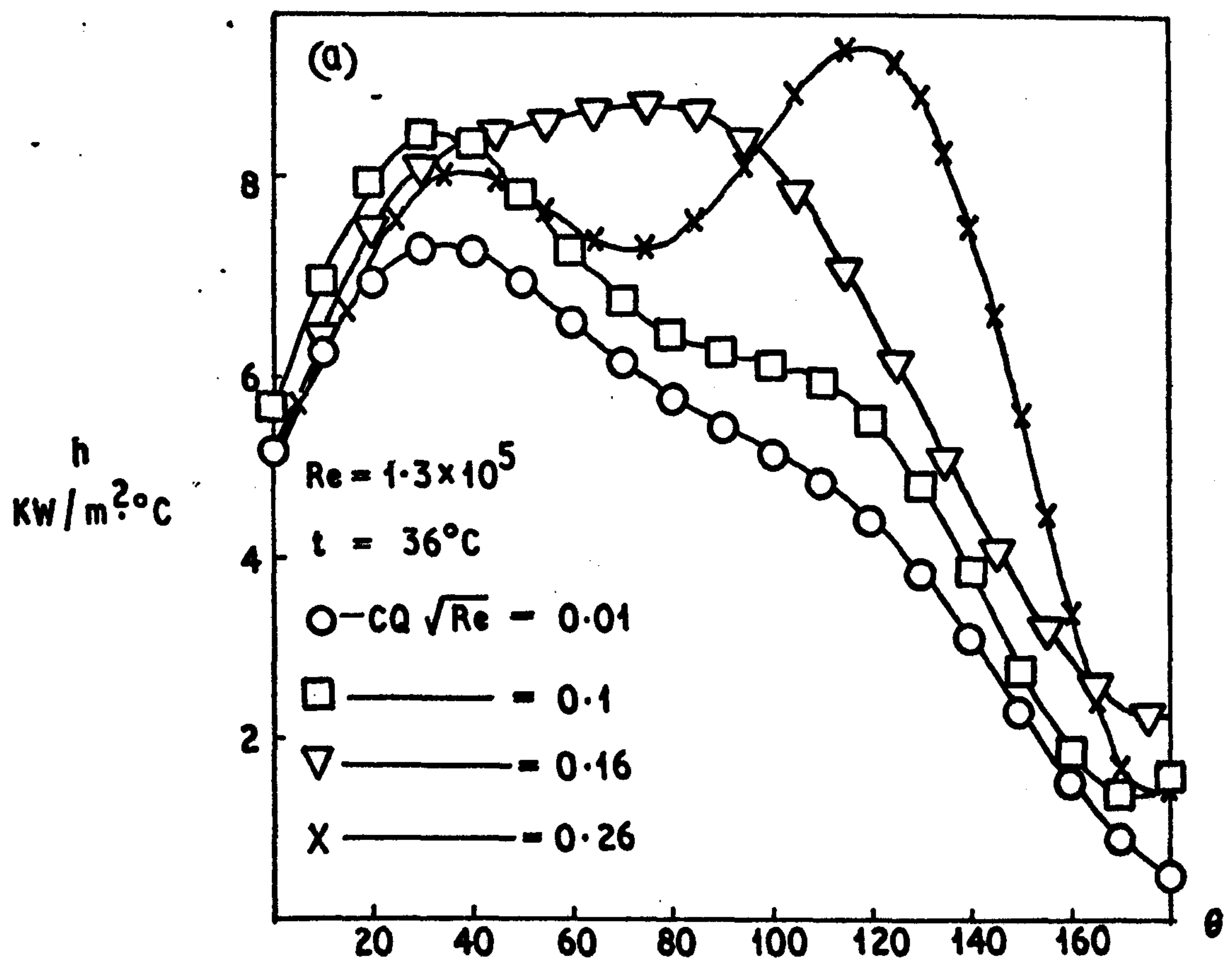


Fig. 9.27

HEAT TRANSFER WITH MASS TRANSFER  
FOR SECOND ROW IN THE BANK

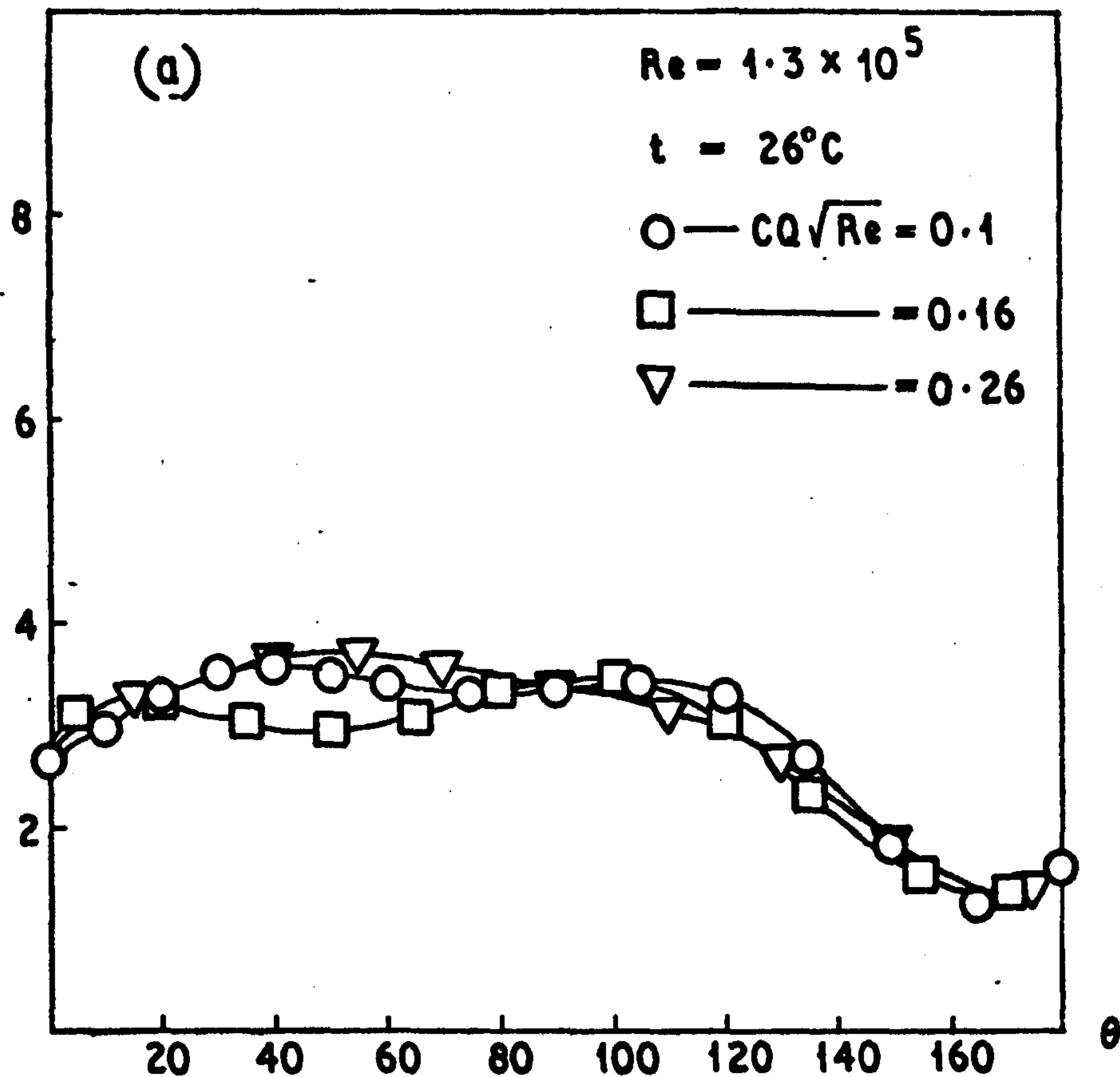


**Fig.9.28**

**HEAT TRANSFER WITH MASS TRANSFER  
FOR SECOND ROW IN THE BANK**



$h$   
 $\text{KW/m}^2\cdot^\circ\text{C}$



$h$   
 $\text{KW/m}^2\cdot^\circ\text{C}$

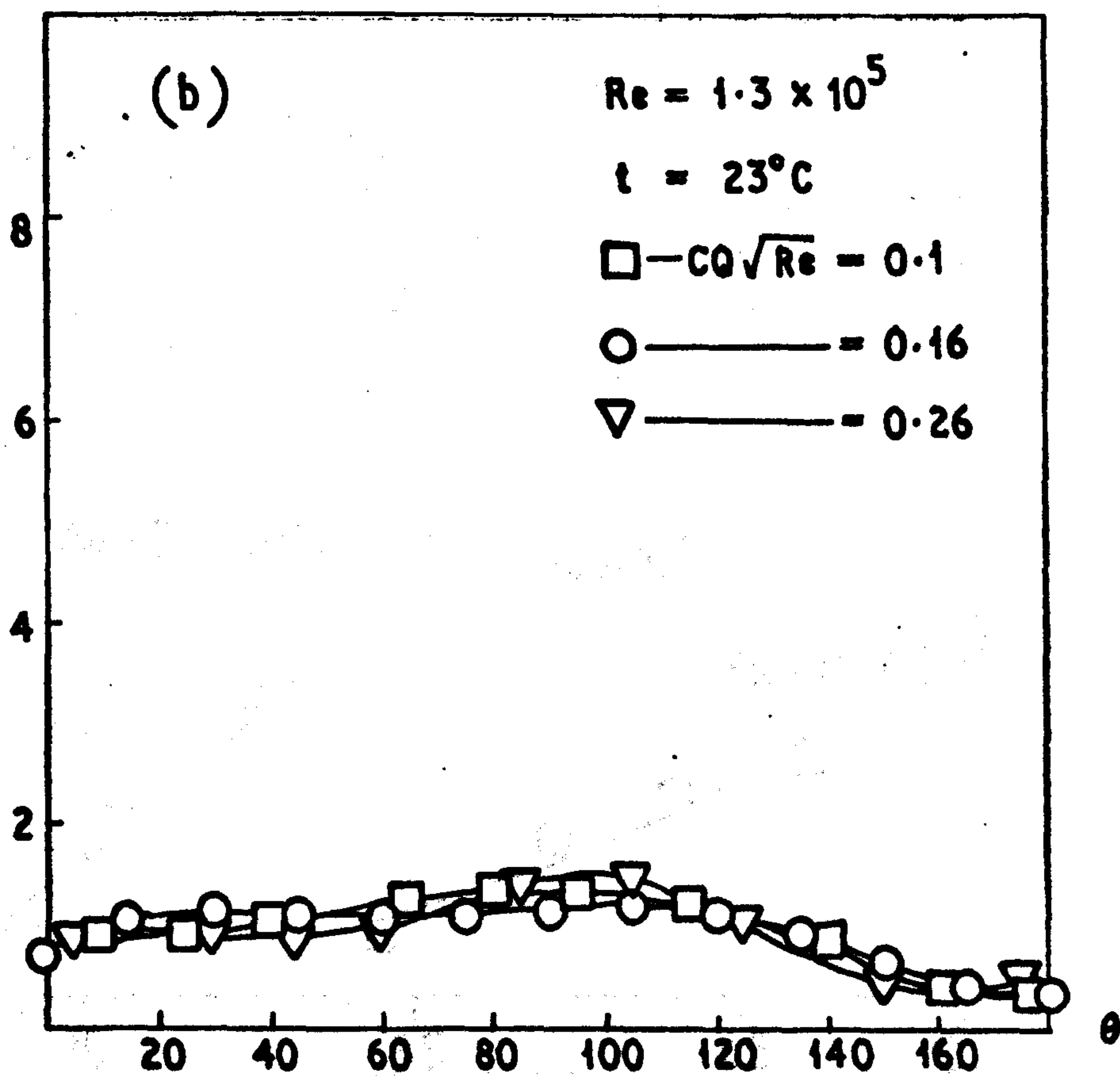


**Fig. 9.29**

**HEAT TRANSFER WITH MASS TRANSFER  
FOR SECOND ROW IN THE BANK**

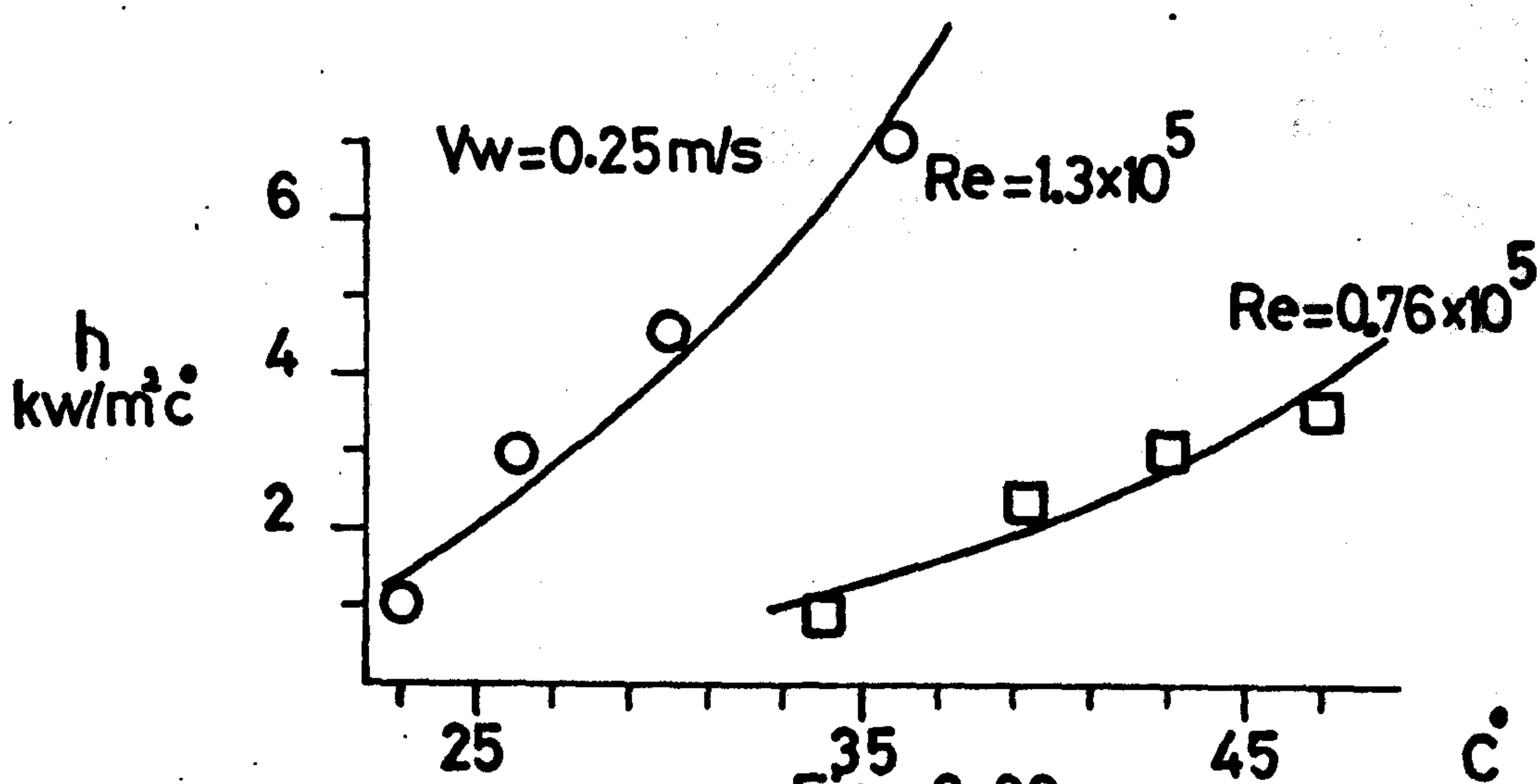
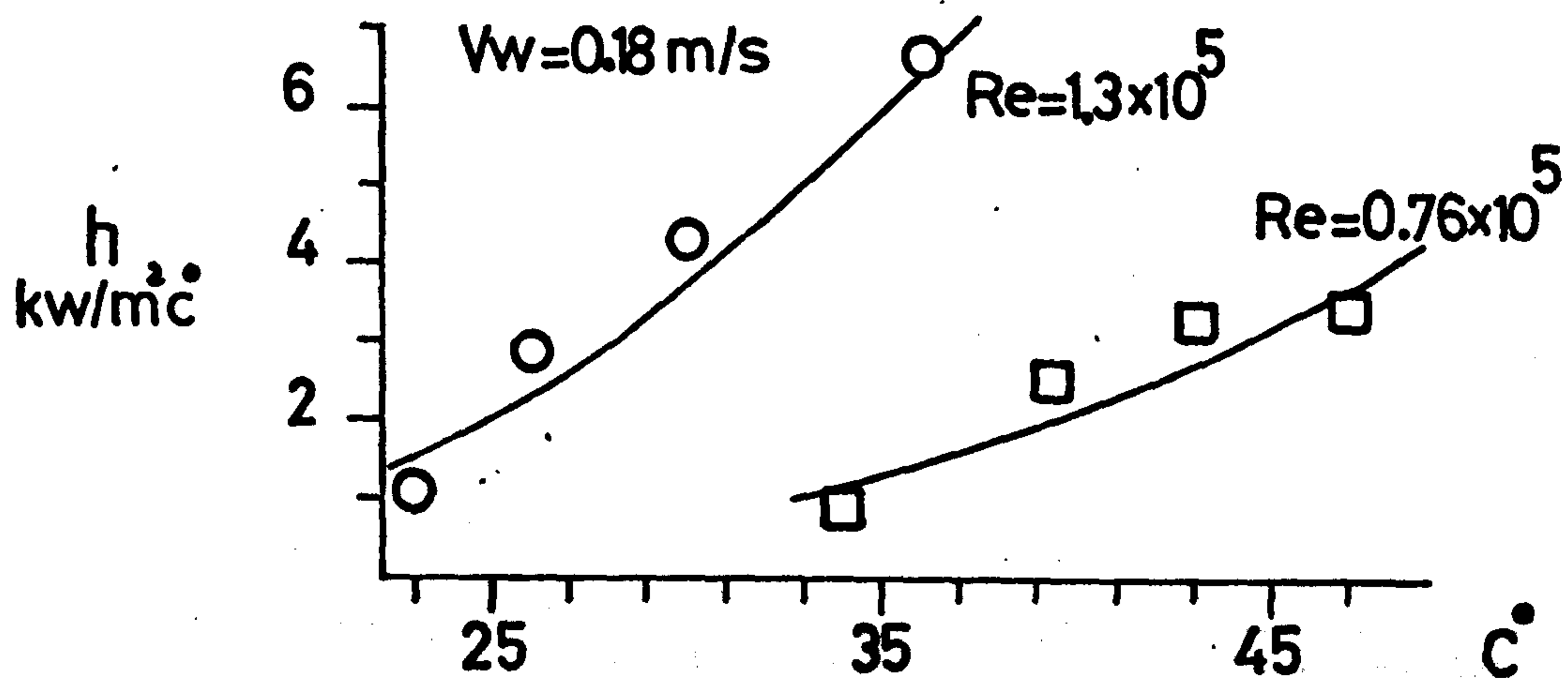
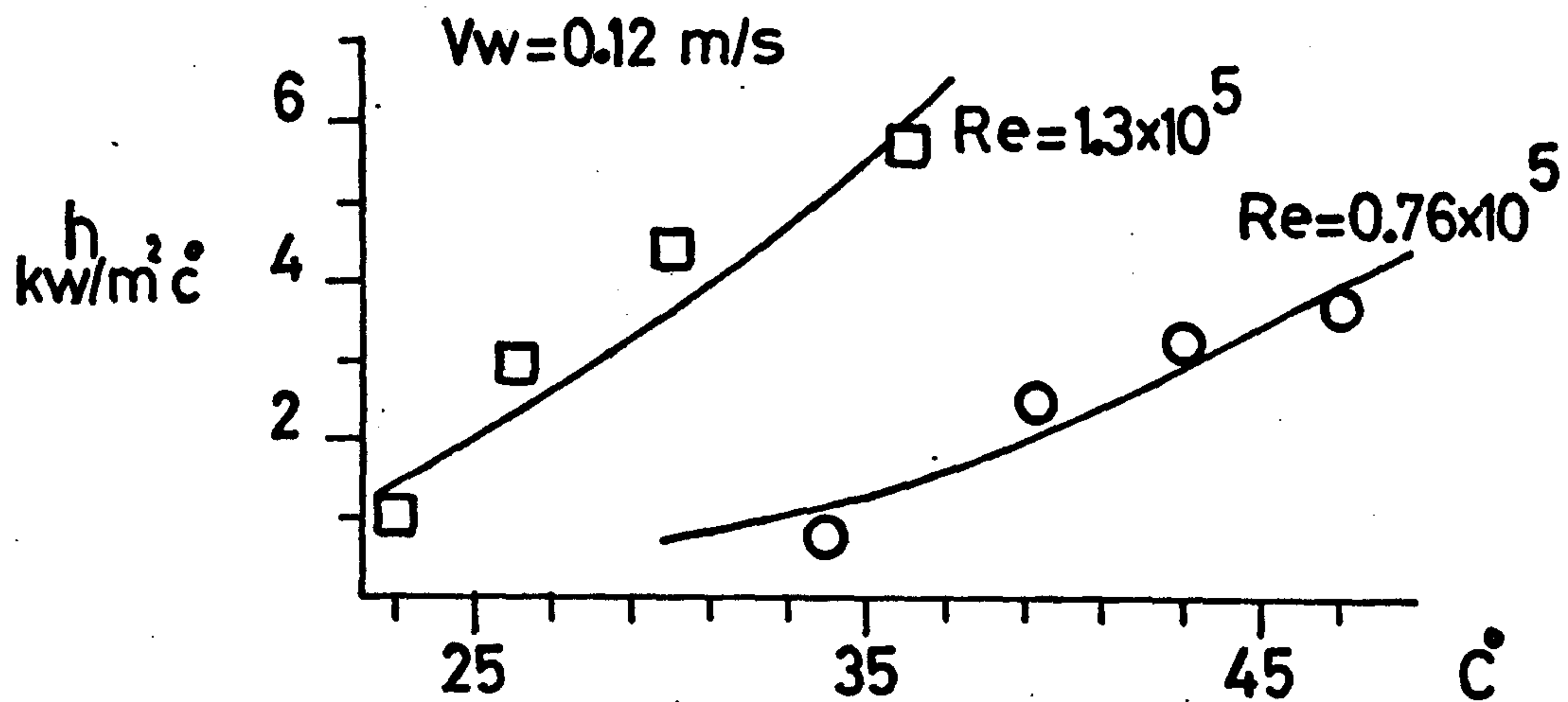
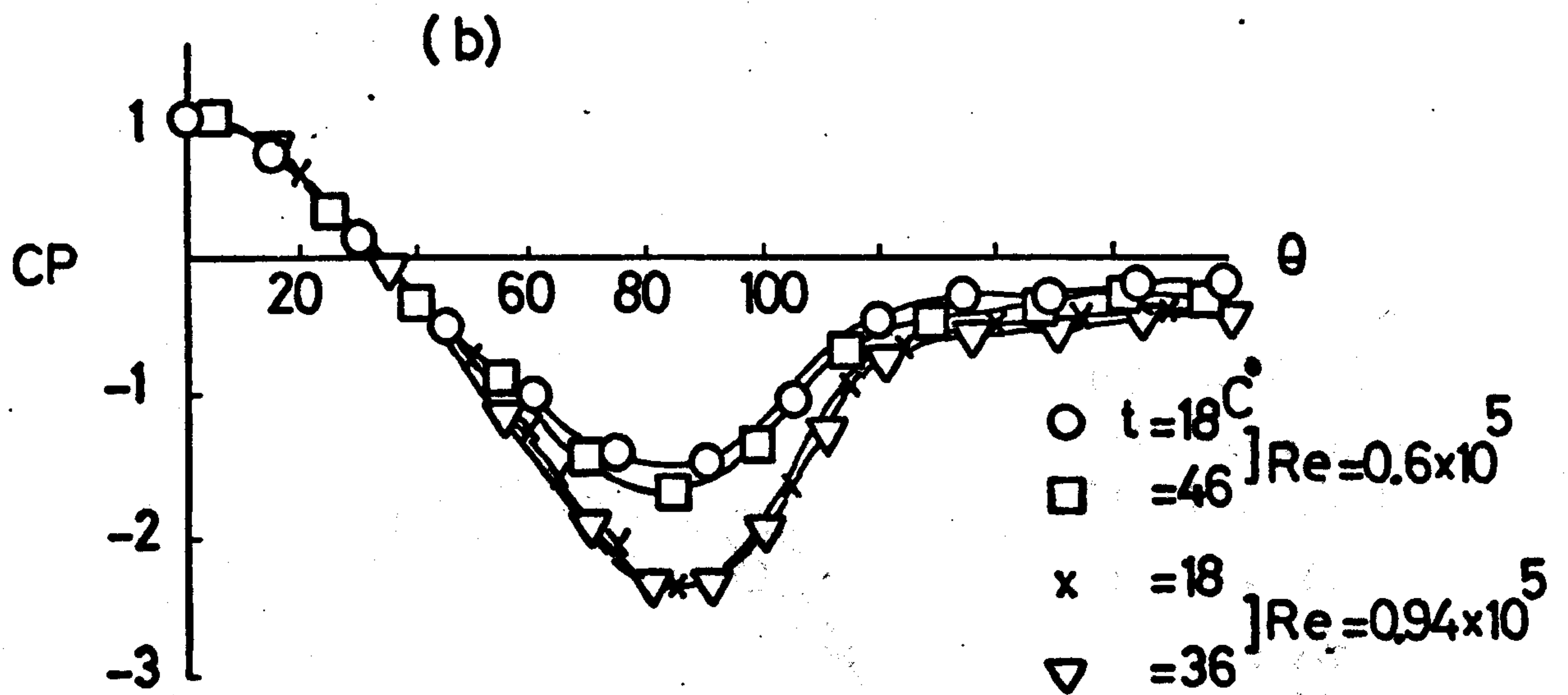
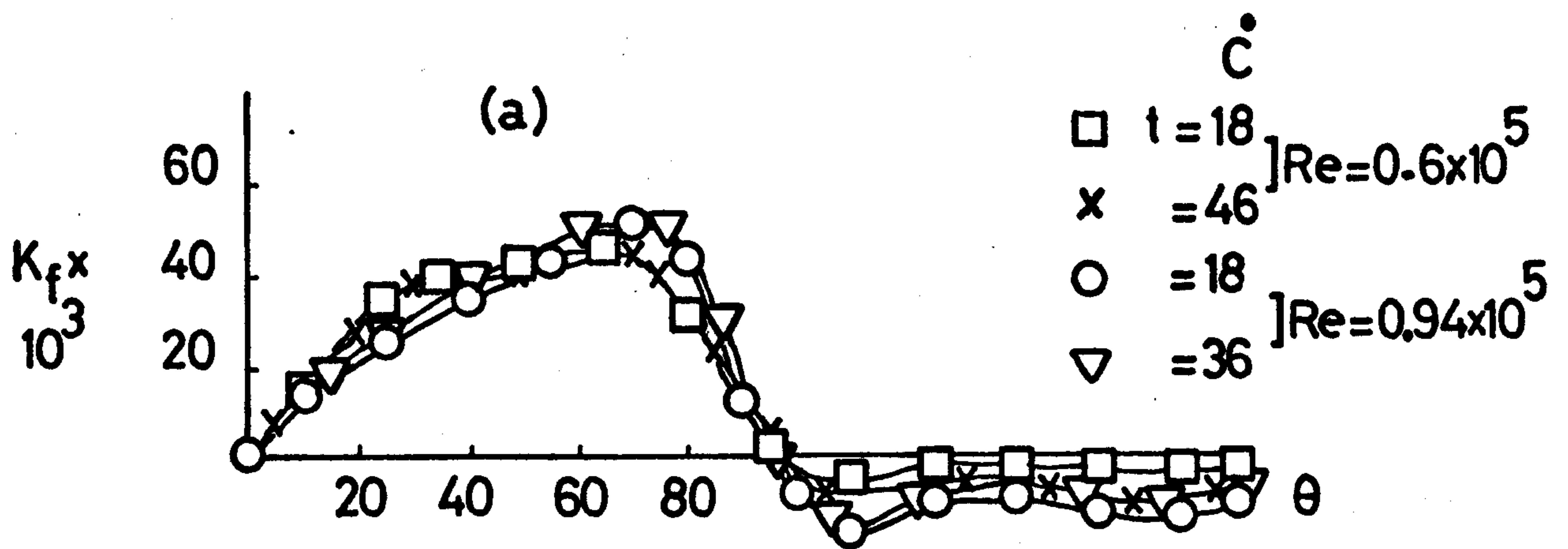


Fig. 9.30

Average HTC for second row  
in the bank



**Fig. 9.31**  
**Effect of main stream temperature**  
**on third row in the bank**



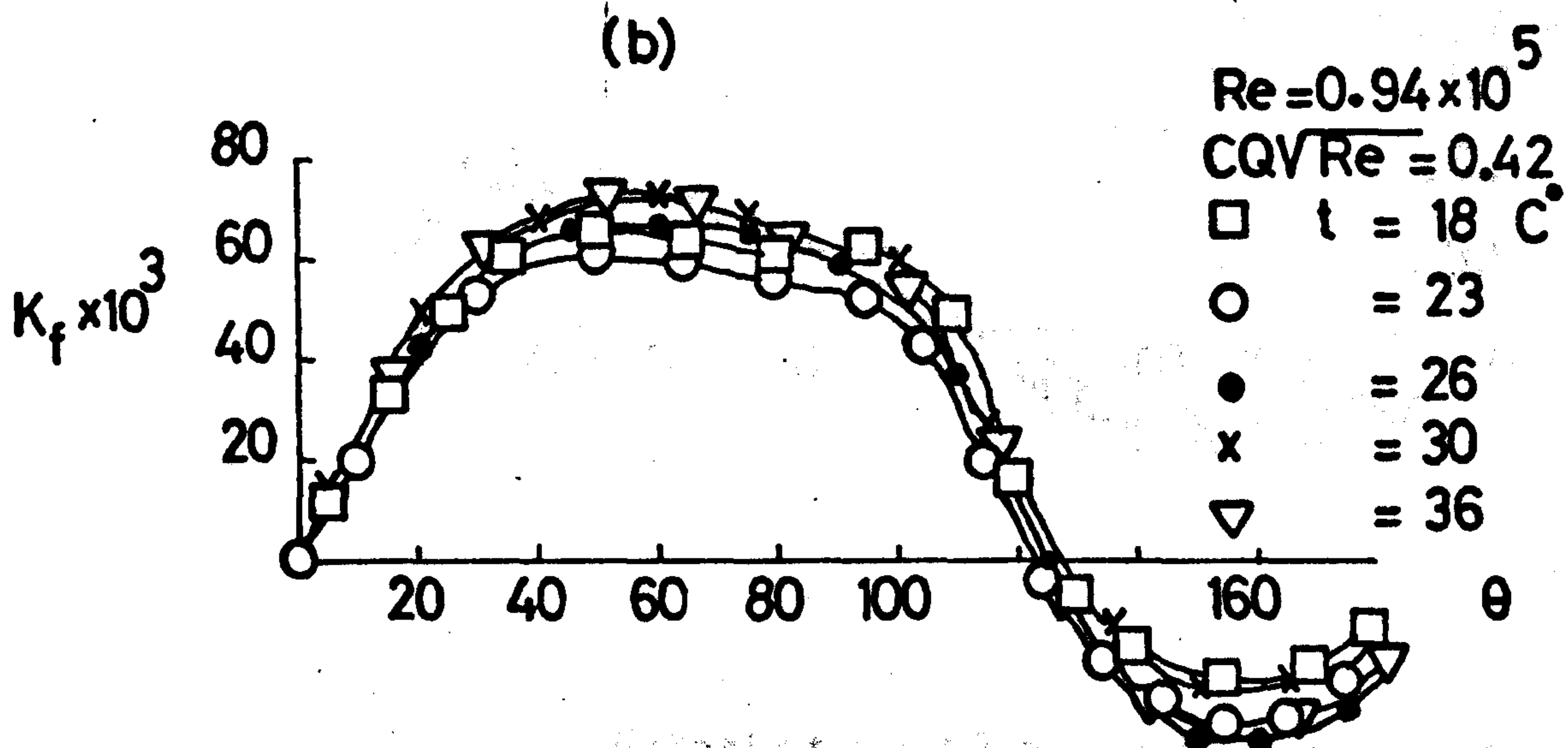
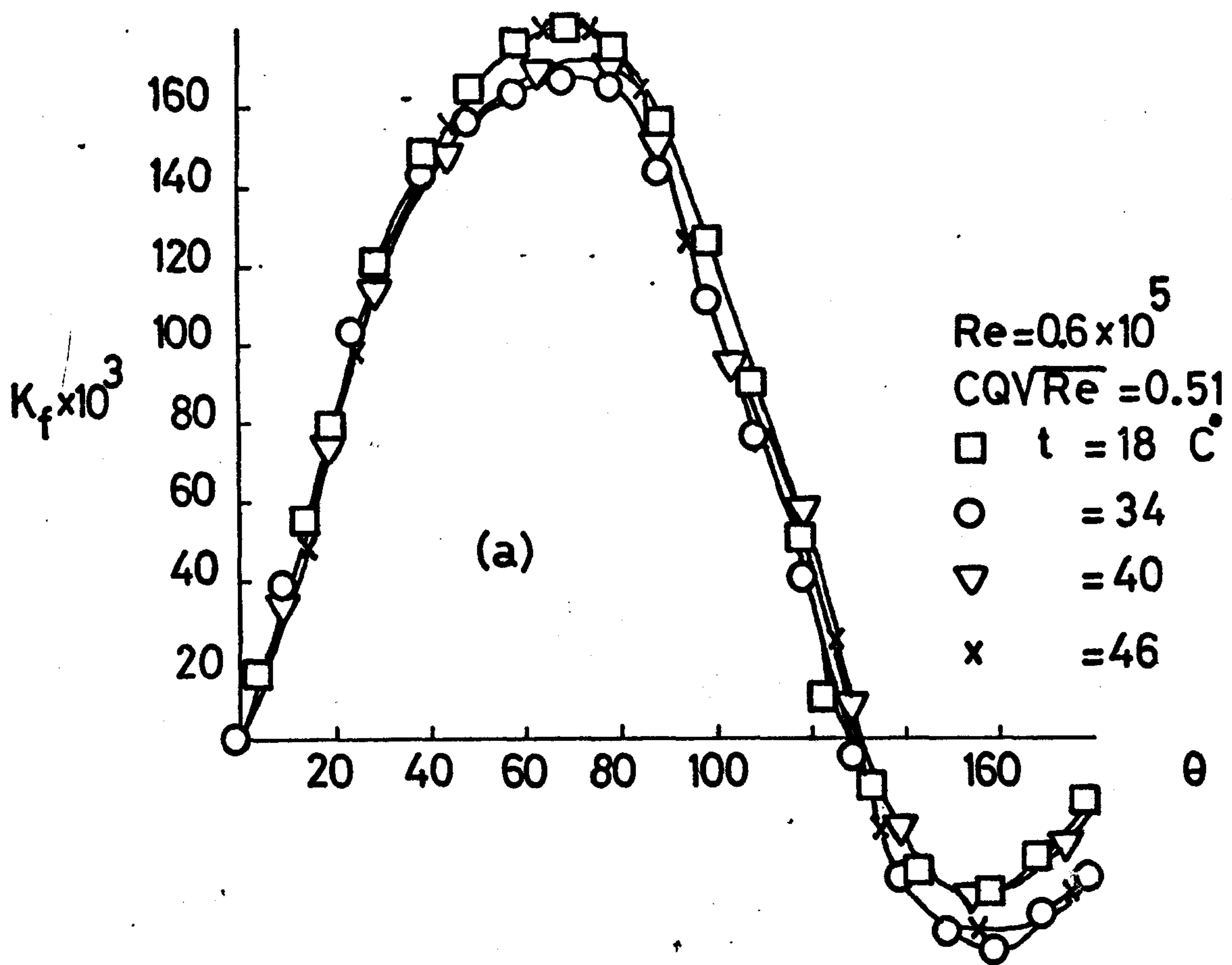
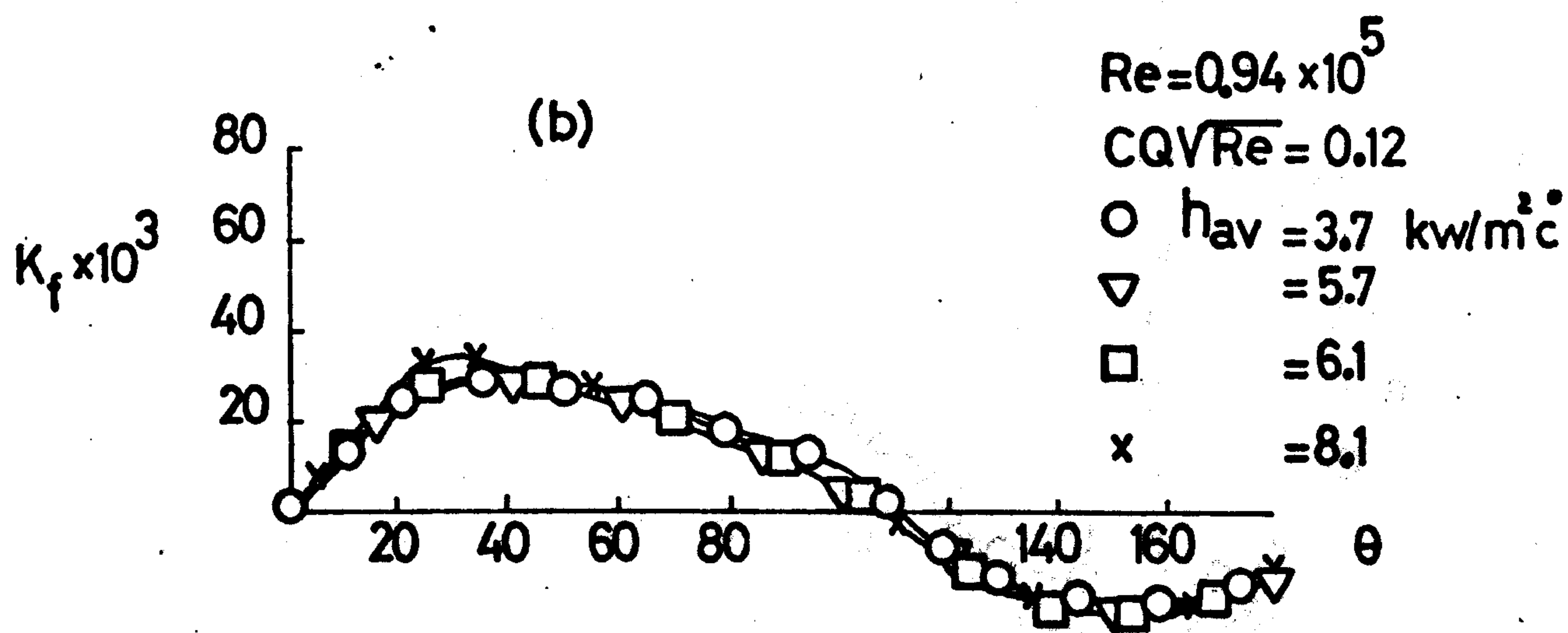
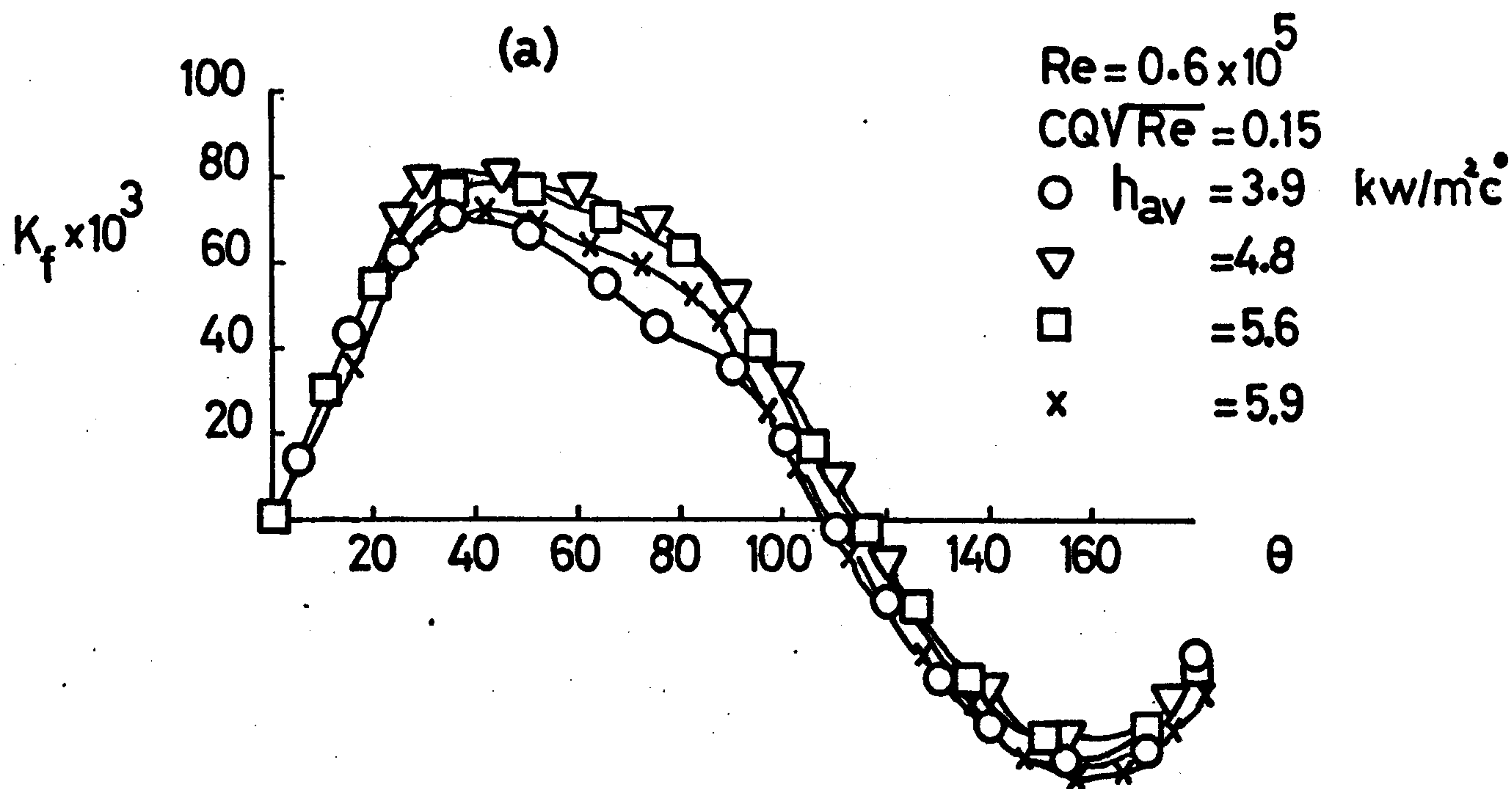
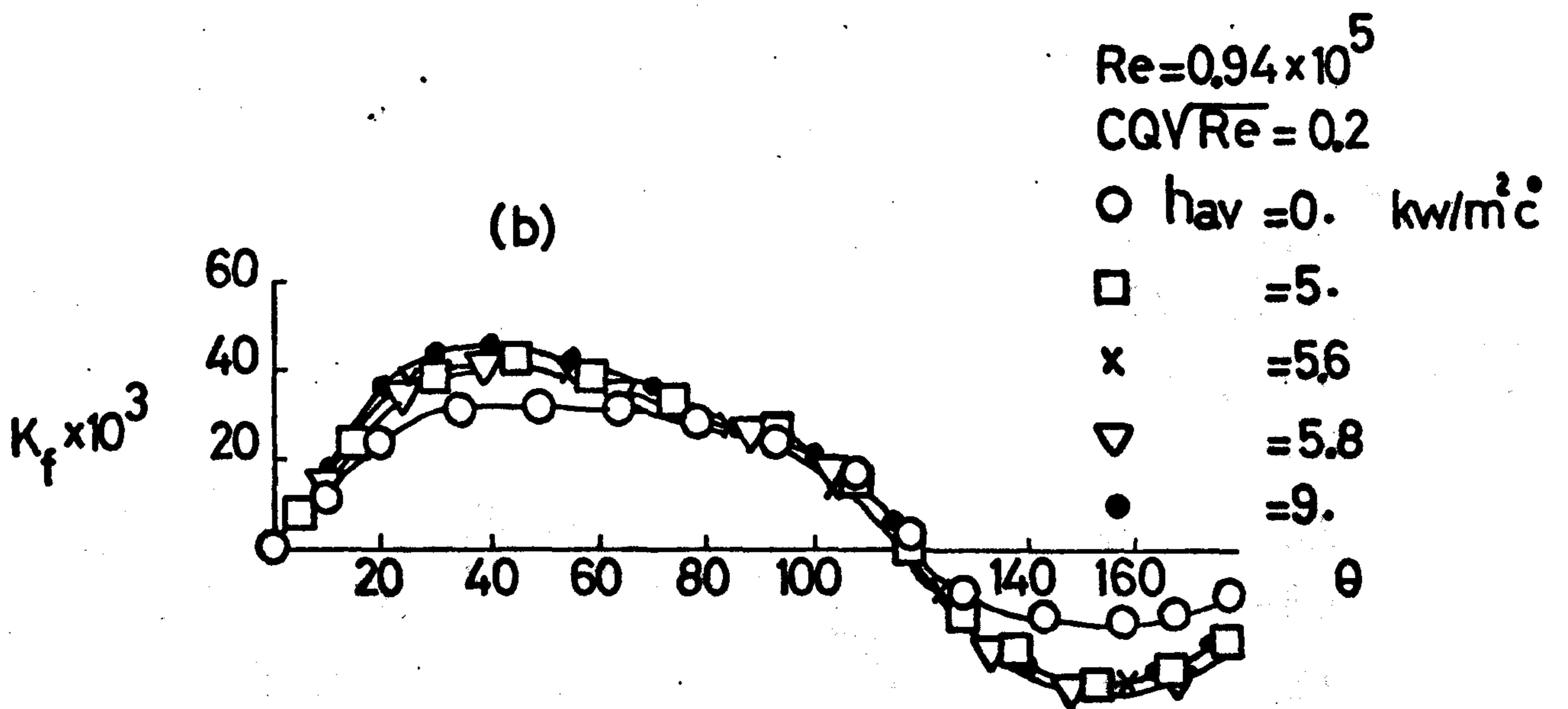
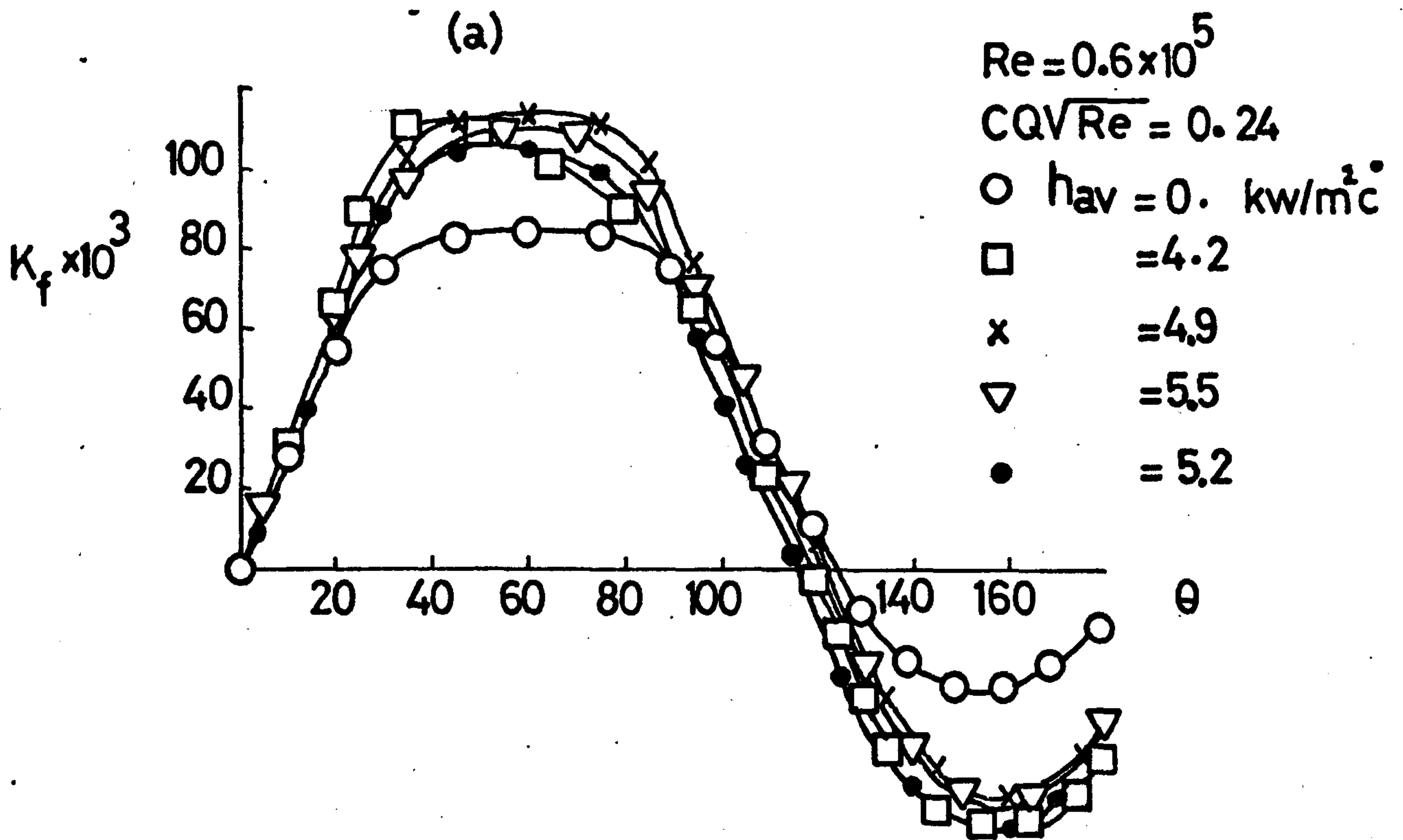


**Fig. 9.32**  
Effect of main stream temp. with mass transfer on third row in the bank



Effect of heat & mass transfer on shear stress, third row in the bank

Fig. 9.33



Effect of heat and mass transfer on shear stress, third row in the bank

Fig. 9.34



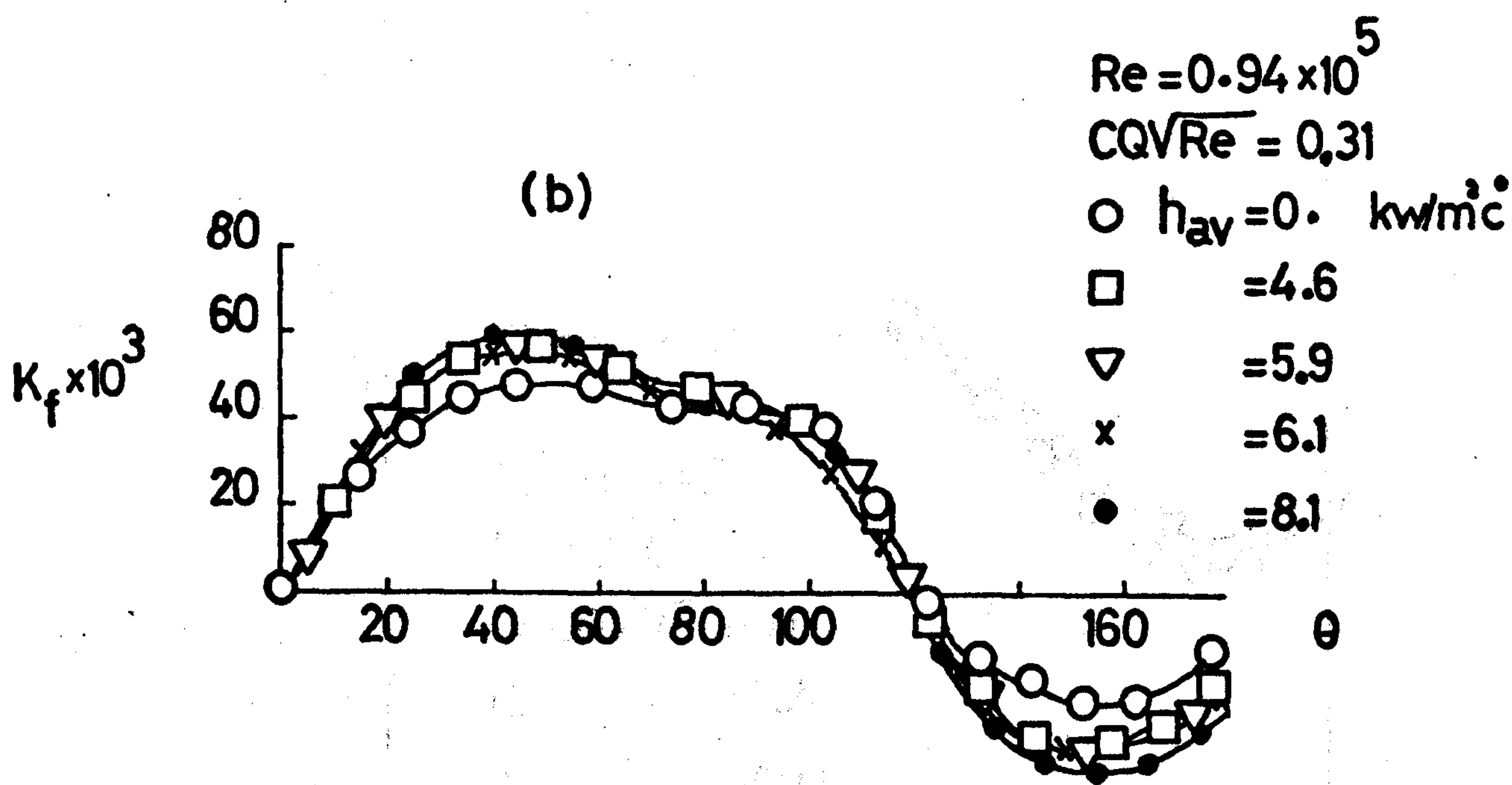
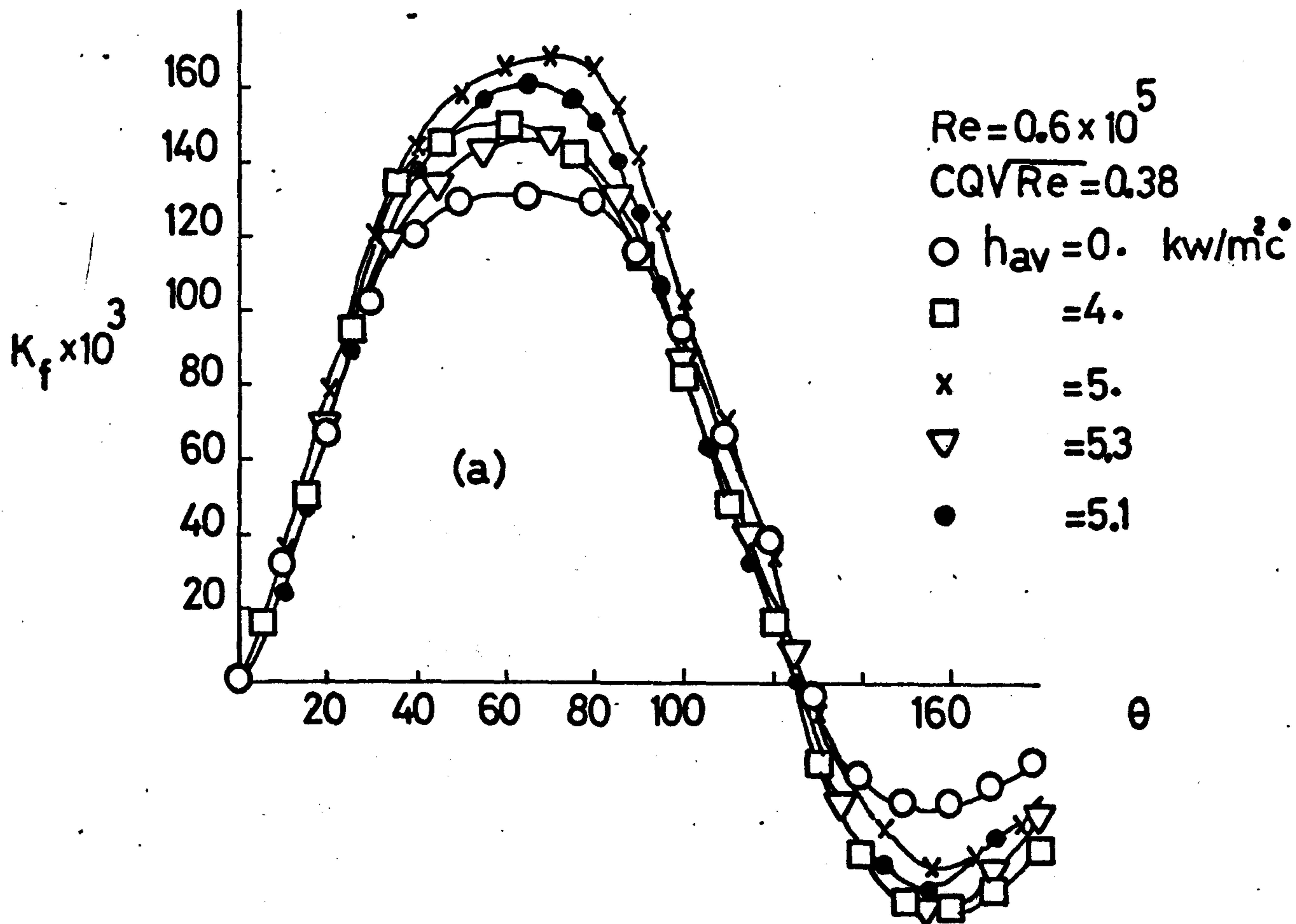


**Fig. 9.35**  
Shear stress with heat and mass transfer,  
third row in the bank

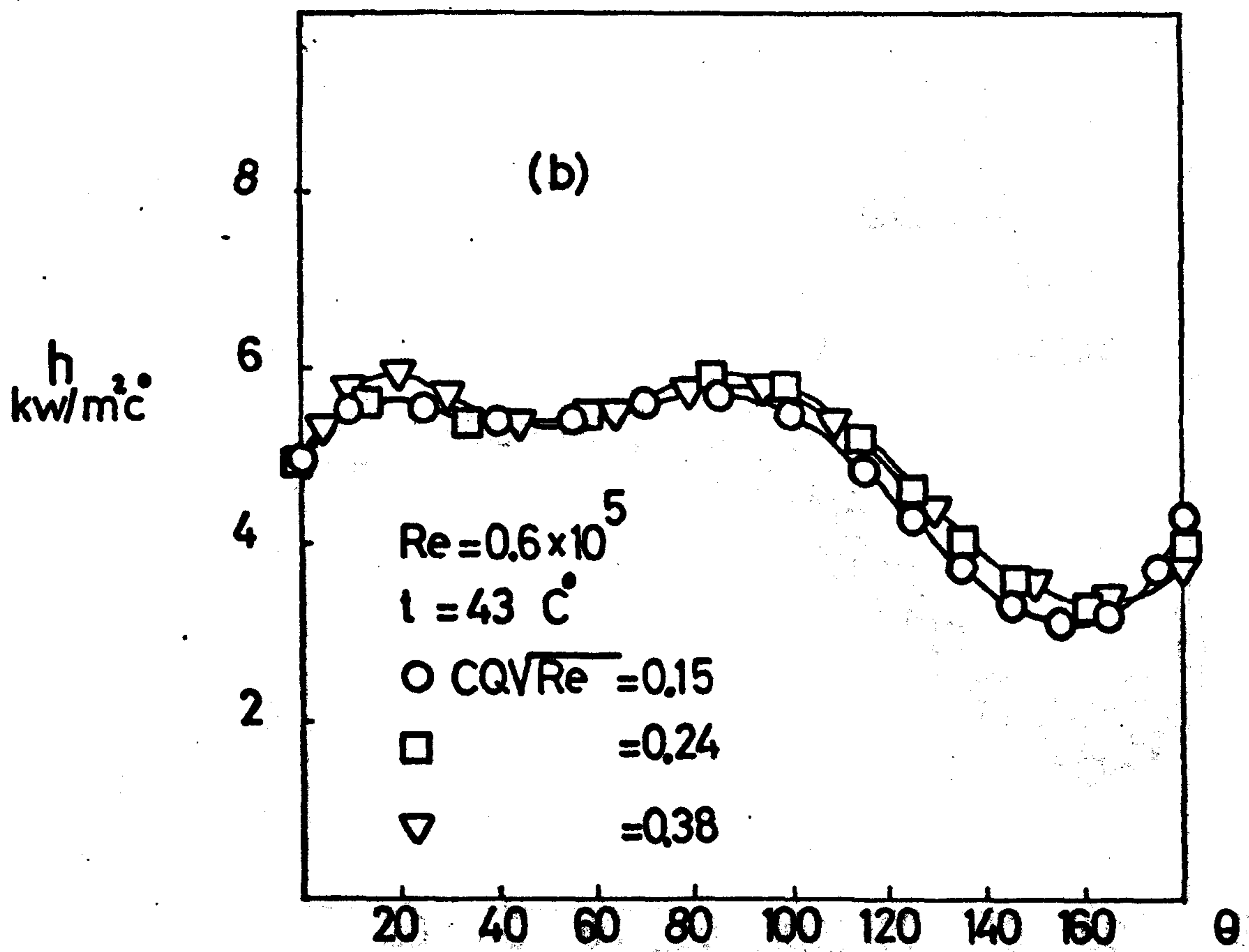
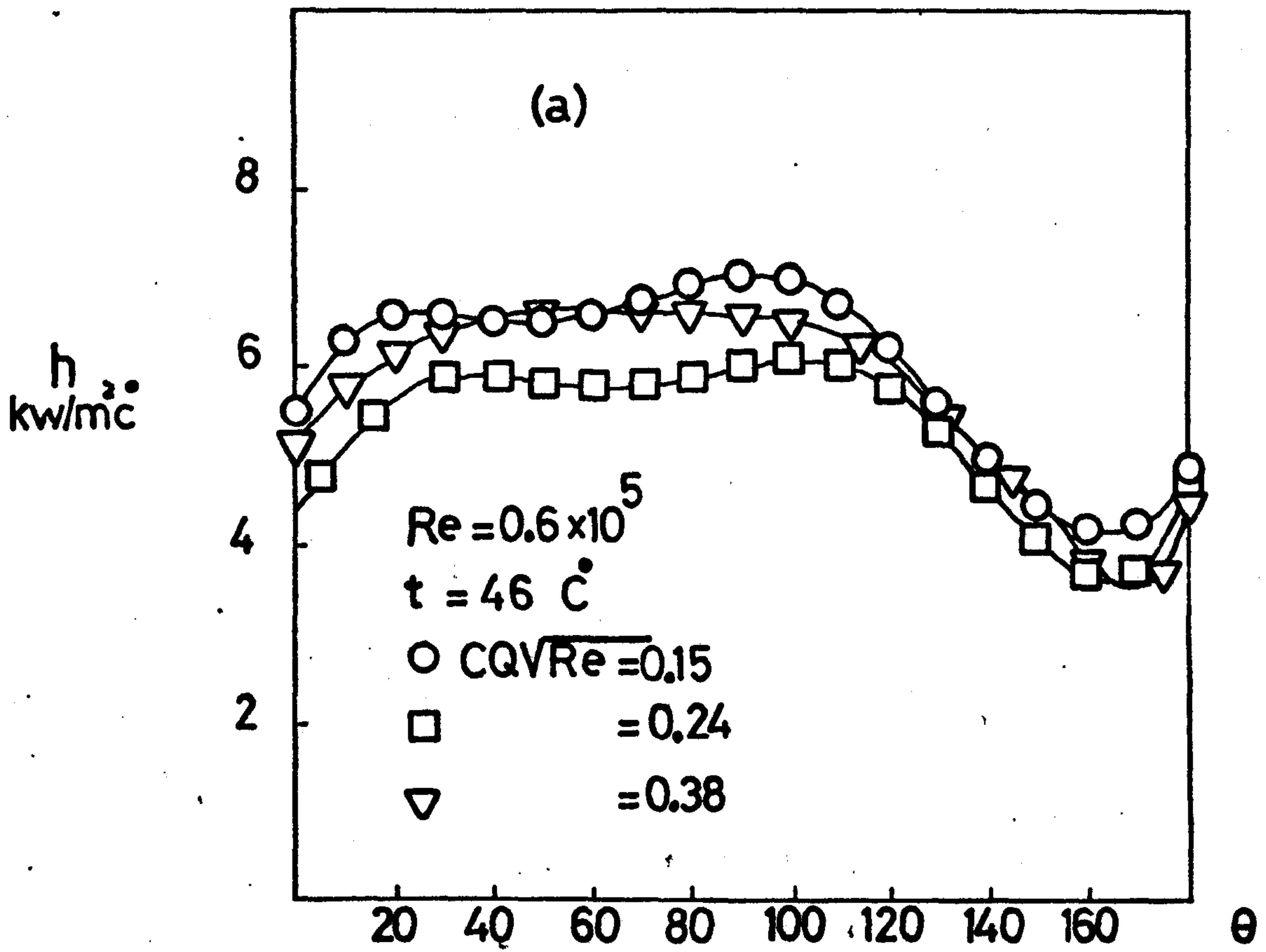


Fig. 9.36  
Heat transfer with mass transfer,  
third row in the bank

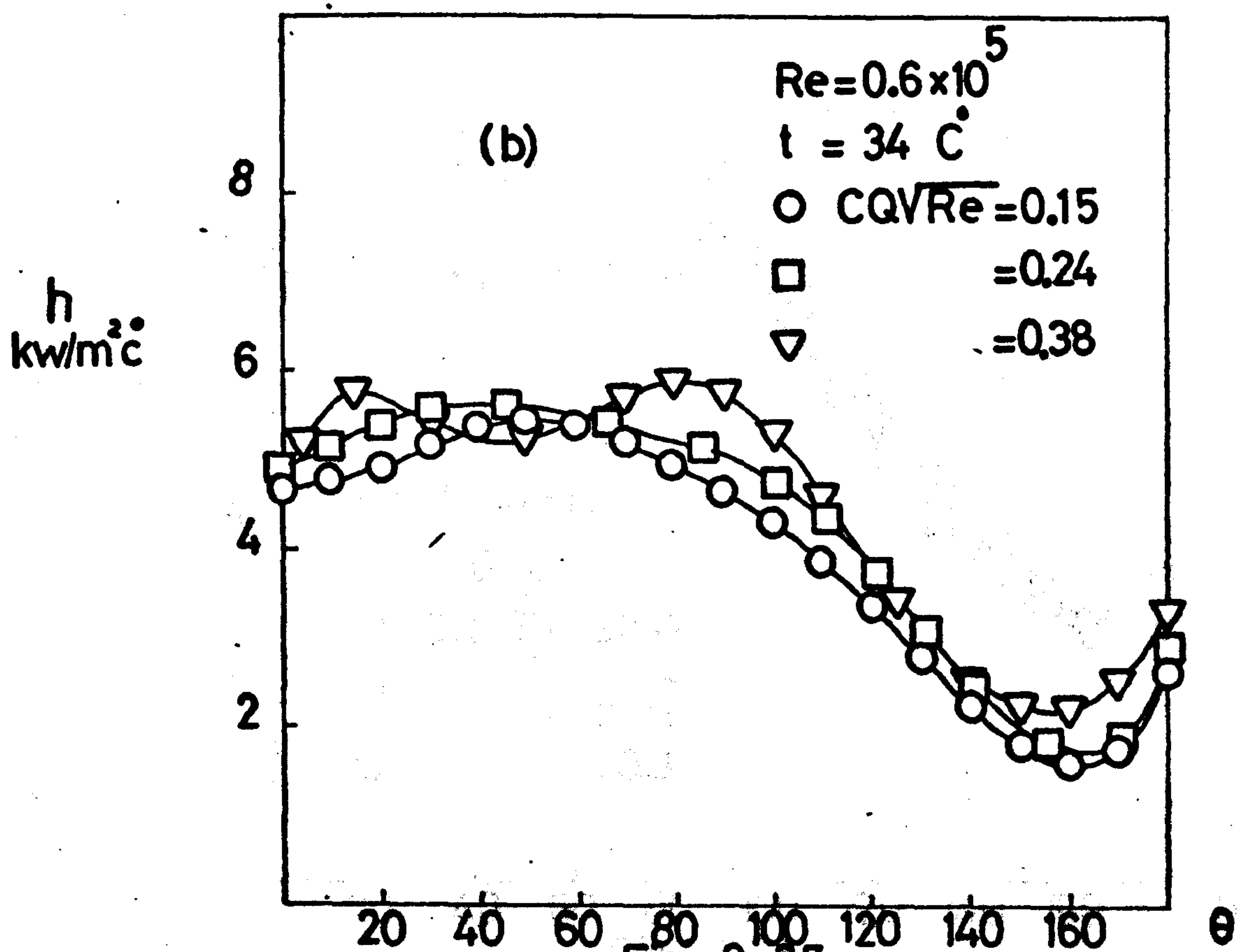
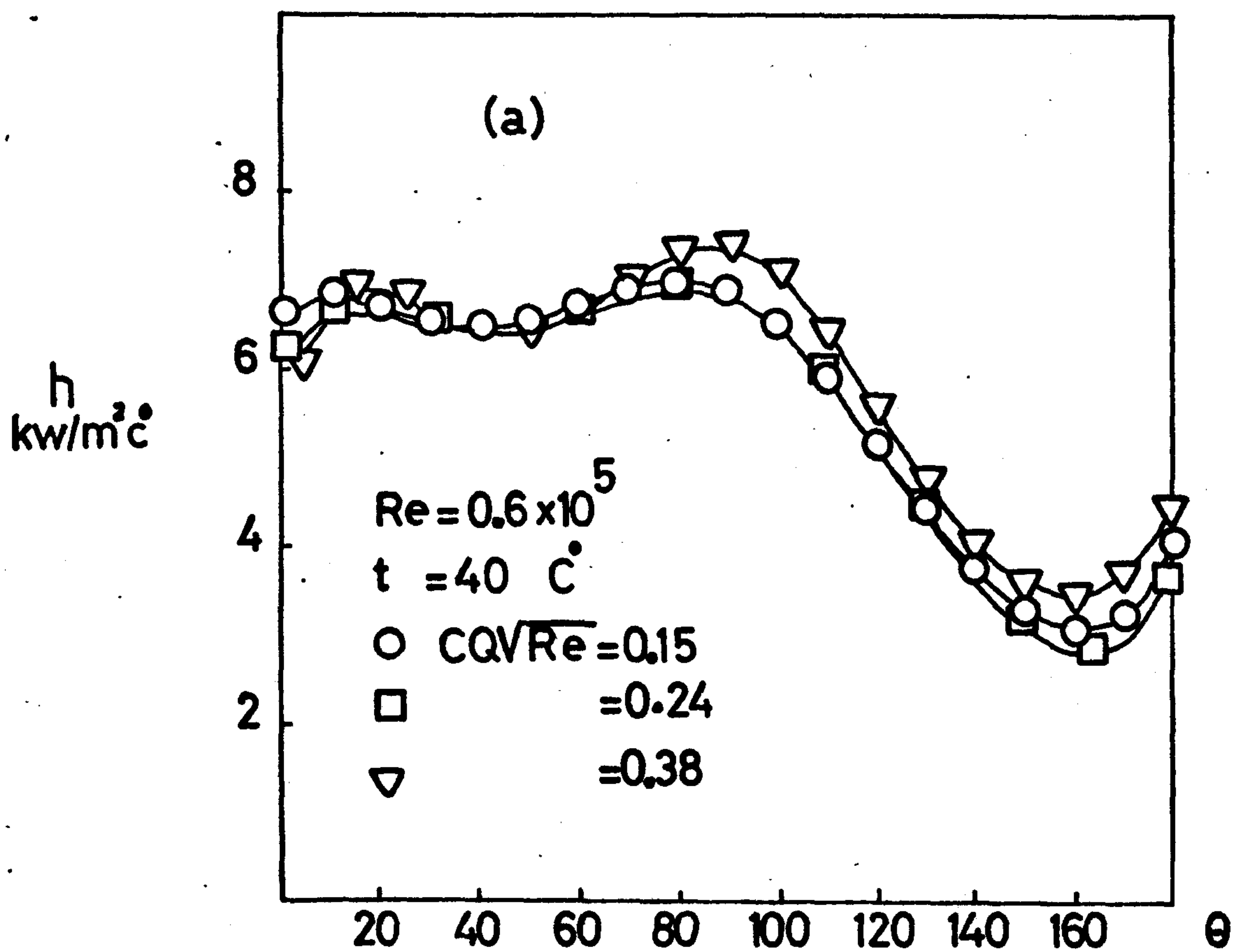
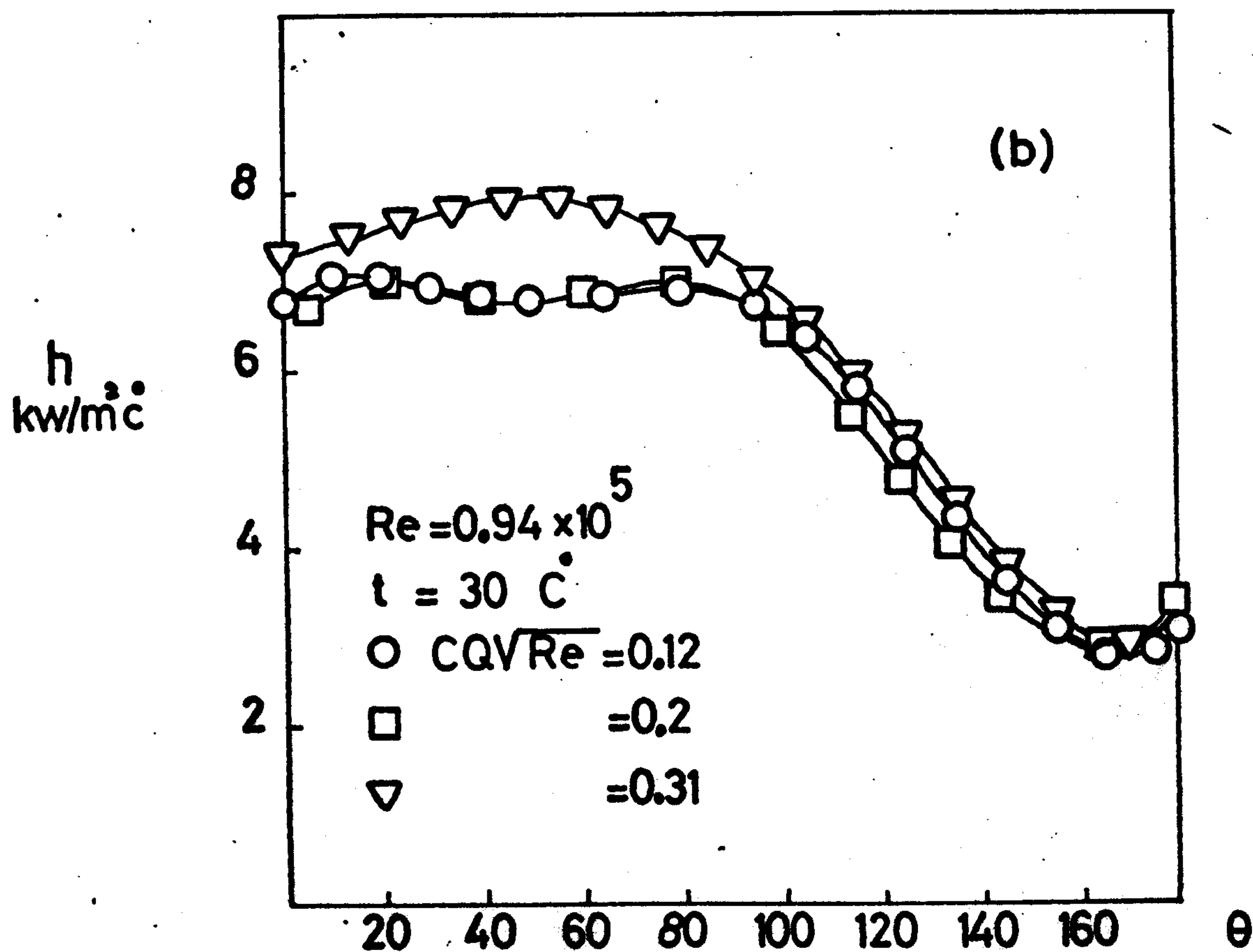
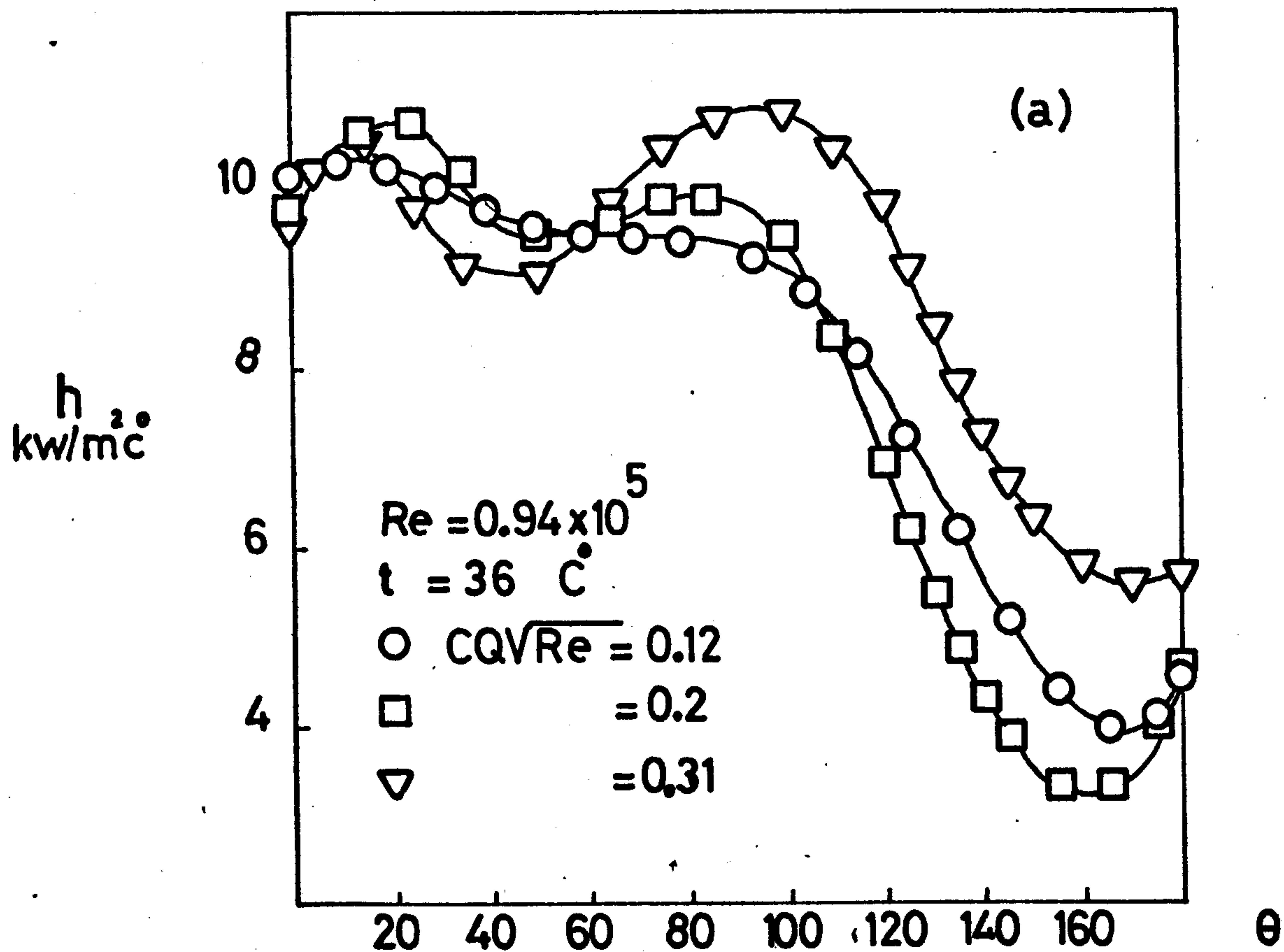


Fig. 9.37

Heat transfer with mass transfer,  
third row in the bank





**Fig. 9.38**  
Heat transfer with mass transfer,  
third row in the bank

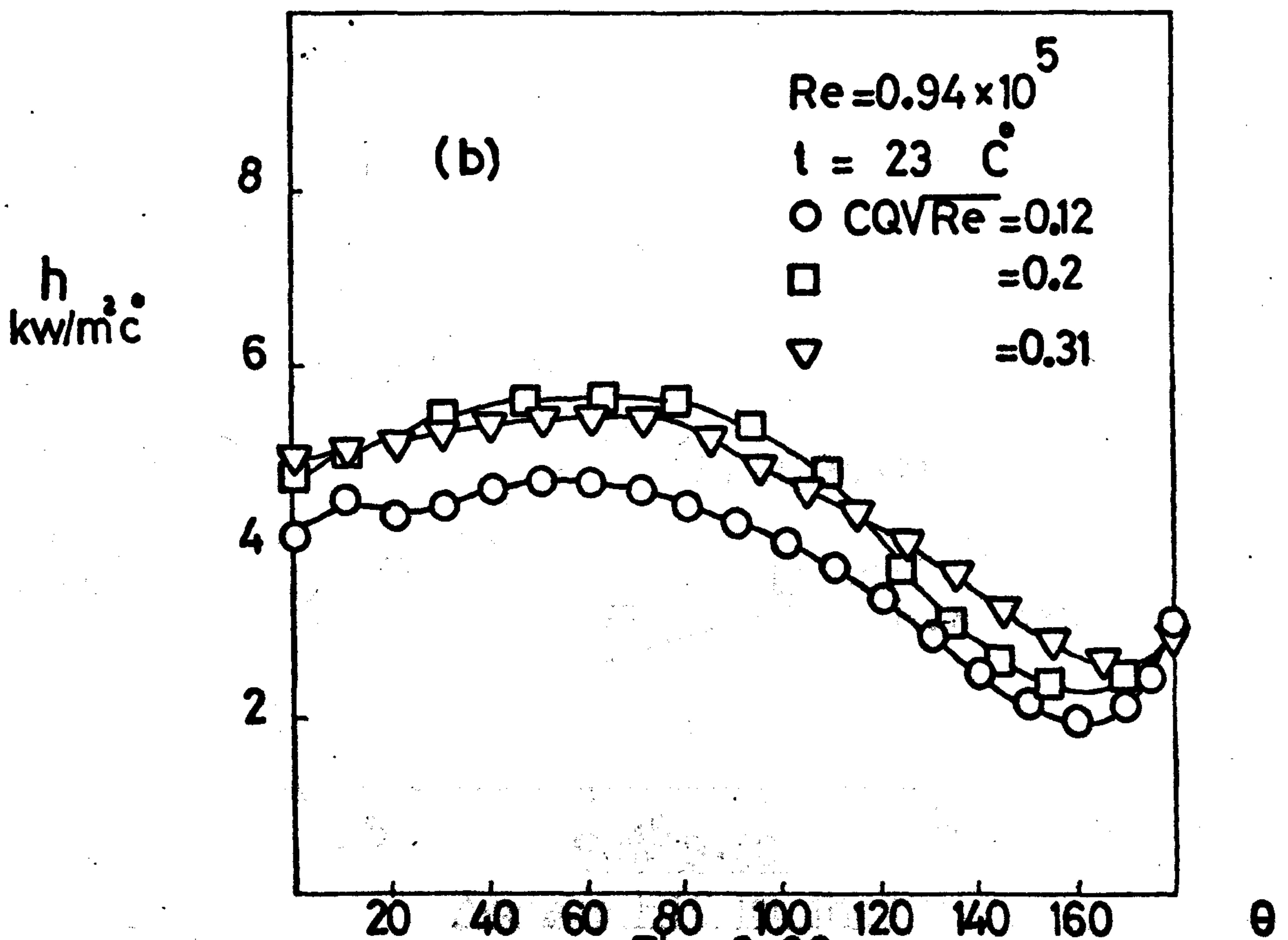
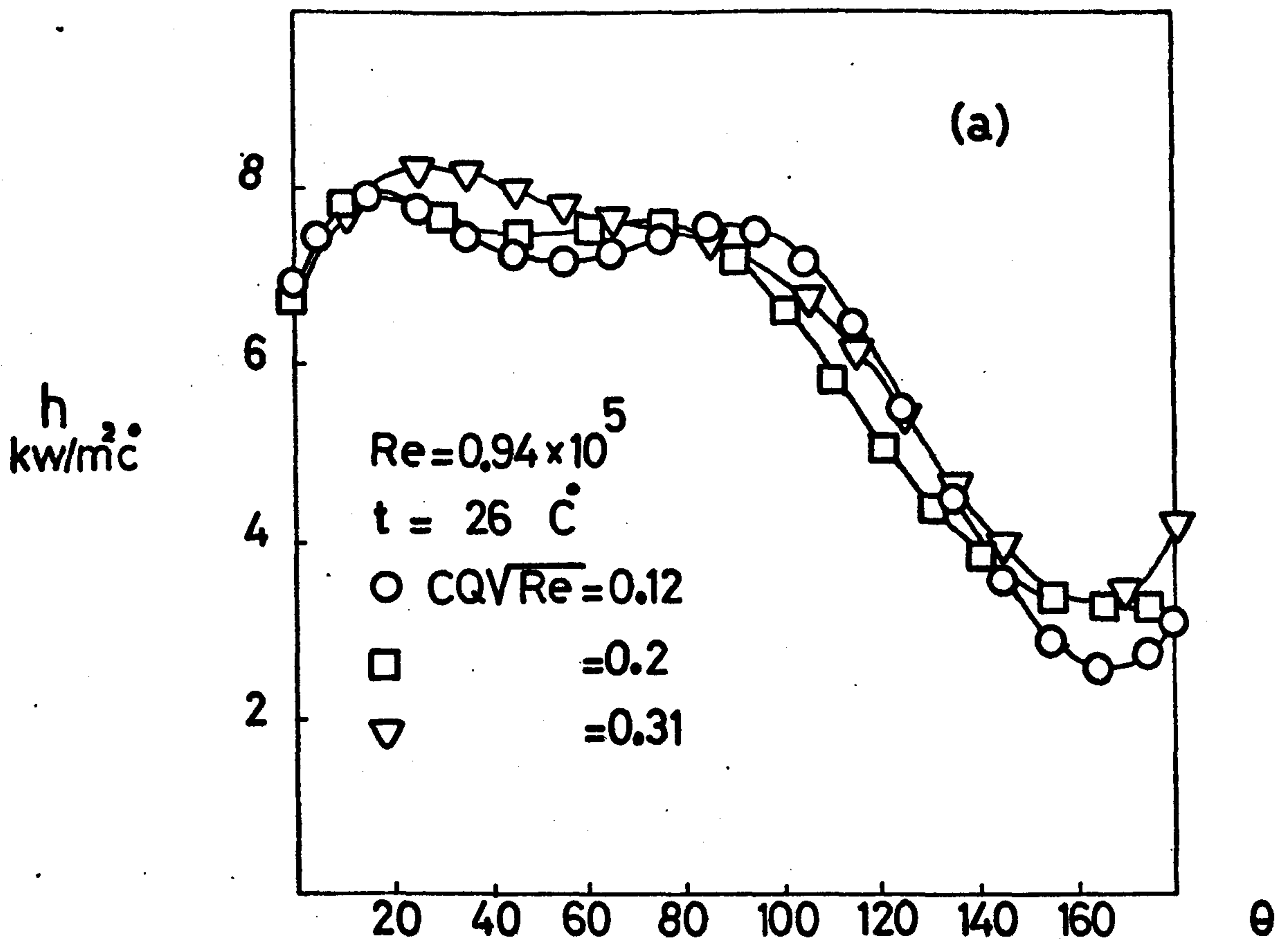


Fig. 9.39

Heat transfer with mass transfer,  
third row in the bank

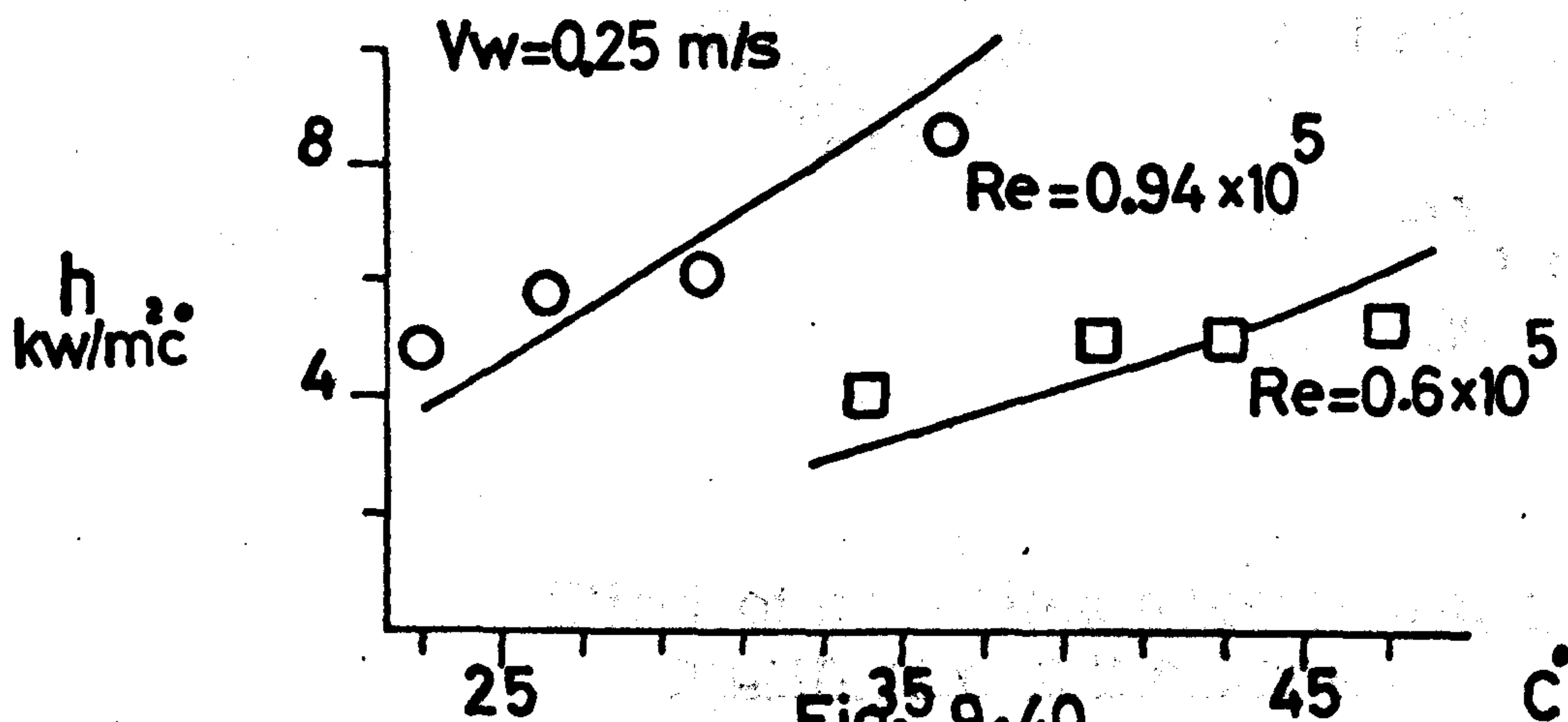
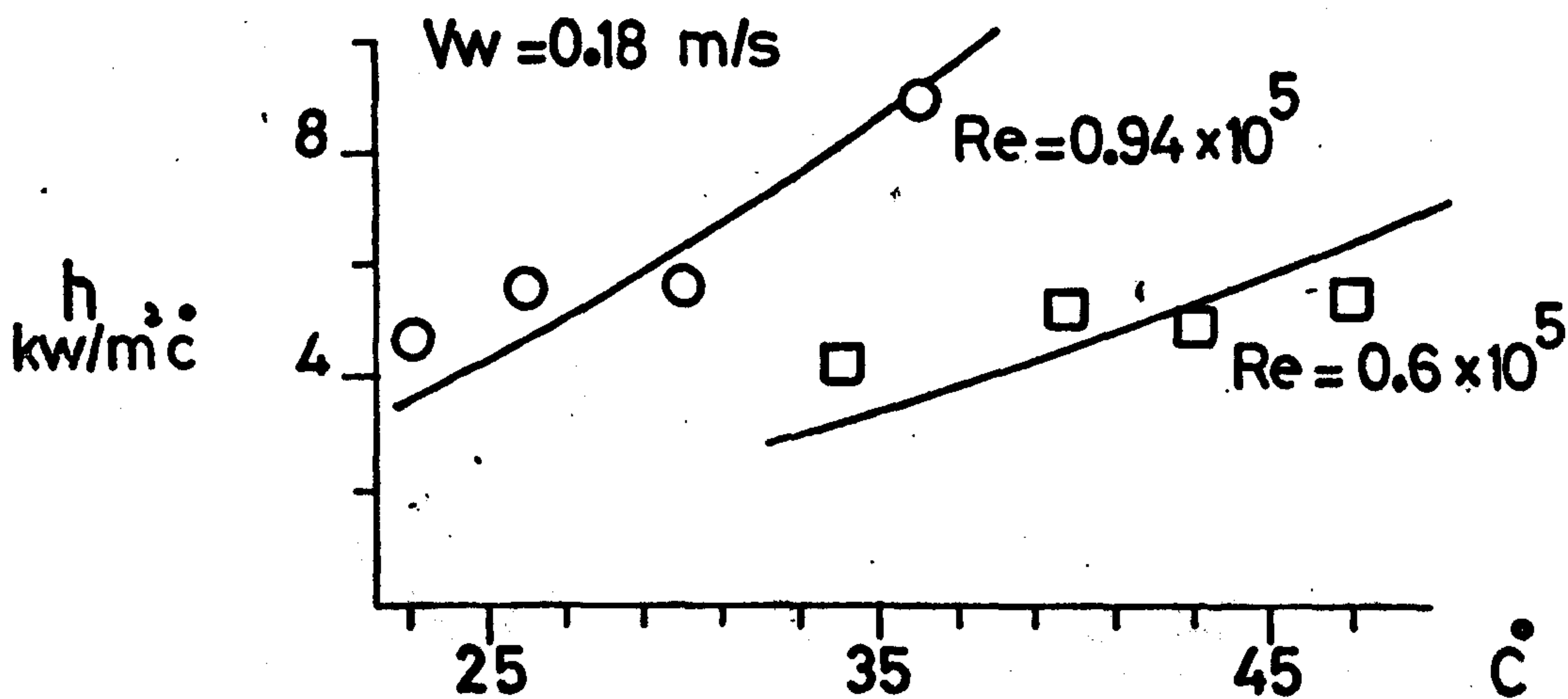
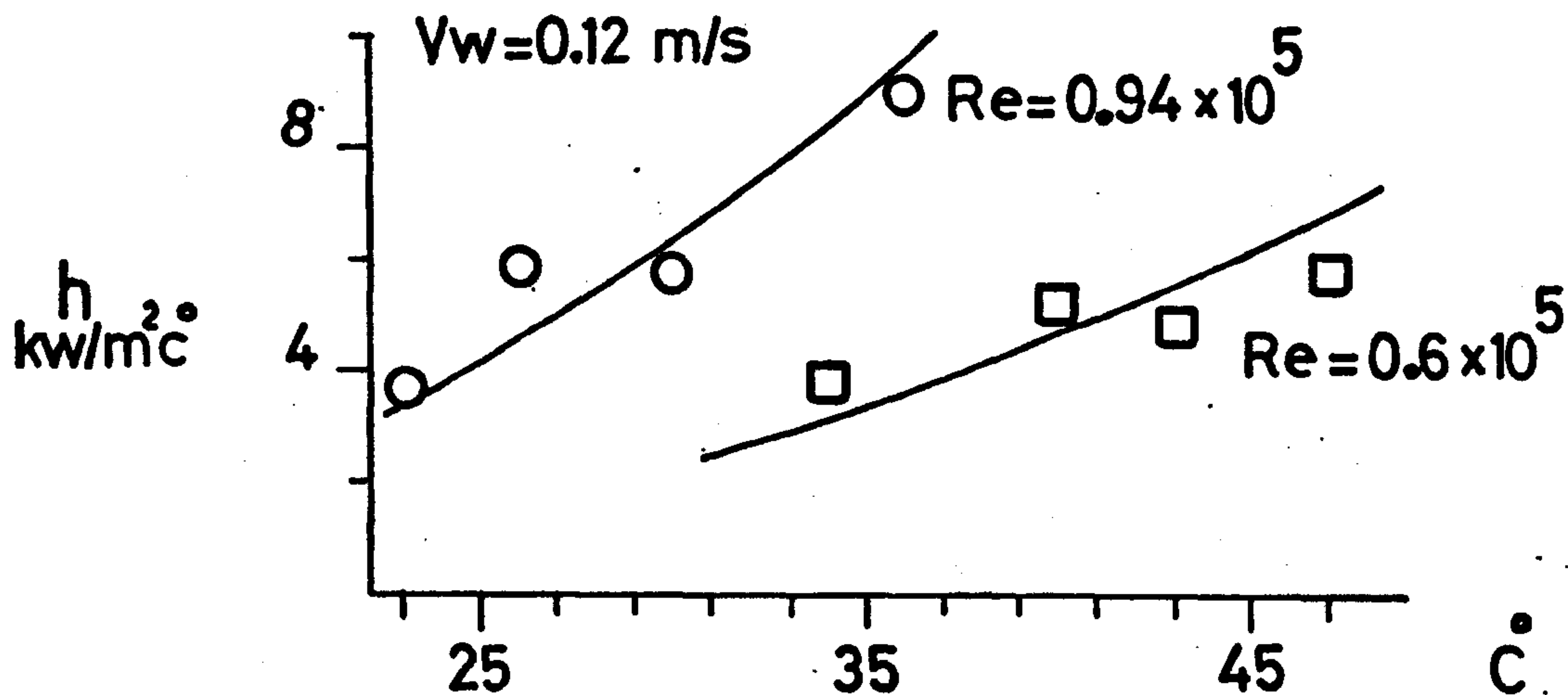
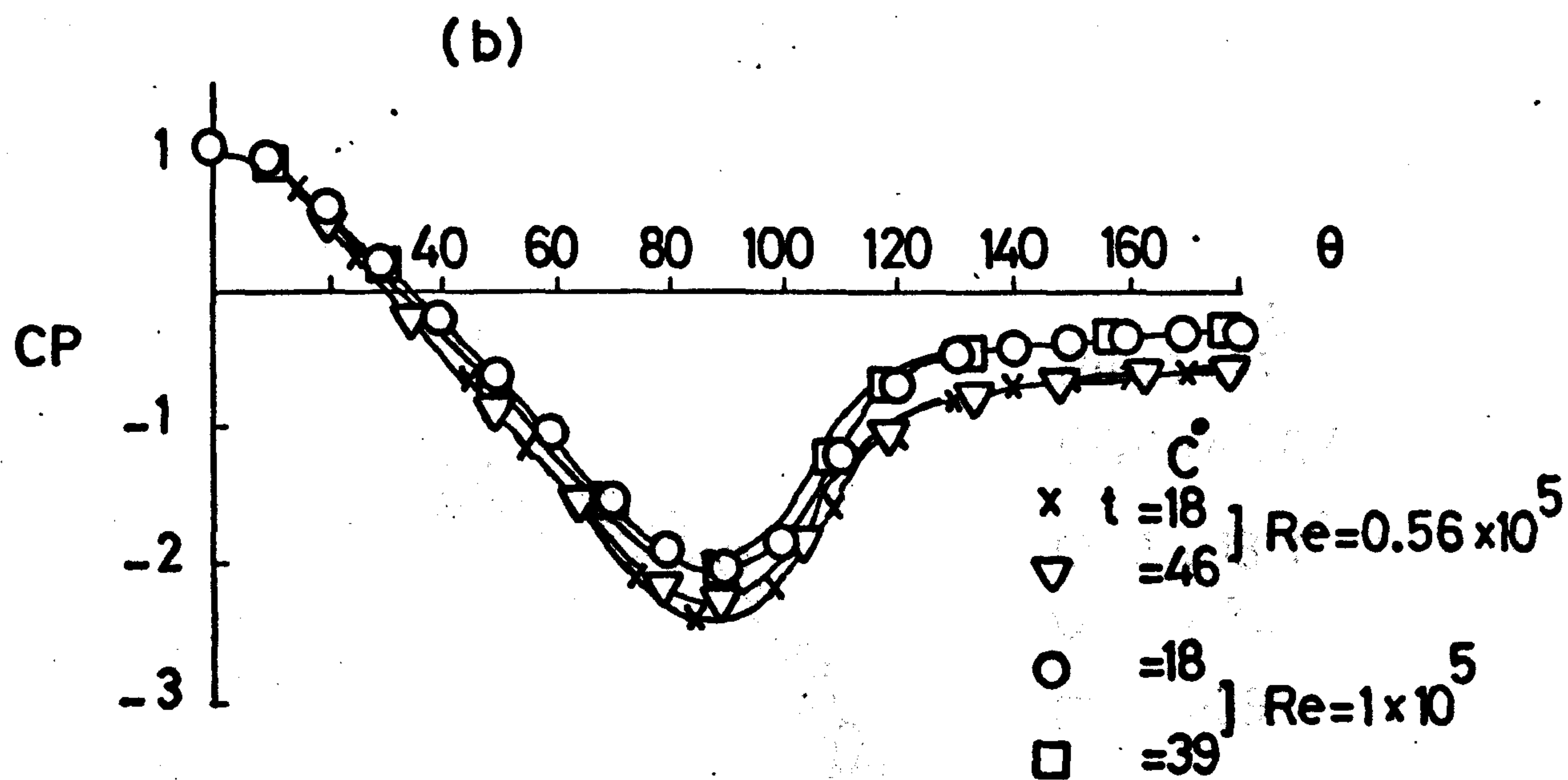
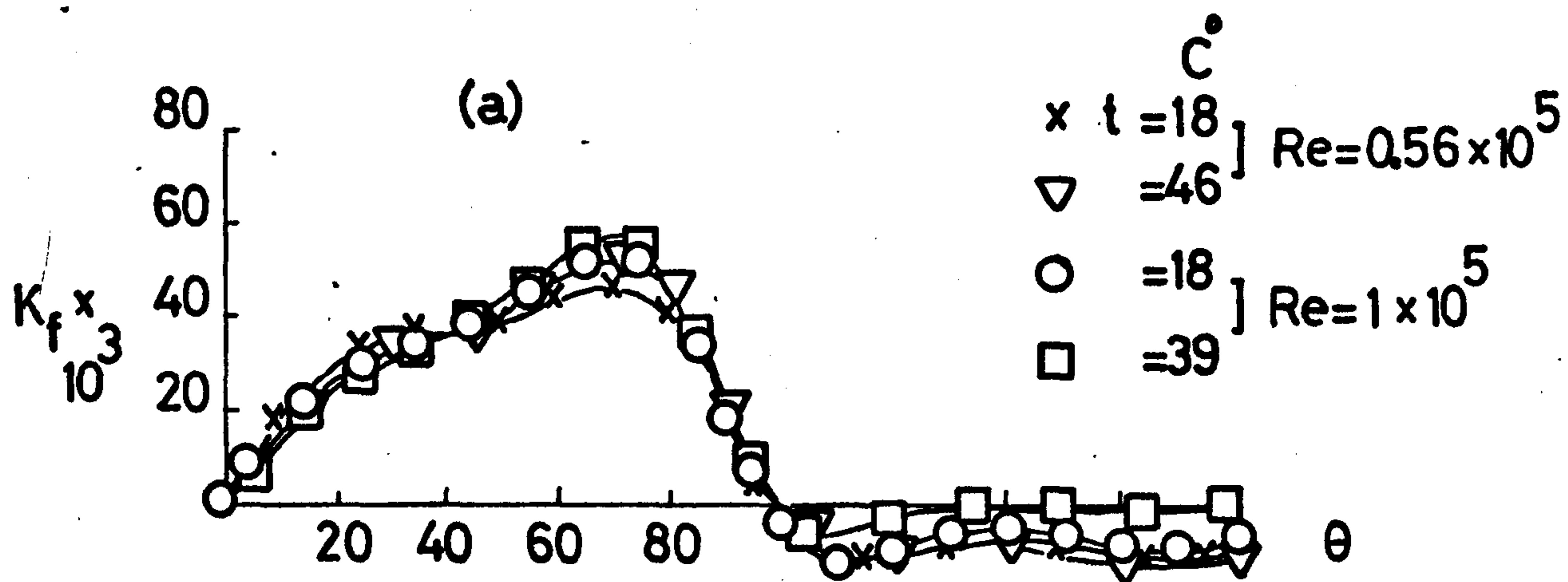


Fig. 9.40  
Average HTC for third row  
in the bank





Effect of main stream temperature,  
fourth row in the bank

Fig. 9.41

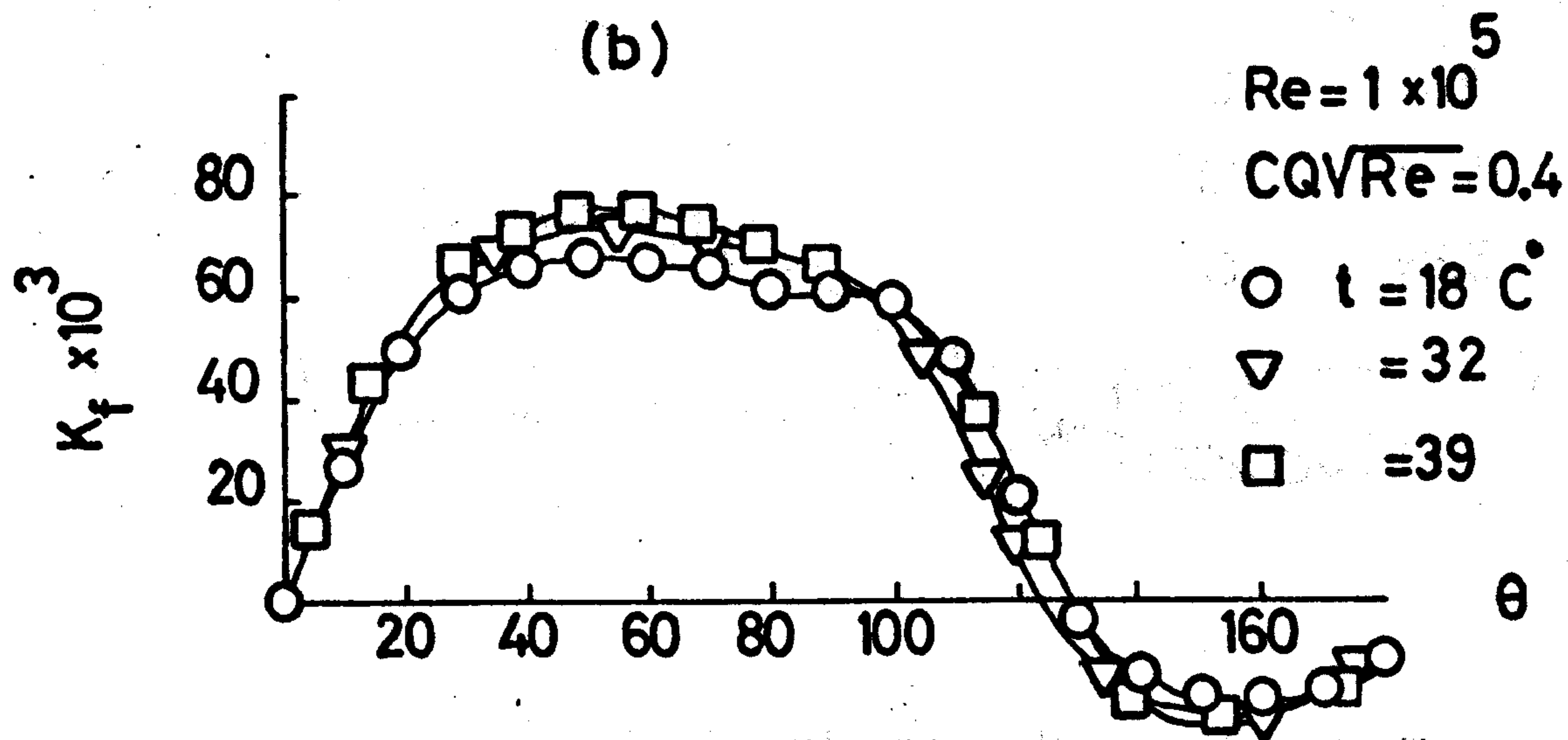
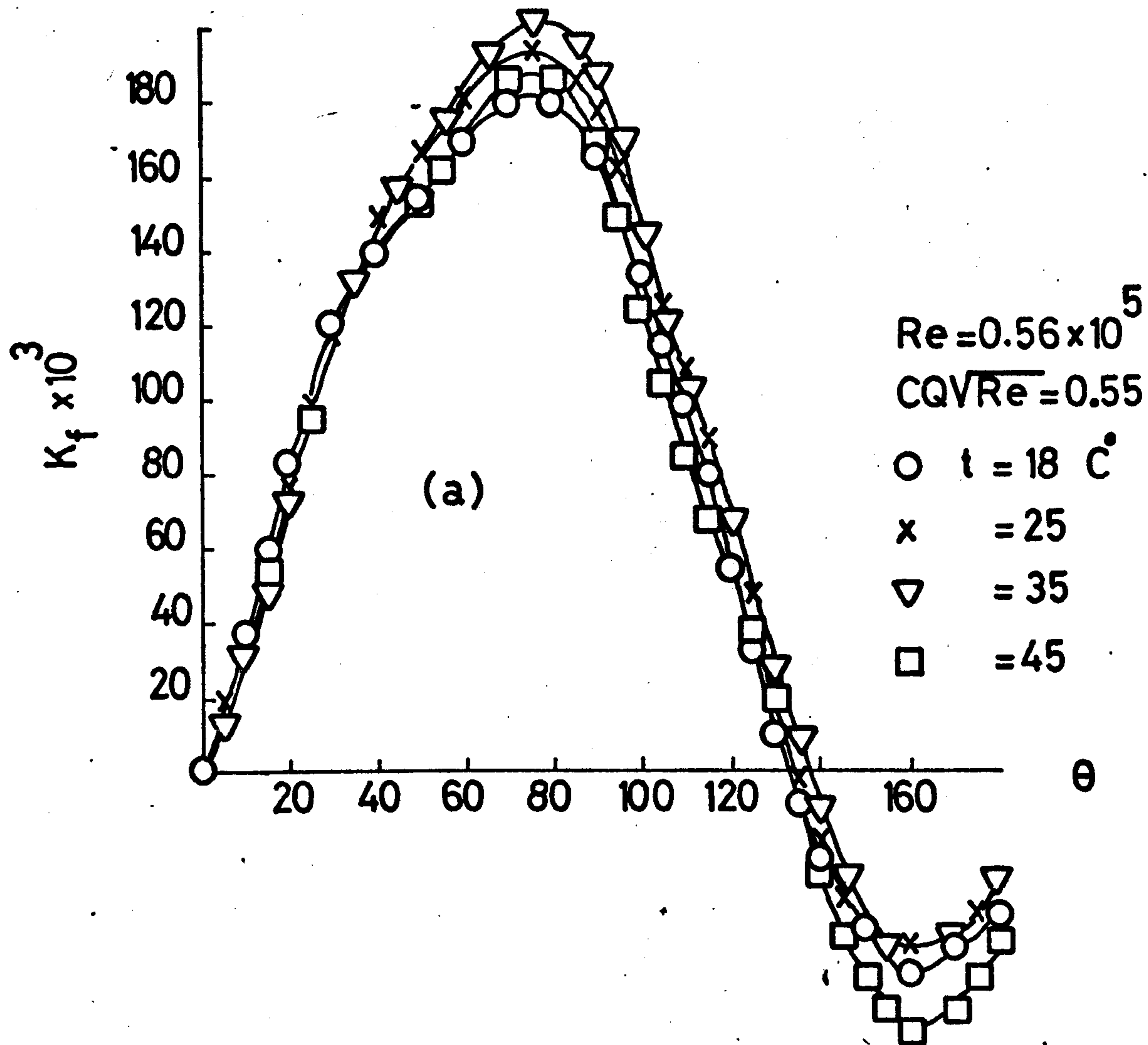
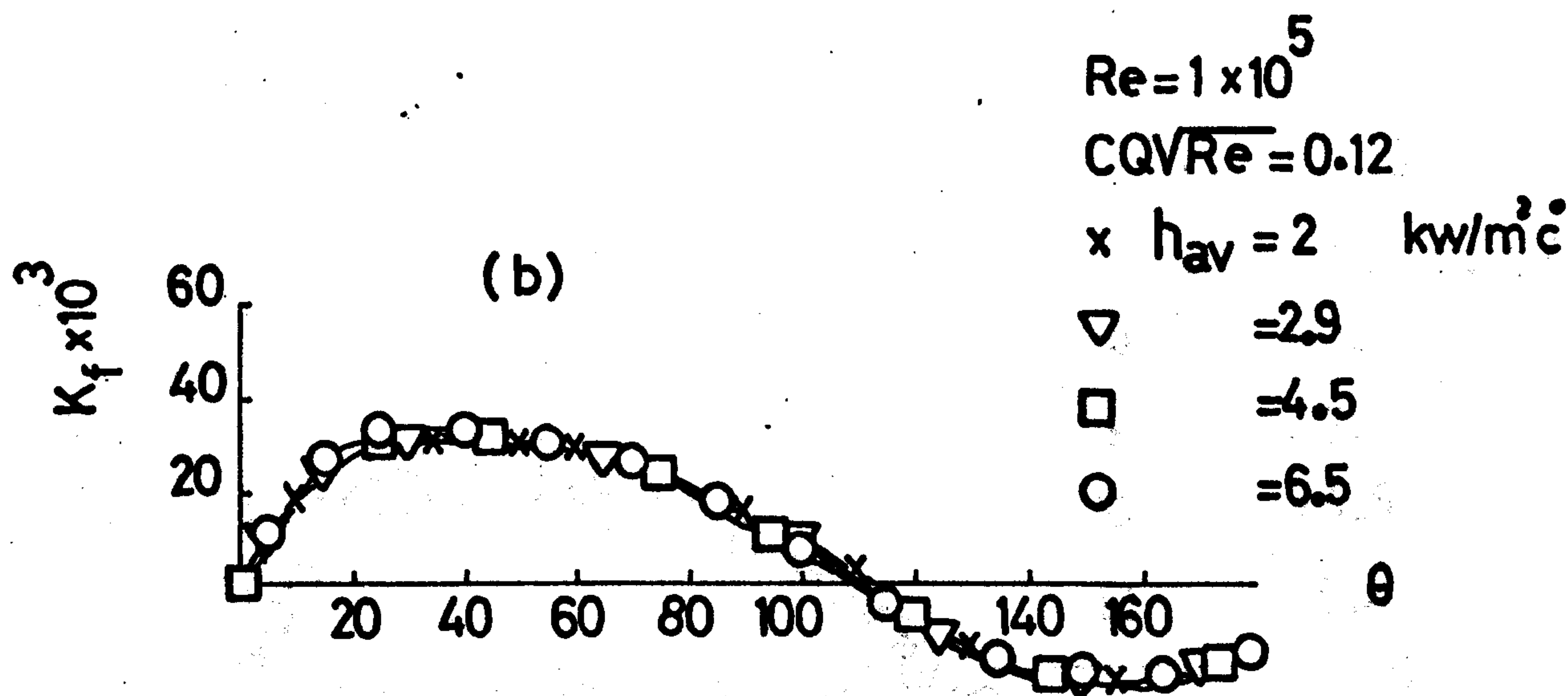
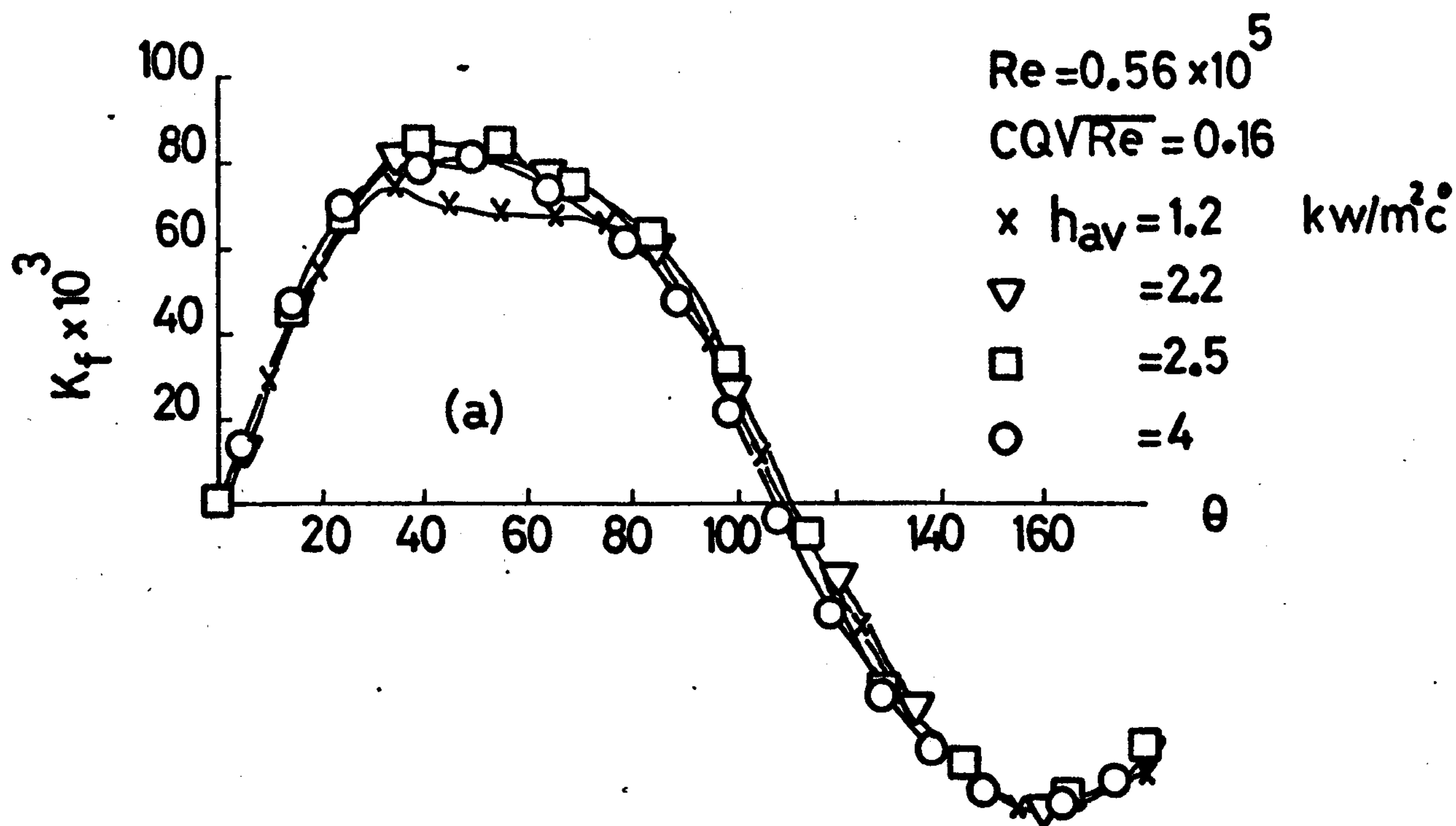


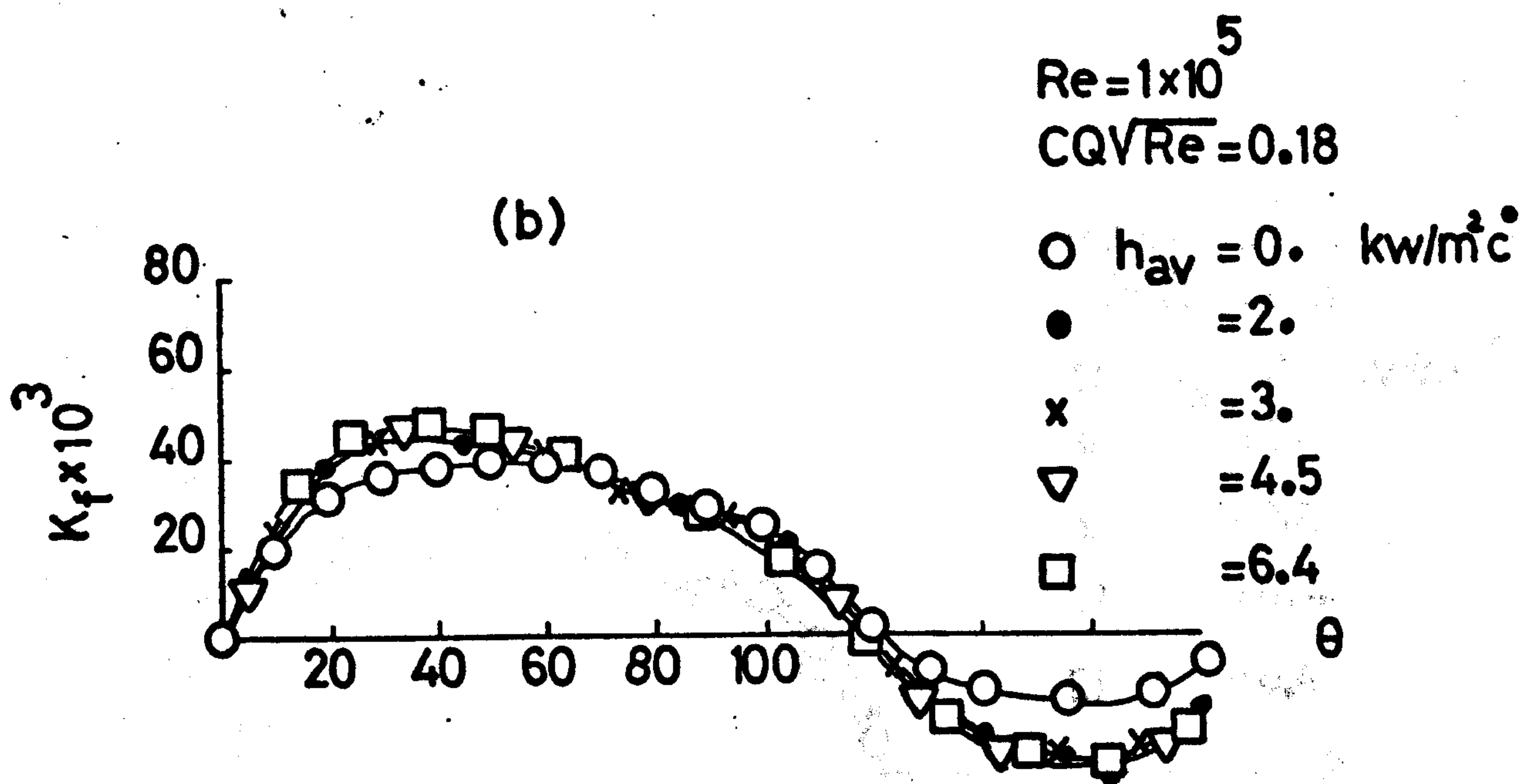
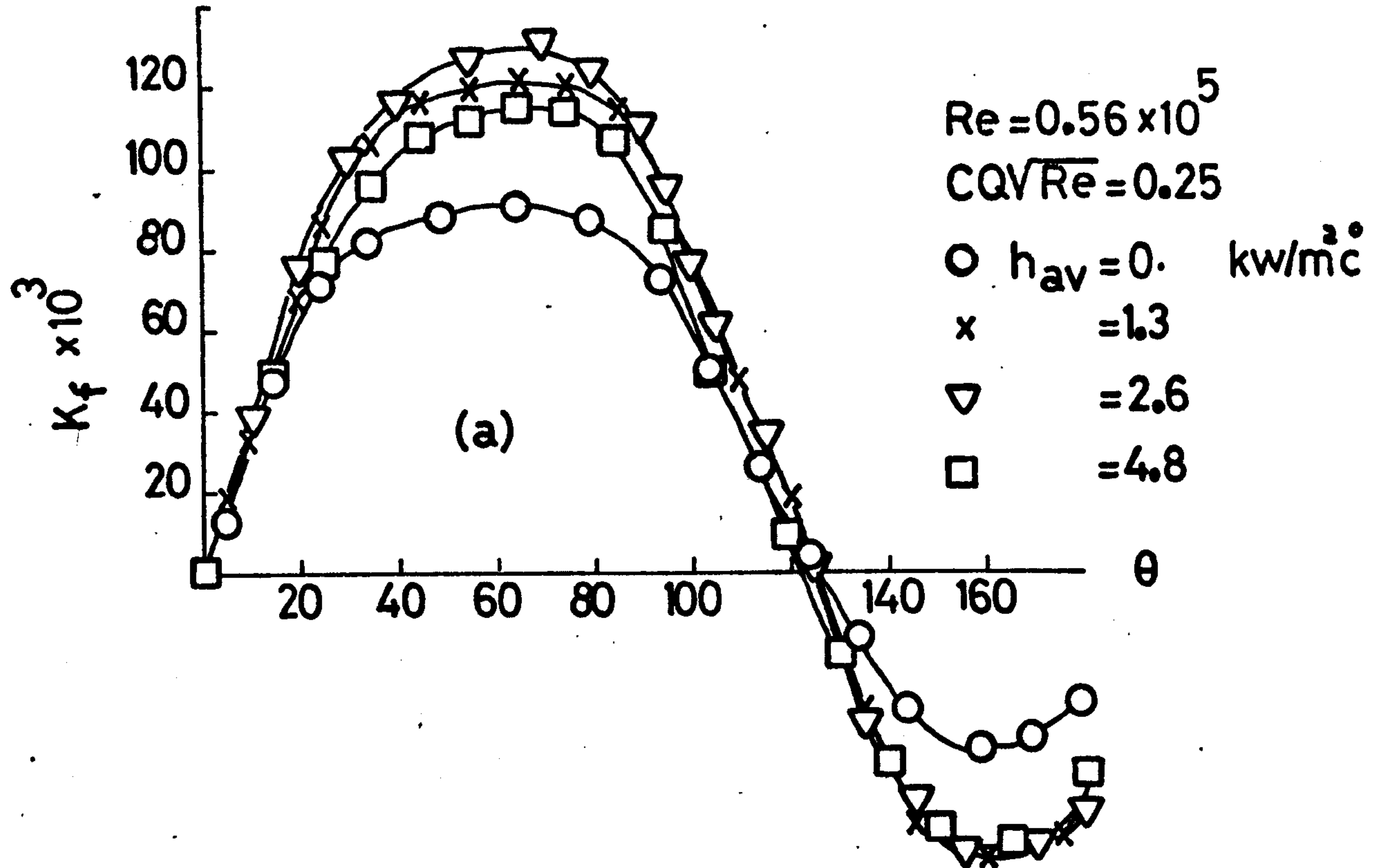
**Fig. 9.42**  
Shear stress at different main stream temp.  
with suction, fourth row in the bank



Shear stress with heat and mass transfer, fourth row in the bank

Fig. 9.43





Shear stress with heat and mass transfer,  
fourth row in the bank

Fig. 9.44

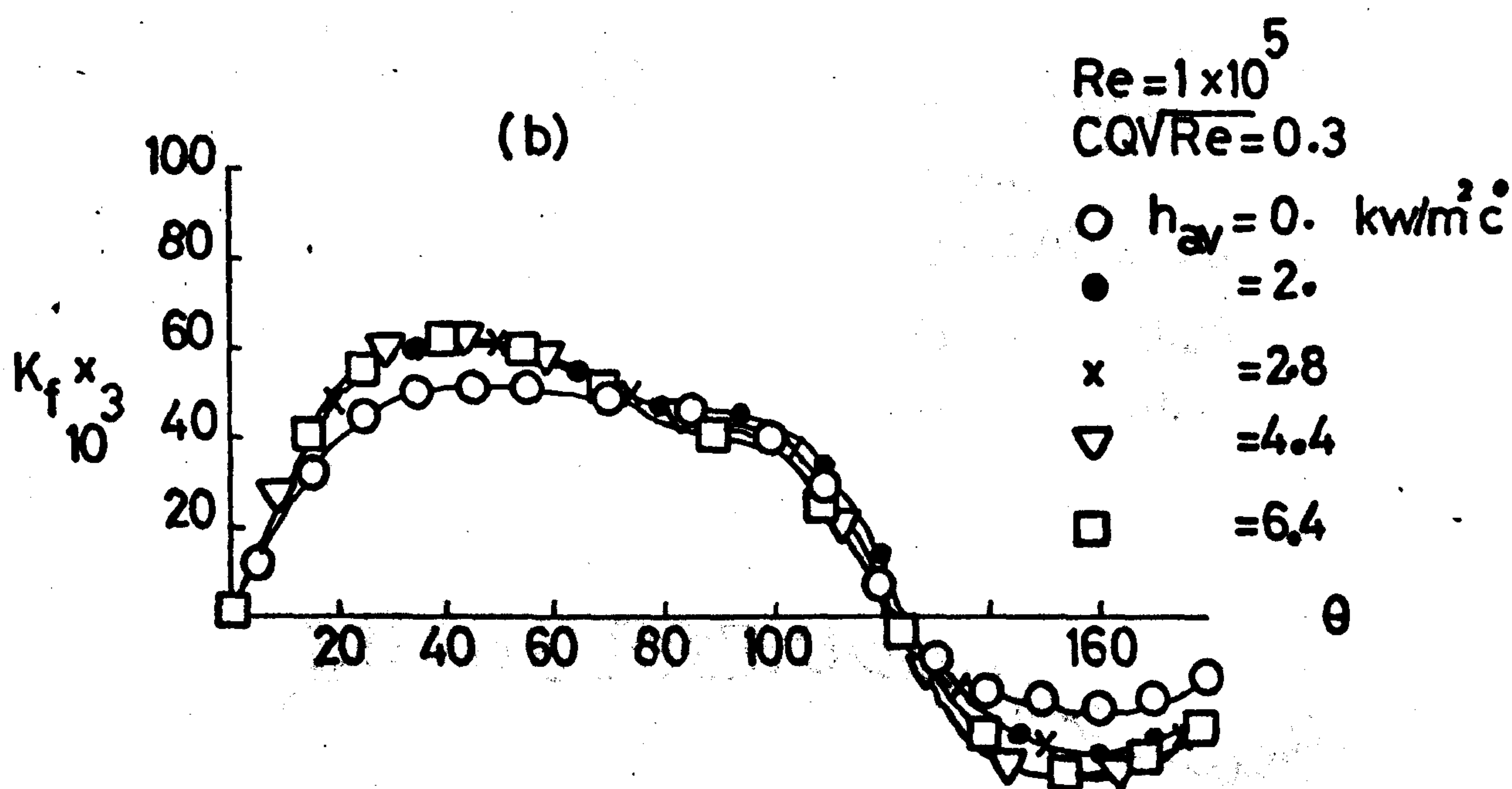
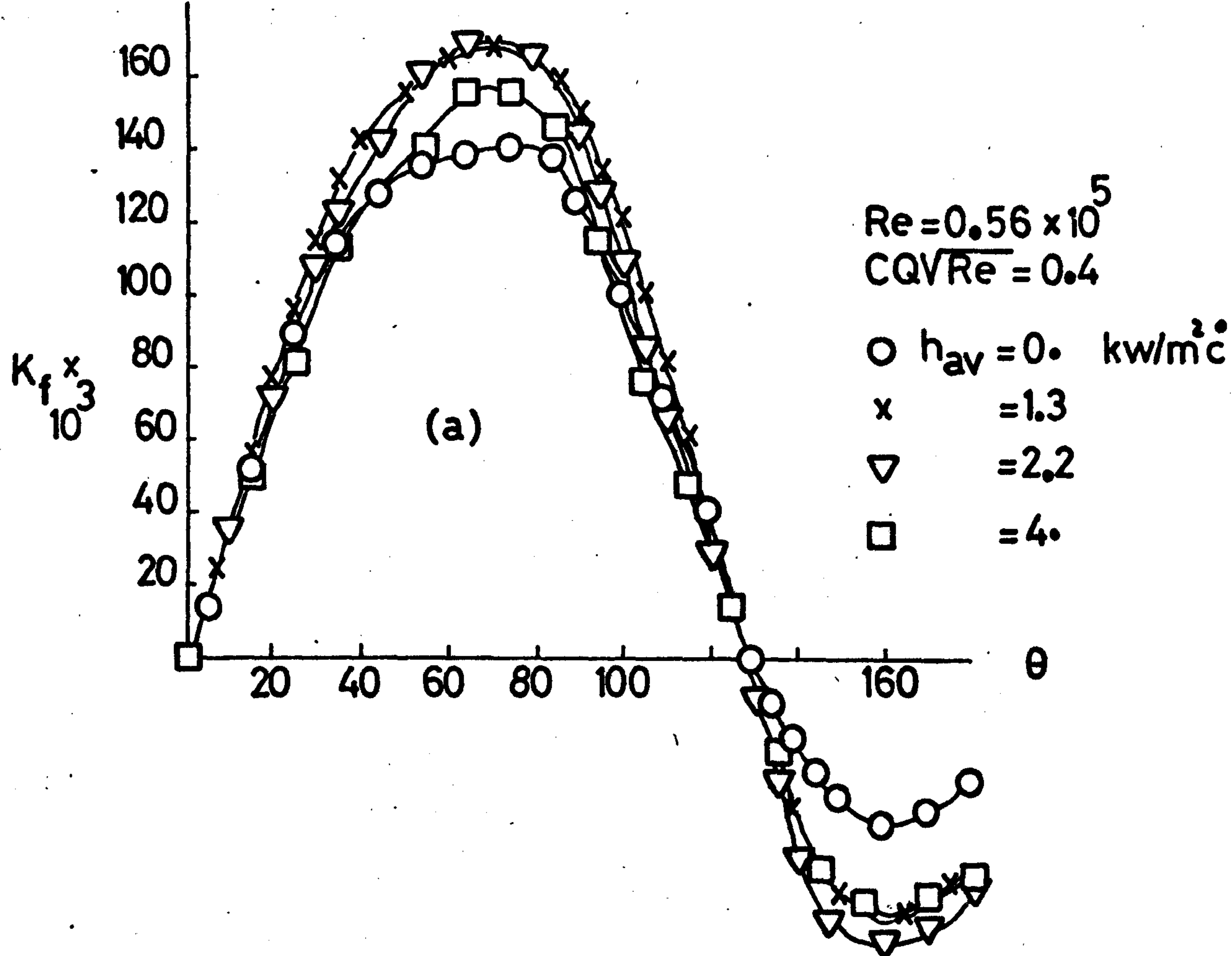


**Fig. 9.45**  
Shear stress with heat and mass transfer,  
fourth row in the bank

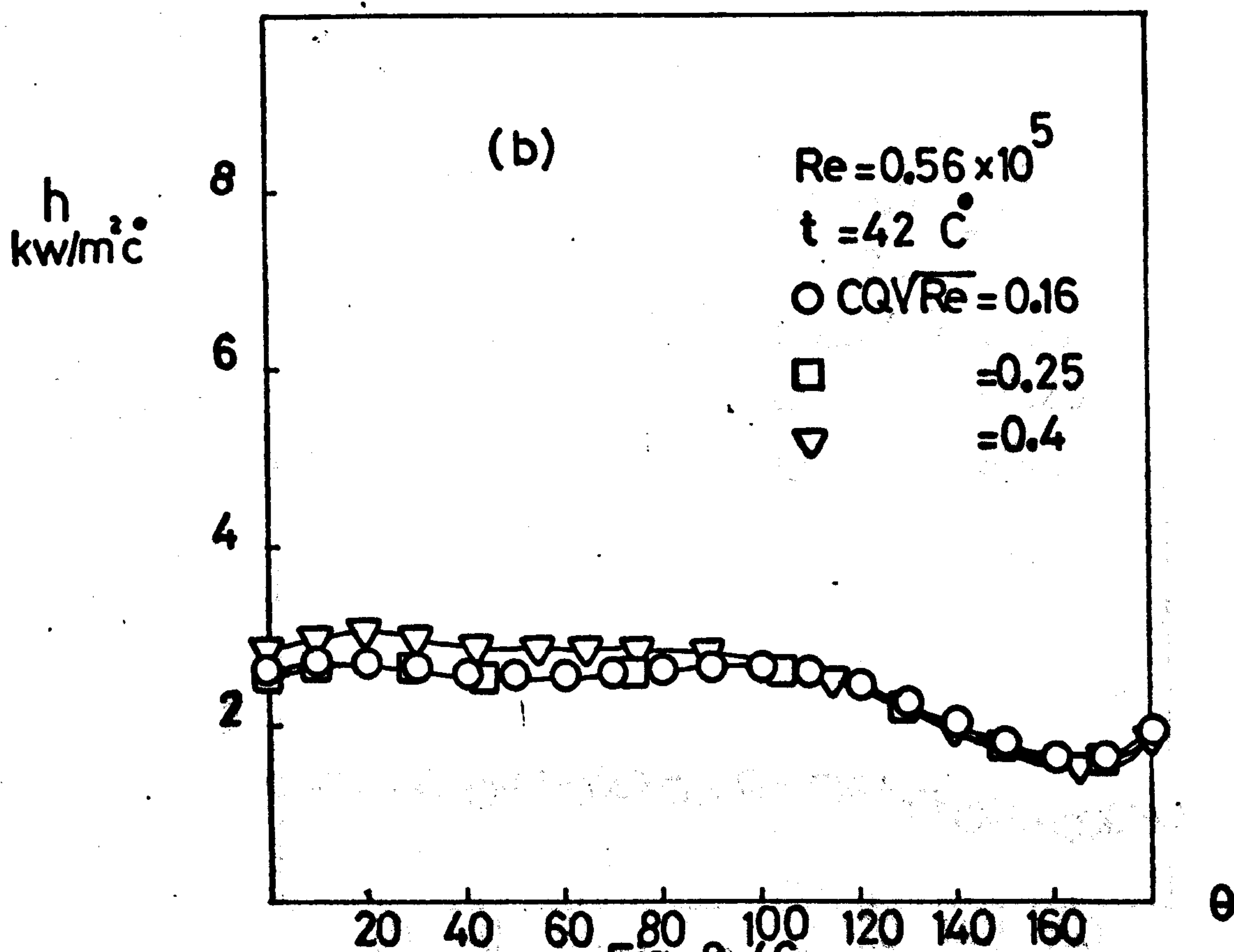
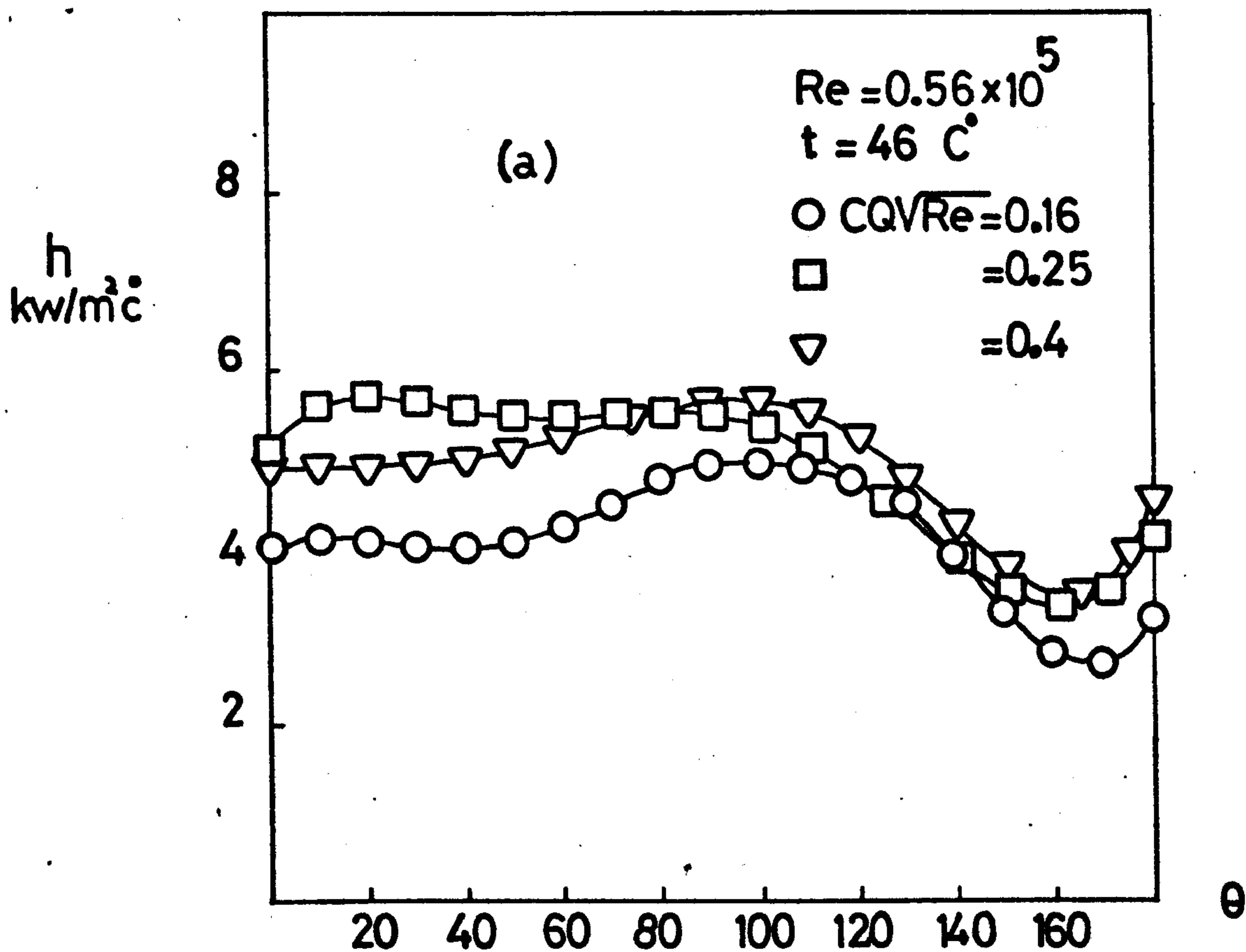


Fig. 9.46  
Heat transfer with suction, fourth  
row in the bank.



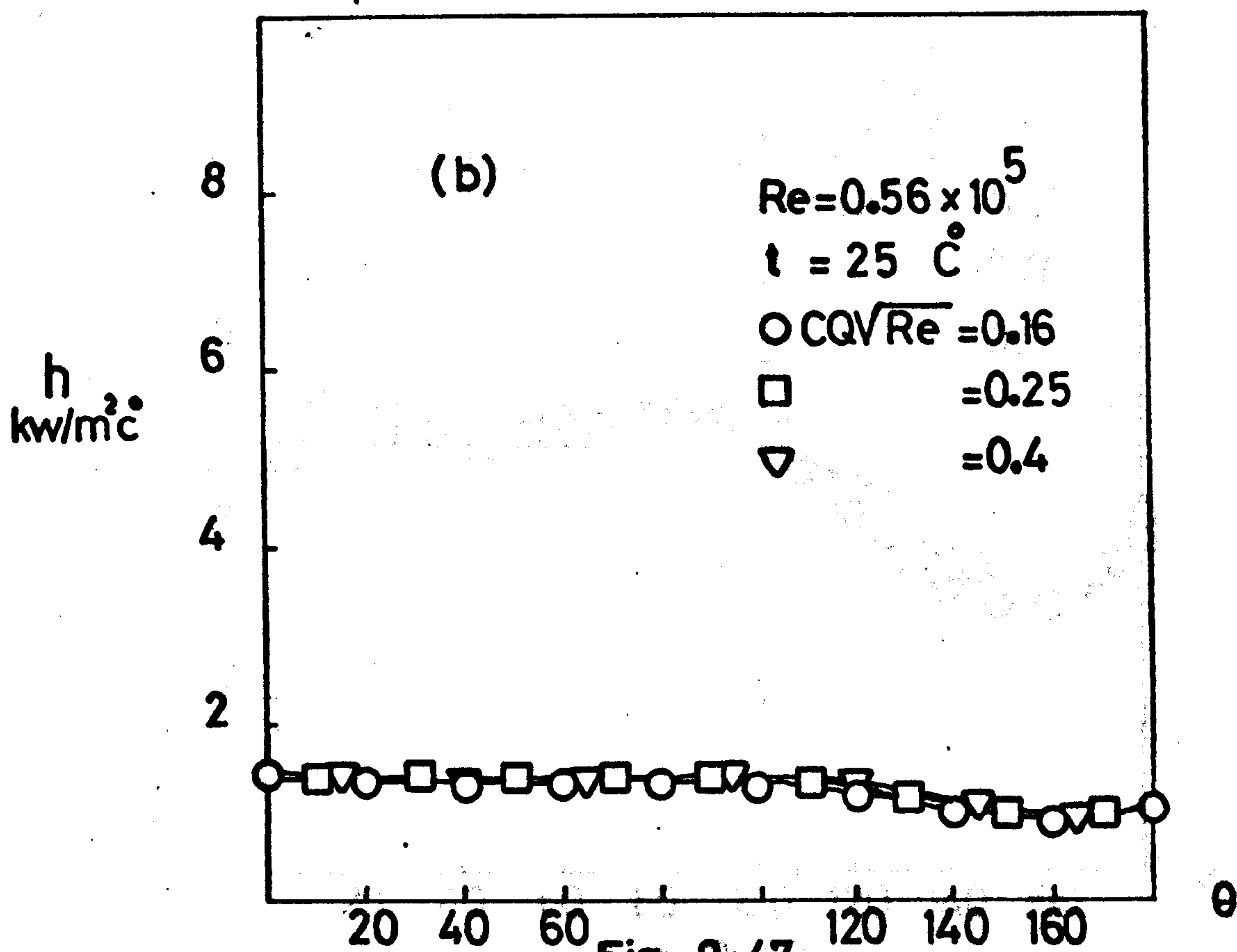
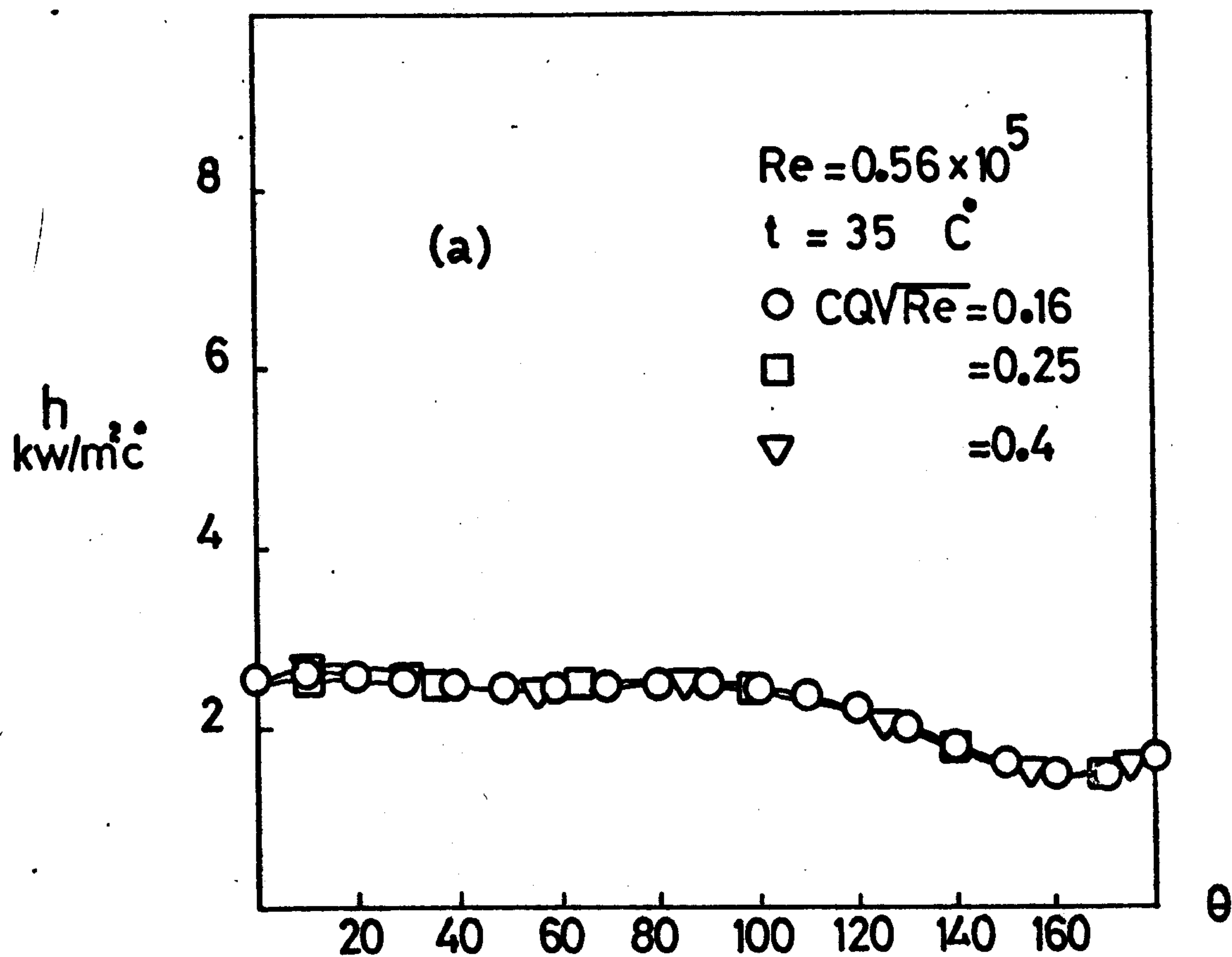
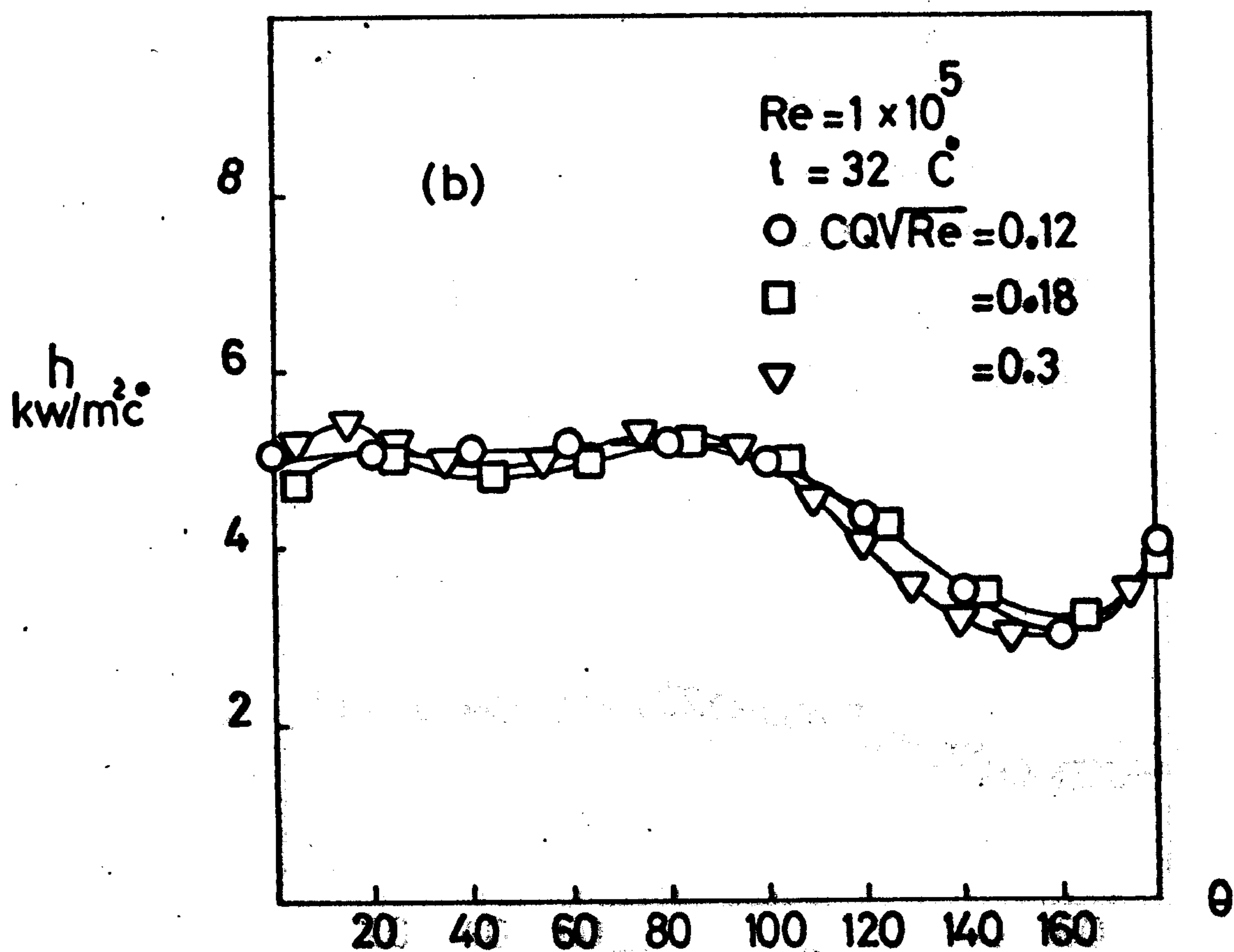
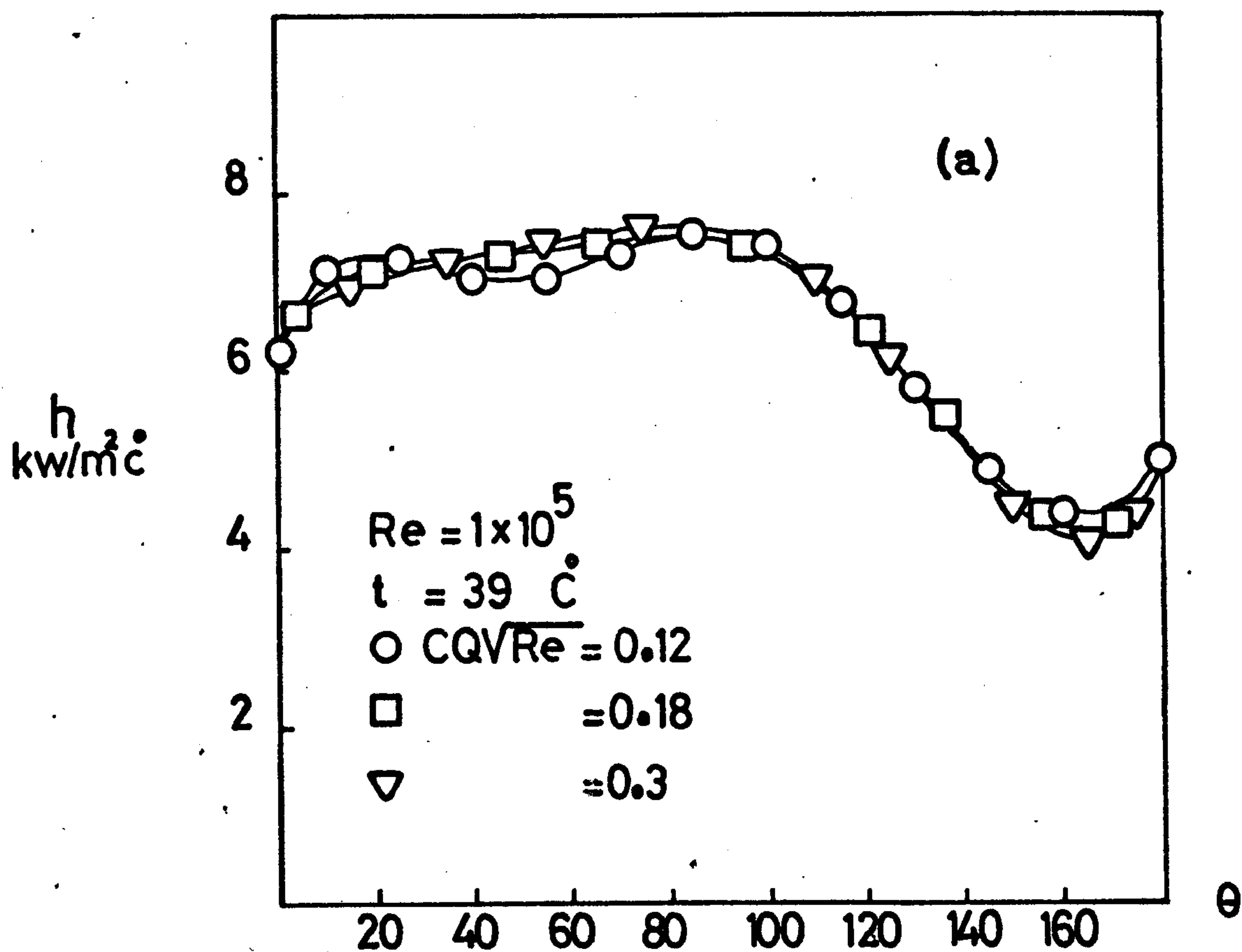
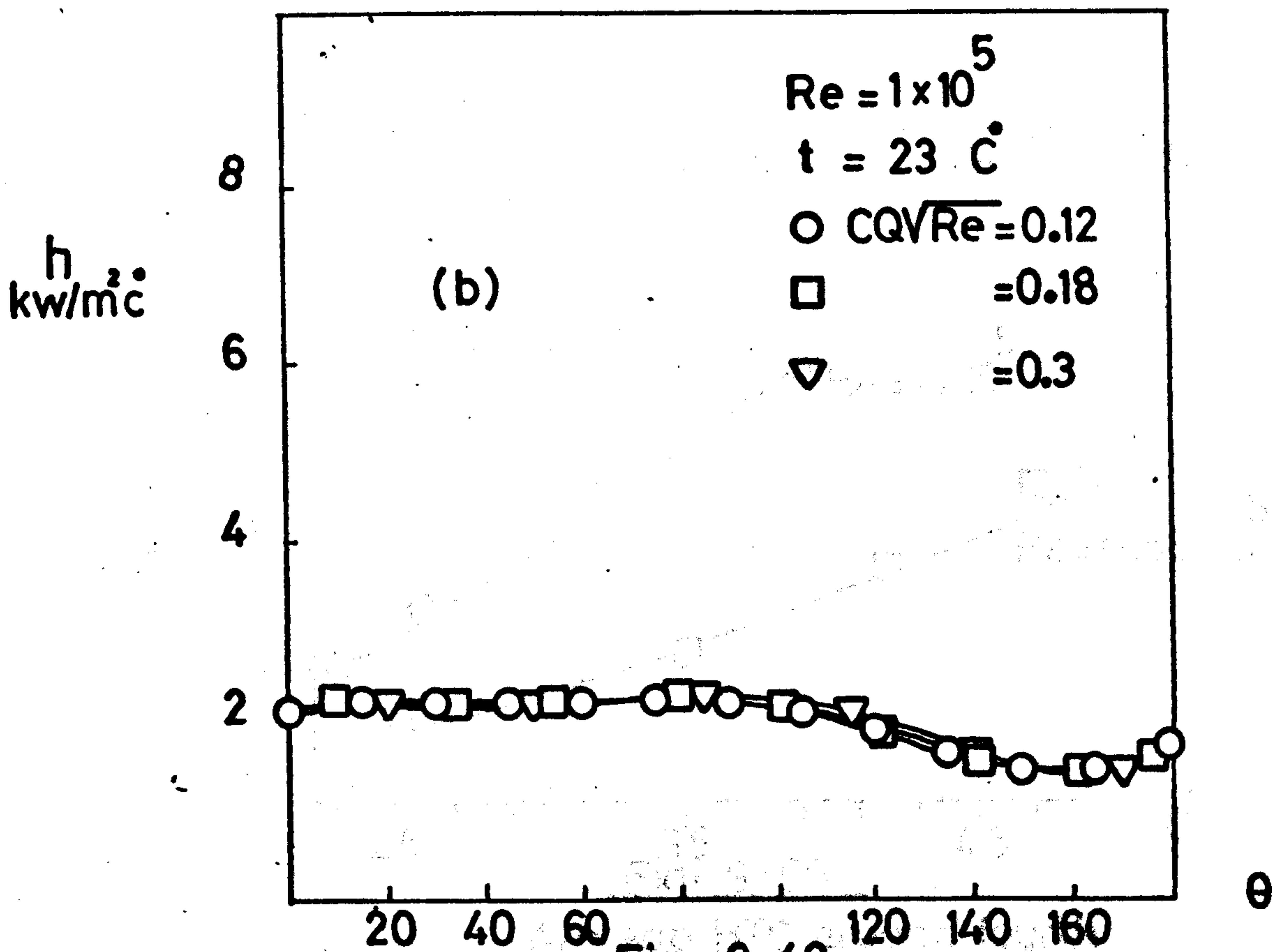
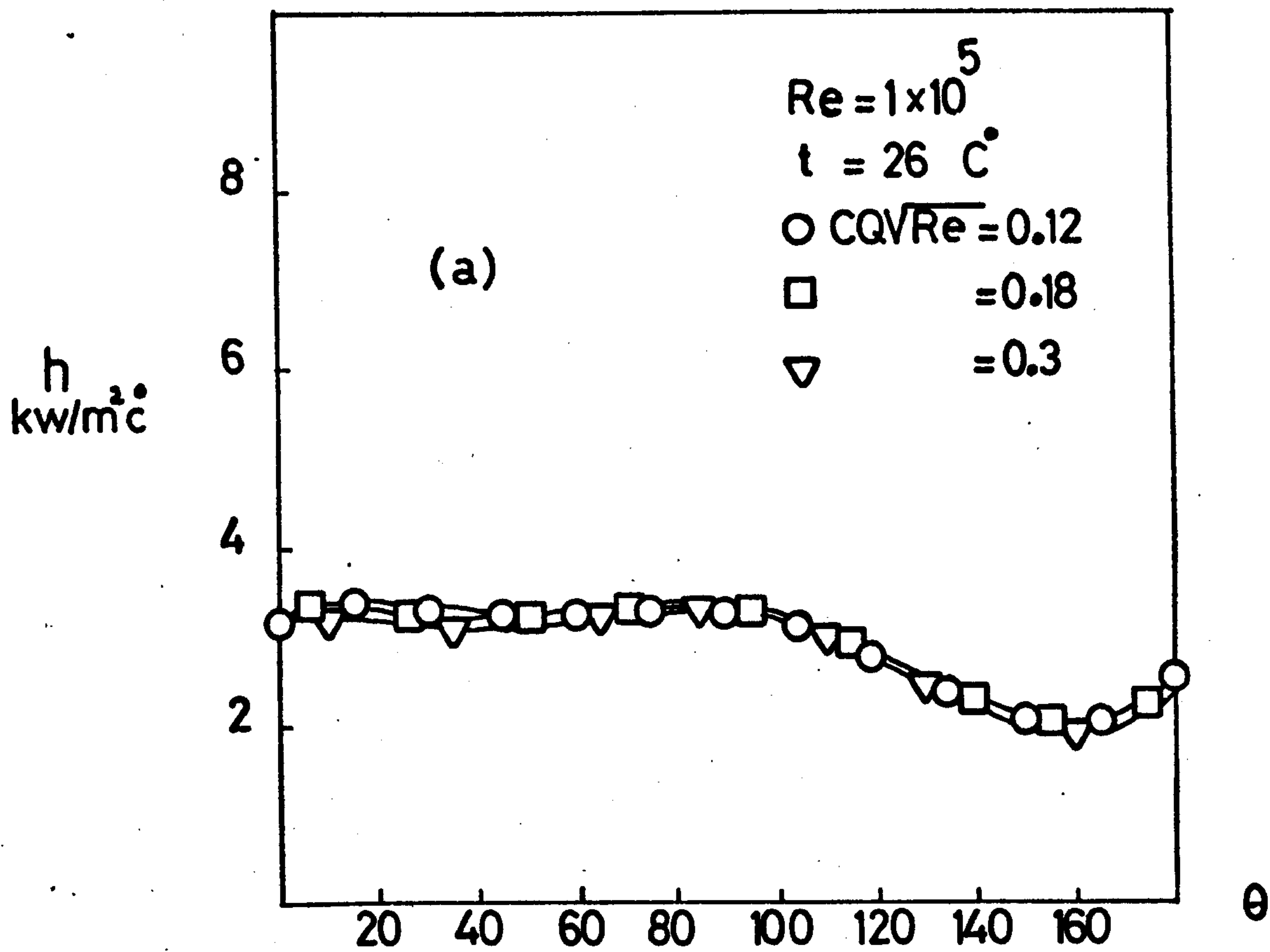


Fig. 9.47

Heat transfer with mass transfer,  
fourth row in the bank



**Fig. 9.48**  
Heat transfer with mass transfer,  
fourth row in the bank



**Fig. 9.49**  
Heat transfer with mass transfer,  
fourth row in the bank.



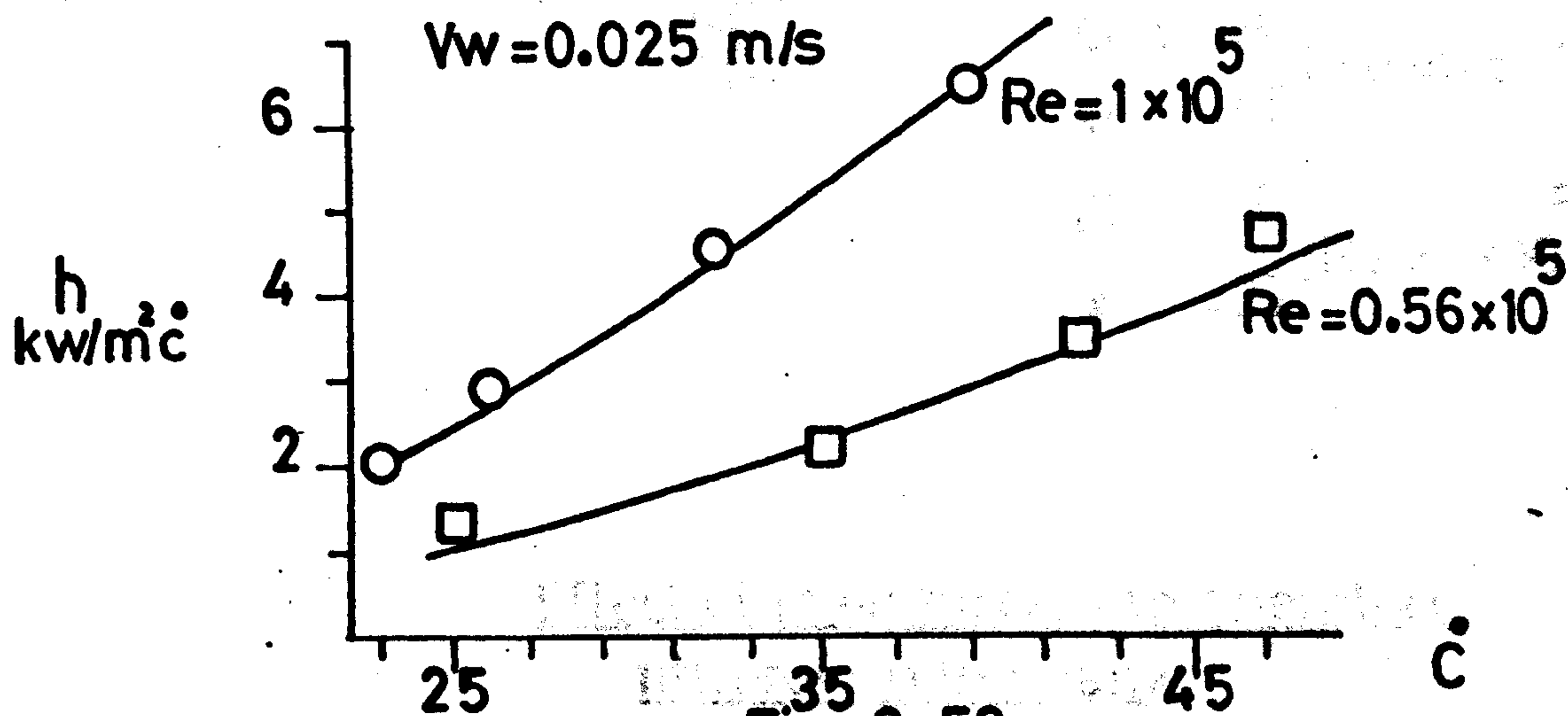
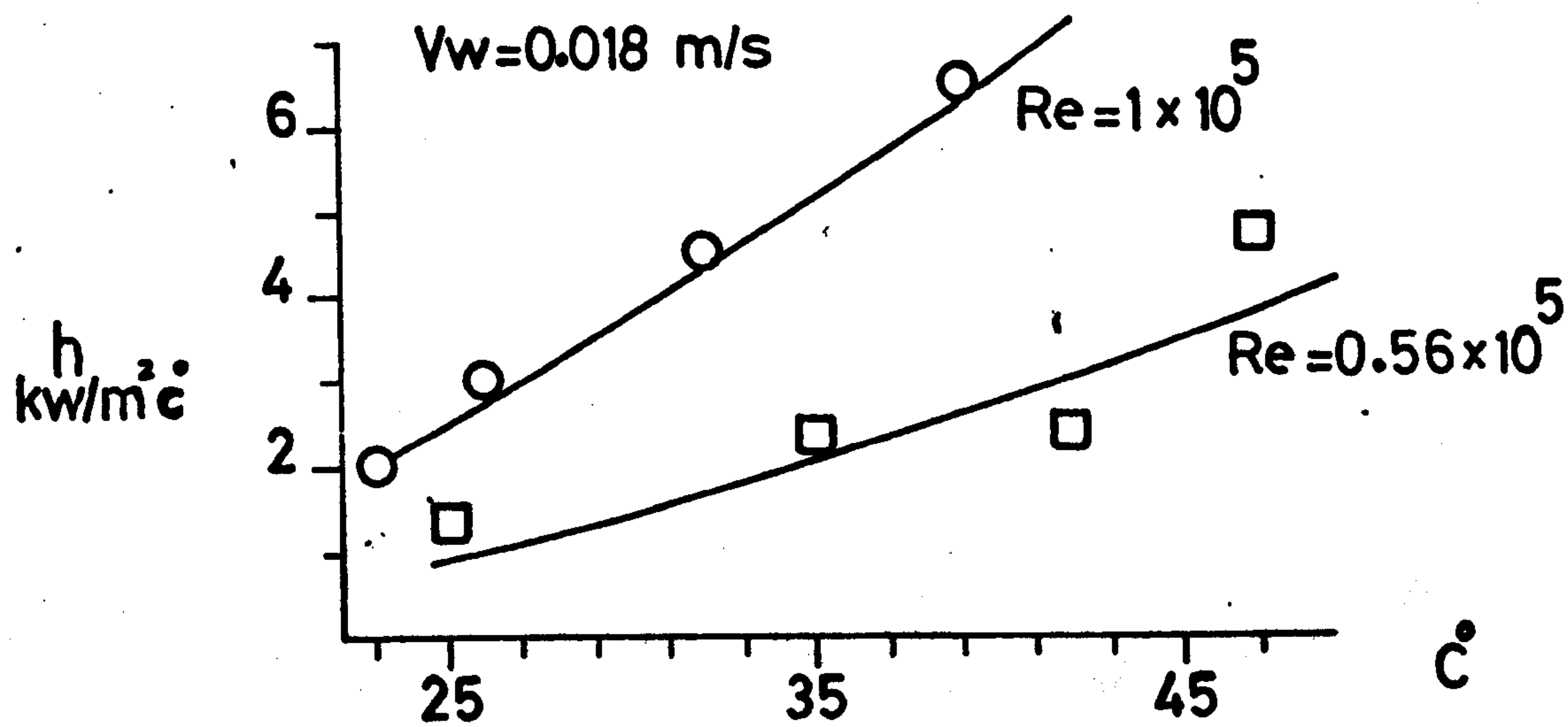
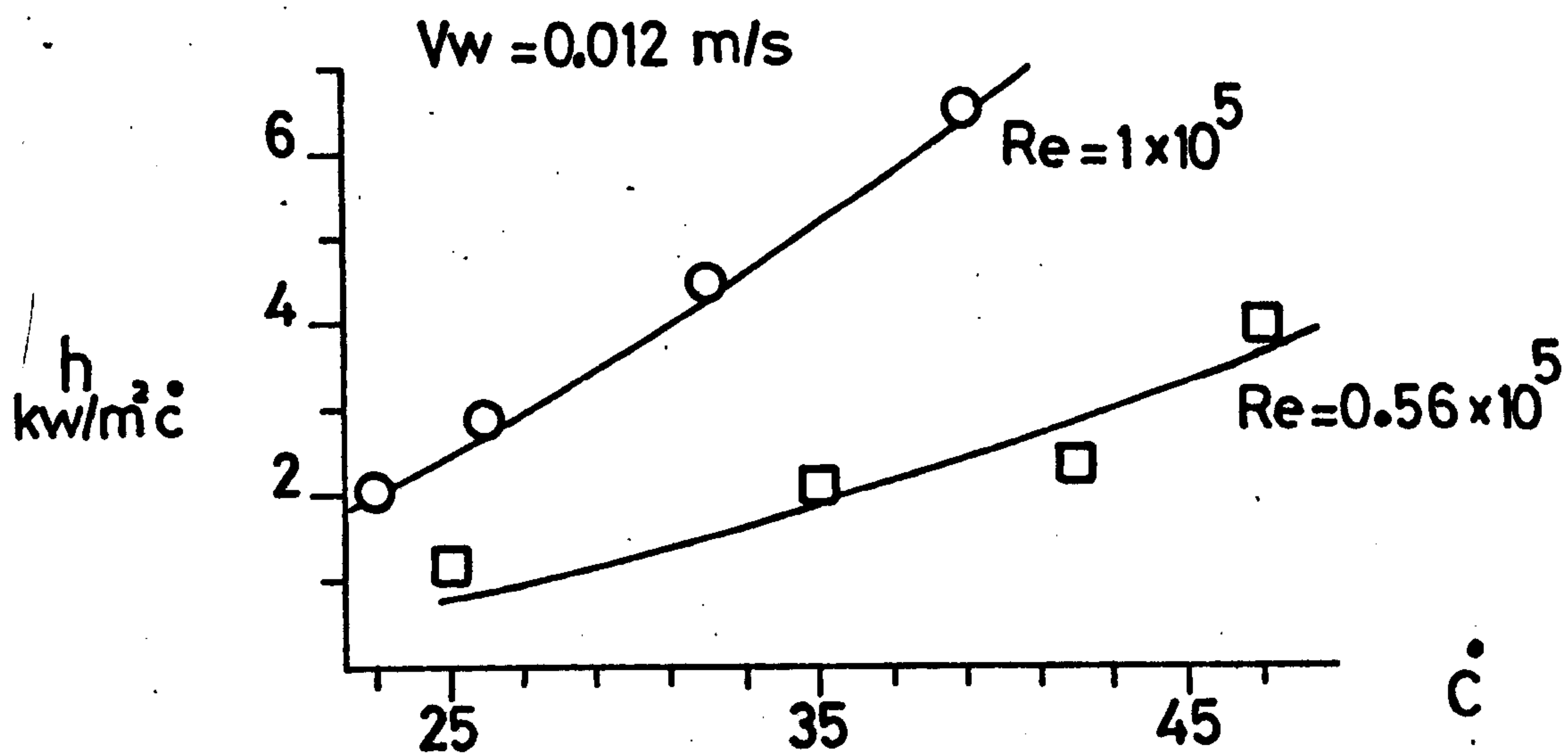
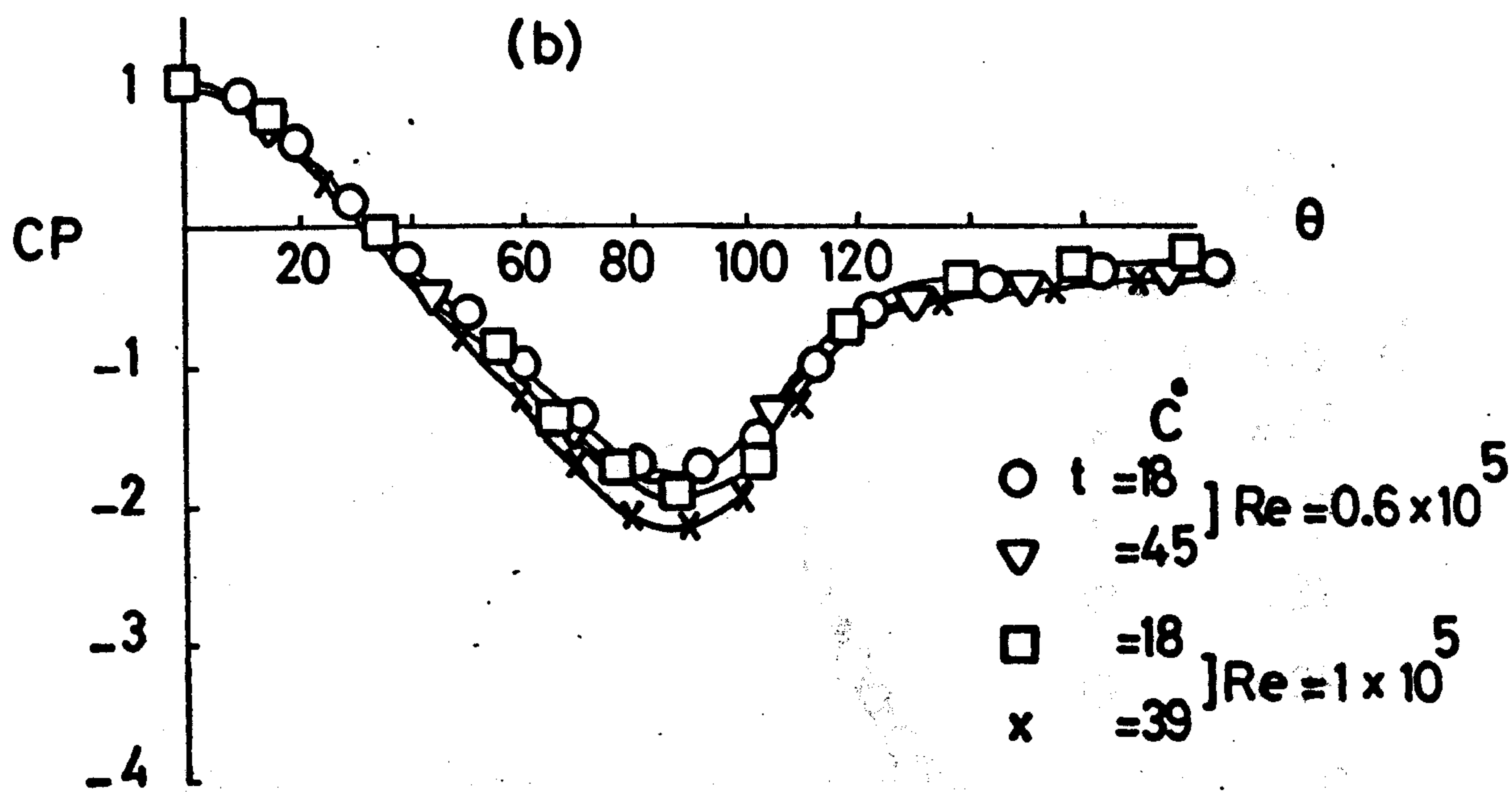
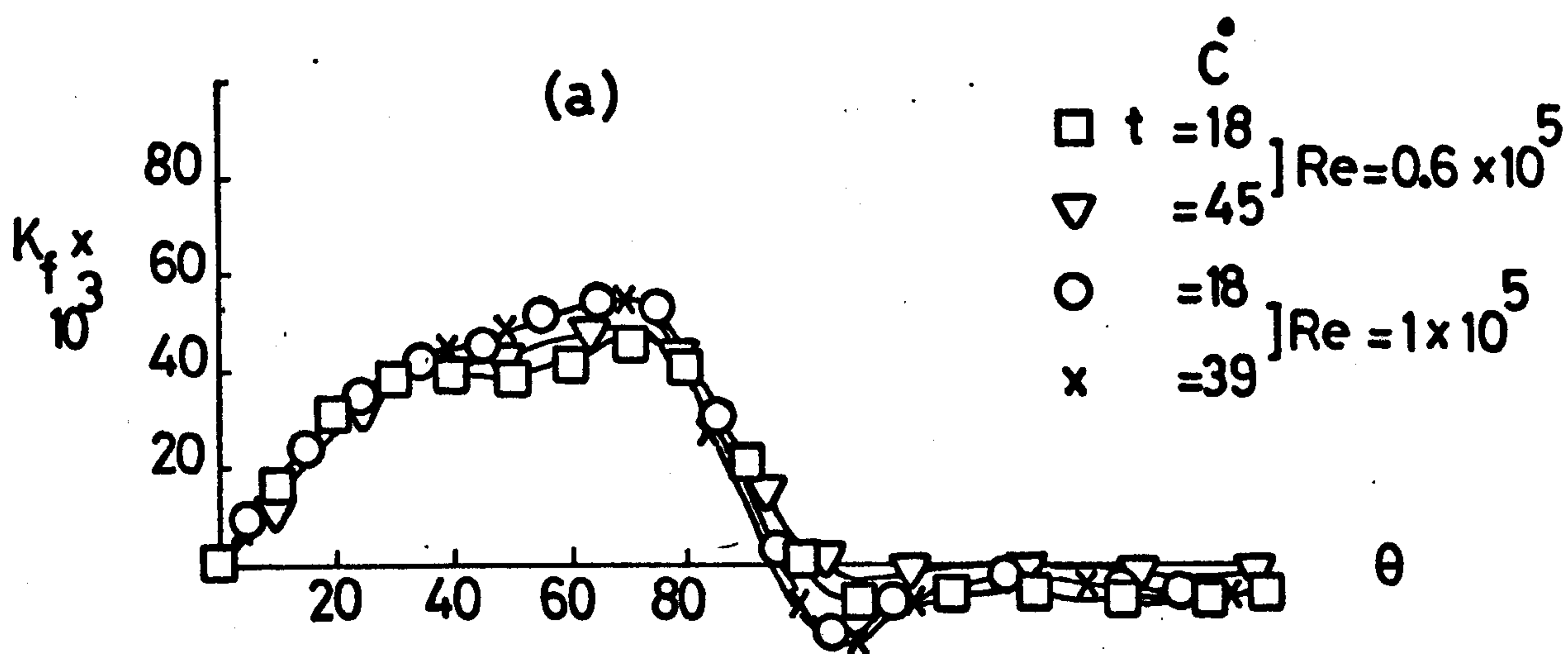


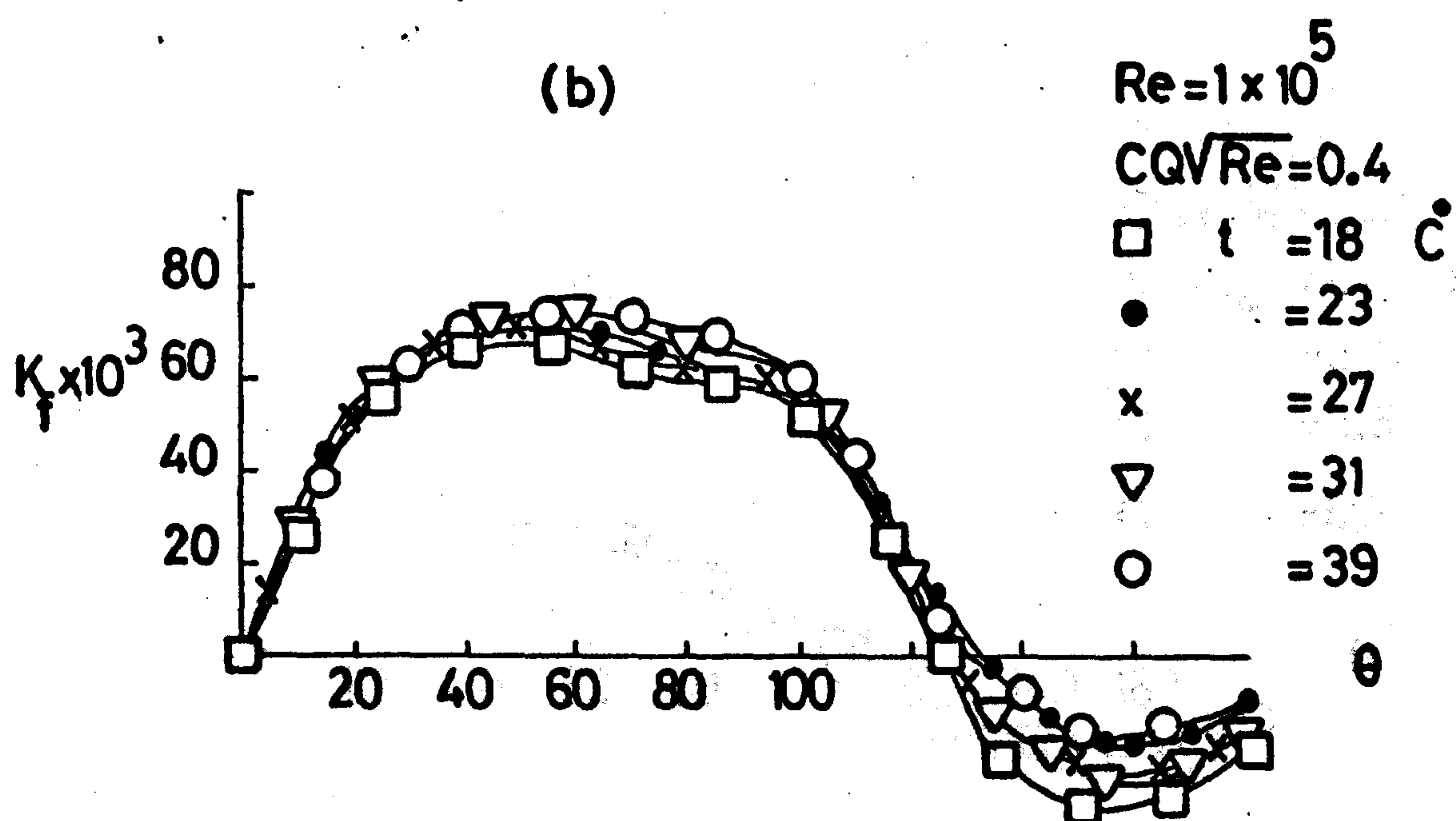
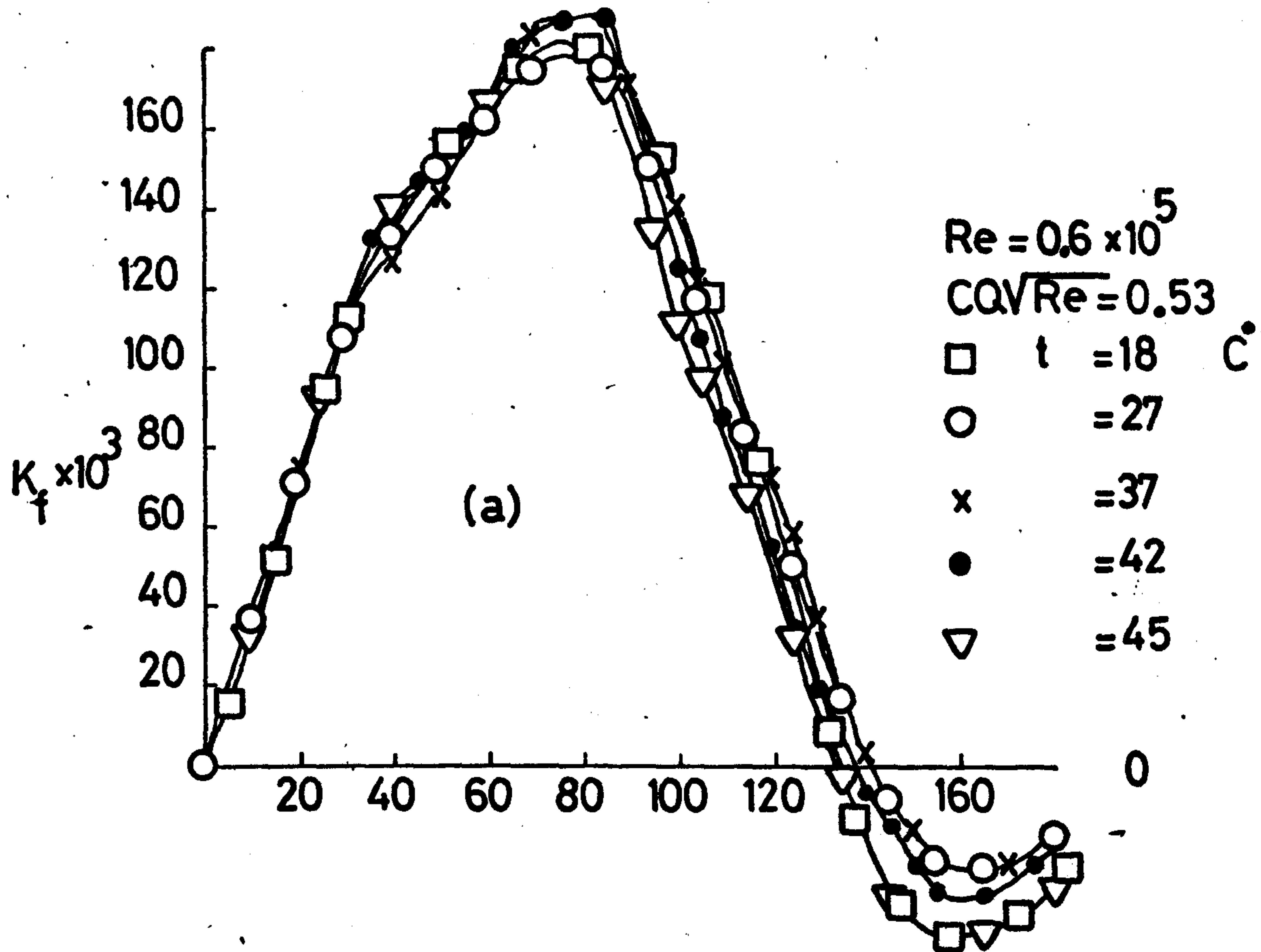
**Fig. 9.50**

Average HTC around fourth row in the bank.



Effect of main stream temperature,  
fifth row in the bank

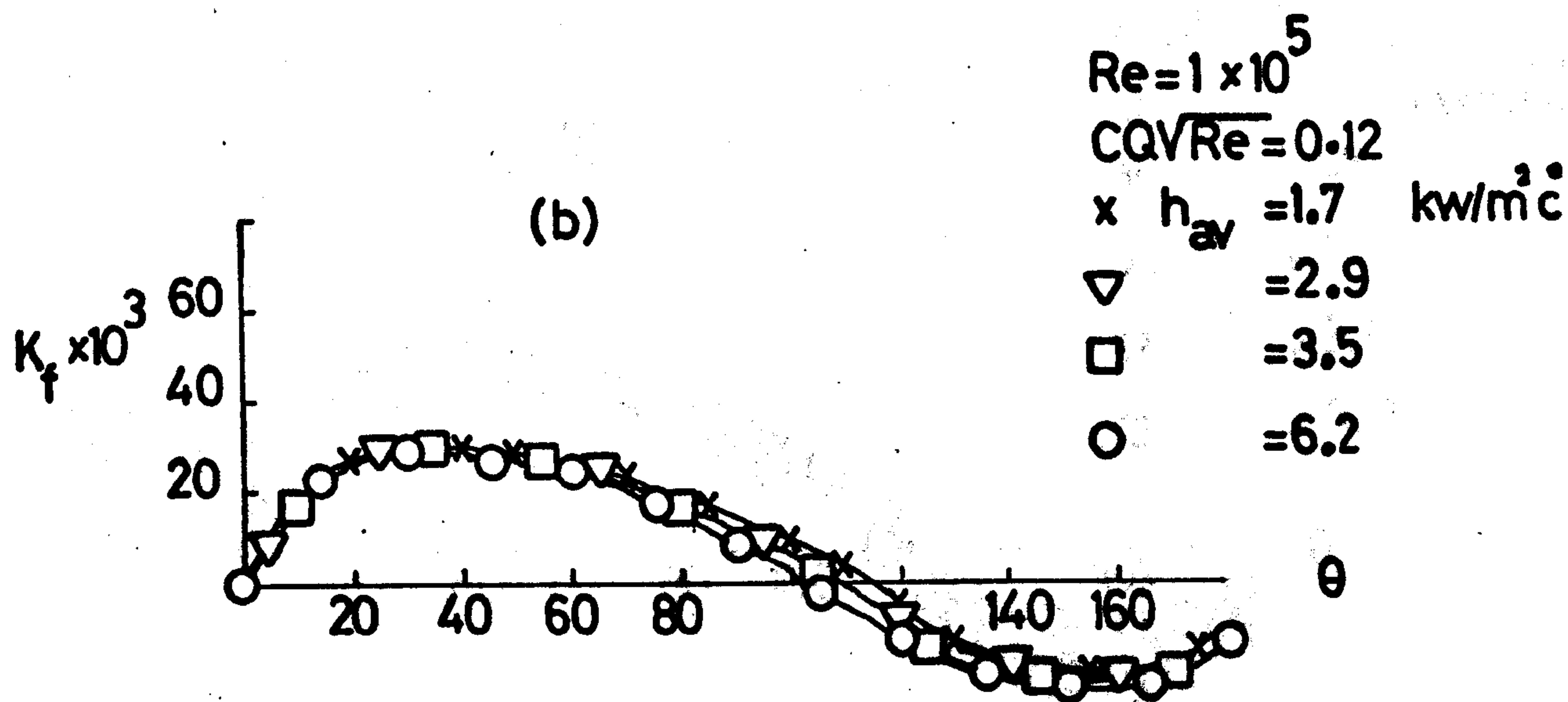
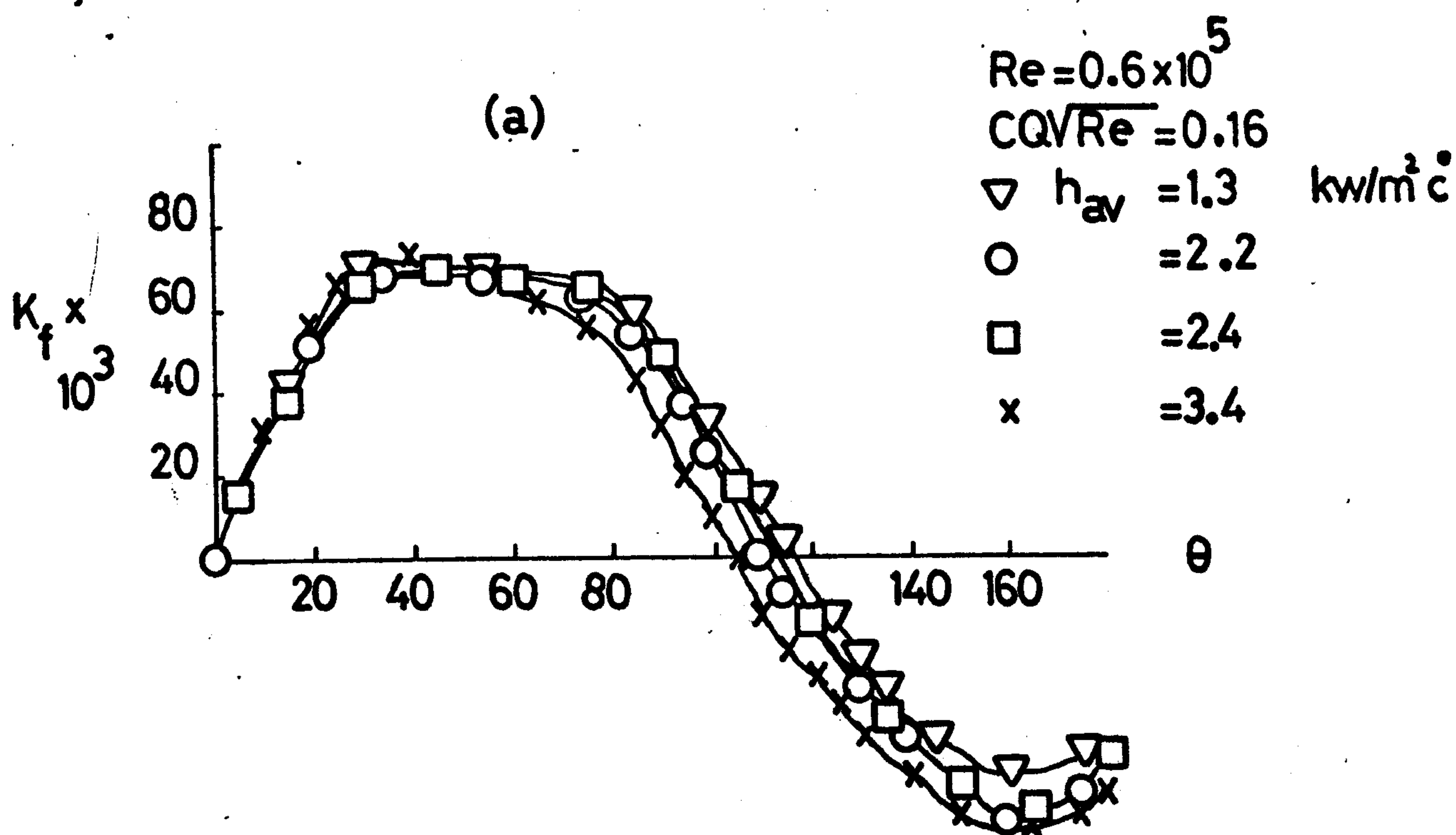
Fig. 9.51



Shear stress with mass transfer for different main stream temp, fifth row in the bank

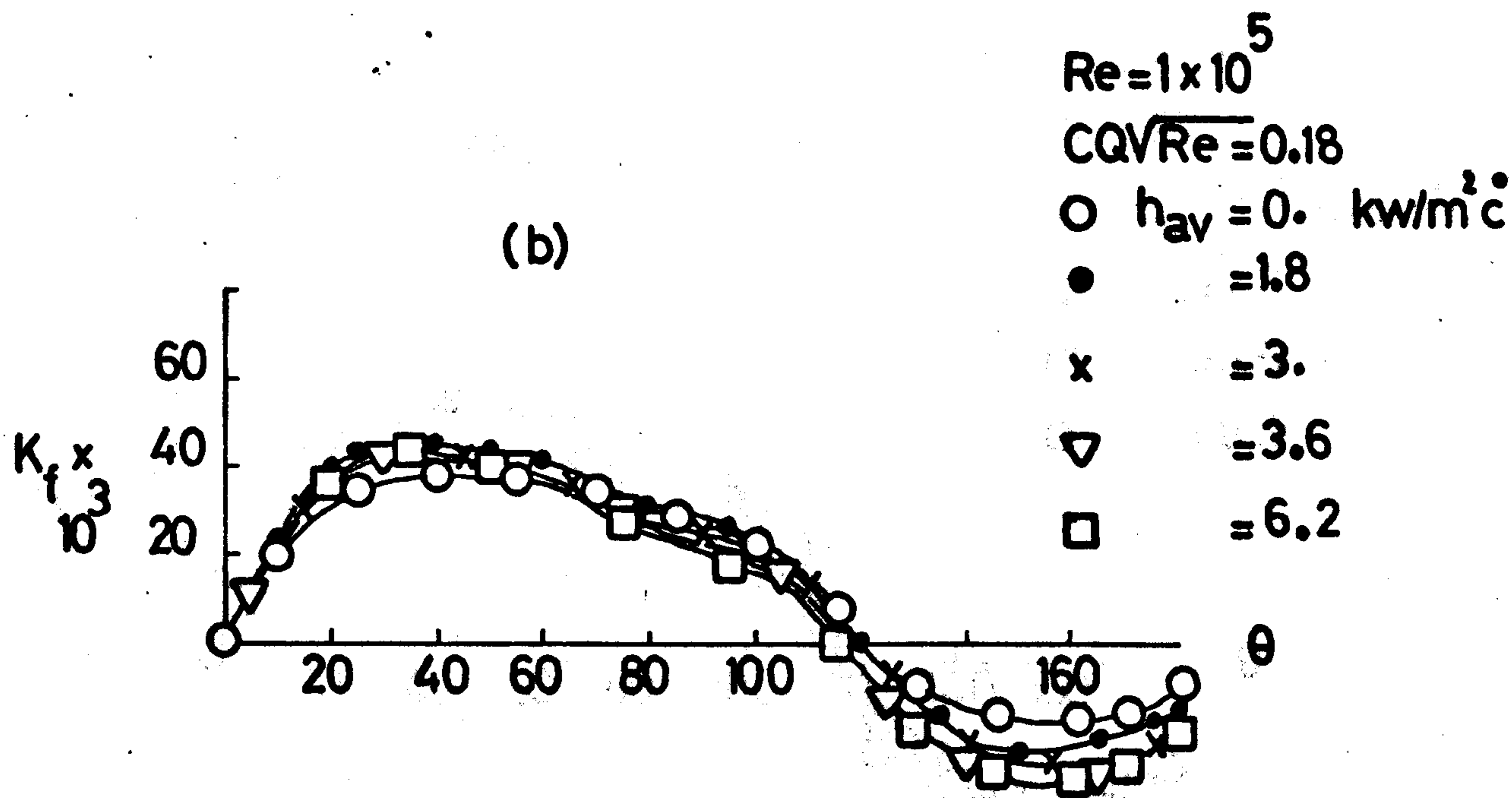
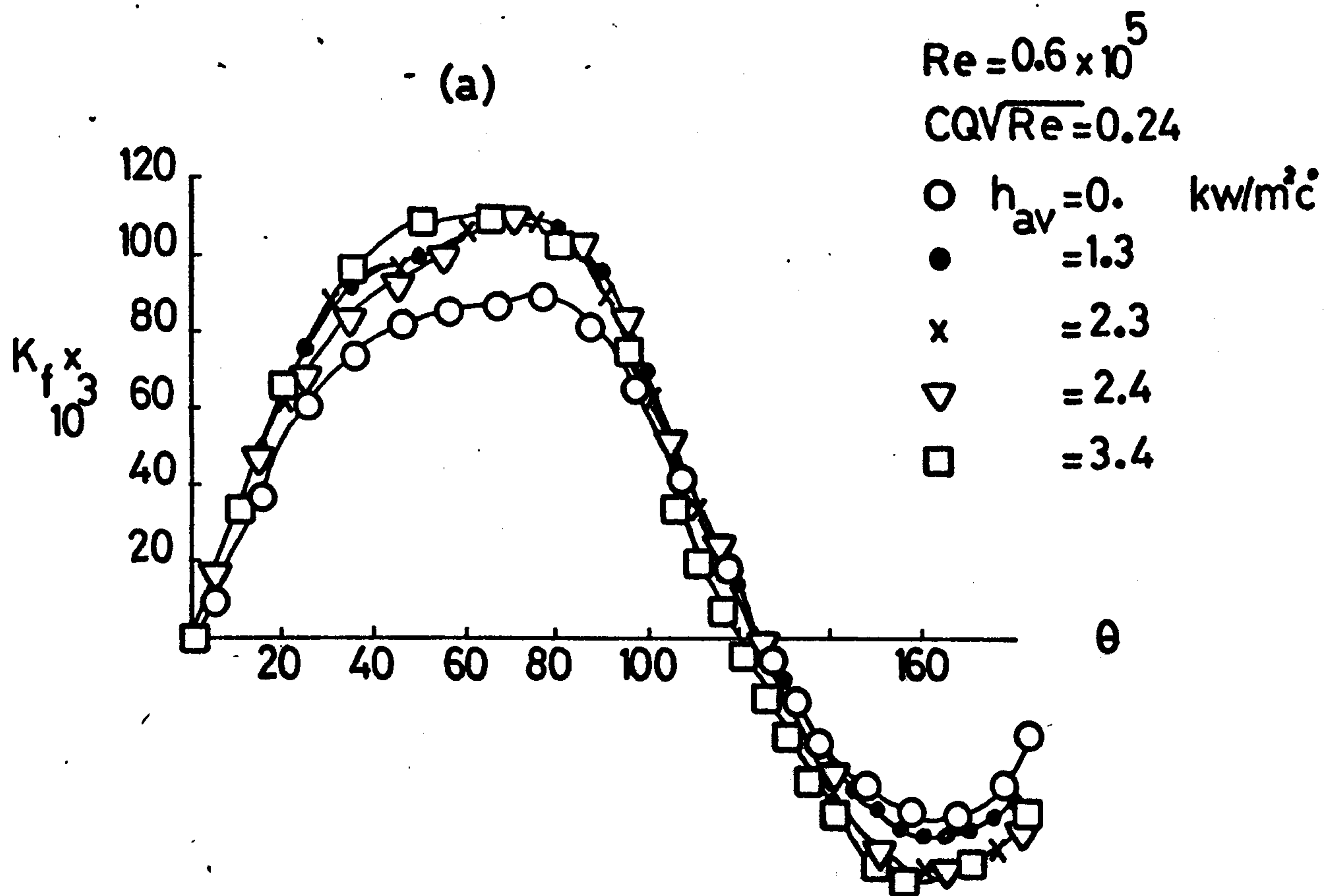
Fig. 9.52





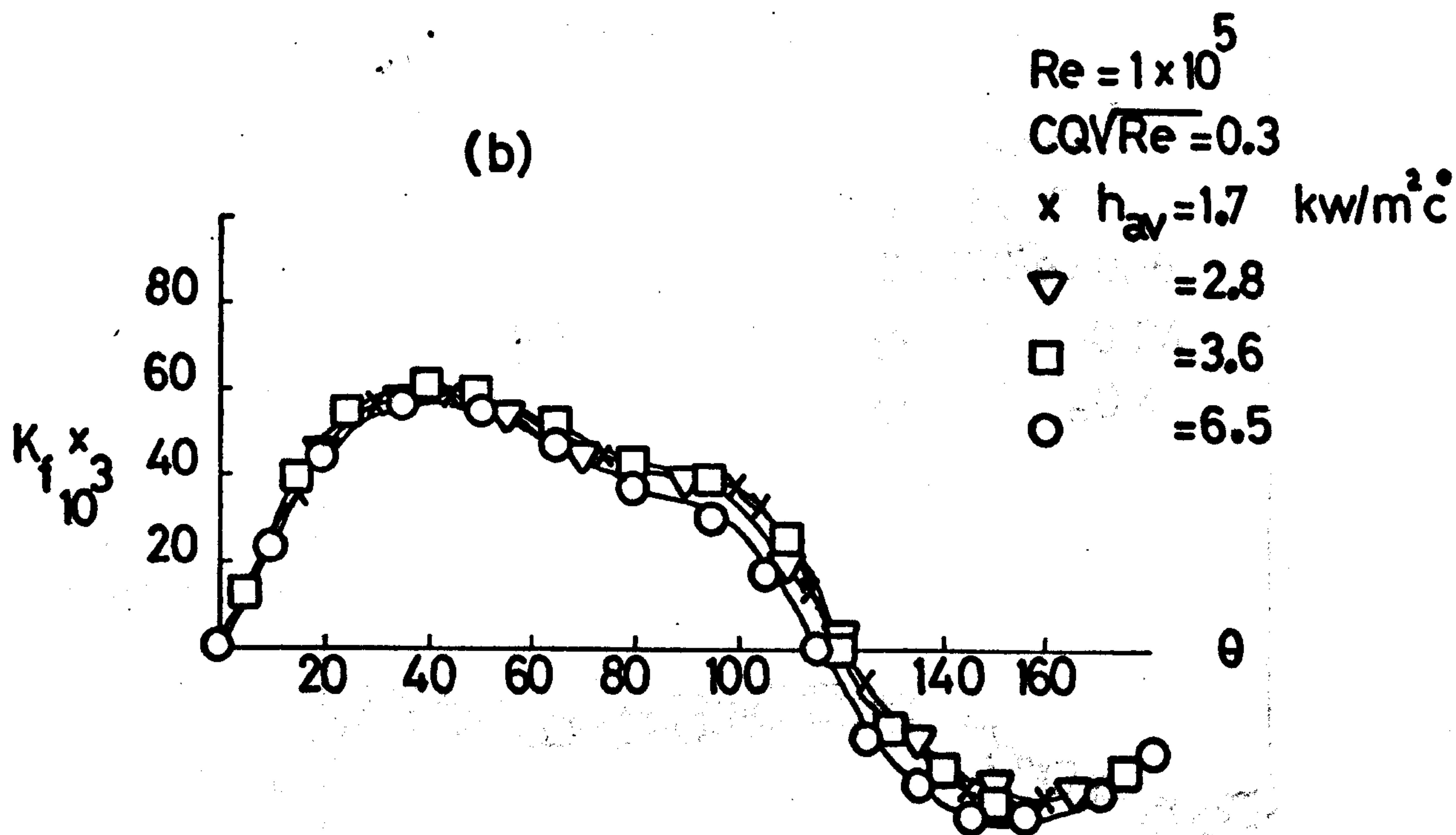
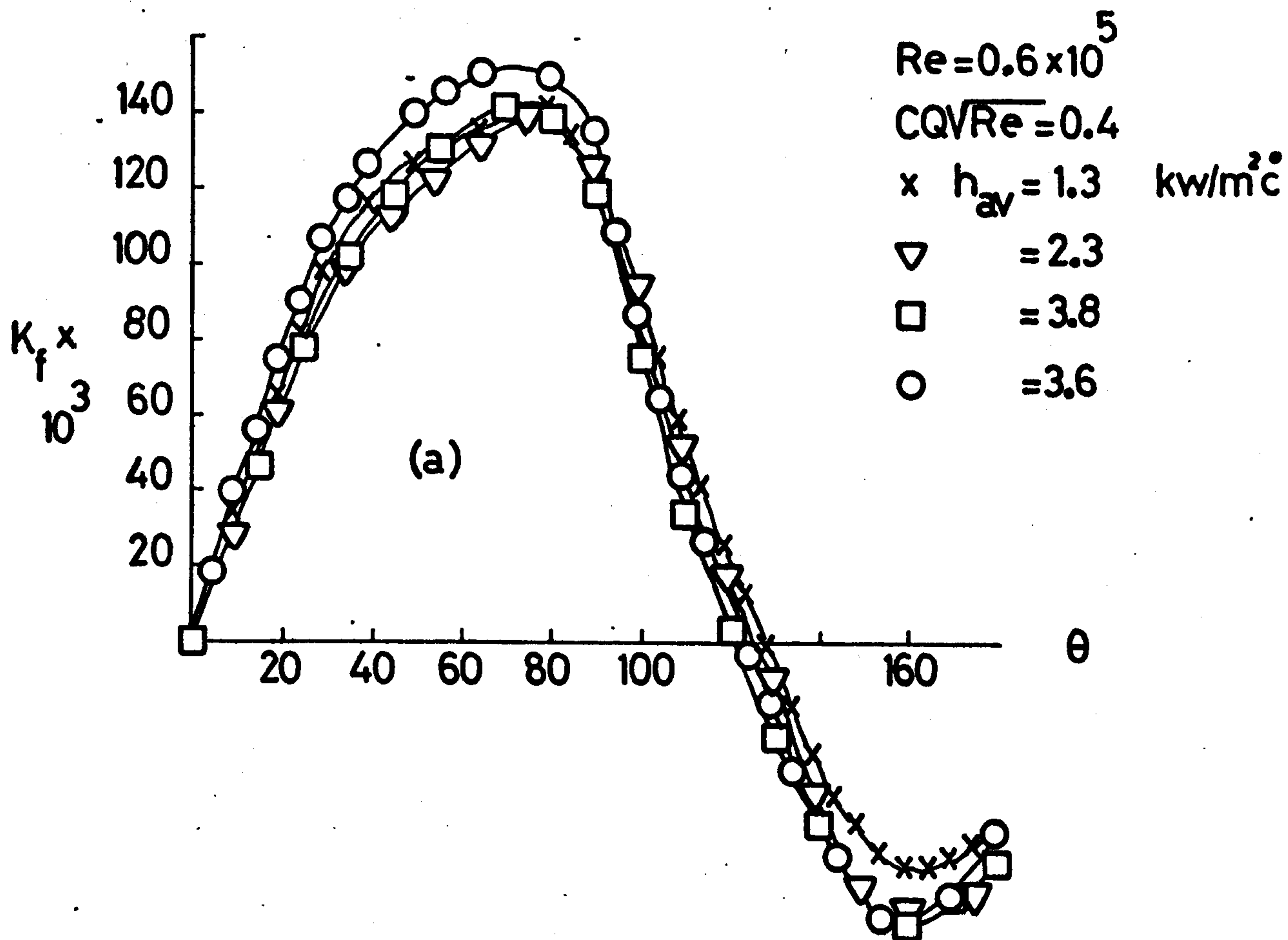
Shear stress with heat and mass transfer,  
fifth row in the bank

Fig. 9.53



Shear stress with heat and mass transfer,  
fifth row in the bank

Fig. 9.54



**Fig. 9.55**  
Shear stress with heat and mass transfer,  
fifth row in the bank



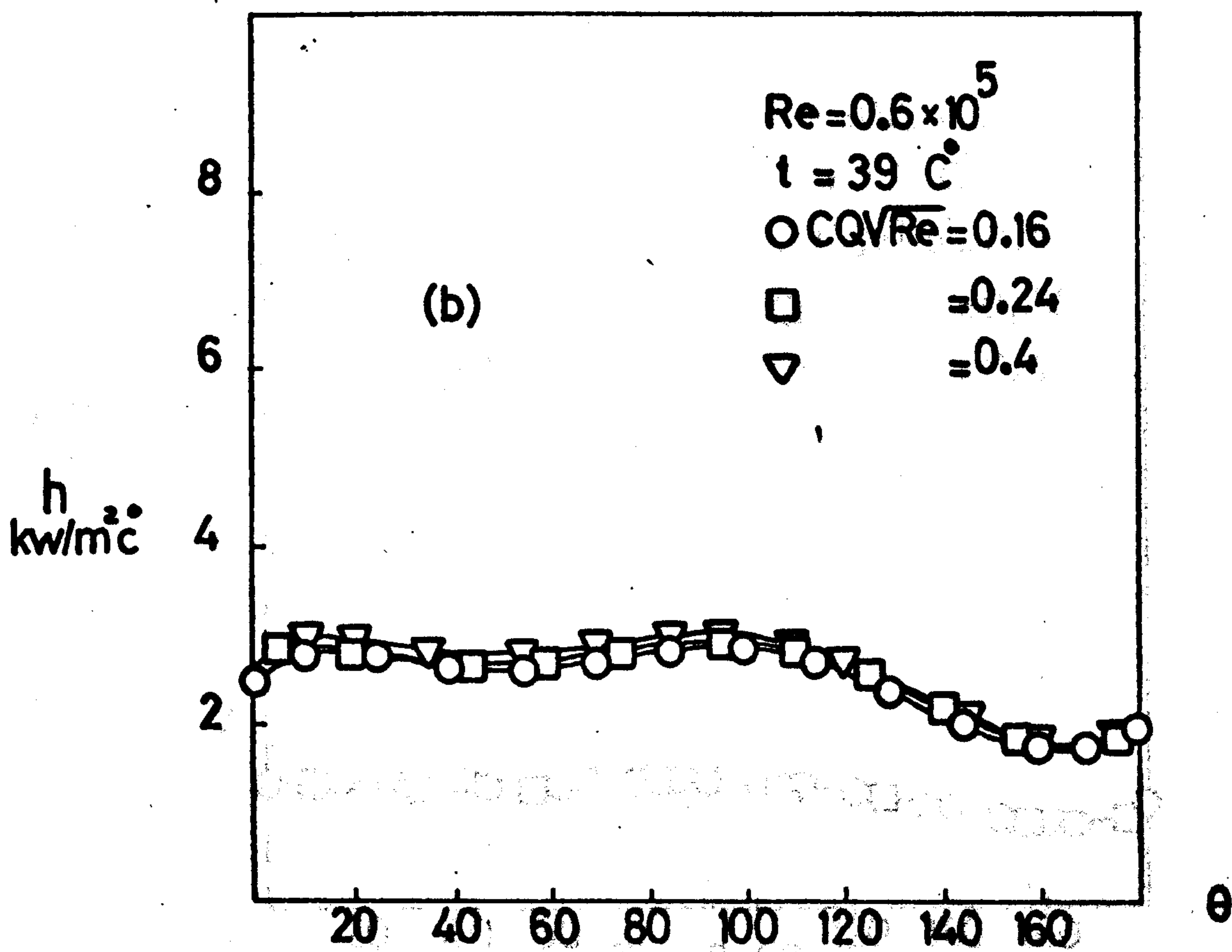
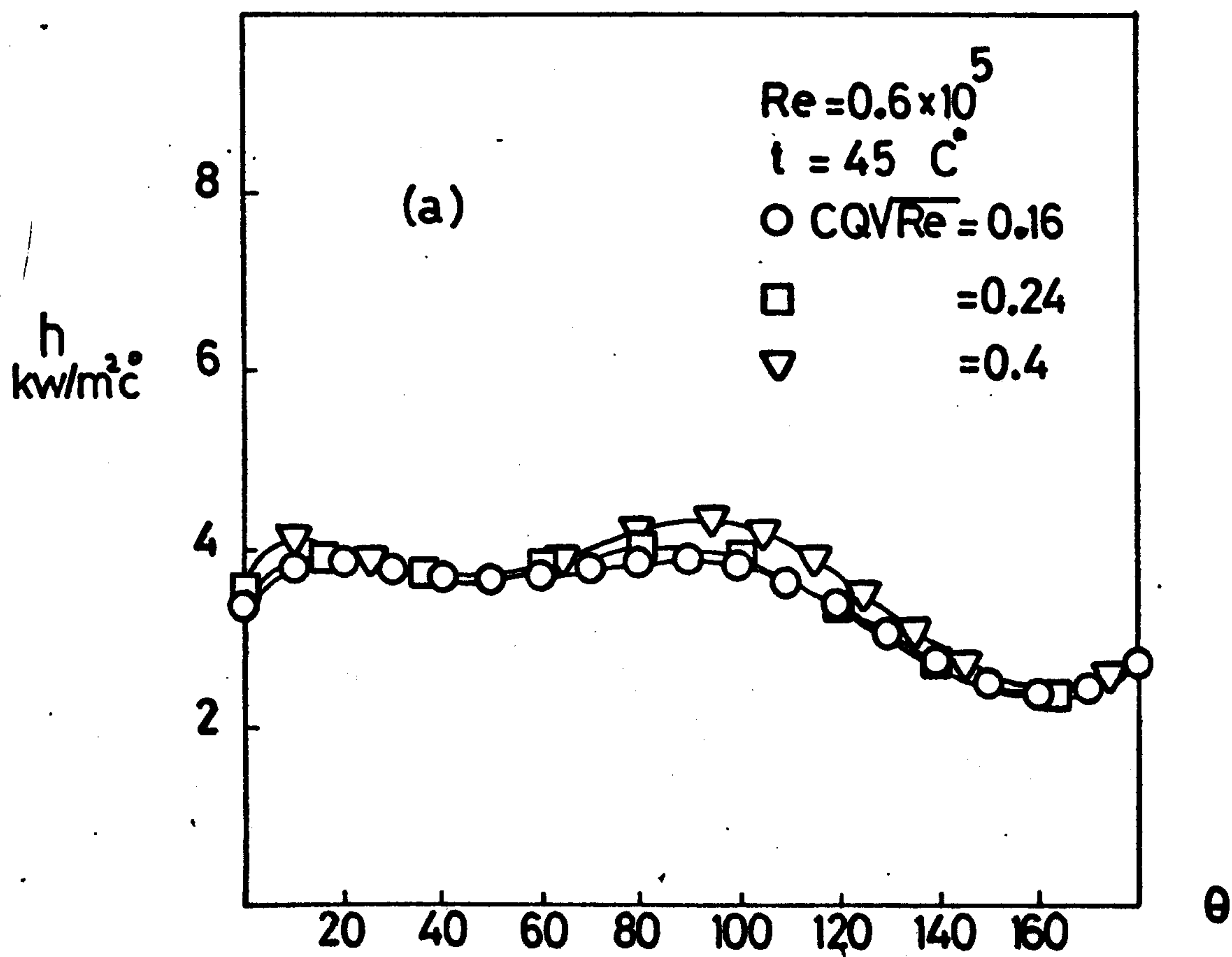
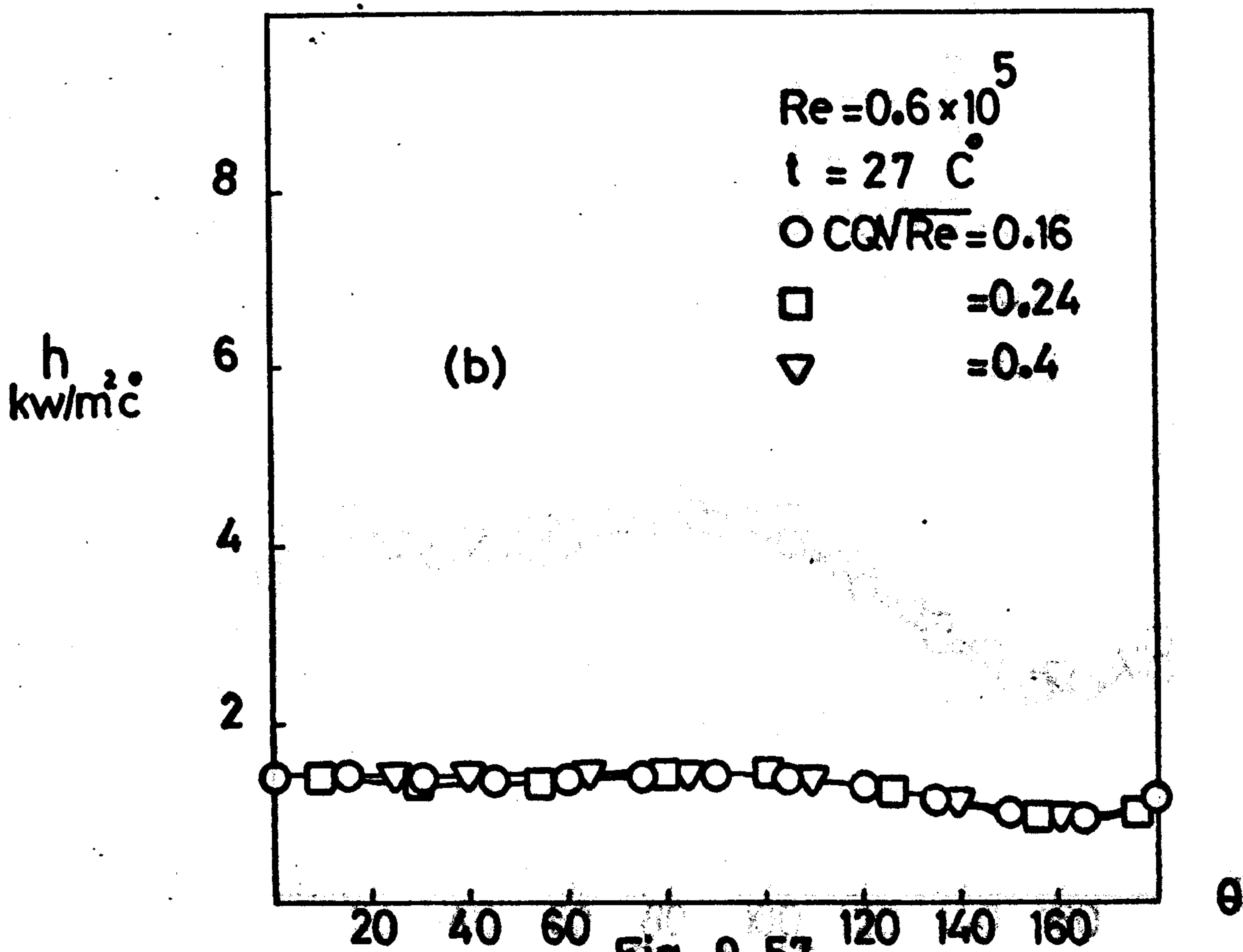
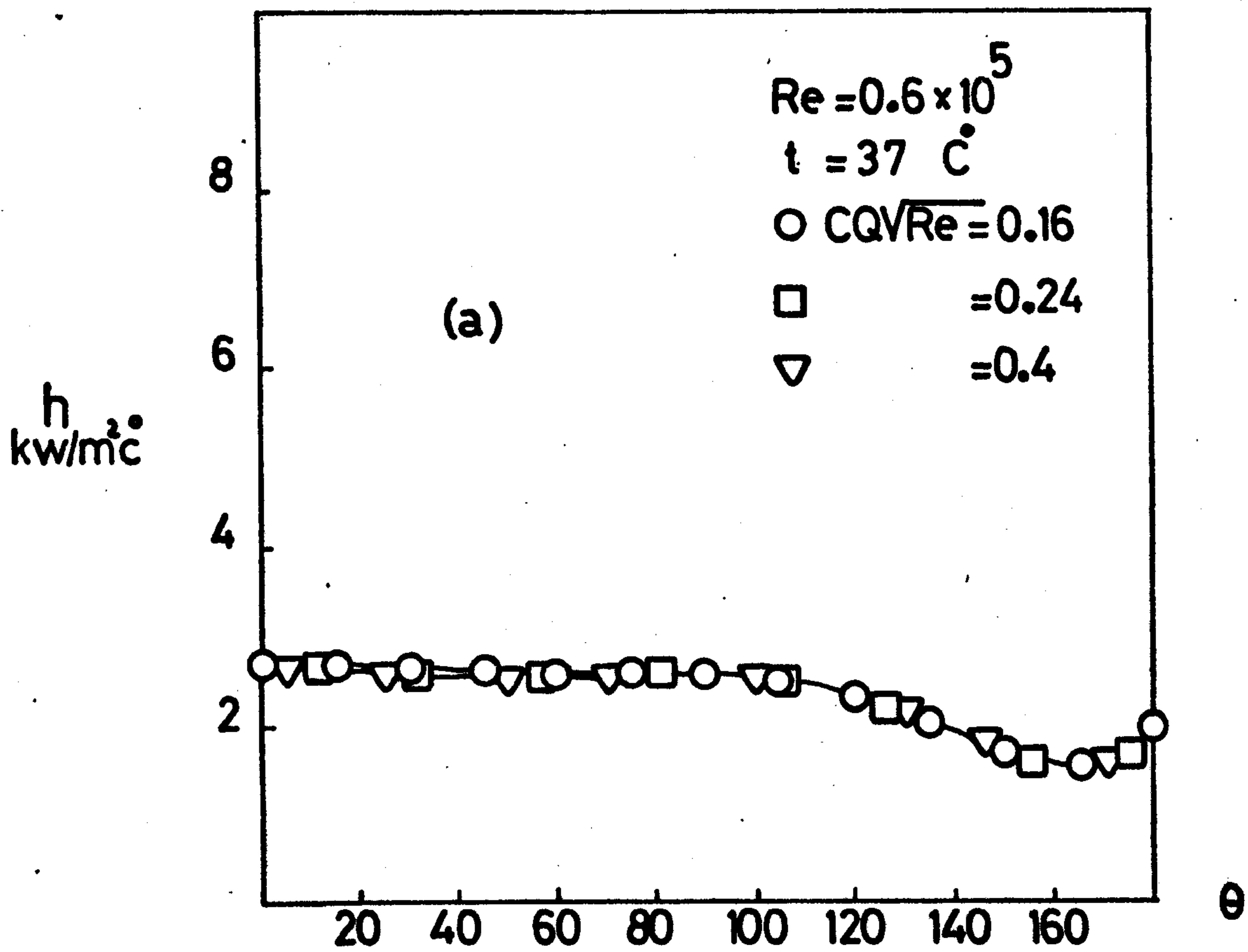
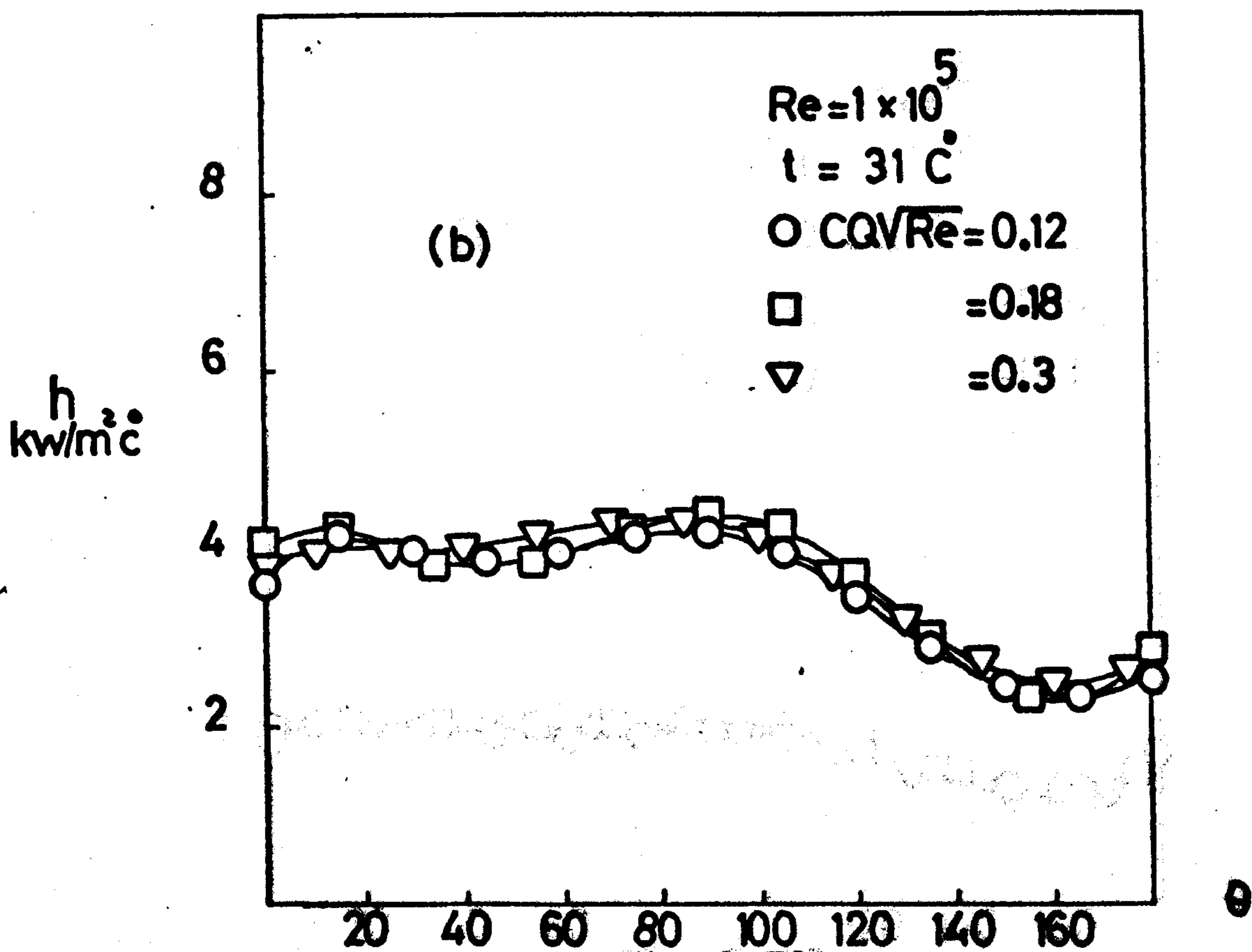
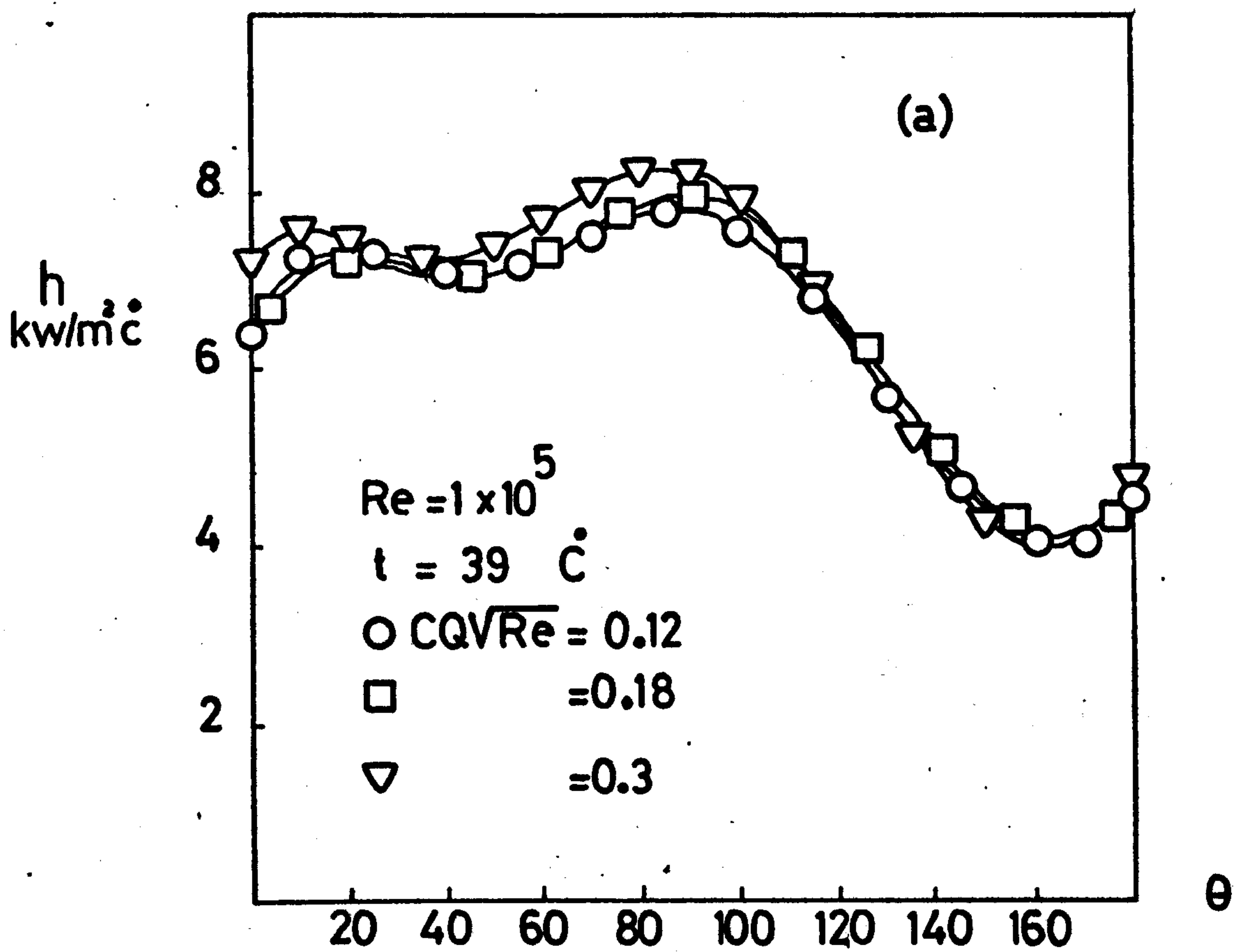


Fig. 9.56  
Heat transfer with mass transfer,  
fifth row in the bank



**Fig. 9.57**  
Heat transfer with suction, fifth row in the bank



**Fig. 9.58**  
Heat transfer with suction, fifth row in the bank



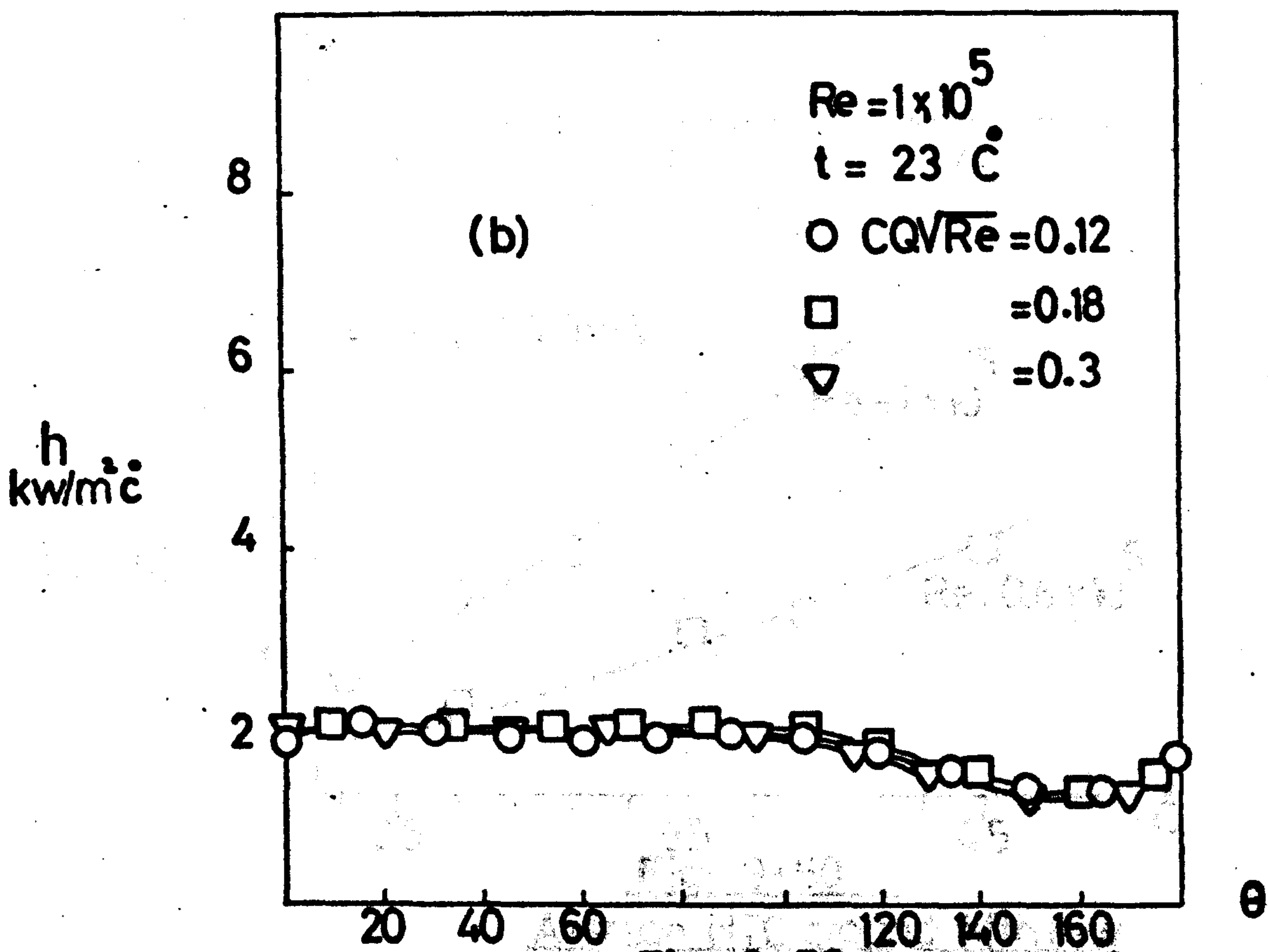
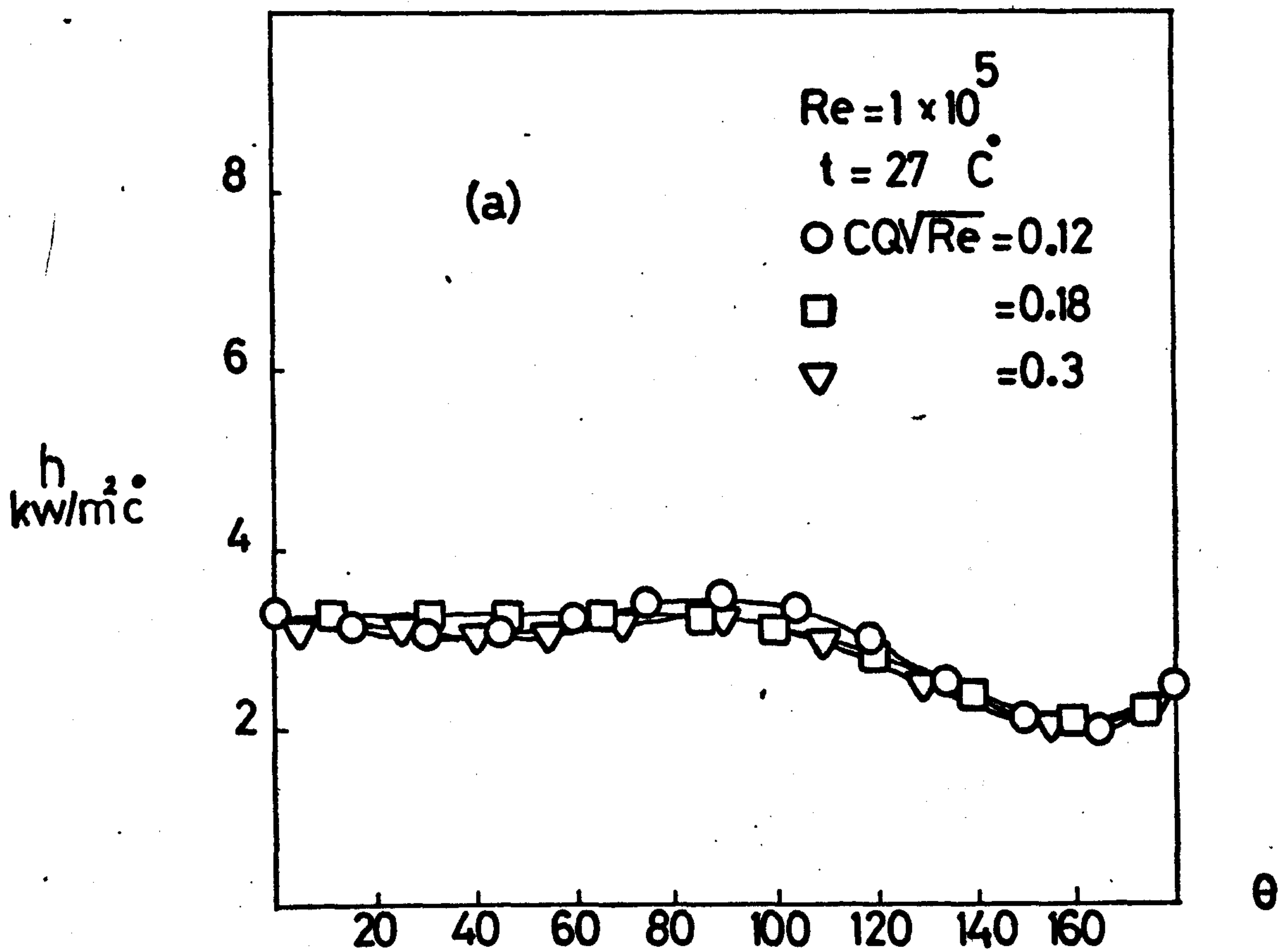


Fig. 9.59.  
Heat transfer with suction, fifth  
row in the bank

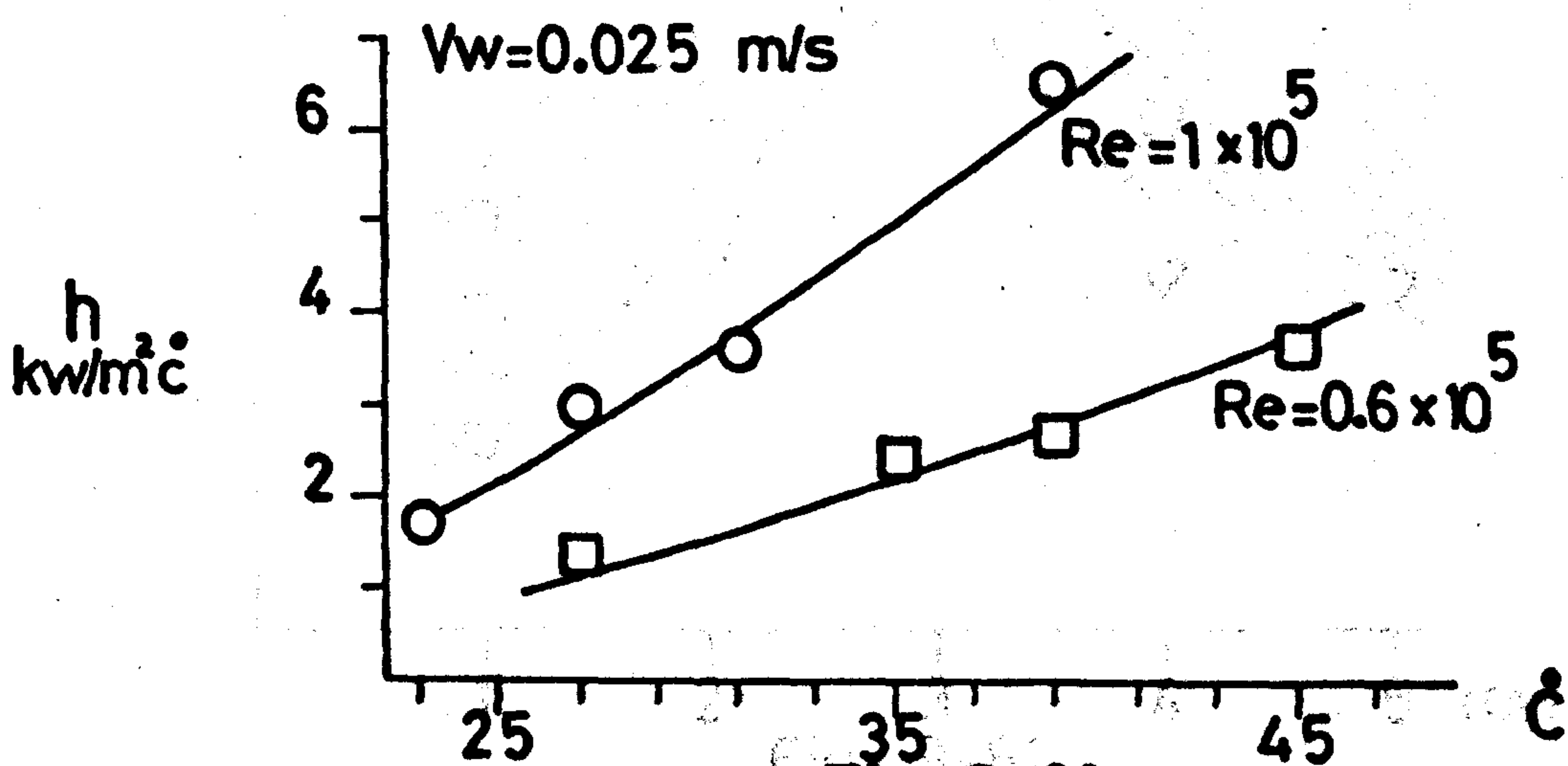
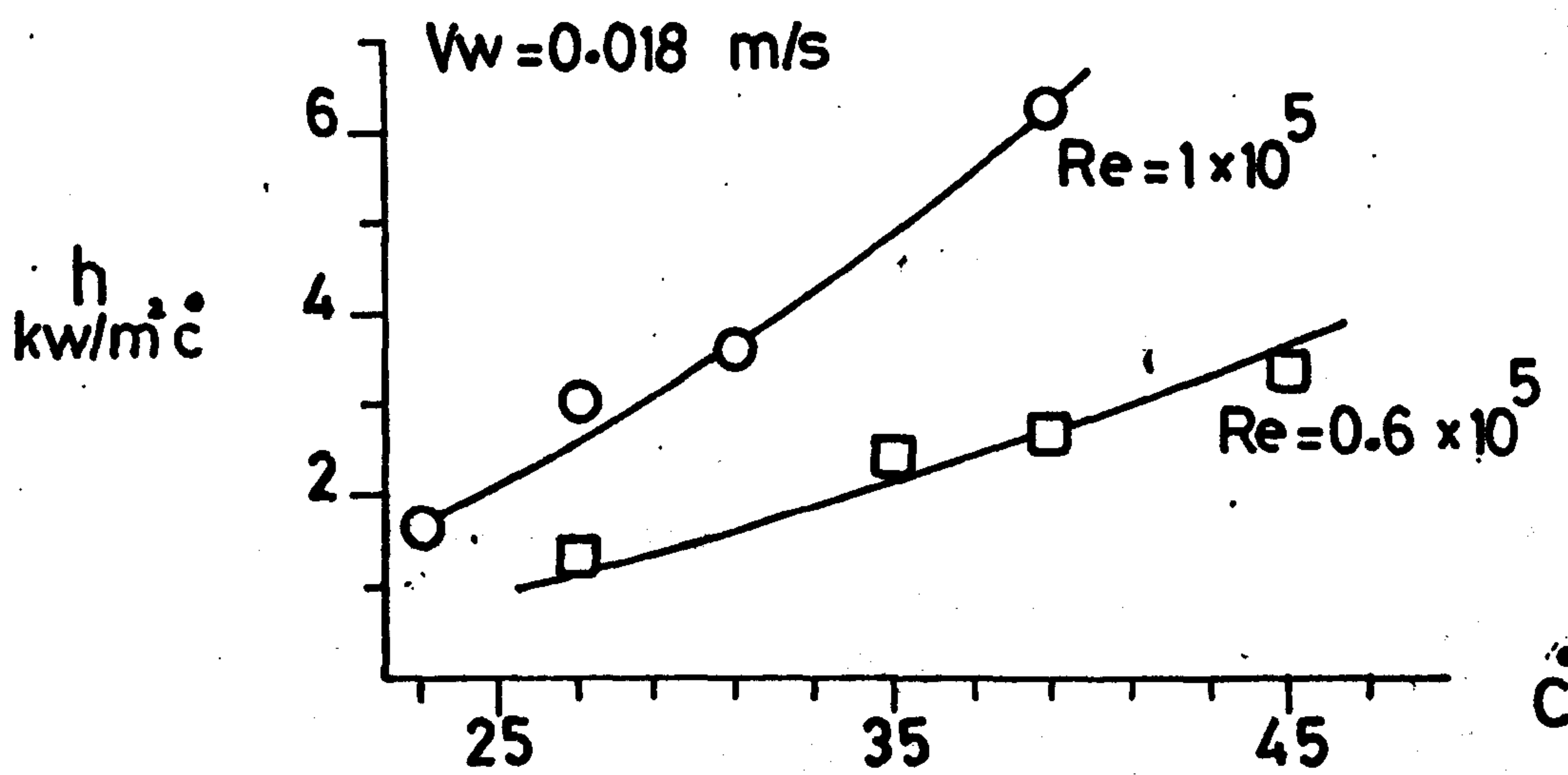
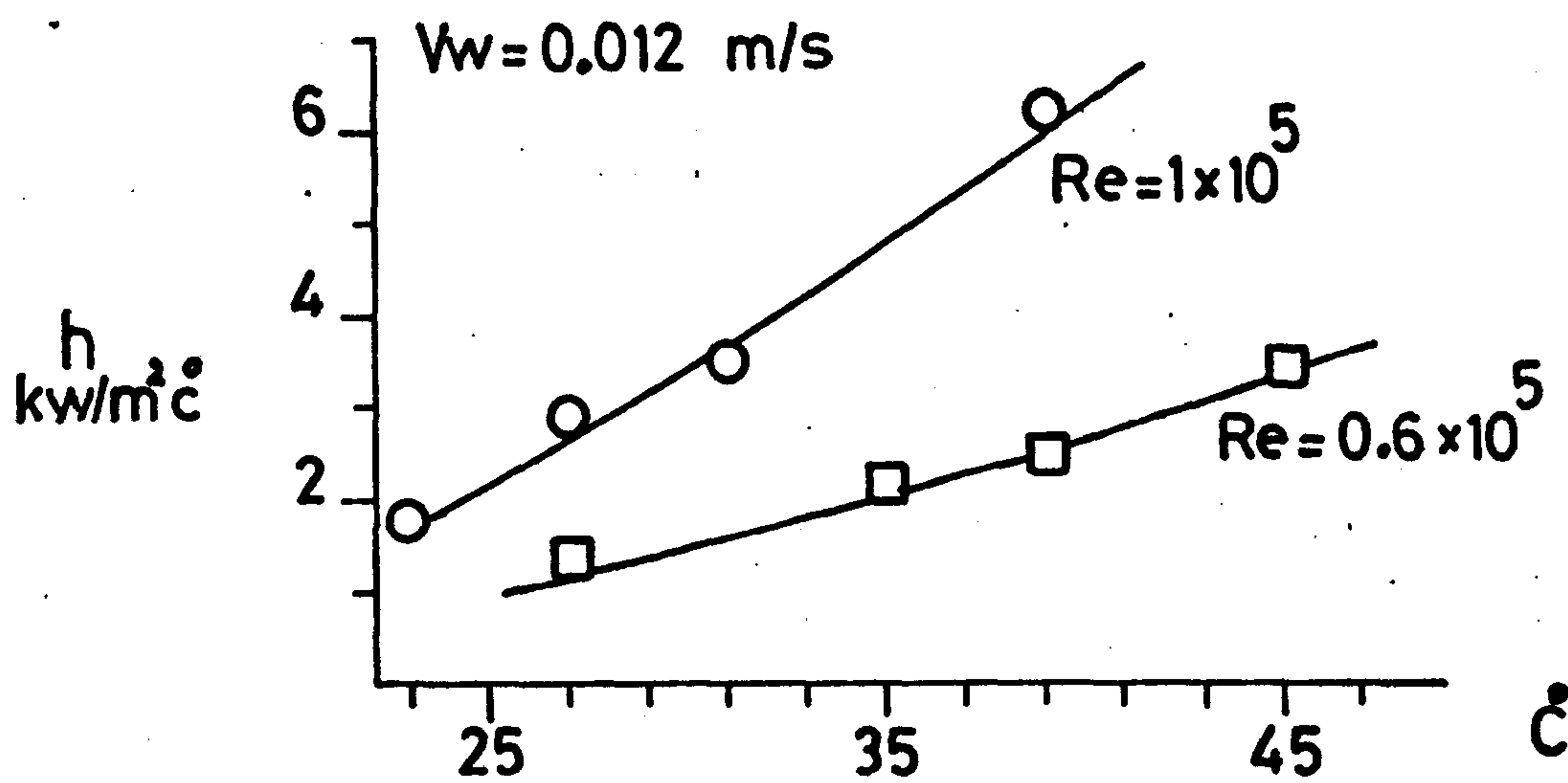


Fig. 9-60

Average HTC around fifth row  
in the bank

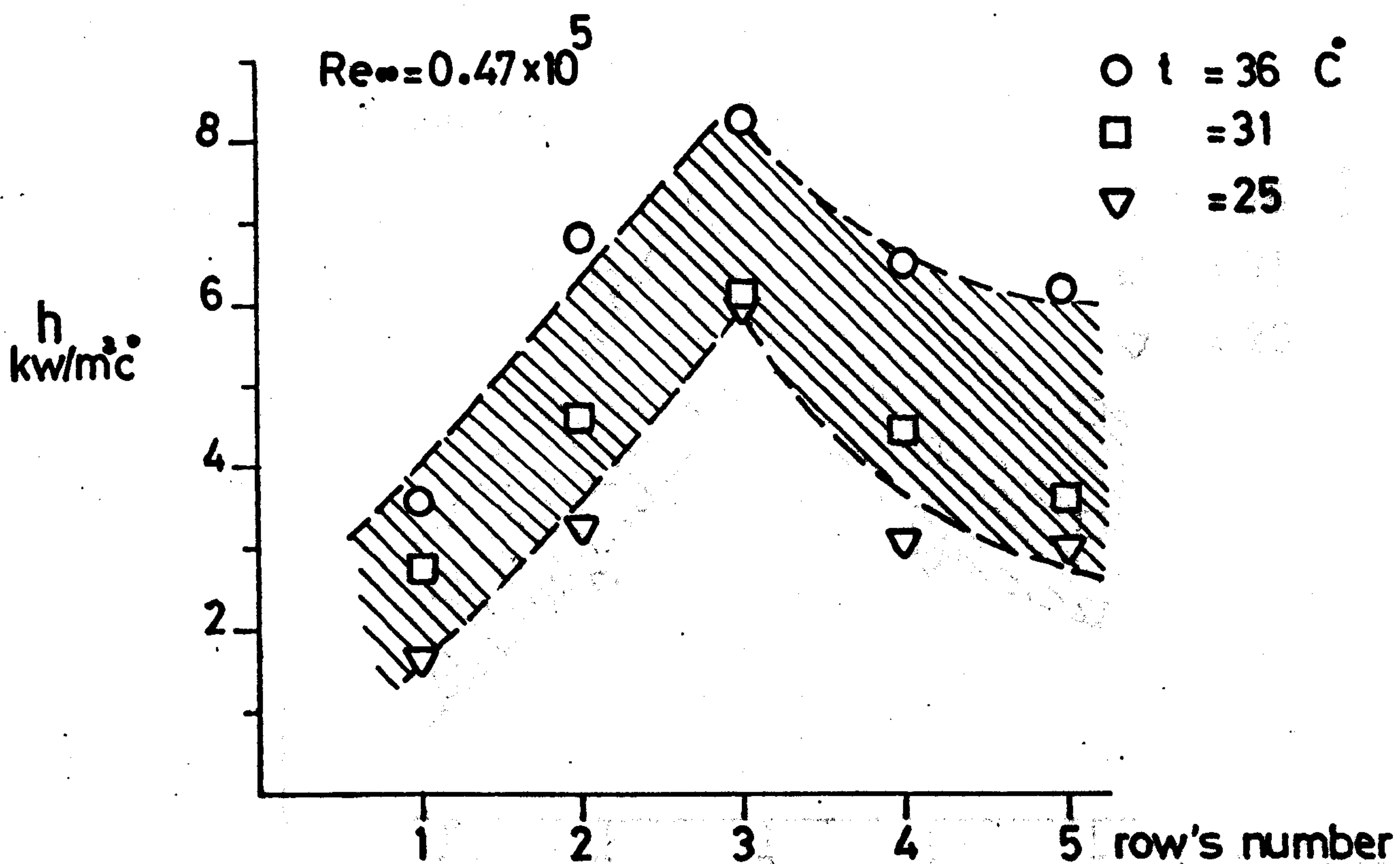
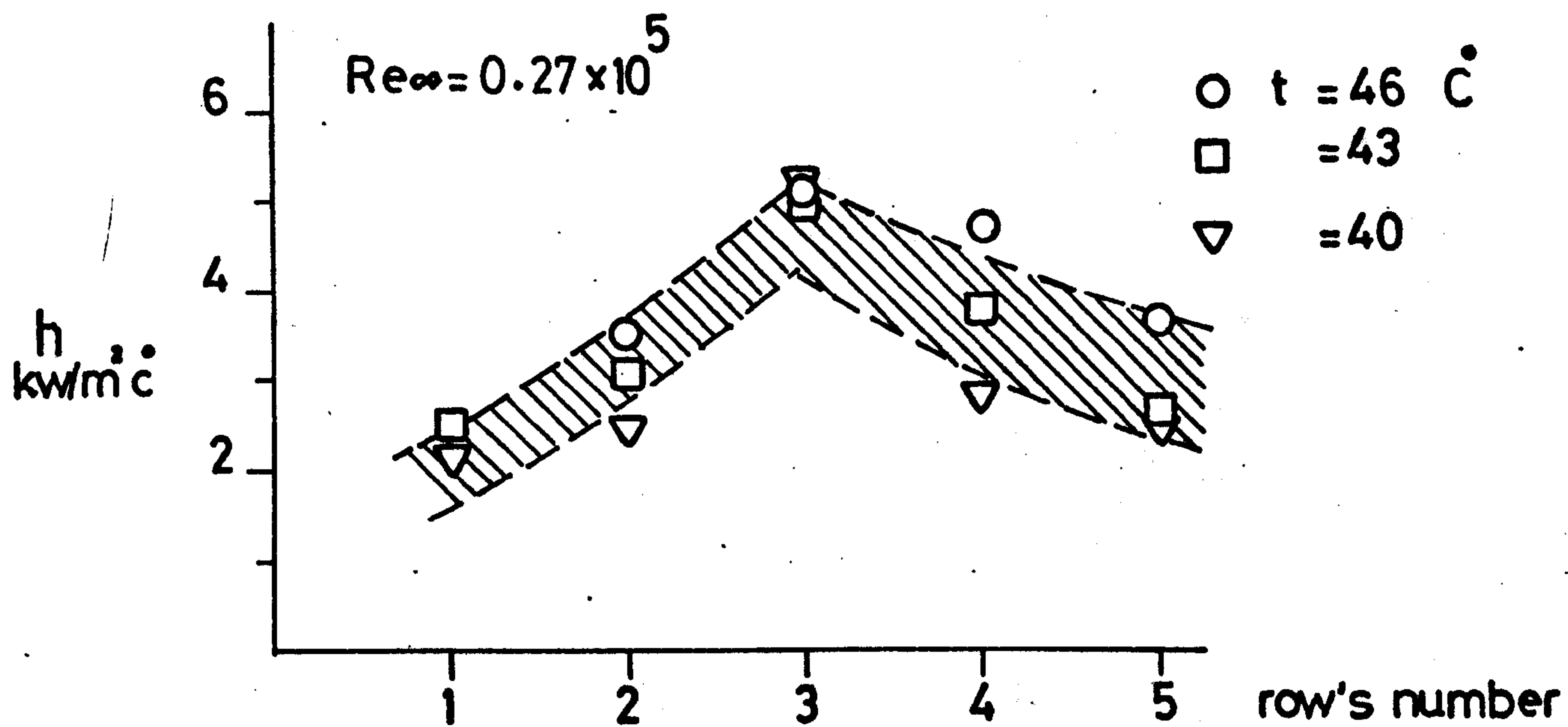


Fig. 9.61  
Heat transfer with tube position,  
 $V_w = 0.012$  m/s



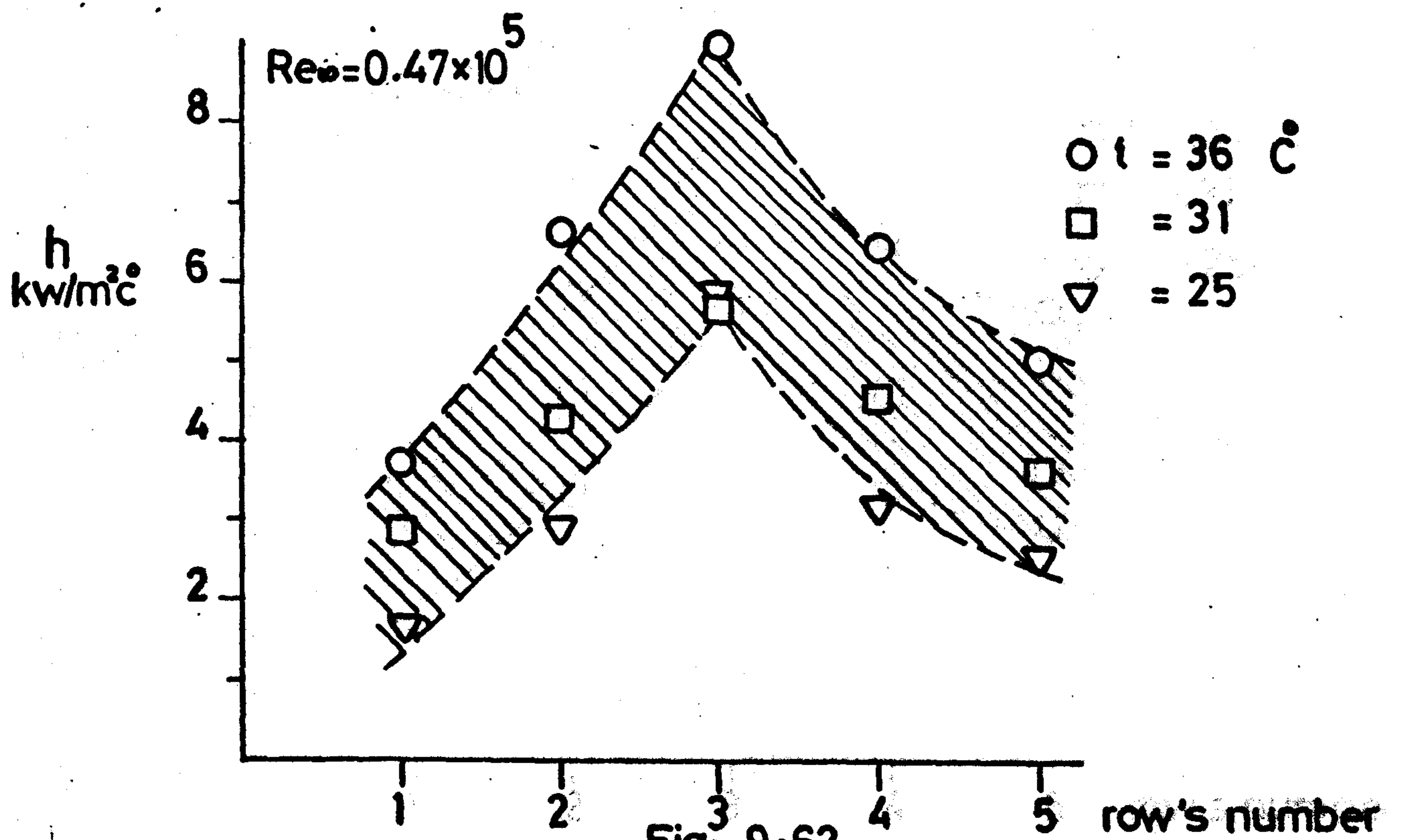
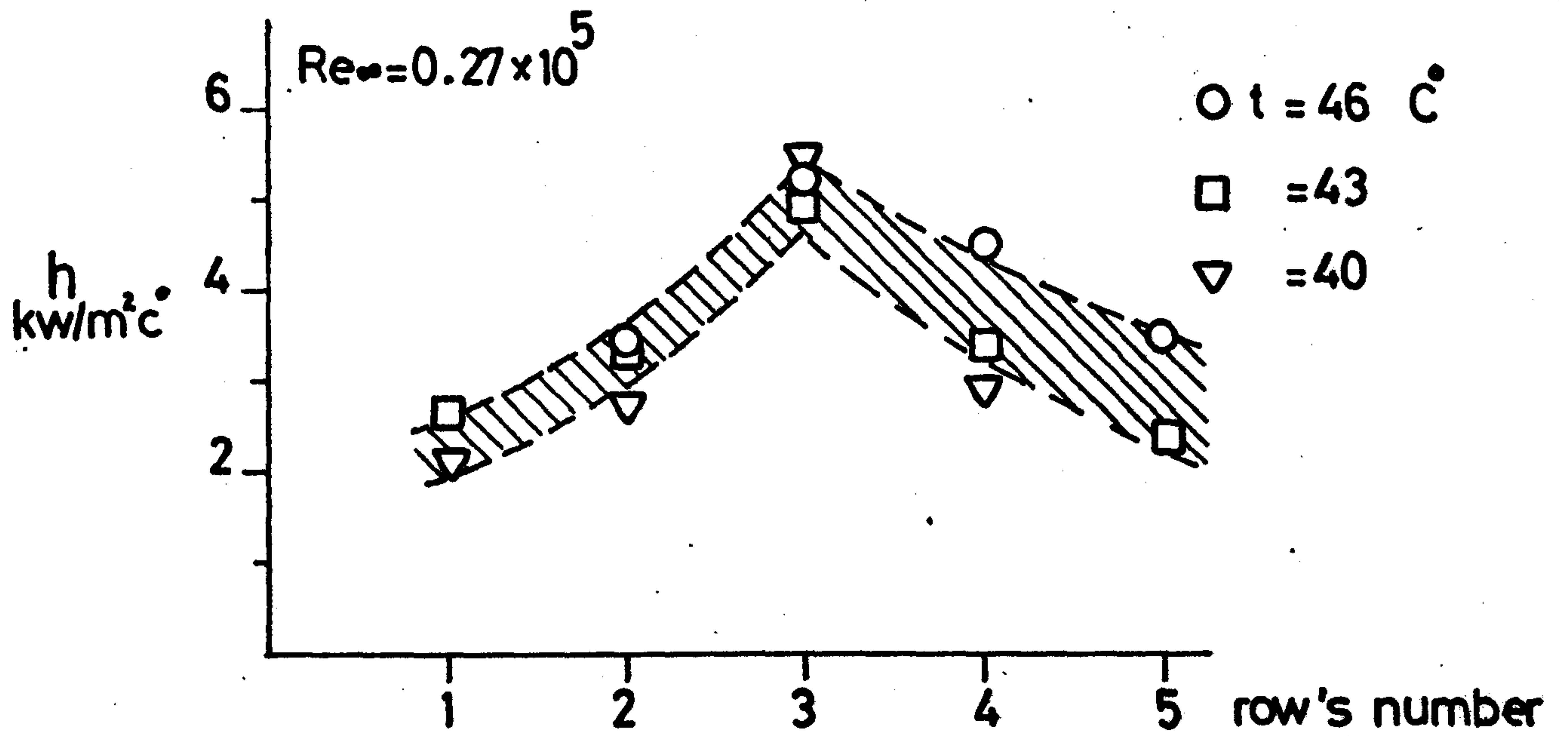
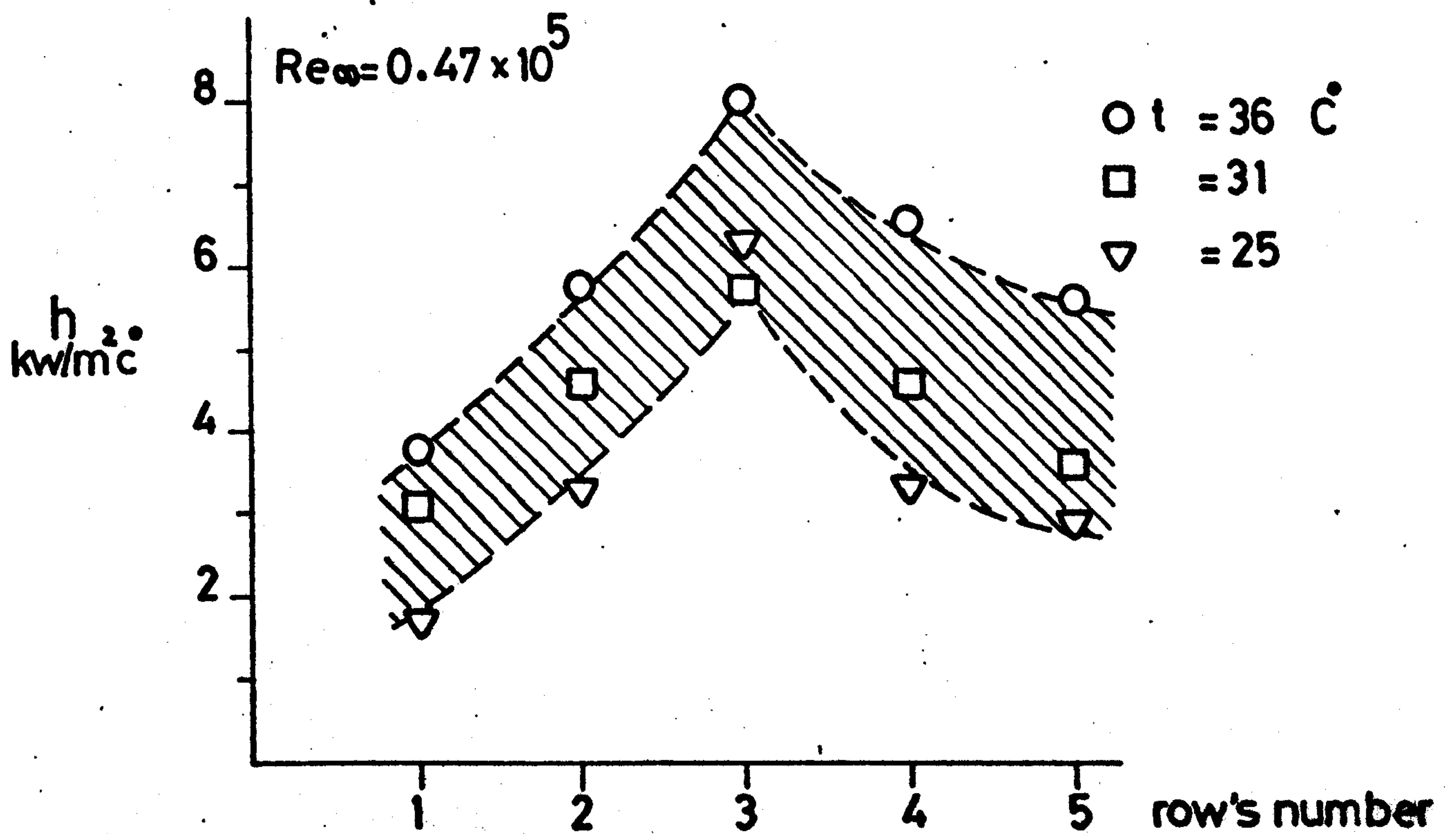
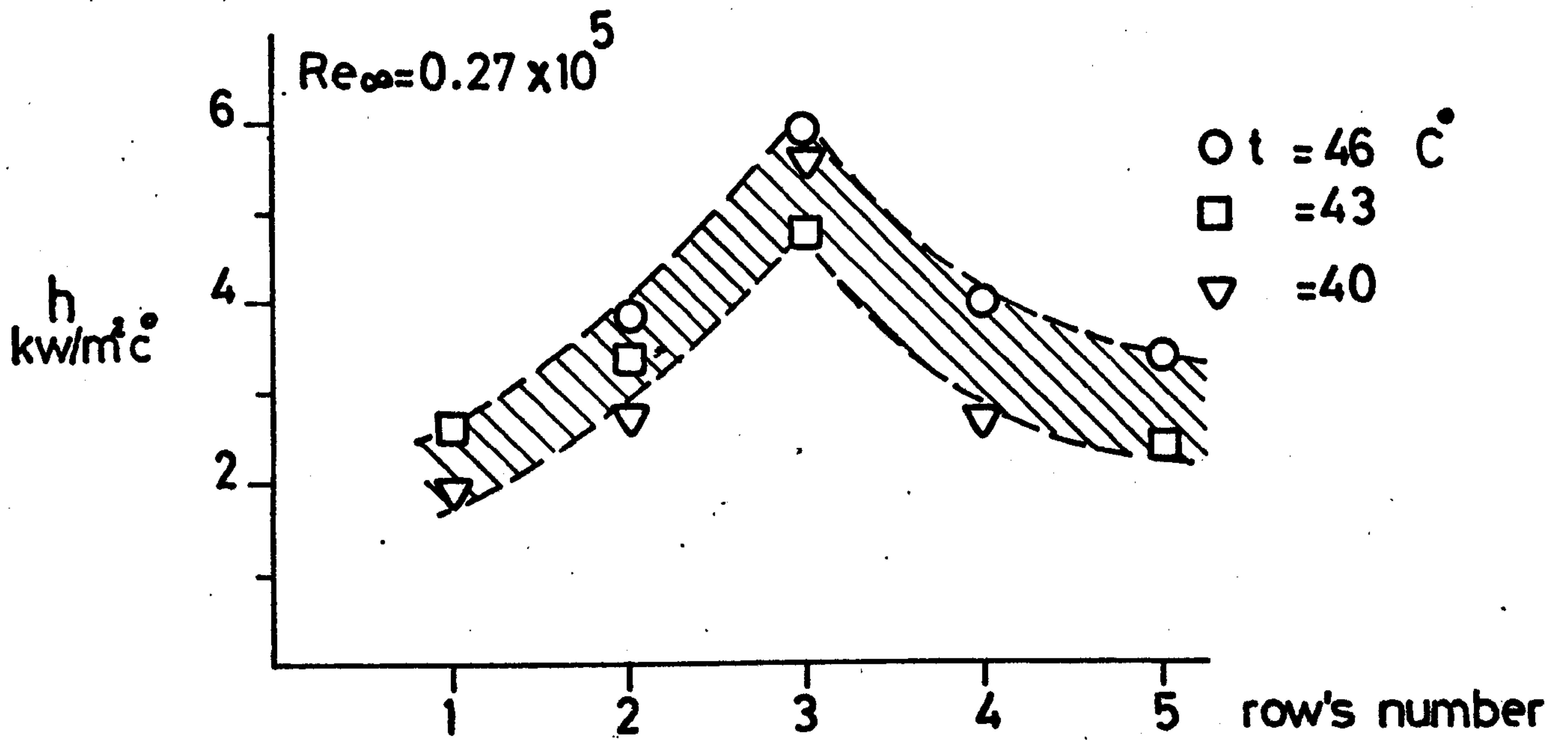


Fig. 9.62

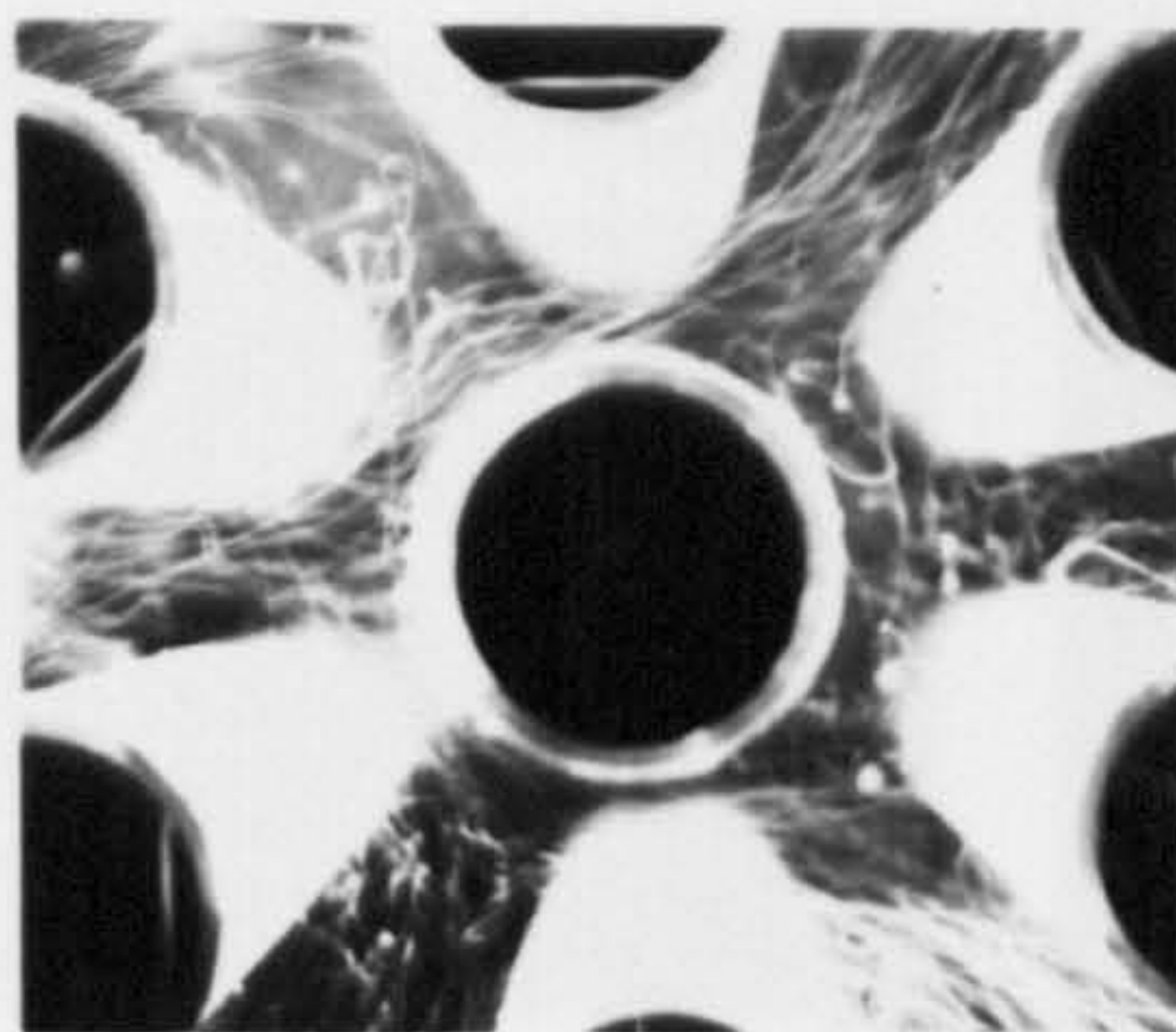
Heat transfer with tube position,

$V_w = 0.018$  m/s.

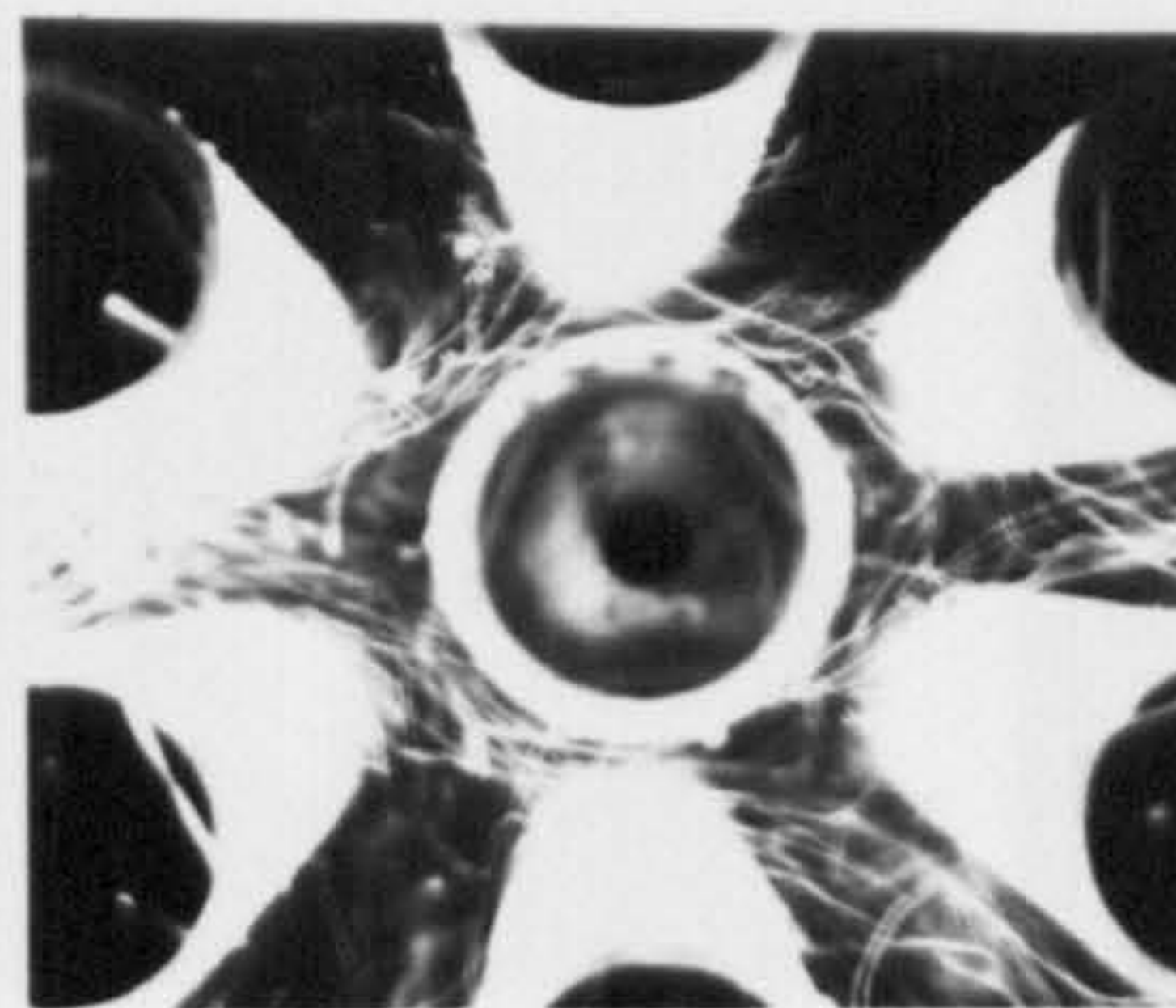


**Fig. 9.63**  
Heat transfer with tube position,  
 $V_w = 0.025$  m/s

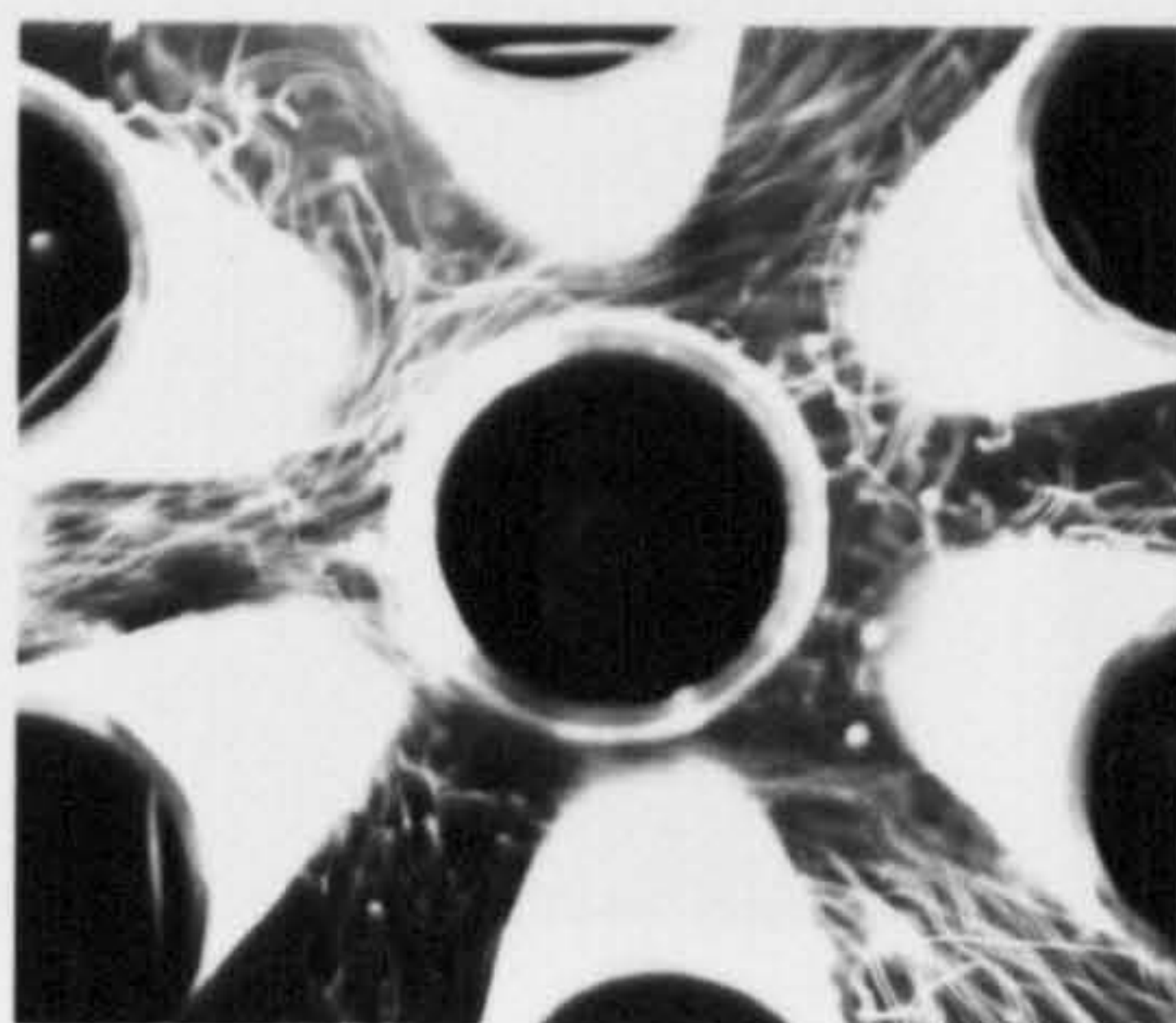




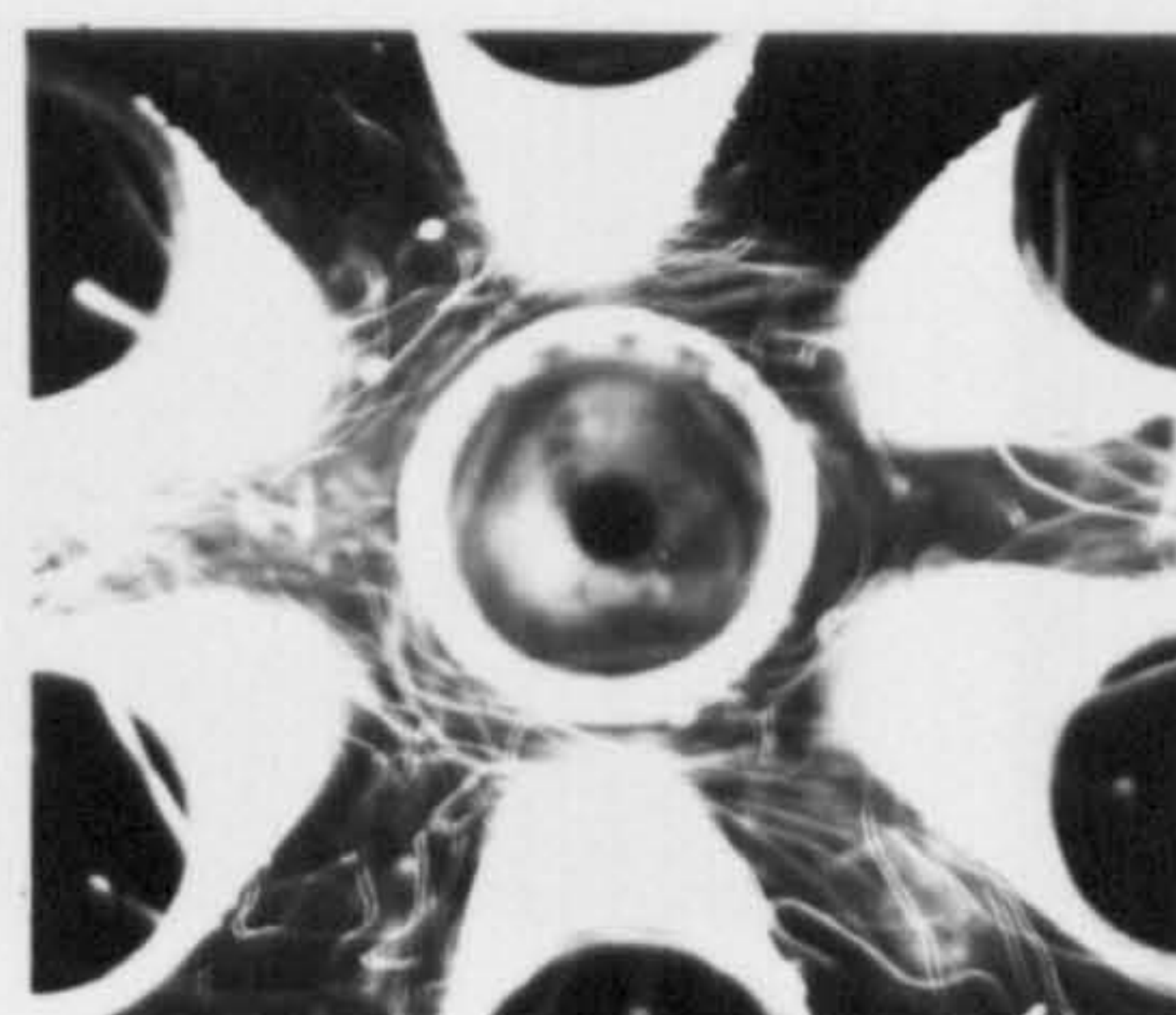
$Re=19500$  ,  $V_w/U = 0.0$



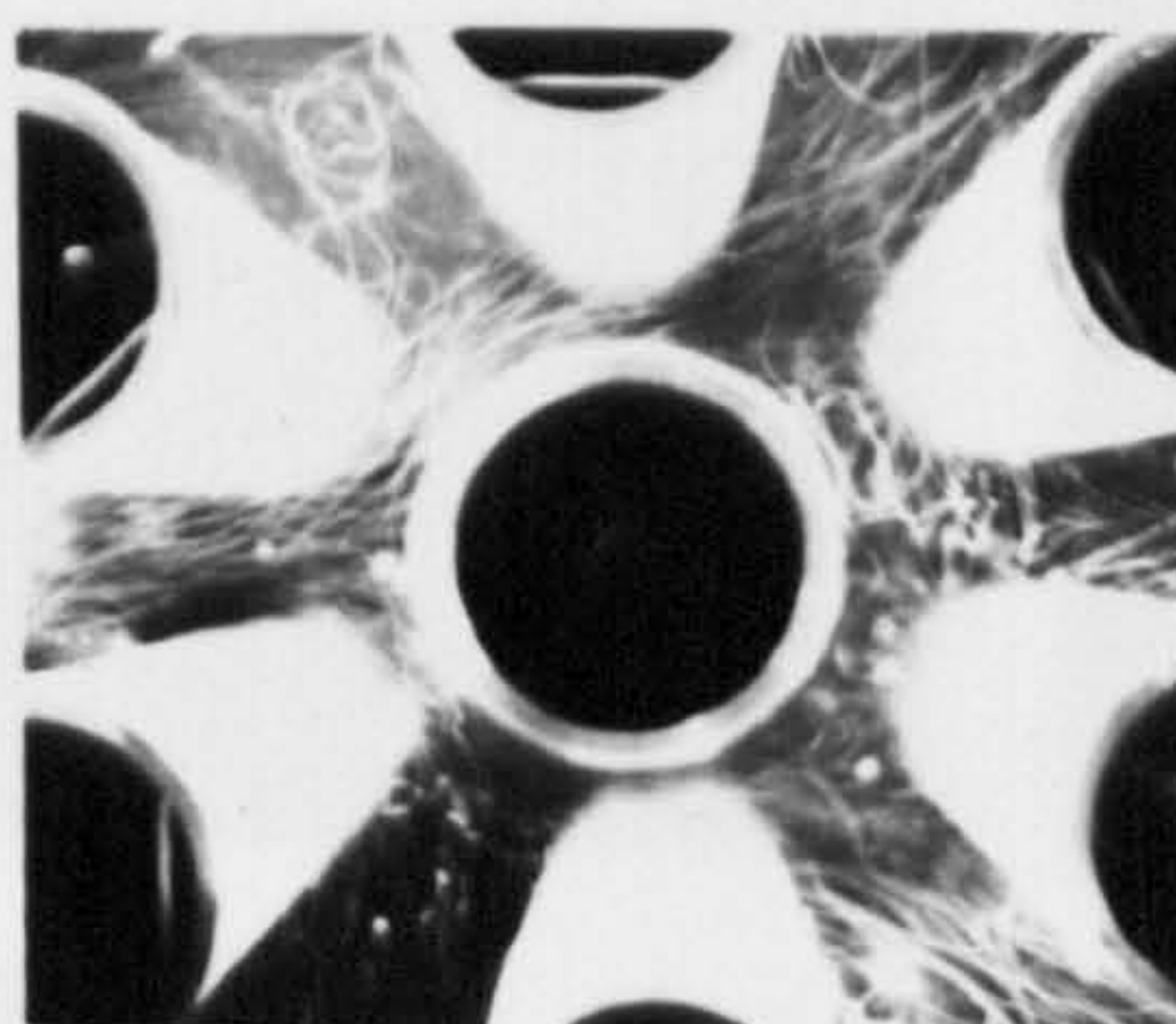
$Re=19500$  ,  $V_w/U = 0.017$



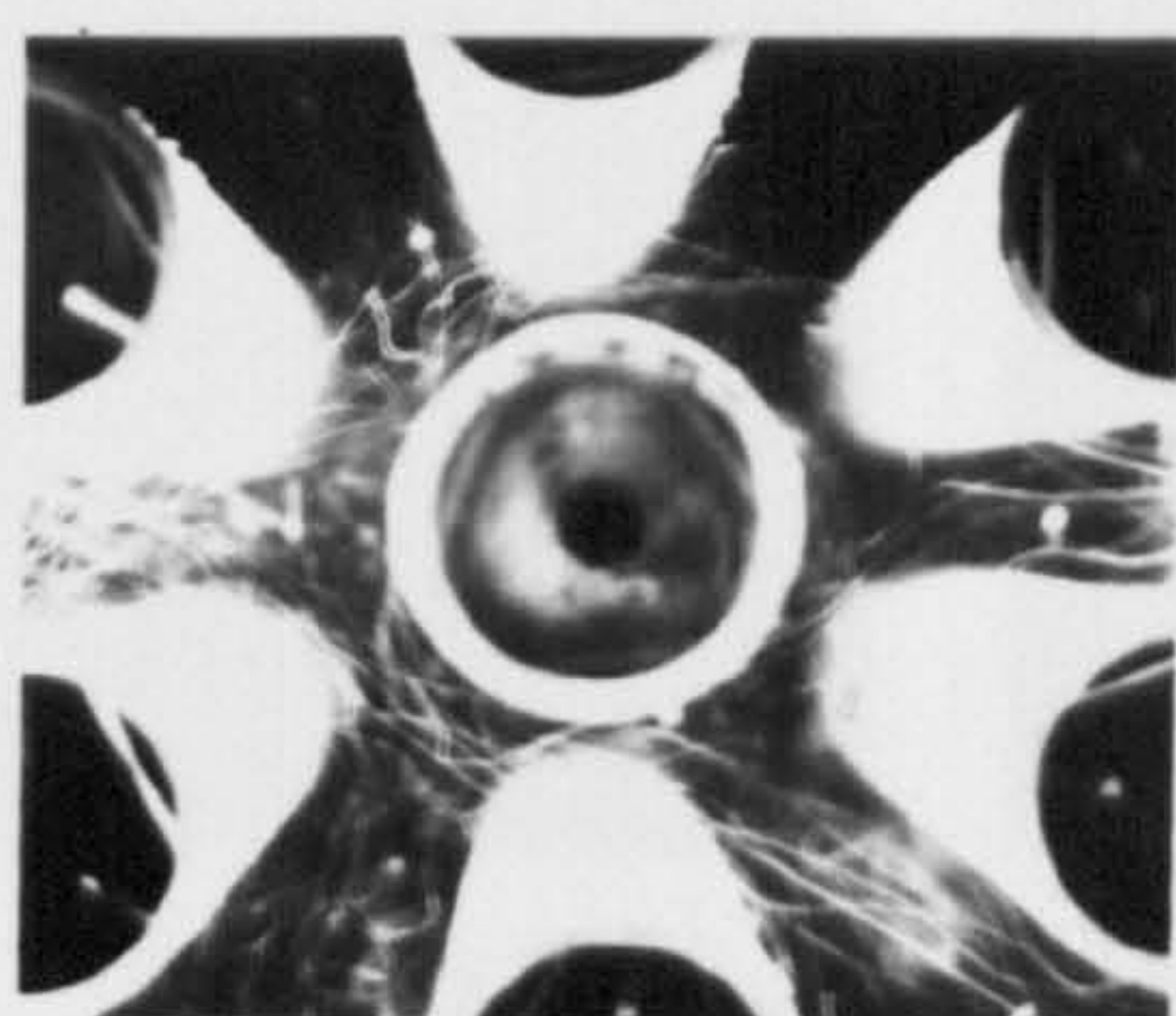
$Re=23000$  ,  $V_w/U = 0.0$



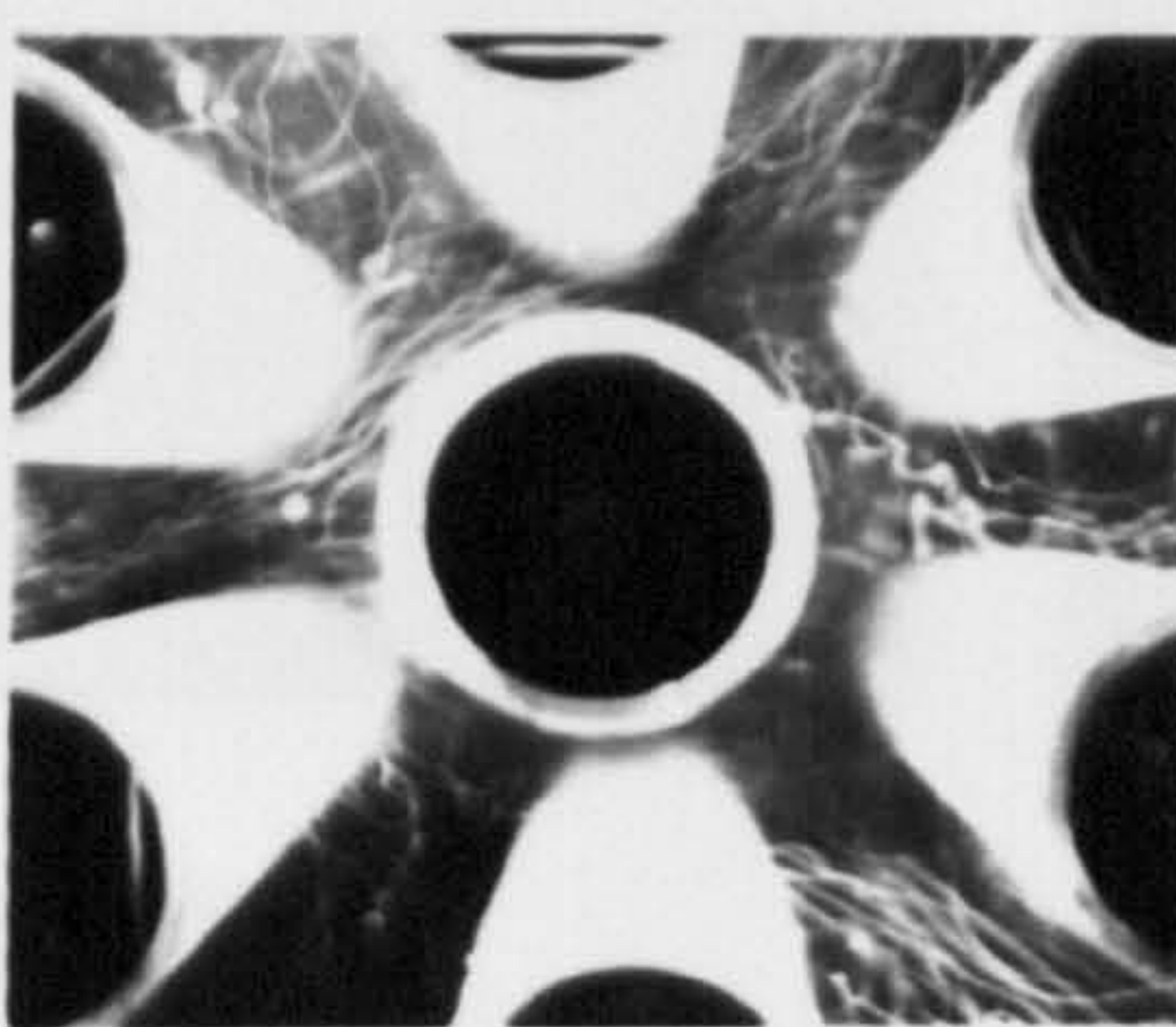
$Re=23000$  ,  $V_w/U = 0.015$



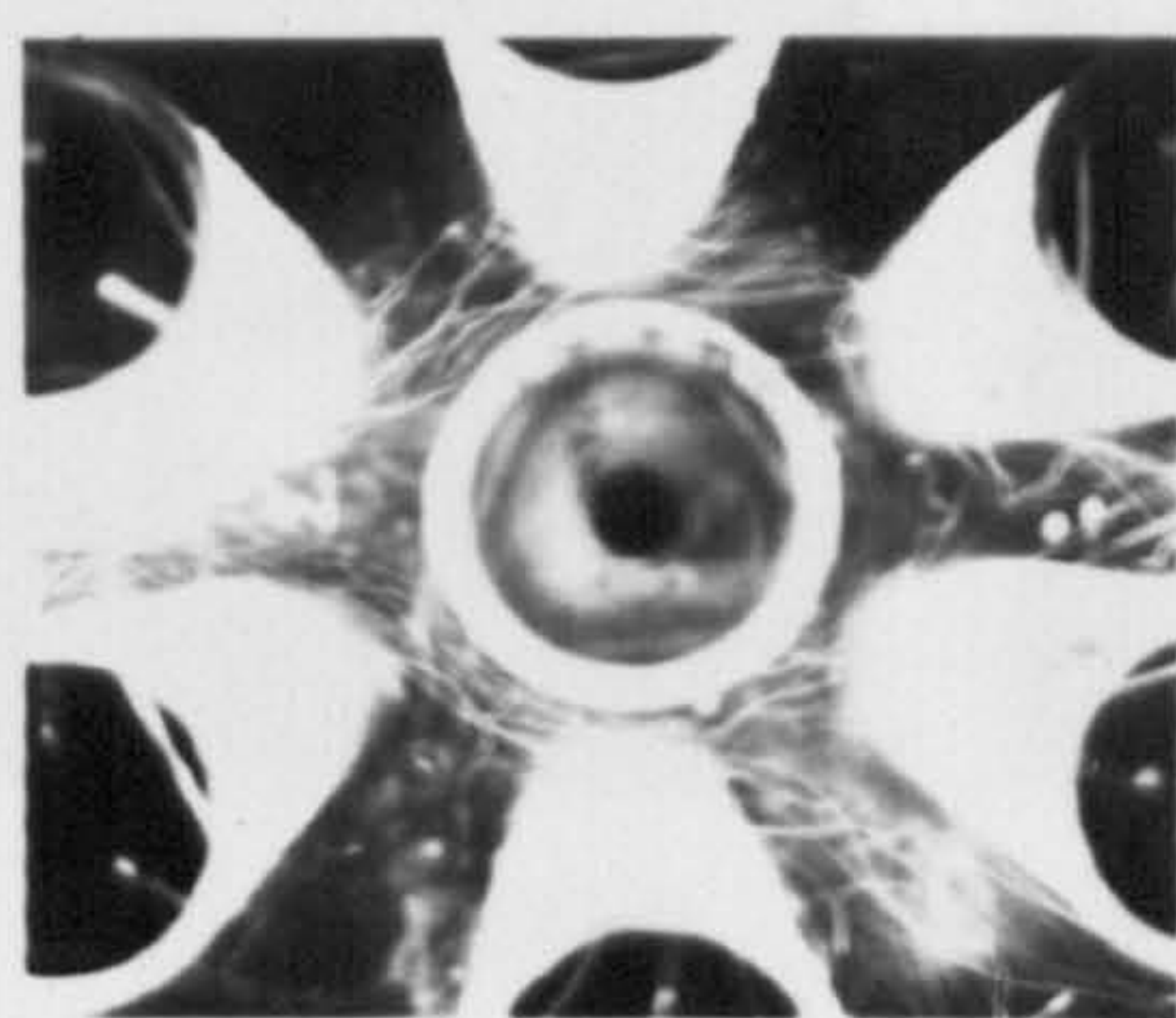
$Re=25000$  ,  $V_w/U = 0.0$



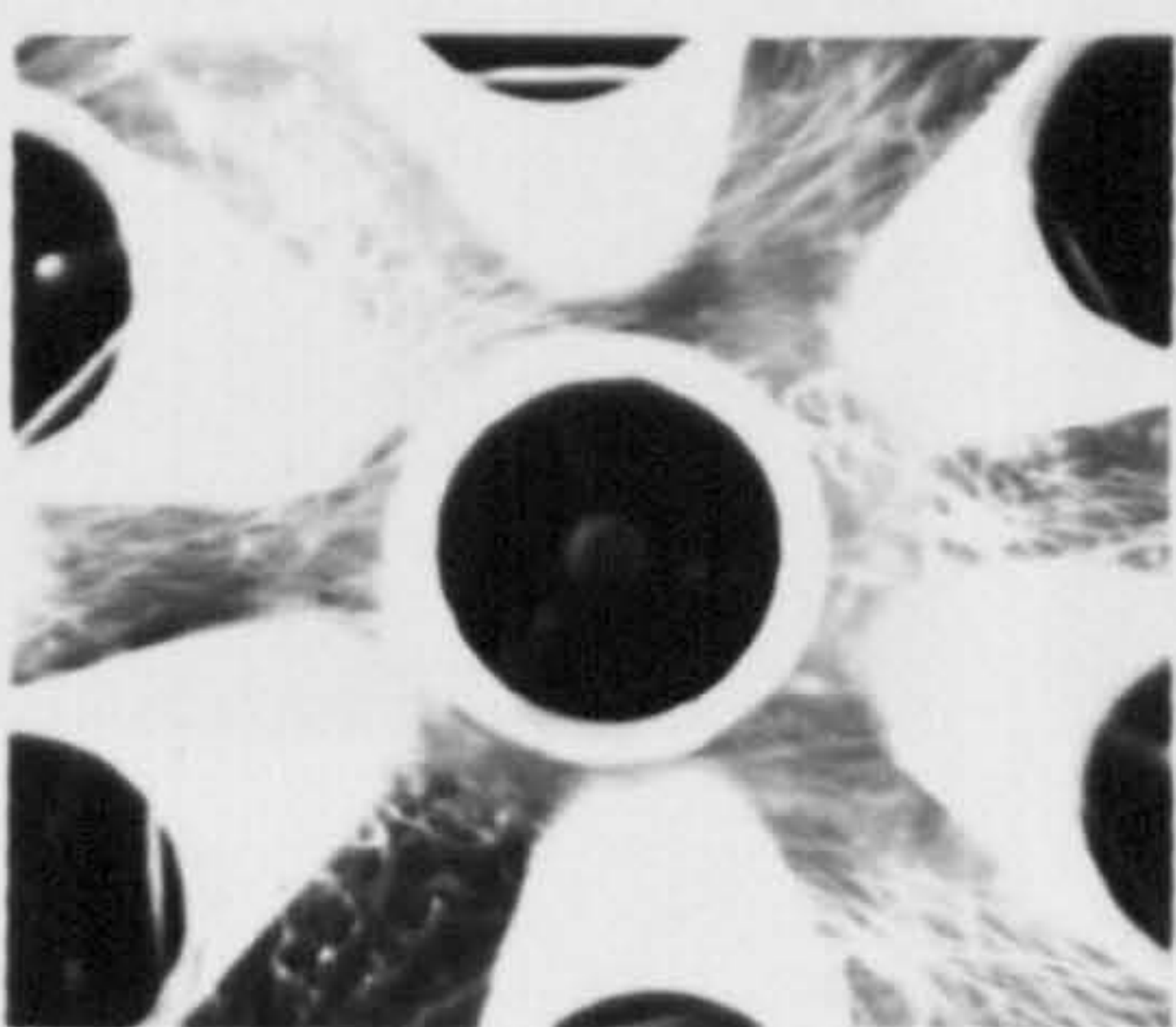
$Re=25000$  ,  $V_w/U = 0.013$



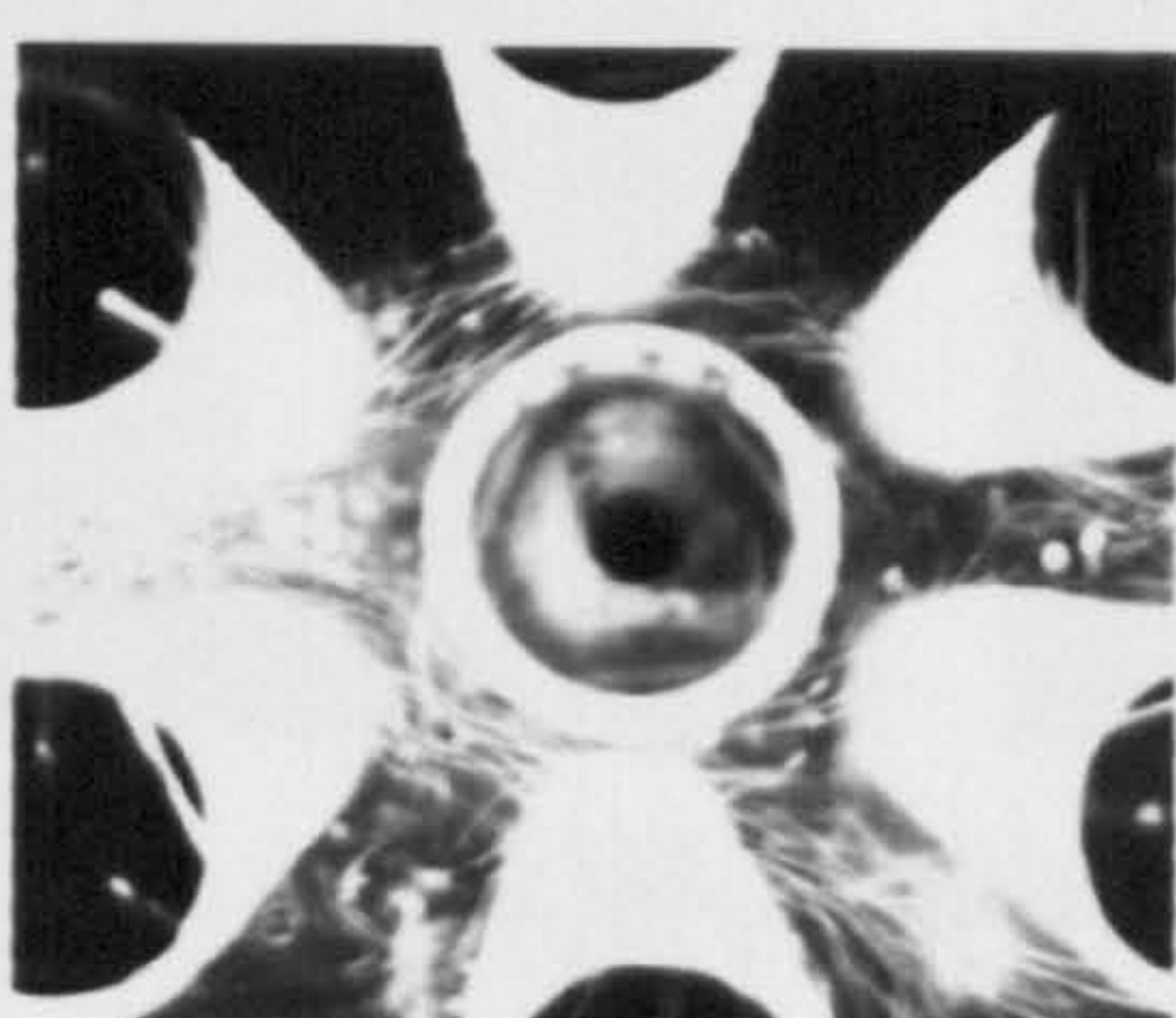
$Re=29000$  ,  $V_w/U = 0.0$



$Re=29000$  ,  $V_w/U = 0.011$



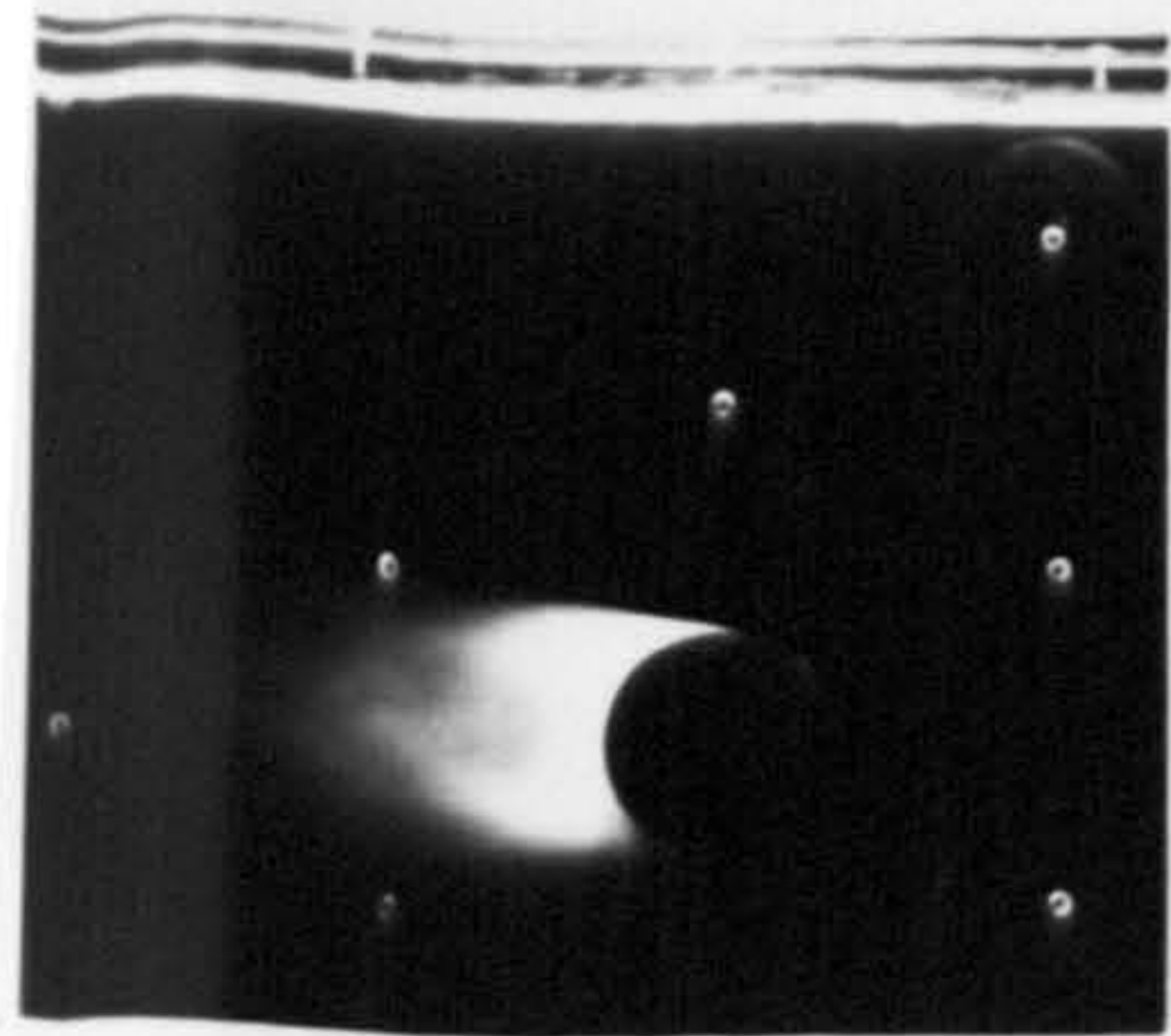
$Re=32000$  ,  $V_w/U = 0.0$



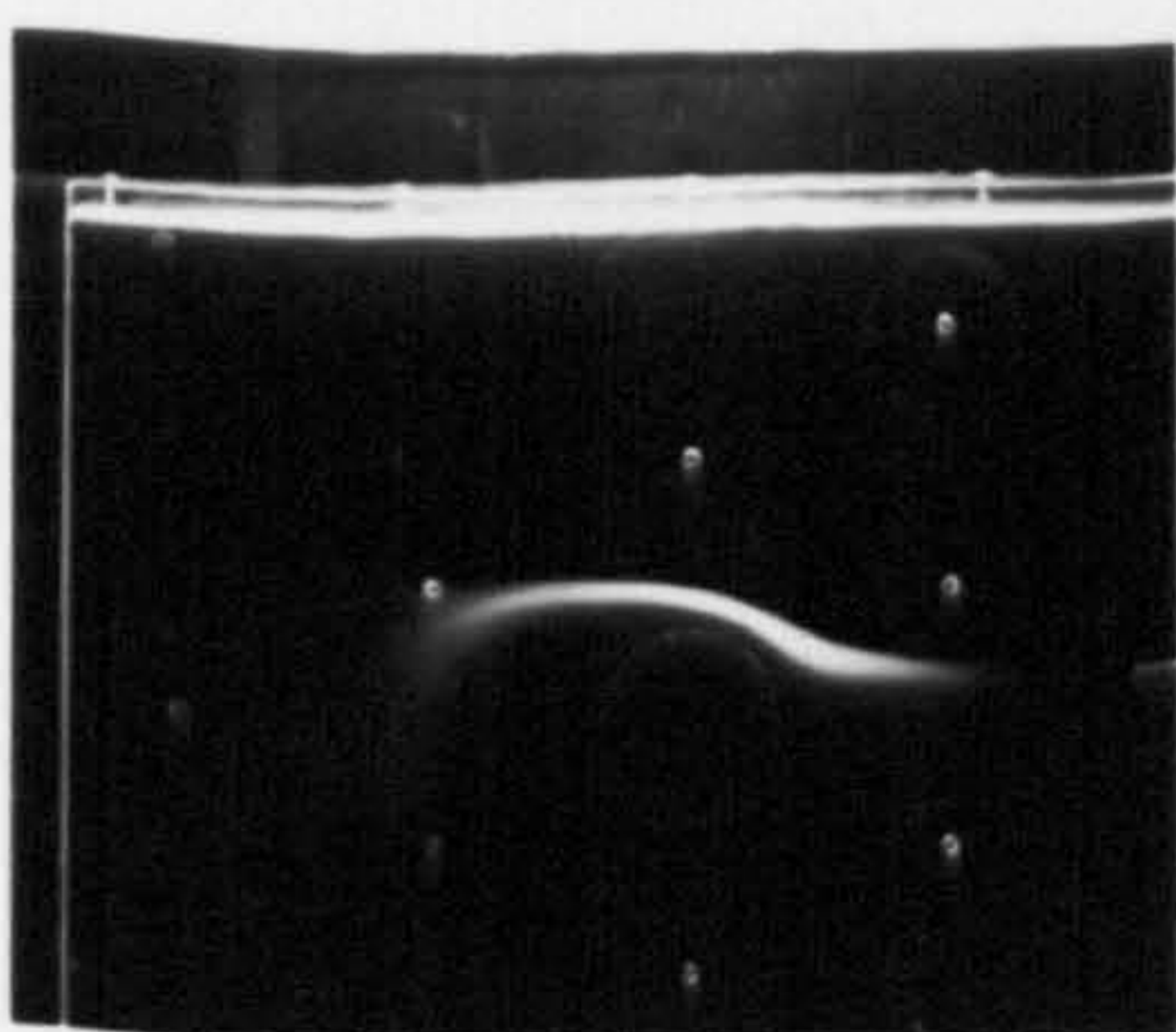
$Re=32000$  ,  $V_w/U = 0.01$

Fig. 10.1  
row number 3

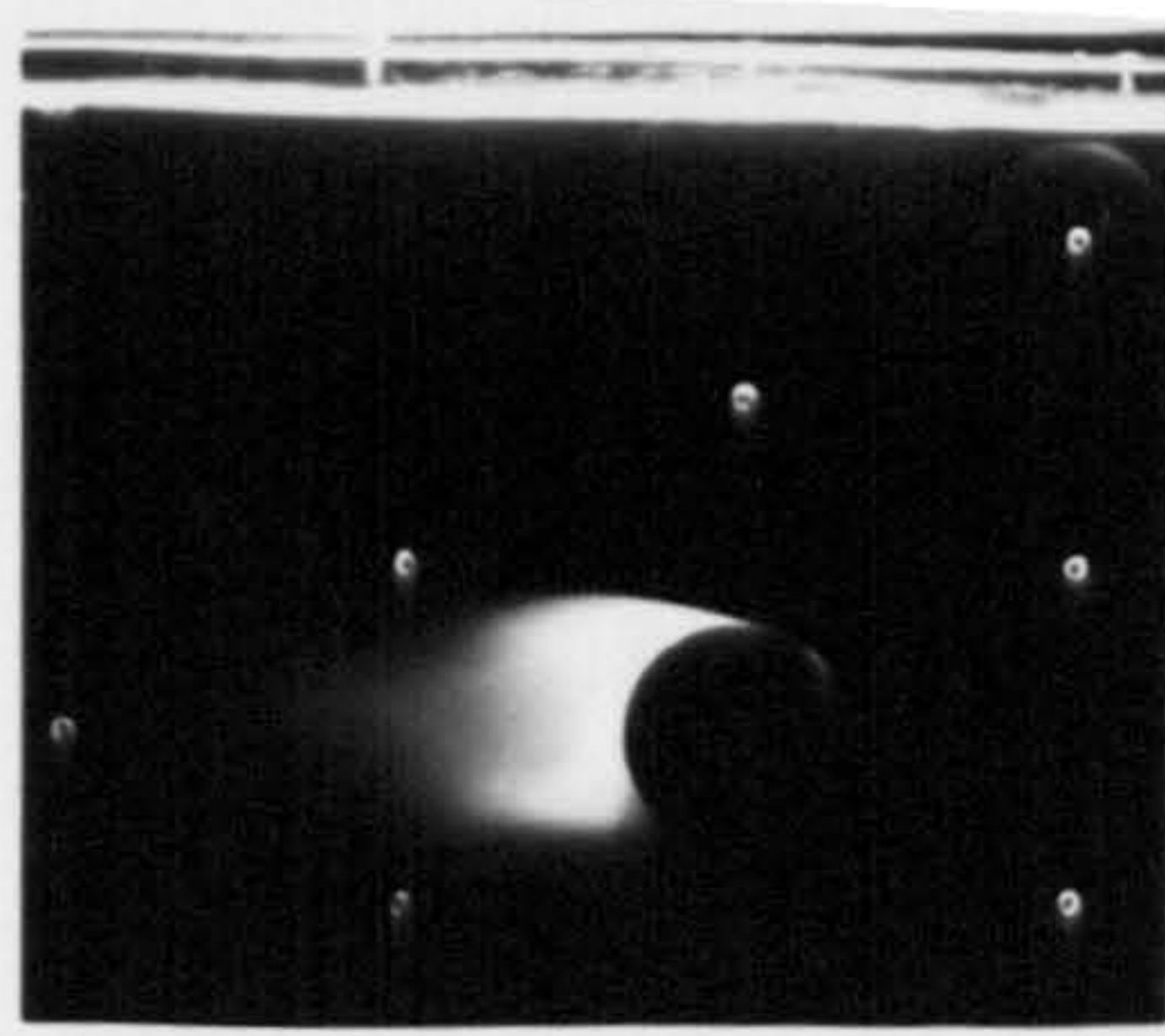




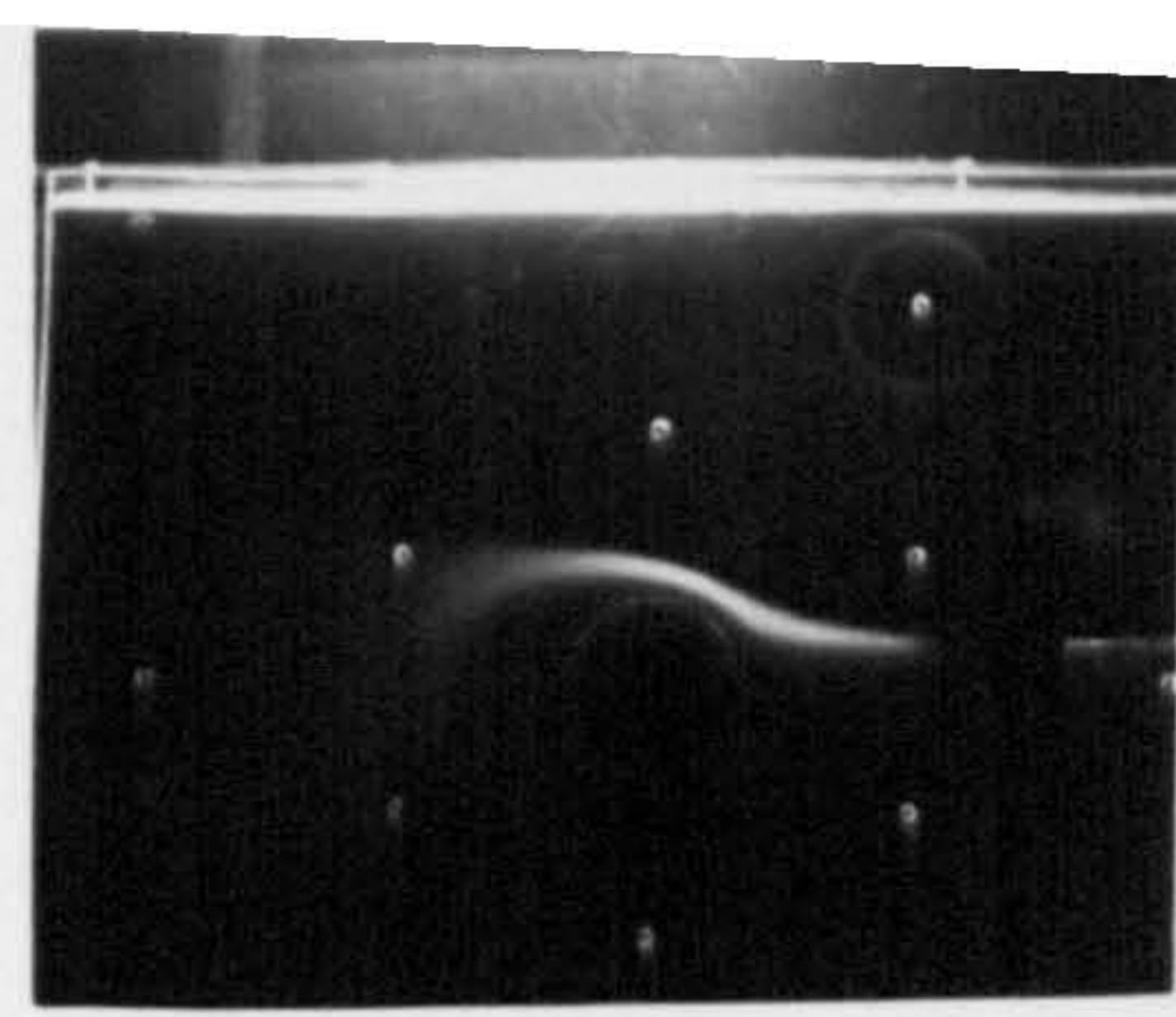
Re=13600 ,  $V_w/U=0.0$



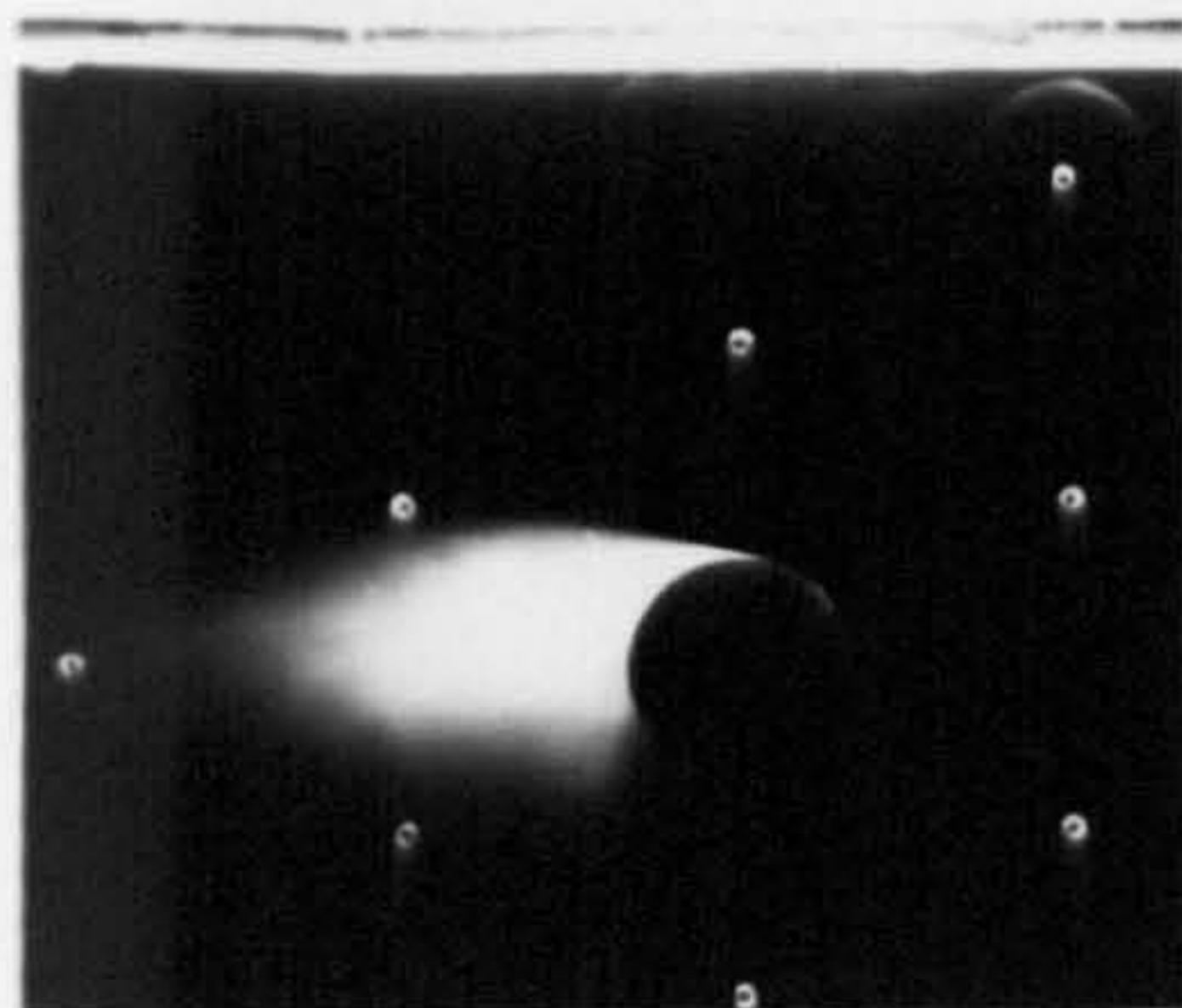
Re=13600 ,  $V_w/U=0.011$



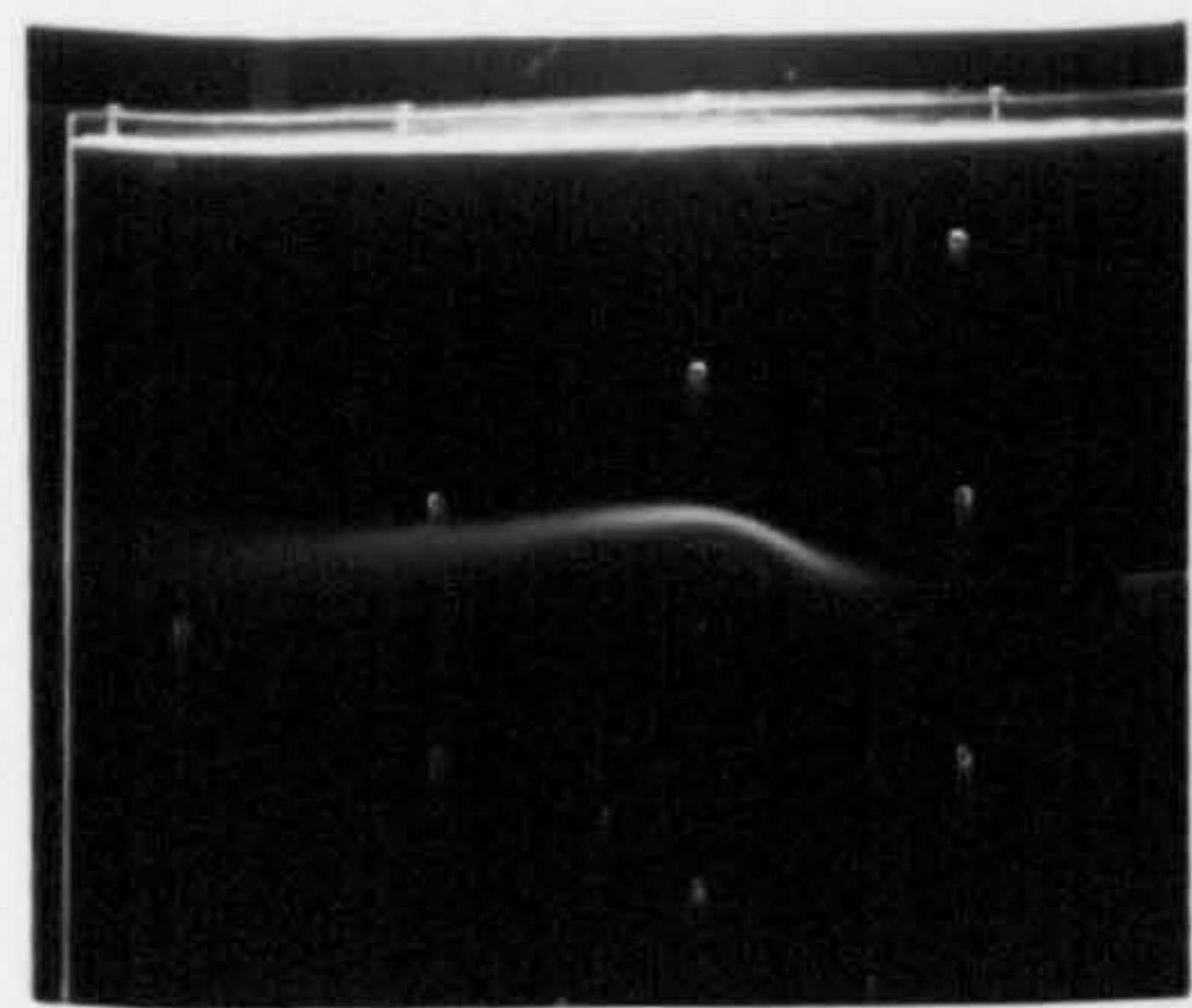
Re=24000 ,  $V_w/U=0.0$



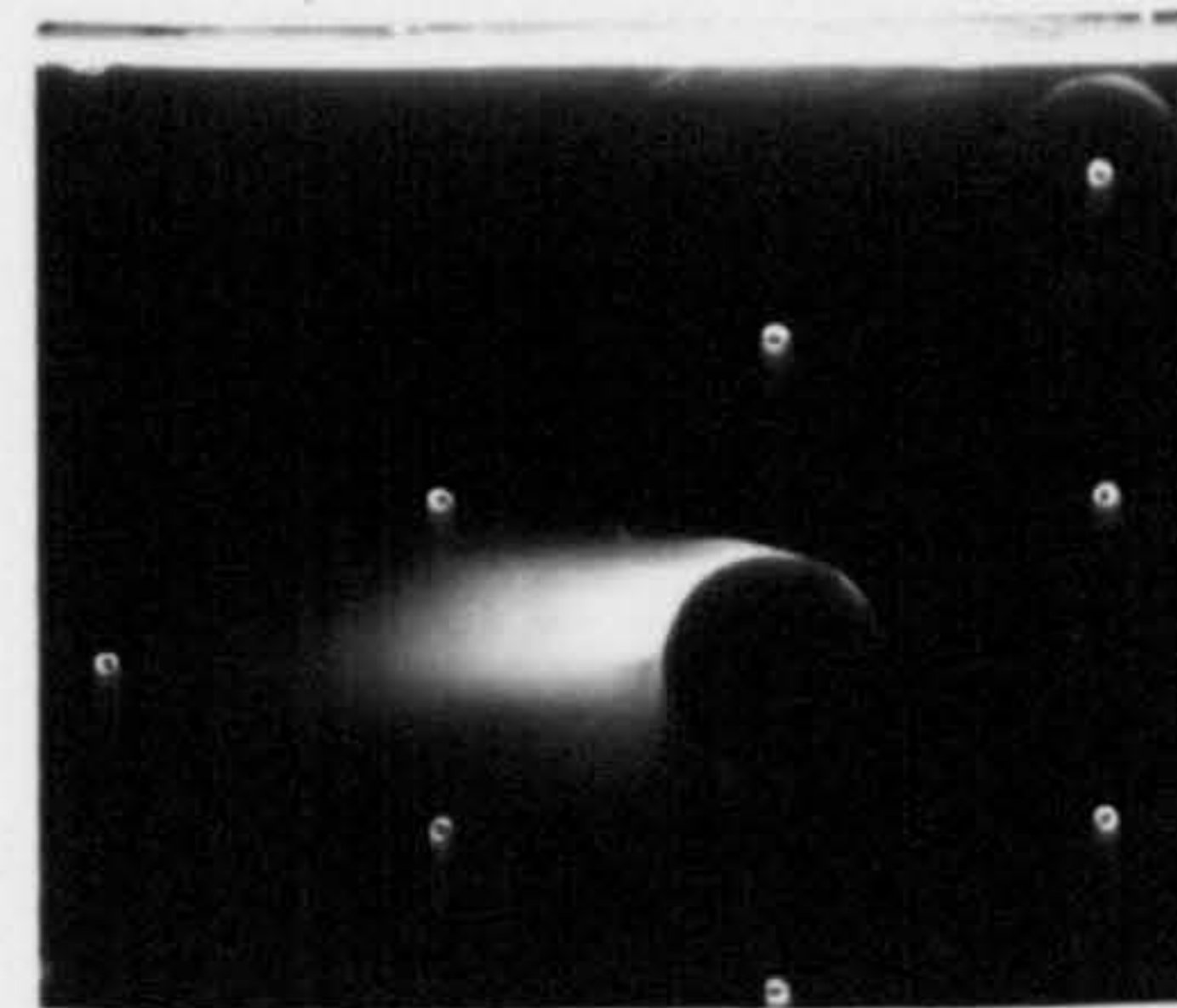
Re=24000 ,  $V_w/U=0.006$



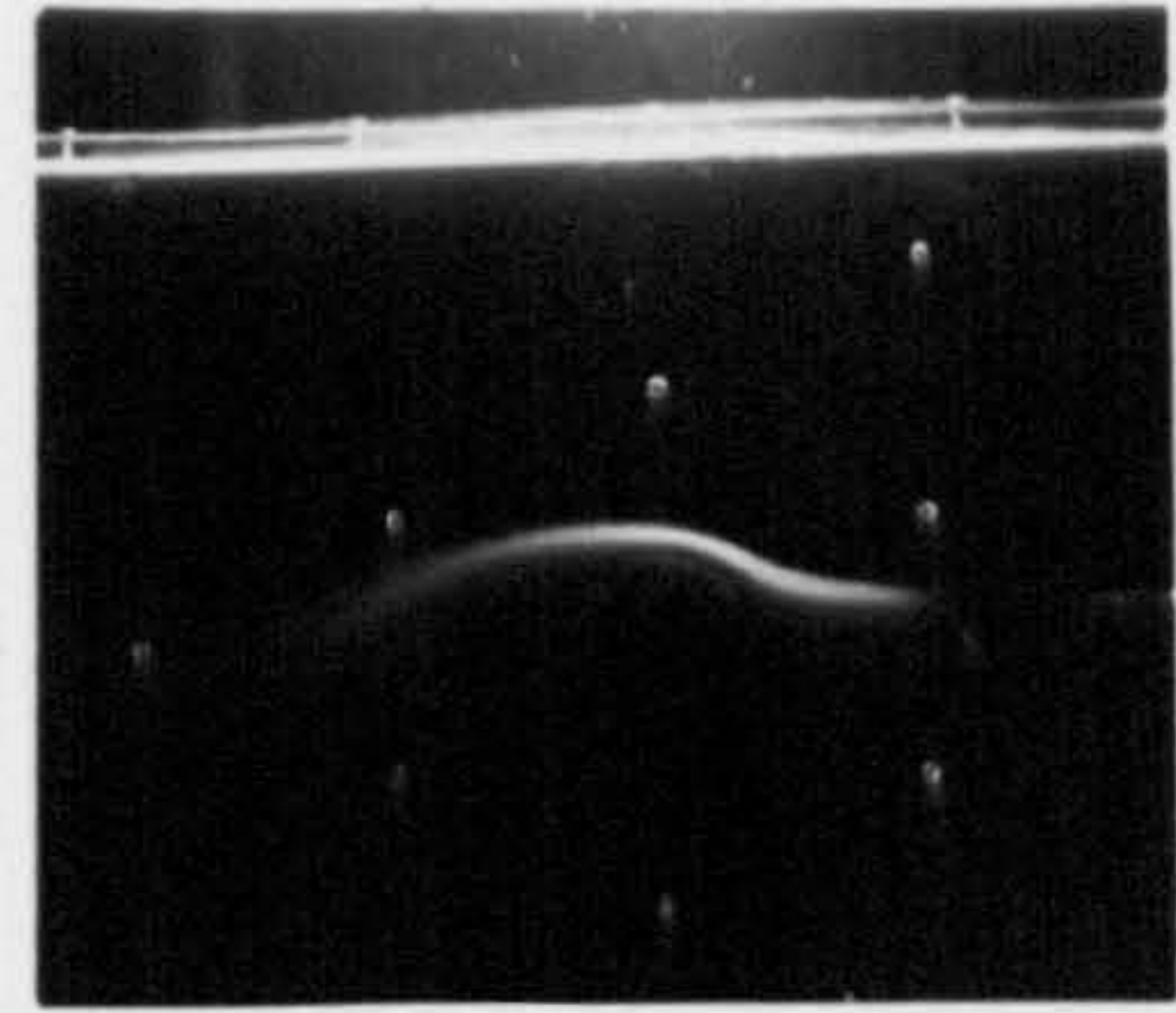
Re=13600 ,  $V_w/U=0.023$



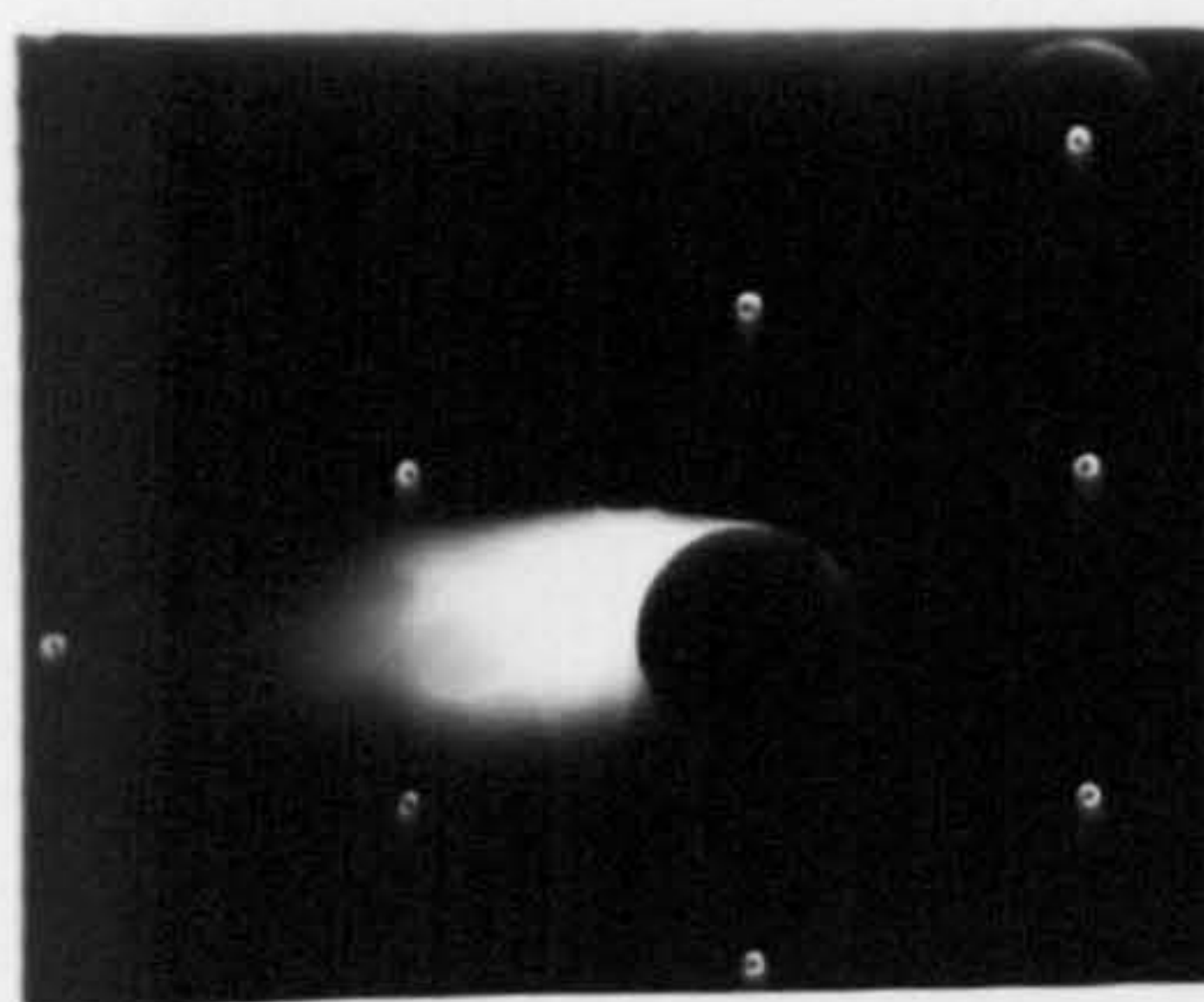
Re=13600 ,  $V_w/U=0.035$



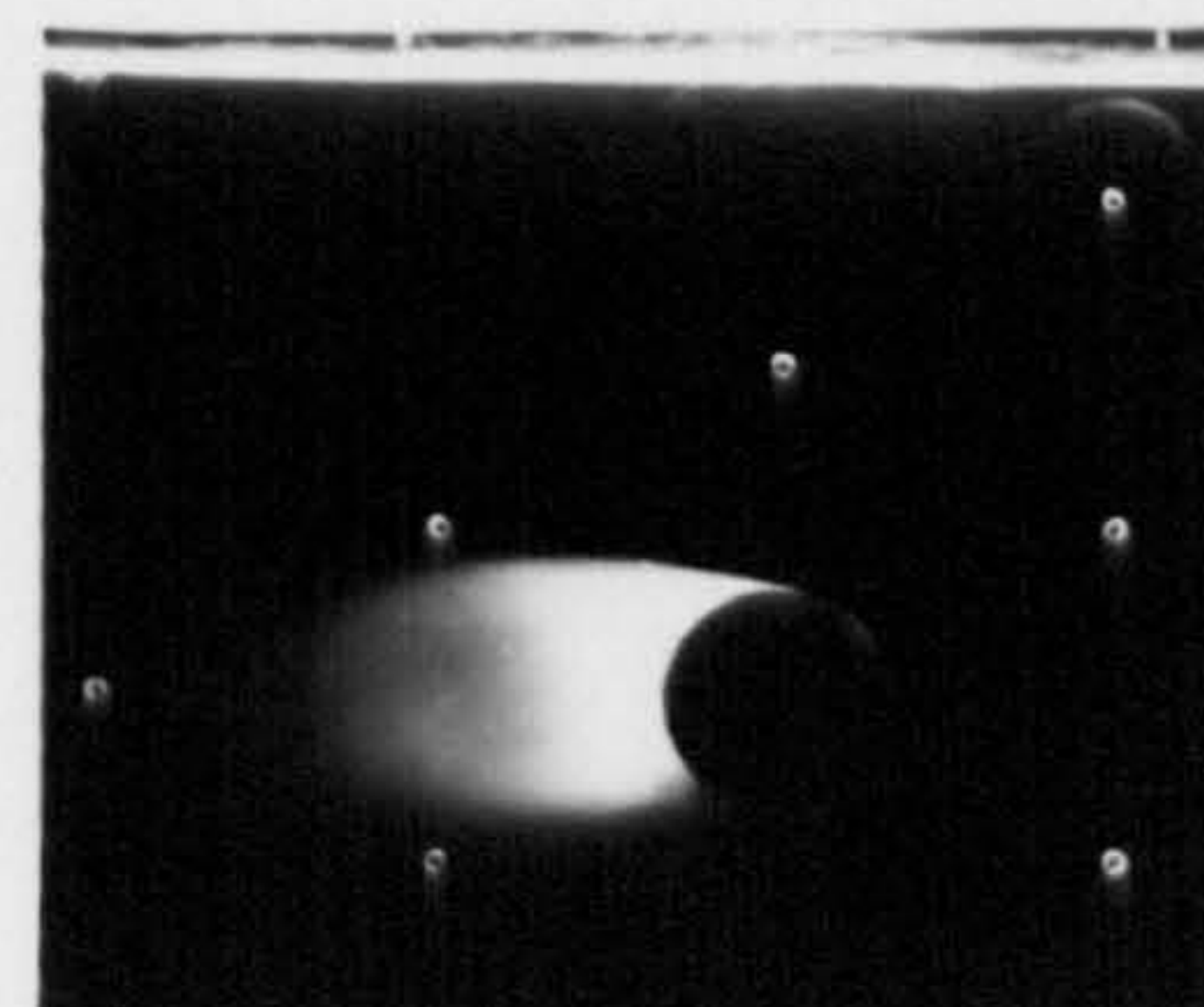
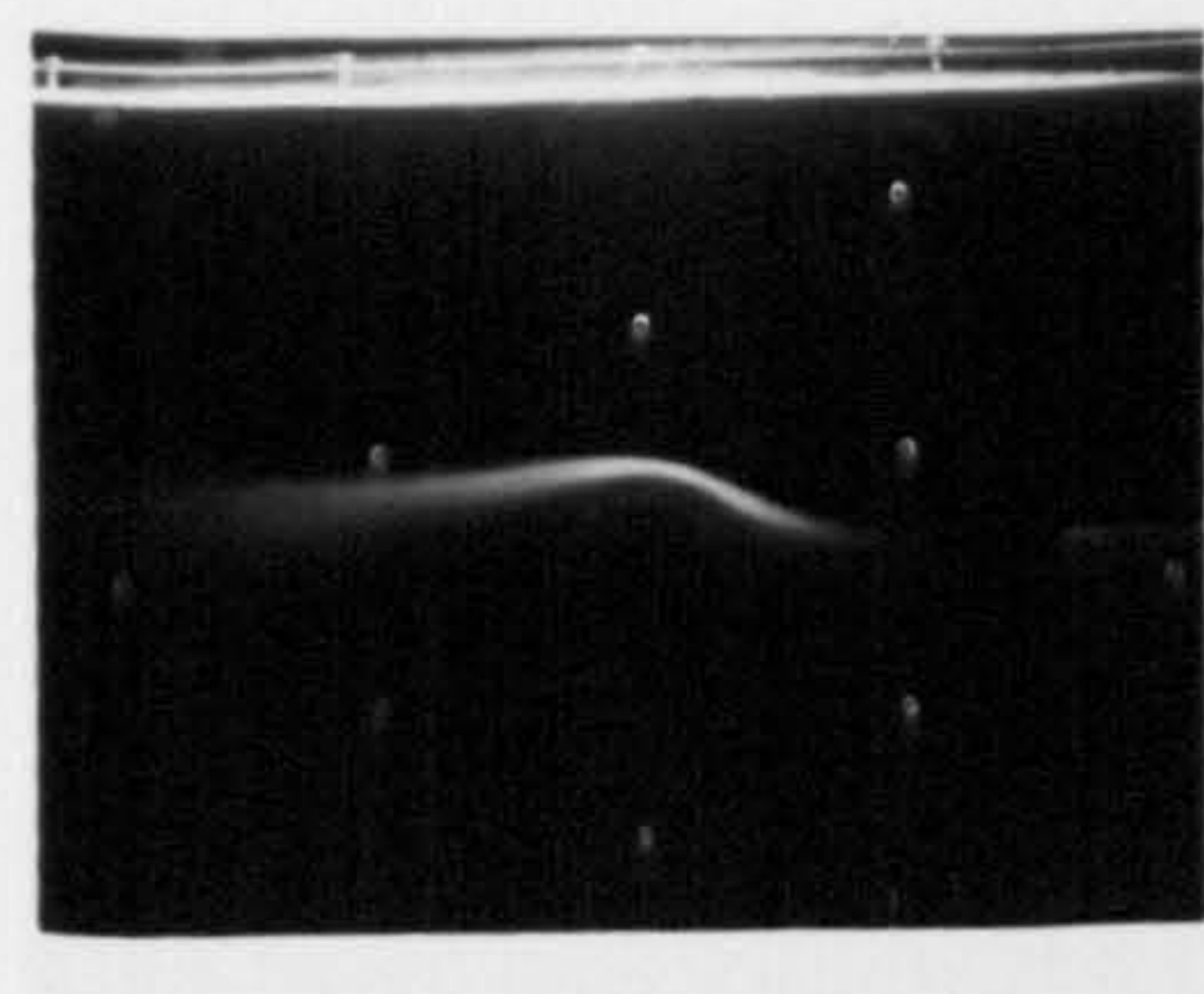
Re=24000 ,  $V_w/U=0.013$



Re=24000 ,  $V_w/U=0.019$



Re=13600 ,  $V_w/U=0.044$



Re=24000 ,  $V_w/U=0.025$

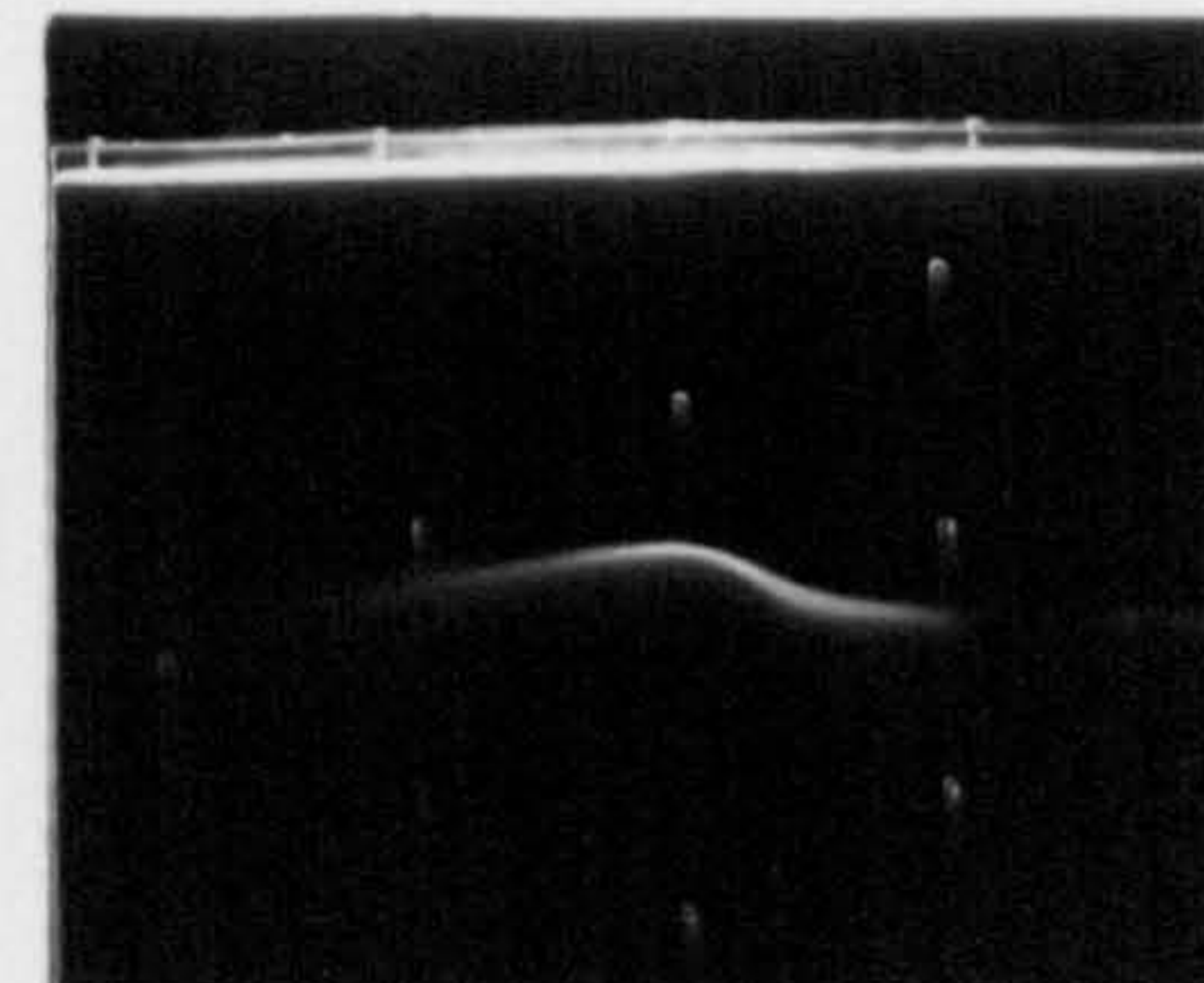
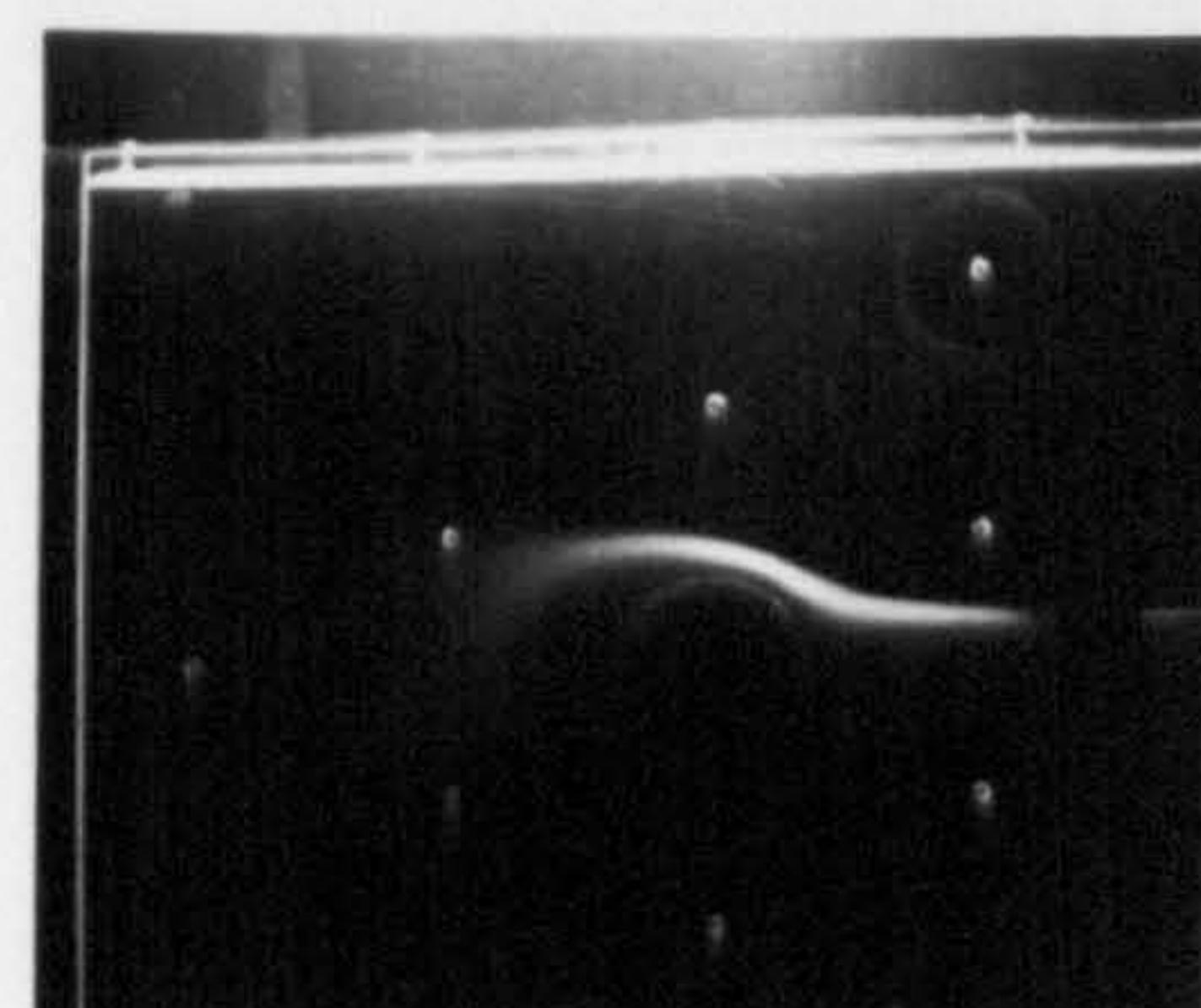
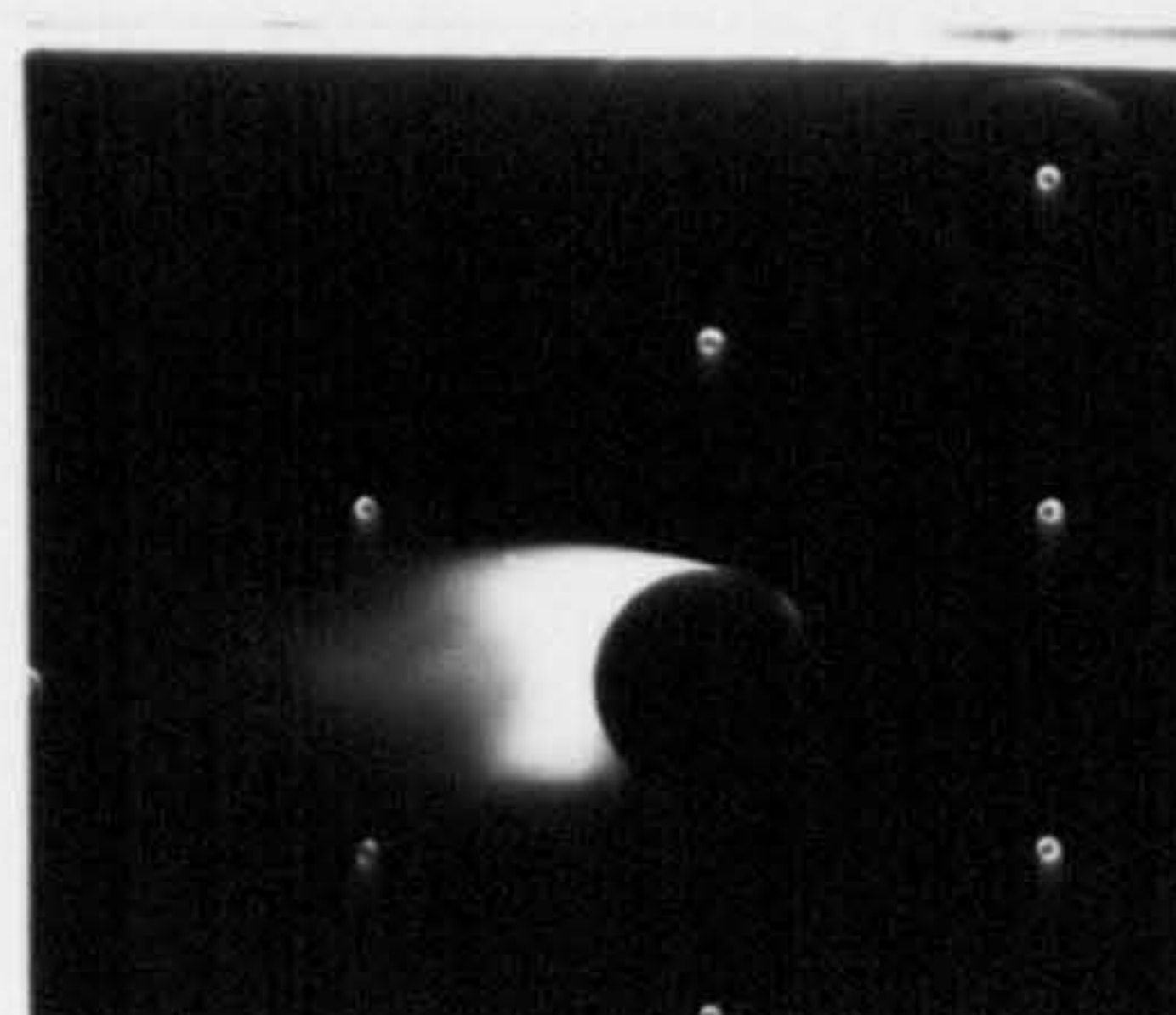
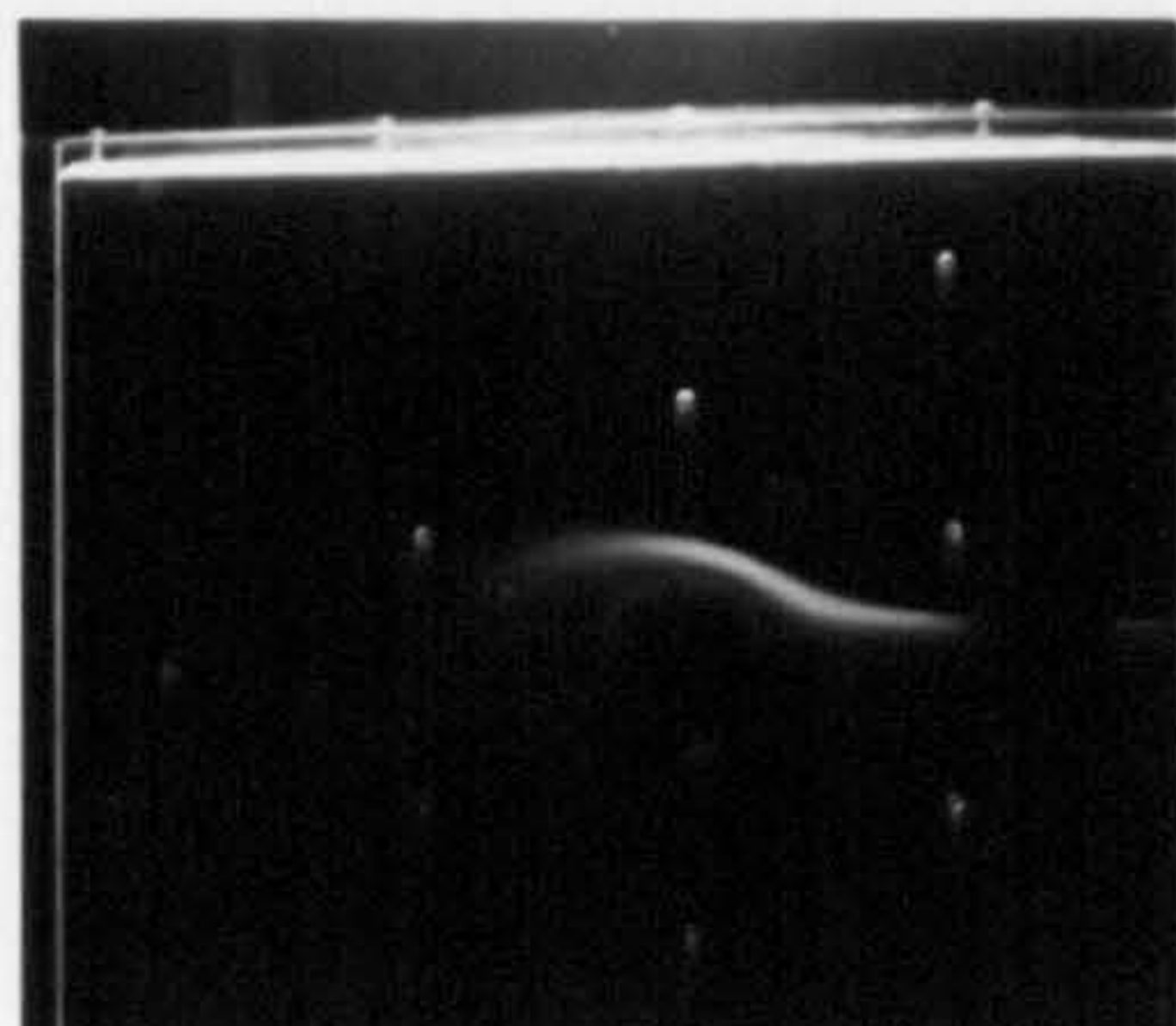
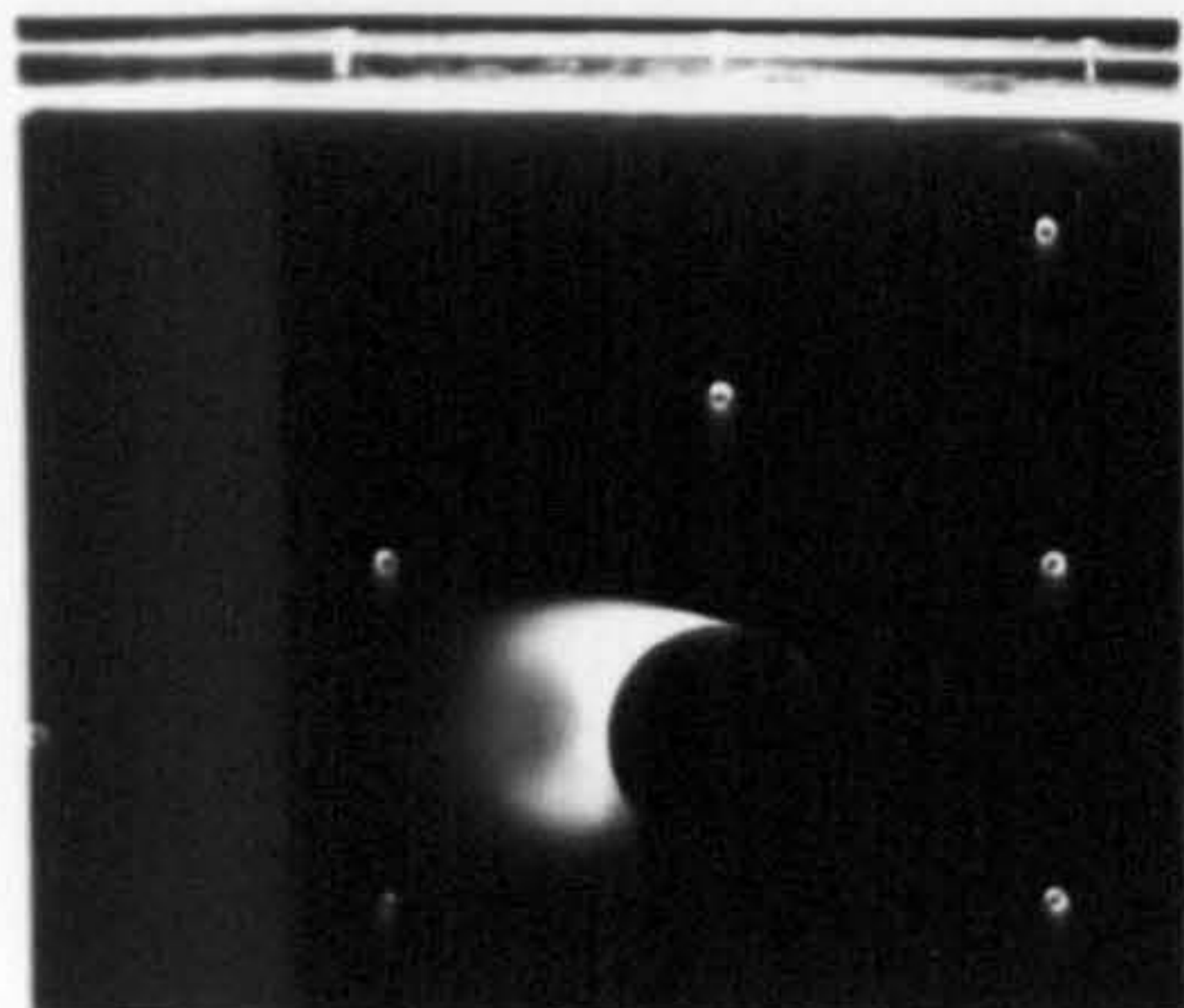


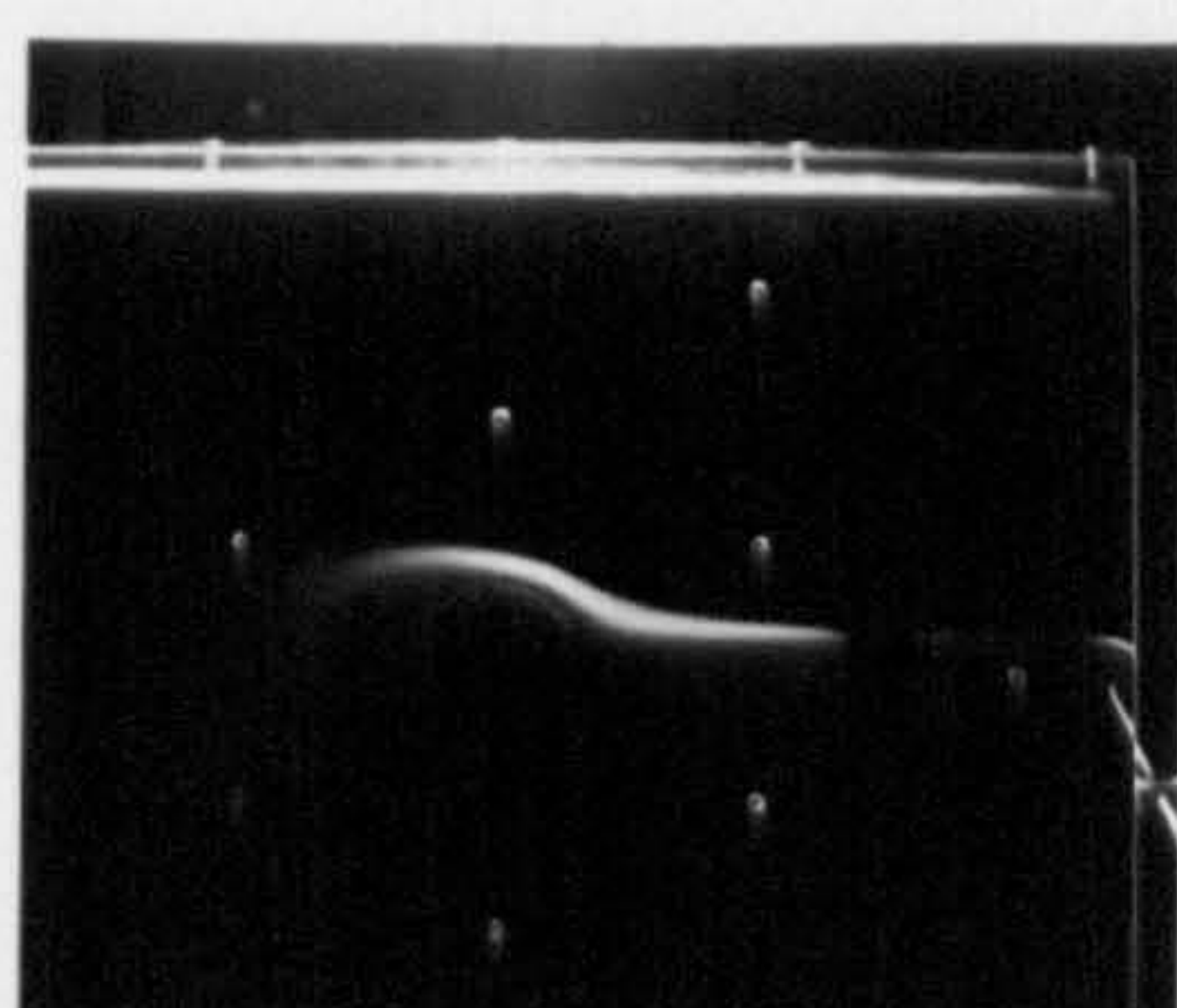
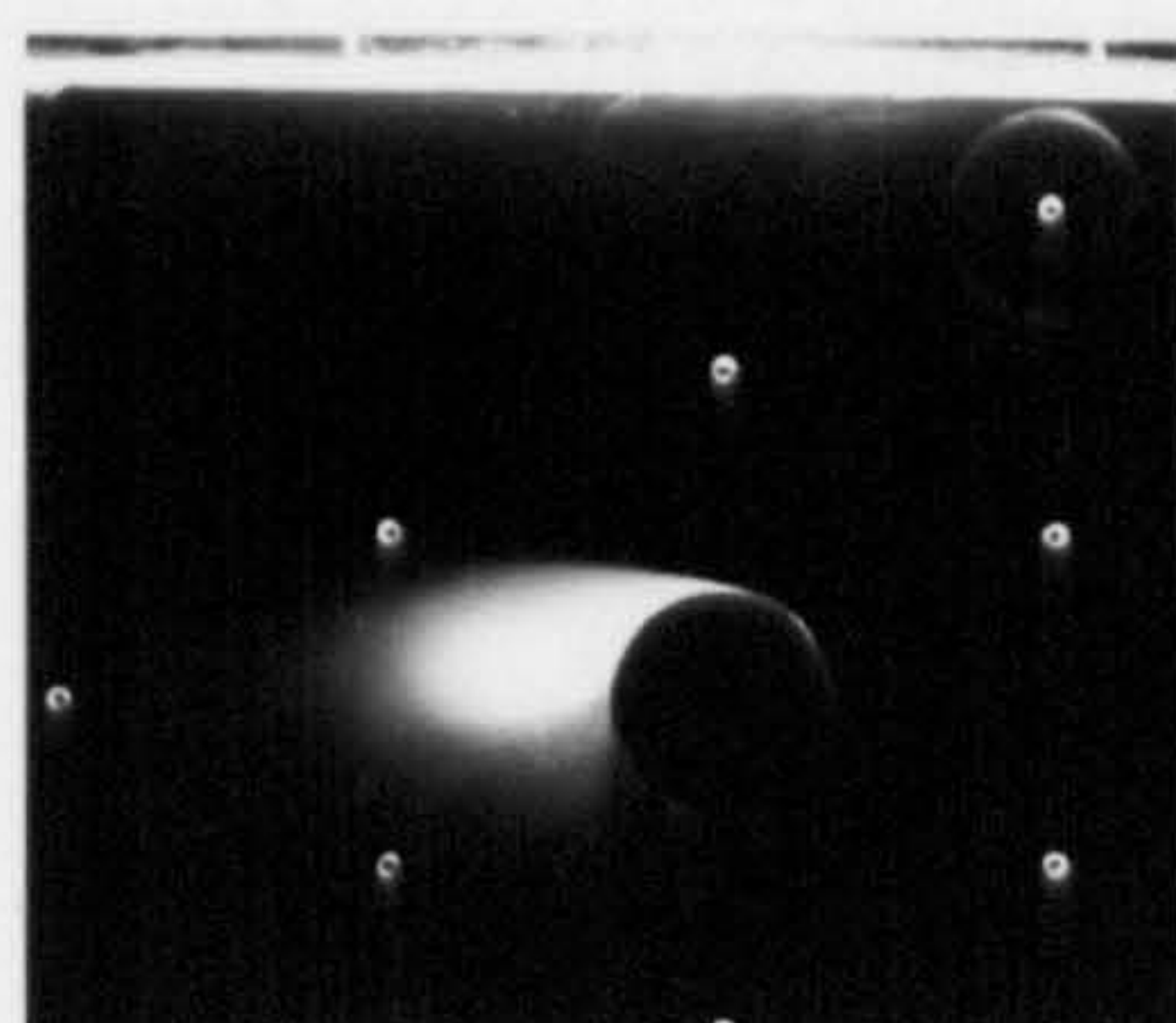
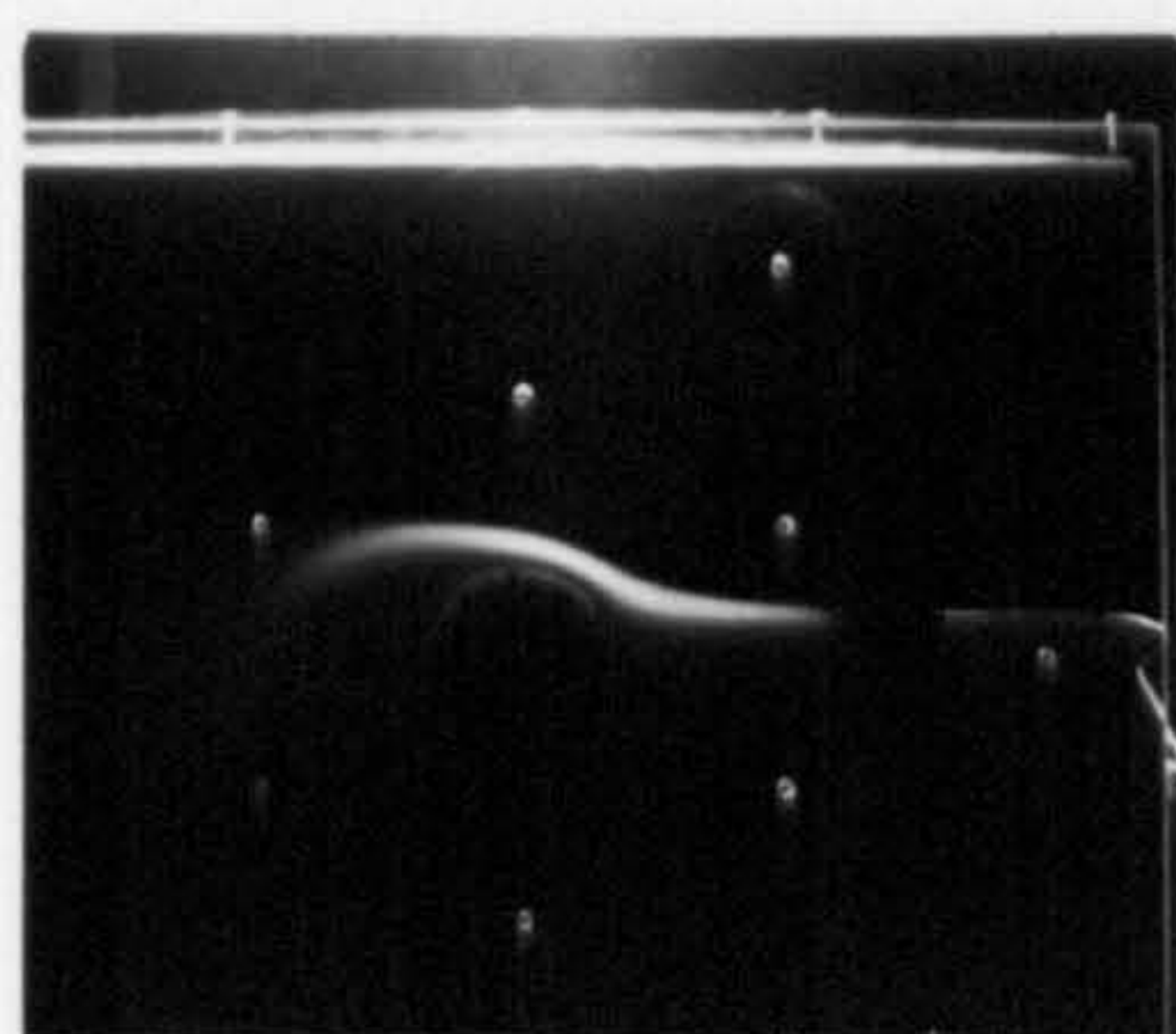
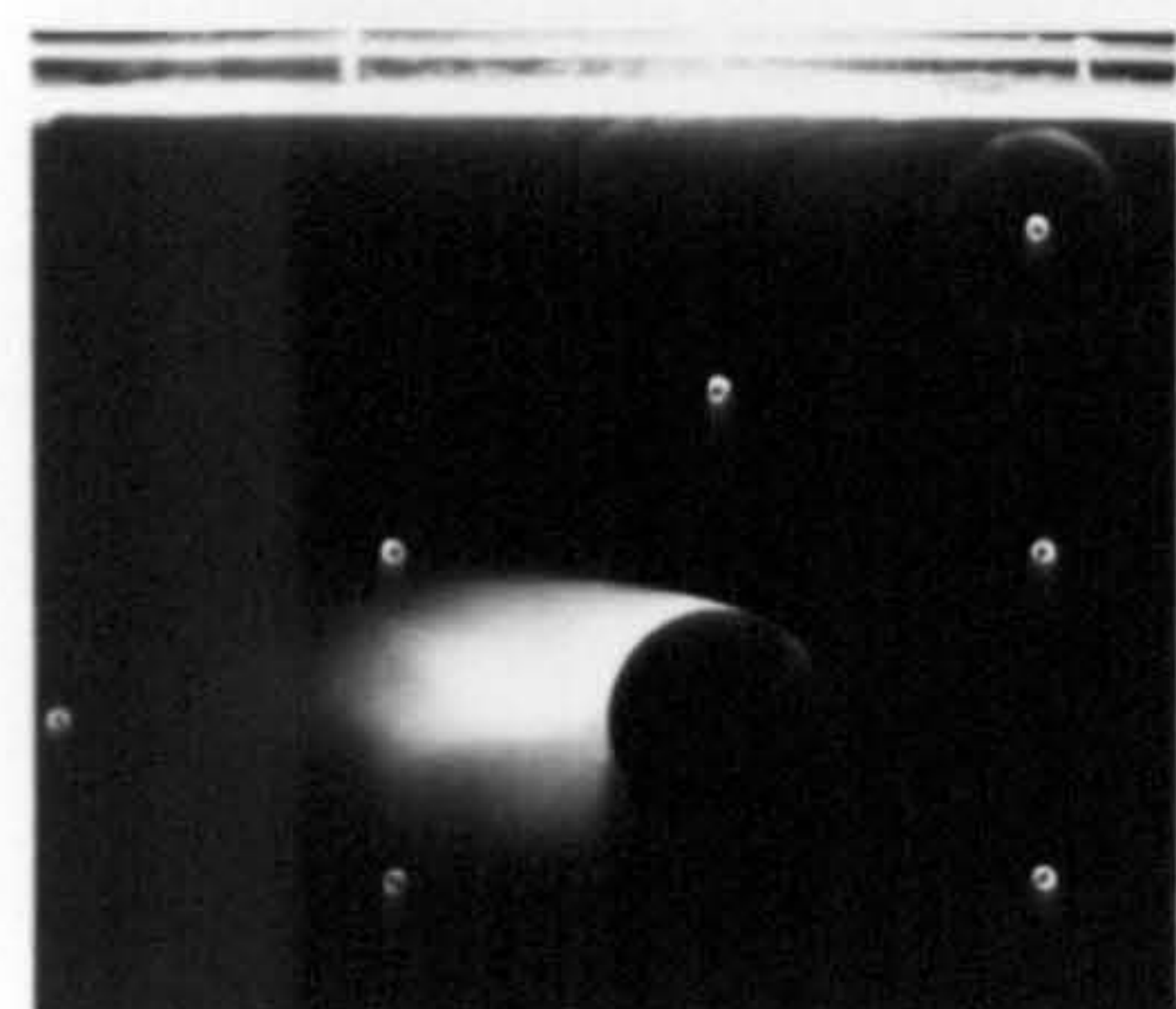
FIGURE 10.2  
single cylinder





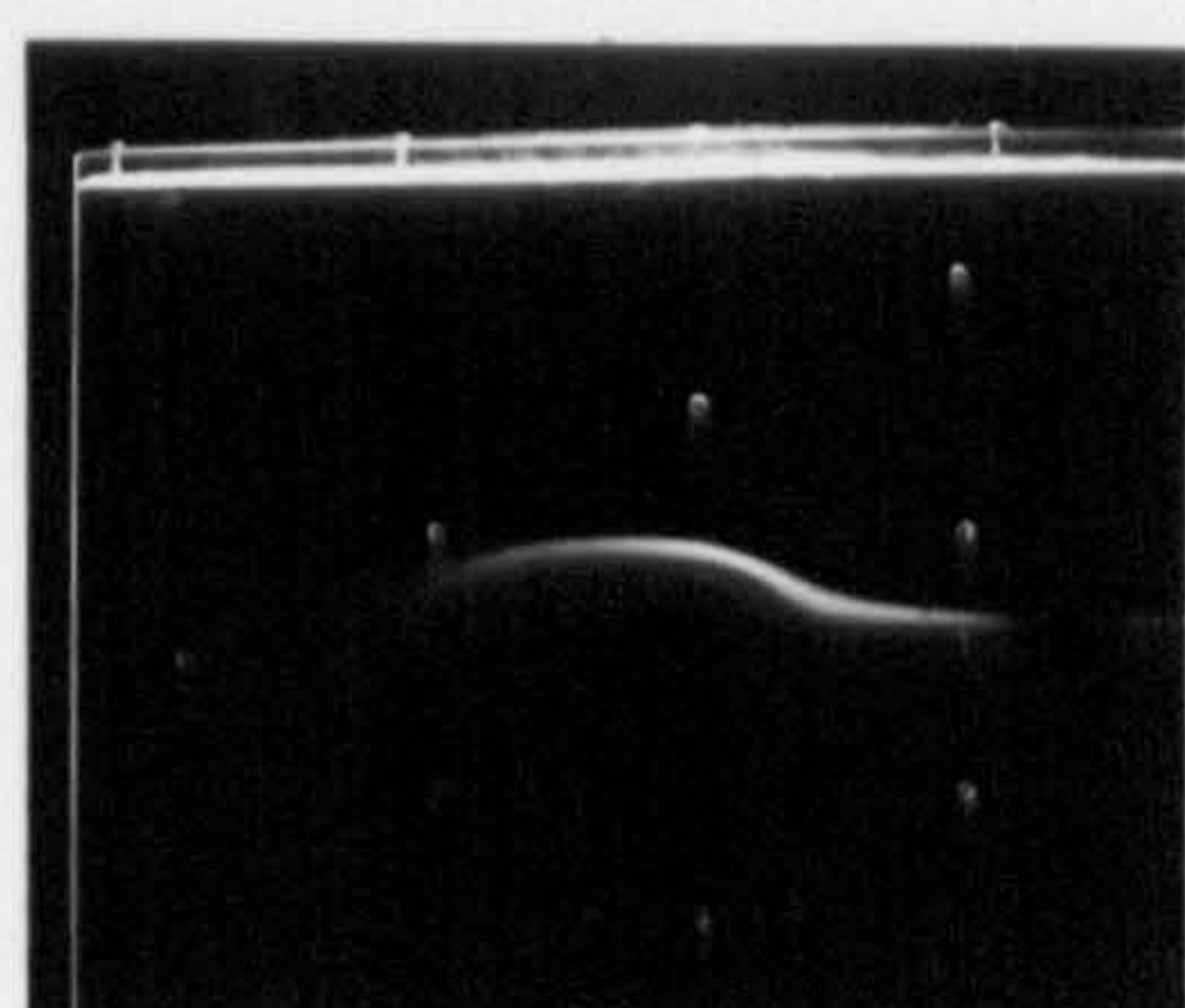
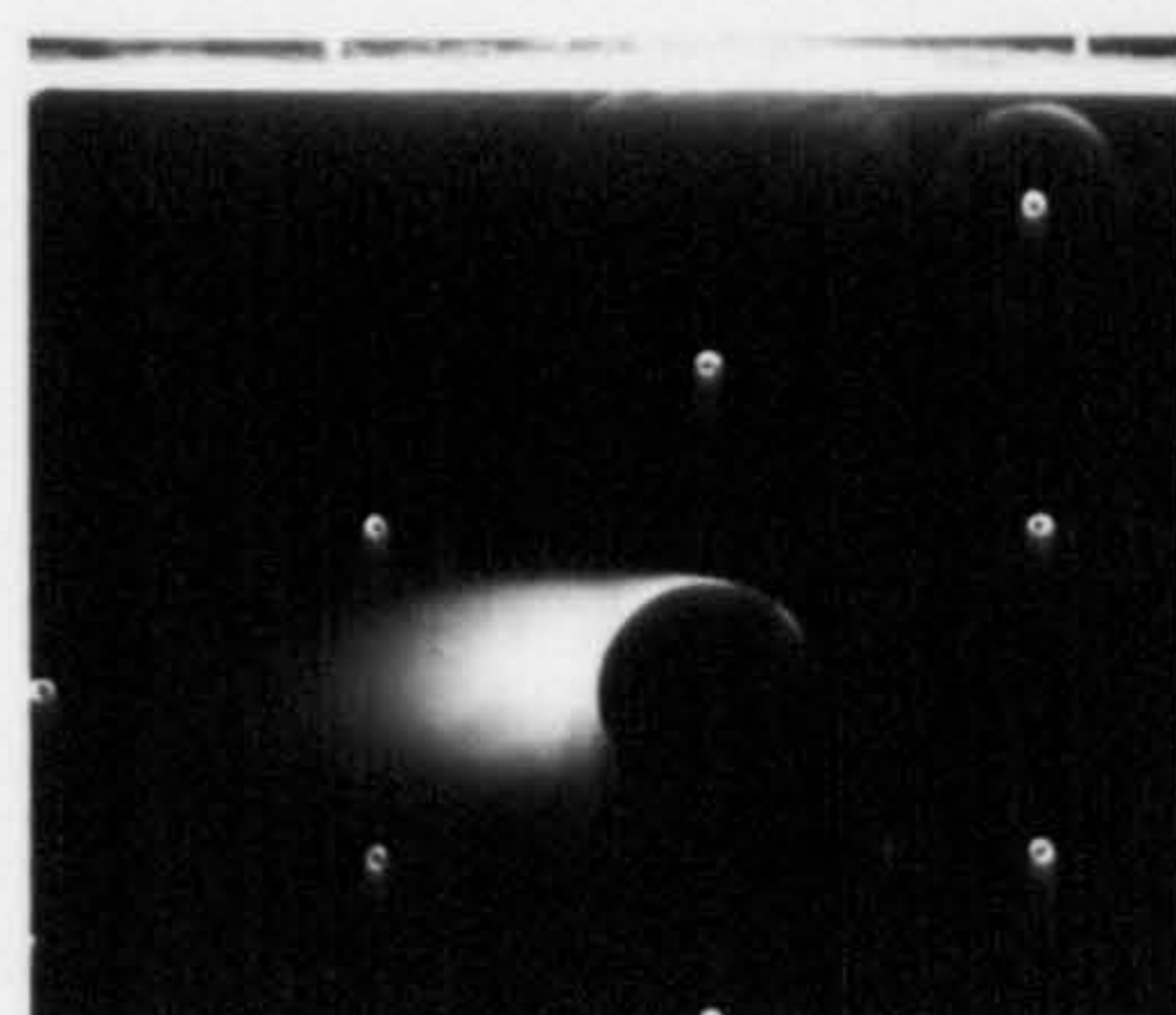
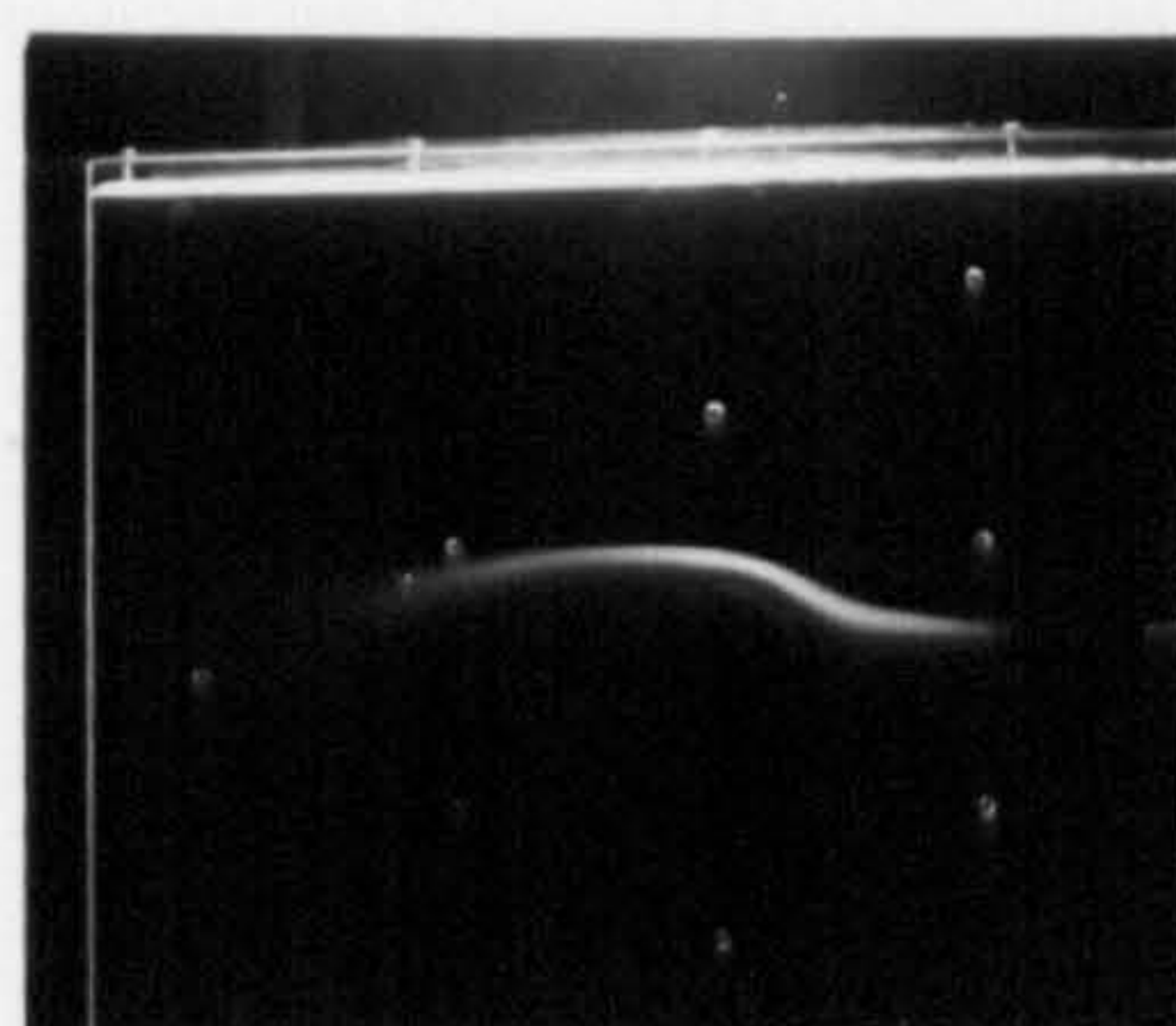
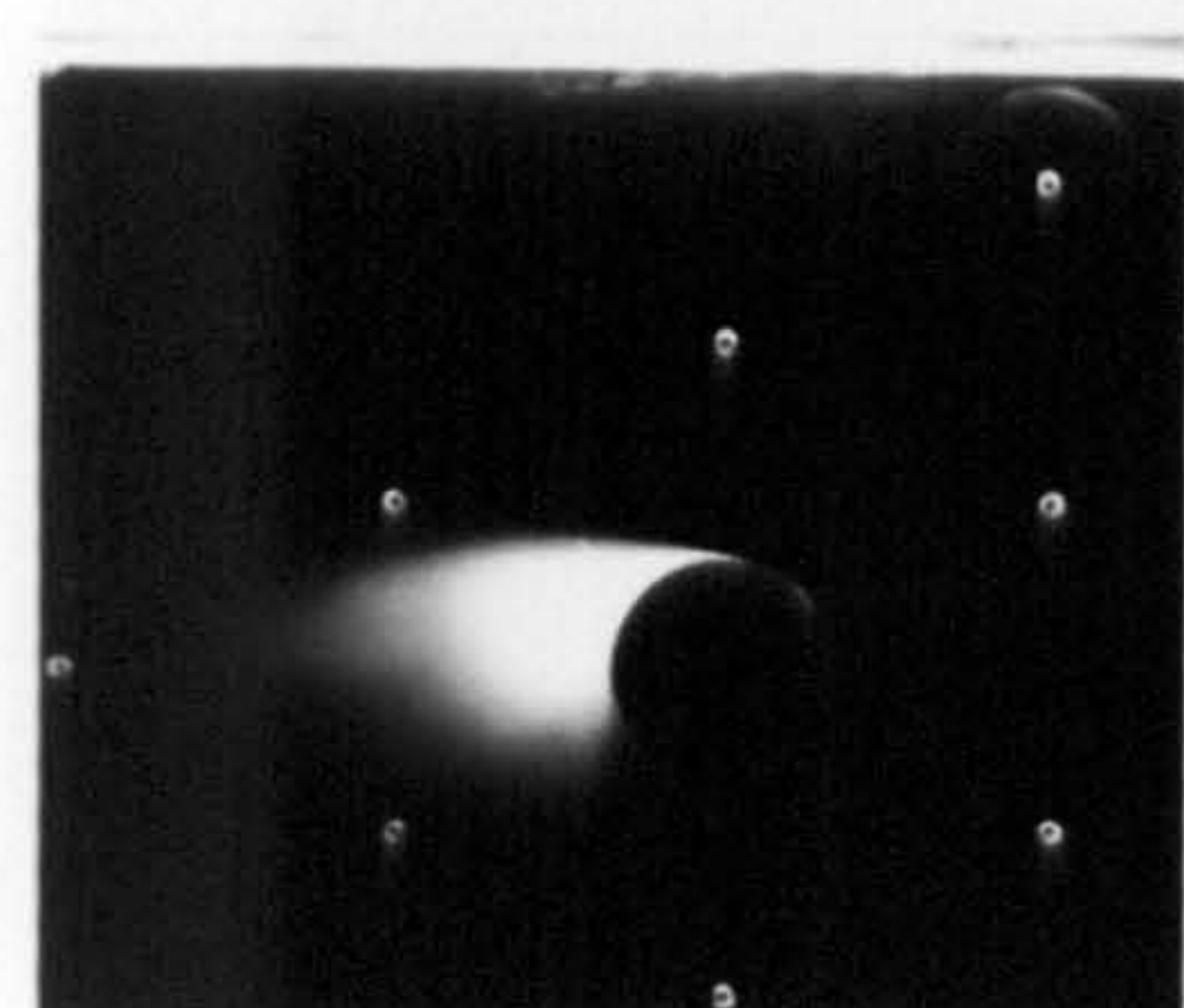
Re=35000 ,  $V_w/U=0.0$

Re=45000 ,  $V_w/U=0.0$



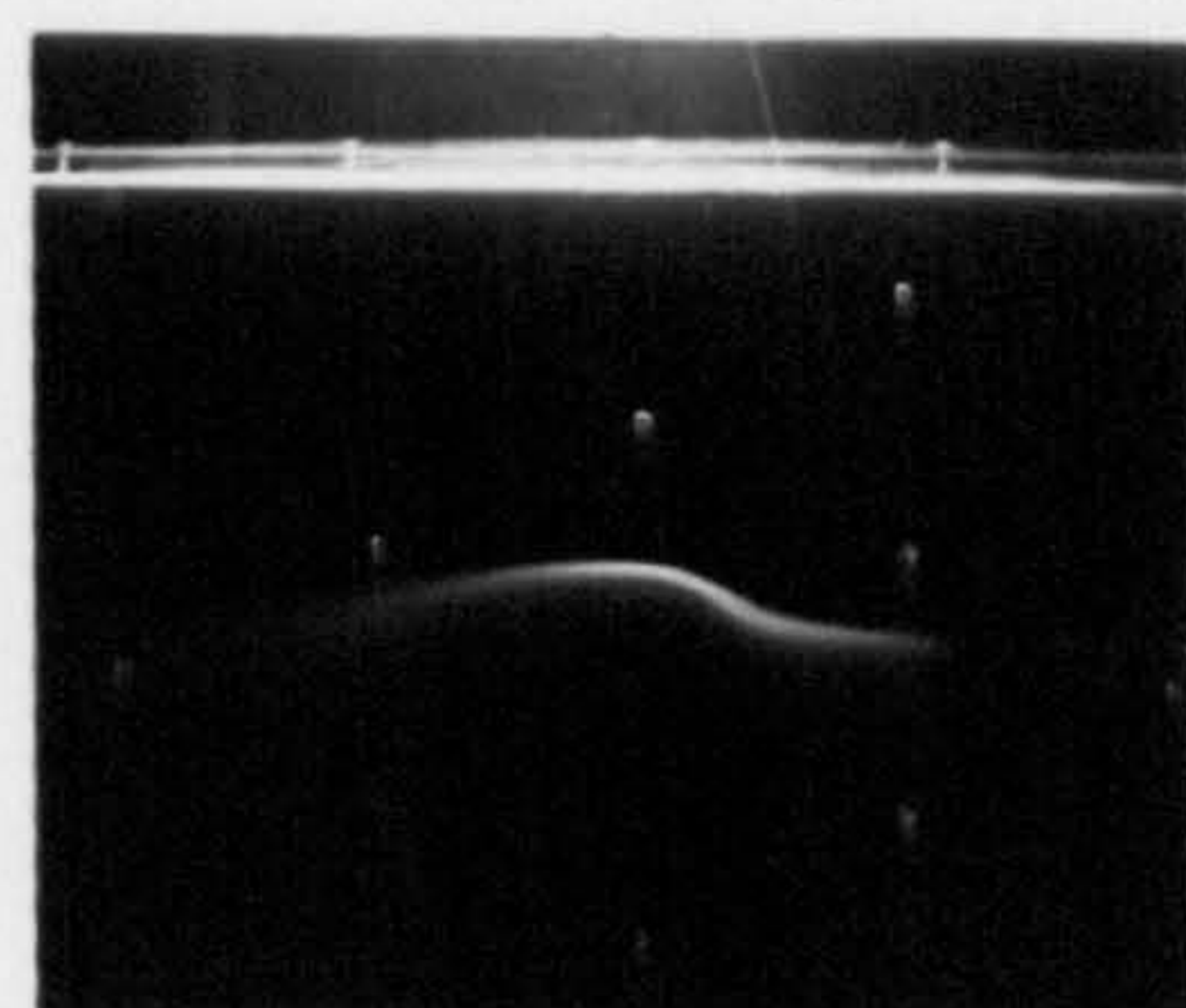
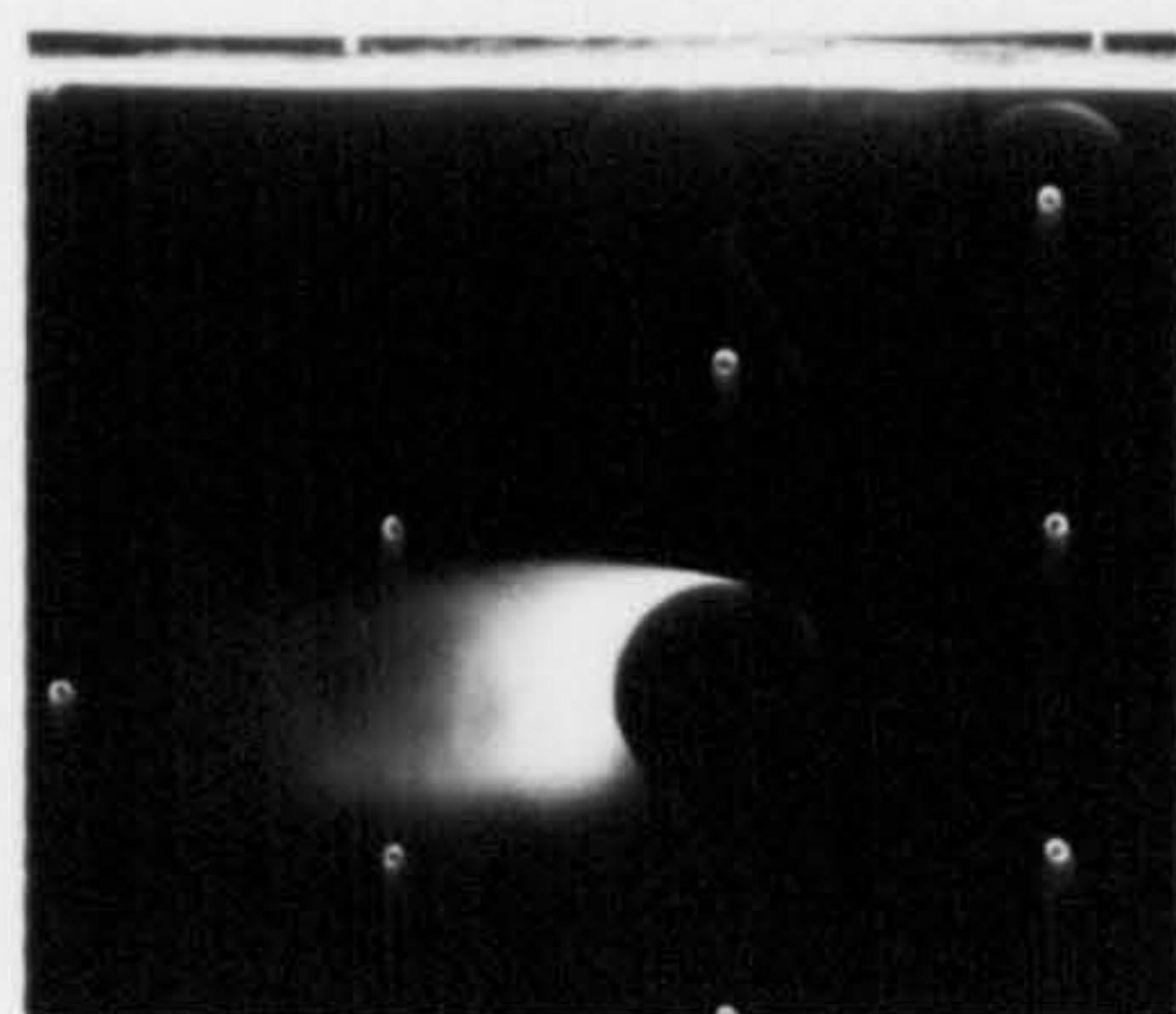
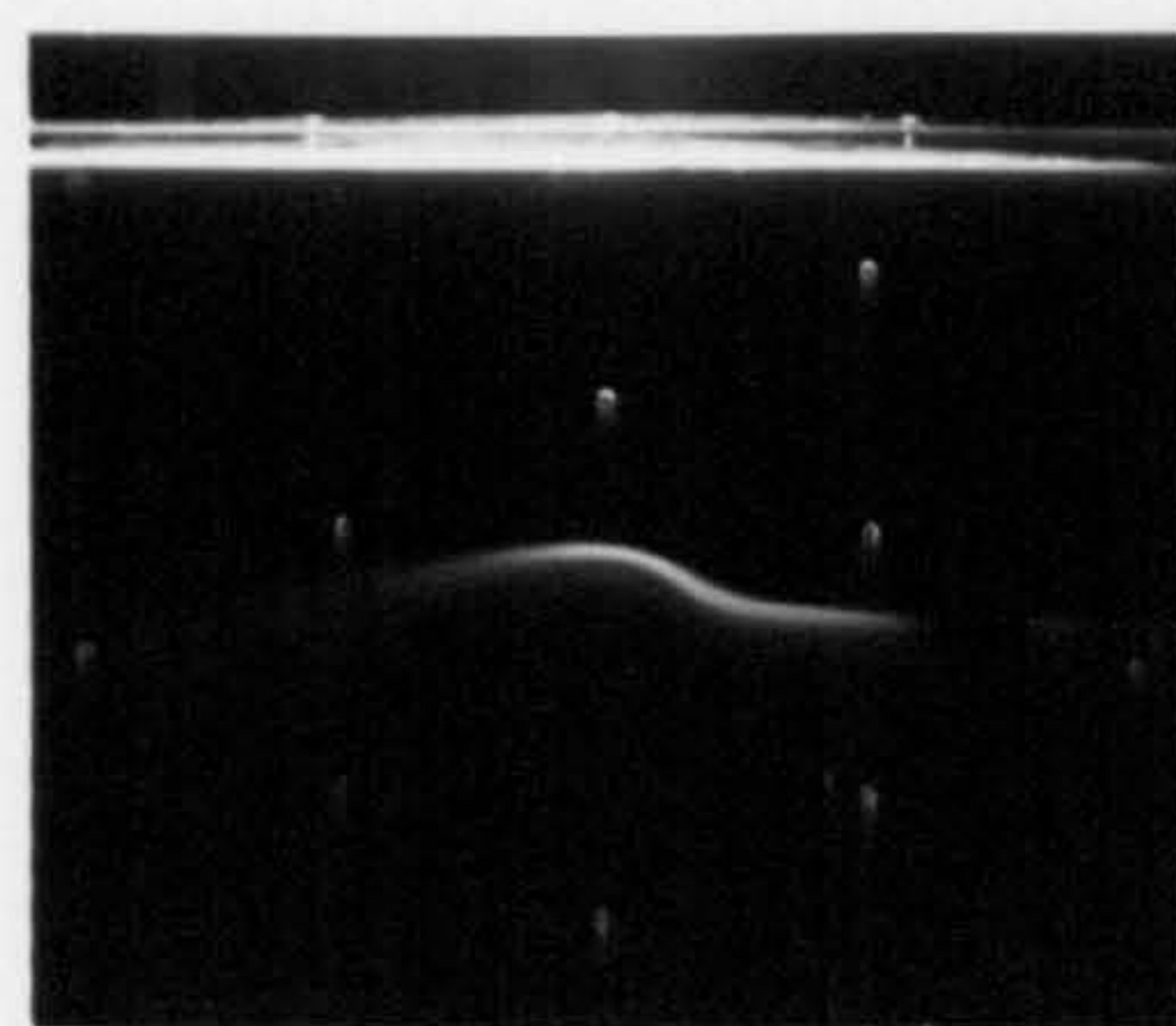
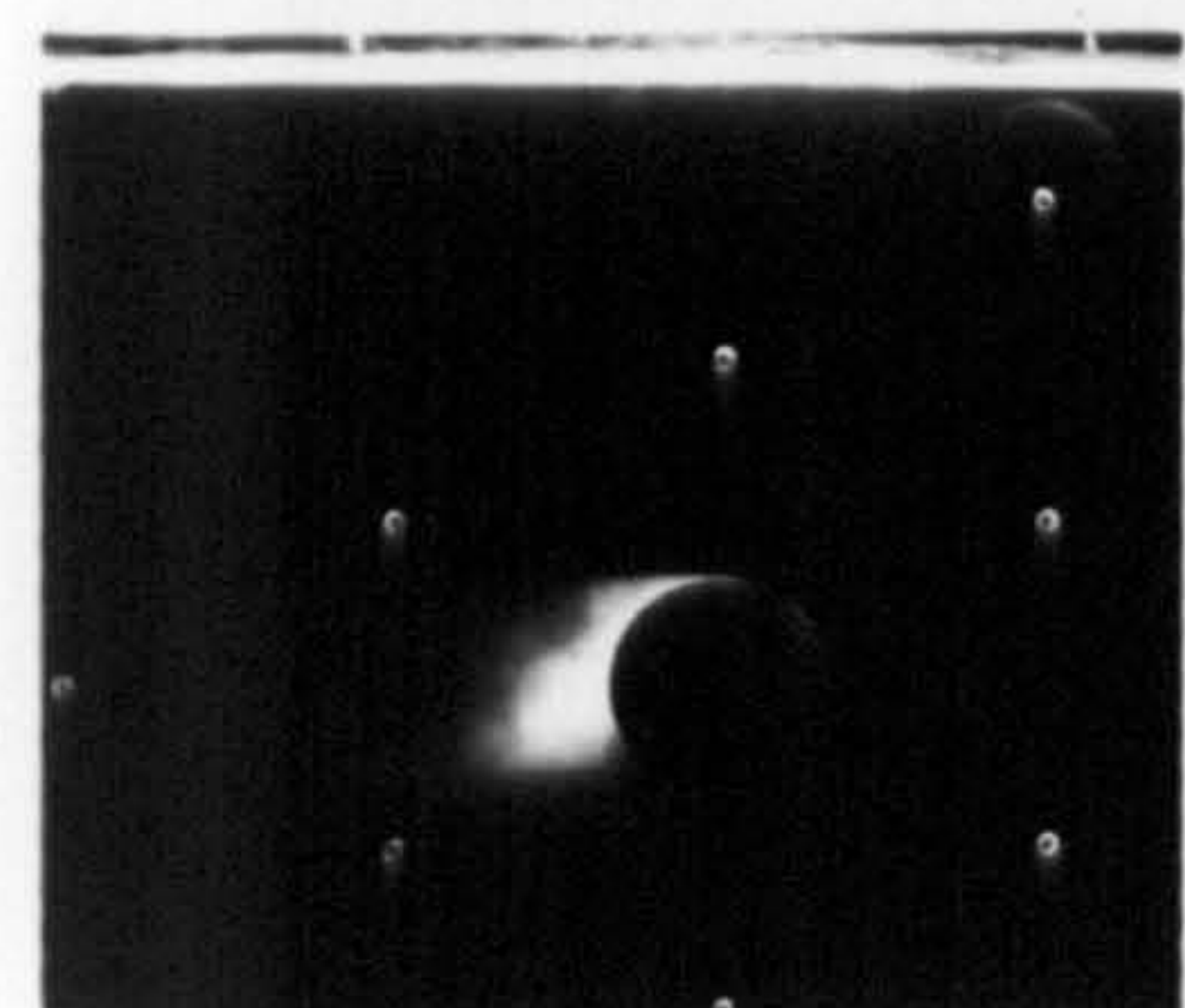
Re=35000 ,  $V_w/U=0.004$

Re=45000 ,  $V_w/U=0.0035$



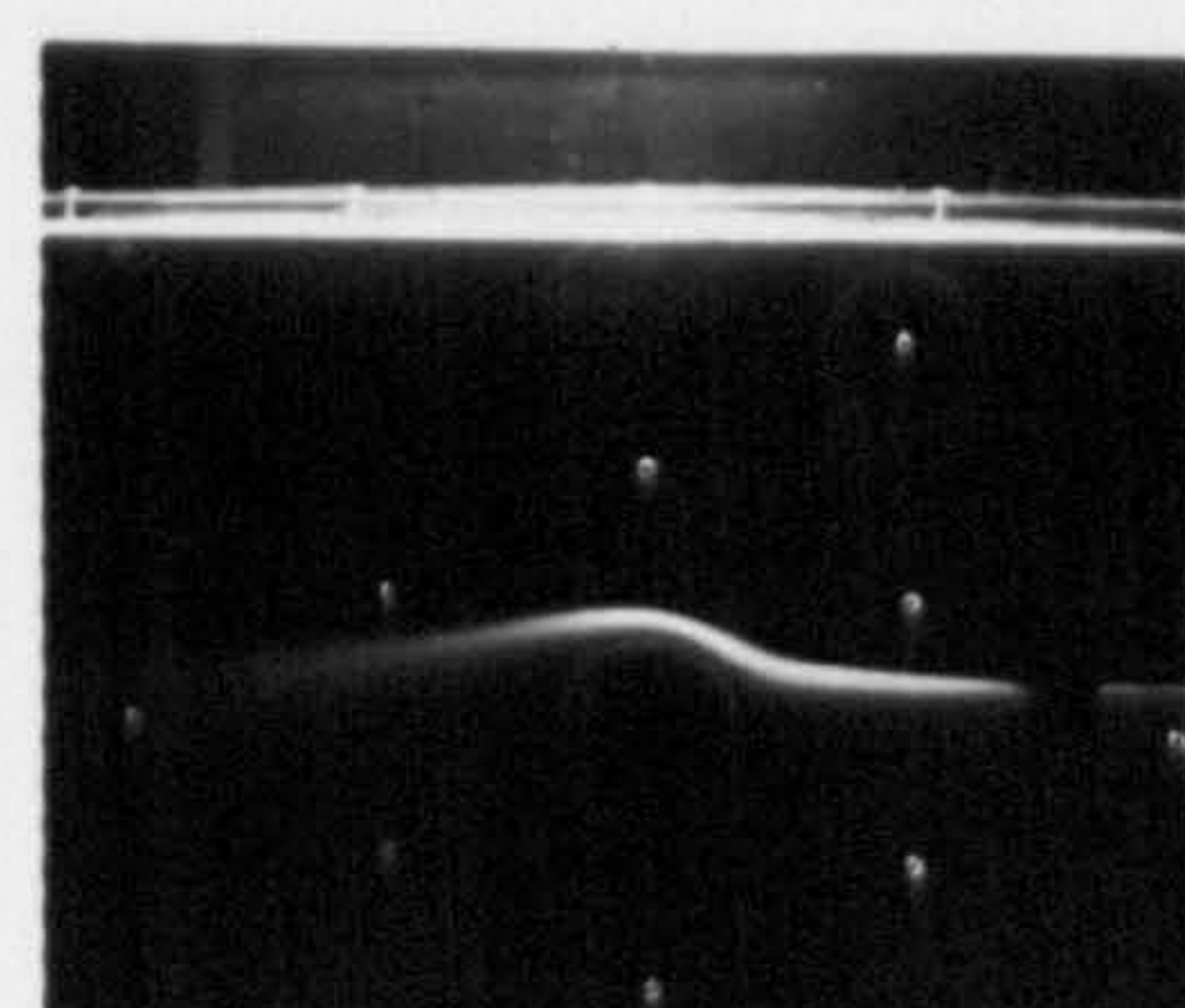
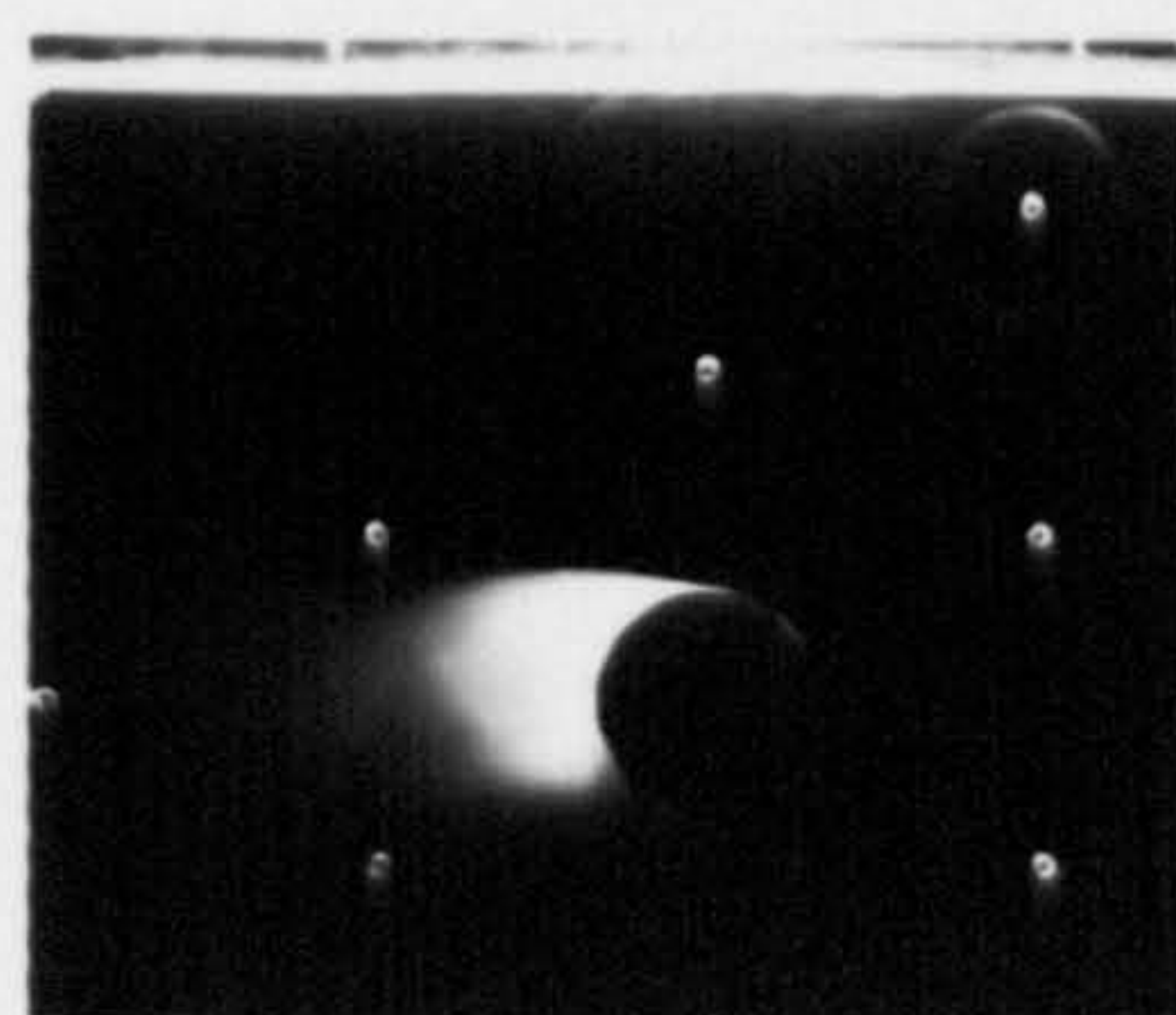
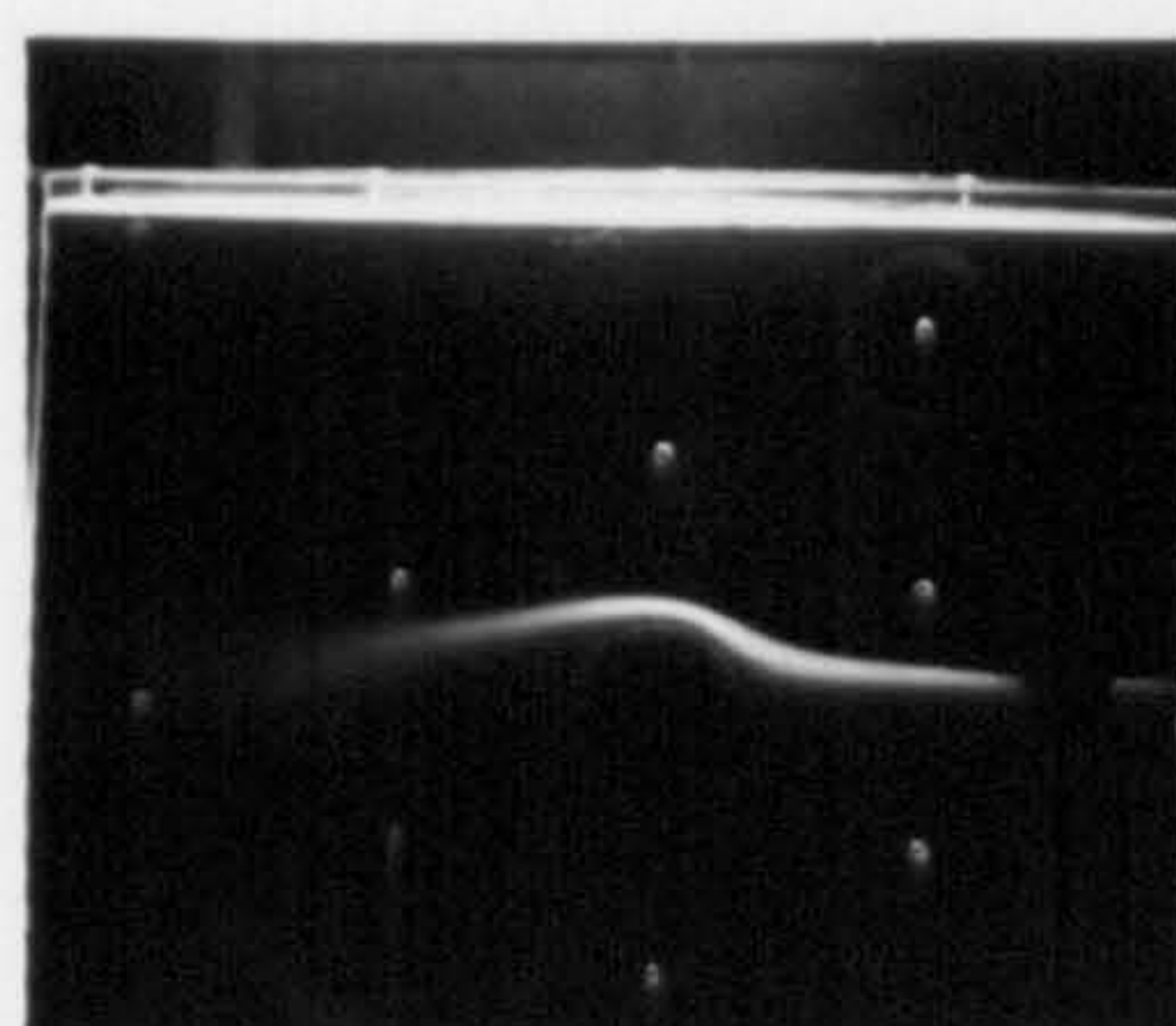
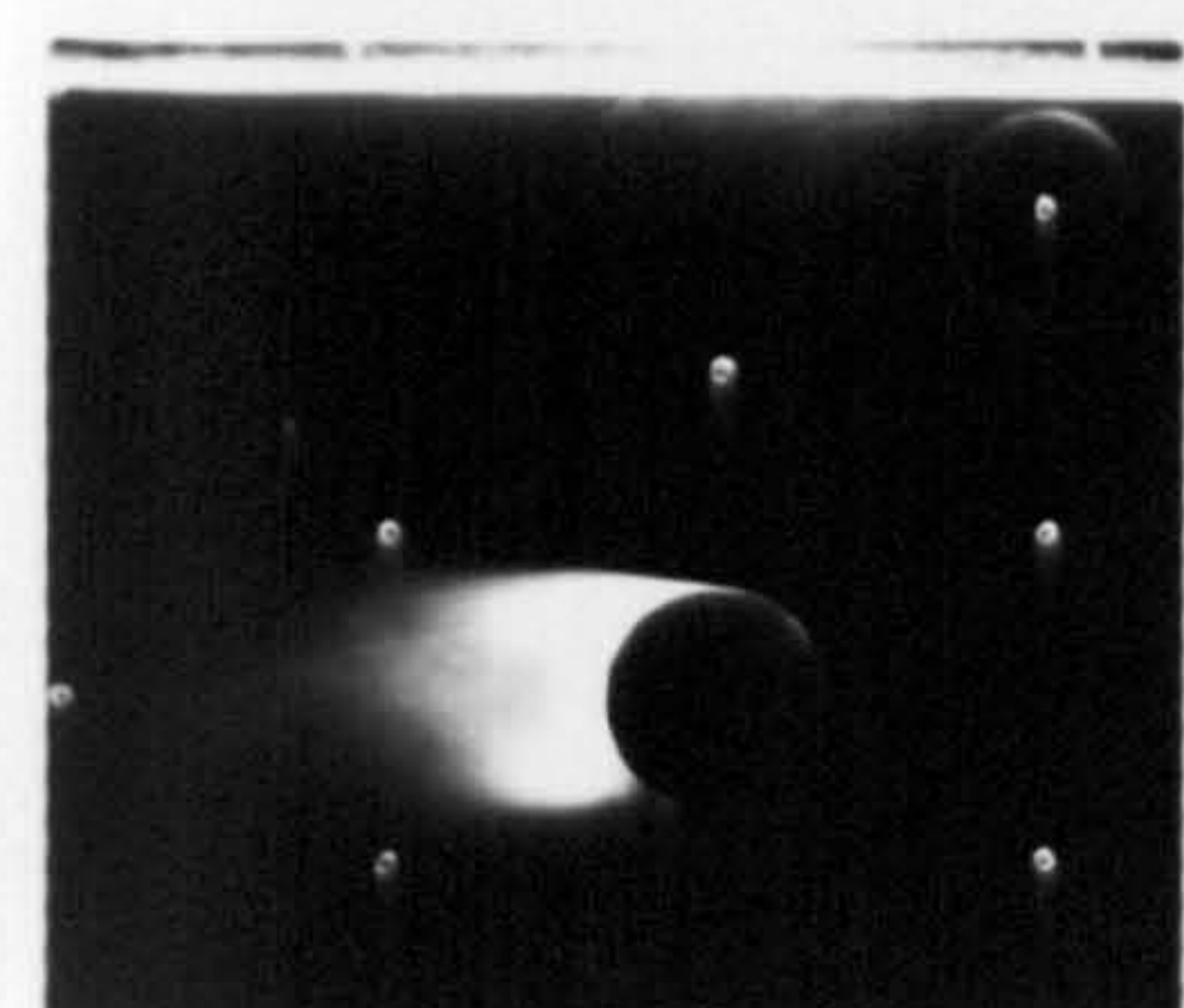
Re=35000 ,  $V_w/U=0.009$

Re=45000 ,  $V_w/U=0.007$



Re=35000 ,  $V_w/U=0.013$

Re=45000 ,  $V_w/U=0.01$

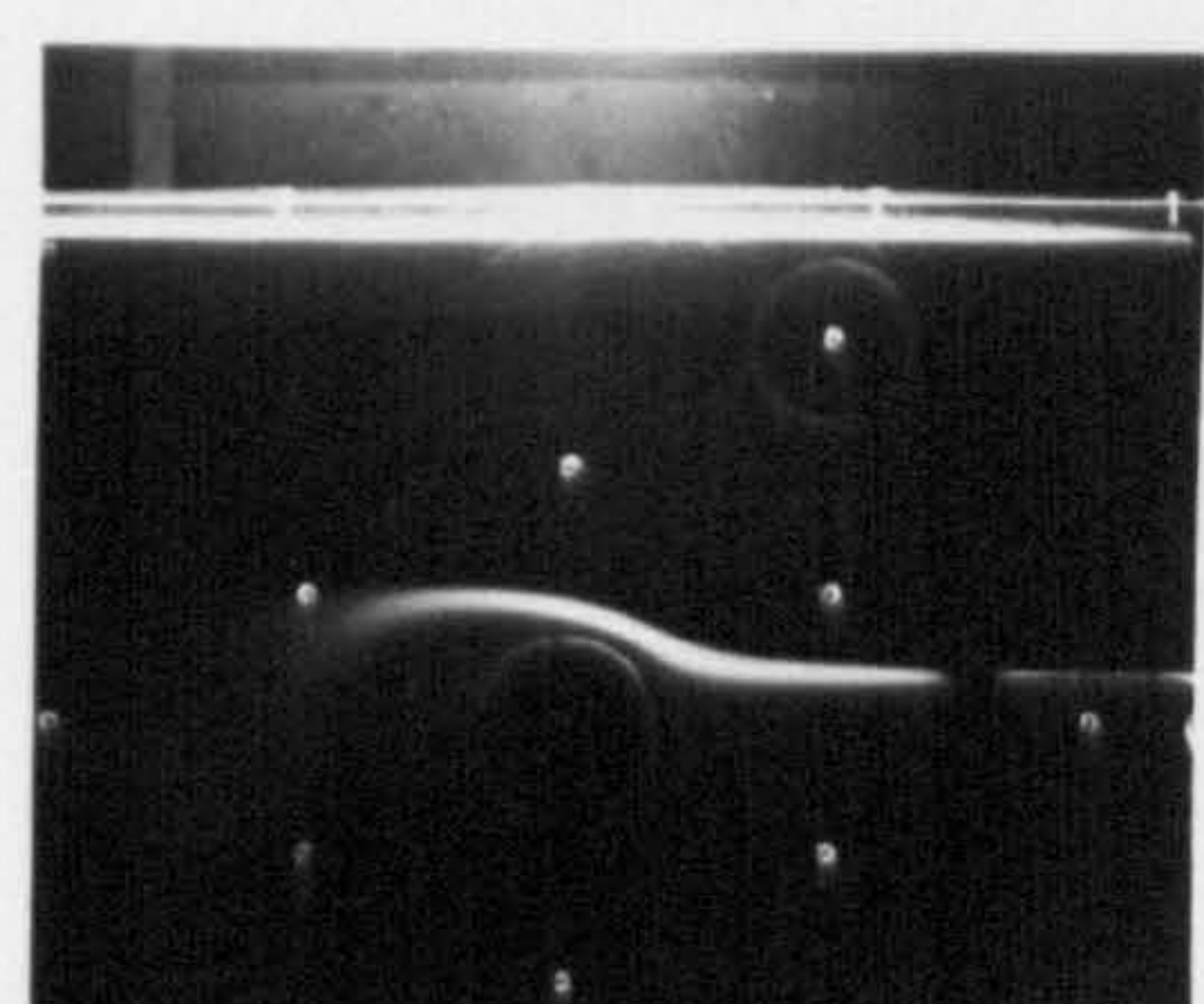
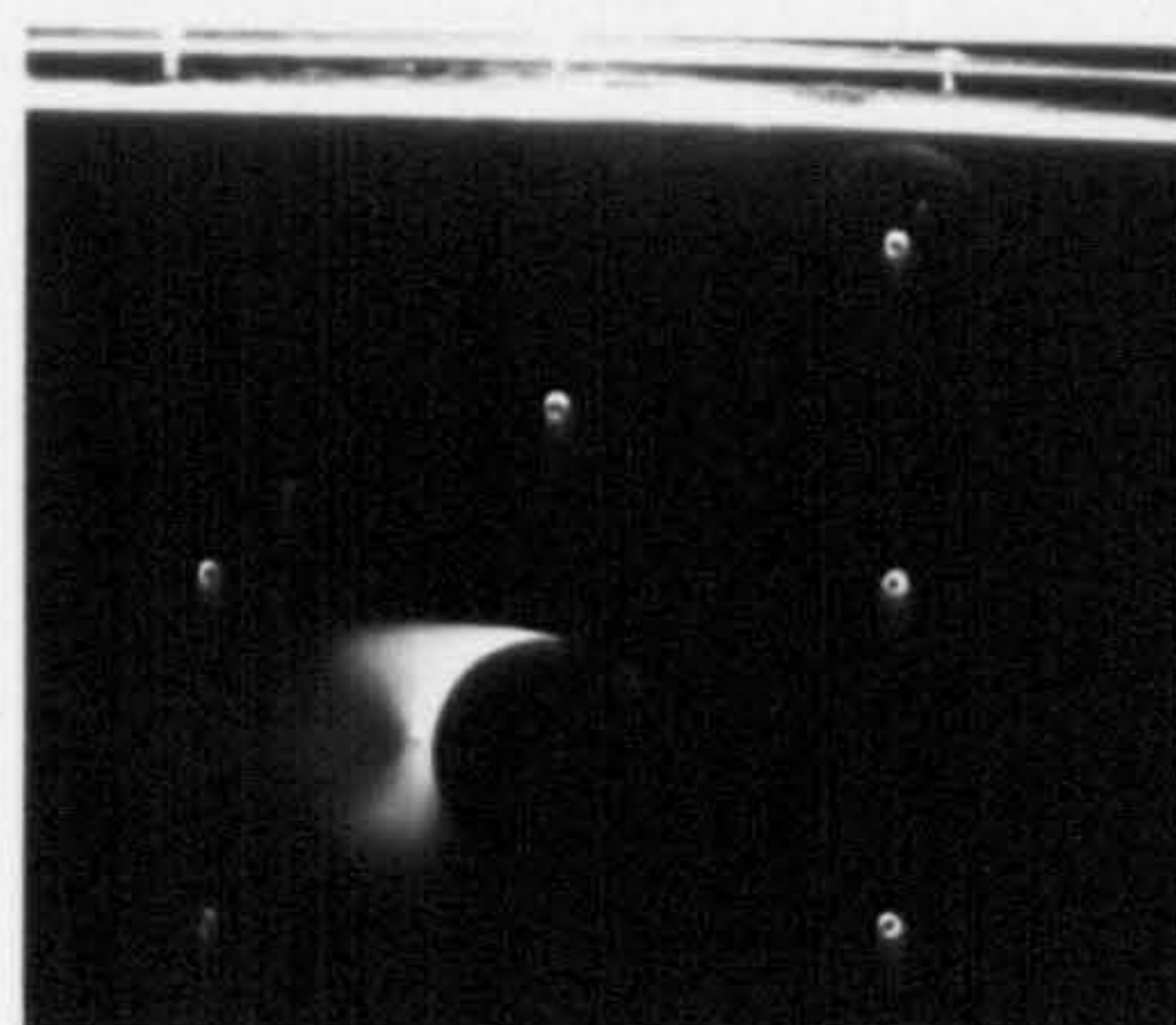
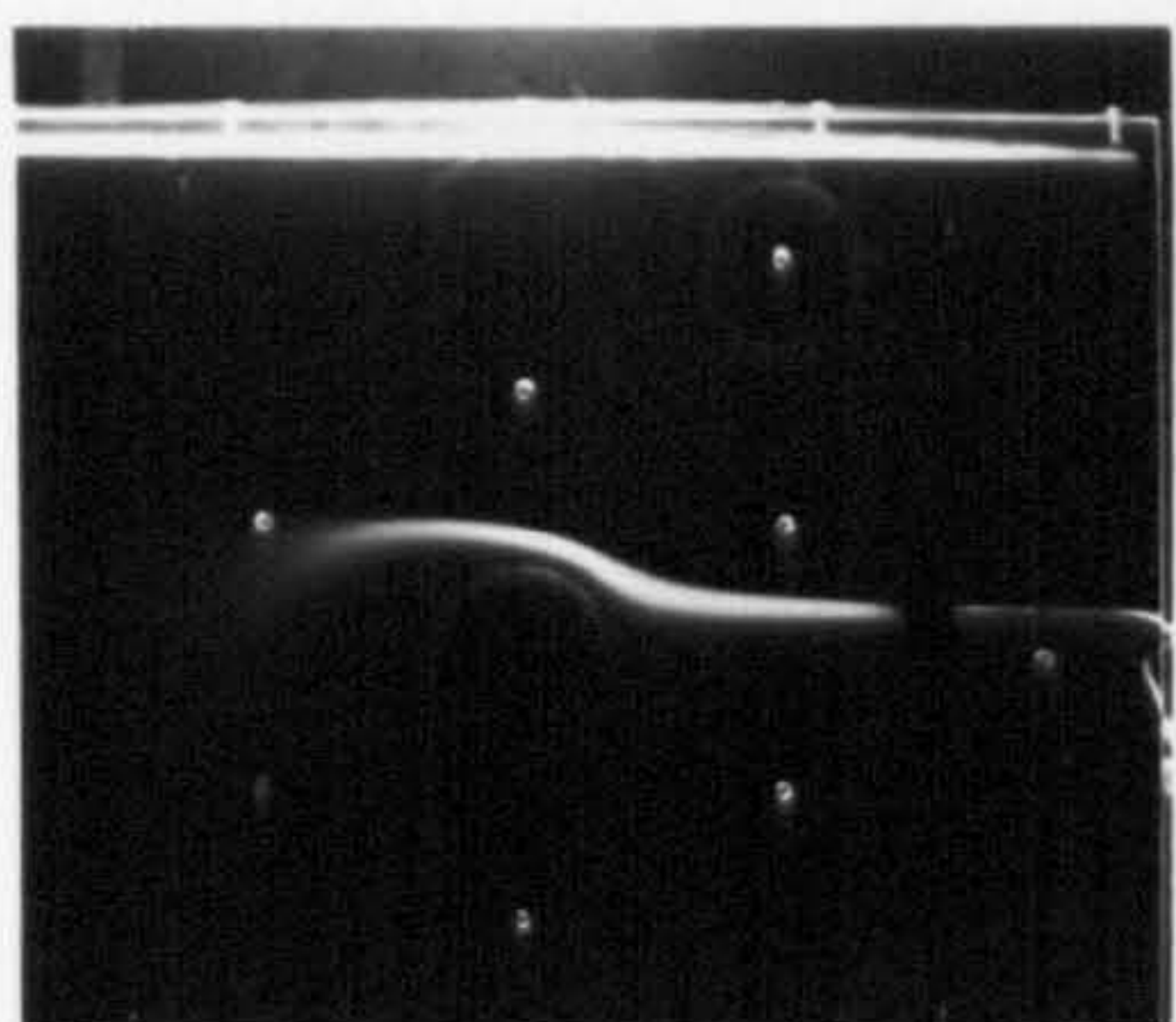
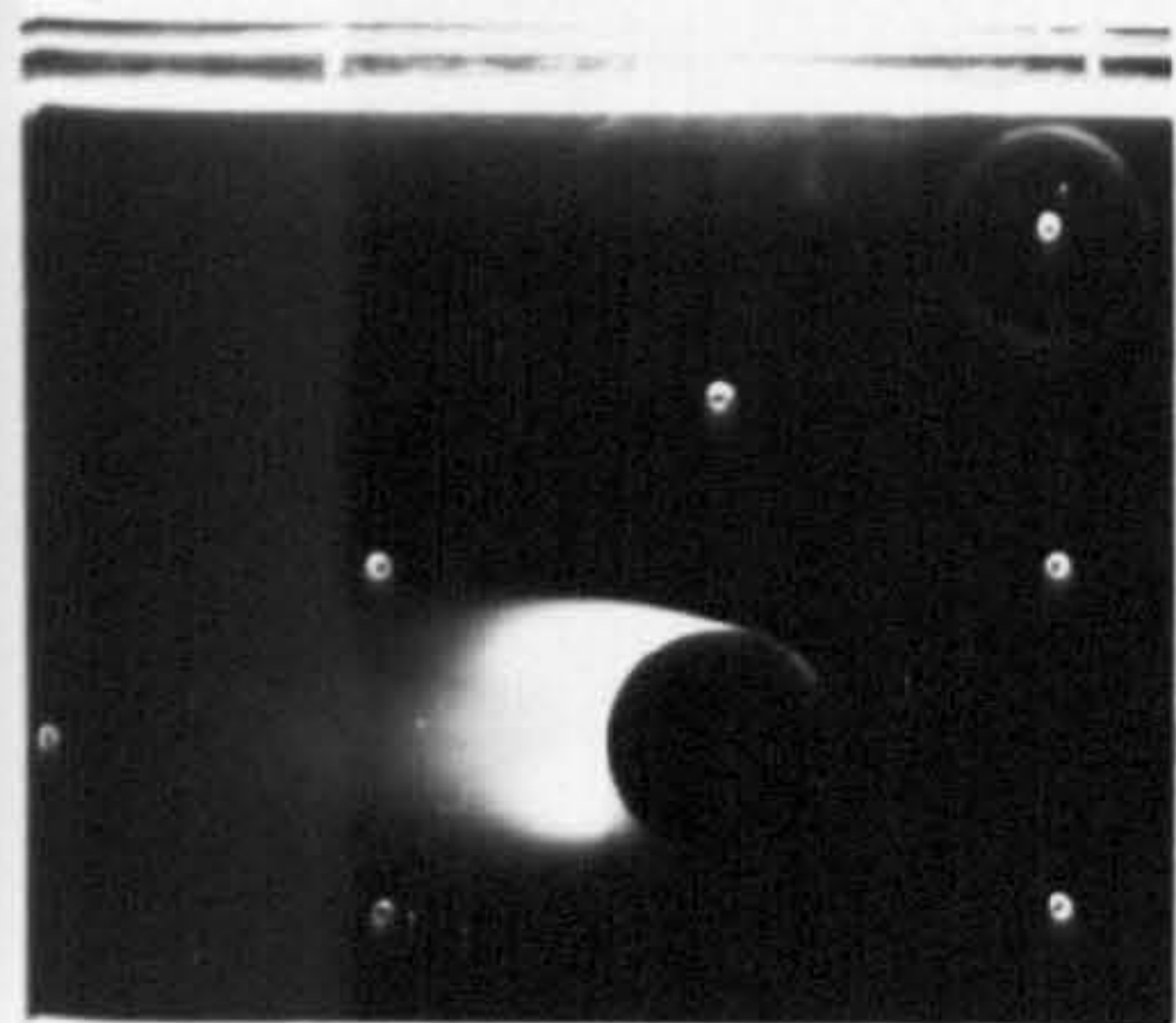


Re=35000 ,  $V_w/U=0.017$

Re=45000 ,  $V_w/U=0.013$

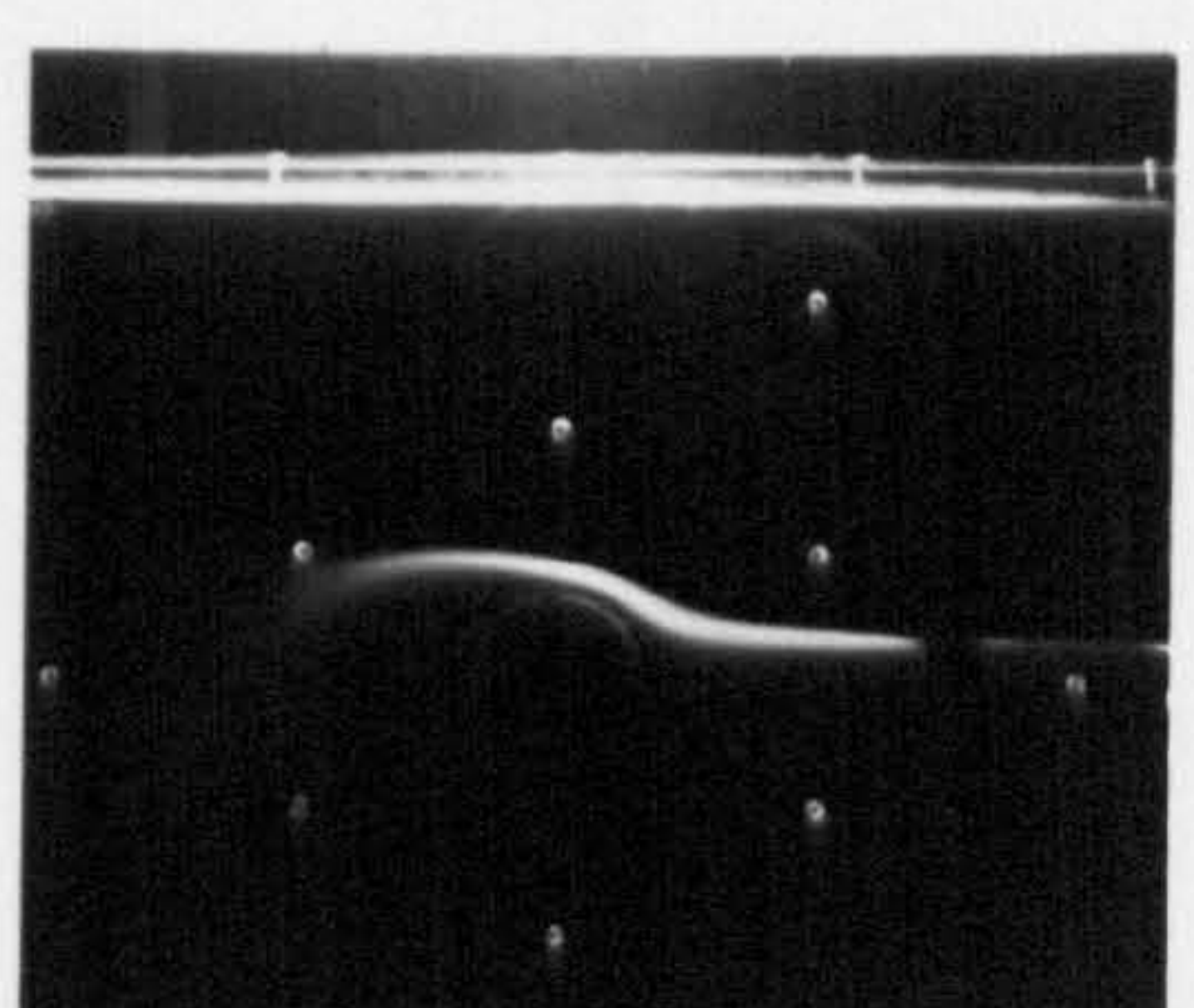
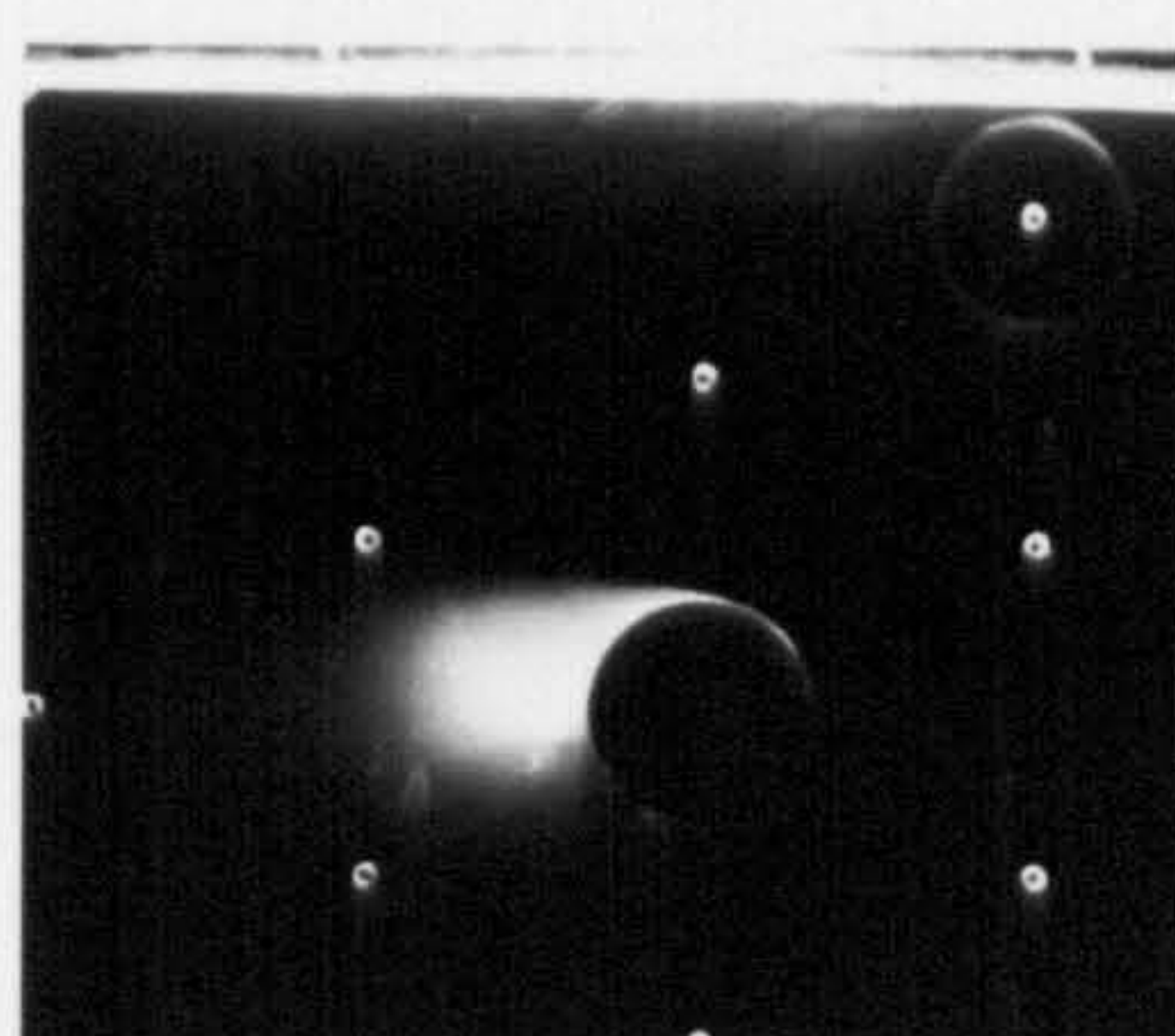
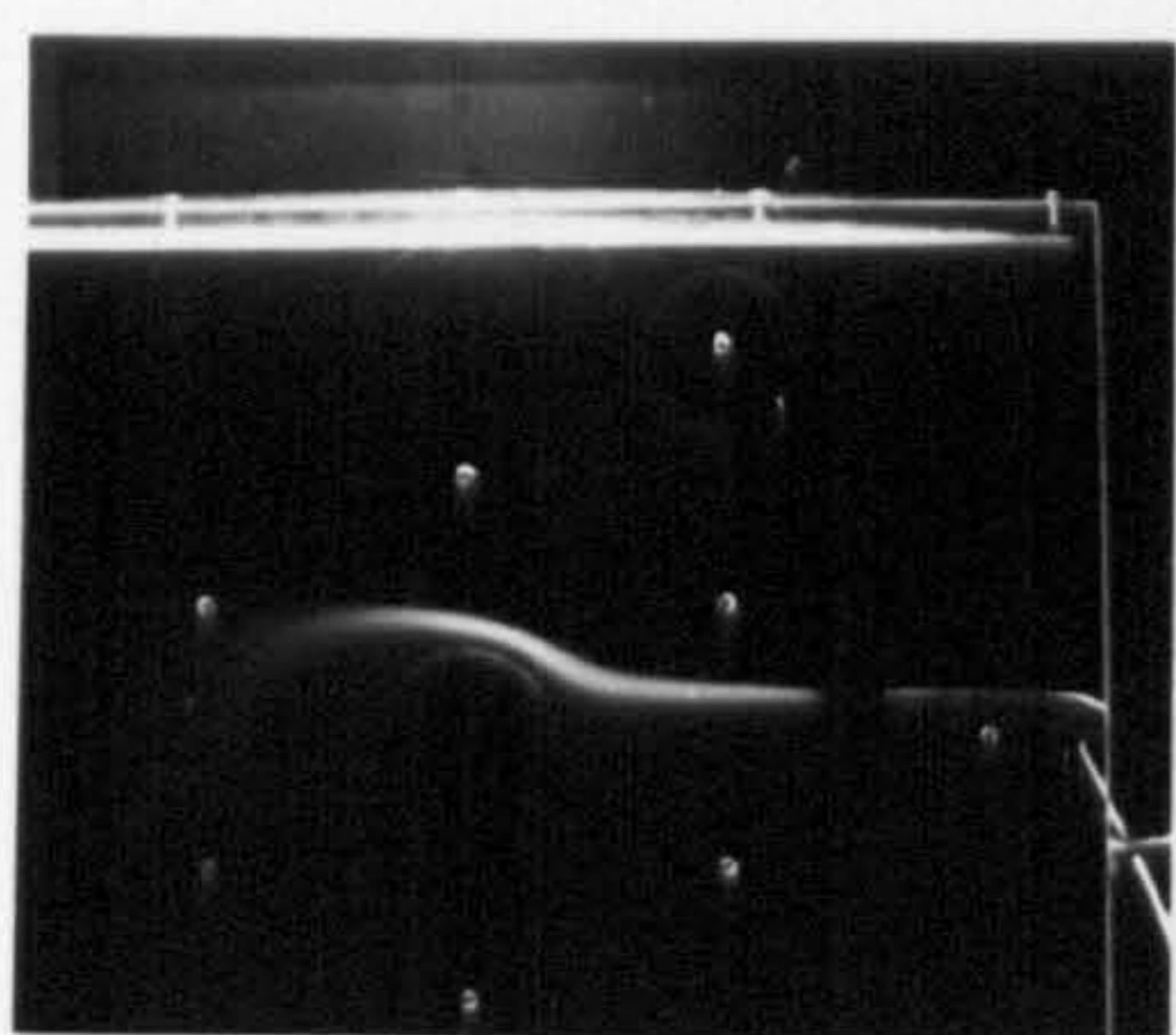
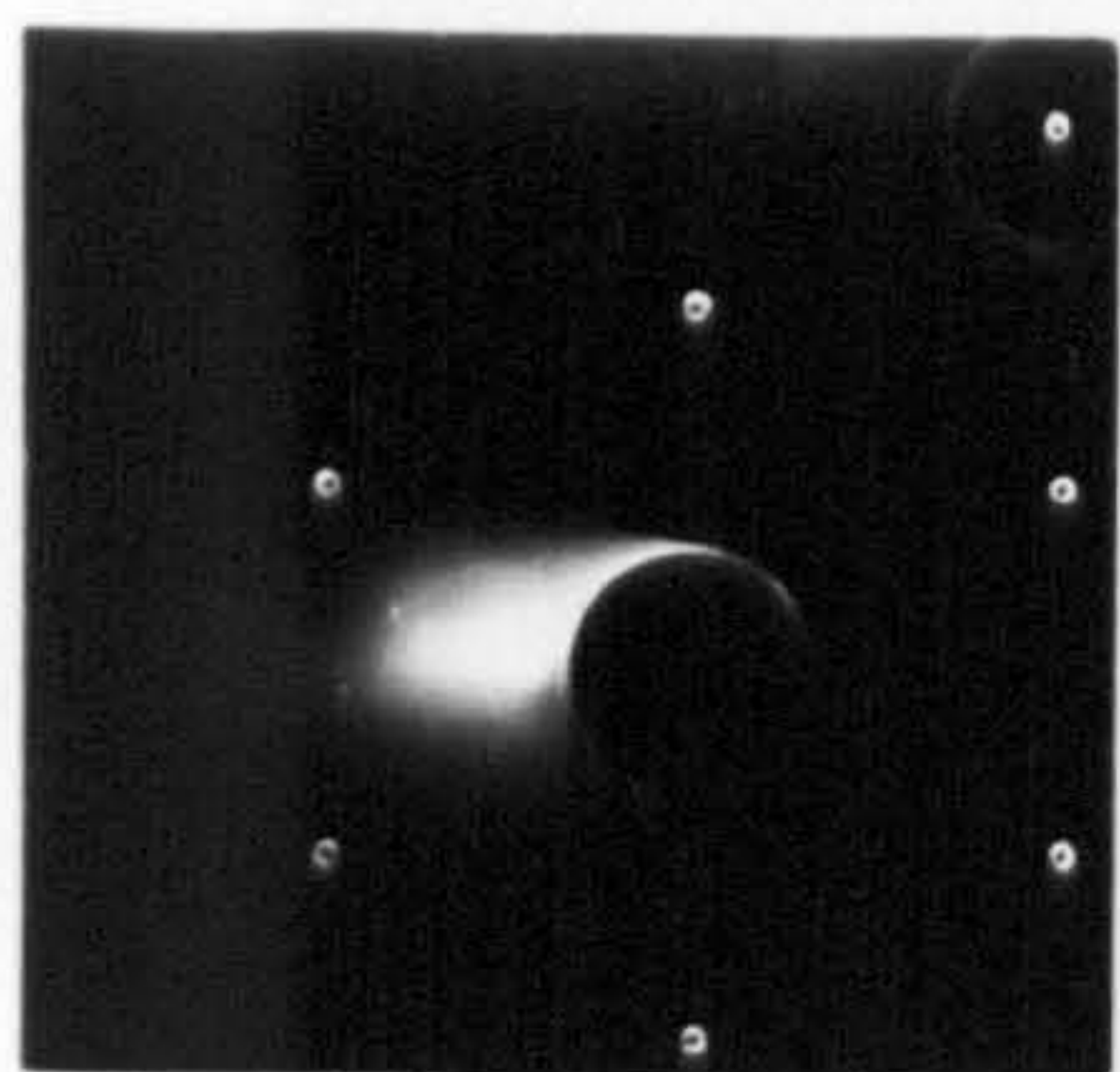
FIGURE 10.3





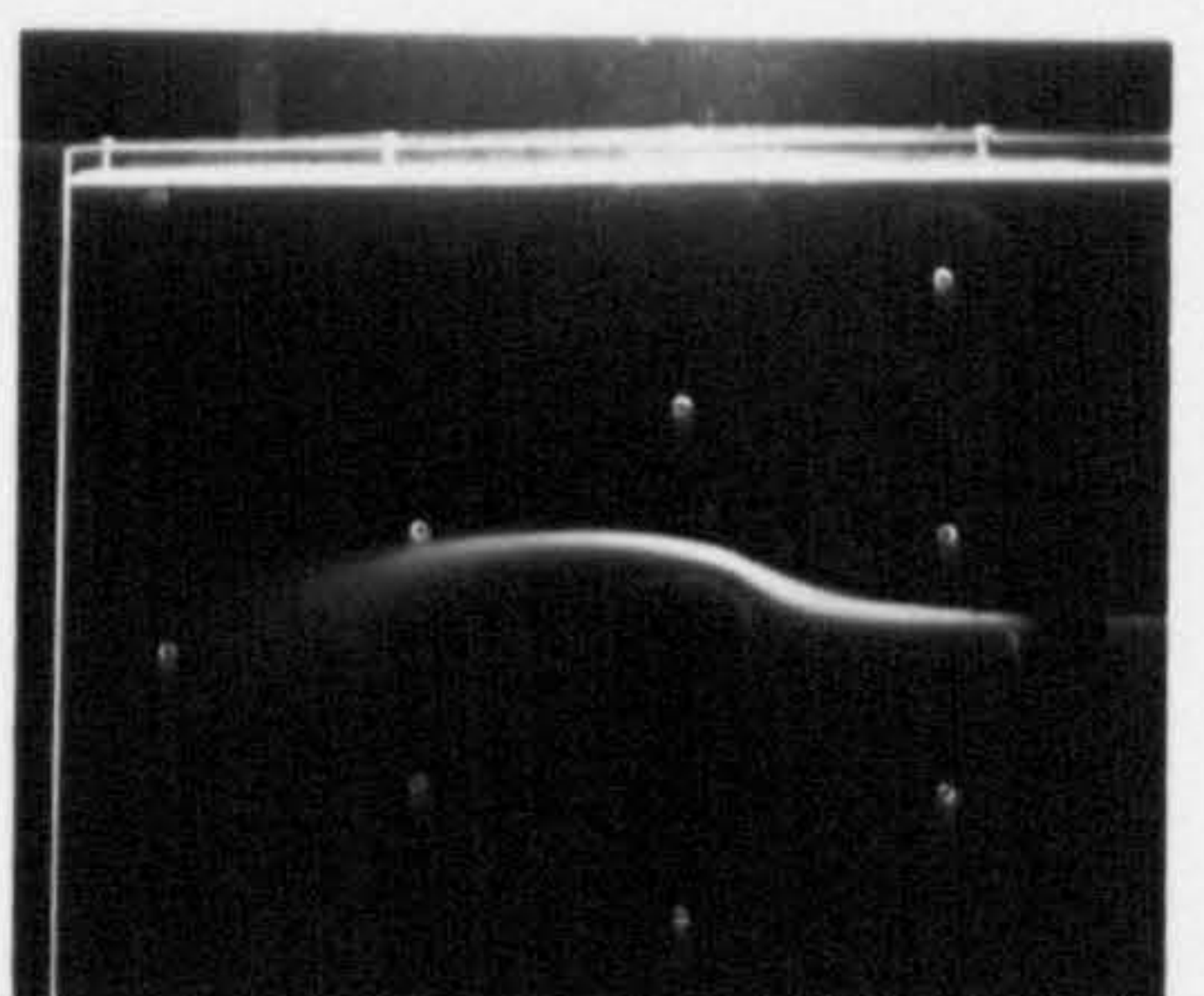
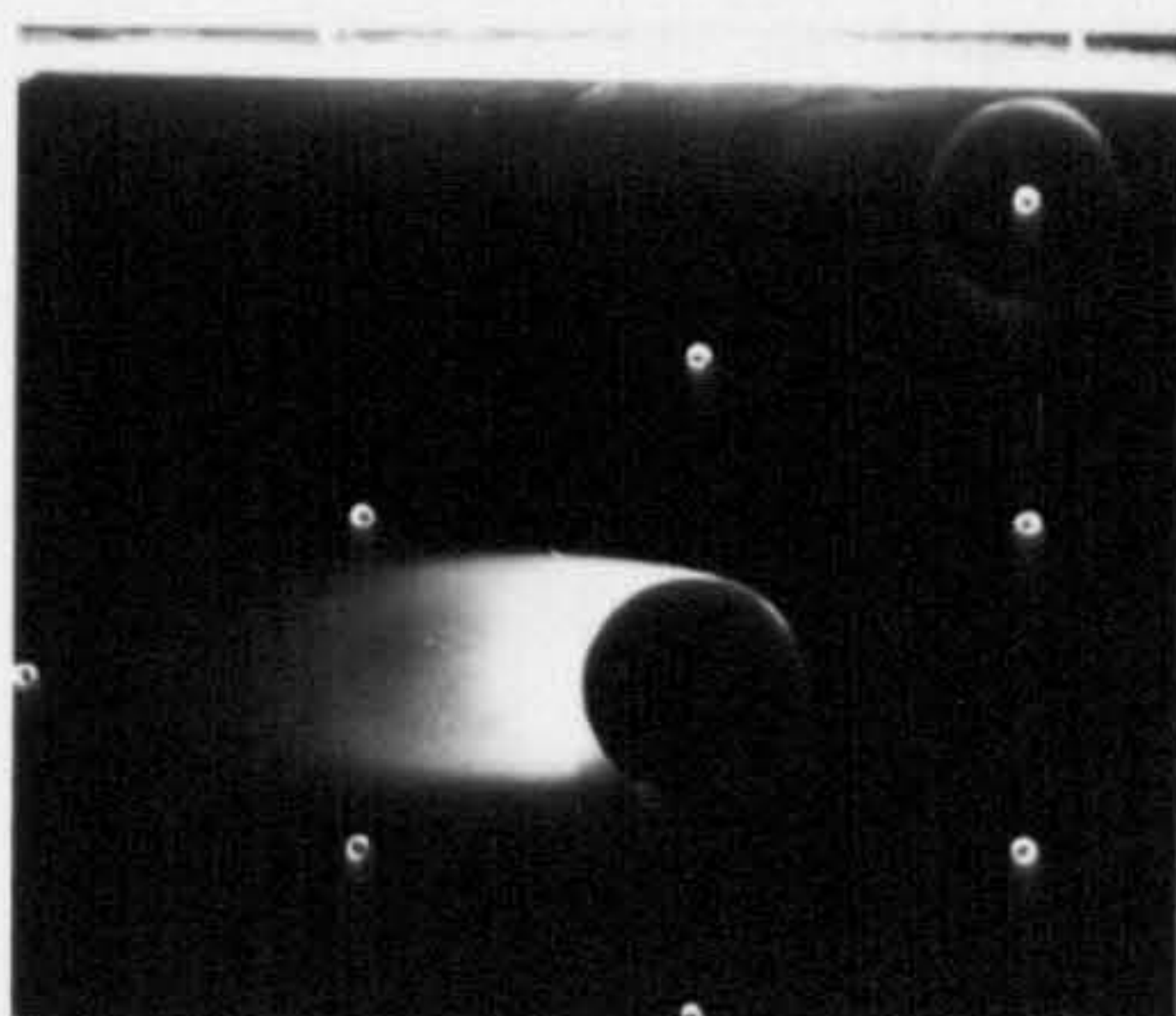
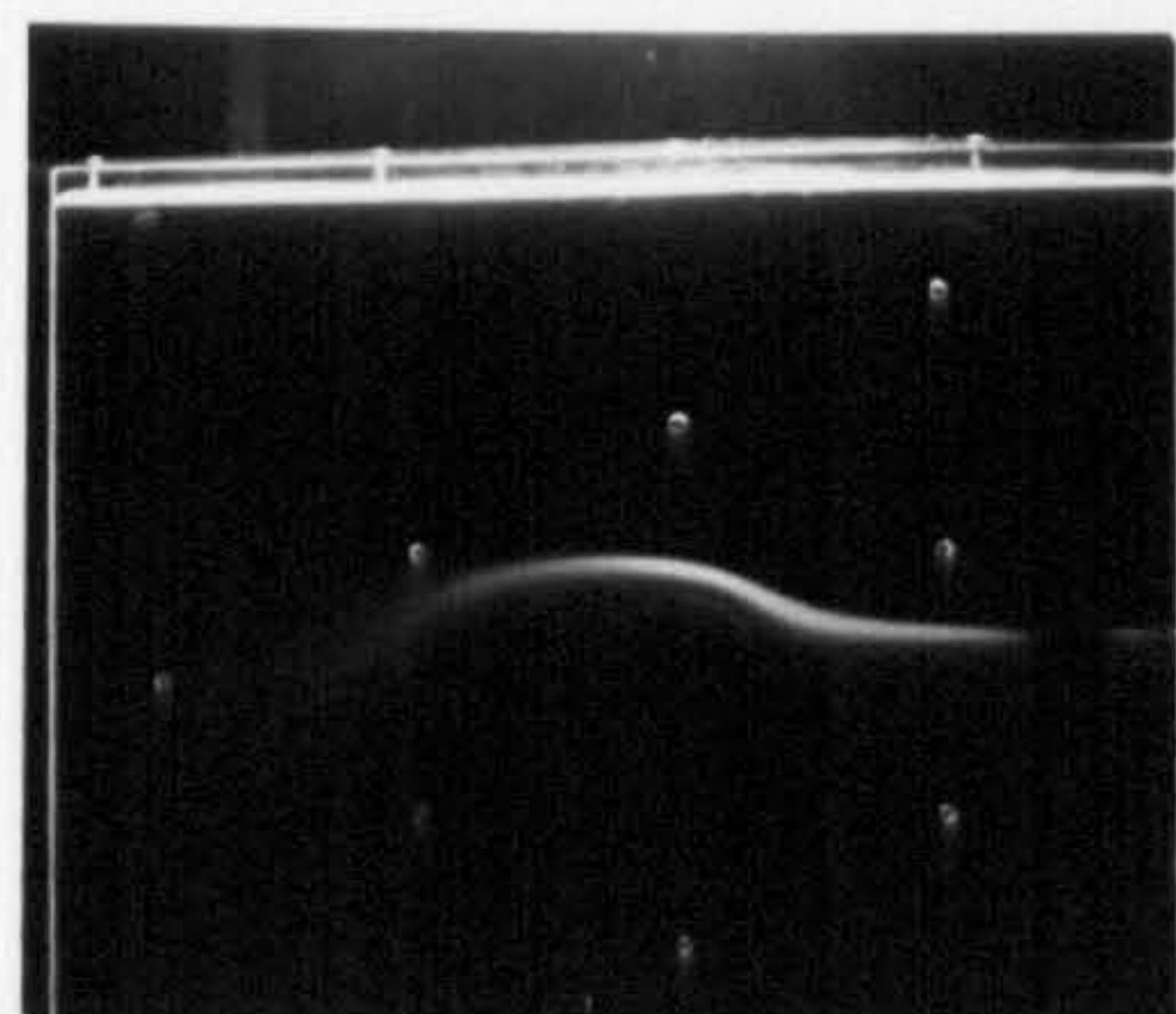
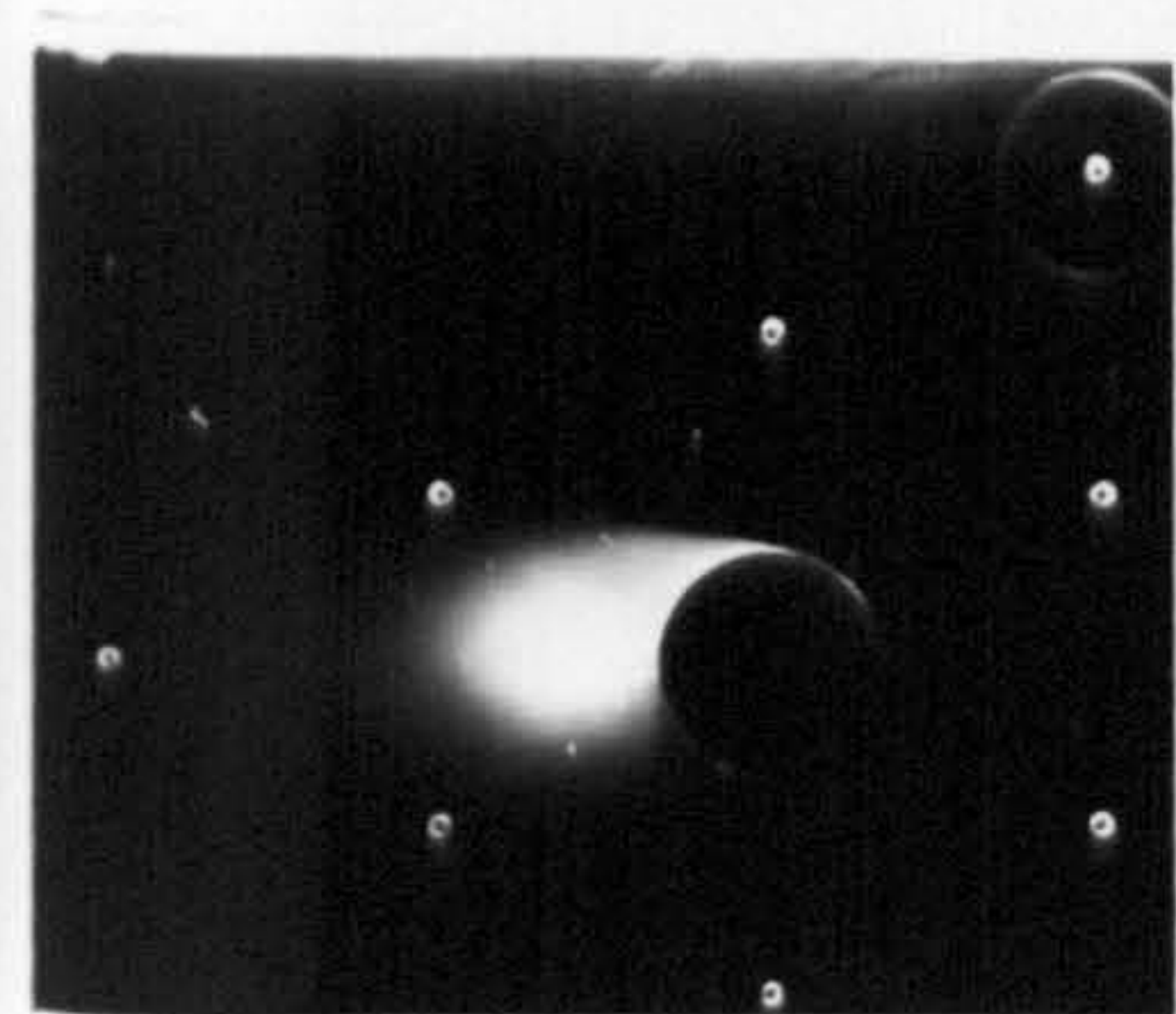
Re=55000 ,  $V_w/U=0.0$

Re= 66000 ,  $V_w/U=0.0$



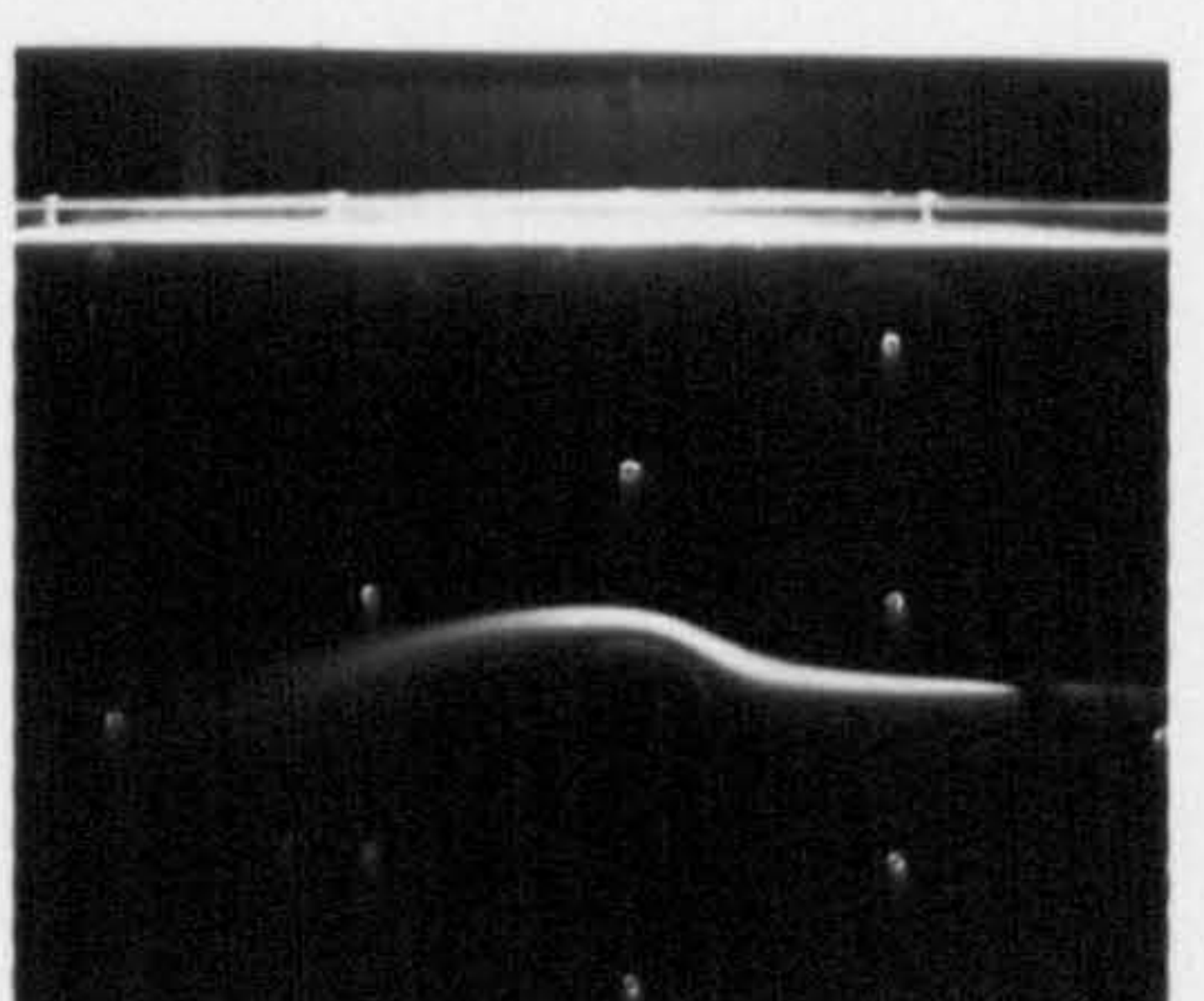
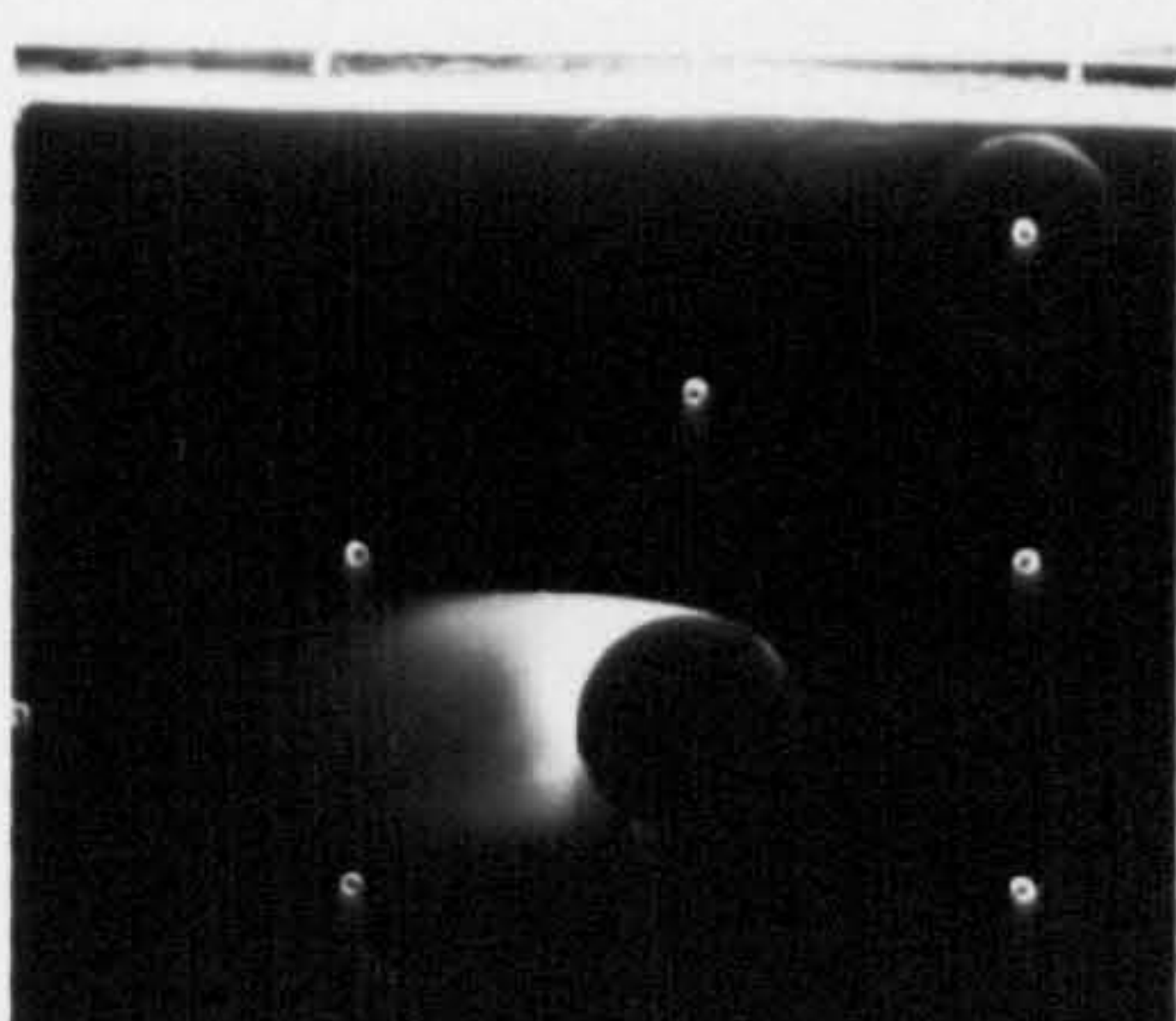
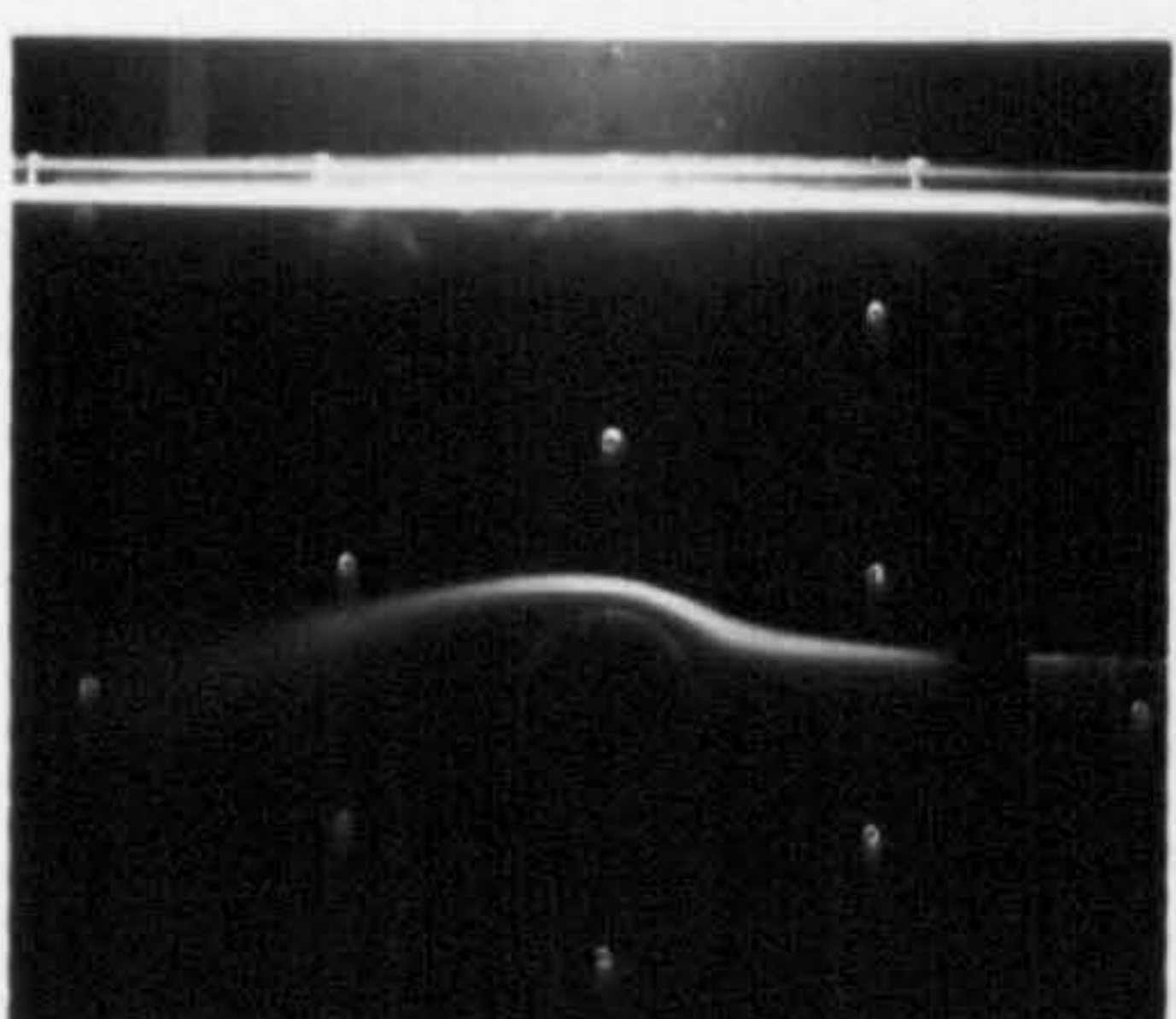
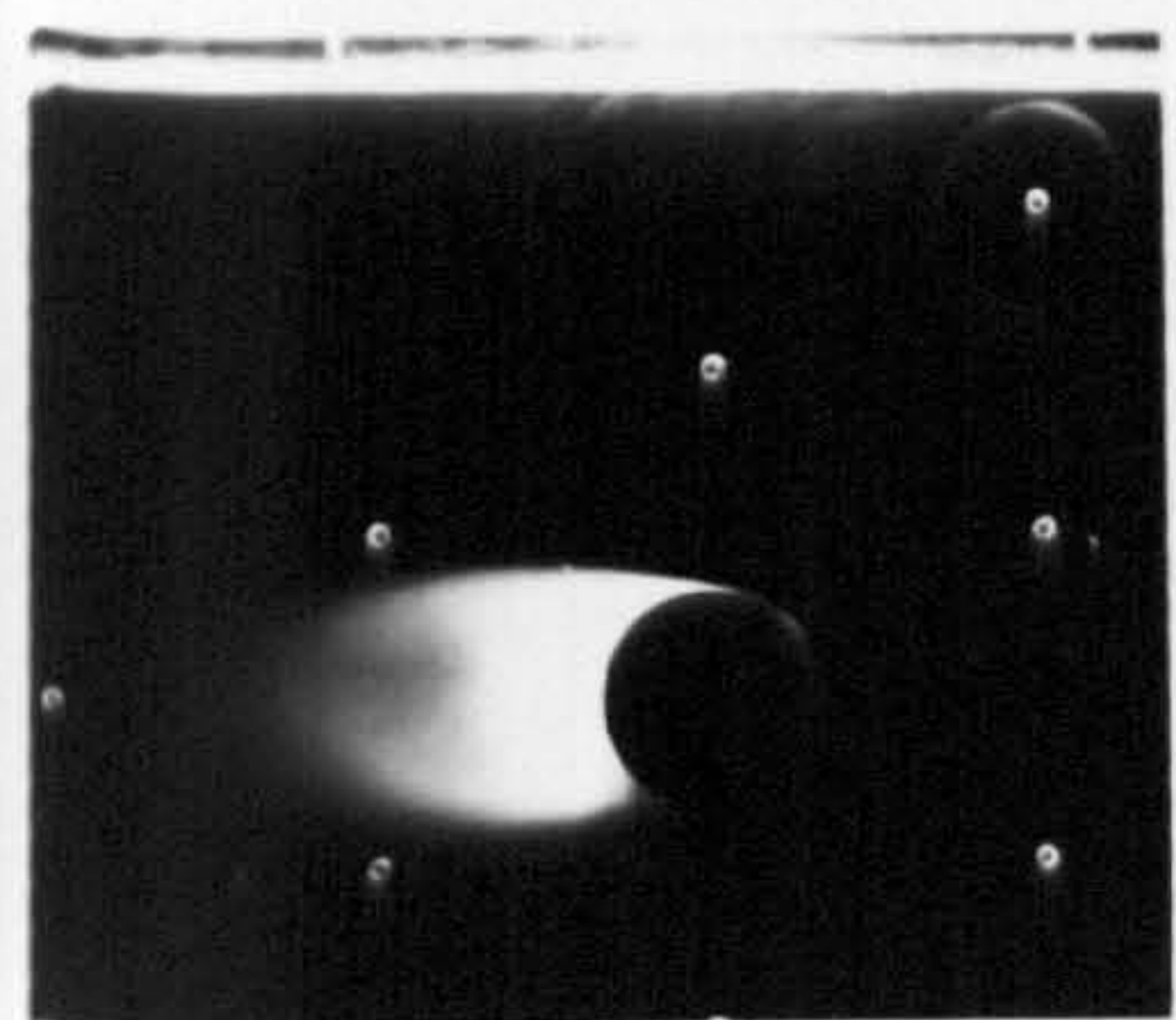
Re= 55000 ,  $V_w/U=0.003$

Re=66000 ,  $V_w/U=0.0023$



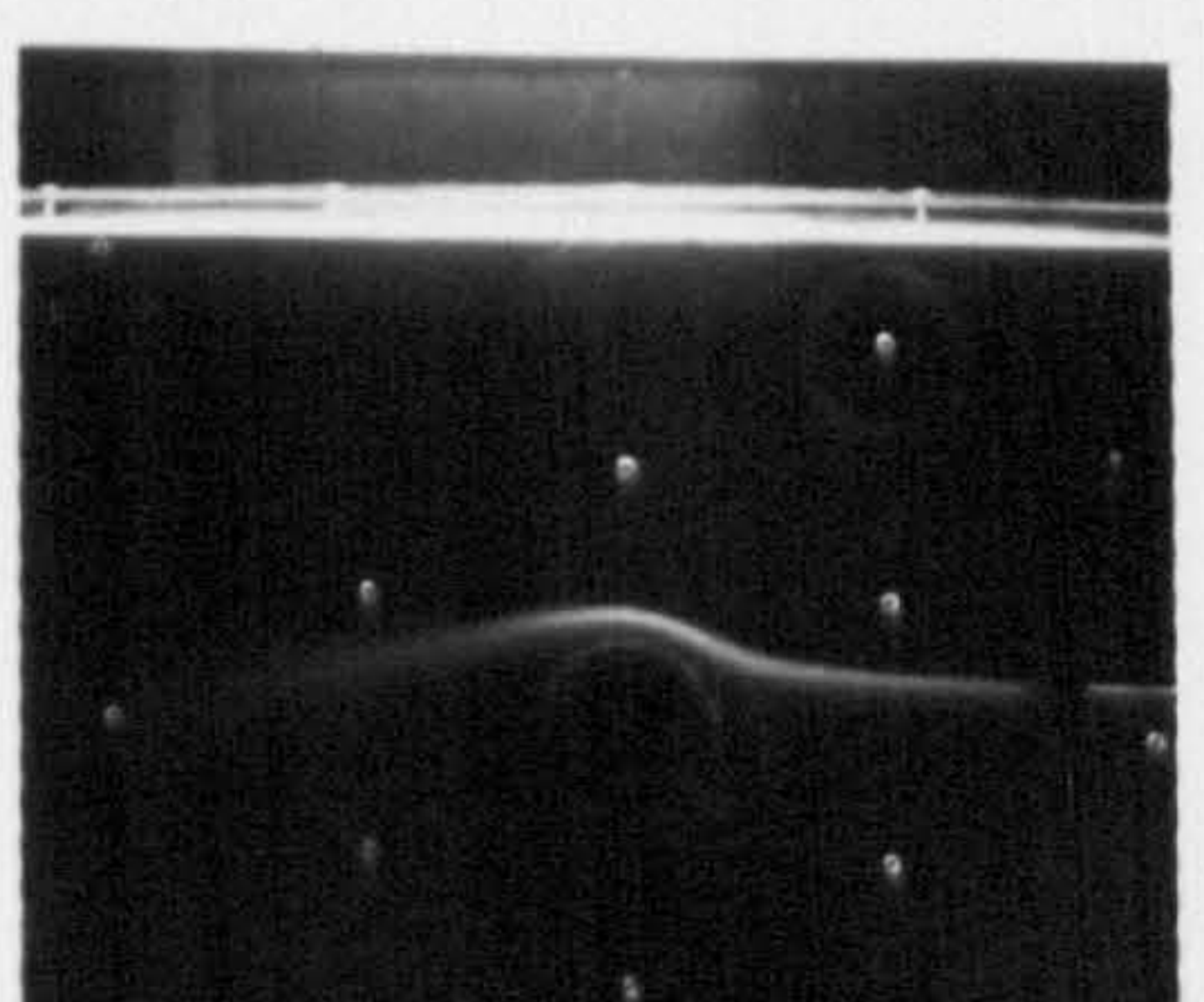
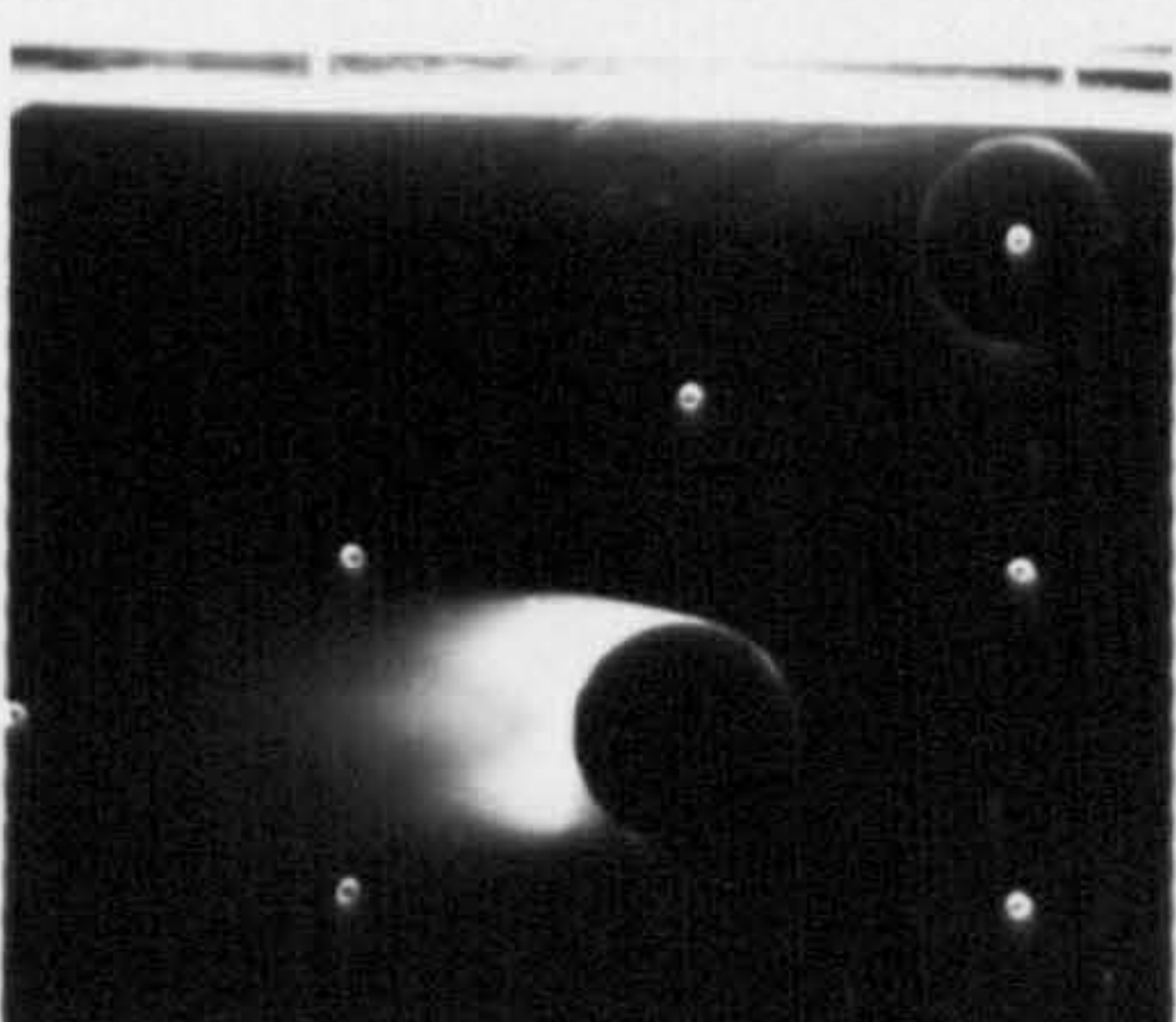
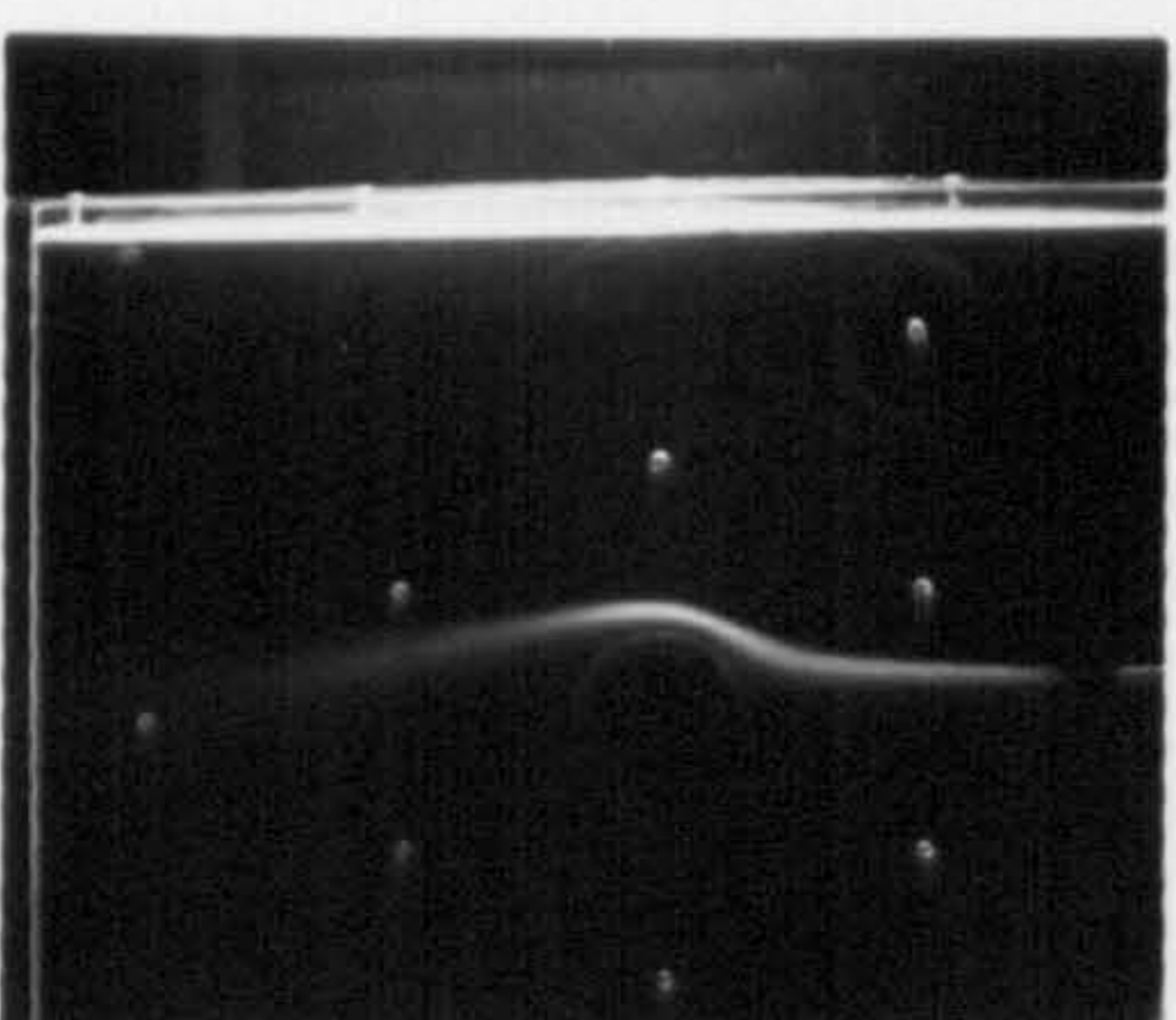
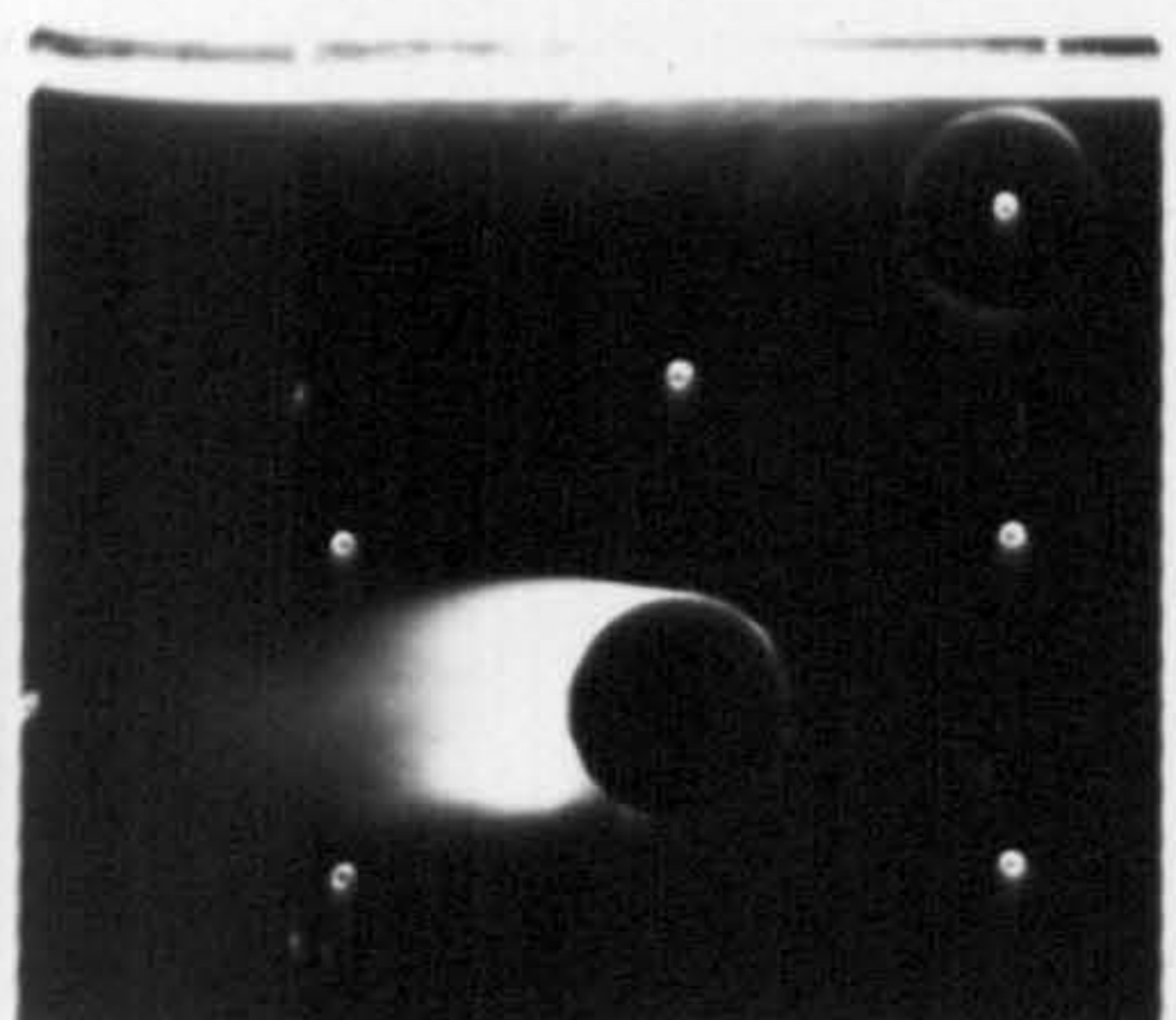
Re=55000 ,  $V_w/U=0.0057$

Re=66000 ,  $V_w/U=0.005$



Re=55000 ,  $V_w/U=0.0086$

Re=66000 ,  $V_w/U=0.0072$

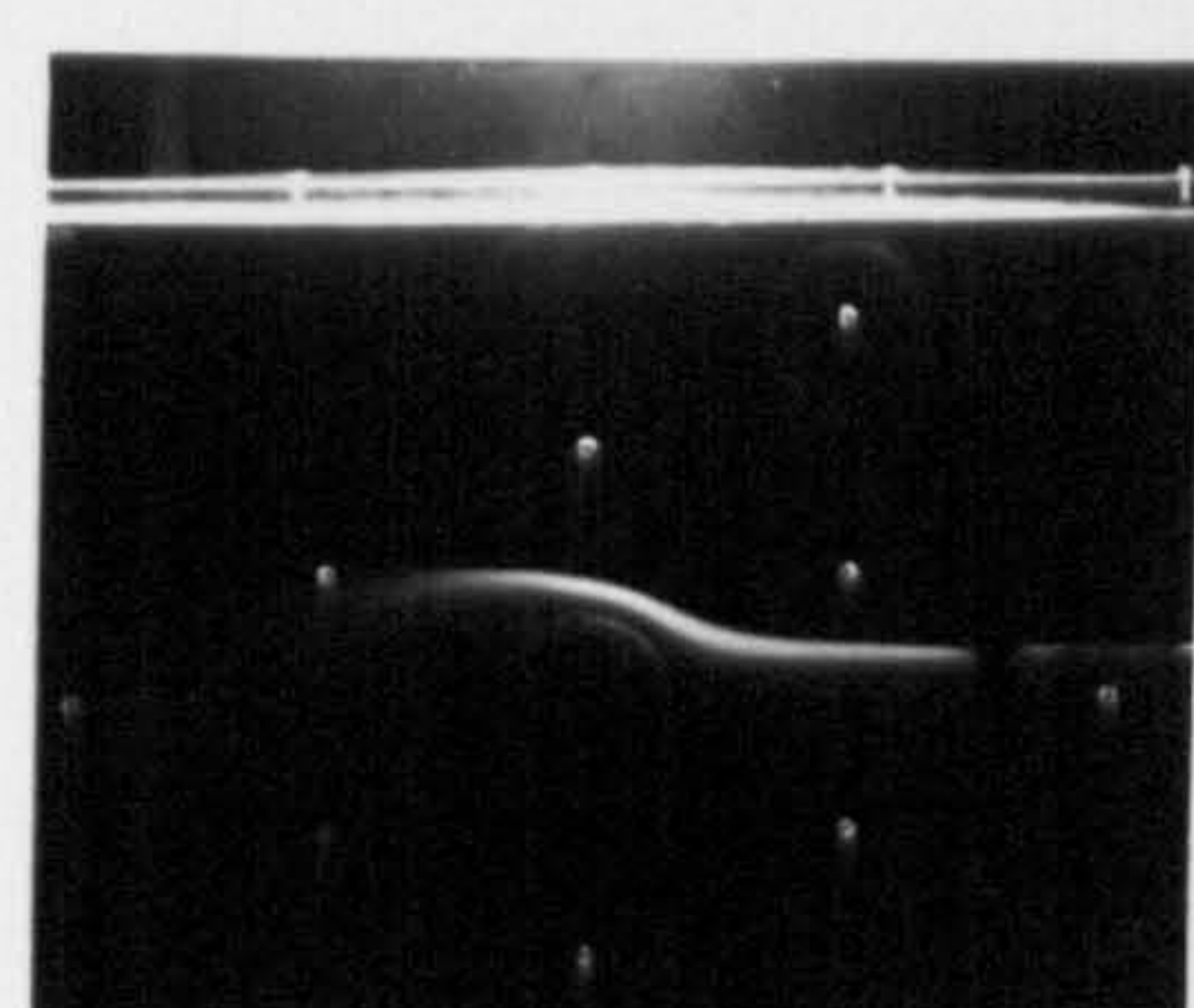
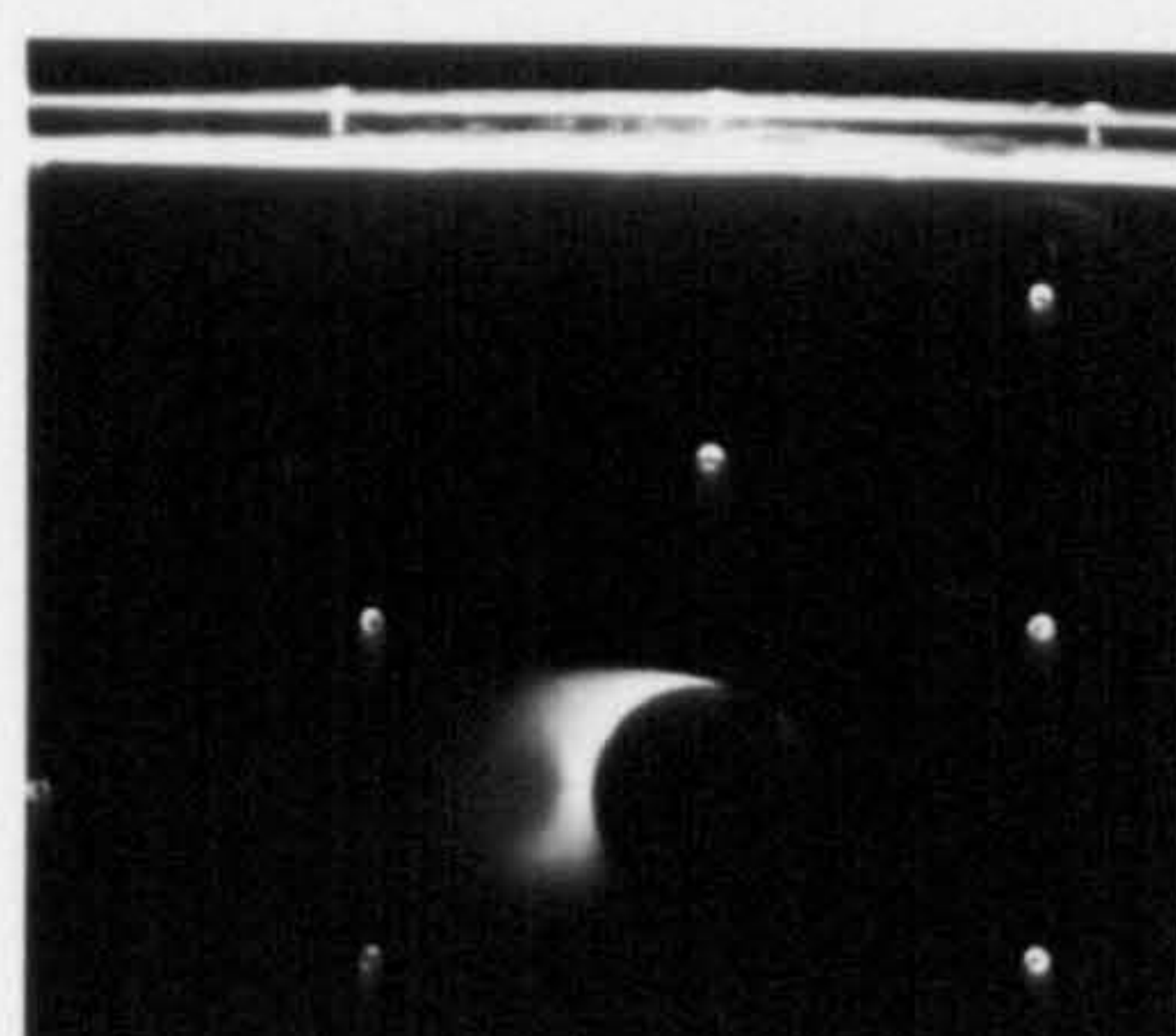
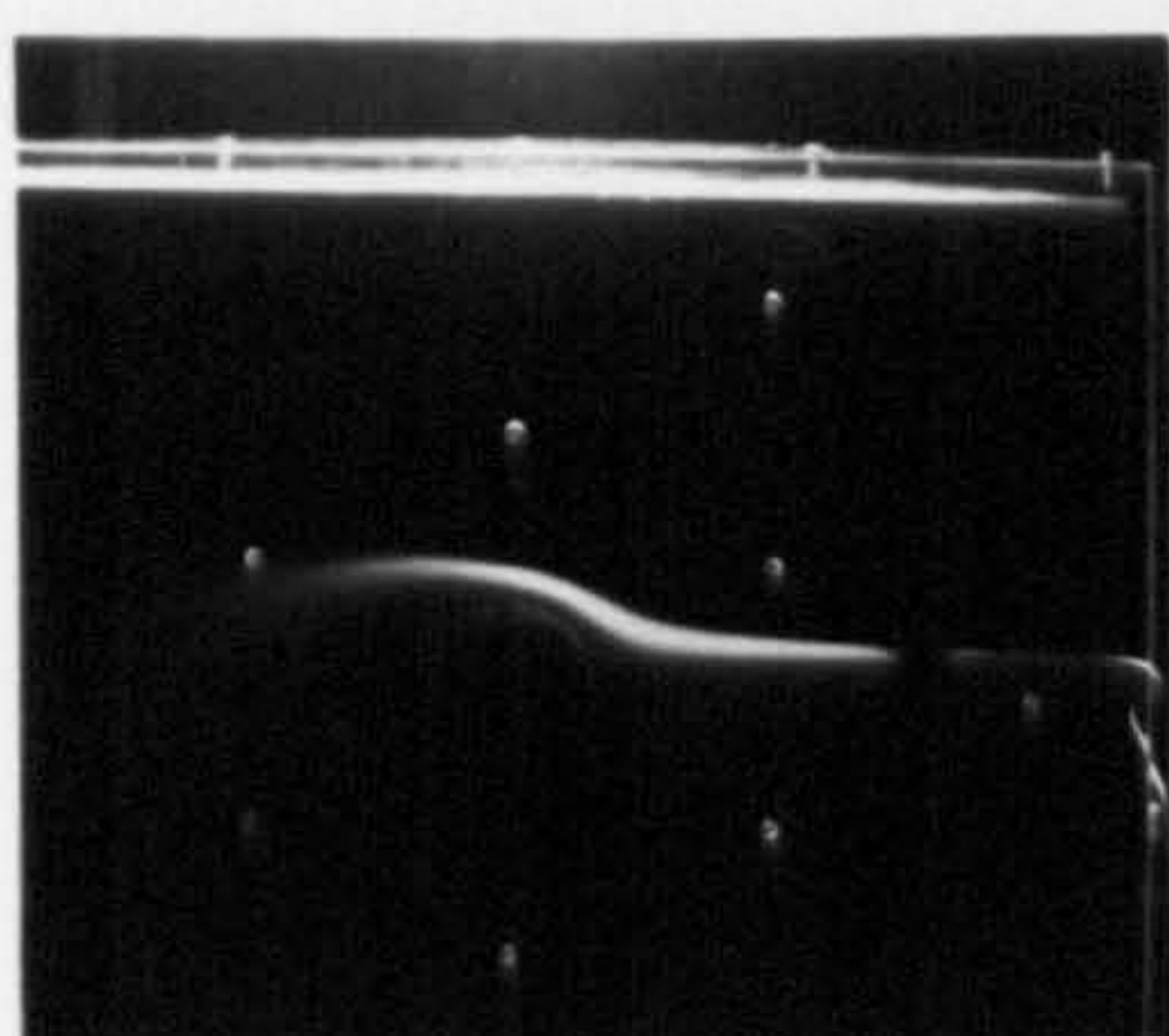
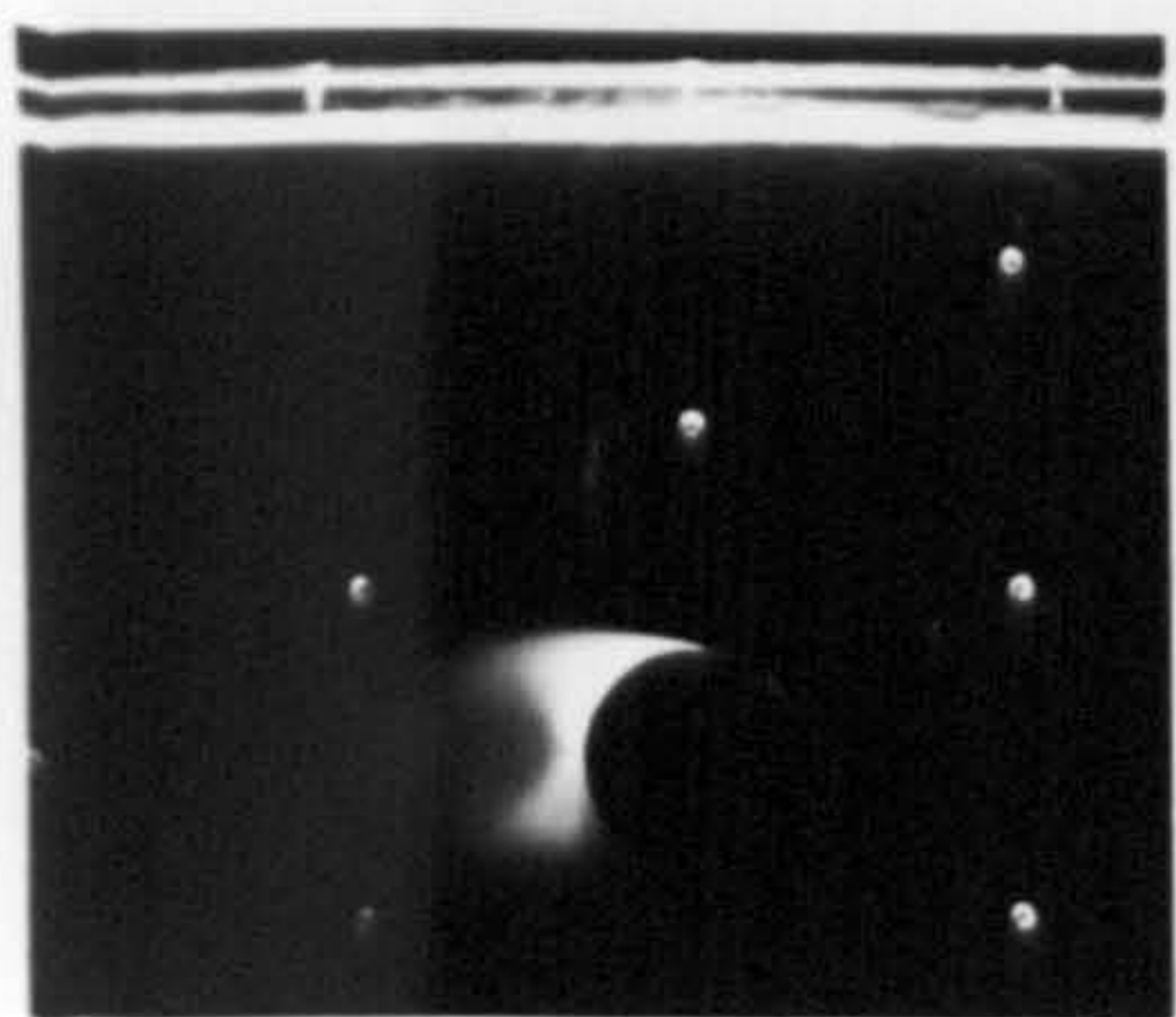


Re=55000 ,  $V_w/U=0.011$

Re=66000 ,  $V_w/U=0.0095$

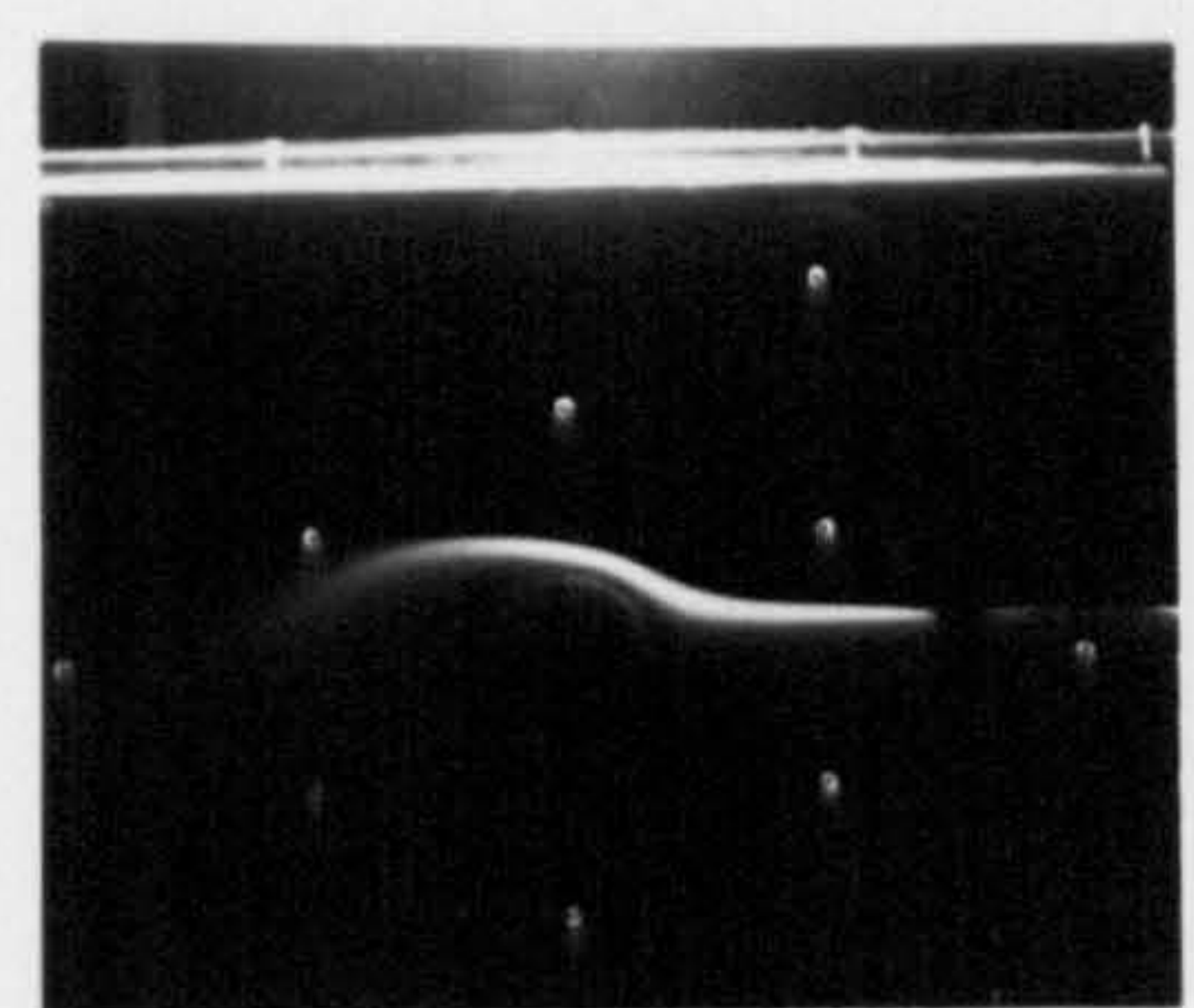
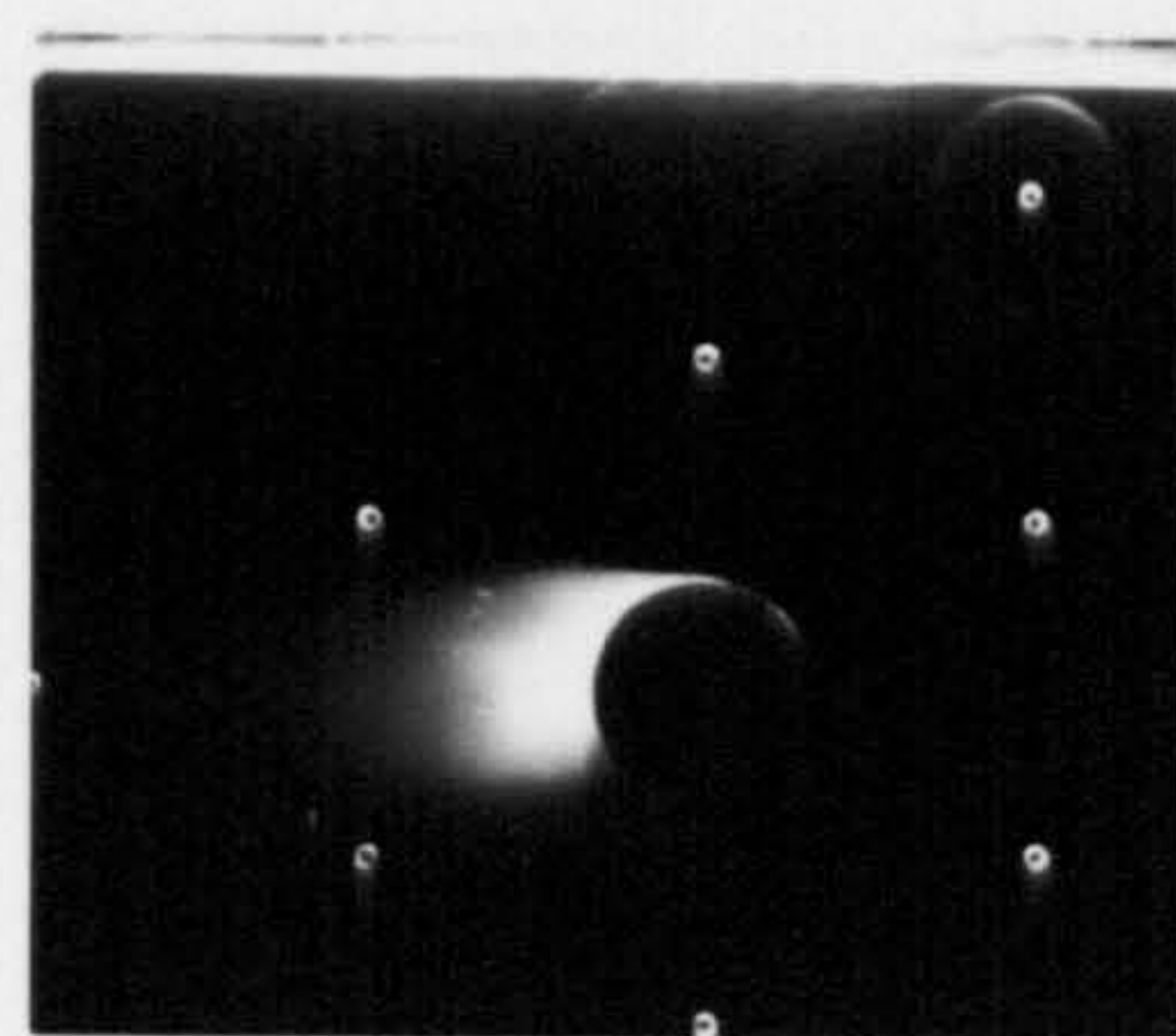
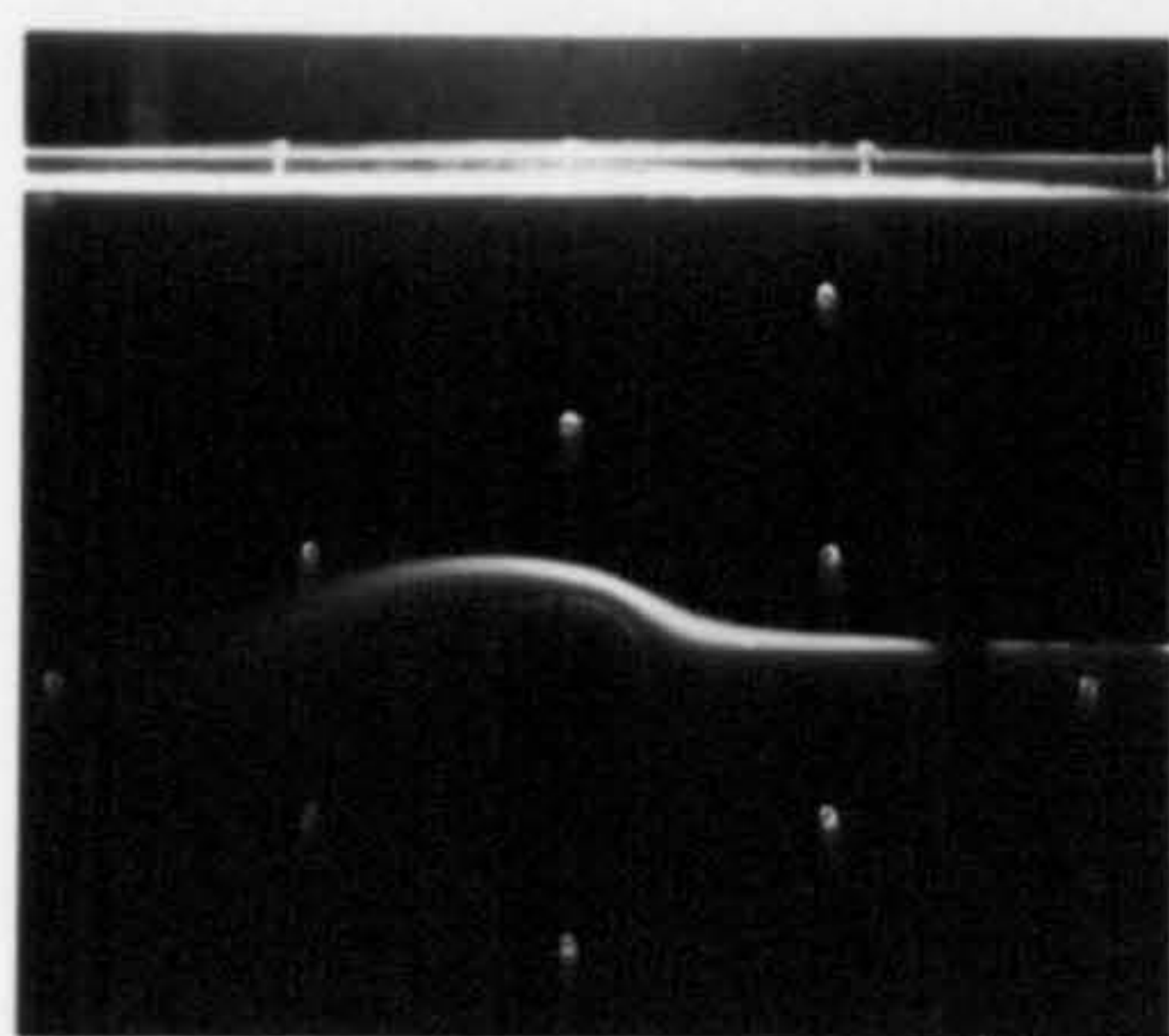
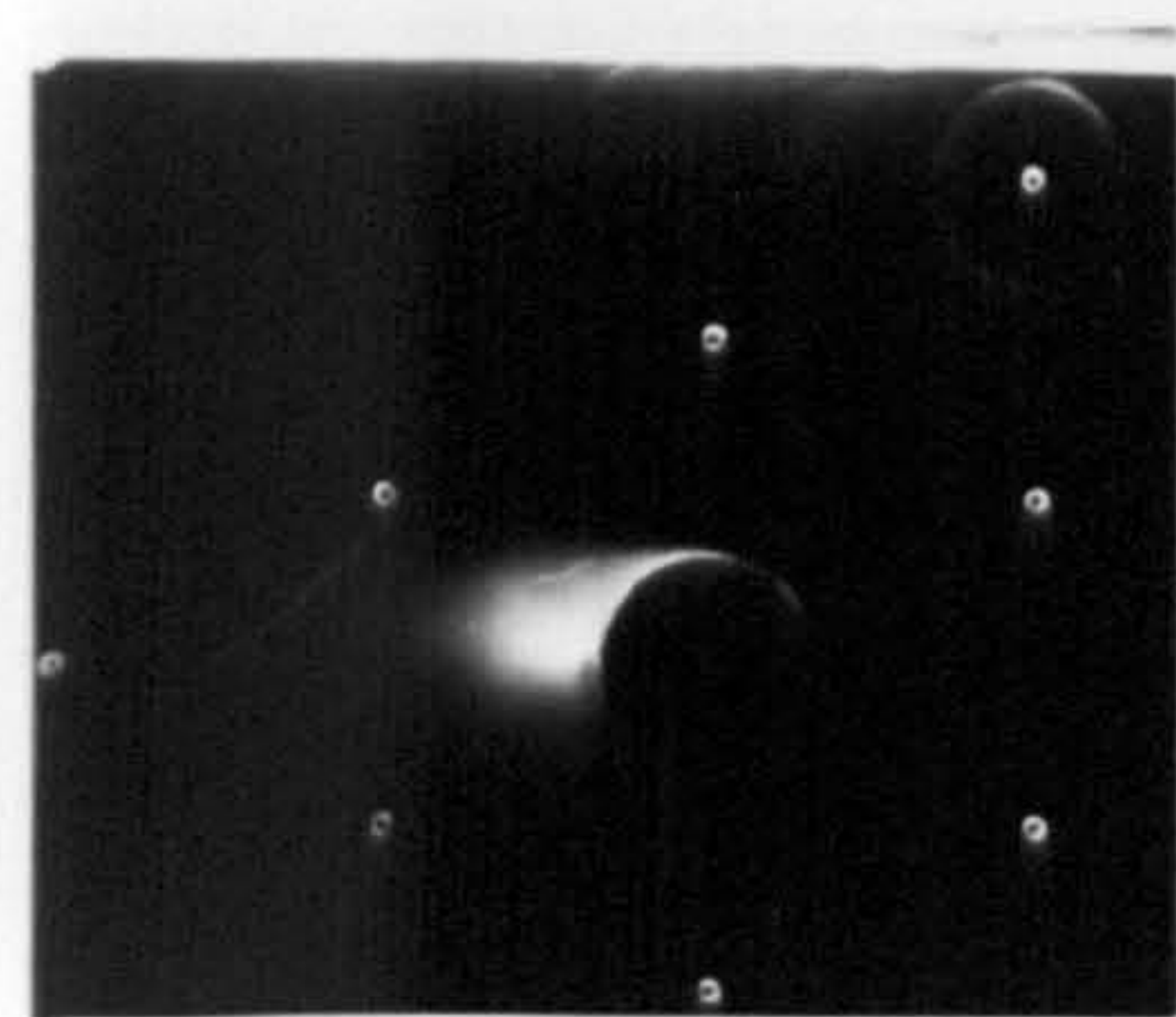
FIGURE 10.4





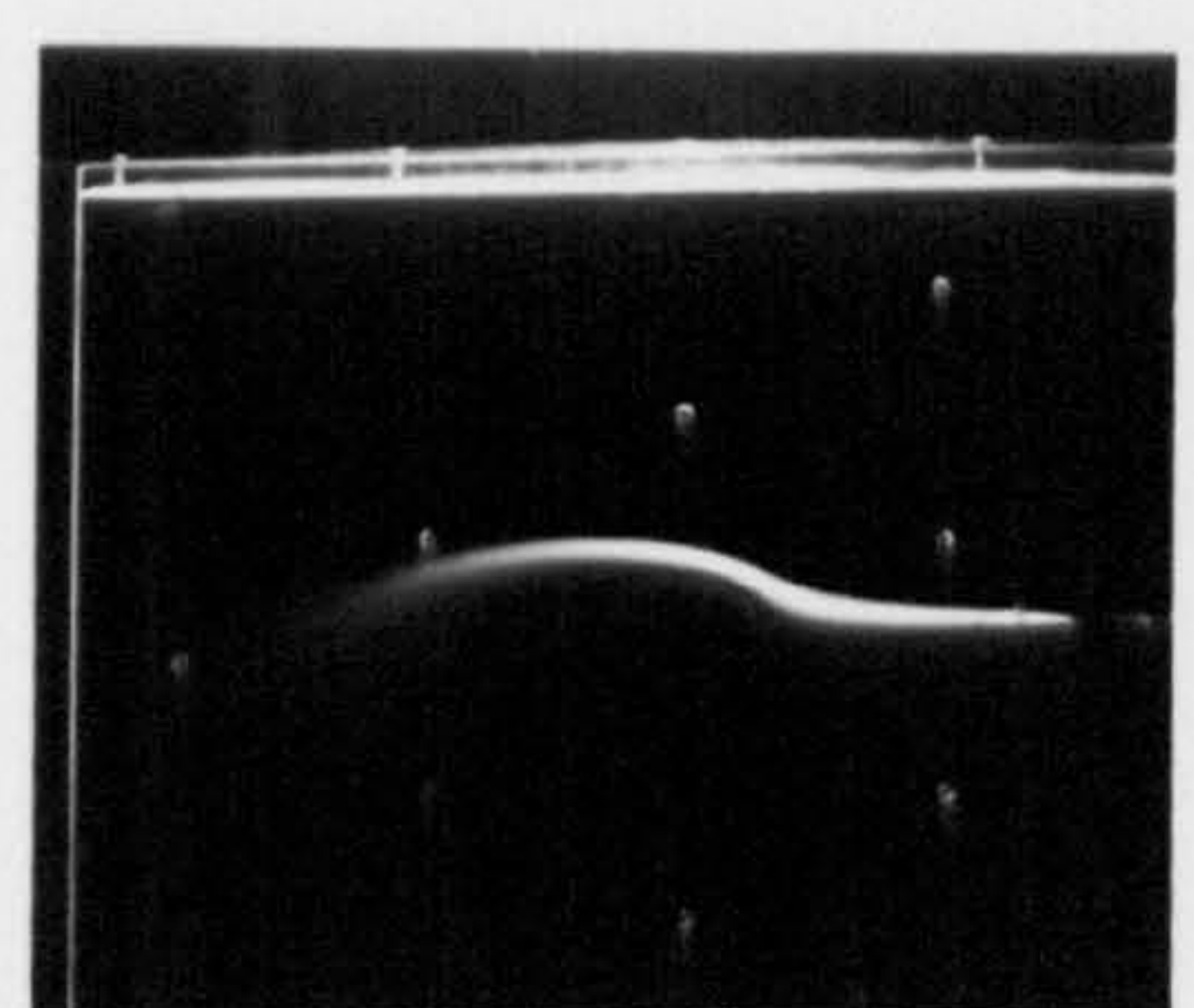
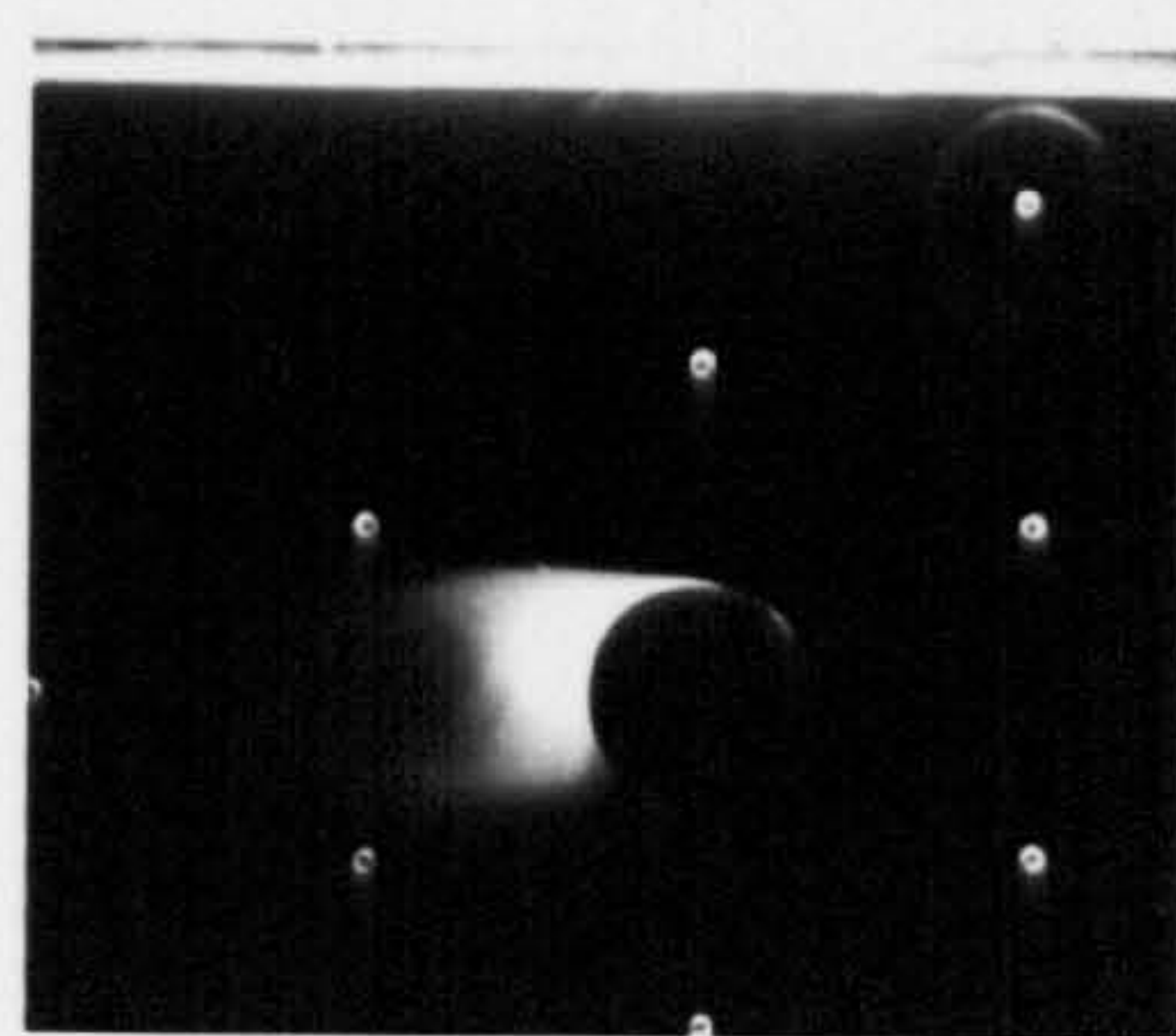
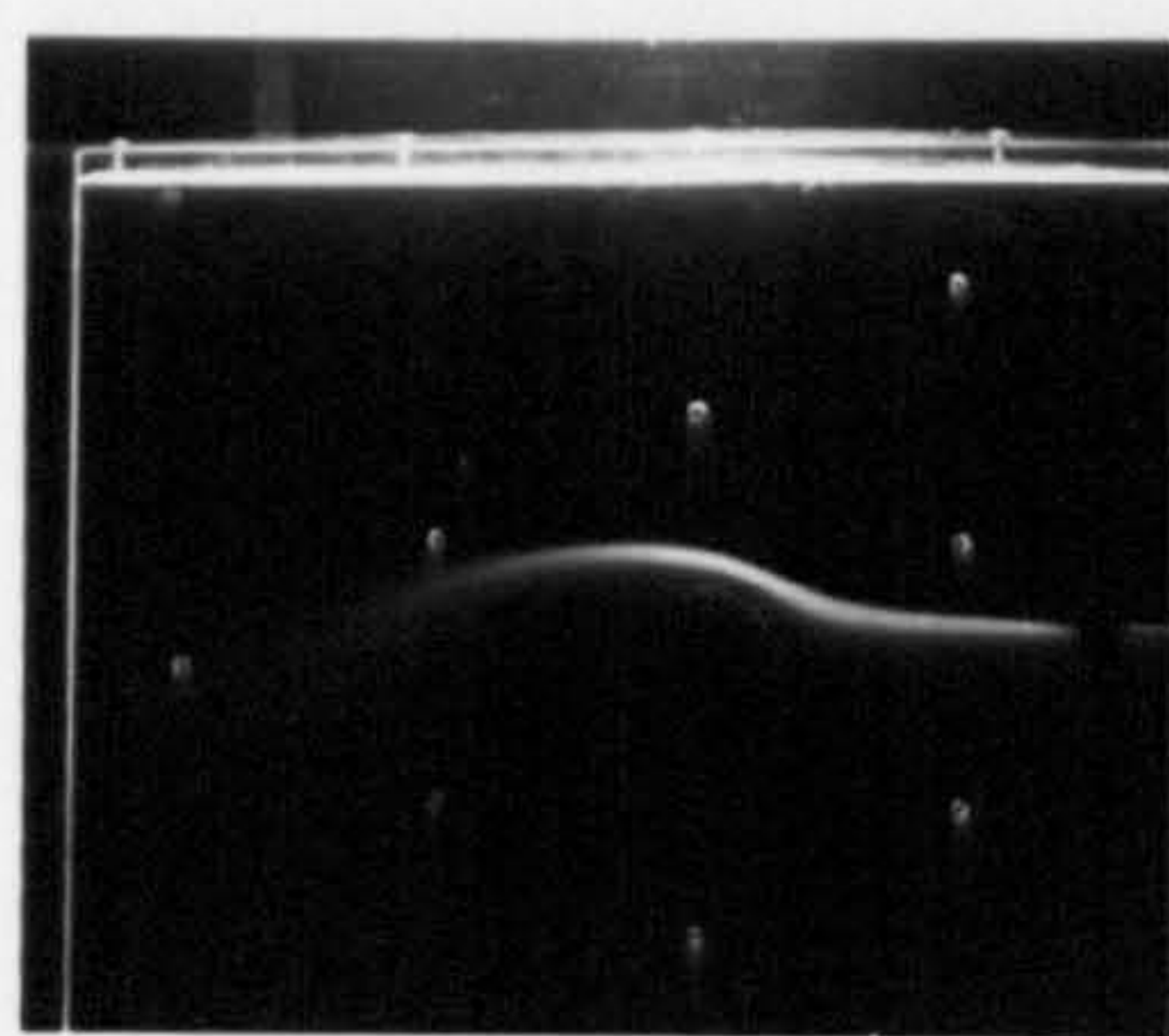
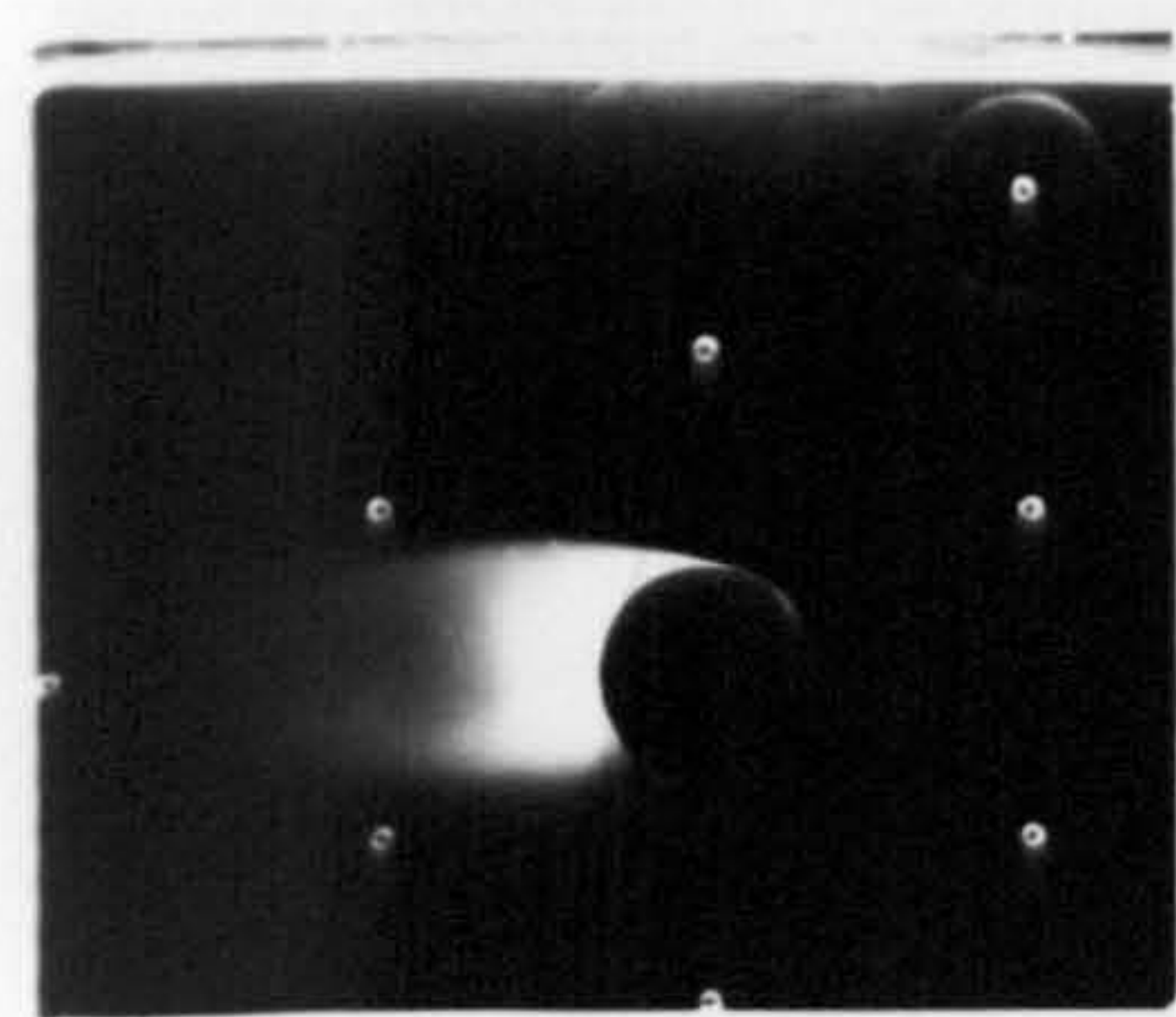
Re=77000 ,  $V_w/U = 0.0$

Re=87000 ,  $V_w/U = 0.0$



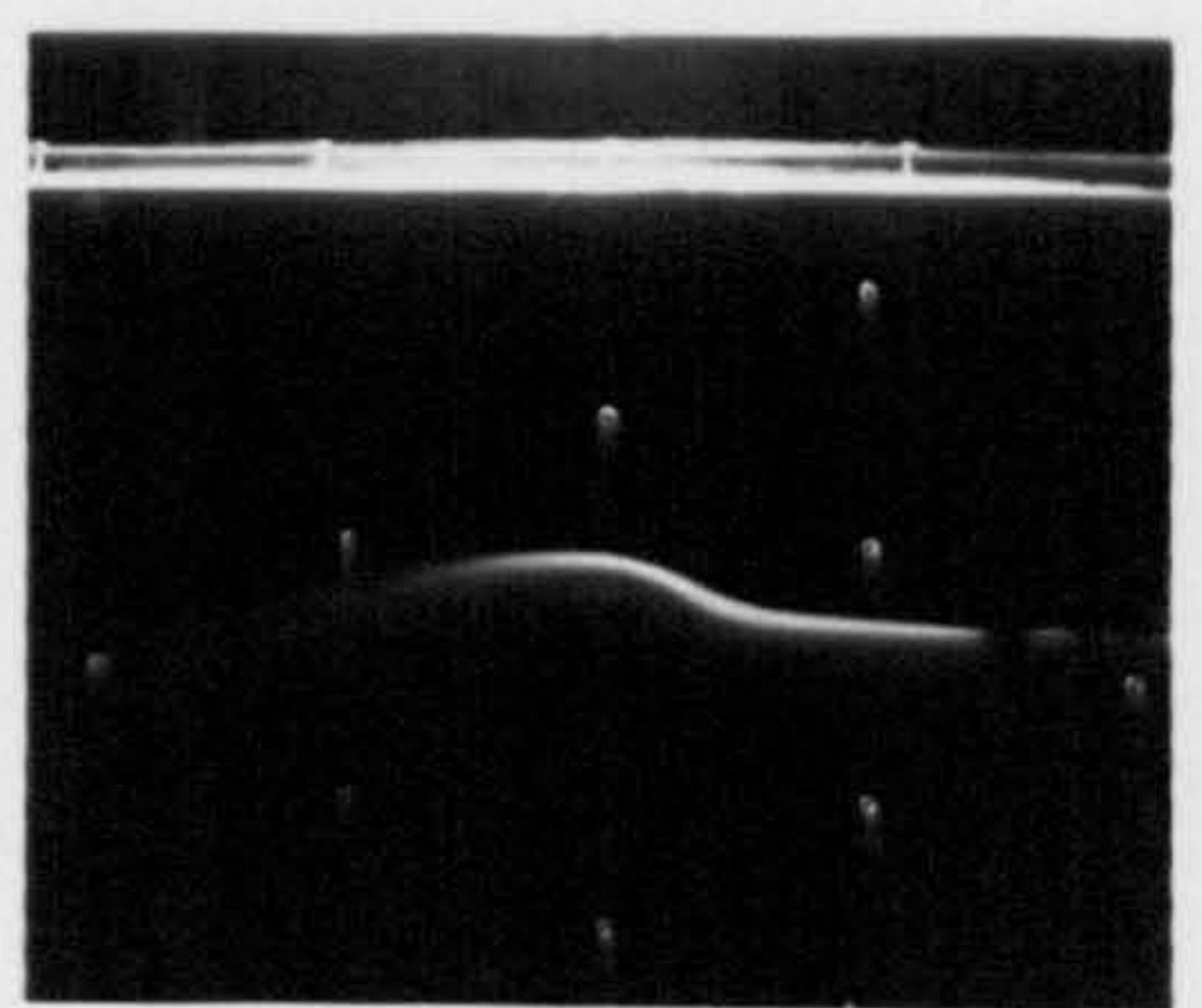
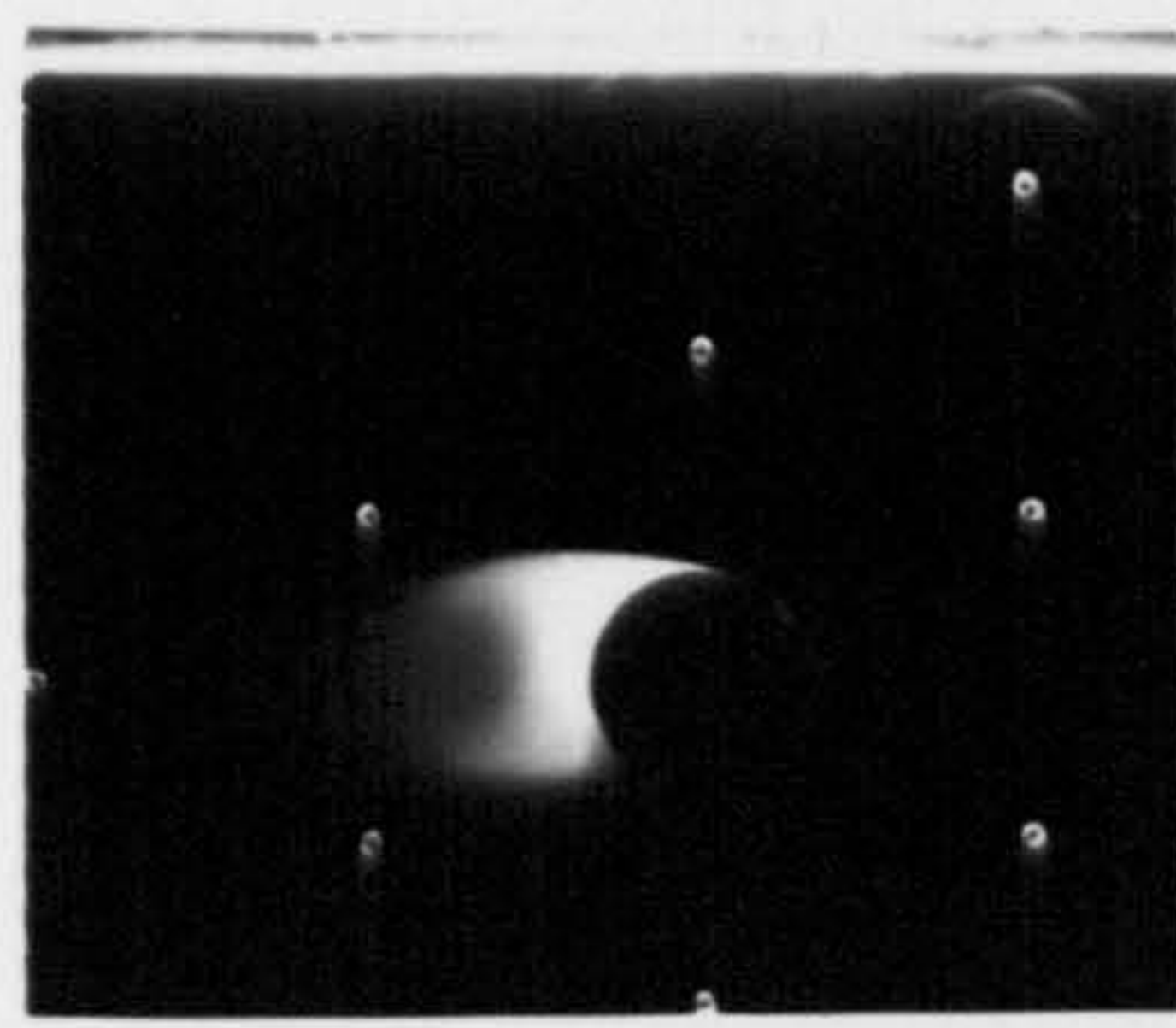
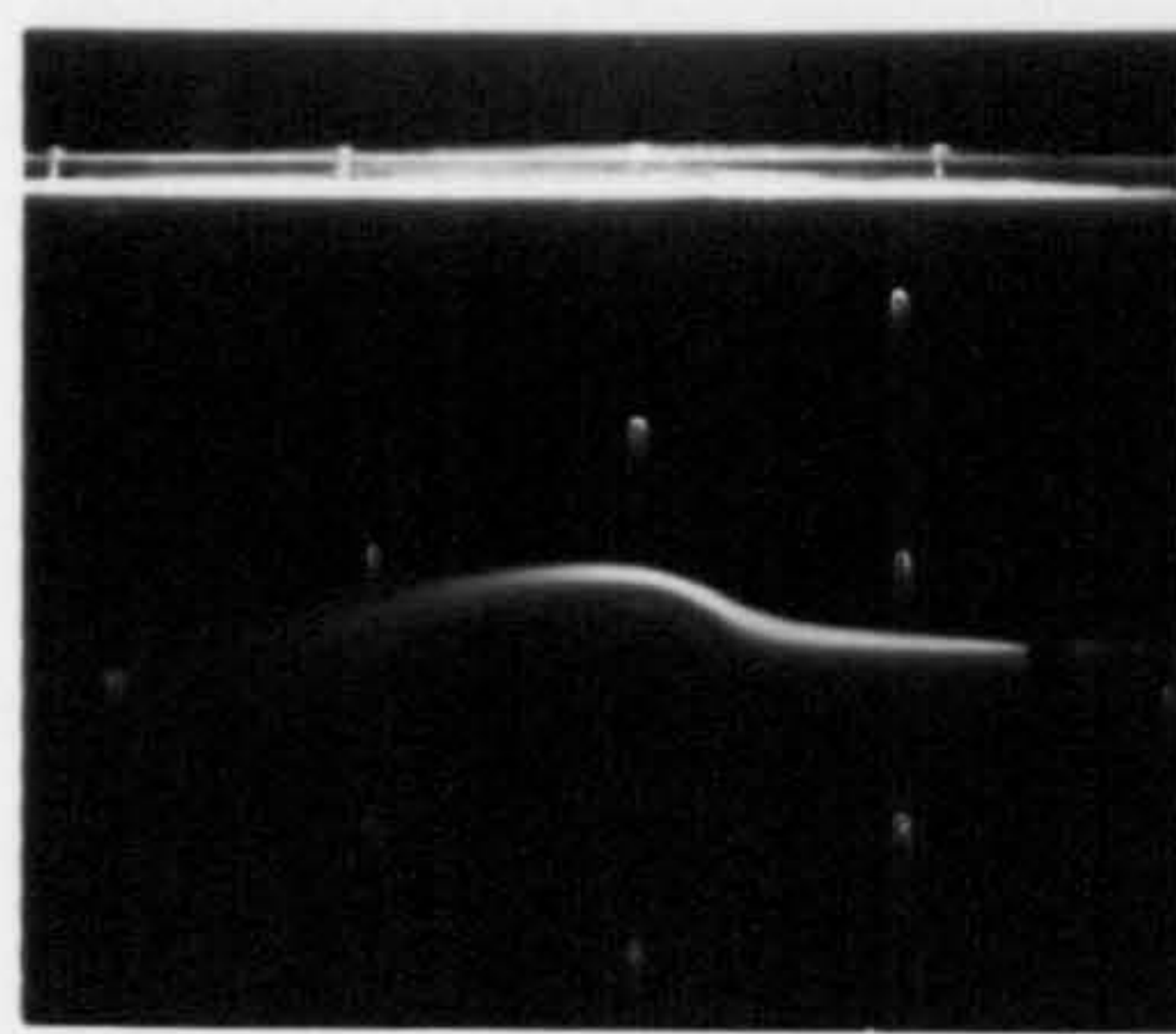
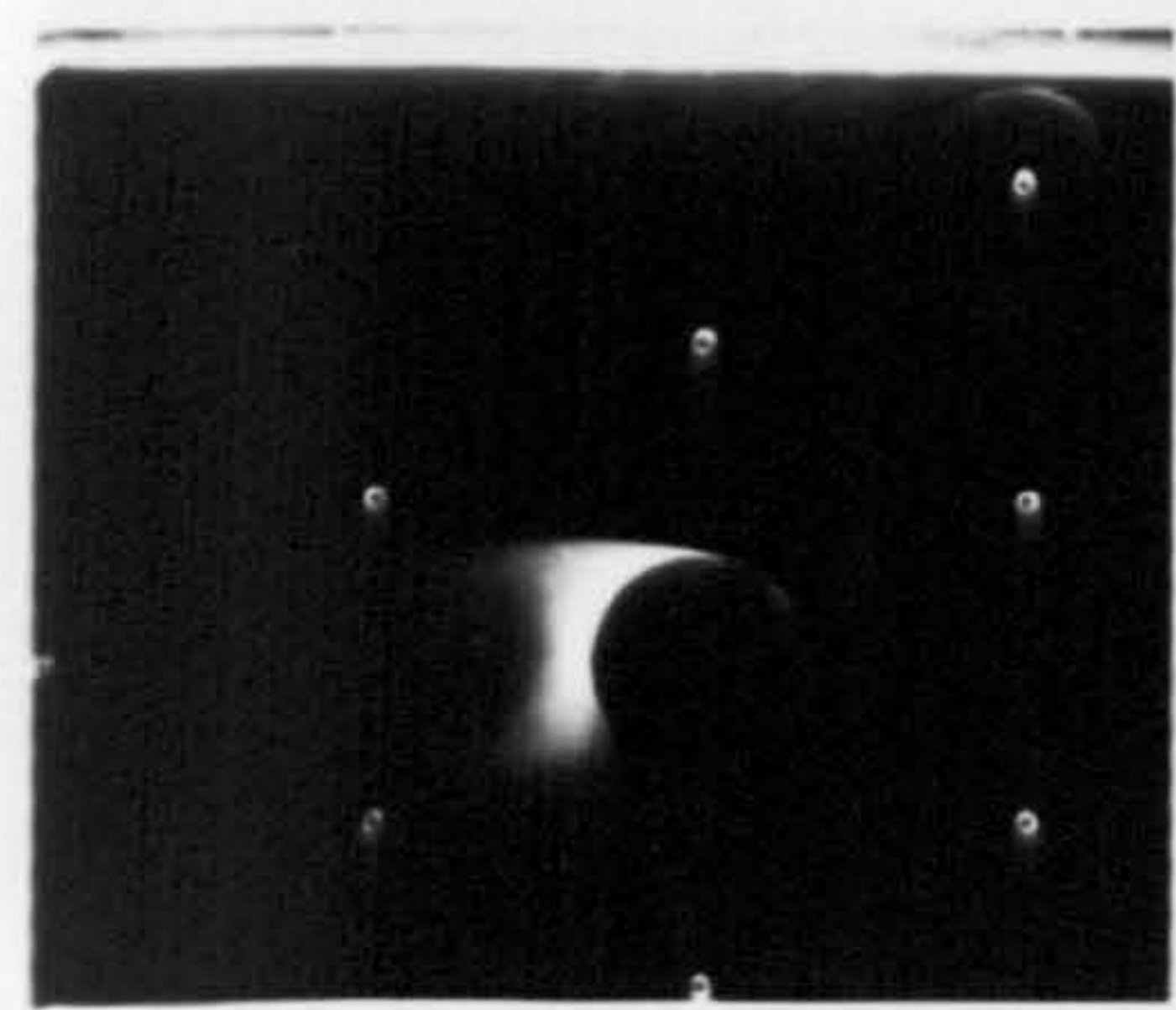
Re=77000 ,  $V_w/U = 0.002$

Re=87000 ,  $V_w/U = 0.0017$



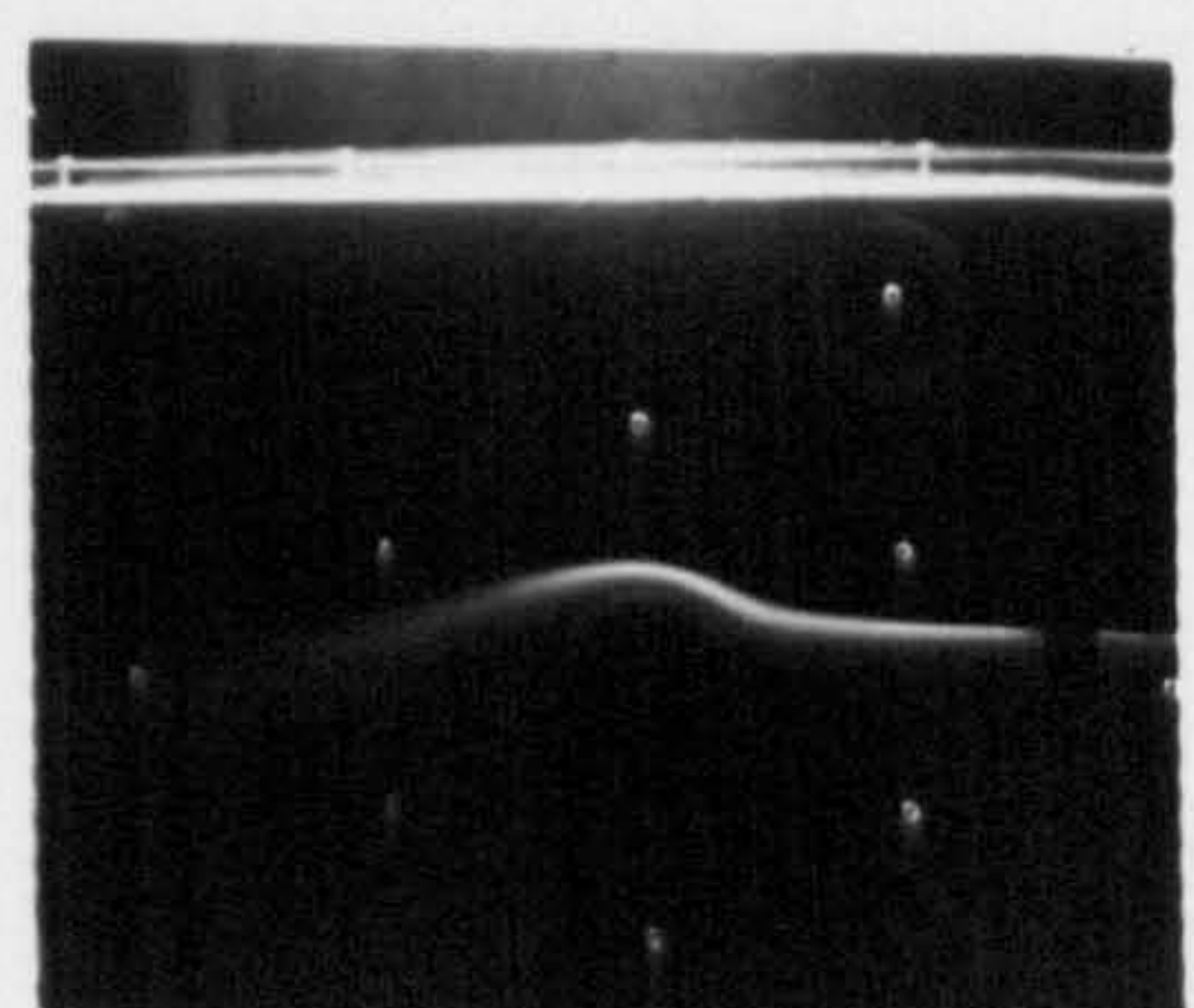
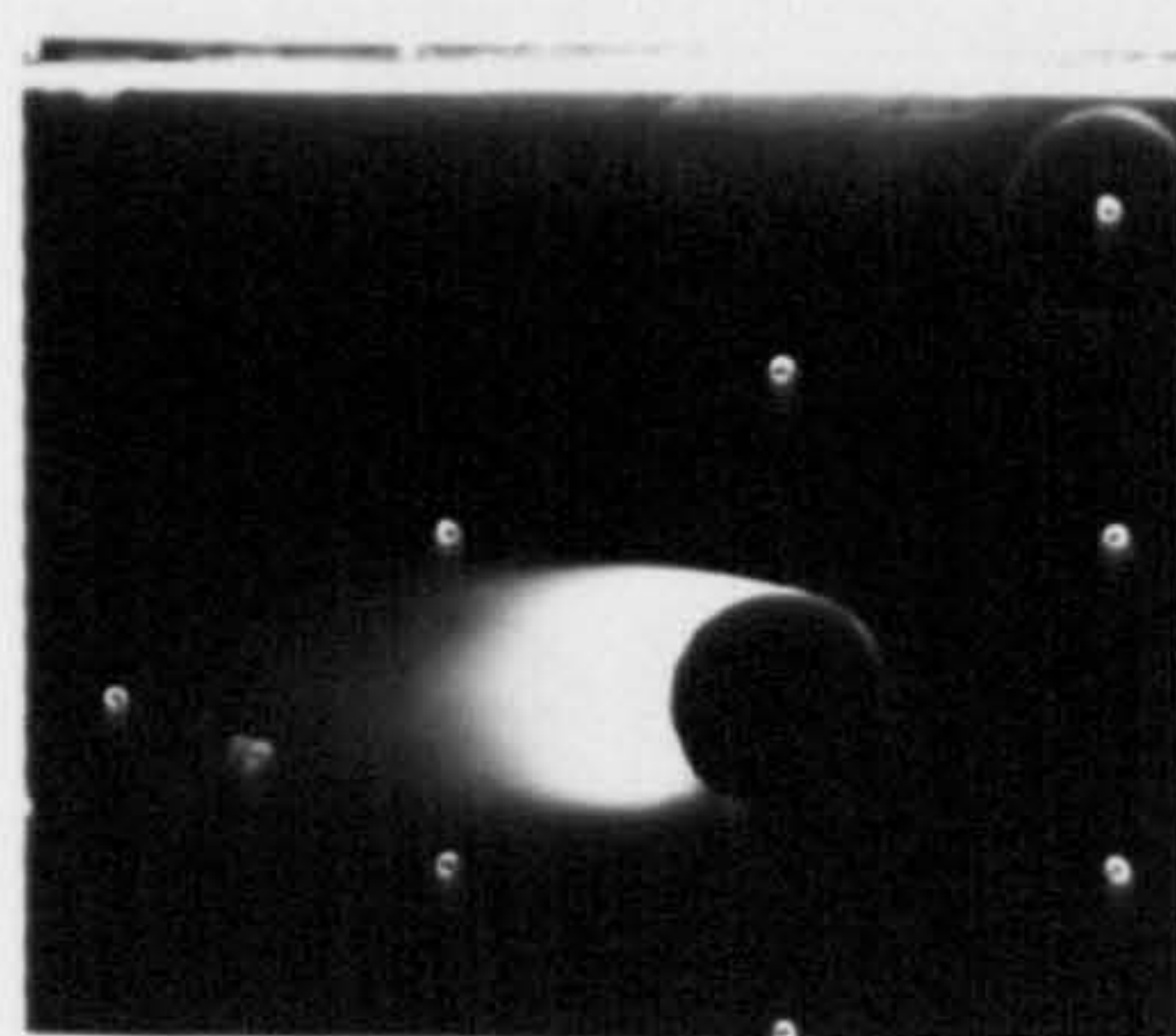
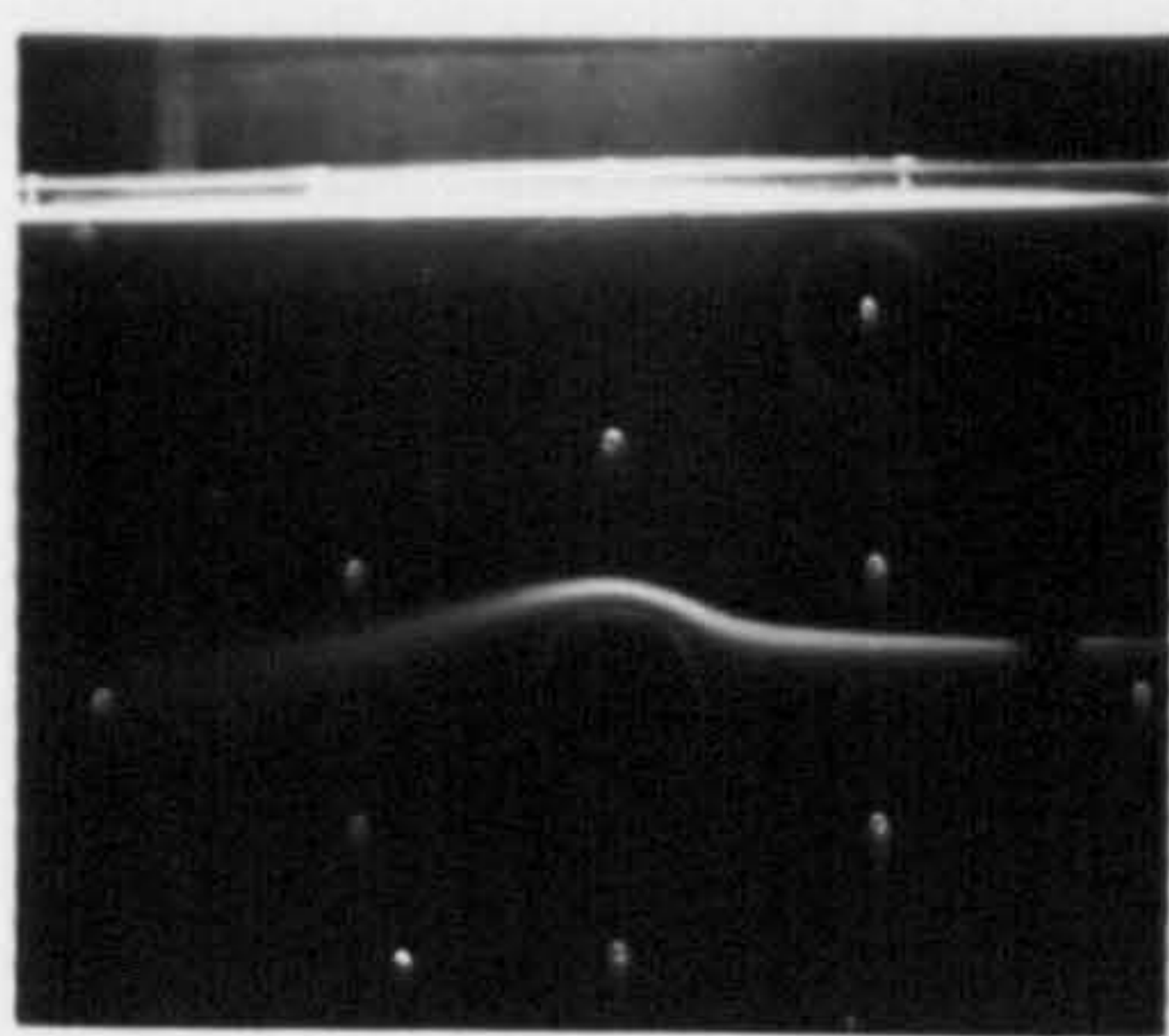
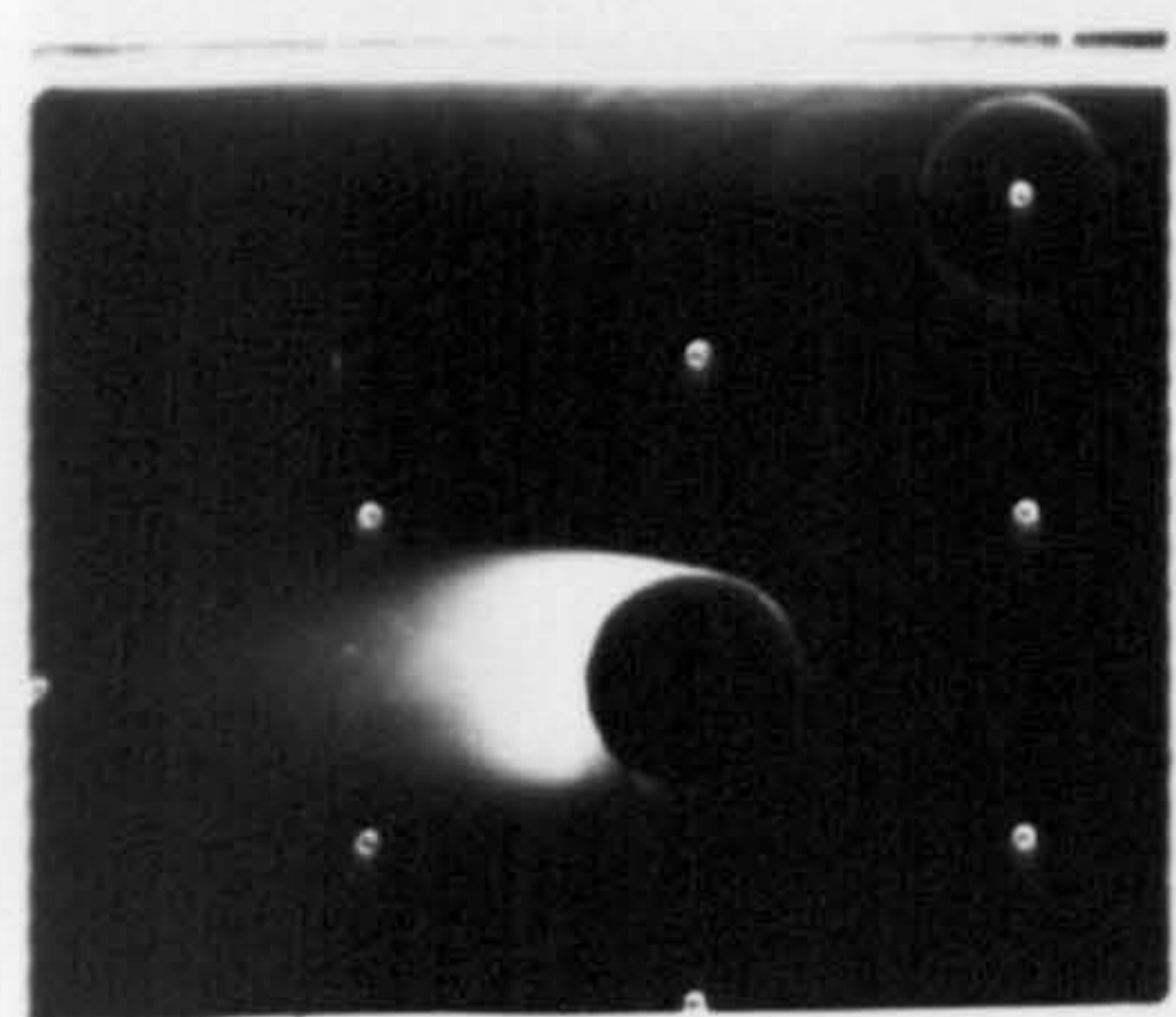
Re=77000 ,  $V_w/U = 0.004$

Re=87000 ,  $V_w/U = 0.0036$



Re=77000 ,  $V_w/U = 0.006$

Re=87000 ,  $V_w/U = 0.005$

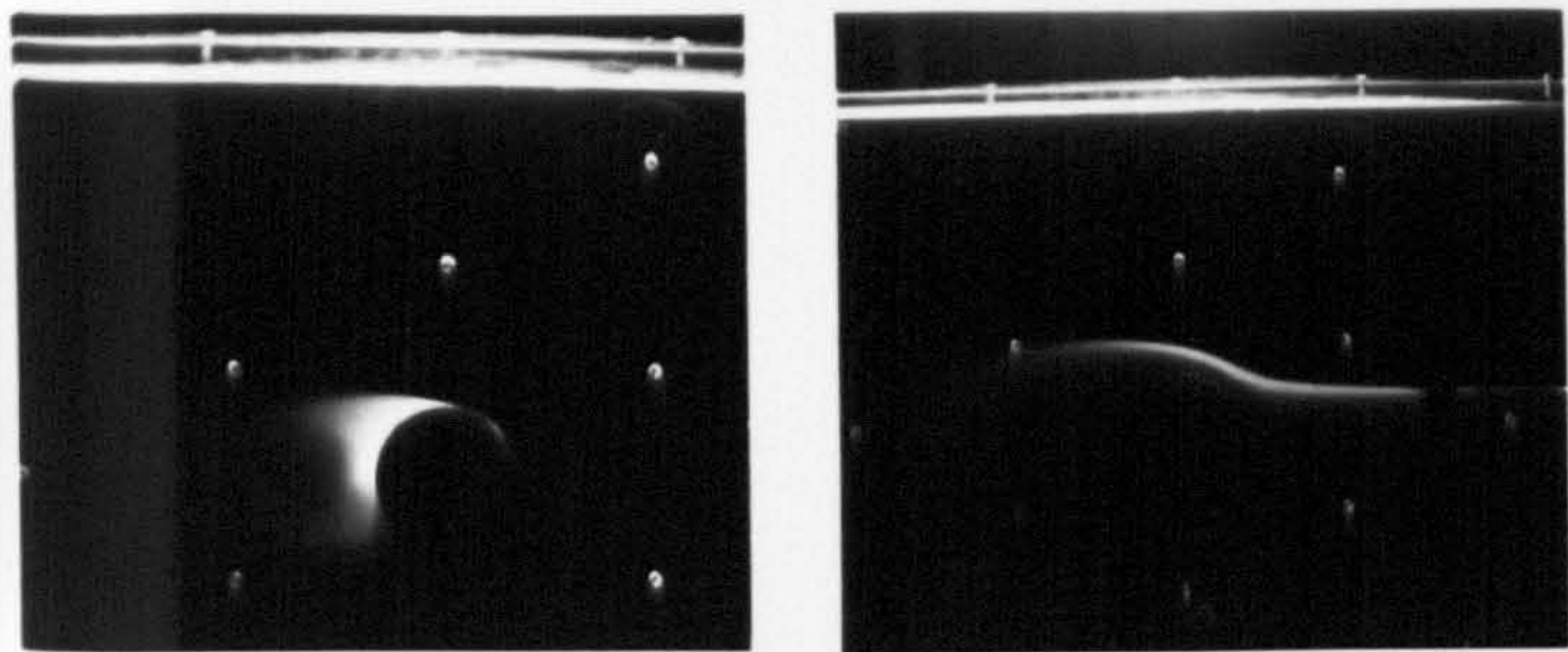


Re=77000 ,  $V_w/U = 0.008$

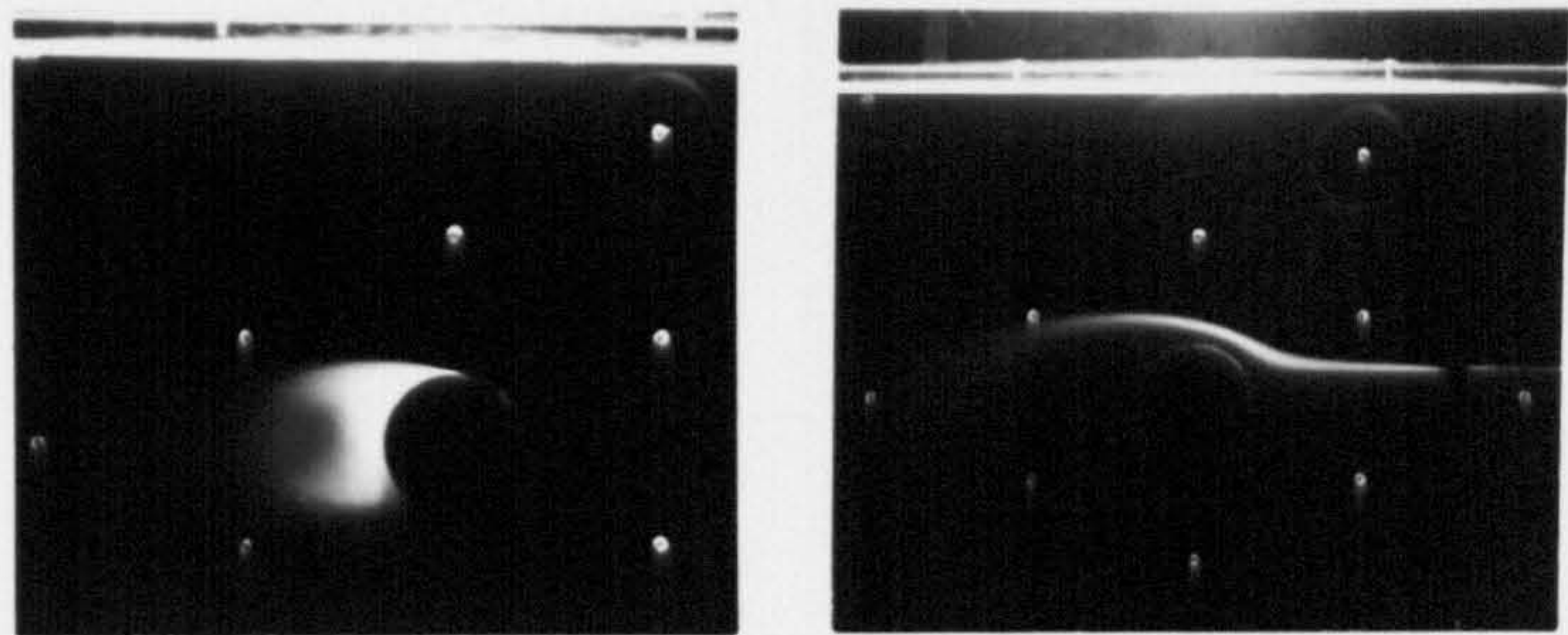
Re=87000 ,  $V_w/U = 0.007$

FIGURE 10.5

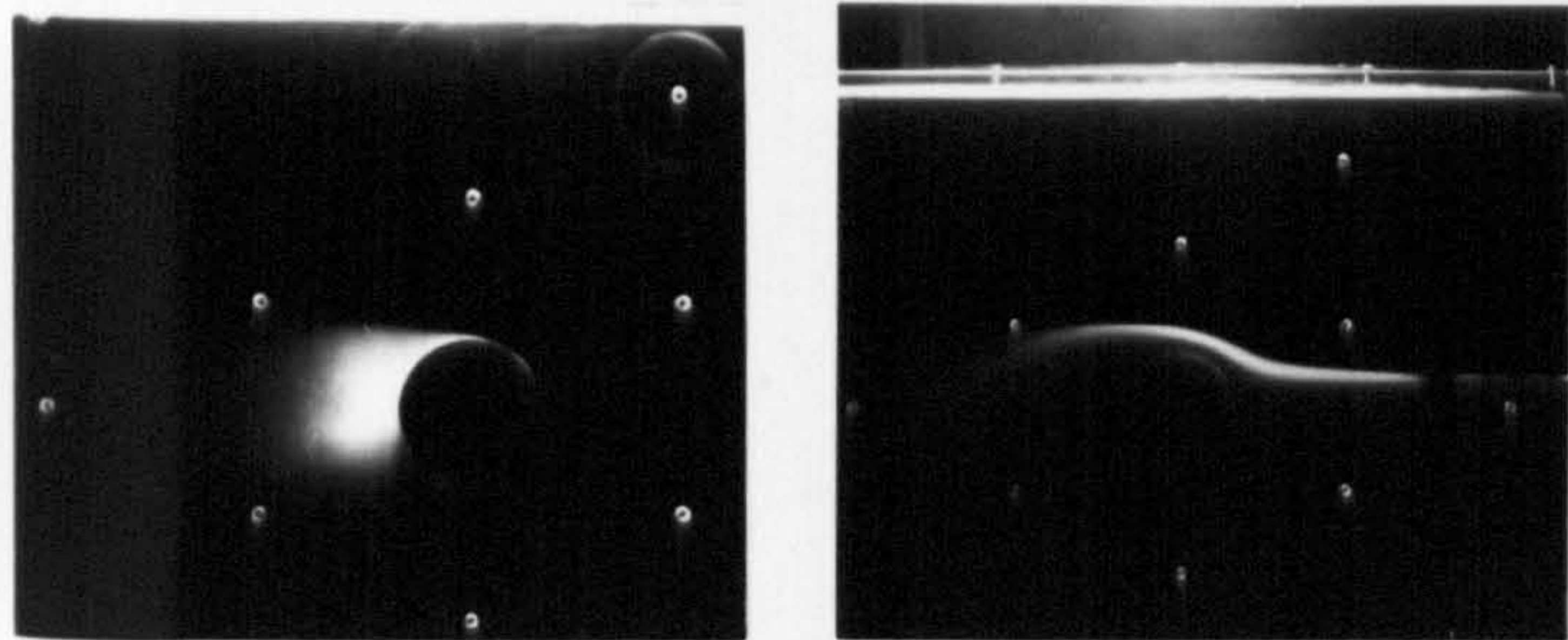




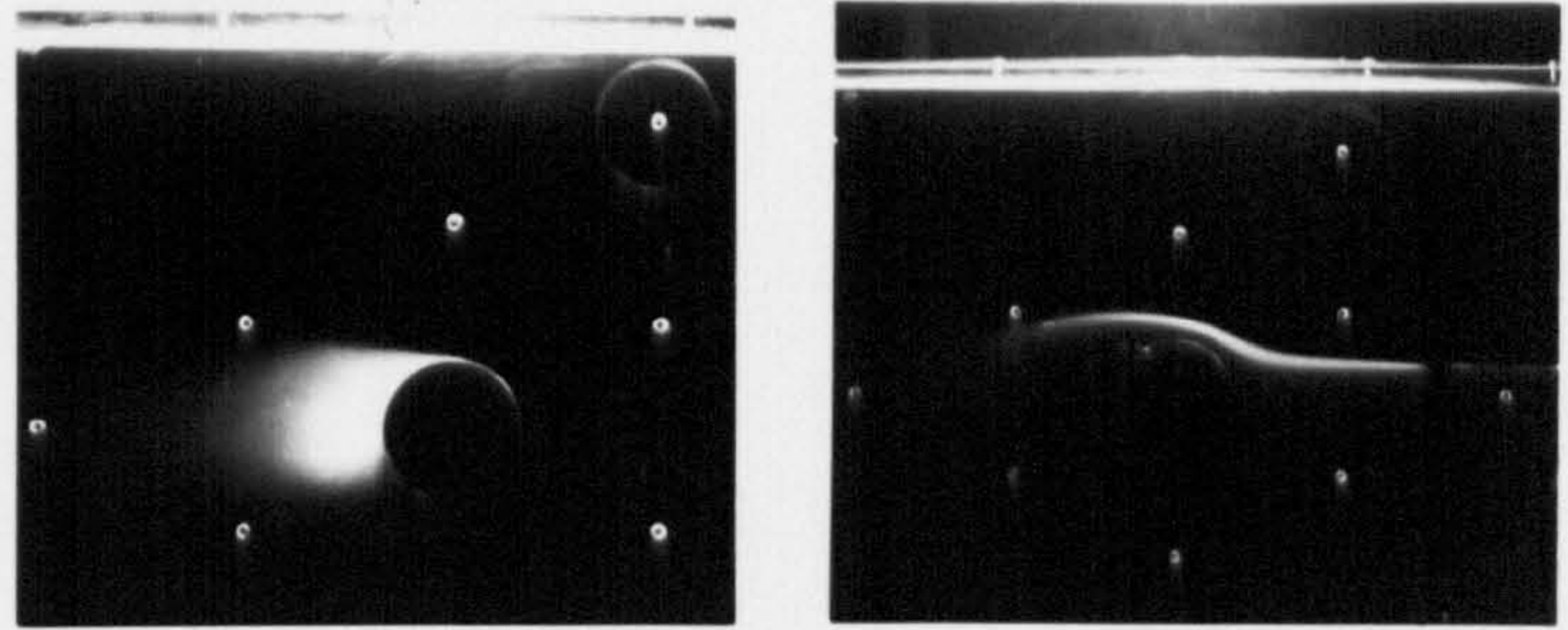
Re=98000 ,  $V_w/U=0.0$



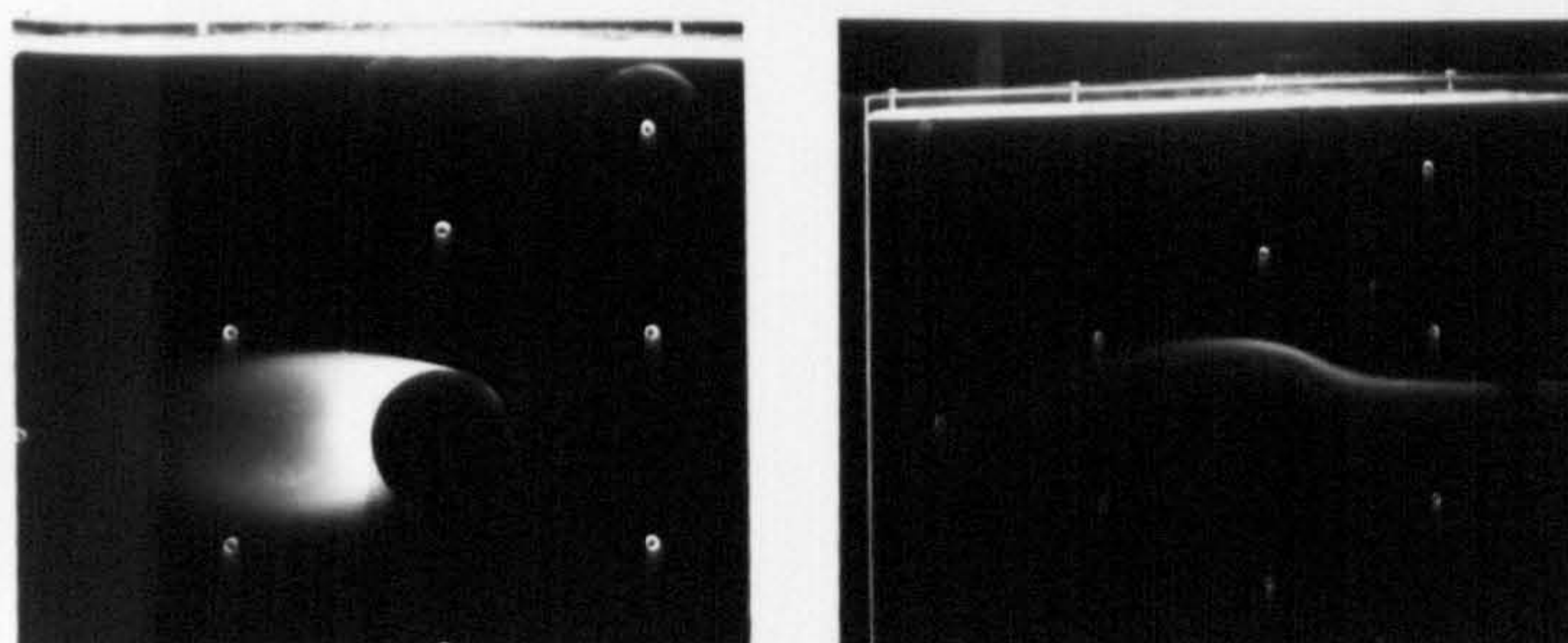
Re=108000 ,  $V_w/U=0.0$



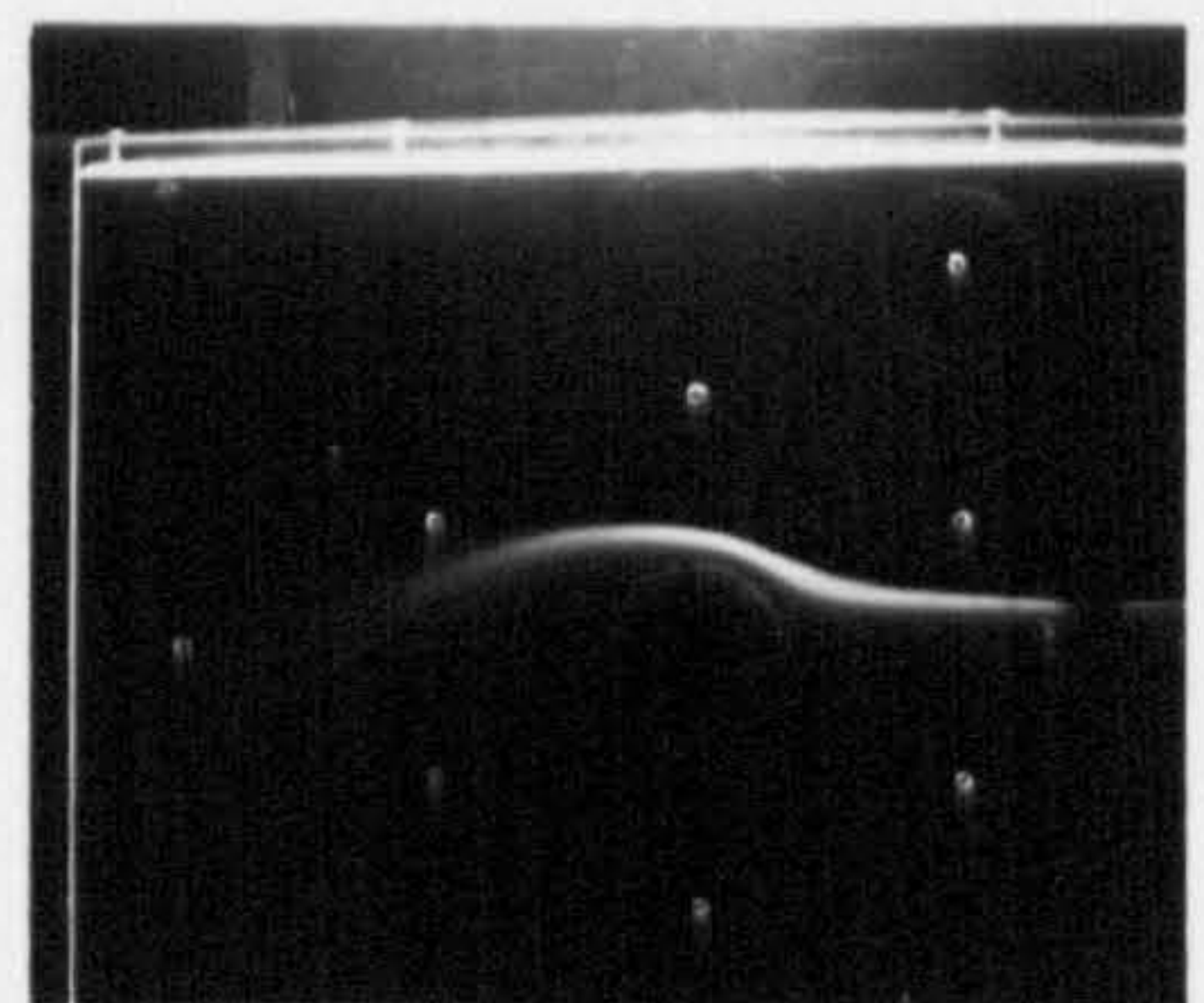
Re=98000 ,  $V_w/U=0.0016$



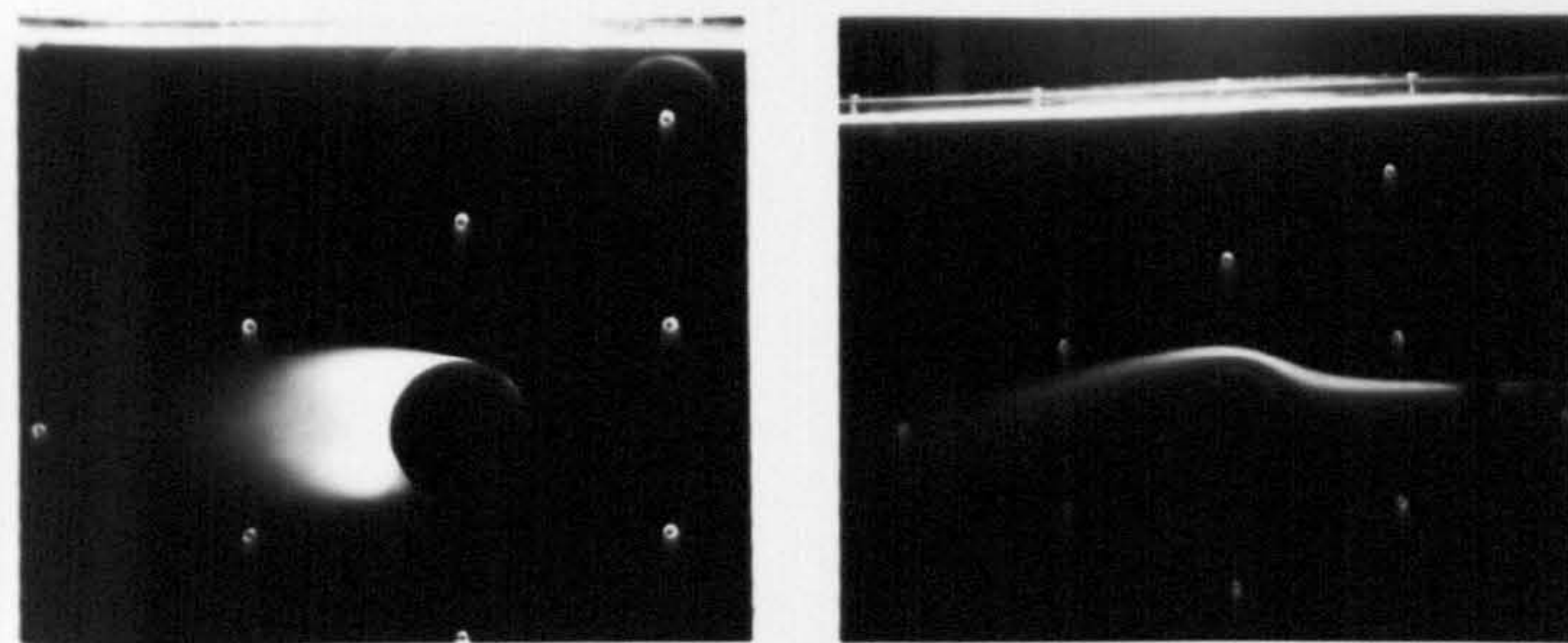
Re=108000 ,  $V_w/U=0.0014$



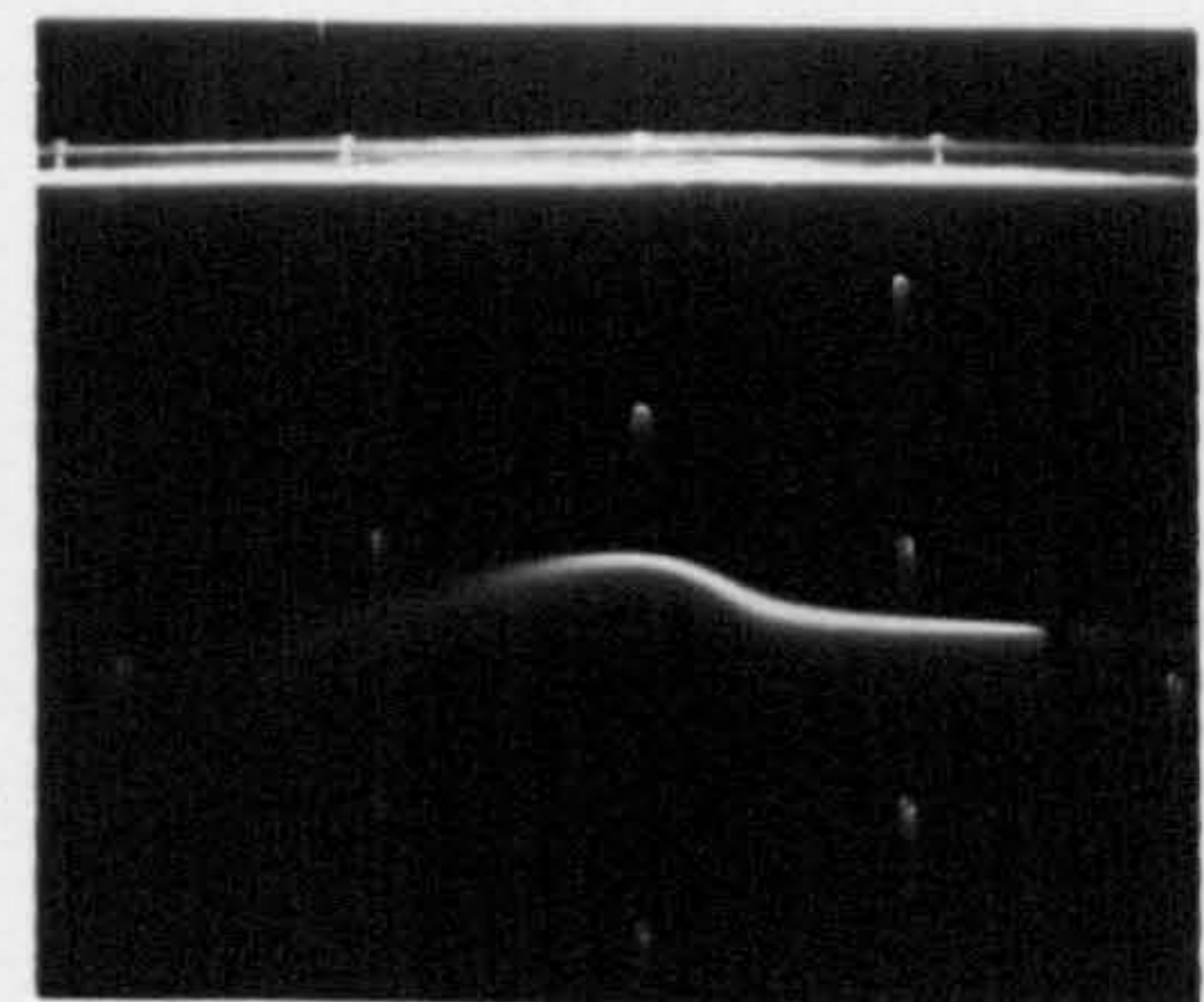
Re=98000 ,  $V_w/U=0.0032$



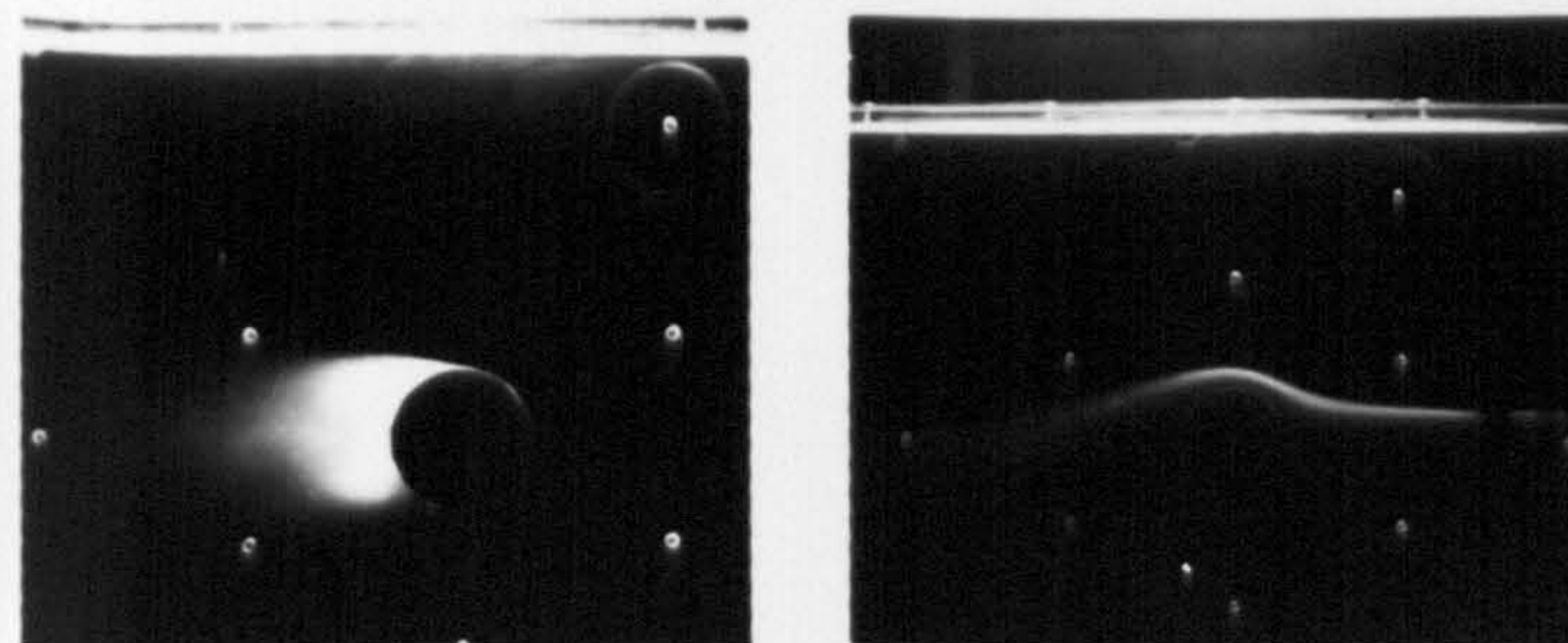
Re=108000 ,  $V_w/U=0.003$



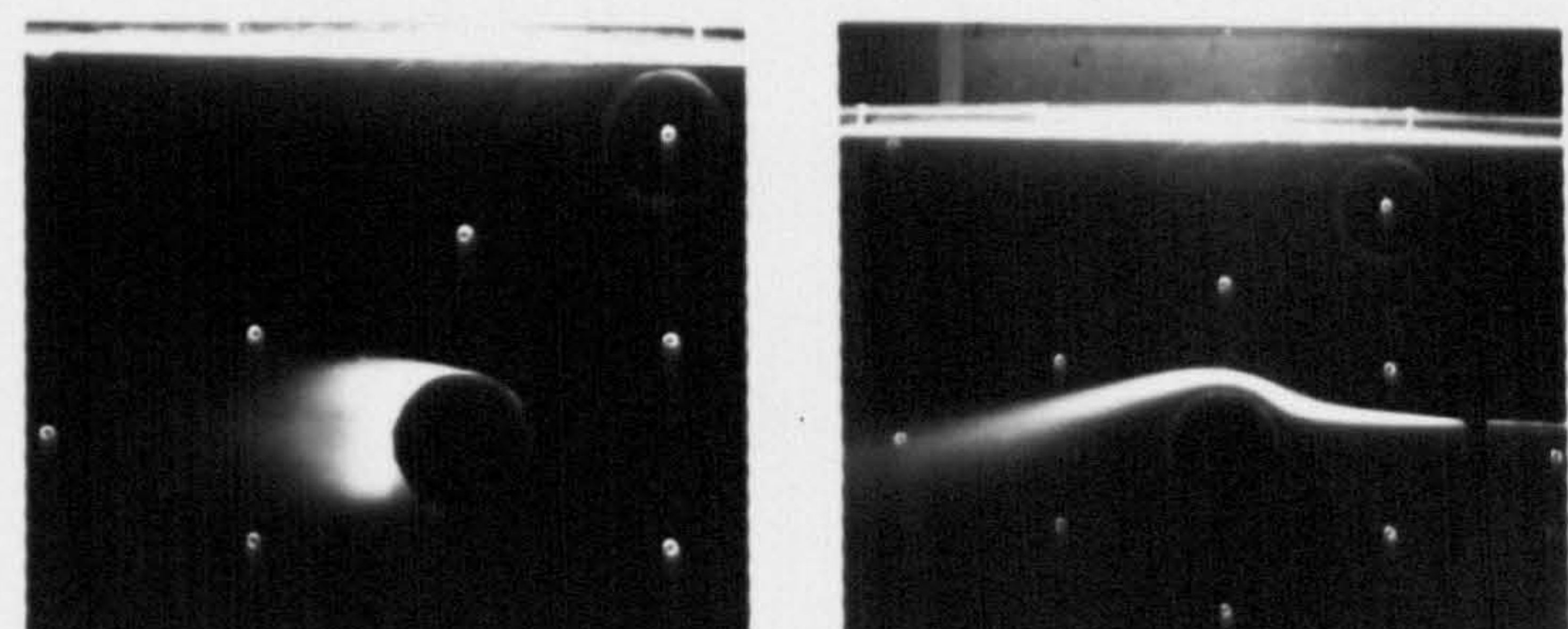
Re=98000 ,  $V_w/U=0.0048$



Re=108000 ,  $V_w/U=0.0043$



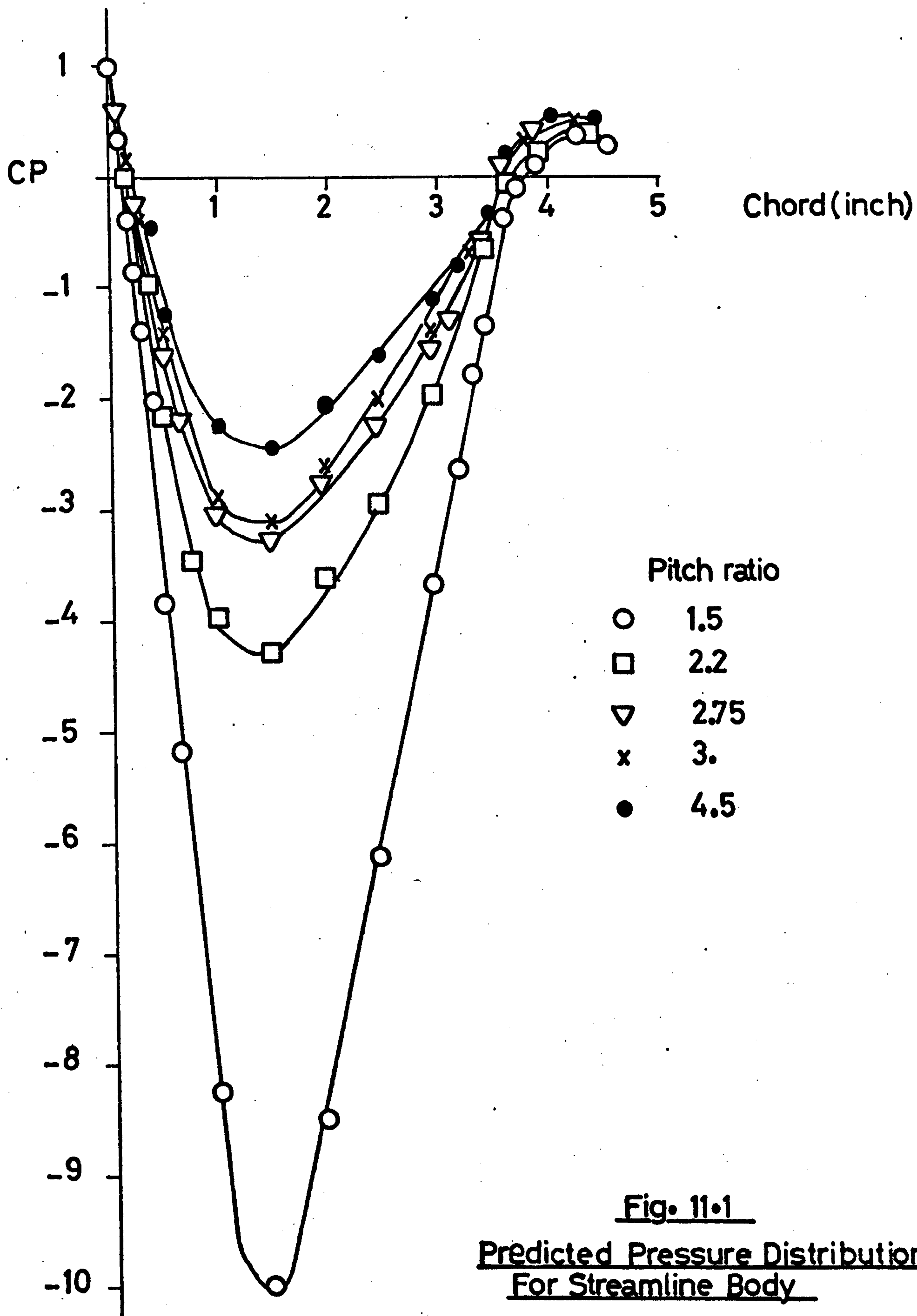
Re=98000 ,  $V_w/U=0.006$



Re=108000 ,  $V_w/U=0.0057$

FIGURE 10.6

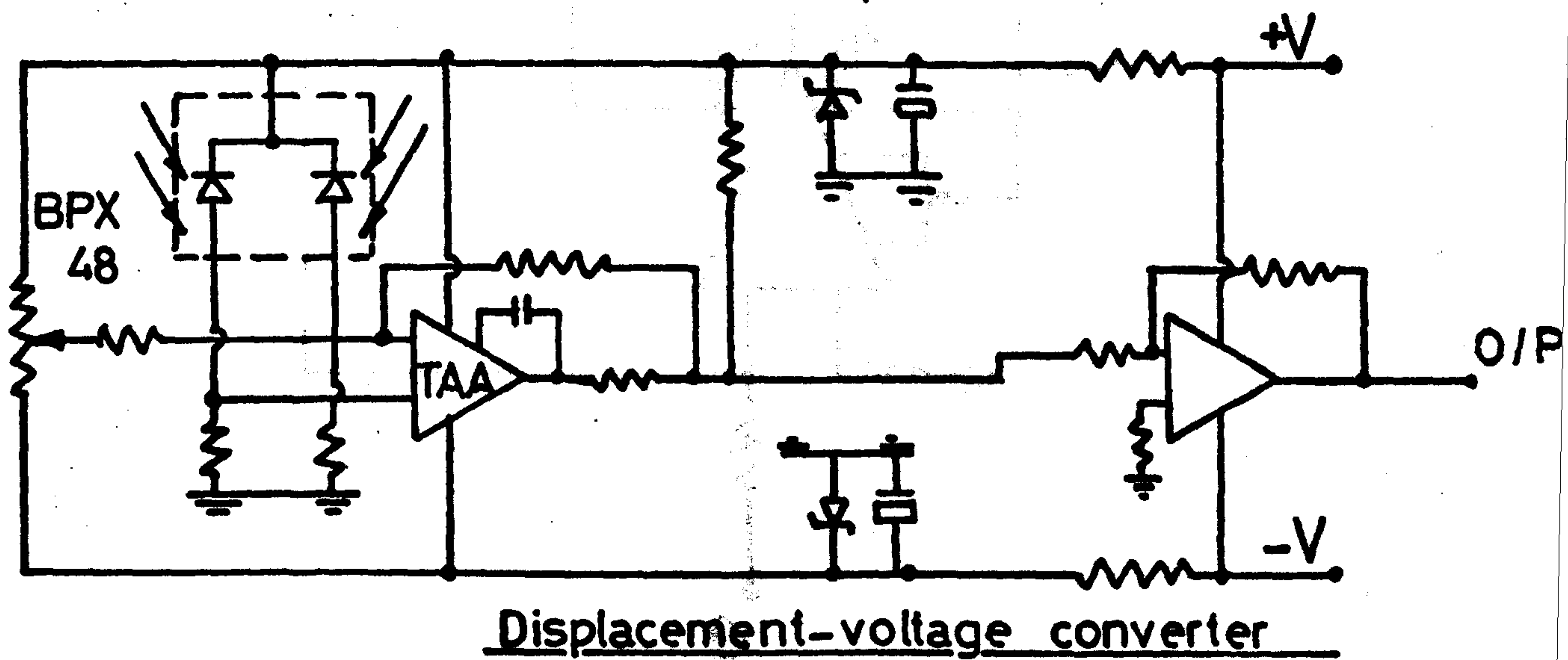
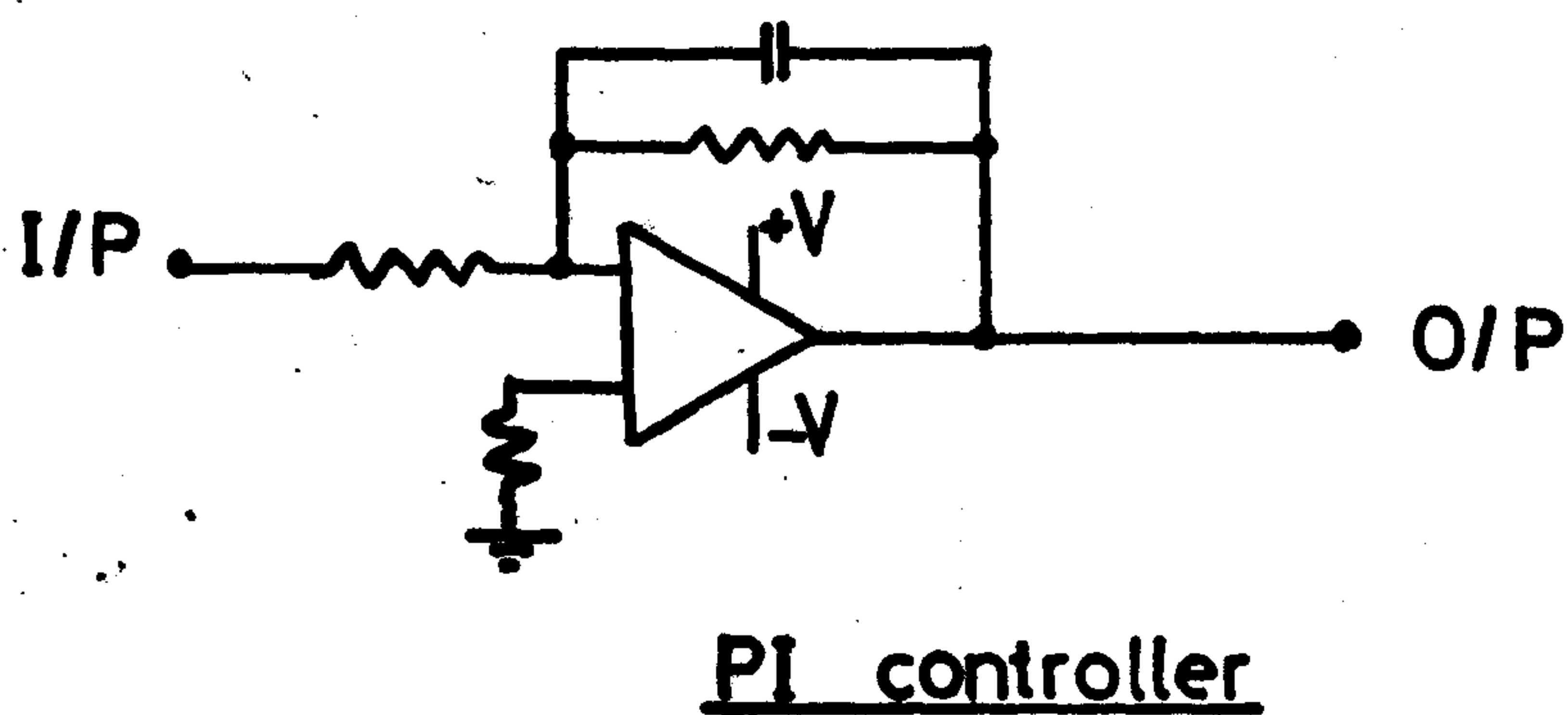
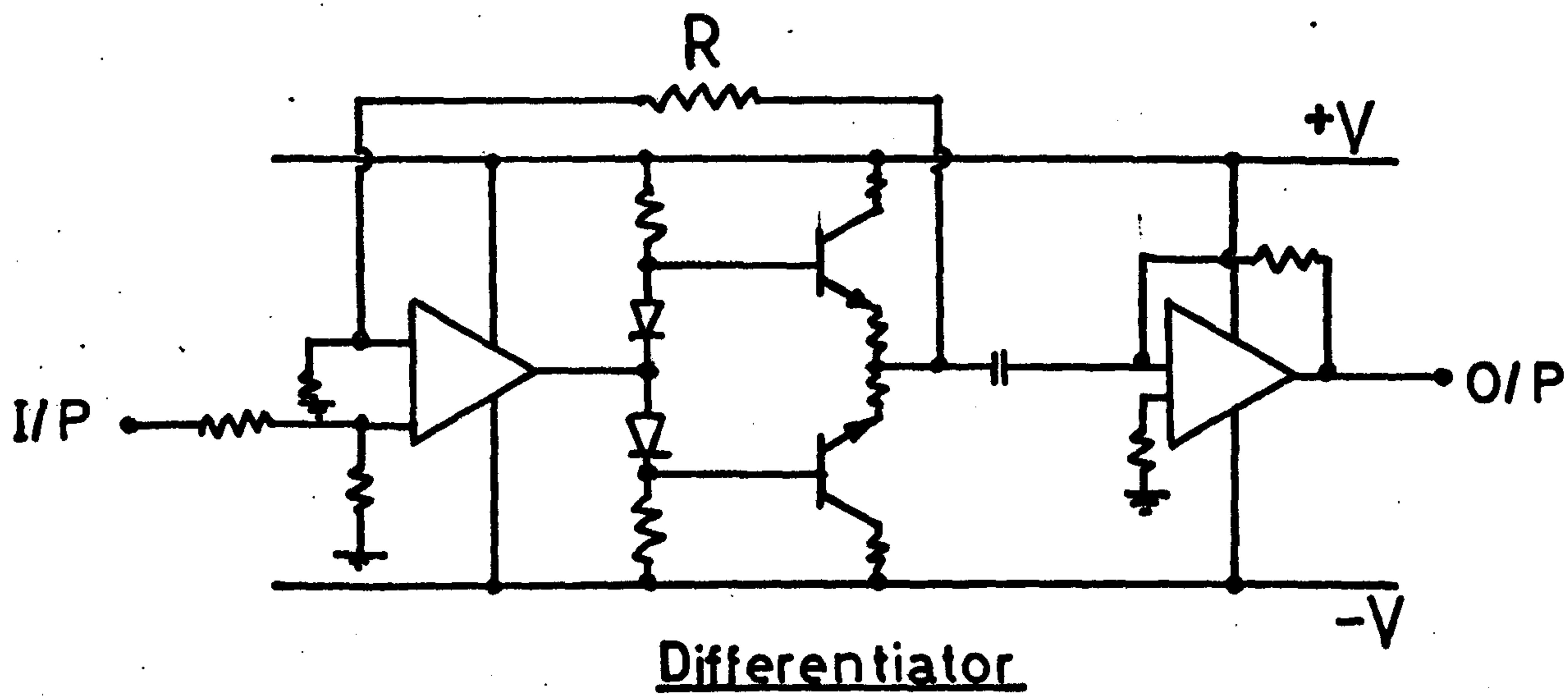


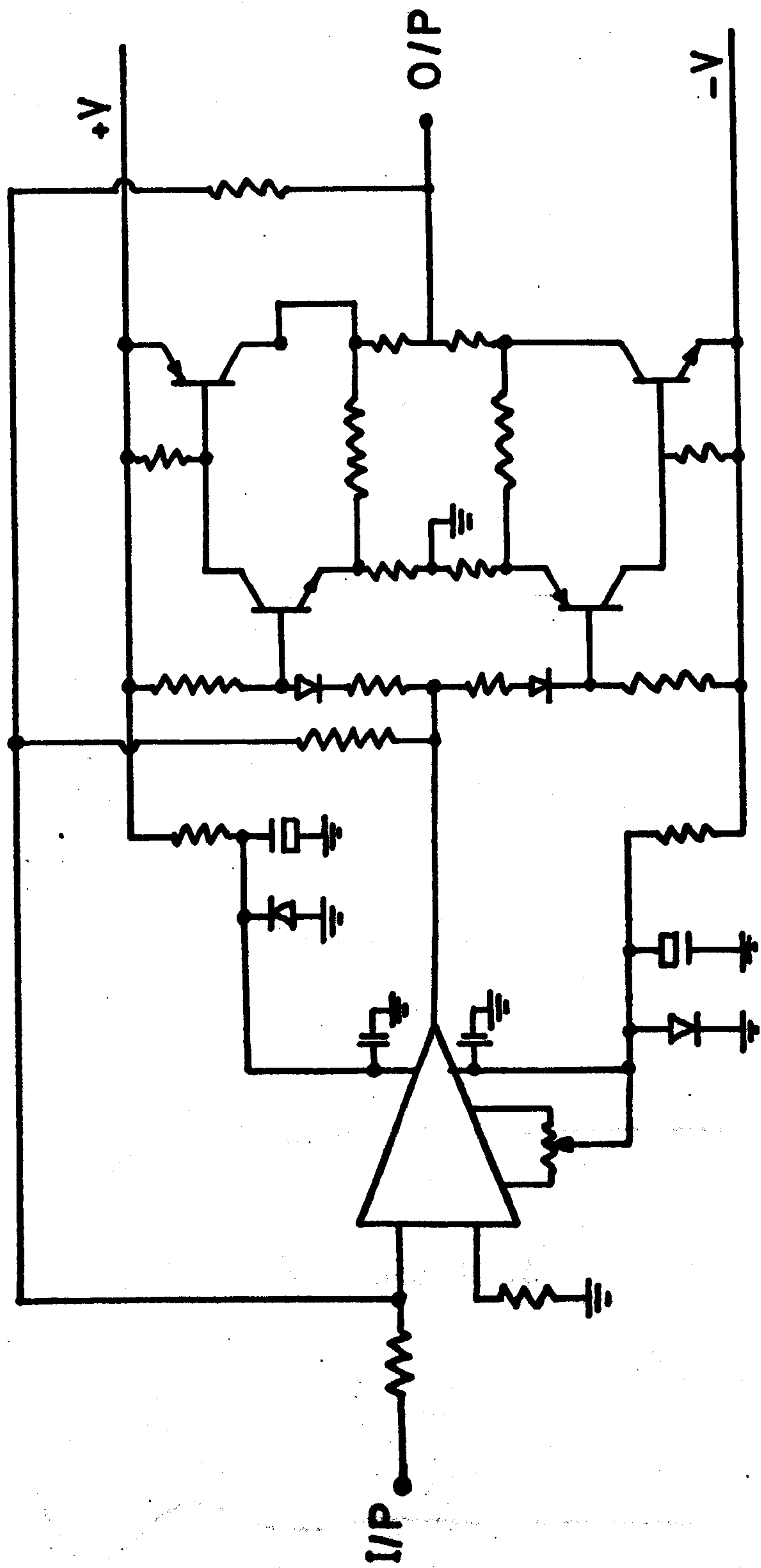




APPENDIX 1.

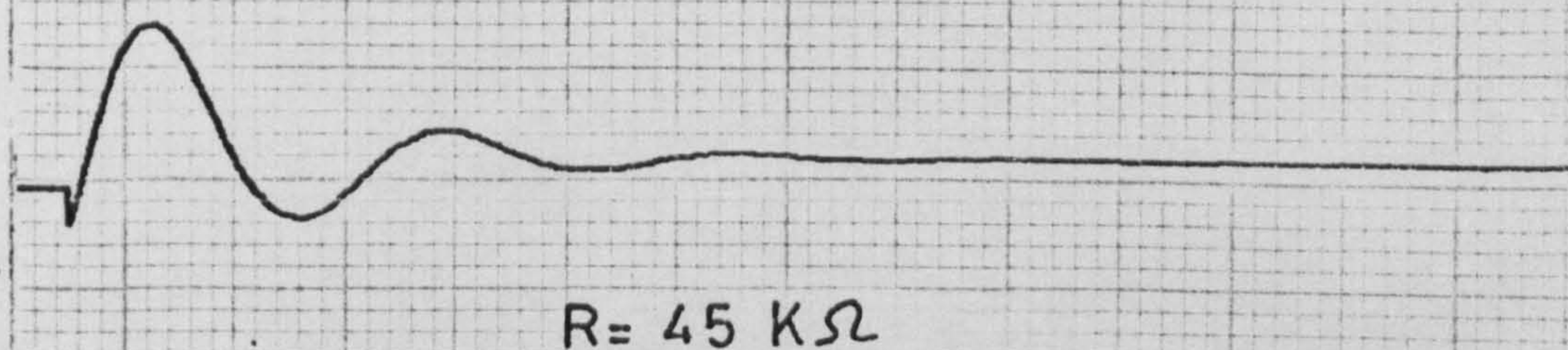
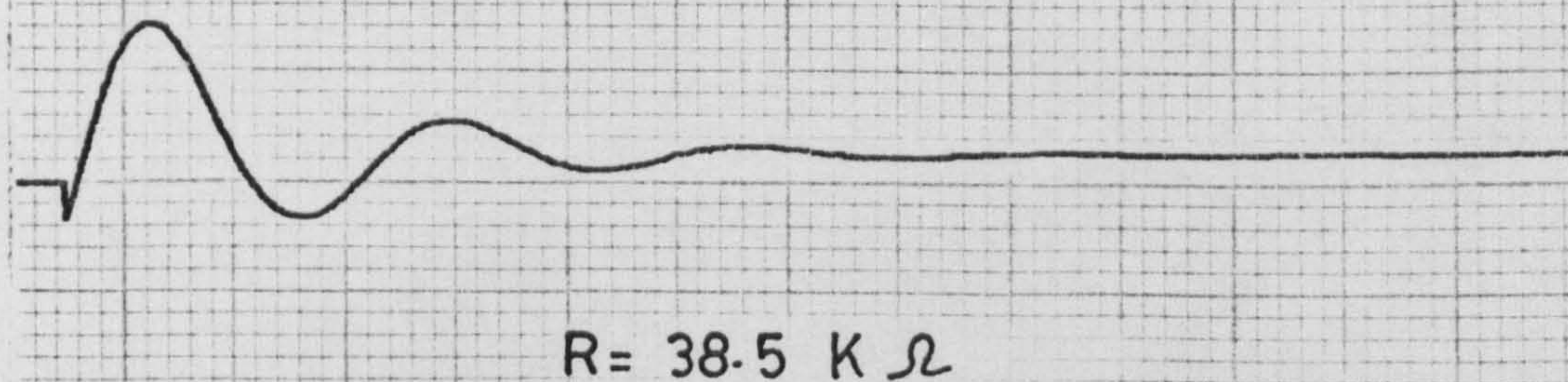
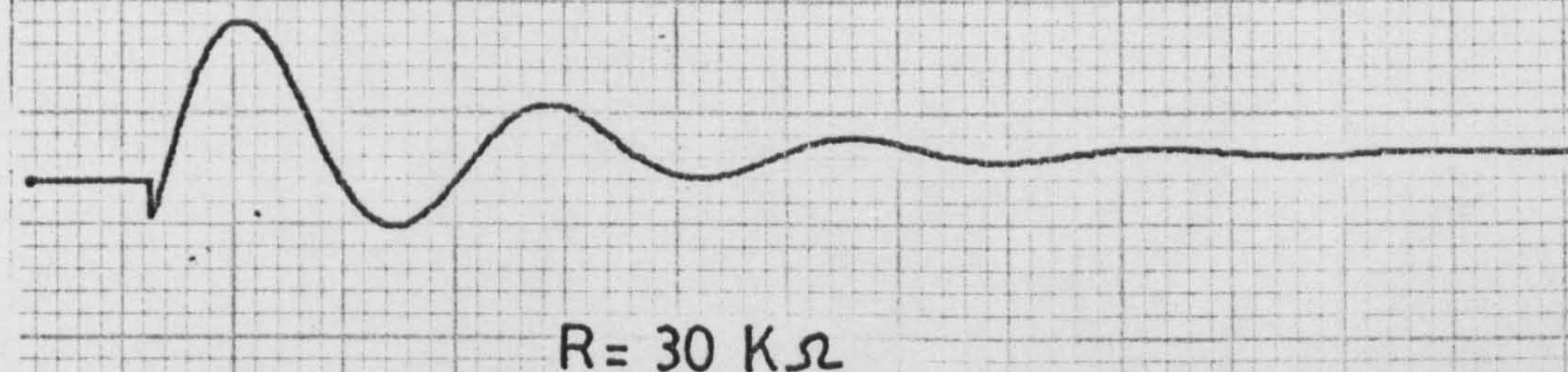
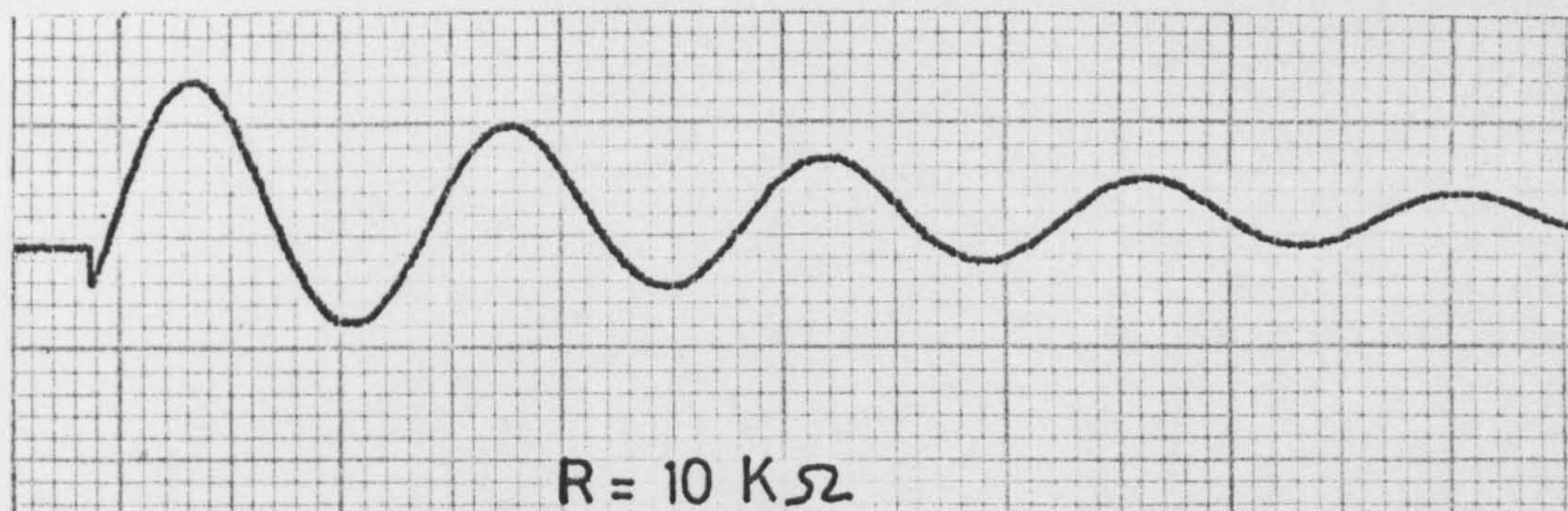
Electronic circuit and computer programme





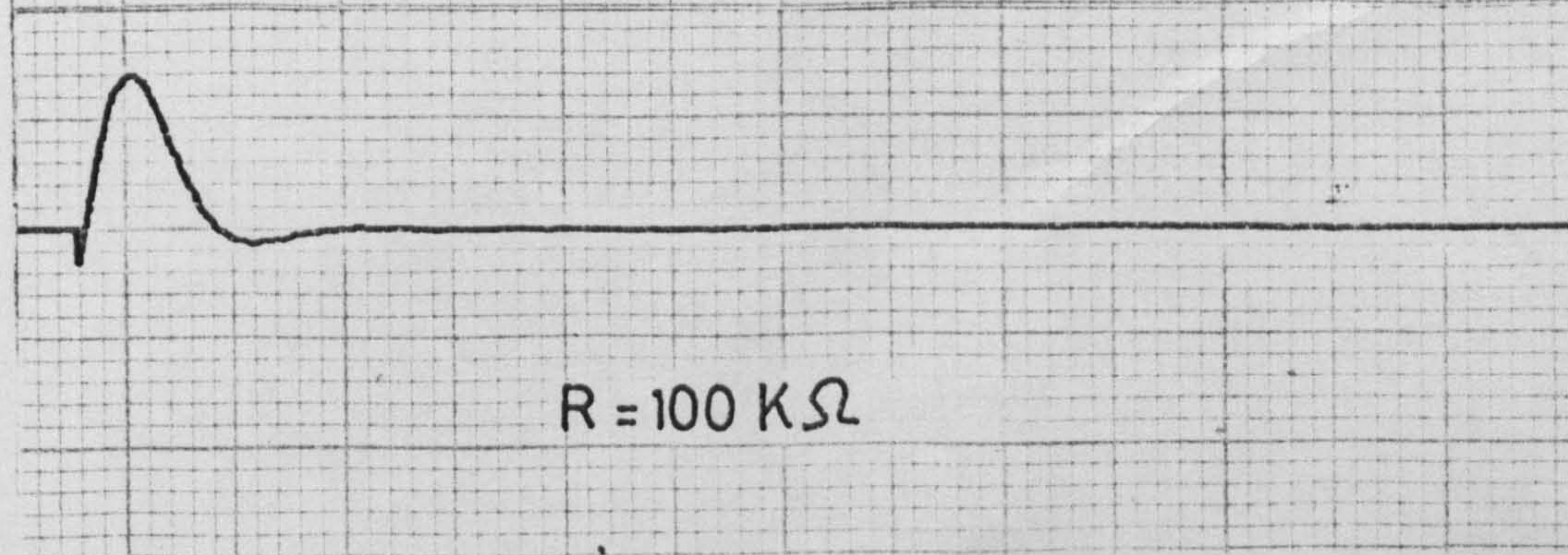
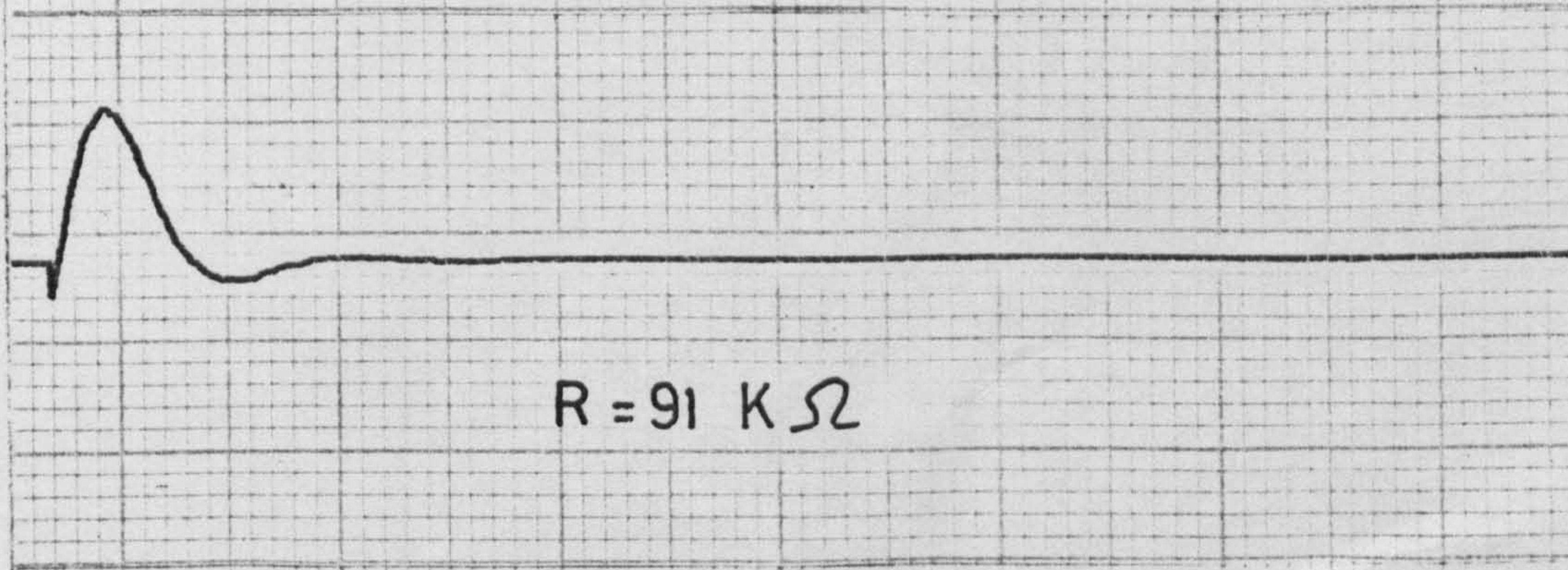
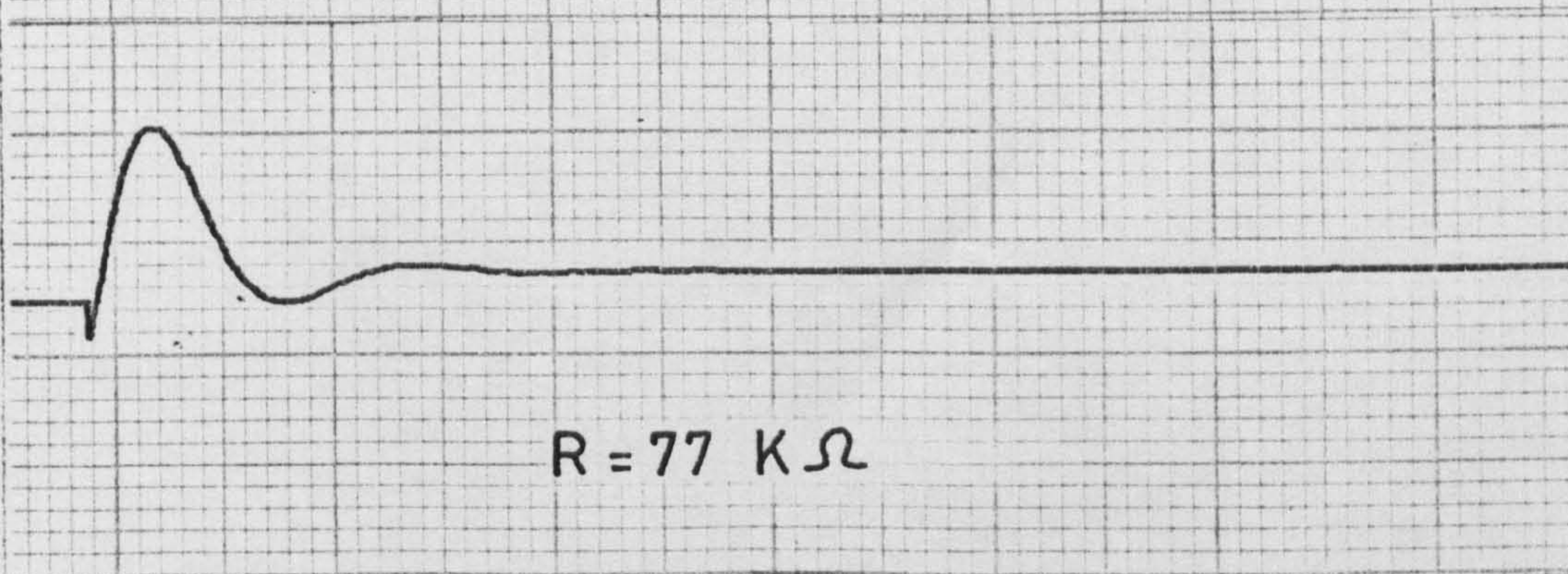
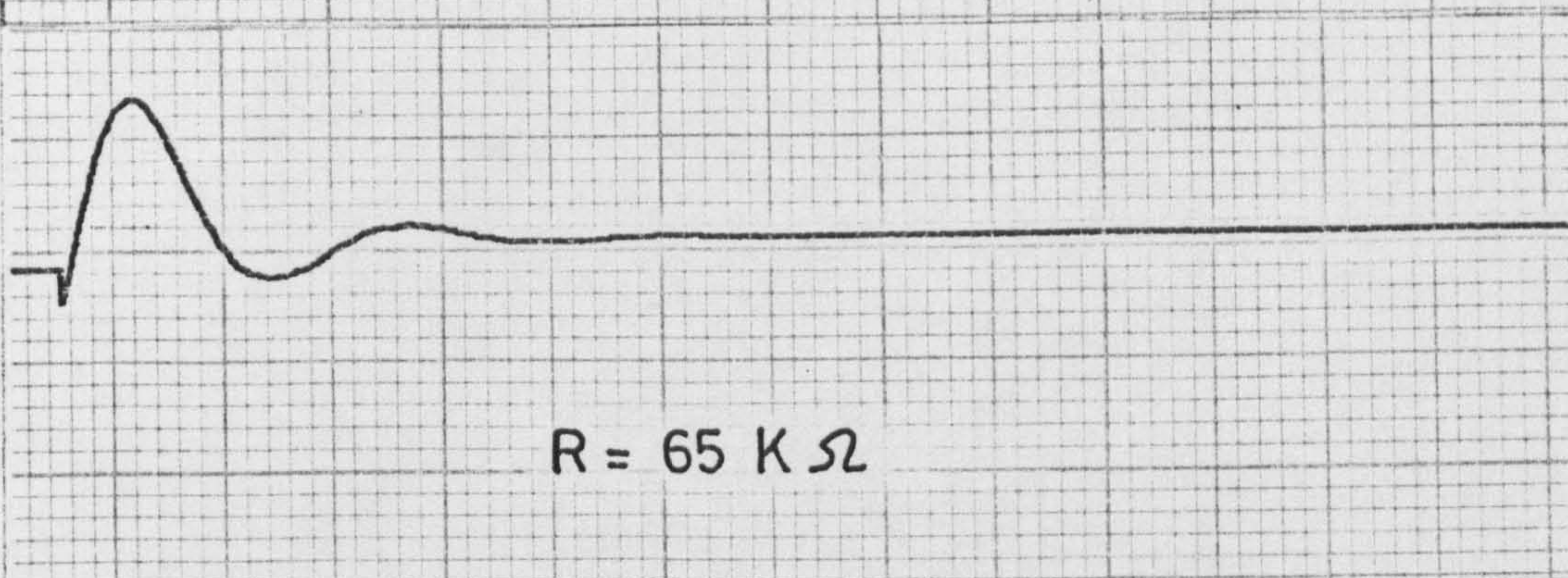
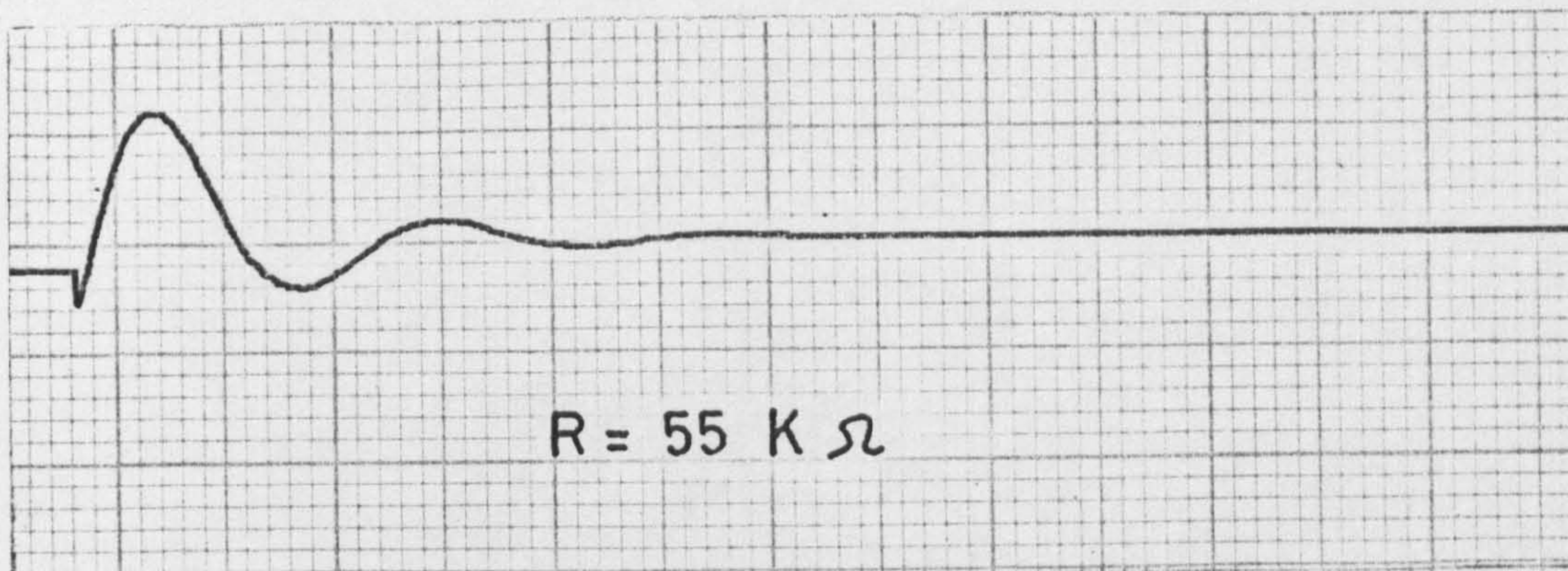
Servo-amplifier circuit





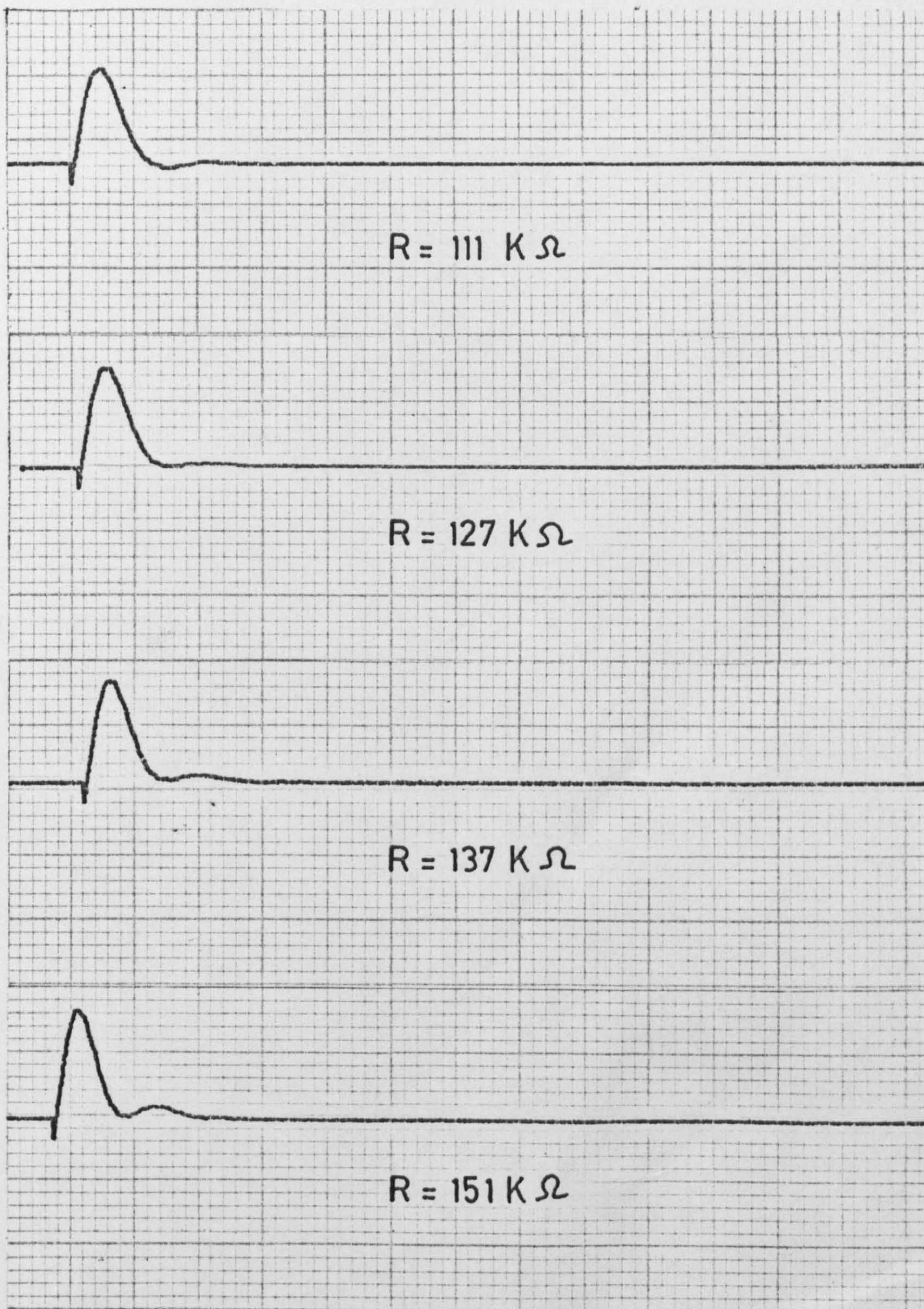
Damping with various velocity  
feed back





Damping with various velocity  
feed back





[The indicated values are referred to resistor  $R$  in the differentiator circuit]

Damping with various velocity  
feed back



EDINBURGH FORTRAN(G) COMPILER VERSION 30.3

```

1      IMPLICIT REAL*8(A-H,O-Z)
2      INTEGER TEST
3      DIMENSION V(1),FD(1,4),DFDYD(1,1),DIFD(1,7,2),TOL(3)
4      COMMON GAM,VV,AP,AKP,PP,VW,VWSO,U1,L1M,DEL,TDEL,S,XX,B,JK,KKK
5      EXTERNAL AUXD,OUTD
6      C  CALL ICL9HERRORTABLE(4,1,0,0,0,0,0,1,0,0,0,IRES)
7      KKK=0
8      GAM=15.0D-6
9      READ(5,11) X,V(1),DEL
10     11  FORMAT(3E15.5)
11     XEND=0.059700
12     S=1.00
13     TABD=0.0033200
14     N=1
15     TEST=1
16     IFAIL=0
17     HT=0.000
18     TOL(1)=1.0-4
19     CALL D02AJF(X,XEND,V,N,AUXD,HT,TOL,TEST,TABD,OUTD,FD,DFDYD,DIFD,
20     1IFAIL)
21     WRITE(6,100)
22     100  FORMAT(17X,'X',17X,'V',17X,'DEL')
23     WRITE(6,200) X,V,DEL
24     200  FORMAT(3(6X,D12.4))
25     STOP
26     END

```

```

27     SUBROUTINE AUXD(FD,V,X,N)
28     IMPLICIT REAL*8(A-H,O-Z)
29     INTEGER TEST
30     DIMENSION TOL(3),FD(1),V(1),A(3),F(3),YPP(3),D(3,15),DP(3,15)
31     COMMON GAM,VV,AP,AKP,PP,VW,VWSO,U1,L1M,DEL,TDEL,S,XX,B,JK,KKK
32     EXTERNAL AUXABC
33     C  EQUATION IN X
34     KKK=KKK+1
35     XX=X
36     Y=0.00
37     YEND=DEL*1.5+1.0-7
38     A(1)=V(1)*V(1)/GAM
39     A(2)=0.00
40     L=2
41     DO 20 I=1,3
42     TOL(I)=1.0D-3
43     20  CONTINUE
44     VV=V(1)
45     TEST=1
46     TAB=0.00100

```

```

47      IFAIL=0
48      VW=-.1117D0
49      UENF=5.3D0
50      R=0.0381D0
51      PROW=1.18
52      U1=2.*UENF*DSIN(X/R)
53      ALF=0.D0
54      IF(X.EQ.0.D0) GO TO 21
55      ALF=-GAM*U1*2.*UENF*DCOS(X/R)/(R*VV**3)
56      PP=-ALF
57      AKP=4D.*V(1)/15.
58      VWS0=VW/V(1)
59      21 U1M=0.99*U1
60      JK=0
61      HT=1.D-7
62      C      WRITE(6,300)
63      300 FORMAT(' RESULTS A,B,C')
64      C      WRITE(6,400)
65      400 FORMAT(17X,'Y',17X,'U',17X,'Z',17X,'T')
66      CALL D02AHF(Y,A,TOL,TEST,L,YEND-Y,HT,AUXABC,F,YPP,D,DP,L,IQ,IFAIL
67      WRITE(6,800) X,YEND,DEL,A(1),U1
68      800 FORMAT(' X,YEND,DEL,A(1),U1',(5(5X,D12.4)))
69      IF(JK.EQ.0) STOP 3
70      DELP=DEL*V(1)/GAM
71      DUDYP=2./(1.+DSQRT(S))
72      FD(1)=1.D7
73      IF(TDEL.EQ.0.D0) GO TO 31
74      FD(1)=((DUDYP-ALF*DELP-1.D0)*VV*VV-VW*U1)/(GAM*TDEL)
75      31 WRITE(6,700) Y,(A(I),I=1,2),FD(1)
76      700 FORMAT(' Y,A(I),DV/DX',(5(6X,D12.4)))
77      RETURN
78      END

```

```

79      SUBROUTINE AUXABC(F,A,Y)
80      IMPLICIT REAL*8(A-H,O-Z)
81      DIMENSION F(3),A(3),TWAS(3)
82      COMMON/KEEP/FLAST
83      COMMON GAM,VV,AP,AKP,PP,VW,VWS0,U1,U1M,DEL,TDEL,S,XX,B,JK,KKK
84      C      EQUATIONS IN Y
85      YP=Y*VV/GAM
86      F(1)=VV*VV/GAM
87      IF(XX.EQ.0.D0) GO TO 121
88      T3=0.774D0*YP*YP
89      T4=F(1)
90      IF(Y.EQ.0.D0) FLAST=T4
91      KOUNT=0
92      KK=0
93      12 F1OLD=FLAST
94      KOUNT=KOUNT+1
95      KK=KK+1
96      IF(KOUNT.GT.50) GO TO 88
97      TWAS(KK)=F1OLD
98      TAUP=F1OLD/T4
99      TAUPSQ=DSQRT(TAUP)
100     VXY=VV*TAUPSQ
101     VWS=VW/VXY

```

```

102      B=DUXP(11.8D0*VWS)
103      23 IF(PP.LE.0.012) GO TO 24
104      EF1=2133.*PP-12.
105      GO TO 25
106      24 EF1=1133.*PP
107      25 IF(VWS.GE.0.) GO TO 26
108      EF2=6.78*PP**0.7*(-VWS)**1.4
109      GO TO 27
110      26 EF2=1990.*(PP*VWS**0.25)**1.1
111      27 AP=26./(1.+5.9*VWS)+EF1+EF2
112      11 T1=YP/AP
113      T2=T1*60.D0/AKP
114      SS=1.D0+T3*(1.D0-DUXP(-T1*TAUPSQ) +DUXP(-T2*TAUPSQ))**2
115      FLAST=2.D0*T4/(1.D0+DSQRT(SS))
116      IF(KK.EQ.1) GO TO 15
117      KK=0
118      TWAS(3)=FLAST
119      FLAST=TWAS(1)-(TWAS(2)-TWAS(1))**2/(TWAS(3)-TWAS(2)-TWAS(2)+
120      1 TWAS(1))
121      99 FORMAT(I4,4E14.4)
122      16 IF(DABS(1.D0-F1OLD/FLAST).GT.1.D-4) GO TO 12
123      F(1)=FLAST
124      88 JJ=MIN0(KOUNT,3)
125      IF(JJ.NE.1)WRITE(6,99) KOUNT,(TWAS(J),J=1,JJ),FLAST
126      IF(KOUNT.GT.50) STOP 11
127      121 CONTINUE
128      F(2)=0.D0
129      IF(VV.NE.0.D0) F(2)=A(1)*A(1)/(GAM*VV)
130      IF(JK.EQ.1.OR.A(1).LT.3*U1M.OR.A(2).EQ.0.0.AND.XX.NE.0.0) GO TO 7
131      JK=1
132      DEL=Y
133      S=SS
134      TDEL=A(2)
135      7 RETURN
136      END

```

```

137      SUBROUTINE OUTD(X,V,HT,N,TABD)
138      IMPLICIT REAL*8(A-H,O-Z)
139      DIMENSION V(1)
140      WRITE(6,500) X,V
141      500 FORMAT(' X,V',(2(10X,D12.4)))
142      RETURN
143      END

```

```

144      FUNCTION DUXP(X)
145      IMPLICIT REAL*8 (A-H,O-Z)
146      IF(X.LT.-180.) GO TO 17
147      DUXP=DEXP(X)
148      RETURN
149      17 DUXP=0.D0
150      RETURN
151      END

```



## APPENDIX 2.

### Difficulties and failures

## DIFFICULTIES AND FAILURES

The first major difficulty, faced in the programme, appeared during the period of construction of the control system for the servo-force balance. It proved to be a mysterious mechanical hysteresis in the suspension pivots when the system was tested using the transfer function analyser (TFA).

The hysteresis loop is shown in figure A in this Appendix. This item undoubtedly caused a great deal of confusion at the earlier stages and was only identifiable with any certainty when dynamic measurements were made in order to assist in the development of the control system.

After long and careful consideration it was finally deemed necessary to dismantle the mechanical system, specifically the vane and the bearings, and remount. This stage was highly successful and led to a suspension which is entirely free from any mechanical hysteresis and of extremely low damping. This is shown in figure B in this Appendix but the reason for that mechanical hysteresis or why it happened is not yet known.

The second major problem in the programme was the cooling of the inside walls of the porous test cylinder. Ideas such as using refrigeration coils were rejected due to their possible effect on the porosity of the surface. Cooling the wall using a sprayed cooling water on to the surface created problems especially when the suction rate was increased. The stability of the cooling water layer on the surface/...

surface was affected to a great extent by the amount of suction applied. This put an upper limit on the suction rates in the non-isothermal tests. Exceeding this limit caused the cooling water to be sucked into the air lines which caused a great deal of trouble in the suction pump.

On the other hand, decreasing the suction rate below a certain minimum value caused the cooling water to leak from inside to outside of the porous surface with possibility of flooding the shear stress sensor. Indeed, this caused an inability to reach the situation where there was only heat transfer without mass transfer. Of course this made it difficult to compare our results with other investigations as far as the heat transfer distribution is concerned.

Carrying the cooling water away from the test cylinder without disturbing the conditions inside the cylinder was also a problem. This was solved by making a perspex extension to the bottom of the cylinder and the stability of pumping the cooling water was established when the upper part of this extension was subjected to the same pressure inside the cylinder via a valve.

The third major difficulty was the estimation of the buoyancy effect on the recorded shear stress due to the pressure difference on the upstream and downstream sides of the drag piece. Due to the nature of such pressure differences being sometimes quite small together with high oscillations of the pressure inside the leads, it was necessary to use a Casella manometer to be able to read such small pressure differences./...



differences.

Since this was a very slow process, such measurements of the pressure differences were made at time intervals in some selected runs and the results were considered to be applicable for the whole programme. Whilst this was not exactly true, this assumption seemed reasonable compared with the experimental difficulties and length of time involved if these measurements were to be carried out for each individual test.

One of the main failures in the present study was the inability to reach general correlations for the obtained data in terms of the different parameters studied. Unfortunately, it was estimated that such an aim required at least as much as three times the period used in the present programme. Therefore, the obtained results were presented in such a way as to demonstrate the general behaviour of the flow structure, rather than providing empirical correlations, under the effect of different parameters involved in the study.

The second main failure was the inability to develop a successful theoretical model for the case under study. Keeping in mind that such a situation is known to be a difficult one, as pointed out by many investigators, it was hoped, however, to provide at least an approximate model for that case. Nevertheless, it is hoped that whenever time allows, this situation will again be approached from different aspects.

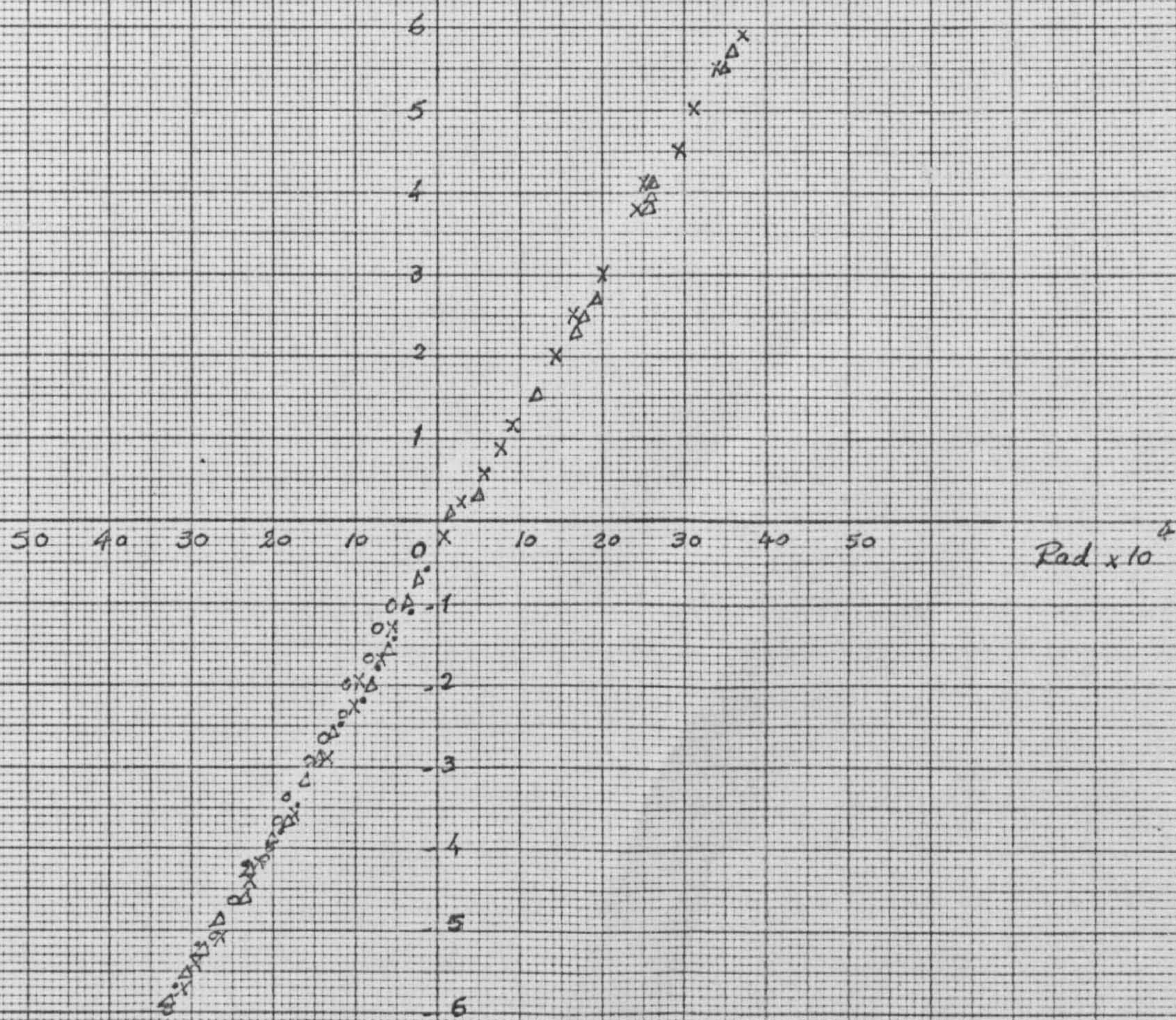




TAA Hysteresis Loop



TAA  
V



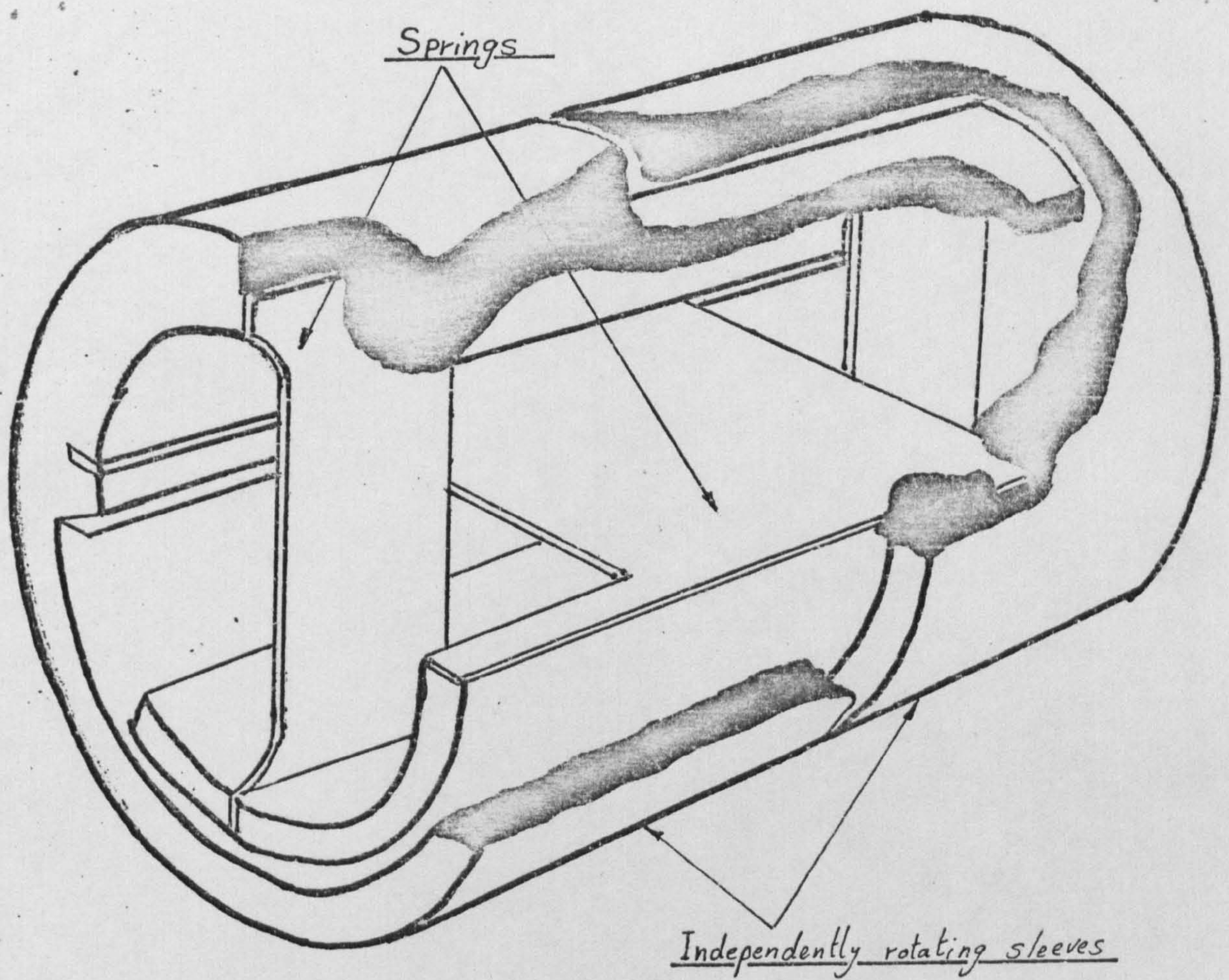
TAA response after rassembling



APPENDIX 5.

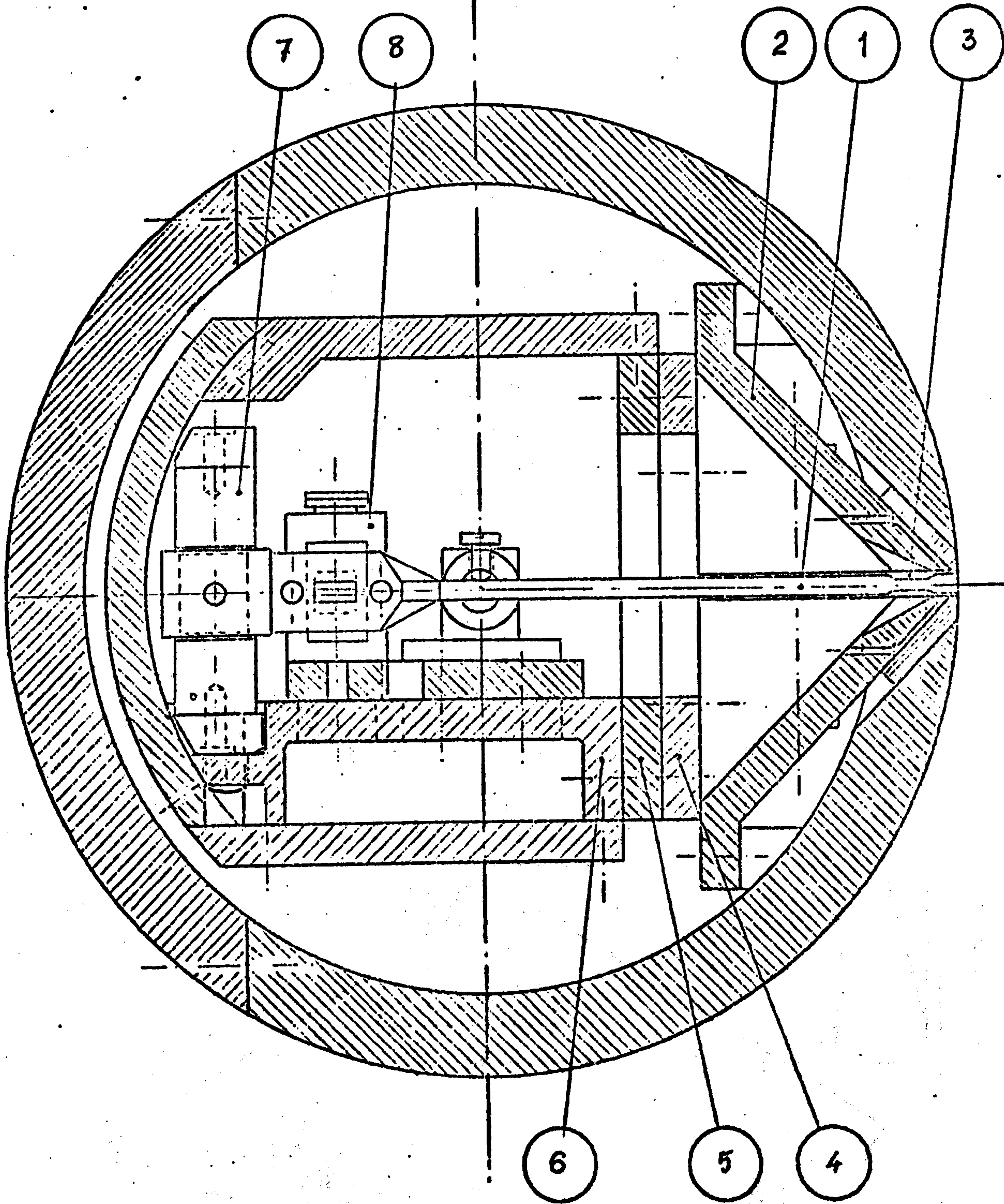
Mechanical description of the shear stress sensor





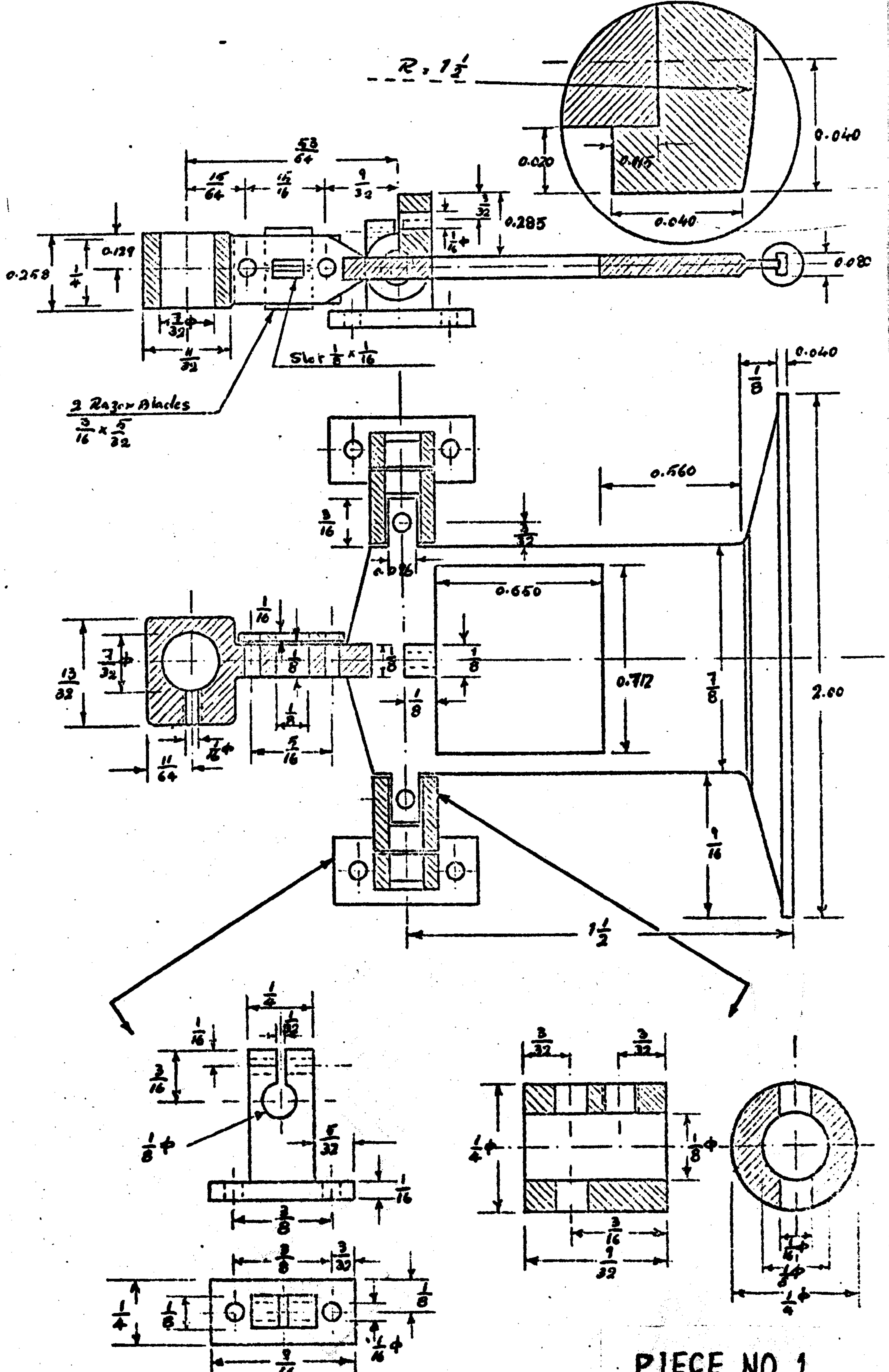
Spring-supported flexural pivot



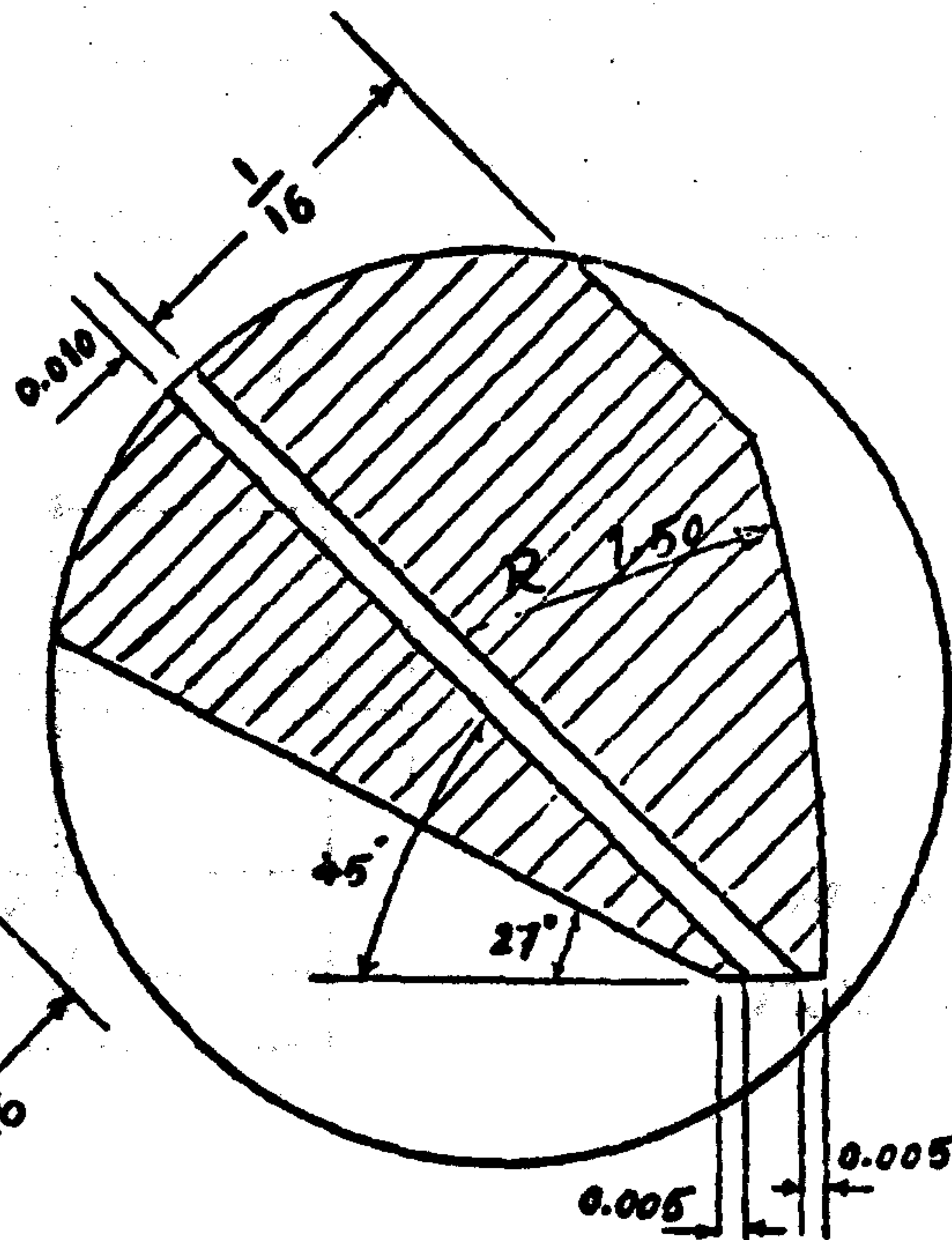
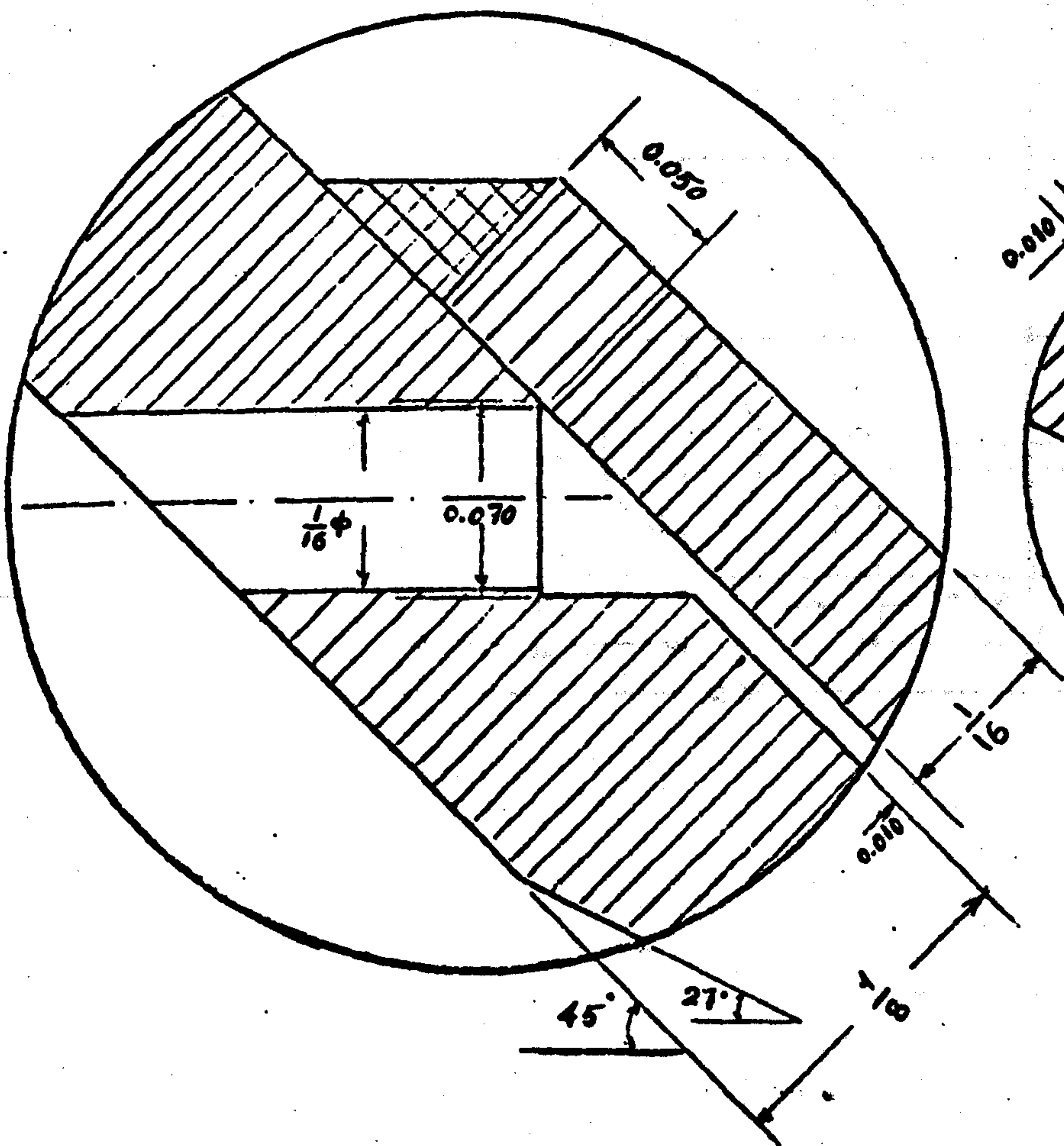
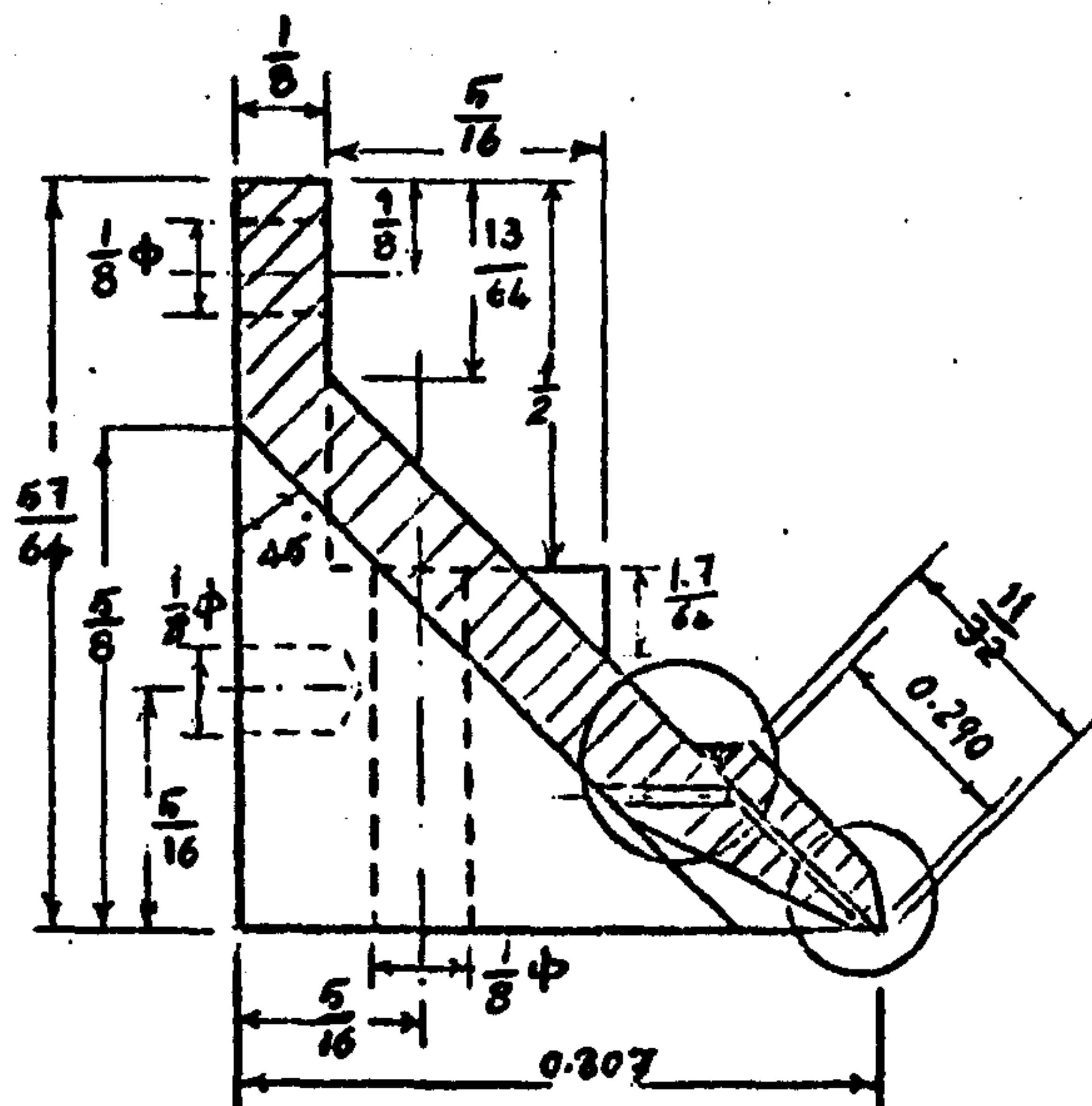
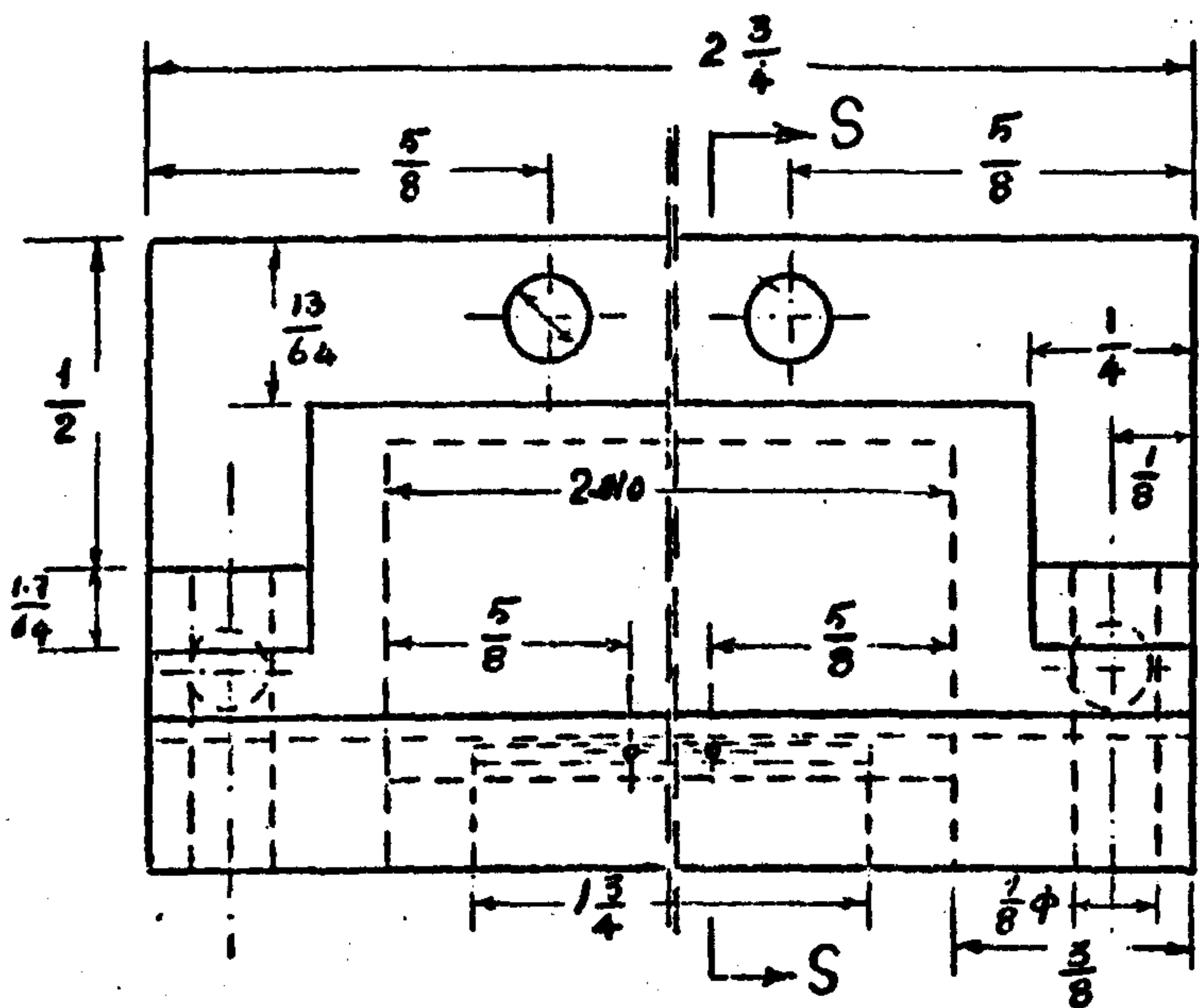


SKIN FRICTION SENSOR  
ASSEMBLY





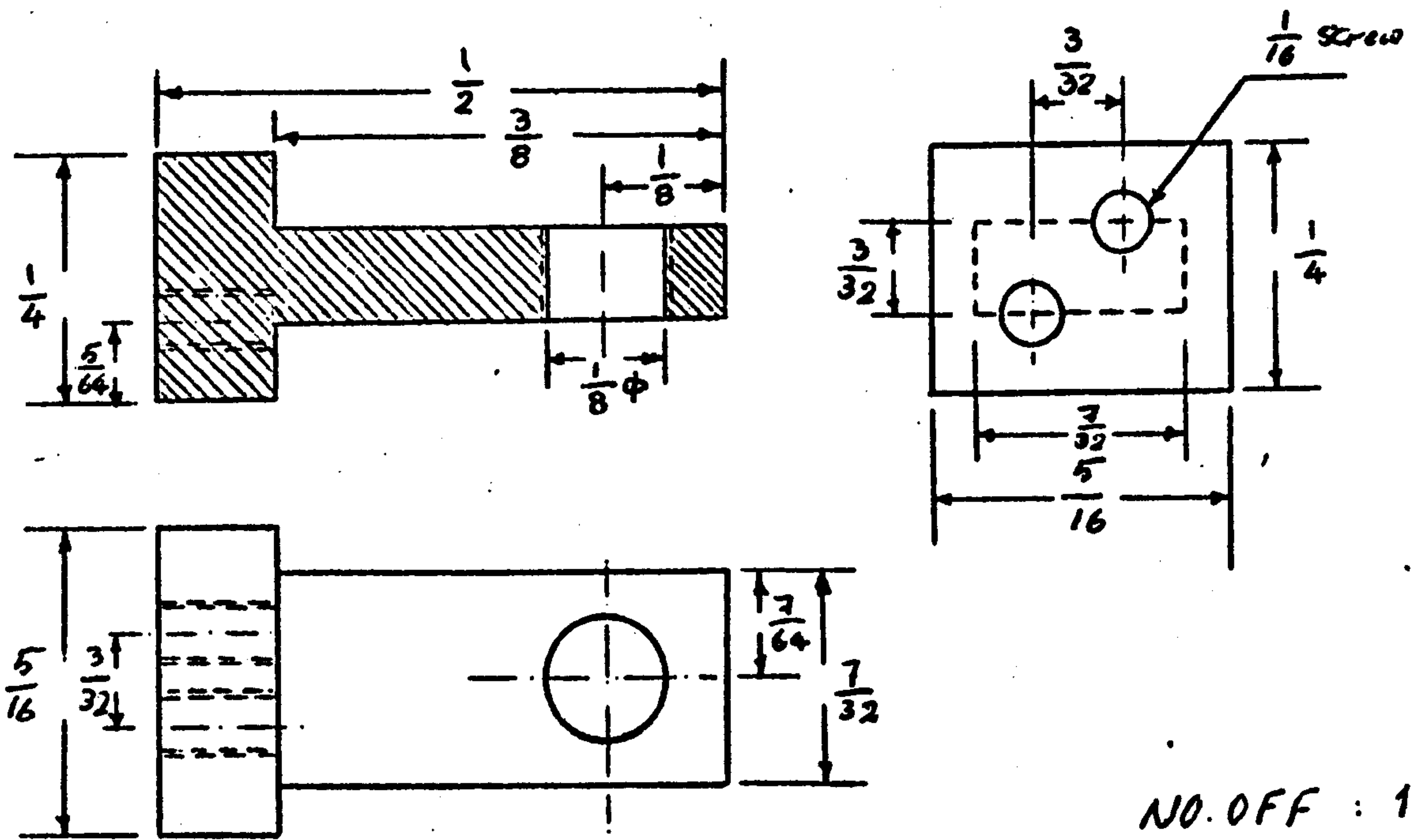
PIECE NO. 1  
DIMS IN IN  $\pm 0.009$



PIECE NO. 2

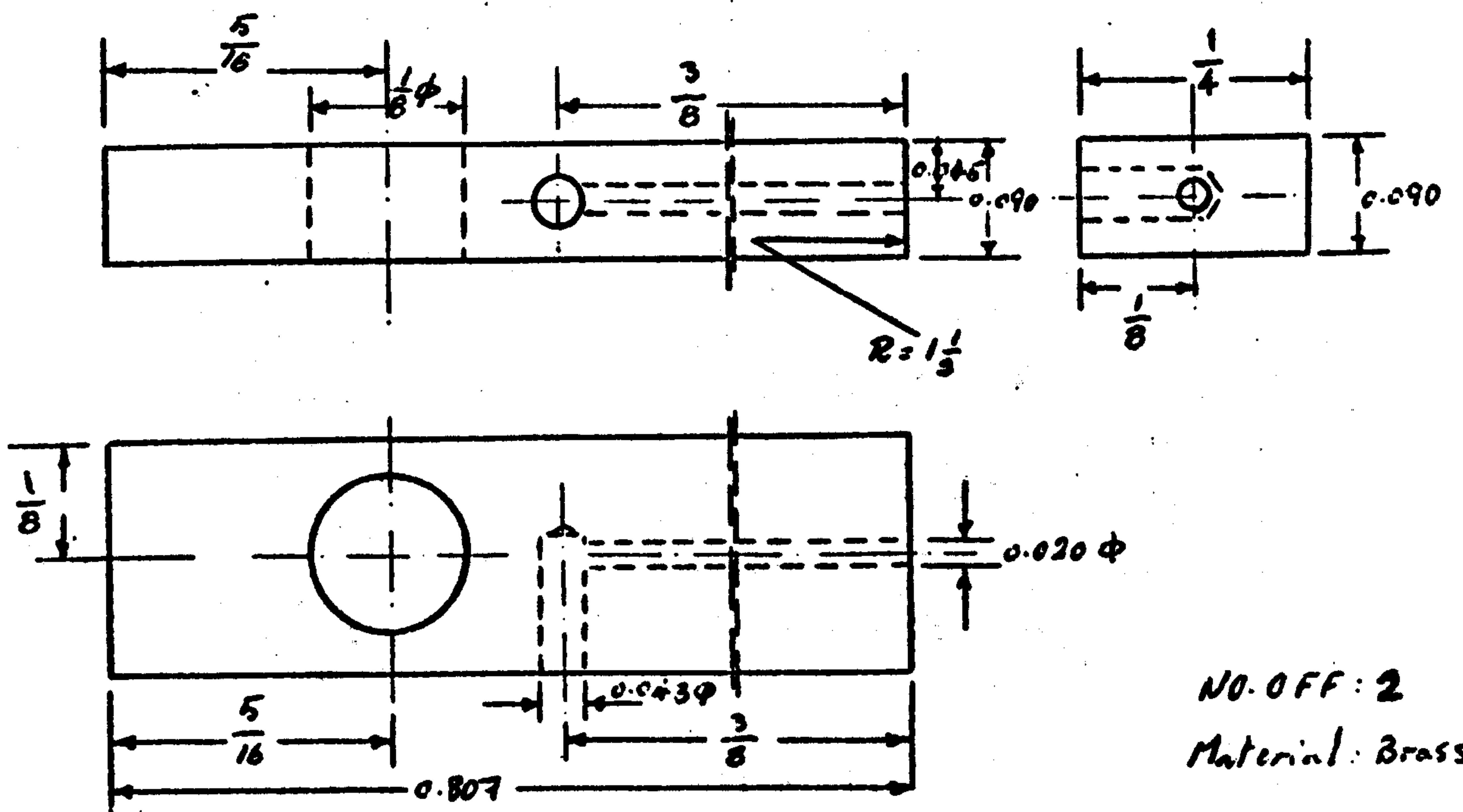
DIMS. IN. IN.  $\pm 0.001$





NO. OFF : 1

Material : Brass



NO. OFF : 2

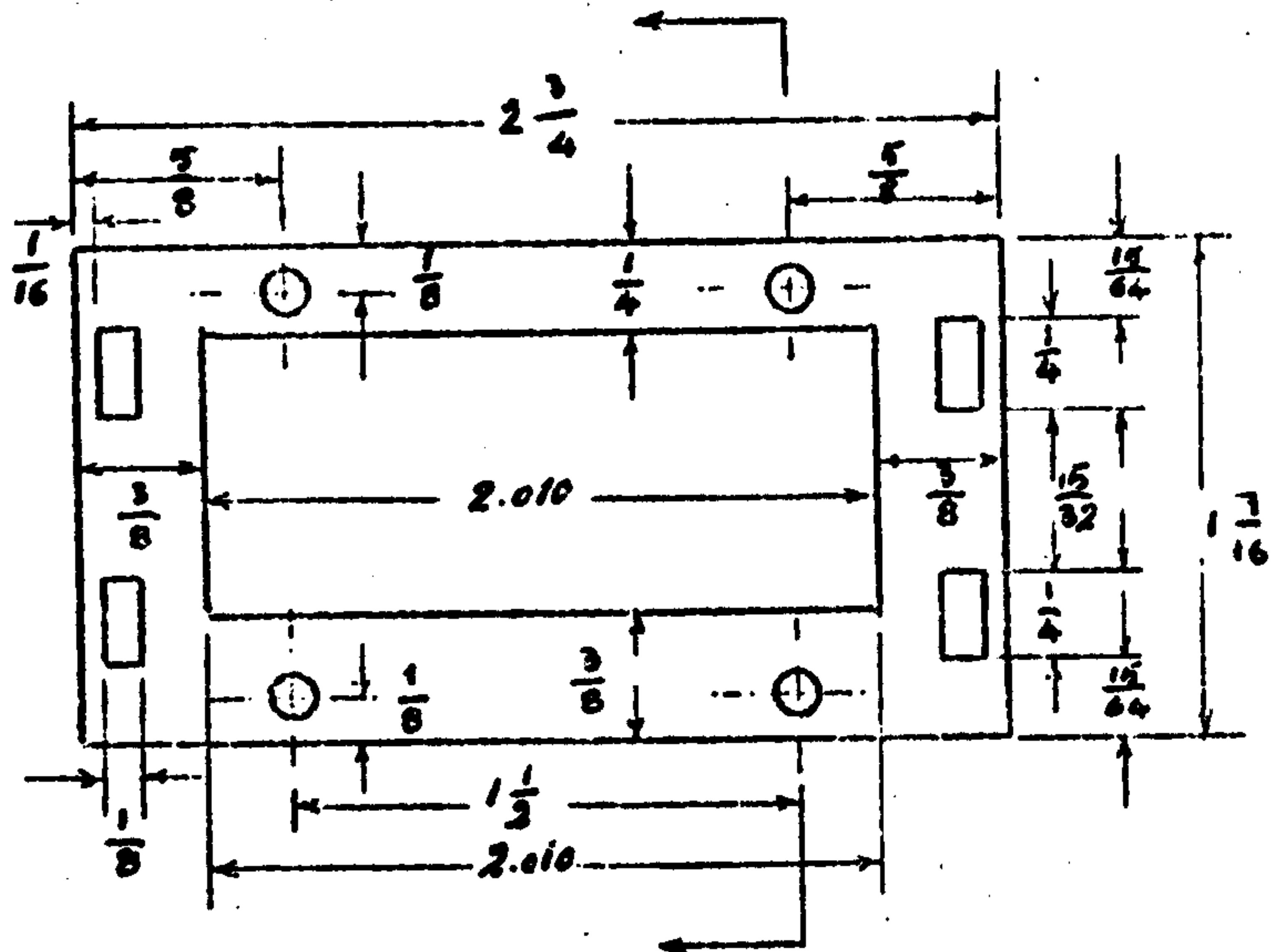
Material : Brass

PIECE NO. 3

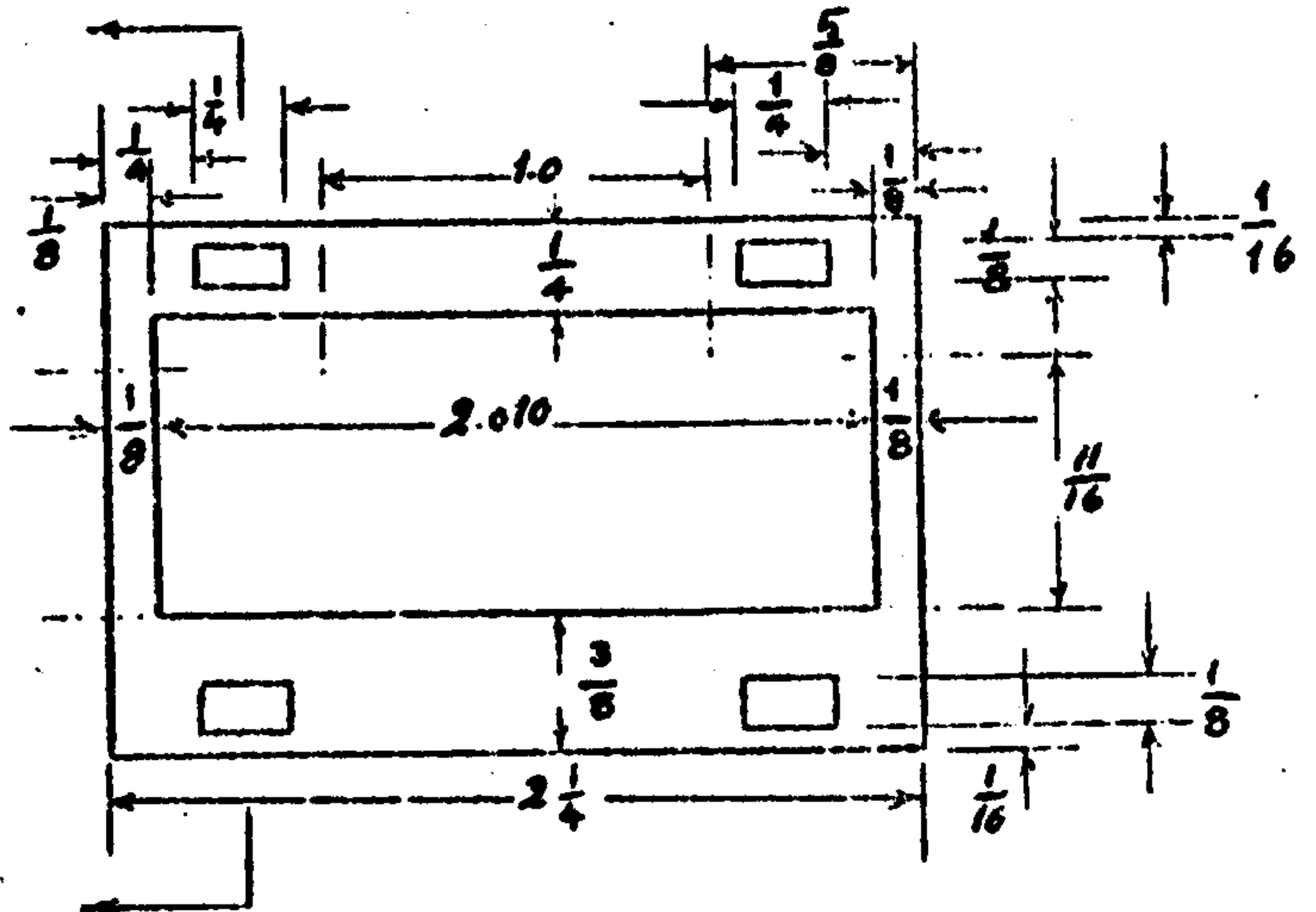
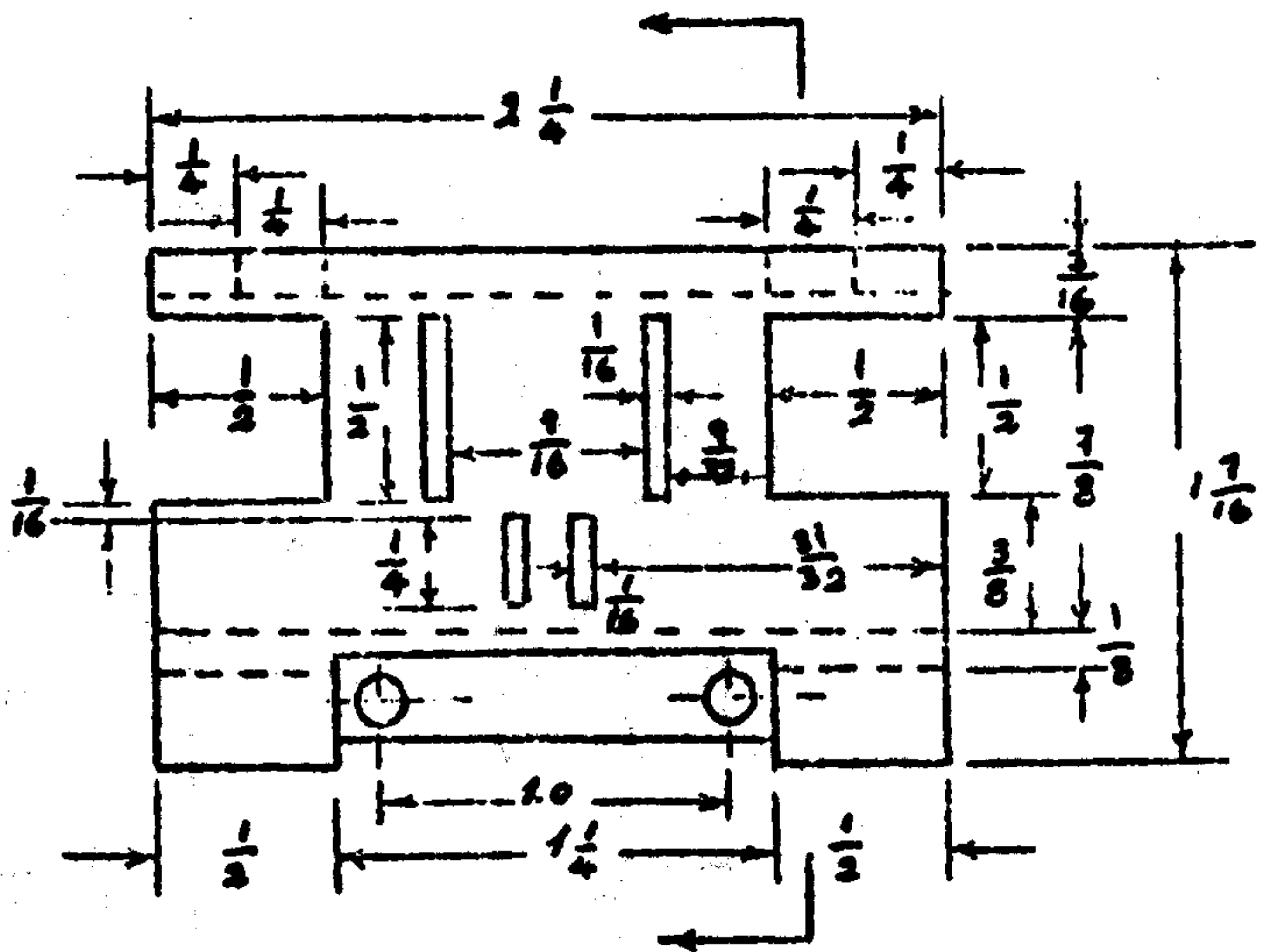
DIMS. IN. IN.

$\pm 0.001$





A vertical column of total height 17/16 is shown. It is divided into four segments of height 1/8, 3/8, 1/8, and 1/8 from top to bottom. The top segment is labeled '1' and has a horizontal load 'P' applied at its top. The second segment is labeled '3' and has a horizontal load 'P' applied at its top. The third segment is labeled '1' and has a horizontal load 'P' applied at its top. The bottom segment is labeled '1' and has a horizontal load 'P' applied at its top. The column is supported by a base at the bottom. The total height is indicated as 17/16 on the left. The height of the top segment is 1/8, the second segment is 3/8, the third segment is 1/8, and the bottom segment is 1/8. The height of the top three segments is indicated as 13/16 on the right. The height of the bottom segment is indicated as 1/8 on the right.

[illegible]

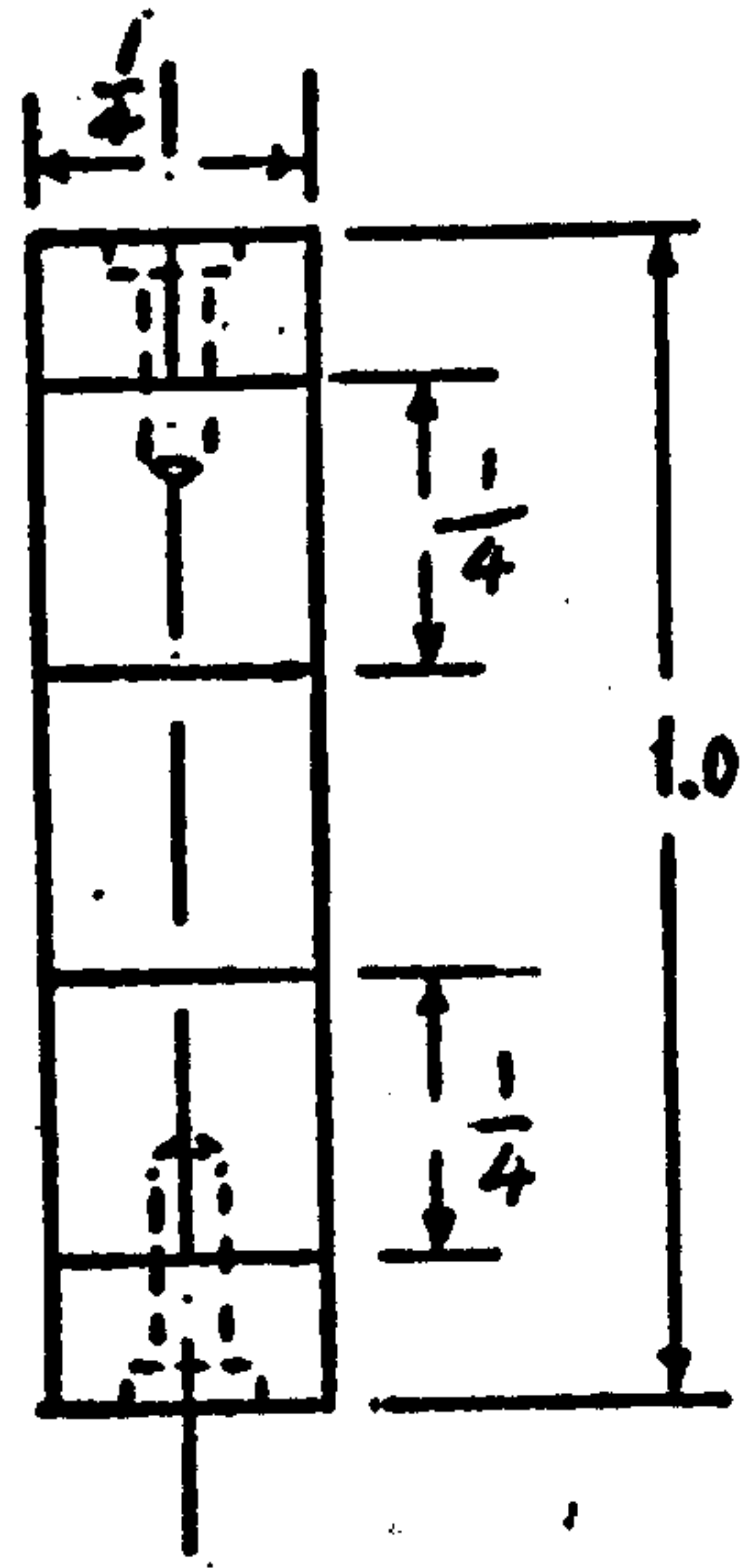
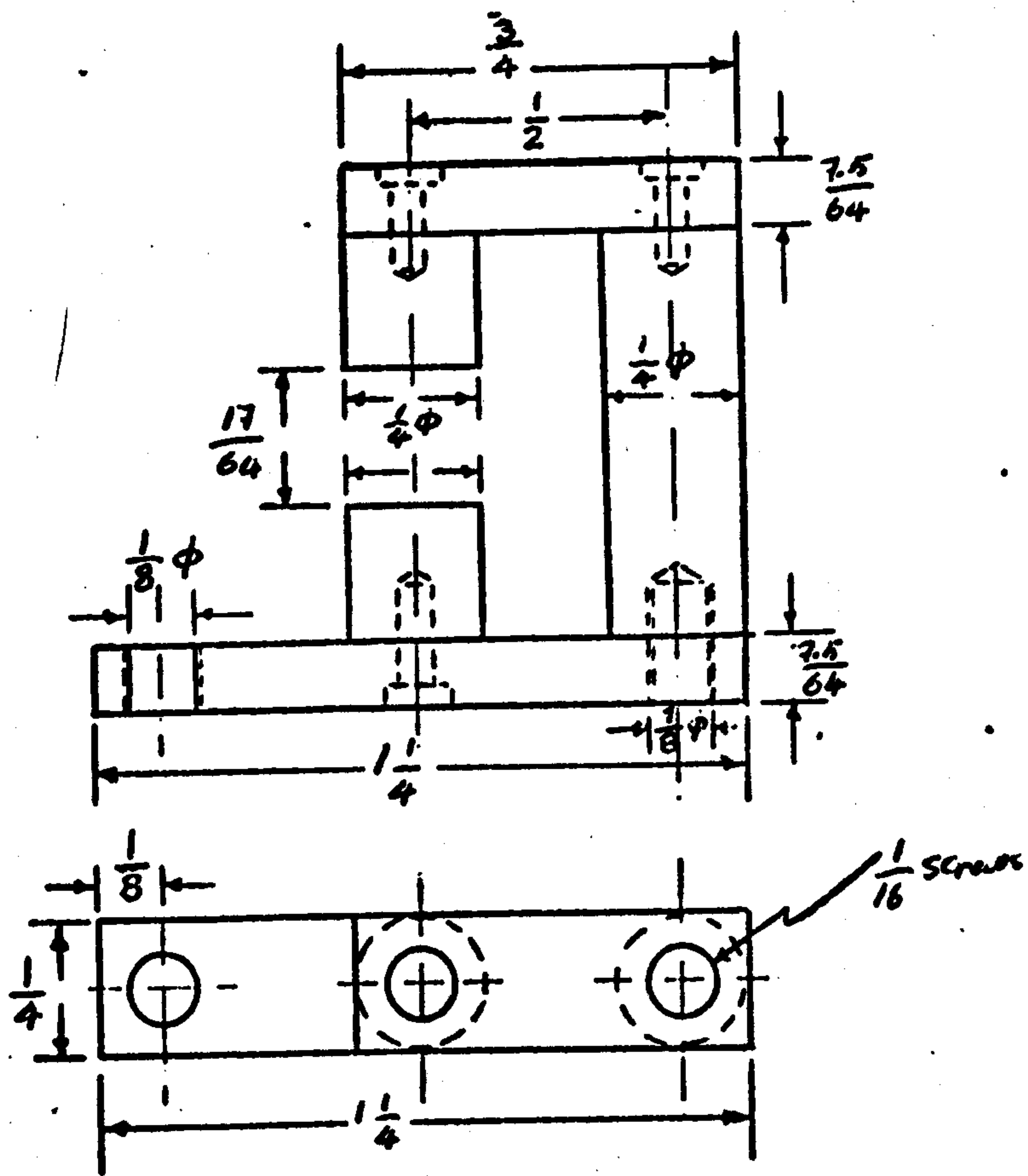
Technical drawing of a mechanical part, likely a bracket or plate, showing dimensions in inches. The drawing includes a top view and a side view.

**Top View Dimensions:**

- Overall width:  $2\frac{1}{16}$
- Overall height:  $3\frac{3}{4}$
- Distance from left edge to first vertical slot:  $\frac{1}{8}$
- Distance between first and second vertical slots:  $\frac{3}{16}$
- Distance from second vertical slot to right edge:  $\frac{9}{16}$
- Distance from left edge to first horizontal slot:  $\frac{1}{16}$
- Distance between first and second horizontal slots:  $\frac{1}{16}$
- Distance from second horizontal slot to bottom edge:  $\frac{1}{16}$
- Distance from left edge to first rectangular slot:  $\frac{1}{8}$
- Distance between first and second rectangular slots:  $\frac{11}{16}$
- Distance from second rectangular slot to right edge:  $\frac{11}{32}$
- Distance from left edge to first circular hole:  $\frac{1}{8}$
- Distance between first and second circular holes:  $\frac{11}{16}$
- Distance from second circular hole to right edge:  $\frac{11}{32}$
- Distance from left edge to first rectangular slot:  $\frac{1}{8}$
- Distance between first and second rectangular slots:  $\frac{11}{16}$
- Distance from second rectangular slot to right edge:  $\frac{11}{32}$

**Side View Dimensions:**

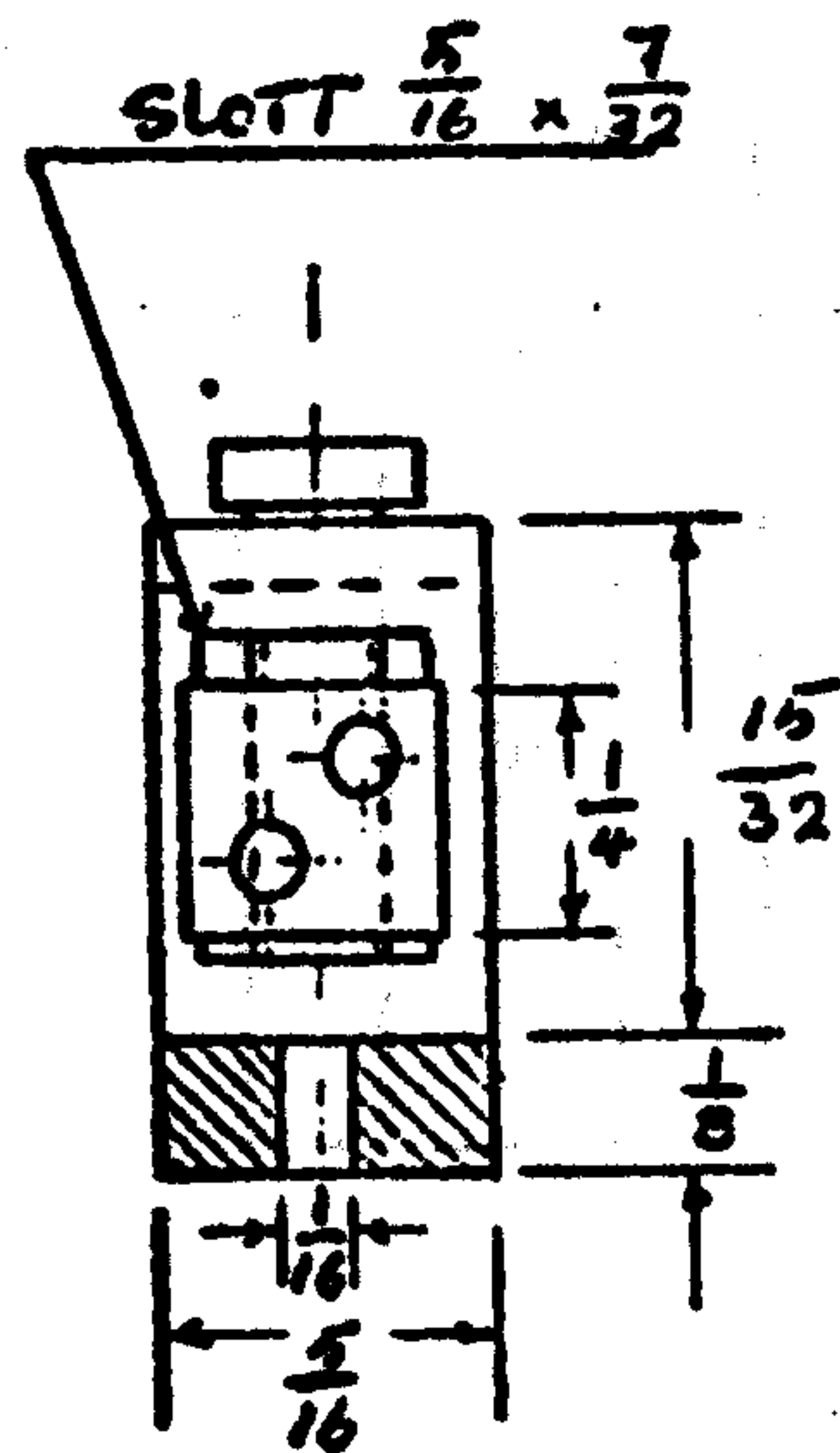
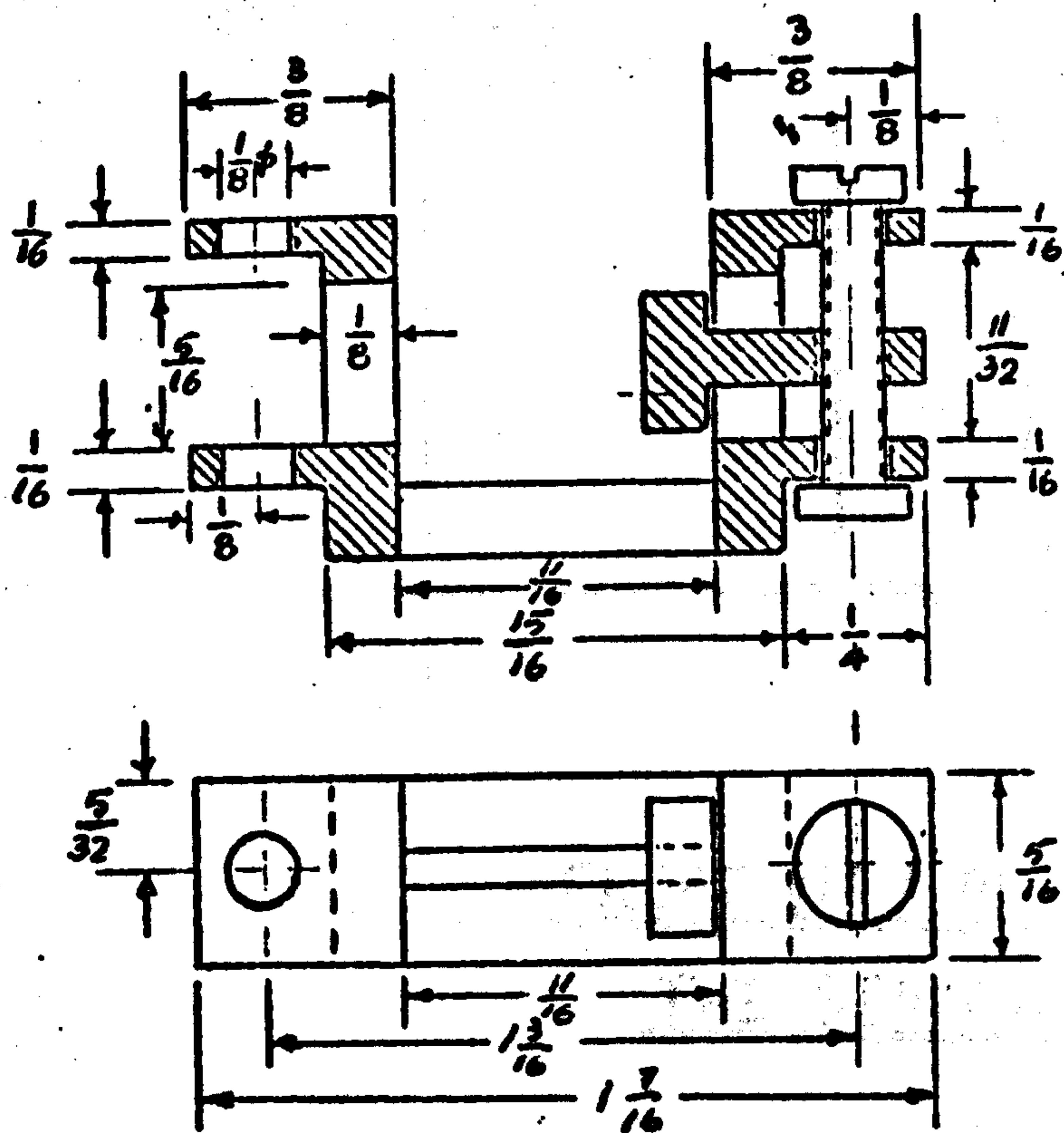
- Overall width:  $2\frac{1}{16}$
- Overall height:  $3\frac{3}{4}$
- Distance from left edge to first vertical slot:  $\frac{1}{8}$
- Distance between first and second vertical slots:  $\frac{3}{16}$
- Distance from second vertical slot to right edge:  $\frac{9}{16}$
- Distance from left edge to first horizontal slot:  $\frac{1}{16}$
- Distance between first and second horizontal slots:  $\frac{1}{16}$
- Distance from second horizontal slot to bottom edge:  $\frac{1}{16}$
- Distance from left edge to first rectangular slot:  $\frac{1}{8}$
- Distance between first and second rectangular slots:  $\frac{11}{16}$
- Distance from second rectangular slot to right edge:  $\frac{11}{32}$
- Distance from left edge to first circular hole:  $\frac{1}{8}$
- Distance between first and second circular holes:  $\frac{11}{16}$
- Distance from second circular hole to right edge:  $\frac{11}{32}$
- Distance from left edge to first rectangular slot:  $\frac{1}{8}$
- Distance between first and second rectangular slots:  $\frac{11}{16}$
- Distance from second rectangular slot to right edge:  $\frac{11}{32}$



PIECE NO. 7

NO. OFF : 1

Material : Soft Iron.



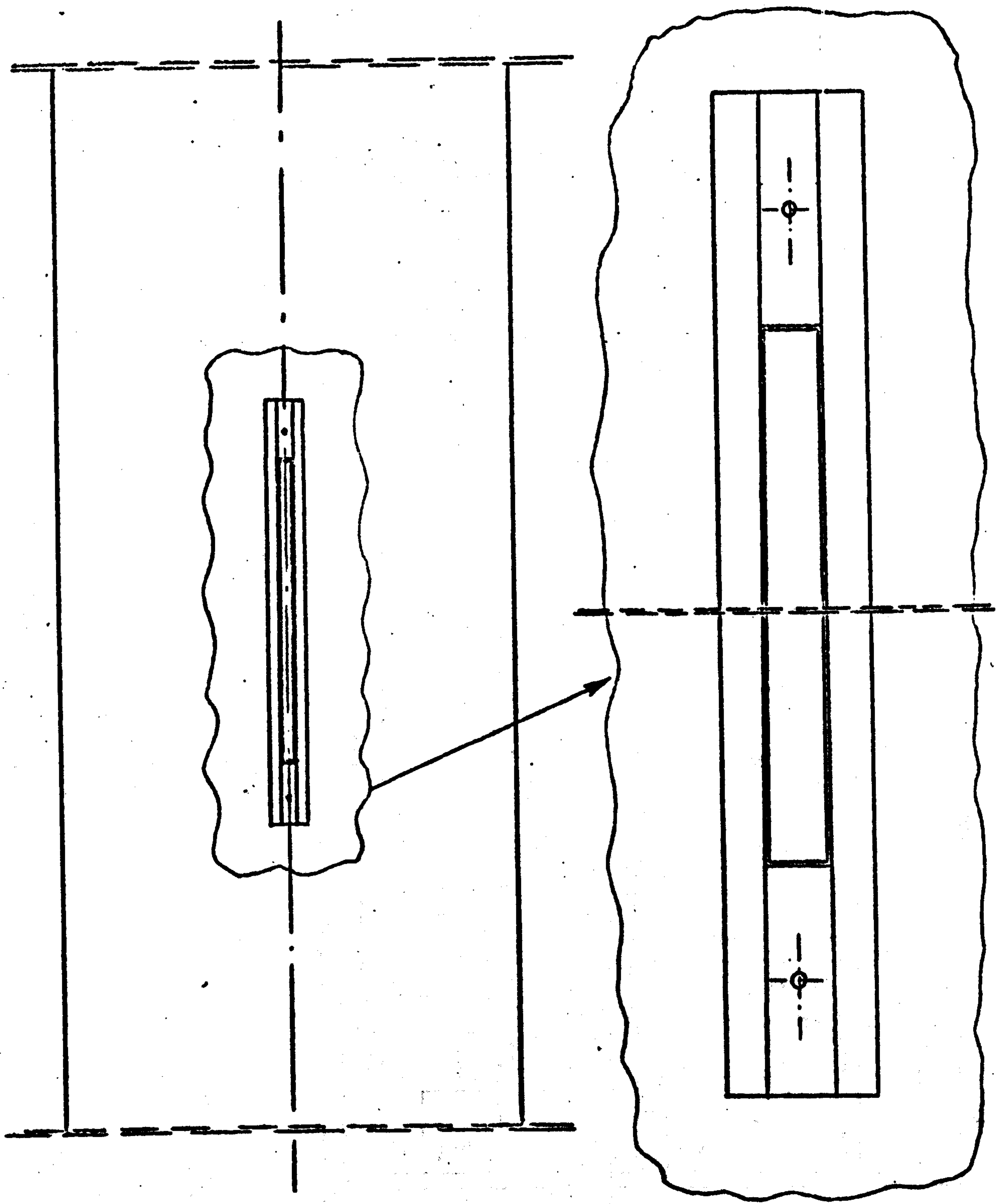
PIECE NO. 8

DIMS. IN. IN.

$\pm 0.002$

NO. OFF : 1

Material : Brass



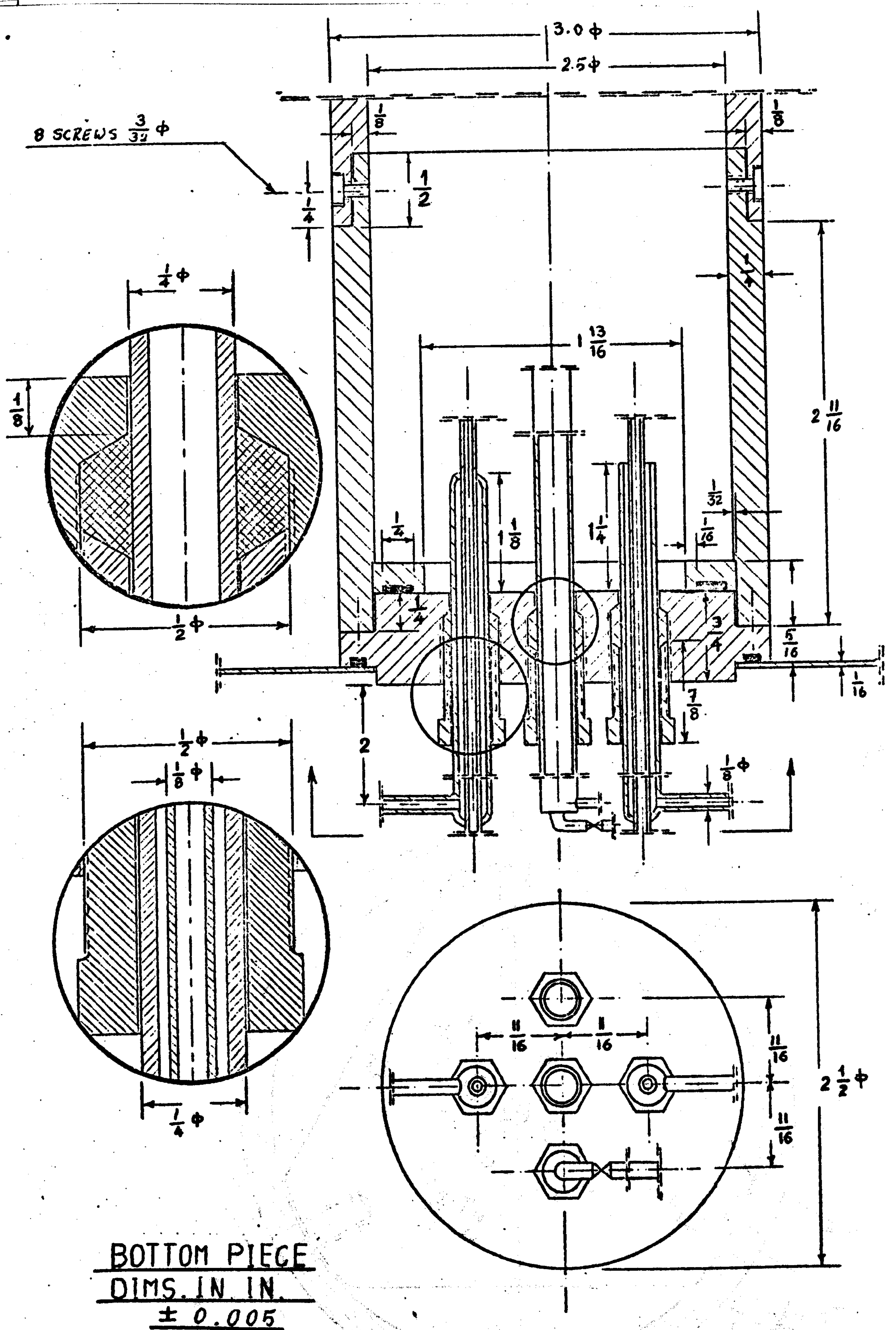
FRONT VIEW OF  
THE SENSOR

TOP PIECE



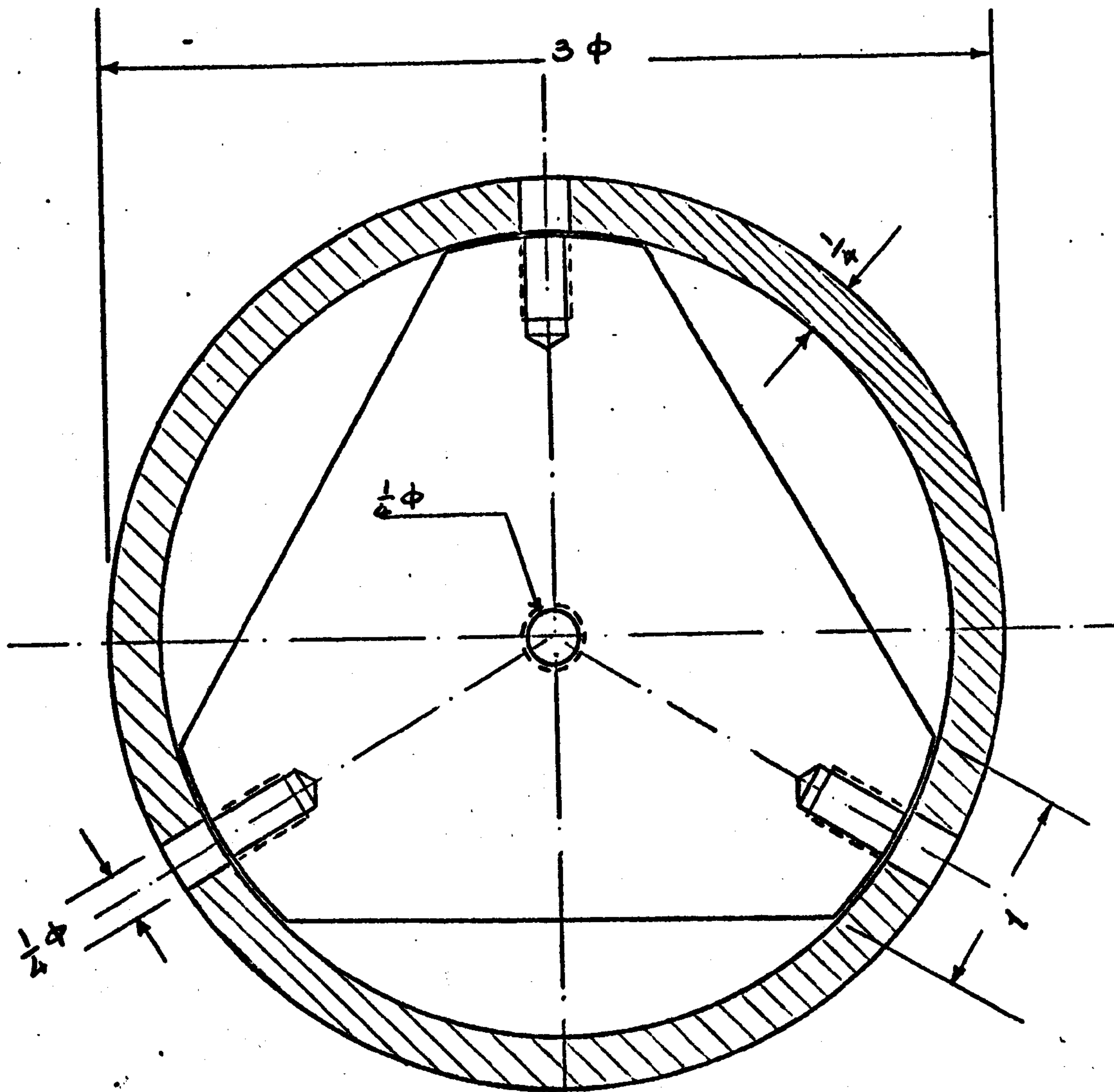




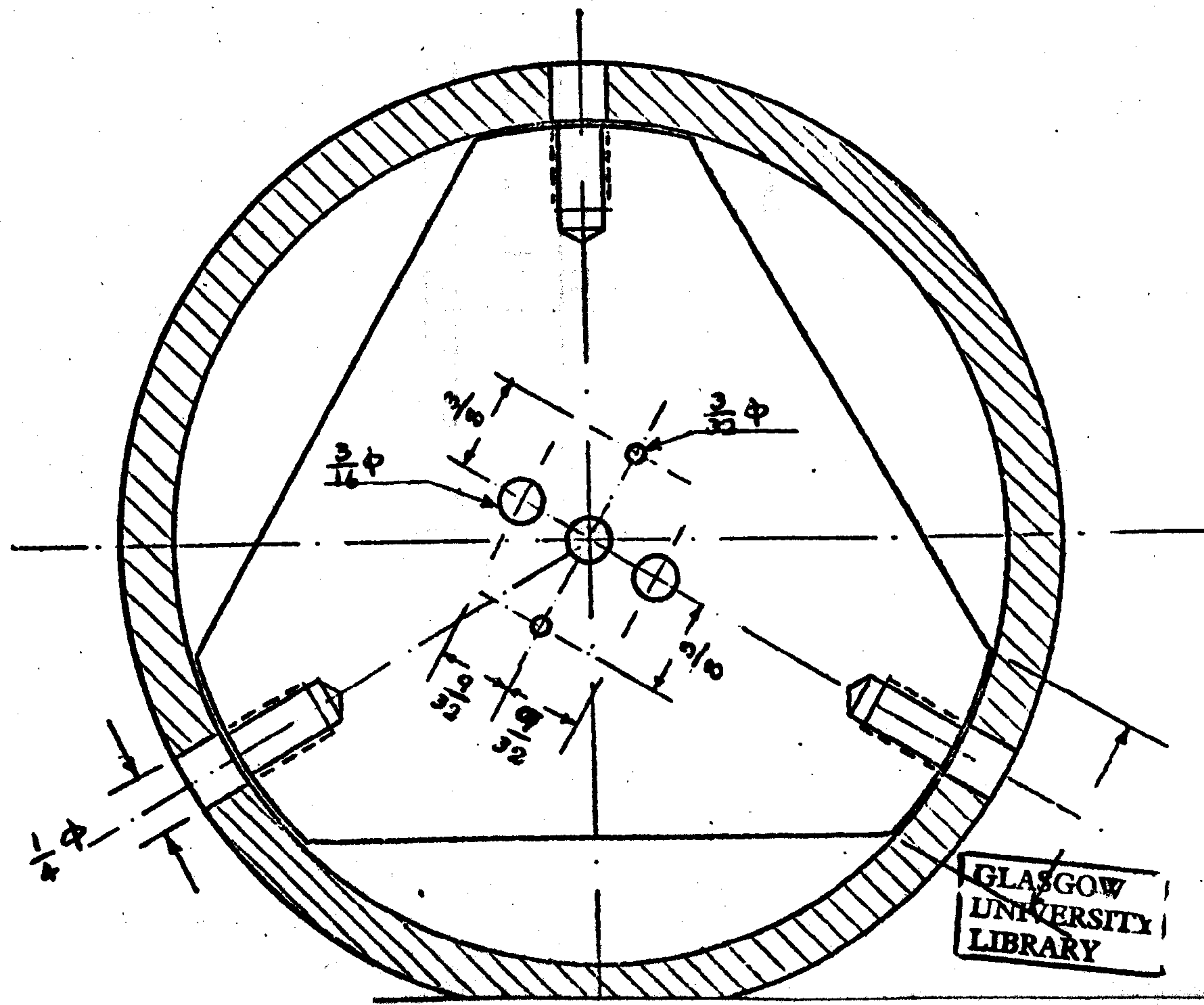




NO.OFF:  
33



NO.OFF:  
1



GLASGOW  
UNIVERSITY  
LIBRARY

